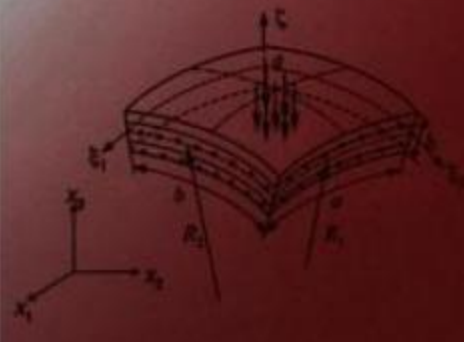
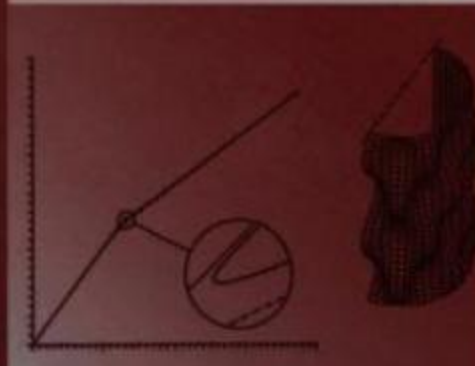
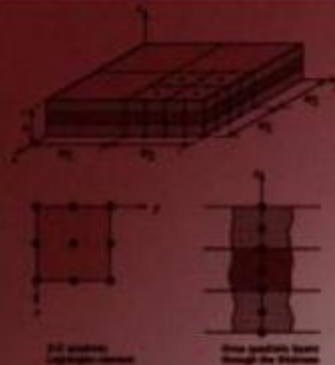


MECHANICS of LAMINATED COMPOSITE PLATES and SHELLS

Theory and Analysis

SECOND EDITION



**MECHANICS of
LAMINATED COMPOSITE
PLATES and SHELLS
Theory and Analysis**

S E C O N D E D I T I O N

J.N. REDDY



CRC PRESS

Boca Raton London New York Washington, D.C.

Library of Congress Cataloging-in-Publication Data

Reddy, J. N. (Junuthula Narasimha), 1945-

Mechanics of laminated composite plates and shells : theory and analysis / J.N. Reddy.—
2nd ed.

p. cm.

Rev. ed. of: Mechanics of laminated composite plates. c1997.

Includes bibliographical references and index.

ISBN 0-8493-1592-1 (alk. paper)

1. Plates (Engineering)—Mathematical models. 2. Shells (Engineering)—Mathematical
models. 3. Laminated materials—Mechanical properties—Mathematical models. 4.

Composite materials—Mechanical properties—Mathematical models. I. Reddy, J. N.
(Junuthula Narasimha), 1945-. Mechanics of laminated composite plates. II. Title.

TA660.P6R42 2003

624.1'7765—dc22

2003061067

This book contains information obtained from authentic and highly regarded sources. Reprinted material is quoted with permission, and sources are indicated. A wide variety of references are listed. Reasonable efforts have been made to publish reliable data and information, but the author and the publisher cannot assume responsibility for the validity of all materials or for the consequences of their use.

Neither this book nor any part may be reproduced or transmitted in any form or by any means, electronic or mechanical, including photocopying, microfilming, and recording, or by any information storage or retrieval system, without prior permission in writing from the publisher.

The consent of CRC Press LLC does not extend to copying for general distribution, for promotion, for creating new works, or for resale. Specific permission must be obtained in writing from CRC Press LLC for such copying.

Direct all inquiries to CRC Press LLC, 2000 N.W. Corporate Blvd., Boca Raton, Florida 33431.

Trademark Notice: Product or corporate names may be trademarks or registered trademarks, and are used only for identification and explanation, without intent to infringe.

Visit the CRC Press Web site at www.crcpress.com

© 2004 by CRC Press LLC

No claim to original U.S. Government works

International Standard Book Number 0-8493-1592-1

Library of Congress Card Number 2003061067

Printed in the United States of America 1 2 3 4 5 6 7 8 9 0

Printed on acid-free paper

To the Memory of

*My parents,
My brother,
My brother in-law,
My father in-law,
Hans Eggers,
Kalpana Chawla, ...*

About the Author

J. N. Reddy is a Distinguished Professor and the inaugural holder of the Oscar S. Wyatt Endowed Chair in the Department of Mechanical Engineering at Texas A&M University, College Station, Texas. Prior to his current position, he worked as a postdoctoral fellow at the University of Texas at Austin (1973–74), as a research scientist for Lockheed Missiles and Space Company (1974), and taught at the University of Oklahoma (1975–1980) and Virginia Polytechnic Institute and State University (1980–1992), where he was the inaugural holder of the Clifton C. Garvin Endowed Professorship.

Professor Reddy is the author of over 300 journal papers and 13 text books on theoretical formulations and finite-element analysis of problems in solid and structural mechanics (plates and shells), composite materials, computational fluid dynamics and heat transfer, and applied mathematics. His contributions to mechanics of composite materials and structures are well known through his research on refined plate and shell theories and their finite element models.

Professor Reddy is the first recipient of the University of Oklahoma College of Engineering's Award for Outstanding Faculty Achievement in Research, the 1984 *Walter L. Huber Civil Engineering Research Prize* of the American Society of Civil Engineers (ASCE), the 1985 Alumni Research Award at Virginia Polytechnic Institute, and 1992 *Worcester Reed Warner Medal* and 1995 *Charles Russ Richards Memorial Award* of the American Society of Mechanical Engineers (ASME). He received German Academic Exchange (DAAD) and von Humboldt Foundation (Germany) research awards. Recently, he received the 1997 *Melvin R. Lohmann Medal* from Oklahoma State University's College of Engineering, Architecture and Technology, the 1997 *Archie Higdon Distinguished Educator Award* from the Mechanics Division of the American Society of Engineering Education, the 1998 *Nathan M. Newmark Medal* from the American Society of Civil Engineers, the 2000 *Excellence in the Field of Composites Award* from the American Society of Composite Materials, the 2000 *Faculty Distinguished Achievement Award for Research*, the 2003 *Bush Excellence Award for Faculty in International Research* award from Texas A&M University, and 2003 *Computational Structural Mechanics Award* from the U.S. Association for Computational Mechanics.

Professor Reddy is a fellow of the American Academy of Mechanics (AAM), the American Society of Civil Engineers (ASCE), the American Society of Mechanical Engineers (ASME), the American Society of Composites (ASC), International Association of Computational Mechanics (IACM), U.S. Association of Computational Mechanics (USACM), the Aeronautical Society of India (ASI), and the American Society of Composite Materials. Dr. Reddy is the Editor-in-Chief of the journals *Mechanics of Advanced Materials and Structures* (Taylor and Francis), *International Journal of Computational Engineering Science* and *International Journal Structural Stability and Dynamics* (both from World Scientific), and he serves on the editorial boards of over two dozen other journals.

Contents

Preface to the Second Edition	xix
Preface to the First Edition	xxi
1 Equations of Anisotropic Elasticity, Virtual Work Principles, and Variational Methods	1
1.1 Fiber-Reinforced Composite Materials	1
1.2 Mathematical Preliminaries.....	3
1.2.1 General Comments	3
1.2.2 Vectors and Tensors.....	3
1.3 Equations of Anisotropic Entropy.....	12
1.3.1 Introduction	12
1.3.2 Strain-Displacement Equations.....	13
1.3.3 Strain Compatibility Equations.....	18
1.3.4 Stress Measures	18
1.3.5 Equations of Motion	19
1.3.6 Generalized Hooke's Law.....	22
1.3.7 Thermodynamic Principles.....	34
1.4 Virtual Work Principles	38
1.4.1 Introduction	38
1.4.2 Virtual Displacements and Virtual Work	38
1.4.3 Variational Operator and Euler Equations.....	40
1.4.4 Principle of Virtual Displacements.....	44
1.5 Variational Methods.....	58
1.5.1 Introduction	58
1.5.2 The Ritz Method	58
1.5.3 Weighted-Residual Methods.....	64
1.6 Summary	71
Problems	72
References for Additional Reading.....	78
2 Introduction to Composite Materials	81
2.1 Basic Concepts and Terminology	81
2.1.1 Fibers and Matrix	81
2.1.2 Laminae and Laminates.....	83
2.2 Constitutive Equations of a Lamina	85
2.2.1 Generalized Hooke's Law	85
2.2.2 Characteristics of a Unidirectional Lamina.....	86

2.3 Transformation of Stresses and Strains.....	89
2.3.1 Coordinate Transformations.....	89
2.3.2 Transformation of Stress Components	90
2.3.3 Transformation of Strain Components	93
2.3.4 Transformation of Material Coefficients.....	96
2.4 Plan Stress Constitutive Relations	99
Problems	103
References for Additional Reading.....	106
3 Classical and First-Order Theories of Laminated Composite Plates	109
3.1 Introduction	109
3.1.1 Preliminary Comments.....	109
3.1.2 Classification of Structural Theories.....	109
3.2 An Overview of Laminated Plate Theories.....	110
3.3 The Classical Laminated Plate Theory.....	112
3.3.1 Assumptions	112
3.3.2 Displacements and Strains	113
3.3.3 Lamina Constitutive Relations	117
3.3.4 Equations of Motion	119
3.3.5 Laminate Constitutive Equations.....	127
3.3.6 Equations of Motion in Terms of Displacements	129
3.4 The First-Order Laminated Plate Theory	132
3.4.1 Displacements and Strains	132
3.4.2 Equations of Motion	134
3.4.3 Laminate Constitutive Equations.....	137
3.4.4 Equations of Motion in Terms of Displacements	139
3.5 Laminate Stiffnesses for Selected Laminates.....	142
3.5.1 General Discussion	142
3.5.2 Single-Layer Plates.....	144
3.5.3 Symmetric Laminates	148
3.5.4 Antisymmetric Laminates	152
3.5.5 Balanced and Quasi-Isotropic Laminates	156
Problems	157
References for Additional Reading.....	161
4 One-Dimensional Analysis of Laminated Composite Plates	165
4.1 Introduction	165
4.2 Analysis of Laminated Beams Using CLPT	167
4.2.1 Governing Equations.....	167
4.2.2 Bending	169
4.2.3 Buckling	176
4.2.4 Vibration	182

4.3 Analysis of Laminated Beams Using FSDT	187
4.3.1 Governing Equations	187
4.3.2 Bending	188
4.3.3 Buckling	192
4.3.4 Vibration	197
4.4 Cylindrical Bending Using CLPT	200
4.4.1 Governing Equations	200
4.4.2 Bending	203
4.4.3 Buckling	208
4.4.4 Vibration	209
4.5 Cylindrical Bending Using FSDT	214
4.5.1 Governing Equations	214
4.5.2 Bending	215
4.5.3 Buckling	216
4.5.4 Vibration	219
4.6 Vibration Suppression in Beams	222
4.6.1 Introduction	222
4.6.2 Theoretical Formulation	222
4.6.3 Analytical Solution	227
4.6.4 Numerical Results	230
4.7 Closing Remarks	232
Problems	232
References for Additional Reading	242
5 Analysis of Specially Orthotropic Laminates Using CLPT	245
5.1 Introduction	245
5.2 Bending of Simply Supported Rectangular Plates	246
5.2.1 Governing Equations	246
5.2.2 The Navier Solution	247
5.3 Bending of Plates with Two Opposite Edges Simply Supported	255
5.3.1 The Lévy Solution Procedure	255
5.3.2 Analytical Solutions	257
5.3.3 Ritz Solution	262
5.4 Bending of Rectangular Plates with Various Boundary Conditions	265
5.4.1 Virtual Work Statements	265
5.4.2 Clamped Plates	266
5.4.3 Approximation Functions for Other Boundary Conditions	269
5.5 Buckling of Simply Supported Plates Under Compressive Loads	271
5.5.1 Governing Equations	271
5.5.2 The Navier Solution	272
5.5.3 Biaxial Compression of a Square Laminate ($k = 1$)	273
5.5.4 Biaxial Loading of a Square Laminate	274
5.5.5 Uniaxial Compression of a Rectangular Laminate ($k = 0$)	274

5.6 Buckling of Rectangular Plates Under In-Plane Shear Load	278
5.6.1 Governing Equation.....	278
5.6.2 Simply Supported Plates.....	278
5.6.3 Clamped Plates.....	280
5.7 Vibration of Simply Supported Plates	282
5.7.1 Governing Equations.....	282
5.7.2 Solution	282
5.8 Buckling and Vibration of Plates with Two Parallel Edges	
Simply Supported	285
5.8.1 Introduction	285
5.8.2 Buckling by Direct Integration	287
5.8.3 Vibration by Direct Integration	288
5.8.4 Buckling and Vibration by the State-Space Approach.....	288
5.9 Transient Analysis	290
5.9.1 Preliminary Comments.....	290
5.9.2 Spatial Variation of the Solution	290
5.9.3 Time Integration.....	292
5.10 Closure	293
Problems	293
References for Additional Reading.....	296
6 Analytical Solutions of Rectangular Laminated Plates Using CLPT	297
6.1 Governing Equations in Terms of Displacements	297
6.2 Admissible Boundary Conditions for the Navier Solutions.....	299
6.3 Navier Solutions of Antisymmetric Cross-Ply Laminates	301
6.3.1 Boundary Conditions	301
6.3.2 Solution	304
6.3.3 Bending	308
6.3.4 Determination of Stresses	309
6.3.5 Buckling	317
6.3.6 Vibration	323
6.4 Navier Solutions of Antisymmetric Angle-Ply Laminates	326
6.4.1 Boundary Conditions	326
6.4.2 Solution	328
6.4.3 Bending	329
6.4.4 Determination of Stresses	330
6.4.5 Buckling	335
6.4.6 Vibration	337
6.5 The Lévy Solutions.....	339
6.5.1 Introduction	339
6.5.2 Solution Procedure.....	342
6.5.3 Antisymmetric Cross-Ply Laminates.....	348
6.5.4 Antisymmetric Angle-Ply Laminates	353

6.6 Analysis of Midplane Symmetric Laminates.....	356
6.6.1 Introduction	356
6.6.2 Governing Equations.....	356
6.6.3 Weak Forms	357
6.6.4 The Ritz Solution.....	358
6.6.5 Simply Supported Plates.....	358
6.6.6 Other Boundary Conditions.....	360
6.7 Transient Analysis	361
6.7.1 Preliminary Comments.....	361
6.7.2 Equations of Motion	361
6.7.3 Numerical Time Integration.....	362
6.7.4 Numerical Results	364
6.8 Summary	371
Problems	371
References for Additional Reading.....	375
7 Analytical Solutions of Rectangular Laminated Plates Using FSDT	377
7.1 Introduction	377
7.2 Simply Supported Antisymmetric Cross-Ply Laminated Plates	379
7.2.1 Solution for the General Case	379
7.2.2 Bending	381
7.2.3 Buckling	388
7.2.4 Vibration.....	394
7.3 Simply Supported Antisymmetric Angle-Ply Laminated Plates	400
7.3.1 Boundary Conditions	400
7.3.2 The Navier Solution	402
7.3.3 Bending	404
7.3.4 Buckling	405
7.3.5 Vibration.....	406
7.4 Antisymmetric Cross-Ply Laminates with Two Opposite Edges Simply Supported.....	412
7.4.1 Introduction	412
7.4.2 The Lévy Type Solution	413
7.4.3 Numerical Examples	415
7.5 Antisymmetric Angle-Ply Laminates with Two Opposite Edges Simply Supported.....	421
7.5.1 Introduction	421
7.5.2 Governing Equations.....	421
7.5.3 The Lévy Solution	423
7.5.4 Numerical Examples	425
7.6 Transient Solutions	430
7.7 Vibration Control of Laminated Plates	437
7.7.1 Preliminary Comments.....	437
7.7.2 Theoretical Formulation.....	438

7.7.3 Velocity Feedback Control	438
7.7.4 Analytical Solution	439
7.7.5 Numerical Results and Discussion	441
7.8 Summary	442
Problems	444
References for Additional Reading	445
8 Theory and Analysis of Laminated Shells	449
8.1 Introduction	449
8.2 Governing Equations	450
8.2.1 Geometric Properties of the Shell	450
8.2.2 Kinetics of the Shell	454
8.2.3 Kinematics of the Shell	455
8.2.4 Equations of Motion	457
8.2.5 Laminate Constitutive Relations	461
8.3 Theory of Doubly-Curved Shells	462
8.3.1 Equations of Motion	462
8.3.2 Analytical Solution	463
8.4 Vibration and Buckling of Cross-Ply Laminated Circular Cylindrical Shells	473
8.4.1 Equations of Motion	473
8.4.2 Analytical Solution Procedure	475
8.4.3 Boundary Conditions	479
8.4.4 Numerical Results	480
Problems	483
References for Additional Reading	483
9 Linear Finite Element Analysis of Composite Plates and Shells	487
9.1 Introduction	487
9.2 Finite Element Models of the Classical Plate Theory (CLPT)	488
9.2.1 Weak Forms	488
9.2.2 Spatial Approximations	490
9.2.3 Semidiscrete Finite Element Model	499
9.2.4 Fully Discretized Finite Element Models	500
9.2.5 Quadrilateral Elements and Numerical Integration	503
9.2.6 Post-Computation of Stresses	510
9.2.7 Numerical Results	510
9.3 Finite Element Models of Shear Deformation Plate Theory (FSDT)	515
9.3.1 Weak Forms	515
9.3.2 Finite Element Model	516
9.3.3 Penalty Function Formulation and Shear Locking	520
9.3.4 Post-Computation of Stresses	524
9.3.5 Bending Analysis	525
9.3.6 Vibration Analysis	540
9.3.7 Transient Analysis	542

9.4 Finite Element Analysis of Shells	543
9.4.1 Weak Forms	543
9.4.2 Finite Element Model	546
9.4.3 Numerical Results	549
9.5 Summary	558
Problems	560
References for Additional Reading	560
10 Nonlinear Analysis of Composite Plates and Shells	567
10.1 Introduction	567
10.2 Classical Plate Theory	568
10.2.1 Governing Equations	568
10.2.2 Virtual Work Statement	569
10.2.3 Finite Element Model	572
10.3 First-Order Shear Deformation Plate Theory	575
10.3.1 Governing Equations	575
10.3.2 Virtual Work Statements	576
10.3.3 Finite Element Model	578
10.4 Time Approximation and the Newton-Raphson Method	583
10.4.1 Time Approximations	583
10.4.2 The Newton-Raphson Method	584
10.4.3 Tangent Stiffness Coefficients for CLPT	586
10.4.4 Tangent Stiffness Coefficients for FSDT	590
10.4.5 Membrane Locking	594
10.5 Numerical Examples of Plates	596
10.5.1 Preliminary Comments	596
10.5.2 Isotropic and Orthotropic Plates	596
10.5.3 Laminated Composite Plates	601
10.5.4 Effect of Symmetry Boundary Conditions on Nonlinear Response	604
10.5.5 Nonlinear Response Under In-Plane Compressive Loads	608
10.5.6 Nonlinear Response of Antisymmetric Cross-Ply Laminated Plate Strips	608
10.5.7 Transient Analysis of Composite Plates	612
10.6 Functionally Graded Plates	613
10.6.1 Background	613
10.6.2 Theoretical Formulation	615
10.6.3 Thermomechanical Coupling	616
10.6.4 Numerical Results	617
10.7 Finite Element Models of Laminated Shell Theory	621
10.7.1 Governing Equations	621
10.7.2 Finite Element Model	622
10.7.3 Numerical Examples	625

10.8 Continuum Shell Finite Element.....	627
10.8.1 Introduction	627
10.8.2 Incremental Equations of Motion.....	628
10.8.3 Continuum Finite Element Mode.....	631
10.8.4 Shell Finite Element	633
10.8.5 Numerical Examples	638
10.8.6 Closure.....	644
10.9 Postbuckling Response and Progressive Failure of Composite Panels in Compression.....	645
10.9.1 Preliminary Comments	645
10.9.2 Experimental Study.....	645
10.9.3 Finite Element Models.....	647
10.9.4 Failure Analysis	648
10.9.5 Results for Panel C4	650
10.9.6 Results for Panel H4.....	655
10.10 Closure	658
Problems	658
References for Additional Reading.....	664
11 Third-Order Theory of Laminated Composite Plates and Shells ..	671
11.1 Introduction	671
11.2 A Third-Order Plate Theory	671
11.2.1 Displacement Field	671
11.2.2 Strains and Stresses.....	674
11.2.3 Equations of Motion	674
11.3 Higher-Order Laminate Stiffness Characteristics	677
11.3.1 Single-Layer Plates	678
11.3.2 Symmetric Laminates.....	680
11.3.3 Antisymmetric Laminates.....	681
11.4 The Navier Solutions.....	682
11.4.1 Preliminary Comments	682
11.4.2 Antisymmetric Cross-Ply Laminates.....	684
11.4.3 Antisymmetric Angle-Ply Laminates	687
11.4.4 Numerical Results	689
11.5 Lévy Solutions of Cross-Ply Laminates	699
11.5.1 Preliminary Comments	699
11.5.2 Solution Procedure	701
11.5.3 Numerical Results	704
11.6 Finite Element Model of Plates.....	706
11.6.1 Introduction	706
11.6.2 Finite Element Model.....	707
11.6.3 Numerical Results	712
11.6.4 Closure.....	714

11.7 Equations of Motion of the Third-Order Theory of Doubly-Curved Shells	718
Problems	720
References for Additional Reading.....	721
12 Layerwise Theory and Variable Kinematic Models	725
12.1 Introduction	725
12.1.1 Motivation.....	725
12.1.2 An Overview of Layerwise Theories	726
12.2 Development of the Theory.....	730
12.2.1 Displacement Field	730
12.2.2 Strains and Stresses.....	733
12.2.3 Equations of Motion	734
12.2.4 Laminate Constitutive Equations.....	736
12.3 Finite Element Model.....	738
12.3.1 Layerwise Model.....	738
12.3.2 Full Layerwise Model Versus 3-D Finite Element Model	739
12.3.3 Considerations for Modeling Relatively Thin Laminates	742
12.3.4 Bending of a Simply Supported (0/90/0) Laminate	746
12.3.5 Free Edge Stresses in a (45/-45) _s Laminate	753
12.4 Variable Kinematic Formulations.....	759
12.4.1 Introduction	759
12.4.2 Multiple Assumed Displacement Fields.....	762
12.4.3 Incorporation of Delamination Kinematics.....	764
12.4.4 Finite Element Model.....	766
12.4.5 Illustrative Examples	769
12.5 Application to Adaptive Structures.....	780
12.5.1 Introduction	780
12.5.2 Governing Equations.....	783
12.5.3 Finite Element Model.....	785
12.5.4 An Example	787
12.6 Layerwise Theory of Cylindrical Shells.....	794
12.6.1 Introduction	794
12.6.2 Unstiffened Shells.....	794
12.6.3 Stiffened Shells	798
12.6.4 Postbuckling of Laminated Cylinders.....	806
12.7 Closure	812
References for Additional Reading.....	816
Subject Index.....	821

Preface to the Second Edition

In the seven years since the first edition of this book appeared some significant developments have taken place in the area of materials modeling in general and in composite materials and structures in particular. Foremost among these developments have been the smart materials and structures, functionally graded materials (FGMs), and nanoscience and technology -- each topic deserves to be treated in a separate monograph. While the author's expertise and contributions in these areas are limited, it is felt that the reader should be made aware of the developments in the analysis of smart and FGM structures. The subject of nanoscience and technology, of course, is outside the scope of the present study. Also, the first edition of this book did not contain any material on the theory and analysis of laminated shells. It should be an integral part of any study on laminated composite structures.

The focus for the present edition of this book remains the same – the education of the individual who is interested in gaining a good understanding of the mechanics theories and associated finite element models of laminated composite structures. Very little material has been deleted. New material has been added in most chapters along with some rearrangement of topics to improve the clarity of the overall presentation. In particular, the material from the first three chapters is condensed into a single chapter (Chapter 1) in this second edition to make room for the new material. Thus Chapter 1 contains certain mathematical preliminaries, a study of the equations of anisotropic elasticity, and an introduction to the principle of virtual displacements and classical variational methods (the Ritz and Galerkin methods). Chapters 2 through 7 correspond to Chapters 4 through 9, respectively, from the first edition, and they have been revised to include smart structures and functionally graded materials. A completely new chapter, Chapter 8, on theory and analysis of laminated shells is added to overcome the glaring omission in the first edition of this book. Chapters 9 and 10 (corresponding to Chapters 10 and 13 in the first edition) are devoted to linear and nonlinear finite element analysis, respectively, of laminated plates and shells. These chapters are extensively revised to include more details on the derivation of tangent stiffness matrices and finite element models of shells with numerical examples. Chapters 11 and 12 in the present edition correspond to Chapters 11 and 12 of the first edition, which underwent significant revisions to include laminated shells. The problem sets essentially remained the same with the addition of a few problems here and there.

The acknowledgments and sincere thanks and feelings expressed in the preface to the first edition still hold but they are not repeated here. It is a pleasure to acknowledge the help of my colleagues, especially Dr. Zhen-Qiang Cheng, for their help with the proofreading of the manuscript. Thanks are also due to Mr. Román

Arciniega for providing the numerical results of some examples on shells included in Chapter 9.

J. N. Reddy
College Station, Texas

Preface to the First Edition

The dramatic increase in the use of composite materials in all types of engineering structures (e.g., aerospace, automotive, and underwater structures, as well as in medical prosthetic devices, electronic circuit boards, and sports equipment) and the number of journals and research papers published in the last two decades attest to the fact that there has been a major effort to develop composite material systems, and to analyze and design structural components made from composite materials.

The subject of composite materials is truly an interdisciplinary area where chemists, material scientists, chemical engineers, mechanical engineers, and structural engineers contribute to the overall product. The number of students taking courses in composite materials and structures has steadily increased in recent years, and the students are drawn to these courses from a variety of disciplines. The courses offered at universities and the books published on composite materials are of three types: material science, mechanics, and design. The present book belongs to the *mechanics* category.

The motivation for the present book has come from many years of the author's research and teaching in laminated composite structures and from the fact there does not exist a book that contains a detailed coverage of various laminate theories, analytical solutions, and finite element models. The book is largely based on the author's original work on refined theories of laminated composite plates and shells, and analytical and finite element solutions he and his collaborators have developed over the last two decades.

Some mathematical preliminaries, equations of anisotropic elasticity, and virtual work principles and variational methods are reviewed in Chapters 1 through 3. A reader who has had a course in elasticity or energy and variational principles of mechanics may skip these chapters and go directly to Chapter 4, where certain terminology common to composite materials is introduced, followed by a discussion of the constitutive equations of a lamina and transformation of stresses and strains. Readers who have had a basic course in composites may skip Chapter 4 also.

The major journey of the book begins with Chapter 5, where a complete derivation of the equations of motion of the classical and first-order shear deformation laminated plate theories is presented, and laminate stiffness characteristics of selected laminates are discussed. Chapter 6 includes applications of the classical and first-order shear deformation theories to laminated beams and plate strips in cylindrical bending. Here analytical solutions are developed for bending, buckling, natural vibration, and transient response of simple beam and plate structures. Chapter 7 deals with the analysis of specially orthotropic rectangular laminates using the classical laminated plate theory (CLPT). Here, the parametric effects of material anisotropy, lamination scheme, and plate aspect ratio on bending deflections and stresses, buckling loads, vibration frequencies, and transient response are discussed.

Analytical solutions for bending, buckling, natural vibration, and transient response of rectangular laminates based on the Navier and Lévy solution approaches are presented in Chapters 8 and 9 for the classical and first-order shear deformation plate theories (FSDT), respectively. The Rayleigh-Ritz solutions are also discussed for laminates that do not admit the Navier solutions. Chapter 10 deals with finite element analysis of composite laminates. One-dimensional (for beams and plate strips) as well as two-dimensional (plates) finite element models based on CLPT and FSDT are discussed and numerical examples are presented.

Chapters 11 and 12 are devoted to higher-order (third-order) laminate theories and layerwise theories, respectively. Analytical as well as finite element models are discussed. The material included in these chapters is up to date at the time of this writing. Finally, Chapter 13 is concerned about the geometrically nonlinear analysis of composite laminates. Displacement finite element models of laminated plates with the von Kármán nonlinearity are derived, and numerical results are presented for some typical problems.

The book is suitable as a reference for engineers and scientists working in industry and academia, and it can be used as a textbook in a graduate course on theory and/or analysis of composite laminates. It can also be used for a course on stress analysis of laminated composite plates. An introductory course on mechanics of composite materials may prove to be helpful but not necessary because a review of the basics is included in the first four chapters of this book. The first course may cover Chapters 1 through 8 or 9, and a second course may cover Chapters 8 through 13.

The author wishes to thank all his former doctoral students for their research collaboration on the subject. In particular, Chapters 7 through 13 contain results of the research conducted by Drs. Ahmed Khdeir, Stephen Engelstad, Asghar Nosier, and Donald Robbins, Jr. on the development of theories, analytical solutions, and finite element analysis of equivalent single-layer and layerwise theories of composite laminates. The research of the author in composite materials was influenced by many researchers. The author wishes to thank Professor Charles W. Bert of the University of Oklahoma, Professor Robert M. Jones of the Virginia Polytechnic Institute and State University, Professor A. V. Krishna Murty of the Indian Institute of Science, and Dr. Nicholas J. Pagano of Wright-Patterson Air Force Base. It is also the author's pleasure to acknowledge the help of Mr. Praveen Grama, Mr. Dakshina Moorthy, and Mr. Govind Rengarajan for their help with the proofreading of the manuscript. The author is indebted to Dr. Filis Kokkinos for his dedication and innovative and creative production of the final artwork in this book. Indeed, without his imagination and hundreds of hours of effort the artwork would not have looked as beautiful, professional, and technical as it does.

The author gratefully acknowledges the support of his research in composite materials in the last two decades by the Office of Naval Research (ONR), the Air Force Office of Scientific Research (AFOSR), the U.S. Army Research Office (ARO), the National Aeronautics and Space Administration (NASA Lewis and NASA Langley), the U.S. National Science Foundation (NSF), and the *Oscar S. Wyatt Chair* in the Department of Mechanical Engineering at Texas A&M University. Without this support, it would not have been possible to contribute to the subject of this book. The author is also grateful to Professor G. P. Peterson, a colleague

and friend, for his encouragement and support of the author's professional activities at Texas A&M University.

The writing of this book took thousands of hours over the last ten years. Most of these hours came from evenings and holidays that could have been devoted to family matters. While no words of gratitude can replace the time lost with family, it should be recorded that the author is grateful to his wife Aruna for her care, devotion, and love, and to his daughter Anita and son Anil for their understanding and support.

During the long period of writing this book, the author has lost his father, brother, brother in-law, father in-law, and a friend (Hans Eggars) - all suddenly. While death is imminent, the suddenness makes it more difficult to accept. This book is dedicated to the memory of these individuals.

J. N. Reddy
College Station, Texas

All that is not given is lost

Equations of Anisotropic Elasticity, Virtual Work Principles, and Variational Methods

1.1 Fiber-Reinforced Composite Materials

Composite materials consist of two or more materials which together produce desirable properties that cannot be achieved with any of the constituents alone. Fiber-reinforced composite materials, for example, contain high strength and high modulus *fibers* in a *matrix* material. Reinforced steel bars embedded in concrete provide an example of fiber-reinforced composites. In these composites, fibers are the principal load-carrying members, and the matrix material keeps the fibers together, acts as a load-transfer medium between fibers, and protects fibers from being exposed to the environment (e.g., moisture, humidity, etc.).

It is known that fibers are stiffer and stronger than the same material in bulk form, whereas matrix materials have their usual bulk-form properties. Geometrically, fibers have near crystal-sized diameter and a very high length-to-diameter ratio. Short fibers, called *whiskers*, paradoxically exhibit better structural properties than long fibers. To gain a full understanding of the behavior of fibers, matrix materials, agents that are used to enhance bonding between fibers and matrix, and other properties of fiber-reinforced materials, it is necessary to know certain aspects of material science. Since the present study is entirely devoted to mechanics aspects and analysis methods of fiber-reinforced composite materials, no attempt is made here to present basic material science aspects, such as the molecular structure or inter-atomic forces those hold the matter together. However, an abstract understanding of the material behavior is useful.

Materials are studied at various levels: atomic level, nano-level, single-crystal level, a group of crystals, and so on. For the purpose of gaining some insight into the material behavior, we consider a basic unit of material as one that has properties, such as the modulus, strength, thermal coefficient of expansion, electrical resistance, etc., whose magnitudes depend on the direction. The directional dependence of properties is a result of the inter-atomic bonds, which are “stronger” in one direction than in other directions. Materials are “processed” such that the basic units are aligned so that the desired property is maximized in a given direction. Fibers provide an example of such materials. When a property is maximized in one direction, it may be achieved at the expense of the same property in other directions and other properties in the same direction. When materials are processed such that the basic

units are randomly oriented, the resulting material tends to have the same value of the property, in an average statistical sense, in all directions. Such materials are called *isotropic* materials. A matrix material, which is made in bulk form, provides an example of isotropic materials. Material scientists are continuously striving to develop better materials for specific applications. The fibers and matrix materials used in composites are either metallic or non-metallic. The fiber materials in use are common metals like aluminum, copper, iron, nickel, steel, and titanium, and organic materials like glass, boron, and graphite materials.

Fiber-reinforced composite materials for structural applications are often made in the form of a thin layer, called *lamina*. A lamina is a macro unit of material whose material properties are determined through appropriate laboratory tests. Structural elements, such as bars, beams or plates are then formed by stacking the layers to achieve desired strength and stiffness. Fiber orientation in each lamina and stacking sequence of the layers can be chosen to achieve desired strength and stiffness for a specific application. It is the purpose of the present study to develop equations that describe appropriate kinematics of deformation, govern force equilibrium, and represent the material response of laminated structural elements.

Analysis of structural elements made of laminated composite materials involves several steps. As shown in Figure 1.1.1, the analysis requires a knowledge of anisotropic elasticity, structural theories (i.e., kinematics of deformation) of laminates, analytical or computational methods to determine solutions of the governing equations, and failure theories to predict modes of failures and to determine failure loads. A detailed study of the theoretical formulations and solutions of governing equations of laminated composite plate structures constitutes the objective of the present book.

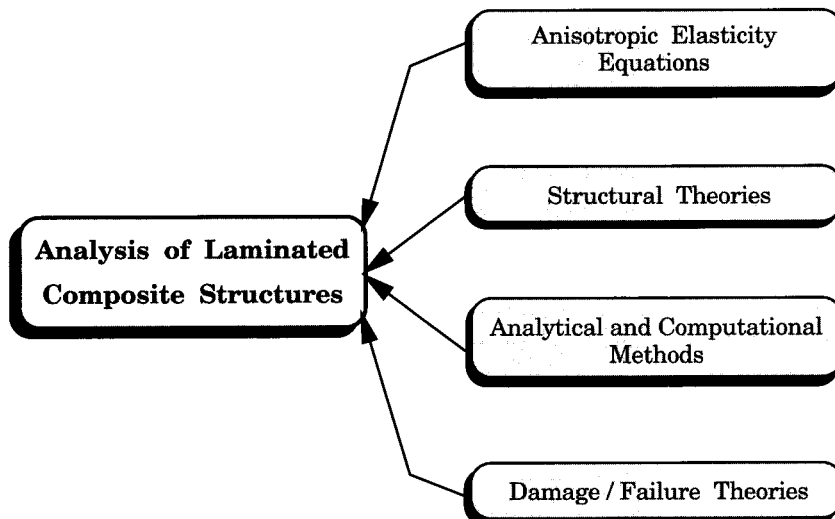


Figure 1.1.1: Basic blocks in the analysis of composite materials.

Following this general introduction, a review of vectors and tensors, integral relations, equations governing a deformable anisotropic medium, and virtual work principles and variational methods is presented, as they are needed in the sequel. Readers familiar with these topics can skip the remaining portion of this chapter and go directly to Chapter 2.

1.2 Mathematical Preliminaries

1.2.1 General Comments

The quantities used to express physical laws can be classified into two classes, according to the information needed to specify them completely: scalars and nonscalars. The scalars are given by a single number. Nonscalar quantities require not only a magnitude specified, but also additional information, such as direction. Time, temperature, volume, and mass density provide examples of scalars. Displacement, temperature gradient, force, moment, and acceleration are examples of nonscalars.

The term *vector* is used to imply a nonscalar that has magnitude and “direction” and obeys the parallelogram law of vector addition and rules of scalar multiplication. Vector in modern mathematical analysis is an abstraction of the elementary notion of a *physical vector*, and it is “an element from a linear vector space.” While the definition of a vector in abstract analysis does not require the vector to have a magnitude, in nearly all cases of practical interest the vector is endowed with a magnitude. In this book, we need only vectors with magnitude. Some nonscalar quantities require the specification of magnitude and two directions. For example, the specification of stress requires not only a force, but also an area upon which the force acts. A stress is a second-order *tensor*. Sometimes a vector is referred to as a tensor of order one, and a tensor of order 2 is also called a *dyad*. First- and second-order tensors (i.e., vectors and dyads) will be of primary interest in the present study (see [1-8] for additional details). We also encounter third-order and fourth-order tensors in the discussion of constitutive equations. A brief discussion of vectors and tensors is presented next.

1.2.2 Vectors and Tensors

In the analytical description of physical phenomena, a coordinate system in the chosen frame of reference is introduced, and various physical quantities involved in the description are expressed in terms of measurements made in that system. The description thus depends upon the chosen coordinate system and may appear different in another type of coordinate system. The laws of nature, however, should be independent of the choice of a coordinate system, and we may seek to represent the law in a manner independent of a particular coordinate system. A way of doing this is provided by vector and tensor notation. When vector notation is used, a particular coordinate system need not be introduced. Consequently, use of vector notation in formulating natural laws leaves them *invariant* to coordinate transformations.

Vectors

Often a specific coordinate system is chosen to express governing equations of a problem to facilitate their solution. Then the vector and tensor quantities are expressed in terms of their components in that coordinate system. For example, a vector \mathbf{A} in a three-dimensional space may be expressed in terms of its components (a_1, a_2, a_3) and *basis vectors* $(\mathbf{e}_1, \mathbf{e}_2, \mathbf{e}_3)$ (\mathbf{e}_i are not necessarily unit vectors) as

$$\mathbf{A} = a_1 \mathbf{e}_1 + a_2 \mathbf{e}_2 + a_3 \mathbf{e}_3 \quad (1.2.1)$$

When the basis vectors of a coordinate system are constants, i.e., with fixed lengths and directions, the coordinate system is called a *Cartesian coordinate system*. The general Cartesian system is oblique. When the Cartesian system is orthogonal, it is called *rectangular Cartesian*. The Cartesian coordinates are denoted by

$$(x_1, x_2, x_3) \text{ or } (x, y, z) \quad (1.2.2)$$

The familiar rectangular Cartesian coordinate system is shown in Figure 1.2.1. We shall always use a right-hand coordinate system. When the basis vectors are of unit lengths and mutually orthogonal, they are called *orthonormal*. In many situations an *orthonormal basis* simplifies calculations. We denote an orthonormal Cartesian basis by

$$(\hat{\mathbf{e}}_1, \hat{\mathbf{e}}_2, \hat{\mathbf{e}}_3) \text{ or } (\hat{\mathbf{e}}_x, \hat{\mathbf{e}}_y, \hat{\mathbf{e}}_z) \quad (1.2.3)$$

For an orthonormal basis the vectors \mathbf{A} and \mathbf{B} can be written as

$$\mathbf{A} = A_1 \hat{\mathbf{e}}_1 + A_2 \hat{\mathbf{e}}_2 + A_3 \hat{\mathbf{e}}_3$$

$$\mathbf{B} = B_1 \hat{\mathbf{e}}_1 + B_2 \hat{\mathbf{e}}_2 + B_3 \hat{\mathbf{e}}_3$$

where $\hat{\mathbf{e}}_i$ ($i = 1, 2, 3$) is the orthonormal basis, and A_i and B_i are the corresponding *physical components* (i.e., the components have the same physical dimensions as the vector).

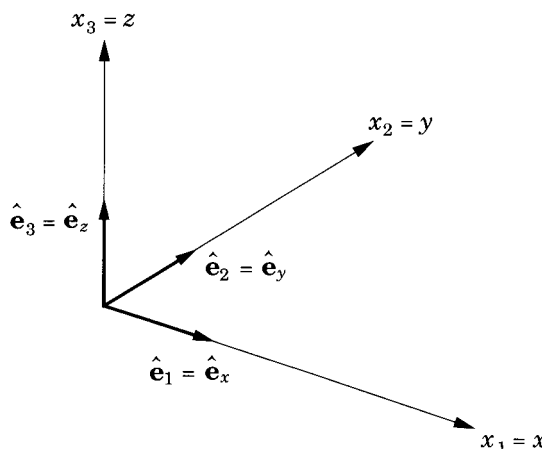


Figure 1.2.1: A rectangular Cartesian coordinate system, $(x_1, x_2, x_3) = (x, y, z)$; $(\hat{\mathbf{e}}_1, \hat{\mathbf{e}}_2, \hat{\mathbf{e}}_3) = (\hat{\mathbf{e}}_x, \hat{\mathbf{e}}_y, \hat{\mathbf{e}}_z)$ are the unit basis vectors.

Summation Convention

It is convenient to abbreviate a summation of terms by understanding that a repeated index means summation over all values of that index. For example, the component form of vector \mathbf{A}

$$\mathbf{A} = a^1 \mathbf{e}_1 + a^2 \mathbf{e}_2 + a^3 \mathbf{e}_3$$

where $(\mathbf{e}_1, \mathbf{e}_2, \mathbf{e}_3)$ are basis vectors (not necessarily unit), can be expressed in the form

$$\mathbf{A} = \sum_{j=1}^3 a^j \mathbf{e}_j = a^j \mathbf{e}_j \quad (1.2.4)$$

The repeated index is a *dummy index* in the sense that any other symbol that is not already used in that expression can be employed:

$$\mathbf{A} = a^j \mathbf{e}_j = a^k \mathbf{e}_k = a^m \mathbf{e}_m$$

The range of summation is always known in the context of the discussion. For example, in the present context the range of j, k and m is 1 to 3 because we are discussing vectors in a three-dimensional space.

In an orthonormal basis the *scalar product* (also called the “dot product”) and *vector product* (also called the “cross product”) can be expressed in the index form using the *Kronecker delta symbol* δ_{ij} and the *alternating symbol* (or permutation symbol) ϵ_{ijk} :

$$\mathbf{A} \cdot \mathbf{B} = (A_i \hat{\mathbf{e}}_i) \cdot (B_j \hat{\mathbf{e}}_j) = A_i B_j \delta_{ij} = A_i B_i \quad (1.2.5a)$$

$$\mathbf{A} \times \mathbf{B} = (A_i \hat{\mathbf{e}}_i) \times (B_j \hat{\mathbf{e}}_j) = A_i B_j \epsilon_{ijk} \hat{\mathbf{e}}_k \quad (1.2.5b)$$

where

$$\delta_{ij} \equiv \hat{\mathbf{e}}_i \cdot \hat{\mathbf{e}}_j = \begin{cases} 1, & \text{if } i = j \\ 0, & \text{if } i \neq j \end{cases} \quad (1.2.6)$$

$$\epsilon_{ijk} \equiv \begin{cases} 1, & \text{if } i, j, k \text{ are in cyclic order} \\ & \text{and not repeated } (i \neq j \neq k) \\ -1, & \text{if } i, j, k \text{ are not in cyclic order} \\ & \text{and not repeated } (i \neq j \neq k) \\ 0, & \text{if any of } i, j, k \text{ are repeated} \end{cases} \quad (1.2.7)$$

Further, the Kronecker delta and the permutation symbol are related by the identity, known as the ϵ - δ *identity*,

$$\epsilon_{ijk} \epsilon_{imn} = \delta_{jm} \delta_{kn} - \delta_{jn} \delta_{km} \quad (1.2.8)$$

Differentiation of vector functions with respect to the coordinates is a common occurrence in mechanics. Most of the operations involve the “del operator,” denoted by ∇ . In a rectangular Cartesian system it has the form

$$\nabla \equiv \hat{\mathbf{e}}_x \frac{\partial}{\partial x} + \hat{\mathbf{e}}_y \frac{\partial}{\partial y} + \hat{\mathbf{e}}_z \frac{\partial}{\partial z} \quad (1.2.9)$$

or, in the summation convention, we have

$$\nabla \equiv \hat{\mathbf{e}}_i \frac{\partial}{\partial x_i} \quad (1.2.10)$$

It is important to note that the del operator has some of the properties of a vector but it does not have them all, because it is an operator. For instance $\nabla \cdot \mathbf{A}$ is a scalar, called the *divergence* of \mathbf{A} ,

$$\nabla \cdot \mathbf{A} = \left(\hat{\mathbf{e}}_i \frac{\partial}{\partial x_i} \right) \cdot (A_j \hat{\mathbf{e}}_j) = (\hat{\mathbf{e}}_i \cdot \hat{\mathbf{e}}_j) \frac{\partial A_j}{\partial x_i} = \frac{\partial A_i}{\partial x_i} = \frac{\partial A_j}{\partial x_j} \quad (1.2.11)$$

whereas $\mathbf{A} \cdot \nabla$

$$\mathbf{A} \cdot \nabla = (A_j \hat{\mathbf{e}}_j) \cdot \left(\hat{\mathbf{e}}_i \frac{\partial}{\partial x_i} \right) = A_j (\hat{\mathbf{e}}_j \cdot \hat{\mathbf{e}}_i) \frac{\partial}{\partial x_i} = A_i \frac{\partial}{\partial x_i} \quad (1.2.12)$$

is a scalar differential operator. Thus the del operator does not commute in this sense. The operation $\nabla \phi(\mathbf{x})$ is called the *gradient* of a scalar function ϕ whereas $\nabla \times \mathbf{A}(\mathbf{x})$ is called the *curl* of a vector function \mathbf{A} .

We have the following relations between the rectangular Cartesian coordinates (x, y, z) and cylindrical coordinates (r, θ, z) (see Figure 1.2.2):

$$x = r \cos \theta, \quad y = r \sin \theta, \quad z = z \quad (1.2.13)$$

$$\hat{\mathbf{e}}_r = \cos \theta \hat{\mathbf{e}}_x + \sin \theta \hat{\mathbf{e}}_y, \quad \hat{\mathbf{e}}_\theta = -\sin \theta \hat{\mathbf{e}}_x + \cos \theta \hat{\mathbf{e}}_y, \quad \hat{\mathbf{e}}_z = \hat{\mathbf{e}}_z \quad (1.2.14)$$

$$\frac{\partial \hat{\mathbf{e}}_r}{\partial \theta} = -\sin \theta \hat{\mathbf{e}}_x + \cos \theta \hat{\mathbf{e}}_y = \hat{\mathbf{e}}_\theta, \quad \frac{\partial \hat{\mathbf{e}}_\theta}{\partial \theta} = -\cos \theta \hat{\mathbf{e}}_x - \sin \theta \hat{\mathbf{e}}_y = -\hat{\mathbf{e}}_r \quad (1.2.15)$$

and all other derivatives of the base vectors are zero. For more on vector calculus, see Reddy and Rasmussen [5] and Reddy [6], among other references.

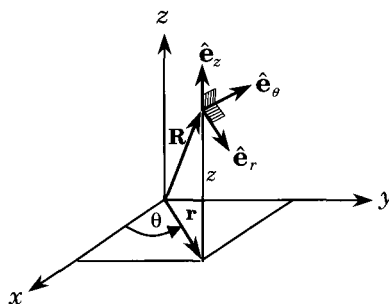


Figure 1.2.2: Cylindrical coordinate system.

Tensor

To introduce the concept of a second-order tensor, also called a *dyad*, we consider the equilibrium of an element of a continuum acted upon by forces. The surface force acting on a small element of area in a continuous medium depends not only on the magnitude of the area but also upon the orientation of the area. It is customary to denote the direction of a plane area by means of a unit vector drawn normal to that plane. To fix the direction of the normal, we assign a *sense of travel* along the contour of the boundary of the plane area in question. The direction of the normal is taken by convention as that in which a right-handed screw advances as it is rotated according to the sense of travel along the boundary curve or contour. Let the unit normal vector be given by $\hat{\mathbf{n}}$. Then the area A can be denoted by $\mathbf{A} = A\hat{\mathbf{n}}$.

If we denote by $\Delta\mathbf{F}(\hat{\mathbf{n}})$ the force on a small area $\hat{\mathbf{n}}\Delta S$ located at the position \mathbf{r} (see Figure 1.2.3a), the *stress vector* can be defined as follows:

$$\mathbf{t}(\hat{\mathbf{n}}) = \lim_{\Delta S \rightarrow 0} \frac{\Delta\mathbf{F}(\hat{\mathbf{n}})}{\Delta S} \quad (1.2.16)$$

We see that the stress vector is a point function of the unit normal $\hat{\mathbf{n}}$ which denotes the orientation of the surface ΔS . The component of \mathbf{t} that is in the direction of $\hat{\mathbf{n}}$ is called the *normal stress*. The component of \mathbf{t} that is normal to $\hat{\mathbf{n}}$ is called a *shear stress*. Because of Newton's third law for action and reaction, we see that $\mathbf{t}(-\hat{\mathbf{n}}) = -\mathbf{t}(\hat{\mathbf{n}})$. Note that $\mathbf{t}(\hat{\mathbf{n}})$ is, in general, not in the direction of $\hat{\mathbf{n}}$.

It is useful to establish a relationship between \mathbf{t} and $\hat{\mathbf{n}}$. To do this we now set up an infinitesimal tetrahedron in Cartesian coordinates as shown in Figure 1.2.3b. If $-\mathbf{t}_1, -\mathbf{t}_2, -\mathbf{t}_3$, and \mathbf{t} denote the stress vectors in the outward directions on the faces of the infinitesimal tetrahedron whose areas are $\Delta S_1, \Delta S_2, \Delta S_3$, and ΔS , respectively, we have by Newton's second law for the mass inside the tetrahedron,

$$\mathbf{t}\Delta S - \mathbf{t}_1\Delta S_1 - \mathbf{t}_2\Delta S_2 - \mathbf{t}_3\Delta S_3 + \rho\Delta V\mathbf{f} = \rho\Delta V\mathbf{a} \quad (1.2.17)$$

where ΔV is the volume of the tetrahedron, ρ the density, \mathbf{f} the body force per unit mass, and \mathbf{a} the acceleration. Since the total vector area of a closed surface is zero

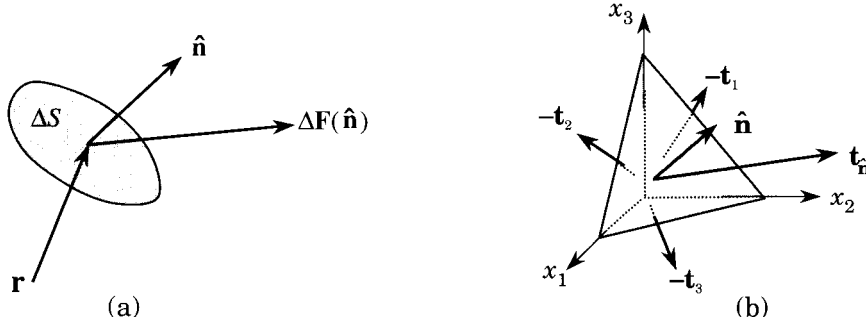


Figure 1.2.3: (a) Force on an area element. (b) Tetrahedral element in Cartesian coordinates.

(see Problem 1.3),

$$\Delta S\hat{\mathbf{n}} - \Delta S_1\hat{\mathbf{e}}_1 - \Delta S_2\hat{\mathbf{e}}_2 - \Delta S_3\hat{\mathbf{e}}_3 = \mathbf{0} \quad (1.2.18)$$

it follows that

$$\Delta S_1 = (\hat{\mathbf{n}} \cdot \hat{\mathbf{e}}_1)\Delta S, \quad \Delta S_2 = (\hat{\mathbf{n}} \cdot \hat{\mathbf{e}}_2)\Delta S, \quad \Delta S_3 = (\hat{\mathbf{n}} \cdot \hat{\mathbf{e}}_3)\Delta S \quad (1.2.19)$$

The volume of the element ΔV can be expressed as

$$\Delta V = \frac{\Delta h}{3}\Delta S \quad (1.2.20)$$

where Δh is the perpendicular distance from the origin to the slant face.

Substitution of Eqs. (1.2.19) and (1.2.20) in (1.2.17) and dividing throughout by ΔS reduces it to

$$\mathbf{t} = (\hat{\mathbf{n}} \cdot \hat{\mathbf{e}}_1)\mathbf{t}_1 + (\hat{\mathbf{n}} \cdot \hat{\mathbf{e}}_2)\mathbf{t}_2 + (\hat{\mathbf{n}} \cdot \hat{\mathbf{e}}_3)\mathbf{t}_3 + \rho \frac{\Delta h}{3}(\mathbf{a} - \mathbf{f}) \quad (1.2.21)$$

In the limit when the tetrahedron shrinks to a point, $\Delta h \rightarrow 0$, we are left with

$$\mathbf{t} = (\hat{\mathbf{n}} \cdot \hat{\mathbf{e}}_1)\mathbf{t}_1 + (\hat{\mathbf{n}} \cdot \hat{\mathbf{e}}_2)\mathbf{t}_2 + (\hat{\mathbf{n}} \cdot \hat{\mathbf{e}}_3)\mathbf{t}_3 = (\hat{\mathbf{n}} \cdot \hat{\mathbf{e}}_i)\mathbf{t}_i \quad (1.2.22)$$

It is now convenient to display the above equation as

$$\mathbf{t} = \hat{\mathbf{n}} \cdot (\hat{\mathbf{e}}_1\mathbf{t}_1 + \hat{\mathbf{e}}_2\mathbf{t}_2 + \hat{\mathbf{e}}_3\mathbf{t}_3) \quad (1.2.23)$$

The terms in the parenthesis are to be treated as a dyadic, called *stress dyadic* or *stress tensor* $\vec{\sigma}$ (we will not use the “double arrow” notation for tensors after this discussion):

$$\vec{\sigma} \equiv \hat{\mathbf{e}}_1\mathbf{t}_1 + \hat{\mathbf{e}}_2\mathbf{t}_2 + \hat{\mathbf{e}}_3\mathbf{t}_3 \quad (1.2.24)$$

Thus, we have

$$\mathbf{t}(\hat{\mathbf{n}}) = \hat{\mathbf{n}} \cdot \vec{\sigma} \quad (1.2.25)$$

and the dependence of \mathbf{t} on $\hat{\mathbf{n}}$ has been explicitly displayed.

It is useful to resolve the stress vectors $\mathbf{t}_1, \mathbf{t}_2$, and \mathbf{t}_3 into their orthogonal components. We have

$$\mathbf{t}_i = \sigma_{i1}\hat{\mathbf{e}}_1 + \sigma_{i2}\hat{\mathbf{e}}_2 + \sigma_{i3}\hat{\mathbf{e}}_3 = \sigma_{ij}\hat{\mathbf{e}}_i\hat{\mathbf{e}}_j \quad (1.2.26)$$

for $i = 1, 2, 3$. Hence, the stress dyadic can be expressed in summation notation as

$$\vec{\sigma} = \hat{\mathbf{e}}_i\mathbf{t}_i = \sigma_{ij}\hat{\mathbf{e}}_i\hat{\mathbf{e}}_j \quad (1.2.27)$$

The component σ_{ij} represents the stress (force per unit area) on an area perpendicular to the i th coordinate and in the j th coordinate direction (see Figure 1.2.4). The stress vector \mathbf{t} represents the vectorial stress on an area perpendicular to the direction $\hat{\mathbf{n}}$. Equation (1.2.25) is known as the *Cauchy stress formula*, and $\vec{\sigma}$ is termed the *Cauchy stress tensor*.

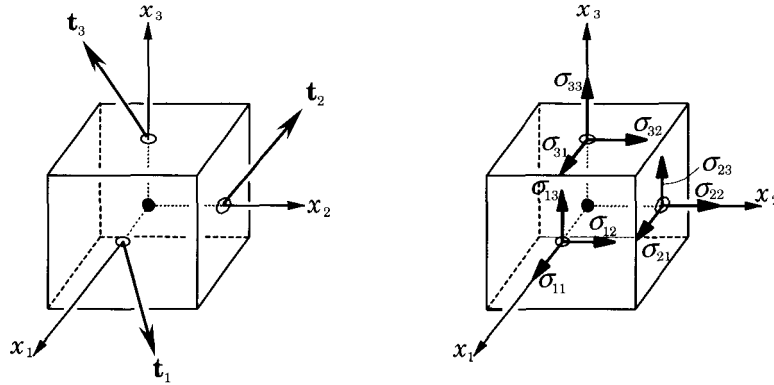


Figure 1.2.4: Notation used for the stress components in Cartesian rectangular coordinates.

One of the properties of a dyadic is defined by the dot product with a vector. For example, dot products of a second-order tensor Φ with a vector \mathbf{A} from the right and left are given, respectively, by

$$\Phi \cdot \mathbf{A} = (\Phi_{ij}\hat{\mathbf{e}}_i\hat{\mathbf{e}}_j) \cdot (A_k\hat{\mathbf{e}}_k) = \Phi_{ij}A_j\hat{\mathbf{e}}_i$$

$$\mathbf{A} \cdot \Phi = (A_k\hat{\mathbf{e}}_k) \cdot (\Phi_{ij}\hat{\mathbf{e}}_i\hat{\mathbf{e}}_j) = \Phi_{ij}A_i\hat{\mathbf{e}}_j$$

Thus the dot operation with a vector produces another vector. The two operations in general produce different vectors. The transpose of a second-order tensor is defined as the result obtained by the interchange of the two basis vectors:

$$\Phi^T = (\Phi_{ij}\hat{\mathbf{e}}_i\hat{\mathbf{e}}_j)^T = \Phi_{ij}\hat{\mathbf{e}}_j\hat{\mathbf{e}}_i \quad (1.2.28)$$

It is clear that we have

$$\mathbf{A} \cdot \Phi = \Phi^T \cdot \mathbf{A}, \quad \Phi \cdot \mathbf{A} = \mathbf{A} \cdot \Phi^T \quad (1.2.29)$$

We can display all of the components Φ_{ij} of a dyad Φ by letting the j index run to the right and the i index run downward:

$$\begin{aligned} \Phi &= \phi_{11}\hat{\mathbf{e}}_1\hat{\mathbf{e}}_1 + \phi_{12}\hat{\mathbf{e}}_1\hat{\mathbf{e}}_2 + \phi_{13}\hat{\mathbf{e}}_1\hat{\mathbf{e}}_3 \\ &\quad + \phi_{21}\hat{\mathbf{e}}_2\hat{\mathbf{e}}_1 + \phi_{22}\hat{\mathbf{e}}_2\hat{\mathbf{e}}_2 + \phi_{23}\hat{\mathbf{e}}_2\hat{\mathbf{e}}_3 \\ &\quad + \phi_{31}\hat{\mathbf{e}}_3\hat{\mathbf{e}}_1 + \phi_{32}\hat{\mathbf{e}}_3\hat{\mathbf{e}}_2 + \phi_{33}\hat{\mathbf{e}}_3\hat{\mathbf{e}}_3 \end{aligned} \quad (1.2.30)$$

This form is called the *nonion* form. Equation (1.2.30) illustrates that a dyad in three-dimensional space, or what we shall call a second-order tensor, has nine independent components in general, each component associated with a certain dyad pair. The components are thus said to be ordered. When the ordering is understood, the explicit writing of the dyads can be suppressed and the dyad is written as an array:

$$[\Phi] = \begin{bmatrix} \phi_{11} & \phi_{12} & \phi_{13} \\ \phi_{21} & \phi_{22} & \phi_{23} \\ \phi_{31} & \phi_{32} & \phi_{33} \end{bmatrix} \quad \text{and} \quad \Phi = \left\{ \begin{array}{c} \hat{\mathbf{e}}_1 \\ \hat{\mathbf{e}}_2 \\ \hat{\mathbf{e}}_3 \end{array} \right\}^T [\Phi] \left\{ \begin{array}{c} \hat{\mathbf{e}}_1 \\ \hat{\mathbf{e}}_2 \\ \hat{\mathbf{e}}_3 \end{array} \right\} \quad (1.2.31)$$

This representation is simpler than Eq. (1.2.30), but it is taken to mean the same. A unit second order tensor \mathbf{I} is defined by

$$\mathbf{I} = \delta_{ij}\hat{\mathbf{e}}_i\hat{\mathbf{e}}_j \quad (1.2.32)$$

In the general scheme that is developed, vectors are called *first-order tensors* and dyads are called *second-order tensors*. Scalars are called *zeroth-order tensors*. The generalization to *third-order tensors* thus leads, or is derived from, *triadics*, or three vectors standing side by side. It follows that higher order tensors are developed from *polyads*. An n th-order tensor can be expressed in a short form using the summation convention:

$$\Phi = \phi_{ijkl\dots} \hat{\mathbf{e}}_i\hat{\mathbf{e}}_j\hat{\mathbf{e}}_k\hat{\mathbf{e}}_\ell \dots \quad (1.2.33)$$

Here we have selected a rectangular Cartesian basis to represent the tensor.

Tensors are sometimes defined by the transformation law for its components. For example, a vector \mathbf{A} has components A_i with respect to the rectangular Cartesian basis $(\hat{\mathbf{e}}_1, \hat{\mathbf{e}}_2, \hat{\mathbf{e}}_3)$; its components referred to another rectangular Cartesian basis $(\hat{\mathbf{e}}'_1, \hat{\mathbf{e}}'_2, \hat{\mathbf{e}}'_3)$ are A'_{ij} . The two sets of components are related according to

$$A'_i = \ell_{ij}A_j, \quad \ell_{ij} \equiv \hat{\mathbf{e}}'_i \cdot \hat{\mathbf{e}}_j \quad (1.2.34)$$

where ℓ_{ij} are called the direction cosines. Similarly, the components of a second-order tensor Φ transform according to the rule

$$\Phi'_{ij} = \ell_{im}\ell_{jn}\Phi_{mn} \quad \text{or} \quad [\Phi'] = [L][\Phi][L]^T \quad (1.2.35)$$

If the components do not satisfy the above transformation law, then it is not a tensor.

The *double-dot product* between tensors of second order and higher order is encountered in mechanics. The double-dot product between two second-order tensors Φ and Ψ is defined as

$$\begin{aligned} \Phi : \Psi &= (\phi_{ij}\hat{\mathbf{e}}_i\hat{\mathbf{e}}_j) : (\psi_{mn}\hat{\mathbf{e}}_m\hat{\mathbf{e}}_n) \\ &= \phi_{ij}\psi_{mn}(\hat{\mathbf{e}}_j \cdot \hat{\mathbf{e}}_m)(\hat{\mathbf{e}}_i \cdot \hat{\mathbf{e}}_n) \\ &= \phi_{ij}\psi_{mn}\delta_{jm}\delta_{in} \\ &= \phi_{nm}\psi_{mn} \\ &= \phi_{ij}\psi_{ji} \end{aligned} \quad (1.2.36)$$

Integral Relations

Relations between volume integrals and surface integrals of the gradient (∇) of a scalar or a vector and divergence ($\nabla \cdot$) of a vector are needed in the later chapters. We record them here for future reference and use.

Let Ω denote a region in space surrounded by the surface Γ , and let ds be a differential element of the surface whose unit outward normal is denoted by $\hat{\mathbf{n}}$. Let dv be a differential volume element. Let ψ be a scalar function and \mathbf{A} be a vector function defined over the region Ω . Then the following integral identities hold (see Figure 1.2.5):

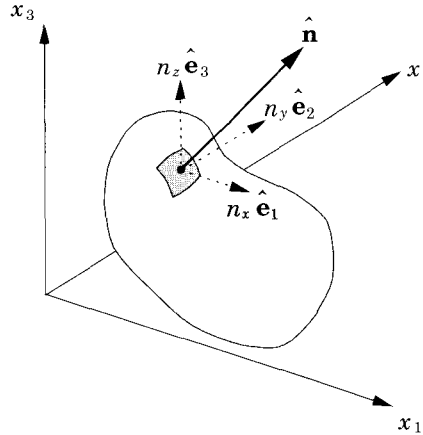


Figure 1.2.5: A solid body with a surface normal vector $\hat{\mathbf{n}}$.

Gradient Theorem

$$\int_{\Omega} \nabla \psi \, dv = \oint_{\Gamma} \hat{\mathbf{n}} \psi \, ds \quad (\text{vector form}) \quad (1.2.37a)$$

$$\int_{\Omega} \frac{\partial \psi}{\partial x_i} \, dv = \oint_{\Gamma} n_i \psi \, ds \quad (\text{component form}) \quad (1.2.37b)$$

Divergence Theorem

$$\int_{\Omega} \nabla \cdot \mathbf{A} \, dv = \oint_{\Gamma} \hat{\mathbf{n}} \cdot \mathbf{A} \, ds \quad (\text{vector form}) \quad (1.2.38a)$$

$$\int_{\Omega} \frac{\partial A_i}{\partial x_i} \, dv = \oint_{\Gamma} n_i A_i \, ds \quad (\text{component form}) \quad (1.2.38b)$$

In the above integral relations, \oint_{Γ} denotes the integral on the *closed* boundary Γ of the domain Ω , and the component forms refer to the usual rectangular Cartesian coordinate system. Equations (1.2.37) and (1.2.38) are valid in two as well as three dimensions. The integral relations in Eqs. (1.2.37) and (1.2.38) can be expressed concisely in the single statement

$$\int_{\Omega} (\nabla * F) \, dv = \oint_{\Gamma} (\hat{\mathbf{n}} * F) \, ds \quad (1.2.39)$$

where $*$ denotes an appropriate operation, i.e., gradient, divergence or curl operation, and F is a scalar or vector function.

Some additional integral relations can be derived from Eqs. (1.2.37) and (1.2.38). Let $\mathbf{A} = \nabla \varphi$ in Eq. (1.2.38a), where φ is a scalar function, and obtain

$$\int_{\Omega} \nabla \cdot (\nabla \varphi) \, dv = \int_{\Omega} \nabla^2 \varphi \, dv = \oint_{\Gamma} \hat{\mathbf{n}} \cdot (\nabla \varphi) \, ds \quad (\text{vector form}) \quad (1.2.40a)$$

or, in component form

$$\int_{\Omega} \frac{\partial^2 \varphi}{\partial x_i \partial x_i} dv = \oint_{\Gamma} n_i \frac{\partial \varphi}{\partial x_i} ds \quad (1.2.40b)$$

The quantity $\hat{\mathbf{n}} \cdot \nabla \varphi$ is called the *normal derivative* of φ on the surface Γ , and is denoted by

$$\begin{aligned} \frac{\partial \varphi}{\partial n} &= \hat{\mathbf{n}} \cdot \nabla \varphi \text{ (invariant form)} \\ &= n_i \frac{\partial \varphi}{\partial x_i} \text{ (rectangular Cartesian component form)} \\ &= n_x \frac{\partial \varphi}{\partial x} + n_y \frac{\partial \varphi}{\partial y} + n_z \frac{\partial \varphi}{\partial z} \end{aligned} \quad (1.2.41)$$

The integral relations presented in this section are useful in developing the so-called weak forms of differential equations in connection with the Ritz method and finite element formulations of boundary value problems.

1.3 Equations of Anisotropic Elasticity

1.3.1 Introduction

The objective of this section is to review the governing equations of a linear anisotropic elastic body. The equations governing the motion of a solid body can be classified into four basic categories:

- (1) Kinematics (strain-displacement equations)
- (2) Kinetics (conservation of momenta)
- (3) Thermodynamics (first and second laws of thermodynamics)
- (4) Constitutive equations (stress-strain relations)

Kinematics is a study of the geometric changes or deformation in a body, without the consideration of forces causing the deformation. *Kinetics* is the study of the static or dynamic equilibrium of forces and moments acting on a body. This leads to equations of motion as well as the symmetry of stress tensor in the absence of body moments. The thermodynamic principles are concerned with the conservation of energy and relations among heat, mechanical work, and thermodynamic properties of the body. The constitutive equations describe thermomechanical behavior of the material of the body, and they relate the dependent variables introduced in the kinetic description to those in the kinematic and thermodynamic descriptions. These equations are supplemented by appropriate boundary and initial conditions of the problem.

In the following sections, an overview of the governing equations of an anisotropic elastic body is presented. The strain-displacement relations, equations of motion, and the constitutive equations for an isothermal state (i.e., no change in the temperature of the body) are presented first. Subsequently, the thermodynamic principles are considered only to determine the temperature distribution in a solid body and to account for the effect of non-uniform temperature distribution on the strains.

A solid body \mathcal{B} is a set of material particles which can be identified as having one-to-one correspondence with the points of a region Ω of Euclidean point space \mathfrak{R}^3 .

The particles of \mathcal{B} are identified by their time-dependent positions relative to the selected frame of reference. The simultaneous position of all material points of \mathcal{B} at a fixed time is called a *configuration* of the structure. The analytical description of configurations at various times of a material body acted on by various loads results in a set of governing equations.

Consider a deformable body \mathcal{B} of known geometry, constitution, and loading. Under given geometric restrictions and loading, the body will undergo motion and/or deformation (i.e., geometric changes within the body). If the applied loads are time dependent, the deformation of the body will be a function of time, i.e., the geometry of the body will change continuously with time. If the loads are applied slowly so that the deformation is only dependent on the loads, the body will take a definitive shape at the end of each load application. Whether the deformation is time dependent or not, the forces acting on the body will be in equilibrium at all times.

Suppose that the body \mathcal{B} under consideration at time $t = 0$ occupies a configuration \mathcal{C}^0 , in which a particle X of the body \mathcal{B} occupies a position \mathbf{X} . Note that X is the name of the particle that occupies the location \mathbf{X} in the reference configuration. At time $t > 0$, the body assumes a new configuration \mathcal{C} and the particle X occupies the new position \mathbf{x} .

There are two commonly used descriptions of motion and deformation in continuum mechanics. In the *referential* or *Lagrangian description*, the motion of a body \mathcal{B} is referred to a reference configuration \mathcal{C}^R . Thus, in the Lagrangian description the current coordinates (x_1, x_2, x_3) are expressed in terms of the reference coordinates (X_1, X_2, X_3) and time t as

$$\mathbf{x} = \mathbf{x}(X_1, X_2, X_3, t) \quad (1.3.1)$$

Often, the reference configuration \mathcal{C}^R is chosen to be the unstressed state of the body, i.e., $\mathcal{C}^R \equiv \mathcal{C}^0$. The coordinates (X_1, X_2, X_3) are called the *material coordinates*.

In the *spatial* or *Eulerian description* of a body \mathcal{B} , the motion is referred to the current configuration \mathcal{C} occupied by the body \mathcal{B} . The spatial description focuses attention on a given region of space instead of on a given body of matter, and is the description most used in fluid mechanics, whereas in the Lagrangian description the coordinate system \mathbf{X} is fixed on a given body of matter in its undeformed configuration, and its position \mathbf{x} at any time is referred to the material coordinates X_i . Thus, during a motion of a body \mathcal{B} , a representative particle X occupies a succession of points which together form a curve in Euclidean space. This curve is called the path of X and is given parametrically by Eq. (1.3.1).

1.3.2 Strain-Displacement Equations

The phrase *deformation of a body* refers to relative displacements and changes in the geometry experienced by the body. Referred to a rectangular Cartesian frame of reference (X_1, X_2, X_3) , every particle X in the body corresponds to a set of coordinates $\mathbf{X} = (X_1, X_2, X_3)$. When the body is deformed under the action of external forces, the particle X moves to a new position $\mathbf{x} = (x_1, x_2, x_3)$. The displacement of the particle X is given by

$$\mathbf{u} = \mathbf{x} - \mathbf{X} \quad \text{or} \quad u_i = x_i - X_i \quad (1.3.2)$$

If the displacement of every particle in the body is known, we can construct the current (deformed) configuration \mathcal{C} from the reference (or undeformed) configuration \mathcal{C}^0 . In the Lagrangian description, the displacements are expressed in terms of the material coordinates X_i , and we have

$$u_i(X_1, X_2, X_3, t) = x_i(X_1, X_2, X_3, t) - X_i \quad (1.3.3)$$

A rigid-body motion is one in which all material particles of the body undergo the same linear and angular displacements. A deformable body is one in which the material particles can move relative to each other. The deformation (i.e., relative motion of material particles) of a deformable body can be determined only by considering the change of distance between any two arbitrary but infinitesimally close points of the body.

Consider two neighboring material particles P and Q which occupy the positions $P : (X_1, X_2, X_3)$ and $Q : (X_1 + dX_1, X_2 + dX_2, X_3 + dX_3)$, respectively, in the undeformed configuration \mathcal{C}^0 of the body \mathcal{B} . The particles are separated by the infinitesimal distance $dS = \sqrt{dX_i d\bar{X}_i}$ (sum on i) in \mathcal{C}^0 , and $d\mathbf{X}$ is the vector connecting the position of P to the position of Q . These two particles move to new places \bar{P} and \bar{Q} , respectively, in the deformed body (see Figure 1.3.1). Suppose that the positions of \bar{P} and \bar{Q} are (x_1, x_2, x_3) and $(x_1 + dx_1, x_2 + dx_2, x_3 + dx_3)$, respectively. The two particles are now separated by the distance $ds = \sqrt{dx_i dx_i}$ in the deformed configuration \mathcal{C} , and $d\mathbf{x}$ is the vector connecting \bar{P} to \bar{Q} . The vector $d\mathbf{x}$ can be interpreted as the position occupied by the deformed material vector $d\mathbf{X}$. When the material vector $d\mathbf{X}$ is small but finite, the line vector $d\mathbf{x}$ in general does not coincide exactly with the deformed position of $d\mathbf{X}$, which lies along a curve in the deformed body. The deformation (or strains) in a body can be measured in a number of ways. Here we use the standard strain measure of solid mechanics, namely the *Green-Lagrange strain* \mathbf{E} , which is defined such that it gives the change

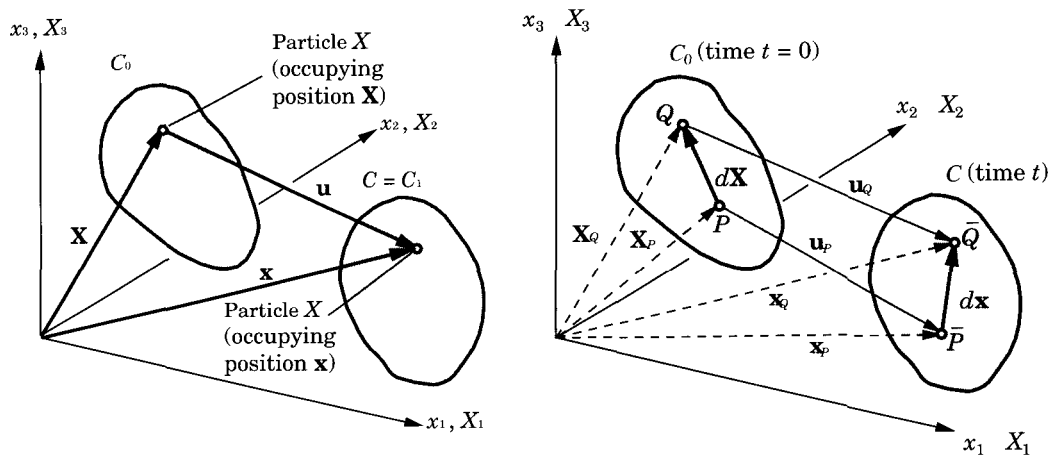


Figure 1.3.1: Kinematics of deformation of a continuous medium.

in the square of the length of the material vector $d\mathbf{X}$

$$2d\mathbf{X} \cdot \mathbf{E} \cdot d\mathbf{X} \equiv (ds)^2 - (dS)^2 = d\mathbf{x} \cdot d\mathbf{x} - d\mathbf{X} \cdot d\mathbf{X} \quad (1.3.4a)$$

and in rectangular Cartesian component form we have

$$2dX_i E_{ij} dX_j \equiv (ds)^2 - (dS)^2 = dx_i dx_i - dX_i dX_i \quad (1.3.4b)$$

In Eq. (1.3.4b) and in the equations that follow, the *summation convention* on repeated indices is used, and the range of summation is 1 to 3.

In order to express the strains in terms of the displacements, we use Eq. (1.3.2) and write

$$\mathbf{x} = \mathbf{X} + \mathbf{u}(X_1, X_2, X_3, t) \quad (1.3.5)$$

Since \mathbf{x} is a function of \mathbf{X} , its total differential is given by [using the chain rule of differentiation and Eq. (1.3.5)]

$$d\mathbf{x} \equiv d\mathbf{X} + d\mathbf{X} \cdot \nabla \mathbf{u} = d\mathbf{X} \cdot (\mathbf{I} + \nabla \mathbf{u}) \quad (1.3.6)$$

where ∇ denotes the gradient operator with respect to the material coordinates, \mathbf{X} . Now the strain tensor or its components from Eqs. (1.3.4a,b) can be expressed in terms of the displacement vector or its components with the help of Eq. (1.3.6):

$$\begin{aligned} 2d\mathbf{X} \cdot \mathbf{E} \cdot d\mathbf{X} &= d\mathbf{x} \cdot d\mathbf{x} - d\mathbf{X} \cdot d\mathbf{X} \\ &= [d\mathbf{X} \cdot (\mathbf{I} + \nabla \mathbf{u})] \cdot [d\mathbf{X} \cdot (\mathbf{I} + \nabla \mathbf{u})] - d\mathbf{X} \cdot d\mathbf{X} \\ &= d\mathbf{X} \cdot (\mathbf{I} + \nabla \mathbf{u}) \cdot (\mathbf{I} + \nabla \mathbf{u})^T \cdot d\mathbf{X} - d\mathbf{X} \cdot d\mathbf{X} \\ &= d\mathbf{X} \cdot [(\mathbf{I} + \nabla \mathbf{u}) \cdot (\mathbf{I} + \nabla \mathbf{u})^T - \mathbf{I}] \cdot d\mathbf{X} \end{aligned} \quad (1.3.7)$$

Thus the Green (or Green-Lagrange) strain tensor \mathbf{E} is given in terms of the displacement gradients as

$$\begin{aligned} \mathbf{E} &= \frac{1}{2} [(\mathbf{I} + \nabla \mathbf{u}) \cdot (\mathbf{I} + \nabla \mathbf{u})^T - \mathbf{I}] \\ &= \frac{1}{2} [\nabla \mathbf{u} + (\nabla \mathbf{u})^T + \nabla \mathbf{u} \cdot (\nabla \mathbf{u})^T] \end{aligned} \quad (1.3.8)$$

Note that the Green-Lagrange strain tensor is symmetric, $\mathbf{E} = \mathbf{E}^T$ ($E_{ij} = E_{ji}$). The strain components defined in Eq. (1.3.8) are called finite strain components because no assumption concerning the smallness (compared to unity) of the strains is made.

The rectangular Cartesian component form is given by

$$\begin{aligned} E_{jk} &= \frac{1}{2} \left[\left(\delta_{ij} + \frac{\partial u_i}{\partial X_j} \right) \left(\delta_{ik} + \frac{\partial u_i}{\partial X_k} \right) - \delta_{jk} \right] \\ &= \frac{1}{2} \left(\frac{\partial u_j}{\partial X_k} + \frac{\partial u_k}{\partial X_j} + \frac{\partial u_m}{\partial X_j} \frac{\partial u_m}{\partial X_k} \right) \end{aligned} \quad (1.3.9)$$

Explicit form of the six Cartesian components of strain are given by

$$\begin{aligned}
 E_{11} &= \frac{\partial u_1}{\partial X_1} + \frac{1}{2} \left[\left(\frac{\partial u_1}{\partial X_1} \right)^2 + \left(\frac{\partial u_2}{\partial X_1} \right)^2 + \left(\frac{\partial u_3}{\partial X_1} \right)^2 \right] \\
 E_{22} &= \frac{\partial u_2}{\partial X_2} + \frac{1}{2} \left[\left(\frac{\partial u_1}{\partial X_2} \right)^2 + \left(\frac{\partial u_2}{\partial X_2} \right)^2 + \left(\frac{\partial u_3}{\partial X_2} \right)^2 \right] \\
 E_{33} &= \frac{\partial u_3}{\partial X_3} + \frac{1}{2} \left[\left(\frac{\partial u_1}{\partial X_3} \right)^2 + \left(\frac{\partial u_2}{\partial X_3} \right)^2 + \left(\frac{\partial u_3}{\partial X_3} \right)^2 \right] \\
 E_{12} &= \frac{1}{2} \left(\frac{\partial u_1}{\partial X_2} + \frac{\partial u_2}{\partial X_1} + \frac{\partial u_1}{\partial X_1} \frac{\partial u_1}{\partial X_2} + \frac{\partial u_2}{\partial X_1} \frac{\partial u_2}{\partial X_2} + \frac{\partial u_3}{\partial X_1} \frac{\partial u_3}{\partial X_2} \right) \\
 E_{13} &= \frac{1}{2} \left(\frac{\partial u_1}{\partial X_3} + \frac{\partial u_3}{\partial X_1} + \frac{\partial u_1}{\partial X_1} \frac{\partial u_1}{\partial X_3} + \frac{\partial u_2}{\partial X_1} \frac{\partial u_2}{\partial X_3} + \frac{\partial u_3}{\partial X_1} \frac{\partial u_3}{\partial X_3} \right) \\
 E_{23} &= \frac{1}{2} \left(\frac{\partial u_2}{\partial X_3} + \frac{\partial u_3}{\partial X_2} + \frac{\partial u_1}{\partial X_2} \frac{\partial u_1}{\partial X_3} + \frac{\partial u_2}{\partial X_2} \frac{\partial u_2}{\partial X_3} + \frac{\partial u_3}{\partial X_2} \frac{\partial u_3}{\partial X_3} \right)
 \end{aligned} \quad (1.3.10)$$

If the displacement gradients are so small, $|\nabla \mathbf{u}| \ll 1$, that their squares and products are negligible compared to $|\nabla \mathbf{u}|$. Then the Green-Lagrange strain tensor reduces to the *infinitesimal strain tensor*, $\mathbf{E} \approx \boldsymbol{\varepsilon}$:

$$\boldsymbol{\varepsilon} = \frac{1}{2} [\nabla \mathbf{u} + (\nabla \mathbf{u})^T], \quad \varepsilon_{ij} = \frac{1}{2} \left(\frac{\partial u_i}{\partial x_j} + \frac{\partial u_j}{\partial x_i} \right) \quad (1.3.11)$$

The explicit form of the infinitesimal strain components (1.3.11) is given by (γ_{ij} denote the engineering shear strains)

$$\begin{aligned}
 \varepsilon_{11} &= \frac{\partial u_1}{\partial x_1}, \quad \varepsilon_{22} = \frac{\partial u_2}{\partial x_2}, \quad \varepsilon_{33} = \frac{\partial u_3}{\partial x_3}, \quad \gamma_{12} \equiv 2\varepsilon_{12} = \frac{\partial u_1}{\partial x_2} + \frac{\partial u_2}{\partial x_1} \\
 \gamma_{13} \equiv 2\varepsilon_{13} &= \frac{\partial u_1}{\partial x_3} + \frac{\partial u_3}{\partial x_1}, \quad \gamma_{23} \equiv 2\varepsilon_{23} = \frac{\partial u_2}{\partial x_3} + \frac{\partial u_3}{\partial x_2}
 \end{aligned} \quad (1.3.12)$$

Example 1.3.1:

(a) A square block is deformed as shown by dotted lines in Figure 1.3.2a. Assuming that the body is very thin and the strains (due to the Poisson effect) associated with the thickness direction are negligible, we wish to determine the two-dimensional strains.

A material particle which occupied position (X_1, X_2, X_3) in the undeformed body takes the position (x_1, x_2, x_3) in the deformed body. The current coordinates of the material particle can be expressed in terms of its original position as

$$x_1 = X_1 + \frac{e}{a} X_2, \quad x_2 = X_2, \quad x_3 = X_3 \quad (1.3.13)$$

The displacements are

$$u_1 \equiv x_1 - X_1 = \frac{e}{a} X_2, \quad u_2 \equiv x_2 - X_2 = 0, \quad u_3 \equiv x_3 - X_3 = 0 \quad (1.3.14)$$

Then the Green-Lagrangian strains can be computed using Eq. (1.3.10). The only nonzero strain component is ($e = 0.2\text{cm}$ and $a = 10\text{cm}$)

$$E_{12} = \frac{e}{2a} = 0.01 \text{ cm/cm} \quad (1.3.15)$$

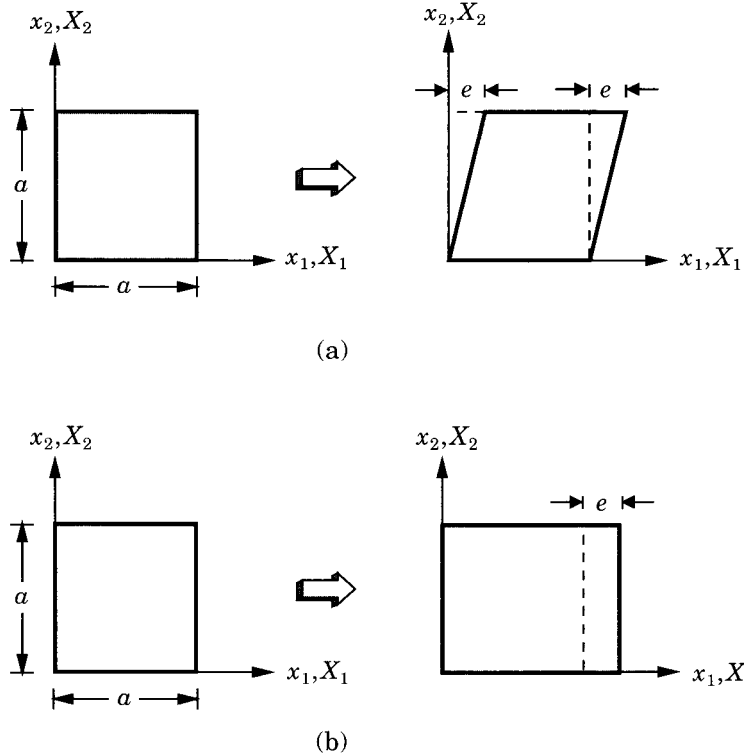


Figure 1.3.2: Undeformed and deformed configurations of a solid square block.
 (a) Pure shear deformation. (b) Pure extensional deformation.

(b) Consider a square block, deformed as shown by dotted lines in Figure 1.3.2b. The current coordinates of the material particle occupying position (X_1, X_2, X_3) in the undeformed body can be expressed as

$$x_1 = X_1 + \frac{e}{a}X_1, \quad x_2 = X_2, \quad x_3 = X_3 \quad (1.3.16)$$

The displacements are

$$u_1 \equiv x_1 - X_1 = \frac{e}{a}X_1, \quad u_2 \equiv x_2 - X_2 = 0, \quad u_3 \equiv x_3 - X_3 = 0 \quad (1.3.17)$$

The only nonzero Lagrangian strain is

$$E_{11} = \frac{e}{a} + \frac{1}{2} \left(\frac{e}{a} \right)^2 = (0.02 + 0.0002) \text{ cm/cm} \quad (1.3.18)$$

The strain is nonlinear. The nonlinear part of the strain is 0.02 percent.

This completes the kinematic description. In the coming chapters, we use only the linear strains and the von Kármán nonlinear strains derived from Eq. (1.3.10).

1.3.3 Strain Compatibility Equations

By definition, the components of the strain tensor can be computed from a differentiable displacement field using Eq. (1.3.8) or Eq. (1.3.11). However, if the *six* components of strain tensor are given and if we are required to find the *three* displacement components, the strains given should be such that a unique solution to the six differential equations relating the strains and displacements exists. The existence of a unique solution is guaranteed if the infinitesimal strain components satisfy the following six compatibility conditions:

$$\frac{\partial^2 \varepsilon_{ij}}{\partial x_m \partial x_n} + \frac{\partial^2 \varepsilon_{mn}}{\partial x_i \partial x_j} - \frac{\partial^2 \varepsilon_{im}}{\partial x_j \partial x_n} - \frac{\partial^2 \varepsilon_{jn}}{\partial x_i \partial x_m} = 0 \quad (1.3.19)$$

for any $i, j, m, n = 1, 2, 3$. For the two-dimensional case, Eq. (1.3.19) reduces to the following single compatibility equation

$$\frac{\partial^2 \varepsilon_{11}}{\partial x_2^2} + \frac{\partial^2 \varepsilon_{22}}{\partial x_1^2} - 2 \frac{\partial^2 \varepsilon_{12}}{\partial x_1 \partial x_2} = 0 \quad (1.3.20)$$

It should be noted that the strain compatibility equations are satisfied automatically when the strains are computed from a displacement field. Thus, one needs to verify the compatibility conditions only when the strains are computed from stresses that are in equilibrium.

1.3.4 Stress Measures

Stress at a point was introduced in Section 1.2 as a measure of force per unit area. Equation (1.2.16) indicates that the stress vector at a point depends on the force vector (its direction and magnitude) and the surface area. The surface area in turn depends on the orientation of the plane used to slice the body. It was shown that the state of stress at a point inside a body can be expressed in terms of stress vectors on three mutually perpendicular planes, say planes perpendicular to the rectangular coordinate axes by Cauchy's formula in Eq. (1.2.25).

In the above discussion, stress vector \mathbf{t} at a point in a deformed body is measured as the force per unit area in the deformed body. The area element Δs in the deformed body corresponds to an area element ΔS in the reference configuration, in much the same way \mathbf{x} is the position of a material particle X in the deformed body whose position in the reference configuration was \mathbf{X} . Thus the *Cauchy stress tensor* σ is defined to be the *current force per unit deformed area*:

$$d\mathbf{f} = \mathbf{t} da = d\mathbf{a} \cdot \sigma, \quad \text{where } d\mathbf{a} = da \hat{\mathbf{n}} \quad (1.3.21)$$

where Cauchy's formula, $\mathbf{t} = \sigma \cdot \hat{\mathbf{n}}$, is used.

Expressing $d\mathbf{f}$ in terms of a stress times the initial undeformed area dA requires a new stress tensor \mathbf{P} ,

$$d\mathbf{f} = d\mathbf{A} \cdot \mathbf{P}, \quad \text{where } d\mathbf{A} = dA \hat{\mathbf{N}} \quad (1.3.22)$$

where $\hat{\mathbf{N}}$ is the unit normal to the undeformed area dA . The stress tensor \mathbf{P} is called the *first Piola-Kirchhoff stress tensor*, and it gives the *current force per unit undeformed area*. The first Piola-Kirchhoff stress tensor is not symmetric.

The *second Piola–Kirchhoff stress tensor* \mathbf{S} is introduced as follows. First, we introduce the *deformation gradient tensor* \mathbf{F}

$$d\mathbf{x} = \mathbf{F} \cdot d\mathbf{X} = d\mathbf{X} \cdot \mathbf{F}^T \quad \text{where } \mathbf{F} = \left(\frac{\partial \mathbf{x}}{\partial \mathbf{X}} \right)^T \equiv (\nabla_0 \mathbf{x})^T \quad (1.3.23)$$

and ∇_0 is the gradient operator with respect to \mathbf{X} . We also have

$$d\mathbf{X} = \mathbf{F}^{-1} \cdot d\mathbf{x} = d\mathbf{x} \cdot \mathbf{F}^{-T}, \quad \text{where } \mathbf{F}^{-T} = \frac{\partial \mathbf{X}}{\partial \mathbf{x}} \equiv \nabla \mathbf{X} \quad (1.3.24)$$

and ∇ is the gradient operator with respect to \mathbf{x} . Analogous to the transformation between \mathbf{X} and \mathbf{x} , we can transform the force $d\mathbf{f}$ on the deformed elemental area $d\mathbf{a}$ to the force $d\mathbf{F}$ on the undeformed elemental area $d\mathbf{A}$ (not to be confused between the force $d\mathbf{F}$ and deformation gradient tensor \mathbf{F})

$$d\mathbf{F} = \mathbf{F}^{-1} \cdot d\mathbf{f} = \mathbf{F}^{-1} \cdot (d\mathbf{A} \cdot \mathbf{P}) = d\mathbf{A} \cdot \mathbf{P} \cdot \mathbf{F}^{-T} \equiv d\mathbf{A} \cdot \mathbf{S} \quad (1.3.25)$$

Thus, the second Piola–Kirchhoff stress tensor gives the *transformed current force per unit undeformed area*. The second Piola–Kirchhoff stress tensor is symmetric whenever the Cauchy stress tensor is symmetric.

1.3.5 Equations of Motion

The principle of conservation of linear momentum states that the rate of change of the total linear momentum of a given continuous medium equals the vector sum of all the external forces acting on the body \mathcal{B} , which initially occupied a configuration \mathcal{C}^0 , provided Newton's third law of action and reaction governs the internal forces. The principle leads to the following equations of motion:

$$\nabla \cdot \sigma + \mathbf{f} = \rho \frac{\partial^2 \mathbf{u}}{\partial t^2} \quad (\text{vector form}) \quad (1.3.26a)$$

$$\frac{\partial \sigma_{ji}}{\partial x_j} + f_i = \rho \frac{\partial^2 u_i}{\partial t^2} \quad (\text{Cartesian component form}) \quad (1.3.26b)$$

where ρ is the density in the deformed configuration and \mathbf{f} is the body force vector (measured per unit volume). The equations of equilibrium are obtained by setting the time derivative term to zero:

$$\nabla \cdot \sigma + \mathbf{f} = 0 \quad (\text{vector form}) \quad (1.3.27a)$$

$$\frac{\partial \sigma_{ji}}{\partial x_j} + f_i = 0 \quad (\text{Cartesian component form}) \quad (1.3.27b)$$

For kinematically infinitesimal deformations, i.e., $|\nabla \mathbf{u}| \ll 1$, we do not distinguish between \mathbf{x} and \mathbf{X} , between σ and \mathbf{S} and between ε and \mathbf{E} , and we use the first symbol of each pair. In much of this book we deal with kinematically infinitesimal deformations (i.e., linearized elasticity).

The strain-displacement relations and the equations of motion in any coordinate system can be obtained from the vector forms in Eqs. (1.3.8), (1.3.11), (1.3.26a) and

(1.3.27a) by expressing σ , \mathbf{f} , \mathbf{u} , and ∇ in the chosen coordinate system. The vector forms of equations are invariant, i.e., independent of the choice of the coordinate system.

The principle of conservation of angular momentum, in the absence of any distributed body couples, leads to the symmetry of the stress tensor:

$$\sigma = \sigma^T \quad (\sigma_{ij} = \sigma_{ji})$$

Thus there are only six independent components of the Cauchy stress tensor. Since the Cauchy stress tensor is a second-order tensor and symmetric, we may write it with a “double arrow” notation as

$$\overleftrightarrow{\sigma} \quad (1.3.28a)$$

This notation is meaningful and descriptive of the nature of the tensor; the notation indicates that the quantity is a dyad (i.e., having two base vectors) and it is symmetric:

$$\overleftrightarrow{\sigma} = \hat{\mathbf{e}}_i \sigma_{ij} \hat{\mathbf{e}}_j \quad (1.3.28b)$$

Note that the equations of motion or equilibrium contain three equations relating six stress components and therefore cannot be solved for all six components uniquely. Additional equations are required. These include the strain-displacement relations discussed in Section 1.3.2 and constitutive relations or stress-strain relations to be discussed in the next section.

Example 1.3.2:

Consider the following stress field in a body that is in equilibrium:

$$\sigma_{11} = c_1 x_1 + c_2 x_2 + c_3 x_1 x_2, \quad \sigma_{12} = -\frac{c_3}{2} (x_2)^2 - c_1 x_2, \quad \sigma_{22} = c_4 x_1 + c_1 x_2$$

and all other components of stress are zero. We wish to determine if the stress field satisfies the equations of equilibrium in the presence of body forces, $f_1 = 0$, $f_2 = -c_1$, and $f_3 = 0$. We assume that the body experienced only a small deformation. We have

$$\begin{aligned} 0 &= \frac{\partial \sigma_{11}}{\partial x_1} + \frac{\partial \sigma_{12}}{\partial x_2} + \frac{\partial \sigma_{13}}{\partial x_3} + f_1 \\ &= (c_1 + c_3 x_2) + (-c_1 - c_3 x_2) + 0 + 0 \\ 0 &= \frac{\partial \sigma_{12}}{\partial x_1} + \frac{\partial \sigma_{22}}{\partial x_2} + \frac{\partial \sigma_{23}}{\partial x_3} + f_2 \\ &= 0 + c_1 + 0 + 0 + (-c_1) \end{aligned}$$

Thus, the first two equations of equilibrium are identically satisfied for any choice of constants, c_1 , c_2 , c_3 , and c_4 . The third equation of equilibrium is trivially satisfied.

Example 1.3.3:

Consider the cantilevered beam under an end load (see Figure 1.3.3). The bending moment about the x_2 -axis at any distance x_1 is given by $M_2 = P(L - x_1)$. Then the stress component σ_{11} can be calculated using the flexure stress formula from elementary strength of materials:

$$\sigma_{11} = -\frac{M_2 x_3}{I_{22}} = -\frac{P}{I_{22}} (L - x_1) x_3 \equiv c_1 (L - x_1) x_3 \quad (1.3.29)$$

where I_{22} is area moment of inertia about the x_2 -axis. Assuming a two-dimensional state of stress (with respect to the x_1 and x_3 coordinates) in the beam, we wish to determine the stress components σ_{13} and σ_{33} in the absence of body forces. Since the stress components σ_{12} , σ_{22} , and σ_{23} are assumed to be zero, the first equation of equilibrium yields

$$\frac{\partial \sigma_{13}}{\partial x_3} = -\frac{\partial \sigma_{11}}{\partial x_1} = c_1 x_3$$

Integration with respect to x_3 gives

$$\sigma_{13} = \frac{c_1}{2} (x_3)^2 + f(x_1) \quad (1.3.30)$$

where f is a function of x_1 only. The second equation of equilibrium is trivially satisfied. The third equation of equilibrium gives

$$\frac{\partial \sigma_{33}}{\partial x_3} = -\frac{\partial \sigma_{13}}{\partial x_1} = -\frac{df}{dx_1}$$

Integration with respect to x_3 yields

$$\sigma_{33} = -\frac{df}{dx_1} x_3 + g(x_1) \quad (1.3.31)$$

The functions f and g can be determined using the boundary conditions of the beam. Note that σ_{13} and σ_{33} must be zero on the top and bottom surfaces of the beam (i.e., at $x_3 = \pm h/2$). Vanishing of σ_{33} at $x_3 = \pm h/2$ gives

$$-\frac{df}{dx_1} \frac{h}{2} + g = 0, \quad -\frac{df}{dx_1} (-\frac{h}{2}) + g = 0$$

which imply that

$$-\frac{df}{dx_1} = 0, \quad g = 0, \quad \text{or} \quad f = c_2 \quad \text{and} \quad g = 0$$

Vanishing of σ_{13} at $x_3 = \pm h/2$ gives

$$c_2 = -\frac{c_1 h^2}{8}$$

Thus the two-dimensional state of stress is given by

$$\sigma_{11} = -\frac{P}{I_{22}} (L - x_1) x_3, \quad \sigma_{13} = \frac{Ph^2}{8I_{22}} \left[1 - \left(\frac{2x_3}{h} \right)^2 \right], \quad \sigma_{33} = 0 \quad (1.3.32)$$

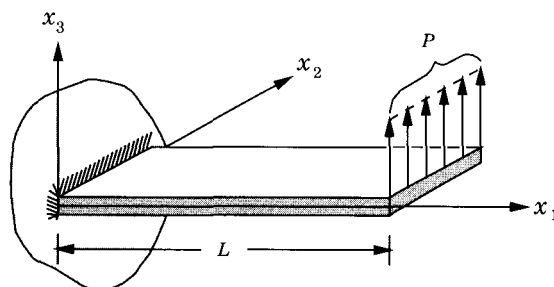


Figure 1.3.3: A cantilevered beam (i.e., fixed at one end and no support at the other end) under an end load.

Since the stress field is derived from stress equilibrium equations, it is necessary to see if the strain compatibility condition in Eq. (1.3.20) is satisfied. Suppose that the strains ε_{11} , ε_{13} , and ε_{33} are related to the stress components σ_{11} , σ_{13} , and σ_{33} by the relations (see the next section for details)

$$\varepsilon_{11} = S_{11}\sigma_{11} + S_{13}\sigma_{33} + S_{15}\sigma_{13}$$

$$\varepsilon_{33} = S_{13}\sigma_{11} + S_{33}\sigma_{33} + S_{35}\sigma_{13}$$

$$\varepsilon_{13} = S_{15}\sigma_{11} + S_{35}\sigma_{33} + S_{55}\sigma_{13}$$

Then

$$\begin{aligned}\varepsilon_{11} &= -S_{11}\frac{P}{I_{22}}(L-x_1)x_3 + S_{15}\frac{Ph^2}{8I_{22}}\left[1-\left(\frac{2x_3}{h}\right)^2\right] \\ \varepsilon_{33} &= -S_{13}\frac{P}{I_{22}}(L-x_1)x_3 + S_{35}\frac{Ph^2}{8I_{22}}\left[1-\left(\frac{2x_3}{h}\right)^2\right] \\ \varepsilon_{13} &= -S_{15}\frac{P}{I_{22}}(L-x_1)x_3 + S_{55}\frac{Ph^2}{8I_{22}}\left[1-\left(\frac{2x_3}{h}\right)^2\right]\end{aligned}\quad (1.3.33)$$

Substituting these strain components into the compatibility equation [see Eq. (1.3.20)],

$$\frac{\partial^2\varepsilon_{11}}{\partial x_3^2} + \frac{\partial^2\varepsilon_{33}}{\partial x_1^2} - 2\frac{\partial^2\varepsilon_{13}}{\partial x_1\partial x_3} = 0 \quad (1.3.34)$$

we obtain

$$-S_{15}\frac{P}{I_{22}} + 0 + 2S_{15}\frac{P}{I_{22}} \neq 0$$

Thus the strains are compatible only if $S_{15} = 0$, which is the case when the material is isotropic or orthotropic with respect to the problem coordinates.

1.3.6 Generalized Hooke's Law

The kinematic relations and the mechanical and thermodynamic principles are applicable to any continuum irrespective of its physical constitution. Here we consider equations characterizing the individual material and its reaction to applied loads. These equations are called the *constitutive equations*.

Materials for which the constitutive behavior is only a function of the current state of deformation are known as *elastic*. In the special case in which the work done by the stresses during a deformation is dependent only on the initial state and the current configuration, the material is called *hyperelastic*.

A material body is said to be *homogeneous* if the material properties are the same throughout the body (i.e., independent of position). In a *heterogeneous* body, the material properties are a function of position. For example, a structure composed of several uniform thickness layers of different materials stacked on top of each other and bonded to each other is heterogeneous through the thickness. An *anisotropic* body is one that has different values of a material property in different directions at a point; i.e., material properties are direction-dependent. An *isotropic* body is one for which every material property in all directions at a point is the same. An isotropic or anisotropic material can be nonhomogeneous or homogeneous.

A material body is said to be *ideally elastic* when, under isothermal conditions, the body recovers its original form completely upon removal of the forces causing deformation, and there is a one-to-one relationship between the state of stress and the state of strain in the current configuration. The constitutive equations described here do not include creep at constant stress and stress relaxation at constant strain. Thus, the material coefficients that specify the constitutive relationship between the stress and strain components are assumed to be constant during the deformation. This does not automatically imply that we neglect temperature effects on deformation. We account for the thermal expansion of the material, which can produce strains or stresses as large as those produced by the applied mechanical forces. Here, we discuss the constitutive equations of linear elasticity (i.e., relations between stress and strain are linear) for the case of infinitesimal deformation (i.e., $|\nabla \mathbf{u}| \ll 1$). Hence, we will not distinguish between various measures of stress and strain, and use $\mathbf{S} \approx \sigma$ for the stress tensor and $\mathbf{E} \approx \varepsilon$ for strain tensor in the material description used in solid mechanics. The linear constitutive model for infinitesimal deformation is referred to as the *generalized Hooke's law*. Suppose that the reference configuration has a (residual) stress state of σ^0 . Then if the stress components are assumed to be linear functions of the components of strain, then the most general form of the linear constitutive equations for infinitesimal deformations is

$$\sigma = \mathbf{C} : \varepsilon + \sigma^0, \quad \sigma_{ij} = C_{ijkl}\varepsilon_{kl} + \sigma_{ij}^0, \quad \varepsilon_{kl} = \varepsilon_{lk} \quad (1.3.35)$$

where \mathbf{C} is the fourth-order tensor of material parameters and is termed *stiffness tensor*. There are, in general, $3^4 = 81$ scalar components of a fourth-order tensor. The number of independent components of \mathbf{C} are considerably less because of the symmetry of σ , symmetry of ε , and symmetry of \mathbf{C} , as discussed next [6].

In the absence of body couples, the principle of conservation of angular momentum requires the stress tensor to be symmetric, $\sigma_{ij} = \sigma_{ji}$. Then it follows from Eq. (1.3.35) that C_{ijkl} must be symmetric in the first two subscripts. Hence the number of independent material stiffness components reduces to $6(3)^2 = 54$. Since the strain tensor is symmetric (by its definition), $\varepsilon_{ij} = \varepsilon_{ji}$, then C_{ijkl} must be symmetric in the last two subscripts as well, further reducing the number of independent material stiffness components to $6 \times 6 = 36$.

If we also assume that the material is hyperelastic, i.e., there exists a strain energy density function $U_0(\varepsilon_{ij})$ such that

$$\sigma_{ij} = \frac{\partial U_0}{\partial \varepsilon_{ij}} = C_{ijkl}\varepsilon_{kl} + \sigma_{ij}^0 \quad (1.3.36)$$

we have

$$\frac{\partial^2 U_0}{\partial \varepsilon_{ij} \partial \varepsilon_{kl}} = C_{ijkl}$$

Since the order of differentiation is arbitrary, $\partial^2 U_0 / \partial \varepsilon_{ij} \partial \varepsilon_{kl} = \partial^2 U_0 / \partial \varepsilon_{kl} \partial \varepsilon_{ij}$, it follows that $C_{ijkl} = C_{klij}$. This reduces the number of independent material stiffness components to 21. To show this we express Eq. (1.3.35) in an alternate form using single subscript notation for stresses and strains and two subscript notation for the

material stiffness coefficients:

$$\begin{aligned}\sigma_1 &= \sigma_{11}, \sigma_2 = \sigma_{22}, \sigma_3 = \sigma_{33}, \sigma_4 = \sigma_{23}, \sigma_5 = \sigma_{13}, \sigma_6 = \sigma_{12} \\ \varepsilon_1 &= \varepsilon_{11}, \varepsilon_2 = \varepsilon_{22}, \varepsilon_3 = \varepsilon_{33}, \varepsilon_4 = 2\varepsilon_{23}, \varepsilon_5 = 2\varepsilon_{13}, \varepsilon_6 = 2\varepsilon_{12}\end{aligned}\quad (1.3.37a)$$

$$11 \rightarrow 1 \quad 22 \rightarrow 2 \quad 33 \rightarrow 3 \quad 23 \rightarrow 4 \quad 13 \rightarrow 5 \quad 12 \rightarrow 6. \quad (1.3.37b)$$

It should be cautioned that the single subscript notation used for stresses and strains and the two-subscript components C_{ij} render them non-tensor components (i.e., σ_i , ε_i , and C_{ij} do not transform like the components of a vector or tensor). The single subscript notation for stresses and strains is called the *engineering notation* or the *Voigt-Kelvin notation*. Equation (1.3.35) now takes the form

$$\sigma_i = C_{ij}\varepsilon_j + \sigma_i^0 \quad (1.3.38a)$$

where summation on repeated subscripts is implied (now from 1 to 6). In matrix notation, Eq. (1.3.38a) can be written as

$$\left\{ \begin{array}{c} \sigma_1 \\ \sigma_2 \\ \sigma_3 \\ \sigma_4 \\ \sigma_5 \\ \sigma_6 \end{array} \right\} = \left[\begin{array}{cccccc} C_{11} & C_{12} & C_{13} & C_{14} & C_{15} & C_{16} \\ C_{21} & C_{22} & C_{23} & C_{24} & C_{25} & C_{26} \\ C_{31} & C_{32} & C_{33} & C_{34} & C_{35} & C_{36} \\ C_{41} & C_{42} & C_{43} & C_{44} & C_{45} & C_{46} \\ C_{51} & C_{52} & C_{53} & C_{54} & C_{55} & C_{56} \\ C_{61} & C_{62} & C_{63} & C_{64} & C_{65} & C_{66} \end{array} \right] \left\{ \begin{array}{c} \varepsilon_1 \\ \varepsilon_2 \\ \varepsilon_3 \\ \varepsilon_4 \\ \varepsilon_5 \\ \varepsilon_6 \end{array} \right\} + \left\{ \begin{array}{c} \sigma_1^0 \\ \sigma_2^0 \\ \sigma_3^0 \\ \sigma_4^0 \\ \sigma_5^0 \\ \sigma_6^0 \end{array} \right\} \quad (1.3.38b)$$

Now the coefficients C_{ij} must be symmetric ($C_{ij} = C_{ji}$) by virtue of the assumption that the material is hyperelastic. Hence, we have $6+5+4+3+2+1 = 21$ independent stiffness coefficients for the most general elastic material.

We assume that the stress-strain relations (1.3.38a,b) are invertible. Thus, the components of strain are related to the components of stress by

$$\varepsilon_i = S_{ij}\sigma_j + \varepsilon_i^0, \quad \varepsilon_i^0 = -S_{ij}\sigma_j^0 \quad (1.3.39a)$$

where S_{ij} are the material compliance parameters with $[S] = [C]^{-1}$ (the compliance tensor is the inverse of the stiffness tensor: $\mathbf{S} = \mathbf{C}^{-1}$). In matrix form Eq. (1.3.39a) becomes

$$\left\{ \begin{array}{c} \varepsilon_1 \\ \varepsilon_2 \\ \varepsilon_3 \\ \varepsilon_4 \\ \varepsilon_5 \\ \varepsilon_6 \end{array} \right\} = \left[\begin{array}{cccccc} S_{11} & S_{12} & S_{13} & S_{14} & S_{15} & S_{16} \\ S_{21} & S_{22} & S_{23} & S_{24} & S_{25} & S_{26} \\ S_{31} & S_{32} & S_{33} & S_{34} & S_{35} & S_{36} \\ S_{41} & S_{42} & S_{43} & S_{44} & S_{45} & S_{46} \\ S_{51} & S_{52} & S_{53} & S_{54} & S_{55} & S_{56} \\ S_{61} & S_{62} & S_{63} & S_{64} & S_{65} & S_{66} \end{array} \right] \left\{ \begin{array}{c} \sigma_1 \\ \sigma_2 \\ \sigma_3 \\ \sigma_4 \\ \sigma_5 \\ \sigma_6 \end{array} \right\} + \left\{ \begin{array}{c} \varepsilon_1^0 \\ \varepsilon_2^0 \\ \varepsilon_3^0 \\ \varepsilon_4^0 \\ \varepsilon_5^0 \\ \varepsilon_6^0 \end{array} \right\} \quad (1.3.39b)$$

In the following discussion we assume that the reference configuration is stress free, $\sigma_i^0 = 0$ and strain free $\varepsilon_i^0 = 0$.

Material Symmetry

Further reduction in the number of independent stiffness (or compliance) parameters comes from the so-called material symmetry. Suppose that (x_1, x_2, x_3) denote the coordinate system with respect to which Eqs. (1.3.38a,b) and (1.3.39a,b) are defined. We shall call them *material coordinate system*. The coordinate system (x, y, z) used to write the equations of motion and strain-displacement equations will be called the *problem coordinates* to distinguish them from the material coordinate system. Note that the phrase “material coordinates” used in connection with the material description should not be confused with the present term. In the remaining discussion, we will use the material description for everything, but we may use one material coordinate system, say (x, y, z) , to describe the kinematics as well as stress state in the body and another material coordinate system (x_1, x_2, x_3) to describe the stress-strain behavior. Both are fixed in the body, and the two systems are oriented with respect to each other. When elastic material parameters at a point have the same values for every pair of coordinate systems that are mirror images of each other in a certain plane, that plane is called a *material plane of symmetry* (e.g., symmetry of internal structure due to crystallographic form, regular arrangement of fibers or molecules, etc.). We note that the symmetry under discussion is a directional property and not a positional property. Thus, a material may have certain elastic symmetry at every point of a material body the properties may vary from point to point. Positional dependence of material properties is what we called the inhomogeneity of the material.

In the following we discuss various planes of symmetry and forms of associated stress-strain relations. Note that use of the tensor components of stress and strain is necessary because the transformation laws of the form (1.2.35) are valid only for the tensor components. The fourth-order tensor, for example, transforms according to the formula

$$C'_{ijkl} = \ell_{ip} \ell_{jq} \ell_{kr} \ell_{ls} C_{pqrs} \quad (1.3.40)$$

where ℓ_{ij} are the direction cosines associated with the coordinate systems (x_1, x_2, x_3) and (x'_1, x'_2, x'_3) , and C'_{ijkl} and C_{pqrs} are the components of the fourth-order tensor \mathbf{C} in the primed and unprimed coordinate systems, respectively.

Monoclinic Materials

When the elastic coefficients at a point have the same value for every pair of coordinate systems which are the mirror images of each other with respect to a plane, the material is called a *monoclinic material*. For example, let (x_1, x_2, x_3) and (x'_1, x'_2, x'_3) be two coordinate systems, with the x_1, x_2 -plane parallel to the plane of symmetry. Choose x'_3 -axis such that $x'_3 = -x_3$ (never mind about the left-handed coordinate system as it does not affect the discussion) so that one system is the mirror image of the other. The definitions and sign conventions of the stress and strain components show that

$$\sigma'_{23} = -\sigma_{23}, \quad \sigma'_{31} = -\sigma_{31}, \quad \varepsilon'_{23} = -\varepsilon_{23}, \quad \varepsilon'_{31} = -\varepsilon_{31}$$

or, in single-subscript notation

$$\sigma'_4 = -\sigma_4, \quad \sigma'_5 = -\sigma_5, \quad \varepsilon'_4 = -\varepsilon_4, \quad \varepsilon'_5 = -\varepsilon_5$$

while all their independent stress and strain components remain unchanged in value by the change from one coordinate system to the other. Using the stress-strain relations of the form in Eq. (1.3.38b), we can write

$$\begin{aligned}\sigma'_1 &= C_{11}\varepsilon'_1 + C_{12}\varepsilon'_2 + C_{13}\varepsilon'_3 + C_{14}\varepsilon'_4 + C_{15}\varepsilon'_5 + C_{16}\varepsilon'_6 \\ \sigma_1 &= C_{11}\varepsilon_1 + C_{12}\varepsilon_2 + C_{13}\varepsilon_3 - C_{14}\varepsilon_4 - C_{15}\varepsilon_5 + C_{16}\varepsilon_6\end{aligned}$$

But we also have

$$\sigma_1 = C_{11}\varepsilon_1 + C_{12}\varepsilon_2 + C_{13}\varepsilon_3 + C_{14}\varepsilon_4 + C_{15}\varepsilon_5 + C_{16}\varepsilon_6$$

Note that the elastic parameters C_{ij} are the same for the two coordinate systems because they are the mirror images in the plane of symmetry. From the above two equations (subtract one from the other) we arrive at

$$C_{14}\varepsilon_4 + C_{15}\varepsilon_5 = 0 \text{ for all values of } \varepsilon_4 \text{ and } \varepsilon_5$$

The above equation holds only if $C_{14} = 0$ and $C_{15} = 0$. Similar discussion with the two alternative expressions of the remaining stress components yield $C_{24} = 0$ and $C_{25} = 0$; $C_{34} = 0$ and $C_{35} = 0$; and $C_{46} = 0$ and $C_{56} = 0$. Thus out of 21 material parameters, we only have $21 - 8 = 13$ independent parameters, as indicated below

$$[C] = \begin{bmatrix} C_{11} & C_{12} & C_{13} & 0 & 0 & C_{16} \\ C_{12} & C_{22} & C_{23} & 0 & 0 & C_{26} \\ C_{13} & C_{23} & C_{33} & 0 & 0 & C_{36} \\ 0 & 0 & 0 & C_{44} & C_{45} & 0 \\ 0 & 0 & 0 & C_{45} & C_{55} & 0 \\ C_{16} & C_{26} & C_{36} & 0 & 0 & C_{66} \end{bmatrix} \quad (1.3.42)$$

Note that monoclinic materials exhibit shear-extensional coupling; i.e., a shear strain can produce a normal stress; for example, $\sigma_{11} = C_{16}\varepsilon_6 = 2C_{16}\varepsilon_{12}$. Therefore, the principal axes of stress do not coincide with those of strain.

The result in Eq. (1.3.42) can also be obtained using the following transformation matrix (which converts the unprimed coordinate system to the primed one) in Eq. (1.3.40):

$$[L] = \begin{bmatrix} 1 & 0 & 0 \\ 0 & 1 & 0 \\ 0 & 0 & -1 \end{bmatrix} \quad (\text{or } \ell_{11} = \ell_{22} = 1, \ell_{33} = -1, \ell_{ij} = 0 \text{ for } i \neq j) \quad (1.3.43)$$

Orthotropic Materials

When three mutually orthogonal planes of material symmetry exist, the number of elastic coefficients is reduced to 9 using arguments similar to those given for single material symmetry plane, and such materials are called *orthotropic*. The stress-strain relations for an orthotropic material take the form

$$\begin{Bmatrix} \sigma_1 \\ \sigma_2 \\ \sigma_3 \\ \sigma_4 \\ \sigma_5 \\ \sigma_6 \end{Bmatrix} = \begin{bmatrix} C_{11} & C_{12} & C_{13} & 0 & 0 & 0 \\ C_{12} & C_{22} & C_{23} & 0 & 0 & 0 \\ C_{13} & C_{23} & C_{33} & 0 & 0 & 0 \\ 0 & 0 & 0 & C_{44} & 0 & 0 \\ 0 & 0 & 0 & 0 & C_{55} & 0 \\ 0 & 0 & 0 & 0 & 0 & C_{66} \end{bmatrix} \begin{Bmatrix} \varepsilon_1 \\ \varepsilon_2 \\ \varepsilon_3 \\ \varepsilon_4 \\ \varepsilon_5 \\ \varepsilon_6 \end{Bmatrix} \quad (1.3.44)$$

The transformation matrices associated with the planes of symmetry are

$$[L^{(1)}] = \begin{bmatrix} 1 & 0 & 0 \\ 0 & 1 & 0 \\ 0 & 0 & -1 \end{bmatrix}; \quad [L^{(2)}] = \begin{bmatrix} -1 & 0 & 0 \\ 0 & 1 & 0 \\ 0 & 0 & 1 \end{bmatrix}; \quad [L^{(3)}] = \begin{bmatrix} 1 & 0 & 0 \\ 0 & -1 & 0 \\ 0 & 0 & 1 \end{bmatrix}$$

Most simple mechanical-property characterization tests are performed with a known load or stress. Hence, it is convenient to write the inverse of relations in (1.3.44). The strain-stress relations of an orthotropic material are given by

$$\begin{Bmatrix} \varepsilon_1 \\ \varepsilon_2 \\ \varepsilon_3 \\ \varepsilon_4 \\ \varepsilon_5 \\ \varepsilon_6 \end{Bmatrix} = \begin{bmatrix} S_{11} & S_{12} & S_{13} & 0 & 0 & 0 \\ S_{12} & S_{22} & S_{23} & 0 & 0 & 0 \\ S_{13} & S_{23} & S_{33} & 0 & 0 & 0 \\ 0 & 0 & 0 & S_{44} & 0 & 0 \\ 0 & 0 & 0 & 0 & S_{55} & 0 \\ 0 & 0 & 0 & 0 & 0 & S_{66} \end{bmatrix} \begin{Bmatrix} \sigma_1 \\ \sigma_2 \\ \sigma_3 \\ \sigma_4 \\ \sigma_5 \\ \sigma_6 \end{Bmatrix} \quad (1.3.45)$$

where S_{ij} are the *compliance coefficients* ($[C] = [S]^{-1}$)

$$\begin{aligned} C_{11} &= \frac{S_{22}S_{33} - S_{23}^2}{S} & C_{12} &= \frac{S_{13}S_{23} - S_{12}S_{33}}{S} \\ C_{22} &= \frac{S_{33}S_{11} - S_{13}^2}{S} & C_{13} &= \frac{S_{12}S_{23} - S_{13}S_{22}}{S} \\ C_{33} &= \frac{S_{11}S_{22} - S_{12}^2}{S} & C_{23} &= \frac{S_{12}S_{13} - S_{23}S_{11}}{S} \\ C_{44} &= \frac{1}{S_{44}} & C_{55} &= \frac{1}{S_{55}} & C_{66} &= \frac{1}{S_{66}} \\ S &= S_{11}S_{22}S_{33} - S_{11}S_{23}^2 - S_{22}S_{13}^2 - S_{33}S_{12}^2 + 2S_{12}S_{23}S_{13} \end{aligned} \quad (1.3.46)$$

Most often, the material properties are determined in a laboratory in terms of the engineering constants such as Young's modulus, shear modulus, and so on. These constants are measured using simple tests like uniaxial tension test or pure shear test. Because of their direct and obvious physical meaning, engineering constants are used in place of the more abstract stiffness coefficients C_{ij} and compliance coefficients S_{ij} . Next we discuss how to relate the compliance coefficients S_{ij} to the engineering constants.

One of the consequences of linearity (both kinematic and material linearizations) is that the principle of superposition applies. That is, if the applied loads and geometric constraints are independent of deformation, the sum of the displacements (and hence strains) produced by two sets of loads is equal to the displacements (and strains) produced by the sum of the two sets of loads. In particular, the strains of the same type produced by the application of individual stress components can be superposed. For example, the extensional strain $\varepsilon_{11}^{(1)}$ in the material coordinate direction x_1 due to the stress σ_{11} in the same direction is σ_{11}/E_1 , where E_1 denotes Young's modulus of the material in the x_1 direction. The extensional strain $\varepsilon_{11}^{(2)}$ due to the stress σ_{22} applied in the x_2 direction is $-\nu_{21}\sigma_{22}/E_2$, where ν_{21} is the Poisson ratio

$$\nu_{21} = -\frac{\varepsilon_{11}}{\varepsilon_{22}}$$

and E_2 is Young's modulus of the material in the x_2 direction. Similarly, σ_{33} produces a strain $\varepsilon_{11}^{(3)}$ equal to $-\nu_{31}\sigma_{33}/E_3$. Hence, the total strain ε_{11} due to the simultaneous application of all three normal stress components is

$$\varepsilon_{11} = \varepsilon_{11}^{(1)} + \varepsilon_{11}^{(2)} + \varepsilon_{11}^{(3)} = \frac{\sigma_{11}}{E_1} - \frac{\sigma_{22}\nu_{21}}{E_2} - \frac{\sigma_{33}\nu_{31}}{E_3} \quad (\text{a})$$

where the direction of loading is denoted by the superscript. Similarly, we can write

$$\varepsilon_{22} = -\frac{\sigma_{11}\nu_{12}}{E_1} + \frac{\sigma_{22}}{E_2} - \frac{\sigma_{33}\nu_{32}}{E_3} \quad (\text{b})$$

$$\varepsilon_{33} = -\frac{\sigma_{11}\nu_{13}}{E_1} - \frac{\sigma_{22}\nu_{23}}{E_2} + \frac{\sigma_{33}}{E_3} \quad (\text{c})$$

The simple shear tests with an orthotropic material give the results

$$2\varepsilon_{12} = \frac{\sigma_{12}}{G_{12}}, \quad 2\varepsilon_{13} = \frac{\sigma_{13}}{G_{13}}, \quad 2\varepsilon_{23} = \frac{\sigma_{23}}{G_{23}} \quad (\text{d})$$

Recall that $2\varepsilon_{ij}$ ($i \neq j$) is the change in the right angle between two lines parallel to the x_1 and x_2 directions at a point, σ_{ij} ($i \neq j$) denotes the corresponding shear stress in the $x_i x_j$ plane, and G_{ij} ($i \neq j$) are the shear moduli in the $x_i x_j$ plane. Writing Eqs. (a)–(d) in matrix form, we obtain

$$\begin{Bmatrix} \varepsilon_1 \\ \varepsilon_2 \\ \varepsilon_3 \\ \varepsilon_4 \\ \varepsilon_5 \\ \varepsilon_6 \end{Bmatrix} = \begin{bmatrix} \frac{1}{E_1} & -\frac{\nu_{21}}{E_2} & -\frac{\nu_{31}}{E_3} & 0 & 0 & 0 \\ -\frac{\nu_{12}}{E_1} & \frac{1}{E_2} & -\frac{\nu_{32}}{E_3} & 0 & 0 & 0 \\ -\frac{\nu_{13}}{E_1} & -\frac{\nu_{23}}{E_2} & \frac{1}{E_3} & 0 & 0 & 0 \\ 0 & 0 & 0 & \frac{1}{G_{23}} & 0 & 0 \\ 0 & 0 & 0 & 0 & \frac{1}{G_{13}} & 0 \\ 0 & 0 & 0 & 0 & 0 & \frac{1}{G_{12}} \end{bmatrix} \begin{Bmatrix} \sigma_1 \\ \sigma_2 \\ \sigma_3 \\ \sigma_4 \\ \sigma_5 \\ \sigma_6 \end{Bmatrix} \quad (1.3.47)$$

where E_1, E_2, E_3 are Young's moduli in 1, 2, and 3 material directions, respectively, ν_{ij} is Poisson's ratio, defined as the ratio of transverse strain in the j th direction to the axial strain in the i th direction when stressed in the i th direction, and G_{23}, G_{13}, G_{12} are shear moduli in the 2-3, 1-3, and 1-2 planes, respectively. Since the compliance matrix $[S]$ is the inverse of the stiffness matrix $[C]$ and the inverse of a symmetric matrix is symmetric, it follows that the compliance matrix $[S]$ is also a symmetric matrix. This in turn implies that the following reciprocal relations hold [see Eq. (1.3.47)]:

$$\frac{\nu_{21}}{E_2} = \frac{\nu_{12}}{E_1}; \quad \frac{\nu_{31}}{E_3} = \frac{\nu_{13}}{E_1}; \quad \frac{\nu_{32}}{E_3} = \frac{\nu_{23}}{E_2}$$

or, in short

$$\frac{\nu_{ij}}{E_i} = \frac{\nu_{ji}}{E_j} \quad (\text{no sum on } i, j) \quad (1.3.48)$$

for $i, j = 1, 2, 3$. The 9 independent material coefficients for an orthotropic material are

$$E_1, E_2, E_3, G_{23}, G_{13}, G_{12}, \nu_{12}, \nu_{13}, \nu_{23} \quad (1.3.49)$$

It is important to note the difference, for example, between ν_{ij} and ν_{ji} for $i \neq j$ for an orthotropic material [10]. For example the difference between ν_{12} and ν_{21} for an orthotropic material is illustrated in Figure 1.3.4 with two cases of uniaxial stress for a square element of length a . First a stress σ is applied in the x_1 -direction as shown in Figure 1.3.4a. The resulting strains are

$$\varepsilon_{11}^{(1)} = \frac{\sigma}{E_1} \quad \varepsilon_{22}^{(1)} = -\frac{\nu_{12}}{E_1} \sigma \quad (1.3.50)$$

where the direction of loading is denoted by the superscript and negative sign indicates compression. Next, the same value of stress is applied in the x_2 -direction as shown in Figure 1.3.4b. The strains are

$$\varepsilon_{11}^{(2)} = -\frac{\nu_{21}}{E_2} \sigma \quad \varepsilon_{22}^{(2)} = \frac{\sigma}{E_2} \quad (1.3.51)$$

While it is obvious that $\varepsilon_{11}^{(1)} < \varepsilon_{22}^{(2)}$ if $E_1 > E_2$, we have no clue about the relative magnitudes of $\varepsilon_{22}^{(1)}$ and $\varepsilon_{11}^{(2)}$. However, the displacements associated with the two loads are

$$u_1^{(1)} = a \frac{\sigma}{E_1} \quad u_2^{(1)} = -a \frac{\nu_{12}}{E_1} \sigma \quad (1.3.52a)$$

$$u_1^{(2)} = -a \frac{\nu_{21}}{E_2} \sigma \quad u_2^{(2)} = a \frac{\sigma}{E_2} \quad (1.3.52b)$$

and the reciprocal relation (1.3.48) gives $u_2^{(1)} = u_1^{(2)}$, which is the statement of *Betti's reciprocity theorem* (see Reddy [6]).

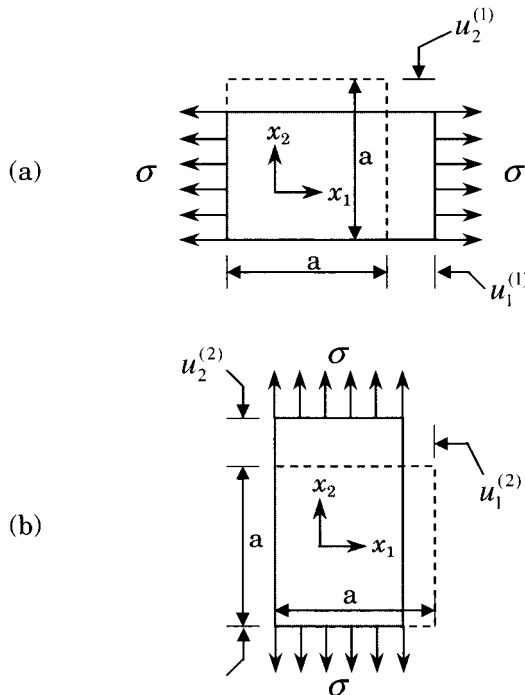


Figure 1.3.4: Distinction between ν_{12} and ν_{21} .

Comparing Eqs. (1.3.45) and (1.3.47), we note that

$$\begin{aligned} S_{11} &= \frac{1}{E_1}, & S_{12} &= -\frac{\nu_{12}}{E_1}, & S_{13} &= -\frac{\nu_{13}}{E_1} \\ S_{22} &= \frac{1}{E_2}, & S_{23} &= -\frac{\nu_{23}}{E_2}, & S_{33} &= \frac{1}{E_3} \\ S_{44} &= \frac{1}{G_{23}}, & S_{55} &= \frac{1}{G_{13}}, & S_{66} &= \frac{1}{G_{12}} \end{aligned} \quad (1.3.53)$$

and using Eq. (1.3.46) the stiffness coefficients can be expressed in terms of the engineering constants

$$\begin{aligned} C_{11} &= \frac{1 - \nu_{23}\nu_{32}}{E_2 E_3 \Delta}, & C_{12} &= \frac{\nu_{21} + \nu_{31}\nu_{23}}{E_2 E_3 \Delta} = \frac{\nu_{12} + \nu_{32}\nu_{13}}{E_1 E_3 \Delta} \\ C_{13} &= \frac{\nu_{31} + \nu_{21}\nu_{32}}{E_2 E_3 \Delta} = \frac{\nu_{13} + \nu_{12}\nu_{23}}{E_1 E_2 \Delta} \\ C_{22} &= \frac{1 - \nu_{13}\nu_{31}}{E_1 E_3 \Delta}, & C_{23} &= \frac{\nu_{32} + \nu_{12}\nu_{31}}{E_1 E_3 \Delta} = \frac{\nu_{23} + \nu_{21}\nu_{13}}{E_1 E_3 \Delta} \\ C_{33} &= \frac{1 - \nu_{12}\nu_{21}}{E_1 E_2 \Delta}, & C_{44} &= G_{23} \quad C_{55} = G_{31} \quad C_{66} = G_{12} \\ \Delta &= \frac{1 - \nu_{12}\nu_{21} - \nu_{23}\nu_{32} - \nu_{31}\nu_{13} - 2\nu_{21}\nu_{32}\nu_{13}}{E_1 E_2 E_3} \end{aligned} \quad (1.3.54)$$

Example 1.3.4:

The material properties of graphite fabric-carbon matrix layers, which are characterized as orthotropic, are:

$$E_1 = 25.1 \times 10^6 \text{ psi}, \quad E_2 = 4.8 \times 10^6 \text{ psi}, \quad E_3 = 0.75 \times 10^6 \text{ psi}$$

$$G_{12} = 1.36 \times 10^6 \text{ psi}, \quad G_{13} = 1.2 \times 10^6 \text{ psi}, \quad G_{23} = 0.47 \times 10^6 \text{ psi}$$

$$\nu_{12} = 0.036, \quad \nu_{13} = 0.25, \quad \nu_{23} = 0.171$$

The matrix of elastic coefficients for the material can be calculated using Eq. (1.3.54) as

$$[C] = \begin{bmatrix} 25.16 & 0.2063 & 0.1934 & 0 & 0 & 0 \\ 0.2063 & 4.8240 & 0.1304 & 0 & 0 & 0 \\ 0.1934 & 0.1304 & 4.8320 & 0 & 0 & 0 \\ 0 & 0 & 0 & 0.47 & 0 & 0 \\ 0 & 0 & 0 & 0 & 1.2 & 0 \\ 0 & 0 & 0 & 0 & 0 & 1.36 \end{bmatrix} \text{ (msi)}$$

A qualitative understanding of the anisotropic behavior of a material can be obtained by simple tension and shear tests [10]. Application of a normal stress to a rectangular block of isotropic or orthotropic material leads to only extension in the direction of the applied stress and contraction perpendicular to it, whereas an anisotropic material experiences extension in the direction of the applied normal stress, contraction perpendicular to it, as well as shearing strain (see Figure 1.3.5). Conversely, the application of a shearing stress to an anisotropic material causes

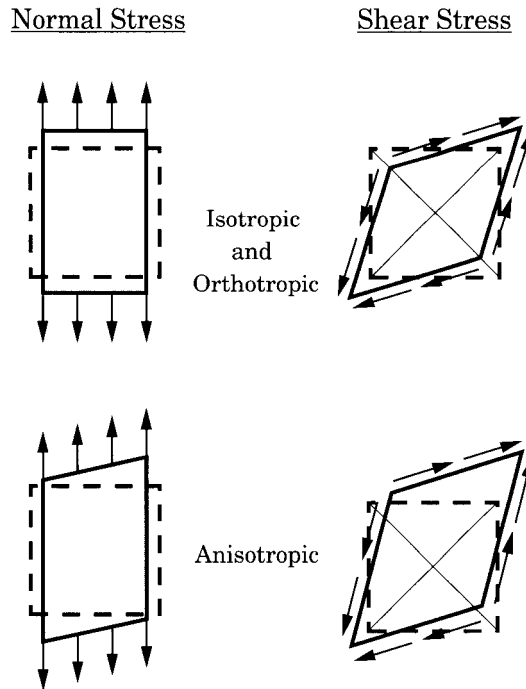


Figure 1.3.5: Deformation of orthotropic and anisotropic rectangular block under uniaxial tension.

shearing strain as well as normal strains. Normal stress applied to an orthotropic material at an angle to its principal material directions causes it to behave like an anisotropic material. The coupling between the two loading modes and the two deformation modes plays a significant role in the testing, analysis, and design of composite materials.

Isotropic Materials

When there exist no preferred directions in the material (i.e., the material has infinite number of planes of material symmetry), the number of independent elastic coefficients reduces to 2. Such materials are called *isotropic*. For isotropic materials we have

$$E_1 = E_2 = E_3 = E, \quad G_{12} = G_{13} = G_{23} \equiv G, \quad \nu_{12} = \nu_{23} = \nu_{13} \equiv \nu \quad (1.3.55)$$

Consequently, Eqs. (1.3.44) and (1.3.47), in view of the relations (1.3.53), (1.3.54) and (1.3.55), take the form

$$\begin{Bmatrix} \sigma_1 \\ \sigma_2 \\ \sigma_3 \\ \sigma_4 \\ \sigma_5 \\ \sigma_6 \end{Bmatrix} = \Lambda \begin{bmatrix} 1 - \nu & \nu & \nu & 0 & 0 & 0 \\ \nu & 1 - \nu & \nu & 0 & 0 & 0 \\ \nu & \nu & 1 - \nu & 0 & 0 & 0 \\ 0 & 0 & 0 & \frac{1}{2}(1 - 2\nu) & 0 & 0 \\ 0 & 0 & 0 & 0 & \frac{1}{2}(1 - 2\nu) & 0 \\ 0 & 0 & 0 & 0 & 0 & \frac{1}{2}(1 - 2\nu) \end{bmatrix} \begin{Bmatrix} \varepsilon_1 \\ \varepsilon_2 \\ \varepsilon_3 \\ \varepsilon_4 \\ \varepsilon_5 \\ \varepsilon_6 \end{Bmatrix} \quad (1.3.56)$$

$$\begin{Bmatrix} \varepsilon_1 \\ \varepsilon_2 \\ \varepsilon_3 \\ \varepsilon_4 \\ \varepsilon_5 \\ \varepsilon_6 \end{Bmatrix} = \frac{1}{E} \begin{bmatrix} 1 & -\nu & -\nu & 0 & 0 & 0 \\ -\nu & 1 & -\nu & 0 & 0 & 0 \\ -\nu & -\nu & 1 & 0 & 0 & 0 \\ 0 & 0 & 0 & 1+\nu & 0 & 0 \\ 0 & 0 & 0 & 0 & 1+\nu & 0 \\ 0 & 0 & 0 & 0 & 0 & 1+\nu \end{bmatrix} \begin{Bmatrix} \sigma_1 \\ \sigma_2 \\ \sigma_3 \\ \sigma_4 \\ \sigma_5 \\ \sigma_6 \end{Bmatrix} \quad (1.3.57)$$

where

$$\Lambda = \frac{E}{(1+\nu)(1-2\nu)} \quad (1.3.58)$$

Alternatively, the stress-strain relations can be written in more compact form using the fact that a fourth-order isotropic tensor can be expressed as

$$C_{ijkl} = \lambda \delta_{ij} \delta_{kl} + \mu (\delta_{ik} \delta_{jl} + \delta_{il} \delta_{jk}) \quad (1.3.59)$$

where λ and μ are called *Lamé constants*. Therefore, the stress-strain relation for the isotropic case takes the form

$$\sigma_{ij} = C_{ijkl} \varepsilon_{kl} = 2\mu \varepsilon_{ij} + \lambda \varepsilon_{kk} \delta_{ij}, \quad \sigma = 2\mu \varepsilon + \lambda \operatorname{tr}(\varepsilon) \mathbf{I} \quad (1.3.60)$$

The strain-stress relations are

$$\varepsilon_{ij} = \frac{1}{2\mu} \left[\sigma_{ij} - \frac{\lambda}{(2\mu+3\lambda)} \sigma_{kk} \delta_{ij} \right], \quad \varepsilon = \frac{1}{2\mu} \left[\sigma - \frac{\lambda}{(2\mu+3\lambda)} \operatorname{tr}(\sigma) \mathbf{I} \right] \quad (1.3.61)$$

We note the following relations between the Lamé constants λ and μ and engineering constants E , ν and G for an isotropic material [8]:

$$E = \frac{\mu(3\lambda+2\mu)}{\lambda+\mu}, \quad \nu = \frac{\lambda}{2(\mu+\lambda)}, \quad G = \mu \quad (1.3.62)$$

The following definitions and constitutive relations are of interest in the sequel:

$$\text{mean stress, } \tilde{\sigma} \equiv \frac{1}{3} \sigma_{ii}, \quad \text{dilatation, } e \equiv \varepsilon_{ii} \quad (1.3.63)$$

$$\text{deviatoric stress, } \sigma' = \sigma - \tilde{\sigma} \mathbf{I}, \quad \text{deviatoric strain, } \varepsilon' = \varepsilon - \frac{1}{3} \operatorname{tr}(\varepsilon) \mathbf{I} \quad (1.3.64)$$

$$\sigma_{ii} = (3\lambda+2\mu)\varepsilon_{ii}, \quad \tilde{\sigma} = K e, \quad K = \lambda + \frac{2}{3}\mu \quad (1.3.65)$$

where K is the bulk modulus and $\mu = G$ is the shear modulus.

In view of the relations between the Lamé constants and engineering constants, Eqs. (1.3.60) and (1.3.61) can be written in terms of engineering constants:

$$\sigma_{ij} = \frac{E}{1+\nu} \varepsilon_{ij} + \frac{\nu E}{(1+\nu)(1-2\nu)} \varepsilon_{kk} \delta_{ij}, \quad \sigma = \frac{E}{1+\nu} \varepsilon + \frac{\nu E}{(1+\nu)(1-2\nu)} \operatorname{tr}(\varepsilon) \mathbf{I} \quad (1.3.66)$$

$$\varepsilon_{ij} = \frac{1}{E} [(1+\nu)\sigma_{ij} - \nu \sigma_{kk} \delta_{ij}], \quad \varepsilon = \frac{1}{E} [(1+\nu)\sigma - \nu \operatorname{tr}(\sigma) \mathbf{I}] \quad (1.3.67)$$

The strain energy density for a linear isotropic material is given by

$$\begin{aligned} U_0 &= \frac{1}{2} C_{ijkl} \varepsilon_{ij} \varepsilon_{kl} = \frac{1}{2} \sigma_{ij} \varepsilon_{ij} \\ &= \frac{1}{2} (\sigma_{11} \varepsilon_{11} + \sigma_{22} \varepsilon_{22} + \sigma_{33} \varepsilon_{33} + 2\sigma_{12} \varepsilon_{12} + 2\sigma_{13} \varepsilon_{13} + 2\sigma_{23} \varepsilon_{23}) \quad (1.3.68) \end{aligned}$$

Plane Stress-Reduced Constitutive Relations

A state of *generalized plane stress* with respect to the x_1x_2 -plane is defined to be one in which

$$\sigma_{\alpha\beta} = \sigma_{\alpha\beta}(x_1, x_2), \quad \sigma_{\alpha 3} = \sigma_{\alpha 3}(x_1, x_2), \quad \sigma_{33} = 0 \quad (1.3.69)$$

where α and β take the values of 1 and 2. Although $\sigma_{33} = 0$, ε_{33} is not zero.

The strain-stress relations of an orthotropic body in plane stress state can be written as [see Eq. (1.3.47)]

$$\begin{Bmatrix} \varepsilon_1 \\ \varepsilon_2 \\ \varepsilon_6 \end{Bmatrix} = \begin{bmatrix} \frac{1}{E_1} & -\frac{\nu_{21}}{E_2} & 0 \\ -\frac{\nu_{12}}{E_1} & \frac{1}{E_2} & 0 \\ 0 & 0 & \frac{1}{G_{12}} \end{bmatrix} \begin{Bmatrix} \sigma_1 \\ \sigma_2 \\ \sigma_6 \end{Bmatrix} = \begin{bmatrix} S_{11} & S_{12} & 0 \\ S_{12} & S_{22} & 0 \\ 0 & 0 & S_{66} \end{bmatrix} \begin{Bmatrix} \sigma_1 \\ \sigma_2 \\ \sigma_6 \end{Bmatrix} \quad (1.3.70a)$$

and the transverse normal strain is given by

$$\varepsilon_{33} = (S_{13}\sigma_1 + S_{23}\sigma_2) = -\frac{\nu_{13}}{E_1}\sigma_1 - \frac{\nu_{23}}{E_2}\sigma_2 \quad (1.3.70b)$$

The strain-stress relations (1.3.70a) are inverted to obtain the stress-strain relations

$$\begin{Bmatrix} \sigma_1 \\ \sigma_2 \\ \sigma_6 \end{Bmatrix} = \begin{bmatrix} Q_{11} & Q_{12} & 0 \\ Q_{12} & Q_{22} & 0 \\ 0 & 0 & Q_{66} \end{bmatrix} \begin{Bmatrix} \varepsilon_1 \\ \varepsilon_2 \\ \varepsilon_6 \end{Bmatrix} \quad (1.3.71)$$

where the Q_{ij} , called the *plane stress-reduced stiffnesses*, are given by

$$\begin{aligned} Q_{11} &= \frac{S_{22}}{S_{11}S_{22} - S_{12}^2} = \frac{E_1}{1 - \nu_{12}\nu_{21}}, \quad Q_{12} = \frac{S_{12}}{S_{11}S_{22} - S_{12}^2} = \frac{\nu_{12}E_2}{1 - \nu_{12}\nu_{21}} \\ Q_{22} &= \frac{S_{11}}{S_{11}S_{22} - S_{12}^2} = \frac{E_2}{1 - \nu_{12}\nu_{21}}, \quad Q_{66} = \frac{1}{S_{66}} = G_{12} \end{aligned} \quad (1.3.72)$$

Note that the reduced stiffnesses involve four independent material constants, E_1 , E_2 , ν_{12} , and G_{12} .

The transverse shear stresses are related to the transverse shear strains in an orthotropic material by the relations

$$\begin{Bmatrix} \sigma_4 \\ \sigma_5 \end{Bmatrix} = \begin{bmatrix} Q_{44} & 0 \\ 0 & Q_{55} \end{bmatrix} \begin{Bmatrix} \varepsilon_4 \\ \varepsilon_5 \end{Bmatrix}, \quad Q_{44} = G_{23}, \quad Q_{55} = G_{13} \quad (1.3.73)$$

1.3.7 Thermodynamic Principles

Of the four principles of thermodynamics, the first law of thermodynamics and the second law of thermodynamics are important in the study of deformable solids. The first law of thermodynamics, also known as the *principle of conservation of energy*, states that the time rate of change of the total energy is equal to the sum of the rate of work done by applied forces and the change of heat content per unit time. The second law of thermodynamics places restrictions on the interconvertibility of heat and work done. For irreversible processes, the second law states that the entropy production is positive.

The thermodynamic principles can be expressed, in the Lagrangian description of deformation of solid bodies, as

$$\rho c_v \frac{\partial T}{\partial t} = -\nabla \cdot \mathbf{q} + Q + \boldsymbol{\sigma} : \dot{\boldsymbol{\epsilon}} \quad (1.3.74)$$

where T is the temperature, \mathbf{q} is the heat flux vector, Q is the internal heat generation (measured per unit volume), ρ is the density, c_v is the specific heat at constant volume or constant strain, $\boldsymbol{\sigma}$ is the stress tensor, and $\dot{\boldsymbol{\epsilon}}$ is the *strain rate tensor* (or time rate of the strain tensor).

Equation (1.3.74), termed the generalized *heat conduction equation*, is used to determine the temperature distribution in the body. The viscous dissipation couples the thermal problem to the stress problem. Even when the viscous dissipation is neglected, the thermal problem is coupled to the stress problem through constitutive relations, as explained in the next section.

The thermal problem for the solid requires the temperature or the heat flux to be specified on all parts of the boundary enclosing the heat transfer region as

$$T = \hat{T}(s, t) \quad \text{on } \Gamma_T \quad (1.3.75a)$$

$$\mathbf{n} \cdot \mathbf{q} + h_c(T - T_c) = \hat{q}_n(s, t) \quad \text{on } \Gamma_q \quad (1.3.75b)$$

where Γ is the total boundary enclosing the heat transfer region, $\Gamma = \Gamma_T \cup \Gamma_q$, $\Gamma_T \cap \Gamma_q = \emptyset$, h_c is the convective heat transfer coefficient, T_c is a reference (or sink) temperature for convective transfer, \hat{q}_n is the specified boundary flux, and s denotes the position of a point on the boundary.

Thermoelasticity

The thermoelastic problem is governed by the strain-displacement equations of Section 1.3.4, equations of motion of Section 1.3.5, thermodynamic equations of this section, and the constitutive equations to be given in this section. The constitutive equation of the thermal problem is the well known Fourier's heat conduction law, which states that heat flux is proportional to the gradient of temperature:

$$\mathbf{q} = -\mathbf{k} \cdot \nabla T \quad \text{or} \quad q_i = -k_{ij} \frac{\partial T}{\partial x_j} \quad (1.3.76)$$

where \mathbf{k} denotes the *thermal conductivity tensor* of order two. The negative sign in Eq. (1.3.51) indicates that heat flows from higher temperatures to lower temperatures.

The constitutive equations of thermoelasticity are derived by assuming the existence of the *Helmholtz free-energy function* $\Psi_0 = \Psi_0(\varepsilon_{ij}, T)$ (see [11–14])

$$\begin{aligned}\Psi_0(\varepsilon_{ij}, T) &= U_0 - \eta T \\ &= \frac{1}{2} C_{ijkl} \varepsilon_{ij} \varepsilon_{kl} - \beta_{ij} \varepsilon_{ij} \theta - \frac{\rho c_v}{2T_0} \theta^2\end{aligned}\quad (1.3.77a)$$

such that

$$\sigma_{ij} = \frac{\partial \Psi_0}{\partial \varepsilon_{ij}} = C_{ijkl} \varepsilon_{kl} - \beta_{ij} \theta \quad (1.3.77b)$$

where $\theta = T - T_0$, T_0 is the reference temperature, η is the entropy density, and β_{ij} are material coefficients. It is assumed that η and σ_{ij} are initially zero. Equation (1.3.77b) is known as the *Duhamel–Neumann law* for an anisotropic body. Inverting relations (1.3.77b), we obtain

$$\varepsilon_{ij} = S_{ijkl} \sigma_{kl} + \alpha_{ij} \theta \quad (1.3.78)$$

where S_{ijkl} are the elastic compliances, and α_{ij} are the thermal coefficients of expansion and related to β_{ij} by $\beta_{ij} = C_{ijkl} \alpha_{kl}$.

Hygrothermal Elasticity

Temperature and moisture concentration in fiber-reinforced composites cause reductions of both strength and stiffness [15–18]. Therefore, it is important to determine the temperature and moisture concentration in composite laminates under given initial and boundary conditions. As described in the previous section, the heat conduction problem described by equations (1.3.74)–(1.3.76) can be used to determine the temperature field.

The moisture concentration problem is mathematically similar to the heat transfer problem. The moisture concentration c in a solid is described by Fick's second law:

$$\frac{\partial c}{\partial t} = -\nabla \cdot \mathbf{q}_f + \phi_f \quad (1.3.79a)$$

$$\mathbf{q}_f = -\mathbf{D} \cdot \nabla c \quad (1.3.79b)$$

where \mathbf{D} denotes the *mass diffusivity tensor* of order two, \mathbf{q}_f is the flux vector, and ϕ_f is the moisture source in the domain. The negative sign in Eq. (1.3.79b) indicates that moisture seeps from higher concentration to lower concentration. The boundary conditions involve specifying the moisture concentration or the flux normal to the boundary:

$$c = \hat{c}(s, t) \quad \text{on } \Gamma_1 \quad (1.3.80a)$$

$$\mathbf{n} \cdot \mathbf{q}_f = \hat{q}_f(s, t) \quad \text{on } \Gamma_2 \quad (1.3.80b)$$

where $\Gamma = \Gamma_1 \cup \Gamma_2$, and $\Gamma_1 \cap \Gamma_2 = \emptyset$ and quantities with a hat are specified functions on the respective boundaries.

The moisture-induced strains $\{\varepsilon\}^M$ are given by

$$\{\varepsilon\}^M = \{\alpha_M\}c \quad (1.3.81)$$

where $\{\alpha_M\}$ is the vector of *coefficients of hygroscopic expansion*. Thus, the hygrothermal strains have the same form as the thermal strains [see Eq. (1.3.76)]. The total strains are given by

$$\{\varepsilon\} = [S]\{\sigma\} + \{\alpha_T\}(T - T_0) + \{\alpha_M\}(c - c_0) \quad (1.3.82)$$

where T_0 and c_0 are reference values from which the strains and stresses are measured. In view of the similarity between the thermal and moisture strains, we will use only thermal strains to show their contribution to governing equations in the sequel.

Electroelasticity

Electroelasticity deals with the phenomena caused by interactions between electric and mechanical fields. The *piezoelectric effect* is one such phenomenon, and it is concerned with the effect of the electric charge on the deformation [14–16]. A laminated structure with piezoelectric laminae receives actuation through an applied electric field, and the piezoelectric laminae send electric signals that are used to measure the motion or deformation of the laminate. In these problems, the electric charge that is applied to actuate a structure provides an additional body force to the stress analysis problem, much the same way a temperature field induces a body force through thermal strains.

The piezoelectric effect is described by the *polarization vector* \mathbf{P} , which represents the electric moment per unit volume or polarization charge per unit area. It is related to the stress tensor by the relation (see [14–17])

$$\mathbf{P} = \mathbf{d} \cdot \boldsymbol{\sigma} \text{ or } P_i = d_{ijk}\sigma_{jk} \quad (1.3.83a)$$

where \mathbf{d} is the third-order tensor of piezoelectric moduli. The inverse effect relates the electric field vector \mathcal{E} to the linear strain tensor ε by

$$\varepsilon = \mathcal{E} \cdot \mathbf{d} \text{ or } \varepsilon_{ij} = d_{kij}\mathcal{E}_k \quad (1.3.83b)$$

Note that d_{kij} is symmetric with respect to indices i and j because of the symmetry of ε_{ij} (note that $i, j, k = 1, 2, 3$).

The *pyroelectric effect* is another phenomenon that relates temperature changes to polarization of a material. For a small temperature change ΔT , the change in polarization vector $\Delta\mathbf{P}$ is given by

$$\Delta\mathbf{P} = \mathbf{p}\Delta T \quad (1.3.84)$$

where \mathbf{p} is the vector of pyroelectric coefficients.

The coupling between the mechanical, thermal, and electrical fields can be established using thermodynamical principles and Maxwell's relations. Analogous to the strain energy function U_0 for elasticity and the Helmholtz free-energy function Ψ_0 for thermoelasticity, we assume the existence of a function Φ_0

$$\begin{aligned} \Phi_0(\varepsilon_{ij}, \mathcal{E}_i, T) &= U_0 - \mathcal{E} \cdot \mathbf{D} - \eta T \\ &= \frac{1}{2}C_{ijkl}\varepsilon_{ij}\varepsilon_{kl} - e_{ijk}\varepsilon_{ij}\mathcal{E}_k - \beta_{ij}\varepsilon_{ij}\theta \\ &\quad - \frac{1}{2}\epsilon_{kl}\mathcal{E}_k\mathcal{E}_l - p_k\mathcal{E}_k\theta - \frac{\rho c_v}{2T_0}\theta^2 \end{aligned} \quad (1.3.85a)$$

which is called the electric *Gibbs free-energy function* or *enthalpy function*, such that

$$\sigma_{ij} = \frac{\partial \Phi_0}{\partial \varepsilon_{ij}}, \quad D_i = -\frac{\partial \Phi_0}{\partial \mathcal{E}_i}, \quad \eta = -\frac{\partial \Phi_0}{\partial T} = -\frac{\partial \Phi_0}{\partial \theta} \quad (1.3.85b)$$

where σ_{ij} are the components of the stress tensor, D_i are the components of the electric displacement vector, and η is the entropy. Use of Eq. (1.3.85a) in Eq. (1.3.85b) gives the constitutive equations of a deformable piezoelectric medium:

$$\sigma_{ij} = C_{ijkl} \varepsilon_{kl} - e_{ijk} \mathcal{E}_k - \beta_{ij} \theta \quad (1.3.86a)$$

$$D_k = e_{ijk} \varepsilon_{ij} + \epsilon_{kl} \mathcal{E}_l + p_k \theta \quad (1.3.86b)$$

$$\eta = \beta_{ij} \varepsilon_{ij} + p_k \mathcal{E}_k + \frac{\rho c_v}{T_0} \theta \quad (1.3.86c)$$

where C_{ijkl} are the elastic moduli, e_{ijk} are the piezoelectric moduli, ϵ_{ij} are the dielectric constants, p_k are the pyroelectric constants, β_{ij} are the stress-temperature expansion coefficients, c_v is the specific heat per unit mass, and T_0 is the reference temperature. In single-subscript notation, Eqs. (1.3.86a–c) can be expressed as

$$\sigma_i = C_{ij} \varepsilon_j - e_{ik} \mathcal{E}_k - \beta_i \theta \quad (1.3.87a)$$

$$D_k = e_{kj} \varepsilon_j + \epsilon_{kl} \mathcal{E}_l + p_k \theta \quad (1.3.87b)$$

$$\eta = \beta_i \varepsilon_i + p_k \mathcal{E}_k + \frac{\rho c_v}{T_0} \theta \quad (1.3.87c)$$

Note that the range of summation in (1.3.87a–c) is different for different terms: $i, j = 1, 2, \dots, 6; k, l = 1, 2, 3$. For the general anisotropic material, there are 21 independent elastic constants, 18 piezoelectric constants, 6 dielectric constants, 3 pyroelectric constants, and 6 thermal expansion coefficients.

Maxwell's equation governing the electric displacement vector is given by

$$\nabla \cdot \mathbf{D} = 0 \quad (1.3.88)$$

It is often assumed that the electric field \mathcal{E} is derivable from an electric scalar potential function ψ :

$$\mathcal{E} = -\nabla \psi \quad (1.3.89)$$

This assumption allows us to write Eq. (1.3.88), in view of Eq. (1.3.87b), as

$$\frac{\partial}{\partial x_1} \left(\epsilon_{11} \frac{\partial \psi}{\partial x_1} \right) + \frac{\partial}{\partial x_2} \left(\epsilon_{22} \frac{\partial \psi}{\partial x_2} \right) + \frac{\partial}{\partial x_3} \left(\epsilon_{33} \frac{\partial \psi}{\partial x_3} \right) + f_e = 0 \quad (1.3.90a)$$

where

$$f_e = -\frac{\partial}{\partial x_k} (e_{kl} \varepsilon_l + p_k \theta) \quad (1.3.90b)$$

This completes a review of the basic equations of solid mechanics. In the coming chapters reference is made to many of the equations presented here.

1.4 Virtual Work Principles

1.4.1 Introduction

In solid mechanics some of the laws of physics take several alternative forms. For example, the principle of conservation of linear momentum, which requires that the vector sum of all applied forces acting on a body be equal to the total time rate of momentum of the body, is known in mechanics as Newton's second law and it is also derivable from a variational principle. The use of Newton's laws to determine the governing equations of a structural problem requires isolation of a typical volume element of the structure with all its applied and reactive forces (i.e., the free-body diagram of the element). For complicated systems the procedure becomes more cumbersome and intractable. In addition, the type of boundary conditions to be used in conjunction with the derived equations is not always clear. In a variational approach, the governing equations are obtained by the principle of virtual displacements or by seeking the minimum of the total potential energy of the system. The variational approach, applicable to linear or nonlinear theories, is useful both in deriving governing equations and boundary conditions, and obtaining approximate solutions by variational methods.

In the context of the present study, the principle of virtual displacements will be used to derive the equations of motion of laminated plates. Hence, it is useful to study variational principles and methods (see Reddy [6] for additional details). We begin with the concepts of virtual displacements and forces.

1.4.2 Virtual Displacements and Virtual Work

From purely geometrical considerations, a given mechanical system can take many possible configurations consistent with the geometric constraints of the system. Of all the possible configurations, only one corresponds to the actual configuration, and it is this configuration that satisfies Newton's second law (i.e., equations of equilibrium or motion of the system). The set of configurations that satisfy the geometric constraints but not necessarily Newton's second law is called the *set of admissible configurations*. These configurations are restricted to a neighborhood of the true configuration so that they are obtained from infinitesimal variations of the true configuration. During such variations, the geometric constraints of the system are not violated and all the forces are fixed at their actual values. When a mechanical system experiences such variations in its configuration, it is said to undergo *virtual displacements* from its true or actual configuration. These displacements need not have any relationship to the actual displacements that might occur due to a change in the applied loads. The displacements are called virtual because they are *imagined* to take place (i.e., hypothetical) while the actual loads acting at their fixed values. The virtual displacements at the boundary points at which the geometric conditions (or displacements) are specified, are necessarily zero.

The work done by the actual forces moving through virtual displacements is called *virtual work*. The virtual work done by actual forces \mathbf{F} in a body Ω_0 in moving through the virtual displacements $\delta\mathbf{u}$ is given by

$$\delta W = \int_{\Omega_0} \mathbf{F} \cdot \delta\mathbf{u} \, dv \quad (1.4.1)$$

where dv denotes the volume element $dv = dx_1 dx_2 dx_3$ in the material body Ω_0 .

The external virtual work done due to virtual displacements $\delta\mathbf{u}$ in a solid body Ω_0 subjected to body forces \mathbf{f} per unit volume and surface tractions \mathbf{t} per unit area of the boundary Γ_σ is given by

$$\delta V = - \left(\int_{\Omega_0} \mathbf{f} \cdot \delta\mathbf{u} \, dv + \int_{\Gamma_\sigma} \mathbf{t} \cdot \delta\mathbf{u} \, ds \right) \quad (1.4.2)$$

where ds denotes a surface element and Γ_σ denotes the portion of the boundary on which stresses are specified. The negative sign in Eq. (1.4.2) indicates that the work is performed on the body. It is understood that the displacements are specified on the remaining portion $\Gamma_u = \Gamma - \Gamma_\sigma$ of the boundary Γ . Therefore, the virtual displacements are zero on Γ_u , irrespective of whether \mathbf{u} is specified to be zero or not. For example, a bar fixed at one end ($x = 0$) and subjected to an axial load at the other end ($x = L$) can be imagined to have a virtual displacement $\delta u(x)$, provided $\delta u(0) = 0$, because the actual displacement is specified at $x = 0$. Thus, one may select $\delta u(x) = cx$, where c is an arbitrary constant.

Recall that the deformation of solid body acted upon by forces can be measured in terms of strains and that the body experiences internal stresses. The forces associated with the stress field move the material particles through displacements corresponding to the strain field in the body, and hence work is done. The work done by these internal forces in moving through displacements of the material particles is called *internal work*. Note that the work done on the body is responsible for the internal work stored in the body.

The internal virtual work due to the virtual displacement $\delta\mathbf{u}$ can be computed as follows. Suppose that an infinitesimal material element of volume $dv = dx_1 dx_2 dx_3$ of the body experiences virtual strains $\delta\varepsilon_{ij}$ due to the virtual displacements δu_i , where [see Eq. (1.3.12)]

$$\delta\varepsilon_{ij} = \frac{1}{2}(\delta u_{i,j} + \delta u_{j,i}), \quad \delta u_{i,j} \equiv \frac{\partial \delta u_i}{\partial x_j} \quad (1.4.3)$$

The work done by the force due to actual stress σ_{11} , for example, in moving through the virtual displacement $\delta u_1 = \delta\varepsilon_{11}dx_1$ is

$$\sigma_{11} dx_2 dx_3 \cdot \delta\varepsilon_{11} dx_1 = \sigma_{11} \delta\varepsilon_{11} dv$$

Here ε_{ij} denote the strain components and σ_{ij} the stress components. Similarly, the work done by the force due to stress σ_{12} in the body is

$$\sigma_{12} dx_2 dx_3 \cdot 2\delta\varepsilon_{12} dx_1 = \sigma_{12} 2\delta\varepsilon_{12} dv$$

Thus, the total virtual work done by forces due to all the stresses in a volume element (that originally occupied the material element dv) in moving through their respective displacements is

$$(\sigma_{11} \cdot \delta\varepsilon_{11} + \sigma_{22} \cdot \delta\varepsilon_{22} + \cdots + \sigma_{12} \cdot 2\delta\varepsilon_{12}) dv = \sigma_{ij} \cdot \delta\varepsilon_{ij} dv \quad (1.4.4)$$

The total internal virtual work done is obtained by integrating the above expression over the entire volume of the body

$$\delta U = \int_{\Omega_0} \sigma_{ij} \delta \varepsilon_{ij} dv \quad (1.4.5)$$

Equation (1.4.5) is valid for any material body irrespective of its constitutive behavior. The expression in Eq. (1.4.5) is called the *virtual strain energy* of a deformable body.

The internal virtual work done by virtual stresses $\delta\sigma_{ij}$ in moving through the actual strains ε_{ij} is

$$\delta U^* = \int_{\Omega_0} \varepsilon_{ij} \delta \sigma_{ij} dv \quad (1.4.6)$$

The expression in Eq. (1.4.6) is also known as the *virtual complementary strain energy*. The virtual forces ($\delta f_i, \delta t_i$) and virtual stresses ($\delta\sigma_{ij}$) should be such that the stress equilibrium equations [see Eq. (1.3.27b)] and stress boundary conditions [see Eq. (1.2.25)] are satisfied:

$$[\delta\sigma_{ji}]_{,j} + \delta f_i = 0 \quad \text{in } \Omega_0 \quad (1.4.7a)$$

$$\delta t_i \equiv \delta\sigma_{ji} n_j = 0 \quad \text{on } \Gamma_\sigma \quad (1.4.7b)$$

In the present study we will not consider complementary energy principles.

1.4.3 Variational Operator and Euler Equations

The delta symbol δ used in conjunction with virtual displacements and forces can be interpreted as an operator, called the *variational operator*. It is used to denote a variation (or change) in a given quantity; i.e., δu denotes a variation in u . Thus δ is an operator that produces virtual change or variation δu in a dependent variable u , in much the same way as dx denotes a change in x , and δu is called the *first variation* of u . The operator proves to be very useful in constructing virtual work statements and deriving governing equations from virtual work principles, as will be shown shortly.

There is an analogy between the variational operator δ and the total differential operator d . To see this consider a function F of the dependent variable u and its derivative $u' = du/dx$ in one dimension. The total differential of F , for fixed x , is

$$dF = \frac{\partial F}{\partial x} dx + \frac{\partial F}{\partial u} du + \frac{\partial F}{\partial u'} du' \quad (1.4.8)$$

The first variation of F is

$$\delta F = \frac{\partial F}{\partial u} \cdot \delta u + \frac{\partial F}{\partial u'} \cdot \delta u' + \frac{1}{2} \frac{\partial^2 F}{\partial u^2} (\delta u)^2 + \frac{1}{2} \frac{\partial^2 F}{\partial u'^2} (\delta u')^2 + \dots \quad (1.4.9)$$

Since δu is small, terms involving squares and higher powers of δu can be neglected. We have

$$\delta F = \frac{\partial F}{\partial u} \delta u + \frac{\partial F}{\partial u'} \delta u' \quad (1.4.10)$$

Since x is fixed during the variation of u to $u + \delta u$, we have $dx = 0$ in Eq. (1.4.8) and the analogy between δF in Eq. (1.4.10) and dF in Eq. (1.4.8) becomes apparent: the variational operator, δ , is a differential operator with respect to the dependent variable, u . Indeed, the laws of variation of sums, products, ratios, powers, and so forth, are completely analogous to the corresponding laws of differentiation. The following properties of the variational operator should be noted:

$$\delta(\nabla u) = \nabla(\delta u) \quad (1.4.11)$$

$$\delta \left(\int_{\Omega} u \, d\Omega \right) = \int_{\Omega} \delta u \, d\Omega \quad (1.4.12)$$

$$\delta(F_1 \pm F_2) = \delta F_1 \pm \delta F_2 \quad (1.4.13)$$

$$\delta(F_1 F_2) = \delta F_1 F_2 + F_1 \delta F_2 \quad (1.4.14)$$

$$\delta \left(\frac{F_1}{F_2} \right) = \frac{\delta F_1}{F_2} - F_1 \left(\frac{\delta F_2}{F_2^2} \right) \quad (1.4.15)$$

$$\delta(F_1)^n = n(F_1)^{n-1} \delta F_1 \quad (1.4.16)$$

where $F_1 = F_1(u)$ and $F_2 = F_2(u)$. If $G = G(u, v, w)$ is a function of several dependent variables (and possibly their derivatives), the total variation is the sum of partial variations:

$$\delta G = \delta_u G + \delta_v G + \delta_w G \quad (1.4.17)$$

where, for example, δ_u denotes the partial variation of G with respect to u .

Functionals

Integral expressions whose integrands are functions of dependent variables and their derivatives are called functionals. Mathematically, a *functional* is a real number (or scalar) obtained by operating on functions (dependent variables) from a given set (or vector space). Thus, a functional $I(\cdot)$ is an operator which maps functions u of a vector space H into a real number $I(u)$ in the set of real numbers, R :

$$I : H \rightarrow R \quad (1.4.18)$$

For example, the integral expression

$$I(u) = \int_0^L [au(x) + bu'(x) + cu''(x)] \, dx$$

qualifies as a functional for all integrable and square-integrable functions $u(x)$. Note that $I(u)$ is a number whose value depends on the choice of u .

A functional is said to be *linear* if

$$I(\alpha u + \beta v) = \alpha I(u) + \beta I(v) \quad (1.4.19)$$

for all constants α and β and dependent variables u and v . A *quadratic functional* is one which satisfies the relation

$$I(\alpha u) = \alpha^2 I(u) \quad (1.4.20)$$

for all constants α and dependent variable u .

The first variation of a functional $I(u)$ of u (and its derivatives) can be calculated using the definition in Eq. (1.4.10). For instance consider the functional $I(u)$ defined in the interval (a, b)

$$I(u) = \int_a^b F(x, u, u') dx \quad (1.4.21)$$

where F is a function, in general, of x , u and $du/dx \equiv u'$. The first variation of the functional I is

$$\delta I = \delta \int_a^b F dx = \int_a^b \delta F dx = \int_a^b \left(\frac{\partial F}{\partial u} \delta u + \frac{\partial F}{\partial u'} \delta u' \right) dx \quad (1.4.22)$$

Thus, the variation of a functional can be readily calculated.

Fundamental Lemma of Variational Calculus

The *fundamental lemma* of calculus of variations can be stated as follows: for any integrable function G , if the statement

$$\int_a^b G \cdot \eta dx = 0 \quad (1.4.23)$$

holds for any arbitrary continuous function $\eta(x)$, for all x in (a, b) , then it follows that $G = 0$ in (a, b) . A mathematical proof of the lemma can be found in most books on variational calculus. A simple proof of the lemma follows. Since η is arbitrary, it can be replaced by G . We have

$$\int_a^b G^2 dx = 0$$

Since an integral of a positive function is positive, the above statement implies that $G = 0$. A more general statement of the fundamental lemma is as follows: If η is arbitrary in $a < x < b$ and $\eta(a)$ is arbitrary, then

$$\text{if } \int_a^b G\eta dx + B(a)\eta(a) = 0 \quad (1.4.24a)$$

$$\text{then } G = 0 \text{ in } a < x < b \text{ and } B(a) = 0 \quad (1.4.24b)$$

In most of our study in this book, we shall be interested in the use of Eqs. (1.4.24a,b) because they provide the means to the determination of the governing equations and boundary conditions and their solution by the variational methods.

Consider the question of finding the extremum (i.e., minimum or maximum) of the functional

$$I(u) = \int_a^b F(x, u, u') dx, \quad u(a) = u_a, \quad u(b) = u_b \quad (1.4.25)$$

The necessary condition for the functional to have a minimum or maximum is (analogous to minima or maxima of functions) that its first variation be zero:

$$\delta I = 0 \quad (1.4.26)$$

Using Eq. (1.4.10) we obtain

$$0 = \int_a^b \left(\frac{\partial F}{\partial u} \delta u + \frac{\partial F}{\partial u'} \delta u' \right) dx$$

Note that $\delta u' = \delta(du/dx) = d(\delta u)/dx$. We cannot use the fundamental lemma in the above equation because it is not in the form of Eq. (1.4.24). To recast the above equation in the form of Eq. (1.4.24), we integrate the second term by parts and obtain

$$\begin{aligned} 0 &= \int_a^b \left(\frac{\partial F}{\partial u} \delta u + \frac{\partial F}{\partial u'} \delta u' \right) dx \\ &= \int_a^b \left(\frac{\partial F}{\partial u} \delta u + \frac{\partial F}{\partial u'} \frac{d \delta u}{dx} \right) dx \\ &= \int_a^b \left[\frac{\partial F}{\partial u} - \frac{d}{dx} \left(\frac{\partial F}{\partial u'} \right) \right] \delta u \, dx + \left[\frac{\partial F}{\partial u'} \delta u \right]_a^b \end{aligned} \quad (1.4.27)$$

Let us first examine the boundary expression:

$$\left[\frac{\partial F}{\partial u'} \right] \cdot \delta u$$

There are two parts to this expression: a varied quantity and its coefficient. The variable u that is subjected to variation is called the *primary variable*. The coefficient of the varied quantity, i.e., the expression next to δu in the boundary term, is called a *secondary variable*. The product of the primary variable (or its variation) with the secondary variable often represents the work done (or virtual work done). The specification of the primary variable at a boundary point is termed the *essential boundary condition*, and the specification of the secondary variable ($\partial F/\partial u'$) is called the *natural boundary condition*. In solid mechanics, these are known as the *geometric* and *force* boundary conditions, respectively. All admissible variations must satisfy the homogeneous form of the essential (or geometric) boundary conditions: $\delta u(a) = 0$ and $\delta u(b) = 0$. Elsewhere, $a < x < b$, δu is arbitrary.

Returning to Eq. (1.4.27), we note that the boundary terms drop out because of the conditions on δu . We have

$$0 = \int_a^b \left[\frac{\partial F}{\partial u} - \frac{d}{dx} \left(\frac{\partial F}{\partial u'} \right) \right] \delta u \, dx$$

which must hold for any δu in (a, b) . In view of the fundamental lemma of calculus of variations ($\eta = \delta u$), it follows that

$$G \equiv \frac{\partial F}{\partial u} - \frac{d}{dx} \left(\frac{\partial F}{\partial u'} \right) = 0 \quad \text{in } a < x < b \quad (1.4.28)$$

Thus the necessary condition for $I(u)$ to be an extremum at $u = u(x)$ is that $u(x)$ be the solution of Eq. (1.4.28).

If $u(a) = u_a$ and $\delta u(b)$ is arbitrary (i.e., $u(a)$ is specified but u is not specified at $x = b$), then $\delta u(a) = 0$ and we have from Eq. (1.4.27) the result

$$0 = \int_a^b \left[\frac{\partial F}{\partial u} - \frac{d}{dx} \left(\frac{\partial F}{\partial u'} \right) \right] \delta u \, dx + \left(\frac{\partial F}{\partial u'} \right)_{x=b} \delta u(b) \quad (1.4.29)$$

Since δu is arbitrary in (a, b) and $\delta u(b)$ is arbitrary, the above equation implies, in view of Eq. (1.4.28), that both the integral expression and the boundary term be zero separately:

$$\frac{\partial F}{\partial u} - \frac{d}{dx} \left(\frac{\partial F}{\partial u'} \right) = 0, \quad a < x < b \quad (1.4.30a)$$

$$\left(\frac{\partial F}{\partial u'} \right) = 0 \quad \text{at } x = b \quad (1.4.30b)$$

Both Eq. (1.4.30a) and Eq. (1.4.30b) are called the Euler–Lagrange equations. Note that the boundary conditions that are a part of the Euler–Lagrange equations always belong to the class of natural boundary conditions.

Now we have all the necessary concepts and tools in place to study the principles of virtual work. In the next section, we discuss the principle of virtual displacements and its special case, the principle of minimum total potential energy. For a discussion of the principle of virtual forces and its special cases, consult Reddy [6].

1.4.4 Principle of Virtual Displacements

Recall that the virtual work due to virtual displacements is the work done by actual forces in displacing the body through virtual displacements that are consistent with the geometric constraints. All applied forces are kept constant during the virtual displacements. Consider a rigid body acted upon by a set of applied forces $\mathbf{F}_1, \mathbf{F}_2, \dots, \mathbf{F}_n$, and suppose that the points of application of these forces are subjected to the virtual displacements $\delta \mathbf{u}_1, \delta \mathbf{u}_2, \dots, \delta \mathbf{u}_n$, respectively. The virtual displacement $\delta \mathbf{u}_i$ has no relation to $\delta \mathbf{u}_j$ for $i \neq j$. The external virtual work done by the virtual displacements is

$$\delta V = -[\mathbf{F}_1 \cdot \delta \mathbf{u}_1 + \mathbf{F}_2 \cdot \delta \mathbf{u}_2 + \dots + \mathbf{F}_n \cdot \delta \mathbf{u}_n] = -\sum_{i=1}^n \mathbf{F}_i \cdot \delta \mathbf{u}_i \quad (1.4.31)$$

The internal virtual work done δU is zero because a rigid body does not undergo any strains (hence virtual strains are zero). In addition, the virtual displacements $\delta \mathbf{u}_1, \delta \mathbf{u}_2, \dots, \delta \mathbf{u}_n$ should all be the same, say $\delta \mathbf{u}$, for a rigid body. Thus, we have

$$\delta V = -\sum_{i=1}^n \mathbf{F}_i \cdot \delta \mathbf{u}_i = -\left(\sum_{i=1}^n \mathbf{F}_i \right) \cdot \delta \mathbf{u} \quad \text{and} \quad \delta U = 0 \quad (1.4.32)$$

But by Newton's second law, the vector sum of the forces acting on a body in static equilibrium is zero. This implies that the total virtual work, $\delta U + \delta V$, is equal to zero. Thus, for a body in equilibrium the total virtual work done due to

virtual displacements is zero. This statement is known as *the principle of virtual displacements*. The principle also holds for continuous, deformable bodies, for which δU is not zero. In this section, the principle of virtual displacements and its special case are described since they play an important role in the formulation of theories (e.g., plate theories) and their analysis by variational methods of approximation.

Consider a continuous body \mathcal{B} in equilibrium under the action of body forces \mathbf{f} and surface tractions \mathbf{t} . Let the reference configuration be the initial configuration \mathcal{C}^0 , whose volume is denoted as Ω_0 . Suppose that over portion Γ_u of the total boundary Γ of the region Ω_0 the displacements are specified to be $\hat{\mathbf{u}}$, and on portion Γ_σ the tractions are specified to be $\hat{\mathbf{t}}$. The boundary portions Γ_u and Γ_σ are disjoint (i.e., do not overlap), and their sum is the total boundary Γ . Let \mathbf{u} be the displacement vector corresponding to the equilibrium configuration of the body, and let σ and ε be the associated stress and strain tensors, respectively. The set of admissible configurations are defined by sufficiently differentiable functions that satisfy the geometric boundary conditions: $\mathbf{u} = \hat{\mathbf{u}}$ on Γ_u .

If the body is in equilibrium, then of all admissible configurations, the actual one corresponding to the equilibrium configuration makes the total virtual work done zero. In order to determine the equations governing the equilibrium configuration \mathcal{C} , we let the body experience a virtual displacement $\delta\mathbf{u}$ from the true configuration \mathcal{C} . The virtual displacements are arbitrary, continuous functions except that they satisfy the homogeneous form of geometric boundary conditions; i.e., they must belong to the set of admissible variations.

The principle of virtual displacements can be stated as: *if a continuous body is in equilibrium, the virtual work of all actual forces in moving through a virtual displacement is zero:*

$$\delta U + \delta V \equiv \delta W = 0 \quad (1.4.33)$$

Just as we derived the Euler–Lagrange equations associated with the statement $\delta I = 0$, we can derive them for the statement in Eq. (1.4.33). However, first we must identify δU and δV for a given problem. The principle of virtual work is independent of any constitutive law and applies to both elastic (linear and nonlinear) and inelastic continua.

For a solid body, the external and internal virtual work expressions are given in Eqs. (1.4.2) and (1.4.5), respectively. The principle can be expressed as

$$\int_{\Omega_0} \sigma : \delta \varepsilon \, dv - \int_{\Omega_0} \mathbf{f} \cdot \delta \mathbf{u} \, dv - \int_{\Gamma_\sigma} \mathbf{t} \cdot \delta \mathbf{u} \, ds = 0 \quad (1.4.34)$$

where $\sigma : \delta \varepsilon$ denotes the “double dot product,” Ω_0 is the volume of the undeformed body, and dv and ds denote the volume and surface elements of Ω_0 . Writing in terms of the Cartesian rectangular components, Eq. (1.4.34) takes the form

$$\int_{\Omega_0} (\sigma_{ij} \delta \varepsilon_{ij} - f_i \delta u_i) \, dv - \int_{\Gamma_\sigma} t_i \delta u_i \, ds = 0 \quad (1.4.35)$$

where the summation on repeated subscripts is implied.

The Euler–Lagrange equations associated with the statement (1.4.35) of the principle of virtual displacements are nothing but the equilibrium equations of the

3-D elasticity theory. Recall the strain-displacement equations from Eq. (1.3.11). The virtual strains $\delta\varepsilon_{ij}$ are related to the virtual displacements δu_i by

$$\delta\varepsilon_{ij} = \frac{1}{2}(\delta u_{i,j} + \delta u_{j,i}), \quad \delta u_{i,j} \equiv \frac{\partial \delta u_i}{\partial x_j} \quad (1.4.36)$$

Substituting $\delta\varepsilon_{ij}$ from the above equation into Eq. (1.4.35), and using the divergence theorem, Eq. (1.2.38), to transfer differentiation from δu_i to its coefficient, one obtains ($\sigma_{ij} = \sigma_{ji}$)

$$\begin{aligned} 0 &= \int_{\Omega_0} \left[\frac{1}{2} \sigma_{ij} (\delta u_{i,j} + \delta u_{j,i}) - f_i \delta u_i \right] dv - \int_{\Gamma_\sigma} t_i \delta u_i \, ds \\ &= \int_{\Omega_0} (\sigma_{ij} \delta u_{i,j} - f_i \delta u_i) \, dv - \int_{\Gamma_\sigma} t_i \delta u_i \, ds \\ &= - \int_{\Omega_0} (\sigma_{ij,j} + f_i) \delta u_i \, dv - \int_{\Gamma_\sigma} t_i \delta u_i \, ds + \oint_{\Gamma} \sigma_{ij} n_j \delta u_i \, ds \end{aligned} \quad (1.4.37)$$

Since $\Gamma = \Gamma_u \cup \Gamma_\sigma$ and $\delta u_i = 0$ on Γ_u , we have

$$0 = - \int_{\Omega_0} (\sigma_{ij,j} + f_i) \delta u_i \, dv + \int_{\Gamma_\sigma} (\sigma_{ij} n_j - t_i) \delta u_i \, ds \quad (1.4.38)$$

Because the virtual displacements are arbitrary in Ω_0 and on Γ_σ , Eq. (1.4.38) yields the following equations [cf., Eq. (1.3.27b)]

$$\frac{\partial \sigma_{ij}}{\partial x_j} + f_i = 0 \text{ in } \Omega_0 \quad (1.4.39)$$

$$\sigma_{ij} n_j - t_i = 0 \text{ on } \Gamma_\sigma \quad (1.4.40)$$

Equations (1.4.39) and (1.4.40) are the Euler–Lagrange equations associated with the principle of virtual displacements for a body undergoing small deformation. The stress boundary conditions in Eq. (1.4.40) are the natural boundary conditions. The principle of virtual displacements is applicable to any continuous body with arbitrary constitutive behavior (i.e., elastic or inelastic).

Example 1.4.1: (Euler–Bernoulli beam theory) —

Consider the bending of a beam of length L , Young's modulus E and moment of inertia I , and subjected to distributed axial force $f(x)$ and transverse load q (see Figure 1.4.1). Under the assumption of small strains and displacements, we derive the governing differential equation of the beam using the Euler–Bernoulli hypotheses, which assumes that straight lines perpendicular to the beam axis before deformation remain (1) straight, (2) perpendicular to the tangent line to the beam axis, and (3) inextensible after deformation. These assumptions lead to the displacement field (see Figure 1.4.1a)

$$u = u_0(x) - z \frac{dw_0}{dx}, \quad v = 0, \quad w = w_0(x) \quad (1.4.41)$$

where (u, v, w) are the displacements of a point (x, y, z) along the x, y and z coordinates, respectively, and (u_0, w_0) are the displacements of the point $(x, 0, 0)$. Under the assumption of smallness of strains

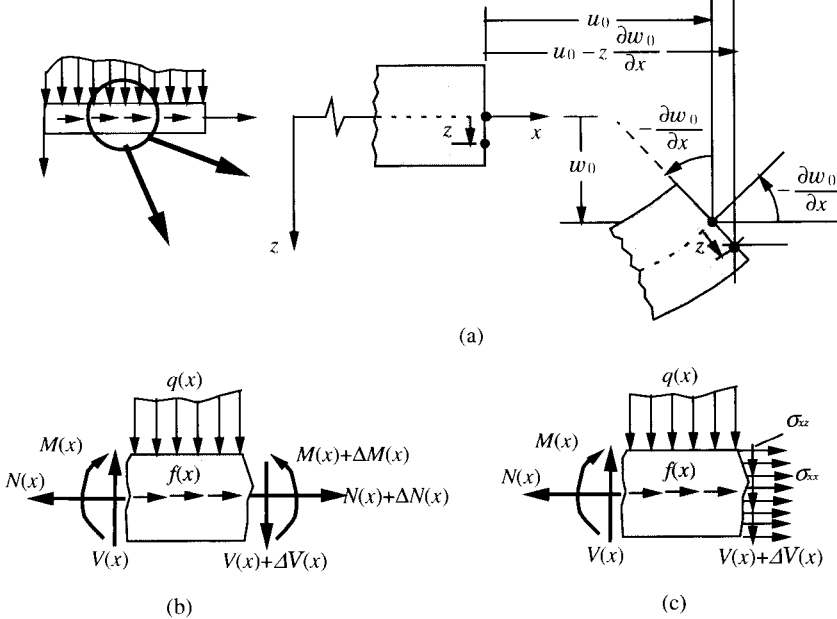


Figure 1.4.1: Bending of beams. (a) Kinematics of deformation of an Euler-Bernoulli beam. (b) Equilibrium of a beam element. (c) Definitions (or internal equilibrium) of stress resultants.

and rotations, the only nonzero strain is

$$\varepsilon_{xx} = \frac{du_0}{dx} - z \frac{d^2 w_0}{dx^2} \quad (1.4.42)$$

First we derive the equilibrium equations using Newton's second law of motion. Summing the forces and moments on an element of the beam (see Figure 1.4.1b) gives the following equilibrium equations:

$$\sum F_x = 0 : \quad - \frac{dN}{dx} = f(x). \quad (1.4.43a)$$

$$\sum F_z = 0 : \quad - \frac{dV}{dx} = q(x) \quad (1.4.43b)$$

$$\sum M_y = 0 : \quad V - \frac{dM}{dx} = 0 \quad (1.4.43c)$$

where $N(x)$ is the net axial force, $M(x)$ the bending moment, and $V(x)$ the shear force, which are known as the stress resultants, and they are defined in terms of the stresses σ_{xx} and σ_{xz} on a cross section as (see Figure 1.4.1c)

$$N(x) = \int_A \sigma_{xx} dA, \quad M(x) = \int_A \sigma_{xx} z dA, \quad V(x) = \int_A \sigma_{xz} dA \quad (1.4.44)$$

Here A denotes the area of cross section. Equations (1.4.43b) and (1.4.43c) can be combined into the single equation so that Eqs. (1.4.43a–c) reduce to

$$-\frac{dN}{dx} = f(x), \quad -\frac{d^2 M}{dx^2} = q(x) \quad (1.4.45a, b)$$

The stress resultants (N, M) can be related back to the stress σ_{xx} using the linear elastic constitutive relation for an isotropic material as [see Eq. (1.4.42)]

$$\sigma_{xx} = E\varepsilon_{xx} = E \left(\frac{du_0}{dx} - z \frac{d^2w_0}{dx^2} \right). \quad (1.4.46)$$

First, note that

$$N(x) = \int_A \sigma_{xx} dA = E \frac{du_0}{dx} \int_A dA = EA \frac{du_0}{dx} \quad (1.4.47a)$$

$$M(x) = \int_A \sigma_{xx} z dA = E \int_A \left(\frac{du_0}{dx} - z \frac{d^2w_0}{dx^2} \right) z dA = -EI \frac{d^2w_0}{dx^2} \quad (1.4.47b)$$

or

$$\frac{du_0}{dx} = \frac{N}{EA}, \quad \frac{d^2w_0}{dx^2} = -\frac{M}{EI} \quad (1.4.48)$$

where I is the moment of inertia about the axis of bending (y -axis) and z is the transverse coordinate. Note that the x -axis is taken through the geometric centroid of the cross section so that $\int_A z dA = 0$. Using the relations in Eq. (1.4.48) in Eq. (1.4.46), we obtain

$$\sigma_{xx} = \frac{N}{A} + \frac{Mz}{I}, \quad (1.4.49)$$

Next, we derive the governing equations (1.4.45a,b) using the principle of virtual displacements. Note that for the problem at hand the only nonzero stress is σ_{xx} . Hence, the internal virtual work done per unit length of the beam by the actual internal force $\sigma_{xx} dA$ in moving through the virtual displacements $\delta\varepsilon_{xx} dx$ is given by $\sigma_{xx} dA \cdot \delta\varepsilon_{xx} dx$. The total internal virtual work done is

$$\delta U = \int_0^L \int_A \sigma_{xx} \delta\varepsilon_{xx} dAdx \quad (1.4.50)$$

where all other stresses are assumed to be zero; i.e., the Euler–Bernoulli assumptions are invoked. The actual strain in the Euler–Bernoulli beam theory is given by Eq. (1.4.42). The virtual strain $\delta\varepsilon_{xx}$ is related to the virtual displacements $(\delta u_0, \delta w_0)$ by $\delta\varepsilon_{xx} = (d\delta u_0/dx) - z(d^2\delta w_0/dx^2)$. Substituting this expression into (1.4.50), we obtain

$$\delta U = \int_0^L \int_A \sigma_{xx} \left(\frac{d\delta u_0}{dx} - z \frac{d^2\delta w_0}{dx^2} \right) dx = \int_0^L \left(N \frac{d\delta u_0}{dx} - M \frac{d^2\delta w_0}{dx^2} \right) dx \quad (1.4.51a)$$

The virtual work done by the external distributed forces $f(x)$ and $q(x)$ in moving through the displacements δu_0 and δw_0 , respectively, is

$$\delta V = - \int_0^L (f\delta u_0 + q\delta w_0) dx \quad (1.4.51b)$$

The virtual work done by any applied point loads (and moments) must be added to δV in Eq. (1.4.51b). For example, the virtual work done by the counterclockwise moment M_L at $x = L$ in rotating through the virtual rotation $\frac{d\delta w_0}{dx}(L)$ is

$$M_L \left(-\frac{d\delta w_0}{dx} \right)_L$$

and the virtual work done by an axial point load P_L in moving through $\delta u_0(L)$ and a transverse point load F_L in moving through the virtual displacement $\delta w_0(L)$ is (see Figure 1.4.2)

$$-[P_L \delta u_0(L) + F_L \delta w_0(L)]$$

Thus, the total external virtual work done is

$$\delta V = - \left[\int_0^L (f \delta u_0 + q \delta w_0) dx + M_L \left(-\frac{d \delta w_0}{dx} \right)_{x=L} + P_L \delta u_0(L) + F_L \delta w_0(L) \right] \quad (1.4.52)$$

The principle of virtual displacements states that if the beam is in equilibrium we must have $\delta U + \delta V = 0$ or

$$\int_0^L \left(N \frac{d \delta u_0}{dx} - M \frac{d^2 \delta w_0}{dx^2} - f \delta u_0 - q \delta w_0 \right) dx - M_L \left(-\frac{d \delta w_0}{dx} \right)_{x=L} - P_L \delta u_0(L) - F_L \delta w_0(L) = 0 \quad (1.4.53)$$

To obtain the Euler–Lagrange equations associated with the virtual work statement (1.4.47), integrate the first term by parts once and the second term by parts twice and obtain

$$\begin{aligned} & \int_0^L \left[\left(-\frac{dN}{dx} - f \right) \delta u_0 + \left(-\frac{d^2 M}{dx^2} - q \right) \delta w_0 \right] dx + \left[N \delta u_0 - M \frac{d \delta w_0}{dx} + \frac{dM}{dx} \delta w_0 \right]_0^L \\ & - M_L \left(-\frac{d \delta w_0}{dx} \right)_{x=L} - P_L \delta u_0(L) - F_L \delta w_0(L) = 0 \end{aligned}$$

Note from the boundary terms that u_0 , w_0 and dw_0/dx are primary variables and N , $dM/dx = V$ and M are the secondary variables of the problem. We have

$$\begin{aligned} & \int_0^L \left[\left(-\frac{dN}{dx} - f \right) \delta u_0 + \left(-\frac{d^2 M}{dx^2} - q \right) \delta w_0 \right] dx + [N(L) - P_L] \delta u_0(L) - N(0) \delta u_0(0) \\ & - [M(L) - M_L] \left(\frac{d \delta w_0}{dx} \right)_{x=L} + M(0) \left(\frac{d \delta w_0}{dx} \right)_{x=0} \\ & + \left[\left(\frac{dM}{dx} \right)_{x=L} - F_L \right] \delta w_0(L) - \left(\frac{dM}{dx} \right)_{x=0} \delta w_0(0) = 0 \end{aligned} \quad (1.4.54)$$

First, consider the integral expressions in (1.4.54). Since δu_0 and δw_0 are independent and arbitrary in $0 < x < L$, we obtain the Euler equations

$$\delta u_0 : \quad -\frac{dN}{dx} - f = 0, \quad 0 < x < L \quad (1.4.55a)$$

$$\delta w_0 : \quad -\frac{d^2 M}{dx^2} - q = 0, \quad 0 < x < L \quad (1.4.55b)$$

which are the same as those in Eqs. (1.4.45a,b).

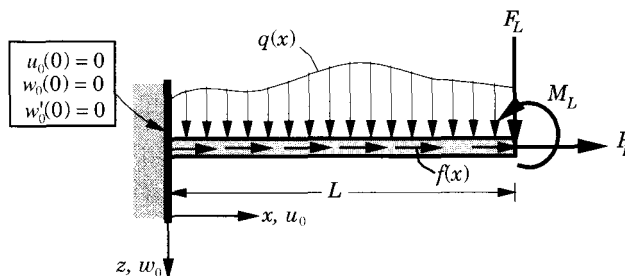


Figure 1.4.2: A cantilever beam with distributed loads f and q , and concentrated loads P_L , F_L and M_L at the right end.

Next, consider the boundary expressions in (1.4.54). If the beam is fixed at $x = 0$ and subjected to forces P_L , M_L , and F_L , the virtual displacements δu_0 and δw_0 must satisfy the conditions

$$\delta u_0(0) = 0, \quad \delta w_0(0) = 0, \quad \left(\frac{d\delta w_0}{dx}\right)_{x=0} = 0 \quad (1.4.56)$$

and they are arbitrary at $x = L$. Consequently, the second, fourth and sixth boundary expressions vanish, and we have the (natural) boundary conditions resulting from the virtual work principle:

$$\delta u_0(L) : \quad N(L) - P_L = 0, \quad \text{at } x = L \quad (1.4.57)$$

$$\delta w_0(L) : \quad \left(\frac{dM}{dx}\right)_{x=L} - F_L = 0, \quad \text{at } x = L \quad (1.4.58)$$

$$\left(\frac{d\delta w_0}{dx}\right)_{x=L} : \quad M(L) - M_L = 0, \quad \text{at } x = L \quad (1.4.59)$$

We note that Eqs. (1.4.55a) and (1.4.57) together define axial deformation, while Eqs. (1.4.55b), (1.4.58) and (1.4.59) describe bending deformation of the beam. These sets of equations can be solved independently as N is only a function of u_0 and M is a function of only w_0 [see Eq. (1.4.48)].

The Principle of Minimum Total Potential Energy

A special case of the principle of virtual displacements that deals with linear as well as nonlinear elastic bodies is known as the *principle of minimum total potential energy*. For elastic bodies (in the absence of temperature variations) there exists a *strain energy density* function U_0 such that

$$\sigma = \frac{\partial U_0}{\partial \varepsilon} \quad \text{or} \quad \sigma_{ij} = \frac{\partial U_0}{\partial \varepsilon_{ij}} \quad (1.4.60)$$

Equation (1.4.60) represents the constitutive equation of an hyperelastic material. The strain energy density U_0 is a single-valued function of strains at a point and is assumed to be positive definite. The statement of the principle of virtual displacements, Eq. (1.4.34), can be expressed in terms of the strain energy density U_0 :

$$\int_{\Omega_0} \frac{\partial U_0}{\partial \varepsilon} : \delta \mathbf{E} \, dv - \left[\int_{\Omega_0} \mathbf{f} \cdot \delta \mathbf{u} \, dv + \int_{\Gamma_\sigma} \mathbf{t} \cdot \delta \mathbf{u} \, ds \right] = 0 \quad (1.4.61a)$$

or, in component form,

$$\int_{\Omega_0} \frac{\partial U_0}{\partial \varepsilon_{ij}} \delta \varepsilon_{ij} \, dv - \left[\int_{\Omega_0} f_i \delta u_i \, dv + \int_{\Gamma_\sigma} t_i \delta u_i \, ds \right] = 0 \quad (1.4.61b)$$

The first integral is equal to

$$\int_{\Omega_0} \delta U_0 \, dv = \delta U$$

where U is the internal strain energy functional

$$U = \int_{\Omega_0} U_0 \, dv \quad (1.4.62a)$$

Suppose that there exists a potential V whose first variation is

$$\begin{aligned}\delta V &= - \left[\int_{\Omega_0} \mathbf{f} \cdot \delta \mathbf{u} \, dv + \int_{\Gamma_\sigma} \mathbf{t} \cdot \delta \mathbf{u} \, ds \right] \\ &= - \left[\int_{\Omega_0} f_i \delta u_i \, dv + \int_{\Gamma_\sigma} t_i \delta u_i \, ds \right]\end{aligned}\quad (1.4.62b)$$

Then the principle of virtual work takes the form

$$\delta U + \delta V = \delta(U + V) \equiv \delta \Pi = 0 \quad (1.4.63)$$

The sum $U + V = \Pi$ is called the *total potential energy* of the elastic body. The statement in Eq. (1.4.63) is known as the *principle of minimum total potential energy*. It means that *of all admissible displacements, those which satisfy the equilibrium equations make the total potential energy a minimum*:

$$\Pi(\mathbf{u}) \leq \Pi(\bar{\mathbf{u}}) \quad (1.4.64)$$

where \mathbf{u} is the true solution and $\bar{\mathbf{u}}$ is any admissible displacement field. The equality holds only if $\mathbf{u} = \bar{\mathbf{u}}$.

Example 1.4.2:

We consider the cantilever beam problem of Example 1.4.1 (see Figure 1.4.2). The minimum total potential energy principle requires us to construct the total potential energy (i.e., sum of the strain energy and potential energy due to applied loads) of the beam and set its first variation to zero to obtain the Euler–Lagrange equations of the functional.

The total strain energy stored in the beam is

$$U = \frac{1}{2} \int_0^L \left(N \frac{du_0}{dx} - M \frac{d^2 w_0}{dx^2} \right) dx = \frac{1}{2} \int_0^L \left[EA \left(\frac{du_0}{dx} \right)^2 + EI \left(\frac{d^2 w_0}{dx^2} \right)^2 \right] dx \quad (1.4.65)$$

where Eq. (1.4.48) is used to write the last expression for U . The work done by external applied loads f , q , M_L , P_L and F_L is

$$V = - \left[\int_0^L (fu_0 + qw_0) dx + P_L u_0(L) + M_L \left(-\frac{dw_0}{dx} \right)_{x=L} + F_L w_0(L) \right] \quad (1.4.66)$$

The total potential energy of the beam is given by

$$\begin{aligned}\Pi = U + V &= \int_0^L \left[\frac{EA}{2} \left(\frac{du_0}{dx} \right)^2 + \frac{EI}{2} \left(\frac{d^2 w_0}{dx^2} \right)^2 - fu_0 - qw_0 \right] dx \\ &\quad - P_L u_0(L) - M_L \left(-\frac{dw_0}{dx} \right)_{x=L} - F_L w_0(L)\end{aligned}\quad (1.4.67)$$

The total potential energy principle requires that $\delta(U + V) = 0$:

$$\begin{aligned}0 &= \int_0^L \left(EA \frac{du_0}{dx} \frac{d\delta u_0}{dx} + EI \frac{d^2 w_0}{dx^2} \frac{d^2 \delta w_0}{dx^2} - f\delta u_0 - q\delta w_0 \right) dx \\ &\quad - P_L \delta u_0(L) - M_L \left(-\frac{d\delta w_0}{dx} \right)_{x=L} - F_L \delta w_0(L)\end{aligned}$$

Integration by parts of the first two terms, and use of Eq. (1.4.56) and the property that δu_0 and δw_0 are arbitrary both in $(0, L)$ and at $x = L$, yields the Euler equations

$$-\frac{d}{dx} \left(EA \frac{du_0}{dx} \right) - f = 0, \quad 0 < x < L \quad (1.4.68a)$$

$$\frac{d^2}{dx^2} \left(EI \frac{d^2 w_0}{dx^2} \right) - q = 0, \quad 0 < x < L \quad (1.4.68b)$$

$$\left(EA \frac{du_0}{dx} \right)_{x=L} - P_L = 0 \quad (1.4.68c)$$

$$\left(-EI \frac{d^2 w_0}{dx^2} \right)_{x=L} - M_L = 0 \quad (1.4.68d)$$

$$\left[-\frac{d}{dx} \left(EI \frac{d^2 w_0}{dx^2} \right) \right]_{x=L} - F_L = 0 \quad (1.4.68e)$$

Equations (1.4.55a,b), and (1.4.57)–(1.4.59) are the same as above when N and M are replaced in terms of u_0 and w_0 using Eq. (1.4.47a,b), i.e., when the beam constitutive equations are used.

The minimum property of the total potential energy can be established by considering an arbitrary admissible displacement field, (\bar{u}, \bar{w})

$$\bar{u} = u_0 + \alpha v_1, \quad \alpha \text{ small}, \quad v_1(0) = 0 \quad (1.4.69a)$$

$$\bar{w} = w_0 + \beta v_2, \quad \beta \text{ small}, \quad v_2(0) = 0, \quad \left(\frac{dv_2}{dx} \right)_{x=0} = 0 \quad (1.4.69b)$$

For the example problem we have

$$\begin{aligned} \Pi(\bar{u}, \bar{w}) &= \int_0^L \left[\frac{EA}{2} \left(\frac{d\bar{u}}{dx} \right)^2 + \frac{EI}{2} \left(\frac{d^2 \bar{w}}{dx^2} \right)^2 - f\bar{u} - q\bar{w} \right] dx - P_L \bar{u}(L) - M_L \left(-\frac{d\bar{w}}{dx} \right)_{x=L} - F_L \bar{w}(L) \\ &= \int_0^L \left\{ \frac{EA}{2} \left[\left(\frac{du_0}{dx} \right)^2 + \alpha^2 \left(\frac{dv_1}{dx} \right)^2 + 2\alpha \frac{du_0}{dx} \frac{dv_1}{dx} \right] - f(u_0 + \alpha v_1) \right\} dx \\ &\quad - P_L [u_0(L) + \alpha v_1(L)] \\ &\quad + \frac{EI}{2} \left[\left(\frac{d^2 w_0}{dx^2} \right)^2 + \beta^2 \left(\frac{d^2 v_2}{dx^2} \right)^2 + 2\beta \frac{d^2 w_0}{dx^2} \frac{d^2 v_2}{dx^2} \right] - q(w_0 + \beta v_2) \} dx \\ &\quad - M_L \left[\left(-\frac{dw_0}{dx} \right)_{x=L} + \beta \left(-\frac{dv_2}{dx} \right)_{x=L} \right] - F_L [w_0(L) + \beta v_2(L)] \\ &= \Pi(u_0, w_0) + \int_0^L \left[\alpha^2 \frac{EA}{2} \left(\frac{dv_1}{dx} \right)^2 + \beta^2 \frac{EI}{2} \left(\frac{d^2 v_2}{dx^2} \right)^2 \right] dx \\ &\quad + \alpha \int_0^L \left[EA \frac{du_0}{dx} \frac{dv_1}{dx} + EI \frac{d^2 w_0}{dx^2} \frac{d^2 v_2}{dx^2} - fv_1 - qv_2 \right] dx \\ &\quad - \left[\alpha P_L v_1(L) + \beta M_L \left(-\frac{dv_2}{dx} \right)_{x=L} + \beta F_L v_2(L) \right] \end{aligned} \quad (1.4.70a)$$

Now, consider the second integral and the boundary terms

$$\begin{aligned} &\alpha \left\{ \int_0^L \left(EA \frac{du_0}{dx} \frac{dv_1}{dx} - fv_1 \right) dx - P_L v_1(L) \right\} \\ &+ \beta \left\{ \int_0^L \left(EI \frac{d^2 w_0}{dx^2} \frac{d^2 v_2}{dx^2} - qv_2 \right) dx - M_L \left(-\frac{dv_2}{dx} \right)_{x=L} - F_L v_2(L) \right\} \end{aligned}$$

$$\begin{aligned}
&= \alpha \left\{ \int_0^L \left[-\frac{d}{dx} \left(EA \frac{du_0}{dx} \right) - f \right] v_1 \, dx + \left[\left(EA \frac{du_0}{dx} - P_L \right) v_1 \right]_{x=L} \right\} \\
&\quad + \beta \left\{ \int_0^L \left[\frac{d^2}{dx^2} \left(EI \frac{d^2 w_0}{dx^2} \right) - q \right] v_2 \, dx + \left[-EI \frac{d^2 w_0}{dx^2} - M_L \right]_{x=L} \left(-\frac{dv_2}{dx} \right)_{x=L} \right. \\
&\quad \left. + \left[-\frac{d}{dx} \left(EI \frac{d^2 w_0}{dx^2} \right) - F_L \right]_{x=L} v_2(L) \right\} \tag{1.4.70b}
\end{aligned}$$

The boundary terms at $x = 0$ are zero because of the conditions in Eq. (1.4.69a,b). Since (u_0, w_0) is the true solution of the problem, all terms in Eq. (1.4.70b) are zero. Thus, Eq. (1.4.70a) becomes

$$\begin{aligned}
\Pi(\bar{u}, \bar{w}) &= \Pi(u_0, w_0) + \int_0^L \left[\alpha^2 \frac{EA}{2} \left(\frac{dv_1}{dx} \right)^2 + \beta^2 \frac{EI}{2} \left(\frac{d^2 v_2}{dx^2} \right)^2 \right] dx \\
&\geq \Pi(u_0, w_0)
\end{aligned} \tag{1.4.71}$$

and the equality holds only when $\bar{u} = u_0$ and $\bar{w} = w_0$. Thus $\Pi(\bar{u}, \bar{w})$ is greater than $\Pi(u_0, w_0)$ when $\bar{w} \neq w_0$ and $\bar{u} \neq u_0$, establishing the minimum character of the total potential energy of the beam.

One may note that in this example, we considered axial deformation of a bar (set $w_0 = 0$) as well as pure bending of a beam (set $u_0 = 0$). These equations are uncoupled for the case of small strains. The total potential energy is the minimum with respect to both u_0 and w_0 .

Hamilton's Principle

Hamilton's principle is a generalization of the principle of virtual displacements to dynamics of systems. The principle assumes that the system under consideration is characterized by two energy functions; a *kinetic energy* K and a *potential energy* Π . For deformable bodies, the energies can be expressed in terms of the dependent variables (which are functions of position) of the problem. Hamilton's principle may be considered as dynamics version of the principle of virtual displacements [6].

Newton's second law of motion applied to deformable bodies expresses the global statement of the principle of conservation of linear momentum. However, it should be noted that Newton's second law of motion for continuous media is not sufficient to determine its motion $\mathbf{u} = \mathbf{u}(\mathbf{x}, t)$; the kinematic conditions and constitutive equations discussed in the previous sections are needed to completely determine the motion.

Newton's second law of motion for a continuous body can be written in general terms as

$$\mathbf{F} - m\mathbf{a} = \mathbf{0} \tag{1.4.72}$$

where m is the mass, \mathbf{a} the acceleration vector, and \mathbf{F} is the resultant of *all* forces acting on the body. The actual path $\mathbf{u} = \mathbf{u}(\mathbf{x}, t)$ followed by a material particle in position \mathbf{x} in the body is varied, consistent with kinematic (essential) boundary conditions, to $\mathbf{u} + \delta\mathbf{u}$, where $\delta\mathbf{u}$ is the admissible variation (or virtual displacement) of the path. We suppose that the varied path differs from the actual path except at initial and final times, t_1 and t_2 , respectively. Thus, an admissible variation $\delta\mathbf{u}$ satisfies the conditions,

$$\delta\mathbf{u} = \mathbf{0} \text{ on } S_1 \text{ for all } t \tag{1.4.73a}$$

$$\delta\mathbf{u}(\mathbf{x}, t_1) = \delta\mathbf{u}(\mathbf{x}, t_2) = \mathbf{0} \text{ for all } \mathbf{x} \tag{1.4.73b}$$

where S_1 denotes the portion of the boundary of the body where the displacement vector \mathbf{u} is specified. Note that the scalar product of Eq. (1.4.72) with $\delta\mathbf{u}$ gives work done at point \mathbf{x} , because \mathbf{F} , \mathbf{a} , and \mathbf{u} are vector functions of position (whereas the work is a scalar). Integration of the product over the volume (and surface) of the body gives the total work done by all points.

The *work done on the body* at time t by the resultant force in moving through the virtual displacement $\delta\mathbf{u}$ is given by

$$\int_V \mathbf{f} \cdot \delta\mathbf{u} \, dV + \int_{S_2} \hat{\mathbf{t}} \cdot \delta\mathbf{u} \, dS - \int_V \vec{\sigma} : \vec{\varepsilon} \, dV \quad (1.4.74)$$

where \mathbf{f} is the body force vector, $\hat{\mathbf{t}}$ the specified surface traction vector, and $\vec{\sigma}$ and $\vec{\varepsilon}$ are the stress and strain tensors. The last term in Eq. (1.4.74) represents the *virtual work* of internal forces *stored in the body*. The strains $\vec{\varepsilon}$ are assumed to be compatible in the sense that the strain-displacement relations (1.3.11) are satisfied. The work done by the inertia force $m\mathbf{a}$ in moving through the virtual displacement $\delta\mathbf{u}$ is given by

$$\int_V \rho \frac{\partial^2 \mathbf{u}}{\partial t^2} \cdot \delta\mathbf{u} \, dV \quad (1.4.75)$$

where ρ is the mass density (can be a function of position) of the medium. We have the result

$$\int_{t_1}^{t_2} \left\{ \int_V \rho \frac{\partial^2 \mathbf{u}}{\partial t^2} \cdot \delta\mathbf{u} \, dV - \left[\int_V (\mathbf{f} \cdot \delta\mathbf{u} - \vec{\sigma} : \vec{\varepsilon}) \, dV + \int_{S_2} \hat{\mathbf{t}} \cdot \delta\mathbf{u} \, dS \right] \right\} dt = 0$$

or

$$-\int_{t_1}^{t_2} \left[\int_V \rho \frac{\partial \mathbf{u}}{\partial t} \cdot \frac{\partial \delta\mathbf{u}}{\partial t} \, dV + \int_V (\mathbf{f} \cdot \delta\mathbf{u} - \vec{\sigma} : \vec{\varepsilon}) \, dV + \int_{S_2} \hat{\mathbf{t}} \cdot \delta\mathbf{u} \, dS \right] dt = 0 \quad (1.4.76)$$

In arriving at the expression in Eq. (1.4.76), integration-by-parts is used on the first term; the integrated terms vanish because of the initial and final conditions in Eq. (1.4.73b). Equation (1.4.76) is known as the general form of Hamilton's principle for a continuous medium (conservative or not, and elastic or not).

For an ideal elastic body, we recall from the previous discussions that the forces \mathbf{f} and \mathbf{t} are conservative,

$$\delta V = - \left(\int_V \mathbf{f} \cdot \delta\mathbf{u} \, dV + \int_{S_2} \hat{\mathbf{t}} \cdot \delta\mathbf{u} \, dS \right) \quad (1.4.77a)$$

and that there exists a strain energy density function $U_0 = U_0(\varepsilon_{ij})$ such that

$$\sigma_{ij} = \frac{\partial U_0}{\partial \varepsilon_{ij}} \quad (1.4.77b)$$

Substituting Eqs. (1.4.77a,b) into Eq. (1.4.76), we obtain

$$\delta \int_{t_1}^{t_2} [K - (V + U)] dt = 0 \quad (1.4.78)$$

where K and U are the kinetic and strain energies:

$$K = \int_V \frac{\rho}{2} \frac{\partial \mathbf{u}}{\partial t} \cdot \frac{\partial \mathbf{u}}{\partial t} dV, \quad U = \int_V U_0 dV \quad (1.4.79)$$

Equation(1.4.78) represents Hamilton's principle for an elastic body (linear or nonlinear). Recall that the sum of the strain energy and potential energy of external forces, $U + V$, is called the total potential energy, Π , of the body. For bodies involving no motion (i.e., forces are applied sufficiently slowly such that the motion is independent of time, and the inertia forces are negligible), Hamilton's principle (1.4.78) reduces to the principle of virtual displacements.

The Euler-Lagrange equations associated with the Lagrangian, $L = K - \Pi$, ($\Pi = U + V$) can be obtained from Eq. (1.4.78):

$$\begin{aligned} 0 &= \delta \int_{t_1}^{t_2} L(\mathbf{u}, \nabla \mathbf{u}, \dot{\mathbf{u}}) dt \\ &= \int_{t_1}^{t_2} \left[\int_V \left(\rho \frac{\partial^2 \mathbf{u}}{\partial t^2} - \operatorname{div} \vec{\sigma} - \mathbf{f} \right) \cdot \delta \mathbf{u} dV + \int_{S_2} (\mathbf{t} - \hat{\mathbf{t}}) \cdot \delta \mathbf{u} dS \right] dt \end{aligned} \quad (1.4.80)$$

where integration-by-parts, gradient theorems, and Eqs. (1.4.73a,b) were used in arriving at Eq. (1.4.80) from Eq. (1.4.78). Because $\delta \mathbf{u}$ is arbitrary for $t, t_1 < t < t_2$, and for \mathbf{x} in V and also on S_2 , it follows that

$$\begin{aligned} \rho \frac{\partial^2 \mathbf{u}}{\partial t^2} - \operatorname{div} \vec{\sigma} - \mathbf{f} &= \mathbf{0} \quad \text{in } V \\ \mathbf{t} - \hat{\mathbf{t}} &= \mathbf{0} \quad \text{on } S_2 \end{aligned} \quad (1.4.81)$$

Equations (1.4.81) are the Euler-Lagrange equations for an elastic body.

Example 1.4.3 (*Third-order beam theory*)

Consider the displacement field

$$\begin{aligned} u(x, z, t) &= u_0(x, t) + z\phi(x, t) - c_1 z^3 \left(\phi + \frac{\partial w_0}{\partial x} \right) \\ w(x, z, t) &= w_0(x, t) \end{aligned} \quad (1.4.82)$$

where $c_1 = 4/(3h^2)$, u_0 is the axial displacement, w_0 the transverse displacement, and ϕ the rotation of a point on the centroidal axis x of the beam. The displacement field is arrived by (a) relaxing the Euler-Bernoulli hypotheses to let the straight lines normal to the beam axis before deformation to become (cubic) curves with arbitrary slope at $z = 0$, and (b) requiring the transverse shear stress to vanish at the top and bottom of the beam. Thus, only restriction from the Euler-Bernoulli beam theory that is kept is $w(x, z, t) = w_0(x, t)$ (i.e., transverse deflection is independent of the thickness coordinate z). The displacement field (1.4.82) accommodates quadratic variation of transverse shear strain ε_{xz} and shear stress σ_{xz} through the beam height, as can be seen from the strains computed next.

Now suppose that the beam is subjected to distributed axial force $f(x)$ and transverse load of $q(x, t)$ along the length of the beam. Since we are primarily interested in deriving the equations of motion and the nature of the boundary conditions of the beam that experiences a displacement field of the form in Eq. (1.4.82), we will not consider specific geometric or force boundary conditions here. The procedure to obtain the equations of motion and boundary conditions involves the

following steps: (i) compute the strains, (ii) compute the virtual energies required in Hamilton's principle, and (iii) use Hamilton's principle, derive the Euler-Lagrange equations of motion and identify the primary and secondary variables of the theory (which in turn help identify the nature of the boundary conditions).

Although one can use the general nonlinear strain-displacement relations, here we restrict the development to small strains and displacements. The linear strains associated with the displacement field are

$$\begin{aligned}\varepsilon_{xx} &= \varepsilon_{xx}^{(0)} + z\varepsilon_{xx}^{(1)} + z^3\varepsilon_{xx}^{(3)} \\ \gamma_{xz} &= \gamma_{xz}^{(0)} + z^2\gamma_{xz}^{(2)}\end{aligned}\quad (1.4.83a)$$

where

$$\begin{aligned}\varepsilon_{xx}^{(0)} &= \frac{\partial u_0}{\partial x}, \quad \varepsilon_{xx}^{(1)} = \frac{\partial \phi}{\partial x}, \quad \varepsilon_{xx}^{(3)} = -c_1 \left(\frac{\partial \phi}{\partial x} + \frac{\partial^2 w_0}{\partial x^2} \right) \\ \gamma_{xz}^{(0)} &= \phi + \frac{\partial w_0}{\partial x}, \quad \gamma_{xz}^{(2)} = -c_2 \left(\phi + \frac{\partial w_0}{\partial x} \right)\end{aligned}\quad (1.4.83b)$$

and $c_2 = 4/h^2$. Note that $\gamma_{xz} = 2\varepsilon_{xz}$ is a quadratic function of z . Hence, $\sigma_{xz} = G\gamma_{xz}$ is also quadratic in z .

From the dynamic version of the principle of virtual displacements (i.e. Hamilton's principle) we have

$$\begin{aligned}0 &= \int_0^T \int_0^L \int_A \left[\sigma_{xx} \left(\delta\varepsilon_{xx}^{(0)} + z\delta\varepsilon_{xx}^{(1)} + z^3\delta\varepsilon_{xx}^{(3)} \right) + \sigma_{xz} \left(\delta\gamma_{xz}^{(0)} + z^2\delta\gamma_{xz}^{(2)} \right) \right] dA dx dt \\ &\quad - \int_0^T \int_0^L \int_A \rho \left\{ \left[\dot{u}_0 + z\dot{\phi} - c_1 z^3 \left(\dot{\phi} + \frac{\partial \dot{w}_0}{\partial x} \right) \right] \left[\delta\dot{u}_0 + z\delta\dot{\phi} - c_1 z^3 \left(\delta\dot{\phi} + \frac{\partial \delta\dot{w}_0}{\partial x} \right) \right] \right. \\ &\quad \left. + \dot{w}_0 \delta\dot{w}_0 \right\} dA dx dt - \int_0^T \int_0^L (f\delta u_0 + q\delta w_0) dx dt \\ &= \int_0^T \int_0^L \left(N_{xx} \delta\varepsilon_{xx}^{(0)} + M_{xx} \delta\varepsilon_{xx}^{(1)} + P_{xx} \delta\varepsilon_{xx}^{(3)} + Q_x \delta\gamma_{xz}^{(0)} + R_x \delta\gamma_{xz}^{(2)} \right) dx dt \\ &\quad - \int_0^T \int_0^L \left\{ I_0 \dot{u}_0 \delta\dot{u}_0 + \left[I_2 \dot{\phi} - c_1 I_4 \left(\dot{\phi} + \frac{\partial \dot{w}_0}{\partial x} \right) \right] \delta\dot{\phi} + f\delta u_0 + q\delta w_0 \right\} dx dt \\ &\quad - \int_0^T \int_0^L \left\{ -c_1 \left[I_4 \dot{\phi} - c_1 I_6 \left(\dot{\phi} + \frac{\partial \dot{w}_0}{\partial x} \right) \right] \left(\delta\dot{\phi} + \frac{\partial \delta\dot{w}_0}{\partial x} \right) + I_0 \dot{w}_0 \delta\dot{w}_0 \right\} dx dt \\ &= \int_0^T \int_0^L \left\{ \left(-\frac{\partial N_{xx}}{\partial x} - f + I_0 \frac{\partial^2 u_0}{\partial t^2} \right) \delta u_0 + \left(-\frac{\partial \bar{M}_{xx}}{\partial x} + \bar{Q}_x + K_2 \frac{\partial^2 \phi}{\partial t^2} - c_1 J_4 \frac{\partial^3 w_0}{\partial x \partial t^2} \right) \delta\phi \right. \\ &\quad \left. + \left[-c_1 \frac{\partial^2 P_{xx}}{\partial x^2} - \frac{\partial \bar{Q}_x}{\partial x} - q + c_1 \left(J_4 \frac{\partial^3 \phi}{\partial x \partial t^2} - c_1 I_6 \frac{\partial^4 w_0}{\partial x^2 \partial t^2} \right) + I_0 \frac{\partial^2 w_0}{\partial t^2} \right] \delta w_0 \right\} dx dt \\ &\quad + \int_0^T \left\{ N_{xx} \delta u_0 + \bar{M}_{xx} \delta\phi - c_1 P_{xx} \frac{\partial \delta w_0}{\partial x} + \left[\bar{Q}_x + c_1 \left(\frac{\partial P_{xx}}{\partial x} - J_4 \frac{\partial^2 \phi}{\partial t^2} + c_1 I_6 \frac{\partial^3 w_0}{\partial x \partial t^2} \right) \right] \delta w_0 \right\}_0^L dt\end{aligned}\quad (1.4.84)$$

where all the terms involving $[\cdot]_0^L$ vanish on account of the assumption that all variations and their derivatives are zero at $t = 0$ and $t = T$, and the new variables introduced in arriving at the last expression are defined as follows:

$$\begin{Bmatrix} N_{xx} \\ M_{xx} \\ P_{xx} \end{Bmatrix} = \int_{-h/2}^{h/2} \begin{Bmatrix} 1 \\ z \\ z^3 \end{Bmatrix} \sigma_{xx} dz, \quad \begin{Bmatrix} Q_x \\ R_x \end{Bmatrix} = \int_{-h/2}^{h/2} \begin{Bmatrix} 1 \\ z^2 \end{Bmatrix} \sigma_{xz} dz \quad (1.4.85)$$

$$\bar{M}_{xx} = M_{xx} - c_1 P_{xx}, \quad \bar{Q}_x = Q_x - c_2 R_x, \quad c_1 = \frac{4}{3h^2}, \quad c_2 = \frac{4}{h^2} \quad (1.4.86a)$$

$$J_4 = I_4 - c_1 I_6, \quad K_2 = I_2 - 2c_1 I_4 + c_1^2 I_6, \quad I_i = \int_{-h/2}^{h/2} \rho(z)^i dz \quad (1.4.86b)$$

Note that I_i are zero for odd values of i (i.e., $I_1 = I_3 = I_5 = 0$).

Thus, the Euler–Lagrange equations are

$$\delta u_0 : \quad \frac{\partial N_{xx}}{\partial x} + f = I_0 \frac{\partial^2 u_0}{\partial t^2} \quad (1.4.87)$$

$$\begin{aligned} \delta w_0 : \quad & \frac{\partial \bar{Q}_x}{\partial x} + c_1 \frac{\partial^2 P_{xx}}{\partial x^2} + q \\ &= I_0 \frac{\partial^2 w_0}{\partial t^2} + c_1 \left(J_4 \frac{\partial^3 \phi}{\partial x \partial t^2} - c_1 I_6 \frac{\partial^4 w_0}{\partial x^2 \partial t^2} \right) \end{aligned} \quad (1.4.88a)$$

$$\delta \phi : \quad \frac{\partial \bar{M}_{xx}}{\partial x} - \bar{Q}_x = K_2 \frac{\partial^2 \phi}{\partial t^2} - c_1 J_4 \frac{\partial^3 w_0}{\partial x \partial t^2} \quad (1.4.88b)$$

The last line of Eq. (1.4.84) includes boundary terms, which indicate that the primary variables of the theory are (those with the variational symbol) u_0 , w_0 , ϕ , and $\partial w_0/\partial x$. The corresponding secondary variables are the coefficients of δu_0 , δw_0 , $\delta \phi$, and $\partial \delta w_0/\partial x$:

$$N_{xx}, \quad \bar{Q}_x + c_1 \left(\frac{\partial P_{xx}}{\partial x} - J_4 \frac{\partial^2 \phi}{\partial t^2} + c_1 I_6 \frac{\partial^3 w_0}{\partial x \partial t^2} \right), \quad \bar{M}_{xx}, \quad -c_1 P_{xx} \quad (1.4.89)$$

When $c_1 = 0$ in Eq. (1.4.82), it corresponds to the displacement field of the *Timoshenko beam theory*. Thus, the equations of motion of the Timoshenko beam theory can be obtained directly from Eqs. (1.4.87) and (1.4.88a,b) by setting $c_1 = c_2 = 0$:

$$\frac{\partial N_{xx}}{\partial x} + f = I_0 \frac{\partial^2 u_0}{\partial t^2} \quad (1.4.90)$$

$$\frac{\partial Q_x}{\partial x} + q = I_0 \frac{\partial^2 w_0}{\partial t^2} \quad (1.4.91a)$$

$$\frac{\partial M_{xx}}{\partial x} - Q_x = I_2 \frac{\partial^2 \phi}{\partial t^2} \quad (1.4.91b)$$

The primary and secondary variables of the Timoshenko beam theory are: (u_0, w_0, ϕ) and (N_{xx}, Q_x, M_{xx}) . Note that the Timoshenko beam theory accounts for transverse shear strain $\gamma_{xz} = \gamma_{xz}^0$ and hence Q_x . In the Timoshenko beam theory Q_x is defined, in place of the definition (1.4.85), by

$$Q_x = K \int_A \sigma_{xz} dA \quad (1.4.92)$$

where K is the *shear correction factor*.

A *simplified third-order beam theory* can be obtained from Eqs. (1.4.87) and (1.4.88a,b) by setting $c_1 = 0$ (but not c_2):

$$\frac{\partial N_{xx}}{\partial x} + f = I_0 \frac{\partial^2 u_0}{\partial t^2} \quad (1.4.93)$$

$$\frac{\partial \bar{Q}_x}{\partial x} + q = I_0 \frac{\partial^2 w_0}{\partial t^2} \quad (1.4.94)$$

$$\frac{\partial \bar{M}_{xx}}{\partial x} - \bar{Q}_x = I_2 \frac{\partial^2 \phi}{\partial t^2} \quad (1.4.95)$$

These equations are lower-order than those in Eqs. (1.4.87) and (1.4.88a,b).

1.5 Variational Methods

1.5.1 Introduction

In Section 1.4, we saw how virtual work and variational principles can be used to obtain governing differential equations and associated boundary conditions. Here we study the direct use of the variational principles in the solution of the underlying equations. The methods to be described here are known as the *classical* variational methods. In these methods, we seek an approximate solution to the problem in terms of adjustable parameters that are determined by substituting the assumed solution into a variational statement equivalent to the governing equations of the problem. Such solution methods are called *direct methods* because the approximate solutions are obtained directly by applying the same variational principle that was used to derive the governing (i.e., Euler–Lagrange) equations.

The assumed solutions in the variational methods are in the form of a finite linear combination of *undetermined parameters* with appropriately chosen functions. This amounts to representing a continuous function by a finite set of functions. Since the solution of a continuum problem in general cannot be represented by a finite set of functions, error is introduced into the solution. Therefore, the solution obtained is an approximation to the true solution of the equations describing a physical problem. As the number of linearly independent terms in the assumed solution is increased, the error in the approximation will be reduced, and the assumed solution converges to the exact solution.

It should be understood that the equations governing a physical problem are themselves approximate. The approximations are introduced by several sources, including the geometry, representation of specified loads and boundary conditions, and material behavior. Therefore, when one thinks of permissible error in an approximate solution, it is understood to be relative to exact solutions of the governing equations that inherently contain approximations. The variational methods of approximation to be described here are limited to the Ritz method, and the weighted-residual methods (e.g., the least-squares method, collocation method, and so on). The weighted-residual methods will be visited only briefly. Interested readers may consult the references at the end of the chapter for additional details [6].

1.5.2 The Ritz Method

As noted in Section 1.4 the principle of virtual displacements gives the equilibrium equations as the Euler–Lagrange equations. These governing equations are in the form of differential equations that are not always solvable by exact methods of solution. There exists a number of approximate methods that can be used to solve differential equations (e.g., finite-difference methods, the finite element method, etc.). The most direct methods are those which bypass the derivation of the Euler–Lagrange equations, and go directly from a variational statement of the problem to the solution of the equations. One such direct method was proposed by Ritz [26]. The Ritz method is based on variational statements, such as those provided by the principles of virtual displacements or the minimum total potential energy, which are

equivalent to the governing differential equations as well as the natural boundary conditions, and they are also known as the *weak forms*.

The basic idea of the Ritz method is described here using the principle of virtual displacements or the minimum total potential energy principle. In the Ritz method we approximate a dependent unknown (e.g., the displacement) u of a given problem by a finite linear combination of the form

$$u \approx U_N = \sum_{j=1}^N c_j \varphi_j + \varphi_0 \quad (1.5.1)$$

and then determine the parameters c_j by requiring that the principle of virtual displacements holds for the approximate solution, i.e., minimize $\Pi(U_N)$ with respect to c_j , $j = 1, 2, \dots, N$. In Eq. (1.5.1) c_j denote undetermined parameters, and φ_0 and φ_j are the *approximation functions*, which are appropriately selected functions of position x . Equation (1.5.1) can be viewed as a representation of u in a finite component form; c_j are termed the *Ritz coefficients*. The selection of φ_j is discussed next.

Properties of Approximation Functions

Substitution of Eq. (1.5.1) into $\Pi(u)$ for u and the minimization of $\Pi(c_j)$ results in a set of algebraic equations among the parameters c_j . In order to ensure that the algebraic equations resulting from the Ritz procedure have a solution, and the approximate solution converges to the true solution of the problem as the number of parameters N is increased, we must choose φ_j ($j = 1, 2, 3, \dots, N$) and φ_0 such that they meet the following requirements:

1. φ_0 has the principal purpose of satisfying the specified *essential* (or geometric) boundary conditions associated with the variational formulation; φ_0 plays the role of *particular solution*. It should be the lowest order possible for completeness.
2. φ_j ($j = 1, 2, \dots, N$) should satisfy the following three conditions:
 - (a) be continuous as required in the variational statement (i.e., φ_j should be such that it has a nonzero contribution to the virtual work statement);
 - (b) satisfy the homogeneous form of the specified essential boundary conditions;
 - (c) the set $\{\varphi_j\}$ is linearly independent and complete. (1.5.2)

The completeness property is defined mathematically as follows. Given a function u and a real number $\varepsilon > 0$, the sequence $\{\varphi_j\}$ is said to be *complete* if there exists an integer N (which depends on ε) and scalars c_1, c_2, \dots, c_N such that

$$\|u - \sum_{j=1}^N c_j \varphi_j\| < \varepsilon \quad (1.5.3)$$

where $\|\cdot\|$ denotes a norm in the vector space of functions u . The set $\{\varphi_j\}$ is called the *spanning set*. A sequence of algebraic polynomials, for example, is complete if it contains terms of all degrees up to the highest degree (N).

Linear independence of a set of functions $\{\varphi_j\}$ refers to the property that there exists no trivial relation among them; i.e., the relation

$$\alpha_1\varphi_1 + \alpha_2\varphi_2 + \cdots + \alpha_N\varphi_N = 0$$

holds only for all $\alpha_j = 0$. Thus no function is expressible as a linear combination of others in the set.

For polynomial approximations functions, the linear independence and completeness properties require φ_j to be increasingly higher-order polynomials. For example, if φ_1 is a linear polynomial, φ_2 should be a quadratic polynomial, φ_3 should be a cubic polynomial, and so on (but each φ_j need not be complete by itself):

$$\varphi_1 = a_1 + b_1x, \quad \varphi_2 = a_2 + b_2x + c_2x^2, \quad a_2 + c_2x^2, \quad \text{or} \quad b_2x + c_2x^2, \quad \dots$$

The completeness property is essential for the convergence of the Ritz approximation (see Reddy [29], p. 262).

Since the natural boundary conditions of the problem are included in the variational statements, we require the Ritz approximation U_N to satisfy only the specified essential boundary conditions of the problem. This is done by selecting φ_i to satisfy the homogeneous form and φ_0 to satisfy the actual form of the essential boundary conditions. For instance, if u is specified to be \hat{u} on the boundary $x = L$, we require

$$\varphi_0 = \hat{u} \quad \text{at} \quad x = L \quad \text{and} \quad \varphi_i = 0 \quad \text{at} \quad x = L \quad \text{for } i = 1, 2, \dots, N$$

The requirement on φ_i to satisfy the homogeneous form of the specified essential boundary conditions follows from the approximation adopted in Eq. (1.5.1). Since $U_N = \hat{u}$ and $\varphi_0 = \hat{u}$ at $x = L$, we have

$$U_N(L) = \sum_{j=1}^N c_j \varphi_j(L) + \varphi_0(L)$$

$$\hat{u} = \sum_{j=1}^N c_j \varphi_j(L) + \hat{u}$$

and, therefore, it follows that $\sum_{j=1}^N c_j \varphi_j(L) = 0$. Since this condition must hold for any set of parameters c_j , it follows that

$$\varphi_j(L) = 0 \quad \text{for } j = 1, 2, \dots, N$$

Note that when the specified values are zero, i.e., $\hat{u} = 0$, there is no need to include φ_0 (or equivalently, $\varphi_0 = 0$); however, φ_j are still required to satisfy the specified (homogeneous) essential boundary conditions.

The conditions in Eq. (1.5.2) provide guidelines for selecting the coordinate functions; they do not give any formula for generating the functions. As a general rule, coordinate functions should be selected from the admissible set, from the lowest order to a desirable order without missing any intermediate admissible terms in the

representation of U_N (*i.e.*, satisfy the completeness property). The function φ_0 has no other role to play than to satisfy specified (nonhomogeneous) essential boundary conditions; there are no continuity conditions on φ_0 . Therefore, one should select the lowest order φ_o that satisfies the essential boundary conditions.

Algebraic Equations for the Ritz Parameters

Once the functions φ_0 and φ_i are selected, the parameters c_j in Eq. (1.5.1) are determined by requiring U_N to minimize the total potential energy functional Π (or satisfy the principle of virtual work) of the problem: $\delta\Pi(U_N) = 0$. Note that $\Pi(U_N)$ is now a real-valued function of variables, c_1, c_2, \dots, c_N . Hence minimization of the functional $\Pi(U_N)$ is reduced to the minimization of a function of several variables:

$$0 = \delta\Pi(U_N) = \delta\Pi(c_i) = \sum_{i=1}^N \frac{\partial\Pi}{\partial c_i} \delta c_i \quad \text{or} \quad \frac{\partial\Pi}{\partial c_i} = 0 \quad (1.5.4)$$

This gives N algebraic equations in the N coefficients (c_1, c_2, \dots, c_N)

$$0 = \frac{\partial\Pi}{\partial c_i} = \sum_{j=1}^N A_{ij} c_j - b_i \quad \text{or} \quad [A]\{c\} = \{b\} \quad (1.5.5)$$

where A_{ij} and b_i are known coefficients that depend on the problem parameters (*e.g.*, geometry, material coefficients, and loads) and the approximation functions. These coefficients will be defined for each problem discussed in the sequel. Equations (1.5.5) are then solved for $\{c\}$ and substituted back into Eq. (1.5.1) to obtain the N -parameter Ritz solution.

Some general features of the Ritz method based on the principle of virtual displacements are listed below:

1. If the approximate functions φ_i are selected to satisfy the conditions in Eq. (1.5.2), the assumed approximation for the displacements converges to the true solution with an increase in the number of parameters (*i.e.*, as $N \rightarrow \infty$). A mathematical proof of such an assertion can be found in [20–22, 29].
2. For increasing values of N , the previously computed coefficients A_{ij} and b_i of the algebraic equations (1.5.5) remain unchanged, provided the previously selected coordinate functions are not changed. One must add only the newly computed coefficients to the system of equations. Of course, c_j will be different for different values of N .
3. If the resulting algebraic equations are symmetric, one needs to compute only upper or lower diagonal elements in the coefficient matrix, $[A]$. The symmetry of the coefficient matrix depends on the variational statement of the problem.
4. If the variational (or virtual work) statement is nonlinear in u , then the resulting algebraic equations will also be nonlinear in the parameters c_i . To solve such nonlinear equations, a variety of numerical methods are available (*e.g.*, Newton's method, the Newton–Raphson method, the Picard method), which will be discussed later in this book (see Chapter 13).

5. Since the strains are computed from an approximate displacement field, the strains and stresses are generally less accurate than the displacement.
6. The equilibrium equations of the problem are satisfied only in the energy sense, not in the differential equation sense. Therefore the displacements obtained from the Ritz approximation, in general do not satisfy the equations of equilibrium pointwise, unless the solution converged to the exact solution.
7. Since a continuous system is approximated by a finite number of coordinates (or degrees of freedom), the approximate system is less flexible than the actual system. Consequently, the displacements obtained using the principle of minimum total potential energy by the Ritz method converge to the exact displacements from below:

$$U_1 < U_2 < \dots < U_N < U_{M\dots} < u(\text{exact}), \text{ for } M > N$$

where U_N denotes the N -parameter Ritz approximation of u obtained from the principle of virtual displacements or the principle of minimum total potential energy. It should be noted that the displacements obtained from the Ritz method based on the total complementary energy (maximum) principle provide the upper bound.

8. The Ritz method can be applied, in principle, to any physical problem that can be cast in a *weak form* — a form that is equivalent to the governing equations and natural boundary conditions of the problem. In particular, the Ritz method can be applied to all structural problems since a virtual work principle exists.

Example 1.5.1:

Consider the cantilever beam shown in Figure 1.4.2. We consider the pure bending case (i.e., $u_0 = 0$). We set up the coordinate system such that the origin is at the fixed end. For this case the geometric (or essential) boundary conditions are

$$w_0(0) = 0, \quad \frac{dw_0}{dx}(0) = 0$$

The force (or natural) boundary conditions can be arbitrary. For example, the beam can be subjected to uniformly distributed transverse load $q(x) = q_0$, concentrated point load F_0 , and moment M_0 , as in Figure 1.4.2. The applied loads will have no bearing on the selection of φ_0 and φ_i . The applied loads will enter the analysis through the expression for the external work done [see Eq. (1.4.52)], which will alter the expression for the coefficients F_i of Eq. (1.5.5).

An N -parameter Ritz approximation of the transverse deflection $w_0(x)$ is chosen in the form

$$w_0(x) \approx W_N = \sum_{j=1}^N c_j \varphi_j + \varphi_0 \quad (1.5.6)$$

Since the specified essential boundary conditions are homogeneous, $\varphi_0 = 0$. Next, we must select φ_i to satisfy the homogeneous form of the specified essential boundary conditions

$$\varphi_i(0) = 0 \quad \text{and} \quad \frac{d\varphi_i}{dx}(0) = 0 \quad (1.5.7)$$

and φ_i must be differentiable as required by the total potential energy functional in Eq. (1.4.67) of Example 1.4.2. Since there are two conditions to satisfy, we begin with $\varphi_1 = a + bx + cx^2$ and

determine two of the three constants using Eq. (1.5.7). The third constant will remain arbitrary. Conditions (1.5.7) give $a = b = 0$, and $\varphi_1(x) = cx^2$. We can arbitrarily take $c = 1$. Using the same procedure, we can determine φ_2, φ_3 , etc. One may set the coefficients of lower order terms to zero, since they are already accounted in the preceding φ_i :

$$\varphi_1 = x^2, \varphi_2 = x^3, \varphi_3 = x^4, \dots, \varphi_N = x^{N+1}$$

The Ritz approximation becomes

$$W_N = c_1 x^2 + c_2 x^3 + \dots + c_N x^{N+1} \quad (1.5.8)$$

Substituting Eq. (1.5.8) into Eq. (1.4.67) we obtain Π as a function of the coefficients c_1, c_2, \dots, c_N :

$$\begin{aligned} \Pi(c_1, c_2, \dots, c_N) &= \int_0^L \left\{ \frac{EI}{2} [2c_1 + 6c_2 x + \dots + N(N+1)c_N x^{N-1}]^2 \right. \\ &\quad \left. - q(c_1 x^2 + c_2 x^3 + \dots + c_N x^{N+1}) \right\} dx \\ &\quad - F_L [c_1 x^2 + c_2 x^3 + \dots + c_N x^{N+1}]_{x=L} \\ &\quad - M_L [2c_1 x + 3c_2 x^2 + \dots + (N+1)c_N x^N]_{x=L} \end{aligned} \quad (1.5.9)$$

Using the total potential energy principle, $\delta\Pi = 0$, which requires that Π be a minimum with respect to each of c_1, c_2, \dots, c_N , we arrive at the conditions

$$\frac{\partial\Pi}{\partial c_1} = 0, \frac{\partial\Pi}{\partial c_2} = 0, \dots, \frac{\partial\Pi}{\partial c_N} = 0 \quad (1.5.10)$$

The i th equation in (1.5.10) has the form

$$\begin{aligned} 0 &= \frac{\partial\Pi}{\partial c_i} = \int_0^L \left\{ EI [2c_1 + 6c_2 x + \dots + N(N+1)c_N x^{N-1}] i(i+1)x^{i-1} - q x^{i+1} \right\} dx \\ &\quad - F_L L^{i+1} - M_L (i+1)L^i \\ &= c_1 \left[\int_0^L 2EI \cdot i(i+1)x^{i-1} dx \right] + c_2 \left[\int_0^L 6EI x \cdot i(i+1)x^{i-1} dx \right] + \dots \\ &\quad + c_N \left[\int_0^L EI N(N+1)x^{N-1} i(i+1)x^{i-1} dx \right] - \int_0^L q(x) x^{i+1} dx - F_L L^{i+1} - M_L (i+1)L^i \\ &= c_1 A_{i1} + c_2 A_{i2} + \dots + c_N A_{iN} - F_i = \sum_{j=1}^N A_{ij} c_j - b_i, \quad (i = 1, 2, \dots, N) \end{aligned} \quad (1.5.11a)$$

where

$$A_{ij} = EI \int_0^L j(j+1)x^{j-1} \cdot i(i+1)x^{i-1} dx, \quad b_i = \int_0^L q(x) x^{i+1} dx + F_L L^{i+1} + M_L (i+1)L^i \quad (1.5.11b)$$

For one- and two-parameter approximations we have the following equations:

$$\begin{aligned} N = 1 : \quad A_{11} &= 4EIL, \quad b_1 = \frac{q_0 L^3}{3} + F_L L^2 + 2M_L L \\ c_1 &= \frac{q_0 L^2}{12EI} + \frac{F_L L}{4EI} + \frac{M_L}{2EI}, \\ W_1(x) &= \left(\frac{q_0 L^4}{12EI} + \frac{F_L L^3}{4EI} + \frac{M_L L^2}{2EI} \right) \frac{x^2}{L^2} \end{aligned} \quad (1.5.12a)$$

$$\begin{aligned} N = 2 : \quad A_{11} &= 4EIL, \quad A_{12} = 6EIL^2 = A_{21}, \quad A_{22} = 12EIL^3 \\ b_1 &= \frac{q_0 L^3}{3} + F_L L^2 + 2M_L L, \quad b_2 = \frac{q_0 L^4}{4} + F_L L^3 + 3M_L L^2 \\ c_1 &= \frac{1}{EI} \left(\frac{5}{24} q_0 L^2 + \frac{1}{2} F_L L + \frac{1}{2} M_L \right), \quad c_2 = -\frac{1}{12EI} (q_0 L + 2F_L) \\ W_2(x) &= \left(\frac{5q_0 L^4}{24EI} + \frac{F_L L^3}{2EI} + \frac{M_L L^2}{2EI} \right) \frac{x^2}{L^2} - \left(\frac{q_0 L^4}{12EI} + \frac{F_L L^3}{6EI} \right) \frac{x^3}{L^3} \end{aligned} \quad (1.5.12b)$$

The exact solution is

$$w_0(x) = \frac{q_0 L^4}{24EI} \left(6 \frac{x^2}{L^2} - 4 \frac{x^3}{L^3} + \frac{x^4}{L^4} \right) + \frac{F_L L^3}{6EI} \left(3 \frac{x^2}{L^2} - \frac{x^3}{L^3} \right) + \frac{M_L L^2}{2EI} \frac{x^2}{L^2} \quad (1.5.13)$$

The two-parameter solution is exact for the case in which $q_0 = 0$. For $q_0 \neq 0$, the solution is not exact for every x but the maximum deflection $W_2(L)$ coincides with the exact value $w_0(L)$. The three-parameter solution, with $\phi_3 = x^4$, would be exact for this problem.

If we were to choose trigonometric functions for φ_i , we may select the functions $\varphi_i(x) = 1 - \cos[(2i-1)\pi x/2L]$. This particular choice would not give the exact solution for a finite value of N , because the applied load q_0 , when expanded in terms of φ_i , would involve infinite number of terms. Thus, a proper choice of the coordinate functions is important in realizing the exact solution. Of course, both algebraic and trigonometric functions would yield acceptable results with finite number of terms.

1.5.3 Weighted-Residual Methods

Consider an operator equation in the form

$$\begin{aligned} A(u) &= f \text{ in } \Omega \\ B_1(u) &= \hat{u} \text{ on } \Gamma_1, \quad B_2(u) = \hat{g} \text{ on } \Gamma_2 \end{aligned} \quad (1.5.14)$$

where A is a linear or nonlinear differential operator, u is the dependent variable, f is a given force term in the domain Ω , B_1 and B_2 are boundary operators associated with essential and natural boundary conditions of the operator A , and \hat{u} and \hat{g} are specified values on the portions Γ_1 and Γ_2 of the boundary Γ of the domain. An example of Eq. (1.5.14) is given by

$$A(u) = -\frac{d}{dx} \left(a \frac{du}{dx} \right), \quad B_1(u) = u, \quad B_2(u) = a \frac{du}{dx}$$

Γ_1 is the point $x = 0$, Γ_2 is the point $x = L$

We seek a solution in the form

$$U_N = \sum_{j=1}^N c_j \varphi_j + \varphi_0 \quad (1.5.15)$$

where the parameters c_j are determined by requiring the residual of the approximation

$$R_N = A \left(\sum_{j=1}^N c_j \varphi_j + \varphi_0 \right) - f \neq 0 \quad (1.5.16a)$$

be orthogonal to N linearly independent set of *weight functions* ψ_i :

$$\int_{\Omega} \psi_i R_N(c_i, \varphi_i, f) d\mathbf{x} = 0, \quad i = 1, 2, \dots, N \quad (1.5.16b)$$

The method based on this procedure is called, for obvious reason, a *weighted-residual method*.

The coordinate function φ_0 and φ_i in a weighted-residual method should satisfy the properties in Eq. (1.5.2), except that they should satisfy *all* specified boundary conditions:

- φ_0 should satisfy *all* specified boundary conditions.
- φ_i should satisfy homogeneous form of *all* specified boundary conditions. (1.5.17)

The variational statement referred to in Property 2a of (1.5.2) is now given in Eq. (1.5.16b). Properties in (1.5.17) are required because the boundary conditions, both essential and natural, are not included in Eq. (1.5.16b). Both properties now require φ_i to be of higher order than those used in the Ritz method. On the other hand, ψ_i can be any linearly independent set, such as $\{1, x, \dots\}$, and no continuity requirements are placed on ψ_i .

Various special cases of the weighted-residual method differ from each other due to the choice of the weight function ψ_i . The most commonly used weight functions are

$$\text{Galerkin's method: } \psi_i = \varphi_i$$

$$\text{Least-squares method: } \psi_i = A(\varphi_i)$$

$$\text{Collocation method: } \psi_i = \delta(\mathbf{x} - \mathbf{x}_i)$$

Here $\delta(\cdot)$ denotes the Dirac delta function. The weighted-residual method in the general form (1.5.16b) (with $\psi_i \neq \varphi_i$) is known as the *Petrov-Galerkin method*. Equation (1.5.16b) provides N linearly independent equations for the determination of the parameters c_i . If A is a nonlinear operator, the resulting algebraic equations will be nonlinear. Whenever A is linear, we have

$$A \left(\sum_{j=1}^N c_j \varphi_j + \varphi_0 \right) = \sum_{j=1}^N c_j A(\varphi_j) + A(\varphi_0) \quad (1.5.18)$$

and Eq. (1.5.16b) becomes

$$\begin{aligned} \sum_{j=1}^N \left[\int_{\Omega} \psi_i A(\varphi_j) d\mathbf{x} \right] c_j - \int_{\Omega} \psi_i [f - A(\varphi_0)] d\mathbf{x} &= 0 \\ \sum_{j=1}^N G_{ij} c_j - q_i &= 0, \quad i = 1, 2, \dots, N \end{aligned} \quad (1.5.19a)$$

where

$$G_{ij} = \int_{\Omega} \psi_i A(\varphi_j) d\mathbf{x}, \quad q_i = \int_{\Omega} \psi_i [f - A(\varphi_0)] d\mathbf{x} \quad (1.5.19b)$$

Note that G_{ij} is not symmetric in general, even when $\psi_i = \varphi_i$ (Galerkin's method). It is symmetric when A is a linear operator and $\psi_i = A(\varphi_i)$ (the least-squares method).

It should be noted that in most problems of interest in solid mechanics, the operator A is of the form that permits the use of integration by parts to transfer

half of the differentiation to the weight functions ψ_i and include natural boundary conditions in the integral statement (see Reddy [6]). For problems for which there exists a quadratic functional or a virtual work statement, the Ritz method is most suitable. The least-squares method is applicable to all types operators A but requires higher-order differentiability of φ_i .

The Galerkin Method

The Galerkin method is a special case of the Petrov–Galerkin method in which the coordinate functions and the weighted functions are the same ($\varphi_i = \psi_i$). It constitutes a generalization of the Ritz method. When the governing equation has even order of highest derivative, it is possible to construct a weak form of the equation, and use the Ritz method. If the Galerkin method is used in such cases, it would involve the use of higher-order coordinate functions and the solution of unsymmetric equations.

The Ritz and Galerkin methods yield the same set of algebraic equations for the following two cases:

1. The specified boundary conditions of the problem are all essential type, and therefore the requirements on φ_i in both methods are the same.
2. The problem has both essential and natural boundary conditions, but the coordinate functions used in the Galerkin method are also used in the Ritz method.

Least-Squares Method

The least-squares method is a variational method in which the integral of the square of the residual in the approximation of a given differential equation is minimized with respect to the parameters in the approximation:

$$\min I(c_i) \equiv \int_{\Omega} |R_N(c_j, \varphi_j, f)|^2 d\mathbf{x} \quad (1.5.20a)$$

or

$$\int_{\Omega} 2R_N(c_j, \varphi_j, f) \frac{\partial R_N}{\partial c_i} d\mathbf{x} = 0, \quad i = 1, 2, \dots, N \quad (1.5.20b)$$

where R_N is the residual defined in Eq. (1.5.16a). Equation (1.5.20) provides N algebraic equations for the constants c_i .

First we note that the least-squares method is a special case of the weighted-residual method for the weight function, $\psi_i = 2(\partial R_N / \partial c_i)$ [compare Eqs. (1.5.16b) and (1.5.20b)]. Therefore, the coordinate functions φ_i should satisfy the same conditions as in the case of the weighted-residual method. Next, if the operator A in the governing equation is linear, the weight function ψ_i becomes

$$\psi_i = \frac{\partial R_N}{\partial c_i} = A(\varphi_i) \quad (1.5.21)$$

Then from Eq. (1.5.20) we have

$$\sum_{j=1}^N \left[\int_{\Omega} A(\varphi_i) A(\varphi_j) d\mathbf{x} \right] c_j - \int_{\Omega} [A(\varphi_i) f - A(\varphi_i) A(\varphi_0)] d\mathbf{x} = 0$$

or

$$\sum_{j=1}^N L_{ij} c_j - h_i = 0, \quad i = 1, 2, \dots, N \quad (1.5.22a)$$

where

$$L_{ij} = \int_{\Omega} A(\varphi_i) A(\varphi_j) \, d\mathbf{x}, \quad h_i = \int_{\Omega} A(\varphi_i) [f - A(\varphi_0)] \, d\mathbf{x} \quad (1.5.22b)$$

Note that the coefficient matrix is symmetric. The least-squares method requires higher-order coordinate functions than the Ritz method because the coefficient matrix L_{ij} involves the same operator as in the original differential equation and no trading of differentiation can be achieved. For first-order differential equations the least-squares method yields a symmetric coefficient matrix, whereas the Ritz and Galerkin methods yield unsymmetric coefficient matrices. Note that in the least-squares method the boundary conditions can also be included in the functional. For example, consider Eq. (1.5.14). The least-squares functional is given by

$$I(u) = \frac{1}{2} \left\{ \int_{\Omega} [A(u) - f]^2 \, d\Omega + \int_{\Gamma_1} [B_1(u) - \hat{u}]^2 \, d\Gamma + \int_{\Gamma_2} [B_2(u) - \hat{g}]^2 \, d\Gamma \right\} \quad (1.5.23)$$

Collocation Method

In the collocation method, we require the residual to vanish at a selected number of points \mathbf{x}^i in the domain:

$$R_N(\mathbf{x}^i, \{c\}, \{\phi\}, f) = 0, \quad (i = 1, 2, \dots, N) \quad (1.5.24a)$$

which can be written, with the help of the Dirac delta function, as

$$\int_{\Omega} \delta(\mathbf{x} - \mathbf{x}^i) R_N(\mathbf{x}, \{c\}, \{\phi\}, f) \, d\mathbf{x} = 0, \quad (i = 1, 2, \dots, N) \quad (1.5.24b)$$

Thus, the collocation method is a special case of the weighted-residual method (1.5.16b) with $\psi_i(\mathbf{x}) = \delta(\mathbf{x} - \mathbf{x}^i)$. In the collocation method, one must choose as many collocation points as there are undetermined parameters. In general, these points should be distributed uniformly in the domain. Otherwise, ill-conditioned equations among c_j may result.

Eigenvalue and Time-Dependent Problems

It should be noted that if the problem at hand is an eigenvalue problem or a time-dependent problem, the operator equation in Eq. (1.5.14) takes the following alternative forms:

Eigenvalue problem

$$A(u) - \lambda C(u) = 0 \quad (1.5.25)$$

Time-dependent problem

$$A_t(u) + A(u) = f(x, t) \quad (1.5.26)$$

In Eq. (1.5.25), parameter λ is called the eigenvalue, which is to be determined along with the eigenvector $u(x)$, and A and C are spatial differential operators. An example of the equation is provided by the buckling of a beam-column

$$\frac{d^2}{dx^2} \left(EI \frac{d^2 u}{dx^2} \right) + P \frac{d^2 u}{dx^2} = 0 \quad (1.5.27)$$

where u denotes the lateral deflection and P is the axial compressive load. The problem involves determining the value of P and mode shape $u(x)$ such that the governing equation and certain end conditions of the beam are satisfied. The minimum value of P is called the *critical buckling load*. Comparing Eq. (1.5.27) with Eq. (1.5.25), we note that

$$A(u) = \frac{d^2}{dx^2} \left(EI \frac{d^2 u}{dx^2} \right), \quad \lambda = P, \quad C(u) = -\frac{d^2 u}{dx^2}$$

In Eq. (1.5.26) A is a spatial differential operator and A_t is a temporal differential operator. Examples of Eq. (1.5.26) are provided by the equations governing the axial motion of a bar:

$$-\rho \frac{\partial^2 u}{\partial t^2} - \frac{\partial}{\partial x} \left(EA_0 \frac{\partial u}{\partial x} \right) = f(x, t) \quad (1.5.28)$$

where u denotes the axial displacement, ρ the density, E Young's modulus, A_0 area of cross section, and f body force per unit length. In this case, we have

$$A_t(u) = -\rho \frac{\partial^2 u}{\partial t^2}, \quad A(u) = -\frac{\partial}{\partial x} \left(EA_0 \frac{\partial u}{\partial x} \right)$$

Application of the weighted-residual method to Eqs. (1.5.25) and (1.5.26) follows the same idea, i.e., Eq. (1.5.16b) holds. For additional details and examples, the reader may consult [6].

Example 1.5.2:

Consider the eigenvalue problem described by the equations

$$-\frac{d^2 u}{dx^2} - \lambda u = 0, \quad u(0) = 0, \quad \frac{du}{dx} + u = 0 \quad \text{at } x = 1 \quad (1.5.29)$$

In a weighted-residual method, φ_i must satisfy not only the condition $\varphi_i(0) = 0$ but also the condition $\varphi'_i(1) + \varphi_i(1) = 0$. The lowest-order function that satisfies the two conditions is

$$\varphi_1(x) = 3x - 2x^2 \quad (1.5.30)$$

The one-parameter Galerkin's solution for the natural frequency can be computed using

$$0 = c_1 \int_0^1 \varphi_1 \left(\frac{d^2 \varphi_1}{dx^2} + \lambda \varphi_1 \right) dx \quad \text{or} \quad \left(-\frac{10}{3} + \frac{4}{5} \lambda \right) c_1 = 0 \quad (1.5.31)$$

which gives (for nonzero c_1) $\lambda = 50/12 = 4.167$. If the same function is used for φ_1 in the one-parameter Ritz solution, we obtain the same result as in the one-parameter Galerkin solution.

For one-parameter collocation method with the collocation point at $x = 0.5$, we obtain [$\varphi_1(0.5) \approx 1.0$ and $(d^2\varphi_1/dx^2) = -4.0$]

$$0 = c_1 \varphi_1(0.5) \left[\left(\frac{d^2\varphi_1}{dx^2} \right) \Big|_{x=0.5} + \lambda \varphi_1(0.5) \right] \quad \text{or} \quad (-4 + \lambda) c_1 = 0 \quad (1.5.32)$$

which gives $\lambda = 4$.

The one-parameter least-squares approximation with $\psi_1 = A(\varphi_1)$ gives

$$0 = c_1 \int_0^1 \frac{d^2\varphi_1}{dx^2} \left(\frac{d^2\varphi_1}{dx^2} + \lambda \varphi_1 \right) dx \quad \text{or} \quad \left(-4 + \frac{5}{6}\lambda \right) c_1 = 0 \quad (1.5.33)$$

and $\lambda = 4.8$. If we use $\psi_1 = A(\varphi_1) - \lambda \varphi_1$, we obtain

$$\begin{aligned} 0 &= c_1 \int_0^1 \left(\frac{d^2\varphi_1}{dx^2} + \lambda \varphi_1 \right) \left(\frac{d^2\varphi_1}{dx^2} + \lambda \varphi_1 \right) dx \\ &= \left(\frac{4}{5}\lambda^2 - \frac{20}{3}\lambda + 16 \right) c_1 \end{aligned} \quad (1.5.34)$$

whose roots are

$$\lambda_{1,2} = \frac{25}{6} \pm \frac{1}{6}\sqrt{445} \quad \rightarrow \quad \lambda_1 = 7.6825, \quad \lambda_2 = 0.6508 \quad (1.5.35)$$

Neither root is closer to the exact value of 4.116. This indicates that the least-squares method with $\psi_i = A(\varphi_i)$ is perhaps more suitable than $\psi_i = A(\varphi_i) - \lambda C(\varphi_i)$.

Let us consider a two-parameter weighted-residual solution to the problem

$$U_2(x) = c_1 \varphi_1(x) + c_2 \varphi_2(x) \quad (1.5.36)$$

where $\varphi_1(x)$ is given by Eq. (1.5.30). To determine $\varphi_2(x)$, we begin with a polynomial that is one degree higher than that used for φ_1 :

$$\varphi_2(x) = a + bx + cx^2 + dx^3$$

and obtain

$$\varphi_2(0) = 0 \rightarrow a = 0; \quad \varphi'_2(1) + \varphi_2(1) = 0 \rightarrow 2b + 3c + 4d = 0 \quad \text{or} \quad d = -\frac{2}{4}b - \frac{3}{4}c$$

We can arbitrarily pick the values of b and c , except that not both are equal to zero (for obvious reasons). Thus we have infinite number of possibilities. If we pick $b = 0$ and $c = 4$, we have $d = -3$, and φ_2 becomes

$$\varphi_2(x) = a + bx + cx^2 + dx^3 = 4x^2 - 3x^3 \quad (1.5.37a)$$

On the other hand, if we choose $b = 1$ and $c = 2$, we have $d = -2$, and φ_2 becomes

$$\varphi_2(x) = a + bx + cx^2 + dx^3 = x + 2x^2 - 2x^3 \equiv \bar{\varphi}_2(x) \quad (1.5.37b)$$

The set $\{\varphi_1, \varphi_2\}$ is equivalent to the set $\{\varphi_1, \bar{\varphi}_2\}$. Note that

$$\begin{aligned} U_2(x) &= c_1 \varphi_1(x) + c_2 \varphi_2(x) \\ &= c_1(3x - 2x^2) + c_2(4x^2 - 3x^3) \\ &= 3c_1 x + (-2c_1 + 4c_2)x^2 - 3c_2 x^3 \\ U_2(x) &\approx c_1 \varphi_1(x) + c_2 \bar{\varphi}_2(x) \\ &= \bar{c}_1(3x - 2x^2) + \bar{c}_2(x + 2x^2 - 2x^3) \\ &= (3\bar{c}_1 + \bar{c}_2)x + (-2\bar{c}_1 + 2\bar{c}_2)x^2 - 2\bar{c}_2 x^3 \end{aligned}$$

Comparing the two relations we can show that

$$\bar{c}_1 = c_1 - 0.5c_2, \quad \bar{c}_2 = 1.5c_2$$

Hence, either set will yield the same final solution for $U_2(x)$ or λ .

Using φ_1 from (1.5.30) and φ_2 from Eq. (1.5.37a), we compute the residual of the approximation as

$$\begin{aligned} R &= -\frac{d^2U_2}{dx^2} - \lambda U_2 = -c_1 \frac{d^2\varphi_1}{dx^2} - c_2 \frac{d^2\varphi_1}{dx^2} - \lambda(c_1\varphi_1 + c_2\varphi_2) \\ &= c_1 \left(-\frac{d^2\varphi_1}{dx^2} - \lambda\varphi_1 \right) + c_2 \left(-\frac{d^2\varphi_1}{dx^2} - \lambda\varphi_2 \right) \end{aligned} \quad (1.5.38)$$

For the Galerkin method, we set the integral of the weighted-residual to zero and obtain

$$\begin{aligned} 0 &= \int_0^1 \varphi_1(x)R dx = \int_0^1 \varphi_1(x) \left[-c_1 \frac{d^2\varphi_1}{dx^2} - c_2 \frac{d^2\varphi_1}{dx^2} - \lambda(c_1\varphi_1 + c_2\varphi_2) \right] dx \\ &= K_{11}c_1 + K_{12}c_2 - \lambda(M_{11}c_1 + M_{12}c_2) \\ 0 &= \int_0^1 \varphi_2(x)R dx = \int_0^1 \varphi_2(x) \left[-c_1 \frac{d^2\varphi_1}{dx^2} - c_2 \frac{d^2\varphi_1}{dx^2} - \lambda(c_1\varphi_1 + c_2\varphi_2) \right] dx \\ &= K_{21}c_1 + K_{22}c_2 - \lambda(M_{21}c_1 + M_{22}c_2) \end{aligned}$$

In matrix form, we have

$$[K]\{c\} - \lambda[M]\{c\} = \{0\}$$

where

$$K_{ij} = - \int_0^1 \varphi_i \frac{d^2\varphi_j}{dx^2} dx, \quad M_{ij} = \int_0^1 \varphi_i \varphi_j dx$$

First, for the choice of functions in Eqs. (1.5.30) and (1.5.37a), we have

$$\frac{d^2\varphi_1}{dx^2} = -4, \quad \frac{d^2\varphi_2}{dx^2} = 8 - 18x$$

Evaluating the integrals, we obtain

$$\begin{aligned} K_{11} &= - \int_0^1 \phi_1 \frac{d^2\phi_1}{dx^2} dx = \int_0^1 (3x - 2x^2)(4)dx = \frac{10}{3} \\ K_{12} &= - \int_0^1 \phi_1 \frac{d^2\phi_2}{dx^2} dx = \int_0^1 (3x - 2x^2)(-8 + 18x)dx = \frac{7}{3} \\ K_{21} &= - \int_0^1 \phi_2 \frac{d^2\phi_1}{dx^2} dx = \int_0^1 (4x^2 - 3x^3)(4)dx = \frac{7}{3} \\ K_{22} &= - \int_0^1 \phi_2 \frac{d^2\phi_2}{dx^2} dx = \int_0^1 (4x^2 - 3x^3)(-8 + 18x)dx = \frac{38}{15} \\ M_{11} &= \int_0^1 \phi_1 \phi_1 dx = \int_0^1 (3x - 2x^2)(3x - 2x^2)dx = \frac{4}{5} \\ M_{12} &= \int_0^1 \phi_1 \phi_2 dx = \int_0^1 (3x - 2x^2)(4x^2 - 3x^3)dx = \frac{3}{5} = M_{21} \\ M_{22} &= \int_0^1 \phi_2 \phi_2 dx = \int_0^1 (4x^2 - 3x^3)(4x^2 - 3x^3)dx = \frac{17}{35} \end{aligned}$$

and

$$\left(\frac{1}{15} \begin{bmatrix} 50 & 35 \\ 35 & 38 \end{bmatrix} - \frac{\lambda}{35} \begin{bmatrix} 28 & 21 \\ 21 & 17 \end{bmatrix} \right) \begin{Bmatrix} c_1 \\ c_2 \end{Bmatrix} = \begin{Bmatrix} 0 \\ 0 \end{Bmatrix}$$

For nontrivial solution, $c_1 \neq 0$ and $c_2 \neq 0$, we set the determinant of the coefficient matrix to zero to obtain the characteristic polynomial

$$675 - \frac{1332}{7}\lambda + \frac{315}{49}\lambda^2 = 0 \quad \text{or} \quad 525 - 148\lambda + 5\lambda^2 = 0 \quad (1.5.39)$$

which gives

$$\lambda_1 = 4.121, \lambda_2 = 25.479 \quad (1.5.40)$$

Clearly, the value of λ_1 has improved over that computed using the one-parameter approximation. The exact value of the second eigenvalue is 24.139.

If we were to use the collocation method, we may select $x = 1/3$ and $x = 2/3$ as the collocation points, among other choices. We leave this as an exercise to the reader.

1.6 Summary

In this chapter a review of the linear and nonlinear strain-displacement relations, equations of motion in terms of stresses and displacements, compatibility conditions on strains, and linear constitutive equations of elasticity, thermoelasticity and electroelasticity is presented. Also, an introduction to the principle of virtual displacements and its special case, the principle of minimum total potential energy, is also presented. The virtual work principles provide a means for the derivation of the governing equations of structural systems, provided one can write the internal and external virtual work expressions for the system. They also yield the natural boundary conditions and give the form of the essential and natural boundary conditions. The last feature proves to be very helpful in the derivation of higher-order plate theories, as will be shown in the sequel. A brief but complete introduction to the Ritz method and weighted-residual methods (Galerkin, least-squares, and collocation methods) is also included in this chapter.

The principle of virtual displacements will be used in this book to derive governing equations of plates according to various theories, and the Ritz and Galerkin methods will be used to determine solutions of simple beam and plate problems. The ideas introduced in connection with classical variational methods are also useful in the study of the finite element method (see Chapter 9).

The single most difficult step in all classical variational methods is the selection of the coordinate functions. The selection of coordinate functions becomes more difficult for problems with irregular domains or discontinuous data (i.e., loading or geometry). Further, the generation of coefficient matrices for the resulting algebraic equations cannot be automated for a *class* of problems that differ from each other only in the geometry of the domain, boundary conditions, or loading. These limitations of the classical variational methods are overcome by the finite element method. In the finite element method, the domain is represented as an assemblage (called mesh) of subdomains, called finite elements, that permit the construction of the approximation functions required in Ritz and Galerkin methods. Traditionally, the choice of the approximation functions in the finite element method is limited to algebraic polynomials. Recent trend in computational mechanics is to return to traditional variational methods that are meshless and find ways to construct approximation functions for arbitrary domains [31–36]. The traditional finite element method is discussed in Chapter 9.

Problems

- 1.1** The nine cross-product (or vector product) relations among the basis $(\hat{\mathbf{e}}_1, \hat{\mathbf{e}}_2, \hat{\mathbf{e}}_3)$ can be expressed using the index notation as

$$\hat{\mathbf{e}}_i \times \hat{\mathbf{e}}_j = \epsilon_{ijk} \hat{\mathbf{e}}_k$$

where ϵ_{ijk} is the *permutation symbol*. Prove the following properties of δ_{ij} and ϵ_{ijk} :

- (a) $F_{ij}\delta_{jk} = F_{ik}$
- (b) $\delta_{ij}\delta_{ij} = \delta_{ii}$
- (c) $\epsilon_{ijk}\epsilon_{ijk} = 6$, (for i, j, k over a range of 1 to 3)
- (d) $\epsilon_{ijk}A_i A_j = 0$
- (e) $\epsilon_{ijk} = \epsilon_{kij} = \epsilon_{jki} = -\epsilon_{jik} = -\epsilon_{ikj} = -\epsilon_{kji}$

- 1.2** Prove the following vector identities using the summation convention and the $\epsilon - \delta$ identity (1.2.8). In the first three identities **A**, **B**, **C** and **D** denote vectors:

- (a) $(\mathbf{A} \times \mathbf{B}) \times (\mathbf{C} \times \mathbf{D}) = [\mathbf{A} \cdot (\mathbf{C} \times \mathbf{D})]\mathbf{B} - [\mathbf{B} \cdot (\mathbf{C} \times \mathbf{D})]\mathbf{A}$
- (b) $(\mathbf{A} \times \mathbf{B}) \cdot (\mathbf{C} \times \mathbf{D}) = (\mathbf{A} \cdot \mathbf{C})(\mathbf{B} \cdot \mathbf{D}) - (\mathbf{A} \cdot \mathbf{D})(\mathbf{B} \cdot \mathbf{C})$
- (c) $(\mathbf{A} \times \mathbf{B}) \cdot [(\mathbf{B} \times \mathbf{C}) \times (\mathbf{C} \times \mathbf{A})] = [\mathbf{A} \cdot (\mathbf{B} \times \mathbf{C})]^2$
- (d) $(\mathbf{AB})^T = (\mathbf{B})^T(\mathbf{A})^T$, where **A** and **B** are dyads

- 1.3** Use the integral theorems to establish the following results:

- (a) The total vector area of a closed surface is zero.
- (b) Show that $\Delta V = \frac{\Delta h}{3} \Delta S$ (see Figure 1.2.3b).

- 1.4** Derive the following integral identities:

- (a) $-\int_{\Omega} w_i \left[\frac{\partial}{\partial x_j} \left(\frac{\partial u_i}{\partial x_j} + \frac{\partial u_j}{\partial x_i} \right) \right] d\Omega = \int_{\Omega} \frac{\partial w_i}{\partial x_j} \left(\frac{\partial u_i}{\partial x_j} + \frac{\partial u_j}{\partial x_i} \right) d\Omega - \oint_{\Gamma} w_i n_j \left(\frac{\partial u_i}{\partial x_j} + \frac{\partial u_j}{\partial x_i} \right) d\Gamma$
- (b) $\int_{\Omega} (\varphi \nabla^4 \psi - \nabla^2 \varphi \nabla^2 \psi) d\Omega = \oint_{\Gamma} \left[\varphi \frac{\partial}{\partial n} (\nabla^2 \psi) - \nabla^2 \psi \frac{\partial \varphi}{\partial n} \right] d\Gamma$

where w_i and u_i are functions of position in Ω , and Γ is the boundary of Ω . The summation convention on repeated subscripts is used.

- 1.5** If **A** is an arbitrary vector and **Φ** is an arbitrary second-order tensor, show that

- (a) $(\mathbf{I} \times \mathbf{A}) \cdot \mathbf{\Phi} = \mathbf{A} \times \mathbf{\Phi}$, **I** = unit tensor
- (b) $(\mathbf{\Phi} \times \mathbf{A})^T = -\mathbf{A} \times \mathbf{\Phi}^T$

- 1.6** Write the position of an arbitrary point (x_1, x_2, x_3) in the deformed body (solid lines) in terms of its coordinates in the undeformed body (broken lines) and compute the nonlinear Lagrangian strains for the body shown in Figure P1.6.

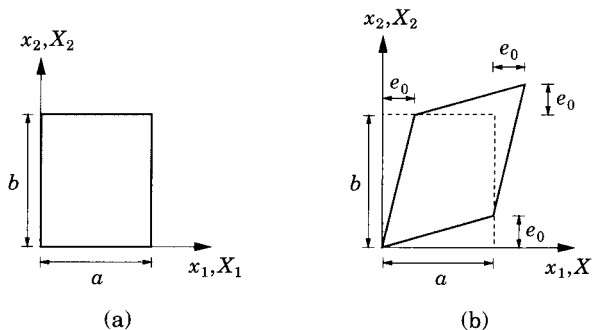


Figure P1.6

- 1.7 Write the position of an arbitrary point (x_1, x_2, x_3) in the deformed body (solid lines) in terms of its coordinates in the undeformed body (broken lines) and compute the nonlinear Lagrangian strains for the body shown in Figure P1.7.

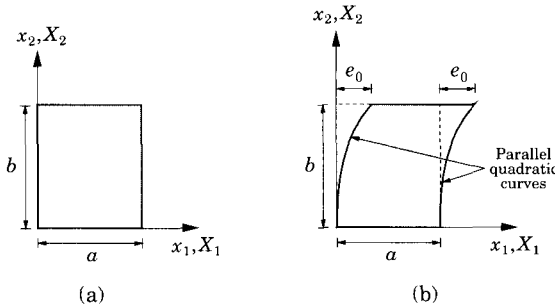


Figure P1.7

- 1.8 Compute the axial strain in the line element AB and the shear strain at point O of the rectangular block shown in Figure P1.8 using the engineering definitions.

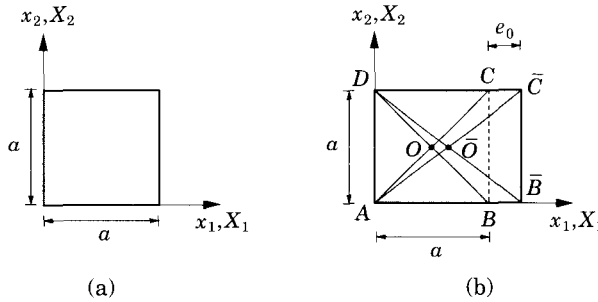


Figure P1.8

- 1.9 Compute the nonlinear strain components E_{ij} associated with the displacement field

$$u_1 = \frac{e_o}{b} X_2, \quad u_2 = \frac{e_o}{a} X_1, \quad u_3 = 0$$

where e_o , a , and b are constants.

- 1.10 Consider the uniform deformation of a square of side 2 units initially centered at $\mathbf{X} = (0, 0)$. The deformation is given by the mapping .

$$x_1 = \frac{1}{4}(18 + 4X_1 + 6X_2), \quad x_2 = \frac{1}{4}(14 + 6X_2)$$

- (a) Sketch the deformed configuration of the body.
- (b) Compute the components of the deformation gradient tensor \mathbf{F} and its inverse (display them in matrix form).
- (c) Compute the Green's strain tensor components (display them in matrix form).

- 1.11 Find the linear strains associated with the 2-D displacement field

$$u_1 = -\frac{Px_1^2 x_2}{2EI} + \frac{PL^2}{2EI} x_2 + \frac{(2+\nu)P}{6EI} x_3^3$$

$$u_2 = \frac{\nu h^2(1+\nu)}{EI} (L - x_1) + \frac{\nu P}{2EI} x_1 x_2^2 + \frac{P}{6EI} x_1^3 - \frac{PL^2}{2EI} x_1 + \frac{PL^3}{3EI}$$

where P , h , ν , and EI are constants.

- 1.12** Find the linear strains associated with the 2-D displacement field ($u_3 = 0$)

$$\begin{aligned} u_1 &= -c_0 x_1 x_2 + c_1 x_2 + c_2 x_3 + c_4 \\ u_2 &= \frac{1}{2} c_0 [\nu (x_2^2 - x_1^2) + x_1^2] + c_4 x_3 + c_5 x_1 + c_6 \end{aligned}$$

where c_0, c_1, \dots, c_6 are constants.

- 1.13** Use the definition (1.3.11) and the vector form of the displacement field and the del operator (∇) in the cylindrical coordinate system

$$\mathbf{u} = u_r \hat{\mathbf{e}}_r + u_\theta \hat{\mathbf{e}}_\theta + u_z \hat{\mathbf{e}}_z \quad \text{and} \quad \nabla = \hat{\mathbf{e}}_r \frac{\partial}{\partial r} + \hat{\mathbf{e}}_\theta \frac{1}{r} \frac{\partial}{\partial \theta} + \hat{\mathbf{e}}_z \frac{\partial}{\partial z}$$

to compute the linear strain-displacement relations in the cylindrical coordinate system:

$$\begin{aligned} \varepsilon_{rr} &= \frac{\partial u_r}{\partial r}, \quad \gamma_{r\theta} = \frac{1}{r} \frac{\partial u_r}{\partial \theta} + \frac{\partial u_\theta}{\partial r} - \frac{u_\theta}{r}, \quad \varepsilon_{\theta\theta} = \frac{1}{r} \frac{\partial u_\theta}{\partial \theta} + \frac{u_r}{r} \\ \gamma_{\theta z} &= \frac{1}{r} \frac{\partial u_z}{\partial \theta} + \frac{\partial u_\theta}{\partial z}, \quad \varepsilon_{zz} = \frac{\partial u_z}{\partial z}, \quad \gamma_{rz} = \frac{\partial u_r}{\partial z} + \frac{\partial u_z}{\partial r} \end{aligned}$$

- 1.14** Show that in order to have a valid displacement field corresponding to a given infinitesimal strain tensor ε , it must satisfy the compatibility relation

$$\nabla \times (\nabla \times \varepsilon)^T = \mathbf{0} \quad \text{or} \quad \epsilon_{imp} \epsilon_{jnq} \varepsilon_{ij,mn} = 0$$

where ϵ_{ijk} is the permutation symbol [see Eqs. (1.2.5b) and (1.2.7)] and ε_{ij} are the Cartesian components of the strain tensor. *Hints:* Begin with $\nabla \times \varepsilon$ and use the requirement $u_{i,jk} = u_{i,kj}$.

- 1.15** Consider the Cartesian components of an infinitesimal strain field for an elastic body [8]:

$$\begin{aligned} \varepsilon_{31} &= \varepsilon_{32} = \varepsilon_{33} = 0 \\ \varepsilon_{11} &= Ax_2^2, \quad \varepsilon_{22} = Ax_1^2, \quad 2\varepsilon_{12} = Bx_1 x_2 \end{aligned}$$

where A and B are constants.

- (a) Determine the relation between A and B required for there to exist a continuous, single-valued displacement field that corresponds to this strain field.
- (b) Determine the most general form of the corresponding displacement field with the A and B from Part (a).
- (c) Determine the specific corresponding displacement field that is fixed at the origin so that $\mathbf{u} = \mathbf{0}$ and $\nabla \times \mathbf{u} = \mathbf{0}$ when $\mathbf{x} = \mathbf{0}$.

- 1.16** Use the del operator (∇) and the dyadic form of σ in the cylindrical coordinate system (r, θ, z) to express the equations of motion (1.3.26a) in the cylindrical coordinate system:

$$\begin{aligned} \frac{\partial \sigma_{rr}}{\partial r} + \frac{1}{r} \frac{\partial \sigma_{r\theta}}{\partial \theta} + \frac{\partial \sigma_{rz}}{\partial z} + \frac{\sigma_{rr} - \sigma_{\theta\theta}}{r} + f_r &= \rho_0 \frac{\partial^2 u_r}{\partial t^2} \\ \frac{\partial \sigma_{r\theta}}{\partial r} + \frac{1}{r} \frac{\partial \sigma_{\theta\theta}}{\partial \theta} + \frac{\partial \sigma_{\theta z}}{\partial z} + 2 \frac{\sigma_{r\theta}}{r} + f_\theta &= \rho_0 \frac{\partial^2 u_\theta}{\partial t^2} \\ \frac{\partial \sigma_{rz}}{\partial r} + \frac{1}{r} \frac{\partial \sigma_{\theta z}}{\partial \theta} + \frac{\partial \sigma_{zz}}{\partial z} + \frac{\sigma_{rz}}{r} + f_z &= \rho_0 \frac{\partial^2 u_z}{\partial t^2} \end{aligned}$$

- 1.17** The components of a stress dyadic σ at a point, referred to the rectangular Cartesian system (x_1, x_2, x_3), are:

$$[\sigma] = \begin{bmatrix} 12 & 9 & 0 \\ 9 & -12 & 0 \\ 0 & 0 & 6 \end{bmatrix} \text{ MPa}$$

Find the following:

- (a) The *stress vector* acting on a plane perpendicular to the vector $2\hat{\mathbf{e}}_1 - 2\hat{\mathbf{e}}_2 + \hat{\mathbf{e}}_3$ passing through the point. Here $\hat{\mathbf{e}}_i$ denote the basis vectors in (x_1, x_2, x_3) system.
 - (b) The magnitude of the stress vector and the angle between the stress vector and the normal to the plane.
 - (c) The magnitudes of the normal and tangential components of the stress vector.
 - (d) Principal stresses.
- 1.18** The problem of pulling a fiber imbedded in a matrix material can be idealized (in the interest of gaining qualitative understanding of the stress distributions at the fiber-matrix interface) as one of studying the following problem [8]: consider a hollow circular cylinder with outer radius a , inner radius b , and length L . The outer surface of the hollow cylinder is assumed to be fixed and its inner surface ideally bonded to a rigid circular cylindrical core of radius b and length L , as shown in Fig. P1.18. Suppose that an axial force $\mathbf{F} = P\hat{\mathbf{e}}_z$ is applied to the rigid core along its centroidal axis.
- (a) Find the axial displacement δ of the rigid core by assuming the following displacement field in the hollow cylinder:
- $$u_r = u_\theta = 0, \quad u_z = u_z(r)$$
- (b) Find the relationship between the applied load P and displacement δ of the rigid core.
 - (c) Determine the work done by the load P .

Here the hollow cylinder represents the matrix around the fiber while the fiber is idealized as the rigid core.

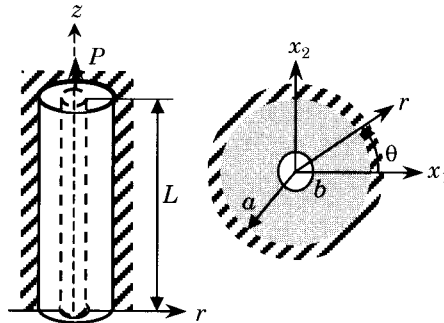


Figure P1.18

- 1.19–1.20** Write expressions for the total virtual work done, $\delta W = \delta U + \delta V$, for each of the beam structures shown in Figs. P1.19 and P1.20.

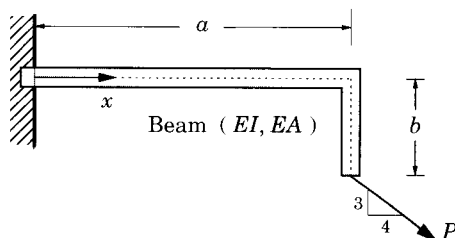


Figure P1.19

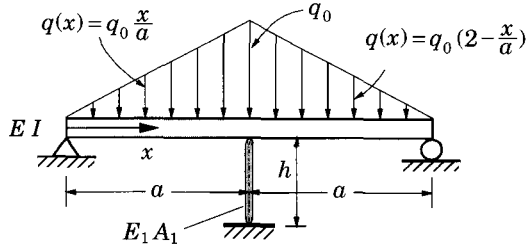


Figure P1.20

Find the Euler–Lagrange equations and the natural boundary conditions associated with each of the functionals in Problems 1.21 through 1.25. The dependent variables are listed as the arguments of the functional. All other variables are not functions of the dependent variables.

1.21

$$\Pi(u_0) = \int_0^L \left[\frac{EA}{2} \left(\frac{du_0}{dx} \right)^2 - fu_0 \right] dx + \frac{k}{2} [u_0(L)]^2 - Pu_0(L), \quad u_0(0) = 0$$

1.22

$$\Pi(w_0) = \int_0^L \left[\frac{EI}{2} \left(\frac{d^2w_0}{dx^2} \right)^2 + \frac{k}{2} w_0^2 - qw_0 \right] dx, \quad w_0(0) = 0, \quad w_0(L) = 0$$

1.23

$$\begin{aligned} \Pi(u_0, w_0) = & \int_0^L \left\{ \frac{EA}{2} \left[\frac{du_0}{dx} + \frac{1}{2} \left(\frac{dw_0}{dx} \right)^2 \right]^2 + \frac{EI}{2} \left(\frac{d^2w_0}{dx^2} \right)^2 \right\} dx \\ & - F_0 w_0(L) - Pu_0(L) \end{aligned}$$

$$u_0(0) = 0, \quad w_0(0) = 0, \quad \frac{dw_0}{dx}(0) = 0$$

1.24

$$\Pi(w_0) = \int_{\Omega} \left[\frac{D_{11}}{2} \left(\frac{\partial^2 w_0}{\partial x^2} \right)^2 + \frac{D_{22}}{2} \left(\frac{\partial^2 w_0}{\partial y^2} \right)^2 + 2D_{12} \left(\frac{\partial^2 w_0}{\partial x \partial y} \right)^2 - qw_0 \right] dxdy$$

$$w_0 = 0, \quad \frac{\partial w_0}{\partial n} = 0 \quad \text{on the boundary } \Gamma$$

1.25

$$\begin{aligned} I(u, v) = & \int_{\Omega} \left\{ \frac{1}{2} \left[\left(c_{11} \frac{\partial u}{\partial x} + c_{12} \frac{\partial v}{\partial y} \right)^2 + \left(c_{12} \frac{\partial u}{\partial x} + c_{22} \frac{\partial v}{\partial y} \right)^2 \right. \right. \\ & \left. \left. + c_{33} \left(\frac{\partial u}{\partial y} + \frac{\partial v}{\partial x} \right)^2 \right] - f_1 u - f_2 v \right\} dxdy - \int_{\Gamma_2} (t_1 u + t_2 v) ds \end{aligned}$$

$$u = \hat{u} \text{ and } v = \hat{v} \quad \text{on } \Gamma_1, \quad \Gamma_1 + \Gamma_2 = \Gamma$$

- 1.26** Suppose that the total displacements (u, v, w) along the three coordinate axes (x, y, z) in a laminated beam can be expressed as

$$\begin{aligned} u(x, z) &= u_0(x) + z\phi_x(x) + z^2\psi_x(x) + z^3\theta_x(x) \\ v(x, z) &= 0 \\ w(x, z) &= w_0(x) + z\phi_z(x) + z^2\psi_z(x) + z^3\theta_z(x) \end{aligned}$$

where (u_0, w_0) denote the displacements of a point $(x, y, 0)$ along the x and z directions, respectively, ϕ_x denotes the rotation of a transverse normal about the y -axis, and $\psi_x, \theta_x, \phi_z, \psi_z$, and θ_z are functions of x . Construct the total potential energy functional for the theory. Assume that the beam is subjected to a distributed load $q(x)$ at the top surface of the beam.

- 1.27** Give the approximation functions φ_1 and φ_0 required in the (i) Ritz and (ii) weighted-residual methods to solve the following problems:

- (a) A bar fixed at the left end and connected to an axial elastic spring (spring constant, k) at the right end.
- (b) A beam clamped at the left end and simply supported at the right end.

- 1.28** Consider a uniform beam fixed at one end and supported by an elastic spring (spring constant k) in the vertical direction. Assume that the beam is loaded by uniformly distributed load q_0 . Determine a one-parameter Ritz solution using algebraic functions.

- 1.29** Use the total potential energy functional in Eq. (1.4.67) to determine a two-parameter Ritz solution of a simply supported beam subjected a transverse point load F_0 at the center. You may use the symmetry about the center ($x = L/2$) of the beam to set up the solution.

- 1.30** Determine a two-parameter Galerkin solution of the cantilever beam problem in Example 1.5.1.

- 1.31** Determine a two-parameter collocation solution of the cantilever beam problem in Example 1.5.1. Use collocation points $x = L/2$ and $x = L$.

- 1.32** Determine the one-parameter Galerkin solution of the equation

$$\frac{d^2}{dx^2} \left[\left(2 + \frac{x}{L} \right) \frac{d^2 w_0}{dx^2} \right] + k w_0 = q_0 \frac{x}{L}$$

that governs a cantilever beam on elastic foundation and subjected to linearly varying load (from zero at the free end to q_0 at the fixed end). Take $k = L = 1$ and $q_0 = 3$, and use algebraic polynomials.

- 1.33** Find the first two eigenvalues associated with the differential equation

$$-\frac{d^2 u}{dx^2} = \lambda u, \quad 0 < x < 1; \quad u(0) = 0, \quad u(1) + u'(1) = 0$$

Use the least-squares method. Use the operator definition to be $A = -(d^2/dx^2)$ to avoid increasing the degree of the characteristic polynomial for λ .

- 1.34** Solve the Poisson equation

$$-\nabla^2 u = f_0 \quad \text{in a unit square, } u = 0 \quad \text{on the boundary}$$

using the following N -parameter Galerkin approximation

$$U_N = \sum_{i,j=1}^N c_{ij} \sin i\pi x \sin j\pi y$$

References for Additional Reading

1. Aris, R., *Vectors, Tensors, and the Basic Equations of Fluid Mechanics*, Prentice-Hall, Englewood Cliffs, NJ (1962).
2. Hildebrand, F. B., *Methods of Applied Mathematics*, Second Edition, Prentice-Hall, Englewood Cliffs, NJ (1965).
3. Jeffreys, H., *Cartesian Tensors*, Cambridge University Press, London, UK (1965).
4. Kreyszig, E., *Advanced Engineering Mathematics*, 6th Edition, John Wiley, New York (1988).
5. Reddy, J. N. and Rasmussen, M. L., *Advanced Engineering Analysis*, John Wiley, New York, 1982; reprinted by Krieger, Melbourne, FL, 1990.
6. Reddy, J. N., *Energy Principles and Variational Methods in Applied Mechanics*, Second Edition, John Wiley, New York (2002).
7. Malvern, L. E., *Introduction to the Mechanics of a Continuous Medium*, Prentice-Hall, Englewood Cliffs, NJ (1969).
8. Slaughter, W. S., *The Linearized Theory of Elasticity*, Birkhäuser, Boston, MA (2002).
9. Lekhnitskii, S. G., *Theory of Elasticity of an Anisotropic Elastic Body*, Holden-Day, San Francisco, CA (1963).
10. Jones, R. M., *Mechanics of Composite Materials*, Second Edition, Taylor & Francis, Philadelphia, PA (1999).
11. Nowinski, J. L., *Theory of Thermoelasticity with Applications*, Sijthoff & Noordhoff, Alphen aan den Rijn, The Netherlands (1978).
12. Carslaw, H. S. and Jaeger, J. C., *Conduction of Heat in Solids*, Second Edition, Oxford University Press, London, UK (1959).
13. Jost, W., *Diffusion in Solids, Liquids, and Gases*, Academic Press, New York (1952).
14. Tiersten, H. F., *Linear Piezoelectric Plate Vibrations*, Plenum, New York (1969).
15. Penfield, P., Jr. and Hermann, A. H., *Electrodynamics of Moving Media*, Research Monograph No. 40, The M. I. T. Press, Cambridge, MA (1967).
16. Gandhi, M. V. and Thompson, B. S., *Smart Materials and Structures*, Chapman & Hall, London, UK (1992).
17. Parton, V. Z. and Kudryavtsev, B. A., *Engineering Mechanics of Composite Structures*, CRC Press, Boca Raton, FL (1993).
18. Reddy, J. N. (Ed.), *Mechanics of Composite Materials. Selected Works of Nicholas J. Pagano*, Kluwer, The Netherlands (1994).
19. Lanczos, C., *The Variational Principles of Mechanics*, The University of Toronto Press, Toronto (1964).
20. Mikhlin, S. G., *Variational Methods in Mathematical Physics*, (translated from the 1957 Russian edition by T. Boddington) The MacMillan Company, New York (1964).
21. Mikhlin, S. G., *The Problem of the Minimum of a Quadratic Functional* (translated from the 1952 Russian edition by A. Feinstein), Holden-Day, San Francisco, CA (1965).
22. Mikhlin, S. G., *An Advanced Course of Mathematical Physics*, American Elsevier, New York (1970).
23. Kantorovitch, L. V. and Krylov, V. I., *Approximate Methods of Higher Analysis* (translated by C. D. Benster), Noordhoff, The Netherlands (1958).
24. Galerkin, B. G., "Series-Solutions of Some Cases of Equilibrium of Elastic Beams and Plates" (in Russian), *Vestn. Inshenernov.*, 1, 897–903 (1915).
25. Galerkin, B. G., "Berechnung der frei galagerten elliptischen Platte auf Biegung," *Z Agnew. Math. Mech.* (1923).

26. Ritz, W., "Über eine neue Methode zur Lösung gewisser Variationsprobleme der mathematischen Physik," *J. Reine Angew. Math.*, **135**, 1-61 (1908).
27. Oden, J. T. and Reddy, J. N., *Variational Methods in Theoretical Mechanics*, Second Edition, Springer Verlag, Berlin (1982).
28. Oden, J. T. and Ripperger, E. A., *Mechanics of Elastic Structures*, Second Edition, Hemisphere, New York (1981).
29. Reddy, J. N., *Applied Functional Analysis and Variational Methods in Engineering*, McGraw-Hill, New York (1986); reprinted by Krieger, Melbourne, FL (1992).
30. Washizu, K., *Variational Methods in Elasticity and Plasticity*, Third Edition, Pergamon Press, New York (1982).
31. Belytschko, T., Lu, Y., and Gu, L., "Element Free Galerkin Methods," *International Journal for Numerical Methods in Engineering*, **37**, 229-256 (1994).
32. Melenk, J. M., and Babuska, I., "The Partition of Unity Finite Element Method: Basic Theory and Applications," *Computer Methods in Applied Mechanics and Engineering*, **139**, 289-314 (1996).
33. Duarte, A. C., and Oden, J. T., "An $h-p$ Adaptive Method Using Clouds," *Computer Methods in Applied Mechanics and Engineering*, **139**, 237-262 (1996).
34. Liew, K. M., Huang, Y. Q., and Reddy, J. N., "A Hybrid Moving Least Squares and Differential Quadrature (MLSDQ) Meshfree Method," *International Journal of Computational Engineering Science*, **3**(1), 1-12 (2002).
35. Liew, K. M., T.Y. Ng, T. Y., Zhoa, X., Zou, G. P., and Reddy, J. N., "Harmonic Reproducing Kernel Particle Method for Free Vibration Analysis of Rotating Cylindrical Shells," *Computer Methods in Applied Mechanics and Engineering*, (to appear).
36. Liew, K. M., Huang, Y. Q., and Reddy, J. N., "Moving Least Square Differential Quadrature Method and Its Application to the Analysis of Shear Deformable Plates," *International Journal for Numerical Methods in Engineering*, (to appear).

Introduction to Composite Materials

2.1 Basic Concepts and Terminology

2.1.1 Fibers and Matrix

Composite materials are those formed by combining two or more materials on a macroscopic scale such that they have better engineering properties than the conventional materials, for example, metals. Some of the properties that can be improved by forming a composite material are stiffness, strength, weight reduction, corrosion resistance, thermal properties, fatigue life, and wear resistance. Most man-made composite materials are made from two materials: a reinforcement material called *fiber* and a base material, called *matrix* material.

Composite materials are commonly formed in three different types: (1) *fibrous composites*, which consist of fibers of one material in a matrix material of another; (2) *particulate composites*, which are composed of macro size particles of one material in a matrix of another; and (3) *laminated composites*, which are made of layers of different materials, including composites of the first two types. The particles and matrix in particulate composites can be either metallic or nonmetallic. Thus, there exist four possible combinations: metallic in nonmetallic, nonmetallic in metallic, nonmetallic in nonmetallic, and metallic in metallic.

The stiffness and strength of fibrous composites come from fibers which are stiffer and stronger than the same material in bulk form. Shorter fibers, called whiskers, exhibit better strength and stiffness properties than long fibers. Whiskers are about 1 to 10 microns (i.e., micro inches or μ in.) in diameter and 10 to 100 times as long. Fibers may be 5 microns to 0.005 inches. Some forms of graphite fibers are 5 to 10 microns in diameter, and they are handled as a bundle of several thousand fibers. The matrix material keeps the fibers together, acts as a load-transfer medium between fibers, and protects fibers from being exposed to the environment. Matrix materials have their usual bulk-form properties whereas fibers have directionally dependent properties.

The basic mechanism of load transfer between the matrix and a fiber can be explained by considering a cylindrical bar of single fiber in a matrix material (see Figure 2.1.1a). The load transfer between the matrix material and fiber takes place through shear stress. When the applied load P on the matrix is tensile, shear stress τ develops on the outer surface of the fiber, and its magnitude decreases from a high value at the end of the fiber to zero at a distance from the end. The tensile stress σ in the fiber cross section has the opposite trend, starting from zero value at the end of the fiber to its maximum at a distance from the end. The two stresses together balance the applied load, P , on the matrix. The distance from the free end to the

point at which the normal stress attains its maximum and shear stress becomes zero is known as the *characteristic distance*. The pure tensile state continues along the rest of the fiber.

When a compressive load is applied on the matrix, the stresses in the region of characteristic length are reversed in sign; in the compressive region, i.e., rest of the fiber length, the fiber tends to buckle, much like a wire subjected to compressive load. At this stage, the matrix provides a lateral support to reduce the tendency of the fiber to buckle (Figure 2.1.1b). When a fiber is broken, the load carried by the fiber is transferred through shear stress to the neighboring two fibers (see Figure 2.1.1c), elevating the fiber axial stress level to a value of 1.5σ .

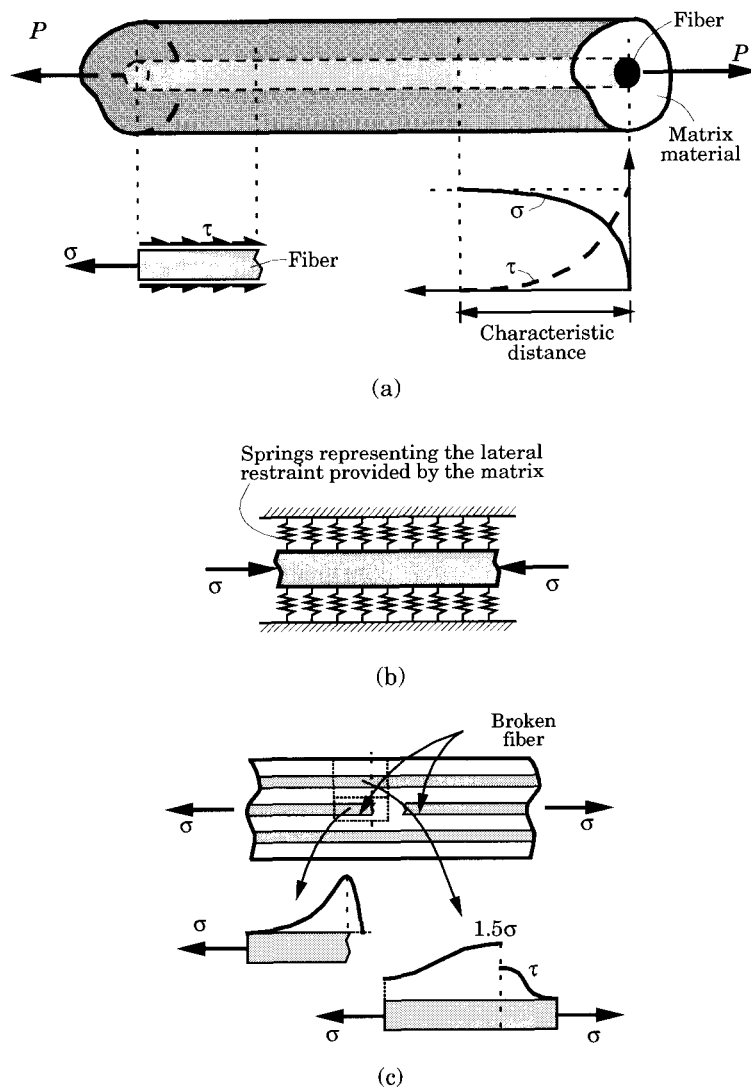


Figure 2.1.1: Load transfer and stress distributions in a single fiber embedded in a matrix material and subjected to an axial load.

2.1.2 Laminae and Laminates

A *lamina* or *ply* is a typical sheet of composite material. It represents a fundamental building block. A fiber-reinforced lamina consists of many fibers embedded in a matrix material, which can be a metal like aluminum, or a nonmetal like thermoset or thermoplastic polymer. Often, coupling (chemical) agents and fillers are added to improve the bonding between fibers and matrix material and increase toughness. The fibers can be continuous or discontinuous, woven, unidirectional, bidirectional, or randomly distributed (see Figure 2.1.2). Unidirectional fiber-reinforced laminae exhibit the highest strength and modulus in the direction of the fibers, but they have very low strength and modulus in the direction transverse to the fibers. A poor bonding between a fiber and matrix results in poor transverse properties and failures in the form of fiber pull out, fiber breakage, and fiber buckling. Discontinuous fiber-reinforced composites have lower strength and modulus than continuous fiber-reinforced composites.

A *laminate* is a collection of laminae stacked to achieve the desired stiffness and thickness. For example, unidirectional fiber-reinforced laminae can be stacked so that the fibers in each lamina are oriented in the same or different directions (see Figure 2.1.3). The sequence of various orientations of a fiber-reinforced composite layer in a laminate is termed the *lamination scheme* or *stacking sequence*. The layers are usually bonded together with the same matrix material as that in a lamina. If a laminate has layers with fibers oriented at 30° or 45° , it can take shear loads. The lamination scheme and material properties of individual lamina provide an added flexibility to designers to tailor the stiffness and strength of the laminate to match the structural stiffness and strength requirements.

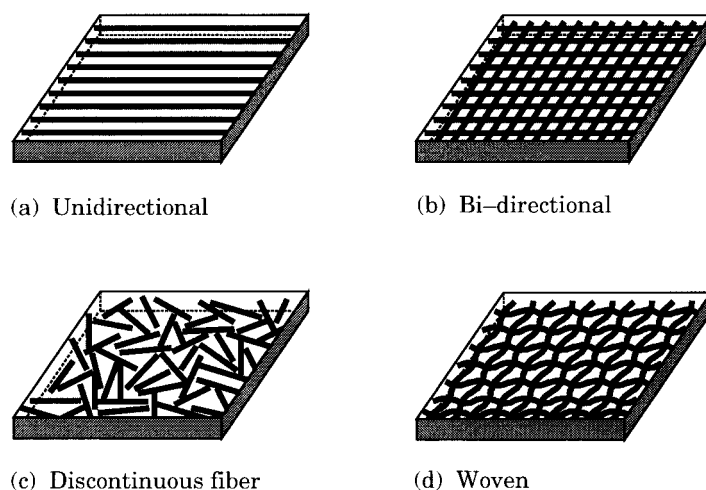


Figure 2.1.2: Various types of fiber-reinforced composite laminae.

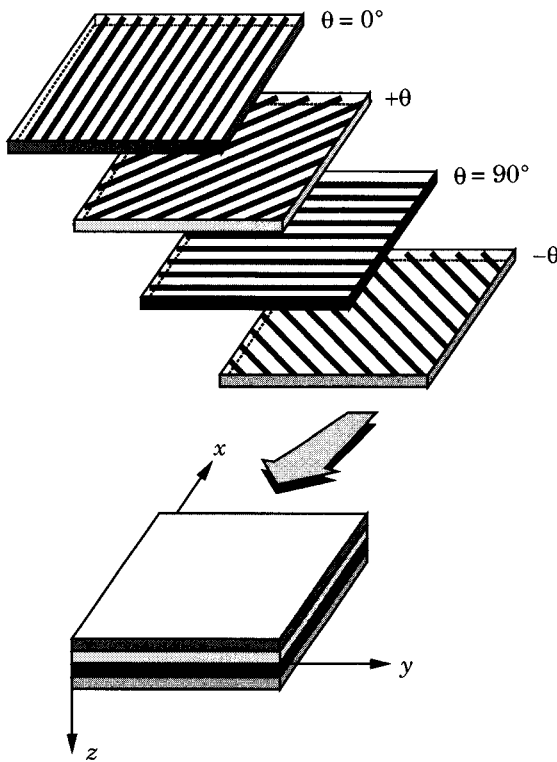


Figure 2.1.3: A laminate made up of laminae with different fiber orientations.

Laminates made of fiber-reinforced composite materials also have disadvantages. Because of the mismatch of material properties between layers, the shear stresses produced between the layers, especially at the edges of a laminate, may cause delamination. Similarly, because of the mismatch of material properties between matrix and fiber, fiber debonding may take place. Also, during manufacturing of laminates, material defects such as interlaminar voids, delamination, incorrect orientation, damaged fibers, and variation in thickness may be introduced. It is impossible to eliminate manufacturing defects altogether; therefore, analysis and design methodologies must account for various mechanisms of failure.

This book is devoted to the theoretical study of laminated structures. Determination of static, transient, vibration, and buckling characteristics of fiber-reinforced composite laminates with different lamination schemes, thicknesses, loads, and boundary conditions constitutes the major objective of the study. The theoretical concepts and analysis methods presented herein can help structural engineers in aerospace, civil, and mechanical engineering industries to select suitable materials and the number and orientations of fiber-reinforced laminae for the best performance in a particular application.

In the remaining portion of this chapter, we study the mechanical behavior of a single lamina, treating it as an orthotropic, linear elastic continuum. The generalized Hooke's law is revisited (see Section 1.3.6) for an orthotropic material, the elastic coefficients of an orthotropic material are expressed in terms of engineering constants of a lamina, and the fiber-matrix interactions in a unidirectional lamina are discussed. Transformation of stresses, strains, and elasticity coefficients from the lamina material coordinates to the problem coordinates are also presented.

2.2 Constitutive Equations of a Lamina

2.2.1 Generalized Hooke's Law

In this section we study the mechanical behavior of a typical fiber-reinforced composite lamina, which is the basic building block of a composite laminate. In formulating the constitutive equations of a lamina we assume that:

- (1) a lamina is a continuum; i.e., no gaps or empty spaces exist.
- (2) a lamina behaves as a linear elastic material.

The first assumption amounts to considering the *macromechanical behavior* of a lamina. If fiber-matrix debonding and fiber breakage, for example, are to be included in the formulation of the constitutive equations of a lamina, then we must consider the *micromechanics* approach, which treats the constituent materials as continua and accounts for the mechanical behavior of the constituents and possibly their interactions. The second assumption implies that the generalized Hooke's law is valid. It should be noted that both assumptions can be removed if we were to develop micromechanical constitutive models for inelastic (e.g., plastic, viscoelastic, etc.) behavior of a lamina.

Composite materials are inherently heterogeneous from the microscopic point of view. From the macroscopic point of view, wherein the material properties of a composite are derived from a weighted average of the constituent materials, fiber and matrix, composite materials are assumed to be homogeneous. The following discussion of constitutive equations is independent of whether the material is homogeneous or not, because the stress-strain relations hold for a typical point in the body.

The generalized Hooke's law for an anisotropic material under isothermal conditions is given in contracted notation [see Eq. (1.3.37a,b)] by

$$\sigma_i = C_{ij}\varepsilon_j \quad (2.2.1)$$

where σ_{ij} (σ_i) are the stress components, ε_{ij} (ε_i) are the strain components, and C_{ij} are the material coefficients, all referred to an orthogonal Cartesian coordinate system (x_1, x_2, x_3) . In general, there are 21 independent elastic constants for the most general hyperelastic material as discussed in detail in Section 1.3.6. When materials possess one or more planes of material symmetry, the number of independent elastic coefficients can be reduced. For materials with one plane of material symmetry, called *monoclinic materials*, there are only 13 independent parameters, and for materials with three mutually orthogonal planes of symmetry, called *orthotropic materials*, the number of material parameters is reduced to 9 in three-dimensional cases.

2.2.2 Characterization of a Unidirectional Lamina

A unidirectional fiber-reinforced lamina is treated as an orthotropic material whose material symmetry planes are parallel and transverse to the fiber direction. The material coordinate axis x_1 is taken to be parallel to the fiber, the x_2 -axis transverse to the fiber direction in the plane of the lamina, and the x_3 -axis is perpendicular to the plane of the lamina (see Figure 2.2.1). The orthotropic material properties of a lamina are obtained either by the theoretical approach or through suitable laboratory tests.

The theoretical approach, called a *micromechanics approach*, used to determine the engineering constants of a continuous fiber-reinforced composite material is based on the following assumptions:

1. Perfect bonding exists between fibers and matrix.
2. Fibers are parallel, and uniformly distributed throughout.
3. The matrix is free of voids or microcracks and initially in a stress-free state.
4. Both fibers and matrix are isotropic and obey Hooke's law.
5. The applied loads are either parallel or perpendicular to the fiber direction.

The moduli and Poisson's ratio of a fiber-reinforced material can be expressed in terms of the moduli, Poisson's ratios, and volume fractions of the constituents. To this end, let

$$\begin{aligned} E_f &= \text{modulus of the fiber;} & E_m &= \text{modulus of the matrix} \\ \nu_f &= \text{Poisson's ratio of the fiber;} & \nu_m &= \text{Poisson's ratio of the matrix} \\ v_f &= \text{fiber volume fraction;} & v_m &= \text{matrix volume fraction} \end{aligned}$$

Then it can be shown (see Problems 2.1 and 2.2) that the lamina engineering constants are given by

$$\begin{aligned} E_1 &= E_f v_f + E_m v_m, & \nu_{12} &= \nu_f v_f + \nu_m v_m \\ E_2 &= \frac{E_f E_m}{E_f v_m + E_m v_f}, & G_{12} &= \frac{G_f G_m}{G_f v_m + G_m v_f} \end{aligned} \quad (2.2.2)$$

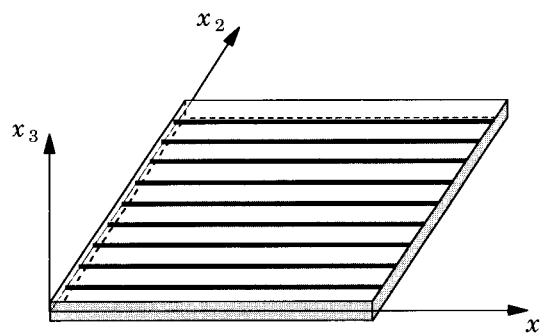


Figure 2.2.1: A unidirectional fiber-reinforced composite layer with the material coordinate system (x_1, x_2, x_3) (with the x_1 -axis oriented along the fiber direction).

where E_1 is the longitudinal modulus, E_2 is transverse modulus, ν_{12} is the major Poisson's ratio, and G_{12} is the shear modulus, and

$$G_f = \frac{E_f}{2(1 + \nu_f)}, \quad G_m = \frac{E_m}{2(1 + \nu_m)} \quad (2.2.3)$$

Other micromechanics approaches use elasticity, as opposed to mechanics of materials approaches. Interested readers may consult Chapter 3 of Jones [3] and the references given there (also see [18-20]).

The engineering parameters E_1 , E_2 , E_3 , G_{12} , G_{13} , G_{23} , ν_{12} , ν_{13} , and ν_{23} of an orthotropic material can be determined experimentally using an appropriate test specimen made up of the material. At least four tests are required to determine the four constants E_1 , E_2 , E_3 and G_{12} and the longitudinal strength X , transverse strength Y and shear strength S (and additional tests to determine G_{13} and G_{23}). These are shown schematically in Figure 2.2.2a-d.

For example, E_1 , ν_{12} and X of a fiber-reinforced material are measured using a uniaxial test shown in Figure 2.2.2a. The specimen consists of several layers of the material with fibers in each layer being aligned with the longitudinal direction. The specimen is then loaded along the longitudinal direction and strains along and perpendicular to the fiber directions are measured using strain gauges (see Figure 2.2.2e). By measuring the applied load P , the cross-sectional area A , the longitudinal strain $\varepsilon_\ell = \varepsilon_1$ and transverse strain $\varepsilon_t = \varepsilon_2$, we can calculate

$$E_\ell = E_1 = \frac{P}{A\varepsilon_1}, \quad \nu_{\ell t} = \nu_{12} = -\frac{\varepsilon_2}{\varepsilon_1}, \quad X = \frac{P_{\text{ult}}}{A}$$

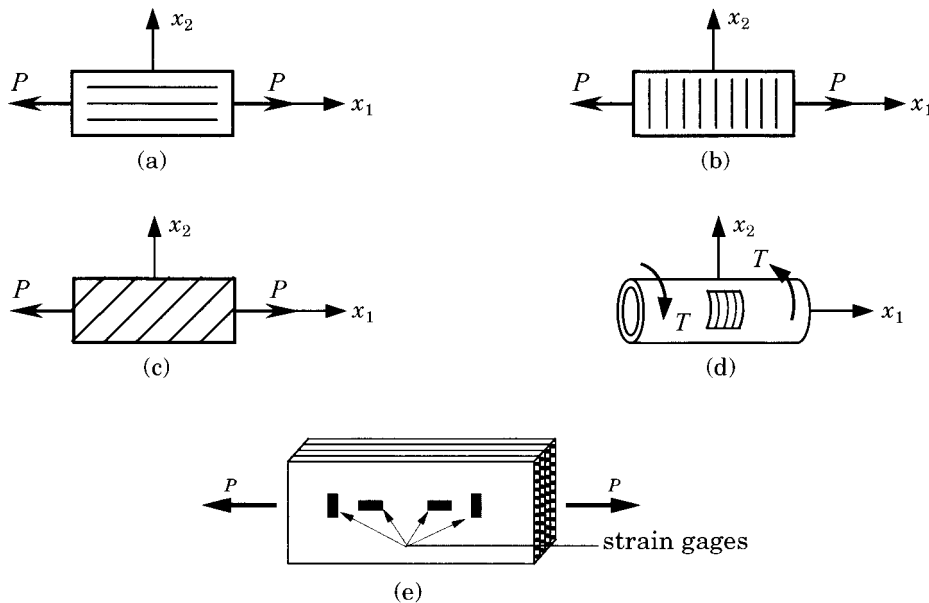


Figure 2.2.2: Tests required for the mechanical characterization of a laminate.

where P_{ult} is the ultimate load (say, load at which the material reaches its elastic limit). Similarly, E_2 , ν_{12} and Y can be determined from the test shown in Figure 2.2.2b:

$$E_t = E_1 = \frac{P}{A\varepsilon_1}, \quad \nu_{t\ell} = \nu_{12} = -\frac{\varepsilon_2}{\varepsilon_1}, \quad Y = \frac{P_{\text{ult}}}{A}$$

The shear modulus is determined from the test shown in Figure 2.2.2c by measuring $E_1 = P/A\varepsilon_1$, E_ℓ , E_t and $\nu_{\ell t}$, and using the transformation equation (4a) of Problem 2.3:

$$\frac{1}{E_1} = \frac{1}{4} \left(\frac{1}{E_\ell} + \frac{1}{E_t} + \frac{1}{G_{\ell t}} - \frac{2\nu_{\ell t}}{E_\ell} \right)$$

wherein $G_{\ell t}$ is the only unknown. The shear strength S is determined from the test shown in Figure 2.2.2d:

$$S = \tau_{\text{ult}} = \frac{T_{\text{ult}}}{2\pi r^2 h}$$

where T is the applied torque, and r and h are the mean radius and thickness of the tube, respectively. The values of the engineering constants for several materials are presented in Tables 2.2.1 and 2.2.2.

Table 2.2.1: Values of the engineering constants for several materials*.

Material†	E_1	E_2	G_{12}	G_{13}	G_{23}	ν_{12}
Aluminum	10.6	10.6	3.38	3.38	3.38	0.33
Copper	18.0	18.0	6.39	6.39	6.39	0.33
Steel	30.0	30.0	11.24	11.24	11.24	0.29
Gr.-Ep (AS)	20.0	1.3	1.03	1.03	0.90	0.30
Gr.-Ep (T)	19.0	1.5	1.00	0.90	0.90	0.22
Gl.-Ep (1)	7.8	2.6	1.30	1.30	0.50	0.25
Gl.-Ep (2)	5.6	1.2	0.60	0.60	0.50	0.26
Br.-Ep	30.0	3.0	1.00	1.00	0.60	0.30

*Moduli are in msi = million psi; 1 psi = 6,894.76 N/m²; Pa = N/m²; kPa = 10³ Pa; MPa = 10⁶ Pa; GPa = 10⁹ Pa.

† The following abbreviations are used for various material systems: Gr.-Ep (AS) = graphite-epoxy (AS/3501); Gr.-Ep (T) = graphite-epoxy (T300/934); Gl.-Ep = glass-epoxy; Br.-Ep = boron-epoxy.

Table 2.2.2: Values of additional engineering constants for the materials listed in Table 2.2.1*.

Material	E_3	ν_{13}	ν_{23}	α_1	α_2
Aluminum	10.6	0.33	0.33	13.1	13.1
Copper	18.0	0.33	0.33	18.0	18.0
Steel	30.0	0.29	0.29	10.0	10.0
Gr.-Ep (AS)	1.3	0.30	0.49	1.0	30.0
Gr.-Ep (T)	1.5	0.22	0.49	-0.167	15.6
Gl.-Ep (1)	2.6	0.25	0.34	3.5	11.4
Gl.-Ep (2)	1.3	0.26	0.34	4.8	12.3
Br.-Ep	3.0	0.25	0.25	2.5	8.0

* Units of E_3 are msi, and the units of α_1 and α_2 are 10⁻⁶ in./in./°F.

2.3 Transformation of Stresses and Strains

2.3.1 Coordinate Transformations

The constitutive relations (1.3.44) and (1.3.45) for an orthotropic material were written in terms of the stress and strain components that are referred to a coordinate system that coincides with the principal material coordinate system. The coordinate system used in the problem formulation, in general, does not coincide with the principal material coordinate system. Further, composite laminates have several layers, each with different orientation of their material coordinates with respect to the laminate coordinates. Thus, there is a need to establish transformation relations among stresses and strains in one coordinate system to the corresponding quantities in another coordinate system. These relations can be used to transform constitutive equations from the material coordinates of each layer to the coordinates used in the problem description.

In forming flat laminates, fiber-reinforced laminae are stacked with their x_1x_2 -planes parallel but each having its own fiber direction. If the z -coordinate of the problem is taken along the laminate thickness, the x_3 -coordinate of each lamina we will always coincide with the z -coordinate of the problem. Thus we have a special type of coordinate transformation between the material coordinates and the coordinates used in the problem description.

Let (x, y, z) denote the coordinate system used to write the governing equations of a laminate, and let (x_1, x_2, x_3) be the principal material coordinates of a typical layer in the laminate such that x_3 -axis is parallel to the z -axis (i.e., the x_1x_2 -plane and the xy -plane are parallel) and the x_1 -axis is oriented at an angle of $+\theta$ counterclockwise (when looking down on the lamina) from the x -axis (see Figure 2.3.1). The coordinates of a material point in the two coordinate systems are related as follows ($z = x_3$):

$$\begin{Bmatrix} x_1 \\ x_2 \\ x_3 \end{Bmatrix} = \begin{bmatrix} \cos \theta & \sin \theta & 0 \\ -\sin \theta & \cos \theta & 0 \\ 0 & 0 & 1 \end{bmatrix} \begin{Bmatrix} x \\ y \\ z \end{Bmatrix} = [L] \begin{Bmatrix} x \\ y \\ z \end{Bmatrix} \quad (2.3.1)$$

The inverse of Eq. (2.3.1) is

$$\begin{Bmatrix} x \\ y \\ z \end{Bmatrix} = \begin{bmatrix} \cos \theta & -\sin \theta & 0 \\ \sin \theta & \cos \theta & 0 \\ 0 & 0 & 1 \end{bmatrix} \begin{Bmatrix} x_1 \\ x_2 \\ x_3 \end{Bmatrix} = [L]^T \begin{Bmatrix} x_1 \\ x_2 \\ x_3 \end{Bmatrix} \quad (2.3.2)$$

Note that the inverse of $[L]$ is equal to its transpose: $[L]^{-1} = [L]^T$.

The transformation relations (2.3.1) and (2.3.2) are also valid for the unit vectors associated with the two coordinate systems:

$$\begin{Bmatrix} \hat{\mathbf{e}}_1 \\ \hat{\mathbf{e}}_2 \\ \hat{\mathbf{e}}_3 \end{Bmatrix} = [L] \begin{Bmatrix} \hat{\mathbf{e}}_x \\ \hat{\mathbf{e}}_y \\ \hat{\mathbf{e}}_z \end{Bmatrix}, \quad \begin{Bmatrix} \hat{\mathbf{e}}_x \\ \hat{\mathbf{e}}_y \\ \hat{\mathbf{e}}_z \end{Bmatrix} = [L]^T \begin{Bmatrix} \hat{\mathbf{e}}_1 \\ \hat{\mathbf{e}}_2 \\ \hat{\mathbf{e}}_3 \end{Bmatrix} \quad (2.3.3)$$

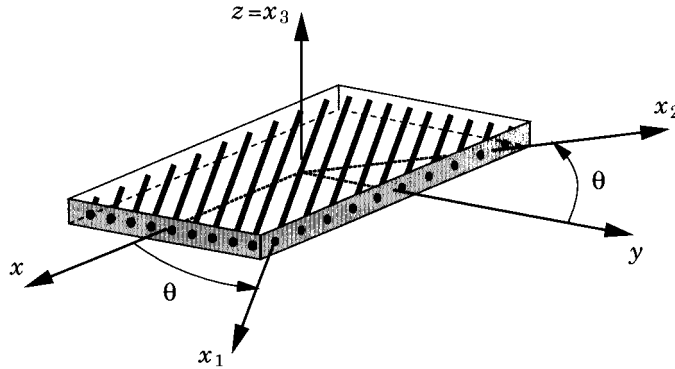


Figure 2.3.1: A lamina with material and problem coordinate systems.

2.3.2 Transformation of Stress Components

Next we consider the relationship between the components of stress in (x, y, z) and (x_1, x_2, x_3) coordinate systems. Let σ denote the stress tensor, which has components $\sigma_{11}, \sigma_{12}, \dots, \sigma_{33}$ in the material (m) coordinates (x_1, x_2, x_3) and components $\sigma_{xx}, \sigma_{xy}, \dots, \sigma_{zz}$ in the problem (p) coordinates (x, y, z) . Since stress tensor is a second-order tensor, it transforms according to the formula

$$(\sigma_{kq})_m = \ell_{ki} \ell_{qj} (\sigma_{ij})_p, \quad (\sigma_{kq})_p = \ell_{ik} \ell_{jq} (\sigma_{ij})_m \quad (2.3.4)$$

where $(\sigma_{ij})_m$ are the components of the stress tensor σ in the material coordinates (x_1, x_2, x_3) , whereas $(\sigma_{ij})_p$ are the components of the same stress tensor σ in the problem coordinates (x, y, z) , and ℓ_{ij} are the direction cosines defined by

$$\ell_{ij} = (\hat{\mathbf{e}}_i)_m \cdot (\hat{\mathbf{e}}_j)_p$$

and $(\hat{\mathbf{e}}_i)_m$ and $(\hat{\mathbf{e}}_i)_p$ are the orthonormal basis vectors in the material and problem coordinate systems, respectively. Note that the tensor transformation equations (2.3.4) hold among tensor components only. Equations (2.3.4) can be expressed in matrix forms. First, we introduce the 3×3 arrays of the stress components in the two coordinate systems:

$$[\sigma]_p = \begin{bmatrix} \sigma_{xx} & \sigma_{xy} & \sigma_{xz} \\ \sigma_{xy} & \sigma_{yy} & \sigma_{yz} \\ \sigma_{xz} & \sigma_{yz} & \sigma_{zz} \end{bmatrix}, \quad [\sigma]_m = \begin{bmatrix} \sigma_{11} & \sigma_{12} & \sigma_{13} \\ \sigma_{12} & \sigma_{22} & \sigma_{23} \\ \sigma_{13} & \sigma_{23} & \sigma_{33} \end{bmatrix} \quad (2.3.5)$$

Then Eqs. (2.3.4) can be expressed in matrix form as

$$[\sigma]_m = [L][\sigma]_p[L]^T, \quad [\sigma]_p = [L]^T[\sigma]_m[L] \quad (2.3.6a, b)$$

where $[L]$ is the 3×3 matrix of direction cosines ℓ_{ij} .

Equation (2.3.6a) provides a means to convert stress components referred to the problem (laminate) coordinate system to those referred to the material (lamina) coordinate system, while Eq. (2.3.6b) allows computation of stress components referred to the problem coordinates in terms of stress components referred to the material coordinates. Equations (2.3.6a,b) hold for any general coordinate transformation, and hence it holds for the special transformation in Eqs. (2.3.1).

Carrying out the matrix multiplications in Eq. (2.3.6b), with $[L]$ defined by Eq. (2.3.1), and rearranging the equations in terms of the single-subscript stress components in (x, y, z) and (x_1, x_2, x_3) coordinate systems, we obtain

$$\begin{Bmatrix} \sigma_{xx} \\ \sigma_{yy} \\ \sigma_{zz} \\ \sigma_{yz} \\ \sigma_{xz} \\ \sigma_{xy} \end{Bmatrix} = \begin{bmatrix} \cos^2 \theta & \sin^2 \theta & 0 & 0 & 0 & -\sin 2\theta \\ \sin^2 \theta & \cos^2 \theta & 0 & 0 & 0 & \sin 2\theta \\ 0 & 0 & 1 & 0 & 0 & 0 \\ 0 & 0 & 0 & \cos \theta & \sin \theta & 0 \\ 0 & 0 & 0 & -\sin \theta & \cos \theta & 0 \\ \sin \theta \cos \theta & -\sin \theta \cos \theta & 0 & 0 & 0 & \cos^2 \theta - \sin^2 \theta \end{bmatrix} \begin{Bmatrix} \sigma_1 \\ \sigma_2 \\ \sigma_3 \\ \sigma_4 \\ \sigma_5 \\ \sigma_6 \end{Bmatrix} \quad (2.3.7)$$

or

$$\{\sigma\}_p = [T]\{\sigma\}_m \quad (2.3.8)$$

The inverse relationship between $\{\sigma\}_m$ and $\{\sigma\}_p$, Eq. (2.3.6a), is given by

$$\begin{Bmatrix} \sigma_1 \\ \sigma_2 \\ \sigma_3 \\ \sigma_4 \\ \sigma_5 \\ \sigma_6 \end{Bmatrix} = \begin{bmatrix} \cos^2 \theta & \sin^2 \theta & 0 & 0 & 0 & \sin 2\theta \\ \sin^2 \theta & \cos^2 \theta & 0 & 0 & 0 & -\sin 2\theta \\ 0 & 0 & 1 & 0 & 0 & 0 \\ 0 & 0 & 0 & \cos \theta & -\sin \theta & 0 \\ 0 & 0 & 0 & \sin \theta & \cos \theta & 0 \\ -\sin \theta \cos \theta & \sin \theta \cos \theta & 0 & 0 & 0 & \cos^2 \theta - \sin^2 \theta \end{bmatrix} \begin{Bmatrix} \sigma_{xx} \\ \sigma_{yy} \\ \sigma_{zz} \\ \sigma_{yz} \\ \sigma_{xz} \\ \sigma_{xy} \end{Bmatrix} \quad (2.3.9)$$

or

$$\{\sigma\}_m = [R]\{\sigma\}_p \quad (2.3.10)$$

The result in Eq. (2.3.9) can also be obtained from Eq. (2.3.7) by replacing θ with $-\theta$.

Example 2.3.1:

The stress transformation equations (2.3.9) can be derived directly by considering the equilibrium of an element of the lamina (see Figure 2.3.2). Consider a wedge element whose slant face is parallel to the fibers. Suppose that the thickness of the lamina is h , and the length of the slant face is ΔS . Then the horizontal and vertical sides of the wedges are of lengths $\Delta S \cos \theta$ and $\Delta S \sin \theta$, respectively. The forces acting on any face of the wedge are obtained by multiplying the stresses acting on the face with the area of the surface.

Suppose that we wish to determine σ_{22} in terms of $(\sigma_{xx}, \sigma_{yy}, \sigma_{xy})$. Then by summing all forces acting on the wedge along coordinate x_2 (i.e., equilibrium of forces along x_2) we obtain

$$\begin{aligned} \sigma_{22}\Delta S h - (\sigma_{xx}\Delta S \sin \theta h) \sin \theta + (\sigma_{xy}\Delta S \sin \theta h) \cos \theta - (\sigma_{yy}\Delta S \cos \theta h) \cos \theta \\ + (\sigma_{xy}\Delta S \cos \theta h) \sin \theta = 0 \end{aligned}$$

or

$$\sigma_{22} = \sigma_{xx} \sin^2 \theta + \sigma_{yy} \cos^2 \theta - 2\sigma_{xy} \cos \theta \sin \theta$$

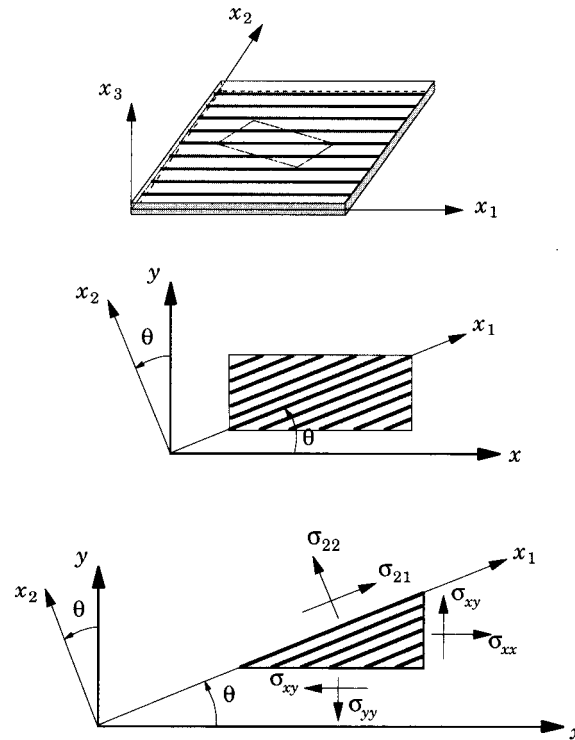


Figure 2.3.2: A free-body diagram of a wedge element with stress components.

Similarly, summing the forces along x_1 coordinate, we obtain

$$\begin{aligned} \sigma_{12}\Delta S h + (\sigma_{xx}\Delta S \sin \theta h) \cos \theta + (\sigma_{xy}\Delta S \sin \theta h) \sin \theta - (\sigma_{yy}\Delta S \cos \theta h) \sin \theta \\ - (\sigma_{xy}\Delta S \cos \theta h) \cos \theta = 0 \end{aligned}$$

or

$$\sigma_{12} = -\sigma_{xx} \sin \theta \cos \theta + \sigma_{yy} \cos \theta \sin \theta + \sigma_{xy}(\cos^2 \theta - \sin^2 \theta)$$

Clearly, the expressions for σ_{22} and σ_{12} derived here are the same as those for σ_1 and σ_6 , respectively, in Eq. (2.3.9). The stress component σ_{11} can be determined in terms of $(\sigma_{xx}, \sigma_{yy}, \sigma_{xy})$ by considering a wedge element whose slant face is perpendicular to the fibers (see Figure 2.3.2). By summing forces along the x - and y -coordinates we can obtain stresses σ_{xx} and σ_{xy} in terms of $(\sigma_{11}, \sigma_{22}, \sigma_{12})$.

Example 2.3.2:

Consider a thin (i.e., the thickness is about one-tenth of the radius), filament-wound, closed cylindrical pressure vessel (see Figure 2.3.3). The vessel is of 63.5 cm (25 in.) internal diameter and pressurized to 1.379 MPa (200 psi). We wish to determine the shear and normal forces per unit length of filament winding. Assume a filament winding angle of $\theta = 53.125^\circ$ from the longitudinal axis of the pressure vessel, and use the following material properties, typical of graphite-epoxy material: $E_1 = 140$ MPa (20.3 Ms), $E_2 = 10$ MPa (1.45 Ms), $G_{12} = 7$ MPa (1.02 Ms), and $\nu_{12} = 0.3$. Note that MPa means mega (10^6) Pascal (Pa) and Pa = N/m² (1 psi = 6,894.76 Pa).

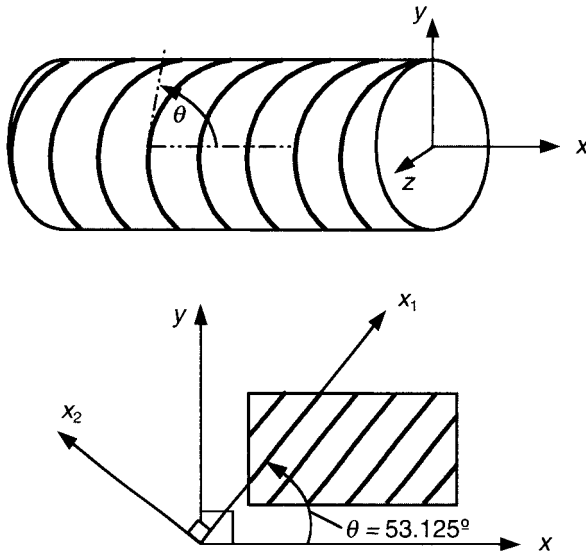


Figure 2.3.3: A filament-wound cylindrical pressure vessel.

The equations of equilibrium of forces in a structure do not depend on the material properties. Hence, equations derived for the longitudinal (σ_{xx}) and circumferential (σ_{yy}) stresses in a thin-walled cylindrical pressure vessel are valid here:

$$\sigma_{xx} = \frac{pD_i}{4h}, \quad \sigma_{yy} = \frac{pD_i}{2h}$$

where p is internal pressure, D_i is internal diameter, and h is thickness of the pressure vessel. We obtain

$$\sigma_{xx} = \frac{1.379 \times 0.635}{4h} = \frac{0.2189}{h} \text{ MPa}, \quad \sigma_{yy} = \frac{1.379 \times 0.635}{2h} = \frac{0.4378}{h} \text{ MPa}$$

The shear stress σ_{xy} is zero.

Next we determine the shear stress along the fiber and the normal stress in the fiber using the transformation equations (2.3.9) or from the equations derived in Example 2.3.1. We obtain

$$\begin{aligned}\sigma_{11} &= \frac{0.2189}{h}(0.6)^2 + \frac{0.4378}{h}(0.8)^2 = \frac{0.3590}{h} \text{ MPa} \\ \sigma_{22} &= \frac{0.2189}{h}(0.8)^2 + \frac{0.4378}{h}(0.6)^2 = \frac{0.2977}{h} \text{ MPa} \\ \sigma_{12} &= \left(\frac{0.4378}{h} - \frac{0.2189}{h} \right) \times 0.6 \times 0.8 = \frac{0.1051}{h} \text{ MPa}\end{aligned}$$

Thus the normal and shear forces per unit length along the fiber-matrix interface are $F_{22} = 0.2977$ MN and $F_{12} = 0.1051$ MN, whereas the force per unit length in the fiber direction is $F_{11} = 0.359$ MN.

2.3.3 Transformation of Strain Components

Since strains are also second-order tensor quantities, transformation equations derived for stresses, Eqs. (2.3.6a,b), are also valid for tensor components of strains:

$$[\varepsilon]_m = [L][\varepsilon]_p[L]^T \quad (2.3.11a)$$

$$[\varepsilon]_p = [L]^T [\varepsilon]_m [L] \quad (2.3.11b)$$

Therefore, Eqs. (2.3.7) and (2.3.9) are valid for strains when the stress components are replaced with tensor components of strains from the two coordinate systems. However, the single-column formats in Eqs. (2.3.7) and (2.3.9) for stresses are not valid for single-column formats of strains because of the definition:

$$2\varepsilon_{12} = \varepsilon_6, \quad 2\varepsilon_{13} = \varepsilon_5, \quad 2\varepsilon_{23} = \varepsilon_4 \quad (2.3.12)$$

Slight modification of the results in Eqs. (2.3.7) and (2.3.9) will yield the proper relations for the engineering components of strains. We have

$$\begin{Bmatrix} \varepsilon_{xx} \\ \varepsilon_{yy} \\ \varepsilon_{zz} \\ 2\varepsilon_{yz} \\ 2\varepsilon_{xz} \\ 2\varepsilon_{xy} \end{Bmatrix} = \begin{bmatrix} \cos^2 \theta & \sin^2 \theta & 0 & 0 & 0 & -\sin \theta \cos \theta \\ \sin^2 \theta & \cos^2 \theta & 0 & 0 & 0 & \sin \theta \cos \theta \\ 0 & 0 & 1 & 0 & 0 & 0 \\ 0 & 0 & 0 & \cos \theta & \sin \theta & 0 \\ 0 & 0 & 0 & -\sin \theta & \cos \theta & 0 \\ \sin 2\theta & -\sin 2\theta & 0 & 0 & 0 & \cos^2 \theta - \sin^2 \theta \end{bmatrix} \begin{Bmatrix} \varepsilon_1 \\ \varepsilon_2 \\ \varepsilon_3 \\ \varepsilon_4 \\ \varepsilon_5 \\ \varepsilon_6 \end{Bmatrix} \quad (2.3.13)$$

The inverse relation is given by

$$\begin{Bmatrix} \varepsilon_1 \\ \varepsilon_2 \\ \varepsilon_3 \\ \varepsilon_4 \\ \varepsilon_5 \\ \varepsilon_6 \end{Bmatrix} = \begin{bmatrix} \cos^2 \theta & \sin^2 \theta & 0 & 0 & 0 & \sin \theta \cos \theta \\ \sin^2 \theta & \cos^2 \theta & 0 & 0 & 0 & -\sin \theta \cos \theta \\ 0 & 0 & 1 & 0 & 0 & 0 \\ 0 & 0 & 0 & \cos \theta & -\sin \theta & 0 \\ 0 & 0 & 0 & \sin \theta & \cos \theta & 0 \\ -\sin 2\theta & \sin 2\theta & 0 & 0 & 0 & \cos^2 \theta - \sin^2 \theta \end{bmatrix} \begin{Bmatrix} \varepsilon_{xx} \\ \varepsilon_{yy} \\ \varepsilon_{zz} \\ 2\varepsilon_{yz} \\ 2\varepsilon_{xz} \\ 2\varepsilon_{xy} \end{Bmatrix} \quad (2.3.14)$$

We note that the transformation matrix $[T]$ in Eq. (2.3.8) is the transpose of the square matrix in Eq. (2.3.14). Similarly, the transformation matrix in Eq. (2.3.13) is the transpose of the matrix $[R]$ in Eq. (2.3.10):

$$\{\varepsilon\}_p = [R]^T \{\varepsilon\}_m, \quad \{\varepsilon\}_m = [T]^T \{\varepsilon\}_p \quad (2.3.15)$$

Example 2.3.3:

A square lamina of thickness h and planar dimension a is made of glass-epoxy material ($E_1 = 40 \times 10^3$ MPa, $E_2 = 10 \times 10^3$ MPa, $G_{12} = 3.5 \times 10^3$ MPa, and $\nu_{12} = 0.25$). When the lamina is deformed as shown in Figure 2.3.4, we wish to determine the longitudinal strain in the fiber and shear strain at the center of the lamina. The fibers are oriented at 45° to the horizontal.

From Eq. (2.3.14), the only nonzero strain is $\varepsilon_{xy} = 0.01$. Hence, longitudinal strain in the fiber is

$$\varepsilon_1 = \varepsilon_{11} = 0 + 0 + 2\varepsilon_{xy} \frac{1}{\sqrt{2}} \frac{1}{\sqrt{2}} = 0.01 \text{ cm/cm}$$

and the shear strain is given by

$$\varepsilon_6 = 2\varepsilon_{12} = 0 + 0 + 2\varepsilon_{xy} \left(\frac{1}{2} - \frac{1}{2} \right) = 0.0$$

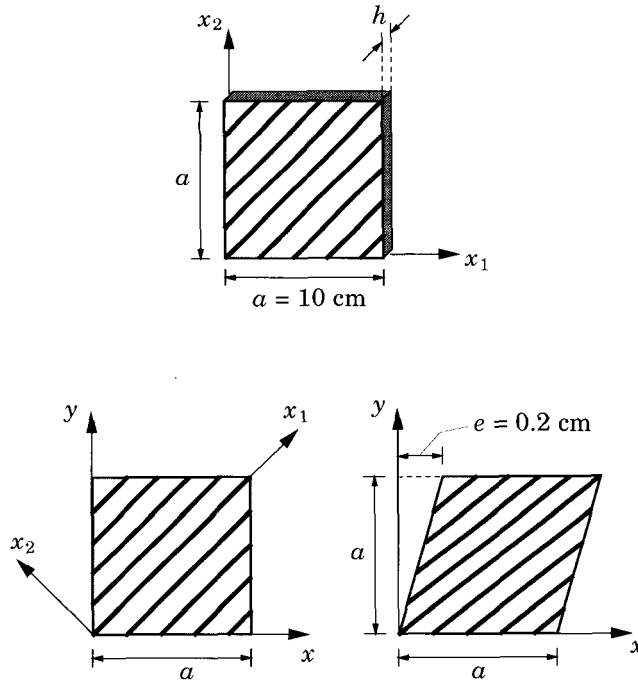


Figure 2.3.4: Deformation of a fiber-reinforced lamina.

Example 2.3.4:

Suppose that the thickness of the cylindrical pressure vessel of Example 2.3.2 is \$h = 2 \text{ cm}\$. Then the stress field in the material coordinates becomes

$$\sigma_{11} = 17.95 \text{ MPa}, \sigma_{22} = 14.885 \text{ MPa}, \sigma_{12} = 5.255 \text{ MPa}$$

The strains in the material coordinates can be calculated using the strain-stress relations (1.3.47). We have (\$\nu_{21}/E_2 = \nu_{12}/E_1\$)

$$\varepsilon_{11} = \frac{\sigma_{11}}{E_1} - \frac{\sigma_{22}\nu_{12}}{E_1} = \frac{17.95}{140} - \frac{14.885 \times 0.3}{140} = 0.0963 \text{ m/m}$$

$$\varepsilon_{22} = -\frac{\sigma_{11}\nu_{12}}{E_1} + \frac{\sigma_{22}}{E_2} = -\frac{17.95 \times 0.3}{140} + \frac{14.885}{10} = 1.45 \text{ m/m}$$

$$\varepsilon_{12} = \frac{\sigma_{12}}{2G_{12}} = \frac{5.255}{2 \times 7} = 0.3757$$

The strains in the \$(x, y)\$ coordinates can be computed using Eq. (2.3.13):

$$\varepsilon_{xx} = 0.0963 \times (0.6)^2 + 1.45 \times (0.8)^2 - 0.3757 \times 0.6 \times 0.8 = 0.782 \text{ m/m}$$

$$\varepsilon_{yy} = 0.0963 \times (0.8)^2 + 1.45 \times (0.6)^2 + 0.3757 \times 0.6 \times 0.8 = 0.764 \text{ m/m}$$

$$\varepsilon_{xy} = 2(0.0963 - 1.45) \times (0.6) \times 0.8 + 0.3757[(0.6)^2 - (0.8)^2] = -1.405$$

2.3.4 Transformation of Material Coefficients

In formulating the problem of a laminated structure, we must write the governing equations, with all their variables and coefficients, in the problem coordinates. In the previous section we discussed transformation of coordinates (which are also valid for displacements and forces), stresses, and strains. The only remaining quantities that need to be transformed from the material coordinate system to the problem coordinates are the material stiffnesses C_{ij} and thermal coefficients of expansion α_{ij} .

The material stiffnesses C_{ij} in their original form [see Eq. (1.3.35)] are the components of a fourth-order tensor. Hence, the tensor transformation law holds. The fourth-order elasticity tensor components \bar{C}_{ijkl} in the problem coordinates can be related to the components C_{mnpq} in the material coordinates by the tensor transformation law

$$\bar{C}_{ijkl} = a_{im}a_{jn}a_{kp}a_{lq}C_{mnpq}$$

However, the above equation involves five matrix multiplications with four-subscript material coefficients. Alternatively, the same result can be obtained by using the stress-strain and strain-stress relations (1.3.38a,b), and the stress and strain transformation equations in (2.3.8) and (2.3.15):

$$\{\sigma\}_p = [T]\{\sigma\}_m = [T][C]_m\{\varepsilon\}_m = [T][C]_m[T]^T\{\varepsilon\}_p \equiv [C]_p\{\varepsilon\}_p \quad (2.3.16)$$

where $[C]_m$ is the 6×6 material stiffness matrix [see Eq. (1.3.38a)] in the material coordinates and $[T]$ is the transformation matrix defined in Eq. (2.3.8). Thus the transformed material stiffness matrix is given by ($[\bar{C}] = [C]_p$ and $[C] = [C]_m$)

$$[\bar{C}] = [T][C][T]^T \quad (2.3.17)$$

Equation (2.3.17) is valid for general constitutive matrix $[C]$ (i.e., for orthotropic as well as anisotropic). Of course, $[T]$ is the matrix based on the particular transformation (2.3.1) (rotation about a transverse normal to the lamina).

Carrying out the matrix multiplications in (2.3.17) for the general anisotropic case, we obtain

$$\begin{aligned}\bar{C}_{11} &= C_{11} \cos^4 \theta - 4C_{16} \cos^3 \theta \sin \theta + 2(C_{12} + 2C_{66}) \cos^2 \theta \sin^2 \theta \\ &\quad - 4C_{26} \cos \theta \sin^3 \theta + C_{22} \sin^4 \theta \\ \bar{C}_{12} &= C_{12} \cos^4 \theta + 2(C_{16} - C_{26}) \cos^3 \theta \sin \theta + (C_{11} + C_{22} - 4C_{66}) \cos^2 \theta \sin^2 \theta \\ &\quad + 2(C_{26} - C_{16}) \cos \theta \sin^3 \theta + C_{12} \sin^4 \theta \\ \bar{C}_{13} &= C_{13} \cos^2 \theta - 2C_{36} \cos \theta \sin \theta + C_{23} \sin^2 \theta \\ \bar{C}_{16} &= C_{16} \cos^4 \theta + (C_{11} - C_{12} - 2C_{66}) \cos^3 \theta \sin \theta + 3(C_{26} - C_{16}) \cos^2 \theta \sin^2 \theta \\ &\quad + (2C_{66} + C_{12} - C_{22}) \cos \theta \sin^3 \theta - C_{26} \sin^4 \theta \\ \bar{C}_{22} &= C_{22} \cos^4 \theta + 4C_{26} \cos^3 \theta \sin \theta + 2(C_{12} + 2C_{66}) \cos^2 \theta \sin^2 \theta \\ &\quad + 4C_{16} \cos \theta \sin^3 \theta + C_{11} \sin^4 \theta \\ \bar{C}_{23} &= C_{23} \cos^2 \theta + 2C_{36} \cos \theta \sin \theta + C_{13} \sin^2 \theta\end{aligned}$$

$$\begin{aligned}
\bar{C}_{26} &= C_{26} \cos^4 \theta + (C_{12} - C_{22} + 2C_{66}) \cos^3 \theta \sin \theta + 3(C_{16} - C_{26}) \cos^2 \theta \sin^2 \theta \\
&\quad + (C_{11} - C_{12} - 2C_{66}) \cos \theta \sin^3 \theta - C_{16} \sin^4 \theta \\
\bar{C}_{33} &= C_{33} \\
\bar{C}_{36} &= (C_{13} - C_{23}) \cos \theta \sin \theta + C_{36}(\cos^2 \theta - \sin^2 \theta) \\
\bar{C}_{66} &= 2(C_{16} - C_{26}) \cos^3 \theta \sin \theta + (C_{11} + C_{22} - 2C_{12} - 2C_{66}) \cos^2 \theta \sin^2 \theta \\
&\quad + 2(C_{26} - C_{16}) \cos \theta \sin^3 \theta + C_{66}(\cos^4 \theta + \sin^4 \theta) \\
\bar{C}_{44} &= C_{44} \cos^2 \theta + C_{55} \sin^2 \theta + 2C_{45} \cos \theta \sin \theta \\
\bar{C}_{45} &= C_{45}(\cos^2 \theta - \sin^2 \theta) + (C_{55} - C_{44}) \cos \theta \sin \theta \\
\bar{C}_{55} &= C_{55} \cos^2 \theta + C_{44} \sin^2 \theta - 2C_{45} \cos \theta \sin \theta \\
\bar{C}_{14} &= C_{14} \cos^3 \theta + (C_{15} - 2C_{46}) \cos^2 \theta \sin \theta + (C_{24} - 2C_{56}) \cos \theta \sin^2 \theta + C_{25} \sin^3 \theta \\
\bar{C}_{15} &= C_{15} \cos^3 \theta - (C_{14} + 2C_{56}) \cos^2 \theta \sin \theta + (C_{25} + 2C_{46}) \cos \theta \sin^2 \theta - C_{24} \sin^3 \theta \\
\bar{C}_{24} &= C_{24} \cos^3 \theta + (C_{25} + 2C_{46}) \cos^2 \theta \sin \theta + (C_{14} + 2C_{56}) \cos \theta \sin^2 \theta + C_{15} \sin^3 \theta \\
\bar{C}_{25} &= C_{25} \cos^3 \theta + (2C_{56} - C_{24}) \cos^2 \theta \sin \theta + (C_{15} - 2C_{46}) \cos \theta \sin^2 \theta - C_{14} \sin^3 \theta \\
\bar{C}_{34} &= C_{34} \cos \theta + C_{35} \sin \theta \\
\bar{C}_{35} &= C_{35} \cos \theta - C_{34} \sin \theta \\
\bar{C}_{46} &= C_{46} \cos^3 \theta + (C_{56} + C_{14} - C_{24}) \cos^2 \theta \sin \theta + (C_{15} - C_{25} - C_{46}) \cos \theta \sin^2 \theta \\
&\quad - C_{56} \sin^3 \theta \\
\bar{C}_{56} &= C_{56} \cos^3 \theta + (C_{15} - C_{25} - C_{46}) \cos^2 \theta \sin \theta + (C_{24} - C_{14} - C_{56}) \cos \theta \sin^2 \theta \\
&\quad + C_{46} \sin^3 \theta
\end{aligned} \tag{2.3.18}$$

When $[C]$ is the matrix corresponding to an orthotropic material, it has the form shown in Eq. (1.3.44); then Eq. (2.3.16) has the explicit form [cf. Eq. (1.3.42) for monoclinic materials]

$$\left\{ \begin{array}{l} \sigma_{xx} \\ \sigma_{yy} \\ \sigma_{zz} \\ \sigma_{yz} \\ \sigma_{xz} \\ \sigma_{xy} \end{array} \right\} = \left[\begin{array}{cccccc} \bar{C}_{11} & \bar{C}_{12} & \bar{C}_{13} & 0 & 0 & \bar{C}_{16} \\ \bar{C}_{21} & \bar{C}_{22} & \bar{C}_{23} & 0 & 0 & \bar{C}_{26} \\ \bar{C}_{31} & \bar{C}_{32} & \bar{C}_{33} & 0 & 0 & \bar{C}_{36} \\ 0 & 0 & 0 & \bar{C}_{44} & \bar{C}_{45} & 0 \\ 0 & 0 & 0 & \bar{C}_{45} & \bar{C}_{55} & 0 \\ \bar{C}_{16} & \bar{C}_{26} & \bar{C}_{36} & 0 & 0 & \bar{C}_{66} \end{array} \right] \left\{ \begin{array}{l} \varepsilon_{xx} \\ \varepsilon_{yy} \\ \varepsilon_{zz} \\ 2\varepsilon_{yz} \\ 2\varepsilon_{xz} \\ 2\varepsilon_{xy} \end{array} \right\} \tag{2.3.19}$$

where the \bar{C}_{ij} are the transformed elastic coefficients referred to the (x, y, z) coordinate system, which are related to the elastic coefficients in the material coordinates C_{ij} by Eq. (2.3.18). Note that C_{14} , C_{15} , C_{16} , C_{24} , C_{25} , C_{26} , C_{34} , C_{35} , C_{36} , C_{45} , C_{46} , and C_{56} are zero for an orthotropic material.

In order to relate compliance coefficients in the two coordinate systems, we use the strain transformation equation in Eq. (2.3.15):

$$\begin{aligned}
\{\varepsilon\}_p &= [R]^T \{\varepsilon\}_m = [R]^T ([S]_m \{\sigma\}_m) = [R]^T [S]_m ([R] \{\sigma\}_p) \\
&\equiv [S]_p \{\sigma\}_p
\end{aligned} \tag{2.3.20a}$$

Thus the compliance coefficients \bar{S}_{ij} referred to the (x, y, z) system are related to the compliance coefficients S_{ij} in the material coordinates by ($[S]_p \equiv [\bar{S}]$ and $[S]_m \equiv [S]$)

$$[\bar{S}] = [R]^T [S] [R] \tag{2.3.20b}$$

Expanded form of the relations in Eq. (2.3.20b) is

$$\begin{aligned}
 \bar{S}_{11} &= S_{11} \cos^4 \theta - 2S_{16} \cos^3 \theta \sin \theta + (2S_{12} + S_{66}) \cos^2 \theta \sin^2 \theta \\
 &\quad - 2S_{26} \cos \theta \sin^3 \theta + S_{22} \sin^4 \theta \\
 \bar{S}_{12} &= S_{12} \cos^4 \theta + (S_{16} - S_{26}) \cos^3 \theta \sin \theta + (S_{11} + S_{22} - S_{66}) \cos^2 \theta \sin^2 \theta \\
 &\quad + (S_{26} - S_{16}) \cos \theta \sin^3 \theta + S_{12} \sin^4 \theta \\
 \bar{S}_{13} &= S_{13} \cos^2 \theta - S_{36} \cos \theta \sin \theta + S_{23} \sin^2 \theta \\
 \bar{S}_{16} &= S_{16} \cos^4 \theta + (2S_{11} - 2S_{12} - S_{66}) \cos^3 \theta \sin \theta + 3(S_{26} - S_{16}) \cos^2 \theta \sin^2 \theta \\
 &\quad + (S_{66} + 2S_{12} - 2S_{22}) \cos \theta \sin^3 \theta - S_{26} \sin^4 \theta \\
 \bar{S}_{22} &= S_{22} \cos^4 \theta + 2S_{26} \cos^3 \theta \sin \theta + (2S_{12} + S_{66}) \cos^2 \theta \sin^2 \theta \\
 &\quad + 2S_{16} \cos \theta \sin^3 \theta + S_{11} \sin^4 \theta \\
 \bar{S}_{23} &= S_{23} \cos^2 \theta + S_{36} \cos \theta \sin \theta + S_{13} \sin^2 \theta \\
 \bar{S}_{26} &= S_{26} \cos^4 \theta + (2S_{12} - 2S_{22} + S_{66}) \cos^3 \theta \sin \theta + 3(S_{16} - S_{26}) \cos^2 \theta \sin^2 \theta \\
 &\quad + (2S_{11} - 2S_{12} - S_{66}) \cos \theta \sin^3 \theta - S_{16} \sin^4 \theta \\
 \bar{S}_{33} &= S_{33} \\
 \bar{S}_{36} &= 2(S_{13} - S_{23}) \cos \theta \sin \theta + S_{36}(\cos^2 \theta - \sin^2 \theta) \\
 \bar{S}_{66} &= S_{66}(\cos^2 \theta - \sin^2 \theta)^2 + 4(S_{16} - S_{26})(\cos^2 \theta - \sin^2 \theta) \cos \theta \sin \theta \\
 &\quad + 4(S_{11} + S_{22} - 2S_{12}) \cos^2 \theta \sin^2 \theta \\
 \bar{S}_{44} &= S_{44} \cos^2 \theta + 2S_{45} \cos \theta \sin \theta + S_{55} \sin^2 \theta \\
 \bar{S}_{45} &= S_{45}(\cos^2 \theta - \sin^2 \theta) + (S_{55} - S_{44}) \cos \theta \sin \theta \\
 \bar{S}_{55} &= S_{55} \cos^2 \theta + S_{44} \sin^2 \theta - 2S_{45} \cos \theta \sin \theta \\
 \bar{S}_{14} &= S_{14} \cos^3 \theta + (S_{15} - S_{46}) \cos^2 \theta \sin \theta + (S_{24} - S_{56}) \cos \theta \sin^2 \theta + S_{25} \sin^3 \theta \\
 \bar{S}_{15} &= S_{15} \cos^3 \theta - (S_{14} + S_{56}) \cos^2 \theta \sin \theta + (S_{25} + S_{46}) \cos \theta \sin^2 \theta - S_{24} \sin^3 \theta \\
 \bar{S}_{24} &= S_{24} \cos^3 \theta + (S_{25} + S_{46}) \cos^2 \theta \sin \theta + (S_{14} + S_{56}) \cos \theta \sin^2 \theta + S_{15} \sin^3 \theta \\
 \bar{S}_{25} &= S_{25} \cos^3 \theta + (-S_{24} + S_{56}) \cos^2 \theta \sin \theta + (S_{15} - S_{46}) \cos \theta \sin^2 \theta - S_{14} \sin^3 \theta \\
 \bar{S}_{34} &= S_{34} \cos \theta + S_{35} \sin \theta \\
 \bar{S}_{35} &= S_{35} \cos \theta - S_{34} \sin \theta \\
 \bar{S}_{46} &= (2S_{14} - 2S_{24} + S_{56}) \cos^2 \theta \sin \theta + (2S_{15} - 2S_{25} - S_{46}) \cos \theta \sin^2 \theta \\
 &\quad + S_{46} \cos^3 \theta - S_{56} \sin^3 \theta \\
 \bar{S}_{56} &= (2S_{15} - 2S_{25} - S_{46}) \cos^2 \theta \sin \theta + (2S_{24} - 2S_{14} - S_{56}) \cos \theta \sin^2 \theta \\
 &\quad + S_{56} \cos^3 \theta + S_{46} \sin^3 \theta
 \end{aligned} \tag{2.3.21}$$

For an orthotropic material, the compliance matrix $[S]$ has the form shown in Eq. (1.3.45), and the strain-stress relations in the problem coordinates are given by

$$\left\{ \begin{array}{l} \varepsilon_{xx} \\ \varepsilon_{yy} \\ \varepsilon_{zz} \\ 2\varepsilon_{yz} \\ 2\varepsilon_{xz} \\ 2\varepsilon_{xy} \end{array} \right\} = \left[\begin{array}{cccccc} \bar{S}_{11} & \bar{S}_{12} & \bar{S}_{13} & 0 & 0 & \bar{S}_{16} \\ \bar{S}_{21} & \bar{S}_{22} & \bar{S}_{13} & 0 & 0 & \bar{S}_{26} \\ \bar{S}_{31} & \bar{S}_{32} & \bar{S}_{33} & 0 & 0 & \bar{S}_{36} \\ 0 & 0 & 0 & \bar{S}_{44} & \bar{S}_{45} & 0 \\ 0 & 0 & 0 & \bar{S}_{45} & \bar{S}_{55} & 0 \\ \bar{S}_{16} & \bar{S}_{26} & \bar{S}_{36} & 0 & 0 & \bar{S}_{66} \end{array} \right] \left\{ \begin{array}{l} \sigma_{xx} \\ \sigma_{yy} \\ \sigma_{zz} \\ \sigma_{yz} \\ \sigma_{xz} \\ \sigma_{xy} \end{array} \right\} \tag{2.3.22}$$

Note that Eq. (2.3.22) relates stresses to strains in the problem coordinates while Eq. (1.3.45) relates the stresses to strains in the material coordinates.

The thermal coefficients α_{ij} are the components of a second-order tensor, and therefore they transform like the strain components (because $\alpha_6 = 2\alpha_{12}$, and so on). In the context of the present study, only nonzero components of thermal expansion tensor are $\alpha_{11} \equiv \alpha_1$, $\alpha_{22} \equiv \alpha_2$, and $\alpha_{33} \equiv \alpha_3$. All other components are zero. Hence, following Eq. (2.3.7), we can write the transformation relations ($\alpha_6 = \alpha_{12} = 0$, $\alpha_5 = \alpha_{13} = 0$, $\alpha_4 = \alpha_{23} = 0$)

$$\begin{aligned}\alpha_{xx} &= \alpha_{11} \cos^2 \theta + \alpha_{22} \sin^2 \theta \\ \alpha_{yy} &= \alpha_{11} \sin^2 \theta + \alpha_{22} \cos^2 \theta \\ 2\alpha_{xy} &= 2(\alpha_{11} - \alpha_{22}) \sin \theta \cos \theta \\ 2\alpha_{xz} &= 0, \quad 2\alpha_{yz} = 0, \quad \alpha_{zz} = \alpha_{33}\end{aligned}\tag{2.3.23}$$

The same transformations hold for the coefficients of hygroscopic expansion. The transformation relations (2.3.18), (2.3.21), and (2.3.23) are valid for a rectangular coordinate system (x_1, x_2, x_3) which is oriented at an angle θ (in the xy -plane) from the (x, y, z) coordinate system (see Figure 2.3.1). The orientation angle θ is measured counterclockwise from the x -axis to the x_1 -axis.

In summary, Eq. (1.3.44) represents the stress-strain relations in the principal material coordinates (x_1, x_2, x_3) , and Eq. (2.3.19) represents the stress-strain relations in the (x, y, z) coordinate system. The material coefficients of the lamina in the (x, y, z) coordinate system are related to material coefficients in the material coordinates by Eq. (2.3.18). In general, for the k th layer of a laminate, the hygro-thermo-elastic stress-strain relations in the laminate coordinate system can be written as

$$\begin{aligned}\{\sigma\}_p^{(k)} &= [\bar{C}]^{(k)} \left(\{\varepsilon\}_p^{(k)} - \{\alpha_T\}_p^{(k)}(T - T_0) - \{\alpha_M\}_p^{(k)}(c - c_0) \right) \\ \{\varepsilon\}_p^{(k)} &= [\bar{S}]^{(k)} \{\sigma\}_p^{(k)} + \{\alpha_T\}_p^{(k)}(T - T_0) + \{\alpha_M\}_p^{(k)}(c - c_0)\end{aligned}\tag{2.3.24}$$

where all quantities are referred to the (x, y, z) coordinate system, and $\{\alpha_T\}$ and $\{\alpha_M\}$ are vectors of thermal and hygroscopic coefficients of expansion, respectively.

2.4 Plane Stress Constitutive Relations

Most laminates are typically thin and experience a plane state of stress (see Section 1.3.6). For a lamina in the x_1x_2 -plane, the transverse stress components are σ_{33} , σ_{13} , and σ_{23} (see Figure 2.4.1). Although these stress components are small in comparison to σ_{11} , σ_{22} , and σ_{12} , they can induce failures because fiber-reinforced composite laminates are weak in the transverse direction (because the strength providing fibers are in the x_1x_2 -plane). For this reason, the transverse shear stress components are not neglected in shear deformation theories. However, in most equivalent-single layer theories the transverse normal stress σ_{33} is neglected. Then the constitutive equations must be modified to account for this fact.

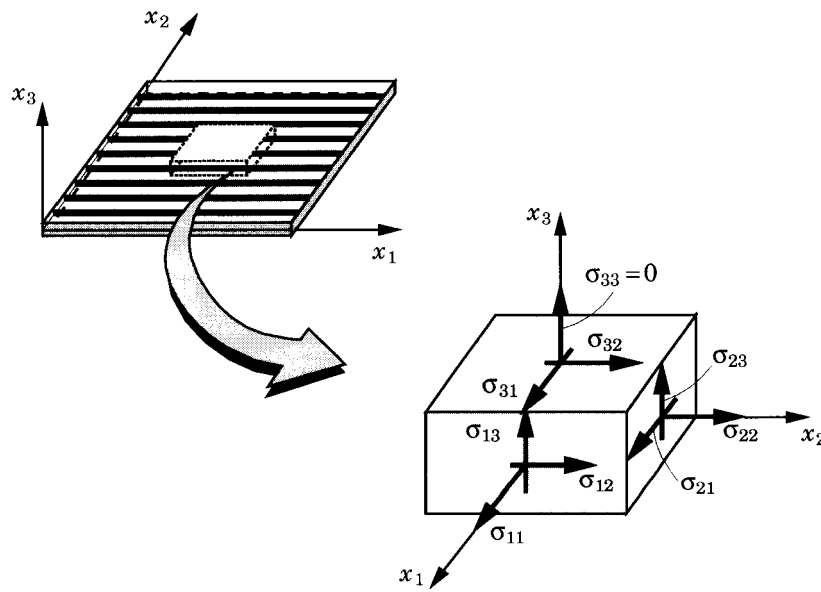


Figure 2.4.1: A lamina in a plane state of stress.

The condition $\sigma_{33} = 0$ results in the following thermoelastic constitutive equations for the k th layer that is characterized as an orthotropic lamina with piezoelectric effect:

$$\begin{Bmatrix} \sigma_1 \\ \sigma_2 \\ \sigma_6 \end{Bmatrix}^{(k)} = \begin{bmatrix} Q_{11} & Q_{12} & 0 \\ Q_{12} & Q_{22} & 0 \\ 0 & 0 & Q_{66} \end{bmatrix}^{(k)} \begin{Bmatrix} \varepsilon_1 - \alpha_1 \Delta T \\ \varepsilon_2 - \alpha_2 \Delta T \\ \varepsilon_6 \end{Bmatrix}^{(k)} - \begin{bmatrix} 0 & 0 & e_{31} \\ 0 & 0 & e_{32} \\ 0 & 0 & 0 \end{bmatrix}^{(k)} \begin{Bmatrix} \mathcal{E}_1 \\ \mathcal{E}_2 \\ \mathcal{E}_3 \end{Bmatrix}^{(k)} \quad (2.4.1)$$

$$\begin{Bmatrix} \sigma_4 \\ \sigma_5 \end{Bmatrix}^{(k)} = \begin{bmatrix} Q_{44} & 0 \\ 0 & Q_{55} \end{bmatrix}^{(k)} \begin{Bmatrix} \varepsilon_4 \\ \varepsilon_5 \end{Bmatrix}^{(k)} - \begin{bmatrix} 0 & e_{24} & 0 \\ e_{15} & 0 & 0 \end{bmatrix}^{(k)} \begin{Bmatrix} \mathcal{E}_1 \\ \mathcal{E}_2 \\ \mathcal{E}_3 \end{Bmatrix}^{(k)} \quad (2.4.2)$$

$$\begin{Bmatrix} D_1 \\ D_2 \\ D_3 \end{Bmatrix}^{(k)} = \begin{bmatrix} 0 & 0 & 0 & e_{15} & 0 \\ 0 & 0 & e_{24} & 0 & 0 \\ e_{31} & e_{32} & 0 & 0 & 0 \end{bmatrix}^{(k)} \begin{Bmatrix} \varepsilon_1 \\ \varepsilon_2 \\ \varepsilon_4 \\ \varepsilon_5 \\ \varepsilon_6 \end{Bmatrix}^{(k)} + \begin{bmatrix} \epsilon_{11} & 0 & 0 \\ 0 & \epsilon_{22} & 0 \\ 0 & 0 & \epsilon_{33} \end{bmatrix}^{(k)} \begin{Bmatrix} \mathcal{E}_1 \\ \mathcal{E}_2 \\ \mathcal{E}_3 \end{Bmatrix}^{(k)} \quad (2.4.3)$$

where $Q_{ij}^{(k)}$ are the *plane stress-reduced stiffnesses*, $e_{ij}^{(k)}$ are the piezoelectric moduli, and ϵ_{ij} are the dielectric constants of the k th lamina in its material coordinate system, $(\sigma_i, \varepsilon_i, \mathcal{E}_i, D_i)$ are the stress, strain, electric field, and electric displacement components, respectively, referred to the material coordinate system (x_1, x_2, x_3) , α_1 and α_2 are the coefficients of thermal expansion along the x_1 and x_2 directions,

respectively, and ΔT is the temperature increment from a reference state, $\Delta T = T - T_0$. Recall from Eq. (1.3.72) that $Q_{ij}^{(k)}$ are related to the engineering constants as follows:

$$Q_{11}^{(k)} = \frac{E_1^{(k)}}{1 - \nu_{12}^{(k)} \nu_{21}^{(k)}}, \quad Q_{12}^{(k)} = \frac{\nu_{12}^{(k)} E_2^{(k)}}{1 - \nu_{12}^{(k)} \nu_{21}^{(k)}}, \quad Q_{22}^{(k)} = \frac{E_2^{(k)}}{1 - \nu_{12}^{(k)} \nu_{21}^{(k)}} \quad (2.4.4a)$$

$$Q_{66}^{(k)} = G_{12}^{(k)}, \quad Q_{44}^{(k)} = G_{23}^{(k)}, \quad Q_{55}^{(k)} = G_{13}^{(k)} \quad (2.4.4b)$$

Note that the reduced stiffnesses involve six independent engineering constants: E_1 , E_2 , ν_{12} , G_{12} , G_{13} , and G_{23} .

The transformed stress-strain relations of an orthotropic lamina in a plane state of stress are (the superscript k is omitted in the interest of brevity)

$$\begin{Bmatrix} \sigma_{xx} \\ \sigma_{yy} \\ \sigma_{xy} \end{Bmatrix} = \begin{bmatrix} \bar{Q}_{11} & \bar{Q}_{12} & \bar{Q}_{16} \\ \bar{Q}_{12} & \bar{Q}_{22} & \bar{Q}_{26} \\ \bar{Q}_{16} & \bar{Q}_{26} & \bar{Q}_{66} \end{bmatrix} \left(\begin{Bmatrix} \varepsilon_{xx} \\ \varepsilon_{yy} \\ \gamma_{xy} \end{Bmatrix} - \begin{Bmatrix} \alpha_{xx} \\ \alpha_{yy} \\ 2\alpha_{xy} \end{Bmatrix} \Delta T \right) + \begin{bmatrix} 0 & 0 & \bar{e}_{31} \\ 0 & 0 & \bar{e}_{32} \\ 0 & 0 & \bar{e}_{36} \end{bmatrix} \begin{Bmatrix} \frac{\partial \psi}{\partial x} \\ \frac{\partial \psi}{\partial y} \\ \frac{\partial \psi}{\partial z} \end{Bmatrix} \quad (2.4.5)$$

$$\begin{Bmatrix} \sigma_{yz} \\ \sigma_{xz} \end{Bmatrix} = \begin{bmatrix} \bar{Q}_{44} & \bar{Q}_{45} \\ \bar{Q}_{45} & \bar{Q}_{55} \end{bmatrix} \begin{Bmatrix} \gamma_{yz} \\ \gamma_{xz} \end{Bmatrix} + \begin{bmatrix} \bar{e}_{14} & \bar{e}_{24} & 0 \\ \bar{e}_{15} & \bar{e}_{25} & 0 \end{bmatrix} \begin{Bmatrix} \frac{\partial \psi}{\partial x} \\ \frac{\partial \psi}{\partial y} \\ \frac{\partial \psi}{\partial z} \end{Bmatrix} \quad (2.4.6)$$

$$\begin{Bmatrix} D_x \\ D_y \\ D_z \end{Bmatrix} = \begin{bmatrix} 0 & 0 & \bar{e}_{14} & \bar{e}_{15} & 0 \\ 0 & 0 & \bar{e}_{24} & \bar{e}_{25} & 0 \\ \bar{e}_{31} & \bar{e}_{32} & 0 & 0 & \bar{e}_{36} \end{bmatrix} \begin{Bmatrix} \varepsilon_{xx} \\ \varepsilon_{yy} \\ \gamma_{yz} \\ \gamma_{xz} \\ \gamma_{xy} \end{Bmatrix} - \begin{bmatrix} \epsilon_{xx} & \epsilon_{xy} & 0 \\ \epsilon_{xy} & \epsilon_{yy} & 0 \\ 0 & 0 & \epsilon_{zz} \end{bmatrix} \begin{Bmatrix} \frac{\partial \psi}{\partial x} \\ \frac{\partial \psi}{\partial y} \\ \frac{\partial \psi}{\partial z} \end{Bmatrix} \quad (2.4.7)$$

where ψ denotes the scalar electric potential [see Eq. (1.3.89)] and

$$\begin{aligned} \bar{Q}_{11} &= Q_{11} \cos^4 \theta + 2(Q_{12} + 2Q_{66}) \sin^2 \theta \cos^2 \theta + Q_{22} \sin^4 \theta \\ \bar{Q}_{12} &= (Q_{11} + Q_{22} - 4Q_{66}) \sin^2 \theta \cos^2 \theta + Q_{12}(\sin^4 \theta + \cos^4 \theta) \\ \bar{Q}_{22} &= Q_{11} \sin^4 \theta + 2(Q_{12} + 2Q_{66}) \sin^2 \theta \cos^2 \theta + Q_{22} \cos^4 \theta \\ \bar{Q}_{16} &= (Q_{11} - Q_{12} - 2Q_{66}) \sin \theta \cos^3 \theta + (Q_{12} - Q_{22} + 2Q_{66}) \sin^3 \theta \cos \theta \\ \bar{Q}_{26} &= (Q_{11} - Q_{12} - 2Q_{66}) \sin^3 \theta \cos \theta + (Q_{12} - Q_{22} + 2Q_{66}) \sin \theta \cos^3 \theta \\ \bar{Q}_{66} &= (Q_{11} + Q_{22} - 2Q_{12} - 2Q_{66}) \sin^2 \theta \cos^2 \theta + Q_{66}(\sin^4 \theta + \cos^4 \theta) \\ \bar{Q}_{44} &= Q_{44} \cos^2 \theta + Q_{55} \sin^2 \theta \\ \bar{Q}_{45} &= (Q_{55} - Q_{44}) \cos \theta \sin \theta \\ \bar{Q}_{55} &= Q_{55} \cos^2 \theta + Q_{44} \sin^2 \theta \end{aligned} \quad (2.4.8)$$

α_{xx} , α_{yy} , and α_{xy} are the transformed thermal coefficients of expansion [see Eq. (2.3.23)]

$$\alpha_{xx} = \alpha_1 \cos^2 \theta + \alpha_2 \sin^2 \theta, \quad \alpha_{yy} = \alpha_1 \sin^2 \theta + \alpha_2 \cos^2 \theta, \quad \alpha_{xy} = (\alpha_1 - \alpha_2) \sin \theta \cos \theta \quad (2.4.9)$$

and \bar{e}_{ij} are the transformed piezoelectric moduli, and ϵ_{xx} , ϵ_{xy} , and ϵ_{yy} are transformed dielectric coefficients

$$\begin{aligned}\bar{e}_{31} &= e_{31} \cos^2 \theta + e_{32} \sin^2 \theta, \quad \bar{e}_{32} = e_{31} \sin^2 \theta + e_{32} \cos^2 \theta, \quad \bar{e}_{33} = e_{33} \\ \bar{e}_{36} &= (e_{31} - e_{32}) \sin \theta \cos \theta, \quad \bar{e}_{14} = (e_{15} - e_{24}) \sin \theta \cos \theta \\ \bar{e}_{24} &= e_{24} \cos^2 \theta + e_{15} \sin^2 \theta, \quad \bar{e}_{15} = e_{15} \cos^2 \theta + e_{24} \sin^2 \theta \\ \bar{e}_{25} &= (e_{15} - e_{24}) \sin \theta \cos \theta, \quad \epsilon_{xx} = \epsilon_{11} \cos^2 \theta + \epsilon_{22} \sin^2 \theta \\ \epsilon_{yy} &= \epsilon_{11} \sin^2 \theta + \epsilon_{22} \cos^2 \theta, \quad \epsilon_{xy} = (\epsilon_{11} - \epsilon_{22}) \sin \theta \cos \theta\end{aligned}\quad (2.4.10)$$

This completes the development of constitutive relations for an orthotropic lamina in a plane state of stress.

Example 2.4.1:

The material properties of graphite fabric-carbon matrix layers are (see Example 1.3.4):

$$E_1 = 25.1 \times 10^6 \text{ psi}, \quad E_2 = 4.8 \times 10^6 \text{ psi}, \quad E_3 = 0.75 \times 10^6 \text{ psi}$$

$$G_{12} = 1.36 \times 10^6 \text{ psi}, \quad G_{13} = 1.2 \times 10^6 \text{ psi}, \quad G_{23} = 0.47 \times 10^6 \text{ psi}$$

$$\nu_{12} = 0.036, \quad \nu_{13} = 0.25, \quad \nu_{23} = 0.171$$

The matrix of plane stress-reduced elastic coefficients for the material can be calculated using Eqs. (2.4.4) and (2.4.8) for various values of θ as

$$[Q]_{\theta=0} = \begin{bmatrix} 25.11 & 0.1728 & 0 & 0 & 0 \\ 0.1728 & 4.8010 & 0 & 0 & 0 \\ 0 & 0 & 0.47 & 0 & 0 \\ 0 & 0 & 0 & 1.20 & 0 \\ 0 & 0 & 0 & 0 & 1.36 \end{bmatrix} \text{ msi} \quad (2.4.11)$$

The transformed coefficients for various angles of orientation are given below:

$$[\bar{Q}]_{\theta=90} = \begin{bmatrix} 4.8010 & 0.1728 & 0 & 0 & 0 \\ 0.1728 & 25.11 & 0 & 0 & 0 \\ 0 & 0 & 1.20 & 0 & 0 \\ 0 & 0 & 0 & 0.47 & 0 \\ 0 & 0 & 0 & 0 & 1.36 \end{bmatrix} \text{ msi} \quad (2.4.12)$$

$$[\bar{Q}]_{\theta=45} = \begin{bmatrix} 8.923 & 6.203 & 0 & 0 & 5.076 \\ 6.203 & 8.923 & 0 & 0 & 5.076 \\ 0 & 0 & 0.835 & 0.365 & 0 \\ 0 & 0 & 0.365 & 0.835 & 0 \\ 5.076 & 5.076 & 0 & 0 & 7.390 \end{bmatrix} \text{ msi} \quad (2.4.13)$$

$$[\bar{Q}]_{\theta=-45} = \begin{bmatrix} 8.923 & 6.203 & 0 & 0 & -5.076 \\ 6.203 & 8.923 & 0 & 0 & -5.076 \\ 0 & 0 & 0.835 & -0.365 & 0 \\ 0 & 0 & -0.365 & 0.835 & 0 \\ -5.076 & -5.076 & 0 & 0 & 7.390 \end{bmatrix} \text{ msi} \quad (2.4.14)$$

$$[\bar{Q}]_{\theta=30} = \begin{bmatrix} 15.51 & 4.696 & 0 & 0 & 7.007 \\ 4.696 & 5.355 & 0 & 0 & 1.785 \\ 0 & 0 & 0.6525 & 0.3161 & 0 \\ 0 & 0 & 0.3161 & 1.0175 & 0 \\ 7.007 & 1.785 & 0 & 0 & 5.883 \end{bmatrix} \text{ msi} \quad (2.4.15)$$

Problems

- 2.1** Consider the composite lamina subjected to axial stress σ_1 , as shown in Fig. P2.1 below. Let E_f , v_f and A_f denote Young's modulus, volume fraction and area of cross section of the fiber, and (E_m, v_m, A_m) be the same quantities for the matrix. Assuming that plane sections remain plane during the deformation process and both matrix and fiber undergo the same longitudinal deformation Δx_1 , derive the *law of mixtures*,

$$E_1 \equiv \frac{\sigma_1}{\varepsilon_1} = v_f E_f + v_m E_m, \quad \nu_{12} \equiv -\frac{\varepsilon_2}{\varepsilon_1} = v_f v_f + v_m v_m$$

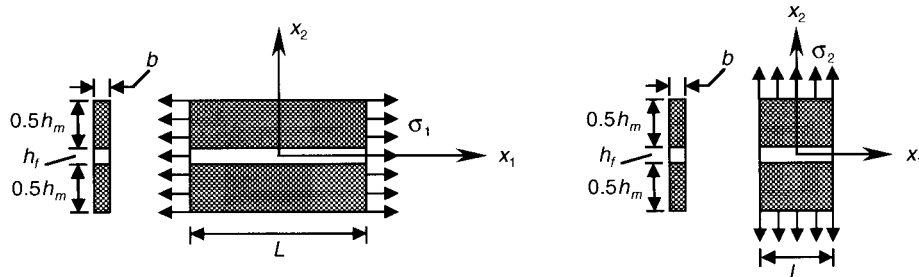


Figure P2.1

Figure P2.2

- 2.2** Consider the composite lamina of Problem 2.1 but subjected to axial stress σ_2 alone, as shown in Fig. P2.2. Derive the result

$$E_2 = \frac{E_f E_m}{E_f v_m + E_m v_f}$$

- 2.3** (Apparent moduli of an orthotropic material) Note that the transformed material compliance matrix $[\bar{S}]$ is relatively full and is in the same form as that for a monoclinic material. For an orthotropic material, we have

$$\begin{Bmatrix} \varepsilon_{xx} \\ \varepsilon_{yy} \\ 2\varepsilon_{xy} \end{Bmatrix} = \begin{bmatrix} \bar{S}_{11} & \bar{S}_{12} & \bar{S}_{16} \\ \bar{S}_{21} & \bar{S}_{22} & \bar{S}_{26} \\ \bar{S}_{16} & \bar{S}_{26} & \bar{S}_{66} \end{bmatrix} \begin{Bmatrix} \sigma_{xx} \\ \sigma_{yy} \\ \sigma_{xy} \end{Bmatrix} \quad (1)$$

where \bar{S}_{ij} are the transformed compliances defined in Eq. (2.3.21). Guided by the form of the strain-stress relations (1.3.47) in the material coordinates, we can write strain-stress relations in the problem coordinates as

$$\begin{Bmatrix} \varepsilon_{xx} \\ \varepsilon_{yy} \\ 2\varepsilon_{xy} \end{Bmatrix} = \begin{bmatrix} \frac{1}{E_x} & -\frac{\nu_{yx}}{E_y} & \frac{\eta_{xy,x}}{E_x} \\ -\frac{\nu_{xy}}{E_x} & \frac{1}{E_y} & \frac{\eta_{xy,y}}{E_y} \\ \frac{\eta_{xy,x}}{E_x} & \frac{\eta_{xy,y}}{E_y} & \frac{1}{G_{xy}} \end{bmatrix} \begin{Bmatrix} \sigma_{xx} \\ \sigma_{yy} \\ \sigma_{xy} \end{Bmatrix} \quad (2)$$

Comparing Eq. (2) with Eq. (1), we note that

$$\frac{1}{E_x} = \bar{S}_{11}, \quad -\frac{\nu_{yx}}{E_y} = \bar{S}_{12}, \quad \frac{\eta_{xy,x}}{E_x} = \bar{S}_{16}, \quad \frac{\eta_{xy,y}}{E_y} = \bar{S}_{26} \quad (3)$$

and so on. Thus, the equivalent modulus of elasticity E_x in the problem coordinates, for example, can be evaluated using the engineering constants in the material coordinate system:

$$\frac{1}{E_x} \equiv \bar{S}_{11} = S_{11} \cos^4 \theta + (2S_{12} + S_{66}) \sin^2 \theta \cos^2 \theta + S_{22} \sin^4 \theta \quad (4a)$$

where

$$S_{11} = \frac{1}{E_1}, \quad S_{12} = -\frac{\nu_{21}}{E_2}, \quad S_{22} = \frac{1}{E_2}, \quad S_{66} = \frac{1}{G_{12}} \quad (4b)$$

Thus, the apparent compliance \bar{S}_{11} in the (x, y, z) coordinate system is contributed by the compliances S_{11} , S_{12} , S_{22} , and S_{66} and the lamination angle θ :

$$\frac{1}{E_x} = \frac{1}{E_1} \cos^4 \theta + \left(-\frac{2\nu_{21}}{E_2} + \frac{1}{G_{12}} \right) \sin^2 \theta \cos^2 \theta + \frac{1}{E_2} \sin^4 \theta \quad (5)$$

We note that the compliance \bar{S}_{16} , which was zero in the material coordinates, is contributed by S_{11} , S_{12} , S_{22} , and S_{66} :

$$\bar{S}_{16} = \left(\frac{2}{E_1} + \frac{2\nu_{21}}{E_2} - \frac{1}{G_{12}} \right) \sin \theta \cos^3 \theta - \left(\frac{2}{E_2} + \frac{2\nu_{21}}{E_2} - \frac{1}{G_{12}} \right) \sin^3 \theta \cos \theta \quad (6)$$

Physically, \bar{S}_{16} represents the normal strain in the x -direction caused by the shear stress in the xy -plane, when all other stresses are zero. Since $\bar{S}_{16} = \bar{S}_{61}$, it also represents the shear strain in the xy -plane caused by the normal stress along the x -direction, when all other stresses are zero. Guided by these observations, Lekhnitskii [4] introduced the following engineering constants, called *coefficients of mutual influence*:

$\eta_{ij,i}$ = characterizes shearing in the $x_i x_j$ -plane caused by a normal stress
in the x_i -direction ($i \neq j$)

$$= \frac{2\varepsilon_{ij}}{\varepsilon_{ii}}, \quad \text{for } \sigma_{ii} \neq 0 \text{ and all other stresses being zero} \quad (7)$$

The compliance \bar{S}_{16} and \bar{S}_{26} are related, by definition, to the coefficients $\eta_{xy,x}$ and $\eta_{xy,y}$ by

$$\bar{S}_{16} = \eta_{xy,x}/E_x, \quad \bar{S}_{26} = \eta_{xy,y}/E_y \quad (8)$$

Show that

$$\frac{\eta_{xy,x}}{E_x} = \left(\frac{2}{E_1} + \frac{2\nu_{21}}{E_2} - \frac{1}{G_{12}} \right) \sin \theta \cos^3 \theta - \left(\frac{2}{E_1} + \frac{2\nu_{21}}{E_2} - \frac{1}{G_{12}} \right) \sin^3 \theta \cos \theta \quad (9)$$

$$\frac{\eta_{xy,y}}{E_y} = \left(\frac{2}{E_1} + \frac{2\nu_{21}}{E_2} - \frac{1}{G_{12}} \right) \sin^3 \theta \cos \theta - \left(\frac{2}{E_2} + \frac{2\nu_{21}}{E_2} - \frac{1}{G_{12}} \right) \sin \theta \cos^3 \theta \quad (10)$$

2.4 (Continuation of Problem 2.3) Derive an expression for G_{xy} in terms of E_1 , E_2 , ν_{12} , G_{12} , and θ .

2.5 (Continuation of Problem 2.3) Show that G_{xy} is a maximum for $\theta = 45^\circ$. Make use of the following trigonometric identities:

$$\cos^4 \theta = \frac{1}{8}(3 + 4 \cos 2\theta + \cos 4\theta)$$

$$\sin^4 \theta = \frac{1}{8}(3 - 4 \cos 2\theta + \cos 4\theta)$$

$$\cos^2 \theta \sin^2 \theta = \frac{1}{8}(1 - \cos 4\theta)$$

2.6 (Continuation of Problem 2.3) Show that the coefficient of mutual influence is zero at $\theta = 0^\circ$ and $\theta = 90^\circ$.

- 2.7** (Continuation of Problem 2.3) Show that the moduli E_x (and E_y) varies between E_1 and E_2 , but it can either exceed or get smaller than both E_1 and E_2 .
- 2.8** (Continuation of Problem 2.3) Derive the expression for E_x in terms of E_1 , E_2 , ν_{12} , G_{12} , α_1 , α_2 , and θ for the nonisothermal case.
- 2.9** (Continuation of Problem 2.3) Derive the expression for G_{xy} in terms of E_1 , E_2 , ν_{12} , G_{12} , α_1 , α_2 , and θ for the nonisothermal case.
- 2.10** Show that the following combinations of stiffness coefficients are invariant:

$$\begin{aligned} S_1 &= (3Q_{11} + 3Q_{22} + 2Q_{12} + 4Q_{66}) \\ S_2 &= (Q_{12} - Q_{66}) \\ S_3 &= (Q_{11} + Q_{22} + 2Q_{66}) \\ S_4 &= (Q_{11} + Q_{22} + 2Q_{12}) \end{aligned}$$

- 2.11** Rewrite the transformation equations (2.4.8) as

$$\begin{aligned} \bar{Q}_{11} &= U_1 + U_2 \cos 2\theta + U_3 \cos 4\theta \\ \bar{Q}_{12} &= U_4 - U_3 \cos 4\theta \\ \bar{Q}_{22} &= U_1 - U_2 \cos 2\theta + U_3 \cos 4\theta \\ \bar{Q}_{16} &= \frac{1}{2}U_2 \sin 2\theta + U_3 \sin 4\theta \\ \bar{Q}_{26} &= \frac{1}{2}U_2 \sin 2\theta - U_3 \sin 4\theta \\ \bar{Q}_{66} &= \frac{1}{2}(U_1 - U_4) - U_3 \cos 4\theta \end{aligned}$$

where

$$\begin{aligned} U_1 &= \frac{1}{8}(3Q_{11} + 3Q_{22} + 2Q_{12} + 4Q_{66}) \\ U_2 &= \frac{1}{2}(Q_{11} - Q_{22}) \\ U_3 &= \frac{1}{8}(Q_{11} + Q_{22} - 2Q_{12} - 4Q_{66}) \\ U_4 &= \frac{1}{8}(Q_{11} + Q_{22} + 6Q_{12} - 4Q_{66}) \end{aligned}$$

- 2.12** Determine the transformation matrix (i.e., direction cosines) relating the orthonormal basis vectors $(\hat{\mathbf{e}}_1, \hat{\mathbf{e}}_2, \hat{\mathbf{e}}_3)$ of the system (x_1, x_2, x_3) to the orthonormal basis $(\hat{\mathbf{e}}'_1, \hat{\mathbf{e}}'_2, \hat{\mathbf{e}}'_3)$ of the system (x'_1, x'_2, x'_3) , when $\hat{\mathbf{e}}'_1$ are given as follows: $\hat{\mathbf{e}}'_1$ is along the vector $\hat{\mathbf{e}}_1 - \hat{\mathbf{e}}_2 + \hat{\mathbf{e}}_3$ and $\hat{\mathbf{e}}'_2$ is perpendicular to the plane $2x_1 + 3x_2 + x_3 - 5 = 0$.
- 2.13** Verify the transformation relations for the piezoelectric moduli given in Eq. (2.4.10).
- 2.14** Consider a square, graphite-epoxy lamina of length 8 in., width 2 in., and thickness 0.005 in., and subjected to an axial load of 1000 lbs. Determine the transverse normal strain ε_3 . Assume that the load is applied parallel to the fibers, and use $E_1 = 20$ msi, $E_2 = 1.3$ msi, $G_{12} = G_{13} = 1.03$ msi, $G_{23} = 0.9$ msi, $\nu_{12} = \nu_{13} = 0.3$, and $\nu_{23} = 0.49$.
- 2.15** Compute the numerical values of the reduced stiffnesses Q_{ij} for the graphite-epoxy material of Problem 2.14. *Ans:*

$$[Q] = \begin{bmatrix} 20.118 & 0.392 & 0 & 0 & 0 \\ 0.392 & 1.308 & 0 & 0 & 0 \\ 0 & 0 & 0.9 & 0 & 0 \\ 0 & 0 & 0 & 1.03 & 0 \\ 0 & 0 & 0 & 0 & 1.03 \end{bmatrix} \text{ msi}$$

2.16 The material properties of AS/3501 graphite-epoxy material layers are

$$E_1 = 140 \times 10^3 \text{ MPa}, E_2 = 10 \times 10^3 \text{ MPa}, G_{12} = 7 \times 10^3 \text{ MPa}$$

$$G_{13} = 7 \times 10^3 \text{ MPa}, G_{23} = 7 \times 10^3 \text{ MPa}, \nu_{12} = 0.3$$

$$\alpha_1 = 1.0 \times 10^{-6} \text{ m/m/}^\circ\text{K}, \alpha_2 = 30 \times 10^{-6} \text{ m/m/}^\circ\text{K}$$

Show that (1 GPa = 10^3 MPa = 10^9 Pa)

$$[Q] = \begin{bmatrix} 140.90 & 3.02 & 0 & 0 & 0 \\ 3.02 & 10.06 & 0 & 0 & 0 \\ 0 & 0 & 7 & 0 & 0 \\ 0 & 0 & 0 & 7 & 0 \\ 0 & 0 & 0 & 0 & 7 \end{bmatrix} \text{ GPa}$$

The transformed coefficients for various angles of orientation are given below:

$$[\bar{Q}]_{\theta=90} = \begin{bmatrix} 10.06 & 3.02 & 0 & 0 & 0 \\ 3.02 & 140.9 & 0 & 0 & 0 \\ 0 & 0 & 7 & 0 & 0 \\ 0 & 0 & 0 & 7 & 0 \\ 0 & 0 & 0 & 0 & 7 \end{bmatrix} \text{ GPa}$$

$$[\bar{Q}]_{\theta=45} = \begin{bmatrix} 46.25 & 32.25 & 0 & 0 & 32.71 \\ 32.25 & 46.25 & 0 & 0 & 32.71 \\ 0 & 0 & 7 & 0 & 0 \\ 0 & 0 & 0 & 7 & 0 \\ 32.71 & 32.71 & 0 & 0 & 36.23 \end{bmatrix} \text{ GPa}$$

Also, compute the transformed thermal coefficients of expansion for $\theta = 45^\circ$.

References for Additional Reading

1. Ambartsumyan, S. A., *Theory of Anisotropic Shells*, NASA Report TT F-118 (1964).
2. Ambartsumyan, S. A., *Theory of Anisotropic Plates*, Izdat. Nauka, Moskva (1967), English translation by Technomic, Stamford, CT (1969).
3. Jones, R. M., *Mechanics of Composite Materials*, Second Edition, Taylor & Francis, PA (1999).
4. Lekhnitskii, S. G., *Theory of Elasticity of an Anisotropic Body*, Mir Publishers, Moscow (1982).
5. Christensen, R. M., *Mechanics of Composite Materials*, John Wiley, New York (1979).
6. Tsai, S. W. and Hahn, H. T., *Introduction to Composite Materials*, Technomic, Lancaster, PA (1980).
7. Agarwal, B. D. and Broutman, L. J., *Analysis and Performance of Fiber Composites*, John Wiley, New York (1980).
8. Reddy, J. N., *Energy Principles and Variational Methods in Applied Mechanics*, Second Edition, John Wiley, New York (2002).
9. Vinson, J. R. and Sierakowski, R. L., *The Behavior of Structures Composed of Composite Materials*, Kluwer, The Netherlands (1986).
10. Mallick, P. K., *Fiber-Reinforced Composites*, Marcel Dekker, New York (1988).
11. Gibson, R. F., *Principles of Composite Material Mechanics*, McGraw-Hill, New York (1994).
12. Parton, V. Z. and Kudryavtsev, B. A., *Engineering Mechanics of Composite Structures*, CRC Press, Boca Raton, FL (1993).

13. Reddy, J. N. (Ed.), *Mechanics of Composite Materials. Selected Works of Nicholas J. Pagano*, Kluwer, The Netherlands (1994).
14. Adams, D. F. and Doner, D. R., "Longitudinal Shear Loading of a Unidirectional Composite," *Journal of Composite Materials*, **1**, 4–17 (1967).
15. Adams, D. F. and Doner, D. R., "Transverse Normal Loading of a Unidirectional Composite," *Journal of Composite Materials*, **1**, 152–164 (1967).
16. Ishikawa, T., Koyama, K., and Kobayashi, S., "Thermal Expansion Coefficients of Unidirectional Composites," *Journal of Composite Materials*, **12**, 153–168 (1978).
17. Halpin, J. C. and Tsai, S. W., "Effects of Environmental Factors on Composite Materials," AFML-TR-67-423, Air Force Flight Mechanics Laboratory, Dayton, OH (1969).
18. Tsai, S. W., *Structural Behavior of Composite Materials*, NASA CR-71, (1964).
19. Chamis, C. C. and Sendeckyj, G. P., "Critique on Theories Predicting Thermoelastic Properties of Fibrous Composites," *Journal of Composite Materials*, 332–358 (1968).
20. Zhang, G. and June, R. R., "An Analytical and Numerical Study of Fiber Microp buckling," *Composite Science and Technology*, **51**, 95–109 (1994).

Classical and First-Order Theories of Laminated Composite Plates

3.1 Introduction

3.1.1 Preliminary Comments

Composite laminates are formed by stacking layers of different composite materials and/or fiber orientation. By construction, composite laminates have their planar dimensions one to two orders of magnitude larger than their thickness. Often laminates are used in applications that require membrane and bending strengths. Therefore, composite laminates are treated as plate elements.

The objective of this chapter is to develop two commonly used laminate plate theories, namely the classical plate theory and the first-order shear deformation plate theory. To provide a background for the theories discussed in this chapter, an overview of pertinent literature on laminate plate theories is included here.

3.1.2 Classification of Structural Theories

Analyses of composite plates in the past have been based on one of the following approaches:

- (1) Equivalent single-layer theories (2-D)
 - (a) Classical laminated plate theory
 - (b) Shear deformation laminated plate theories
- (2) Three-dimensional elasticity theory (3-D)
 - (a) Traditional 3-D elasticity formulations
 - (b) Layerwise theories
- (3) Multiple model methods (2-D and 3-D)

The equivalent single layer (ESL) plate theories are derived from the 3-D elasticity theory by making suitable assumptions concerning the kinematics of deformation or the stress state through the thickness of the laminate. These assumptions allow the reduction of a 3-D problem to a 2-D problem. In the three-dimensional elasticity theory or in a layerwise theory, each layer is modeled as a 3-D solid. In this chapter, we present the classical plate theory and the first-order shear deformation plate theory as applied to laminated plates. Literature reviews and development of the governing equations of the third-order shear deformation plate theory and the layerwise theory will be presented in later chapters (see Chapters 11 and 12).

3.2 An Overview of Laminated Plate Theories

The equivalent single layer laminated plate theories are those in which a heterogeneous laminated plate is treated as a statically equivalent single layer having a complex constitutive behavior, reducing the 3-D continuum problem to a 2-D problem. The ESL theories are developed by assuming the form of the displacement field or stress field as a linear combination of unknown functions and the thickness coordinate [1–13]:

$$\varphi_i(x, y, z, t) = \sum_{j=0}^N (z)^j \varphi_i^j(x, y, t) \quad (3.2.1)$$

where φ_i is the i th component of displacement or stress, (x, y) the in-plane coordinates, z the thickness coordinate, t the time, and φ_i^j are functions to be determined.

When φ_i are displacements, then the equations governing φ_i^j are determined by the principle of virtual displacements (or its dynamic version when time dependency is to be included; see Section 1.4):

$$0 = \int_0^T (\delta U + \delta V - \delta K) dt \quad (3.2.2)$$

where δU , δV , and δK denote the virtual strain energy, virtual work done by external applied forces, and the virtual kinetic energy, respectively. These quantities are determined in terms of actual stresses and virtual strains, which depend on the assumed displacement functions, φ_i and their variations. For plate structures, laminated or not, the integration over the domain of the plate is represented as the (tensor) product of integration over the plane of the plate and integration over the thickness of the plate, because of the explicit nature of the assumed displacement field in the thickness coordinate:

$$\int_{Vol.} (\cdot) dV = \int_{-\frac{h}{2}}^{\frac{h}{2}} \int_{\Omega_0} (\cdot) d\Omega dz \quad (3.2.3)$$

where h denotes the total thickness of the plate, and Ω_0 denotes the undeformed midplane of the plate, which is chosen as the reference plane. Since all functions are explicit in the thickness coordinate, the integration over plate thickness is carried out explicitly, reducing the problem to a two dimensional one. Consequently, the Euler–Lagrange equations of Eq. (3.2.2) consist of differential equations involving the dependent variables $\varphi_i^j(x, y, t)$ and thickness-averaged stress resultants, $R_{ij}^{(m)}$:

$$R_{ij}^{(m)} = \int_{-\frac{h}{2}}^{\frac{h}{2}} (z)^m \sigma_{ij} dz \quad (3.2.4)$$

The resultants can be written in terms of φ_i with the help of the assumed constitutive equations (stress-strain relations) and strain-displacement relations. More complete development of this procedure is forthcoming in this chapter.

The same approach is used when φ_i denote stress components, except that the basis of the derivation of the governing equations is the principle of virtual forces. In

the present book, the stress-based theories will not be developed. Readers interested in stress-based theories may consult the book by Panc [14].

The simplest ESL laminated plate theory is the *classical laminated plate theory* (or CLPT) [15–20], which is an extension of the Kirchhoff (classical) plate theory to laminated composite plates. It is based on the displacement field

$$\begin{aligned} u(x, y, z, t) &= u_0(x, y, t) - z \frac{\partial w_0}{\partial x} \\ v(x, y, z, t) &= v_0(x, y, t) - z \frac{\partial w_0}{\partial y} \\ w(x, y, z, t) &= w_0(x, y, t) \end{aligned} \quad (3.2.5)$$

where (u_0, v_0, w_0) are the displacement components along the (x, y, z) coordinate directions, respectively, of a point on the midplane (i.e., $z = 0$). The displacement field (3.2.5) implies that straight lines normal to the xy -plane before deformation remain straight and normal to the midsurface after deformation. The Kirchhoff assumption amounts to neglecting both transverse shear and transverse normal effects; i.e., deformation is due entirely to bending and in-plane stretching.

The next theory in the hierarchy of ESL laminated plate theories is the *first-order shear deformation theory* (or FSDT) [21–27], which is based on the displacement field

$$\begin{aligned} u(x, y, z, t) &= u_0(x, y, t) + z\phi_x(x, y, t) \\ v(x, y, z, t) &= v_0(x, y, t) + z\phi_y(x, y, t) \\ w(x, y, z, t) &= w_0(x, y, t) \end{aligned} \quad (3.2.6)$$

where ϕ_x and $-\phi_y$ denote rotations about the y and x axes, respectively. The FSDT extends the kinematics of the CLPT by including a gross transverse shear deformation in its kinematic assumptions; i.e., the transverse shear strain is assumed to be constant with respect to the thickness coordinate. Inclusion of this rudimentary form of shear deformation allows the normality restriction of the classical laminate theory to be relaxed. The first-order shear deformation theory requires shear correction factors (see [28–32]), which are difficult to determine for arbitrarily laminated composite plate structures. The shear correction factors depend not only on the lamination and geometric parameters, but also on the loading and boundary conditions.

In both CLPT and FSDT, the plane-stress state assumption is used and plane-stress reduced form of the constitutive law of Section 2.4 is used. In both theories the inextensibility and/or straightness of transverse normals can be removed. Such extensions lead to second- and higher-order theories of plates.

Second- and higher-order ESL laminated plate theories use higher-order polynomials [i.e., $N > 1$ in Eq. (3.2.1)] in the expansion of the displacement components through the thickness of the laminate (see [33–38], among many others). The higher-order theories introduce additional unknowns that are often difficult to interpret in physical terms. The second-order theory with transverse inextensibility is based on the displacement field

$$\begin{aligned} u(x, y, z, t) &= u_0(x, y, t) + z\phi_x(x, y, t) + z^2\psi_x(x, y, t) \\ v(x, y, z, t) &= v_0(x, y, t) + z\phi_y(x, y, t) + z^2\psi_y(x, y, t) \\ w(x, y, z, t) &= w_0(x, y, t) \end{aligned} \quad (3.2.7)$$

The *third-order laminated plate theory* of Reddy [38,39] with transverse inextensibility is based on the displacement field

$$\begin{aligned} u(x, y, z, t) &= u_0(x, y, t) + z\phi_x(x, y, t) + z^3 \left(-\frac{4}{3h^2} \right) \left(\phi_x + \frac{\partial w_0}{\partial x} \right) \\ v(x, y, z, t) &= v_0(x, y, t) + z\phi_y(x, y, t) + z^3 \left(-\frac{4}{3h^2} \right) \left(\phi_y + \frac{\partial w_0}{\partial y} \right) \\ w(x, y, z, t) &= w_0(x, y, t) \end{aligned} \quad (3.2.8)$$

The displacement field accommodates quadratic variation of transverse shear strains (and hence stresses) and vanishing of transverse shear stresses on the top and bottom of a general laminate composed of monoclinic layers. Thus there is no need to use shear correction factors in a third-order theory. The third-order theories provide a slight increase in accuracy relative to the FSDT solution, at the expense of an increase in computational effort. Further, finite element models of third-order theories that satisfy the vanishing of transverse shear stresses on the bounding planes require continuity of the transverse deflection and its derivatives between elements. Complete derivations of the governing equations of the third-order laminated plate theory and their solutions are presented in Chapter 11.

In addition to their inherent simplicity and low computational cost, the ESL models often provide a sufficiently accurate description of global response for thin to moderately thick laminates, e.g., gross deflections, critical buckling loads, and fundamental vibration frequencies and associated mode shapes. Of the ESL theories, the FSDT with transverse extensibility appears to provide the best compromise of solution accuracy, economy, and simplicity. However, the ESL models have limitations that prevent them from being used to solve the whole spectrum of composite laminate problems. First, the accuracy of the global response predicted by the ESL models deteriorates as the laminate becomes thicker. Second, the ESL models are often incapable of accurately describing the state of stress and strain at the ply level near geometric and material discontinuities or near regions of intense loading – the areas where accurate stresses are needed most. In such cases, 3-D theories or multiple model approaches are required (see Chapter 12 for the layerwise theory and multiple model approaches).

This completes an overview of various ESL theories. For additional discussion and references, one may consult the review articles [40–43]. In the remaining sections of this chapter, we study the classical and first-order shear deformation plate theories for laminated plates [44–52].

3.3 The Classical Laminated Plate Theory

3.3.1 Assumptions

The classical laminated plate theory is an extension of the classical plate theory to composite laminates. In the *classical laminated plate theory* (CLPT) it is assumed[†] that the *Kirchhoff hypothesis* holds:

[†] An assumption is that which is necessary for the development of the mathematical model, whereas a restriction is not a necessary condition for the development of the theory.

- (1) Straight lines perpendicular to the midsurface (i.e., transverse normals) before deformation remain straight after deformation.
- (2) The transverse normals do not experience elongation (i.e., they are inextensible).
- (3) The transverse normals rotate such that they remain perpendicular to the midsurface after deformation.

The first two assumptions imply that the transverse displacement is independent of the transverse (or thickness) coordinate and the transverse normal strain ε_{zz} is zero. The third assumption results in zero transverse shear strains, $\varepsilon_{xz} = 0, \varepsilon_{yz} = 0$.

3.3.2 Displacements and Strains

Consider a plate of total thickness h composed of N orthotropic layers with the principal material coordinates (x_1^k, x_2^k, x_3^k) of the k th lamina oriented at an angle θ_k to the laminate coordinate, x . Although not necessary, it is convenient to take the xy -plane of the problem in the undeformed midplane Ω_0 of the laminate (see Figure 3.3.1). The z -axis is taken positive downward from the midplane. The k th layer is located between the points $z = z_k$ and $z = z_{k+1}$ in the thickness direction.

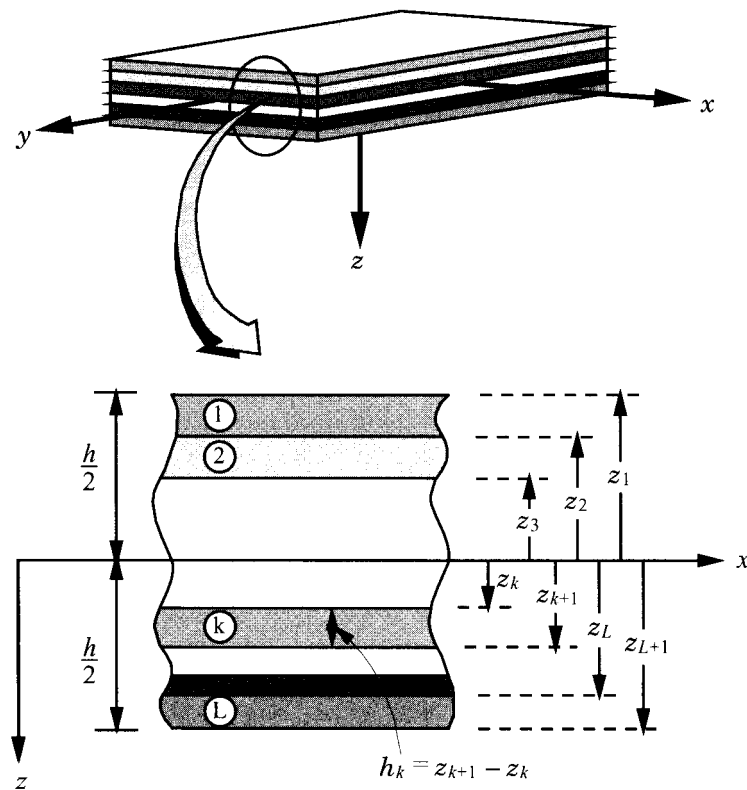


Figure 3.3.1: Coordinate system and layer numbering used for a laminated plate.

The total domain $\bar{\Omega}_0$ of the laminate is the tensor product of $\Omega_0 \times (-h/2, h/2)$. The boundary of $\bar{\Omega}_0$ consists of top surface $S_t(z = -h/2)$ and bottom surfaces $S_b(z = h/2)$, and the edge $\bar{\Gamma} \equiv \Gamma \times (-h/2, h/2)$ of the laminate. In general, Γ is a curved surface, with outward normal $\hat{\mathbf{n}} = n_x \hat{\mathbf{e}}_x + n_y \hat{\mathbf{e}}_y$. Different parts of the boundary $\bar{\Gamma}$ are subjected to, in general, a combination of generalized forces and generalized displacements. A discussion of the boundary conditions is presented in the sequel.

In formulating the theory, we make certain assumptions or place restrictions, as stated here:

- The layers are perfectly bonded together (assumption).
- The material of each layer is linearly elastic and has three planes of material symmetry (i.e., orthotropic) (restriction).
- Each layer is of uniform thickness (restriction).
- The strains and displacements are small (restriction).
- The transverse shear stresses on the top and bottom surfaces of the laminate are zero (restriction).

By the Kirchhoff assumptions, a material point occupying the position (x, y, z) in the undeformed laminate moves to the position $(x + u, y + v, z + w)$ in the deformed laminate, where (u, v, w) are the components of the total displacement vector \mathbf{u} along the (x, y, z) coordinates. We have

$$\mathbf{u} = u\hat{\mathbf{e}}_x + v\hat{\mathbf{e}}_y + w\hat{\mathbf{e}}_z \quad (3.3.1)$$

where $(\hat{\mathbf{e}}_x, \hat{\mathbf{e}}_y, \hat{\mathbf{e}}_z)$ are unit vectors along the (x, y, z) coordinates. Due to small strain and small displacement assumption, no distinction is made between the material coordinates and spatial coordinates, between the finite Green strain tensor and infinitesimal strain tensor, and between the second Piola–Kirchhoff stress tensor and the Cauchy stress tensor (see Chapter 1). The Kirchhoff hypothesis requires the displacements (u, v, w) to be such that (see Figure 3.3.2)

$$\begin{aligned} u(x, y, z, t) &= u_0(x, y, t) - z \frac{\partial w_0}{\partial x} \\ v(x, y, z, t) &= v_0(x, y, t) - z \frac{\partial w_0}{\partial y} \\ w(x, y, z, t) &= w_0(x, y, t) \end{aligned} \quad (3.3.2)$$

where (u_0, v_0, w_0) are the displacements along the coordinate lines of a material point on the xy -plane. Note that the form of the displacement field (3.3.1) allows reduction of the 3-D problem to one of studying the deformation of the reference plane $z = 0$ (or midplane). Once the midplane displacements (u_0, v_0, w_0) are known, the displacements of any arbitrary point (x, y, z) in the 3-D continuum can be determined using Eq. (3.3.2).

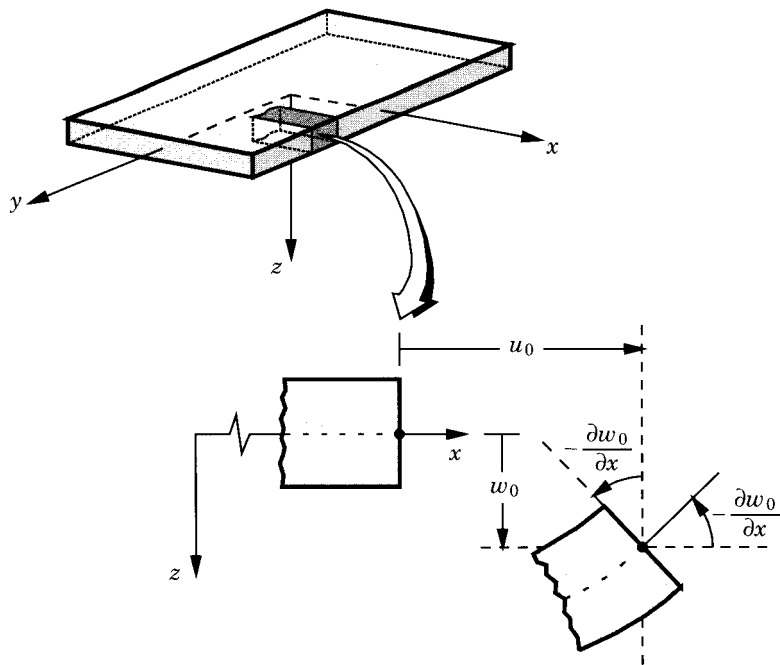


Figure 3.3.2: Undeformed and deformed geometries of an edge of a plate under the Kirchhoff assumptions.

The strains associated with the displacement field (3.3.2) can be computed using either the nonlinear strain-displacement relations (1.3.10) or the linear strain-displacement relations (1.3.12). The nonlinear strains are given by

$$\begin{aligned}
 E_{xx} &= \frac{\partial u}{\partial x} + \frac{1}{2} \left[\left(\frac{\partial u}{\partial x} \right)^2 + \left(\frac{\partial v}{\partial x} \right)^2 + \left(\frac{\partial w}{\partial x} \right)^2 \right] \\
 E_{yy} &= \frac{\partial v}{\partial y} + \frac{1}{2} \left[\left(\frac{\partial u}{\partial y} \right)^2 + \left(\frac{\partial v}{\partial y} \right)^2 + \left(\frac{\partial w}{\partial y} \right)^2 \right] \\
 E_{zz} &= \frac{\partial w}{\partial z} + \frac{1}{2} \left[\left(\frac{\partial u}{\partial z} \right)^2 + \left(\frac{\partial v}{\partial z} \right)^2 + \left(\frac{\partial w}{\partial z} \right)^2 \right] \\
 E_{xy} &= \frac{1}{2} \left(\frac{\partial u}{\partial y} + \frac{\partial v}{\partial x} + \frac{\partial u}{\partial x} \frac{\partial u}{\partial y} + \frac{\partial v}{\partial x} \frac{\partial v}{\partial y} + \frac{\partial w}{\partial x} \frac{\partial w}{\partial y} \right) \\
 E_{xz} &= \frac{1}{2} \left(\frac{\partial u}{\partial z} + \frac{\partial w}{\partial x} + \frac{\partial u}{\partial x} \frac{\partial u}{\partial z} + \frac{\partial v}{\partial x} \frac{\partial v}{\partial z} + \frac{\partial w}{\partial x} \frac{\partial w}{\partial z} \right) \\
 E_{yz} &= \frac{1}{2} \left(\frac{\partial v}{\partial z} + \frac{\partial w}{\partial y} + \frac{\partial u}{\partial y} \frac{\partial u}{\partial z} + \frac{\partial v}{\partial y} \frac{\partial v}{\partial z} + \frac{\partial w}{\partial y} \frac{\partial w}{\partial z} \right)
 \end{aligned} \tag{3.3.3}$$

If the components of the displacement gradients are of the order ϵ , i.e.,

$$\frac{\partial u}{\partial x}, \frac{\partial u}{\partial y}, \frac{\partial v}{\partial x}, \frac{\partial v}{\partial y}, \frac{\partial w}{\partial z} = O(\epsilon) \quad (3.3.4)$$

then the small strain assumption implies that terms of the order ϵ^2 are negligible in the strains. Terms of order ϵ^2 are

$$\begin{aligned} & \left(\frac{\partial u}{\partial x} \right)^2, \left(\frac{\partial u}{\partial y} \right)^2, \left(\frac{\partial u}{\partial z} \right)^2, \left(\frac{\partial u}{\partial x} \right) \left(\frac{\partial u}{\partial y} \right), \left(\frac{\partial u}{\partial x} \right) \left(\frac{\partial u}{\partial z} \right), \left(\frac{\partial u}{\partial y} \right) \left(\frac{\partial u}{\partial z} \right) \\ & \left(\frac{\partial v}{\partial x} \right)^2, \left(\frac{\partial v}{\partial y} \right)^2, \left(\frac{\partial v}{\partial z} \right)^2, \left(\frac{\partial v}{\partial x} \right) \left(\frac{\partial v}{\partial y} \right), \left(\frac{\partial v}{\partial x} \right) \left(\frac{\partial v}{\partial z} \right), \left(\frac{\partial v}{\partial y} \right) \left(\frac{\partial v}{\partial z} \right) \\ & \left(\frac{\partial w}{\partial x} \right) \left(\frac{\partial w}{\partial z} \right), \left(\frac{\partial w}{\partial y} \right) \left(\frac{\partial w}{\partial z} \right), \left(\frac{\partial w}{\partial z} \right)^2 \end{aligned} \quad (3.3.5)$$

If the rotations $\partial w_0/\partial x$ and $\partial w_0/\partial y$ of transverse normals are moderate (say 10° – 15°), then the following terms are small but *not* negligible compared to ϵ :

$$\left(\frac{\partial w}{\partial x} \right)^2, \left(\frac{\partial w}{\partial y} \right)^2, \frac{\partial w}{\partial x} \frac{\partial w}{\partial y} \quad (3.3.6)$$

and they should be included in the strain-displacement relations. Thus for small strains and moderate rotations cases the strain-displacement relations (3.3.3) take the form

$$\begin{aligned} \varepsilon_{xx} &= \frac{\partial u}{\partial x} + \frac{1}{2} \left(\frac{\partial w}{\partial x} \right)^2, \quad \varepsilon_{xy} = \frac{1}{2} \left(\frac{\partial u}{\partial y} + \frac{\partial v}{\partial x} + \frac{\partial w}{\partial x} \frac{\partial w}{\partial y} \right) \\ \varepsilon_{xz} &= \frac{1}{2} \left(\frac{\partial u}{\partial z} + \frac{\partial w}{\partial x} \right), \quad \varepsilon_{yy} = \frac{\partial v}{\partial y} + \frac{1}{2} \left(\frac{\partial w}{\partial y} \right)^2 \\ \varepsilon_{yz} &= \frac{1}{2} \left(\frac{\partial v}{\partial z} + \frac{\partial w}{\partial y} \right), \quad \varepsilon_{zz} = \frac{\partial w}{\partial z} \end{aligned} \quad (3.3.7)$$

where, for this special case of geometric nonlinearity (i.e., small strains but moderate rotations), the notation ε_{ij} is used in place of E_{ij} . The corresponding second Piola-Kirchhoff stresses will be denoted σ_{ij} .

For the assumed displacement field in Eq. (3.3.2), $\partial w/\partial z = 0$. In view of the assumptions in Eqs. (3.3.4)–(3.3.6), the strains in Eq. (3.3.7) reduce to

$$\begin{aligned} \varepsilon_{xx} &= \frac{\partial u_0}{\partial x} + \frac{1}{2} \left(\frac{\partial w_0}{\partial x} \right)^2 - z \frac{\partial^2 w_0}{\partial x^2} \\ \varepsilon_{xy} &= \frac{1}{2} \left(\frac{\partial u_0}{\partial y} + \frac{\partial v_0}{\partial x} + \frac{\partial w_0}{\partial x} \frac{\partial w_0}{\partial y} \right) - z \frac{\partial^2 w_0}{\partial x \partial y} \\ \varepsilon_{yy} &= \frac{\partial v_0}{\partial y} + \frac{1}{2} \left(\frac{\partial w_0}{\partial y} \right)^2 - z \frac{\partial^2 w_0}{\partial y^2} \\ \varepsilon_{xz} &= \frac{1}{2} \left(-\frac{\partial w_0}{\partial x} + \frac{\partial w_0}{\partial x} \right) = 0 \\ \varepsilon_{yz} &= \frac{1}{2} \left(-\frac{\partial w_0}{\partial y} + \frac{\partial w_0}{\partial y} \right) = 0 \\ \varepsilon_{zz} &= 0 \end{aligned} \quad (3.3.8)$$

The strains in Eqs. (3.3.8) are called the *von Kármán strains*, and the associated plate theory is termed the *von Kármán plate theory*. Note that the transverse strains ($\varepsilon_{xz}, \varepsilon_{yz}, \varepsilon_{zz}$) are identically zero in the classical plate theory.

The first three strains in Eq. (3.3.8) have the form

$$\begin{Bmatrix} \varepsilon_{xx} \\ \varepsilon_{yy} \\ \gamma_{xy} \end{Bmatrix} = \begin{Bmatrix} \varepsilon_{xx}^{(0)} \\ \varepsilon_{yy}^{(0)} \\ \gamma_{xy}^{(0)} \end{Bmatrix} + z \begin{Bmatrix} \varepsilon_{xx}^{(1)} \\ \varepsilon_{yy}^{(1)} \\ \gamma_{xy}^{(1)} \end{Bmatrix} \quad (3.3.9)$$

$$\{\varepsilon^0\} = \begin{Bmatrix} \varepsilon_{xx}^{(0)} \\ \varepsilon_{yy}^{(0)} \\ \gamma_{xy}^{(0)} \end{Bmatrix} = \begin{Bmatrix} \frac{\partial u_0}{\partial x} + \frac{1}{2} \left(\frac{\partial w_0}{\partial x} \right)^2 \\ \frac{\partial v_0}{\partial y} + \frac{1}{2} \left(\frac{\partial w_0}{\partial y} \right)^2 \\ \frac{\partial u_0}{\partial y} + \frac{\partial v_0}{\partial x} + \frac{\partial w_0}{\partial x} \frac{\partial w_0}{\partial y} \end{Bmatrix}, \quad \{\varepsilon^1\} = \begin{Bmatrix} \varepsilon_{xx}^{(1)} \\ \varepsilon_{yy}^{(1)} \\ \gamma_{xy}^{(1)} \end{Bmatrix} = \begin{Bmatrix} -\frac{\partial^2 w_0}{\partial x^2} \\ -\frac{\partial^2 w_0}{\partial y^2} \\ -2 \frac{\partial^2 w_0}{\partial x \partial y} \end{Bmatrix} \quad (3.3.10)$$

where $(\varepsilon_{xx}^{(0)}, \varepsilon_{yy}^{(0)}, \gamma_{xy}^{(0)})$ are the *membrane strains*, and $(\varepsilon_{xx}^{(1)}, \varepsilon_{yy}^{(1)}, \gamma_{xy}^{(1)})$ are the flexural (bending) strains, known as the *curvatures*.

Once the displacements (u_0, v_0, w_0) of the midplane are known, strains at any point (x, y, z) in the plate can be computed using Eqs. (3.3.9) and (3.3.10). Note from Eq. (3.3.9) that all strain components vary linearly through the laminate thickness, and they are independent of the material variations through the laminate thickness (see Figure 3.3.3a). For a fixed value of z , the strains are, in general, nonlinear functions of x and y , and they depend on time t for dynamic problems.

3.3.3 Lamina Constitutive Relations

In the classical laminated plate theory, all three transverse strain components ($\varepsilon_{zz}, \varepsilon_{xz}, \varepsilon_{yz}$) are zero by definition. For a laminate composed of orthotropic layers, with their x_1x_2 -plane oriented arbitrarily with respect to the xy -plane ($x_3 = z$),

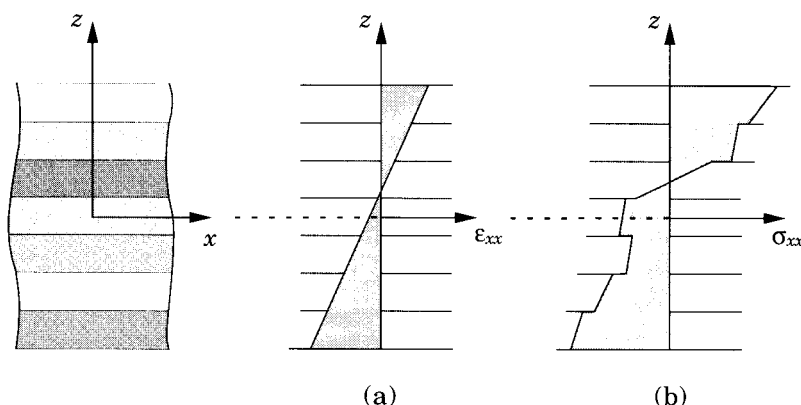


Figure 3.3.3: Variations of strains and stresses through layer and laminate thicknesses. (a) Variation of a typical in-plane strain. (b) Variation of corresponding stress.

the transverse shear stresses (σ_{xz}, σ_{yz}) are also zero. Since $\varepsilon_{zz} = 0$, the transverse normal stress σ_{zz} , although not zero identically, does not appear in the virtual work statement and hence in the equations of motion. Consequently, it amounts to neglecting the transverse normal stress. Thus we have, in theory, a case of both plane strain and plane stress. However, from practical considerations, a thin or moderately thick plate is in a state of plane stress because of thickness being small compared to the in-plane dimensions. Hence, the plane-stress reduced constitutive relations of Section 2.4 may be used.

The linear constitutive relations for the k th orthotropic (piezoelectric) lamina in the principal material coordinates of a lamina are

$$\begin{Bmatrix} \sigma_1 \\ \sigma_2 \\ \sigma_6 \end{Bmatrix}^{(k)} = \begin{bmatrix} Q_{11} & Q_{12} & 0 \\ Q_{12} & Q_{22} & 0 \\ 0 & 0 & Q_{66} \end{bmatrix}^{(k)} \begin{Bmatrix} \varepsilon_1 - \alpha_1 \Delta T \\ \varepsilon_2 - \alpha_2 \Delta T \\ \varepsilon_6 \end{Bmatrix} - \begin{bmatrix} 0 & 0 & e_{31} \\ 0 & 0 & e_{32} \\ 0 & 0 & 0 \end{bmatrix}^{(k)} \begin{Bmatrix} \mathcal{E}_1 \\ \mathcal{E}_2 \\ \mathcal{E}_3 \end{Bmatrix} \quad (3.3.11a)$$

where $Q_{ij}^{(k)}$ are the plane stress-reduced stiffnesses and $e_{ij}^{(k)}$ are the piezoelectric moduli of the k th lamina [cf., Eq. (2.4.4a,b)], $(\sigma_i, \varepsilon_i, \mathcal{E}_i)$ are the stress, strain, and electric field components, respectively, referred to the material coordinate system (x_1, x_2, x_3) , α_1 and α_2 are the coefficients of thermal expansion along the x_1 and x_2 directions, respectively, and ΔT is the temperature increment from a reference state, $\Delta T = T - T_{\text{ref}}$. When piezoelectric effects are not present, the part containing the piezoelectric moduli $e_{ij}^{(k)}$ should be omitted. The coefficients $Q_{ij}^{(k)}$ are known in terms of the engineering constants of the k th layer:

$$\begin{aligned} Q_{11} &= \frac{E_1}{1 - \nu_{12}\nu_{21}}, & Q_{12} &= \frac{\nu_{12}E_2}{1 - \nu_{12}\nu_{21}} = \frac{\nu_{21}E_1}{1 - \nu_{12}\nu_{21}} \\ Q_{22} &= \frac{E_2}{1 - \nu_{12}\nu_{21}}, & Q_{66} &= G_{12} \end{aligned} \quad (3.3.11b)$$

Since the laminate is made of several orthotropic layers, with their material axes oriented arbitrarily with respect to the laminate coordinates, the constitutive equations of each layer must be transformed to the laminate coordinates (x, y, z) , as explained in Section 2.3. The stress-strain relations (3.3.11a) when transformed to the laminate coordinates (x, y, z) relate the stresses $(\sigma_{xx}, \sigma_{yy}, \sigma_{xy})$ to the strains $(\varepsilon_{xx}, \varepsilon_{yy}, \gamma_{xy})$ and components of the electric field vector $(\mathcal{E}_x, \mathcal{E}_y, \mathcal{E}_z)$ in the laminate coordinates [see Eq. (2.4.5)]

$$\begin{Bmatrix} \sigma_{xx} \\ \sigma_{yy} \\ \sigma_{xy} \end{Bmatrix}^{(k)} = \begin{bmatrix} \bar{Q}_{11} & \bar{Q}_{12} & \bar{Q}_{16} \\ \bar{Q}_{12} & \bar{Q}_{22} & \bar{Q}_{26} \\ \bar{Q}_{16} & \bar{Q}_{26} & \bar{Q}_{66} \end{bmatrix}^{(k)} \left(\begin{Bmatrix} \varepsilon_{xx} \\ \varepsilon_{yy} \\ \gamma_{xy} \end{Bmatrix} - \begin{Bmatrix} \alpha_{xx} \\ \alpha_{yy} \\ 2\alpha_{xy} \end{Bmatrix} \Delta T \right) - \begin{bmatrix} 0 & 0 & \bar{e}_{31} \\ 0 & 0 & \bar{e}_{32} \\ 0 & 0 & \bar{e}_{36} \end{bmatrix}^{(k)} \begin{Bmatrix} \mathcal{E}_x \\ \mathcal{E}_y \\ \mathcal{E}_z \end{Bmatrix} \quad (3.3.12a)$$

where

$$\begin{aligned}\bar{Q}_{11} &= Q_{11} \cos^4 \theta + 2(Q_{12} + 2Q_{66}) \sin^2 \theta \cos^2 \theta + Q_{22} \sin^4 \theta \\ \bar{Q}_{12} &= (Q_{11} + Q_{22} - 4Q_{66}) \sin^2 \theta \cos^2 \theta + Q_{12}(\sin^4 \theta + \cos^4 \theta) \\ \bar{Q}_{22} &= Q_{11} \sin^4 \theta + 2(Q_{12} + 2Q_{66}) \sin^2 \theta \cos^2 \theta + Q_{22} \cos^4 \theta \\ \bar{Q}_{16} &= (Q_{11} - Q_{12} - 2Q_{66}) \sin \theta \cos^3 \theta + (Q_{12} - Q_{22} + 2Q_{66}) \sin^3 \theta \cos \theta \\ \bar{Q}_{26} &= (Q_{11} - Q_{12} - 2Q_{66}) \sin^3 \theta \cos \theta + (Q_{12} - Q_{22} + 2Q_{66}) \sin \theta \cos^3 \theta \\ \bar{Q}_{66} &= (Q_{11} + Q_{22} - 2Q_{12} - 2Q_{66}) \sin^2 \theta \cos^2 \theta + Q_{66}(\sin^4 \theta + \cos^4 \theta)\end{aligned}\quad (3.3.12b)$$

and α_{xx} , α_{yy} , and α_{xy} are the transformed thermal coefficients of expansion [see Eq. (2.3.23)]

$$\begin{aligned}\alpha_{xx} &= \alpha_1 \cos^2 \theta + \alpha_2 \sin^2 \theta \\ \alpha_{yy} &= \alpha_1 \sin^2 \theta + \alpha_2 \cos^2 \theta \\ 2\alpha_{xy} &= 2(\alpha_1 - \alpha_2) \sin \theta \cos \theta\end{aligned}\quad (3.3.12c)$$

and \bar{e}_{ij} are the transformed piezoelectric moduli

$$\begin{aligned}\bar{e}_{31} &= e_{31} \cos^2 \theta + e_{32} \sin^2 \theta \\ \bar{e}_{32} &= e_{31} \sin^2 \theta + e_{32} \cos^2 \theta \\ \bar{e}_{36} &= (e_{31} - e_{32}) \sin \theta \cos \theta\end{aligned}\quad (3.3.12d)$$

Here θ is the angle measured counterclockwise from the x -coordinate to the x_1 -coordinate. Note that stresses are also linear through the thickness of each layer; however, they will have different linear variation in different material layers when $\bar{Q}_{ij}^{(k)}$ change from layer to layer (see Fig. 3.3.3b). If we assume that the temperature increment varies linearly, consistent with the mechanical strains, we can write

$$\Delta T = T_0(x, y, t) + zT_1(x, y, t) \quad (3.3.13)$$

and the total strains are of the form in Eq. (3.3.9) with

$$\{\varepsilon^0\} = \left\{ \begin{array}{l} \varepsilon_{xx}^{(0)} - \alpha_{xx} T_0 \\ \varepsilon_{yy}^{(0)} - \alpha_{yy} T_0 \\ \gamma_{xy}^{(0)} - 2\alpha_{xy} T_0 \end{array} \right\}, \quad \{\varepsilon^1\} = \left\{ \begin{array}{l} \varepsilon_{xx}^{(1)} - \alpha_{xx} T_1 \\ \varepsilon_{yy}^{(1)} - \alpha_{yy} T_1 \\ \gamma_{xy}^{(1)} - 2\alpha_{xy} T_1 \end{array} \right\} \quad (3.3.14)$$

3.3.4 Equations of Motion

As noted earlier, the transverse strains (γ_{xz} , γ_{yz} , ε_{zz}) are identically zero in the classical plate theory. Consequently, the transverse shear stresses (σ_{xz} , σ_{yz}) are zero for a laminate made of orthotropic layers if they are computed from the constitutive relations. The transverse normal stress σ_{zz} is not zero by the constitutive relation because of the Poisson effect. However, all three stress components do not enter the formulation because the virtual strain energy of these stresses is zero due to the fact that kinematically consistent virtual strains must be zero [see Eq. (3.3.8)]:

$$\delta\varepsilon_{xz} = 0, \quad \delta\varepsilon_{yz} = 0, \quad \delta\varepsilon_{zz} = 0$$

Whether the transverse stresses are accounted for or not in a theory, they are present in reality to keep the plate in equilibrium. In addition, these stress components may be specified on the boundary. Thus, the transverse stresses do not enter the virtual strain energy expression, but they must be accounted for in the boundary conditions and equilibrium of forces.

Here, the governing equations are derived using the principle of virtual displacements. In the derivations, we account for thermal (and hence, moisture) and piezoelectric effects only with the understanding that the material properties are independent of temperature and electric fields, and that the temperature T and electric field vector \mathcal{E} are known functions of position (hence, $\delta T = 0$ and $\delta \mathcal{E} = \mathbf{0}$). Thus temperature and electric fields enter the formulation only through constitutive equations [see Eq. (3.3.12a)].

The dynamic version of the principle of virtual work [see Eq. (1.4.78)] is

$$0 = \int_0^T (\delta U + \delta V - \delta K) dt \quad (3.3.15)$$

where the virtual strain energy δU (volume integral of δU_0), virtual work done by applied forces δV , and the virtual kinetic energy δK are given by

$$\begin{aligned} \delta U &= \int_{\Omega_0} \int_{-\frac{h}{2}}^{\frac{h}{2}} (\sigma_{xx} \delta \varepsilon_{xx} + \sigma_{yy} \delta \varepsilon_{yy} + 2\sigma_{xy} \delta \varepsilon_{xy}) dz dx dy \\ &= \int_{\Omega_0} \left\{ \int_{-\frac{h}{2}}^{\frac{h}{2}} [\sigma_{xx} (\delta \varepsilon_{xx}^{(0)} + z \delta \varepsilon_{xx}^{(1)}) + \sigma_{yy} (\delta \varepsilon_{yy}^{(0)} + z \delta \varepsilon_{yy}^{(1)}) \right. \\ &\quad \left. + \sigma_{xy} (\delta \gamma_{xy}^{(0)} + z \delta \gamma_{xy}^{(1)})] dz \right\} dx dy \end{aligned} \quad (3.3.16)$$

$$\begin{aligned} \delta V &= - \int_{\Omega_0} \left[q_b(x, y) \delta w(x, y, \frac{h}{2}) + q_t(x, y) \delta w(x, y, -\frac{h}{2}) \right] dx dy \\ &\quad - \int_{\Gamma_\sigma} \int_{-\frac{h}{2}}^{\frac{h}{2}} [\hat{\sigma}_{nn} \delta u_n + \hat{\sigma}_{ns} \delta u_s + \hat{\sigma}_{nz} \delta w] dz ds \\ &= - \int_{\Omega_0} \{ [q_b(x, y) + q_t(x, y)] \delta w_0(x, y) \} dx dy \\ &\quad - \int_{\Gamma_\sigma} \int_{-\frac{h}{2}}^{\frac{h}{2}} \left[\hat{\sigma}_{nn} \left(\delta u_{0n} - z \frac{\partial \delta w_0}{\partial n} \right) + \hat{\sigma}_{ns} \left(\delta u_{0s} - z \frac{\partial \delta w_0}{\partial s} \right) \right. \\ &\quad \left. + \hat{\sigma}_{nz} \delta w_0 \right] dz ds \end{aligned} \quad (3.3.17)$$

$$\begin{aligned} \delta K &= \int_{\Omega_0} \int_{-\frac{h}{2}}^{\frac{h}{2}} \rho_0 \left[\left(\dot{u}_0 - z \frac{\partial \dot{w}_0}{\partial x} \right) \left(\delta \dot{u}_0 - z \frac{\partial \delta \dot{w}_0}{\partial x} \right) \right. \\ &\quad \left. + \left(\dot{v}_0 - z \frac{\partial \dot{w}_0}{\partial y} \right) \left(\delta \dot{v}_0 - z \frac{\partial \delta \dot{w}_0}{\partial y} \right) + \dot{w}_0 \delta \dot{w}_0 \right] dz dx dy \end{aligned} \quad (3.3.18)$$

where q_b is the distributed force at the bottom ($z = h/2$) of the laminate, q_t is the distributed force at the top ($z = -h/2$) of the laminate, $(\hat{\sigma}_{nn}, \hat{\sigma}_{ns}, \hat{\sigma}_{nz})$ are the

specified stress components on the portion Γ_σ of the boundary Γ , $(\delta u_{0n}, \delta u_{0s})$ are the virtual displacements along the normal and tangential directions, respectively, on the boundary Γ (see Figure 3.3.4), ρ_0 is the density of the plate material, and a superposed dot on a variable indicates its time derivative, $\dot{u}_0 = \partial u_0 / \partial t$. Details of how (u_{0n}, u_{0s}) and $(\sigma_{nn}, \sigma_{ns})$ are related to (u_0, v_0) and $(\sigma_{xx}, \sigma_{yy}, \sigma_{xy})$, respectively, will be presented shortly.

The virtual displacements are zero on the portion of the boundary where the corresponding actual displacements are specified. For time-dependent problems, the admissible virtual displacements must also vanish at time $t = 0$ and $t = T$ [see Eq. (1.4.73b)]. Since we are interested in the governing differential equations and the form of the boundary conditions of the theory, we can assume that the stresses are specified on either a part or whole of the boundary. If a stress component is specified only on a part of the boundary, on the remaining part of the boundary the corresponding displacement must be known and hence the virtual displacement must be zero there, contributing nothing to the virtual work done.

Substituting for δU , δV , and δK from Eqs. (3.3.16)–(3.3.18) into the virtual work statement in Eq. (3.3.15) and integrating through the thickness of the laminate, we obtain

$$0 = \int_0^T \left\{ \int_{\Omega_0} \left[N_{xx} \delta \varepsilon_{xx}^{(0)} + M_{xx} \delta \varepsilon_{xx}^{(1)} + N_{yy} \delta \varepsilon_{yy}^{(0)} + M_{yy} \delta \varepsilon_{yy}^{(1)} + N_{xy} \delta \gamma_{xy}^{(0)} \right. \right. \\ \left. \left. + M_{xy} \delta \gamma_{xy}^{(1)} - q \delta w_0 - I_0 (\dot{u}_0 \delta \dot{u}_0 + \dot{v}_0 \delta \dot{v}_0 + \dot{w}_0 \delta \dot{w}_0) \right. \right. \\ \left. \left. + I_1 \left(\frac{\partial \delta \dot{w}_0}{\partial x} \dot{u}_0 + \frac{\partial \dot{w}_0}{\partial x} \delta \dot{u}_0 + \frac{\partial \delta \dot{w}_0}{\partial y} \dot{v}_0 + \frac{\partial \dot{w}_0}{\partial y} \delta \dot{v}_0 \right) \right. \right. \\ \left. \left. - I_2 \left(\frac{\partial \dot{w}_0}{\partial x} \frac{\partial \delta \dot{w}_0}{\partial x} + \frac{\partial \dot{w}_0}{\partial y} \frac{\partial \delta \dot{w}_0}{\partial y} \right) \right] dx dy \right. \\ \left. - \int_{\Gamma_\sigma} \left(\hat{N}_{nn} \delta u_{0n} + \hat{N}_{ns} \delta u_{0s} - \hat{M}_{nn} \frac{\partial \delta w_0}{\partial n} - \hat{M}_{ns} \frac{\partial \delta w_0}{\partial s} + \hat{Q}_n \delta w_0 \right) ds \right\} dt \quad (3.3.19)$$

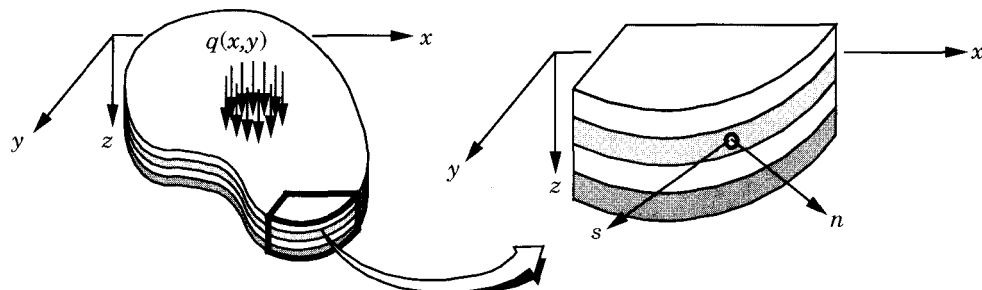


Figure 3.3.4: Geometry of a laminated plate with curved boundary.

where $q = q_b + q_t$ is the total transverse load and

$$\begin{Bmatrix} N_{xx} \\ N_{yy} \\ N_{xy} \end{Bmatrix} = \int_{-\frac{h}{2}}^{\frac{h}{2}} \begin{Bmatrix} \sigma_{xx} \\ \sigma_{yy} \\ \sigma_{xy} \end{Bmatrix} dz, \quad \begin{Bmatrix} M_{xx} \\ M_{yy} \\ M_{xy} \end{Bmatrix} = \int_{-\frac{h}{2}}^{\frac{h}{2}} \begin{Bmatrix} \sigma_{xx} \\ \sigma_{yy} \\ \sigma_{xy} \end{Bmatrix} z \, dz \quad (3.3.20a)$$

$$\begin{Bmatrix} \hat{N}_{nn} \\ \hat{N}_{ns} \end{Bmatrix} = \int_{-\frac{h}{2}}^{\frac{h}{2}} \begin{Bmatrix} \hat{\sigma}_{nn} \\ \hat{\sigma}_{ns} \end{Bmatrix} dz, \quad \begin{Bmatrix} \hat{M}_{nn} \\ \hat{M}_{ns} \end{Bmatrix} = \int_{-\frac{h}{2}}^{\frac{h}{2}} \begin{Bmatrix} \hat{\sigma}_{nn} \\ \hat{\sigma}_{ns} \end{Bmatrix} z \, dz \quad (3.3.20b)$$

$$\begin{Bmatrix} I_0 \\ I_1 \\ I_2 \end{Bmatrix} = \int_{-\frac{h}{2}}^{\frac{h}{2}} \begin{Bmatrix} 1 \\ z \\ z^2 \end{Bmatrix} \rho_0 \, dz, \quad \hat{Q}_n = \int_{-\frac{h}{2}}^{\frac{h}{2}} \hat{\sigma}_{nz} \, dz \quad (3.3.20c)$$

The quantities (N_{xx}, N_{yy}, N_{xy}) are called the in-plane force resultants, and (M_{xx}, M_{yy}, M_{xy}) are called the moment resultants (see Figure 3.3.5); Q_n denotes the transverse force resultant, and (I_0, I_1, I_2) are the mass moments of inertia. All stress resultants are measured per unit length (e.g., N_i and Q_i in lb/in. and M_i in lb-in/in.).

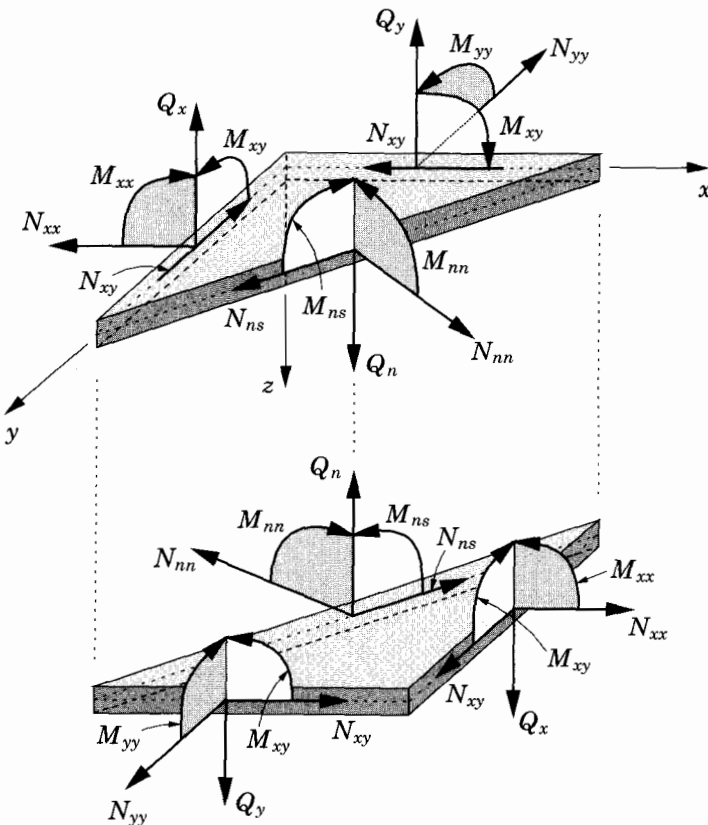


Figure 3.3.5: Force and moment resultants on a plate element.

The virtual strains are known in terms of the virtual displacements in the same way as the true strains in terms of the true displacements [see Eq. (3.3.10)]:

$$\begin{aligned}\delta\varepsilon_{xx}^{(0)} &= \frac{\partial\delta u_0}{\partial x} + \frac{\partial w_0}{\partial x} \frac{\partial\delta w_0}{\partial x}, \quad \delta\varepsilon_{xx}^{(1)} = -\frac{\partial^2\delta w_0}{\partial x^2} \\ \delta\varepsilon_{yy}^{(0)} &= \frac{\partial\delta v_0}{\partial y} + \frac{\partial w_0}{\partial y} \frac{\partial\delta w_0}{\partial y}, \quad \delta\varepsilon_{yy}^{(1)} = -\frac{\partial^2\delta w_0}{\partial y^2} \\ \delta\gamma_{xy}^{(0)} &= \frac{\partial\delta u_0}{\partial y} + \frac{\partial\delta v_0}{\partial x} + \frac{\partial\delta w_0}{\partial x} \frac{\partial w_0}{\partial y} + \frac{\partial w_0}{\partial x} \frac{\partial\delta w_0}{\partial y} \\ \delta\gamma_{xy}^{(1)} &= -2\frac{\partial^2\delta w_0}{\partial x\partial y}\end{aligned}\tag{3.3.21}$$

Substituting for the virtual strains from Eq. (3.3.21) into Eq. (3.3.19) and integrating by parts to relieve the virtual displacements ($\delta u_0, \delta v_0, \delta w_0$) in Ω_0 of any differentiation, so that we can use the fundamental lemma of variational calculus, we obtain

$$\begin{aligned}0 &= \int_0^T \left\{ \int_{\Omega_0} \left[-N_{xx,x}\delta u_0 - \left(N_{xx} \frac{\partial w_0}{\partial x} \right)_{,x} \delta w_0 - M_{xx,xx}\delta w_0 - N_{yy,y}\delta v_0 \right. \right. \\ &\quad - \left(N_{yy} \frac{\partial w_0}{\partial y} \right)_{,y} \delta w_0 - M_{yy,yy}\delta w_0 - N_{xy,y}\delta u_0 - N_{xy,x}\delta v_0 \\ &\quad - \left(N_{xy} \frac{\partial w_0}{\partial y} \right)_{,x} \delta w_0 - \left(N_{xy} \frac{\partial w_0}{\partial x} \right)_{,y} \delta w_0 - 2M_{xy,xy}\delta w_0 - q\delta w_0 \\ &\quad + I_0 (\ddot{u}_0\delta u_0 + \ddot{v}_0\delta v_0 + \ddot{w}_0\delta w_0) - I_2 \left(\frac{\partial^2\ddot{w}_0}{\partial x^2} + \frac{\partial^2\ddot{w}_0}{\partial y^2} \right) \delta w_0 \\ &\quad \left. \left. + I_1 \left(\frac{\partial\ddot{u}_0}{\partial x} \delta w_0 - \frac{\partial\ddot{w}_0}{\partial x} \delta u_0 + \frac{\partial\ddot{v}_0}{\partial y} \delta w_0 - \frac{\partial\ddot{w}_0}{\partial y} \delta v_0 \right) \right] dx dy \right. \\ &\quad \left. + \oint_{\Gamma} \left[N_{xx}n_x\delta u_0 + \left(N_{xx} \frac{\partial w_0}{\partial x} \right) n_x \delta w_0 - M_{xx}n_x \frac{\partial\delta w_0}{\partial x} + M_{xx,x}n_x\delta w_0 \right. \right. \\ &\quad + N_{yy}n_y\delta v_0 + \left(N_{yy} \frac{\partial w_0}{\partial y} \right) n_y \delta w_0 - M_{yy}n_y \frac{\partial\delta w_0}{\partial y} + M_{yy,y}n_y\delta w_0 \\ &\quad - M_{xy}n_x \frac{\partial\delta w_0}{\partial y} + M_{xy,x}n_y\delta w_0 - M_{xy}n_y \frac{\partial\delta w_0}{\partial x} + M_{xy,y}n_x\delta w_0 \\ &\quad \left. \left. + N_{xy}n_y\delta u_0 + N_{xy}n_x\delta v_0 + N_{xy} \frac{\partial w_0}{\partial y} n_x \delta w_0 + N_{xy} \frac{\partial w_0}{\partial x} n_y \delta w_0 \right] ds \right. \\ &\quad \left. - \int_{\Gamma_\sigma} \left(\hat{N}_{nn}\delta u_{0n} + \hat{N}_{ns}\delta u_{0s} - \hat{M}_{nn} \frac{\partial\delta w_0}{\partial n} - \hat{M}_{ns} \frac{\partial\delta w_0}{\partial s} + \hat{Q}_n \delta w_0 \right) ds \right. \\ &\quad \left. + \oint_{\Gamma} \left[-I_1 (\ddot{u}_0 n_x + \ddot{v}_0 n_y) + I_2 \left(\frac{\partial\ddot{w}_0}{\partial x} n_x + \frac{\partial\ddot{w}_0}{\partial y} n_y \right) \right] \delta w_0 ds \right\} dt\end{aligned}\tag{3.3.22}$$

where a comma followed by subscripts denotes differentiation with respect to the subscripts: $N_{xx,x} = \partial N_{xx}/\partial x$, and so on. Note that both spatial and time integration-by-parts were used in arriving at the last expression. The terms obtained

in Ω_0 but evaluated at $t = 0$ and $t = T$ were set to zero because the virtual displacements are zero there.

Collecting the coefficients of each of the virtual displacements $(\delta u_0, \delta v_0, \delta w_0)$ together and noting that the virtual displacements are zero on Γ_u , we obtain

$$\begin{aligned}
 0 = \int_0^T \left\{ \int_{\Omega_0} \left[- \left(N_{xx,x} + N_{xy,y} - I_0 \ddot{u}_0 + I_1 \frac{\partial \ddot{w}_0}{\partial x} \right) \delta u_0 \right. \right. \\
 \left. \left. - \left(N_{xy,x} + N_{yy,y} - I_0 \ddot{v}_0 + I_1 \frac{\partial \ddot{w}_0}{\partial y} \right) \delta v_0 \right. \right. \\
 \left. \left. - \left(M_{xx,xx} + 2M_{xy,xy} + M_{yy,yy} + \mathcal{N}(w_0) + q \right. \right. \right. \\
 \left. \left. \left. - I_1 \ddot{w}_0 - I_1 \frac{\partial \ddot{u}_0}{\partial x} - I_1 \frac{\partial \ddot{v}_0}{\partial y} + I_2 \frac{\partial^2 \ddot{w}_0}{\partial x^2} + I_2 \frac{\partial^2 \ddot{w}_0}{\partial y^2} \right) \delta w_0 \right] dx dy \right] \\
 + \int_{\Gamma_\sigma} \left[(N_{xx} n_x + N_{xy} n_y) \delta u_0 + (N_{xy} n_x + N_{yy} n_y) \delta v_0 \right. \\
 \left. + \left(M_{xx,x} n_x + M_{xy,y} n_x + M_{yy,y} n_y + M_{xy,x} n_y + \mathcal{P}(w_0) \right. \right. \\
 \left. \left. - I_1 \ddot{u}_0 n_x - I_1 \ddot{v}_0 n_y + I_2 \frac{\partial \ddot{w}_0}{\partial x} n_x + I_2 \frac{\partial \ddot{w}_0}{\partial y} n_y \right) \delta w_0 \right. \\
 \left. - (M_{xx} n_x + M_{xy} n_y) \frac{\partial \delta w_0}{\partial x} - (M_{xy} n_x + M_{yy} n_y) \frac{\partial \delta w_0}{\partial y} \right] ds \\
 \left. - \int_{\Gamma_\sigma} \left(\hat{N}_{nn} \delta u_{0n} + \hat{N}_{ns} \delta u_{0s} - \hat{M}_{nn} \frac{\partial \delta w_0}{\partial n} - \hat{M}_{ns} \frac{\partial \delta w_0}{\partial s} + \hat{Q}_n \delta w_0 \right) ds \right\} dt
 \end{aligned} \tag{3.3.23}$$

where

$$\mathcal{N}(w_0) = \frac{\partial}{\partial x} \left(N_{xx} \frac{\partial w_0}{\partial x} + N_{xy} \frac{\partial w_0}{\partial y} \right) + \frac{\partial}{\partial y} \left(N_{xy} \frac{\partial w_0}{\partial x} + N_{yy} \frac{\partial w_0}{\partial y} \right) \tag{3.3.24a}$$

$$\mathcal{P}(w_0) = \left(N_{xx} \frac{\partial w_0}{\partial x} + N_{xy} \frac{\partial w_0}{\partial y} \right) n_x + \left(N_{xy} \frac{\partial w_0}{\partial x} + N_{yy} \frac{\partial w_0}{\partial y} \right) n_y \tag{3.3.24b}$$

The Euler–Lagrange equations of the theory are obtained by setting the coefficients of δu_0 , δv_0 , and δw_0 over Ω_0 of Eq. (3.3.23) to zero separately:

$$\begin{aligned}
 \delta u_0 : \quad & \frac{\partial N_{xx}}{\partial x} + \frac{\partial N_{xy}}{\partial y} = I_0 \frac{\partial^2 u_0}{\partial t^2} - I_1 \frac{\partial^2}{\partial t^2} \left(\frac{\partial w_0}{\partial x} \right) \\
 \delta v_0 : \quad & \frac{\partial N_{xy}}{\partial x} + \frac{\partial N_{yy}}{\partial y} = I_0 \frac{\partial^2 v_0}{\partial t^2} - I_1 \frac{\partial^2}{\partial t^2} \left(\frac{\partial w_0}{\partial y} \right) \\
 \delta w_0 : \quad & \frac{\partial^2 M_{xx}}{\partial x^2} + 2 \frac{\partial^2 M_{xy}}{\partial y \partial x} + \frac{\partial^2 M_{yy}}{\partial y^2} + \mathcal{N}(w_0) + q = I_0 \frac{\partial^2 w_0}{\partial t^2} \\
 & - I_2 \frac{\partial^2}{\partial t^2} \left(\frac{\partial^2 w_0}{\partial x^2} + \frac{\partial^2 w_0}{\partial y^2} \right) + I_1 \frac{\partial^2}{\partial t^2} \left(\frac{\partial u_0}{\partial x} + \frac{\partial v_0}{\partial y} \right)
 \end{aligned} \tag{3.3.25}$$

The terms involving I_2 are called *rotary* inertia terms, and are often neglected in most books. The term can contribute to higher-order vibration or frequency modes.

Next we obtain the boundary conditions of the theory from Eq. (3.3.23). In order to collect the coefficients of the virtual displacements and their derivatives on the boundary, we should express $(\delta u_0, \delta v_0)$ in terms of $(\delta u_{0n}, \delta u_{0s})$. If the unit outward normal vector $\hat{\mathbf{n}}$ is oriented at an angle θ from the x -axis, then its direction cosines are $n_x = \cos \theta$ and $n_y = \sin \theta$. Hence, the transformation between the coordinate system (n, s, r) and (x, y, z) is given by

$$\begin{aligned}\hat{\mathbf{e}}_x &= \cos \theta \hat{\mathbf{e}}_n - \sin \theta \hat{\mathbf{e}}_s \\ \hat{\mathbf{e}}_y &= \sin \theta \hat{\mathbf{e}}_n + \cos \theta \hat{\mathbf{e}}_s \\ \hat{\mathbf{e}}_z &= \hat{\mathbf{e}}_r\end{aligned}\quad (3.3.26)$$

Therefore, the displacements (u_{0n}, u_{0s}) are related to (u_0, v_0) by

$$u_0 = n_x u_{0n} - n_y u_{0s}, \quad v_0 = n_y u_{0n} + n_x u_{0s} \quad (3.3.27a)$$

Similarly, the normal and tangential derivatives $(w_{0,n}, w_{0,s})$ are related to the derivatives $(w_{0,x}, w_{0,y})$ by

$$\frac{\partial w_0}{\partial x} = n_x \frac{\partial w_0}{\partial n} - n_y \frac{\partial w_0}{\partial s}, \quad \frac{\partial w_0}{\partial y} = n_y \frac{\partial w_0}{\partial n} + n_x \frac{\partial w_0}{\partial s} \quad (3.3.27b)$$

Now we can rewrite the boundary expressions in terms of (u_{0n}, u_{0s}) and $(w_{0,n}, w_{0,s})$. We have

$$\begin{aligned}& (N_{xx} n_x + N_{xy} n_y) \delta u_0 + (N_{xy} n_x + N_{yy} n_y) \delta v_0 \\&= (N_{xx} n_x + N_{xy} n_y) (n_x \delta u_n - n_y \delta u_s) + (N_{xy} n_x + N_{yy} n_y) (n_y \delta u_n + n_x \delta u_s) \\&= \left(N_{xx} n_x^2 + 2N_{xy} n_x n_y + N_{yy} n_y^2 \right) \delta u_n + \left[(N_{yy} - N_{xx}) n_x n_y + N_{xy} (n_x^2 - n_y^2) \right] \delta u_s\end{aligned}\quad (3.3.28a)$$

We recognize that the coefficients of δu_{0n} and δu_{0s} in the right-hand side of the above equation are equal to N_{nn} and N_{ns} , respectively. This follows from the fact that the stresses $(\sigma_{nn}, \sigma_{ns})$ are related to $(\sigma_{xx}, \sigma_{yy}, \sigma_{xy})$ by the transformation in Eq. (2.3.9):

$$\begin{Bmatrix} \sigma_{nn} \\ \sigma_{ns} \end{Bmatrix} = \begin{bmatrix} n_x^2 & n_y^2 & 2n_x n_y \\ -n_x n_y & n_x n_y & n_x^2 - n_y^2 \end{bmatrix} \begin{Bmatrix} \sigma_{xx} \\ \sigma_{yy} \\ \sigma_{xy} \end{Bmatrix} \quad (3.3.28b)$$

Hence we have

$$\begin{Bmatrix} N_{nn} \\ N_{ns} \end{Bmatrix} = \begin{bmatrix} n_x^2 & n_y^2 & 2n_x n_y \\ -n_x n_y & n_x n_y & n_x^2 - n_y^2 \end{bmatrix} \begin{Bmatrix} N_{xx} \\ N_{yy} \\ N_{xy} \end{Bmatrix} \quad (3.3.29a)$$

$$\begin{Bmatrix} M_{nn} \\ M_{ns} \end{Bmatrix} = \begin{bmatrix} n_x^2 & n_y^2 & 2n_x n_y \\ -n_x n_y & n_x n_y & n_x^2 - n_y^2 \end{bmatrix} \begin{Bmatrix} M_{xx} \\ M_{yy} \\ M_{xy} \end{Bmatrix} \quad (3.3.29b)$$

In view of the above relations, the boundary integrals in Eq. (3.3.23) can be written as

$$0 = \int_0^T \int_{\Gamma_\sigma} \left[\begin{aligned} & \left(N_{nn} - \hat{N}_{nn} \right) \delta u_{0n} + \left(N_{ns} - \hat{N}_{ns} \right) \delta u_{0s} \\ & + \left(M_{xx,x} n_x + M_{xy,y} n_x + M_{yy,y} n_y + M_{xy,x} n_y + \mathcal{P}(w_0) \right. \\ & \left. - I_1 \ddot{u}_0 n_x - I_1 \ddot{v}_0 n_y + I_2 \frac{\partial \ddot{w}_0}{\partial x} n_x + I_2 \frac{\partial \ddot{w}_0}{\partial y} n_y - \hat{Q}_n \right) \delta w_0 \\ & - \left(M_{nn} - \hat{M}_{nn} \right) \frac{\partial \delta w_0}{\partial n} - \left(M_{ns} - \hat{M}_{ns} \right) \frac{\partial \delta w_0}{\partial s} \end{aligned} \right] ds dt \quad (3.3.30)$$

The natural boundary conditions are then given by

$$\begin{aligned} N_{nn} - \hat{N}_{nn} &= 0, \quad N_{ns} - \hat{N}_{ns} = 0, \quad Q_n - \hat{Q}_n = 0 \\ M_{nn} - \hat{M}_{nn} &= 0, \quad M_{ns} - \hat{M}_{ns} = 0 \end{aligned} \quad (3.3.31a)$$

on Γ_σ , where

$$\begin{aligned} Q_n \equiv & \left(M_{xx,x} + M_{xy,y} - I_1 \ddot{u}_0 + I_2 \frac{\partial \ddot{w}_0}{\partial x} \right) n_x + \\ & \left(M_{yy,y} + M_{xy,x} - I_1 \ddot{v}_0 + I_2 \frac{\partial \ddot{w}_0}{\partial y} \right) n_y + \mathcal{P}(w_0) \end{aligned} \quad (3.3.31b)$$

Thus the primary variables (i.e., generalized displacements) and secondary variables (i.e., generalized forces) of the theory are

$$\begin{aligned} \text{primary variables: } & u_n, u_s, w_0, \frac{\partial w_0}{\partial n}, \frac{\partial w_0}{\partial s} \\ \text{secondary variables: } & N_{nn}, N_{ns}, Q_n, M_{nn}, M_{ns} \end{aligned} \quad (3.3.32)$$

The generalized displacements are specified on Γ_u , which constitutes the essential (or geometric) boundary conditions.

We note that the equations in Eq. (3.3.25) have the total spatial differential order of eight. In other words, if the equations are expressed in terms of the displacements (u_0, v_0, w_0), they would contain second-order spatial derivatives of u_0 and v_0 and fourth-order spatial derivatives of w_0 . Hence, the classical laminated plate theory is said to be an eighth-order theory. This implies that there should be only eight boundary conditions, whereas Eq. (3.3.32) shows five essential and five natural boundary conditions, giving a total of ten boundary conditions. To eliminate this discrepancy, one integrates the tangential derivative term by parts to obtain the boundary term

$$-\oint_{\Gamma} M_{ns} \frac{\partial \delta w_0}{\partial s} ds = \oint_{\Gamma} \frac{\partial M_{ns}}{\partial s} \delta w_0 ds - [M_{ns} \delta w_0]_{\Gamma} \quad (3.3.33a)$$

The term in the square bracket is zero since the end points of a closed curve coincide. This term now must be added to Q_n (because it is a coefficient of δw_0):

$$V_n \equiv Q_n + \frac{\partial M_{ns}}{\partial s} \quad (3.3.33b)$$

which should be balanced by the applied force \hat{Q}_n . This boundary condition, $V_n = \hat{Q}_n$, is known as the *Kirchhoff free-edge condition*. The boundary conditions of the classical laminated plate theory are

$$\begin{aligned} u_n, u_s, w_0, \frac{\partial w_0}{\partial n} & \text{ (essential)} \\ N_{nn}, N_{ns}, V_n, M_{nn} & \text{ (natural)} \end{aligned} \quad (3.3.34)$$

The initial conditions of the theory involve specifying the values of the displacements and their first derivatives with respect to time at $t = 0$:

$$\begin{aligned} u_n = u_n^0, u_s = u_s^0, w_0 = w_0^0 \\ \dot{u}_n = \dot{u}_n^0, \dot{u}_s = \dot{u}_s^0, \dot{w}_0 = \dot{w}_0^0 \end{aligned} \quad (3.3.35)$$

where variables with superscript ‘0’ denotes values at time $t = 0$. We note that both the displacement and velocities must be specified.

This completes the basic development of the classical laminated plate theory for nonlinear and dynamic analyses. As a special case, one can obtain the equations of equilibrium from (3.3.25) by setting all terms involving time derivatives to zero. For linear analysis, we set $\mathcal{N}(w_0)$ and $\mathcal{P}(w_0)$ to zero, in addition to setting the nonlinear terms in the strain-displacement equations to zero. Equations (3.3.25) are applicable to linear and nonlinear elastic bodies, since the constitutive equations were not utilized in deriving the governing equations of motion.

3.3.5 Laminate Constitutive Equations

Here we derive the constitutive equations that relate the force and moment resultants in Eq. (3.3.20a) to the strains of a laminate. To this end, we assume that each layer is orthotropic with respect to its material symmetry lines and obeys Hooke’s law; i.e., Eq. (3.3.12a) holds for the k th lamina in the problem coordinates. For the moment we consider the case in which the temperature and piezoelectric effects are not included. Although the strains are continuous through the thickness, stresses are not, due to the change in material coefficients through the thickness (i.e., each lamina). Hence, the integration of stresses through the laminate thickness requires lamina-wise integration. The force resultants are given by

$$\begin{aligned} \left\{ \begin{array}{c} N_{xx} \\ N_{yy} \\ N_{xy} \end{array} \right\} &= \sum_{k=1}^N \int_{z_k}^{z_{k+1}} \left\{ \begin{array}{c} \sigma_{xx} \\ \sigma_{yy} \\ \sigma_{xy} \end{array} \right\} dz \\ &= \sum_{k=1}^N \int_{z_k}^{z_{k+1}} \begin{bmatrix} \bar{Q}_{11} & \bar{Q}_{12} & \bar{Q}_{16} \\ \bar{Q}_{12} & \bar{Q}_{22} & \bar{Q}_{26} \\ \bar{Q}_{16} & \bar{Q}_{26} & \bar{Q}_{66} \end{bmatrix}^{(k)} \left\{ \begin{array}{c} \varepsilon_{xx}^{(0)} + z\varepsilon_{xx}^{(1)} \\ \varepsilon_{yy}^{(0)} + z\varepsilon_{yy}^{(1)} \\ \gamma_{xy}^{(0)} + z\gamma_{xy}^{(1)} \end{array} \right\} dz \end{aligned}$$

$$\begin{Bmatrix} N_{xx} \\ N_{yy} \\ N_{xy} \end{Bmatrix} = \begin{bmatrix} A_{11} & A_{12} & A_{16} \\ A_{12} & A_{22} & A_{26} \\ A_{16} & A_{26} & A_{66} \end{bmatrix} \begin{Bmatrix} \varepsilon_{xx}^{(0)} \\ \varepsilon_{yy}^{(0)} \\ \gamma_{xy}^{(0)} \end{Bmatrix} + \begin{bmatrix} B_{11} & B_{12} & B_{16} \\ B_{12} & B_{22} & B_{26} \\ B_{16} & B_{26} & B_{66} \end{bmatrix} \begin{Bmatrix} \varepsilon_{xx}^{(1)} \\ \varepsilon_{yy}^{(1)} \\ \gamma_{xy}^{(1)} \end{Bmatrix} \quad (3.3.36)$$

$$\begin{aligned} \begin{Bmatrix} M_{xx} \\ M_{yy} \\ M_{xy} \end{Bmatrix} &= \sum_{k=1}^N \int_{z_k}^{z_{k+1}} \begin{Bmatrix} \sigma_{xx} \\ \sigma_{yy} \\ \sigma_{xy} \end{Bmatrix} z \, dz \\ &= \sum_{k=1}^N \int_{z_k}^{z_{k+1}} \begin{bmatrix} \bar{Q}_{11} & \bar{Q}_{12} & \bar{Q}_{16} \\ \bar{Q}_{12} & \bar{Q}_{22} & \bar{Q}_{26} \\ \bar{Q}_{16} & \bar{Q}_{26} & \bar{Q}_{66} \end{bmatrix}^{(k)} \begin{Bmatrix} \varepsilon_{xx}^{(0)} + z\varepsilon_{xx}^{(1)} \\ \varepsilon_{yy}^{(0)} + z\varepsilon_{yy}^{(1)} \\ \gamma_{xy}^{(0)} + z\gamma_{xy}^{(1)} \end{Bmatrix} z \, dz \\ \begin{Bmatrix} M_{xx} \\ M_{yy} \\ M_{xy} \end{Bmatrix} &= \begin{bmatrix} B_{11} & B_{12} & B_{16} \\ B_{12} & B_{22} & B_{26} \\ B_{16} & B_{26} & B_{66} \end{bmatrix} \begin{Bmatrix} \varepsilon_{xx}^{(0)} \\ \varepsilon_{yy}^{(0)} \\ \gamma_{xy}^{(0)} \end{Bmatrix} + \begin{bmatrix} D_{11} & D_{12} & D_{16} \\ D_{12} & D_{22} & D_{26} \\ D_{16} & D_{26} & D_{66} \end{bmatrix} \begin{Bmatrix} \varepsilon_{xx}^{(1)} \\ \varepsilon_{yy}^{(1)} \\ \gamma_{xy}^{(1)} \end{Bmatrix} \end{aligned} \quad (3.3.37)$$

where A_{ij} are called *extensional stiffnesses*, D_{ij} the *bending stiffnesses*, and B_{ij} the *bending-extensional coupling stiffnesses*, which are defined in terms of the lamina stiffnesses $\bar{Q}_{ij}^{(k)}$ as

$$(A_{ij}, B_{ij}, D_{ij}) = \int_{-\frac{h}{2}}^{\frac{h}{2}} \bar{Q}_{ij}(1, z, z^2) dz = \sum_{k=1}^N \int_{z_k}^{z_{k+1}} \bar{Q}_{ij}^{(k)}(1, z, z^2) dz \quad (3.3.38a)$$

or

$$\begin{aligned} A_{ij} &= \sum_{k=1}^N \bar{Q}_{ij}^{(k)}(z_{k+1} - z_k), \quad B_{ij} = \frac{1}{2} \sum_{k=1}^N \bar{Q}_{ij}^{(k)}(z_{k+1}^2 - z_k^2) \\ D_{ij} &= \frac{1}{3} \sum_{k=1}^N \bar{Q}_{ij}^{(k)}(z_{k+1}^3 - z_k^3) \end{aligned} \quad (3.3.38b)$$

Note that \bar{Q} 's, and therefore A 's, B 's, and D 's, are, in general, functions of position (x, y) . Equations (3.3.36) and (3.3.37) can be written in a compact form as

$$\begin{Bmatrix} \{N\} \\ \{M\} \end{Bmatrix} = \begin{bmatrix} [A] & [B] \\ [B] & [D] \end{bmatrix} \begin{Bmatrix} \{\varepsilon^0\} \\ \{\varepsilon^1\} \end{Bmatrix} \quad (3.3.39)$$

where $\{\varepsilon^0\}$ and $\{\varepsilon^1\}$ are vectors of the membrane and bending strains defined in Eq. (3.3.10), and $[A]$, $[B]$, and $[D]$ are the 3×3 symmetric matrices of laminate coefficients defined in Eqs. (3.3.38a,b). Values of the laminate stiffnesses for various stacking sequences will be presented in Section 3.5.

For the nonisothermal case, the strains are given by Eq. (3.3.14) and the laminate constitutive equations (39) become

$$\begin{Bmatrix} \{N\} \\ \{M\} \end{Bmatrix} = \begin{bmatrix} [A] & [B] \\ [B] & [D] \end{bmatrix} \begin{Bmatrix} \{\varepsilon^0\} \\ \{\varepsilon^1\} \end{Bmatrix} - \begin{Bmatrix} \{N^T\} \\ \{M^T\} \end{Bmatrix} - \begin{Bmatrix} \{N^P\} \\ \{M^P\} \end{Bmatrix} \quad (3.3.40)$$

where $\{N^T\}$ and $\{M^T\}$ are thermal force resultants

$$\{N^T\} = \sum_{k=1}^N \int_{z_k}^{z_{k+1}} [\bar{Q}]^{(k)} \{\bar{\alpha}\}^{(k)} \Delta T \, dz \quad (3.3.41a)$$

$$\{M^T\} = \sum_{k=1}^N \int_{z_k}^{z_{k+1}} [\bar{Q}]^{(k)} \{\bar{\alpha}\}^{(k)} \Delta T \, z \, dz \quad (3.3.41b)$$

and $\{N^P\}$ and $\{M^P\}$ are the piezoelectric resultants

$$\{N^P\} = \sum_{k=1}^N \int_{z_k}^{z_{k+1}} [\bar{e}]^{(k)} \{E\}^{(k)} dz \quad (3.3.42a)$$

$$\{M^P\} = \sum_{k=1}^N \int_{z_k}^{z_{k+1}} [\bar{e}]^{(k)} \{E\}^{(k)} z dz \quad (3.3.42b)$$

Relations similar to Eqs. (3.3.41a,b) can be written for hygroscopic effects.

3.3.6 Equations of Motion in Terms of Displacements

The stress resultants (N 's and M 's) are related to the displacement gradients, temperature increment, and electric field. In the absence of the temperature and electric effects, the force and moment resultants can be expressed in terms of the displacements (u_0, v_0, w_0) by the relations

$$\begin{aligned} \begin{Bmatrix} N_{xx} \\ N_{yy} \\ N_{xy} \end{Bmatrix} &= \begin{bmatrix} A_{11} & A_{12} & A_{16} \\ A_{12} & A_{22} & A_{26} \\ A_{16} & A_{26} & A_{66} \end{bmatrix} \begin{Bmatrix} \frac{\partial u_0}{\partial x} + \frac{1}{2} \left(\frac{\partial w_0}{\partial x} \right)^2 \\ \frac{\partial v_0}{\partial y} + \frac{1}{2} \left(\frac{\partial w_0}{\partial y} \right)^2 \\ \frac{\partial u_0}{\partial y} + \frac{\partial v_0}{\partial x} + \frac{\partial w_0}{\partial x} \frac{\partial w_0}{\partial y} \end{Bmatrix} \\ &\quad - \begin{bmatrix} B_{11} & B_{12} & B_{16} \\ B_{12} & B_{22} & B_{26} \\ B_{16} & B_{26} & B_{66} \end{bmatrix} \begin{Bmatrix} \frac{\partial^2 w_0}{\partial x^2} \\ \frac{\partial^2 w_0}{\partial y^2} \\ 2 \frac{\partial^2 w_0}{\partial x \partial y} \end{Bmatrix} \end{aligned} \quad (3.3.43)$$

$$\begin{aligned} \begin{Bmatrix} M_{xx} \\ M_{yy} \\ M_{xy} \end{Bmatrix} &= \begin{bmatrix} B_{11} & B_{12} & B_{16} \\ B_{12} & B_{22} & B_{26} \\ B_{16} & B_{26} & B_{66} \end{bmatrix} \begin{Bmatrix} \frac{\partial u_0}{\partial x} + \frac{1}{2} \left(\frac{\partial w_0}{\partial x} \right)^2 \\ \frac{\partial v_0}{\partial y} + \frac{1}{2} \left(\frac{\partial w_0}{\partial y} \right)^2 \\ \frac{\partial u_0}{\partial y} + \frac{\partial v_0}{\partial x} + \frac{\partial w_0}{\partial x} \frac{\partial w_0}{\partial y} \end{Bmatrix} \\ &\quad - \begin{bmatrix} D_{11} & D_{12} & D_{16} \\ D_{12} & D_{22} & D_{26} \\ D_{16} & D_{26} & D_{66} \end{bmatrix} \begin{Bmatrix} \frac{\partial^2 w_0}{\partial x^2} \\ \frac{\partial^2 w_0}{\partial y^2} \\ 2 \frac{\partial^2 w_0}{\partial x \partial y} \end{Bmatrix} \end{aligned} \quad (3.3.44)$$

The equations of motion (3.3.25) can be expressed in terms of displacements (u_0, v_0, w_0) by substituting for the force and moment resultants from Eqs. (3.3.43) and (3.3.44). In general, the laminate stiffnesses can be functions of position (x, y) (i.e., nonhomogeneous plates). For homogeneous laminates (i.e., for laminates with constant A 's, B 's, and D 's), the equations of motion (3.3.25) take the form

$$\begin{aligned} A_{11} \left(\frac{\partial^2 u_0}{\partial x^2} + \frac{\partial w_0}{\partial x} \frac{\partial^2 w_0}{\partial x^2} \right) &+ A_{12} \left(\frac{\partial^2 v_0}{\partial x \partial y} + \frac{\partial w_0}{\partial y} \frac{\partial^2 w_0}{\partial x \partial y} \right) \\ &+ A_{16} \left(\frac{\partial^2 u_0}{\partial x \partial y} + \frac{\partial^2 v_0}{\partial x^2} + \frac{\partial^2 w_0}{\partial x^2} \frac{\partial w_0}{\partial y} + \frac{\partial w_0}{\partial x} \frac{\partial^2 w_0}{\partial x \partial y} \right) \\ &- B_{11} \frac{\partial^3 w_0}{\partial x^3} - B_{12} \frac{\partial^3 w_0}{\partial x \partial y^2} - 2B_{16} \frac{\partial^3 w_0}{\partial x^2 \partial y} \end{aligned}$$

$$\begin{aligned}
& + A_{16} \left(\frac{\partial^2 u_0}{\partial x \partial y} + \frac{\partial w_0}{\partial x} \frac{\partial^2 w_0}{\partial x \partial y} \right) + A_{26} \left(\frac{\partial^2 v_0}{\partial y^2} + \frac{\partial w_0}{\partial y} \frac{\partial^2 w_0}{\partial y^2} \right) \\
& + A_{66} \left(\frac{\partial^2 u_0}{\partial y^2} + \frac{\partial^2 v_0}{\partial x \partial y} + \frac{\partial^2 w_0}{\partial x \partial y} \frac{\partial w_0}{\partial y} + \frac{\partial w_0}{\partial x} \frac{\partial^2 w_0}{\partial y^2} \right) \\
& - B_{16} \frac{\partial^3 w_0}{\partial x^2 \partial y} - B_{26} \frac{\partial^3 w_0}{\partial y^3} - 2B_{66} \frac{\partial^3 w_0}{\partial x \partial y^2} \\
& - \left(\frac{\partial N_{xx}^T}{\partial x} + \frac{\partial N_{xy}^T}{\partial y} \right) = I_0 \frac{\partial^2 u_0}{\partial t^2} - I_1 \frac{\partial^3 w_0}{\partial x \partial t^2}
\end{aligned} \tag{3.3.45}$$

$$\begin{aligned}
& A_{16} \left(\frac{\partial^2 u_0}{\partial x^2} + \frac{\partial w_0}{\partial x} \frac{\partial^2 w_0}{\partial x^2} \right) + A_{26} \left(\frac{\partial^2 v_0}{\partial x \partial y} + \frac{\partial w_0}{\partial y} \frac{\partial^2 w_0}{\partial x \partial y} \right) \\
& + A_{66} \left(\frac{\partial^2 u_0}{\partial x \partial y} + \frac{\partial^2 v_0}{\partial x^2} + \frac{\partial^2 w_0}{\partial x^2} \frac{\partial w_0}{\partial y} + \frac{\partial w_0}{\partial x} \frac{\partial^2 w_0}{\partial x \partial y} \right) \\
& - B_{16} \frac{\partial^3 w_0}{\partial x^3} - B_{26} \frac{\partial^3 w_0}{\partial x \partial y^2} - 2B_{66} \frac{\partial^3 w_0}{\partial x^2 \partial y} \\
& + A_{12} \left(\frac{\partial^2 u_0}{\partial x \partial y} + \frac{\partial w_0}{\partial x} \frac{\partial^2 w_0}{\partial x \partial y} \right) + A_{22} \left(\frac{\partial^2 v_0}{\partial y^2} + \frac{\partial w_0}{\partial y} \frac{\partial^2 w_0}{\partial y^2} \right) \\
& + A_{26} \left(\frac{\partial^2 u_0}{\partial y^2} + \frac{\partial^2 v_0}{\partial x \partial y} + \frac{\partial^2 w_0}{\partial x \partial y} \frac{\partial w_0}{\partial y} + \frac{\partial w_0}{\partial x} \frac{\partial^2 w_0}{\partial y^2} \right) \\
& - B_{12} \frac{\partial^3 w_0}{\partial x^2 \partial y} - B_{22} \frac{\partial^3 w_0}{\partial y^3} - 2B_{26} \frac{\partial^3 w_0}{\partial x \partial y^2} \\
& - \left(\frac{\partial N_{xy}^T}{\partial x} + \frac{\partial N_{yy}^T}{\partial y} \right) = I_0 \frac{\partial^2 v_0}{\partial t^2} - I_1 \frac{\partial^3 w_0}{\partial y \partial t^2}
\end{aligned} \tag{3.3.46}$$

$$\begin{aligned}
& B_{11} \left(\frac{\partial^3 u_0}{\partial x^3} + \frac{\partial^2 w_0}{\partial x^2} \frac{\partial^2 w_0}{\partial x^2} + \frac{\partial w_0}{\partial x} \frac{\partial^3 w_0}{\partial x^3} \right) + B_{12} \left(\frac{\partial^3 v_0}{\partial x^2 \partial y} + \frac{\partial^2 w_0}{\partial x \partial y} \frac{\partial^2 w_0}{\partial x \partial y} \right. \\
& \left. + \frac{\partial w_0}{\partial y} \frac{\partial^3 w_0}{\partial x^2 \partial y} \right) + B_{16} \left(\frac{\partial^3 u_0}{\partial x^2 \partial y} + \frac{\partial^3 v_0}{\partial x^3} + \frac{\partial^3 w_0}{\partial x^3} \frac{\partial w_0}{\partial y} + 2 \frac{\partial^2 w_0}{\partial x^2} \frac{\partial^2 w_0}{\partial x \partial y} \right. \\
& \left. + \frac{\partial w_0}{\partial x} \frac{\partial^3 w_0}{\partial x^2 \partial y} \right) - D_{11} \frac{\partial^4 w_0}{\partial x^4} - D_{12} \frac{\partial^4 w_0}{\partial x^2 \partial y^2} - 2D_{16} \frac{\partial^4 w_0}{\partial x^3 \partial y} \\
& + 2B_{16} \left(\frac{\partial^3 u_0}{\partial x^2 \partial y} + \frac{\partial^2 w_0}{\partial x^2} \frac{\partial^2 w_0}{\partial x \partial y} + \frac{\partial w_0}{\partial x} \frac{\partial^3 w_0}{\partial x^2 \partial y} \right) + 2B_{26} \left(\frac{\partial^3 v_0}{\partial x \partial y^2} + \frac{\partial^2 w_0}{\partial x \partial y} \frac{\partial^2 w_0}{\partial y^2} \right. \\
& \left. + \frac{\partial w_0}{\partial y} \frac{\partial^3 w_0}{\partial x \partial y^2} \right) + 2B_{66} \left(\frac{\partial^3 u_0}{\partial x \partial y^2} + \frac{\partial^3 v_0}{\partial x^2 \partial y} + \frac{\partial^3 w_0}{\partial x^2 \partial y} \frac{\partial w_0}{\partial y} + \frac{\partial^2 w_0}{\partial x \partial y} \frac{\partial^2 w_0}{\partial x \partial y} \right. \\
& \left. + \frac{\partial^2 w_0}{\partial x^2} \frac{\partial^2 w_0}{\partial y^2} + \frac{\partial w_0}{\partial x} \frac{\partial^3 w_0}{\partial x \partial y^2} \right) - 2D_{16} \frac{\partial^4 w_0}{\partial x^3 \partial y} - 2D_{26} \frac{\partial^4 w_0}{\partial x \partial y^3} \\
& - 4D_{66} \frac{\partial^4 w_0}{\partial x^2 \partial y^2} + B_{12} \left(\frac{\partial^3 u_0}{\partial x \partial y^2} + \frac{\partial^2 w_0}{\partial x \partial y} \frac{\partial^2 w_0}{\partial x \partial y} + \frac{\partial w_0}{\partial x} \frac{\partial^3 w_0}{\partial x \partial y^2} \right)
\end{aligned}$$

$$\begin{aligned}
& + B_{22} \left(\frac{\partial^3 v_0}{\partial y^3} + \frac{\partial^2 w_0}{\partial y^2} \frac{\partial^2 w_0}{\partial y^2} + \frac{\partial w_0}{\partial y} \frac{\partial^3 w_0}{\partial y^3} \right) + B_{26} \left(\frac{\partial^3 u_0}{\partial y^3} + \frac{\partial^3 v_0}{\partial x \partial y^2} \right. \\
& \left. + \frac{\partial^3 w_0}{\partial x \partial y^2} \frac{\partial w_0}{\partial y} + 2 \frac{\partial^2 w_0}{\partial x \partial y} \frac{\partial^2 w_0}{\partial y^2} + \frac{\partial w_0}{\partial x} \frac{\partial^3 w_0}{\partial y^3} \right) \\
& - D_{12} \frac{\partial^4 w_0}{\partial x^2 \partial y^2} - D_{22} \frac{\partial^4 w_0}{\partial y^4} - 2D_{26} \frac{\partial^4 w_0}{\partial x \partial y^3} + \mathcal{N}(w_0) + q \\
& - \left(\frac{\partial^2 M_{xx}^T}{\partial x^2} + 2 \frac{\partial^2 M_{xy}^T}{\partial y \partial x} + \frac{\partial^2 M_{yy}^T}{\partial y^2} \right) \\
& = I_0 \frac{\partial^2 w_0}{\partial t^2} - I_2 \frac{\partial^2}{\partial t^2} \left(\frac{\partial^2 w_0}{\partial x^2} + \frac{\partial^2 w_0}{\partial y^2} \right) + I_1 \frac{\partial^2}{\partial t^2} \left(\frac{\partial u_0}{\partial x} + \frac{\partial v_0}{\partial y} \right) \tag{3.3.47}
\end{aligned}$$

where $\mathcal{N}(w_0)$ was defined in Eq. (3.3.24a).

The nonlinear partial differential equations (3.3.45)–(3.3.47) can be simplified for linear analyses, static analyses, and lamination schemes for which some of the stiffnesses (A_{ij} , B_{ij} , D_{ij}) are zero. These cases will be considered in the sequel. Once the displacements are determined by solving Eqs. (3.3.45)–(3.3.47), analytically or numerically for a given problem, the strains and stresses in each lamina can be computed using Eqs. (3.3.10) and (3.3.12), respectively.

Example 3.3.1: (Cylindrical Bending)

If a plate is infinitely long in one direction, the plate becomes a *plate strip*. Consider a plate strip that has a finite dimension along the x -axis and subjected to a transverse load $q(x)$ that is uniform at any section parallel to the x -axis. In such a case, the deflection w_0 and displacements (u_0, v_0) of the plate are functions of only x . Therefore, all derivatives with respect to y are zero. In such cases, the deflected surface of the plate strip is cylindrical, and it is referred to as the *cylindrical bending*. For this case, the governing equations (3.3.45)–(3.3.47) reduce to

$$A_{11} \left(\frac{\partial^2 u_0}{\partial x^2} + \frac{\partial w_0}{\partial x} \frac{\partial^2 w_0}{\partial x^2} \right) + A_{16} \frac{\partial^2 v_0}{\partial x^2} - B_{11} \frac{\partial^3 w_0}{\partial x^3} - \frac{\partial N_{xx}^T}{\partial x} = I_0 \frac{\partial^2 u_0}{\partial t^2} - I_1 \frac{\partial^3 w_0}{\partial x \partial t^2} \tag{3.3.48a}$$

$$A_{16} \left(\frac{\partial^2 u_0}{\partial x^2} + \frac{\partial w_0}{\partial x} \frac{\partial^2 w_0}{\partial x^2} \right) + A_{66} \frac{\partial^2 v_0}{\partial x^2} - B_{16} \frac{\partial^3 w_0}{\partial x^3} - \frac{\partial N_{xy}^T}{\partial x} = I_0 \frac{\partial^2 v_0}{\partial t^2} \tag{3.3.48b}$$

$$\begin{aligned}
& B_{11} \left(\frac{\partial^3 u_0}{\partial x^3} + \frac{\partial^2 w_0}{\partial x^2} \frac{\partial^2 w_0}{\partial x^2} + \frac{\partial w_0}{\partial x} \frac{\partial^3 w_0}{\partial x^3} \right) + B_{16} \frac{\partial^3 v_0}{\partial x^3} - D_{11} \frac{\partial^4 w_0}{\partial x^4} - \frac{\partial^2 M_{xx}^T}{\partial x^2} \\
& + \frac{\partial}{\partial x} \left(N_{xx} \frac{\partial w_0}{\partial x} \right) + q = I_0 \frac{\partial^2 w_0}{\partial t^2} - I_2 \frac{\partial^4 w_0}{\partial x^2 \partial t^2} + I_1 \frac{\partial^3 u_0}{\partial x \partial t^2} \tag{3.3.48c}
\end{aligned}$$

Example 3.3.2:

Suppose that a six-layer ($\pm 60/0$)_s symmetric laminate is subjected to loads such that the only nonzero strains at a point (x, y) are $\varepsilon_{xx}^{(0)} = \varepsilon_0$ in./in. and $\varepsilon_{xx}^{(1)} = \kappa_0$ /in. Assume that layers are of thickness 0.005 in. with material properties $E_1 = 7.8$ psi, $E_2 = 2.6$ psi, $G_{12} = G_{13} = 1.3$ psi, $G_{23} = 0.5$ psi, and $\nu_{12} = 0.25$. We wish to determine the state of stress $(\sigma_{xx}, \sigma_{yy}, \sigma_{xy})$ and force resultants in the laminate.

The only nonzero strain is $\varepsilon_{xx} = \varepsilon_0 + z\kappa_0$. Hence, the stresses in k th lamina are given by

$$\sigma_{xx}^{(k)} = \bar{Q}_{11}^{(k)} (\varepsilon_0 + z\kappa_0), \quad \sigma_{yy}^{(k)} = \bar{Q}_{12}^{(k)} (\varepsilon_0 + z\kappa_0), \quad \sigma_{xy}^{(k)} = \bar{Q}_{16}^{(k)} (\varepsilon_0 + z\kappa_0)$$

where

$$[\bar{Q}]_{\pm 60^\circ} = \begin{bmatrix} 3.215 & 1.431 & \pm 0.707 \\ 1.431 & 5.871 & \pm 1.593 \\ \pm 0.707 & \pm 1.593 & 2.068 \end{bmatrix} \text{ msi}, \quad [\bar{Q}]_{0^\circ} = \begin{bmatrix} 7.966 & 0.664 & 0 \\ 0.664 & 2.655 & 0 \\ 0 & 0 & 1.3 \end{bmatrix} \text{ msi}$$

The stress resultants are given by

$$\begin{Bmatrix} N_{xx} \\ N_{yy} \\ N_{xy} \end{Bmatrix} = \begin{Bmatrix} 0.1440 \\ 0.0353 \\ 0 \end{Bmatrix} \varepsilon_0 \times 10^6 \text{ lb/in.}, \quad \begin{Bmatrix} M_{xx} \\ M_{yy} \\ M_{xy} \end{Bmatrix} = \begin{Bmatrix} 7.6306 \\ 3.1566 \\ 0.7066 \end{Bmatrix} \kappa_0 \text{ lb-in/in.}$$

If $\varepsilon_0 = 1000 \times 10^{-6}$ in./in. and $\kappa_0 = 0$, we have

$$\begin{Bmatrix} N_{xx} \\ N_{yy} \\ N_{xy} \end{Bmatrix} = \begin{Bmatrix} 144 \\ 35.3 \\ 0 \end{Bmatrix} \text{ lb/in.}, \quad \begin{Bmatrix} M_{xx} \\ M_{yy} \\ M_{xy} \end{Bmatrix} = \begin{Bmatrix} 0 \\ 0 \\ 0 \end{Bmatrix} \text{ lb-in/in.}$$

If $\varepsilon_0 = 0$ in./in. and $\kappa_0 = 1.0$ /in., we have

$$\begin{Bmatrix} N_{xx} \\ N_{yy} \\ N_{xy} \end{Bmatrix} = \begin{Bmatrix} 0 \\ 0 \\ 0 \end{Bmatrix} \text{ lb/in.}, \quad \begin{Bmatrix} M_{xx} \\ M_{yy} \\ M_{xy} \end{Bmatrix} = \begin{Bmatrix} 7.6306 \\ 3.1566 \\ 0.7066 \end{Bmatrix} \text{ lb-in/in.}$$

3.4 The First-Order Laminated Plate Theory

3.4.1 Displacements and Strains

In the *first-order shear deformation laminated plate theory* (FSDT), the *Kirchhoff hypothesis* is relaxed by removing the third part; i.e., the transverse normals *do not* remain perpendicular to the midsurface after deformation (see Figure 3.4.1). This amounts to including transverse shear strains in the theory. The inextensibility of transverse normals requires that w not be a function of the thickness coordinate, z .

Under the same assumptions and restrictions as in the classical laminate theory, the displacement field of the first-order theory is of the form

$$\begin{aligned} u(x, y, z, t) &= u_0(x, y, t) + z\phi_x(x, y, t) \\ v(x, y, z, t) &= v_0(x, y, t) + z\phi_y(x, y, t) \\ w(x, y, z, t) &= w_0(x, y, t) \end{aligned} \tag{3.4.1}$$

where $(u_0, v_0, w_0, \phi_x, \phi_y)$ are unknown functions to be determined. As before, (u_0, v_0, w_0) denote the displacements of a point on the plane $z = 0$. Note that

$$\frac{\partial u}{\partial z} = \phi_x, \quad \frac{\partial v}{\partial z} = \phi_y \tag{3.4.2a}$$

which indicate that ϕ_x and ϕ_y are the rotations of a transverse normal about the y - and x -axes, respectively (see Figure 3.4.1). The notation that ϕ_x denotes the rotation of a transverse normal about the y -axis and ϕ_y denotes the rotation about the x -axis may be confusing to some, and they do not follow the right-hand rule. However, the notation has been used extensively in the literature, and we will not

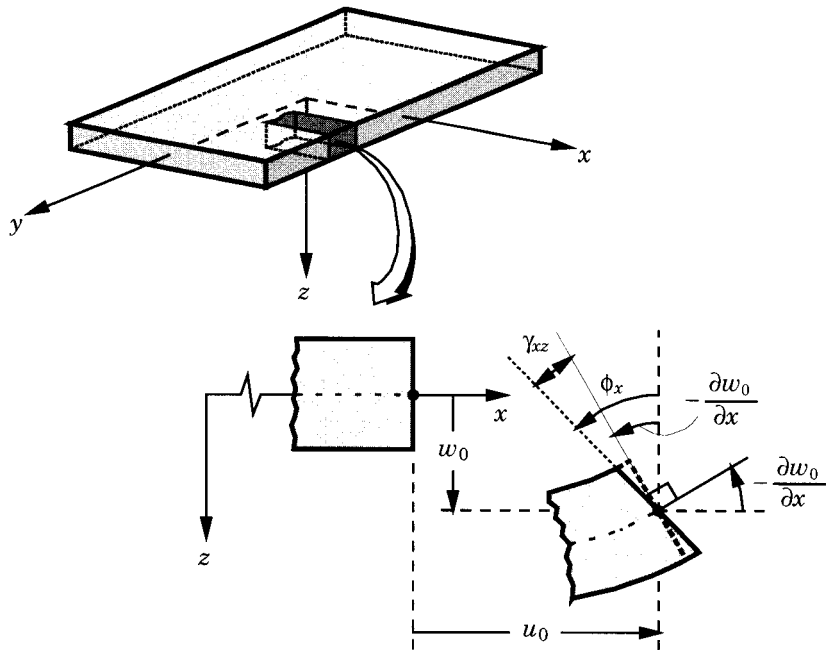


Figure 3.4.1: Undeformed and deformed geometries of an edge of a plate under the assumptions of the first-order plate theory.

depart from it. If (β_x, β_y) denote the rotations about the x and y axes, respectively, that follow the right-hand rule, then

$$\beta_x = -\phi_y, \quad \beta_y = \phi_x \quad (3.4.2b)$$

The quantities $(u_0, v_0, w_0, \phi_x, \phi_y)$ will be called the *generalized displacements*. For thin plates, i.e., when the plate in-plane characteristic dimension to thickness ratio is on the order 50 or greater, the rotation functions ϕ_x and ϕ_y should approach the respective slopes of the transverse deflection:

$$\phi_x = -\frac{\partial w_0}{\partial x}, \quad \phi_y = -\frac{\partial w_0}{\partial y}$$

The nonlinear strains associated with the displacement field (3.4.1) are obtained by using Eq. (3.4.1) in Eq. (3.3.7):

$$\begin{aligned} \varepsilon_{xx} &= \frac{\partial u_0}{\partial x} + \frac{1}{2} \left(\frac{\partial w_0}{\partial x} \right)^2 + z \frac{\partial \phi_x}{\partial x} \\ \gamma_{xy} &= \left(\frac{\partial u_0}{\partial y} + \frac{\partial v_0}{\partial x} + \frac{\partial w_0}{\partial x} \frac{\partial w_0}{\partial y} \right) + z \left(\frac{\partial \phi_x}{\partial y} + \frac{\partial \phi_y}{\partial x} \right) \end{aligned}$$

$$\begin{aligned}\varepsilon_{yy} &= \frac{\partial v_0}{\partial y} + \frac{1}{2} \left(\frac{\partial w_0}{\partial y} \right)^2 + z \frac{\partial \phi_y}{\partial y} \\ \gamma_{xz} &= \frac{\partial w_0}{\partial x} + \phi_x, \quad \gamma_{yz} = \frac{\partial w_0}{\partial y} + \phi_y, \quad \varepsilon_{zz} = 0\end{aligned}\quad (3.4.3)$$

Note that the strains ($\varepsilon_{xx}, \varepsilon_{yy}, \gamma_{xy}$) are linear through the laminate thickness, while the transverse shear strains (γ_{xz}, γ_{yz}) are constant through the thickness of the laminate in the first-order laminated plate theory. Of course, the constant state of transverse shear strains through the laminate thickness is a gross approximation of the true stress field, which is at least quadratic through the thickness.

The strains in Eq. (3.4.3) have the form

$$\begin{Bmatrix} \varepsilon_{xx} \\ \varepsilon_{yy} \\ \gamma_{yz} \\ \gamma_{xz} \\ \gamma_{xy} \end{Bmatrix} = \begin{Bmatrix} \varepsilon_{xx}^{(0)} \\ \varepsilon_{yy}^{(0)} \\ \gamma_{yz}^{(0)} \\ \gamma_{xz}^{(0)} \\ \gamma_{xy}^{(0)} \end{Bmatrix} + z \begin{Bmatrix} \varepsilon_{xx}^{(1)} \\ \varepsilon_{yy}^{(1)} \\ \gamma_{yz}^{(1)} \\ \gamma_{xz}^{(1)} \\ \gamma_{xy}^{(1)} \end{Bmatrix} = \begin{Bmatrix} \frac{\partial u_0}{\partial x} + \frac{1}{2} \left(\frac{\partial w_0}{\partial x} \right)^2 \\ \frac{\partial v_0}{\partial y} + \frac{1}{2} \left(\frac{\partial w_0}{\partial y} \right)^2 \\ \frac{\partial w_0}{\partial y} + \phi_y \\ \frac{\partial w_0}{\partial x} + \phi_x \\ \frac{\partial u_0}{\partial y} + \frac{\partial v_0}{\partial x} + \frac{\partial w_0}{\partial x} \frac{\partial w_0}{\partial y} \end{Bmatrix} + z \begin{Bmatrix} \frac{\partial \phi_x}{\partial x} \\ \frac{\partial \phi_y}{\partial y} \\ 0 \\ 0 \\ \frac{\partial \phi_x}{\partial y} + \frac{\partial \phi_y}{\partial x} \end{Bmatrix} \quad (3.4.4)$$

3.4.2 Equations of Motion

The governing equations of the first-order theory will be derived using the dynamic version of the principle of virtual displacements:

$$0 = \int_0^T (\delta U + \delta V - \delta K) dt \quad (3.4.5)$$

where the virtual strain energy δU , virtual work done by applied forces δV , and the virtual kinetic energy δK are given by

$$\begin{aligned}\delta U &= \int_{\Omega_0} \left\{ \int_{-\frac{h}{2}}^{\frac{h}{2}} \left[\sigma_{xx} \left(\delta \varepsilon_{xx}^{(0)} + z \delta \varepsilon_{xx}^{(1)} \right) + \sigma_{yy} \left(\delta \varepsilon_{yy}^{(0)} + z \delta \varepsilon_{yy}^{(1)} \right) \right. \right. \\ &\quad \left. \left. + \sigma_{xy} \left(\delta \gamma_{xy}^{(0)} + z \delta \gamma_{xy}^{(1)} \right) + \sigma_{xz} \delta \gamma_{xz}^{(0)} + \sigma_{yz} \delta \gamma_{yz}^{(0)} \right] dz \right\} dx dy \quad (3.4.6)\end{aligned}$$

$$\begin{aligned}\delta V &= - \int_{\Omega_0} [(q_b + q_t) \delta w_0] dx dy - \int_{\Gamma_\sigma} \int_{-\frac{h}{2}}^{\frac{h}{2}} [\hat{\sigma}_{nn} (\delta u_n + z \delta \phi_n) \\ &\quad + \hat{\sigma}_{ns} (\delta u_s + z \delta \phi_s) + \hat{\sigma}_{nz} \delta w_0] dz ds \quad (3.4.7)\end{aligned}$$

$$\begin{aligned}\delta K &= \int_{\Omega_0} \int_{-\frac{h}{2}}^{\frac{h}{2}} \rho_0 \left[\left(\dot{u}_0 + z \dot{\phi}_x \right) \left(\delta \dot{u}_0 + z \delta \dot{\phi}_x \right) + \left(\dot{v}_0 + z \dot{\phi}_y \right) \left(\delta \dot{v}_0 + z \delta \dot{\phi}_y \right) \right. \\ &\quad \left. + \dot{w}_0 \delta \dot{w}_0 \right] dz dx dy \quad (3.4.8)\end{aligned}$$

where all variables were previously introduced [see Eqs. (3.3.16)–(3.3.18) and the paragraph following the equations].

Substituting for δU , δV , and δK from Eqs. (3.4.6)–(3.4.8) into the virtual work statement in Eq. (3.4.5) and integrating through the thickness of the laminate, we obtain

$$0 = \int_0^T \left\{ \int_{\Omega_0} \left[N_{xx} \delta \varepsilon_{xx}^{(0)} + M_{xx} \delta \varepsilon_{xx}^{(1)} + N_{yy} \delta \varepsilon_{yy}^{(0)} + M_{yy} \delta \varepsilon_{yy}^{(1)} + N_{xy} \delta \gamma_{xy}^{(0)} + M_{xy} \delta \gamma_{xy}^{(1)} \right. \right. \\ \left. \left. + Q_x \delta \gamma_{xz}^{(0)} + Q_y \delta \gamma_{yz}^{(0)} - q \delta w_0 - I_0 (\dot{u}_0 \delta \dot{u}_0 + \dot{v}_0 \delta \dot{v}_0 + \dot{w}_0 \delta \dot{w}_0) \right. \right. \\ \left. \left. - I_1 (\dot{\phi}_x \delta \dot{u}_0 + \dot{\phi}_y \delta \dot{v}_0 + \delta \dot{\phi}_x \dot{u}_0 + \delta \dot{\phi}_y \dot{v}_0) - I_2 (\dot{\phi}_x \delta \dot{\phi}_x + \dot{\phi}_y \delta \dot{\phi}_y) \right] dx dy \right. \\ \left. - \int_{\Gamma_\sigma} (\hat{N}_{nn} \delta u_n + \hat{N}_{ns} \delta u_s + \hat{M}_{nn} \delta \phi_n + \hat{M}_{ns} \delta \phi_s + \hat{Q}_n \delta w_0) ds \right\} dt \quad (3.4.9)$$

where $q = q_b + q_t$, the stress resultants ($N_{xx}, N_{yy}, N_{xy}, M_{xx}, M_{yy}, M_{xy}$) and the inertias (I_0, I_1, I_2) are as defined in Eq. (3.3.20), ($N_{nn}, N_{ns}, M_{nn}, M_{ns}$) are as defined in Eq. (3.3.29a,b), and

$$\begin{Bmatrix} Q_x \\ Q_y \end{Bmatrix} = \int_{-\frac{h}{2}}^{\frac{h}{2}} \begin{Bmatrix} \sigma_{xz} \\ \sigma_{yz} \end{Bmatrix} dz \quad (3.4.10a)$$

The quantities (Q_x, Q_y) are called the *transverse force resultants*.

Shear Correction Factors

Since the transverse shear strains are represented as constant through the laminate thickness, it follows that the transverse shear stresses will also be constant. It is well known from elementary theory of homogeneous beams that the transverse shear stress varies parabolically through the beam thickness. In composite laminated beams and plates, the transverse shear stresses vary at least quadratically through layer thickness. This discrepancy between the actual stress state and the constant stress state predicted by the first-order theory is often corrected in computing the transverse shear force resultants (Q_x, Q_y) by multiplying the integrals in Eq. (3.4.10a) with a parameter K , called *shear correction coefficient*:

$$\begin{Bmatrix} Q_x \\ Q_y \end{Bmatrix} = K \int_{-\frac{h}{2}}^{\frac{h}{2}} \begin{Bmatrix} \sigma_{xz} \\ \sigma_{yz} \end{Bmatrix} dz \quad (3.4.10b)$$

This amounts to modifying the plate transverse shear stiffnesses. The factor K is computed such that the strain energy due to transverse shear stresses in Eq. (3.4.10b) equals the strain energy due to the true transverse stresses predicted by the three-dimensional elasticity theory.

For example, consider a homogeneous beam with rectangular cross section, with width b and height h . The actual shear stress distribution through the thickness of the beam, from a course on mechanics of materials, is given by

$$\sigma_{xz}^c = \frac{3Q}{2bh} \left[1 - \left(\frac{2z}{h} \right)^2 \right], \quad -\frac{h}{2} \leq z \leq \frac{h}{2}$$

where Q is the transverse shear force. The transverse shear stress in the first-order theory is a constant, $\sigma_{xz}^f = Q/bh$. The strain energies due to transverse shear stresses in the two theories are

$$U_s^c = \frac{1}{2G_{13}} \int_A (\sigma_{xz}^c)^2 dA = \frac{3Q^2}{5G_{13}bh}$$

$$U_s^f = \frac{1}{2G_{13}} \int_A (\sigma_{xz}^f)^2 dA = \frac{Q^2}{2G_{13}bh}$$

The shear correction factor is the ratio of U_s^f to U_s^c , which gives $K = 5/6$. The shear correction factor for a general laminate depends on lamina properties and lamination scheme.

Returning to the virtual work statement in Eq. (3.4.9), we substitute for the virtual strains into Eq. (3.4.9) and integrate by parts to relieve the virtual generalized displacements ($\delta u_0, \delta v_0, \delta w_0, \delta \phi_x, \delta \phi_y$) in Ω_0 of any differentiation, so that we can use the fundamental lemma of variational calculus; we obtain

$$0 = \int_0^T \int_{\Omega_0} \left[- \left(N_{xx,x} + N_{xy,y} - I_0 \ddot{u}_0 - I_1 \ddot{\phi}_x \right) \delta u_0 \right. \\ - \left(N_{xy,x} + N_{yy,y} - I_0 \ddot{v}_0 - I_1 \ddot{\phi}_y \right) \delta v_0 \\ - \left(M_{xx,x} + M_{xy,y} - Q_x - I_2 \ddot{\phi}_x - I_1 \ddot{u}_0 \right) \delta \phi_x \\ - \left(M_{xy,x} + M_{yy,y} - Q_y - I_2 \ddot{\phi}_y - I_1 \ddot{v}_0 \right) \delta \phi_y \\ \left. - (Q_{x,x} + Q_{y,y} + \mathcal{N}(w_0) + q - I_0 \ddot{w}_0) \delta w_0 \right] dx dy \\ + \int_0^T \int_{\Gamma} \left[(N_{nn} - \hat{N}_{nn}) \delta u_n + (N_{ns} - \hat{N}_{ns}) \delta u_s + (Q_n - \hat{Q}_n) \delta w_0 \right. \\ \left. + (M_{nn} - \hat{M}_{nn}) \delta \phi_n + (M_{ns} - \hat{M}_{ns}) \delta \phi_s \right] ds dt \quad (3.4.11)$$

where $\mathcal{N}(w_0)$ and $\mathcal{P}(w_0)$ were defined in Eq. (3.3.24), and the boundary expressions were arrived by expressing ϕ_x and ϕ_y in terms of the normal and tangential rotations, (ϕ_n, ϕ_s):

$$\phi_x = n_x \phi_n - n_y \phi_s, \quad \phi_y = n_y \delta \phi_n + n_x \delta \phi_s \quad (3.4.12)$$

The Euler–Lagrange equations are obtained by setting the coefficients of $\delta u_0, \delta v_0, \delta w_0, \delta \phi_x$, and $\delta \phi_y$ in Ω_0 to zero separately:

$$\delta u_0 : \quad \frac{\partial N_{xx}}{\partial x} + \frac{\partial N_{xy}}{\partial y} = I_0 \frac{\partial^2 u_0}{\partial t^2} + I_1 \frac{\partial^2 \phi_x}{\partial t^2}$$

$$\delta v_0 : \quad \frac{\partial N_{xy}}{\partial x} + \frac{\partial N_{yy}}{\partial y} = I_0 \frac{\partial^2 v_0}{\partial t^2} + I_1 \frac{\partial^2 \phi_y}{\partial t^2}$$

$$\delta w_0 : \quad \frac{\partial Q_x}{\partial x} + \frac{\partial Q_y}{\partial y} + \mathcal{N}(w_0) + q = I_0 \frac{\partial^2 w_0}{\partial t^2}$$

$$\begin{aligned}\delta\phi_x : \quad & \frac{\partial M_{xx}}{\partial x} + \frac{\partial M_{xy}}{\partial y} - Q_x = I_2 \frac{\partial^2 \phi_x}{\partial t^2} + I_1 \frac{\partial^2 u_0}{\partial t^2} \\ \delta\phi_y : \quad & \frac{\partial M_{xy}}{\partial x} + \frac{\partial M_{yy}}{\partial y} - Q_y = I_2 \frac{\partial^2 \phi_y}{\partial t^2} + I_1 \frac{\partial^2 v_0}{\partial t^2}\end{aligned}\quad (3.4.13)$$

The natural boundary conditions are obtained by setting the coefficients of δu_n , δu_s , δw_0 , $\delta\phi_n$, and $\delta\phi_s$ on Γ to zero separately:

$$\begin{aligned}N_{nn} - \hat{N}_{nn} &= 0, \quad N_{ns} - \hat{N}_{ns} = 0, \quad Q_n - \hat{Q}_n = 0 \\ M_{nn} - \hat{M}_{nn} &= 0, \quad M_{ns} - \hat{M}_{ns} = 0\end{aligned}\quad (3.4.14a)$$

where

$$Q_n \equiv Q_x n_x + Q_y n_y + \mathcal{P}(w_0) \quad (3.4.14b)$$

Thus the primary and secondary variables of the theory are

$$\begin{aligned}\text{primary variables: } & u_n, u_s, w_0, \phi_n, \phi_s \\ \text{secondary variables: } & N_{nn}, N_{ns}, Q_n, M_{nn}, M_{ns}\end{aligned}\quad (3.4.15)$$

Note that Q_n defined in Eq. (3.4.14b) is the same as that defined in Eq. (3.3.31b). This follows from the last two equations of (3.4.13).

The initial conditions of the theory involve specifying the values of the displacements and their first derivatives with respect to time at $t = 0$:

$$\begin{aligned}u_n &= u_n^0, \quad u_s = u_s^0, \quad w_0 = w_0^0, \quad \phi_n = \phi_n^0, \quad \phi_s = \phi_s^0 \\ \dot{u}_n &= \dot{u}_n^0, \quad \dot{u}_s = \dot{u}_s^0, \quad \dot{w}_0 = \dot{w}_0^0, \quad \dot{\phi}_n = \dot{\phi}_n^0, \quad \dot{\phi}_s = \dot{\phi}_s^0\end{aligned}\quad (3.4.16)$$

for all points in Ω_0 .

3.4.3 Laminate Constitutive Equations

The laminate constitutive equations for the first-order theory are obtained using the lamina constitutive equations (3.3.12a) and the following relations:

$$\left\{ \begin{array}{l} \sigma_{yz} \\ \sigma_{xz} \end{array} \right\}^{(k)} = \begin{bmatrix} \bar{Q}_{44} & \bar{Q}_{45} \\ \bar{Q}_{45} & \bar{Q}_{55} \end{bmatrix}^{(k)} \left\{ \begin{array}{l} \gamma_{yz}^{(0)} \\ \gamma_{xz}^{(0)} \end{array} \right\} - \begin{bmatrix} \bar{e}_{14} & \bar{e}_{24} & 0 \\ \bar{e}_{15} & \bar{e}_{25} & 0 \end{bmatrix}^{(k)} \left\{ \begin{array}{l} \mathcal{E}_x \\ \mathcal{E}_y \\ \mathcal{E}_z \end{array} \right\}^{(k)} \quad (3.4.17a)$$

where [see Eq. (2.4.10)]

$$\begin{aligned}\bar{Q}_{44} &= Q_{44} \cos^2 \theta + Q_{55} \sin^2 \theta \\ \bar{Q}_{45} &= (Q_{55} - Q_{44}) \cos \theta \sin \theta \\ \bar{Q}_{55} &= Q_{44} \sin^2 \theta + Q_{55} \cos^2 \theta\end{aligned}\quad (3.4.17b)$$

$$\begin{aligned}\bar{e}_{14} &= (e_{15} - e_{24}) \sin \theta \cos \theta, \quad \bar{e}_{24} = e_{24} \cos^2 \theta + e_{15} \sin^2 \theta \\ \bar{e}_{15} &= e_{15} \cos^2 \theta + e_{24} \sin^2 \theta, \quad \bar{e}_{25} = (e_{15} - e_{24}) \sin \theta \cos \theta\end{aligned}\quad (3.4.17c)$$

The laminate constitutive equations in Eqs. (3.3.36) and (3.3.37) are valid also for the first-order laminate theory. In addition, we have the following laminate constitutive equations:

$$\begin{Bmatrix} Q_y \\ Q_x \end{Bmatrix} = K \sum_{k=1}^N \int_{z_k}^{z_{k+1}} \begin{Bmatrix} \sigma_{yz} \\ \sigma_{xz} \end{Bmatrix} dz$$

or

$$\begin{Bmatrix} Q_y \\ Q_x \end{Bmatrix} = K \begin{bmatrix} A_{44} & A_{45} \\ A_{45} & A_{55} \end{bmatrix} \begin{Bmatrix} \gamma_{yz}^{(0)} \\ \gamma_{xz}^{(0)} \end{Bmatrix} - \begin{Bmatrix} Q_y^P \\ Q_x^P \end{Bmatrix} \quad (3.4.18)$$

where the extensional stiffnesses A_{44} , A_{45} , and A_{55} are defined by

$$\begin{aligned} (A_{44}, A_{45}, A_{55}) &= \int_{-\frac{h}{2}}^{\frac{h}{2}} (\bar{Q}_{44}, \bar{Q}_{45}, \bar{Q}_{55}) dz \\ &= \sum_{k=1}^N \int_{z_k}^{z_{k+1}} (\bar{Q}_{44}^{(k)}, \bar{Q}_{45}^{(k)}, \bar{Q}_{55}^{(k)}) dz \\ &= \sum_{k=1}^N (\bar{Q}_{44}^{(k)}, \bar{Q}_{45}^{(k)}, \bar{Q}_{55}^{(k)})(z_{k+1} - z_k) \end{aligned} \quad (3.4.19a)$$

and the piezoelectric forces Q_x^P and Q_y^P are defined by

$$\begin{Bmatrix} Q_x^P \\ Q_y^P \end{Bmatrix} = \sum_{k=1}^N \int_{z_k}^{z_{k+1}} \begin{bmatrix} \bar{e}_{14} & \bar{e}_{24} & 0 \\ \bar{e}_{15} & \bar{e}_{25} & 0 \end{bmatrix}^{(k)} \begin{Bmatrix} \mathcal{E}_x \\ \mathcal{E}_y \\ \mathcal{E}_z \end{Bmatrix} dz \quad (3.4.19b)$$

When thermal and piezoelectric effects are not present, the stress resultants (N 's and M 's) are related to the generalized displacements ($u_0, v_0, w_0, \phi_x, \phi_y$) by the relations

$$\begin{Bmatrix} N_{xx} \\ N_{yy} \\ N_{xy} \end{Bmatrix} = \begin{bmatrix} A_{11} & A_{12} & A_{16} \\ A_{12} & A_{22} & A_{26} \\ A_{16} & A_{26} & A_{66} \end{bmatrix} \begin{Bmatrix} \frac{\partial u_0}{\partial x} + \frac{1}{2} \left(\frac{\partial w_0}{\partial x} \right)^2 \\ \frac{\partial v_0}{\partial y} + \frac{1}{2} \left(\frac{\partial w_0}{\partial y} \right)^2 \\ \frac{\partial u_0}{\partial y} + \frac{\partial v_0}{\partial x} + \frac{\partial w_0}{\partial x} \frac{\partial w_0}{\partial y} \end{Bmatrix} + \begin{bmatrix} B_{11} & B_{12} & B_{16} \\ B_{12} & B_{22} & B_{26} \\ B_{16} & B_{26} & B_{66} \end{bmatrix} \begin{Bmatrix} \frac{\partial \phi_x}{\partial x} \\ \frac{\partial \phi_y}{\partial y} \\ \frac{\partial \phi_x}{\partial y} + \frac{\partial \phi_y}{\partial x} \end{Bmatrix} \quad (3.4.20)$$

$$\begin{Bmatrix} M_{xx} \\ M_{yy} \\ M_{xy} \end{Bmatrix} = \begin{bmatrix} B_{11} & B_{12} & B_{16} \\ B_{12} & B_{22} & B_{26} \\ B_{16} & B_{26} & B_{66} \end{bmatrix} \begin{Bmatrix} \frac{\partial u_0}{\partial x} + \frac{1}{2} \left(\frac{\partial w_0}{\partial x} \right)^2 \\ \frac{\partial v_0}{\partial y} + \frac{1}{2} \left(\frac{\partial w_0}{\partial y} \right)^2 \\ \frac{\partial u_0}{\partial y} + \frac{\partial v_0}{\partial x} + \frac{\partial w_0}{\partial x} \frac{\partial w_0}{\partial y} \end{Bmatrix} + \begin{bmatrix} D_{11} & D_{12} & D_{16} \\ D_{12} & D_{22} & D_{26} \\ D_{16} & D_{26} & D_{66} \end{bmatrix} \begin{Bmatrix} \frac{\partial \phi_x}{\partial x} \\ \frac{\partial \phi_y}{\partial y} \\ \frac{\partial \phi_x}{\partial y} + \frac{\partial \phi_y}{\partial x} \end{Bmatrix} \quad (3.4.21)$$

$$\begin{Bmatrix} Q_y \\ Q_x \end{Bmatrix} = K \begin{bmatrix} A_{44} & A_{45} \\ A_{45} & A_{55} \end{bmatrix} \begin{Bmatrix} \frac{\partial w_0}{\partial y} + \phi_y \\ \frac{\partial w_0}{\partial x} + \phi_x \end{Bmatrix} \quad (3.4.22)$$

When thermal and piezoelectric effects are present, Eqs. (3.4.20) and (3.4.21) take the same form as Eq. (3.3.40), and Eq. (3.4.22) will contain the column of piezoelectric forces given in Eq. (3.4.18).

3.4.4 Equations of Motion in Terms of Displacements

The equations of motion (3.4.13) can be expressed in terms of displacements ($u_0, v_0, w_0, \phi_x, \phi_y$) by substituting for the force and moment resultants from Eqs. (3.4.20)–(3.4.22). For homogeneous laminates, the equations of motion (3.4.13) take the form (including thermal and piezoelectric effects)

$$\begin{aligned} & A_{11} \left(\frac{\partial^2 u_0}{\partial x^2} + \frac{\partial w_0}{\partial x} \frac{\partial^2 w_0}{\partial x^2} \right) + A_{12} \left(\frac{\partial^2 v_0}{\partial y \partial x} + \frac{\partial w_0}{\partial y} \frac{\partial^2 w_0}{\partial y \partial x} \right) + \\ & A_{16} \left(\frac{\partial^2 u_0}{\partial y \partial x} + \frac{\partial^2 v_0}{\partial x^2} + \frac{\partial^2 w_0}{\partial x^2} \frac{\partial w_0}{\partial y} + \frac{\partial w_0}{\partial x} \frac{\partial^2 w_0}{\partial y \partial x} \right) + \\ & B_{11} \frac{\partial^2 \phi_x}{\partial x^2} + B_{12} \frac{\partial^2 \phi_y}{\partial y \partial x} + B_{16} \left(\frac{\partial^2 \phi_x}{\partial x \partial y} + \frac{\partial^2 \phi_y}{\partial x^2} \right) + \\ & A_{16} \left(\frac{\partial^2 u_0}{\partial x \partial y} + \frac{\partial w_0}{\partial x} \frac{\partial^2 w_0}{\partial x \partial y} \right) + A_{26} \left(\frac{\partial^2 v_0}{\partial y^2} + \frac{\partial w_0}{\partial y} \frac{\partial^2 w_0}{\partial y^2} \right) + \\ & A_{66} \left(\frac{\partial^2 u_0}{\partial y^2} + \frac{\partial^2 v_0}{\partial x \partial y} + \frac{\partial^2 w_0}{\partial x \partial y} \frac{\partial w_0}{\partial y} + \frac{\partial w_0}{\partial x} \frac{\partial^2 w_0}{\partial y^2} \right) + \\ & B_{16} \frac{\partial^2 \phi_x}{\partial x \partial y} + B_{26} \frac{\partial^2 \phi_y}{\partial y^2} + B_{66} \left(\frac{\partial^2 \phi_x}{\partial y^2} + \frac{\partial^2 \phi_y}{\partial y \partial x} \right) - \\ & \left(\frac{\partial N_{xx}^T}{\partial x} + \frac{\partial N_{xy}^T}{\partial y} \right) - \left(\frac{\partial N_{xx}^P}{\partial x} + \frac{\partial N_{xy}^P}{\partial y} \right) = I_0 \frac{\partial^2 u_0}{\partial t^2} + I_1 \frac{\partial^2 \phi_x}{\partial t^2} \quad (3.4.23) \end{aligned}$$

$$\begin{aligned} & A_{16} \left(\frac{\partial^2 u_0}{\partial x^2} + \frac{\partial w_0}{\partial x} \frac{\partial^2 w_0}{\partial x^2} \right) + A_{26} \left(\frac{\partial^2 v_0}{\partial y \partial x} + \frac{\partial w_0}{\partial y} \frac{\partial^2 w_0}{\partial y \partial x} \right) + \\ & A_{66} \left(\frac{\partial^2 u_0}{\partial y \partial x} + \frac{\partial^2 v_0}{\partial x^2} + \frac{\partial^2 w_0}{\partial x^2} \frac{\partial w_0}{\partial y} + \frac{\partial w_0}{\partial x} \frac{\partial^2 w_0}{\partial y \partial x} \right) + \\ & B_{16} \frac{\partial^2 \phi_x}{\partial x^2} + B_{26} \frac{\partial^2 \phi_y}{\partial y \partial x} + B_{66} \left(\frac{\partial^2 \phi_x}{\partial x \partial y} + \frac{\partial^2 \phi_y}{\partial x^2} \right) + \\ & A_{12} \left(\frac{\partial^2 u_0}{\partial x \partial y} + \frac{\partial w_0}{\partial x} \frac{\partial^2 w_0}{\partial x \partial y} \right) + A_{22} \left(\frac{\partial^2 v_0}{\partial y^2} + \frac{\partial w_0}{\partial y} \frac{\partial^2 w_0}{\partial y^2} \right) + \\ & A_{26} \left(\frac{\partial^2 u_0}{\partial y^2} + \frac{\partial^2 v_0}{\partial x \partial y} + \frac{\partial^2 w_0}{\partial x \partial y} \frac{\partial w_0}{\partial y} + \frac{\partial w_0}{\partial x} \frac{\partial^2 w_0}{\partial y^2} \right) + \end{aligned}$$

$$B_{12} \frac{\partial^2 \phi_x}{\partial x \partial y} + B_{22} \frac{\partial^2 \phi_y}{\partial y^2} + B_{26} \left(\frac{\partial^2 \phi_x}{\partial y^2} + \frac{\partial^2 \phi_y}{\partial x \partial y} \right) - \\ \left(\frac{\partial N_{xy}^T}{\partial x} + \frac{\partial N_{yy}^T}{\partial y} \right) - \left(\frac{\partial N_{xy}^P}{\partial x} + \frac{\partial N_{yy}^P}{\partial y} \right) = I_0 \frac{\partial^2 v_0}{\partial t^2} + I_1 \frac{\partial^2 \phi_y}{\partial t^2} \quad (3.4.24)$$

$$KA_{55} \left(\frac{\partial^2 w_0}{\partial x^2} + \frac{\partial \phi_x}{\partial x} \right) + KA_{45} \left(\frac{\partial^2 w_0}{\partial y \partial x} + \frac{\partial \phi_y}{\partial x} \right) + \\ KA_{45} \left(\frac{\partial^2 w_0}{\partial x \partial y} + \frac{\partial \phi_x}{\partial y} \right) + KA_{44} \left(\frac{\partial^2 w_0}{\partial y^2} + \frac{\partial \phi_y}{\partial y} \right) + \\ \mathcal{N}(w) + q - \left(\frac{\partial Q_x^P}{\partial x} + \frac{\partial Q_y^P}{\partial y} \right) = I_0 \frac{\partial^2 w_0}{\partial t^2} \quad (3.4.25)$$

$$B_{11} \left(\frac{\partial^2 u_0}{\partial x^2} + \frac{\partial w_0}{\partial x} \frac{\partial^2 w_0}{\partial x^2} \right) + B_{12} \left(\frac{\partial^2 v_0}{\partial y \partial x} + \frac{\partial w_0}{\partial y} \frac{\partial^2 w_0}{\partial y \partial x} \right) + \\ B_{16} \left(\frac{\partial^2 u_0}{\partial y \partial x} + \frac{\partial^2 v_0}{\partial x^2} + \frac{\partial^2 w_0}{\partial x^2} \frac{\partial w_0}{\partial y} + \frac{\partial w_0}{\partial x} \frac{\partial^2 w_0}{\partial y \partial x} \right) + \\ D_{11} \frac{\partial^2 \phi_x}{\partial x^2} + D_{12} \frac{\partial^2 \phi_y}{\partial y \partial x} + D_{16} \left(\frac{\partial^2 \phi_x}{\partial x \partial y} + \frac{\partial^2 \phi_y}{\partial x^2} \right) + \\ B_{16} \left(\frac{\partial^2 u_0}{\partial x \partial y} + \frac{\partial w_0}{\partial x} \frac{\partial^2 w_0}{\partial x \partial y} \right) + B_{26} \left(\frac{\partial^2 v_0}{\partial y^2} + \frac{\partial w_0}{\partial y} \frac{\partial^2 w_0}{\partial y^2} \right) + \\ B_{66} \left(\frac{\partial^2 u_0}{\partial y^2} + \frac{\partial^2 v_0}{\partial x \partial y} + \frac{\partial^2 w_0}{\partial x \partial y} \frac{\partial w_0}{\partial y} + \frac{\partial w_0}{\partial x} \frac{\partial^2 w_0}{\partial y^2} \right) + \\ D_{16} \frac{\partial^2 \phi_x}{\partial x \partial y} + D_{26} \frac{\partial^2 \phi_y}{\partial y^2} + D_{66} \left(\frac{\partial^2 \phi_x}{\partial y^2} + \frac{\partial^2 \phi_y}{\partial y \partial x} \right) - \\ KA_{55} \left(\frac{\partial w_0}{\partial x} + \phi_x \right) - KA_{45} \left(\frac{\partial w_0}{\partial y} + \phi_y \right) - \\ \left(\frac{\partial M_{xx}^T}{\partial x} + \frac{\partial M_{xy}^T}{\partial y} \right) - \left(\frac{\partial M_{xx}^P}{\partial x} + \frac{\partial M_{xy}^P}{\partial y} - Q_x^P \right) \\ = I_2 \frac{\partial^2 \phi_x}{\partial t^2} + I_1 \frac{\partial^2 u_0}{\partial t^2} \quad (3.4.26)$$

$$B_{16} \left(\frac{\partial^2 u_0}{\partial x^2} + \frac{\partial w_0}{\partial x} \frac{\partial^2 w_0}{\partial x^2} \right) + B_{26} \left(\frac{\partial^2 v_0}{\partial y \partial x} + \frac{\partial w_0}{\partial y} \frac{\partial^2 w_0}{\partial y \partial x} \right) + \\ B_{66} \left(\frac{\partial^2 u_0}{\partial y \partial x} + \frac{\partial^2 v_0}{\partial x^2} + \frac{\partial^2 w_0}{\partial x^2} \frac{\partial w_0}{\partial y} + \frac{\partial w_0}{\partial x} \frac{\partial^2 w_0}{\partial y \partial x} \right) + \\ D_{16} \frac{\partial^2 \phi_x}{\partial x^2} + D_{26} \frac{\partial^2 \phi_y}{\partial y \partial x} + D_{66} \left(\frac{\partial^2 \phi_x}{\partial x \partial y} + \frac{\partial^2 \phi_y}{\partial x^2} \right) +$$

$$\begin{aligned}
& B_{12} \left(\frac{\partial^2 u_0}{\partial x \partial y} + \frac{\partial w_0}{\partial x} \frac{\partial^2 w_0}{\partial x \partial y} \right) + B_{22} \left(\frac{\partial^2 v_0}{\partial y^2} + \frac{\partial w_0}{\partial y} \frac{\partial^2 w_0}{\partial y^2} \right) + \\
& B_{26} \left(\frac{\partial^2 u_0}{\partial y^2} + \frac{\partial^2 v_0}{\partial x \partial y} + \frac{\partial^2 w_0}{\partial x \partial y} \frac{\partial w_0}{\partial y} + \frac{\partial w_0}{\partial x} \frac{\partial^2 w_0}{\partial y^2} \right) + \\
& D_{12} \frac{\partial^2 \phi_x}{\partial x \partial y} + D_{22} \frac{\partial^2 \phi_y}{\partial y^2} + D_{26} \left(\frac{\partial^2 \phi_x}{\partial y^2} + \frac{\partial^2 \phi_y}{\partial x \partial y} \right) - \\
& K A_{45} \left(\frac{\partial w_0}{\partial x} + \phi_x \right) - K A_{44} \left(\frac{\partial w_0}{\partial y} + \phi_y \right) - \\
& \left(\frac{\partial M_{xy}^T}{\partial x} + \frac{\partial M_{yy}^T}{\partial y} \right) - \left(\frac{\partial M_{xy}^P}{\partial x} + \frac{\partial M_{yy}^P}{\partial y} - Q_y^P \right) \\
& = I_2 \frac{\partial^2 \phi_y}{\partial t^2} + I_1 \frac{\partial^2 v_0}{\partial t^2}
\end{aligned} \tag{3.4.27}$$

Equations (3.4.23)–(3.4.27) describe five second-order, nonlinear, partial differential equations in terms of the five generalized displacements. Hence, the first-order laminated plate theory is a tenth-order theory and there are ten boundary conditions, as stated earlier in Eqs. (3.4.14) and (3.4.15). Note that the displacement field of the classical plate theory can be obtained from that of the first-order theory by setting

$$\phi_x = -\frac{\partial w_0}{\partial x} \quad \text{and} \quad \phi_y = -\frac{\partial w_0}{\partial y} \tag{3.4.28}$$

Conversely, the relations in Eq. (3.4.28) can be used to derive the first-order theory from the classical plate theory via the penalty function method (see Chapter 10).

Example 3.4.1:

The linearized equations of motion for cylindrical bending according to the first-order shear deformation theory are given by setting all derivatives with respect to y in Eqs. (3.4.23)–(3.4.27):

$$\begin{aligned}
& A_{11} \frac{\partial^2 u_0}{\partial x^2} + A_{16} \frac{\partial^2 v_0}{\partial x^2} + B_{11} \frac{\partial^2 \phi_x}{\partial x^2} + B_{16} \frac{\partial^2 \phi_y}{\partial x^2} - \frac{\partial N_{xx}^T}{\partial x} - \frac{\partial N_{xx}^P}{\partial x} \\
& = I_0 \frac{\partial^2 u_0}{\partial t^2} + I_1 \frac{\partial^2 \phi_x}{\partial t^2}
\end{aligned} \tag{3.4.29}$$

$$\begin{aligned}
& A_{16} \frac{\partial^2 u_0}{\partial x^2} + A_{66} \frac{\partial^2 v_0}{\partial x^2} + B_{16} \frac{\partial^2 \phi_x}{\partial x^2} + B_{66} \frac{\partial^2 \phi_y}{\partial x^2} - \frac{\partial N_{xy}^T}{\partial x} - \frac{\partial N_{xy}^P}{\partial x} \\
& = I_0 \frac{\partial^2 v_0}{\partial t^2} + I_1 \frac{\partial^2 \phi_y}{\partial t^2}
\end{aligned} \tag{3.4.30}$$

$$\begin{aligned}
& B_{11} \frac{\partial^2 u_0}{\partial x^2} + B_{16} \frac{\partial^2 v_0}{\partial x^2} + D_{11} \frac{\partial^2 \phi_x}{\partial x^2} + D_{16} \frac{\partial^2 \phi_y}{\partial x^2} - K A_{55} \left(\frac{\partial w_0}{\partial x} + \phi_x \right) \\
& - K A_{45} \phi_y - \frac{\partial M_{xx}^T}{\partial x} - \frac{\partial M_{xx}^P}{\partial x} + Q_x^P = I_2 \frac{\partial^2 \phi_x}{\partial t^2} + I_1 \frac{\partial^2 u_0}{\partial t^2}
\end{aligned} \tag{3.4.31}$$

$$\begin{aligned}
& B_{16} \frac{\partial^2 u_0}{\partial x^2} + B_{66} \frac{\partial^2 v_0}{\partial x^2} + D_{16} \frac{\partial^2 \phi_x}{\partial x^2} + D_{66} \frac{\partial^2 \phi_y}{\partial x^2} - K A_{44} \phi_y \\
& - K A_{45} \left(\frac{\partial w_0}{\partial x} + \phi_x \right) - \frac{\partial M_{xy}^T}{\partial x} - \frac{\partial M_{xy}^P}{\partial x} + Q_y^P = I_2 \frac{\partial^2 \phi_y}{\partial t^2} + I_1 \frac{\partial^2 v_0}{\partial t^2}
\end{aligned} \tag{3.4.32}$$

$$KA_{55} \left(\frac{\partial^2 w_0}{\partial x^2} + \frac{\partial \phi_x}{\partial x} \right) + KA_{45} \frac{\partial \phi_y}{\partial x} + \frac{\partial}{\partial x} \left(N_{xx} \frac{\partial w_0}{\partial x} \right) + q - \frac{\partial Q_x^P}{\partial x} = I_0 \frac{\partial^2 w_0}{\partial t^2} \quad (3.4.33)$$

3.5 Laminate Stiffnesses for Selected Laminates

3.5.1 General Discussion

A close examination of the laminate stiffnesses defined in Eqs. (3.3.38) and (3.4.19a) show that their values depend on the material stiffnesses, layer thicknesses, and the lamination scheme. Symmetry or antisymmetry of the lamination scheme and material properties about the midplane of the laminate reduce some of the laminate stiffnesses to zero. The book by Jones [44] has an excellent discussion of the laminate stiffnesses for various types of laminated plates. In this section, we review selective lamination schemes for their laminate stiffness characteristics.

Before we embark on the discussion of laminate stiffnesses, it is useful to introduce the terminology and notation associated with special lamination schemes. The lamination scheme of a laminate will be denoted by $(\alpha/\beta/\gamma/\delta/\varepsilon/\dots)$, where α is the orientation of the first ply, β is the orientation of the second ply, and so on (see Figure 3.5.1). The plies are counted in the positive z direction (see Figure 3.3.1). Unless stated otherwise, this notation also implies that all layers are of the same thickness and made of the same material.

A general laminate has layers of different orientations θ where $-90^\circ \leq \theta \leq 90^\circ$. For example, $(0/15/-35/45/90/-45)$ is a six-ply laminate. General *angle-ply* laminates (see Figure 3.5.2) have ply orientations of θ and $-\theta$ where $0^\circ \leq \theta \leq 90^\circ$, and with at least one layer having an orientation other than 0° or 90° . An example

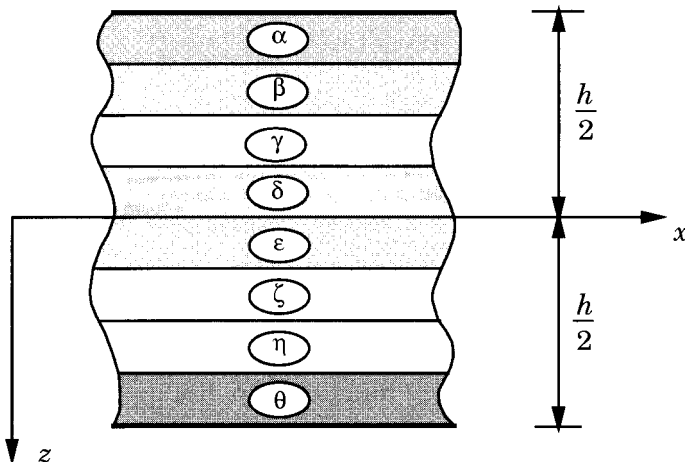


Figure 3.5.1: A laminate with general stacking sequence.

of angle-ply laminates is provided by (15/-30/0/90/45/-45). *Cross-ply* laminates are those which have ply orientations of 0° or 90° (see Figure 3.5.3). An example of a cross-ply laminate is (0/90/90/0/0/90). For layers with 0° or 90° orientations, the layer stiffnesses \bar{Q}_{16} , \bar{Q}_{26} , \bar{Q}_{45} are zero. Hence, $A_{16} = A_{26} = A_{45} = D_{16} = D_{26} = 0$.

When ply stacking sequence, material, and geometry (i.e., ply thicknesses) are symmetric about the midplane of the laminate, the laminate is called a *symmetric laminate* (see Figure 3.5.4). For a symmetric laminate, the upper half through the laminate thickness is a mirror image of the lower half. The laminates $(-45/45/45/-45)=(-45/45)_s$ and $(45/-45/-45/45)=(45/-45)_s$, with all layers having the same thickness and material, are examples of a symmetric angle-ply laminate, $(0/90/90/0)=(0/90)_s$ is a symmetric cross-ply laminate, and $(30/-45/0/90/90/0/-45/30)=(30/-45/0/90)_s$ is a general symmetric laminate.

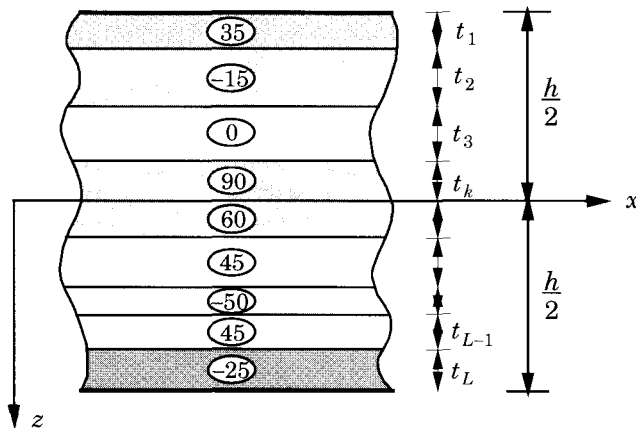


Figure 3.5.2: A general angle-ply laminate.

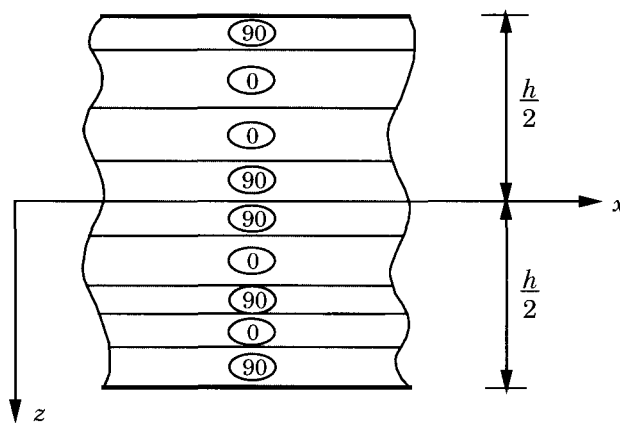


Figure 3.5.3: A cross-ply laminated plate with the 0° and 90° layers.

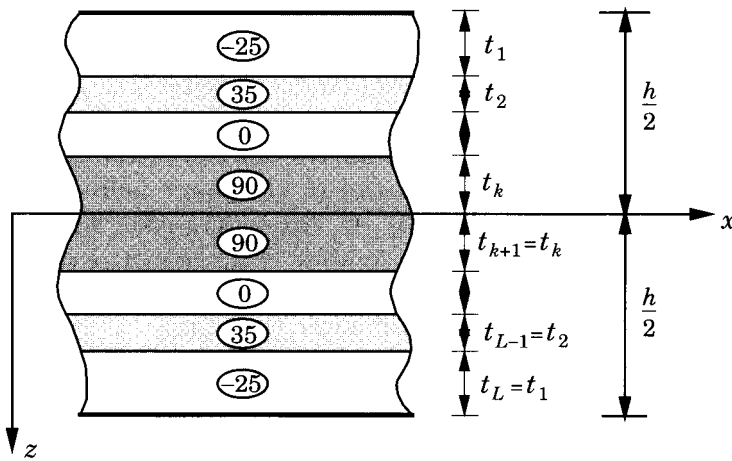


Figure 3.5.4: A symmetric laminate.

Note that symmetric laminates are also denoted by displaying only the lamination scheme of the upper half. The symmetric laminate $(-25/35/0/90/90/0/35/-25)$ is denoted as $(-25/35/0/90)_s$.

An unsymmetric or *asymmetric laminate* is a laminate that is not symmetric. An *antisymmetric laminate* is one whose lamination scheme is antisymmetric and material and thicknesses are symmetric about the midplane. Examples of antisymmetric angle-ply and cross-ply laminates are provided, respectively, by $(-30/30/-30/30/-30/30) \equiv (-30/30)_3$ and $(0/90/0/90/0/90) \equiv (0/90)_3$.

Laminate stiffnesses A_{ij} depend on only on the thicknesses and stiffnesses of the layers but not on their placement in the laminate. On the other hand, laminate stiffnesses D_{ij} depend not only on the layer thickness and stiffnesses but also on their location relative to the midplane. For example, both $(0/90)_s$ and $(90/0)_s$ laminates will have the same in-plane stiffnesses A_{ij} . However, $(0/90)_s$ laminate will have larger bending stiffnesses D_{ij} about an axis perpendicular to the fiber direction than the $(90/0)_s$ laminate, because the 0° layers are located farther from the midplane in the $(0/90)_s$ laminate. Both A_{ij} and D_{ij} are always positive. Laminate stiffnesses B_{ij} also depend on the layer thickness, stiffnesses and location relative to the midplane, and they can be negative, depending on the lamination scheme and the number of layers.

3.5.2 Single-Layer Plates

Here we discuss some special cases of single-layered configurations and their stiffnesses. The special single layer plates discussed here include: isotropic, specially orthotropic (i.e., the principal material coordinates coincide with those of the plate), generally orthotropic (i.e., the principal material coordinates *do not* coincide with those of the plate), and anisotropic. The bending-stretching coupling coefficients

B_{ij} and the shear stiffnesses A_{16} , A_{26} , D_{16} , and D_{26} can be shown to be zero for all single-layer plates except for generally orthotropic and anisotropic single-layer plates. The units of N_i and M_i , in the U.S. Customary System (USCS), are lb-in. and lb-in/in., respectively.

Single Isotropic Layer

For a single isotropic layer with material constants E and ν [$G = \frac{E}{2(1+\nu)}$] and thickness h , the nonzero laminate stiffnesses of Eqs. (3.3.38) and (3.4.19a) become

$$\begin{aligned} A_{11} &= \frac{Eh}{1-\nu^2}, \quad A_{12} = \nu A_{11}, \quad A_{22} = A_{11}, \quad A_{66} = \frac{1-\nu}{2} A_{11}, \quad A_{44} = A_{55} = \frac{1-\nu}{2} A_{11} \\ D_{11} &= \frac{Eh^3}{12(1-\nu^2)}, \quad D_{12} = \nu D_{11}, \quad D_{22} = D_{11}, \quad D_{66} = \frac{1-\nu}{2} D_{11} \end{aligned} \quad (3.5.1)$$

The plate constitutive equations for the classical and first-order theories become

$$\begin{Bmatrix} N_{xx} \\ N_{yy} \\ N_{xy} \end{Bmatrix} = \begin{bmatrix} A_{11} & \nu A_{11} & 0 \\ \nu A_{11} & A_{11} & 0 \\ 0 & 0 & \frac{1-\nu}{2} A_{11} \end{bmatrix} \begin{Bmatrix} \varepsilon_{xx}^{(0)} \\ \varepsilon_{yy}^{(0)} \\ \gamma_{xy}^{(0)} \end{Bmatrix} \quad (\text{lb/in.}) \quad (3.5.2)$$

$$\begin{Bmatrix} M_{xx} \\ M_{yy} \\ M_{xy} \end{Bmatrix} = \begin{bmatrix} D_{11} & \nu D_{11} & 0 \\ \nu D_{11} & D_{11} & 0 \\ 0 & 0 & \frac{1-\nu}{2} D_{11} \end{bmatrix} \begin{Bmatrix} \varepsilon_{xx}^{(1)} \\ \varepsilon_{yy}^{(1)} \\ \gamma_{xy}^{(1)} \end{Bmatrix} \quad (\text{lb-in/in.}) \quad (3.5.3)$$

$$\begin{Bmatrix} Q_y \\ Q_x \end{Bmatrix} = K \frac{1-\nu}{2} \begin{bmatrix} A_{11} & 0 \\ 0 & A_{11} \end{bmatrix} \begin{Bmatrix} \gamma_{yz}^{(0)} \\ \gamma_{xz}^{(0)} \end{Bmatrix} \quad (\text{lb-in}) \quad (3.5.4)$$

The nonzero thermal stress resultants $\{N^T\}$ and $\{M^T\}$ are given by

$$N_{xx}^T = N_{yy}^T = \frac{E\alpha}{(1-\nu)} \int_{-\frac{h}{2}}^{\frac{h}{2}} \Delta T \, dz, \quad M_{xx}^T = M_{yy}^T = \frac{E\alpha}{(1-\nu)} \int_{-\frac{h}{2}}^{\frac{h}{2}} \Delta T z \, dz \quad (3.5.5)$$

Single Specially Orthotropic Layer

For a single specially orthotropic layer, the stiffnesses can be expressed in terms of the Q_{ij} and thickness h . The nonzero stiffnesses of Eqs. (3.3.38) and (3.4.19a) become

$$\begin{aligned} A_{11} &= Q_{11}h, \quad A_{12} = Q_{12}h, \quad A_{22} = Q_{22}h \\ A_{66} &= Q_{66}h, \quad A_{44} = Q_{44}h, \quad A_{55} = Q_{55}h \\ D_{11} &= \frac{Q_{11}h^3}{12}, \quad D_{12} = \frac{Q_{12}h^3}{12}, \quad D_{22} = \frac{Q_{22}h^3}{12}, \quad D_{66} = \frac{Q_{66}h^3}{12} \end{aligned} \quad (3.5.6)$$

where Q_{ij} are the plane-stress-reduced stiffnesses, and they are given in terms of the engineering constants [see Eq. (3.3.11b)] as

$$Q_{11} = \frac{E_1}{1-\nu_{12}\nu_{21}}, \quad Q_{12} = \frac{\nu_{12}E_2}{1-\nu_{12}\nu_{21}}, \quad Q_{22} = \frac{E_2}{1-\nu_{12}\nu_{21}}$$

$$Q_{66} = G_{12}, \quad Q_{44} = G_{23}, \quad Q_{55} = G_{13} \quad (3.5.7)$$

The plate constitutive equations for the classical and first-order theories become

$$\begin{Bmatrix} N_{xx} \\ N_{yy} \\ N_{xy} \end{Bmatrix} = h \begin{bmatrix} Q_{11} & Q_{12} & 0 \\ Q_{12} & Q_{22} & 0 \\ 0 & 0 & Q_{66} \end{bmatrix} \begin{Bmatrix} \varepsilon_{xx}^{(0)} \\ \varepsilon_{yy}^{(0)} \\ \gamma_{xy}^{(0)} \end{Bmatrix} \quad (3.5.8)$$

$$\begin{Bmatrix} M_{xx} \\ M_{yy} \\ M_{xy} \end{Bmatrix} = \frac{h^3}{12} \begin{bmatrix} Q_{11} & Q_{12} & 0 \\ Q_{12} & Q_{22} & 0 \\ 0 & 0 & Q_{66} \end{bmatrix} \begin{Bmatrix} \varepsilon_{xx}^{(1)} \\ \varepsilon_{yy}^{(1)} \\ \gamma_{xy}^{(1)} \end{Bmatrix} \quad (3.5.9)$$

$$\begin{Bmatrix} Q_y \\ Q_x \end{Bmatrix} = K h \begin{bmatrix} Q_{44} & 0 \\ 0 & Q_{55} \end{bmatrix} \begin{Bmatrix} \gamma_{yz}^{(0)} \\ \gamma_{xz}^{(0)} \end{Bmatrix} \quad (3.5.10)$$

The nonzero thermal stress resultants are given by

$$\begin{Bmatrix} N_{xx}^T \\ N_{yy}^T \end{Bmatrix} = \begin{bmatrix} Q_{11} & Q_{12} \\ Q_{12} & Q_{22} \end{bmatrix} \begin{Bmatrix} \alpha_1 \\ \alpha_2 \end{Bmatrix} \int_{-\frac{h}{2}}^{\frac{h}{2}} \Delta T \, dz \quad (3.5.11a)$$

$$\begin{Bmatrix} M_{xx}^T \\ M_{yy}^T \end{Bmatrix} = \begin{bmatrix} Q_{11} & Q_{12} \\ Q_{12} & Q_{22} \end{bmatrix} \begin{Bmatrix} \alpha_1 \\ \alpha_2 \end{Bmatrix} \int_{-\frac{h}{2}}^{\frac{h}{2}} \Delta T z \, dz \quad (3.5.11b)$$

Single Generally Orthotropic Layer

For a single generally orthotropic layer (i.e., the principal material coordinates do not coincide with those of the plate), the stiffnesses can be expressed in terms of the transformed coefficients \bar{Q}_{ij} and thickness h . The nonzero stiffnesses are ($B_{ij} = 0$)

$$A_{ij} = \bar{Q}_{ij} h, \quad D_{ij} = \frac{\bar{Q}_{ij} h^3}{12}, \quad A_{44} = h \bar{Q}_{44}, \quad A_{55} = h \bar{Q}_{55} \quad (3.5.12)$$

The plate constitutive equations are

$$\begin{Bmatrix} N_{xx} \\ N_{yy} \\ N_{xy} \end{Bmatrix} = \begin{bmatrix} A_{11} & A_{12} & A_{16} \\ A_{12} & A_{22} & A_{26} \\ A_{16} & A_{26} & A_{66} \end{bmatrix} \begin{Bmatrix} \varepsilon_{xx}^{(0)} \\ \varepsilon_{yy}^{(0)} \\ \gamma_{xy}^{(0)} \end{Bmatrix} \quad (3.5.13)$$

$$\begin{Bmatrix} M_{xx} \\ M_{yy} \\ M_{xy} \end{Bmatrix} = \begin{bmatrix} D_{11} & D_{12} & D_{16} \\ D_{12} & D_{22} & D_{26} \\ D_{16} & D_{26} & D_{66} \end{bmatrix} \begin{Bmatrix} \varepsilon_{xx}^{(1)} \\ \varepsilon_{yy}^{(1)} \\ \gamma_{xy}^{(1)} \end{Bmatrix} \quad (3.5.14)$$

$$\begin{Bmatrix} Q_y \\ Q_x \end{Bmatrix} = K \begin{bmatrix} A_{44} & A_{45} \\ A_{45} & A_{55} \end{bmatrix} \begin{Bmatrix} \gamma_{yz}^{(0)} \\ \gamma_{xz}^{(0)} \end{Bmatrix} \quad (3.5.15)$$

The thermal stress resultants for this case are given by

$$\begin{Bmatrix} N_{xx}^T \\ N_{yy}^T \\ N_{xy}^T \end{Bmatrix} = \begin{bmatrix} \bar{Q}_{11} & \bar{Q}_{12} & \bar{Q}_{16} \\ \bar{Q}_{12} & \bar{Q}_{22} & \bar{Q}_{26} \\ \bar{Q}_{16} & \bar{Q}_{26} & \bar{Q}_{66} \end{bmatrix} \begin{Bmatrix} \alpha_{xx} \\ \alpha_{yy} \\ 2\alpha_{xy} \end{Bmatrix} \int_{-\frac{h}{2}}^{\frac{h}{2}} \Delta T dz \quad (3.5.16)$$

A similar expression holds for $\{M^T\}$.

If the temperature increment is linear through the layer thickness, $\Delta T = T_0 + zT_1$, the thermal stress resultants have the form

$$\begin{aligned}\left\{\begin{array}{l}N_{xx}^T \\ N_{yy}^T \\ N_{xy}^T\end{array}\right\} &= \begin{bmatrix}\bar{Q}_{11} & \bar{Q}_{12} & \bar{Q}_{16} \\ \bar{Q}_{12} & \bar{Q}_{22} & \bar{Q}_{26} \\ Q_{16} & Q_{26} & Q_{66}\end{bmatrix} \left\{\begin{array}{l}\alpha_{xx} \\ \alpha_{yy} \\ 2\alpha_{xy}\end{array}\right\} T_0 h \\ \left\{\begin{array}{l}M_{xx}^T \\ M_{yy}^T \\ M_{xy}^T\end{array}\right\} &= \begin{bmatrix}\bar{Q}_{11} & \bar{Q}_{12} & \bar{Q}_{16} \\ \bar{Q}_{12} & \bar{Q}_{22} & \bar{Q}_{26} \\ Q_{16} & Q_{26} & Q_{66}\end{bmatrix} \left\{\begin{array}{l}\alpha_{xx} \\ \alpha_{yy} \\ 2\alpha_{xy}\end{array}\right\} \frac{T_1 h^3}{12}\end{aligned}\quad (3.5.17)$$

Single Anisotropic Layer

For a single anisotropic layer, the stiffnesses are expressed in terms of the coefficients C_{ij} and thickness h . The nonzero stiffnesses are ($B_{ij} = 0$)

$$A_{ij} = C_{ij}h, \quad D_{ij} = \frac{C_{ij}h^3}{12} \quad (3.5.18)$$

for $i, j = 1, 2, 3, 4, 5$ and 6 [see Eq. (2.4.3a)]. The plate constitutive equations are the same as in Eqs. (3.5.13)–(3.5.16) with the plate stiffnesses given by Eq. (3.5.18).

Example 3.5.1:

The material properties of boron-epoxy material layers are

$$\begin{aligned}E_1 &= 30 \times 10^6 \text{ psi}, \quad E_2 = E_3 = 3 \times 10^6 \text{ psi}, \quad G_{12} = G_{13} = 1.5 \times 10^6 \text{ psi} \\ G_{23} &= 0.6 \times 10^6 \text{ psi}, \quad \nu_{12} = 0.25, \quad \nu_{13} = 0.25, \quad \nu_{23} = 0.25\end{aligned}\quad (3.5.19)$$

The matrix of elastic coefficients for the material is [see Eq. (1.3.44)]

$$[C] = \begin{bmatrix}30.508 & 1.017 & 1.017 & 0 & 0 & 0 \\ 1.017 & 3.234 & 0.834 & 0 & 0 & 0 \\ 1.017 & 0.834 & 3.234 & 0 & 0 & 0 \\ 0 & 0 & 0 & 0.6 & 0 & 0 \\ 0 & 0 & 0 & 0 & 1.5 & 0 \\ 0 & 0 & 0 & 0 & 0 & 1.5\end{bmatrix} \text{msi}$$

The plane stress-reduced elastic coefficient matrix in the material coordinates is

$$[Q] = \begin{bmatrix}30.189 & 0.755 & 0 & 0 & 0 \\ 0.755 & 3.019 & 0 & 0 & 0 \\ 0 & 0 & 0.6 & 0 & 0 \\ 0 & 0 & 0 & 1.5 & 0 \\ 0 & 0 & 0 & 0 & 1.5\end{bmatrix} \text{msi}$$

The transformed stiffness matrix $[\bar{Q}]$ for $\theta = 60^\circ$ is given by

$$[\bar{Q}]_{60} = \begin{bmatrix}4.993 & 5.573 & 0 & 0 & 3.101 \\ 5.573 & 18.578 & 0 & 0 & 8.664 \\ 0 & 0 & 1.275 & 0.390 & 0 \\ 0 & 0 & 0.390 & 0.825 & 0 \\ 3.101 & 8.664 & 0 & 0 & 6.318\end{bmatrix} \text{msi}$$

The laminate stiffnesses A_{ij} and D_{ij} for $i, j = 1, 2, 6$ may be computed using Eq. (3.5.12). The transverse shear stiffnesses A_{44} , A_{45} , and A_{55} are given by $A_{ij} = \bar{Q}_{ij}h$ for $i, j = 4, 5$.

Suppose that the thermal coefficients of expansion of the material are

$$\alpha_1 = 2.5 \times 10^{-6} \text{ in./in./}^{\circ}\text{F}, \quad \alpha_2 = 8.0 \times 10^{-6} \text{ in./in./}^{\circ}\text{F} \quad (3.5.20)$$

The transformed coefficients are

$$\left\{ \begin{array}{c} \alpha_{xx} \\ \alpha_{yy} \\ 2\alpha_{xy} \end{array} \right\}_{60^\circ} = \left\{ \begin{array}{c} 6.625 \\ 3.875 \\ -4.763 \end{array} \right\} \times 10^{-6} \text{ in./in./}^{\circ}\text{F}$$

3.5.3 Symmetric Laminates

When the material properties, locations, and lamination scheme are symmetric about the midplane, the laminate is called a *symmetric laminate*. If a laminate is not symmetric, it is said to be an *unsymmetric laminate*. Due to the symmetry of the layer material coefficients $\bar{Q}_{ij}^{(k)}$, distances z_k , and thicknesses h_k about the midplane of the laminate for every layer, the coupling stiffnesses B_{ij} are zero for symmetric laminates (see Figure 3.5.5). The elimination of the coupling between bending and extension simplifies the governing equations. When the strain-displacement equations are linear, the equations governing the in-plane deformation can be uncoupled from those governing bending of symmetric laminates. Further, if there are no applied in-plane forces or displacements, the in-plane deformation (i.e., strains) will be zero, and only the bending equations must be analyzed. From production point of view, symmetric laminates do not have the tendency to twist from the thermally induced contractions that occur during cooling following the curing process.

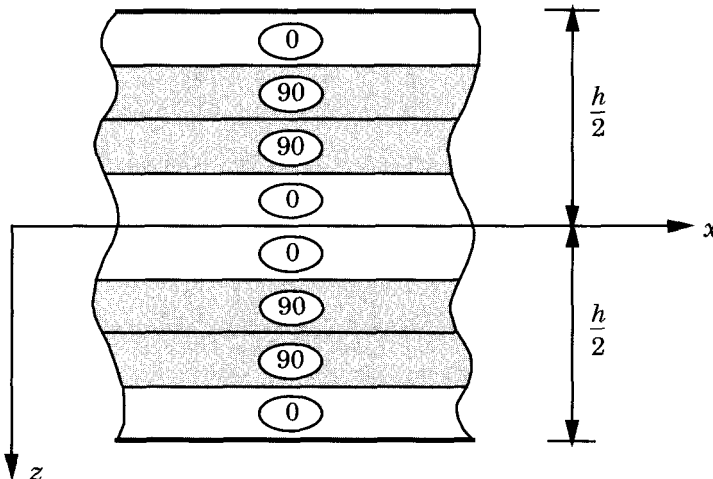


Figure 3.5.5: A symmetric cross-ply laminate.

The force and moment resultants for a symmetric laminate, in general, have the same form as the generally orthotropic single-layer plates [see Eqs. (3.5.13)–(3.5.15)]. For certain special cases of symmetric laminates, the relations between strains and resultants can be further simplified, as explained next.

Symmetric Laminates with Multiple Isotropic Layers

When isotropic layers of possibly different material properties and thicknesses are arranged symmetrically from both a geometric and a material property standpoint, the resulting laminate will have the following laminate constitutive equations for the classical or first-order theories:

$$\begin{Bmatrix} N_{xx} \\ N_{yy} \\ N_{xy} \end{Bmatrix} = \begin{bmatrix} A_{11} & A_{12} & 0 \\ A_{12} & A_{11} & 0 \\ 0 & 0 & A_{66} \end{bmatrix} \begin{Bmatrix} \varepsilon_{xx}^{(0)} \\ \varepsilon_{yy}^{(0)} \\ \gamma_{xy}^{(0)} \end{Bmatrix} \quad (3.5.21a)$$

$$\begin{Bmatrix} M_{xx} \\ M_{yy} \\ M_{xy} \end{Bmatrix} = \begin{bmatrix} D_{11} & D_{12} & 0 \\ D_{12} & D_{11} & 0 \\ 0 & 0 & D_{66} \end{bmatrix} \begin{Bmatrix} \varepsilon_{xx}^{(1)} \\ \varepsilon_{yy}^{(1)} \\ \gamma_{xy}^{(1)} \end{Bmatrix} \quad (3.5.21b)$$

$$\begin{Bmatrix} Q_y \\ Q_x \end{Bmatrix} = K \begin{bmatrix} A_{44} & 0 \\ 0 & A_{55} \end{bmatrix} \begin{Bmatrix} \gamma_{yz}^{(0)} \\ \gamma_{xz}^{(0)} \end{Bmatrix} \quad (3.5.21c)$$

where the laminate stiffnesses A_{ij} and D_{ij} are defined by Eqs. (3.3.38) and (3.4.19a) with

$$\begin{aligned} \bar{Q}_{11}^{(k)} &= \bar{Q}_{22}^{(k)} = \frac{E^k}{1 - \nu_k^2}, \quad \bar{Q}_{16}^{(k)} = \bar{Q}_{26}^{(k)} = 0 \\ \bar{Q}_{12}^{(k)} &= \frac{\nu_k E^k}{1 - \nu_k^2}, \quad \bar{Q}_{44}^{(k)} = \bar{Q}_{55}^{(k)} = \bar{Q}_{66}^{(k)} = \frac{E^k}{2(1 + \nu_k)} \end{aligned} \quad (3.5.22)$$

The thermal stress resultants for this case are given by

$$\begin{Bmatrix} N_{xx}^T \\ N_{yy}^T \end{Bmatrix} = \sum_{k=1}^L \int_{z_k}^{z_{k+1}} \begin{bmatrix} \bar{Q}_{11} & \bar{Q}_{12} \\ \bar{Q}_{12} & \bar{Q}_{22} \end{bmatrix}^{(k)} \begin{Bmatrix} \alpha_{xx} \\ \alpha_{yy} \end{Bmatrix} \Delta T \, dz \quad (3.5.23)$$

and similar expression holds for $\{M^T\}$.

If $\Delta T = T_0 + zT_1$, then Eq. (3.5.23) can be written as

$$\begin{Bmatrix} N_{xx}^T \\ N_{yy}^T \end{Bmatrix} = T_0 \begin{bmatrix} A_{11} & A_{12} \\ A_{12} & A_{22} \end{bmatrix} \begin{Bmatrix} \alpha_{xx} \\ \alpha_{yy} \end{Bmatrix}, \quad \begin{Bmatrix} M_{xx}^T \\ M_{yy}^T \end{Bmatrix} = T_1 \begin{bmatrix} D_{11} & D_{12} \\ D_{12} & D_{22} \end{bmatrix} \begin{Bmatrix} \alpha_{xx} \\ \alpha_{yy} \end{Bmatrix} \quad (3.5.24)$$

Symmetric Laminates with Multiple Specially Orthotropic Layers

A laminate composed of multiple specially orthotropic layers that are symmetrically disposed, both from a material and geometric properties standpoint, about the midplane of the laminate does not exhibit coupling between bending and extension

i.e., $B_{ij} = 0$. The laminate constitutive equations are again given by Eqs. (3.5.21a-c), where the laminate stiffnesses A_{ij} and D_{ij} are defined by Eqs. (3.3.38) and (3.4.19a) with

$$\begin{aligned}\bar{Q}_{11}^{(k)} &= \frac{E_1^k}{1 - \nu_{12}^k \nu_{21}^k}, \quad \bar{Q}_{12}^{(k)} = \frac{\nu_{21}^k E_1^k}{1 - \nu_{12}^k \nu_{21}^k}, \quad \bar{Q}_{22}^{(k)} = \frac{E_2^k}{1 - \nu_{12}^k \nu_{21}^k} \\ \bar{Q}_{16}^{(k)} &= 0, \quad \bar{Q}_{26}^{(k)} = 0, \quad \bar{Q}_{66}^{(k)} = G_{12}^k, \quad \bar{Q}_{44}^{(k)} = G_{23}^k, \quad \bar{Q}_{55}^{(k)} = G_{13}^k\end{aligned}\quad (3.5.25)$$

Such laminates are also called *specially orthotropic laminates*. The thermal stress resultants have the same form as those given in Eq. (3.5.23).

A common example of specially orthotropic laminates is provided by the *regular symmetric cross-ply laminates*, which consist of laminae of the same thickness and material properties but have their major principal material coordinates (i.e., x_1 and x_2) alternating at 0° and 90° to the laminate axes x and y : $(0/90/0/90/\dots)$. The regular symmetric cross-ply laminates necessarily contain an odd number of layers; otherwise, they are not symmetric. Of course, a general symmetric cross-ply laminate can have either an even or odd number of layers: $(0/90/0/90/90/0/90/0)$ or $(0/90/90/0/0/90/90/0)$ (see Figure 3.5.5).

Symmetric Laminates with Multiple Generally Orthotropic Layers

Laminates can be composed of generally orthotropic layers whose principal material directions are aligned with the laminate axes at an angle θ degrees. If the thicknesses, locations, and material properties of the layers are symmetric about the midplane of the laminate, the coupling between bending and extension is zero, $B_{ij} = 0$, and the laminate constitutive equations are given by Eqs. (3.5.13)–(3.5.15). Note that the coupling between normal forces and shearing strain, shearing force and normal strains, normal moments and twist, and twisting moment and normal curvatures is not zero for these laminates (i.e., A_{16} , A_{26} , D_{16} , and D_{26} are not zero). An example of a general symmetric laminate with generally orthotropic laminae is provided by $(30/-60_3/15_5/-60_3/30)$, where the subscript denotes the number of layers of the same orientation and thickness.

Regular symmetric angle-ply laminates are those that have an *odd* number of orthotropic laminae of equal thicknesses and alternating orientations: $(\alpha/-\alpha/\alpha/-\alpha/\alpha/\dots)$, $0^\circ < \alpha < 90^\circ$ (see Figure 3.5.6). A general symmetric angle-ply laminate has the form $(\theta/\beta/\gamma/\dots)_s$, where θ , β , and γ can take any values between -90° and 90° , and each layer can have any thickness, but they should be symmetrically placed about the midplane. It can be shown that the stiffnesses A_{16} , A_{26} , D_{16} , and D_{26} of a regular symmetric angle-ply laminate are the largest when the number of layers N is equal to 3, and they decrease in proportion to $1/N$ as N increases. Thus, for symmetric angle-ply laminates with many layers, the values of A_{16} , A_{26} , D_{16} , and D_{26} can be quite small compared to other A_{ij} and D_{ij} .

A laminate composed of multiple anisotropic layers that are symmetrically disposed about the midplane of the laminate does not have any stiffness simplification other than $B_{ij} = 0$, which holds for *all* symmetric laminates. Stiffnesses A_{16} , A_{26} , D_{16} , and D_{26} are not zero, and they do not necessarily go to zero as the number of layers is increased.

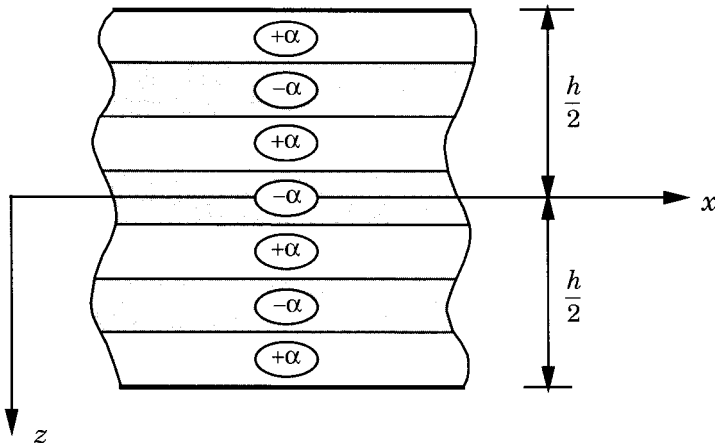


Figure 3.5.6: A symmetric angle-ply laminate.

In general, symmetric laminates are preferred wherever they meet the application requirements. Symmetric laminates are much easier to analyze than general or unsymmetric laminates. Further, symmetric laminates do not have a tendency to twist due to thermally induced contractions that occur during cooling following the curing process.

Example 3.5.2:

A general symmetric laminate (30/0/90/-45)_s of total thickness 1 in. and made of boron-epoxy layers [see Eqs. (3.5.19) and (3.5.20) for material properties] has the following laminate stiffnesses:

$$[A] = \begin{bmatrix} 15.491 & 3.565 & 0.468 \\ 3.565 & 12.095 & -0.923 \\ 0.468 & -0.923 & 4.311 \end{bmatrix} 10^6 \text{ lb/in.}, \quad [D] = \begin{bmatrix} 1.683 & 0.303 & 0.409 \\ 0.303 & 0.604 & 0.141 \\ 0.409 & 0.141 & 0.366 \end{bmatrix} 10^6 \text{ lb-in.}$$

The transverse shear stiffnesses are (in 10^6 lb/in.)

$$A_{44} = 0.9938, \quad A_{45} = -0.0151, \quad A_{55} = 1.1063$$

The thermal stress resultants are ($T_0 \neq 0, T_1 = 0$)

$$\begin{Bmatrix} N_{xx}^T \\ N_{yy}^T \\ N_{xy}^T \end{Bmatrix} = \begin{Bmatrix} 57.241 \\ 50.307 \\ -0.929 \end{Bmatrix} 10^6 T_0 \text{ lb/in.}, \quad \begin{Bmatrix} M_{xx}^T \\ M_{yy}^T \\ M_{xy}^T \end{Bmatrix} = \begin{Bmatrix} 0 \\ 0 \\ 0 \end{Bmatrix} \text{ lb-in./in.}$$

A symmetric cross-ply laminate (0/90/0/90)_s of boron-epoxy layers has the stiffnesses

$$[A] = \begin{bmatrix} 16.604 & 0.755 & 0 \\ 0.755 & 16.604 & 0 \\ 0 & 0 & 1.5 \end{bmatrix} 10^6 \text{ lb/in.}, \quad [D] = \begin{bmatrix} 1.808 & 0.063 & 0 \\ 0.063 & 0.959 & 0 \\ 0 & 0 & 0.125 \end{bmatrix} 10^6 \text{ lb-in.}$$

The transverse shear stiffnesses are (in 10^6 lb/in.)

$$A_{44} = 1.05, \quad A_{45} = 0.0, \quad A_{55} = 1.05$$

Note that the cross-ply laminate considered here is equivalent to (0/90/0/90/0/90/0) where all layers except the middle layer having a thickness of $h/8$ and the middle layer (90) has a thickness of $h/4$; here h is the total thickness of the laminate.

A symmetric angle-ply laminate (30/-30/45/-45)_s of boron-epoxy layers has the stiffnesses

$$[A] = \begin{bmatrix} 14.379 & 6.376 & 0 \\ 6.376 & 7.586 & 0 \\ 0 & 0 & 7.122 \end{bmatrix} 10^6 \text{ lb/in.}, [D] = \begin{bmatrix} 1.461 & 0.481 & 0.256 \\ 0.481 & 0.470 & 0.126 \\ 0.256 & 0.126 & 0.543 \end{bmatrix} 10^6 \text{ lb-in.}$$

The transverse shear stiffnesses are

$$A_{44} = 0.9375 \times 10^6 \text{ lb/in.}, A_{45} = 0.0 \text{ lb/in.}, A_{55} = 1.1625 \times 10^6 \text{ lb/in.}$$

Example 3.5.3:

Consider a symmetric laminate (0/90)_s made of boron-epoxy layers of thickness 0.005 in. Suppose that the laminate is subjected to loads such that it experiences only nonzero strain of $\varepsilon_{xx}^0 = 10^3 \mu$ in./in. We wish to determine the forces and moment resultants.

The only nonzero strain is $\varepsilon_{xx} = \varepsilon_{xx}^{(0)}$. Hence the force resultants in the laminate are given by

$$\begin{aligned} \begin{Bmatrix} N_{xx} \\ N_{yy} \\ N_{xy} \end{Bmatrix} &= \begin{bmatrix} A_{11} & A_{12} & 0 \\ A_{12} & A_{22} & 0 \\ 0 & 0 & A_{66} \end{bmatrix} \begin{Bmatrix} \varepsilon_{xx}^{(0)} \\ \varepsilon_{yy}^{(0)} \\ \gamma_{xy}^{(0)} \end{Bmatrix} \\ &= \begin{bmatrix} 0.3321 & 0.0151 & 0 \\ 0.0151 & 0.3321 & 0 \\ 0 & 0 & 0.03 \end{bmatrix} \begin{Bmatrix} 1,000 \\ 0 \\ 0 \end{Bmatrix} = \begin{Bmatrix} 332.1 \\ 15.1 \\ 0 \end{Bmatrix} \text{ lb/in.} \end{aligned}$$

All moments will be zero on account of the fact that there are no bending strains and the coupling stiffnesses B_{ij} are zero.

Now suppose that the laminate is subjected to loads such that it experiences only nonzero strain of $\varepsilon_{xx}^{(1)} = 0.1$. Hence, the only nonzero strain is $\varepsilon_{xx} = \varepsilon_{xx}^{(1)} z$. Then the force resultants are zero, and the moment resultants are given by

$$\begin{aligned} \begin{Bmatrix} M_{xx} \\ M_{yy} \\ M_{xy} \end{Bmatrix} &= \begin{bmatrix} D_{11} & D_{12} & 0 \\ D_{12} & D_{22} & 0 \\ 0 & 0 & D_{66} \end{bmatrix} \begin{Bmatrix} \varepsilon_{xx}^{(1)} \\ \varepsilon_{yy}^{(1)} \\ \gamma_{xy}^{(1)} \end{Bmatrix} \\ &= \begin{bmatrix} 17.862 & 0.503 & 0 \\ 0.503 & 4.277 & 0 \\ 0 & 0 & 1 \end{bmatrix} \begin{Bmatrix} 0.1 \\ 0.0 \\ 0.0 \end{Bmatrix} = \begin{Bmatrix} 1.7862 \\ 0.0503 \\ 0 \end{Bmatrix} \text{ lb-in./in.} \end{aligned}$$

3.5.4 Antisymmetric Laminates

Although symmetric laminates are more desirable from an analysis standpoint, they may not meet the design requirements in some applications. For example, a heat shield receives heat from one side and thus requires nonsymmetric laminates to effectively shield the heat. Another example that requires coupling is provided by turbine blades with pretwist. Moreover, the shear stiffness of laminates can be increased by orienting the layers at angle to the laminate coordinates.

The general class of antisymmetric laminates must have an *even* number of orthotropic laminae if adjacent laminae have equal thicknesses and alternating orientations: $(\theta/-\theta)$, $0^\circ \leq \theta \leq 90^\circ$. Due to the antisymmetry of the lamination

scheme (see Figure 3.5.7) but symmetry of the thicknesses of each pair of layers, this class of antisymmetric laminates has the feature that $A_{16} = A_{26} = D_{16} = D_{26} = 0$. The coupling stiffnesses B_{ij} are not all zero; they go to zero as the number of layers is increased. For a general antisymmetric laminate, the relations between the stress resultants and the strains are given by

$$\begin{Bmatrix} N_{xx} \\ N_{yy} \\ N_{xy} \end{Bmatrix} = \begin{bmatrix} A_{11} & A_{12} & 0 \\ A_{12} & A_{22} & 0 \\ 0 & 0 & A_{66} \end{bmatrix} \begin{Bmatrix} \varepsilon_{xx}^{(0)} \\ \varepsilon_{yy}^{(0)} \\ \gamma_{xy}^{(0)} \end{Bmatrix} + \begin{bmatrix} B_{11} & B_{12} & B_{16} \\ B_{12} & B_{22} & B_{26} \\ B_{16} & B_{26} & B_{66} \end{bmatrix} \begin{Bmatrix} \varepsilon_{xx}^{(1)} \\ \varepsilon_{yy}^{(1)} \\ \gamma_{xy}^{(1)} \end{Bmatrix} \quad (3.5.26a)$$

$$\begin{Bmatrix} M_{xx} \\ M_{yy} \\ M_{xy} \end{Bmatrix} = \begin{bmatrix} B_{11} & B_{12} & B_{16} \\ B_{12} & B_{22} & B_{26} \\ B_{16} & B_{26} & B_{66} \end{bmatrix} \begin{Bmatrix} \varepsilon_{xx}^{(0)} \\ \varepsilon_{yy}^{(0)} \\ \gamma_{xy}^{(0)} \end{Bmatrix} + \begin{bmatrix} D_{11} & D_{12} & 0 \\ D_{12} & D_{22} & 0 \\ 0 & 0 & D_{66} \end{bmatrix} \begin{Bmatrix} \varepsilon_{xx}^{(1)} \\ \varepsilon_{yy}^{(1)} \\ \gamma_{xy}^{(1)} \end{Bmatrix} \quad (3.5.26b)$$

$$\begin{Bmatrix} Q_y \\ Q_x \end{Bmatrix} = K \begin{bmatrix} A_{44} & 0 \\ 0 & A_{55} \end{bmatrix} \begin{Bmatrix} \gamma_{yz}^{(0)} \\ \gamma_{xz}^{(0)} \end{Bmatrix} \quad (3.5.26c)$$

The thermal force resultants are given by

$$\begin{Bmatrix} N_{xx}^T \\ N_{yy}^T \\ N_{xy}^T \end{Bmatrix} = \sum_{k=1}^L \int_{z_k}^{z_{k+1}} \begin{bmatrix} \bar{Q}_{11} & \bar{Q}_{12} & \bar{Q}_{16} \\ \bar{Q}_{12} & \bar{Q}_{22} & \bar{Q}_{26} \\ \bar{Q}_{16} & \bar{Q}_{26} & \bar{Q}_{66} \end{bmatrix} \begin{Bmatrix} \alpha_{xx} \\ \alpha_{yy} \\ 2\alpha_{xy} \end{Bmatrix} \Delta T dz \quad (3.5.27)$$

Similar expression holds for $\{M^T\}$.

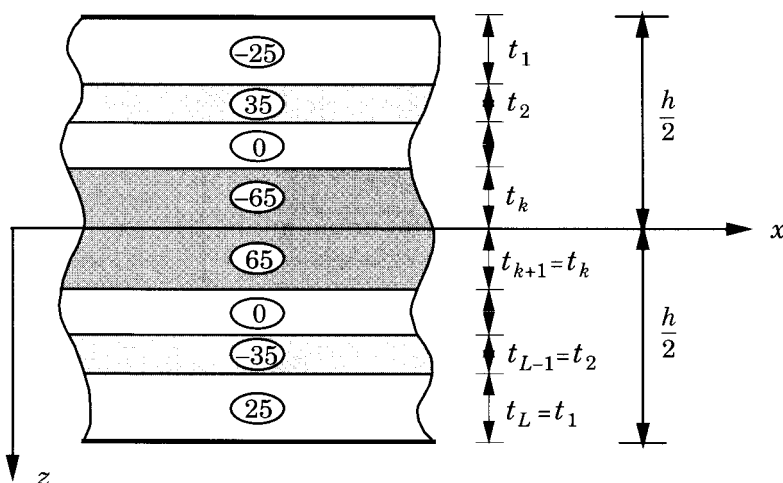


Figure 3.5.7: An antisymmetric laminate.

In the following pages, we discuss some special cases of the class of antisymmetric laminates described above (i.e., laminates that have an even number of orthotropic laminae, each pair having equal thicknesses and alternating orientations).

Antisymmetric Cross-ply Laminates

A special case of antisymmetric laminates are those which have an even number of orthotropic layers with principal material directions alternating at 0° to 90° to the laminate axes. Such laminates are called *antisymmetric cross-ply laminates*. Examples of antisymmetric cross-ply laminates are $(0/90/0/90/\dots)$ with all layers of the same thickness, and $(0/90/90/0/0/90)$ with layers of the thicknesses $(h_1/h_2/h_3/h_3/h_2/h_1)$. Note that for every 0° layer of a given thickness and location, there is a 90° layer of the same thickness and location on the other side of the midplane (see Figure 3.5.8). For these laminates, the coupling stiffnesses B_{ij} have the properties

$$B_{22} = -B_{11}, \text{ and all other } B_{ij} = 0 \quad (3.5.28)$$

The relations between the stress resultants and the strains are

$$\begin{Bmatrix} N_{xx} \\ N_{yy} \\ N_{xy} \end{Bmatrix} = \begin{bmatrix} A_{11} & A_{12} & 0 \\ A_{12} & A_{22} & 0 \\ 0 & 0 & A_{66} \end{bmatrix} \begin{Bmatrix} \varepsilon_{xx}^{(0)} \\ \varepsilon_{yy}^{(0)} \\ \gamma_{xy}^{(0)} \end{Bmatrix} + \begin{bmatrix} B_{11} & 0 & 0 \\ 0 & -B_{11} & 0 \\ 0 & 0 & 0 \end{bmatrix} \begin{Bmatrix} \varepsilon_{xx}^{(1)} \\ \varepsilon_{yy}^{(1)} \\ \gamma_{xy}^{(1)} \end{Bmatrix} \quad (3.5.29a)$$

$$\begin{Bmatrix} M_{xx} \\ M_{yy} \\ M_{xy} \end{Bmatrix} = \begin{bmatrix} B_{11} & 0 & 0 \\ 0 & -B_{11} & 0 \\ 0 & 0 & 0 \end{bmatrix} \begin{Bmatrix} \varepsilon_{xx}^{(0)} \\ \varepsilon_{yy}^{(0)} \\ \gamma_{xy}^{(0)} \end{Bmatrix} + \begin{bmatrix} D_{11} & D_{12} & 0 \\ D_{12} & D_{22} & 0 \\ 0 & 0 & D_{66} \end{bmatrix} \begin{Bmatrix} \varepsilon_{xx}^{(1)} \\ \varepsilon_{yy}^{(1)} \\ \gamma_{xy}^{(1)} \end{Bmatrix} \quad (3.5.29b)$$

$$\begin{Bmatrix} Q_y \\ Q_x \end{Bmatrix} = K \begin{bmatrix} A_{44} & 0 \\ 0 & A_{55} \end{bmatrix} \begin{Bmatrix} \gamma_{yz}^{(0)} \\ \gamma_{xz}^{(0)} \end{Bmatrix} \quad (3.5.30)$$

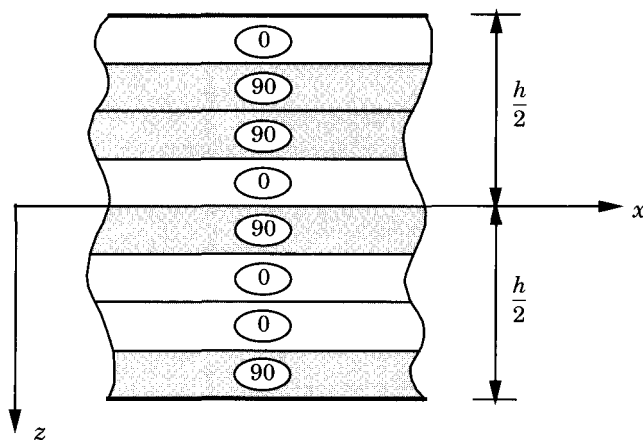


Figure 3.5.8: An antisymmetric cross-ply laminate.

A *regular antisymmetric cross-ply laminate* is one that has an even number of layers of equal thickness and the same material properties and which have alternating 0° and 90° orientations. For these laminates, the coupling coefficient B_{11} approaches zero as the number of layers is increased.

Antisymmetric Angle-ply Laminates

An antisymmetric angle-ply laminate has an even number of orthotropic layers with principal material directions alternating at θ degrees to the laminate axes on one side of the midplane and corresponding equal thickness laminae oriented at $-\theta$ degrees on the other side. When $\theta = 0$, $-\theta$ should be interpreted as 90° or vice versa. A *regular antisymmetric angle-ply laminate* is one that has an even number of layers of equal thickness and material properties. An example is given by (-45/40/-15/15/-40/45).

For antisymmetric angle-ply laminates without 90° layers, the stiffnesses can be simplified as

$$A_{16} = A_{26} = D_{16} = D_{26} = 0; \quad B_{11} = B_{22} = B_{12} = B_{66} = 0 \quad (3.5.31)$$

The relations between the stress resultants and the strains are

$$\begin{Bmatrix} N_{xx} \\ N_{yy} \\ N_{xy} \end{Bmatrix} = \begin{bmatrix} A_{11} & A_{12} & 0 \\ A_{12} & A_{22} & 0 \\ 0 & 0 & A_{66} \end{bmatrix} \begin{Bmatrix} \varepsilon_{xx}^{(0)} \\ \varepsilon_{yy}^{(0)} \\ \gamma_{xy}^{(0)} \end{Bmatrix} + \begin{bmatrix} 0 & 0 & B_{16} \\ 0 & 0 & B_{26} \\ B_{16} & B_{26} & 0 \end{bmatrix} \begin{Bmatrix} \varepsilon_{xx}^{(1)} \\ \varepsilon_{yy}^{(1)} \\ \gamma_{xy}^{(1)} \end{Bmatrix} \quad (3.5.32)$$

$$\begin{Bmatrix} M_{xx} \\ M_{yy} \\ M_{xy} \end{Bmatrix} = \begin{bmatrix} 0 & 0 & B_{16} \\ 0 & 0 & B_{26} \\ B_{16} & B_{26} & 0 \end{bmatrix} \begin{Bmatrix} \varepsilon_{xx}^{(0)} \\ \varepsilon_{yy}^{(0)} \\ \gamma_{xy}^{(0)} \end{Bmatrix} + \begin{bmatrix} D_{11} & D_{12} & 0 \\ D_{12} & D_{22} & 0 \\ 0 & 0 & D_{66} \end{bmatrix} \begin{Bmatrix} \varepsilon_{xx}^{(1)} \\ \varepsilon_{yy}^{(1)} \\ \gamma_{xy}^{(1)} \end{Bmatrix} \quad (3.5.33)$$

$$\begin{Bmatrix} Q_y \\ Q_x \end{Bmatrix} = K \begin{bmatrix} A_{44} & 0 \\ 0 & A_{55} \end{bmatrix} \begin{Bmatrix} \gamma_{yz}^{(0)} \\ \gamma_{xz}^{(0)} \end{Bmatrix} \quad (3.5.34)$$

For a fixed laminate thickness, the stiffnesses B_{16} and B_{26} go to zero as the number of layers in the laminate increases.

Example 3.5.4:

A regular antisymmetric cross-ply laminate (0/90/0/90/0/90/0/90) of boron-epoxy layers has the laminate stiffnesses

$$[A] = \begin{bmatrix} 16.604 & 0.755 & 0 \\ 0.755 & 16.604 & 0 \\ 0 & 0 & 1.5 \end{bmatrix} 10^6 \text{ lb/in.}, \quad [B] = \begin{bmatrix} -0.849 & 0 & 0 \\ 0 & 0.849 & 0 \\ 0 & 0 & 0 \end{bmatrix} 10^6 \text{ lb}$$

$$[D] = \begin{bmatrix} 1.384 & 0.063 & 0 \\ 0.063 & 1.384 & 0 \\ 0 & 0 & 0.125 \end{bmatrix} 10^6 \text{ lb-in.}, \quad \begin{Bmatrix} A_{44} \\ A_{45} \\ A_{55} \end{Bmatrix} = \begin{Bmatrix} 1.050 \\ 0 \\ 1.050 \end{Bmatrix} 10^6 \text{ lb/in.}$$

Note that if the same 0° and 90° layers are positioned differently, say (0/90/90/0/90/0/0/90), then the coefficients B_{ij} would vanish (why?).

An antisymmetric angle-ply laminate (-45/45/30/0/0/-30/-45/45) of boron-epoxy layers has the laminate stiffnesses

$$[A] = \begin{bmatrix} 17.281 & 5.172 & 0 \\ 5.172 & 7.093 & 0 \\ 0 & 0 & 5.917 \end{bmatrix} 10^6 \text{ lb/in.}, \quad [B] = \begin{bmatrix} 0 & 0 & -0.194 \\ 0 & 0 & 0.067 \\ -0.194 & 0.067 & 0 \end{bmatrix} 10^6 \text{ lb}$$

$$[D] = \begin{bmatrix} 0.951 & 0.575 & 0 \\ 0.575 & 0.792 & 0 \\ 0 & 0 & 0.637 \end{bmatrix} 10^6 \text{ lb-in.}, \quad \begin{Bmatrix} A_{44} \\ A_{45} \\ A_{55} \end{Bmatrix} = \begin{Bmatrix} 0.881 \\ 0 \\ 1.219 \end{Bmatrix} 10^6 \text{ lb/in.}$$

A general antisymmetric laminate (30/0/90/45)_{as} \equiv (30/0/90/-45/45/ 0/90/-30) of total thickness 1 in. and composed of boron-epoxy layers has the following laminate stiffnesses and thermal resultants:

$$[A] = \begin{bmatrix} 15.491 & 3.565 & 0 \\ 3.565 & 12.095 & 0 \\ 0 & 0 & 4.311 \end{bmatrix} 10^6 \text{ lb/in.}, \quad [B] = \begin{bmatrix} -0.425 & 0 & -0.842 \\ 0 & 0.425 & -0.233 \\ -0.842 & -0.233 & 0 \end{bmatrix} 10^6 \text{ lb}$$

$$[D] = \begin{bmatrix} 1.470 & 0.303 & 0 \\ 0.303 & 0.816 & 0 \\ 0 & 0 & 0.366 \end{bmatrix} 10^6 \text{ lb-in.}, \quad \begin{Bmatrix} A_{44} \\ A_{45} \\ A_{55} \end{Bmatrix} = \begin{Bmatrix} 0.9938 \\ 0 \\ 1.1063 \end{Bmatrix} 10^6 \text{ lb/in.}$$

$$\begin{Bmatrix} N_{xx}^T \\ N_{yy}^T \\ N_{xy}^T \end{Bmatrix} = \begin{Bmatrix} 5573.6 \\ 5958.5 \\ 0 \end{Bmatrix} 10^6 \text{ lb/in.}, \quad \begin{Bmatrix} M_{xx}^T \\ M_{yy}^T \\ M_{xy}^T \end{Bmatrix} = \begin{Bmatrix} 48.113 \\ -48.113 \\ 121.78 \end{Bmatrix} 10^6 \text{ lb-in./in.}$$

3.5.5 Balanced and Quasi-Isotropic Laminates

A laminate is said to be *balanced* if for every layer in the laminate there exists, somewhere in the laminate, another layer with identical material and thickness but opposite fiber orientation. The two layers are not necessarily symmetrically located with respect to the midplane. Thus, the unsymmetric laminate ($\pm 35/0$)_T = (35/-35/0) as well as the symmetric laminate ($\pm 35/0$)_s are balanced laminates. The characteristic feature of any balanced laminate is that the in-plane shear stiffnesses A_{16} and A_{26} are zero. The reason is that Q_{16} and Q_{26} from opposite orientations of the pair of layers are of opposite sign and therefore the net contribution from the pair to A_{16} and A_{26} is zero:

$$(Q_{16})_\theta = -(Q_{16})_{(-\theta)}, \quad (Q_{26})_\theta = -(Q_{26})_{(-\theta)}$$

For a general balanced laminate, the laminate constitutive relations are not that much simpler than for a general laminate. However, for a symmetric balanced laminate they are given by Eqs. (3.5.13)–(3.5.15) with $A_{16} = A_{26} = 0$.

Laminates consisting of three or more orthotropic laminae of identical material and thickness which are oriented at the same angle relative to adjacent laminae exhibit in-plane isotropy in the sense that $A_{11} = A_{22}$, $A_{66} = (A_{11} - A_{12})/2$, and $A_{16} = A_{26} = 0$. Such laminates are called *quasi-isotropic* laminates. Examples of quasi-isotropic laminates are provided by (90/45/0/-45) and (60/0/-60) (see Example 3.3.2). When the bending-stretching coupling coefficients are zero, the relations between force resultants and membrane strains are the same as those for isotropic plates. The stress resultants are given by

$$\begin{Bmatrix} N_{xx} \\ N_{yy} \\ N_{xy} \end{Bmatrix} = \begin{bmatrix} A_{11} & A_{12} & 0 \\ A_{12} & A_{11} & 0 \\ 0 & 0 & (A_{11} - A_{12})/2 \end{bmatrix} \begin{Bmatrix} \varepsilon_{xx}^{(0)} \\ \varepsilon_{yy}^{(0)} \\ \gamma_{xy}^{(0)} \end{Bmatrix}$$

Problems

- 3.1** Suppose that the displacements (u, v, w) along the three coordinate axes (x, y, z) in a laminated beam can be expressed as

$$\begin{aligned} u(x, z) &= u_0(x) + z \left[c_0 \frac{dw_0}{dx} + c_1 \phi(x) \right] \\ v(x, z) &= 0 \\ w(x, z) &= w_0(x) \end{aligned} \quad (1)$$

where (u_0, w_0) denote the displacements of a point $(x, y, 0)$ along the x and z directions, respectively, and ϕ denotes the rotation of a transverse normal about the y -axis. Show that the nonzero linear strains are given by

$$\varepsilon_{xx} = \varepsilon_{xx}^{(0)} + z\varepsilon_{xx}^{(1)}, \quad 2\varepsilon_{xz} = 2\varepsilon_{xz}^{(0)} \quad (2a)$$

where

$$\varepsilon_{xx}^{(0)} = \frac{du_0}{dx}, \quad \varepsilon_x^{(1)} = c_0 \frac{d^2w_0}{dx^2} + c_1 \frac{d\phi}{dx}, \quad 2\varepsilon_{xz}^{(0)} = (1 + c_0) \frac{dw_0}{dx} + c_1 \phi \quad (2b)$$

- 3.2** (Continuation of Problem 3.1) Use the principle of virtual displacements to derive the equations of equilibrium and the natural and essential boundary conditions associated with the displacement field of Problem 3.1, when the beam is subjected to axial distributed load $p(x)$ and transverse distributed load $q(x)$. In particular, show that

$$\begin{aligned} \delta u_0 : \quad & \frac{dN_{xx}}{dx} + p = 0 \\ \delta \phi : \quad & \frac{d}{dx}(c_1 M_{xx}) - c_1 Q_x = 0 \\ \delta w_0 : \quad & \frac{d^2}{dx^2}(c_0 M_{xx}) - (1 + c_0) \frac{dQ_x}{dx} - q = 0 \end{aligned} \quad (3)$$

and the boundary conditions are of the form

$$\begin{aligned} N_{xx} &\text{ or } u_0 \\ c_1 M_{xx} &\text{ or } \phi \\ -\frac{d}{dx}(c_0 M_{xx}) + (1 + c_0)Q_x &\text{ or } w_0 \\ c_0 M_{xx} &\text{ or } \frac{dw_0}{dx} \end{aligned} \quad (4)$$

where

$$N_{xx} = \int_A \sigma_{xx} dA, \quad M_{xx} = \int_A \sigma_{xx} z dA, \quad Q_x = \int_A \sigma_{xz} dA \quad (5)$$

Note that the displacement field (1), hence the equations of equilibrium (3), contain those of the classical (Euler-Bernoulli) beam theory ($c_0 = -1$, $c_1 = 0$) and the first-order (Timoshenko) beam theory ($c_0 = 0$, $c_1 = 1$).

- 3.3** (Continuation of Problem 3.1) Assume linear elastic constitutive behavior and show that the laminated beam's constitutive equations are given by

$$\begin{Bmatrix} N_{xx} \\ M_{xx} \end{Bmatrix} = \begin{bmatrix} A_{11} & B_{11} \\ B_{11} & D_{11} \end{bmatrix} \begin{Bmatrix} \varepsilon_{xx}^{(0)} \\ \varepsilon_x^{(1)} \end{Bmatrix}, \quad Q_x = 2A_{55}\varepsilon_{xz}^{(0)} \quad (6a)$$

where

$$(A_{11}, B_{11}, D_{11}) = \int_A E_1(1, z, z^2) dA, \quad A_{55} = \int_A G_{13} dA \quad (6b)$$

- 3.4** The 3-D equilibrium equations of a k th layer, in the absence of body forces, can be expressed in index notation as

$$\frac{\partial \sigma_{\alpha\beta}^k}{\partial x_\beta} + \frac{\partial \sigma_{\alpha 3}^k}{\partial x_3} = 0 \quad (1)$$

$$\frac{\partial \sigma_{\alpha 3}^k}{\partial x_\alpha} + \frac{\partial \sigma_{33}^k}{\partial x_3} = 0 \quad (2)$$

where summation on repeated subscripts ($\alpha, \beta = 1, 2$) is implied. Integrate the equations over the thickness (z_k, z_{k+1}) with respect to $z = x_3$ to obtain:

$$\frac{\partial N_{\alpha\beta}^{(k)}}{\partial x_\beta} + \sigma_{\alpha 3}^{(k+1)} - \sigma_{\alpha 3}^{(k)} = 0 \quad (3)$$

$$\frac{\partial Q_\alpha^{(k)}}{\partial x_\alpha} + \sigma_{33}^{(k+1)} - \sigma_{33}^{(k)} = 0 \quad (4)$$

for $k = 1, 2, \dots, N$ and $\alpha, \beta = 1, 2$ ($x_1 = x, x_2 = y, x_3 = z$), where N is the total number of layers, and

$$(N_{\alpha\beta}^{(k)}, M_{\alpha\beta}^{(k)}) = \int_{z_k}^{z_{k+1}} (1, z) \sigma_{\alpha\beta}^{(k)} dz, \quad Q_\alpha^{(k)} = \int_{z_k}^{z_{k+1}} \sigma_{\alpha 3}^{(k)} dz \quad (5)$$

$$\sigma_{ij}^{(k)} = \sigma_{ij}(x_\beta, z_k) \quad (6)$$

- 3.5** (Continuation of Problem 3.4) Multiply the equilibrium equations

$$\frac{\partial \sigma_{\alpha\beta}^k}{\partial x_\beta} + \frac{\partial \sigma_{\alpha 3}^k}{\partial x_3} = 0 \quad (1)$$

with z and integrate over the lamina thickness to obtain the third equation

$$\frac{\partial M_{\alpha\beta}^{(k)}}{\partial x_\beta} + \sigma_{\alpha 3}^{(k+1)} z_{k+1} - \sigma_{\alpha 3}^{(k)} z_k - Q_\alpha^k = 0 \quad (2)$$

- 3.6** Starting with a linear distribution of the displacements through the laminate thickness in terms of unknown functions ($u_0, v_0, w_0, F_1, F_2, F_3$)

$$\begin{aligned} u(x, y, z, t) &= u_0(x, y, t) + zF_1(x, y, t) \\ v(x, y, z, t) &= v_0(x, y, t) + zF_2(x, y, t) \\ w(x, y, z, t) &= w_0(x, y, t) + zF_3(x, y, t) \end{aligned}$$

determine the functions (F_1, F_2, F_3) such that the Kirchhoff hypothesis holds:

$$\frac{\partial w}{\partial z} = 0, \quad \frac{\partial u}{\partial z} = -\frac{\partial w}{\partial x}, \quad \frac{\partial v}{\partial z} = -\frac{\partial w}{\partial y}$$

- 3.7** Consider a single, orthotropic layer plate ($Q_{45} = 0$), and assume that the material coordinates coincide with the plate coordinates. Compute the stresses ($\sigma_{xx}, \sigma_{yy}, \sigma_{xy}$) using the constitutive equations of the first-order plate theory, and then use the equilibrium equations of the three-dimensional elasticity theory to determine the transverse stresses ($\sigma_{xz}, \sigma_{yz}, \sigma_{zz}$) as a function of the thickness coordinate.

- 3.8** Consider a single, orthotropic layer plate ($Q_{45} = 0$), and assume that the material coordinates coincide with the plate coordinates. According to the first-order theory, the strain energy due to transverse shear stresses is given by

$$\begin{aligned} U_s &= \frac{1}{2} \int_{\Omega_0} \int_{-\frac{h}{2}}^{\frac{h}{2}} \left(\sigma_{xz} \gamma_{xz}^{(0)} + \sigma_{yz} \gamma_{yz}^{(0)} \right) dz dx dy \\ &= \frac{1}{2} \int_{\Omega_0} \int_{-\frac{h}{2}}^{\frac{h}{2}} \left[Q_{55} \left(\gamma_{xz}^{(0)} \right)^2 + Q_{44} \left(\gamma_{yz}^{(0)} \right)^2 \right] dz dx dy \\ &= \frac{1}{2K} \int_{\Omega_0} \left(\frac{Q_x^2}{A_{55}} + \frac{Q_y^2}{A_{44}} \right) dx dy \end{aligned}$$

Compute \bar{U}_s using the transverse shear stresses obtained in Problem 3.7 from the three-dimensional elasticity, and equate it with U_s to determine the shear correction coefficient, K .

- 3.9** Consider the equations of motion of 3-D elasticity [see Eq. (1.3.26)] in the absence of body forces:

$$\begin{aligned} \frac{\partial \sigma_{xx}}{\partial x} + \frac{\partial \sigma_{xy}}{\partial y} + \frac{\partial \sigma_{xz}}{\partial z} &= \rho_0 \frac{\partial^2 u}{\partial t^2} \\ \frac{\partial \sigma_{xy}}{\partial x} + \frac{\partial \sigma_{yy}}{\partial y} + \frac{\partial \sigma_{yz}}{\partial z} &= \rho_0 \frac{\partial^2 v}{\partial t^2} \\ \frac{\partial \sigma_{xz}}{\partial x} + \frac{\partial \sigma_{yz}}{\partial y} + \frac{\partial \sigma_{zz}}{\partial z} &= \rho_0 \frac{\partial^2 w}{\partial t^2} \end{aligned}$$

Integrate the above equations with respect to z over the interval $(-h/2, h/2)$ and express the results in terms of the force resultants defined in Eq. (3.3.20a). Use the following boundary conditions:

$$\begin{aligned} \sigma_{xz}(x, y, -\frac{h}{2}) &= 0, \quad \sigma_{xz}(x, y, \frac{h}{2}) = 0, \quad \sigma_{yz}(x, y, -\frac{h}{2}) = 0, \quad \sigma_{yz}(x, y, \frac{h}{2}) = 0 \\ \sigma_{zz}(x, y, -\frac{h}{2}) &= -q_b, \quad \sigma_{zz}(x, y, \frac{h}{2}) = q_t \end{aligned}$$

Next, multiply the equations of motion with z and integrate with respect to z over the interval $(-h/2, h/2)$ and express the results in terms of the moment resultants defined in Eq. (3.3.20a).

- 3.10** Show that the membrane strains $\{\varepsilon^0\}$ and the moment resultants $\{M\}$ in the classical or first-order laminated plate theory can be expressed in terms of force resultants $\{N\}$ and bending strains $\{\varepsilon^1\}$ as

$$\begin{aligned} \{\varepsilon^0\} &= [A]^{-1} (\{N\} - [B]\{\varepsilon^1\}) \\ \{M\} &= ([B][A]^{-1}) \{N\} - ([B][A]^{-1}[B] - [D]) \{\varepsilon^1\} \end{aligned}$$

These equations bring out the bending-extensional coupling for laminates with nonzero $[B]$. For example, when the bending strains are zero, the applied in-plane forces induce bending moments for laminates with nonzero coupling coefficients $[B]$.

- 3.11** Show that if $B_{ij} = 0$ (e.g., for symmetric laminates), the equation of motion governing the transverse deflection w_0 in the classical laminate theory is

$$\begin{aligned} D_{11} \frac{\partial^4 w_0}{\partial x^4} + 4D_{16} \frac{\partial^4 w_0}{\partial x^3 \partial y} + 2(D_{12} + 2D_{66}) \frac{\partial^4 w_0}{\partial x^2 \partial y^2} + 4D_{26} \frac{\partial^4 w_0}{\partial x \partial y^3} + D_{22} \frac{\partial^4 w_0}{\partial y^4} \\ - \mathcal{N}(w) = q - I_0 \frac{\partial^2 w_0}{\partial t^2} + I_2 \frac{\partial^2}{\partial t^2} \left(\frac{\partial^2 w_0}{\partial x^2} + \frac{\partial^2 w_0}{\partial y^2} \right) - I_1 \frac{\partial^2}{\partial t^2} \left(\frac{\partial w_0}{\partial x} + \frac{\partial w_0}{\partial y} \right) \end{aligned}$$

- 3.12** Show that for a general laminate composed of multiple isotropic layers, the laminate stiffness $A_{16}, A_{26}, B_{16}, B_{26}, D_{16}$, and D_{26} are zero, and that $A_{22} = A_{11}, B_{22} = B_{11}$, and $D_{22} = D_{11}$.
- 3.13** Show that for a general laminate composed of multiple specially orthotropic layers, the laminate stiffness $A_{16}, A_{26}, B_{16}, B_{26}, D_{16}$, and D_{26} are zero.
- 3.14** Show that for antisymmetric laminates the stiffnesses, A_{16}, A_{26}, D_{16} , and D_{26} are zero, and the coupling stiffnesses B_{ij} are not zero.
- 3.15** Show that for antisymmetric cross-ply laminates, the coupling stiffnesses B_{ij} have the properties: $B_{22} = -B_{11}$ and all other $B_{ij} = 0$.
- 3.16** Show that for antisymmetric angle-ply laminated plates, the following stiffnesses are zero: $A_{16}, A_{26}, D_{16}, D_{26}, B_{11}, B_{22}, B_{12}$, and B_{66} .
- 3.17** Show that for laminates $(\alpha/\beta/\beta/\alpha/\beta/\alpha/\alpha/\beta)$ where $-90^\circ \leq \alpha \leq 90^\circ$ and $-90^\circ \leq \beta \leq 90^\circ$, coefficients B_{ij} are zero.
- 3.18** The material properties of AS/3501 graphite-epoxy material layers are:

$$E_1 = 140 \times 10^3 \text{ MPa}, E_2 = 10 \times 10^3 \text{ MPa}, G_{12} = 7 \times 10^3 \text{ MPa}$$

$$G_{13} = 7 \times 10^3 \text{ MPa}, G_{23} = 7 \times 10^3 \text{ MPa}, \nu_{12} = 0.3$$

$$\alpha_1 = -0.3 \times 10^{-6} \text{ m/m/}^\circ \text{ K}, \alpha_2 = 28 \times 10^{-6} \text{ m/m/}^\circ \text{ K}$$

Determine the stiffnesses $[A]$, $[B]$, and $[D]$ for the antisymmetric laminate $(0/90)$ composed of equal thickness (0.5 mm) layers.

- 3.19** Determine the stiffnesses $[A]$, $[B]$, and $[D]$ for an antisymmetric laminate $(-45/45)$ composed of equal thickness (0.5 mm) layers of AS/3501 graphite-epoxy layers (see Problem 3.18 for the material properties).
- 3.20** If the laminate of Problem 3.18 is heated from 20° to 90° , determine the thermal forces and moments generated in the laminate, if it were restrained from free expansion.
- 3.21** If the laminate in Problem 3.19 is made of four layers $(-45/45/-45/45)$ of thickness 0.25 mm each, show that the stiffnesses $[A]$ and $[D]$ remain unchanged. Compare the stiffnesses B_{ij} for the two laminates (do they increase or decrease in values?).
- 3.22** Suppose that a four-layer $(0/90)_s$ symmetric laminate is subjected to loads such that the only nonzero strain at a point (x, y) is $\varepsilon_{xx}^{(0)} = 10^3 \mu \text{ in./in.}$. The material properties of a lamina are (typical of a graphite-epoxy material) $E_1 = 20 \text{ ksi}$, $E_2 = 1.30 \text{ ksi}$, $G_{12} = 1.03 \text{ ksi}$, $\nu_{12} = 0.3$. Assume that each layer is of thickness 0.005 in. Determine the state of stress $(\sigma_{xx}, \sigma_{yy}, \sigma_{xy})$ with respect to the laminate coordinates in each layer. Interpret the results you obtain in light of the assumed strains.
- 3.23** Compute the stains and stresses in the principal material coordinate system of each layer for the problem in Problem 3.22.
- 3.24** Compute the stress resultants N 's and M 's for the problem in Problem 3.22.
- 3.25** Repeat Problem 3.22 for the case in which the laminate is subjected to loads such that the only nonzero strain at a point (x, y) is $\varepsilon_{xx}^{(1)} = (1/12) / \text{in.}$
- 3.26** Compute the stains and stresses in the principal material coordinate system of each layer for the problem in Problem 3.25.
- 3.27** Compute the stress resultants N 's and M 's for the problem in Problem 3.25.
- 3.28** Determine the displacement associated with the assumed strain field in Problem 3.25.
- 3.29** Suppose that a six-layer $(\pm 45/0)_s$ symmetric laminate is subjected to loads such that the only nonzero strain at a point (x, y) is $\varepsilon_{xx}^{(0)} = 10^3 \mu \text{ in./in.}$. The thickness and material properties of a lamina are the same as those listed in Problem 3.22. Determine the state of stress $(\sigma_{xx}, \sigma_{yy}, \sigma_{xy})$ and force resultants.

- 3.30** Repeat Problem 3.29 for the case in which the laminate is subjected to loads such that the only nonzero strain at a point (x, y) is $\varepsilon_{xx}^{(1)} = (1/12) / \text{in.}$
- 3.31** Suppose that a three-layer ($\pm 45/0$) unsymmetric laminate is subjected to loads such that the only nonzero strain at a point (x, y) is $\varepsilon_{xx}^{(0)} = 10^{-3} \text{ in./in.}$ The thickness and material properties of a lamina are the same as those listed in Problem 3.22. Determine the state of stress $(\sigma_{xx}, \sigma_{yy}, \sigma_{xy})$ and stress resultants.

References for Additional Reading

1. Cauchy, A. L., "Sur l'équilibre et le mouvement d'une plaque solide," *Exercices de Mathematique*, **3**, 328–355 (1828).
2. Poisson, S. D., "Memoire sur l'équilibre et le mouvement des corps élastiques," *Mem. Acad. Sci.*, **8**(2), 357–570 (1829).
3. Kirchhoff, G., "Über das Gleichgewicht und die Bewegung einer Elastischen Scheibe," *J. Angew. Math.*, **40**, 51–88 (1850).
4. Basset, A. B., "On the Extension and Flexure of Cylindrical and Spherical Thin Elastic Shells," *Philosophical Transactions of the Royal Society*, (London) Ser. A, **181** (6), 433–480 (1890).
5. Goodier, J. N., "On the Problem of the Beam and the Plate in the Theory of Elasticity," *Transactions of the Royal Society of Canada*, **32**, 65–88 (1938).
6. Reissner, E., "On the Theory of Bending of Elastic Plates," *Journal of Mathematical Physics*, **23**, 184–191 (1944).
7. Reissner, E., "The Effect of Transverse Shear Deformation on the Bending of Elastic Plates," *Journal of Applied Mechanics*, **12**, 69–77 (1945).
8. Reissner, E., "Reflections on the Theory of Elastic Plates," *Applied Mechanics Reviews*, **38**(11), 1453–1464 (1985).
9. Bollé, E., "Contribution au Problème Linéaire de Flexion d'une Plaque Élastique," *Bull. Tech. Suisse. Romande.*, **73**, 281–285 and 293–298 (1947).
10. Hencky, H., "Über die Berücksichtigung der Schubverzerrung in ebenen Platten," *Ing. Arch.*, **16**, 72–76 (1947).
11. Hildebrand, F. B., Reissner, E., and Thomas, G. B., "Notes on the Foundations of the Theory of Small Displacements of Orthotropic Shells," NACA TN-1833, Washington, D.C. (1949).
12. Mindlin, R. D., "Influence of Rotatory Inertia and Shear on Flexural Motions of Isotropic, Elastic Plates," *Journal of Applied Mechanics, Transactions of ASME*, **18**, 31–38 (1951).
13. Vlasov, B. F., "Ob uravneniyakh teorii isgiba plastinok (On the Equations of the Theory of Bending of Plates)," *Izv. Akad. Nauk SSR, OTN*, **4**, 102–109 (1958).
14. Panc, V., *Theories of Elastic Plates*, Noordhoff, Leyden, The Netherlands (1975).
15. Reissner, E. and Stavsky, Y., "Bending and Stretching of Certain Types of Aeolotropic Elastic Plates," *Journal of Applied Mechanics*, **28**, 402–408 (1961).
16. Stavsky, Y., "Bending and Stretching of Laminated Aeolotropic Plates," *Journal of Engineering Mechanics, ASCE*, **87** (EM6), 31–56 (1961).
17. Dong, S. B., Pister, K. S., and Taylor, R. L., "On the Theory of Laminated Anisotropic Shells and Plates," *Journal of Aeronautical Science*, **29**(8), 969–975 (1962).
18. Yang, P. C., Norris, C. H., and Stavsky, Y., "Elastic Wave Propagation in Heterogeneous Plates," *International Journal of Solids and Structures*, **2**, 665–684 (1966).
19. Ambartsumyan, S. A., *Theory of Anisotropic Plates*, translated from Russian by T. Cheron, Technomic, Stamford, CT (1969).

20. Whitney, J. M. and Leissa, A. W., "Analysis of Heterogeneous Anisotropic Plates," *Journal of Applied Mechanics*, **36**(2), 261–266 (1969).
21. Whitney, J. M., "The Effect of Transverse Shear Deformation in the Bending of Laminated Plates," *Journal of Composite Materials*, **3**, 534–547 (1969).
22. Whitney, J. M. and Pagano, N. J., "Shear Deformation in Heterogeneous Anisotropic Plates," *Journal of Applied Mechanics*, **37**(4), 1031–1036 (1970).
23. Reissner, E., "A Consistent Treatment of Transverse Shear Deformations in Laminated Anisotropic Plates," *AIAA Journal*, **10**(5), 716–718 (1972).
24. Librescu, L., *Elastostatics and Kinetics of Anisotropic and Heterogeneous Shell-Type Structures*, Noordhoff, Leyden, The Netherlands (1975).
25. Reissner, E., "Note on the Effect of Transverse Shear Deformation in Laminated Anisotropic Plates," *Computer Methods in Applied Mechanics and Engineering*, **20**, 203–209 (1979).
26. Reddy, J. N., *Energy Principles and Variational Methods in Applied Mechanics*, Second Edition, John Wiley, New York (2002).
27. Librescu, L. and Reddy, J. N., "A Critical Review and Generalization of Transverse Shear Deformable Anisotropic Plate Theories," Euromech Colloquium 219, Kassel, Germany, Sept. 1986, *Refined Dynamical Theories of Beams, Plates and Shells and Their Applications*, I. Elishakoff and H. Irretier (Eds.), Springer-Verlag, Berlin, pp. 32–43 (1987).
28. Whitney, J. M., "Shear Correction Factors for Orthotropic Laminates Under Static Load," *Journal of Applied Mechanics*, **40**(1), 302–304 (1973).
29. Bert, C. W., "Simplified Analysis of Static Shear Correction Factors for Beams of Non-Homogeneous Cross Section," *Journal of Composite Materials*, **7**, 525–529 (1973).
30. Chow, T. S., "On the Propagation of Flexural Waves in an Orthotropic Laminated Plate and Its Response to an Impulsive Load," *Journal of Composite Materials*, **5**, 306–319 (1971).
31. Srinivas, S. R., Joga Rao, C. V., and Rao, A. K., "An Exact Analysis for Vibration of Simply-Supported Homogeneous and Laminated Thick Rectangular Plates," *Journal of Sound and Vibration*, **12**, 187–199 (1970).
32. Wittrick, W. H., "Analytical Three-Dimensional Elasticity Solutions to Some Plate Problems and Some Observations on Mindlin's Plate Theory," *International Journal of Solids and Structures*, **23**, 441–464 (1987).
33. Whitney, J. M. and Sun, C. T., "A Higher Order Theory for Extensional Motion of Laminated Composites," *Journal of Sound and Vibration*, **30**, 85–97 (1973).
34. Sun, C. T. and Whitney, J. M., "Theories for the Dynamic Response of Laminated Plates," *AIAA Journal*, **11**(2), 178–183 (1973).
35. Lo, K. H., Christensen, R. M., and Wu, E. M., "A Higher Order Theory of Plate Deformation, Part 2; Laminated Plates," *Journal of Applied Mechanics*, **44**, 669–676 (1977).
36. Krishna Murty, A. V., "Higher Order Theory for Vibration of Thick Plates," *AIAA Journal*, **15**(12), 1823–1824 (1977).
37. Murthy, M. V. V., "An Improved Transverse Shear Deformation Theory for Laminated Anisotropic Plates," NASA Technical Paper 1903, 1–37 (1981).
38. Reddy, J. N., "A Simple Higher-Order Theory for Laminated Composite Plates," *Journal of Applied Mechanics*, **51**, 745–752 (1984).
39. Reddy, J. N., "A General Non-Linear Third-Order Theory of Plates with Moderate Thickness," *International Journal of Non-Linear Mechanics*, **25**(6), 677–686 (1990).
40. Noor, A. K. and Burton, W. S., "Assessment of shear deformation theories for multilayered composite plates," *Applied Mechanics Reviews*, **42**(1), 1–13 (1989).
41. Carrera, E., "An Assessment of Mixed and Classical Theories on Global and Local Response of Multilayered Orthotropic Plates," *Composite Structures*, **50**, 183–198 (2000).

42. Carrera, E., "Developments, Ideas, and Evaluations Based upon Reissner's Mixed Variational Theorem in the Modeling of Multilayered Plates and Shells," *Applied Mechanics Reviews*, **54**(4), 301–329 (2001).
43. Carrera, E., "Theories and Finite Elements for Multilayered, Anisotropic, Composite Plates and Shells," *Archives of Computational Methods in Engineering*, **9**(2), 87–140 (2002).
44. Jones, R. M., *Mechanics of Composite Materials*, Second Edition, Taylor and Francis, Philadelphia, PA (1999).
45. Lekhnitskii, S. G., *Anisotropic Plates*, Translated from Russian by S. W. Tsai and T. Cheron, Gordon and Breach, Newark, NJ (1968).
46. Ashton, J. E. and Whitney, J. M., *Theory of Laminated Plates*, Technomic, Stamford, CT (1970).
47. Vinson, J. R. and Sierakowski, R. L., *The Behavior of Structures Composed of Composite Materials*, Kluwer, The Netherlands (1986).
48. Whitney, J. M., *Structural Analysis of Laminated Anisotropic Plates*, Technomic, Lancaster, PA (1987).
49. Vasiliev, V. V., *Mechanics of Composite Structures*, Translated from Russian by L. I. Man, Taylor and Francis, Washington, DC (1988).
50. Ochoa, O. O. and Reddy, J. N., *Finite Element Analysis of Composite Laminates*, Kluwer, The Netherlands (1992).
51. Reddy, J. N. (Ed.), *Mechanics of Composite Materials. Selected Works of Nicholas J. Pagano*, Kluwer, The Netherlands (1994).
52. Reddy, J. N. and Miravete, A., *Practical Analysis of Composite Laminates*, CRC Press, Boca Raton, FL (1995).

One-Dimensional Analysis of Laminated Composite Plates

4.1 Introduction

There are two cases of laminated plates that can be treated as one-dimensional problems; i.e., the displacements are functions of just one coordinate: (1) laminated beams, and (2) cylindrical bending of laminated plate strips. When the width b (length along the y -axis) of a laminated plate is very small compared to the length along the x -axis and the lamination scheme, and loading is such that the displacements are functions of x only, the laminate is treated as a beam (see Figure 4.1.1). In cylindrical bending, the laminated plate is assumed to be a plate strip that is very long along the y -axis and has a finite dimension a along the x -axis (see Figure 4.1.2). The transverse load q is assumed to be a function of x only. In such a case, the deflection w_0 and displacements (u_0, v_0) of the plate are functions of only x , and all derivatives with respect to y are zero. The cylindrical bending problem is a *plane strain* problem, whereas the beam problem is a *plane stress* problem.

In this chapter we develop exact analytical solutions for the two classes of problems. An *exact solution* of a problem is one that satisfies the governing equations at every point of the domain and the boundary and initial conditions of the problem. A numerical solution is one that is obtained by satisfying the governing equations and boundary conditions of the problem in an approximate sense. The solutions obtained with any of the variational methods (see Chapter 1) and numerical methods, such as the finite difference, finite element, and boundary element methods, are termed *numerical solutions*. An exact solution can be either

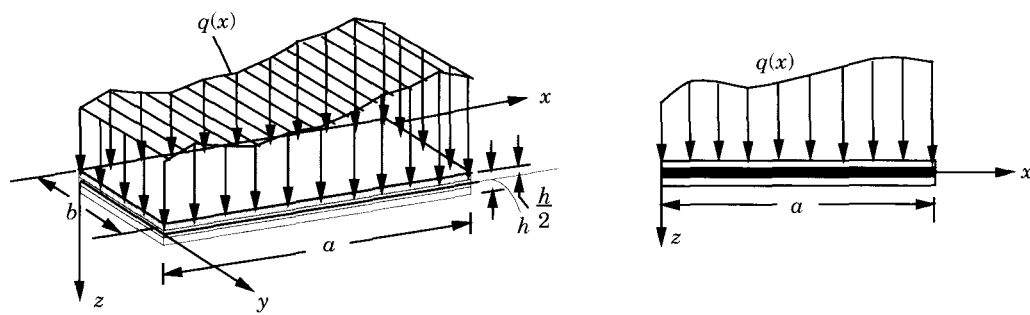


Figure 4.1.1: Geometry of a laminated beam.

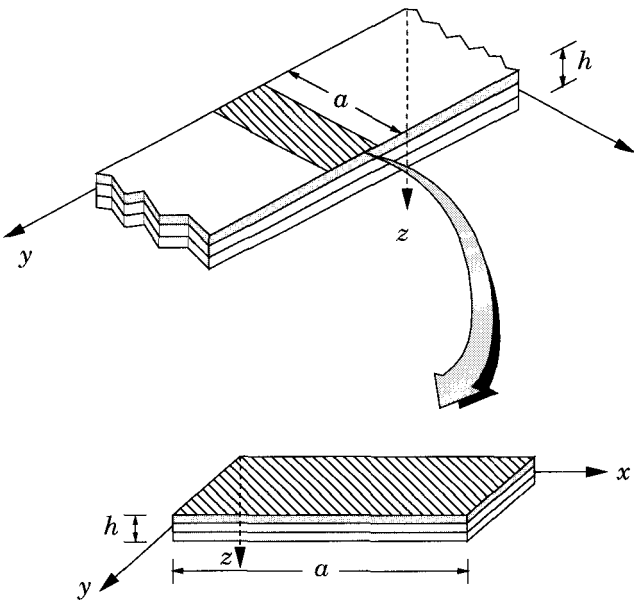


Figure 4.1.2: Geometry of a plate strip in cylindrical bending.

closed-form or an infinite series. *Closed-form solutions* are those that can be expressed in terms of a finite number of terms. For example, $u(x) = 2 - x + 3x^2 + 4 \sin n\pi x$ is a closed-form solution, whereas a solution in the form of a convergent series

$$u(x) = \sum_{n=1}^{\infty} a_n \sin n\pi x \quad (4.1.1)$$

where a_n are real numbers, is *not* a closed-form solution because the number of terms in the series is not finite. Since the series solution, in reality, is evaluated for a finite number of terms, it is, in a sense, approximate. The finite-sum series solution

$$u_N(x) = \sum_{n=1}^{N} a_n \sin n\pi x \quad (4.1.2)$$

will be termed an analytical solution, although it is approximate because not all terms of the series (4.1.1) are included in (4.1.2). For all practical purposes, it is “exact.”

Due to their one-dimensional nature, analytical – exact as well as numerical – solutions can be developed for a number of laminated beams and plate strips. The analytical solutions presented here for simple problems serve as a basis for understanding the response. In addition, the results can serve as a reference for verification of computational methods designed to analyze more complicated problems.

4.2 Analysis of Laminated Beams Using CLPT

4.2.1 Governing Equations

Here we consider the bending of symmetrically laminated beams according to CLPT. For symmetric laminates, the equations for bending deflection are uncoupled from those of the stretching displacements. If the in-plane forces are zero, the in-plane displacements (u_0, v_0) are zero, and the problem is reduced to one of solving for bending deflection and stresses.

In deriving the laminated beam theory we assume that

$$M_{yy} = M_{xy} = 0 \quad (4.2.1)$$

everywhere in the beam. The classical laminated plate theory constitutive equations for symmetric laminates, in the absence of in-plane forces, are given by [see Eqs. (3.3.44)]

$$\begin{Bmatrix} M_{xx} \\ M_{yy} \\ M_{xy} \end{Bmatrix} = - \begin{bmatrix} D_{11} & D_{12} & D_{16} \\ D_{12} & D_{22} & D_{26} \\ D_{16} & D_{26} & D_{66} \end{bmatrix} \begin{Bmatrix} \frac{\partial^2 w_0}{\partial x^2} \\ \frac{\partial^2 w_0}{\partial y^2} \\ 2 \frac{\partial^2 w_0}{\partial x \partial y} \end{Bmatrix} \quad (4.2.2a)$$

or, in inverse form, we have

$$\begin{Bmatrix} \frac{\partial^2 w_0}{\partial x^2} \\ \frac{\partial^2 w_0}{\partial y^2} \\ 2 \frac{\partial^2 w_0}{\partial x \partial y} \end{Bmatrix} = - \begin{bmatrix} D_{11}^* & D_{12}^* & D_{16}^* \\ D_{12}^* & D_{22}^* & D_{26}^* \\ D_{16}^* & D_{26}^* & D_{66}^* \end{bmatrix} \begin{Bmatrix} M_{xx} \\ M_{yy} \\ M_{xy} \end{Bmatrix} \quad (4.2.2b)$$

where D_{ij}^* denote the elements of the inverse matrix of D_{ij} . In view of the assumption (4.2.1), we have

$$\frac{\partial^2 w_0}{\partial x^2} = -D_{11}^* M_{xx}, \quad \frac{\partial^2 w_0}{\partial y^2} = -D_{12}^* M_{xx}, \quad 2 \frac{\partial^2 w_0}{\partial x \partial y} = -D_{16}^* M_{xx} \quad (4.2.3a)$$

where

$$\begin{aligned} D_{11}^* &= (D_{22} D_{66} - D_{26} D_{16}) / D^* \\ D_{12}^* &= (D_{16} D_{26} - D_{12} D_{66}) / D^* \\ D_{16}^* &= (D_{12} D_{26} - D_{22} D_{16}) / D^* \\ D^* &= D_{11} D_1 + D_{12} D_2 + D_{16} D_3, \quad D_1 = D_{22} D_{66} - D_{26} D_{16} \\ D_2 &= D_{16} D_{26} - D_{12} D_{66}, \quad D_3 = D_{12} D_{26} - D_{22} D_{16} \end{aligned} \quad (4.2.3b)$$

Equations (4.2.3a) indicate that the transverse deflection w_0 cannot be independent of the coordinate y due to the Poisson effect (D_{12}^*) and anisotropic shear coupling (D_{16}^*). These effects can be neglected only for long beams (i.e., when the length-to-width ratio is large). The length-to-width ratio for which the transverse deflection can be assumed to be independent of y is a function of the lamination scheme. For angle-ply laminates this ratio must be rather large to make the twisting curvature negligible.

In the following derivations we assume that the laminated beam under consideration is long enough to make the effects of the Poisson ratio and shear coupling on the deflection negligible. Then the transverse deflection can be treated only as a function of coordinate x (along the length of the beam) and time t :

$$w_0 = w_0(x, t) \quad (4.2.4)$$

Then we can write

$$\frac{\partial^2 w_0}{\partial x^2} = -D_{11}^* M_{xx} \quad (4.2.5)$$

In order to cast Eq. (4.2.5) in the familiar form used in the classical Euler–Bernoulli beam theory, we introduce the quantities

$$M = bM_{xx}, \quad Q = bQ_x, \quad E_{xx}^b = \frac{12}{h^3 D_{11}^*} = \frac{b}{I_{yy} D_{11}^*}, \quad I_{yy} = \frac{bh^3}{12} \quad (4.2.6)$$

and write Eq. (4.2.5) as

$$\frac{\partial^2 w_0}{\partial x^2} = -\frac{M}{E_{xx}^b I_{yy}} \quad \text{or} \quad M(x) = -E_{xx}^b I_{yy} \frac{\partial^2 w_0}{\partial x^2} \quad (4.2.7a)$$

and the shear force and bending moments are related by

$$Q_x = \frac{\partial M_{xx}}{\partial x} \quad \text{or} \quad Q = \frac{\partial M}{\partial x} \quad (4.2.7b)$$

where b is the width and h is the total thickness of the laminate.

The equation of motion of laminated beams can be obtained directly from Eq. (3.3.25) by setting all terms involving differentiation with respect to y to zero:

$$\frac{\partial^2 M_{xx}}{\partial x^2} + \hat{N}_{xx} \frac{\partial^2 w_0}{\partial x^2} + q = I_0 \frac{\partial^2 w_0}{\partial t^2} - I_2 \frac{\partial^4 w_0}{\partial x^2 \partial t^2} \quad (4.2.8a)$$

or, for symmetrically laminated long beams, we have

$$-\frac{\partial^2}{\partial x^2} \left(E_{xx}^b I_{yy} \frac{\partial^2 w_0}{\partial x^2} \right) + b\hat{N}_{xx} \frac{\partial^2 w_0}{\partial x^2} + \hat{q} = \hat{I}_0 \frac{\partial^2 w_0}{\partial t^2} - \hat{I}_2 \frac{\partial^4 w_0}{\partial x^2 \partial t^2} \quad (4.2.8b)$$

where \hat{N}_{xx} is the applied axial load, and

$$\hat{q} = bq, \quad \hat{I}_0 = bI_0, \quad \hat{I}_2 = bI_2, \quad I_i = b \int_{-\frac{h}{2}}^{\frac{h}{2}} \rho(z)^i dz \quad (i = 0, 1, 2) \quad (4.2.8c)$$

The boundary conditions are of the form

$$\text{Geometric :} \quad \text{specify} \quad w_0, \quad \frac{\partial w_0}{\partial x} \quad (4.2.9a)$$

$$\text{Force :} \quad \text{specify} \quad Q \equiv \frac{\partial M}{\partial x}, \quad M \quad (4.2.9b)$$

Equations (4.2.7)–(4.2.9) are identical, in form, to those of the Euler–Bernoulli beam theory of homogeneous, isotropic beams. Hence, the solutions available for deflections of isotropic beams under various boundary conditions can be readily used for laminated beams by replacing the modulus E with E_{xx}^b and multiplying loads and mass inertias with b . Note that the rotary (or rotatory) inertia I_2 is not neglected in Eqs. (4.2.8a-c).

4.2.2 Bending

For static bending without the axial force, $\hat{N}_{xx} = 0$, Eqs. (4.2.7a) and (4.2.8b) take the form [cf., Eqs. (1.4.47b) and (1.4.45b); see Figure 1.4.1 for the sign convention]

$$\frac{d^2w_0}{dx^2} = -\frac{M}{E_{xx}^b I_{yy}} , \quad E_{xx}^b I_{yy} \frac{d^4w_0}{dx^4} = \hat{q} \quad (4.2.10a, b)$$

where $\hat{q} = bq$. Equation (4.2.10a) is the most convenient when it is possible to express the bending moment M in terms of the applied loads. For indeterminate beams, use of Eq. (4.2.10b) is more convenient.

General Solutions

The general solutions of Eqs. (4.2.10a,b) are obtained by direct integration. We obtain from Eq. (4.2.10a)

$$E_{xx}^b I_{yy} w_0(x) = - \int_0^x \left[\int_0^\eta M(\xi) d\xi \right] d\eta + b_1 x + b_2 \quad (4.2.11a)$$

and from Eq. (4.2.10b)

$$\begin{aligned} E_{xx}^b I_{yy} w_0(x) &= \int_0^x \left\{ \int_0^\xi \left[\int_0^\eta \left(\int_0^\zeta \hat{q}(\mu) d\mu \right) d\zeta \right] d\eta \right\} d\xi \\ &\quad + c_1 \frac{x^3}{6} + c_2 \frac{x^2}{2} + c_3 x + c_4 \end{aligned} \quad (4.2.11b)$$

The constants of integration, b_1 , b_2 , and c_1 through c_4 , can be determined using the boundary conditions of the problem. The boundary conditions for various types of supports are defined below:

$$\begin{aligned} \text{Free : } \quad Q &\equiv \frac{dM}{dx} = 0 , \quad M = 0 \\ \text{Simply Supported : } \quad w_0 &= 0 , \quad M = 0 \\ \text{Clamped : } \quad w_0 &= 0 , \quad \frac{dw_0}{dx} = 0 \end{aligned} \quad (4.2.11c)$$

Calculation of Stresses

The in-plane stresses in the k th layer can be computed from the equations [see Eqs. (3.3.12a) and (4.2.2b)]

$$\begin{Bmatrix} \sigma_{xx} \\ \sigma_{yy} \\ \sigma_{xy} \end{Bmatrix}^{(k)} = z \begin{bmatrix} \bar{Q}_{11} & \bar{Q}_{12} & \bar{Q}_{16} \\ \bar{Q}_{12} & \bar{Q}_{22} & \bar{Q}_{26} \\ \bar{Q}_{16} & \bar{Q}_{26} & \bar{Q}_{66} \end{bmatrix}^{(k)} \begin{Bmatrix} -\frac{\partial^2 w_0}{\partial x^2} \\ -\frac{\partial^2 w_0}{\partial y^2} \\ -2 \frac{\partial^2 w_0}{\partial x \partial y} \end{Bmatrix}$$

$$= \frac{z}{b} \begin{bmatrix} \bar{Q}_{11} & \bar{Q}_{12} & \bar{Q}_{16} \\ \bar{Q}_{12} & \bar{Q}_{22} & \bar{Q}_{26} \\ Q_{16} & Q_{26} & Q_{66} \end{bmatrix}^{(k)} \begin{bmatrix} D_{11}^* & D_{12}^* & D_{16}^* \\ D_{12}^* & D_{22}^* & D_{26}^* \\ D_{16}^* & D_{26}^* & D_{66}^* \end{bmatrix} \begin{Bmatrix} M \\ 0 \\ 0 \end{Bmatrix} \quad (4.2.12a)$$

or

$$\begin{aligned} \sigma_{xx}^{(k)}(x, z) &= \frac{M(x)z}{b} \left(\bar{Q}_{11}^{(k)} D_{11}^* + \bar{Q}_{12}^{(k)} D_{12}^* + \bar{Q}_{16}^{(k)} D_{16}^* \right) \\ \sigma_{yy}^{(k)}(x, z) &= \frac{M(x)z}{b} \left(\bar{Q}_{12}^{(k)} D_{11}^* + \bar{Q}_{22}^{(k)} D_{12}^* + \bar{Q}_{26}^{(k)} D_{16}^* \right) \\ \sigma_{xy}^{(k)}(x, z) &= \frac{M(x)z}{b} \left(\bar{Q}_{16}^{(k)} D_{11}^* + \bar{Q}_{26}^{(k)} D_{12}^* + \bar{Q}_{66}^{(k)} D_{16}^* \right) \end{aligned} \quad (4.2.12b)$$

In general, the maximum stress does not occur at the top or bottom of a laminated beam. The maximum stress location through the beam thickness depends on the lamination scheme. As will be seen later in this section, the 0° layers take the most axial stress.

The stresses given by Eq. (4.2.12b) are approximate for the purpose of analyzing laminated beams. They are not valid especially in the free-edge zone, where the stress state is three dimensional. The width of the edge zone is about the order of the thickness of the beam.

In the classical beam theory, the interlaminar stresses (σ_{xz}, σ_{zz}) are identically zero when computed using the constitutive equations. However, these stresses do exist in reality, and they can be responsible for failures in composite laminates because of the relatively low shear and transverse normal strengths of materials used. Interlaminar stresses may be computed using the equilibrium equations of 3-D elasticity [see Eq. (1.3.27)]:

$$\begin{aligned} 0 &= \frac{\partial \sigma_{xx}}{\partial x} + \frac{\partial \sigma_{xy}}{\partial y} + \frac{\partial \sigma_{xz}}{\partial z} \\ 0 &= \frac{\partial \sigma_{xy}}{\partial x} + \frac{\partial \sigma_{yy}}{\partial y} + \frac{\partial \sigma_{yz}}{\partial z} \\ 0 &= \frac{\partial \sigma_{xz}}{\partial x} + \frac{\partial \sigma_{yz}}{\partial y} + \frac{\partial \sigma_{zz}}{\partial z} \end{aligned} \quad (4.2.13)$$

For each layer, these equations may be integrated with respect to z to obtain the interlaminar stresses within each layer ($z_k \leq z \leq z_{k+1}$):

$$\sigma_{xz}^{(k)} = - \int_{z_k}^z \left(\frac{\partial \sigma_{xx}^{(k)}}{\partial x} + \frac{\partial \sigma_{xy}^{(k)}}{\partial y} \right) dz + G^{(k)} \quad (4.2.14a)$$

$$\sigma_{yz}^{(k)} = - \int_{z_k}^z \left(\frac{\partial \sigma_{xy}^{(k)}}{\partial x} + \frac{\partial \sigma_{yy}^{(k)}}{\partial y} \right) dz + F^{(k)} \quad (4.2.14b)$$

$$\sigma_{zz}^{(k)} = - \int_{z_k}^z \left(\frac{\partial \sigma_{xz}^{(k)}}{\partial x} + \frac{\partial \sigma_{yz}^{(k)}}{\partial y} \right) dz + H^{(k)} \quad (4.2.14c)$$

where $(\sigma_{xx}^{(k)}, \sigma_{xy}^{(k)}, \sigma_{yy}^{(k)})$ are known from Eq. (4.2.12), and $G^{(k)}$, $F^{(k)}$, and $H^{(k)}$ are constants.

For beams, all variables are independent of y and $v = 0$. Hence, derivatives with respect to y are zero. For example, from Eqs. (4.2.14a,c) and (4.2.12b), we obtain

$$\sigma_{xz}^{(k)}(x, z) = -Q_x(x) \left(\bar{Q}_{11}^{(k)} D_{11}^* + \bar{Q}_{12}^{(k)} D_{12}^* + \bar{Q}_{16}^{(k)} D_{16}^* \right) \left(\frac{z^2 - z_k^2}{2} \right) + G^{(k)} \quad (4.2.15a)$$

$$\sigma_{zz}^{(k)}(x, z) = -\frac{dQ_x}{dx} \left(\bar{Q}_{11}^{(k)} D_{11}^* + \bar{Q}_{12}^{(k)} D_{12}^* + \bar{Q}_{16}^{(k)} D_{16}^* \right) \left(\frac{z^3 - z_k^3}{6} \right) + H^{(k)} \quad (4.2.15b)$$

where Eqs. (4.2.6) and (4.2.7b) are used to replace dM/dx with $Q = bQ_x$, and $G^{(k)}$ and $H^{(k)}$ are the integration constants, which are evaluated using the boundary and interface continuity conditions. For layer 1, the constants should be such that σ_{xz} and σ_{zz} equal the shear and normal stresses at the bottom face of the laminate. For example, if the laminate bottom is stress free, we have $G^{(1)} = 0$ and $H^{(1)} = 0$. The constants $G^{(k)}$ and $H^{(k)}$ for $k = 2, 3, \dots$ are determined by requiring that $\sigma_{xz}^{(k)}$ and $\sigma_{zz}^{(k)}$ be continuous at the layer interfaces (see Figure 4.2.1):

$$\sigma_{xz}^{(k)}(x, z_{k+1}) = \sigma_{xz}^{(k+1)}(x, z_{k+1}), \quad \sigma_{zz}^{(k)}(x, z_{k+1}) = \sigma_{zz}^{(k+1)}(x, z_{k+1})$$

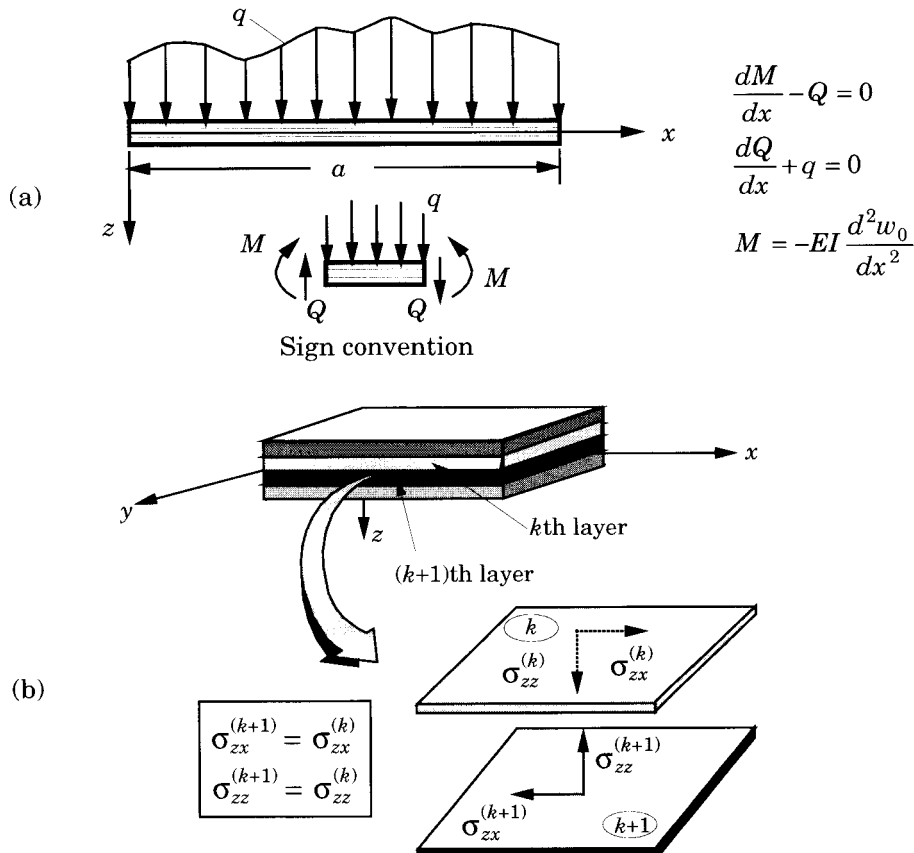


Figure 4.2.1: (a) Sign convention. (b) Equilibrium of interlaminar stresses in a laminated beam.

This gives, for $k = 1, 2, \dots$, the result

$$\begin{aligned} G^{(k+1)} &= -Q_x(x) \left(\bar{Q}_{11}^{(k)} D_{11}^* + \bar{Q}_{12}^{(k)} D_{12}^* + \bar{Q}_{16}^{(k)} D_{16}^* \right) \left(\frac{z_{k+1}^2 - z_k^2}{2} \right) + G^{(k)} \\ &= \sigma_{xz}^{(k)}(x, z_{k+1}) \end{aligned} \quad (4.2.16a)$$

$$\begin{aligned} H^{(k+1)} &= -\frac{dQ_x}{dx} \left(\bar{Q}_{11}^{(k)} D_{11}^* + \bar{Q}_{12}^{(k)} D_{12}^* + \bar{Q}_{16}^{(k)} D_{16}^* \right) \left(\frac{z_{k+1}^3 - z_k^3}{6} \right) + H^{(k)} \\ &= \sigma_{zz}^{(k)}(x, z_{k+1}) \end{aligned} \quad (4.2.16b)$$

Note from Eqs. (4.2.15a,b) that the transverse shear stress σ_{xz} is quadratic and normal stress σ_{zz} is cubic through the thickness of each lamina. The distributions are described by different functions in different layers but they are continuous across layers.

Example 4.2.1 (Simply supported beam):

Consider a simply supported beam with a center point load (see Figure 4.2.2). This case is known as the *three-point bending*. The deflection is symmetric about the point $x = a/2$. The expression for the bending moment is

$$M(x) = \frac{(F_0 b)x}{2}, \quad \text{for } 0 \leq x \leq \frac{a}{2} \quad (4.2.17)$$

Substituting this expression into Eq. (4.2.11a) and evaluating the integrals, we obtain

$$E_{xx}^b I_{yy} w_0(x) = -\frac{F_0 b x^3}{12} + c_1 x + c_2$$

The constants c_1 and c_2 are evaluated using the boundary conditions of the problem

$$w_0(0) = 0, \quad \frac{dw_0}{dx}(a/2) = 0$$

We obtain ($c_1 = F_0 b a^2 / 16$, $c_2 = 0$)

$$w_0(x) = \frac{F_0 b a^3}{48 E_{xx}^b I_{yy}} \left[3 \left(\frac{x}{a} \right) - 4 \left(\frac{x}{a} \right)^3 \right] \quad (4.2.18)$$

The deflection is the maximum at $x = a/2$, which is given by

$$w_{max} = \frac{F_0 b a^3}{48 E_{xx}^b I_{yy}} \equiv w_c \quad (4.2.19)$$

This expression can be used to determine the modulus of the material in terms of the measured center deflection w_c , applied load F_0 , and the geometric parameters of the laminated beam in a three-point bend test:

$$E_{xx}^b = \frac{F_0 b a^3}{4 b h^3 w_c} \quad (4.2.20)$$

The maximum in-plane stress σ_{xx} occurs at $x = a/2$ ($M(a/2) = F_0 b a / 4$)

$$\sigma_{xx}^{(k)}(a/2, z) = \frac{F_0 a z}{4} \left(\bar{Q}_{11}^{(k)} D_{11}^* + \bar{Q}_{12}^{(k)} D_{12}^* + \bar{Q}_{16}^{(k)} D_{16}^* \right) \quad (4.2.21)$$

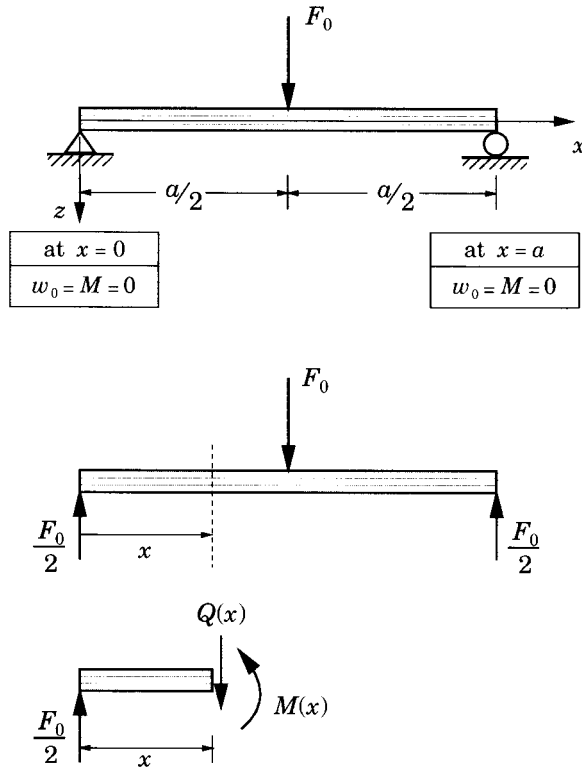


Figure 4.2.2: Three-point bending of a laminated beam (see Figure 4.2.1a for the sign convention).

Example 4.2.2 (Clamped beam):

Consider a laminated beam, clamped at both ends, and subjected to uniformly distributed load acting downward, \$q = q_0\$ (see Figure 4.2.3). The deflection is symmetric about the point \$x = a/2\$. We have from Eq. (4.2.11b) the result

$$E_{xx}^b I_{yy} w_0(x) = \frac{q_0 b x^4}{24} + c_1 \frac{x^3}{6} + c_2 \frac{x^2}{2} + c_3 x + c_4$$

The constants \$c_1\$ through \$c_4\$ are evaluated using the boundary conditions of the half (because of the symmetry) or full beam case. For the full beam case we have

$$w_0(0) = 0, \quad w_0(a) = 0, \quad \frac{dw_0}{dx}(0) = 0, \quad \frac{dw_0}{dx}(a) = 0$$

and for the half beam model we have

$$w_0(0) = 0, \quad \frac{dw_0}{dx}(0) = 0, \quad \frac{dw_0}{dx}\left(\frac{a}{2}\right) = 0, \quad Q\left(\frac{a}{2}\right) = \frac{dM}{dx} = -E_{xx}^b I_{yy} \frac{d^3 w_0}{dx^3}\left(\frac{a}{2}\right) = 0$$

Either set of boundary conditions will yield the same solution. We obtain (\$c_1 = -q_0 ba/2\$, \$c_2 = q_0 ba^2/12\$, \$c_3 = c_4 = 0\$)

$$w_0(x) = \frac{q_0 b a^4}{24 E_{xx}^b I_{yy}} \left[\left(\frac{x}{a}\right)^2 - \left(\frac{x}{a}\right) \right]^2 \quad (4.2.22)$$

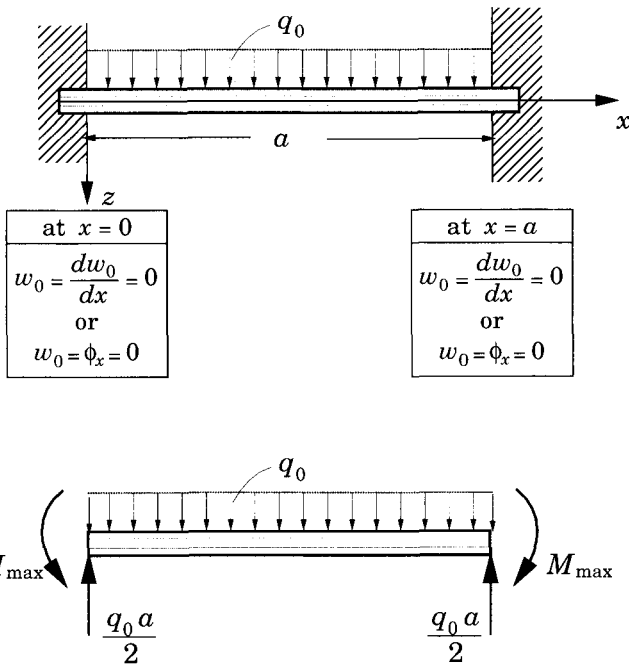


Figure 4.2.3: Clamped beam under uniformly distributed load.

The deflection is the maximum at $x = a/2$, which is given by

$$w_{max} = \frac{q_0 ba^4}{384 E_{xx}^b I_{yy}} \quad (4.2.23)$$

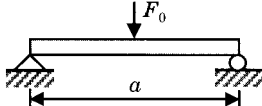
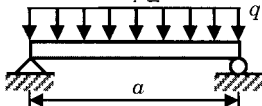
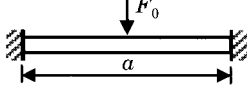
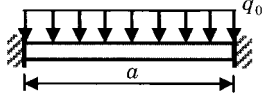
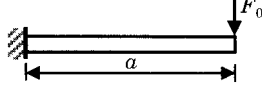
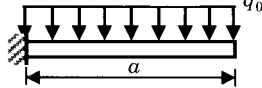
The maximum bending moment, and hence the maximum in-plane stress σ_{xx} , occurs at $x = 0, a$:

$$M(x) = -\frac{q_0 ba^2}{12} \left[1 - 6 \left(\frac{x}{a} \right) + 6 \left(\frac{x}{a} \right)^2 \right], \quad M_{max} = -\frac{q_0 ba^2}{12}$$

$$\sigma_{xx}^{(k)}(0, z) = -\frac{q_0 a^2 z}{12} \left(Q_{11}^{(k)} D_{11}^* + Q_{12}^{(k)} D_{12}^* + Q_{16}^{(k)} D_{16}^* \right) \quad (4.2.24)$$

Expressions for the transverse deflection of laminated beams with simple supports, clamped edges, and clamped-free (cantilever) supports and subjected to a transverse point load or uniformly distributed load are presented in Table 4.2.1. The maximum deflections and bending moments are also listed (note that the loads are assumed to be applied in the downward direction). Recall that $w_0(x)$ is taken positive upward and $M(x)$ is positive clockwise on the right end. When both point load and uniformly distributed load are applied simultaneously, the solution can be obtained by superposing (i.e., adding) the expressions corresponding to each load. Expressions for other boundary conditions can be found in textbooks on a first course in deformable solids. The effects of material properties and stacking sequence are accounted for through the bending stiffness $E_{xx}^b I_{yy} = b/D_{11}^*$, as can be seen from Eqs. (4.2.6) and (4.2.3b).

Table 4.2.1: Transverse deflections of laminated composite beams with various boundary conditions and subjected to point load or uniformly distributed load (acting downward) according to the classical beam theory.

Laminated Beam	Deflection, $w_0(x)$	w_{max} and M_{max}
• Hinged-Hinged		
Central point load	$\frac{c_1}{48} \left[3\left(\frac{x}{a}\right) - 4\left(\frac{x}{a}\right)^3 \right]$	$w_{max}^c = \frac{1}{48}c_1$ $M_{max}^c = -\frac{1}{4}c_3$
		
Uniform load	$\frac{c_2}{24} \left[\left(\frac{x}{a}\right) - 2\left(\frac{x}{a}\right)^3 + \left(\frac{x}{a}\right)^4 \right]$	$w_{max}^c = \frac{5}{384}c_2$ $M_{max}^c = -\frac{1}{8}c_4$
		
• Fixed-Fixed		
Central point load	$\frac{c_1}{48} \left[3\left(\frac{x}{a}\right)^2 - 4\left(\frac{x}{a}\right)^3 \right]$	$w_{max}^c = \frac{1}{192}c_1$ $M_{max}^0 = \frac{1}{8}c_3$
		
Uniform load	$\frac{c_2}{24} \left[\left(\frac{x}{a}\right)^2 - \left(\frac{x}{a}\right)^3 \right]^2$	$w_{max}^c = \frac{1}{384}c_2$ $M_{max}^0 = \frac{1}{12}c_4$
		
• Fixed-Free		
Point load at free end	$\frac{c_1}{6} \left[3\left(\frac{x}{a}\right)^2 - \left(\frac{x}{a}\right)^3 \right]$	$w_{max}^a = \frac{1}{3}c_1$ $M_{max}^0 = c_3$
		
Uniform load	$\frac{c_2}{24} \left[6\left(\frac{x}{a}\right)^2 - 4\left(\frac{x}{a}\right)^3 + \left(\frac{x}{a}\right)^4 \right]$	$w_{max}^a = \frac{1}{8}c_2$ $M_{max}^0 = \frac{1}{2}c_4$
		

Superscript “c” refers to the center (at $x = a/2$), “a” to the end $x = a$, and “0” refers to $x = 0$. The constants in the expressions for the deflection are defined as

$$c_1 = \frac{F_0 ba^3}{E_{xx}^b I_{yy}} , \quad c_2 = \frac{q_0 ba^4}{E_{xx}^b I_{yy}} , \quad c_3 = -F_0 ba , \quad c_4 = -q_0 ba^2$$

Figures 4.2.4 and 4.2.5 show the maximum normal stress distribution, as predicted by Eq. (4.2.12b), through the thickness of $(0/45/-45/90)_s$ (0° corresponds to outer layers) and $(90/45/-45/0)_s$ (90° corresponds to outer layers) laminated beams, respectively, subjected to three-point bending ($F_0 = 1.0, b = 0.2, a = 1.0, h = 0.1$). The following layer material properties are used ($E_2 = 1 \text{ msi}$):

$$\frac{E_1}{E_2} = 25, \quad G_{12} = G_{13} = 0.5E_2, \quad G_{23} = 0.2E_2, \quad \nu = 0.25 \quad (4.2.25)$$

The maximum normal stress distribution in an orthotropic beam (with eight 0° layers) is shown in the figures by dashed lines. It is clear the 0° layer carries the most axial stress while the 90° layer carries the least axial stress, in proportion to their axial stiffness.

Figures 4.2.6 and 4.2.7 show the effect of stacking sequence on maximum transverse shear stress, as predicted by Eq. (4.2.15a), for laminates $(0/45/-45/90)_s$ and $(90/45/-45/0)_s$, respectively ($F_0 = 1.0, b = 0.2, a = 1.0, h = 0.1$). The parabolic distribution of transverse shear stress through an orthotropic beam is shown in dashed lines for comparison. The maximum stress value is dependent on the stacking sequence and considerably different from that in a homogeneous beam.

4.2.3 Buckling

A beam subjected to axial compressive load $\hat{N}_{xx} = -N_{xx}^0$ remains straight but shortens as the load increases from zero to a certain magnitude. If a small additional axial or lateral disturbance applied to the beam keeps it in equilibrium, then the beam is said to be *stable*. If the small additional disturbance results in a large response and the beam does not return to its original equilibrium configuration, the beam is said to be *unstable*. The onset of instability is called *buckling* (see Figure 4.2.8). The magnitude of the compressive axial load at which the beam becomes unstable is termed the *critical buckling load*. If the load is increased beyond this critical buckling load, it results in a large deflection and the beam seeks another equilibrium configuration. Thus, the load at which a beam becomes unstable is of practical importance in the design of structural elements. Here we determine critical buckling loads for laminated straight beams. The equation governing buckling of laminated beams is also given by Eq. (4.2.8b), wherein the applied transverse load and inertia terms are set to zero, and axial force is assumed to be unknown. In addition, the deflection is measured from onset of buckling, and it is termed *buckling deflection*.

Setting $\hat{N}_{xx} = -N_{xx}^0$, $\hat{q} = 0$, and all inertia terms to zero in Eqs. (4.2.8b), we obtain the equation

$$\frac{d^4 W}{dx^4} + \frac{bN_{xx}^0}{E_{xx}^b I_{yy}} \frac{d^2 W}{dx^2} = 0 \quad (4.2.26)$$

where W denotes the buckling deflection. Equation (4.2.26) is obtained from the nonlinear equilibrium equation

$$E_{xx}^b I_{yy} \frac{d^4 w_0}{dx^4} + bN_{xx}(w_0) \frac{d^2 w_0}{dx^2} = 0$$

by substituting $w_0 = w_0^e + W$, where w_0^e is the original equilibrium (prebuckling) deflection and W is the buckling deflection. Note that w_0^e satisfies the equation

$$E_{xx}^b I_{yy} \frac{d^4 w_0^e}{dx^4} + bN_{xx}(w_0^e) \frac{d^2 w_0^e}{dx^2} = 0$$

[The reader is asked to verify the result in Eq. (4.2.26).]

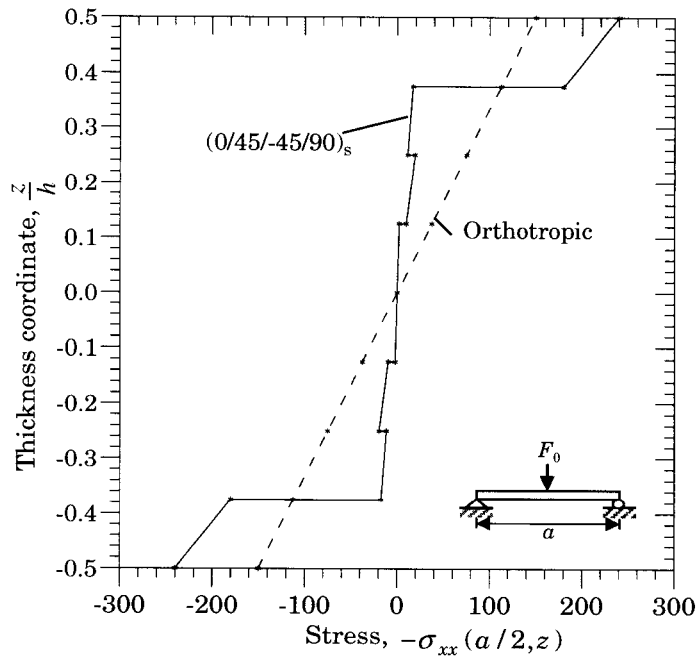


Figure 4.2.4: Maximum normal stress, $-\sigma_{xx}(a/2, z)$, distribution through the thickness of a symmetrically laminated $(0/\pm 45/90)_s$ beam.

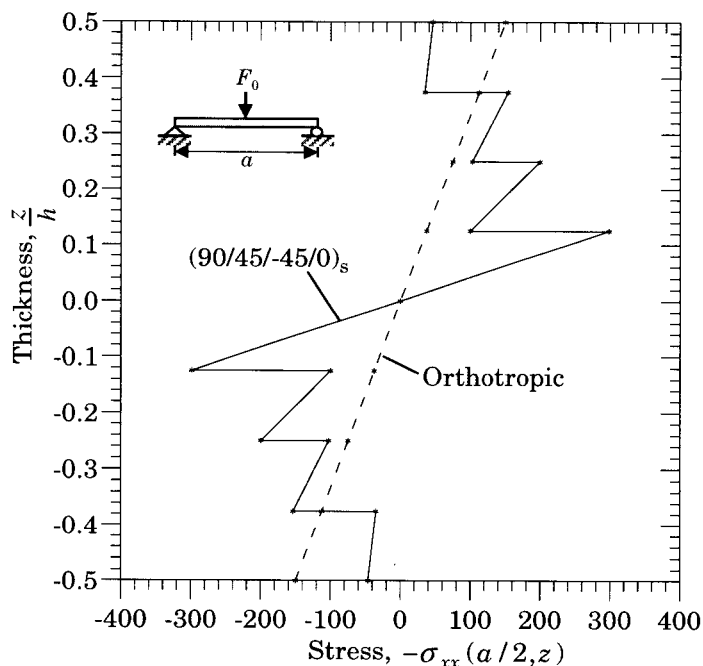


Figure 4.2.5: Maximum normal stress, $-\sigma_{xx}(a/2, z)$, distribution through the thickness of a symmetrically laminated $(90/\pm 45/0)_s$ beam.

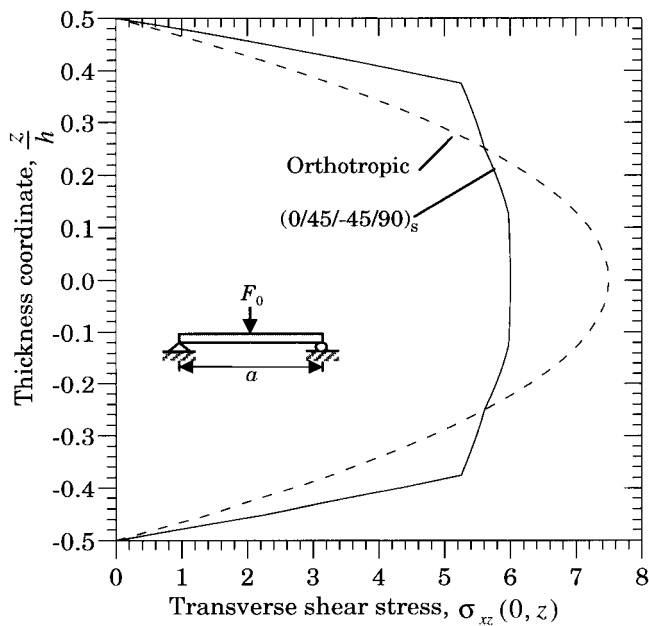


Figure 4.2.6: Variation of transverse shear stress ($-\sigma_{xz}$) through the thickness of a symmetrically laminated $(0/\pm 45/90)_s$ beam subjected to three-point bending ($F_0 = 1.0$, $b = 0.2$, $a = 1.0$, $h = 0.1$).

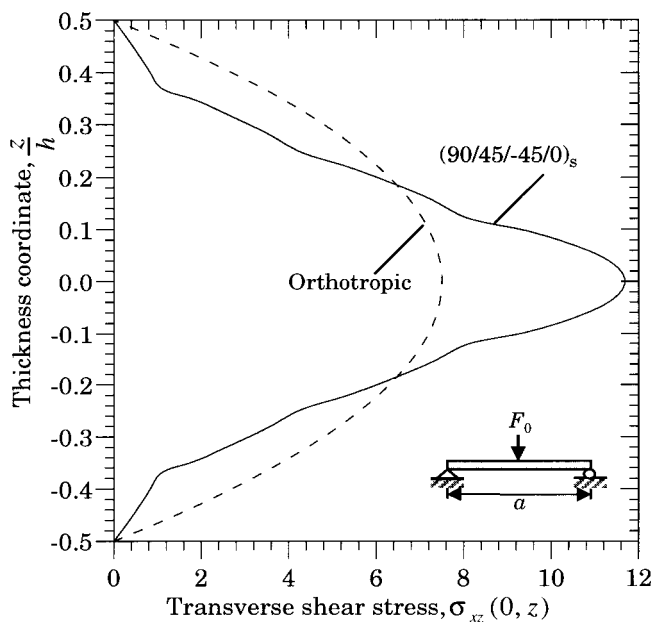


Figure 4.2.7: Variation of transverse shear stress ($-\sigma_{xz}$) through the thickness of a symmetrically laminated $90/\pm 45/0)_s$ beam subjected to three-point bending (see Figure 4.2.6 for data).

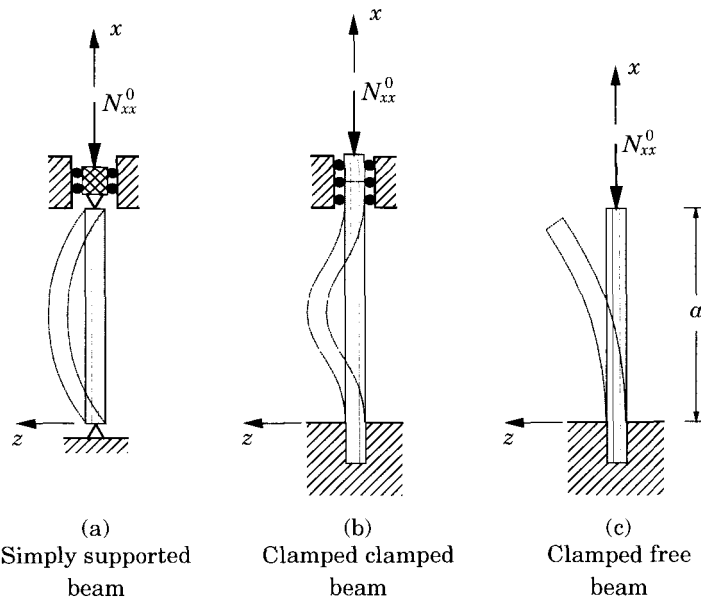


Figure 4.2.8: Buckling of laminated beams under various edge conditions.

Integrating Eq. (4.2.26) twice with respect to x , we obtain

$$\frac{d^2W}{dx^2} + \frac{bN_{xx}^0}{E_{xx}^b I_{yy}} W = K_1 x + K_2 \quad (4.2.27)$$

The general solution of Eq. (4.2.27) is

$$W(x) = c_1 \sin \lambda_b x + c_2 \cos \lambda_b x + c_3 x + c_4 \quad (4.2.28)$$

where

$$\lambda_b^2 = \frac{bN_{xx}^0}{E_{xx}^b I_{yy}}, \quad c_3 = \frac{K_1}{\lambda_b^2}, \quad c_4 = \frac{K_2}{\lambda_b^2} \quad (4.2.29)$$

and the constants c_1, c_2, c_3 , and c_4 can be determined using the boundary conditions of the beam.

We are interested in determining the values of λ_b for which there exists a nonzero solution $W(x)$, i.e., when beam experiences deflection. Once such a λ_b is known (often there will be many), the buckling load is determined from Eq. (4.2.29):

$$N_{xx}^0 = \left(\frac{E_{xx}^b I_{yy}}{b} \right) \lambda_b^2 \quad (4.2.30)$$

The smallest value of N_{xx}^0 , which is given by the smallest value of λ_b , is the critical buckling load. The buckling shape (or mode) is given by $W(x)$. In the following, we consider beams with different boundary conditions to determine λ_b and then the critical buckling load for each beam.

Example 4.2.3 (Simply supported beam): _____

For a simply supported beam, the boundary conditions are

$$w_0(0) = 0, \quad w_0(a) = 0, \quad M_{xx}(0) = 0, \quad M_{xx}(a) = 0 \quad (4.2.31a)$$

These boundary conditions imply

$$W(0) = 0, \quad W(a) = 0, \quad \frac{d^2W}{dx^2}(0) = 0, \quad \frac{d^2W}{dx^2}(a) = 0 \quad (4.2.31b)$$

We have

$$\begin{aligned} W(0) = 0 &: c_2 + c_4 = 0 \\ W''(0) = 0 &: -c_2\lambda_b^2 = 0 \text{ which implies } c_2 = 0, c_4 = 0 \\ W(a) = 0 &: c_1 \sin \lambda_b a + c_3 a = 0 \\ W''(a) = 0 &: c_1 \sin \lambda_b a = 0 \text{ which implies } c_3 = 0 \end{aligned} \quad (4.2.32)$$

For a nontrivial solution, the condition

$$c_1 \sin \lambda_b a = 0 \text{ implies that } \lambda_b a = n\pi, \quad n = 1, 2, \dots \quad (4.2.33)$$

and the buckling load is given by

$$bN_{xx}^0 = E_{xx}^b I_{yy} \left(\frac{n\pi}{a} \right)^2 \quad (4.2.34a)$$

The buckling mode is

$$W(x) = c_1 \sin \frac{n\pi x}{a}, \quad c_1 \neq 0 \quad (4.2.34b)$$

The critical buckling load becomes ($n = 1$)

$$N_{cr} = \left(\frac{\pi}{a} \right)^2 \frac{E_{xx}^b I_{yy}}{b} = \left(\frac{\pi^2}{12} \right) \frac{E_{xx}^b h^3}{a^2} \quad (4.2.35)$$

and the buckling mode (eigenfunction) associated with it is

$$W(x) = c_1 \sin \frac{\pi x}{a}$$

Example 4.2.4 (Clamped beam): _____

When the beam is fixed at both ends, the boundary conditions are

$$w_0(0) = 0, \quad \frac{dw_0}{dx}(0) = 0, \quad w_0(a) = 0, \quad \frac{dw_0}{dx}(a) = 0 \quad (4.2.36a)$$

which can be expressed as

$$W(0) = 0, \quad \frac{dW}{dx}(0) = 0, \quad W(a) = 0, \quad \frac{dW}{dx}(a) = 0 \quad (4.2.36b)$$

We have

$$\begin{aligned} W(0) = 0 &: c_2 + c_4 = 0 \\ W'(0) = 0 &: c_1 \lambda_b + c_3 = 0 \\ W(a) = 0 &: c_1 \sin \lambda_b a + c_2 \cos \lambda_b a + c_3 a + c_4 = 0 \\ W'(a) = 0 &: c_1 \lambda_b \cos \lambda_b a - c_2 \lambda_b \sin \lambda_b a + c_3 = 0 \end{aligned} \quad (4.2.37)$$

Expressing these equations in terms of constants c_1 and c_2 , we obtain

$$\begin{aligned} c_1 (\sin \lambda_b a - \lambda_b a) + c_2 (\cos \lambda_b a - 1) &= 0 \\ c_1 (\cos \lambda_b a - 1) - c_2 \sin \lambda_b a &= 0 \end{aligned} \quad (4.2.38a)$$

For a nontrivial solution, the determinant of the coefficient matrix of the above two equations must be zero (eigenvalue problem):

$$\begin{aligned} 0 &= \begin{vmatrix} \sin \lambda_b a - \lambda_b a & \cos \lambda_b a - 1 \\ \cos \lambda_b a - 1 & -\sin \lambda_b a \end{vmatrix} \\ &= \lambda_b a \sin \lambda_b a + 2 \cos \lambda_b a - 2 \end{aligned} \quad (4.2.38b)$$

The solution of equation (4.2.38b), known as the *characteristic equation*, gives the eigenvalues $e_n \equiv \lambda_b a$, and the buckling load is calculated from Eq. (4.2.30). Equations (4.2.38b) is a transcendental equation, i.e., nonlinear equation involving trigonometric functions. A plot of the function $f(e_n) = e_n \sin e_n + 2 \cos e_n - 2$ against e_n shows that $f(e_n)$ is zero at $e_n = 0, 6.2832 (= 2\pi), 8.9868, 12.5664 (= 4\pi), 15.4505, 6\pi, \dots (\lambda_{2n-1}a = 2n\pi)$. Hence, the critical (i.e., smallest) buckling load is [see Eq. (4.2.30)]

$$\begin{aligned} N_{cr} &= \left(\frac{e_n}{a} \right)^2 \left(\frac{E_{xx}^b I_{yy}}{b} \right) = \left(\frac{2\pi}{a} \right)^2 \left(\frac{E_{xx}^b I_{yy}}{b} \right) \\ &= \left(\frac{\pi^2}{3} \right) \left(\frac{E_{xx}^b h^3}{a^2} \right) \end{aligned} \quad (4.2.39)$$

Table 4.2.2 contains governing equations for λ_b , with some typical values, and values of the constants c_1, c_2, c_3 , and c_4 for several combinations of simply supported (hinged), clamped (fixed), and free-edge conditions. For example, for the critical buckling load of a cantilever beam (i.e., fixed at one end and free at the other end), the boundary conditions are

$$w_0(0) = 0, \quad \frac{dw_0}{dx}(0) = 0, \quad Q_x(a) = 0, \quad M_{xx}(a) = 0 \quad (4.2.40a)$$

which are equivalent to

$$\begin{aligned} W &= 0, \quad \frac{dW}{dx} = 0 \quad \text{at } x = 0 \\ \left(\frac{d^3W}{dx^3} + \lambda_b^2 \frac{dW}{dx} \right) &= 0, \quad \frac{d^2W}{dx^2} = 0 \quad \text{at } x = a \end{aligned} \quad (4.2.40b)$$

The critical buckling load is given by

$$N_{cr} = \left(\frac{\pi}{2a} \right)^2 \frac{E_{xx}^b I_{yy}}{b} = \frac{\pi^2 h^3 E_{xx}^b}{48a^2} \quad (4.2.41)$$

Table 4.2.2: Values of the constants and eigenvalues for buckling of laminated composite beams with various boundary conditions ($\lambda^2 \equiv bN_{xx}^0/E_{xx}^b I_{yy} = (e_n/a)^2$). The classical laminate theory is used.

End conditions at $x = 0$ and $x = a$	Constants†	Characteristic equation and values* of $e_n \equiv \lambda_n a$
• Hinged-Hinged	$c_1 \neq 0, c_2 = c_3 = c_4 = 0$	$\sin e_n = 0$ $e_n = n\pi$
• Fixed-Fixed	$c_1 = 1/(\sin e_n - e_n)$ $c_3 = -1/\lambda_n$ $c_2 = -c_4 = 1/(\cos e_n - 1)$	$e_n \sin e_n = 2(1 - \cos e_n)$ $e_n = 2\pi, 8.987, 4\pi, \dots$
• Fixed-Free	$c_1 = c_3 = 0$ $c_2 = -c_4 \neq 0$	$\cos e_n = 0$ $e_n = (2n - 1)\pi/2$
• Free-Free	$c_1 = c_3 = 0$ $c_2 \neq 0, c_4 \neq 0$	$\sin e_n = 0$ $e_n = n\pi$
• Hinged-Fixed	$c_1 = 1/e_n \cos e_n, c_3 = -1$ $c_2 = c_4 = 0$	$\tan e_n = e_n$ $e_n = 4.493, 7.725, \dots$

† See Eq. (4.2.28): $W(x) = c_1 \sin \lambda_b x + c_2 \cos \lambda_b x + c_3 x + c_4$.

*For critical buckling load, only the first (minimum) value of $e = \lambda a$ is needed.

4.2.4 Vibration

For natural vibration, the solution is assumed to be periodic

$$w_0(x, t) = W(x)e^{i\omega t}, \quad i = \sqrt{-1} \quad (4.2.42)$$

In the absence of applied transverse load q , the governing equation (4.2.8b) reduces to

$$E_{xx}^b I_{yy} \frac{d^4 W}{dx^4} - b\hat{N}_{xx} \frac{d^2 W}{dx^2} = \omega^2 \hat{I}_0 W - \omega^2 \hat{I}_2 \frac{d^2 W}{dx^2} \quad (4.2.43)$$

Equation (4.2.43) has the general form

$$p \frac{d^4 W}{dx^4} + q \frac{d^2 W}{dx^2} - r W = 0 \quad (4.2.44)$$

where

$$p = E_{xx}^b I_{yy}, \quad q = \omega^2 \hat{I}_2 - b\hat{N}_{xx}, \quad r = \omega^2 \hat{I}_0 \quad (4.2.45)$$

The general solution of Eq. (4.2.44) is

$$W(x) = c_1 \sin \lambda x + c_2 \cos \lambda x + c_3 \sinh \mu x + c_4 \cosh \mu x \quad (4.2.46a)$$

$$\lambda = \sqrt{\frac{1}{2p} \left(q + \sqrt{q^2 + 4pr} \right)}, \quad \mu = \sqrt{\frac{1}{2p} \left(-q + \sqrt{q^2 + 4pr} \right)} \quad (4.2.46b)$$

and c_1, c_2, c_3 , and c_4 are constants, which are to be determined using the boundary conditions.

From Eqs. (4.2.46b), we have

$$(2p\lambda^2 - q)^2 = q^2 + 4pr \quad \text{or} \quad p\lambda^4 - q\lambda^2 - r = 0 \quad (4.2.47a)$$

$$(2p\mu^2 + q)^2 = q^2 + 4pr \quad \text{or} \quad p\mu^4 + q\mu^2 - r = 0 \quad (4.2.47b)$$

Substituting for p , q , and r from Eq. (4.2.45) into Eq. (4.2.47a,b) and solving for ω^2 , we obtain

$$\omega^2 = \lambda^4 \left(\frac{E_{xx}^b I_{yy}}{\hat{I}_0} \right) \left(\frac{1 + P_1}{1 + R_1} \right), \quad P_1 = \frac{b\hat{N}_{xx}}{E_{xx}^b I_{yy} \lambda^2}, \quad R_1 = \frac{\hat{I}_2}{\hat{I}_0} \lambda^2 \quad (4.2.48a)$$

$$\omega^2 = \mu^4 \left(\frac{E_{xx}^b I_{yy}}{\hat{I}_0} \right) \left(\frac{1 - P_2}{1 - R_2} \right), \quad P_2 = \frac{b\hat{N}_{xx}}{E_{xx}^b I_{yy} \mu^2}, \quad R_2 = \frac{\hat{I}_2}{\hat{I}_0} \mu^2 \quad (4.2.48b)$$

The two expressions for ω in Eqs. (4.2.48a,b) are the same and hence either one can be used to calculate the frequency once λ is known.

When the applied axial load is zero, the frequency of vibration can be calculated from

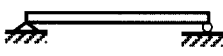
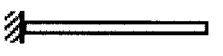
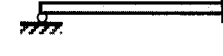
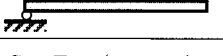
$$\omega^2 = \lambda^4 \frac{E_{xx}^b I_{yy}}{\hat{I}_0} \left(1 - \frac{\hat{I}_2 \lambda^2}{\hat{I}_0 + \hat{I}_2 \lambda^2} \right) = \mu^4 \frac{E_{xx}^b I_{yy}}{\hat{I}_0} \left(1 + \frac{\hat{I}_2 \mu^2}{\hat{I}_0 - \hat{I}_2 \mu^2} \right) \quad (4.2.49)$$

It is clear from the first expression that rotary inertia decreases the frequency of natural vibration. If the rotary inertia is neglected, we have $\lambda = \mu$ and

$$\omega = \lambda^2 a_0, \quad a_0 = \sqrt{\frac{E_{xx}^b I_{yy}}{\hat{I}_0}} \quad (4.2.50)$$

In the following discussion beams with both ends simply supported or clamped are considered to illustrate the procedure to evaluate the constants c_1 through c_4 , and more importantly, to determine λ so that Eqs. (4.2.46)–(4.2.48) can be used to find ω . The smallest frequency ω is known as the *fundamental frequency*. For other boundary conditions, the reader is referred to Table 4.2.3. For boundary conditions other than simply supported, one must solve a transcendental equation for $e_n \equiv \lambda_n a$.

Table 4.2.3: Values of the constants and eigenvalues for natural vibration of laminated composite beams with various boundary conditions ($\lambda_n^4 \equiv \omega_n^2 I_0 / E_{xx}^b I_{yy} = (e_n/a)^4$). The classical laminate theory *without* rotary inertia is used.

End conditions at $x = 0$ and $x = a$	Constants [†]	Characteristic equation and values of $e_n \equiv \lambda_n a$
• Hinged-Hinged	$c_1 \neq 0, c_2 = c_3 = c_4 = 0$ 	$\sin e_n = 0$ $e_n = n\pi$
• Fixed-Fixed	$c_1 = -c_3 = 1/(\sin e_n - \sinh e_n)$ $-c_2 = c_4 = 1/(\cos e_n - \cosh e_n)$ 	$\cos e_n \cosh e_n - 1 = 0$ $e_n = 4.730, 7.853, \dots$
• Fixed-Free	$c_1 = -c_3 = 1/(\sin e_n + \sinh e_n)$ $-c_2 = c_4 = 1/(\cos e_n + \cosh e_n)$ 	$\cos e_n \cosh e_n + 1 = 0$ $e_n = 1.875, 4.694, \dots$
• Free-Free	$c_1 = c_3 = 1/(\sin e_n - \sinh e_n)$ $c_2 = c_4 = -1/(\cos e_n - \cosh e_n)$ 	$\cos e_n \cosh e_n - 1 = 0$ $e_n = 4.730, 7.853, \dots$
• Hinged-Fixed	$c_1 = 1/\sin e_n, c_3 = 1/\sinh e_n$ $c_2 = c_4 = 0$ 	$\tan e_n = \tanh e_n$ $e_n = 3.927, 7.069, \dots$
• Hinged-Free	$c_1 = 1/\sin e_n, c_3 = -1/\sinh e_n$ $c_2 = c_4 = 0$ 	$\tan e_n = \tanh e_n$ $e_n = 3.927, 7.069, \dots$

[†] See Eq. (4.2.46a): $W(x) = c_1 \sin \lambda x + c_2 \cos \lambda x + c_3 \sinh \mu x + c_4 \cosh \mu x$.

Example 4.2.5 (Simply supported beam):

For a simply supported beam, the boundary conditions in Eq. (4.2.31b) give

$$c_2 = c_3 = c_4 = 0 \quad (4.2.51)$$

$$c_1 \sin \lambda a = 0, \text{ which implies } \lambda = \frac{n\pi}{a} \quad (4.2.52)$$

Substituting for λ from Eqs. (4.2.45) and (4.2.46a) into Eq. (4.2.48a), we obtain

$$\omega_n = \left(\frac{n\pi}{a} \right)^2 a_0 \sqrt{1 + \frac{b \hat{N}_{xx}}{\left(\frac{n\pi}{a} \right)^2 E_{xx}^b I_{yy}}} \sqrt{\frac{1}{1 + \left(\frac{n\pi}{a} \right)^2 \frac{I_2}{I_0}}} \quad (4.2.53a)$$

If the rotary inertia is neglected, we obtain

$$\omega_n = \left(\frac{n\pi}{a} \right)^2 a_0 \sqrt{1 + \frac{b \hat{N}_{xx}}{\left(\frac{n\pi}{a} \right)^2 E_{xx}^b I_{yy}}} \quad (4.2.53b)$$

Thus the effect of the axial tensile force \hat{N}_{xx} is to increase the natural frequencies. If we have a very flexible beam, say a cable under large tension, the second term under the radical in Eq. (4.2.53b) becomes very large in comparison with unity; if n is not large, we have

$$\omega_n \approx \frac{n\pi}{a} \sqrt{\frac{\hat{N}_{xx}}{\hat{I}_0}} \quad (4.2.53c)$$

which are natural frequencies of a stretched laminated cable. We also note from Eq. (4.2.53b) that frequencies of natural vibration decrease when a compressive force instead of a tensile force is acting on the beam.

When $\hat{N}_{xx} = 0$, we obtain from Eq. (4.2.53a)

$$\begin{aligned}\omega_n &= \left(\frac{n\pi}{a}\right)^2 a_0 \sqrt{\frac{1}{1 + \left(\frac{n\pi}{a}\right)^2 \frac{\hat{I}_2}{\hat{I}_0}}} \\ &= \left(\frac{n\pi}{a}\right)^2 \sqrt{\frac{E_{xx}^b I_{yy}}{\hat{I}_0}} \sqrt{1 - \frac{\hat{I}_2 \left(\frac{n\pi}{a}\right)^2}{\left(\frac{n\pi}{a}\right)^2 \hat{I}_2 + \hat{I}_0}}\end{aligned}\quad (4.2.54)$$

Thus, rotatory inertia decreases frequencies of natural vibration. If the rotatory inertia is neglected, we obtain

$$\omega_n = \left(\frac{n\pi}{a}\right)^2 \sqrt{\frac{E_{xx}^b I_{yy}}{\hat{I}_0}} \quad (4.2.55)$$

Example 4.2.6 (Clamped beam):

For a beam clamped at both ends, the boundary conditions in Eq. (4.2.36) lead to

$$c_2 + c_4 = 0, \quad \lambda c_1 + \mu c_3 = 0 \quad (4.2.56)$$

and the eigenvalue problem

$$\begin{bmatrix} \sin \lambda a - \left(\frac{\lambda}{\mu}\right) \sinh \mu a & \cos \lambda a - \cosh \mu a \\ \cos \lambda a - \cosh \mu a & -\sin \lambda a - \left(\frac{\mu}{\lambda}\right) \sinh \mu a \end{bmatrix} \begin{Bmatrix} c_1 \\ c_2 \end{Bmatrix} = \begin{Bmatrix} 0 \\ 0 \end{Bmatrix} \quad (4.2.57)$$

where relations (4.2.56) are used to eliminate c_3 and c_4 . For nonzero c_1 and c_2 , we require the determinant of the coefficient matrix of the above equations to vanish, which yields the characteristic polynomial

$$-2 + 2 \cos \lambda a \cosh \mu a + \left(\frac{\lambda}{\mu} - \frac{\mu}{\lambda}\right) \sin \lambda a \sinh \mu a = 0 \quad (4.2.58)$$

The solution of this nonlinear equation gives λ and μ . Then the natural frequency of vibration can be calculated from Eq. (4.2.48a) or (4.2.48b); if the applied axial force is zero, Eq. (4.2.49) can be used to calculate the frequency of vibration.

For natural vibration without rotatory inertia and applied in-plane force (i.e., $q = 0$ in Eq. (4.2.46b) and $\lambda = \mu$), Eq. (4.2.58) takes the simpler form

$$\cos \lambda a \cosh \lambda a - 1 = 0 \quad (4.2.59)$$

Equation (4.2.59) is satisfied for the following values of λ :

$$\lambda_1 a = 4.730, \quad \lambda_2 a = 7.853, \quad \dots, \quad \lambda_n a = \left(n + \frac{1}{2}\right)\pi \quad (4.2.60)$$

Maximum transverse deflections, critical buckling loads, and fundamental natural frequencies of various laminated beams, according to the classical beam theory, are presented in Table 4.2.4 for simply supported (hinged-hinged), clamped (fixed-fixed), and cantilever (clamped-free) boundary conditions. In the case of bending, the point load is $F_0 b$, where F_0 is the line load across the width of the beam (force/unit length), and the distributed line load along the length is $q_0 b$, where q_0 is the intensity of the distributed load (force/unit square area). In Table 4.2.4, the first row corresponds to deflections due to point load F_0 , and the second row corresponds to deflections due to uniformly distributed load q_0 . Also, on the second and third rows, frequencies corresponding to $a/h = 100$

and $a/h = 10$ are listed when rotary inertia is included. All other frequencies were computed by neglecting the rotary inertia. The following nondimensionalizations are used:

$$\bar{w} = w_{max} E_2 h^3 \times 10^2 / q_0 a^4 \quad (F_0 = q_0 a)$$

$$\bar{N} = N_{xx}^0 a^2 / E_2 h^3, \quad \bar{\omega} = \omega_1 a^2 \sqrt{I_0 / E_2 h^3} \quad (4.2.61)$$

The stiffness in a laminate is largest in the fiber direction because $E_1 > E_2$. Also, the bending stiffness increases with (cube of) the distance of the 0° layers from the midplane. Thus, the 0° -laminated beam is stiffer in bending than the 90° -laminated beam, and therefore, 0° beam has smaller deflection and larger buckling load and natural frequencies when compared to the 90° beam. Since the 0° laminae are placed farther from the midplane in $(0/90)_s$ laminate, it has smaller deflection and larger buckling load and natural frequencies when compared to the $(90/0)_s$ beams. Similarly, due to the placement of the 0° layers, laminate *A* is stiffer than laminate *B*, and laminate *B* is stiffer than laminate *C*. Symmetric angle-ply laminated beams ($\theta/-\theta$)_s have the same stiffness characteristics as ($-\theta/\theta$)_s, and they are less stiff compared to the symmetric cross-ply laminated beams.

Table 4.2.4: Maximum transverse deflections, critical buckling loads, and fundamental frequencies of laminated beams according to the classical beam theory ($E_1/E_2 = 25$, $G_{12} = G_{13} = 0.5E_2$, $G_{23} = 0.2E_2$, $\nu_{12} = 0.25$).

Laminate	Hinged-Hinged			Clamped-Clamped			Clamped-Free		
	\bar{w}	\bar{N}	$\bar{\omega}$	\bar{w}	\bar{N}	$\bar{\omega}$	\bar{w}	\bar{N}	$\bar{\omega}$
0	1.000	20.562	14.246	0.250	82.247	32.292	16.000	5.140	5.074
	0.625		14.245	0.125		32.291	6.000		5.074
			14.187			32.129			5.071
90	25.000	0.822	2.849	6.250	3.290	6.458	400.00	0.205	1.015
	15.625			3.125			150.00		
$(0/90)_s$	1.134	18.127	13.375	0.283	72.507	30.320	18.149	4.532	4.764
	0.709			0.142			6.806		
$(90/0)_s$	6.239	3.296	5.703	1.560	13.183	12.929	99.821	0.824	2.032
	3.899			0.780			37.433		
$(45/-45)_s$	14.308	1.437	3.766	3.577	5.748	8.537	228.93	0.359	1.341
	8.942			1.788			85.847		
Laminate <i>A</i>	1.607	12.790	11.236	0.402	51.162	25.469	25.721	3.197	4.002
	1.005			0.201			9.645		
Laminate <i>B</i>	2.801	7.341	8.512	0.700	29.366	19.296	44.813	1.835	3.032
	1.751			0.350			16.805		
Laminate <i>C</i>	7.945	2.588	5.054	1.986	10.351	11.456	127.13	0.647	1.800
	4.966			0.993			47.673		

Laminate *A* = $(0/\pm 45/90)_s$, Laminate *B* = $(45/0/-45/90)_s$, Laminate *C* = $(90/\pm 45/0)_s$.

We note that for clamped-clamped and clamped-free beams, the calculation of natural frequencies require the solutions of transcendental equations for λ . For the case where rotary inertia is negligible, the roots of these equations are given in Table 4.2.3. To see the effect of rotary inertia, Eq. (4.2.58) were solved for λ and the frequencies were calculated. From the frequencies listed in rows 2 and 3 of Table 4.2.4, it is clear that the effect of rotary inertia on fundamental frequencies is negligible for small length-to-height ratios. Except for second and third rows, all other frequencies listed in the table were calculated by neglecting the rotary inertia, in which case the values of λ_1 given in Table 4.2.3 are applicable.

4.3 Analysis of Laminated Beams Using FSDT

4.3.1 Governing Equations

Here we consider the bending of symmetrically laminated beams using the first-order shear deformation theory. When applied to beams, FSDT is known as the *Timoshenko beam theory*. The governing equations can be readily obtained from the results of Section 3.4.

The laminate constitutive equations for symmetric laminates, in the absence of in-plane forces, are given by [see Eqs. (3.4.21) and (3.4.22)]

$$\begin{Bmatrix} M_{xx} \\ M_{yy} \\ M_{xy} \end{Bmatrix} = \begin{bmatrix} D_{11} & D_{12} & D_{16} \\ D_{12} & D_{22} & D_{26} \\ D_{16} & D_{26} & D_{66} \end{bmatrix} \begin{Bmatrix} \frac{\partial \phi_x}{\partial x} \\ \frac{\partial \phi_y}{\partial y} \\ \frac{\partial \phi_x}{\partial y} + \frac{\partial \phi_y}{\partial x} \end{Bmatrix} \quad (4.3.1a)$$

$$\begin{Bmatrix} Q_y \\ Q_x \end{Bmatrix} = K \begin{bmatrix} A_{44} & A_{45} \\ A_{45} & A_{55} \end{bmatrix} \begin{Bmatrix} \frac{\partial w_0}{\partial y} + \phi_y \\ \frac{\partial w_0}{\partial x} + \phi_x \end{Bmatrix} \quad (4.3.1b)$$

or, in inverse form, we have

$$\begin{Bmatrix} \frac{\partial \phi_x}{\partial x} \\ \frac{\partial \phi_y}{\partial y} \\ \frac{\partial \phi_x}{\partial y} + \frac{\partial \phi_y}{\partial x} \end{Bmatrix} = \begin{bmatrix} D_{11}^* & D_{12}^* & D_{16}^* \\ D_{12}^* & D_{22}^* & D_{26}^* \\ D_{16}^* & D_{26}^* & D_{66}^* \end{bmatrix} \begin{Bmatrix} M_{xx} \\ M_{yy} \\ M_{xy} \end{Bmatrix} \quad (4.3.2a)$$

$$\begin{Bmatrix} \frac{\partial w_0}{\partial y} + \phi_y \\ \frac{\partial w_0}{\partial x} + \phi_x \end{Bmatrix} = \frac{1}{K} \begin{bmatrix} A_{44}^* & A_{45}^* \\ A_{45}^* & A_{55}^* \end{bmatrix} \begin{Bmatrix} Q_y \\ Q_x \end{Bmatrix} \quad (4.3.2b)$$

where K is the shear correction coefficient, D_{ij}^* , ($i, j = 1, 2, 6$) denote the elements of the inverse of $[D]$, and A_{ij}^* , ($i, j = 4, 5$) denote elements of the inverse of $[A]$:

$$A_{44}^* = \frac{A_{55}}{A}, \quad A_{55}^* = \frac{A_{44}}{A}, \quad A_{45}^* = -\frac{A_{45}}{A}, \quad A = A_{44}A_{55} - A_{45}A_{45} \quad (4.3.3)$$

As in Section 4.2, we assume that $M_{yy} = M_{xy} = Q_y = \phi_y = 0$ and both w_0 and ϕ_x are functions of only x and t :

$$w_0 = w_0(x, t), \quad \phi_x = \phi_x(x, t) \quad (4.3.4)$$

From Eq. (3.4.1) the displacement field takes the form (when the in-plane displacements u_0 and v_0 are zero)

$$u(x, z) = z\phi_x(x), \quad w(x, z) = w_0(x) \quad (4.3.5a)$$

and the linear strain-displacement relations give

$$\varepsilon_{xx} = z \frac{\partial \phi_x}{\partial x}, \quad 2\varepsilon_{xz} = \frac{\partial w_0}{\partial x} + \phi_x \quad (4.3.5b)$$

From Eqs. (4.3.2a,b) we have

$$\frac{\partial \phi_x}{\partial x} = D_{11}^* M_{xx}, \quad \frac{\partial w_0}{\partial x} + \phi_x = \frac{A_{55}^*}{K} Q_x \quad (4.3.6)$$

or

$$E_{xx}^b I_{yy} \frac{\partial \phi_x}{\partial x} = M(x), \quad M(x) = bM_{xx}, \quad E_{xx}^b = \frac{12}{D_{11}^* h^3} \quad (4.3.7a)$$

$$KG_{xz}^b bh \left(\frac{\partial w_0}{\partial x} + \phi_x \right) = Q(x), \quad Q(x) = bQ_x, \quad G_{xz}^b = \frac{1}{A_{55}^* h} \quad (4.3.7b)$$

The equations of motion from Eq. (3.4.13) are

$$\frac{\partial Q_x}{\partial x} + \hat{N}_{xx} \frac{\partial^2 w_0}{\partial x^2} + q = I_0 \frac{\partial^2 w_0}{\partial t^2} \quad (4.3.8a)$$

$$\frac{\partial M_{xx}}{\partial x} - Q_x = I_2 \frac{\partial^2 \phi_x}{\partial t^2} \quad (4.3.8b)$$

Using Eq. (4.3.7) in Eq. (4.3.8), the equations of motion can be recast in terms of the displacement functions:

$$\begin{aligned} KG_{xz}^b bh \left(\frac{\partial^2 w_0}{\partial x^2} + \frac{\partial \phi_x}{\partial x} \right) + b\hat{N}_{xx} \frac{\partial^2 w_0}{\partial x^2} + \hat{q} &= \hat{I}_0 \frac{\partial^2 w_0}{\partial t^2} \\ E_{xx}^b I_{yy} \frac{\partial^2 \phi_x}{\partial x^2} - KG_{xz}^b bh \left(\frac{\partial w_0}{\partial x} + \phi_x \right) &= \hat{I}_2 \frac{\partial^2 \phi_x}{\partial t^2} \end{aligned} \quad (4.3.9a, b)$$

where

$$\hat{q} = bq, \quad \hat{I}_0 = bI_0, \quad \hat{I}_2 = bI_2 \quad (4.3.9c)$$

4.3.2 Bending

Note that when the laminated beam problem is such that the bending moment $M(x)$ and $Q(x)$ can be written readily in terms of known applied loads (like in statically determinate beam problems), Eq. (4.3.7a) can be utilized to determine ϕ_x , and then w_0 can be determined using Eq. (4.3.7b). When $M(x)$ and $Q(x)$ cannot be expressed in terms of known loads, Eqs. (4.3.9a,b) are used to determine $w_0(x)$ and $\phi_x(x)$. In the latter case, the following relations prove to be useful.

For bending analysis, Eqs. (4.3.9a,b) reduce to

$$\begin{aligned} KG_{xz}^b bh \left(\frac{d^2 w_0}{dx^2} + \frac{d\phi_x}{dx} \right) + \hat{q} &= 0 \\ E_{xx}^b I_{yy} \frac{d^2 \phi_x}{dx^2} - KG_{xz}^b bh \left(\frac{dw_0}{dx} + \phi_x \right) &= 0 \end{aligned} \quad (4.3.10a, b)$$

Integrating Eq. (4.3.10a) with respect to x , we obtain

$$KG_{xz}^b bh \left(\frac{dw_0}{dx} + \phi_x \right) = - \int_0^x \hat{q}(\xi) d\xi + c_1 \quad (4.3.11)$$

Substituting the result into Eq. (4.3.10b) and integrating with respect to x , we obtain

$$E_{xx}^b I_{yy} \frac{d\phi_x}{dx} = - \int_0^x \int_0^\eta \hat{q}(\xi) d\xi d\eta + c_1 x + c_2 \quad (4.3.12a)$$

$$E_{xx}^b I_{yy} \phi_x(x) = - \int_0^x \int_0^\zeta \int_0^\eta \hat{q}(\xi) d\xi d\eta d\zeta + c_1 \frac{x^2}{2} + c_2 x + c_3 \quad (4.3.12b)$$

Substituting for $\phi(x)$ from Eq. (4.3.12b) into Eq. (4.3.11), we arrive at

$$\begin{aligned} \frac{dw_0}{dx} &= - \frac{1}{E_{xx}^b I_{yy}} \left[- \int_0^x \int_0^\zeta \int_0^\eta \hat{q}(\xi) d\xi d\eta d\zeta + c_1 \frac{x^2}{2} + c_2 x + c_3 \right] \\ &\quad + \frac{1}{KG_{xz}^b bh} \left[- \int_0^x \hat{q}(\xi) d\xi + c_1 \right] \end{aligned} \quad (4.3.13a)$$

$$\begin{aligned} w_0(x) &= - \frac{1}{E_{xx}^b I_{yy}} \left[- \int_0^x \int_0^\xi \int_0^\eta \int_0^\mu \hat{q}(\zeta) d\zeta d\mu d\eta d\xi + c_1 \frac{x^3}{6} + c_2 \frac{x^2}{2} + c_3 x + c_4 \right] \\ &\quad + \frac{1}{KG_{xz}^b bh} \left[- \int_0^x \int_0^\xi \hat{q}(\zeta) d\zeta d\xi + c_1 x \right] \end{aligned} \quad (4.3.13b)$$

where the constants of integration c_1 through c_4 can be determined using the boundary conditions of the beam.

It is informative to note from Eq. (4.3.13) that the transverse deflection of the Timoshenko beam theory consists of two parts, one due to pure bending and the other due to transverse shear:

$$w_0(x) = w_0^b(x) + w_0^s(x) \quad (4.3.14a)$$

where

$$\begin{aligned} w_0^b(x) &= \frac{1}{E_{xx}^b I_{yy}} \left[\int_0^x \int_0^\xi \int_0^\eta \int_0^\mu \hat{q}(\zeta) d\zeta d\mu d\eta d\xi - c_1 \frac{x^3}{6} - c_2 \frac{x^2}{2} - c_3 x - c_4 \right] \\ w_0^s(x) &= \frac{1}{KG_{xz}^b bh} \left[- \int_0^x \int_0^\xi \hat{q}(\zeta) d\zeta d\xi + c_1 x \right] \end{aligned} \quad (4.3.14b)$$

The pure bending deflection $w_0^b(x)$ is the same as that derived in the classical beam theory [cf., Eq. (4.2.11b)]. When the transverse shear stiffness is infinite, the shear deflection $w_0^s(x)$ goes to zero, and the Timoshenko beam theory solutions reduce to those of the classical beam theory. In fact, one can establish exact relationships between the solutions of the Euler–Bernoulli beam solutions and Timoshenko beam solutions (see [27–29]). These relationships enable one to obtain the Timoshenko beam solutions from known classical beam solutions for any set of boundary conditions (see Problems 4.33 and 4.36).

The expressions for in-plane stresses of the Timoshenko beam theory remain the same as those in the classical beam theory [see Eq. (4.2.12b)]. The expressions given in Eqs. (4.2.15a,b) for transverse shear stresses derived from 3-D equilibrium are also valid for the present case.

The transverse shear stress can also be computed via constitutive equation in the Timoshenko beam theory. We have

$$\sigma_{xz}^{(k)}(x, z) = \bar{Q}_{55}^{(k)} A_{55}^* \frac{Q(x)}{b} \quad (4.3.15)$$

Example 4.3.1 (Simply supported beam):

Here we consider the three-point bending problem of Section 4.2 (see Figure 4.2.2). For this case, the bending moment [see Eq. (4.2.17)] and shear forces are

$$M(x) = \frac{F_0 b x}{2}, \quad Q(x) = \frac{dM}{dx} = \frac{F_0 b}{2}, \quad 0 \leq x \leq \frac{a}{2} \quad (4.3.16)$$

Using Eq. (4.3.16) for M in Eq. (4.3.7a) and integrating with respect to x , we obtain

$$\phi_x(x) = \frac{F_0 b}{4E_{xx}^b I_{yy}} x^2 + c_1$$

By symmetry, $u_1 = u_0 + z\phi_x$ is zero at $x = a/2$. This implies that $\phi_x(a/2) = 0$. Hence

$$c_1 = -\frac{F_0 b a^2}{16E_{xx}^b I_{yy}}$$

and the solution becomes

$$\phi_x(x) = -\frac{F_0 b a^2}{16E_{xx}^b I_{yy}} \left[1 - 4 \left(\frac{x}{a} \right)^2 \right], \quad 0 \leq x \leq \frac{a}{2} \quad (4.3.17)$$

It is interesting to note from Eq. (4.3.17) that the rotation function $\phi_x(x)$ is the same as the slope $-dw_0/dx$ from the Euler–Bernoulli beam theory (i.e., ϕ_x is independent of transverse shear stiffness). Consequently, the bending moment [see Eq. (4.3.7a)], and therefore the axial stress, is independent of shear deformation. In fact, ϕ_x is independent of shear deformation for all statically determinate beams and indeterminate beams with symmetric boundary conditions and loading (see Wang [27]). However, for general statically indeterminate beams, the rotation ϕ_x will depend on the shear stiffness $KG_{xz}^b bh$ (see Problem 4.11).

Substituting for ϕ_x into Eq. (4.3.7b), we obtain

$$\frac{dw_0}{dx} = \frac{F_0 b a^2}{16E_{xx}^b I_{yy}} \left[1 - 4 \left(\frac{x}{a} \right)^2 \right] + \frac{F_0 b}{2KG_{xz}^b bh} \quad (4.3.18a)$$

Let us denote the first expression in (4.3.18a) by

$$\frac{dw_0^b}{dx} = \frac{F_0 ba^2}{16E_{xx}^b I_{yy}} \left[1 - 4 \left(\frac{x}{a} \right)^2 \right] = -\phi_x(x) \quad (4.3.18b)$$

In light of Eq. (4.3.14a), the first part of Eq. (4.3.18a) can be viewed as the slope (or rotation) due to bending and the second one due to transverse shear strain:

$$\frac{dw_0}{dx} \equiv \frac{dw_0^b}{dx} + \frac{dw_0^s}{dx} \quad (4.3.18c)$$

Indeed, dw_0^s/dx can be interpreted as the transverse shear strain [cf., Eq. (4.3.5b)]

$$\frac{dw_0^s}{dx} = \frac{dw_0}{dx} - \frac{dw_0^b}{dx} = \frac{dw_0}{dx} + \phi_x(x) \equiv \gamma_{xz} \quad (4.3.19)$$

Note from Eq. (4.3.18a) that, in contrast to the classical beam theory, the slope dw_0/dx at the center of the beam in the Timoshenko beam theory is nonzero. We have ($I_{yy} = bh^3/12$)

$$\frac{dw_0}{dx} \left(\frac{a}{2} \right) = \frac{F_0 b}{2KG_{xz}^b bh} \quad (4.3.20)$$

However, $dw_0^b/dx = -\phi_x$ is zero at $x = a/2$. Integrating Eq. (4.3.18a) with respect to x , we arrive at the expression

$$w_0(x) = \frac{F_0 ba^3}{48E_{xx}^b I_{yy}} \left[3 \left(\frac{x}{a} \right) - 4 \left(\frac{x}{a} \right)^3 \right] + \frac{F_0 ba}{2KG_{xz}^b bh} \left(\frac{x}{a} \right) \quad (4.3.21)$$

where the constant of integration is found to be zero on account of the boundary condition $w_0(0) = 0$. Note that the first part (w_0^b) is the same as that obtained in the classical beam theory [cf., Eq. (4.2.18)].

The maximum deflection occurs at $x = a/2$ and it is given by

$$\begin{aligned} w_{max} &= \frac{F_0 ba^3}{48E_{xx}^b I_{yy}} + \frac{F_0 ba}{4KG_{xz}^b bh} \\ &= \frac{F_0 ba^3}{48E_{xx}^b I_{yy}} \left[1 + \left(\frac{E_{xx}^b}{KG_{xz}^b} \right) \left(\frac{h}{a} \right)^2 \right] \end{aligned} \quad (4.3.22)$$

Equation (4.3.22) shows that the effect of shear deformation is to increase the deflection. The contribution due to shear deformation to the deflection depends on the modulus ratio E_{xx}^b/G_{xz}^b as well as the ratio of thickness to length h/a . The effect of shear deformation is negligible for thin and long beams.

Example 4.3.2 (Clamped beam):

Consider a laminated beam fixed at both ends and subjected to uniformly distributed transverse load $q_0 b$ as well as a point load $F_0 b$ at the center, both acting downward. For this case, the boundary conditions are (using half beam)

$$u(0, z) = 0, \quad u\left(\frac{a}{2}, z\right) = 0, \quad w(0, z) = 0, \quad Q_x\left(\frac{a}{2}, z\right) = \left(\frac{F_0 b}{2} + \frac{q_0 b a}{2}\right) - \frac{q_0 b a}{2} = \frac{F_0 b}{2} \quad (4.3.23)$$

which in turn imply that

$$\phi_x(0) = 0, \quad \phi_x\left(\frac{a}{2}\right) = 0, \quad w_0(0) = 0, \quad KG_{xz}^b bh \left(\frac{dw_0}{dx} + \phi_x \right) \left(\frac{a}{2} \right) = \frac{F_0 b}{2} \quad (4.3.24)$$

The solution is

$$\begin{aligned}\phi_x(x) = & \frac{q_0 ba^3}{12E_{xx}^b I_{yy}} \left[-2\left(\frac{x}{a}\right)^3 + 3\left(\frac{x}{a}\right)^2 - \left(\frac{x}{a}\right) \right] \\ & + \frac{F_0 ba^2}{8E_{xx}^b I_{yy}} \left[-2\left(\frac{x}{a}\right)^2 + \left(\frac{x}{a}\right) \right]\end{aligned}\quad (4.3.25)$$

$$\begin{aligned}w_0(x) = & \frac{q_0 ba^4}{24E_{xx}^b I_{yy}} \left[\left(\frac{x}{a}\right)^2 - \left(\frac{x}{a}\right) \right]^2 + \frac{q_0 ba^2}{2KG_{xz}^b bh} \left[\left(\frac{x}{a}\right) - \left(\frac{x}{a}\right)^2 \right] \\ & + \frac{F_0 ba^3}{48E_{xx}^b I_{yy}} \left[3\left(\frac{x}{a}\right)^2 - 4\left(\frac{x}{a}\right)^3 \right] + \frac{F_0 ba}{2KG_{xz}^b bh} \left(\frac{x}{a} \right)\end{aligned}\quad (4.3.26)$$

The maximum deflection is at $x = a/2$ and is given by [cf., Eq. (4.2.23)]

$$\begin{aligned}w_{max} = & \frac{q_0 ba^4}{384E_{xx}^b I_{yy}} + \frac{q_0 a^2}{8KG_{xz}^b h} + \frac{F_0 ba^3}{192E_{xx}^b I_{yy}} + \frac{F_0 a}{4KG_{xz}^b h} \\ = & \left[\frac{q_0 ba^4}{384E_{xx}^b I_{yy}} + \frac{F_0 ba^3}{192E_{xx}^b I_{yy}} \right] (1 + S)\end{aligned}\quad (4.3.27a)$$

where S is the positive parameter that characterizes the contribution due to the transverse shear strain to the displacement field

$$S = 4 \left(\frac{E_{xx}^b}{KG_{xz}^b} \right) \left(\frac{h}{a} \right)^2 \quad (4.3.27b)$$

Table 4.3.1 contains expressions for transverse deflections and maximum transverse deflections of laminated beams according to the first-order shear deformation theory. By comparison to the classical theory (see Table 4.2.1), it is clear that the shear deformation increases the deflection.

Table 4.3.2 contains maximum transverse deflections \bar{w} of various laminated beams according to the Timoshenko shear deformation beam theory. The effect of length-to-height (or thickness) ratios of the beam on the deflections can be seen from the results. Thin or long beams do not experience transverse shear strains. Clamped beams show the most difference in deflections due to transverse shear deformation (i.e., accounting for the transverse shear strain). The effect of shear deformation on maximum deflection can be seen from Figures 4.3.1 and 4.3.2, where the nondimensionalized maximum deflection, $\bar{w} = w_{max} E_2 h^3 / q_0 a^4$ ($F_0 = q_0 a$), of a simply supported beam is plotted as a function of length-to-height ratio a/h for various laminated beams under a point load and uniformly distributed load, respectively. The material properties of a lamina are taken to be those in Eq. (4.2.25). The effect of shear deformation is more significant for beams with length-to-thickness ratios smaller than 10.

4.3.3 Buckling

For buckling analysis, the inertia terms and the applied transverse load q in Eqs. (4.3.9a,b) are set to zero to obtain the governing equations of buckling under compressive edge load $\hat{N}_{xx} = -N_{xx}^0$:

$$KG_{xz}^b bh \left(\frac{d^2 W}{dx^2} + \frac{d \mathcal{X}}{dx} \right) + b \hat{N}_{xx} \frac{d^2 W}{dx^2} = 0 \quad (4.3.28a)$$

$$E_{xx}^b I_{yy} \frac{d^2 \mathcal{X}}{dx^2} - KG_{xz}^b bh \left(\frac{d W}{dx} + \mathcal{X} \right) = 0 \quad (4.3.28b)$$

Table 4.3.1: Transverse deflections of laminated composite beams with various boundary conditions and subjected to point load or uniformly distributed load (acting downward) according to the shear deformation theory.

$$c_1 = \frac{F_0 ba^3}{E_{xx}^b I_{yy}}, \quad c_2 = \frac{q_0 ba^4}{E_{xx}^b I_{yy}}, \quad s_1 = \frac{F_0 ba}{KG_{xz}^b bh}, \quad s_2 = \frac{q_0 ba^2}{G_{xz}^b bh}$$

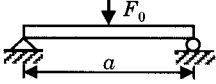
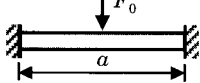
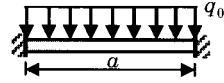
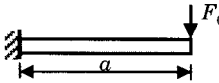
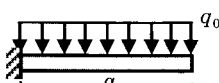
Laminated Beam	Deflection, $w_0(x)$	Max. Deflection
• Hinged-Hinged		
Central point load 	$\frac{c_1}{48} \left[3\left(\frac{x}{a}\right) - 4\left(\frac{x}{a}\right)^3 \right] + \frac{s_1}{2} \left(\frac{x}{a} \right)$	$\frac{1}{48}c_1 + \frac{1}{4}s_1$ at $x = \frac{a}{2}$
• Fixed-Fixed		
Central point load 	$\frac{c_1}{48} \left[3\left(\frac{x}{a}\right)^2 - 4\left(\frac{x}{a}\right)^3 \right] + \frac{s_1}{2} \left(\frac{x}{a} \right)$	$\frac{1}{192}c_1 + \frac{1}{4}s_1$ at $x = \frac{a}{2}$
Uniform load 	$\frac{c_2}{24} \left[\left(\frac{x}{a}\right)^2 - 2\left(\frac{x}{a}\right)^3 + \left(\frac{x}{a}\right)^4 \right] + \frac{s_2}{2} \left[\left(\frac{x}{a}\right) - \left(\frac{x}{a}\right)^2 \right]$	$\frac{5}{384}c_2 + \frac{1}{8}s_2$ at $x = \frac{a}{2}$
• Fixed-Free		
Point load at free end 	$\frac{c_1}{6} \left[3\left(\frac{x}{a}\right)^2 - \left(\frac{x}{a}\right)^3 \right] + s_1 \left(\frac{x}{a} \right)$	$\frac{1}{3}c_1 + s_1$ at $x = a$
Uniform load 	$\frac{c_2}{24} \left[6\left(\frac{x}{a}\right)^2 - 4\left(\frac{x}{a}\right)^3 + \left(\frac{x}{a}\right)^4 \right] + \frac{s_2}{2} \left[\left(2\frac{x}{a}\right) - \left(\frac{x}{a}\right)^2 \right]$	$\frac{1}{8}c_2 + \frac{1}{2}s_2$ at $x = a$

Table 4.3.2: Maximum transverse deflections of laminated beams according to the Timoshenko beam theory[†] ($E_1/E_2 = 25$, $G_{12} = G_{13} = 0.5E_2$, $G_{23} = 0.2E_2$, $\nu_{12} = 0.25$).

Laminate	$\frac{a}{h} \rightarrow$	Hinged-Hinged			Clamped-Clamped			Clamped-Free		
		100	20	10	100	20	10	100	20	10
0		1.001	1.150	1.600	0.256	0.400	0.850	16.02	16.60	18.40
		0.628	0.700	0.925	0.128	0.200	0.425	6.01	6.30	7.20
90		25.015	25.375	26.500	6.265	6.625	7.750	400.00	401.50	406.00
		15.633	15.813	16.375	3.132	3.312	3.875	150.00	150.75	153.00
(90/0) _s		1.143	1.348	1.991	0.292	0.498	1.141	18.18	19.01	21.58
		0.713	0.816	1.137	0.146	0.249	0.570	6.82	7.23	8.52
(45/-45) _s		14.316	14.522	15.165	3.585	3.791	4.434	228.96	229.78	232.35
		8.947	9.049	9.371	1.793	1.895	2.217	85.86	86.28	87.56

[†]The first row of each laminate refers to nondimensionalized maximum deflections under point load ($F_0 b$) and the second one refers to maximum deflections under uniformly distributed load ($q_0 b$). The deflection is nondimensionalized as $\hat{w} = w_{max}(E_2 h^3/q_0 a^4) \times 10^2$ ($F_0 = q_0 a$).

Solving Eq. (4.3.28a) for $d\mathcal{X}/dx$ one obtains

$$KG_{xz}^b bh \frac{d\mathcal{X}}{dx} = - \left(KG_{xz}^b bh - bN_{xx}^0 \right) \frac{d^2 W}{dx^2} \quad (4.3.29)$$

Integration with respect to x yields

$$KG_{xz}^b bh \mathcal{X}(x) = - \left(KG_{xz}^b bh - bN_{xx}^0 \right) \frac{dW}{dx} + K_1 \quad (4.3.30)$$

Next differentiate Eq. (4.3.28b) with respect to x and substitute for $d\mathcal{X}/dx$ from Eq. (4.3.29) to obtain the result

$$\begin{aligned} & -E_{xx}^b I_{yy} \frac{d^2}{dx^2} \left[\left(1 - \frac{bN_{xx}^0}{KG_{xz}^b bh} \right) \frac{d^2 W}{dx^2} \right] \\ & -KG_{xz}^b bh \left[\frac{d^2 W}{dx^2} - \left(1 - \frac{bN_{xx}^0}{KG_{xz}^b bh} \right) \frac{d^2 W}{dx^2} \right] = 0 \end{aligned}$$

or

$$E_{xx}^b I_{yy} \left(1 - \frac{bN_{xx}^0}{KG_{xz}^b bh} \right) \frac{d^4 W}{dx^4} + bN_{xx}^0 \frac{d^2 W}{dx^2} = 0 \quad (4.3.31)$$

The general solution of Eq. (4.3.31) is

$$W(x) = c_1 \sin \lambda x + c_2 \cos \lambda x + c_3 x + c_4 \quad (4.3.32)$$

where

$$\lambda^2 = \frac{bN_{xx}^0}{\left(1 - \frac{bN_{xx}^0}{KG_{xz}^b bh} \right) E_{xx}^b I_{yy}} \quad \text{or} \quad bN_{xx}^0 = \frac{\lambda^2 E_{xx}^b I_{yy}}{\left(1 + \frac{\lambda^2 E_{xx}^b I_{yy}}{KG_{xz}^b bh} \right)} \quad (4.3.33)$$

and c_1 through c_4 are constants of integration, which must be evaluated using the boundary conditions.

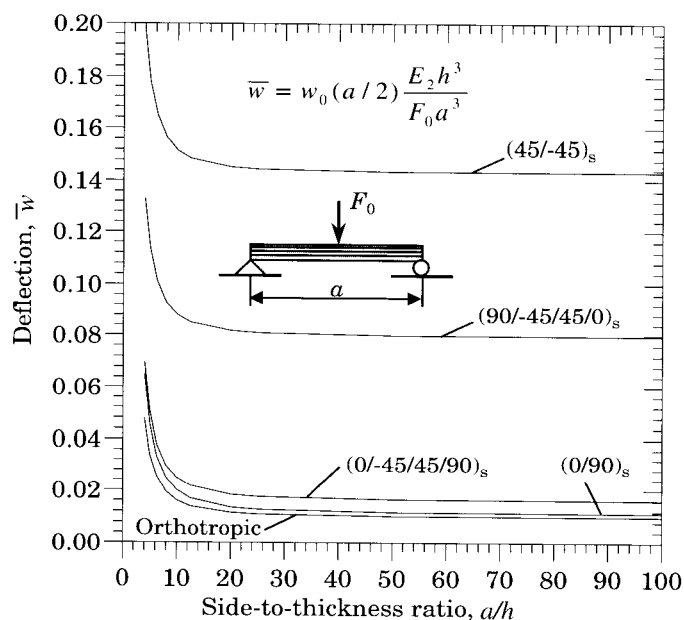


Figure 4.3.1: Transverse deflection (\bar{w}) versus length-to-thickness ratio (a/h) of simply supported beams under center point load.

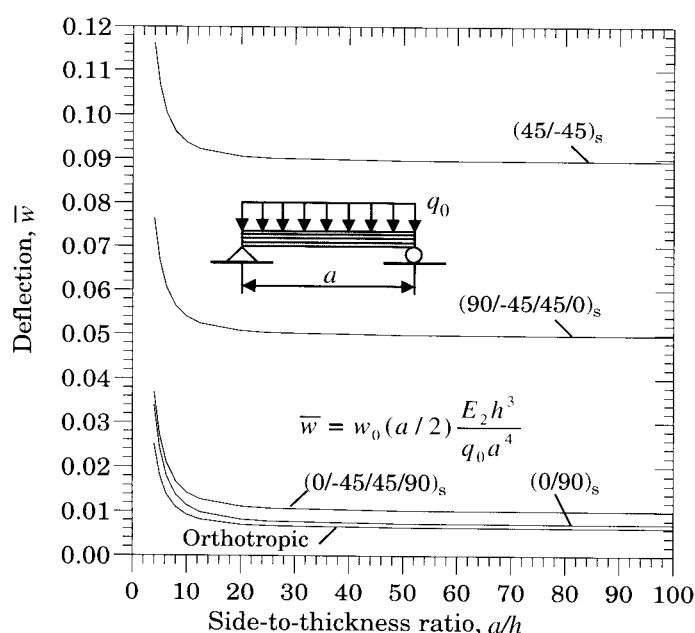


Figure 4.3.2: Transverse deflection (\bar{w}) versus length-to-thickness ratio (a/h) of simply supported beams under uniformly distributed load.

Example 4.3.3 (Simply supported beam): _____

For a simply supported beam, the boundary conditions are [see Eq. (4.2.31a)]

$$W(0) = 0, \quad W(a) = 0, \quad \frac{d\lambda}{dx}(0) = 0, \quad \frac{d\lambda}{dx}(a) = 0 \quad (4.3.34a)$$

In view of Eq. (4.3.29), the above conditions are equivalent to

$$W(0) = 0, \quad W(a) = 0, \quad \frac{d^2W}{dx^2}(0) = 0, \quad \frac{d^2W}{dx^2}(a) = 0 \quad (4.3.34b)$$

The boundary conditions in Eq. (4.3.34b) lead to the result $c_2 = c_3 = c_4 = 0$, and for $c_1 \neq 0$ the requirement

$$\sin \lambda a = 0 \quad \text{implies} \quad \lambda a = n\pi \quad (4.3.35)$$

Substituting for λ from Eq. (4.3.35) into Eq. (4.3.33) for N_{xx}^0 , we obtain

$$\begin{aligned} bN_{xx}^0 &= E_{xx}^b I_{yy} \left(\frac{n\pi}{a} \right)^2 \left[\frac{KG_{xz}^b bh}{KG_{xz}^b bh + E_{xx}^b I_{yy} \left(\frac{n\pi}{a} \right)^2} \right] \\ &= E_{xx}^b I_{yy} \left(\frac{n\pi}{a} \right)^2 \left[1 - \frac{E_{xx}^b I_{yy} \left(\frac{n\pi}{a} \right)^2}{KG_{xz}^b bh + E_{xx}^b I_{yy} \left(\frac{n\pi}{a} \right)^2} \right] \end{aligned} \quad (4.3.36)$$

The critical buckling load is given by the minimum ($n = 1$)

$$bN_{cr} = E_{xx}^b I_{yy} \left(\frac{\pi}{a} \right)^2 \left[1 - \frac{E_{xx}^b I_{yy} \left(\frac{\pi}{a} \right)^2}{KG_{xz}^b bh + E_{xx}^b I_{yy} \left(\frac{\pi}{a} \right)^2} \right] \quad (4.3.37)$$

It is clear from the result in Eq. (4.3.37) that shear deformation has the effect of decreasing the buckling load [cf., Eq. (4.2.35)].

Example 4.3.4 (Clamped beam): _____

For a beam fixed at both ends, the boundary conditions are

$$W(0) = 0, \quad W(a) = 0, \quad \lambda(0) = 0, \quad \lambda(a) = 0 \quad (4.3.38)$$

In order to impose the boundary conditions on λ , we use Eq. (4.3.30). The constant K_1 appearing in Eq. (4.3.30) can be shown (see Problem 4.10) to be equal to $K_1 = -c_3(bN_{xx}^0)$. The boundary conditions yield

$$\begin{aligned} c_2 + c_4 &= 0, \quad c_1 \sin \lambda a + c_2 \cos \lambda a + c_3 a + c_4 = 0 \\ &\quad - \left(1 - \frac{bN_{xx}^0}{KG_{xz}^b bh} \right) \lambda c_1 - c_3 = 0 \\ &\quad - \left(1 - \frac{bN_{xx}^0}{KG_{xz}^b bh} \right) (\lambda c_1 \cos \lambda a - \lambda c_2 \sin \lambda a) - c_3 = 0 \end{aligned}$$

Expressing c_1 and c_2 in terms of c_3 and c_4 , noting that

$$1 - \frac{bN_{xx}^0}{KG_{xz}^b bh} = \frac{1}{1 + \frac{\lambda^2 E_{xx}^b I_{yy}}{KG_{xz}^b bh}}$$

and then setting the determinant of the resulting algebraic equations among c_1 and c_2 to zero, we obtain

$$2(\cos \lambda a - 1) \left(1 + \frac{\lambda^2 E_{xx}^b I_{yy}}{KG_{xz}^b bh} \right) + \lambda a \sin \lambda a = 0 \quad (4.3.39)$$

Once the value of λa is determined by solving the nonlinear equation (4.3.39), the buckling load can be readily determined from Eq. (4.3.33).

4.3.4 Vibration

For natural vibration, we assume that the applied axial force and transverse load are zero and that the motion is periodic. Equations (4.3.9a,b) take the form

$$KG_{xz}^b bh \left(\frac{d^2 W}{dx^2} + \frac{d\mathcal{X}}{dx} \right) + \omega^2 \hat{I}_0 W = 0 \quad (4.3.40a)$$

$$E_{xx}^b I_{yy} \frac{d^2 \mathcal{X}}{dx^2} - KC_{xz}^b bh \left(\frac{dW}{dx} + \mathcal{X} \right) + \omega^2 \hat{I}_2 \mathcal{X} = 0 \quad (4.3.40b)$$

We use the same procedure as before to eliminate \mathcal{X} from Eqs. (4.3.40a,b). From Eq. (4.3.40a), we have

$$KG_{xz}^b bh \frac{d\mathcal{X}}{dx} = -\hat{I}_0 \omega^2 W - KG_{xz}^b bh \frac{d^2 W}{dx^2} \quad (4.3.41)$$

Substitute the above result into the derivative of Eq. (4.3.40b) for $d\mathcal{X}/dx$ and obtain the result

$$E_{xx}^b I_{yy} \frac{d^4 W}{dx^4} + \left(\frac{E_{xx}^b I_{yy} \hat{I}_0}{KG_{xz}^b bh} + \hat{I}_2 \right) \omega^2 \frac{d^2 W}{dx^2} - \left(1 - \frac{\omega^2 \hat{I}_2}{KG_{xz}^b bh} \right) \hat{I}_0 \omega^2 W = 0 \quad (4.3.42a)$$

or

$$p \frac{d^4 W}{dx^4} + q \frac{d^2 W}{dx^2} - r W = 0 \quad (4.3.42b)$$

where

$$p = E_{xx}^b I_{yy}, \quad q = \left(\frac{E_{xx}^b I_{yy}}{KG_{xz}^b bh} + \frac{\hat{I}_2}{\hat{I}_0} \right) \hat{I}_0 \omega^2, \quad r = \left(1 - \frac{\omega^2 \hat{I}_2}{KG_{xz}^b bh} \right) \hat{I}_0 \omega^2 \quad (4.3.42c)$$

The general solution of Eq. (4.3.42b) is

$$W(x) = c_1 \sin \lambda x + c_2 \cos \lambda x + c_3 \sinh \mu x + c_4 \cosh \mu x \quad (4.3.43a)$$

where

$$\lambda = \sqrt{\frac{1}{2p} \left(q + \sqrt{q^2 + 4pr} \right)}, \quad \mu = \sqrt{\frac{1}{2p} \left(-q + \sqrt{q^2 + 4pr} \right)} \quad (4.3.43b)$$

and c_1, c_2, c_3 , and c_4 are constants, which are to be determined using the boundary conditions. Note that we have

$$(2\lambda^2 p - q)^2 = q^2 + 4pr \quad \text{or} \quad p\lambda^4 - q\lambda^2 - r = 0 \quad (4.3.44)$$

Alternatively, Eq. (4.3.42a) can be written, with W given by Eq. (4.3.43), in terms of ω as

$$P\omega^4 - Q\omega^2 + R = 0 \quad (4.3.45a)$$

where

$$P = \frac{\hat{I}_2}{KG_{xz}^b bh}, \quad Q = \left[1 + \left(\frac{E_{xx}^b I_{yy}}{KG_{xz}^b bh} + \frac{\hat{I}_2}{\hat{I}_0} \right) \lambda^2 \right], \quad R = \left(\frac{E_{xx}^b I_{yy}}{\hat{I}_0} \right) \lambda^4 \quad (4.3.45b)$$

Hence, there are two (sets of) roots of this equation (when $\hat{I}_2 \neq 0$)

$$(\omega^2)_1 = \frac{1}{2P} \left(Q - \sqrt{Q^2 - 4PR} \right), \quad (\omega^2)_2 = \frac{1}{2P} \left(Q + \sqrt{Q^2 - 4PR} \right) \quad (4.3.46)$$

It can be shown that $Q^2 - 4PR > 0$ (and $PQ > 0$), and therefore the frequency given by the first equation is the smaller of the two values. When the rotary inertia is neglected, we have $P = 0$ and the frequency is given by

$$\omega^2 = \frac{R}{\bar{Q}}, \quad \bar{Q} = \left[1 + \left(\frac{E_{xx}^b I_{yy}}{KG_{xz}^b bh} \right) \lambda^2 \right], \quad R = \left(\frac{E_{xx}^b I_{yy}}{\hat{I}_0} \right) \lambda^4 \quad (4.3.47)$$

Example 4.3.5 (Simply supported beam):

For a simply supported beam, the boundary conditions in Eq. (4.3.34b) yield $c_2 = c_3 = c_4 = 0$ and

$$c_1 \sin \lambda a = 0, \text{ which implies } \lambda_n = \frac{n\pi}{a} \quad (4.3.48)$$

Substitution of λ from Eq. (4.3.48) into Eq. (4.3.47) and the result into Eq. (4.3.46a,b) gives two frequencies for each value of λ . The fundamental frequency will come from Eq. (4.3.46a).

When the rotary inertia is neglected, we obtain from Eq. (4.3.47) the result

$$\omega_n = \left(\frac{n\pi}{a} \right)^2 \sqrt{\frac{E_{xx}^b I_{yy}}{\hat{I}_0}} \sqrt{1 - \frac{(\frac{n\pi}{a})^2 E_{xx}^b I_{yy}}{KG_{xz}^b bh + (\frac{n\pi}{a})^2 E_{xx}^b I_{yy}}} \quad (4.3.49)$$

Thus, shear deformation decreases the frequencies of natural vibration [see Eq. (4.2.55)].

Example 4.3.6 (Clamped beam):

Using Eq. (4.3.40a) and expression (4.3.43a) for $W(x)$, $d\mathcal{X}/dx$ can be determined in terms of the constants c_1 through c_4 , which then can be integrated with respect to x to obtain an expression for \mathcal{X} . Using the boundary conditions in Eq. (4.3.38), we obtain

$$\begin{aligned} c_2 + c_4 &= 0, \quad c_1 \sin \lambda a + c_2 \cos \lambda a + c_3 \sinh \mu a + c_4 \cosh \mu a = 0 \\ S_{11}c_1 - S_{22}c_3 &= 0, \quad S_{11}c_1 - S_{11}c_2 - S_{22}c_3 - S_{22}c_4 = 0 \end{aligned} \quad (4.3.50a)$$

where

$$S_{11} = \mu \left(\hat{I}_0 \omega^2 - \lambda^2 KG_{xz}^b bh \right), \quad S_{22} = \lambda \left(\hat{I}_0 \omega^2 + \mu^2 KG_{xz}^b bh \right) \quad (4.3.50b)$$

Eliminating c_2 and c_4 from the above equations, and setting the determinant of the resulting equations among c_1 and c_2 to zero (for a nontrivial solution), we obtain

$$-2 + 2 \cos \lambda a \cosh \mu a + \sin \lambda a \sinh \mu a \left(\frac{S_{22}}{S_{11}} - \frac{S_{11}}{S_{22}} \right) = 0 \quad (4.3.51)$$

Table 4.3.3 contains critical buckling loads and fundamental frequencies of various laminated beams according to the Timoshenko beam theory. The first row of each laminate refers to the nondimensionalized critical buckling load, the second row refers to nondimensionalized fundamental frequencies with rotary inertia, and the fourth row refers to fundamental frequencies without rotary inertia. The numbers in rows 3 and 5 refer to the fundamental frequencies calculated using the frequency equations of the classical laminate theory (for the simply supported boundary conditions, the frequency equations are the same in both theories). The following nondimensionalizations are used:

$$\bar{N} = N_{xx}^0(a^2/E_2 h^3), \quad \bar{\omega} = \omega_1 a^2 \sqrt{I_0/E_2 h^3} \quad (4.3.52)$$

The frequency equations (4.3.51) of the Timoshenko theory depend, for clamped-clamped and clamped-free boundary conditions, on the lamination scheme and geometric parameters (through S_{ij}), whereas those of the classical laminate theory [see Eqs. (4.2.58) and (4.2.59)] are independent of the beam geometry or material properties. Thus, there are two different things that influence the frequencies in the Timoshenko theory: (i) the effect of transverse shear deformation [see Eqs. (4.3.47) and (4.3.49)], and (ii) the values of λ , which are governed by different equations than those of the classical theory (for clamped-clamped and clamped-free beams). The second effect is not significant, as can be seen from rows 3 and 5 of Table 4.3.3. Also, for clamped-clamped and clamped-free boundary conditions, the effect of rotary inertia on the frequencies is not as obvious as it was in the case of simply supported beams, where the rotary inertia would decrease the frequencies. From the results presented in Table 4.3.3, it appears that rotary inertia may actually increase the frequencies slightly.

The effect of length-to-height (or thickness) ratios of the beam on critical buckling loads \bar{N} and fundamental frequencies $\bar{\omega}$ is shown in Figures 4.3.3 and 4.3.4, respectively, for various lamination schemes. The material properties used are those listed in Eq. (4.2.25). Transverse shear deformation has the effect of decreasing both buckling loads and natural frequencies. Thus, the classical laminate theory overpredicts buckling loads and natural frequencies. This is primarily due to the assumed infinite rigidity of the transverse normals in the classical laminate theory. Note that the assumption does not yield a conservative result; i.e., if one designs a beam for buckling load based on the classical laminate theory and if no safety factor is used, it will fail for a working load smaller than the critical buckling load.

Once again we note that the relationships between the classical beam theory and the Timoshenko beam theory may be used determine the deflections, buckling loads and fundamental frequencies according to the Timoshenko beam theory from those of the Euler-Bernoulli beam theory [29]. Such relationships exist only for isotropic beams, and the reader may find it challenging to develop the relationships for bending, buckling and vibration of laminated beams (see Section 5.5 of [29]).

Table 4.3.3: Critical buckling loads (\bar{N}) and fundamental frequencies ($\bar{\omega}$) of laminated beams according to the Timoshenko beam theory ($E_1/E_2 = 25$, $G_{12} = G_{13} = 0.5E_2$, $G_{23} = 0.2E_2$, $\nu_{12} = 0.25$).

Laminate	$\frac{a}{h} \rightarrow$	Hinged-Hinged			Clamped-Clamped			Clamped-Free		
		100	20	10	100	20	10	100	20	10
0	\bar{N}	20.461	18.304	13.768	80.655	55.070	27.656	5.134	4.987	4.576
	$\bar{\omega}(\hat{I}_2 \neq 0)$	14.210	13.430	11.635	31.899	25.327	17.212	5.070	4.930	4.528
		14.210	13.430	11.635	32.110	28.506	22.140	5.070	4.965	4.675
	$\bar{\omega}(\hat{I}_2 = 0)$	14.211	13.441	11.657	31.824	24.636	16.680	5.063	4.813	4.229
		14.211	13.441	11.657	32.113	28.547	22.186	5.070	4.966	4.680
90		0.822	0.812	0.784	3.283	3.135	2.747	0.205	0.205	0.203
		2.848	2.829	2.771	6.450	6.260	5.761	1.015	1.012	1.004
		2.848	2.829	2.771	6.454	6.356	6.079	1.015	1.012	1.005
		2.848	2.832	2.781	6.449	6.232	5.681	1.015	1.009	0.993
		2.848	2.832	2.781	6.455	6.370	6.125	1.015	1.013	1.006
(90/0) _s		18.015	15.689	11.179	70.748	44.716	20.800	4.525	4.362	3.922
		13.334	12.434	10.488	29.857	22.672	14.837	4.758	4.594	4.132
		13.334	12.434	10.488	30.106	26.041	19.504	4.759	4.636	4.307
(45/-45) _s		1.436	1.419	1.369	5.737	5.478	4.802	0.359	0.358	0.355
		3.765	3.739	3.663	8.526	8.275	7.616	1.341	1.338	1.326
		3.765	3.739	3.663	8.531	8.402	8.036	1.341	1.338	1.328

4.4 Cylindrical Bending Using CLPT

4.4.1 Governing Equations

Consider a laminated rectangular plate strip, and let the x and y coordinates be parallel to the edges of the strip. Suppose that the plate is long in the y -direction and has a finite dimension along the x -direction, and subjected to a transverse load $q(x)$ that is uniform at any section parallel to the x -axis. In such a case, the deflection w_0 and displacements (u_0, v_0) of the plate are functions of only x . Therefore, all derivatives with respect to y are zero, and the plate bends into a cylindrical surface. For this *cylindrical bending* problem (see Figure 4.1.2), the governing equations of motion according to the linear classical laminate plate theory (CLPT) are given by [see Example 3.3.1; Eqs. (3.3.48)]

$$A_{11} \frac{\partial^2 u_0}{\partial x^2} + A_{16} \frac{\partial^2 v_0}{\partial x^2} - B_{11} \frac{\partial^3 w_0}{\partial x^3} - \frac{\partial N_{xx}^T}{\partial x} = I_0 \frac{\partial^2 u_0}{\partial t^2} - I_1 \frac{\partial^3 w_0}{\partial x \partial t^2} \quad (4.4.1a)$$

$$A_{16} \frac{\partial^2 u_0}{\partial x^2} + A_{66} \frac{\partial^2 v_0}{\partial x^2} - B_{16} \frac{\partial^3 w_0}{\partial x^3} - \frac{\partial N_{xy}^T}{\partial x} = I_0 \frac{\partial^2 v_0}{\partial t^2} \quad (4.4.1b)$$

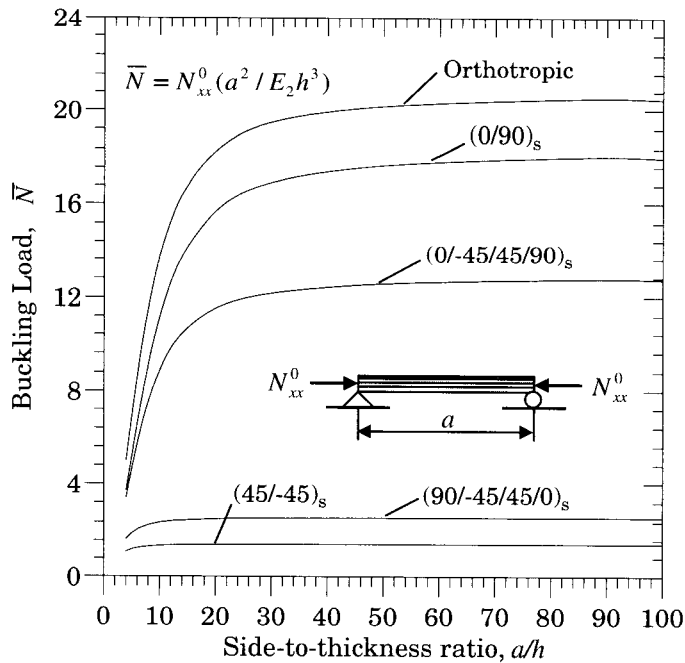


Figure 4.3.3: Nondimensionalized critical buckling load (\bar{N}) versus length-to-thickness ratio (a/h) of simply supported beams.

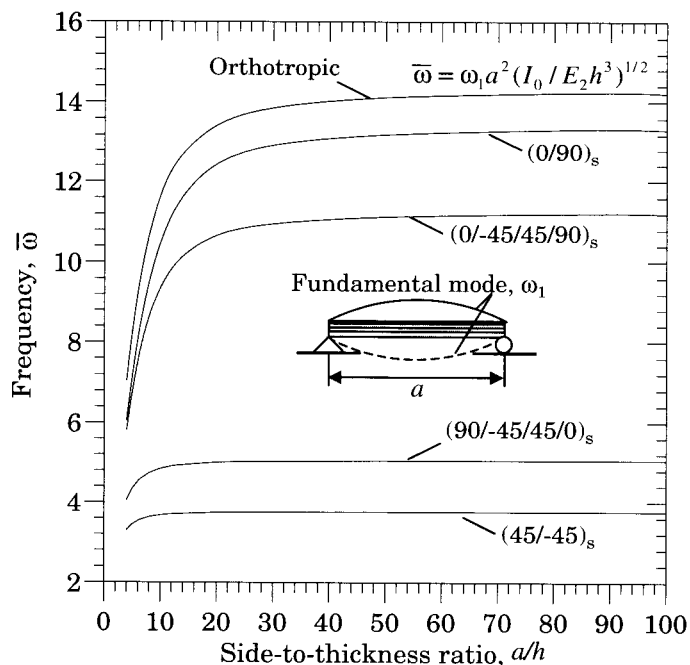


Figure 4.3.4: Nondimensionalized fundamental frequency ($\bar{\omega}$) versus length-to-thickness ratio (a/h) of simply supported beams.

$$\begin{aligned} B_{11} \frac{\partial^3 u_0}{\partial x^3} + B_{16} \frac{\partial^3 v_0}{\partial x^3} - D_{11} \frac{\partial^4 w_0}{\partial x^4} + \frac{\partial}{\partial x} \left(\hat{N}_{xx} \frac{\partial w_0}{\partial x} \right) - \frac{\partial^2 M_{xx}^T}{\partial x^2} + q \\ = I_0 \frac{\partial^2 w_0}{\partial t^2} - I_2 \frac{\partial^4 w_0}{\partial x^2 \partial t^2} + I_1 \frac{\partial^3 u_0}{\partial x \partial t^2} \end{aligned} \quad (4.4.1c)$$

where \hat{N}_{xx} is an applied axial load, and

$$(I_0, I_1, I_2) = \sum_{k=1}^L \int_{z_k}^{z_{k+1}} (1, z, z^2) \rho_0^{(k)} dz \quad (4.4.1d)$$

For a general lamination scheme, the three equations are fully coupled. In the case of cross-ply laminates, the second equation becomes uncoupled from the rest. In the general case, Eqs. (4.4.1a-c) can be expressed in an alternative form by solving the first two equations for u'' and v'' and substituting the results into the third equation

$$\begin{aligned} A \frac{\partial^2 u_0}{\partial x^2} = B \frac{\partial^3 w_0}{\partial x^3} + A_{66} \frac{\partial N_{xy}^T}{\partial x} - A_{16} \frac{\partial N_{xy}^T}{\partial x} + A_{66} I_0 \frac{\partial^2 u_0}{\partial t^2} - A_{16} I_0 \frac{\partial^2 v_0}{\partial t^2} \\ - A_{66} I_1 \frac{\partial^3 w_0}{\partial x \partial t^2} \end{aligned} \quad (4.4.2a)$$

$$\begin{aligned} A \frac{\partial^2 v_0}{\partial x^2} = C \frac{\partial^3 w_0}{\partial x^3} + A_{11} \frac{\partial N_{xy}^T}{\partial x} - A_{16} \frac{\partial N_{xy}^T}{\partial x} + A_{11} I_0 \frac{\partial^2 v_0}{\partial t^2} - A_{16} I_0 \frac{\partial^2 u_0}{\partial t^2} \\ + A_{16} I_1 \frac{\partial^3 w_0}{\partial x \partial t^2} \end{aligned} \quad (4.4.2b)$$

$$\begin{aligned} D \frac{\partial^4 w_0}{\partial x^4} = \bar{B} \frac{\partial^2 N_{xx}^T}{\partial x^2} + \bar{C} \frac{\partial^2 N_{xy}^T}{\partial x^2} - (I_1 - \bar{B} I_0) \frac{\partial^3 u_0}{\partial x \partial t^2} + \bar{C} I_0 \frac{\partial^3 v_0}{\partial x \partial t^2} - I_0 \frac{\partial^2 w_0}{\partial t^2} \\ + (I_2 - \bar{B} I_1) \frac{\partial^4 w_0}{\partial x^2 \partial t^2} - \frac{\partial^2 M_{xx}^T}{\partial x^2} + \frac{\partial}{\partial x} \left(\hat{N}_{xx} \frac{\partial w_0}{\partial x} \right) + q \end{aligned} \quad (4.4.2c)$$

where

$$\begin{aligned} A = A_{11} A_{66} - A_{16} A_{16}, \quad B = B_{11} A_{66} - B_{16} A_{16}, \quad C = A_{11} B_{16} - A_{16} B_{11} \\ D = D_{11} - B_{11} \bar{B} - B_{16} \bar{C}, \quad \bar{B} = \frac{B}{A}, \quad \bar{C} = \frac{C}{A} \end{aligned} \quad (4.4.2d)$$

Note that $C = 0$ for a cross-ply laminate ($A_{16} = B_{16} = D_{16} = 0$), and v is identically zero unless N_{xy}^T is at least a linear function of x .

If the in-plane inertias are neglected, Eq. (4.4.2c) for w_0 is uncoupled from those of u_0 and v_0 . In the absence of thermal forces and axial loads, Eq. (4.4.2c) will have the same form as Eq. (4.2.8b). Therefore, the solutions developed in Sections 4.2.2 through 4.2.4 are also valid for cylindrical bending with appropriate change of the coefficients.

4.4.2 Bending

For static bending analysis, Eqs. (4.4.2a-c) reduce to

$$A \frac{d^2 u_0}{dx^2} = B \frac{d^3 w_0}{dx^3} + A_{66} \frac{dN_{xx}^T}{dx} - A_{16} \frac{dN_{xy}^T}{dx} \quad (4.4.3a)$$

$$A \frac{d^2 v_0}{dx^2} = C \frac{d^3 w_0}{dx^3} + A_{11} \frac{dN_{xy}^T}{dx} - A_{16} \frac{dN_{xx}^T}{dx} \quad (4.4.3b)$$

$$D \frac{d^4 w_0}{dx^4} = \bar{B} \frac{d^2 N_{xx}^T}{dx^2} + \bar{C} \frac{d^2 N_{xy}^T}{dx^2} - \frac{d^2 M_{xx}^T}{dx^2} + q \quad (4.4.3c)$$

Equation (4.4.3c) governing w_0 is uncoupled from those governing (u_0, v_0) . Equation (4.4.3c) closely resembles that for symmetrically laminated beams [see Eq. (4.2.10b)]. While Eq. (4.4.3c) is valid for more general laminates (symmetric as well as nonsymmetric), it differs from Eq. (4.2.10b) mainly in the bending stiffness term. Hence, much of the discussion presented in Section 4.2 on exact solutions applies to Eq. (4.4.3c). The limitation on the lamination scheme in cylindrical bending comes from the boundary conditions on all three displacements of the problem. When both edges are simply supported or clamped, exact solutions can be developed without any restrictions on the lamination scheme. For clamped-free laminated plate strips, satisfaction of the boundary conditions places a restriction on the lamination scheme, as will be seen shortly.

Since Eq. (4.4.3c) is uncoupled from Eqs. (4.4.3a,b), it can be integrated, for given thermal and mechanical loads, to obtain $w_0(x)$, and the result can be used in Eqs. (4.4.3a) and (4.4.3b) to determine $u_0(x)$ and $v_0(x)$:

$$D \frac{d^3 w_0}{dx^3} = \bar{B} \frac{dN_{xx}^T}{dx} + \bar{C} \frac{dN_{xy}^T}{dx} - \frac{dM_{xx}^T}{dx} + \int_0^x q(\xi) d\xi + c_1 \quad (4.4.4a)$$

$$A \frac{d^2 u_0}{dx^2} = \hat{B} \int_0^x q(\xi) d\xi + G_1 \frac{dN_{xx}^T}{dx} + F_1 \frac{dN_{xy}^T}{dx} - \hat{B} \frac{dM_{xx}^T}{dx} + a_1 \quad (4.4.4b)$$

$$A \frac{d^2 v_0}{dx^2} = \hat{C} \int_0^x q(\xi) d\xi + G_2 \frac{dN_{xx}^T}{dx} + F_2 \frac{dN_{xy}^T}{dx} - \hat{C} \frac{dM_{xx}^T}{dx} + b_1 \quad (4.4.4c)$$

where

$$G_1 = \frac{\bar{B}B}{D} + A_{66}, \quad F_1 = \frac{\bar{B}B}{D} - A_{16}, \quad \hat{B} = \frac{B}{D}$$

$$G_2 = \frac{\bar{B}C}{D} - A_{16}, \quad F_2 = \frac{\bar{B}C}{D} + A_{11}, \quad \hat{C} = \frac{C}{D}$$

$$a_1 = \hat{B}c_1, \quad b_1 = \hat{C}c_1 \quad (4.4.5)$$

Further integrations lead to

$$A \frac{du_0}{dx} = \hat{B} \int_0^x \left(\int_0^\xi q(\eta) d\eta \right) d\xi + G_1 N_{xx}^T + F_1 N_{xy}^T - \hat{B} M_{xx}^T + a_1 x + a_2 \quad (4.4.6a)$$

$$A \frac{dv_0}{dx} = \hat{C} \int_0^x \left(\int_0^\xi q(\eta) d\eta \right) d\xi + G_2 N_{xx}^T + F_2 N_{xy}^T - \hat{C} M_{xx}^T + b_1 x + b_2 \quad (4.4.6b)$$

$$D \frac{d^2 w_0}{dx^2} = \bar{B} N_{xx}^T + \bar{C} N_{xy}^T - M_{xx}^T + \int_0^x \left(\int_0^\xi q(\eta) d\eta \right) d\xi + c_1 x + c_2 \quad (4.4.6c)$$

and

$$\begin{aligned} Au_0(x) &= \hat{B} \int_0^x \left[\int_0^\xi \left(\int_0^\eta q(\zeta) d\zeta \right) d\eta \right] d\xi + G_1 \int_0^x N_{xx}^T(\xi) d\xi + F_1 \int_0^x N_{xy}^T(\xi) d\xi \\ &\quad - \hat{B} \int_0^x M_{xx}^T(\xi) d\xi + a_1 \frac{x^2}{2} + a_2 x + a_3 \end{aligned} \quad (4.4.7a)$$

$$\begin{aligned} Av_0(x) &= \hat{C} \int_0^x \left[\int_0^\xi \left(\int_0^\eta q(\zeta) d\zeta \right) d\eta \right] d\xi + G_2 \int_0^x N_{xx}^T(\xi) d\xi + F_2 \int_0^x N_{xy}^T(\xi) d\xi \\ &\quad - \hat{C} \int_0^x M_{xx}^T(\xi) d\xi + b_1 \frac{x^2}{2} + b_2 x + b_3 \end{aligned} \quad (4.4.7b)$$

$$\begin{aligned} D \frac{dw_0}{dx} &= \int_0^x \left[\int_0^\xi \left(\int_0^\eta q(\zeta) d\zeta \right) d\eta \right] d\xi + \bar{B} \int_0^x N_{xx}^T(\xi) d\xi + \bar{C} \int_0^x N_{xy}^T(\xi) d\xi \\ &\quad - \int_0^x M_{xx}^T(\xi) d\xi + c_1 \frac{x^2}{2} + c_2 x + c_3 \end{aligned} \quad (4.4.7c)$$

$$\begin{aligned} Dw_0(x) &= \int_0^x \left\{ \int_0^\xi \left[\int_0^\eta \left(\int_0^\zeta q(\mu) d\mu \right) d\zeta \right] d\eta \right\} d\xi + \bar{B} \int_0^x \left(\int_0^\xi N_{xx}^T(\eta) d\eta \right) d\xi \\ &\quad + \bar{C} \int_0^x \left(\int_0^\xi N_{xy}^T(\eta) d\eta \right) d\xi - \int_0^x \left(\int_0^\xi M_{xx}^T(\eta) d\eta \right) d\xi \\ &\quad + c_1 \frac{x^3}{6} + c_2 \frac{x^2}{2} + c_3 x + c_4 \end{aligned} \quad (4.4.7d)$$

If the temperature distribution in the laminate is of the form

$$\Delta T(x, z) = T_0 + z T_1 \quad (4.4.8)$$

where T_0 and T_1 are constants, then we have

$$\begin{aligned} N_{xx}^T &= \sum_{k=1}^L \int_{z_k}^{z_{k+1}} (\bar{Q}_{11}\alpha_{xx} + \bar{Q}_{12}\alpha_{yy} + 2\bar{Q}_{16}\alpha_{xy})^{(k)} \Delta T dz \\ &= A_1^T T_0 + B_1^T T_1 \end{aligned} \quad (4.4.9a)$$

$$\begin{aligned} N_{xy}^T &= \sum_{k=1}^L \int_{z_k}^{z_{k+1}} (\bar{Q}_{16}\alpha_{xx} + \bar{Q}_{26}\alpha_{yy} + 2\bar{Q}_{66}\alpha_{xy})^{(k)} \Delta T dz \\ &= A_6^T T_0 + B_6^T T_1 \end{aligned} \quad (4.4.9b)$$

$$\begin{aligned} M_{xx}^T &= \sum_{k=1}^L \int_{z_k}^{z_{k+1}} (\bar{Q}_{11}\alpha_{xx} + \bar{Q}_{12}\alpha_{yy} + 2\bar{Q}_{16}\alpha_{xy})^{(k)} \Delta T z dz \\ &= B_1^T T_0 + D_1^T T_1 \end{aligned} \quad (4.4.9c)$$

where

$$\begin{aligned} A_j^T &= \sum_{k=1}^L \int_{z_k}^{z_{k+1}} (\bar{Q}_{j1}\alpha_{xx} + \bar{Q}_{j2}\alpha_{yy} + 2\bar{Q}_{j6}\alpha_{xy})^{(k)} dz \\ B_j^T &= \sum_{k=1}^L \int_{z_k}^{z_{k+1}} (\bar{Q}_{j1}\alpha_{xx} + \bar{Q}_{j2}\alpha_{yy} + 2\bar{Q}_{j6}\alpha_{xy})^{(k)} z dz \\ D_j^T &= \sum_{k=1}^L \int_{z_k}^{z_{k+1}} (\bar{Q}_{j1}\alpha_{xx} + \bar{Q}_{j2}\alpha_{yy} + 2\bar{Q}_{j6}\alpha_{xy})^{(k)} z^2 dz \end{aligned} \quad (4.4.10)$$

In addition, if $q = q_0$, expressions in Eqs. (4.4.7) become

$$\begin{aligned} Au_0(x) &= \hat{B}q_0 \frac{x^3}{6} + G_1 (A_1^T T_0 + B_1^T T_1) x + F_1 (A_6^T T_0 + B_6^T T_1) x \\ &\quad - \hat{B} (B_1^T T_0 + D_1^T T_1) x + a_1 \frac{x^2}{2} + a_2 x + a_3 \\ &\equiv \hat{B}q_0 \frac{x^3}{6} + a_1 \frac{x^2}{2} + \hat{a}_2 x + a_3 \end{aligned} \quad (4.4.11a)$$

$$\begin{aligned} Av_0(x) &= \hat{C}q_0 \frac{x^3}{6} + G_2 (A_1^T T_0 + B_1^T T_1) x + F_2 (A_6^T T_0 + B_6^T T_1) x \\ &\quad - \hat{C} (B_1^T T_0 + D_1^T T_1) x + b_1 \frac{x^2}{2} + b_2 x + b_3 \\ &\equiv \hat{C}q_0 \frac{x^3}{6} + b_1 \frac{x^2}{2} + \hat{b}_2 x + b_3 \end{aligned} \quad (4.4.11b)$$

$$\begin{aligned} Dw_0(x) &= q_0 \frac{x^4}{24} + \bar{B} (A_1^T T_0 + B_1^T T_1) \frac{x^2}{2} + \bar{C} (A_6^T T_0 + B_6^T T_1) \frac{x^2}{2} \\ &\quad - (B_1^T T_0 + D_1^T T_1) \frac{x^2}{2} + c_1 \frac{x^3}{6} + c_2 \frac{x^2}{2} + c_3 x + c_4 \\ &\equiv q_0 \frac{x^4}{24} + c_1 \frac{x^3}{6} + \hat{c}_2 \frac{x^2}{2} + c_3 x + c_4 \end{aligned} \quad (4.4.11c)$$

The constants of integration a_i , b_i , and c_i can be determined using the boundary conditions.

The in-plane stresses in each layer can be computed using the constitutive equations, and the transverse stresses can be determined using equilibrium equations of 3-D elasticity [see Eqs. (4.2.13) and (4.2.14)]. For a cross-ply laminate the only nonzero strain is ε_{xx} .

Example 4.4.1 (Simply supported plate strip):

For a plate strip with simply supported edges at $x = 0$ and $x = a$, the boundary conditions are (see Table 4.4.1)

$$N_{xx} = 0, \quad w_0 = 0, \quad M_{xx} = 0 \quad (4.4.12)$$

where

$$N_{xx} = A_{11} \frac{du_0}{dx} + A_{16} \frac{dv_0}{dx} - B_{11} \frac{d^2w_0}{dx^2} - N_{xx}^T \quad (4.4.13a)$$

$$N_{yy} = A_{12} \frac{du_0}{dx} + A_{26} \frac{dv_0}{dx} - B_{12} \frac{d^2w_0}{dx^2} - N_{yy}^T \quad (4.4.13b)$$

$$N_{xy} = A_{16} \frac{du_0}{dx} + A_{66} \frac{dv_0}{dx} - B_{16} \frac{d^2w_0}{dx^2} - N_{xy}^T \quad (4.4.13c)$$

$$M_{xx} = B_{11} \frac{du_0}{dx} + B_{16} \frac{dv_0}{dx} - D_{11} \frac{d^2w_0}{dx^2} - M_{xx}^T \quad (4.4.14a)$$

$$M_{yy} = B_{12} \frac{du_0}{dx} + B_{26} \frac{dv_0}{dx} - D_{12} \frac{d^2w_0}{dx^2} - M_{yy}^T \quad (4.4.14b)$$

$$M_{xy} = B_{16} \frac{du_0}{dx} + B_{66} \frac{dv_0}{dx} - D_{16} \frac{d^2w_0}{dx^2} - M_{xy}^T \quad (4.4.14c)$$

From Eqs. (4.4.12), (4.4.13a), and (4.4.14a) it follows that, for an arbitrary lamination scheme and $dv_0/dx = 0$, we must have at $x = 0, a$

$$w_0 = 0, \quad \frac{du_0}{dx} = \hat{N}_{xx}^T, \quad \frac{dv_0}{dx} = 0, \quad \frac{d^2w_0}{dx^2} = \hat{M}_{xx}^T \quad (4.4.15a)$$

$$\hat{N}_{xx}^T = \frac{D_{11}N_{xx}^T - B_{11}M_{xx}^T}{A_{11}D_{11} - B_{11}B_{11}}, \quad \hat{M}_{xx}^T = \frac{B_{11}N_{xx}^T - A_{11}M_{xx}^T}{A_{11}D_{11} - B_{11}B_{11}} \quad (4.4.15b)$$

Since only the derivatives of u_0 and v_0 are specified at the boundary points, the solution for u_0 and v_0 can be determined only with an arbitrary constant (i.e., rigid body motion is not eliminated).

Using boundary conditions (4.4.15) in Eq. (4.4.11a-c), we obtain

$$u_0(x) = \frac{B}{AD} \frac{q_0 a^3}{12} \left[2 \left(\frac{x}{a} \right)^3 - 3 \left(\frac{x}{a} \right)^2 \right] + \hat{N}_{xx}^T x + a_3 \quad (4.4.16a)$$

$$v_0(x) = \frac{C}{AD} \frac{q_0 a^3}{12} \left[2 \left(\frac{x}{a} \right)^3 - 3 \left(\frac{x}{a} \right)^2 \right] + b_3 \quad (4.4.16b)$$

$$\begin{aligned} w_0(x) = & \frac{q_0 a^4}{24D} \left[\left(\frac{x}{a} \right)^4 - 2 \left(\frac{x}{a} \right)^3 + \left(\frac{x}{a} \right)^2 \right] \\ & + \frac{\hat{M}_{xx}^T a^2}{2} \left[\left(\frac{x}{a} \right)^2 - \left(\frac{x}{a} \right) \right] \end{aligned} \quad (4.4.16c)$$

where the constants a_3 and b_3 can be interpreted as rigid body displacements. The constants can be determined by setting $u_0(0) = 0$ and $v_0(0) = 0$, which give $a_3 = b_3 = 0$.

The stress resultants for any x are then given by substituting Eqs. (4.4.16) into Eqs. (4.4.13) and (4.4.14):

$$N_{xx} = 0, \quad N_{xy} = A_{16} \hat{N}_{xx}^T - B_{16} \hat{M}_{xx}^T - N_{xy}^T \quad (4.4.17a)$$

$$\begin{aligned} N_{yy} = & \frac{q_0 a^2}{2AD} (A_{12}B + A_{26}C - B_{12}A) \left[\left(\frac{x}{a} \right)^2 - \left(\frac{x}{a} \right) \right] \\ & + A_{16} \hat{N}_{xx}^T - B_{16} \hat{M}_{xx}^T \end{aligned} \quad (4.4.17b)$$

$$M_{xx} = \frac{q_0 a^2}{2} \left[\left(\frac{x}{a} \right)^2 - \left(\frac{x}{a} \right) \right] \quad (4.4.17c)$$

$$\begin{aligned} M_{xy} = & \frac{q_0 a^2}{2AD} (B_{16}B + B_{66}C - D_{16}A) \left[\left(\frac{x}{a} \right)^2 - \left(\frac{x}{a} \right) \right] \\ & + B_{16} \hat{N}_{xx}^T - D_{16} \hat{M}_{xx}^T - M_{xy}^T \end{aligned} \quad (4.4.17d)$$

$$\begin{aligned} M_{yy} = & \frac{q_0 a^2}{2AD} (B_{12}B + B_{26}C - D_{12}A) \left[\left(\frac{x}{a} \right)^2 - \left(\frac{x}{a} \right) \right] \\ & + B_{12} \hat{N}_{xx}^T - D_{12} \hat{M}_{xx}^T - M_{yy}^T \end{aligned} \quad (4.4.17e)$$

The maximum transverse deflection occurs at $x = a/2$, and it is given by

$$w_{max} = \frac{5q_0 a^4}{384D} - \frac{\hat{M}_{xx}^T a^2}{8} \quad (4.4.18)$$

In order to see the effect of the bending-stretching coupling on the transverse deflection, the reciprocal of the bending stiffness D [see Eq. (4.4.2d)] is expressed as

$$\frac{1}{D} = \frac{1}{D_{11}} \left(\frac{D_{11}}{D} \right) = \frac{1}{D_{11}} \left(\frac{D + B_{11}\bar{B} + B_{16}\bar{C}}{D} \right)$$

Hence, the maximum deflection can be expressed in the form

$$w_{max} = \frac{5q_0 a^4}{384D_{11}} \left(1 + \frac{B_{11}\bar{B} + B_{16}\bar{C}}{D} \right) - \frac{\hat{M}_{xx}^T a^2}{8} \quad (4.4.19)$$

For symmetric laminates the coupling terms are zero, and the maximum deflection is given by

$$w_{max} = \frac{5q_0 a^4}{384D_{11}} - \frac{\hat{M}_{xx}^T a^2}{8} \quad (4.4.20)$$

It can be shown that the expression $B_{11}\bar{B} + B_{16}\bar{C}$ is always positive. Therefore, it follows that the effect of the coupling is to increase the maximum transverse deflection of the plate strip. For example, for antisymmetric cross-ply laminates, we have $A_{16} = A_{26} = B_{16} = B_{26} = D_{16} = D_{26} = 0$, $\bar{B} = B_{11}/A_{11}$, $\bar{C} = 0$, and $D = D_{11} - B_{11}^2/A_{11}$. Thus the maximum deflection becomes

$$w_{max} = -\frac{5q_0 a^4}{384D_{11}} \left(1 + \frac{B_{11}^2}{A_{11}D_{11} - B_{11}^2} \right) - \frac{\hat{M}_{xx}^T a^2}{8} \quad (4.4.21)$$

In the case of antisymmetric angle-ply laminates, we have $A_{16} = A_{26} = B_{11} = B_{22} = B_{12} = B_{66} = D_{16} = D_{26} = 0$, $\bar{B} = 0$, $\bar{C} = B_{16}/A_{66}$, and $D = D_{11} - B_{16}^2/A_{66}$. The maximum deflection becomes

$$w_{max} = \frac{5q_0 a^4}{384D_{11}} \left(1 + \frac{B_{16}^2}{A_{66}D_{11} - B_{16}^2} \right) - \frac{\hat{M}_{xx}^T a^2}{8} \quad (4.4.22)$$

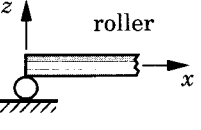
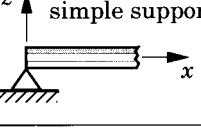
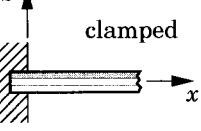
Note that when the bending-stretching coupling terms are zero (e.g., for symmetric laminates), the cylindrical bending and laminated beam solutions have the same form. The difference is only in the bending stiffness term. The bending stiffness D_{11} used in cylindrical bending is given by

$$D_{11} = \frac{E_{xx}^b h^3}{12(1 - \nu_{xy}^b \nu_{yx}^b)} = \frac{E_{xx}^b h^3}{12[1 - (\nu_{xy}^b)^2(E_{xx}^b/E_{yy}^b)]} \quad (4.4.23)$$

whereas the bending stiffness used in the beam theory is $E_{xx}^b I_{yy} = E_{xx}^b b h^3/12$. Thus, the difference is in the expression containing Poisson's ratios, which is due to the plane strain assumption used in cylindrical bending compared to the plane stress assumption used in the beam theory. The difference between the two solutions will be the most for laminates containing angle-ply layers, where ν_{xy}^b can be very large.

Analytical solutions for beams under uniform transverse load with other boundary conditions may be obtained from Eqs. (4.4.11a-c). For loads other than uniformly distributed transverse load, one must use Eqs. (4.4.7a-d).

Table 4.4.1: Boundary conditions in the classical (CLPT) and first-order shear deformation (FSDT) theories of beams and plate strips. The boundary conditions on u_0 and v_0 are only for laminated strips in cylindrical bending.

Edge Condition	CLPT		FSDT	
 free	$N_{xx}=0$	$N_{xy}=0$	$N_{xx}=0$	$N_{xy}=0$
	$M_{xx}=0$	$\frac{dM_{xx}}{dx}=0$	$M_{xx}=0$	$Q_x=0$
 roller	$w_0=0$	$\frac{dv_0}{dx}=0$	$w_0=0$	$\frac{dv_0}{dx}=0$
	$N_{xx}=0$	$M_{xx}=0$	$N_{xx}=0$	$M_{xx}=0$
 simple support	$u_0=0$	$w_0=0$	$u_0=0$	$w_0=0$
	$\frac{dv_0}{dx}=0$	$M_{xx}=0$	$\frac{dv_0}{dx}=0$	$M_{xx}=0$
 clamped	$u_0=0$	$v_0=0$	$u_0=0$	$v_0=0$
	$w_0=0$	$\frac{dw_0}{dx}=0$	$w_0=0$	$\phi_x=0$

4.4.3 Buckling

The equilibrium of the plate strip under the applied in-plane compressive load $\hat{N}_{xx} = -N_{xx}^0$ can be obtained from Eqs. (4.4.2a-c) by omitting the inertia terms and thermal resultants

$$A \frac{d^2U}{dx^2} = B \frac{d^3W}{dx^3} \quad (4.4.24)$$

$$A \frac{d^2V}{dx^2} = C \frac{d^3W}{dx^3} \quad (4.4.25)$$

$$D \frac{d^4W}{dx^4} = -N_{xx}^0 \frac{d^2W}{dx^2} \quad (4.4.26)$$

where (U, V, W) denote the displacements measured from the prebuckling equilibrium state.

Equation (4.4.26), which is uncoupled from (4.4.24) and (4.4.25), can be integrated twice with respect to x to obtain

$$D \frac{d^2W}{dx^2} + N_{xx}^0 W = K_1 x + K_2 \quad (4.4.27)$$

where K_1 and K_2 are constants. The general solution of Eq. (4.4.27) is

$$W(x) = c_1 \sin \lambda x + c_2 \cos \lambda x + c_3 x + c_4 \quad (4.4.28)$$

where $c_3 = K_1/\lambda^2$, $c_4 = K_2/\lambda^2$, and

$$\lambda^2 = \frac{N_{xx}^0}{D} \quad \text{or} \quad N_{xx}^0 = D\lambda^2 \quad (4.4.29)$$

The three of the four constants c_1, c_2, c_3, c_4 , and λ are determined using (four) boundary conditions of the problem. Once λ is known, the buckling load can be determined using Eq. (4.4.29). The results of Section 4.2.3 are applicable here with $b = 1$ and $E_{xx}^b I_{yy} = D$. Here we consider only the case of simply supported boundary conditions for illustrative purposes.

Example 4.4.2:

When the plate strip is simply supported at $x = 0, a$, from Eq. (4.4.15a) we have

$$W = 0, \quad \frac{dU}{dx} = 0, \quad \frac{dV}{dx} = 0, \quad \frac{d^2W}{dx^2} = 0 \quad (4.4.30)$$

Use of the boundary conditions on W gives $c_2 = c_3 = c_4 = 0$ and the result

$$\sin \lambda a \equiv \sin \left(\sqrt{\frac{N_{xx}^0}{D}} \right) = 0, \quad \text{or} \quad N_{xx}^0 = D \left(\frac{n\pi}{a} \right)^2 \quad (4.4.31)$$

The critical buckling load N_{cr} is given by ($n = 1$)

$$N_{cr} = D_{11} \frac{\pi^2}{a^2} \left(1 - \frac{B_{11}\bar{B} + B_{16}\bar{C}}{D_{11}A} \right) \quad (4.4.32)$$

Thus the effect of the bending-extensional coupling is to decrease the critical buckling load.

Recall from Section 4.2.3 that when both edges are clamped, λ is determined by solving the equation

$$\lambda a \sin \lambda a + 2 \cos \lambda a - 2 = 0 \quad (4.4.33)$$

The smallest root of this equation is $\lambda = 2\pi$, and the critical buckling load becomes

$$N_{cr} = D_{11} \frac{4\pi^2}{a^2} \left(1 - \frac{B_{11}\bar{B} + B_{16}\bar{C}}{D_{11}A} \right) \quad (4.4.34)$$

4.4.4 Vibration

For vibration in the absence of in-plane inertias, thermal forces, and transverse load, Eq. (4.4.2c) is reduced to

$$D \frac{\partial^4 w_0}{\partial x^4} = \bar{I}_2 \frac{\partial^4 w_0}{\partial x^2 \partial t^2} - I_0 \frac{\partial^2 w_0}{\partial t^2} + \hat{N}_{xx} \frac{\partial^2 w_0}{\partial x^2} \quad (4.4.35)$$

where $\bar{I}_2 = I_2 - \bar{B}I_1$. For a periodic motion, we assume

$$w_0(x, t) = W(x)e^{i\omega t}, \quad i = \sqrt{-1} \quad (4.4.36)$$

where ω is the natural frequency of vibration. Then Eq. (4.4.35) becomes

$$D \frac{d^4 W}{dx^4} - \hat{N}_{xx} \frac{d^2 W}{dx^2} = I_0 \omega^2 W - \bar{I}_2 \omega^2 \frac{d^2 W}{dx^2} \quad (4.4.37)$$

Equation (4.4.35) has the same form as Eq. (4.2.43). Hence, all of the results of Section 4.2.4 are applicable here with $b = 1$ ($\hat{I}_0 = I_0$, $\hat{I}_2 = \bar{I}_2$) and $E_{xx}^b I_{yy} = D$. We summarize the results here for completeness.

The general solution of Eq. (4.4.37) is

$$W(x) = c_1 \sin \lambda x + c_2 \cos \lambda x + c_3 \sinh \mu x + c_4 \cosh \mu x \quad (4.4.38)$$

where

$$\lambda = \sqrt{\frac{1}{2p} \left(q + \sqrt{q^2 + 4pr} \right)}, \quad \mu = \sqrt{\frac{1}{2p} \left(-q + \sqrt{q^2 + 4pr} \right)} \quad (4.4.39)$$

$$p = D, \quad q = \bar{I}_2 \omega^2 - \hat{N}_{xx}, \quad r = I_0 \omega^2 \quad (4.4.40)$$

and c_1, c_2, c_3 , and c_4 are integration constants, which are determined using the boundary conditions. For natural vibration without rotary inertia and applied axial load, the equation for $\lambda = \mu$ reduces to

$$\lambda^2 = \sqrt{r/p} \quad (4.4.41)$$

If the applied axial force is zero, the natural frequency of vibration, with rotary inertia included, is given by

$$\omega^2 = \lambda^4 \frac{D}{I_0} \left(1 - \frac{\bar{I}_2 \lambda^2}{I_0 + \bar{I}_2 \lambda^2} \right) \quad (4.4.42)$$

When rotary inertia is neglected, we have

$$\omega = \lambda^2 \sqrt{\frac{D}{I_0}} \quad (4.4.43)$$

Example 4.4.3:

For a simply supported plate strip, λ_n is given by $\lambda_n = \frac{n\pi}{a}$ and from Eq. (4.4.42) it follows that

$$\omega_n = \left(\frac{n\pi}{a} \right)^2 \sqrt{\frac{D}{I_0}} \sqrt{\frac{1}{1 + (\frac{n\pi}{a})^2 (\bar{I}_2/I_0)}} \quad (4.4.44)$$

Note that the rotary inertia has the effect of decreasing the natural frequency. When the rotary inertia is zero, we have

$$\omega_n = \left(\frac{n\pi}{a} \right)^2 \sqrt{\frac{D}{I_0}} \quad (4.4.45)$$

For a plate strip clamped at both ends, λ must be determined from [see Eqs. (4.2.56)–(4.2.60)]

$$-2 + 2 \cos \lambda a \cosh \mu a + \left(\frac{\lambda}{\mu} - \frac{\mu}{\lambda} \right) \sin \lambda a \sinh \mu a = 0 \quad (4.4.46)$$

For natural vibration without rotary inertia, Eq. (4.4.46) takes the simpler form

$$\cos \lambda a \cosh \lambda a - 1 = 0 \quad (4.4.47)$$

The roots of Eq. (4.4.47) are

$$\lambda_1 a = 4.730, \quad \lambda_2 a = 7.853, \quad \lambda_3 a = 10.996, \dots, \quad \lambda_n a \approx \left(n + \frac{1}{2}\right)\pi \quad (4.4.48)$$

In general, the roots of the transcendental equation in (4.4.46) are not the same as those of Eq. (4.4.47). If one approximates Eq. (4.4.46) as (4.4.47) (i.e., $\lambda \approx \mu$), the roots in Eq. (4.4.48) can be used to determine the natural frequencies of vibration *with rotary inertia* from Eq. (4.4.42). When rotary inertia is neglected, the frequencies are given by Eq. (4.4.43) with λ as given in Eq. (4.4.48). The frequencies obtained from Eq. (4.4.42) with the values of λ from Eq. (4.4.48) are only an approximation of the frequencies with rotary inertia.

Figure 4.4.1 contains a plot of the nondimensionalized fundamental frequency $\bar{\omega} = \omega a^2 \sqrt{I_0/E_2 h^3}$ of a simply supported plate strip with rotary inertia versus length-to-thickness ratio, a/h . For small values of a/h , rotary inertia is more significant in reducing the frequency than for thin and long plate strips.

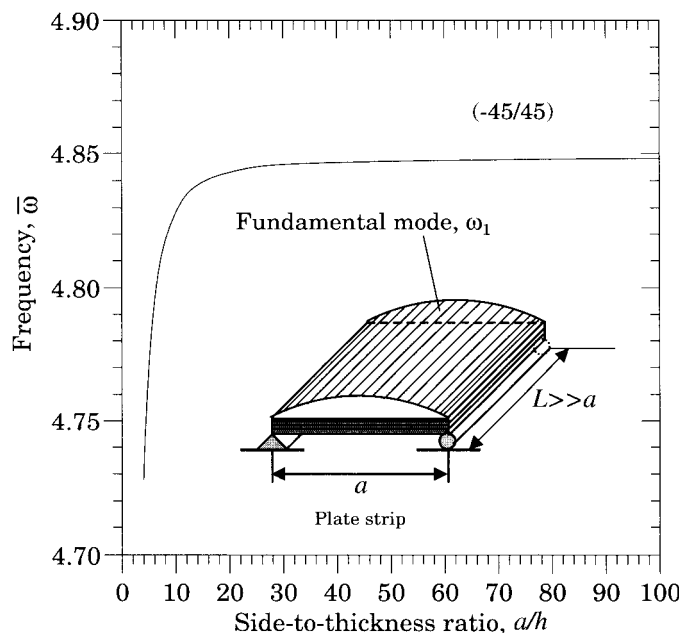


Figure 4.4.1: Effect of rotary inertia on nondimensionalized fundamental frequency of a simply supported $(-45/45)$ laminated plate strip.

Table 4.4.2 contains nondimensionalized maximum deflections, critical buckling loads, and fundamental natural frequencies of simply supported and clamped (at both ends) laminated plate strips with various lamination schemes. Compared to laminated beams (see Table 4.2.4), laminated plates in cylindrical bending undergo smaller displacements and have larger buckling loads and frequencies. This is due to the Poisson effect discussed earlier. All of the frequencies listed in Table 4.4.2 are for the case where rotary inertia is included and $a/h = 10$. The $(0/90/0)$ laminates have larger bending stiffness as well as axial stiffness compared to the $(90/0/90)$ laminates. This is because there are two 0° layers and they are placed farther from the midplane in the first laminate than in the second laminate. Hence, $(0/90/0)$ laminates undergo smaller deflections and have larger buckling loads and natural frequencies. The $(0/90)_s$ laminates have larger bending stiffness than the $(90/0)_s$ laminates; both have the same axial stiffness. The antisymmetric laminates have some of the $B_{ij} \neq 0$ and thus are relatively flexible when compared to symmetric laminates.

Figures 4.4.2 and 4.4.3 show the effect of lamination angle on maximum deflections $\bar{w} = -w_{max}(E_2 h^3/q_0 a^4)$, critical buckling load \bar{N} , and fundamental frequency $\bar{\omega}$ of two-layer antisymmetric angle-ply $(-\theta/\theta)$ plates. It should be noted that antisymmetric angle-ply laminates with more than two plies are stiffer, i.e., deflect less and carry more buckling load.

Table 4.4.2: Maximum deflections (\hat{w}) under uniform load, critical buckling loads (\bar{N}), and fundamental frequencies ($\bar{\omega}$) of laminated plate strips according to the classical laminate theory ($E_1/E_2 = 25$, $G_{12} = G_{13} = 0.5E_2$, $G_{23} = 0.2E_2$, $\nu_{12} = 0.25$).

Laminate	Hinged-Hinged			Clamped-Clamped		
	\hat{w}	\bar{N}	$\bar{\omega}$	\hat{w}	\bar{N}	$\bar{\omega}$
0	0.623	20.613	14.205	0.125	82.453	32.169
90	15.586	0.824	2.841	3.117	3.298	6.434
$(0/90/0)$	0.646	19.880	13.950	0.129	79.521	31.592
$(90/0/90)$	8.251	1.557	3.905	1.650	6.230	8.842
$(0/90)$	3.321	3.869	6.154	0.664	15.476	13.937
$(0/90)_s$	1.427	9.006	9.389	0.285	36.026	21.264
$(0/90)_s$	0.708	18.140	13.326	0.142	72.558	30.177
$(90/0)_s$	3.896	3.298	5.682	0.779	13.192	12.868
$(-45/45)$	5.396	2.382	4.828	1.079	9.526	10.935
$(-45/45)_s$	2.570	5.000	6.996	0.514	20.003	15.845
$(45/-45)_s$	2.188	5.873	7.583	0.437	23.495	17.172
Laminate A	4.035	3.185	5.584	0.807	12.740	12.645
Laminate B	0.897	14.316	11.838	0.179	57.264	26.809

$(\cdot/\cdot)_s$ = symmetric, $(\cdot/\cdot)_{as}$ = antisymmetric (four layers).

Laminate A: $(90/\pm 45/0)_s$; Laminate B: $(0/\pm 45/90)_s$.

$$\hat{w} = -w_{max}(E_2 h^3/q_0 a^4) \times 10^2, \quad \bar{N} = N_{xx}^0(a^2/E_2 h^3), \quad \bar{\omega} = \omega a^2 \sqrt{I_0/E_2 h^3}.$$

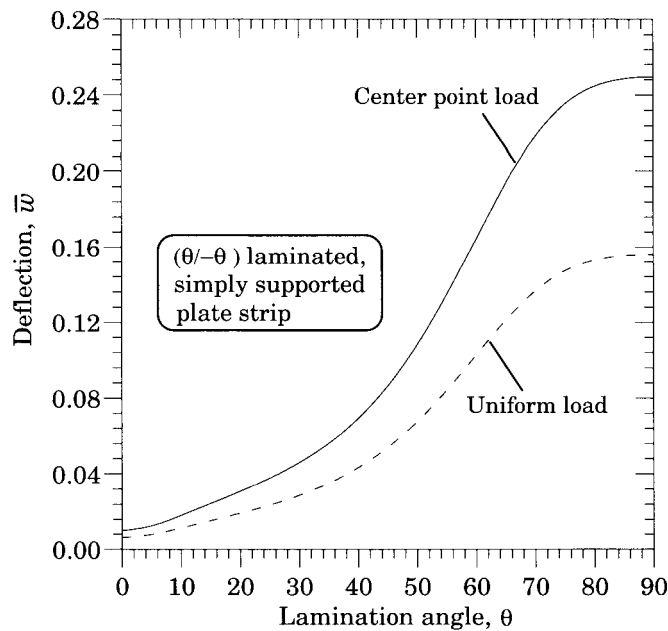


Figure 4.4.2: Nondimensionalized maximum transverse deflection (\bar{w}) versus lamination angle (θ) of a simply supported $(-\theta/\theta)$ laminated plate strip in cylindrical bending (CLPT).

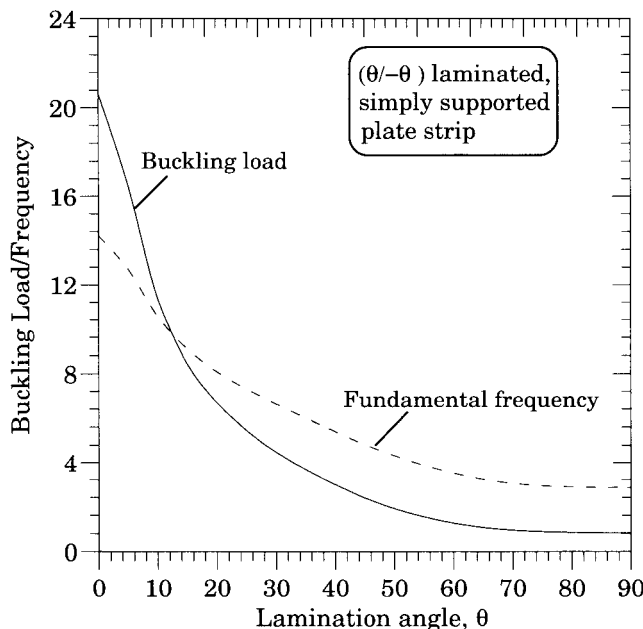


Figure 4.4.3: Nondimensionalized critical buckling load (\bar{N}) and fundamental frequency ($\bar{\omega}$) versus lamination angle (θ) of a simply supported $(-\theta/\theta)$ laminated plate strip in cylindrical bending (CLPT).

4.5 Cylindrical Bending Using FSDT

4.5.1 Governing Equations

In order to see the effect of shear deformation on bending deflections and buckling loads, we consider the equations of motion for cylindrical bending according to the first-order shear deformation theory (FSDT) [see Eqs. (3.4.23)–(3.4.27)]:

$$A_{11} \frac{\partial^2 u_0}{\partial x^2} + A_{16} \frac{\partial^2 v_0}{\partial x^2} + B_{11} \frac{\partial^2 \phi_x}{\partial x^2} + B_{16} \frac{\partial^2 \phi_y}{\partial x^2} - \frac{\partial N_{xx}^T}{\partial x} = I_0 \frac{\partial^2 u_0}{\partial t^2} + I_1 \frac{\partial^2 \phi_x}{\partial t^2} \quad (4.5.1a)$$

$$A_{16} \frac{\partial^2 u_0}{\partial x^2} + A_{66} \frac{\partial^2 v_0}{\partial x^2} + B_{16} \frac{\partial^2 \phi_x}{\partial x^2} + B_{66} \frac{\partial^2 \phi_y}{\partial x^2} - \frac{\partial N_{xy}^T}{\partial x} = I_0 \frac{\partial^2 v_0}{\partial t^2} + I_1 \frac{\partial^2 \phi_y}{\partial t^2} \quad (4.5.1b)$$

$$\begin{aligned} B_{11} \frac{\partial^2 u_0}{\partial x^2} + B_{16} \frac{\partial^2 v_0}{\partial x^2} + D_{11} \frac{\partial^2 \phi_x}{\partial x^2} + D_{16} \frac{\partial^2 \phi_y}{\partial x^2} - K A_{55} \left(\frac{\partial w_0}{\partial x} + \phi_x \right) \\ - K A_{45} \phi_y - \frac{\partial M_{xx}^T}{\partial x} = I_2 \frac{\partial^2 \phi_x}{\partial t^2} + I_1 \frac{\partial^2 u_0}{\partial t^2} \end{aligned} \quad (4.5.1c)$$

$$\begin{aligned} B_{16} \frac{\partial^2 u_0}{\partial x^2} + B_{66} \frac{\partial^2 v_0}{\partial x^2} + D_{16} \frac{\partial^2 \phi_x}{\partial x^2} + D_{66} \frac{\partial^2 \phi_y}{\partial x^2} - K A_{44} \phi_y - K A_{45} \left(\frac{\partial w_0}{\partial x} + \phi_x \right) \\ - \frac{\partial M_{xy}^T}{\partial x} = I_2 \frac{\partial^2 \phi_y}{\partial t^2} + I_1 \frac{\partial^2 v_0}{\partial t^2} \end{aligned} \quad (4.5.1d)$$

$$K A_{55} \left(\frac{\partial^2 w_0}{\partial x^2} + \frac{\partial \phi_x}{\partial x} \right) + K A_{45} \frac{\partial \phi_y}{\partial x} + \frac{\partial}{\partial x} \left(N_{xx} \frac{\partial w_0}{\partial x} \right) + q = I_0 \frac{\partial^2 w_0}{\partial t^2} \quad (4.5.1e)$$

For cylindrical bending we further assume that $\phi_y = 0$ everywhere, and omit Eq. (4.5.1d) from further consideration. For the purpose of developing analytical solutions, we neglect the in-plane inertia terms and assume that there are no thermal effects. Then Eqs. (4.5.1a-e) are simplified to

$$A_{11} \frac{\partial^2 u_0}{\partial x^2} + A_{16} \frac{\partial^2 v_0}{\partial x^2} + B_{11} \frac{\partial^2 \phi_x}{\partial x^2} = I_1 \frac{\partial^2 \phi_x}{\partial t^2} \quad (4.5.2a)$$

$$A_{16} \frac{\partial^2 u_0}{\partial x^2} + A_{66} \frac{\partial^2 v_0}{\partial x^2} + B_{16} \frac{\partial^2 \phi_x}{\partial x^2} = 0 \quad (4.5.2b)$$

$$B_{11} \frac{\partial^2 u_0}{\partial x^2} + B_{16} \frac{\partial^2 v_0}{\partial x^2} + D_{11} \frac{\partial^2 \phi_x}{\partial x^2} - K A_{55} \left(\frac{\partial w_0}{\partial x} + \phi_x \right) = I_2 \frac{\partial^2 \phi_x}{\partial t^2} \quad (4.5.2c)$$

$$K A_{55} \left(\frac{\partial^2 w_0}{\partial x^2} + \frac{\partial \phi_x}{\partial x} \right) + \frac{\partial}{\partial x} \left(N_{xx} \frac{\partial w_0}{\partial x} \right) + q = I_0 \frac{\partial^2 w_0}{\partial t^2} \quad (4.5.2d)$$

Next, we eliminate u_0 and v_0 from Eqs. (4.5.2a-c) by solving (4.5.2a) and (4.5.2b) for u_0 and v_0 in terms of ϕ_x and substituting the result into Eq. (4.5.2c):

$$K A_{55} \left(\frac{\partial^2 w_0}{\partial x^2} + \frac{\partial \phi_x}{\partial x} \right) + \hat{N}_{xx} \frac{\partial^2 w_0}{\partial x^2} + q = I_0 \frac{\partial^2 w_0}{\partial t^2} \quad (4.5.3)$$

$$D \frac{\partial^2 \phi_x}{\partial x^2} - K A_{55} \left(\frac{\partial w_0}{\partial x} + \phi_x \right) = I_2 \frac{\partial^2 \phi_x}{\partial t^2} \quad (4.5.4)$$

Equations (4.5.3) and (4.5.4) are similar to Eqs. (4.3.9a,b) for laminated beams, and therefore all developments of Section 4.3 would apply here.

4.5.2 Bending

For static analysis, Eqs. (4.5.3) and (4.5.4) reduce to

$$KA_{55} \left(\frac{d^2 w_0}{dx^2} + \frac{d\phi_x}{dx} \right) + q = 0 \quad (4.5.5a)$$

$$D \frac{d^2 \phi_x}{dx^2} - KA_{55} \left(\frac{dw_0}{dx} + \phi_x \right) = 0 \quad (4.5.5b)$$

Following the procedure of Section 4.3.2, we obtain [see Eqs. (4.3.12)–(4.3.14)] the general solution for the rotation

$$\phi_x(x) = \frac{1}{D} \left[- \int_0^x \int_0^\xi \int_0^\eta q(\zeta) d\zeta d\eta d\xi + c_1 \frac{x^2}{2} + c_2 x + c_3 \right] \quad (4.5.6)$$

and transverse deflection

$$\begin{aligned} w_0(x) = & - \frac{1}{D} \left[- \int_0^x \int_0^\xi \int_0^\eta \int_0^\mu q(\zeta) d\zeta d\mu d\eta d\xi + c_1 \frac{x^3}{6} + c_2 \frac{x^2}{2} + c_3 x + c_4 \right] \\ & + \frac{1}{KA_{55}} \left[- \int_0^x \int_0^\xi q(\zeta) d\zeta d\xi + c_1 x \right] \end{aligned} \quad (4.5.7)$$

where the constants of integration c_1 through c_4 can be determined using the boundary conditions. The solutions developed are general in the sense that they are applicable to any symmetrically laminated beams. Next we illustrate the procedure to determine the constants for beams with both edges simply supported or clamped.

Example 4.5.1 (*Simply supported beam*): _____

For a plate strip simply supported at both ends and subjected to uniformly distributed load $q = q_0$ as well as a downward point load F_0 at the center, we obtain

$$\phi_x(x) = -\frac{q_0 a^3}{24D} \left[4 \left(\frac{x}{a} \right)^3 - 6 \left(\frac{x}{a} \right)^2 + 1 \right] + \frac{F_0 a^2}{16D} \left[1 - 4 \left(\frac{x}{a} \right)^2 \right] \quad (4.5.8)$$

$$\begin{aligned} w_0(x) = & \frac{q_0 a^4}{24D} \left[\left(\frac{x}{a} \right)^4 - 2 \left(\frac{x}{a} \right)^3 + \left(\frac{x}{a} \right)^2 \right] + \frac{q_0 a^2}{2KA_{55}} \left[\left(\frac{x}{a} \right)^2 - \left(\frac{x}{a} \right)^4 \right] \\ & + \frac{F_0 a^3}{48D} \left[3 \left(\frac{x}{a} \right) - 4 \left(\frac{x}{a} \right)^3 \right] + \frac{F_0 a}{2KA_{55}} \left(\frac{x}{a} \right) \end{aligned} \quad (4.5.9)$$

The maximum deflection occurs at $x = a/2$ and it is given by

$$w_{max} = \left(\frac{5q_0 a^4}{384D} + \frac{q_0 a^2}{8KA_{55}} + \frac{F_0 a^3}{48D} + \frac{F_0 a}{4KA_{55}} \right) \quad (4.5.10)$$

Example 4.5.2 (Clamped beam):

Consider a laminated plate strip fixed at both ends and subjected to uniformly distributed transverse load q_0 and a point load F_0 at the center, both acting downward. For this case, the solution is given by

$$\begin{aligned}\phi_x(x) = & -\frac{q_0 a^3}{12D} \left[2 \left(\frac{x}{a} \right)^3 - 3 \left(\frac{x}{a} \right)^2 + \left(\frac{x}{a} \right) \right] \\ & - \frac{F_0 a^2}{8D} \left[2 \left(\frac{x}{a} \right)^2 - \left(\frac{x}{a} \right) \right]\end{aligned}\quad (4.5.11)$$

$$\begin{aligned}w_0(x) = & \frac{q_0 a^4}{24D} \left[\left(\frac{x}{a} \right)^2 - \left(\frac{x}{a} \right) \right]^2 + \frac{q_0 a^2}{2K A_{55}} \left[\left(\frac{x}{a} \right) - \left(\frac{x}{a} \right)^2 \right] \\ & + \frac{F_0 a^3}{48D} \left[3 \left(\frac{x}{a} \right)^2 - 4 \left(\frac{x}{a} \right)^3 \right] + \frac{F_0 a}{2K A_{55}} \left(\frac{x}{a} \right)\end{aligned}\quad (4.5.12)$$

The maximum deflection is given by

$$w_{max} = \left(\frac{q_0 a^4}{384D} + \frac{q_0 a^2}{8K A_{55}} + \frac{F_0 a^3}{192D} + \frac{F_0 a}{4K A_{55}} \right) \quad (4.5.13)$$

The determination of the shear correction coefficient K for laminated structures is still an unresolved issue. Values of K for various special cases are available in the literature (see [4–8]). The most commonly used value of $K = 5/6$ is based on homogeneous, isotropic plates (see Section 3.4), although K depends, in general, on the lamination scheme, geometry, and material properties.

Figure 4.5.1 shows the effect of shear deformation, shear correction coefficient, and lamination scheme on nondimensionalized deflections $\bar{w} = w_{max}(E_2 h^3 / q_0 a^4)$ of simply supported, cross-ply (0/90) and angle-ply (45/-45) laminates under uniformly distributed load. The shear correction factor has little influence on the global response for the antisymmetric laminates analyzed. The effect of shear deformation is to increase the deflections, especially for $a/h \leq 10$. Antisymmetric angle-ply laminates are relatively more flexible than antisymmetric cross-ply laminates.

Figure 4.5.2 contains plots of nondimensionalized maximum deflection versus length-to-height ratio for two-layer antisymmetric cross-ply (0/90) and angle-ply (45/-45) laminates ($K = 5/6$) under uniformly distributed load and with simply supported edges as well as for clamped edges. For clamped boundary conditions, shear deformation is relatively more significant for $a/h \leq 10$. The effect of orthotropy on deflections is shown in Figure 4.5.3 ($G_{12} = G_{13} = 0.5E_2$, $G_{23} = 0.2E_2$, $\nu_{12} = 0.25$, and $K = 5/6$).

4.5.3 Buckling

For stability analysis, we set $q = 0$, $\hat{N}_{xx} = -N_{xx}^0$, and $I_0 = I_2 = 0$ in Eqs. (4.5.3) and (4.5.4):

$$K A_{55} \left(\frac{d^2 W}{dx^2} + \frac{d\mathcal{X}}{dx} \right) + \hat{N}_{xx} \frac{d^2 W}{dx^2} = 0 \quad (4.5.14a)$$

$$D \frac{d^2 \mathcal{X}}{dx^2} - K A_{55} \left(\frac{dW}{dx} + \mathcal{X} \right) = 0 \quad (4.5.14b)$$

Following the procedure of Section 4.3.3, we obtain

$$\frac{d\mathcal{X}}{dx} = - \left(1 - \frac{N_{xx}^0}{K A_{55}} \right) \frac{d^2 W}{dx^2} \quad (4.5.15)$$

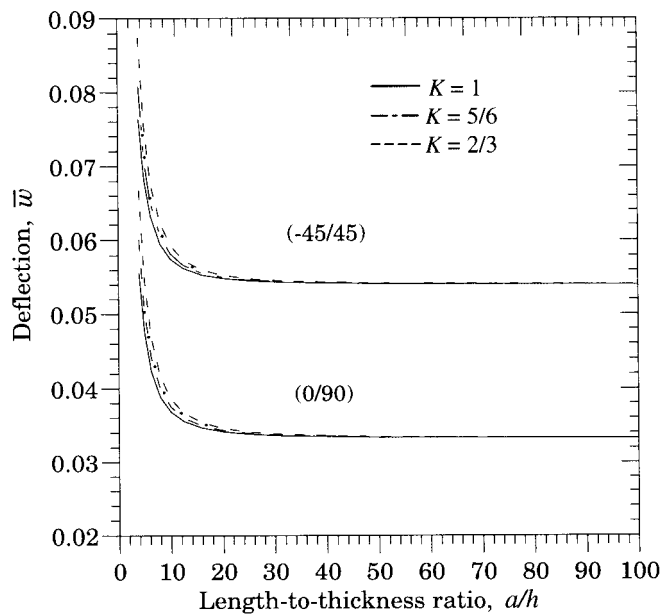


Figure 4.5.1: Transverse deflection (\bar{w}) versus length-to-thickness ratio (a/h) of simply supported plate strips ($K = 1.0, 5/6, 2/3$).

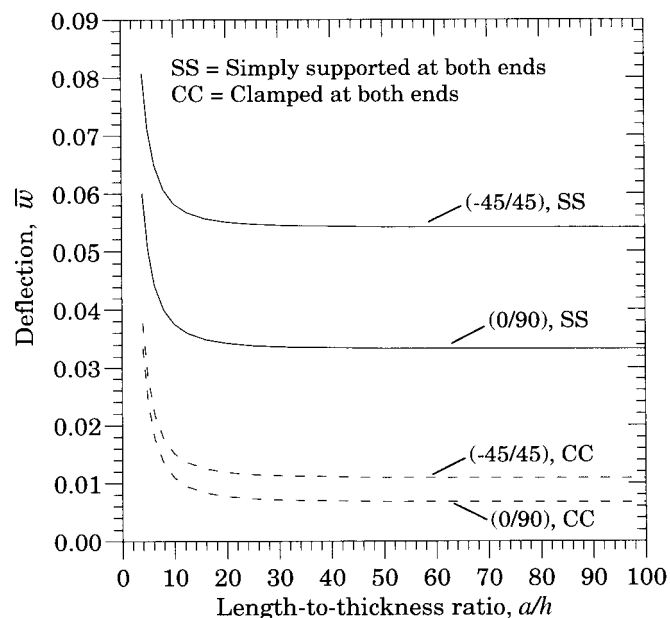


Figure 4.5.2: Transverse deflection (\bar{w}) versus length-to-thickness ratio (a/h) of simply supported (SS) and clamped (CC) plate strips.

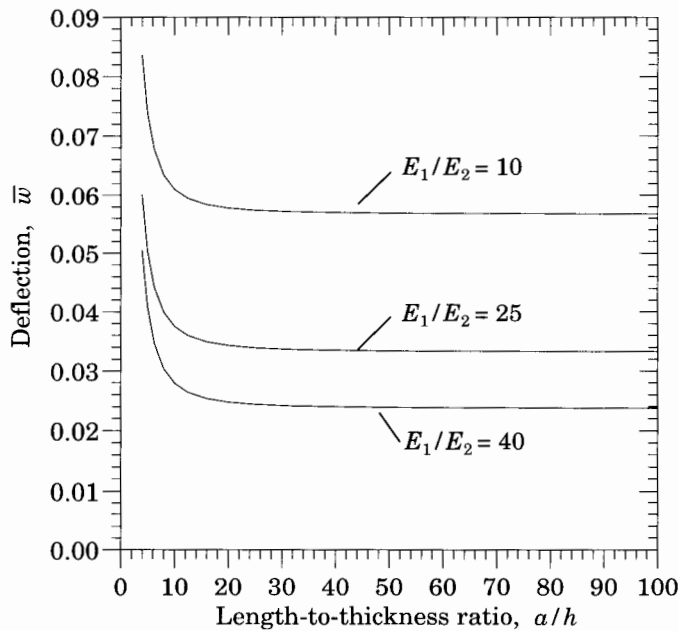


Figure 4.5.3: The effect of material orthotropy and shear deformation on transverse deflections \bar{w} of simply supported cross-ply (0/90) laminated plate strips under uniformly distributed load.

$$\mathcal{X}(x) = - \left(1 - \frac{N_{xx}^0}{KA_{55}} \right) \frac{dW}{dx} + K_1 \quad (4.5.16)$$

$$D \left(1 - \frac{N_{xx}^0}{KA_{55}} \right) \frac{d^4 W}{dx^4} + N_{xx}^0 \frac{d^2 W}{dx^2} = 0 \quad (4.5.17)$$

The general solution of Eq. (4.5.17) is

$$W(x) = c_1 \sin \lambda x + c_2 \cos \lambda x + c_3 x + c_4 \quad (4.5.18)$$

where

$$\lambda^2 = \frac{N_{xx}^0}{\left(1 - \frac{N_{xx}^0}{KA_{55}} \right) D} \quad \text{or} \quad N_{xx}^0 = \frac{\lambda^2 D}{\left(1 + \frac{\lambda^2 D}{KA_{55}} \right)} \quad (4.5.19)$$

and c_1 through c_4 are constants of integration, which are evaluated using the boundary conditions.

Example 4.5.3:

For a simply supported plate strip, the critical buckling load is given by

$$N_{cr} = \left(\frac{\pi}{a} \right)^2 D \left[1 - \frac{D \left(\frac{\pi}{a} \right)^2}{KA_{55} + D \left(\frac{\pi}{a} \right)^2} \right] \quad (4.5.20)$$

Thus, the effect of the transverse shear deformation is to decrease the buckling load. Omission of the transverse shear deformation in the classical theory amounts to assuming infinite rigidity in the transverse direction (i.e., $A_{55} = G_{13} = \infty$); hence, in the classical laminate theory the structure is represented stiffer than it is.

For a plate strip fixed at both ends, λ is governed by the equation

$$2(\cos \lambda a - 1) \left(1 + \frac{\lambda^2 D}{K A_{55}} \right) + \lambda a \sin \lambda a = 0 \quad (4.5.21)$$

The roots of the equation are approximately the same as for the case in which shear deformation is neglected [see Eq. (4.2.38b)]. The first root of the equation is $\lambda_1 = 2\pi$. Hence, the critical buckling load is given by

$$N_{cr} = \left(\frac{2\pi}{a} \right)^2 D \left[1 - \frac{D \left(\frac{2\pi}{a} \right)^2}{K A_{55} + D \left(\frac{2\pi}{a} \right)^2} \right] \quad (4.5.22)$$

Figures 4.5.4 and 4.5.5 show the effect of shear deformation and modulus ratio on nondimensionalized critical buckling loads $N = N_{xx}^0(a^2/E_2 h^3)$ of two-layer antisymmetric angle-ply ($-45/45$) and cross-ply ($0/90$) plate strips ($E_1/E_2 = 25$, $G_{12} = G_{13} = 0.5E_2$, $G_{23} = 0.2E_2$, $\nu = 0.25$, $K = 5/6$). In Figure 4.5.4 results are presented for simply supported as well as clamped boundary conditions. The effect of shear deformation is significant for $a/h \leq 10$ in the case of simply supported boundary conditions, and $a/h \leq 20$ in the case of clamped boundary conditions. The effect of shear deformation is more for materials with larger modulus ratios (see Figure 4.5.5).

4.5.4 Vibration

For a periodic motion, we assume solution in the form

$$w_0(x, t) = W(x)e^{i\omega t}, \quad \phi_x(x, t) = \mathcal{X}(x)e^{i\omega t}, \quad i = \sqrt{-1}$$

where ω is the natural frequency of vibration, and $W(x)$ and $\mathcal{X}(x)$ are the mode shapes. Substitution of the above solution forms into Eqs. (4.5.3) and (4.5.4) yields [cf. Eq. (4.3.40a,b)]

$$D \frac{d^2 \mathcal{X}}{dx^2} - K A_{55} \left(\frac{dW}{dx} + \mathcal{X} \right) + I_2 \omega^2 \mathcal{X} = 0 \quad (4.5.23a)$$

$$K A_{55} \left(\frac{d^2 W}{dx^2} + \frac{d \mathcal{X}}{dx} \right) + I_0 \omega^2 W = 0 \quad (4.5.23b)$$

Following the results of Section 4.3.4, we obtain

$$p \frac{d^4 W}{dx^4} + q \frac{d^2 W}{dx^2} - r W = 0 \quad (4.5.24a)$$

where

$$p = D, \quad q = \frac{I_0 D}{K A_{55}} \omega^2, \quad r = I_0 \omega^2 \quad (4.5.24b)$$

The general solution of Eq. (4.5.24a) is

$$W(x) = c_1 \sin \lambda x + c_2 \cos \lambda x + c_3 \sinh \mu x + c_4 \cosh \mu x \quad (4.5.25a)$$

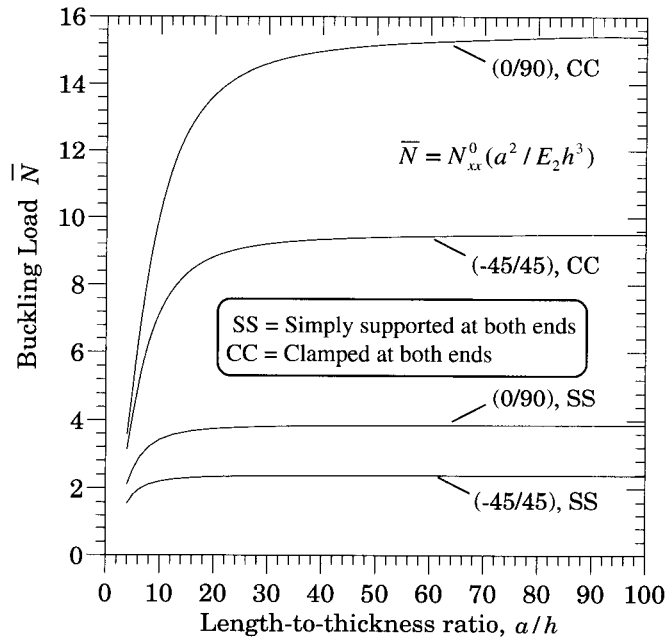


Figure 4.5.4: The effect of shear deformation on the critical buckling loads of simply supported (SS) and clamped (CC) cross-ply and angle-ply plate strips.

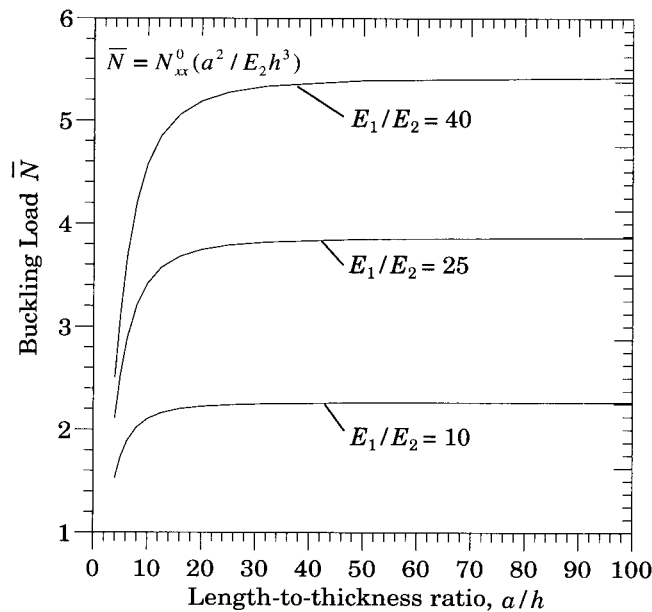


Figure 4.5.5: The effect of material orthotropy and shear deformation on critical buckling loads of simply supported cross-ply (0/90) laminated plate strips.

where

$$\lambda = \sqrt{\frac{1}{2p} \left(q + \sqrt{q^2 + 4pr} \right)}, \quad \mu = \sqrt{\frac{1}{2p} \left(-q + \sqrt{q^2 + 4pr} \right)} \quad (4.5.25b)$$

and c_1, c_2, c_3 , and c_4 are integration constants. Use of the boundary conditions leads to the determination of three of the four constants, the fourth one being arbitrary, and an equation governing λ and μ (see Section 4.3.4 for details). The frequencies ω can be determined from

$$(\omega^2)_1 = \frac{1}{2P} \left(Q - \sqrt{Q^2 - 4PR} \right), \quad (\omega^2)_2 = \frac{1}{2P} \left(Q + \sqrt{Q^2 - 4PR} \right) \quad (4.5.26a)$$

where

$$P = \frac{I_2}{KA_{55}}, \quad Q = \left[1 + \left(\frac{D}{KA_{55}} + \frac{I_2}{I_0} \right) \lambda^2 \right], \quad R = \left(\frac{D}{I_0} \right) \lambda^4 \quad (4.5.26b)$$

When the rotary inertia is neglected, we have $P = 0$ and the frequency is given by

$$\omega^2 = \frac{\bar{Q}}{R}, \quad \bar{Q} = \left[1 + \left(\frac{D}{KA_{55}} \right) \lambda^2 \right], \quad R = \left(\frac{D}{I_0} \right) \lambda^4 \quad (4.5.27)$$

Example 4.5.4:

For a simply supported plate strip, the boundary conditions give $c_2 = c_3 = c_4 = 0$, and

$$\sin \lambda a = 0, \quad \text{or} \quad \lambda_n = \frac{n\pi}{a} \quad (4.5.28)$$

Substitution of λ from Eq. (4.5.28) into Eq. (4.5.26a,b) gives two frequencies for each value of λ . The fundamental frequency will come from Eq. (4.5.26a). When the rotary inertia is neglected, we obtain from Eq. (4.5.27) the result

$$\omega_n = \left(\frac{n\pi}{a} \right)^2 \sqrt{\frac{D}{I_0}} \sqrt{\frac{KA_{55}}{KA_{55} + (\frac{n\pi}{a})^2 D}} \quad (4.5.29)$$

By neglecting the shear deformation (i.e., $A_{55} = G_{13} = \infty$) we obtain the result

$$\omega_n = \left(\frac{n\pi}{a} \right)^2 \sqrt{\frac{D}{I_0}} \quad (4.5.30)$$

which is the same as in Eq. (4.4.45). Thus, the effect of shear deformation is to reduce the frequency of natural vibration.

For a laminated strip with clamped edges, the following equation governs λ :

$$-2 + 2 \cos \lambda a \cosh \mu a + \sin \lambda a \sinh \mu a \left(\frac{S_{22}}{S_{11}} - \frac{S_{11}}{S_{22}} \right) = 0 \quad (4.5.31a)$$

$$S_{11} = \mu (I_0 \omega^2 - \lambda^2 K A_{55}), \quad S_{22} = \lambda (I_0 \omega^2 + \mu^2 K A_{55}) \quad (4.5.31b)$$

Once the value of λ is known, frequencies of vibration can be determined from Eqs. (4.5.26a,b).

Figures 4.5.6 and 4.5.7 show the effect of shear deformation and modulus ratio (E_1/E_2) on nondimensionalized fundamental frequencies $\bar{\omega} = \omega a^2 \sqrt{I_0/E_2 h^3}$ of two-layer antisymmetric angle-ply ($-45/45$) and cross-ply ($0/90$) plate strips ($K = 5/6$, $E_1/E_2 = 25$, $G_{12} = G_{13} = 0.5E_2$, $G_{23} = 0.2E_2$, $\nu_{12} = 0.25$). From Figure 4.5.6 it is clear that shear deformation effect in decreasing frequencies is felt for $a/h \leq 10$ for simply supported boundary conditions, whereas for clamped boundary conditions the effect is felt for $a/h \leq 15$. Also, the effect of shear deformation is more for materials with larger modulus ratio, as can be seen from the results of Figure 4.5.7.

4.6 Vibration Suppression in Beams

4.6.1 Introduction

The grains of certain materials consist of numerous small, randomly oriented magnetic domains that can rotate and align under the influence of an external electric or magnetic field. The electric (magnetic) orientation brings about internal strains in the material. This is known as the *electrostriction*. (*magnetostriction*). For example, a commercially available magnetostrictive material Terfenol-D is an alloy of terbium, iron, and dysprosium. The use of Terfenol-D for vibration suppression has some advantages over other smart materials, in particular, it has easy embedability into host materials, such as the modern carbon fiber-reinforced polymeric (CFRP) composites, without significantly affecting the structural integrity. Considerable effort is spent to understand the interaction between magnetostrictive layers and composite laminates and the feasibility of using magnetostrictive materials for active vibration suppression (see [30–32]). Although there have been important research efforts devoted to characterizing the properties of Terfenol-D material, fundamental information about variation in elasto-magnetic material properties is not available. Few studies [33–35] report experimental evidence of significant variation in material properties such as Young's modulus and magneto-mechanical coupling coefficient.

Here we present a generalized beam theory that contains the classical Euler-Bernoulli beam theory as well as the first-order and the third-order beam theories, and bring out the effects of material properties of a lamina, lamination scheme, and placement of the actuating layers on vibration suppression time.

4.6.2 Theoretical Formulation

Displacement and strain fields

Consider a symmetrically laminated beam of n layers. Suppose that two of the layers, namely, the m th and $(n - m + 1)$ th layers, are made of magnetostrictive material, such as Terfenol-D particles embedded in a resin (see Figure 4.6). The remaining $n - 2$ layers can be made of any fiber-reinforced materials with varying fiber orientation θ but symmetrically disposed about the mid-plane of the beam. We wish to study the problem of vibration suppression in these beams using the Euler–Bernoulli, Timoshenko, and Reddy third-order beam theories. To facilitate the development of all three theories in a unified manner, we introduce tracers whose values will yield the results for a particular theory [29].

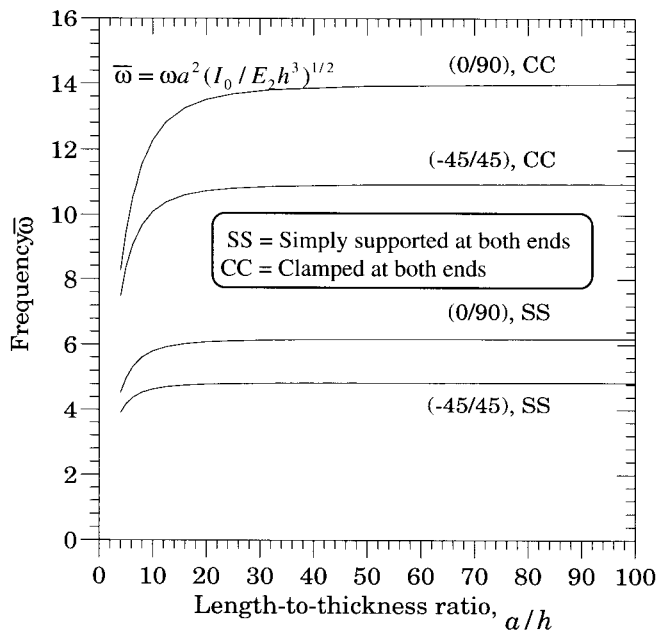


Figure 4.5.6: The effect of shear deformation on the fundamental frequencies of simply supported and clamped cross-ply and angle-ply plate strips.

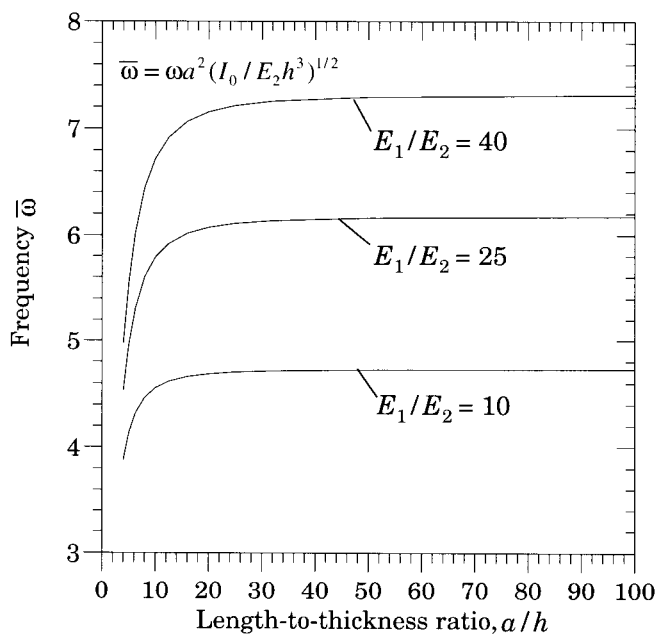


Figure 4.5.7: The effect of material orthotropy and shear deformation on fundamental frequencies of simply supported cross-ply (0/90) laminated plate strips.

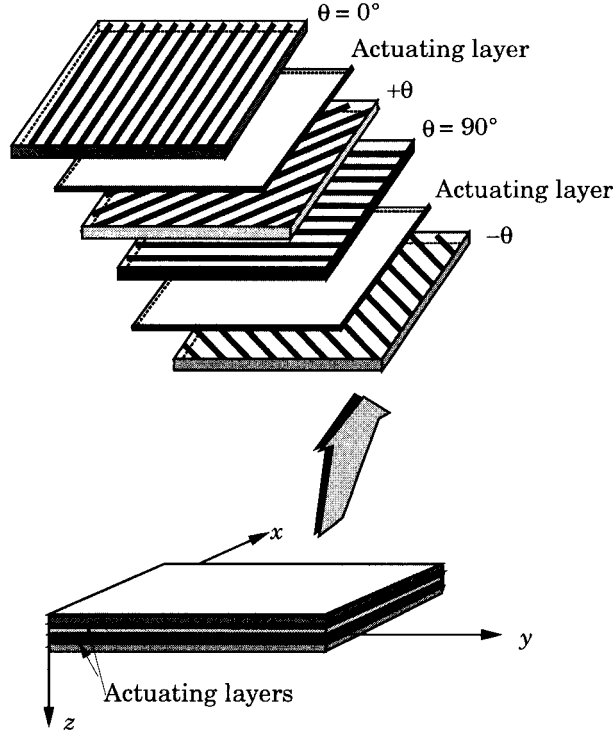


Figure 4.6.1: Layered composite beam with embedded actuating layers.

Consider the displacement field

$$\begin{aligned}
 u(x, y, z, t) &= -zc_0 \frac{\partial w_0}{\partial x} + zc_1 \phi - z^3 c_3 \left(\phi + \frac{\partial w_0}{\partial x} \right) \\
 &\equiv f_1(z) \frac{\partial w_0}{\partial x} + f_2(z) \phi(x, t) \\
 v(x, y, z, t) &= 0 \\
 w(x, y, z, t) &= w_0(x, t)
 \end{aligned} \tag{4.6.1a}$$

where \$(u, v, w)\$ are the displacement components along the \$(x, y, z)\$ coordinate directions, respectively, \$w_0\$ is the transverse deflection of a point on the midplane (i.e., \$z = 0\$), and \$\phi(x, t)\$ is the rotation of a transverse normal line. The functions \$f_1(z)\$ and \$f_2(z)\$ are given by

$$f_1(z) = -c_0 z - c_3 z^3, \quad f_2(z) = c_1 z - c_3 z^3 \tag{4.6.1b}$$

The displacement field (4.6.1a) can be specialized to various beam theories as follows:

Euler–Bernoulli beam theory (EBT): \$\quad c_0 = 1, \quad c_1 = c_3 = 0\$

Timoshenko beam theory (TBT): \$\quad c_1 = 1, \quad c_0 = c_3 = 0\$

Reddy beam theory (RBT): \$\quad c_3 = \frac{4}{3h^2}, \quad c_1 = 1, \quad c_0 = 0\$ (4.6.2)

The non-zero linear strains are given by

$$\begin{aligned}\varepsilon_{xx} &= -zc_0 \frac{\partial^2 w_0}{\partial x^2} + zc_1 \frac{\partial \phi}{\partial x} - z^3 c_3 \left(\frac{\partial \phi}{\partial x} + \frac{\partial^2 w_0}{\partial x^2} \right) = z\varepsilon_{xx}^{(1)} + z^3 \varepsilon_{xx}^{(3)} \\ \gamma_{xz} &= (1 - c_0) \frac{\partial w_0}{\partial x} + c_1 \phi - 3c_3 z^2 \left(\phi + \frac{\partial w_0}{\partial x} \right) = \gamma_{xz}^{(0)} + z^2 \gamma_{xz}^{(2)}\end{aligned}\quad (4.6.3a)$$

where

$$\begin{aligned}\varepsilon_{xx}^{(1)} &= -c_0 \frac{\partial^2 w_0}{\partial x^2} + c_1 \frac{\partial \phi}{\partial x}, \quad \varepsilon_{xx}^{(3)} = -c_3 \left(\frac{\partial \phi}{\partial x} + \frac{\partial^2 w_0}{\partial x^2} \right) \\ \gamma_{xz}^{(0)} &= (1 - c_0) \frac{\partial w_0}{\partial x} + c_1 \phi, \quad \gamma_{xz}^{(2)} = -3c_3 \left(\frac{\partial w_0}{\partial x} + \phi \right)\end{aligned}\quad (4.6.3b)$$

Constitutive relations

The constitutive relations of the k th fiber-reinforced (structural) layer are

$$\sigma_{xx}^{(k)} = \bar{Q}_{11}^{(k)} \varepsilon_{xx}, \quad \sigma_{xz}^{(k)} = \bar{Q}_{55}^{(k)} \gamma_{xz} \quad (4.6.4)$$

where

$$\begin{aligned}\bar{Q}_{11}^{(k)} &= Q_{11}^{(k)} \cos^4 \theta^{(k)} + 2 \left(Q_{12}^{(k)} + 2Q_{66}^{(k)} \right) \cos^2 \theta^{(k)} \sin^2 \theta^{(k)} + Q_{22}^{(k)} \sin^4 \theta^{(k)} \\ \bar{Q}_{55}^{(k)} &= Q_{55}^{(k)} \cos^2 \theta^{(k)} + Q_{44}^{(k)} \sin^2 \theta^{(k)} \\ Q_{11}^{(k)} &= \frac{E_{11}^{(k)}}{1 - \nu_{12}^{(k)} \nu_{21}^{(k)}}, \quad Q_{12}^{(k)} = \frac{\nu_{12}^{(k)} E_{22}^{(k)}}{1 - \nu_{12}^{(k)} \nu_{21}^{(k)}}, \quad Q_{22}^{(k)} = \frac{E_{22}^{(k)}}{1 - \nu_{12}^{(k)} \nu_{21}^{(k)}} \\ Q_{44}^{(k)} &= G_{23}^{(k)}, \quad Q_{55}^{(k)} = G_{13}^{(k)}, \quad Q_{66}^{(k)} = G_{12}^{(k)}, \quad \nu_{21}^{(k)} = \nu_{12}^{(k)} \frac{E_{22}^{(k)}}{E_{11}^{(k)}}\end{aligned}\quad (4.6.5)$$

The constitutive relation for an actuating (say, a magnetostrictive) layer is

$$\sigma_{xx}^{(m)} = \frac{1}{S^{(m)}} \left(\varepsilon_{xx} - d^{(m)} H \right) \equiv Q^{(m)} \varepsilon_{xx} - e^{(m)} H \quad (4.6.6)$$

where H is the magnetic field intensity, $S^{(m)}$ is the compliance of the m th magnetostrictive layer

$$S^{(m)} = \frac{1}{E^{(m)}} = \frac{1}{Q^{(m)}} \quad (4.6.7)$$

and $d^{(m)}$ is the magneto-mechanical coupling coefficient, $E^{(m)}$ being the modulus of the magnetostrictive layer ($e^{(m)} = Q^{(m)} d^{(m)}$).

Velocity feedback control

Considering velocity proportional closed-loop feedback control, the magnetic field intensity H is expressed in terms of coil current $I(x, t)$ as

$$H(x, t) = k_c I(x, t) \quad (4.6.8)$$

and $I(t)$ is related to the velocity \dot{w}_0 by

$$I(x, t) = c(t) \frac{\partial w_0}{\partial t} \quad (4.6.9)$$

where k_c is the coil constant, which can be expressed in terms of the coil width b_c , coil radius r_c , and number of turns n_c in the coil by

$$k_c = \frac{n_c}{\sqrt{b_c^2 + 4r_c^2}} \quad (4.6.10)$$

and $c(t)$ is the control gain.

Equations of motion

Using Hamilton's principle (or the dynamic version of the principle of virtual displacements), we obtain

$$\begin{aligned} 0 &= \int_0^T \int_0^L \int_A \left[\sigma_{xx} \left(z \delta \varepsilon_{xx}^{(1)} + z^3 \delta \varepsilon_{xx}^{(3)} \right) + \sigma_{xz} \left(\delta \gamma_{xz}^{(0)} + z^2 \delta \gamma_{xz}^{(2)} \right) \right] dA dx dt \\ &\quad - \int_0^T \int_0^L \int_A \rho \left[\left(f_1 \frac{\partial \dot{w}_0}{\partial x} + f_2 \dot{\phi} \right) \left(f_1 \frac{\partial \delta \dot{w}_0}{\partial x} + f_2 \delta \dot{\phi} \right) + \dot{w}_0 \delta \dot{w}_0 \right] dA dx dt \\ &\quad - \int_0^T \int_0^L q \delta w_0 dx dt \\ &= \int_0^T \int_0^L \left(M_{xx} \delta \varepsilon_{xx}^{(1)} + P_{xx} \delta \varepsilon_{xx}^{(3)} + Q_x \delta \gamma_{xz}^{(0)} + R_x \delta \gamma_{xz}^{(2)} - q \delta w_0 \right) dx dt \\ &\quad - \int_0^T \int_0^L \left[\left(K_1 \frac{\partial \dot{w}_0}{\partial x} + K_3 \dot{\phi} \right) \frac{\partial \delta \dot{w}_0}{\partial x} + \left(K_3 \frac{\partial \dot{w}_0}{\partial x} + K_2 \dot{\phi} \right) \delta \dot{\phi} + I_0 \dot{w}_0 \delta \dot{w}_0 \right] dx dt \\ &= \int_0^T \int_0^L \left[\left(-\frac{\partial \bar{M}_{xx}}{\partial x} + \bar{Q}_x + K_2 \frac{\partial^2 \phi}{\partial t^2} + K_3 \frac{\partial^3 w_0}{\partial t^2 \partial x} \right) \delta \phi \right. \\ &\quad \left. - \left(-\frac{\partial^2 \tilde{M}_{xx}}{\partial x^2} + \frac{\partial \tilde{Q}_x}{\partial x} + q + K_3 \frac{\partial^3 \phi}{\partial x \partial t^2} + K_1 \frac{\partial^4 w_0}{\partial x^2 \partial t^2} - I_0 \frac{\partial^2 w_0}{\partial t^2} \right) \delta w_0 \right] dx dt \\ &\quad + \int_0^T \left[\bar{M}_{xx} \delta \phi + \tilde{M}_{xx} \frac{\partial \delta w_0}{\partial x} + \left(-\frac{\partial \tilde{M}_{xx}}{\partial x} + \tilde{Q}_x - K_1 \frac{\partial^3 w_0}{\partial x \partial t^2} + K_3 \frac{\partial \phi}{\partial t} \right) \delta w_0 \right]_0^L dt \end{aligned} \quad (4.6.11)$$

where all the terms involving $[\cdot]^T_0$ vanish on account of the assumption that all variations and their derivatives are zero at $t = 0$ and $t = T$. Various symbols introduced in Eq. (4.6.11) are defined as

$$\begin{aligned} \bar{M}_{xx} &= c_1 M_{xx} - c_3 P_{xx}, & \bar{Q}_x &= c_1 Q_x - 3c_3 R_x \\ \tilde{M}_{xx} &= -c_0 M_{xx} - c_3 P_{xx}, & \tilde{Q}_x &= (1 - c_0) Q_x - 3c_3 R_x \end{aligned} \quad (4.6.12)$$

where $(M_{xx}, Q_x, P_{xx}, R_x)$ denote the conventional and higher-order stress resultants

$$\begin{Bmatrix} M_{xx} \\ P_{xx} \end{Bmatrix} = \int_A \begin{Bmatrix} z \\ z^3 \end{Bmatrix} \sigma_{xx} dz = \begin{Bmatrix} D_{11}\varepsilon_{xx}^{(1)} + F_{11}\varepsilon_{xx}^{(3)} \\ F_{11}\varepsilon_{xx}^{(1)} + H_{11}\varepsilon_{xx}^{(3)} \end{Bmatrix} - \begin{Bmatrix} \mathcal{B} \\ \mathcal{E} \end{Bmatrix} \frac{\partial w_0}{\partial t} \quad (4.6.13a)$$

$$\begin{Bmatrix} Q_x \\ R_x \end{Bmatrix} = \int_A \begin{Bmatrix} 1 \\ z^2 \end{Bmatrix} \sigma_{xz} dz = \begin{Bmatrix} A_{55}\gamma_{xz}^{(0)} + D_{55}\gamma_{xz}^{(2)} \\ D_{55}\gamma_{xz}^{(0)} + F_{55}\gamma_{xz}^{(2)} \end{Bmatrix} \quad (4.6.13b)$$

and (K_1, K_2, K_3) are the mass inertias

$$\begin{Bmatrix} K_1 \\ K_2 \\ K_3 \end{Bmatrix} = \int_A \begin{Bmatrix} f_1^2 \\ f_2^2 \\ f_1 f_2 \end{Bmatrix} dz = \begin{Bmatrix} (c_0)^2 I_2 + 2c_0 c_3 I_4 + (c_3)^2 I_6 \\ (c_1)^2 I_2 - 2c_1 c_3 I_4 + (c_3)^2 I_6 \\ -2c_0 c_1 I_2 + (c_0 - c_1)c_3 I_4 + (c_3)^2 I_6 \end{Bmatrix} \quad (4.6.14)$$

$$\begin{Bmatrix} I_2 \\ I_4 \\ I_6 \end{Bmatrix} = \int_A \rho \begin{Bmatrix} z^2 \\ z^4 \\ z^6 \end{Bmatrix} dz, \quad \begin{Bmatrix} \mathcal{B} \\ \mathcal{E} \end{Bmatrix} = k_c c(t) \int_A Q_{11}^{(m)} d^{(m)} \begin{Bmatrix} z \\ z^3 \end{Bmatrix} dz \quad (4.6.15a)$$

$$\begin{Bmatrix} D_{11} \\ F_{11} \\ H_{11} \end{Bmatrix} = \int_A \bar{Q}_{11}^{(k)} \begin{Bmatrix} z^2 \\ z^4 \\ z^6 \end{Bmatrix} dz, \quad \begin{Bmatrix} A_{55} \\ D_{55} \\ F_{55} \end{Bmatrix} = \int_A \bar{Q}_{55}^{(k)} \begin{Bmatrix} 1 \\ z^2 \\ z^4 \end{Bmatrix} dz \quad (4.6.15b)$$

The equations of motion are

$$-\frac{\partial \tilde{M}_{xx}}{\partial x} + \tilde{Q}_x + K_2 \frac{\partial^2 \phi}{\partial t^2} + K_3 \frac{\partial^3 w_0}{\partial t^2 \partial x} = 0 \quad (4.6.16)$$

$$\frac{\partial^2 \tilde{M}_{xx}}{\partial x^2} - \frac{\partial \tilde{Q}_x}{\partial x} - q - K_3 \frac{\partial^3 \phi}{\partial x \partial t^2} - K_1 \frac{\partial^4 w_0}{\partial x^2 \partial t^2} + I_0 \frac{\partial^2 w_0}{\partial t^2} = 0 \quad (4.6.17)$$

The primary and secondary variables of the formulations are

$$\text{Primary Variables : } w_0, \quad \frac{\partial w_0}{\partial x}, \quad \phi \quad (4.6.18a)$$

$$\text{Secondary Variables : } V_x, \quad P_{xx}, \quad \tilde{M}_{xx} \quad (4.6.18b)$$

where

$$V_x \equiv \tilde{Q}_x + \frac{\partial \tilde{M}_{xx}}{\partial x} + K_3 \ddot{\phi} + K_1 \frac{\partial \ddot{w}_0}{\partial x} \quad (4.6.19)$$

4.6.3 Analytical Solution

First we write the equations of motion (4.6.16) and (4.6.17) in terms of the displacement variables (w_0, ϕ) by expressing M_{xx}, Q_x, P_{xx} , and R_x [see Eqs. (4.6.13a,b) and (4.6.12)]. We have

$$\begin{aligned} & -c_1 D_{11} \left(-c_0 \frac{\partial^3 w_0}{\partial x^3} + c_1 \frac{\partial^2 \phi}{\partial x^2} \right) + c_1 c_3 F_{11} \left(\frac{\partial^3 w_0}{\partial x^3} + \frac{\partial^2 \phi}{\partial x^2} \right) \\ & + c_3 F_{11} \left(-c_0 \frac{\partial^3 w_0}{\partial x^3} + c_1 \frac{\partial^2 \phi}{\partial x^2} \right) - (c_3)^2 H_{11} \left(\frac{\partial^3 w_0}{\partial x^3} + \frac{\partial^2 \phi}{\partial x^2} \right) \end{aligned}$$

$$\begin{aligned}
& + c_1 A_{55} \left[(1 - c_0) \frac{\partial w_0}{\partial x} + c_1 \phi \right] - 3c_1 c_3 D_{55} \left(\frac{\partial w_0}{\partial x} + \phi \right) \\
& - 3c_3 D_{55} \left[(1 - c_0) \frac{\partial w_0}{\partial x} + c_1 \phi \right] + 9(c_3)^2 F_{55} \left(\frac{\partial w_0}{\partial x} + \phi \right) \\
& + (c_1 \mathcal{B} - c_3 \mathcal{E}) \frac{\partial^2 w_0}{\partial t \partial x} + [(c_1)^2 I_2 - 2c_1 c_3 I_4 + (c_3)^2 I_6] \frac{\partial^2 \phi}{\partial t^2} \\
& + [-2c_0 c_1 I_2 + (c_0 - c_1) c_3 I_4 + (c_3)^2 I_6] \frac{\partial^3 w_0}{\partial t^2 \partial x} = 0
\end{aligned} \tag{4.6.20}$$

$$\begin{aligned}
& c_0 D_{11} \left(c_0 \frac{\partial^4 w_0}{\partial x^4} - c_1 \frac{\partial^3 \phi}{\partial x^3} \right) + c_0 c_3 F_{11} \left(\frac{\partial^4 w_0}{\partial x^4} + \frac{\partial^3 \phi}{\partial x^3} \right) \\
& + c_3 F_{11} \left(c_0 \frac{\partial^4 w_0}{\partial x^4} - c_1 \frac{\partial^3 \phi}{\partial x^3} \right) + (c_3)^2 H_{11} \left(\frac{\partial^4 w_0}{\partial x^4} + \frac{\partial^3 \phi}{\partial x^3} \right) \\
& - (1 - c_0) A_{55} \left[(1 - c_0) \frac{\partial^2 w_0}{\partial x^2} + c_1 \frac{\partial \phi}{\partial x} \right] + 3(1 - c_0) c_3 D_{55} \left(\frac{\partial^2 w_0}{\partial x^2} + \frac{\partial \phi}{\partial x} \right) \\
& + 3c_3 D_{55} \left[(1 - c_0) \frac{\partial^2 w_0}{\partial x^2} + c_1 \frac{\partial \phi}{\partial x} \right] - 9(c_3)^2 F_{55} \left(\frac{\partial^2 w_0}{\partial x^2} + \frac{\partial \phi}{\partial x} \right) \\
& - q + (c_0 \mathcal{B} + c_3 \mathcal{E}) \frac{\partial^3 w_0}{\partial t \partial x^2} + [2c_0 c_1 I_2 - (c_0 - c_1) c_3 I_4 - (c_3)^2 I_6] \frac{\partial^3 \phi}{\partial x \partial t^2} \\
& - [(c_0)^2 I_2 + 2c_0 c_3 I_4 + (c_3)^2 I_6] \frac{\partial^4 w_0}{\partial t^2 \partial x^2} + I_0 \frac{\partial^2 w_0}{\partial t^2} = 0
\end{aligned} \tag{4.6.21}$$

This completes the development of the governing equations in terms of the displacements (w_0, ϕ) . Of course, the equations can be specialized to any of the three theories.

Here we discuss the Navier's solution of these equations for the case of simply supported boundary conditions. Assuming solution of the form

$$w_0(x, t) = W(t) \sin \frac{n\pi x}{a}, \quad \phi(x, t) = X(t) \cos \frac{n\pi x}{a} \tag{4.6.22}$$

and substituting into Eqs. (4.6.20) and (4.6.21), we obtain

$$\begin{aligned}
& \begin{bmatrix} \hat{S}_{22} & \hat{S}_{23} \\ \hat{S}_{23} & \hat{S}_{33} \end{bmatrix} \begin{Bmatrix} W \\ X \end{Bmatrix} + \begin{bmatrix} \hat{M}_{22} & \hat{M}_{23} \\ \hat{M}_{23} & \hat{M}_{33} \end{bmatrix} \begin{Bmatrix} \ddot{W} \\ \ddot{X} \end{Bmatrix} \\
& + \begin{bmatrix} \hat{C}_{22} & \hat{C}_{23} \\ \hat{C}_{32} & \hat{C}_{33} \end{bmatrix} \begin{Bmatrix} \dot{W} \\ \dot{X} \end{Bmatrix} = \begin{Bmatrix} -Q_n \\ 0 \end{Bmatrix}
\end{aligned} \tag{4.6.23}$$

where the coefficients $\hat{S}_{ij} = \hat{S}_{ji}$ and $\hat{M}_{ij} = \hat{M}_{ji}$ are defined by

$$\begin{aligned}
\hat{S}_{22} &= [(c_0)^2 D_{11} + 2c_0 c_3 F_{11} + (c_3)^2 H_{11}] \left(\frac{n\pi}{a} \right)^4 \\
&+ [(1 - c_0)^2 A_{55} - 6(1 - c_0) c_3 D_{55} + 9(c_3)^2 F_{55}] \left(\frac{n\pi}{a} \right)^2
\end{aligned}$$

$$\begin{aligned}
\hat{S}_{23} &= \left[-c_0 c_1 D_{11} + c_0 c_3 F_{11} - c_1 c_3 F_{11} + (c_3)^2 H_{11} \right] \left(\frac{n\pi}{a} \right)^3 \\
&\quad + \left[(1 - c_0) c_1 A_{55} - 3(1 - c_0 + c_1) c_3 D_{55} + 9(c_3)^2 F_{55} \right] \left(\frac{n\pi}{a} \right) \\
\hat{S}_{33} &= \left[(c_1)^2 D_{11} - 2c_1 c_3 F_{11} + (c_3)^2 H_{11} \right] \left(\frac{n\pi}{a} \right)^2 \\
&\quad + (c_1)^2 A_{55} - 6c_1 c_3 D_{55} + 9(c_3)^2 F_{55} \\
\hat{M}_{22} &= \left[(c_0)^2 I_2 + 2c_0 c_3 I_4 + (c_3)^2 I_6 \right] \left(\frac{n\pi}{a} \right)^2 + I_0 \\
\hat{M}_{23} &= \left[-2c_0 c_1 I_2 + (c_0 - c_1) c_3 I_4 + (c_3)^2 I_6 \right] \left(\frac{n\pi}{a} \right) \\
\hat{M}_{33} &= c_1^2 I_2 - 2c_1 c_3 I_4 + (c_3)^2 I_6 \\
\hat{C}_{22} &= - (c_0 \mathcal{B} + c_3 \mathcal{E}) \left(\frac{n\pi}{a} \right)^2 \\
\hat{C}_{23} &= 0, \quad \hat{C}_{32} = (c_1 \mathcal{B} - c_3 \mathcal{E}) \left(\frac{n\pi}{a} \right), \quad \hat{C}_{33} = 0
\end{aligned} \tag{4.6.24}$$

Equation (4.6.24) can be specialized to various theories as follows (only non-zero coefficients are listed):

Euler–Bernoulli beam theory (EBT) ($c_0 = 1, c_1 = c_3 = 0$)

$$\hat{S}_{22} = D_{11} \left(\frac{n\pi}{a} \right)^4, \quad \hat{M}_{22} = I_2 \left(\frac{n\pi}{a} \right)^2 + I_0, \quad \hat{C}_{22} = -\mathcal{B} \left(\frac{n\pi}{a} \right)^2 \tag{4.6.25}$$

Timoshenko beam theory (TBT) ($c_0 = 0, c_1 = 1, c_3 = 0$)

$$\begin{aligned}
\hat{S}_{22} &= A_{55} \left(\frac{n\pi}{a} \right)^2, \quad \hat{S}_{23} = A_{55} \left(\frac{n\pi}{a} \right), \quad \hat{S}_{33} = D_{11} \left(\frac{n\pi}{a} \right)^2 + A_{55} \\
\hat{M}_{22} &= I_0, \quad \hat{M}_{23} = 0, \quad \hat{M}_{33} = I_2 \\
\hat{C}_{22} &= 0, \quad \hat{C}_{23} = 0, \quad \hat{C}_{32} = \mathcal{B} \left(\frac{n\pi}{a} \right), \quad \hat{C}_{33} = 0
\end{aligned} \tag{4.6.26}$$

Reddy beam theory (RBT) ($c_0 = 0, c_1 = 1, c_3 = \frac{4}{3h^2}$)

$$\begin{aligned}
\hat{S}_{22} &= (c_3)^2 H_{11} \left(\frac{n\pi}{a} \right)^4 + \left[A_{55} - 6c_3 D_{55} + 9(c_3)^2 F_{55} \right] \left(\frac{n\pi}{a} \right)^2 \\
\hat{S}_{23} &= \left[-c_3 F_{11} + (c_3)^2 H_{11} \right] \left(\frac{n\pi}{a} \right)^3 + \left[A_{55} - 6c_3 D_{55} + 9(c_3)^2 F_{55} \right] \left(\frac{n\pi}{a} \right) \\
\hat{S}_{33} &= \left[D_{11} - 2c_3 F_{11} + (c_3)^2 H_{11} \right] \left(\frac{n\pi}{a} \right)^2 + A_{55} - 6c_3 D_{55} + 9(c_3)^2 F_{55} \\
\hat{M}_{22} &= I_0 + (c_3)^2 I_6 \left(\frac{n\pi}{a} \right)^2, \quad \hat{M}_{23} = \left[-c_3 I_4 + (c_3)^2 I_6 \right] \left(\frac{n\pi}{a} \right) \\
\hat{M}_{33} &= I_2 - 2c_3 I_4 + (c_3)^2 I_6, \quad \hat{C}_{22} = -c_3 \mathcal{E} \left(\frac{n\pi}{a} \right)^2 \\
\hat{C}_{23} &= 0, \quad \hat{C}_{32} = (\mathcal{B} - c_3 \mathcal{E}) \left(\frac{n\pi}{a} \right), \quad \hat{C}_{33} = 0
\end{aligned} \tag{4.6.27}$$

For vibration control, we assume $q = 0$ and solution of the ordinary differential equations in Eq. (4.6.23) in the form

$$W(t) = W_0 e^{\lambda t}, \quad X(t) = X_0 e^{\lambda t} \quad (4.6.28)$$

and obtain, for non-trivial solution, the result

$$\bar{S}_{22} = 0 \quad (4.6.29)$$

for the Euler–Bernoulli beam theory, and

$$\begin{vmatrix} \bar{S}_{22} & \bar{S}_{23} \\ \bar{S}_{32} & \bar{S}_{33} \end{vmatrix} = 0 \quad (4.6.30)$$

for the Timoshenko and third-order beam theories, where

$$\begin{aligned} \bar{S}_{22} &= \hat{S}_{22} + \lambda \hat{C}_{22} + \lambda^2 \hat{M}_{22}, & \bar{S}_{23} &= \hat{S}_{23} + \lambda \hat{C}_{23} + \lambda^2 \hat{M}_{23} \\ \bar{S}_{32} &= \hat{S}_{32} + \lambda \hat{C}_{32} + \lambda^2 \hat{M}_{32}, & \bar{S}_{33} &= \hat{S}_{33} + \lambda \hat{C}_{33} + \lambda^2 \hat{M}_{33} \end{aligned} \quad (4.6.31)$$

Equation (4.6.31) gives two sets of eigenvalues. A typical eigenvalue can be expressed as $\lambda = -\alpha + i\omega_d$. The lowest imaginary part (ω_d) corresponds to the transverse motion, and we can write

$$w_0(x, t) = \frac{1}{\omega_d} e^{-\alpha t} \sin \omega_d t \sin \frac{n\pi x}{a} \quad (4.6.32)$$

In arriving at the solution (4.6.32), the following initial conditions were used:

$$w_0(x, 0) = 0, \quad \dot{w}_0(x, 0) = 1, \quad \phi(x, 0) = 0, \quad \dot{\phi}(x, 0) = 0 \quad (4.6.33)$$

The actuation stress is $\sigma_d = -E_m dH$.

4.6.4 Numerical Results

Numerical studies were carried out to analyze damped natural frequencies, damping coefficients, and the vibration suppression time, using the three theories [29]. Different lamination schemes were used to show the influence of the position of magnetostrictive layer from the neutral axis on the vibration suppression time. A time ratio relation between the thickness of the layers and the distance to the neutral axis of the laminated composite beam is also found. All values of the material and structural constants are indicated in the tables. The material properties used are the same as those used in [32].

The numerical values of various coefficients (namely, the inertial and magnetostrictive coefficients) based on different lay-ups and material properties [CFRP, Graphite-Epoxy (AS), Glass-Epoxy and Boron-Epoxy] are listed in Tables 4.6.1 and 4.6.2. Table 4.6.2 also shows the damping coefficients and natural frequencies for different materials and lay-ups. The damping and frequency parameters for transverse modes $n = 1$ to $n = 5$ are shown in Table 4.6.3, and they are compared with the results obtained by Krishna Murty et al. [32] using the Euler–Bernoulli beam theory (EBT). There is some difference between the numerical

Table 4.6.1: Coefficients for Different Lamination Schemes and Materials (from Reddy and Barbosa [30])

Material	Lay-up	$D_{11} (10^3)$	$F_{11} (10^{-2})$	$H_{11} (10^{-7})$	$A_{55} (10^9)$	$D_{55} (10^2)$	$F_{55} (10^{-3})$
CFRP	[±45/m/0/90] _s	3.739	5.246	9.333	6.620	5.185	6.902
	[45/m/-45/0/90] _s	3.552	4.891	8.793	6.620	6.179	8.792
	[m/+45/0/90] _s	3.303	4.069	6.679	6.620	7.506	13.168
	[m/90] _s	1.432	2.567	5.063	6.620	7.506	13.168
	[m/0] _s	7.015	7.927	11.189	6.620	7.506	13.168
Gr.-Ep (AS)	[±45/m/0/90] _s	3.954	5.629	10.053	7.974	6.399	8.881
Gl.-EP	[±45/m/0/90] _s	2.535	3.700	6.589	7.614	6.173	8.384
Br.-Ep	[±45/m/0/90] _s	5.730	8.259	14.865	7.066	5.634	7.569

CFRP : $E_{11}=138.6 \text{ GPa}$, $E_{22}=8.27 \text{ GPa}$, $G_{13}=G_{23}=0.6 E_{22}$, $G_{12}=4.12 \text{ GPa}$, $v_{12}=0.26$, $\rho=1824 \text{ kg.m}^{-3}$
Graphite-Epoxy (AS) : $E_{11}=137.9 \text{ GPa}$, $E_{22}=8.96 \text{ GPa}$, $G_{12}=G_{13}=7.10 \text{ GPa}$, $G_{23}=6.21 \text{ GPa}$, $v_{12}=0.30$, $\rho=1450 \text{ kg.m}^{-3}$
Glass-Epoxy : $E_{11}=53.78 \text{ GPa}$, $E_{22}=17.93 \text{ GPa}$, $G_{12}=G_{13}=8.96 \text{ GPa}$, $G_{23}=3.45 \text{ GPa}$, $v_{12}=0.25$, $\rho=1900 \text{ kg.m}^{-3}$
Boron-Epoxy : $E_{11}=206.9 \text{ GPa}$, $E_{22}=20.69 \text{ GPa}$, $G_{12}=G_{13}=6.9 \text{ GPa}$, $G_{23}=4.14 \text{ GPa}$, $v_{12}=0.30$, $\rho=1950 \text{ kg.m}^{-3}$

Table 4.6.2: Mass Inertias and Magnetostrictive Coefficients, and Parameters α and ω_d for Various Laminates

Material	Lay-up	I_0	$I_2 (10^{-4})$	$I_4 (10^{-9})$	$I_6 (10^{-14})$	$-\beta$	$-\epsilon (10^{-4})$	$-\alpha \pm \omega_{dn} (\text{rad/s})$
CFRP	[±45/m/0/90] _s	33.092	2.461	2.907	4.508	22.128	1.438	3.30±104.85
	[45/m/-45/0/90] _s	33.092	3.352	4.600	7.084	30.979	3.872	4.62±102.15
	[m/+45/0/90] _s	33.092	4.540	8.521	17.171	39.830	8.165	5.94±98.42
	[m/90] _s	33.092	4.540	8.521	17.171	39.830	8.165	5.94±64.65
	[m/0] _s	33.092	4.540	8.521	17.171	39.830	8.165	5.94±143.57
Gr.-Ep	[±45/m/0/90] _s	30.100	2.196	2.471	3.696	22.128	1.438	3.63±113.06
Gl.-EP	[±45/m/0/90] _s	33.700	2.514	2.995	4.674	22.128	1.438	3.24±85.54
Br.-Ep	[±45/m/0/90] _s	34.100	2.550	3.054	4.782	22.128	1.438	3.20±127.90

Table 4.6.3: Comparison of the Damping and Frequency Parameters α and ω_d as Predicted by Various Theories (see Reddy and Barbosa [30])

Mode	$-\alpha \pm \omega_{dn} (\text{rad/s}) - \text{Lay-up } [\pm 45/\text{m}/0/90]\text{s}$			
1	Murty et al	EBT	TBT	RBT
2	3.29±104.88	3.30±104.85	3.30±104.82	3.30±104.82
3	13.19±419.50	13.20±419.37	13.17±418.90	13.16±418.80
4	29.70±943.88	29.68±943.40	29.53±941.05	29.48±940.52
5	52.86±1678.83	52.73±1676.72	52.27±1669.32	52.10±1667.68

CFRP : $E_{11}=138.6 \text{ Gpa}$, $E_{22}=8.27 \text{ GPa}$, $G_{12}=4.12 \text{ GPa}$, $G_{13}=G_{23}=0.6 E_{22}$, $v_{12}=0.26$, $\rho=1824 \text{ kg.m}^{-3}$
Magnetostrictive layer : $E_m=26.5 \text{ GPa}$, $\rho_m=9250 \text{ kg.m}^{-3}$, $d_k=1.67 \times 10^{-8} \text{ m/A}$, $c(t).R_c=10^4$, $v_m=0$, $a=1 \text{ m}$

Table 4.6.4: Damping and Frequency Parameters α and ω_d for Various Lamination Schemes

Lay-up	Murty et al	EBT	TBT	RBT
[45/m/-45/0/90] _s	4.60±102.17	4.62±102.15	4.62±102.12	4.62±102.11
[m/+45/0/90] _s	5.90±98.44	5.94±98.42	5.94±98.39	5.93±98.38
[m/90] _s	5.90±64.65	5.94±64.65	5.94±64.64	5.94±64.64
[m/0] _s	5.90±143.58	5.94±143.57	5.93±143.49	5.93±143.44

CFRP : $E_{11}=138.6 \text{ GPa}$, $E_{22}=8.27 \text{ GPa}$, $G_{12}=4.12 \text{ GPa}$, $G_{13}=G_{23}=0.6 E_{22}$, $v_{12}=0.26$, $\rho=1824 \text{ kg.m}^{-3}$
Magnetostrictive layer : $E_m=26.5 \text{ Gpa}$, $\rho_m=9250 \text{ kg.m}^{-3}$, $d_k=1.67 \times 10^{-8} \text{ m/A}$, $c(t).R_c=10^4$, $v_m=0$, $a=1 \text{ m}$

results predicted by the three theories only in the higher modes. Table 4.6.4 shows the influence of the position of the magnetostrictive layer in the z -direction and the influence of the lamination scheme in the damping and frequency parameters. The value of α increases when the magnetostrictive layer is located further away from the x -axis, indicating faster vibration suppression. The lay-up $[m/90_4]_s$ represents the softest beam and the lay-up $[m/0_4]_s$ the stiffest beam.

A comparison of the fundamental transverse and axial modes, obtained using the three theories show that there is no significant difference between the results. The uncontrolled and controlled motions at the midpoint of the beam, as predicted by RBT, are shown in Figures 4.6.2–4.6.5 for the first mode when the actuating layer (m) is placed at different distances from the midplane of the laminate. These figures show that the vibration suppression time decreases when the distance to the neutral axis is increased, and it remains nearly the same in the laminates with different stiffness. Figures 4.6.6 shows that the vibration suppression time decreases very rapidly for higher modes. Figure 4.6.7 shows the controlled motion of the beam, as predicted by EBT and RBT, for mode $n = 5$. Clearly, the difference between the predictions of the two theories is not significant.

4.7 Closing Remarks

In this chapter analytical solutions are developed for laminated beams and plate strips in cylindrical bending using the classical and first-order shear deformation theories. Analytical solutions are presented for static bending, natural vibration, and buckling problems under a number of boundary conditions.

A unified formulation for laminated beams with embedded actuating layers is presented. The formulation includes the Euler–Bernoulli, Timoshenko, and Reddy third-order beam theories as special cases. Analytical solution for the simply supported beam is presented to bring out the effects of the material properties of a lamina, lamination scheme, and placement of the actuating layers on vibration suppression.

When closed-form solutions can be derived, they are preferred over the series solutions. However, when exact closed-form solutions cannot be developed, the series solutions are the best alternative. When analytical solutions cannot be derived at all, numerical solutions based on the finite element method (see Chapters 9 and 10) can be used to determine the solutions.

Problems

- 4.1 Consider a simply supported laminated beam under point loads F_0 at $x = a/4$ and $x = 3a/4$ (the so-called *four-point bending*). Use the symmetry about $x = a/2$ to determine the deflection $w_0(x)$ using the classical beam theory. (Ans: The maximum deflection is $w_{max} = 11F_0a^3/384E_{xx}^bI_{yy}$.)
- 4.2 Determine the static deflection of a clamped laminated beam under uniformly distributed load q_0 and a point load F_0 at the midspan using the classical beam theory.
- 4.3 Show that the critical buckling load of a clamped-free laminated beam using the classical beam theory is given by

$$N_{cr} = \left(\frac{E_{xx}^b I_{yy}}{b} \right) \left(\frac{\pi}{2a} \right)^2$$

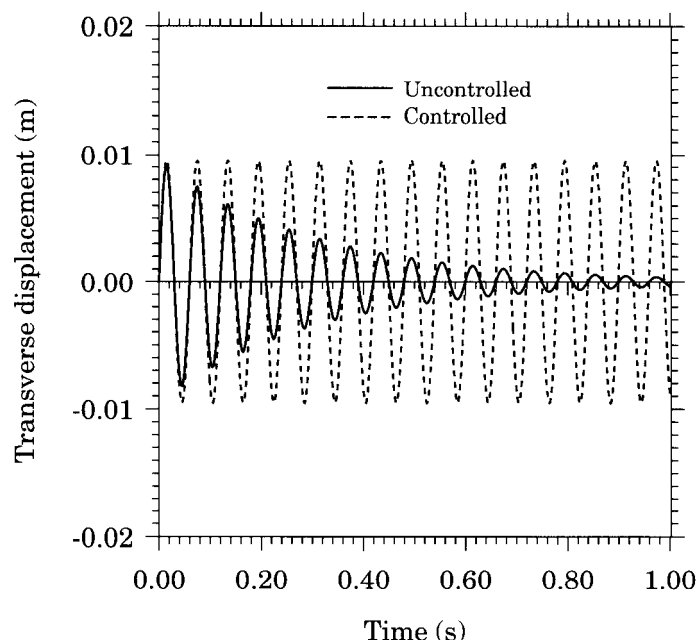


Figure 4.6.2: Comparison of uncontrolled and controlled maximum deflection (at midpoint of the beam) for $(\pm 45/m/0/90)_s$ laminate.

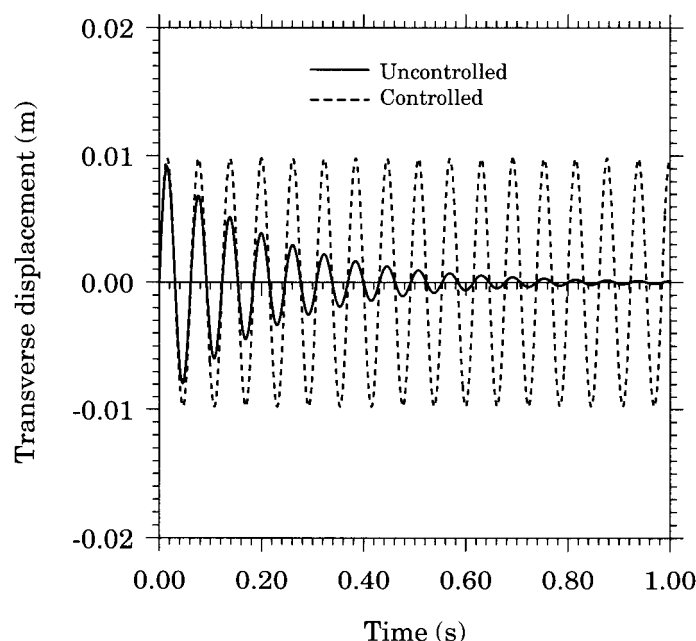


Figure 4.6.3: Comparison of uncontrolled and controlled maximum deflection (at midpoint of the beam) for $(45/m/-45/0/90)_s$ laminate.

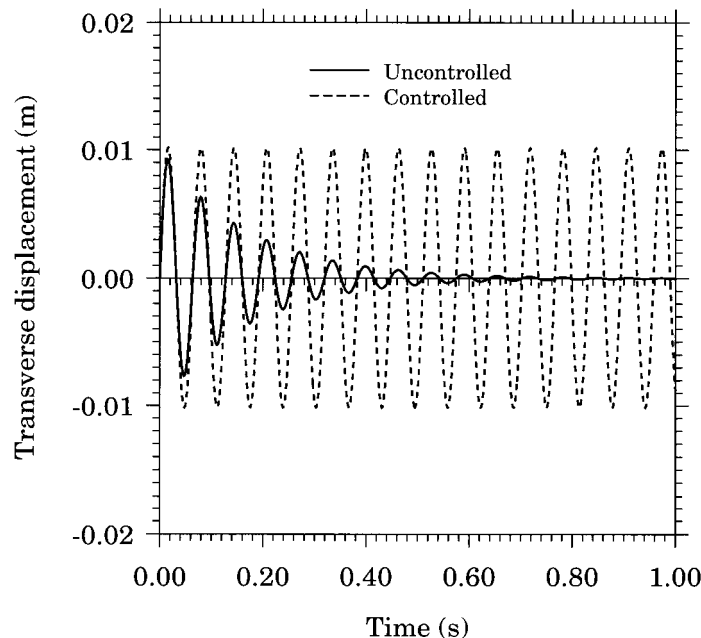


Figure 4.6.4: Comparison of uncontrolled and controlled maximum deflection (at midpoint of the beam) for $(m/\pm 45/0/90)_s$ laminate.

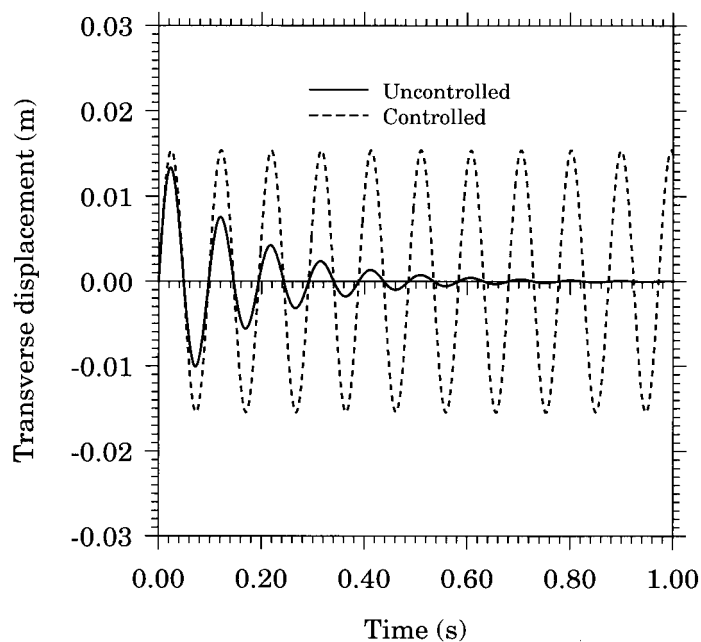


Figure 4.6.5: Comparison of uncontrolled and controlled maximum deflection (at midpoint of the beam) for $(m/90_4)_s$ laminate.

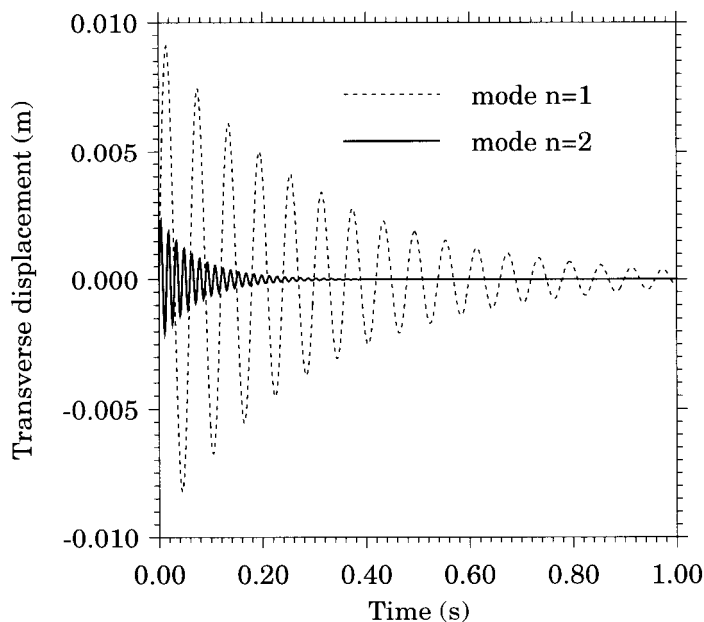


Figure 4.6.6: Controlled motion of the laminated beam $(\pm 45/m/0/90)_s$, as predicted by RBT, for modes $n = 1$ and $n = 2$.

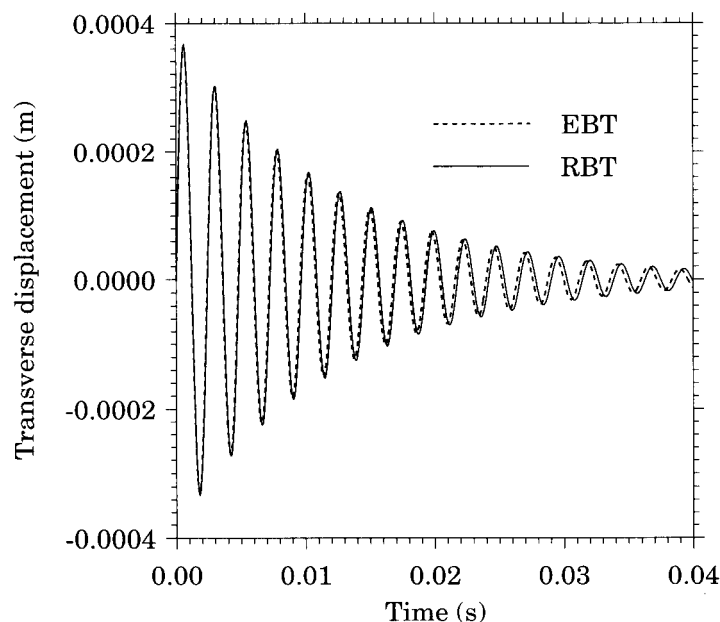


Figure 4.6.7: Controlled motion of the laminated beam $(\pm 45/m/0/90)_s$ as predicted by EBT and RBT for mode $n = 5$.

- 4.4** Show that the characteristic equation governing buckling of a clamped-hinged laminated beam using the classical beam theory is given by

$$\sin \lambda a - \lambda a \cos \lambda a = 0$$

- 4.5** Show that the characteristic equation governing natural vibration of a clamped-free laminated beam using the classical beam theory is given by

$$\cos \lambda a \cosh \lambda a + 1 = 0$$

- 4.6** Show that the characteristic equation governing natural vibration of a clamped-hinged laminated beam using the classical beam theory, when rotary inertia is neglected, is

$$\sin \lambda a \cosh \lambda a - \cos \lambda a \sinh \lambda a = 0$$

- 4.7** Show that the characteristic equation governing natural vibration of a hinged-free laminated beam using the classical beam theory, when rotary inertia is neglected, is the same as that for a clamped-hinged beam.

- 4.8** Derive the characteristic equation governing natural vibration of a clamped-hinged laminated beam using the classical beam theory, when rotary inertia is *not* neglected.

- 4.9** Show that Eqs. (4.3.10a,b) can be reduced to the single equation

$$E_{xx}^b I_{yy} \frac{d^4 w_0}{dx^4} = \hat{q}(x) - \left(\frac{E_{xx}^b I_{yy}}{KG_{xz}^b bh} \right) \frac{d^2 \hat{q}}{dx^2}$$

This equation shows that the deflection of the Timoshenko beam theory can be obtained from that of the classical beam theory by replacing the load \hat{q} [see Eq. (4.2.10b)] with a equivalent load given by the right-hand side of the above equation. Although the effect of shear deformation is zero when the load variation is linear or less, this effect will come through the boundary conditions.

- 4.10** Show that the equations governing the stability of a laminated beam according to the Timoshenko theory can be expressed as

$$KG_{xz}^b bh \chi + (KG_{xz}^b bh - bN_{xx}^0) \frac{dW}{dx} = K_1 \quad (1)$$

$$E_{xx}^b I_{yy} \frac{d\chi}{dx} - bN_{xx}^0 W = K_1 x + K_2 \quad (2)$$

Combine the above two equations to arrive at

$$\frac{d^2 W}{dx^2} + \lambda^2 W + \frac{\lambda^2}{bN_{xx}^0} (K_1 x + K_2) = 0 \quad (3)$$

Show that the general solution of Eq. (3) is

$$W(x) = c_1 \sin \lambda x + c_2 \cos \lambda x + c_3 x + c_4; \quad c_3 = -\frac{1}{bN_{xx}^0} K_1, \quad c_4 = -\frac{1}{bN_{xx}^0} K_2 \quad (4)$$

- 4.11** Show that the solution to the equations governing the bending of a hinged-fixed beam according to the Timoshenko beam theory, under uniformly distributed transverse load, is given by

$$w_0(x) = \frac{q_0 a^4}{48 E_{xx}^b I_{yy}} \left[2 \left(\frac{x}{a} \right)^4 - \left(\frac{5+12\alpha}{1+3\alpha} \right) \left(\frac{x}{a} \right)^3 + 3 \left(\frac{1}{1+3\alpha} \right) \left(\frac{x}{a} \right)^2 \right] + \frac{q_0 a^2}{8 KG_{xz}^b bh} \left[\left(\frac{5+12\alpha}{1+3\alpha} \right) \left(\frac{x}{a} \right) - 4 \left(\frac{x}{a} \right)^2 \right] \quad (1)$$

$$\phi_x(x) = -\frac{q_0 a^3}{48 E_{xx}^b I_{yy}} \left[8 \left(\frac{x}{a} \right)^3 - 3 \left(\frac{5+12\alpha}{1+3\alpha} \right) \left(\frac{x}{a} \right)^2 + 6 \left(\frac{1}{1+3\alpha} \right) \left(\frac{x}{a} \right) \right] \quad (2)$$

where $\alpha = E_{xx}^b I_{yy} / KG_{xz}^b bh a^2$.

- 4.12** Show that the characteristic equation governing the buckling load of a hinged-fixed beam according to the Timoshenko beam theory is given by

$$\lambda a \cos \lambda a - \sin \lambda a \left(1 + \frac{\lambda^2 E_{xx}^b I_{yy}}{K G_{xz}^b b h} \right) = 0$$

Ans: The boundary conditions give

$$w_0(0) = 0 \text{ gives } c_2 + c_4 = 0 \quad (1)$$

$$\phi_x(0) = 0 \text{ gives } \left(1 - \frac{b N_{xx}^0}{K G_{xz}^b b h} \right) \lambda c_1 + c_3 = 0 \quad (2)$$

$$w_0(a) = 0 \text{ gives } c_1 \sin \lambda a + c_2 \cos \lambda a + c_3 a + c_4 = 0 \quad (3)$$

$$\frac{d\phi_x}{dx}(a) = 0 \text{ gives } \lambda^2 \left(1 - \frac{b N_{xx}^0}{K G_{xz}^b b h} \right) (c_1 \sin \lambda a + c_2 \cos \lambda a) = 0 \quad (4)$$

In addition, note that

$$1 - \frac{b N_{xx}^0}{K G_{xz}^b b h} = \frac{1}{1 + \frac{\lambda^2 E_{xx}^b I_{yy}}{K G_{xz}^b b h}} \quad (5)$$

- 4.13** Determine the critical buckling load of a clamped-free laminated beam using the Timoshenko beam theory.

- 4.14** Show that the characteristic equation governing natural vibrations of a clamped-free beam according to the Timoshenko beam theory, when rotary inertia is neglected, is given by

$$\lambda \left(\frac{S_1}{S_2} + \frac{R_1}{R_2} \frac{S_2}{S_1} \right) + \mu \left(1 - \frac{\lambda^2}{\mu^2} \frac{R_1}{R_2} \right) \sin \lambda a \sinh \mu a - \lambda \left(1 + \frac{R_1}{R_2} \right) \cos \lambda a \cosh \mu a = 0 \quad (1)$$

$$\begin{aligned} R_1 &= \beta \hat{I}_0 \omega^2 + K G_{xz}^b b h - \lambda^2 E_{xx}^b I_{yy}, \quad R_2 = \beta \hat{I}_0 \omega^2 + K G_{xz}^b b h + \mu^2 E_{xx}^b I_{yy} \\ S_1 &= \hat{I}_0 \omega^2 - \lambda^2 K G_{xz}^b b h, \quad S_2 = \hat{I}_0 \omega^2 + \mu^2 K G_{xz}^b b h \end{aligned} \quad (2)$$

- 4.15** Show that the characteristic equation governing natural vibrations of a clamped-hinged beam according to the Timoshenko beam theory is given by

$$S_{11} \cos \lambda a \sinh \mu a + S_{22} \sin \lambda a \cosh \mu a = 0 \quad (1)$$

$$\begin{aligned} S_{11} &= \lambda \left(\beta \hat{I}_0 \omega^2 + K G_{xz}^b b h - \lambda^2 E_{xx}^b I_{yy} \right) \\ S_{22} &= \mu \left(\beta \hat{I}_0 \omega^2 + K G_{xz}^b b h + \mu^2 E_{xx}^b I_{yy} \right) \end{aligned} \quad (2)$$

- 4.16** Derive the equations of equilibrium for cylindrical bending using the principle of virtual displacements, $\delta W = 0$, where

$$\begin{aligned} \delta W = \int_0^a & \left\{ N_{xx} \delta \left[\frac{du_0}{dx} + \frac{1}{2} \left(\frac{dw_0}{dx} \right)^2 \right] + N_{xy} \delta \left(\frac{dv_0}{dx} \right) \right. \\ & \left. + M_{xx} \delta \left(-\frac{d^2 w_0}{dx^2} \right) - q \delta w_0 \right\} dx \end{aligned}$$

Use the laminate constitutive equations (4.4.13a), (4.4.13c), and (4.4.14a) to express the resulting Euler-Lagrange equations in terms of the displacements and the thermal stress resultants. These equations are a static version of those in Eqs. (4.4.1).

- 4.17** Consider the equations of equilibrium of cross-ply laminates in cylindrical bending in the absence of thermal effects:

$$A_{11} \frac{d^2 w_0}{dx^2} - B_{11} \frac{d^3 w_0}{dx^3} = 0, \quad -B_{11} \frac{d^3 w_0}{dx^3} + D_{11} \frac{d^4 w_0}{dx^4} = q$$

Show that the Navier solution of these equations for the simply supported boundary conditions is given by

$$u_0(x) = \frac{B_{11}}{D} \sum_{m=1} \frac{Q_m}{\alpha_m^3} \cos \alpha_m x, \quad w_0(x) = \frac{A_{11}}{D} \sum_{m=1} \frac{Q_m}{\alpha_m^4} \sin \alpha_m x$$

where $D = A_{11}D_{11} - B_{11}^2$ and $\alpha_m = \frac{m\pi}{a}$. The load $q(x)$ is also expanded in sine series with coefficient Q_m .

- 4.18** For the cylindrical bending problem of cross-ply plates (see Problem 4.17), show that (a) the stresses in the k th layer are given by

$$\begin{aligned} \sigma_{xx}^k &= \frac{(A_{11}z - B_{11})Q_{11}^k}{D} \sum_{m=1} \frac{Q_m}{\alpha_m^2} \sin \alpha_m x \\ \sigma_{yy}^k &= \frac{(A_{11}z - B_{11})Q_{12}^k}{D} \sum_{m=1} \frac{Q_m}{\alpha_m^2} \sin \alpha_m x \end{aligned}$$

and (b) the transverse stresses from the 3-D equations of equilibrium are given by

$$\begin{aligned} \sigma_{xz}^k &= -\frac{Q_{11}^k}{D} \left(A_{11} \frac{z^2}{2} - B_{11}z + G_i^k \right) \sum_{m=1} \frac{Q_m}{\alpha_m} \cos \alpha_m x \\ \sigma_{zz}^k &= \frac{Q_{11}^k}{D} \left(A_{11} \frac{z^3}{6} - B_{11} \frac{z^2}{2} + G^k z + H^k \right) \sum_{m=1} Q_m \sin \alpha_m x \end{aligned}$$

where G^k and H^k are constants to be determined such that the stress boundary conditions on σ_{xz} and σ_{zz} at $z = \pm h/2$ and the stress continuity conditions at the interfaces are satisfied.

- 4.19** Use the total potential energy functional

$$\Pi(w_0) = \frac{1}{2} \int_0^a \left[E_{xx}^b I_{yy} \left(\frac{d^2 w_0}{dx^2} \right)^2 - b N_{xx}^0 \left(\frac{dw_0}{dx} \right)^2 - I_0 b \omega^2 w_0^2 \right] dx$$

to construct a one-parameter Ritz solution to determine the natural frequency of vibration, ω , of a *simply supported* laminated beam with compressive load N_{xx}^0 . Use algebraic polynomials for the approximate functions. (Ans: $\omega = (1/a) \sqrt{(10/I_0)[(12E_{xx}^b I_{yy}/a^2 b) - N_{xx}^0]}$.)

- 4.20** Repeat Problem 4.19 for a laminated beam with clamped boundary condition at $x = 0$ and free at $x = a$ (i.e., cantilever beam). (Ans: $\omega = (1/a) \sqrt{(5/3I_0)[(12E_{xx}^b I_{yy}/a^2 b) - 4N_{xx}^0]}$.)

- 4.21** Use the total potential energy functional

$$\begin{aligned} \Pi(u_0, v_0, w_0) = & \int_0^a \left[\frac{A_{11}}{2} \left(\frac{du_0}{dx} \right)^2 + A_{16} \frac{du_0}{dx} \frac{dv_0}{dx} + \frac{A_{66}}{2} \left(\frac{dv_0}{dx} \right)^2 \right. \\ & \left. - \frac{d^2 w_0}{dx^2} \left(B_{11} \frac{du_0}{dx} + B_{16} \frac{dv_0}{dx} \right) + \frac{D_{11}}{2} \left(\frac{d^2 w_0}{dx^2} \right)^2 - q w_0 \right] dx \end{aligned}$$

to construct a one-parameter (for each variable) Ritz solution of (u_0, v_0, w_0) for a simply supported plate strip. Use algebraic polynomials for the approximate functions. (Ans: $a_1 = -Bq_0 a^2 / 12AD$, $b_1 = -Cq_0 a^2 / 12AD$, $c_1 = -q_0 a^2 / 24D$.)

- 4.22** Repeat Problem 4.21 for a plate strip with clamped boundary conditions at $x = 0$ and free boundary conditions at $x = a$. (*Ans:* $a_1 = Bq_0a^2/6AD$, $b_1 = Cq_0a^2/6AD$, $c_1 = q_0a^2/12D$.)

- 4.23** Use the total potential energy functional

$$\begin{aligned}\Pi(u_0, v_0, w_0) = \int_0^a & \left[\frac{A_{11}}{2} \left(\frac{du_0}{dx} \right)^2 + A_{16} \frac{du_0}{dx} \frac{dv_0}{dx} + \frac{A_{66}}{2} \left(\frac{dv_0}{dx} \right)^2 - \frac{N_{xx}^0}{2} \left(\frac{dw_0}{dx} \right)^2 \right. \\ & \left. - \frac{d^2 w_0}{dx^2} \left(B_{11} \frac{du_0}{dx} + B_{16} \frac{dv_0}{dx} \right) + \frac{D_{11}}{2} \left(\frac{d^2 w_0}{dx^2} \right)^2 \right] dx\end{aligned}$$

to construct a one-parameter (for each variable) Ritz solution to determine the critical buckling load N_{cr} of a plate strip with clamped boundary conditions at $x = 0$ and free boundary conditions at $x = a$. Use algebraic polynomials for the approximate functions. (*Ans:* $N_{cr} = 3D/a^2$.)

- 4.24** Use the total potential energy functional

$$\begin{aligned}\Pi(u_0, v_0, w_0) = \int_0^a & \left[\frac{A_{11}}{2} \left(\frac{du_0}{dx} \right)^2 + A_{16} \frac{du_0}{dx} \frac{dv_0}{dx} + \frac{A_{66}}{2} \left(\frac{dv_0}{dx} \right)^2 - \frac{N_{xx}^0}{2} \left(\frac{dw_0}{dx} \right)^2 \right. \\ & \left. - \frac{d^2 w_0}{dx^2} \left(B_{11} \frac{du_0}{dx} + B_{16} \frac{dv_0}{dx} \right) + \frac{D_{11}}{2} \left(\frac{d^2 w_0}{dx^2} \right)^2 - \frac{I_0 \omega^2}{2} w_0^2 \right] dx\end{aligned}$$

to construct a one-parameter (for each variable) Ritz solution to determine the natural frequency of vibration, ω , of a simply supported plate strip with edge compressive load N_{xx}^0 . Use algebraic polynomials for the approximate functions. (*Ans:* $\omega = (1/a)\sqrt{(10/I_0)[(12D/a^2) - N_{xx}^0]}$.)

- 4.25** Repeat Exercise 4.24 for a plate strip with clamped boundary condition at $x = 0$ and free at $x = a$. (*Ans:* $\omega = (1/a)\sqrt{(20/3I_0)[(3D/a^2) - N_{xx}^0]}$.)

- 4.26** Repeat Exercise 4.25 for cylindrical bending of a plate strip using the first-order shear deformation theory but neglecting rotary inertia.

- 4.27** Consider the buckling of a uniform beam according to the Timoshenko beam theory. The total potential energy functional for the problem can be written as

$$\Pi(w_0, \phi_x) = \frac{1}{2} \int_0^a \left[D \left(\frac{d\phi_x}{dx} \right)^2 + S \left(\frac{dw_0}{dx} + \phi_x \right)^2 - N_{xx}^0 \left(\frac{dw_0}{dx} \right)^2 \right] dx$$

where $w_0(x)$ is the transverse deflection, ϕ_x is the rotation, D is the flexural stiffness, S is the shear stiffness, and N_{xx}^0 is the axial compressive load. Determine the critical buckling load of a beam clamped at one end and simply supported at the other end. Use one-parameter Rayleigh–Ritz approximation for each variable.

- 4.28** Consider a laminated beam of length L , flexural stiffness $EI=\text{constant}$, and subjected to uniformly distributed transverse load $q(x) = q_0$. Suppose that the beam is subjected to the following geometric boundary conditions

$$w_0(0) = u_1, \quad -\frac{dw_0}{dx}(0) = u_2, \quad w_0(L) = u_3, \quad -\frac{dw_0}{dx}(L) = u_4 \quad (\text{a})$$

and force boundary conditions

$$\begin{aligned}\frac{d}{dx} \left(EI \frac{d^2 w_0}{dx^2} \right)_{x=0} &= Q_1, \quad \left(EI \frac{d^2 w_0}{dx^2} \right)_{x=L} = Q_2 \\ -\frac{d}{dx} \left(EI \frac{d^2 w_0}{dx^2} \right)_{x=L} &= Q_3, \quad -\left(EI \frac{d^2 w_0}{dx^2} \right)_{x=L} = Q_4 \quad (\text{b})\end{aligned}$$

Here (u_1, u_2) and (u_3, u_4) denote the transverse deflections and rotations (clockwise) at the left and right ends, respectively, and (Q_1, Q_3) and (Q_2, Q_4) are the associated shear forces and bending moments at the same points. Note that u_i and Q_i are introduced into the formulation to have the convenience of specifying a geometric or force boundary condition.

Assume Ritz approximation of the form (the exact solution of the homogeneous equation, $EId^4w_0/dx^4 = 0$ suggests this polynomial)

$$w_0(x) = c_1 + c_2x + c_3x^2 + c_4x^3 \quad (c)$$

and express the constants c_1, c_2, c_3 , and c_4 in terms of u_1, u_2, u_3 , and u_4 using the geometric boundary conditions (a) and rewrite (c) in the form

$$w_0(x) = u_1\varphi_1(x) + u_2\varphi_2(x) + u_3\varphi_3(x) + u_4\varphi_4(x) \quad (d)$$

Define the functions $\varphi_i(x)$ ($i = 1, 2, 3, 4$) that you derived. These functions can serve as the approximation functions for the Rayleigh–Ritz method (see the next exercise). (Ans: φ_i are the same as the Hermite cubic interpolation functions given in Section 10.2.)

- 4.29** (Continuation of Problem 4.28) Substitute the approximation

$$w_0(x) = \sum_{j=1}^4 u_j \varphi_j(x) \quad (a)$$

into the total potential energy functional associated with the Euler–Bernoulli beam theory

$$\Pi(w_0) = \frac{1}{2} \int_0^L EI \left(\frac{d^2w_0}{dx^2} \right)^2 dx - \int_0^L q(x) w_0(x) dx - \sum_{j=1}^4 Q_j u_j \quad (b)$$

and express it in the form

$$\Pi(u_1, u_2, u_3, u_4) = \sum_{i=1}^4 \sum_{j=1}^4 \frac{1}{2} K_{ij} u_i u_j - \sum_{j=1}^4 (q_j u_j + Q_j u_j) \quad (c)$$

(a) Define and evaluate the coefficients K_{ij} of the stiffness matrix and q_i of the force vector when $EI = \text{constant}$ and $q(x) = q_0$, a constant, and (b) use the total potential energy principle to determine the four-parameter Ritz solution for the problem. In particular, show that

$$[K]\{u\} = \{q\} + \{Q\} \quad (d)$$

(Ans: The stiffness matrix $[K]$ and force vector $\{q\}$ are the same as those given in Section 10.2 for the Euler–Bernoulli beam element.)

- 4.30** Since Eq. (d) of Problem 4.29 is valid for any boundary conditions, it can be used to determine solutions (which turn out to be exact) even for indeterminate beams. In particular, determine the displacement in the spring that supports the right end of a beam when the left end is fixed and the beam is subjected to uniformly distributed transverse load q_0 .
- 4.31** Equations (4.3.12b) and (4.3.13b) for ϕ_x and w_0 of the Timoshenko beam theory suggest that they can be approximated with quadratic and cubic polynomials

$$\phi_x(x) = a_1 + a_2x + a_3x^2, \quad w_0(x) = c_1 + c_2x + c_3x^2 + c_4x^3$$

Rewrite the constants a_i in terms of the values of ϕ_x at $x = 0$, $x = 0.5L$, and $x = L$ and obtain

$$\phi_x(x) = \Phi_1\psi_1(x) + \Phi_2\psi_2(x) + \Phi_3\psi_3(x) \quad (a)$$

where $\Phi_1 = \phi_x(0)$ etc. Show that $\psi_i(x)$ ($i = 1, 2, 3$) are the quadratic Lagrange interpolation functions derived in Section 10.3.

- 4.32** Use Eq. (a) of Problem 4.31 and Eq. (a) of Exercise 4.29 to express the total potential energy functional in terms of u_j and Φ_j :

$$\begin{aligned}\Pi(w_0, \phi_x) = & \frac{1}{2} \int_0^a \left[E_{xx}^b I_{yy} \left(\frac{d\phi_x}{dx} \right)^2 + KG_{xz}^b bh \left(\frac{dw_0}{dx} + \phi_x \right)^2 \right] dx \\ & - \int_0^a \hat{q} w_0 dx - \sum_{j=1}^4 Q_j u_j - \sum_{j=1}^3 P_j \Phi_j\end{aligned}\quad (\text{a})$$

where P_j ($j = 1, 2, 3$) are the moments corresponding to the rotations Φ_j . Then use the total potential energy principle to derive the Ritz equations for the problem.

- 4.33** The deflection, bending moment, and shear force of the Timoshenko beam theory can be expressed in terms of the corresponding quantities of the Euler–Bernoulli beam theory (see [27,28]). In order to establish these relationships, we use the following equations of the two theories:

$$-D_{xx} \frac{d^4 w_0^E}{dx^4} = -q(x), \quad D_{xx} \frac{d^3 \phi^T}{dx^3} = -q(x), \quad A_{xz} K_s \left(\frac{d\phi^T}{dx} + \frac{d^2 w_0^T}{dx^2} \right) = -q(x) \quad (\text{1a-c})$$

where K_s is the shear correction coefficient, and superscripts E and T on variables refer to the Euler–Bernoulli and Timoshenko beam theories. Show that

$$\begin{aligned}D_{xx} w_0^T(x) = & D_{xx} w_0^E(x) + \frac{D_{xx}}{A_{xz} K_s} M_{xx}^E(x) + C_1 \left(\frac{D_{xx}}{A_{xz} K_s} x - \frac{x^3}{6} \right) \\ & - C_2 \frac{x^2}{2} - C_3 x - C_4 \\ D_{xx} \phi^T(x) = & -D_{xx} \frac{dw_0^E}{dx} + C_1 \frac{x^2}{2} + C_2 x + C_3 \\ M_{xx}^T(x) = & M_{xx}^E(x) + C_1 x + C_2, \quad Q_x^T(x) = Q_x^E(x) + C_1\end{aligned}\quad (2)$$

where C_1, C_2, C_3 , and C_4 are constants of integration, which are to be determined using the boundary conditions of the particular beam.

- 4.34** Show that for simply supported beams all C_i of Problem 4.33 are zero.
- 4.35** Show that for cantilevered beams all C_i except $C_4 = M_{xx}^E(0)D_{xx}/(A_{xz}K_s)$ of Problem 4.33 are zero.
- 4.36** Consider bending of a beam of length L , clamped (or fixed) at the left end and simply supported at the right, and subjected to a uniformly distributed transverse load q_0 . The boundary conditions of the Euler–Bernoulli and Timoshenko beam theories for the problem are as follows:

$$\text{EBT : } w_0^E(0) = w_0^E(L) = \frac{dw_0^E}{dx}(0) = M_{xx}^E(L) = 0 \quad (1)$$

$$\text{TBT : } w_0^T(0) = w_0^T(L) = \phi^T(0) = M_{xx}^T(L) = 0 \quad (2)$$

Show that the constants of integration in Problem 4.33 are given by

$$C_1 = \frac{3\Omega}{(1+3\Omega)L} [M_{xx}^E(0) - M_{xx}^E(L)], \quad C_2 = -C_1 L, \quad C_3 = 0, \quad C_4 = \Omega M_{xx}^E(0)L^2 \quad (3)$$

where $\Omega = D_{xx}/(A_{xz}K_sL^2)$.

References for Additional Reading

1. Reddy, J. N., *Energy Principles and Variational Methods in Applied Mechanics*, Second Edition, John Wiley, New York (2002).
2. Reddy, J. N. (Ed.), *Mechanics of Composite Materials. Selected Works of Nicholas J. Pagano*, Kluwer, The Netherlands (1994).
3. Whitney, J. M. , *Structural Analysis of Laminated Anisotropic Plates*, Technomic, Lancaster, PA (1987).
4. Reissner, E., "The Effect of Transverse Shear Deformation on the Bending of Elastic Plates," *Journal of Applied Mechanics*, **12**, 69–77 (1945).
5. Mindlin, R. D., "Influence of Rotatory Inertia and Shear on Flexural Motions of Isotropic Elastic Plates," *Journal of Applied Mechanics, Transactions of ASME*, **18**, 31–38 (1951).
6. Uflyand, Ya. S., "The Propagation of Waves in the Transverse Vibrations of Bars and Plates," *Akad. Nauk SSSR. Prikl Mat. Mekh.*, **12**, 287–300 (1948) (in Russian).
7. Yang, P. C., Norris, C. H., and Stavsky, Y., "Elastic Wave Propagation in Heterogeneous Plates," *International Journal of Solids and Structures*, **2**, 665–684 (1966).
8. Whitney, J. M., "Shear Correction Factors for Orthotropic Laminates Under Static Load," *Journal of Applied Mechanics*, **40**(1), 302–304 (1973).
9. Brogan, W. L., *Modern Control Theory*, Prentice-Hall, Englewood Cliffs, NJ (1985).
10. Franklin, J. N., *Matrix Theory*, Prentice-Hall, Englewood Cliffs, NJ (1968).
11. Goldberg, J. L. and Schwartz, A. J., *Systems of Ordinary Differential Equations, An Introduction*, Harper and Row, New York, 1972.
12. Khdeir, A. A. and Reddy, J. N., "Free Vibration of Cross-Ply Laminated Beams with Arbitrary Boundary Conditions," *International Journal of Engineering Science*, **32** (12), 1971–1980 (1994).
13. Pagano, N. J., "Exact Solutions for Composite Laminates in Cylindrical Bending," *Journal of Composite Materials*, **3**, 398–411 (1969).
14. Pagano, N. J., "Influence of Shear Coupling in Cylindrical Bending of Anisotropic Laminates," *Journal of Composite Materials*, **4**, 330–343 (1970).
15. Pagano, N. J. and Wang, A. S. D., "Further Study of Composite Laminates Under Cylindrical Bending," *Journal of Composite Materials*, **5**, 521–528 (1971).
16. Weaver, W., Jr., Timoshenko, S. P., and Young, D. H., *Vibration Problems in Engineering*, Fifth Edition, John Wiley, New York (1990).
17. Clough, R. W. and Penzien, J., *Dynamics of Structures*, McGraw-Hill, New York (1975).
18. Pipes, L. A. and Harvill, L. R., *Applied Mathematics for Engineers and Physicists*, Third Edition, McGraw-Hill, New York (1970).
19. Timoshenko, S. P. and Gere, J. P., *Theory of Elastic Stability*, Second Edition, McGraw-Hill, New York (1959).
20. Timoshenko, S. P., "On the Correction for Shear of the Differential Equation for Transverse Vibrations of Prismatic Bars," *Philosophical Magazine*, **41**, 744–746 (1921).
21. Timoshenko, S. P., "On the Transverse Vibrations of Bars of Uniform Cross Section," *Philosophical Magazine*, **43**, 125–131 (1922).
22. Timoshenko, S. P. and Woinowsky-Krieger, S., *Theory of Plates and Shells*, McGraw-Hill, Singapore (1970).
23. Levinson, M., "A New Rectangular Beam Theory," *Journal of Sound and Vibration*, **74**, 81–87 (1981).
24. Bickford, W. B., "A Consistent Higher Order Beam Theory," *Developments in Theoretical and Applied Mechanics*, **11**, 137–150 (1982).
25. Reddy, J. N., "A Simple Higher-Order Theory for Laminated Composite Plates," *Journal of Applied Mechanics*, **51**, 745–752 (1984).
26. Heyliger, P. R. and Reddy, J. N., "A Higher-Order Beam Finite Element for Bending and Vibration Problems," *Journal of Sound and Vibration*, **126**(2), 309–326 (1988).

27. Wang, C. M., "Timoshenko Beam-Bending Solutions in Terms of Euler-Bernoulli Solutions," *Journal of Engineering Mechanics*, ASCE, **121**(6), 763–765 (1995).
28. Reddy, J. N., Wang, C. M., and Lee, K. H., "Relationship Between Bending Solutions of Classical and Shear Deformation Beam Theories," *International Journal of Solids & Structures*, **34**(26), 3373–3384 (1997).
29. Wang, C. M., Reddy, J. N., and Lee, K. H., *Shear Deformable Beams and Plates*, Elsevier, Oxford, UK (2000).
30. Reddy, J. N. and Barbosa, J. I., "On Vibration Suppression of Magnetostrictive Beams," *Smart Materials and Structures*, **9**, 49–58 (2000).
31. Anjanappa, M. and Bi, J., "A Theoretical and Experimental Study of Magnetostrictive Mini Actuators," *Smart Materials and Structures*, **3**, p. 83 (1994).
32. Krishna Murty, A. V., Anjanappa, M. and Wu, Y.-F., "The Use of Magnetostrictive Particle Actuators for Vibration Attenuation of Flexible Beams," *Journal of Sound and Vibration*, **206**(2), 133–149 (1997).
33. Krishna Murty, A. V., Anjanappa, M., Wu, Y.-F., Bhattacharya, B., and Bhat, M. S., "Vibration Suppression of Laminated Composite Beams Using Embedded Magnetostrictive Layers," *IE (I) Journal-AS*, **78**, 38–44 (1998).
34. Dapino, M. J., Flatau, A. B. and Calkins, F. T., "Statistical Analysis of Terfenol-D Materials Properties" *Proceedings of SPIE – Smart Structures and Materials*, paper 3041-20 (1997).
35. Flatau, A. B., Dapino, M. J. and Calkins, F. T., "High Bandwidth Tunability in Smart Absorber" *Proceedings of SPIE – Smart Structures and Integrated Systems*, paper 42, **3327** (1998).
36. Lagoudas, D. C., Dakshina Moorthy, C.M., Qidwai, M. A., and Reddy, J. N., "Modeling of the Thermomechanical Response of Active Laminates with SMA Strips Using the Layerwise Finite Element Method," *Journal of Intelligent Material Systems and Structures*, **8**, 476–488 (1997).
37. Ang, K. K., Reddy, J. N., and Wang, C. M., "Displacement Control of Timoshenko Beams via Induced Strain Actuators," *Smart Materials and Structures*, **9**, 1–4 (2000).

Analysis of Specially Orthotropic Laminates Using CLPT

5.1 Introduction

The governing equations of composite laminates according to various laminate theories were developed in Chapter 3. These equations can be solved either analytically or numerically for the generalized displacements and strains. Stresses can be determined using either the constitutive equations or the 3-D equilibrium equations expressed in terms of stresses. Analytical solutions were developed in Chapter 4 for certain one-dimensional problems, namely laminated beams and cylindrical bending of laminates. Analytical solutions can also be developed for rectangular laminates with certain lamination schemes and boundary conditions.

In this chapter we develop analytical solutions of *specially orthotropic plates*, i.e., plates for which the bending-stretching coupling coefficients B_{ij} and bending-twisting coefficients D_{16} and D_{26} are zero, using the classical laminate theory. The analysis of specially orthotropic laminates is greatly simplified because the bending deformation is uncoupled from the extensional deformation and the fact that $D_{16} = D_{26} = 0$. This class of laminates will be used to gain a basic understanding of the response. Although most laminates of practical interest do not qualify as specially orthotropic plates because of the presence of bending-twisting coupling terms D_{16} and D_{26} , they may represent reasonable approximations to more complex laminates. In the subsequent chapters, the solutions obtained for more complicated laminates will be compared with those of the specially orthotropic plates to assess their behavior.

The solution methods used here are the Navier method, the Lévy method with the state-space approach, and the Ritz method. The Navier solutions can be developed for a rectangular laminate when all four edges of the laminate are simply supported. The Lévy solutions can be developed for plates with two opposite edges simply supported and the remaining two edges having any possible combination of boundary conditions: free, simple support, or fixed support. The Ritz method can be used to determine approximate solutions for more general boundary conditions, as long as we can find suitable approximation functions for the problem.

The equation of motion governing bending deflection w_0 of a specially orthotropic plate can be deduced from Eq. (3.3.47) by omitting the nonlinear terms, bending-stretching terms, and bending-twisting terms. We have

$$\begin{aligned} & - \left[D_{11} \frac{\partial^4 w_0}{\partial x^4} + 2(D_{12} + 2D_{66}) \frac{\partial^4 w_0}{\partial x^2 \partial y^2} + D_{22} \frac{\partial^4 w_0}{\partial y^4} \right] + q \\ & - \left(\frac{\partial^2 M_{xx}^T}{\partial x^2} + 2 \frac{\partial^2 M_{xy}^T}{\partial x \partial y} + \frac{\partial^2 M_{yy}^T}{\partial y^2} \right) + \hat{N}_{xx} \frac{\partial^2 w_0}{\partial x^2} + 2\hat{N}_{xy} \frac{\partial^2 w_0}{\partial x \partial y} + \hat{N}_{yy} \frac{\partial^2 w_0}{\partial y^2} \\ & = I_0 \ddot{w}_0 - I_2 \left(\frac{\partial^2 \ddot{w}_0}{\partial x^2} + \frac{\partial^2 \ddot{w}_0}{\partial y^2} \right) \end{aligned} \quad (5.1.1)$$

Equation (5.1.1) must be solved, in conjunction with appropriate boundary conditions [see Eq. (3.3.34)] and initial conditions of the problem, for the desired response. The boundary conditions at any point on the boundary are of the form

$$w_0 \text{ or } V_n \equiv Q_n + \partial M_{ns} \partial s \quad (5.1.2)$$

and

$$\frac{\partial w_0}{\partial n} \text{ or } M_{nn} \quad (5.1.3)$$

where Q_n and M_{nn} are defined in Eqs. (3.3.31b) and (3.3.29b), respectively.

In this chapter, we wish to determine static deflections and stresses, frequencies of natural vibration, and buckling loads under in-plane compressive or shear loads of specially orthotropic plates. We seek exact solutions whenever possible, and approximate solutions using the Ritz method when exact solutions cannot be developed.

5.2 Bending of Simply Supported Rectangular Plates

5.2.1 Governing Equations

Here we consider the static bending in the absence of thermal effects and in-plane forces. Equation (5.1.1) for this case reduces to

$$D_{11} \frac{\partial^4 w_0}{\partial x^4} + 2(D_{12} + 2D_{66}) \frac{\partial^4 w_0}{\partial x^2 \partial y^2} + D_{22} \frac{\partial^4 w_0}{\partial y^4} = q \quad (5.2.1)$$

The simply supported boundary conditions on all four edges of the rectangular plate (see Figure 5.2.1) can be expressed as

$$w_0(x, 0) = 0, \quad w_0(x, b) = 0, \quad w_0(0, y) = 0, \quad w_0(a, y) = 0 \quad (5.2.2a)$$

$$M_{xx}(0, y) = 0, \quad M_{xx}(a, y) = 0, \quad M_{yy}(x, 0) = 0, \quad M_{yy}(x, b) = 0 \quad (5.2.2b)$$

where the bending moments are related to the transverse deflection by the equations

$$\begin{aligned} M_{xx} &= - \left(D_{11} \frac{\partial^2 w_0}{\partial x^2} + D_{12} \frac{\partial^2 w_0}{\partial y^2} \right) \\ M_{yy} &= - \left(D_{12} \frac{\partial^2 w_0}{\partial x^2} + D_{22} \frac{\partial^2 w_0}{\partial y^2} \right) \\ M_{xy} &= -2D_{66} \frac{\partial^2 w_0}{\partial x \partial y} \end{aligned} \quad (5.2.3)$$

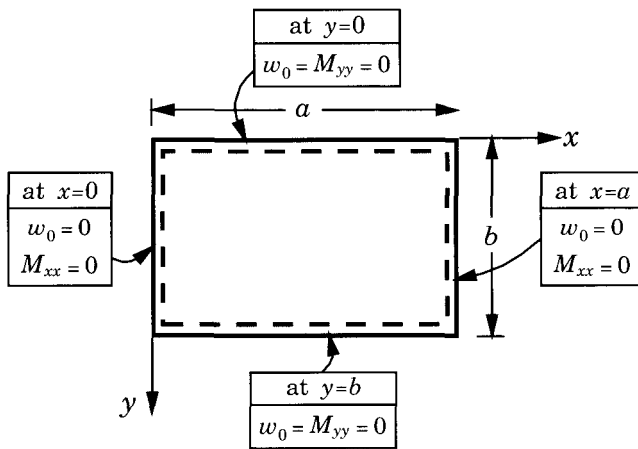


Figure 5.2.1: Geometry, coordinate system, and simply supported boundary conditions for a rectangular plate.

and a and b denote the in-plane dimensions along the x - and y -coordinate directions of the rectangular laminate. The origin of the coordinate system is taken at the lower left corner of the midplane (see Figure 5.2.1).

5.2.2 The Navier Solution

In the Navier method the displacement w_0 is expanded in a double trigonometric (Fourier) series in terms of unknown parameters. The choice of the trigonometric functions in the series is restricted to those which satisfy the boundary conditions of the problem. The load $q(x, y)$ is also expanded in double trigonometric series. Substitution of the displacement and load expansions into the governing equation should result in an invertible set of algebraic equations among the parameters of the displacement expansion. Otherwise, the Navier solution cannot be developed for the problem. The simply supported boundary conditions in Eq. (5.2.2) admit the Navier solution for specially orthotropic rectangular laminates.

The boundary conditions in Eq. (5.2.2) are satisfied by the following form of the transverse deflection

$$w_0(x, y) = \sum_{n=1}^{\infty} \sum_{m=1}^{\infty} W_{mn} \sin \alpha x \sin \beta y \quad (5.2.4)$$

where $\alpha = m\pi/a$ and $\beta = n\pi/b$, and W_{mn} are coefficients to be determined such that the governing equation (5.2.1) is satisfied everywhere in the domain of the plate. We assume that the load can also be expanded in the series form as

$$q(x, y) = \sum_{n=1}^{\infty} \sum_{m=1}^{\infty} Q_{mn} \sin \alpha x \sin \beta y \quad (5.2.5a)$$

where

$$Q_{mn} = \frac{4}{ab} \int_0^b \int_0^a q(x, y) \sin \alpha x \sin \beta y dx dy \quad (5.2.5b)$$

Substitution of the expansions (5.2.4) and (5.2.5) into Eq. (5.2.1) yields

$$\sum_{n=1}^{\infty} \sum_{m=1}^{\infty} \left\{ -W_{mn} [D_{11}\alpha^4 + 2(D_{12} + 2D_{66})\alpha^2\beta^2 + D_{22}\beta^4] + Q_{mn} \right\} \sin \alpha x \sin \beta y = 0 \quad (5.2.6)$$

Since the equation must hold for every point (x, y) of the domain $0 < x < a$ and $0 < y < b$, the expression inside the curl brackets (or braces) should be zero for every m and n . This yields

$$W_{mn} = \frac{Q_{mn}}{d_{mn}} \quad (5.2.7a)$$

$$d_{mn} = \frac{\pi^4}{b^4} [D_{11}m^4s^4 + 2(D_{12} + 2D_{66})m^2n^2s^2 + D_{22}n^4] \quad (5.2.7b)$$

where s denotes the plate aspect ratio, $s = b/a$. Then the solution in Eq. (5.2.4) becomes

$$w_0(x, y) = \sum_{n=1}^{\infty} \sum_{m=1}^{\infty} \frac{Q_{mn}}{d_{mn}} \sin \alpha x \sin \beta y \quad (5.2.8)$$

The load coefficients Q_{mn} for various types of loading [see Eq. (5.2.5b)] are listed in Table 5.2.1. The effect of thermal moments can be easily incorporated into the calculation.

For example, the Navier solution for a sinusoidally distributed transverse load

$$q(x, y) = q_0 \sin \frac{\pi x}{a} \sin \frac{\pi y}{b} \quad (5.2.9)$$

is a one-term solution ($Q_{mn} = q_0$ and $m = n = 1$), and therefore it is a *closed-form solution*. For other types of loads, the Navier solution is a series solution, which can be evaluated for a sufficient number of terms in the series. In particular, for uniformly distributed load $q(x, y) = q_0$, a constant, we have

$$Q_{mn} = \frac{16q_0}{\pi^2 mn} \text{ for } m, n, \text{ odd} \quad (5.2.10)$$

For a point load Q_0 located at (x_0, y_0) , the load coefficients are given by [$q(x, y) = Q_0\delta(x - x_0, y - y_0)$]

$$Q_{mn} = \frac{4Q_0}{ab} \sin \frac{m\pi x_0}{a} \sin \frac{n\pi y_0}{b} \quad (5.2.11)$$

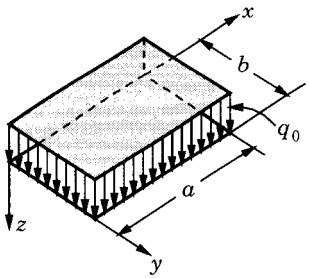
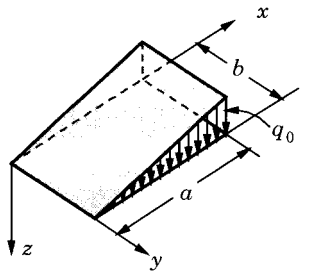
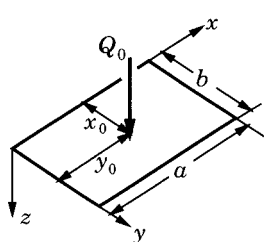
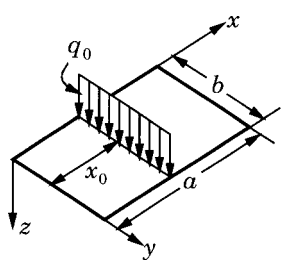
The bending moments can be calculated from

$$M_{xx} = \sum_{n=1}^{\infty} \sum_{m=1}^{\infty} (D_{11}\alpha^2 + D_{12}\beta^2) W_{mn} \sin \frac{m\pi x}{a} \sin \frac{n\pi y}{b} \quad (5.2.12a)$$

$$M_{yy} = \sum_{n=1}^{\infty} \sum_{m=1}^{\infty} (D_{12}\alpha^2 + D_{22}\beta^2) W_{mn} \sin \frac{m\pi x}{a} \sin \frac{n\pi y}{b} \quad (5.2.12b)$$

$$M_{xy} = -2 \sum_{n=1}^{\infty} \sum_{m=1}^{\infty} \alpha\beta D_{66} W_{mn} \cos \frac{m\pi x}{a} \cos \frac{n\pi y}{b} \quad (5.2.12c)$$

Table 5.2.1: Coefficients in the double trigonometric series expansion of loads in the Navier method.

Load $q(x, y)$	Coefficients Q_{mn}
Uniform load, $q = q_0$	 $Q_{mn} = \frac{16q_0}{\pi^2 mn}$ $(m, n = 1, 3, 5, \dots)$
Hydrostatic load, $q(x, y) = q_0 \frac{x}{a}$	 $Q_{mn} = \frac{8q_0 \cos m\pi}{\pi^2 mn}$ $(m, n = 1, 3, 5, \dots)$
Point load, $q(x, y) = Q_0$ at (x_0, y_0)	 $Q_{mn} = \frac{4Q_0}{ab} \sin \frac{m\pi x_0}{a} \sin \frac{n\pi y_0}{b}$ $(m, n = 1, 2, 3, \dots)$
Line load, $q(x, y) = q_0$ at $x = x_0$	 $Q_{mn} = \frac{8q_0}{\pi a n} \sin \frac{m\pi x_0}{a}$ $(m = 1, 3, 5, \dots; n = 1, 2, 3, \dots)$

The in-plane stresses can be computed from Eqs. (4.2.12a)

$$\begin{aligned} \begin{Bmatrix} \sigma_{xx} \\ \sigma_{yy} \\ \sigma_{xy} \end{Bmatrix}^{(k)} &= -z \begin{bmatrix} \bar{Q}_{11} & \bar{Q}_{12} & 0 \\ \bar{Q}_{12} & \bar{Q}_{22} & 0 \\ 0 & 0 & \bar{Q}_{66} \end{bmatrix}^{(k)} \begin{Bmatrix} \frac{\partial^2 w_0}{\partial x^2} \\ \frac{\partial^2 w_0}{\partial y^2} \\ 2 \frac{\partial^2 w_0}{\partial x \partial y} \end{Bmatrix} \\ &= z \sum_{n=1}^{\infty} \sum_{m=1}^{\infty} W_{mn} \begin{Bmatrix} (\bar{Q}_{11}^{(k)} \alpha^2 + \bar{Q}_{12}^{(k)} \beta^2) \sin \frac{m\pi x}{a} \sin \frac{n\pi y}{b} \\ (\bar{Q}_{12}^{(k)} \alpha^2 + \bar{Q}_{22}^{(k)} \beta^2) \sin \frac{m\pi x}{a} \sin \frac{n\pi y}{b} \\ -2\bar{Q}_{66}^{(k)} \alpha \beta \cos \frac{m\pi x}{a} \cos \frac{n\pi y}{b} \end{Bmatrix} \quad (5.2.13) \end{aligned}$$

The maximum normal stresses occur at $(x, y, z) = (a/2, b/2, h/2)$, and the shear stress is maximum at $(x, y, z) = (a, b, -h/2)$ and other three corners.

The interlaminar stresses are identically zero when computed from the constitutive equations in the classical laminate theory. However, they can be computed using the 3-D stress equilibrium equations [see Eqs. (4.2.13)] for any $z_k \leq z \leq z_{k+1}$:

$$\begin{aligned} \sigma_{xz}^{(k)} &= - \int_{z_k}^z \left(\frac{\partial \sigma_{xx}^{(k)}}{\partial x} + \frac{\partial \sigma_{xy}^{(k)}}{\partial y} \right) dz + C_1^{(k)}(x, y) \\ \sigma_{yz}^{(k)} &= - \int_{z_k}^z \left(\frac{\partial \sigma_{xy}^{(k)}}{\partial x} + \frac{\partial \sigma_{yy}^{(k)}}{\partial y} \right) dz + C_2^{(k)}(x, y) \\ \sigma_{zz}^{(k)} &= - \int_{z_k}^z \left(\frac{\partial \sigma_{xz}^{(k)}}{\partial x} + \frac{\partial \sigma_{yz}^{(k)}}{\partial y} \right) dz + C_3^{(k)}(x, y) \quad (5.2.14) \end{aligned}$$

where the stresses $\sigma_{xx}^{(k)}, \sigma_{xy}^{(k)}$, and $\sigma_{yy}^{(k)}$ are known from Eq. (5.2.13), and $C_i^{(k)}$ are functions to be determined using the boundary conditions, $\sigma_{xz}(x, y, -h/2) = \sigma_{yz}(x, y, -h/2) = \sigma_{zz}(x, y, -h/2) = 0$ and continuity of stresses at layer interfaces. We obtain

$$\begin{aligned} \sigma_{xz}^{(k)} &= -\mathcal{X}(z) \sum_{n=1}^{\infty} \sum_{m=1}^{\infty} T_{12}^{(k)} W_{mn} \cos \frac{m\pi x}{a} \sin \frac{n\pi y}{b} + \sigma_{xz}^{(k-1)}(x, y, z_k) \\ \sigma_{yz}^{(k)} &= -\mathcal{Y}(z) \sum_{n=1}^{\infty} \sum_{m=1}^{\infty} T_{13}^{(k)} W_{mn} \sin \frac{m\pi x}{a} \cos \frac{n\pi y}{b} + \sigma_{yz}^{(k-1)}(x, y, z_k) \\ \sigma_{zz}^{(k)} &= -\mathcal{Z}(z) \sum_{n=1}^{\infty} \sum_{m=1}^{\infty} T_{33}^{(k)} W_{mn} \sin \frac{m\pi x}{a} \sin \frac{n\pi y}{b} + \sigma_{zz}^{(k-1)}(x, y, z_k) \\ &\quad + (z - z_k) \left(\frac{\partial \sigma_{xz}^{(k)}}{\partial x} + \frac{\partial \sigma_{yz}^{(k)}}{\partial y} \right)_{z_k} \quad (5.2.15a) \end{aligned}$$

where

$$\mathcal{X}(z) = \mathcal{Y}(z) = \left(\frac{z^2 - z_k^2}{2} \right), \quad \mathcal{Z}(z) = \left[\frac{z_k^3}{3} + \frac{z}{6} (z^2 - 3z_k^2) \right] \quad (5.2.15b)$$

and ($T_{33}^{(k)} = \alpha T_{12} + \beta T_{13}$)

$$\begin{aligned} T_{12}^{(k)} &= \alpha^3 \bar{Q}_{11}^{(k)} + \alpha \beta^2 (2\bar{Q}_{66}^{(k)} + \bar{Q}_{12}^{(k)}) \\ T_{13}^{(k)} &= \beta^3 \bar{Q}_{22}^{(k)} + \alpha^2 \beta (2\bar{Q}_{66}^{(k)} + \bar{Q}_{12}^{(k)}) \\ T_{33}^{(k)} &= \alpha^4 \bar{Q}_{11}^{(k)} + 2\alpha^2 \beta^2 (2\bar{Q}_{66}^{(k)} + \bar{Q}_{12}^{(k)}) + \beta^4 \bar{Q}_{22}^{(k)} \end{aligned} \quad (5.2.15c)$$

For single-layer plates, the expressions in Eq. (5.2.15a) can be simplified to

$$\begin{aligned} \sigma_{xz} &= \frac{h^2}{8} \left[1 - \left(\frac{2z}{h} \right)^2 \right] \sum_{n=1}^{\infty} \sum_{m=1}^{\infty} T_{12}^{(1)} W_{mn} \cos \frac{m\pi x}{a} \sin \frac{n\pi y}{b} \\ \sigma_{yz} &= \frac{h^2}{8} \left[1 - \left(\frac{2z}{h} \right)^2 \right] \sum_{n=1}^{\infty} \sum_{m=1}^{\infty} T_{13}^{(1)} W_{mn} \sin \frac{m\pi x}{a} \cos \frac{n\pi y}{b} \\ \sigma_{zz} &= -\frac{h^3}{48} \left\{ \left[1 + \left(\frac{2z}{h} \right)^3 \right] - 3 \left[1 + \left(\frac{2z}{h} \right) \right] \right\} \times \\ &\quad \sum_{n=1}^{\infty} \sum_{m=1}^{\infty} T_{33}^{(1)} W_{mn} \sin \frac{m\pi x}{a} \sin \frac{n\pi y}{b} \end{aligned} \quad (5.2.16)$$

In integrating the stress-equilibrium equations it is assumed that the stresses ($\sigma_{xz}, \sigma_{yz}, \sigma_{zz}$) are zero at $z = h/2$. Because of the assumptions of the laminate plate theory, $\sigma_{zz} = -q$ at $z = -h/2$.

Table 5.2.2 contains the nondimensionalized maximum transverse deflections and stresses of square laminates under various types of loads. For the case of mechanical loading, the deflection and stresses are nondimensionalized as follows:

$$\begin{aligned} \hat{w} &= w_0(0, 0) \left(\frac{E_2 h^3}{a^4 q_0} \right) \times 10^2; \quad \bar{\sigma}_{xx} = \sigma_{xx} \left(\frac{a}{2}, \frac{b}{2}, \frac{h}{2} \right) \left(\frac{h^2}{a^2 q_0} \right) \\ \bar{\sigma}_{yy} &= \sigma_{yy} \left(\frac{a}{2}, \frac{b}{2}, \frac{h}{2} \right) \left(\frac{h^2}{a^2 q_0} \right); \quad \bar{\sigma}_{xy} = \sigma_{xy} \left(a, b, -\frac{h}{2} \right) \left(\frac{h^2}{a^2 q_0} \right) \\ \bar{\sigma}_{xz} &= \sigma_{xz} \left(0, \frac{b}{2}, 0 \right) \left(\frac{h}{aq_0} \right); \quad \bar{\sigma}_{yz} = \sigma_{yz} \left(\frac{a}{2}, 0, 0 \right) \left(\frac{h}{aq_0} \right) \end{aligned} \quad (5.2.17)$$

For the thermal load case, the nondimensionalized quantities are defined as

$$\begin{aligned} \hat{w} &= w_0(0, 0) \beta \times 10^2; \quad \bar{\sigma}_{xx} = \sigma_{xx} \left(\frac{a}{2}, \frac{b}{2}, \frac{h}{2} \right) \left(\frac{\beta a}{E_2} \right); \quad \beta = \frac{1}{\alpha_1 T_1 h a} \\ \bar{\sigma}_{yy} &= \sigma_{yy} \left(\frac{a}{2}, \frac{b}{2}, \frac{h}{2} \right) \left(\frac{\beta a}{E_2} \right); \quad \bar{\sigma}_{xy} = \sigma_{xy} \left(a, b, -\frac{h}{2} \right) \left(\frac{\beta a}{E_2} \right) \end{aligned} \quad (5.2.18)$$

The mechanical load consists of only the transverse load $q(x, y)$, and the thermal load consists of linear temperature distribution through the laminate thickness, $\Delta T = zT_1(x, y)$. Both q and T_1 are assumed to be sinusoidal, uniform, or point

functions. In the case of uniform and point source distribution, the first ten terms of the double trigonometric series are evaluated.

Plots of nondimensionalized maximum transverse deflection \bar{w} and normal stress $\bar{\sigma}_{xx}$ as a function of the plate aspect ratio a/b are shown in Figures 5.2.2 and 5.2.3, respectively, for symmetric cross-ply (0/90/90/0) laminates under uniformly distributed (UDL) and sinusoidally distributed (SSL) loads. The material properties of the lamina are taken to be: $E_1/E_2 = 25$, $G_{12} = G_{13} = 0.5E_2$, and $\nu_{12} = 0.25$. For uniformly distributed load, the maximum deflection and (negative) stress occur for an aspect ratio around 1.5, whereas for sinusoidally distributed load the maxima are reached around $a/b = 2.5$.

Figures 5.2.4 and 5.2.5 show the distributions of the maximum in-plane normal stresses $\bar{\sigma}_{xx}$ and $\bar{\sigma}_{yy}$, respectively, through the thickness for laminates (0/90/0) and (0/90/90/0) under sinusoidally distributed transverse load, and Figure 5.2.6 shows the distribution of the maximum transverse shear stresses through the thickness for the two laminates ($a/b = 1$, $E_1 = 25E_2$, $G_{12} = G_{13} = 0.5E_2$, $\nu_{12} = 0.25$).

Table 5.2.2: Transverse deflections and stresses in specially orthotropic square laminates subjected to various types of mechanical and thermal loads ($E_1/E_2 = 25$, $G_{12} = G_{13} = 0.5E_2$, $G_{23} = 0.2E_2$, $\nu_{12} = 0.25$, $\alpha_1 = 3\alpha_2$, $T_0 = 0$); all laminates are of the same total thickness.

Laminate	Mechanical					Thermal				
	\hat{w}	$\bar{\sigma}_{xx}$	$\bar{\sigma}_{yy}$	$\bar{\sigma}_{xy}$	$\bar{\sigma}_{xz}^\dagger$	\hat{w}	$\bar{\sigma}_{xx}$	$\bar{\sigma}_{yy}$	$\bar{\sigma}_{xy}$	
SSL*										
0°	0.4312	0.5387	0.0267	0.0213	0.4398	9.1263	0.1172	0.0272	0.0450	
(0°/90°/0°)	0.4312	0.5387	0.0267	0.0213	0.3951	9.1263	0.1172	0.0272	0.0450	
UDL(19)										
0°	0.6497	0.7866	0.0244	0.0463	0.7758	13.246	1.3135	0.0430	0.1893	
(0°/90°/0°)	0.6660	0.8075	0.0306	0.0425	0.7191	13.4863	1.3463	0.0521	0.1811	
CPL(49)										
0°	2.3231	6.7317	1.0119	0.0409	1.8148	6.7273	0.0913	0.0178	19.394	
(0°/90°/0°)	2.1298	6.1582	0.7025	0.0558	1.5076	7.1570	0.0230	0.006	18.810	

* SSL=Sinusoidal load; UDL=Uniformly distributed load; CPL=Central point load; the number in parentheses denotes the number of terms used in the double Fourier series to evaluate the series. The transverse shear stress σ_{xz} is the maximum at $(x, y, z) = (0, b/2, 0)$, σ_{yz} is the maximum at $(x, y, z) = (a/2, 0, 0)$, and the transverse normal stress σ_{zz} is the maximum at $(x, y, z) = (a/2, b/2, h/2)$.

† From equilibrium equations (mechanical load).

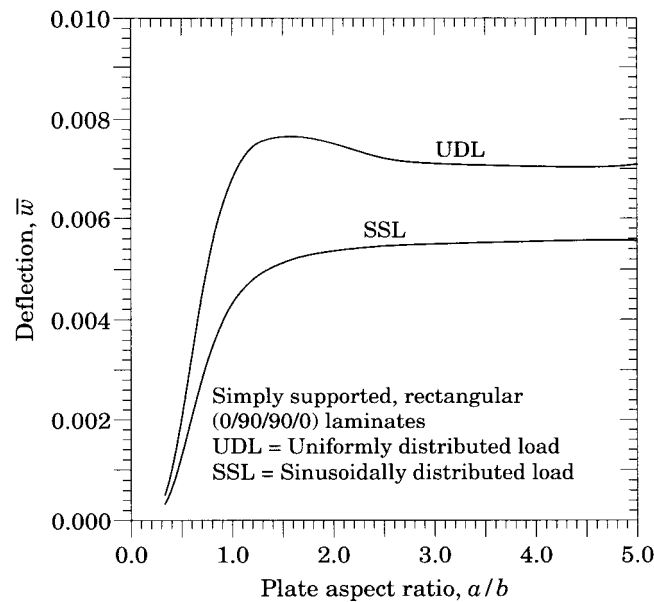


Figure 5.2.2: Nondimensionalized maximum transverse displacement $\bar{w} = w_0(E_2 h^3/a^4 q_0)$ versus plate aspect ratio (a/b) of symmetric cross-ply (0/90/90/0) laminates.

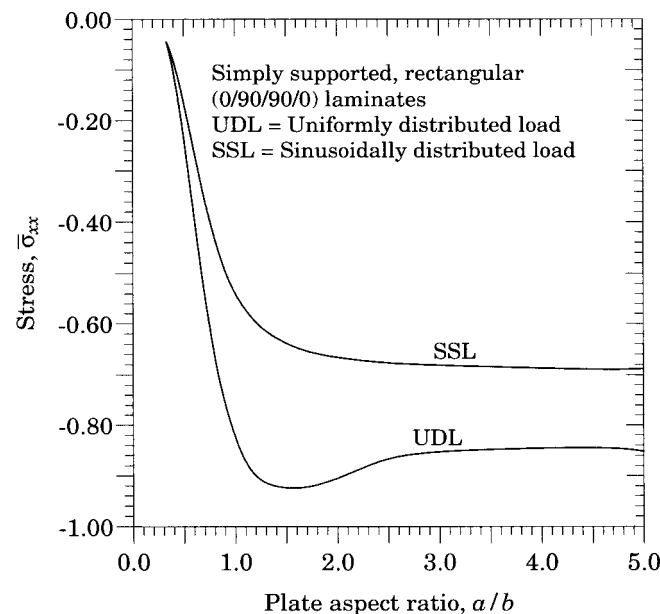


Figure 5.2.3: Nondimensionalized maximum normal stress ($\bar{\sigma}_{xx}$) versus plate aspect ratio (a/b) of symmetric cross-ply (0/90/90/0) laminates.

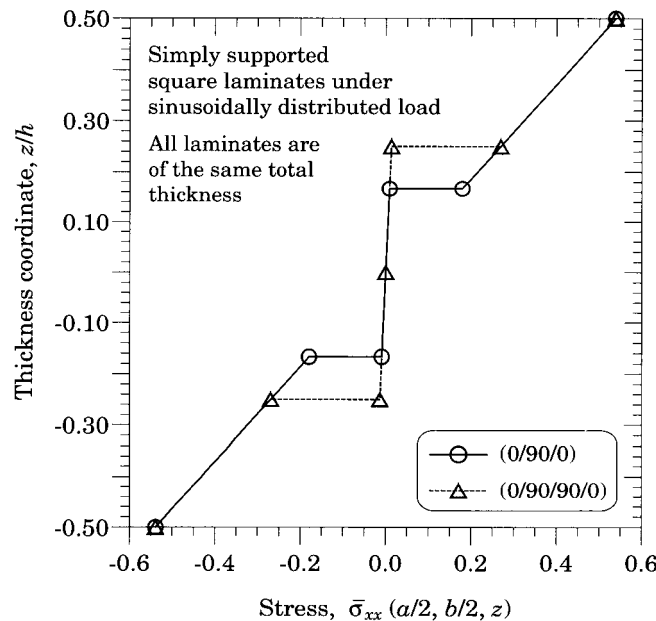


Figure 5.2.4: Variation of nondimensionalized maximum normal stress ($\bar{\sigma}_{xx}$) through the thickness (z/h) of square cross-ply laminates under sinusoidally distributed load.

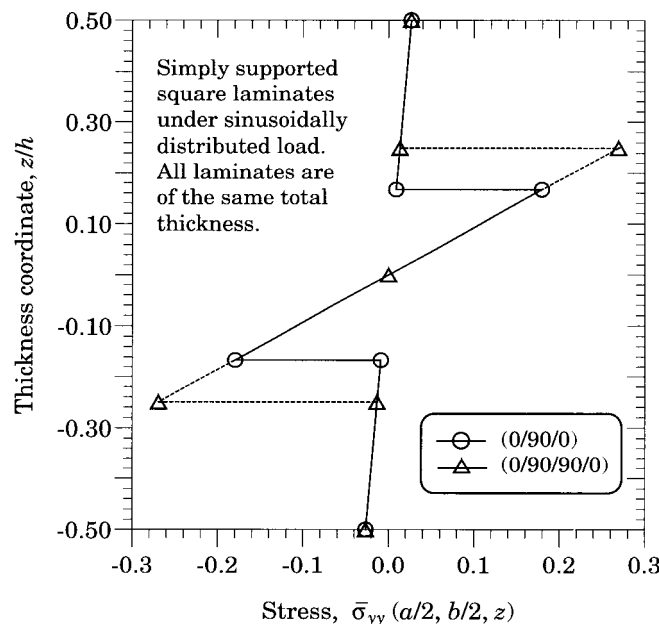


Figure 5.2.5: Variation of nondimensionalized maximum normal stress ($\bar{\sigma}_{yy}$) through the thickness (z/h) of square cross-ply laminates under sinusoidally distributed load.

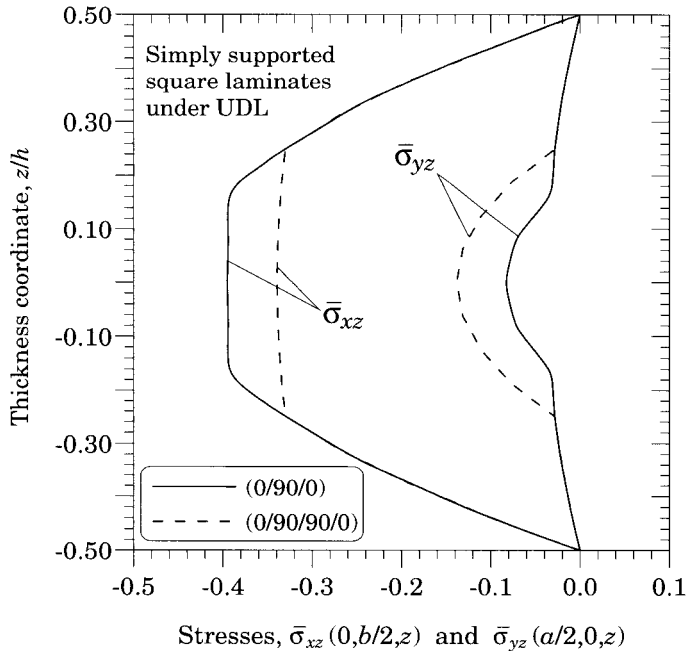


Figure 5.2.6: Variation of nondimensionalized maximum transverse shear stresses, $\bar{\sigma}_{yz}$ and $\bar{\sigma}_{xz}$, through the thickness (z/h) of square cross-ply laminates. The stresses are the same in both laminates.

5.3 Bending of Plates with Two Opposite Edges Simply Supported

5.3.1 The Lévy Solution Procedure

Consider a rectangular plate with simply supported edges along $y = 0, b$ and subjected to a transverse load q . The other two edges at $x = 0, a$, can each be free, simply supported, or clamped, independent of the other. For such problems, the Navier solution cannot be developed. However, the idea of the Navier method can be applied with respect to the simply supported boundary conditions at $y = 0, b$ to reduce the partial differential equation (5.2.1) to an ordinary differential equation with respect to the coordinate x , which may then be solved exactly or approximately. This procedure is known as the Lévy method.

The solution to the problem of a rectangular plate with two opposite edges simply supported and the other two edges having arbitrary boundary conditions can be represented in terms of single Fourier series as

$$w_0(x, y) = \sum_{n=1}^{\infty} W_n(x) \sin \beta y \quad (5.3.1)$$

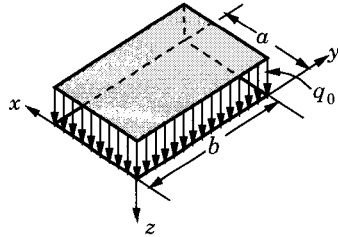
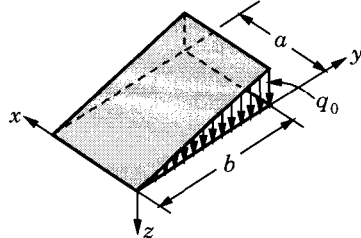
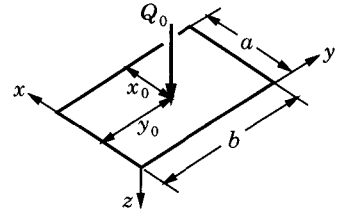
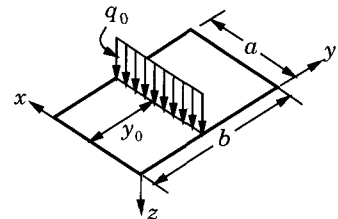
Similarly, the load is represented as

$$q(x, y) = \sum_{n=1}^{\infty} Q_n(x) \sin \beta y \quad (5.3.2a)$$

where $Q_n(x)$ are given by (see Table 5.3.1)

$$Q_n(x) = \frac{2}{b} \int_0^b q(x, y) \sin \beta y dy \quad (5.3.2b)$$

Table 5.3.1: Coefficients in the single trigonometric series expansion of loads in the Lévy method.

Load $q(x)$	Coefficients Q_n
Uniform load, $q = q_0$	 $Q_n = \frac{4q_0}{\pi n}$ $(n = 1, 3, 5, \dots)$
Hydrostatic load, $q(x) = (q_0 y/b)$	 $Q_n = \frac{2q_0}{n\pi} (-1)^{n+1}$ $(n = 1, 2, 3, \dots)$
Point load, $q(x) = Q_0$ at (x_0, y_0)	 $Q_n = \frac{2Q_0}{b} \sin \frac{n\pi y_0}{b}$ $(n = 1, 2, 3, \dots)$
Line load, $q(x) = q_0$ at $y = y_0$	 $Q_n = \frac{2q_0}{b} \delta(x - x_0) \sin \frac{n\pi y_0}{b}$ $(n = 1, 2, 3, \dots)$

The assumed solution in Eq. (5.3.1) satisfies the simply supported boundary conditions on edges $y = 0, b$. In the case of uniformly distributed load of intensity q_0 , the coefficients Q_n are given by

$$Q_n(x) = \frac{4q_0}{n\pi} , \quad n = 1, 3, \dots \quad (5.3.3)$$

Substituting Eqs. (5.3.2a) and (5.3.1) into Eq. (5.2.1), we obtain

$$\sum_{n=1}^{\infty} \left[D_{11} \frac{d^4 W_n}{dx^4} - 2(D_{12} + 2D_{66}) \beta^2 \frac{d^2 W_n}{dx^2} + D_{22} \beta^4 W_n - Q_n \right] \sin \beta y = 0 \quad (5.3.4)$$

Since the result must hold for any y , it follows that the expression in the square brackets must be zero:

$$D_{11} \frac{d^4 W_n}{dx^4} - 2(D_{12} + 2D_{66}) \beta^2 \frac{d^2 W_n}{dx^2} + D_{22} \beta^4 W_n = Q_n \quad (5.3.5)$$

The ordinary fourth-order differential equation (5.3.5) can be solved either analytically or by an approximate method. Analytically, Eq. (5.3.5) can be solved directly or by the so-called state-space approach used in control theory (see [11,12]). As for approximate methods, the Ritz, finite difference, and finite element methods are good candidates. Here we discuss direct analytical solution, analytical solution by the state-space approach, and approximate solution by the Ritz method.

5.3.2 Analytical Solutions

The general form of the analytical (exact) solution to the fourth-order differential equation (5.3.5) consists of two parts: homogeneous and nonhomogeneous (or particular) solutions. The homogeneous solution is of the form

$$W_n^h(x) = C \exp(\lambda x) \quad (5.3.6)$$

where λ denotes a root of the algebraic equation

$$D_{11} \lambda^4 - 2(D_{12} + 2D_{66}) \beta^2 \lambda^2 + D_{22} \beta^4 = 0 \quad (5.3.7)$$

Since there are four roots, the solution (5.3.5) can be written as a linear combination of functions of these four roots. The true form of the solution depends on the nature of the roots, *i.e.*, real or complex and equal or distinct. We consider three cases.

Case 1: Roots are real and distinct

When $(D_{12} + 2D_{66})^2 > D_{11}D_{22}$, the roots are real and unequal:

$$\begin{aligned} (\lambda_1)^2 &= (-\lambda_2)^2 = \frac{\beta^2}{D_{11}} \left[D_{12} + 2D_{66} - \sqrt{(D_{12} + 2D_{66})^2 - D_{11}D_{22}} \right] \\ (\lambda_3)^2 &= (-\lambda_4)^2 = \frac{\beta^2}{D_{11}} \left[D_{12} + 2D_{66} + \sqrt{(D_{12} + 2D_{66})^2 - D_{11}D_{22}} \right] \end{aligned} \quad (5.3.8)$$

The homogeneous part of the solution is of the form

$$W_n^h(x) = A_n \cosh \lambda_1 x + B_n \sinh \lambda_1 x + C_n \cosh \lambda_3 x + D_n \sinh \lambda_3 x \quad (5.3.9)$$

Case 2: Roots are real and equal

When $(D_{12} + 2D_{66})^2 = D_{11}D_{22}$, the roots are real but equal

$$\lambda_1 = \lambda_2 = -\lambda_3 = -\lambda_4 \equiv \lambda, \quad \lambda^2 = \frac{\beta^2}{D_{11}} (D_{12} + 2D_{66}) \quad (5.3.10)$$

and the homogeneous part of the solution is of the form

$$W_n^h(x) = (A_n + B_n x) \cosh \lambda x + (C_n + D_n x) \sinh \lambda x \quad (5.3.11)$$

Case 3: Roots are complex

When $(D_{12} + 2D_{66})^2 < D_{11}D_{22}$, the roots are complex and they appear in complex conjugate pairs $\lambda_1 \pm i\lambda_2$ and $-\lambda_1 \pm i\lambda_2$ ($i = \sqrt{-1}, \lambda_1 > 0, \lambda_2 > 0$):

$$\begin{aligned} (\lambda_1)^2 &= \frac{\beta^2}{2D_{11}} [\sqrt{D_{11}D_{22}} + (D_{12} + 2D_{66})] \\ (\lambda_2)^2 &= \frac{\beta^2}{2D_{11}} [\sqrt{D_{11}D_{22}} - (D_{12} + 2D_{66})] \end{aligned} \quad (5.3.12)$$

The homogeneous part of the solution is of the form

$$\begin{aligned} W_n^h(x) &= (A_n \cos \lambda_2 x + B_n \sin \lambda_2 x) \cosh \lambda_1 x \\ &\quad + (C_n \cos \lambda_2 x + D_n \sin \lambda_2 x) \sinh \lambda_1 x \end{aligned} \quad (5.3.13)$$

The particular solution of the fourth-order differential equation (5.3.5) in the general case in which Q_n is a function of x can be determined using the method of undetermined coefficients (see Pipes and Harvill [10]). When Q_n is a constant the particular solution is a constant k , and it is determined by substituting it into Eq. (5.3.5). We obtain $kD_{22}\beta^4 = Q_n$. Hence, the particular solution becomes

$$W_n^p(x) = \frac{Q_n}{D_{22}\beta^4} \equiv \hat{Q}_n \quad (5.3.14)$$

The four constants A_n, B_n, C_n , and D_n in Eqs. (5.3.9), (5.3.11), and (5.3.13) can be determined using the four boundary conditions associated with the edges $x = 0, a$ (in addition to the simply supported boundary conditions on the edges $y = 0, b$). Note that the particular case (i.e., Case 1, Case 2, or Case 3) in a problem is dictated by the plate stiffnesses, D_{ij} . Here we illustrate the procedure for simply supported and clamped boundary conditions in the case of real and distinct roots. The solution in this case is given by

$$\begin{aligned} w_0(x, y) &= \sum_{n=1}^{\infty} (A_n \cosh \lambda_1 x + B_n \sinh \lambda_1 x + C_n \cosh \lambda_3 x \\ &\quad + D_n \sinh \lambda_3 x + W_n^p) \sin \beta y \end{aligned} \quad (5.3.15)$$

In the following discussion we assume that the applied transverse load is uniformly distributed.

Simply supported plate

The simply supported boundary conditions on edges $x = 0, a$ are

$$w_0 = 0, \quad M_{xx} \equiv - \left(D_{11} \frac{\partial^2 w_0}{\partial x^2} + D_{12} \frac{\partial^2 w_0}{\partial y^2} \right) = 0 \quad (5.3.16)$$

Using (5.3.15) in (5.3.16), we obtain

$$\begin{aligned} A_n + C_n + \hat{Q}_n &= 0 \\ A_n \cosh \lambda_1 a + B_n \sinh \lambda_1 a + C_n \cosh \lambda_3 a + D_n \sinh \lambda_3 a + \hat{Q}_n &= 0 \\ D_{11} (\lambda_1^2 A_n + \lambda_3^2 C_n) - D_{12} (A_n + C_n + \hat{Q}_n) \beta^2 &= 0 \\ D_{11} (A_n \lambda_1^2 \cosh \lambda_1 a + B_n \lambda_1^2 \sinh \lambda_1 a + C_n \lambda_3^2 \cosh \lambda_3 a + D_n \lambda_3^2 \sinh \lambda_3 a) \\ - D_{12} (A_n \cosh \lambda_1 a + B_n \sinh \lambda_1 a + C_n \cosh \lambda_3 a + D_n \sinh \lambda_3 a + \hat{Q}_n) \beta^2 &= 0 \end{aligned}$$

where $\hat{Q}_n = Q_n / \beta^4 D_{22}$. By virtue of the first two equations, the coefficients of D_{12} in the last two equations are identically zero. The four equations can be expressed in matrix form as

$$\begin{bmatrix} 1 & 0 & 1 & 0 \\ \cosh \lambda_1 a & \sinh \lambda_1 a & \cosh \lambda_3 a & \sinh \lambda_3 a \\ \lambda_1^2 & 0 & \lambda_3^2 & 0 \\ \lambda_1^2 \cosh \lambda_1 a & \lambda_1^2 \sinh \lambda_1 a & \lambda_3^2 \cosh \lambda_3 a & \lambda_3^2 \sinh \lambda_3 a \end{bmatrix} \begin{Bmatrix} A_n \\ B_n \\ C_n \\ D_n \end{Bmatrix} = - \begin{Bmatrix} \hat{Q}_n \\ \hat{Q}_n \\ 0 \\ 0 \end{Bmatrix} \quad (5.3.17)$$

The determinant of the 4×4 coefficient matrix in Eq. (5.3.17) is $(\lambda_3^2 - \lambda_1^2)^2 \sinh \lambda_1 a \sinh \lambda_3 a$. The solution of the matrix equation yields

$$\begin{aligned} A_n &= -\hat{Q}_n \frac{\lambda_3^2}{(\lambda_3^2 - \lambda_1^2)}, \quad B_n = -\hat{Q}_n \frac{\lambda_3^2 (1 - \cosh \lambda_1 a)}{\sinh \lambda_1 a (\lambda_3^2 - \lambda_1^2)} \\ C_n &= \hat{Q}_n \frac{\lambda_1^2}{(\lambda_3^2 - \lambda_1^2)}, \quad D_n = \hat{Q}_n \frac{\lambda_1^2 (1 - \cosh \lambda_3 a)}{\sinh \lambda_3 a (\lambda_3^2 - \lambda_1^2)} \end{aligned} \quad (5.3.18)$$

Simply supported at $y=0,b$ and clamped at $x=0,a$

For clamped boundary conditions on edges $x = 0, a$, we require

$$w_0 = 0, \quad \frac{\partial w_0}{\partial x} = 0 \quad (5.3.19)$$

which yield

$$\begin{bmatrix} 1 & 0 & 1 & 0 \\ \cosh \lambda_1 a & \sinh \lambda_1 a & \cosh \lambda_3 a & \sinh \lambda_3 a \\ 0 & \lambda_1 & 0 & \lambda_3 \\ \lambda_1 \sinh \lambda_1 a & \lambda_1 \cosh \lambda_1 a & \lambda_3 \sinh \lambda_3 a & \lambda_3 \cosh \lambda_3 a \end{bmatrix} \begin{Bmatrix} A_n \\ B_n \\ C_n \\ D_n \end{Bmatrix} = - \begin{Bmatrix} \hat{Q}_n \\ \hat{Q}_n \\ 0 \\ 0 \end{Bmatrix} \quad (5.3.20)$$

The solution of the matrix equation (5.3.20) is

$$\begin{aligned} A_n &= \frac{\hat{Q}_n \lambda_3}{E_n} [(\lambda_1 \sinh \lambda_3 a - \lambda_3 \sinh \lambda_1 a) \sinh \lambda_3 a \\ &\quad + \lambda_1 (\cosh \lambda_1 a - \cosh \lambda_3 a) (\cosh \lambda_3 a - 1)] \\ B_n &= \frac{\hat{Q}_n \lambda_3}{E_n} [\lambda_3 \sinh \lambda_3 a (\cosh \lambda_1 a - 1) + \lambda_1 \sinh \lambda_1 a (1 - \cosh \lambda_3 a)] \\ C_n &= -(A_n + Q_n), \quad D_n = -\frac{\lambda_1}{\lambda_3} B_n \end{aligned} \quad (5.3.21)$$

where E_n is the determinant of the coefficient matrix

$$\begin{aligned} E_n &= -(\lambda_3 \sinh \lambda_1 a - \lambda_1 \sinh \lambda_3 a) (\lambda_1 \sinh \lambda_1 a - \lambda_3 \sinh \lambda_3 a) \\ &\quad + \lambda_1 \lambda_3 (\cosh \lambda_3 a - \cosh \lambda_1 a)^2 \end{aligned} \quad (5.3.22)$$

An alternative method of solving Eq. (5.3.5) is provided by the state-space approach [12]. The approach involves writing a higher-order ordinary differential equation as a first-order matrix equation, and its solution is obtained using matrix methods in terms of the eigenvalues of the matrix operator. In the present case, the linear ordinary differential equation in (5.3.5) with constant coefficients can be expressed in the form of a single, first-order matrix differential equation

$$\{Z'\} = [T]\{Z\} + \{F\} \quad (5.3.23)$$

$$\{Z\} = \begin{Bmatrix} W_n \\ W'_n \\ W''_n \\ W'''_n \end{Bmatrix}, \quad [T] = \begin{bmatrix} 0 & 1 & 0 & 0 \\ 0 & 0 & 1 & 0 \\ 0 & 0 & 0 & 1 \\ C_1 & 0 & C_2 & 0 \end{bmatrix}, \quad \{F\} = \begin{Bmatrix} 0 \\ 0 \\ 0 \\ \hat{Q}_n \end{Bmatrix} \quad (5.3.24)$$

$$C_1 = -\frac{D_{22}}{D_{11}} \beta^4, \quad C_2 = 2 \frac{(D_{12} + 2D_{66})}{D_{11}} \beta^2, \quad \hat{Q}_n = \frac{Q_n}{D_{11}} \quad (5.3.25)$$

The general solution of Eq. (5.3.23) is given by

$$\begin{aligned} \mathbf{Z}(x) &= e^{\mathbf{T}x} \left(\mathbf{K} + \int_0^x e^{-\mathbf{T}\xi} \mathbf{F}(\xi) d\xi \right) \\ &\equiv \mathbf{G}(x)\mathbf{K} + \mathbf{H}(x) \end{aligned} \quad (5.3.26)$$

Here $e^{\mathbf{T}x}$ denotes the matrix product

$$e^{\mathbf{T}x} = [E] \begin{bmatrix} e^{\lambda_1 x} & & 0 \\ & \ddots & \\ 0 & & e^{\lambda_4 x} \end{bmatrix} [E]^{-1} \quad (5.3.27)$$

Here $[E]$ is the matrix of distinct eigenvectors of matrix $[T]$, $[E]^{-1}$ denotes its inverse, λ_j ($j = 1, 2, 3, 4$) are the eigenvalues associated with matrix $[T]$, and $\{K\}$ is a vector of constants to be determined using the boundary conditions of the problem.

As an example, consider the case of simply supported boundary condition at $x = 0$ and clamped boundary condition at $x = a$. The simply supported boundary conditions (5.2.2a,b) at $x = 0$ imply [see Eq. (5.3.1)]

$$W_n(0) = 0, \quad D_{11}W_n''(0) - D_{12}\beta^2 W_n(0) = 0 \quad (5.3.28a)$$

The clamped boundary conditions (5.3.19) at $x = a$ imply

$$W_n(a) = 0, \quad W_n'(a) = 0 \quad (5.3.28b)$$

These four conditions in turn yield, in view of Eq. (5.3.26), the following four nonhomogeneous algebraic equations among K_i ($i = 1, 2, 3, 4$):

$$\begin{aligned} & \sum_{j=1}^4 G_{1j}(0)K_j + H_1(0) = 0 \\ & \sum_{j=1}^4 \left(D_{11}G_{3j}(0) - \beta^2 D_{12}G_{1j}(0) \right) K_j + D_{11}H_3(0) - D_{12}\beta^2 H_1(0) = 0 \\ & \sum_{j=1}^4 G_{1j}(a)K_j + H_1(a) = 0 \\ & \sum_{j=1}^4 G_{2j}(a)K_j + H_2(a) = 0 \end{aligned} \quad (5.3.29)$$

These equations can be solved for the four constants. In general, the procedure is algebraically complicated, and therefore all calculations, i.e., matrix multiplication, determination of eigenvalues and constants K_i , and evaluation of the solution, are made using a computer.

Table 5.3.2 contains numerical results for three-layer, cross-ply ($0^\circ/90^\circ/0^\circ$), square laminates under uniformly distributed transverse load. The lamina material properties used are $E_1 = 19.2$ ksi, $E_2 = 1.56$ ksi, $G_{12} = 0.82$ ksi, and $\nu_{12} = 0.24$. The transverse deflection and stresses are nondimensionalized as follows:

$$\begin{aligned} \hat{w} &= w_0(0, 0) \left(\frac{E_2 h^3}{a^4 q_0} \right) \times 10^2; \quad \bar{\sigma}_{xx} = \sigma_{xx}(a/2, b/2, h/2) \left(\frac{h^2}{a^2 q_0} \right) \times 10 \\ \bar{\sigma}_{yy} &= \sigma_{yy}(a/2, b/2, h/6) \left(\frac{h^2}{a^2 q_0} \right) \times 10 \end{aligned} \quad (5.3.30)$$

The notation SF, for example, is used to denote a plate with edge $x = 0$ is simply supported (S) and edge $x = a$ is free (F); of course, edges $y = 0, b$ are simply supported.

Table 5.3.2: Nondimensional center deflections (\hat{w}) and in-plane normal stresses ($\bar{\sigma}_{xx}$ and $\bar{\sigma}_{yy}$) of symmetric cross-ply ($0^\circ/90^\circ/0^\circ$) square plates subjected to uniform distribution of transverse load and for various boundary conditions.

Variable	SS	SC	CC	FF	FS	FC
\hat{w}	1.206	0.544	0.280	10.920	5.992	2.376
$\bar{\sigma}_{xx}$	7.251	4.082	2.787	0.195	3.778	1.685
$\bar{\sigma}_{yy}$	1.938	0.651	0.185	21.597	11.621	4.313

5.3.3 Ritz Solution

Equation (5.3.5) can also be solved using the Ritz method. In the Ritz method, we seek solution of (5.3.5) in the form

$$W_n(x) \approx \sum_{j=1}^N c_j \varphi_j(x) \quad (5.3.31)$$

where $\varphi_j(x)$ are approximation functions that must meet the continuity and completeness conditions and satisfy the homogeneous form of the geometric boundary conditions [see Eq. (1.5.2)]. The parameters c_j are then determined by requiring that the weak form of Eq. (5.3.5) be satisfied:

$$0 = \int_0^a \left[D_{11} \frac{d^2 W_n}{dx^2} \frac{d^2 \delta W_n}{dx^2} + 2(D_{12} + 2D_{66}) \beta^2 \frac{d W_n}{dx} \frac{d \delta W_n}{dx} + D_{22} \beta^4 W_n \delta W_n - Q_n \delta W_n \right] dx \quad (5.3.32)$$

where δW_n denotes the virtual variation in W_n

$$\delta W_n(x) \approx \sum_{i=1}^N \delta c_i \varphi_i(x) \quad (5.3.33)$$

Substituting (5.3.31) and (5.3.33) into (5.3.32), we obtain

$$0 = \sum_{i=1}^N \left\{ \sum_{j=1}^N c_j \int_0^a \left[D_{11} \frac{d^2 \varphi_j}{dx^2} \frac{d^2 \varphi_i}{dx^2} + 2(D_{12} + 2D_{66}) \beta^2 \frac{d \varphi_j}{dx} \frac{d \varphi_i}{dx} + D_{22} \beta^4 \varphi_j \varphi_i \right] dx - \int_0^a Q_n \varphi_i dx \right\} \delta c_i \quad (5.3.34)$$

Since the above expression must hold for all arbitrary values of δc_i , it follows that the expression in the curly bracket must be zero. We have

$$0 = \sum_{j=1}^N A_{ij} c_j - F_i \quad \text{or} \quad [A]\{c\} = \{F\} \quad (5.3.35a)$$

where

$$\begin{aligned} A_{ij} &= \int_0^a \left[D_{11} \frac{d^2 \varphi_j}{dx^2} \frac{d^2 \varphi_i}{dx^2} + 2(D_{12} + 2D_{66}) \beta^2 \frac{d\varphi_j}{dx} \frac{d\varphi_i}{dx} + D_{22} \beta^4 \varphi_j \varphi_i \right] dx \\ F_i &= \int_0^a Q_n \varphi_i dx \end{aligned} \quad (5.3.35b)$$

Equation (5.3.35a) represents a set of N algebraic equations among c_i .

As an example, we consider the case in which the edges $x = 0, a$ are clamped. The geometric boundary conditions are given by Eq. (5.3.19):

$$w_0 = 0, \quad \frac{\partial w_0}{\partial x} = 0 \quad (5.3.36)$$

Hence, the approximation functions φ_i must be selected such that $\varphi_i = 0$ and $(d\varphi_i/dx)$ are zero at $x = 0, a$.

If an algebraic polynomial is to be selected, one may begin with the five-term complete polynomial

$$\varphi_1(x) = K_0 + K_1 x + K_2 x^2 + K_3 x^3 + K_4 x^4$$

and determine four of the five constants K_i in terms of the remaining constant using the four boundary conditions. The constant is arbitrary and may be set to unity. We obtain

$$\varphi_1(x) = \left(\frac{x}{a}\right)^2 \left(1 - \frac{x}{a}\right)^2$$

The i th function can be written as

$$\varphi_i(x) = \left(\frac{x}{a}\right)^{i+1} \left(1 - \frac{x}{a}\right)^2, \quad i = 1, 2, \dots, n \quad (5.3.37)$$

For the choice of $\varphi_i(x)$ in (5.3.37), we have

$$\begin{aligned} \int_0^a \varphi_i dx &= a \left(\frac{1}{i+2} - \frac{2}{i+3} + \frac{1}{i+4} \right) \\ \int_0^a \varphi_i \varphi_j dx &= a \left(\frac{1}{i+j+3} - \frac{4}{i+j+4} + \frac{6}{i+j+5} - \frac{4}{i+j+6} + \frac{1}{i+j+7} \right) \\ \int_0^a \frac{d\varphi_i}{dx} \frac{d\varphi_j}{dx} dx &= \frac{1}{a} \left[\frac{(i+1)(j+1)}{i+j+1} - 2 \frac{(i+1)(j+2) + (j+1)(i+2)}{i+j+2} \right. \\ &\quad \left. + \frac{(i+1)(j+3) + 4(i+2)(j+2) + (i+3)(j+1)}{i+j+3} \right. \\ &\quad \left. - 2 \frac{(i+2)(j+3) + (i+3)(j+2)}{i+j+4} + \frac{(i+3)(j+3)}{i+j+5} \right] \\ \int_0^a \frac{d^2 \varphi_i}{dx^2} \frac{d^2 \varphi_j}{dx^2} dx &= \frac{1}{a^3} \left[\frac{ij(i+1)(j+1)}{i+j-1} - 2(i+1)(j+1) \frac{i(j+2) + (i+2)j}{i+j} \right. \\ &\quad \left. + \frac{i(i+1)(j+2)(j+3) + 4(i+1)(i+2)(j+1)(j+2)}{i+j+1} \right. \\ &\quad \left. + \frac{j(i+2)(i+3)(j+1)}{i+j+1} + \frac{(i+2)(i+3)(j+2)(j+3)}{i+j+3} \right. \\ &\quad \left. - 2(i+2)(j+2) \frac{(i+1)(j+3) + (i+3)(j+1)}{i+j+2} \right] \end{aligned} \quad (5.3.38)$$

For $N = 1$, Eq. (5.3.35a) gives

$$\left[\frac{4}{5a^3} D_{11} + \frac{4}{105a} (D_{12} + 2D_{66}) \beta^2 + \frac{a}{630} D_{22} \beta^4 \right] c_1 = \frac{a}{30} Q_n$$

and the solution (5.3.1) becomes

$$w_0(x, y) \approx \left[\left(\frac{x}{a} \right) - \left(\frac{x}{a} \right)^2 \right]^2 \sum_{n=1}^{\infty} c_1(n) \sin \beta y \quad (5.3.39a)$$

with $\beta = n\pi/b$ and

$$c_1(n) = \frac{1}{30} Q_n a^4 \left[\frac{4}{5} D_{11} + \frac{4}{105} (D_{12} + 2D_{66}) \beta^2 a^2 + \frac{1}{630} D_{22} \beta^4 a^4 \right]^{-1} \quad (5.3.39b)$$

The center deflection is given by

$$\begin{aligned} w_0\left(\frac{a}{2}, \frac{b}{2}\right) &\approx \frac{1}{16} \sum_{n=1}^{\infty} c_1(n) \sin \frac{n\pi}{2} \\ &= \frac{1}{16} [c_1(1) - c_1(3) + c_1(5) - \dots] \end{aligned} \quad (5.3.40)$$

For a symmetric cross-ply laminate (0/90/0) with ply properties $E_1 = 19.2$ ksi, $E_2 = 1.56$ ksi, $G_{12} = 0.82$ ksi, and $\nu_{12} = 0.25$, the bending stiffnesses, for $h = 0.01$, are $D_{11} = 1.5528$, $D_{12} = 0.031347$, $D_{22} = 0.18531$, and $D_{66} = 0.068333$ lb-in. For uniformly distributed load q_0 , we have ($s = a/b$)

$$c_1(n) = \frac{4q_0}{30n\pi (1.24224 + 0.06317n^2s^2 + 0.02865n^4s^4)}$$

for $n = 1, 3, 5, \dots$. For a square plate, the maximum deflection becomes

$$w_0\left(\frac{a}{2}, \frac{b}{2}\right) \approx \frac{q_0 a^4}{16} (0.03181 - 0.003424 + 0.001509 - \dots) q_0 a^4$$

The series converges slowly unless we also increase the number of parameters in the x -coordinate [see Eq. (5.3.31)]. The “exact” solution for a square laminate under uniformly distributed load is

$$w_0\left(\frac{a}{2}, \frac{b}{2}\right) = 0.001795 q_0 a^4 \quad (5.3.41)$$

whereas the one-term ($n = 1$ and $N = 1$) solution predicted by Eq. (5.3.40) is $0.001988 q_0 a^4$. The two-term solution ($n = 1, 3$ and $N = 1$) is $0.001774 q_0 a^4$.

Other choices of $\varphi_i(x)$ are provided by the eigenfunctions $W(x)$ of beams developed in Chapter 4 [see Eq. (4.2.46a)]. For example, for clamped boundary conditions, we use the eigenfunctions of a beam with clamped ends. From Eq. (4.2.46a) and Table 4.2.3, we have

$$\varphi_i(x) = \sin \lambda_i x - \sinh \lambda_i x + \alpha_i (\cosh \lambda_i x - \cos \lambda_i x) \quad (5.3.42a)$$

$$\frac{d\varphi_i}{dx} = \lambda_i [\cos \lambda_i x - \cosh \lambda_i x + \alpha_i (\sinh \lambda_i x + \sin \lambda_i x)] \quad (5.3.42b)$$

where λ_i are the roots of the characteristic equation (4.2.59)

$$\cos \lambda_i a \cosh \lambda_i a - 1 = 0 \quad (5.3.43)$$

and

$$\alpha_i = \frac{\sinh \lambda_i a - \sin \lambda_i a}{\cosh \lambda_i a - \cos \lambda_i a} = \frac{\cosh \lambda_i a - \cos \lambda_i a}{\sinh \lambda_i a + \sin \lambda_i a} \quad (5.3.44)$$

Clearly, φ_i and $(d\varphi_i/dx)$ are zero at $x = 0, a$. Recall from Table 4.2.3 [also see Eq. (4.2.60)] that the roots λ_i of the characteristic equation (5.3.43) are given by

$$\lambda_1 a = 4.730, \lambda_2 a = 7.853, \dots, \lambda_i a \approx (2i + 1) \frac{\pi}{2} \quad (5.3.45)$$

The corresponding values of α_i are

$$\alpha_1 = 1.0178, \alpha_2 = 0.99922, \alpha_i = 1 \text{ for } i > 2 \quad (5.3.46)$$

Hence, the first two eigenfunctions are

$$\begin{aligned} \varphi_1(x) &= \sin \frac{4.73x}{a} - \sinh \frac{4.73x}{a} + 1.0178 \left(\cosh \frac{4.73x}{a} - \cos \frac{4.73x}{a} \right) \\ \varphi_2(x) &= \sin \frac{7.853x}{a} - \sinh \frac{7.853x}{a} + 0.9992 \left(\cosh \frac{7.853x}{a} - \cos \frac{7.853x}{a} \right) \end{aligned} \quad (5.3.47)$$

For $N = 1$, Eq. (5.3.35a) yields

$$\begin{aligned} c_1(n) &= 0.84555 Q_n a^4 \left[518.53135 D_{11} + 12.7442 (D_{12} + 2D_{66}) (n\pi)^2 s^2 \right. \\ &\quad \left. + 1.035965 D_{22} (n\pi)^4 s^4 \right]^{-1} \end{aligned} \quad (5.3.48)$$

For the symmetric cross-ply laminate considered above, the center deflection ($X_1(a/2) = 1.61637$) predicted for $n = 1$ is $0.002009 q_0 a^4$ compared to the exact solution of $0.001795 q_0 a^4$.

5.4 Bending of Rectangular Plates with Various Boundary Conditions

5.4.1 Virtual Work Statements

The Navier and Lévy type solutions do not exist for rectangular plates with all four edges clamped or when two parallel edges are not simply supported. Therefore, an approximate method must be utilized to determine solutions of these plates. In this section, we discuss applications of the Ritz method to determine the bending deflections of specially orthotropic rectangular plates with various boundary conditions.

The virtual work statement (or weak form) and the total potential energy expressions for a specially orthotropic rectangular plate are [see Eq. (3.3.19)]

$$\begin{aligned} 0 &= \int_0^b \int_0^a \left(M_{xx} \delta \varepsilon_{xx}^{(1)} + M_{yy} \delta \varepsilon_{yy}^{(1)} + M_{xy} \delta \gamma_{xy}^{(1)} - q \delta w_0 \right) dx dy \\ &= \int_0^b \int_0^a \left[D_{11} \frac{\partial^2 w_0}{\partial x^2} \frac{\partial^2 \delta w_0}{\partial x^2} + D_{12} \left(\frac{\partial^2 w_0}{\partial y^2} \frac{\partial^2 \delta w_0}{\partial x^2} + \frac{\partial^2 w_0}{\partial x^2} \frac{\partial^2 \delta w_0}{\partial y^2} \right) \right. \\ &\quad \left. + 4D_{66} \frac{\partial^2 w_0}{\partial x \partial y} \frac{\partial^2 \delta w_0}{\partial x \partial y} + D_{22} \frac{\partial^2 w_0}{\partial y^2} \frac{\partial^2 \delta w_0}{\partial y^2} - q \delta w_0 \right] dx dy \end{aligned} \quad (5.4.1)$$

and

$$\begin{aligned} \Pi(w_0) &= \frac{1}{2} \int_0^b \int_0^a \left[D_{11} \left(\frac{\partial^2 w_0}{\partial x^2} \right)^2 + 2D_{12} \frac{\partial^2 w_0}{\partial x^2} \frac{\partial^2 w_0}{\partial y^2} + 4D_{66} \left(\frac{\partial^2 w_0}{\partial x \partial y} \right)^2 \right. \\ &\quad \left. + D_{22} \left(\frac{\partial^2 w_0}{\partial y^2} \right)^2 - 2q w_0 \right] dx dy \end{aligned} \quad (5.4.2)$$

The above expressions should be appended with appropriate terms due to any additional applied edge forces and moments.

5.4.2 Clamped Plates

Consider a rectangular plate with all edges clamped and subjected to distributed transverse load $q(x, y)$. The boundary conditions associated with the clamped plate are

$$w_0 = 0 \text{ and } \frac{\partial w_0}{\partial x} = 0 \text{ at } x = 0, a \quad (5.4.3a)$$

$$w_0 = 0 \text{ and } \frac{\partial w_0}{\partial y} = 0 \text{ at } y = 0, b \quad (5.4.3b)$$

We assume the Ritz approximation in the form

$$w_0(x, y) \approx W_{mn}(x, y) = \sum_i^m \sum_j^n c_{ij} \varphi_{ij}(x, y) \quad (5.4.4)$$

where the approximation functions φ_{ij} satisfy all the (homogeneous) geometric boundary conditions in Eqs. (5.4.3a,b). For this problem, therefore, both the Galerkin and Ritz methods give the same solution for the same choice of approximation functions.

In view of the rectangular geometry and clamped boundary conditions, the approximation functions $\varphi_{ij}(x, y)$ can be expressed as a tensor product of the one-dimensional functions given in Eq. (5.3.37) or (5.3.42a):

$$\varphi_{ij}(x, y) = X_i(x)Y_j(y) \quad (5.4.5)$$

where

$$\begin{aligned} X_i(x) &= \left(\frac{x}{a}\right)^{i+1} \left(1 - \frac{x}{a}\right)^2 \\ Y_j(y) &= \left(\frac{y}{b}\right)^{j+1} \left(1 - \frac{y}{b}\right)^2 \end{aligned} \quad (5.4.6)$$

or

$$\begin{aligned} X_i(x) &= \sin \lambda_i x - \sinh \lambda_i x + \alpha_i (\cosh \lambda_i x - \cos \lambda_i x) \\ Y_j(y) &= \sin \lambda_j y - \sinh \lambda_j y + \alpha_j (\cosh \lambda_j y - \cos \lambda_j y) \end{aligned} \quad (5.4.7)$$

for $i = 1, 2, \dots, m$; $j = 1, 2, \dots, n$. The parameters λ_i and α_i are defined in Eq. (5.3.43) and (5.3.44), respectively.

Substituting Eq. (5.4.4), with φ_{ij} given by Eq. (5.4.5), and

$$\delta w_0 = \sum_p^m \sum_q^n \delta c_{pq} \varphi_{pq}$$

into Eq. (5.4.1), we obtain

$$\begin{aligned} 0 = \sum_p^m \sum_q^n \left\{ \sum_i^m \sum_j^n c_{ij} \int_0^b \int_0^a \left[D_{11} \frac{d^2 X_i}{dx^2} Y_j \frac{d^2 X_p}{dx^2} Y_q + 4D_{66} \frac{dX_i}{dx} \frac{dY_j}{dy} \frac{dX_p}{dx} \frac{dY_q}{dy} \right. \right. \\ \left. \left. + D_{12} \left(X_i \frac{d^2 Y_j}{dy^2} \frac{d^2 X_p}{dx^2} Y_q + \frac{d^2 X_i}{dx^2} Y_j X_p \frac{d^2 Y_q}{dy^2} \right) \right. \right. \\ \left. \left. + D_{22} X_i \frac{d^2 Y_j}{dy^2} X_p \frac{d^2 Y_q}{dy^2} \right] dx dy \right. \\ \left. - \int_0^b \int_0^a q X_p Y_q dx dy \right\} \delta c_{pq} \end{aligned} \quad (5.4.8a)$$

Since the statement should hold for any arbitrary variations δc_{pq} , the expression inside the curly bracket should be zero for all $p, q = 1, 2, \dots$:

$$\begin{aligned} 0 = \sum_i^m \sum_j^n \left\{ \int_0^b \int_0^a \left[D_{11} \frac{d^2 X_i}{dx^2} Y_j \frac{d^2 X_p}{dx^2} Y_q + 4D_{66} \frac{dX_i}{dx} \frac{dY_j}{dy} \frac{dX_p}{dx} \frac{dY_q}{dy} \right. \right. \\ \left. \left. + D_{12} \left(X_i \frac{d^2 Y_j}{dy^2} \frac{d^2 X_p}{dx^2} Y_q + \frac{d^2 X_i}{dx^2} Y_j X_p \frac{d^2 Y_q}{dy^2} \right) \right. \right. \\ \left. \left. + D_{22} X_i \frac{d^2 Y_j}{dy^2} X_p \frac{d^2 Y_q}{dy^2} \right] dx dy \right\} c_{ij} \\ - \int_0^b \int_0^a q X_p Y_q dx dy \end{aligned} \quad (5.4.8b)$$

Equation (5.4.8b) represents $m \times n$ algebraic equations among the coefficients c_{ij} . Note that all integrals in (5.4.8b) are line integrals, and they involve evaluating five different integrals

$$\int_0^a X_i dx, \quad \int_0^a X_i X_p dx, \quad \int_0^a \frac{dX_i}{dx} \frac{dX_p}{dx} dx$$

$$\int_0^a X_i \frac{d^2 X_p}{dx^2} dx, \quad \int_0^a \frac{d^2 X_i}{dx^2} \frac{d^2 X_p}{dx^2} dx \quad (5.4.9a)$$

As an example we consider the algebraic functions in (5.4.6) with $m = n = 1$ and $q = q_0$ (uniformly distributed load). The integrals in Eq. (5.4.9a) for this case are given by

$$\int_0^a X_1 dx = \frac{a}{30}, \quad \int_0^a X_1 X_1 dx = \frac{a}{630}, \quad \int_0^a \frac{dX_1}{dx} \frac{dX_1}{dx} dx = \frac{2}{105a}$$

$$\int_0^a X_1 \frac{d^2 X_1}{dx^2} dx = -\frac{2}{105a}, \quad \int_0^a \frac{d^2 X_1}{dx^2} \frac{d^2 X_1}{dx^2} dx = \frac{4}{5a^3} \quad (5.4.9b)$$

Substituting the integral values into (5.4.8b), we obtain

$$0 = \left[\left(\frac{4}{5a^3} \right) \left(\frac{b}{630} \right) D_{11} + 4D_{66} \left(\frac{2}{105a} \right) \left(\frac{2}{105b} \right) + 2D_{12} \left(-\frac{2}{105a} \right) \left(-\frac{2}{105b} \right) + \left(\frac{a}{630} \right) \left(\frac{4}{5b^3} \right) D_{22} \right] c_{11} - \left(\frac{a}{30} \right) \left(\frac{b}{30} \right) q_0$$

or

$$\left[\frac{7}{a^4} D_{11} + \frac{4}{a^2 b^2} (D_{12} + 2D_{66}) + \frac{7}{b^4} D_{22} \right] c_{11} = \frac{49}{8} q_0 \quad (5.4.10)$$

and the one-parameter solution becomes

$$W_{11}(x, y) = \left(\frac{49}{8} \right) \frac{q_0 a^4 \left[\frac{x}{a} - \left(\frac{x}{a} \right)^2 \right]^2 \left[\frac{y}{b} - \left(\frac{y}{b} \right)^2 \right]^2}{7D_{11} + 4(D_{12} + 2D_{66})s^2 + 7D_{22}s^4} \quad (5.4.11)$$

where $s = a/b$ denotes the plate aspect ratio. The maximum deflection occurs at $x = a/2$ and $y = b/2$:

$$W_{11}\left(\frac{a}{2}, \frac{b}{2}\right) = 0.00342 \frac{q_0 a^4}{D_{11} + 0.5714(D_{12} + 2D_{66})s^2 + D_{22}s^4} \quad (5.4.12)$$

The algebra involved in evaluating the integrals in Eq. (5.4.9a) is quite tedious for the choice of approximation functions in (5.4.7). An algebraic manipulator (e.g., *Maple* or *Mathematica*) may be used to evaluate them. For $m = n = 1$, the functions in (5.4.7) are given by

$$\begin{aligned} X_1(x) &= \sin \frac{4.73x}{a} - \sinh \frac{4.73x}{a} + 1.0178 \left(\cosh \frac{4.73x}{a} - \cos \frac{4.73x}{a} \right) \\ Y_1(y) &= \sin \frac{4.73y}{b} - \sinh \frac{4.73y}{b} + 1.0178 \left(\cosh \frac{4.73y}{b} - \cos \frac{4.73y}{b} \right) \end{aligned} \quad (5.4.13a)$$

and substitution into (5.4.9b) gives

$$\int_0^a X_1 dx = 0.84555a, \quad \int_0^a X_1 X_1 dx = 1.035966a, \quad \int_0^a \frac{dX_1}{dx} \frac{dX_1}{dx} dx = \frac{12.7442}{a}$$

$$\int_0^a X_1 \frac{d^2 X_1}{dx^2} dx = -\frac{12.7442}{a}, \quad \int_0^a \frac{d^2 X_1}{dx^2} \frac{d^2 X_1}{dx^2} dx = \frac{518.531348}{a^3} \quad (5.4.13b)$$

Then Eq. (5.4.8b) becomes

$$\left[\frac{537.181b}{a^3} D_{11} + \frac{324.829}{ab} (D_{12} + 2D_{66}) + \frac{537.181a}{b^3} D_{22} \right] c_{11} = 0.715q_0 ab \quad (5.4.14)$$

The maximum deflection is given by ($X_1(a/2) = Y_1(b/2) = 1.6164$)

$$W_{11}\left(\frac{a}{2}, \frac{b}{2}\right) = 0.00348 \frac{q_0 a^4}{D_{11} b^4 + 0.6047(D_{12} + 2D_{66}) s^2 + D_{22} s^4} \quad (5.4.15)$$

where $s = a/b$ denotes the plate aspect ratio. For an isotropic square plate ($a/b = 1, D_{11} = D_{22} = D_{12} + 2D_{66} = D$), the maximum deflection (5.4.15) becomes

$$W_{11}\left(\frac{a}{2}, \frac{b}{2}\right) = 0.00134 \frac{q_0 a^4}{D}$$

whereas Eq. (5.4.12) gives

$$W_{11}\left(\frac{a}{2}, \frac{b}{2}\right) = 0.00133 \frac{q_0 a^4}{D}$$

The “exact” solution (see Timoshenko and Woinowsky-Krieger [6]) is

$$W_{11}\left(\frac{a}{2}, \frac{b}{2}\right) = 0.00126 \frac{q_0 a^4}{D}$$

5.4.3 Approximation Functions for Other Boundary Conditions

Here we discuss the approximation functions $\varphi_{ij} = X_i(x)Y_j(y)$ required in the Ritz approximation (5.4.4) of specially orthotropic rectangular plates with a variety of boundary conditions (see Hearman [8]). The choice is restricted to the products of eigenfunctions (see Table 4.2.3) of beams with corresponding boundary conditions.

Clamped at $x = 0, a$ and simply supported at $y = 0, b$

$$\begin{aligned} X_i(x) &= \sin \lambda_i x - \sinh \lambda_i x + \alpha_i (\cosh \lambda_i x - \cos \lambda_i x) \\ Y_j(y) &= \sin \frac{j\pi y}{b} \end{aligned} \quad (5.4.16a)$$

where λ_i are the roots of the characteristic equation

$$\cos \lambda_i a \cosh \lambda_i a - 1 = 0 \quad (5.4.16b)$$

and

$$\alpha_i = \frac{\sinh \lambda_i a - \sin \lambda_i a}{\cosh \lambda_i a - \cos \lambda_i a} \quad (5.4.16c)$$

Clamped at $x = 0$, free at $x = a$, and simply supported at $y = 0, b$

$$\begin{aligned} X_i(x) &= \sin \lambda_i x - \sinh \lambda_i x + \alpha_i (\cosh \lambda_i x - \cos \lambda_i x) \\ Y_j(y) &= \sin \frac{j\pi y}{b} \end{aligned} \quad (5.4.17a)$$

where λ_i are the roots of the characteristic equation

$$\cos \lambda_i a \cosh \lambda_i a + 1 = 0 \quad (5.4.17b)$$

and

$$\alpha_i = \frac{\sinh \lambda_i a + \sin \lambda_i a}{\cosh \lambda_i a + \cos \lambda_i a} \quad (5.4.17c)$$

Free at $x = 0, a$ and simply supported at $y = 0, b$

$$\begin{aligned} X_i(x) &= \sin \lambda_i x + \sinh \lambda_i x - \alpha_i (\cosh \lambda_i x + \cos \lambda_i x) \\ Y_j(y) &= \sin \frac{j\pi y}{b} \end{aligned} \quad (5.4.18a)$$

where λ_i are the roots of the characteristic equation

$$\cos \lambda_i a \cosh \lambda_i a - 1 = 0 \quad (5.4.18b)$$

and

$$\alpha_i = \frac{\sinh \lambda_i a - \sin \lambda_i a}{\cosh \lambda_i a - \cos \lambda_i a} \quad (5.4.18c)$$

Simply supported at $x = 0$ and $y = 0, b$, and clamped at $x = a$

$$\begin{aligned} X_i(x) &= \sinh \lambda_i a \sin \lambda_i x + \sin \lambda_i a \sinh \lambda_i x \\ Y_j(y) &= \sin \frac{j\pi y}{b} \end{aligned} \quad (5.4.19a)$$

where λ_i are the roots of the characteristic equation

$$\tan \lambda_i a - \tanh \lambda_i a = 0 \quad (5.4.19b)$$

Simply supported at $x = 0$ and $y = 0, b$, and free at $x = a$

$$\begin{aligned} X_i(x) &= \sinh \lambda_i a \sin \lambda_i x - \sin \lambda_i a \sinh \lambda_i x \\ Y_j(y) &= \sin \frac{j\pi y}{b} \end{aligned} \quad (5.4.20a)$$

where λ_i are the roots of the characteristic equation

$$\tan \lambda_i a - \tanh \lambda_i a = 0 \quad (5.4.20b)$$

Clamped at $x = 0$, and free at $x = a$ and $y = 0, b$

$$\begin{aligned} X_i(x) &= \sin \lambda_i x - \sinh \lambda_i x + \alpha_i (\cosh \lambda_i x - \cos \lambda_i x) \\ Y_j(y) &= \sin \mu_j y + \sinh \mu_j y - \beta_i (\cosh \mu_j y + \cos \mu_j y) \end{aligned} \quad (5.4.21a)$$

where λ_i and μ_j are the roots of the characteristic equations

$$\cos \lambda_i a \cosh \lambda_i a + 1 = 0, \quad \cos \mu_j b \cosh \mu_j b - 1 = 0 \quad (5.4.21b)$$

and

$$\alpha_i = \frac{\sinh \lambda_i a + \sin \lambda_i a}{\cosh \lambda_i a + \cos \lambda_i a}, \quad \beta_j = \frac{\sinh \mu_j b - \sin \mu_j b}{\cosh \mu_j b - \cos \mu_j b} \quad (5.4.21c)$$

Clamped at $x = 0$, simply supported at $y = 0$, and free at $x = a$ and $y = b$

$$\begin{aligned} X_i(x) &= \sin \lambda_i x - \sinh \lambda_i x + \alpha_i (\cosh \lambda_i x - \cos \lambda_i x) \\ Y_j(y) &= \sinh \mu_j b \sin \mu_j y - \sin \mu_j b \sinh \mu_j y \end{aligned} \quad (5.4.22a)$$

where λ_i and μ_j are the roots of the characteristic equations

$$\cos \lambda_i a \cosh \lambda_i a + 1 = 0, \quad \tan \mu_j b - \tanh \mu_j b = 0 \quad (5.4.22b)$$

and

$$\alpha_i = \frac{\sinh \lambda_i a + \sin \lambda_i a}{\cosh \lambda_i a + \cos \lambda_i a} \quad (5.4.22c)$$

Similarly, one can construct the approximation functions for any combination of fixed, hinged, and free boundary conditions on the four edges of a rectangular plate. Of course, the most difficult part is to evaluate the integrals of these functions as required in Eq. (5.4.8b). One may use a symbolic manipulator, such as Mathematica or Maple, to evaluate the integrals. When general laminated plates are considered, products of the beam eigenfunctions can still be used for the approximation of the transverse deflection with appropriate functions for the in-plane displacements. In general, the Ritz method for general rectangular laminates with arbitrary boundary conditions is algebraically more complicated than a numerical method, such as the finite element method.

5.5 Buckling of Simply Supported Plates Under Compressive Loads

5.5.1 Governing Equations

When a plate is subjected to in-plane compressive forces, $\hat{N}_{xx} < 0$, $\hat{N}_{yy} < 0$, and $\hat{N}_{xy} = 0$, and if the forces are sufficiently small, the equilibrium of the plate is stable (see Figure 5.5.1). The plate remains flat until a certain load is reached. At that load, called the buckling load, the stable state of the plate is disturbed and the plate seeks an alternative equilibrium configuration accompanied by a change in the load-deflection behavior. The phenomenon of changing the equilibrium configuration at the same load and without drastic changes in deformation is termed *bifurcation*.

The load-deflection curve for buckled plates is often bilinear. The magnitude of the buckling load depends, as will be shown shortly, on geometry, material properties, as well as on the buckling mode shape. Here we determine the critical buckling loads of simply supported specially orthotropic plates using the Navier method.

For the buckling analysis, we assume that the only applied loads are the in-plane forces and all other mechanical and thermal loads are zero. Since the prebuckling deformation w_0 is that of an equilibrium configuration, it satisfies the equilibrium equations, and the equation governing buckling deflection w_0^b is given by (see Section 4.2.3)

$$D_{11} \frac{\partial^4 w_0^b}{\partial x^4} + 2(D_{12} + 2D_{66}) \frac{\partial^4 w_0^b}{\partial x^2 \partial y^2} + D_{22} \frac{\partial^4 w_0^b}{\partial y^4} = \hat{N}_{xx} \frac{\partial^2 w_0^b}{\partial x^2} + \hat{N}_{yy} \frac{\partial^2 w_0^b}{\partial y^2} \quad (5.5.1)$$

For simplicity, we will omit the superscript “ b ” on buckling deflection w_0^b . We wish to determine a nonzero deflection w_0 that satisfies Eq. (5.5.1) when the in-plane forces are

$$\hat{N}_{xx} = -N_0, \quad \hat{N}_{yy} = -kN_0, \quad k = \frac{\hat{N}_{yy}}{\hat{N}_{xx}} \quad (5.5.2)$$

and the edges are simply supported.

5.5.2 The Navier Solution

As in the case of bending, we select an expansion for w_0 that satisfies the boundary conditions in Eq. (5.2.2)

$$w_0(x, y) = W_{mn} \sin \alpha x \sin \beta y \quad (5.5.3)$$

Substituting Eq. (5.5.3) into Eq. (5.5.1), we obtain (for any m and n)

$$0 = \left\{ - \left[D_{11} \alpha^4 + 2(D_{12} + 2D_{66}) \alpha^2 \beta^2 + D_{22} \beta^4 \right] + (\alpha^2 + k\beta^2) N_0 \right\} \times W_{mn} \sin \alpha x \sin \beta y \quad (5.5.4)$$

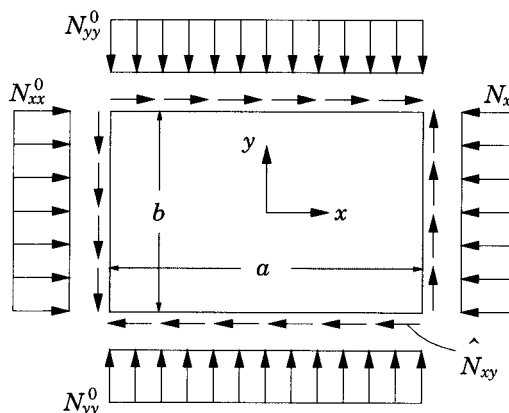


Figure 5.5.1: Buckling of a plate under in-plane compressive edge forces ($N_{xx} = -N_{xx}^0$, $\hat{N}_{yy} = -N_{yy}^0$).

Since the equation must hold for every point (x, y) of the domain for nontrivial w_0 (i.e., $W_{mn} \neq 0$), the expression inside the curl brackets should be zero for every m and n . This yields

$$N_0(m, n) = \frac{d_{mn}}{(\alpha^2 + k\beta^2)} \quad (5.5.5a)$$

where

$$d_{mn} = D_{11}\alpha^4 + 2(D_{12} + 2D_{66})\alpha^2\beta^2 + D_{22}\beta^4, \quad \alpha = \frac{m\pi}{a}, \quad \beta = \frac{n\pi}{b} \quad (5.5.5b)$$

Thus, for each choice of m and n there corresponds a unique value of N_0 . The *critical buckling load* is the smallest of $N_0(m, n)$. For a given laminate this value is dictated by a particular combination of the values of m and n . We investigate critical buckling loads of various laminates next.

5.5.3 Biaxial Compression of a Square Laminate ($k = 1$)

For a square laminate subjected to the same magnitude of compressive load on both edges (i.e., biaxial compression with $k = 1$), Eq. (5.5.5a) yields

$$N_0(m, n) = \left(\frac{\pi^2}{a^2} \right) \frac{[D_{11}m^4 + 2(D_{12} + 2D_{66})m^2n^2 + D_{22}n^4]}{m^2 + n^2} \quad (5.5.6)$$

Now suppose that $D_{11} \geq D_{22}$. Then $D_{11}m^2$ increases more rapidly than the decrease in D_{22}/m^2 with an increase of m . Thus, the minimum of N_0 occurs when $m = 1$:

$$N_0(1, n) = \left(\frac{\pi^2}{a^2} \right) \frac{[D_{11} + 2(D_{12} + 2D_{66})n^2 + D_{22}n^4]}{1 + n^2} \quad (5.5.7)$$

The buckling load is a minimum when n is the nearest integer to the real number R

$$R^2 = -1 + \sqrt{1 + M_1 - 2M_2}, \quad M_1 = \frac{D_{11}}{D_{22}}, \quad M_2 = \frac{D_{12} + 2D_{66}}{D_{22}} \quad (5.5.8)$$

For example, for modulus ratios of $M_1 = 10$ and $M_2 = 1$, we obtain $R = \sqrt{2}$ or $n = 1$. Hence, the critical buckling load becomes

$$N_{cr} \equiv N_0(1, 1) = 6.5 \left(\frac{\pi^2 D_{22}}{a^2} \right) \quad (5.5.9)$$

For modulus ratios of $M_1 = 12$ and $M_2 = 1$, we obtain $R = 1.52$ or $n = 2$, and the critical buckling load becomes

$$N_{cr} = 7.2 \left(\frac{\pi^2 D_{22}}{a^2} \right) \quad (5.5.10)$$

For an isotropic ($D_{11} = D_{22} = D$, $D_{12} = \nu D$, and $2D_{66} = (1 - \nu)D$) square plate under biaxial compression, the buckling can be calculated from Eq. (5.5.6):

$$N_0(m, n) = (m^2 + n^2) \left(\frac{\pi^2 D}{a^2} \right) \quad (5.5.11)$$

and the critical buckling load occurs at $m = n = 1$, and it is equal to

$$N_{cr} \equiv N_0(1, 1) = 2 \left(\frac{\pi^2 D}{a^2} \right) \quad (5.5.12)$$

5.5.4 Biaxial Loading of a Square Laminate

When the edges $x = 0, a$ are subjected to compressive load $\hat{N}_{xx} = -N_0$ and the edges $y = 0, b$ are subjected to tensile load $\hat{N}_{yy} = kN_0$, Eq. (5.5.5a) becomes

$$N_0(m, n) = \frac{\pi^2}{a^2} \frac{[D_{11}m^4 + 2(D_{12} + 2D_{66})m^2n^2 + D_{22}n^4]}{m^2 - kn^2} \quad (5.5.13)$$

for $n^2 < m^2/k$. For example, when $k = 0.5$, the minimum buckling load occurs at $m = 1$ and $n = 1$. For the isotropic material properties used in Section 5.5.3, we have

$$N_{cr} = 26 \left(\frac{\pi^2 D}{a^2} \right) \quad (5.5.14)$$

5.5.5 Uniaxial Compression of a Rectangular Laminate ($k = 0$)

When $k = 0$ ($\hat{N}_{yy} = 0$), we have

$$\begin{aligned} N_0(m, n) &= \frac{a^2}{m^2\pi^2} \left[D_{11} \left(\frac{m\pi}{a} \right)^4 + 2(D_{12} + 2D_{66}) \left(\frac{m\pi}{a} \right)^2 \left(\frac{n\pi}{b} \right)^2 + D_{22} \left(\frac{n\pi}{b} \right)^4 \right] \\ &= \frac{\pi^2}{m^2b^2} \left[D_{11}m^4 \left(\frac{b}{a} \right)^2 + 2(D_{12} + 2D_{66})m^2n^2 + D_{22}n^4 \left(\frac{a}{b} \right)^2 \right] \end{aligned} \quad (5.5.15)$$

An examination of the expression in Eq. (5.5.15) shows that the smallest value of N_0 , for any m , occurs for $n = 1$:

$$N_0(m, 1) = \frac{\pi^2 D_{22}}{b^2} \left[m^2 \frac{D_{11}}{D_{22}} \left(\frac{b}{a} \right)^2 + 2 \frac{(D_{12} + 2D_{66})}{D_{22}} + \frac{1}{m^2} \left(\frac{a}{b} \right)^2 \right] \quad (5.5.16)$$

The critical buckling load is then determined by finding the minimum of $N_0 = N_0(m)$ in Eq. (5.5.16) with respect to m . We have

$$\frac{dN_0}{dm} = 0 \quad \text{gives} \quad m^4 = \frac{D_{22}}{D_{11}} \left(\frac{a}{b} \right)^4 \quad (5.5.17)$$

The second derivative of N_0 with respect to m can be shown to be positive. Since the value of m from Eq. (5.5.17) is not always an integer, the minimum buckling load cannot be predicted by substituting the value of m from Eq. (5.5.17) into Eq. (5.5.16). The minimum value of N_0 is given by Eq. (5.5.16) when m is the nearest integer value given by Eq. (5.5.17). Since the value of m depends on the ratio of the

principal bending stiffnesses as well as plate aspect ratio, we must investigate the variation of N_0 with aspect ratio a/b for different values of m for a given laminate.

As an example, consider a laminate with $D_{11}/D_{22} = 10$ and $a/b = 1.778$. Then we have

$$N_0(m) = \frac{\pi^2 D_{22}}{b^2} \left[10m^2 \left(\frac{b}{a} \right)^2 + 2 + \frac{1}{m^2} \left(\frac{a}{b} \right)^2 \right] \quad (5.5.18a)$$

with

$$m^4 = \frac{D_{22}}{D_{11}} \left(\frac{a}{b} \right)^4 = 0.1 \times (1.778)^4 = 0.9994 \approx 1 \quad (5.5.18b)$$

In fact, for aspect ratios (a/b) less than 2.66, we have

$$m^4 = \frac{D_{22}}{D_{11}} \left(\frac{a}{b} \right)^4 = 0.1 \times (2.66)^4 \quad \text{or } m = 1.496 \quad (5.5.19)$$

Thus the closest integer is $m = 1$. The critical buckling load of a laminate with

$$\frac{D_{11}}{D_{22}} = 10, \quad (D_{12} + 2D_{66}) = D_{22}, \quad \frac{a}{b} < 2.66 \quad (5.5.20)$$

is given by

$$N_{cr} \equiv N_0(1, 1) = \pi^2 \left[10 \left(\frac{b}{a} \right)^2 + 2 + \left(\frac{a}{b} \right)^2 \right] \frac{D_{22}}{b^2} \quad (5.5.21)$$

For various aspect ratios, we have

$$\frac{a}{b} = 1 : \quad N_{cr} = 13 \frac{\pi^2 D_{22}}{b^2}; \quad \frac{a}{b} = 1.5 : \quad N_{cr} = 8.69 \frac{\pi^2 D_{22}}{b^2}$$

$$\frac{a}{b} = 2 : \quad N_{cr} = 8.5 \frac{\pi^2 D_{22}}{b^2}; \quad \frac{a}{b} = 2.5 : \quad N_{cr} = 9.85 \frac{\pi^2 D_{22}}{b^2}$$

It can be shown that if the laminate aspect ratio a/b is greater than 2.66 but less than 4.44, the buckling load is the minimum for $n = 1$ and $m = 2$ [using Eq. (5.5.17)]. For example, for $a/b = 3$, we have from Eq. (5.5.21)

$$N_0(1, 1) = \frac{109}{9} \frac{\pi^2 D_{22}}{b^2} \approx 12.11 \frac{\pi^2 D_{22}}{b^2}$$

$$N_0(1, 2) = \frac{313}{36} \frac{\pi^2 D_{22}}{b^2} \approx 8.69 \frac{\pi^2 D_{22}}{b^2} = N_{cr}$$

$$N_0(1, 3) = 13 \frac{\pi^2 D_{22}}{b^2}$$

Thus, for aspect ratios between 2.66 and 4.44, the plate buckles into two half-waves in the x -direction (and one half-wave in the y -direction). Thus larger aspect ratios lead to higher modes of buckling. Figure 5.5.2 contains a plot of the nondimensionalized buckling load $\bar{N}_0 = N_0 b^2 / (\pi^2 D_{22})$ versus plate aspect ratio a/b for laminates whose material properties are $D_{11}/D_{22} = 10$, $(D_{12}+2D_{66}) = D_{22}$. For aspect ratios less than 2.5, the plate buckles into a single half-wave in the x -direction (see Figure 5.5.3). As the aspect ratio increases, the plate buckles into more and more half-waves in the x -direction. Note that intersections of two consecutive modes

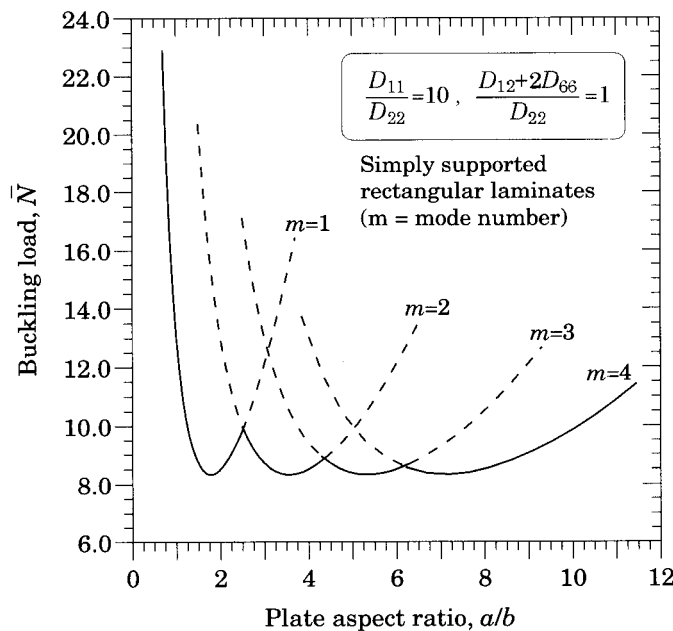


Figure 5.5.2: Nondimensionalized buckling load, $\bar{N} = N_0 b^2 / (\pi^2 D_{22})$, versus plate aspect ratio a/b .

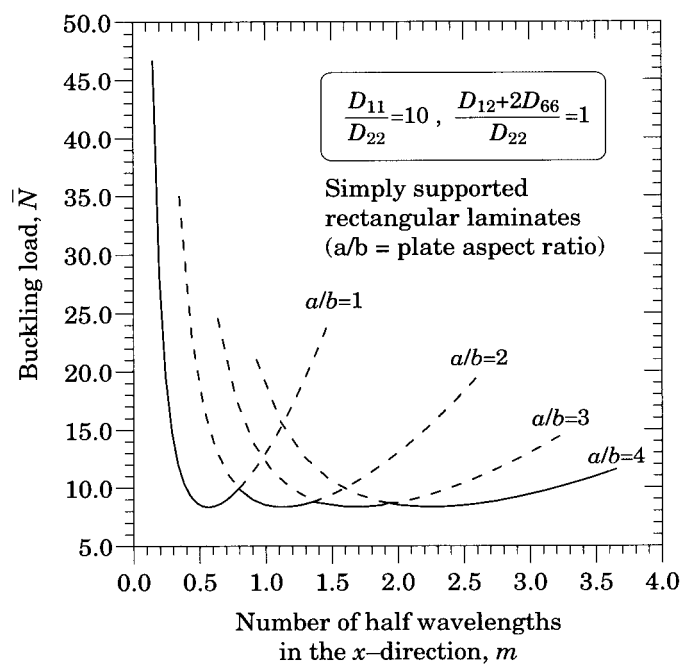


Figure 5.5.3: Nondimensionalized buckling load, \bar{N}_0 , versus number of half-wavelengths m in the x -direction.

correspond to certain aspect ratios (see Figure 5.5.3). Thus, for each of these aspect ratios, there are two possible buckled mode shapes. The \bar{N}_0 versus a/b curve gets flatter with the increasing aspect ratio, and it approaches the value

$$N_{cr} = 2 \left(\frac{\pi^2 D_{22}}{b^2} \right) \left[\sqrt{\frac{D_{11}}{D_{22}}} + \frac{(D_{12} + 2D_{66})}{D_{22}} \right] \quad (5.5.22)$$

which is obtained from Eq. (5.5.16) after substituting for m^2 from Eq. (5.5.17). For the data in Eq. (5.5.20), this limiting value of the critical buckling load is

$$N_{cr} = 8.32456 \left(\frac{\pi^2 D_{22}}{b^2} \right) \quad (5.5.23)$$

For a square isotropic plate ($D_{11} = D_{22} = D$, $D_{12} = \nu D$, and $2D_{66} = (1 - \nu)D$), we have $m = 1$ [from Eq. (5.5.17)], and the critical buckling load from Eq. (5.5.16) is

$$N_{cr} = 4 \left(\frac{\pi^2 D}{a^2} \right) \quad (5.5.24)$$

Table 5.5.1 shows the effect of plate aspect ratio and modulus ratio (anisotropy) on the critical buckling loads $\bar{N} = N_0 b^2 / (\pi^2 D_{22})$ of rectangular laminates (0/90)_s under uniform compression ($k = 0$) and biaxial compression ($k = 1$). In all cases the critical buckling mode is $(m, n) = (1, 1)$, except for $a/b = 0.5$ and $k = 1$, for which case the modes are (1,1), (1,2), (1,2), (1,2), and (1,3) for modulus ratios 5, 10, 20, 25, and 40, respectively. The nondimensionalized buckling load increases as the modulus ratio increases.

Table 5.5.1: Effect of plate aspect ratio and modulus ratio on the nondimensionalized buckling loads \bar{N} of rectangular laminates (0/90)_s under uniform compression ($k = 0$) and biaxial compression ($k = 1$) (E_1/E_2 varied, $G_{12} = G_{13} = 0.5E_2$, $G_{23} = 0.2E_2$, $\nu_{12} = 0.25$; all layers of equal thickness).

k	$\frac{a}{b}$	$\frac{E_1}{E_2} = 5$	10	20	25	40
0	0.5	13.900	18.126	21.878	22.874	24.590
	1.0	5.650	6.347	6.961	7.124	7.404
	1.5	5.233	5.277	5.310	5.318	5.332
1	0.5	11.120	12.694	13.922	14.248	14.766
	1.0	2.825	3.174	3.481	3.562	3.702
	1.5	1.610	1.624	1.634	1.636	1.641

Figure 5.5.4 shows plots of nondimensionalized critical buckling load $\bar{N} = N_0 b^2 / (\pi^2 D_{22})$ as a function of the plate aspect ratio, a/b , for two different materials:

Material 1: $E_1 = 25E_2$, $G_{12} = G_{13} = 0.5E_2$, $\nu_{12} = 0.25$

Material 2: $E_1 = 40E_2$, $G_{12} = G_{13} = 0.6E_2$, $\nu_{12} = 0.25$

There is a mode change around $a/b > 2.2$ from (1,1) to (1,2).

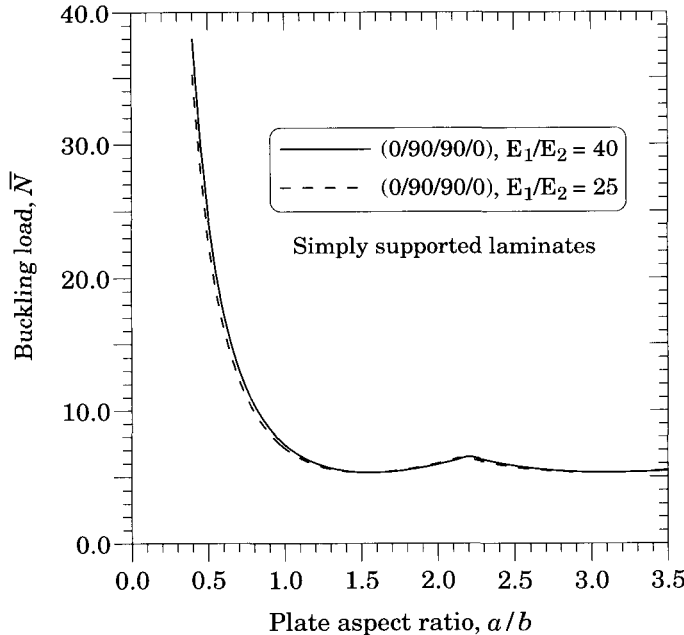


Figure 5.5.4: Nondimensionalized uniaxial critical buckling load (\bar{N}) versus plate aspect ratio (a/b) of symmetric cross-ply laminate $(0/90)_s$ for two different modular ratios.

5.6 Buckling of Rectangular Plates Under In-Plane Shear Load

5.6.1 Governing Equation

In this section we consider buckling of specially orthotropic rectangular plates under in-plane shear load, N_{xy}^0 . The problem does not permit the Navier solution; therefore, we use a variational method to solve the problem. When $\hat{N}_{xx} = \hat{N}_{yy} = 0$ and $\hat{N}_{xy} = N_{xy}^0$ (see Figure 5.5.1), the governing equation (5.5.1) takes the form

$$D_{11} \frac{\partial^4 w_0}{\partial x^4} + 2(D_{12} + 2D_{66}) \frac{\partial^4 w_0}{\partial x^2 \partial y^2} + D_{22} \frac{\partial^4 w_0}{\partial y^4} = 2N_{xy}^0 \frac{\partial^2 w_0}{\partial x \partial y} \quad (5.6.1)$$

5.6.2 Simply Supported Plates

When the plate is simply supported on all its edges and subjected to in-plane shear, the Navier solution does not exist because the cross derivative term involving N_{xy}^0 will have a different coefficient ($\cos \alpha x \cos \beta y$) than the rest of the expression in Eq. (5.6.1). Hence, we will seek the solution by a variational method.

Since the expression given in Eq. (5.5.3) for w_0 satisfies the geometric boundary conditions of the problem, the same functions are admissible in the Ritz method:

$$w_0(x, y) \approx W_{MN} = \sum_{n=1}^N \sum_{m=1}^M c_{mn} \sin \alpha x \sin \beta y \quad (5.6.2)$$

where $\alpha = m\pi/a$ and $\beta = n\pi/b$. Since the approximation functions

$$\varphi_{mn}(x, y) = \sin \frac{m\pi x}{a} \sin \frac{n\pi y}{b} \quad (5.6.3)$$

also satisfy the natural boundary conditions of the problem, the Ritz and Galerkin solutions are the same. Thus, substitution of Eq. (5.6.2) in the total potential energy functional for the Ritz method

$$\begin{aligned} \Pi(w_0) = & \frac{1}{2} \int_0^b \int_0^a \left[D_{11} \left(\frac{\partial^2 w_0}{\partial x^2} \right)^2 + 2D_{12} \frac{\partial^2 w_0}{\partial x^2} \frac{\partial^2 w_0}{\partial y^2} + 4D_{66} \left(\frac{\partial^2 w_0}{\partial x \partial y} \right)^2 \right. \\ & \left. + D_{22} \left(\frac{\partial^2 w_0}{\partial y^2} \right)^2 - 2N_{xy}^0 \left(\frac{\partial w_0}{\partial x} \frac{\partial w_0}{\partial y} \right) \right] dx dy \end{aligned} \quad (5.6.4)$$

or the weighted-integral statement for the Galerkin method

$$0 = \int_0^b \int_0^a \left[D_{11} \frac{\partial^4 w_0}{\partial x^4} + 2(D_{12} + 2D_{66}) \frac{\partial^4 w_0}{\partial x^2 \partial y^2} + D_{22} \frac{\partial^4 w_0}{\partial y^4} - 2N_{xy}^0 \frac{\partial^2 w_0}{\partial x \partial y} \right] \varphi_{pq} dx dy \quad (5.6.5)$$

would lead to the same equations for the coefficients c_{mn} . Using the Galerkin method, we obtain

$$\begin{aligned} 0 = & \sum_{n=1}^N \sum_{m=1}^M \int_0^b \int_0^a \left\{ \left[D_{11} \alpha^4 + (D_{12} + 2D_{66}) \alpha^2 \beta^2 + D_{22} \beta^4 \right] \varphi_{mn} \right. \\ & \left. - 2\alpha\beta N_{xy}^0 \cos \alpha x \cos \beta y \right\} c_{mn} \varphi_{pq} dx dy \end{aligned} \quad (5.6.6)$$

Using the identities

$$\begin{aligned} \int_0^a \sin \frac{m\pi x}{a} \sin \frac{n\pi x}{a} dx &= \begin{cases} 0, & m \neq n \\ \frac{a}{2}, & m = n \end{cases} \\ \int \sin \lambda x \cos \mu x dx &= - \left[\frac{\cos(\lambda - \mu)x}{(\lambda - \mu)} + \frac{\cos(\lambda + \mu)x}{(\lambda + \mu)} \right] \end{aligned} \quad (5.6.7)$$

we arrive at

$$\begin{aligned} 0 = & \frac{ab}{4} \left[D_{11} \left(\frac{p\pi}{a} \right)^4 + (D_{12} + 2D_{66}) \left(\frac{p\pi}{a} \right)^2 \left(\frac{q\pi}{b} \right)^2 + D_{22} \left(\frac{q\pi}{b} \right)^4 \right] c_{pq} \\ & - 2N_{xy}^0 \sum_{m=1}^N \sum_{n=1}^M \left(\frac{m\pi}{a} \right) \left(\frac{n\pi}{b} \right) S_{(mn)(pq)} c_{mn} \end{aligned} \quad (5.6.8a)$$

where

$$\begin{aligned} S_{(mn)(pq)} &= \int_0^b \int_0^a \cos \frac{m\pi x}{a} \cos \frac{n\pi y}{b} \sin \frac{p\pi x}{a} \sin \frac{q\pi y}{b} dx dy \\ &= \left(\frac{4ab}{\pi^2} \right) \frac{pq}{(p^2 - m^2)(q^2 - n^2)} \quad \text{for } p^2 \neq m^2 \text{ and } q^2 \neq n^2 \end{aligned} \quad (7.6.8b)$$

and the coefficients are zero when $p = m, p \pm m$ even, or when $q = n, q \pm n$ even.

The set of mn homogeneous equations (5.6.8a) define an eigenvalue problem

$$\left([A] - N_{xy}^0 [S] \right) \{c\} = \{0\} \quad (5.6.9)$$

which has a nontrivial solution (i.e., $c_{mn} \neq 0$) when the determinant of the coefficient matrix is zero. Note that $[A]$ is a diagonal matrix while $[S]$ is a nonpositive-definite matrix; hence, the solution of (5.6.9) requires an eigenvalue routine that is suitable for nonpositive-definite matrices. It is found that the solution of (5.6.9) converges very slowly with increasing values of M and N (see [3,7]).

5.6.3 Clamped Plates

The total potential energy expression for the clamped rectangular plate under in-plane shear load N_{xy}^0 is

$$\begin{aligned} \Pi(w_0) = & \frac{1}{2} \int_0^b \int_0^a \left[D_{11} \left(\frac{\partial^2 w_0}{\partial x^2} \right)^2 + 2D_{12} \frac{\partial^2 w_0}{\partial x^2} \frac{\partial^2 w_0}{\partial y^2} + 4D_{66} \left(\frac{\partial^2 w_0}{\partial x \partial y} \right)^2 \right. \\ & \left. + D_{22} \left(\frac{\partial^2 w_0}{\partial y^2} \right)^2 - 2N_{xy}^0 \left(\frac{\partial w_0}{\partial x} \frac{\partial w_0}{\partial y} \right) \right] dx dy \end{aligned} \quad (5.6.10a)$$

The minimum total potential energy principle requires that $\delta\Pi = 0$. We have

$$\begin{aligned} 0 = & \int_0^b \int_0^a \left(M_{xx} \delta \varepsilon_{xx}^{(1)} + M_{yy} \delta \varepsilon_{yy}^{(1)} + M_{xy} \delta \gamma_{xy}^{(1)} - q \delta w_0 \right) dx dy \\ = & \int_0^b \int_0^a \left[D_{11} \frac{\partial^2 w_0}{\partial x^2} \frac{\partial^2 \delta w_0}{\partial x^2} + D_{12} \left(\frac{\partial^2 w_0}{\partial y^2} \frac{\partial^2 \delta w_0}{\partial x^2} + \frac{\partial^2 w_0}{\partial x^2} \frac{\partial^2 \delta w_0}{\partial y^2} \right) \right. \\ & + 4D_{66} \frac{\partial^2 w_0}{\partial x \partial y} \frac{\partial^2 \delta w_0}{\partial x \partial y} + D_{22} \frac{\partial^2 w_0}{\partial y^2} \frac{\partial^2 \delta w_0}{\partial y^2} \\ & \left. - N_{xy}^0 \left(\frac{\partial \delta w_0}{\partial x} \frac{\partial w_0}{\partial y} + \frac{\partial w_0}{\partial x} \frac{\partial \delta w_0}{\partial y} \right) \right] dx dy \end{aligned} \quad (5.6.10b)$$

We assume a Ritz approximation of the form

$$w_0(x, y) \approx W_{mn}(x, y) = \sum_{i=1}^m \sum_{j=1}^n c_{ij} \varphi_{ij}(x, y) \quad (5.6.11a)$$

where

$$\varphi_{ij}(x, y) = X_i(x)Y_j(y) \quad (5.6.11b)$$

with

$$X_i(x) = \left(\frac{x}{a} \right)^{i+1} \left(1 - \frac{x}{a} \right)^2, \quad Y_j(y) = \left(\frac{y}{b} \right)^{j+1} \left(1 - \frac{y}{b} \right)^2 \quad (5.6.12)$$

or

$$\begin{aligned} X_i(x) &= \sin \lambda_i x - \sinh \lambda_i x + \alpha_i (\cosh \lambda_i x - \cos \lambda_i x) \\ Y_j(y) &= \sin \lambda_j y - \sinh \lambda_j y + \alpha_j (\cosh \lambda_j y - \cos \lambda_j y) \end{aligned} \quad (5.6.13)$$

for $i = 1, 2, \dots, m$; $j = 1, 2, \dots, n$. The parameters λ_i and α_i of Eq. (5.6.13) are defined in Eq. (5.3.45) and (5.3.46), respectively. Substituting Eq. (5.6.11) into Eq. (5.6.10b) we obtain

$$0 = \left\{ \int_0^b \int_0^a \left[D_{11} \frac{d^2 X_i}{dx^2} Y_j \frac{d^2 X_p}{dx^2} Y_q + 2(D_{12} + 2D_{66}) \frac{dX_i}{dx} \frac{dY_j}{dy} \frac{dX_p}{dx} \frac{dY_q}{dy} \right. \right. \\ \left. \left. + D_{22} X_i \frac{d^2 Y_j}{dy^2} X_p \frac{d^2 Y_q}{dy^2} - N_{xy}^0 \left(\frac{dX_i}{dx} Y_j X_p \frac{dY_q}{dy} + X_i \frac{dY_j}{dy} \frac{dX_p}{dx} Y_q \right) \right] dx dy \right\} c_{pq} \quad (5.6.14)$$

When functions in Eq. (5.6.13) are used, at least two terms should be used because the coefficient of N_{xy}^0 is zero for $m = n = 1$; other coefficients are zero for $m = 1, n = 2$ and $m = 2, n = 1$. Using the approximation

$$w_0(x, y) \approx c_{11} X_1(x) Y_1(y) + c_{22} X_2(x) Y_2(y) \quad (5.6.15a)$$

with [see Eq. (5.3.47)]

$$\begin{aligned} X_1(x) &= \sin \frac{4.73x}{a} - \sinh \frac{4.73x}{a} + 1.0178 \left(\cosh \frac{4.73x}{a} - \cos \frac{4.73x}{a} \right) \\ X_2(x) &= \sin \frac{7.853x}{a} - \sinh \frac{7.853x}{a} + 0.9992 \left(\cosh \frac{7.853x}{a} - \cos \frac{7.853x}{a} \right) \\ Y_1(y) &= \sin \frac{4.73y}{b} - \sinh \frac{4.73y}{b} + 1.0178 \left(\cosh \frac{4.73y}{b} - \cos \frac{4.73y}{b} \right) \\ Y_2(y) &= \sin \frac{7.853y}{b} - \sinh \frac{7.853y}{b} + 0.9992 \left(\cosh \frac{7.853y}{b} - \cos \frac{7.853y}{b} \right) \end{aligned} \quad (5.6.15b)$$

we obtain

$$\begin{aligned} \left[\frac{537.181b}{a^3} D_{11} + \frac{324.829}{ab} (D_{12} + 2D_{66}) + \frac{537.181a}{b^3} D_{22} \right] c_{11} - 23.107 N_{xy}^0 c_{22} &= 0 \\ \left[\frac{3791.532b}{a^3} D_{11} + \frac{4227.255}{ab} (D_{12} + 2D_{66}) + \frac{3791.532a}{b^3} D_{22} \right] c_{22} - 23.107 N_{xy}^0 c_{11} &= 0 \end{aligned}$$

or in matrix form

$$\begin{bmatrix} a_{11} & N_{xy}^0 a_{12} \\ N_{xy}^0 a_{12} & a_{22} \end{bmatrix} \begin{Bmatrix} c_{11} \\ c_{22} \end{Bmatrix} = - \begin{Bmatrix} 0 \\ 0 \end{Bmatrix} \quad (5.6.16a)$$

where

$$\begin{aligned} a_{11} &= \frac{537.181}{a^4} D_{11} + \frac{324.829}{a^2 b^2} (D_{12} + 2D_{66}) + \frac{537.181}{b^4} D_{22}, \quad a_{12} = \frac{23.107}{ab} \\ a_{22} &= \frac{3791.532}{a^4} D_{11} + \frac{4227.255}{a^2 b^2} (D_{12} + 2D_{66}) + \frac{3791.532}{b^4} D_{22} \end{aligned} \quad (5.6.16b)$$

For a nontrivial solution, the determinant of the coefficient matrix should be zero, $a_{11}a_{22} - a_{12}a_{12}(N_{xy}^0)^2 = 0$. Solving for the buckling load N_{xy}^0 , we obtain

$$N_{xy}^0 = \pm \frac{1}{a_{12}} \sqrt{a_{11}a_{22}} \quad (5.6.17)$$

The \pm sign indicates that the shear buckling load may be either positive or negative.

For an isotropic square plate, we have $a = b$ and $D_{11} = D_{22} = (D_{12} + 2D_{66}) = D$, and the shear buckling load predicted by Eq. (5.6.17) is

$$N_{xy}^0 = \pm 176 \frac{D}{a^2} \quad (5.6.18)$$

whereas the “exact” critical buckling load is

$$N_{xy}^0 = \pm 145 \frac{D}{a^2} \quad (5.6.19)$$

The two-term Ritz solution (5.6.18) is over 21% in error.

This concludes the discussion of shear buckling of rectangular plates. The variational solutions presented here for buckling under in-plane shear are only for illustrative purposes. More than two-term variational approximations are required to obtain accurate buckling loads. Once again, a symbolic manipulator proves to be effective in evaluating the integrals in the variational methods.

5.7 Vibration of Simply Supported Plates

5.7.1 Governing Equations

For natural vibration, all applied loads and the in-plane forces are set to zero in Eq. (5.1.1)

$$\begin{aligned} D_{11} \frac{\partial^4 w_0}{\partial x^4} + 2(D_{12} + 2D_{66}) \frac{\partial^4 w_0}{\partial x^2 \partial y^2} + D_{22} \frac{\partial^4 w_0}{\partial y^4} \\ + I_0 \ddot{w}_0 - I_2 \left(\frac{\partial^2 \ddot{w}_0}{\partial x^2} + \frac{\partial^2 \ddot{w}_0}{\partial y^2} \right) = 0 \end{aligned} \quad (5.7.1a)$$

where

$$I_0 = \sum_{k=1}^L \rho_0^{(k)} (z_{k+1} - z_k), \quad I_2 = \frac{1}{3} \sum_{k=1}^L \rho_0^{(k)} (z_{k+1}^3 - z_k^3) \quad (5.7.1b)$$

where L denotes the total number of layers in the laminate.

5.7.2 Solution

We assume a periodic solution of the form

$$W_{mn}(t) = W_{mn}^0 e^{i\omega t} \quad (5.7.2)$$

where $i = \sqrt{-1}$ and ω is the frequency of natural vibration. Substituting (5.7.2) in (5.7.1a), we obtain (for any m and n)

$$\left\{ D_{11}\alpha^4 + 2(D_{12} + 2D_{66})\alpha^2\beta^2 + D_{22}\beta^4 - \omega^2 [I_0 + (\alpha^2 + \beta^2) I_2] \right\} \times W_{mn} \sin \alpha x \sin \beta y = 0 \quad (5.7.3)$$

Since the equation must hold for every point (x, y) of the domain $0 < x < a$ and $0 < y < b$, the expression inside the braces should be zero for every m and n . This yields

$$\omega_{mn}^2 = \frac{\pi^4}{I_0 b^4} \left[D_{11}m^4 \left(\frac{b}{a}\right)^4 + 2(D_{12} + 2D_{66})m^2 n^2 \left(\frac{b}{a}\right)^2 + D_{22}n^4 \right] \quad (5.7.4)$$

where

$$I_0 = I_0 + I_2 \left[\left(\frac{m\pi}{a}\right)^2 + \left(\frac{n\pi}{b}\right)^2 \right] \quad (5.7.5)$$

For different values of m and n there corresponds a unique frequency ω_{mn} and a corresponding mode shape

$$w_0(x, y) = W_{mn}^0 \sin \frac{m\pi x}{a} \sin \frac{n\pi y}{b} \quad (5.7.6)$$

where W_{mn}^0 is the amplitude of the vibration mode (m, n) . For square laminates, Eq. (5.7.4) reduces to

$$\omega_{mn}^2 = \left(\frac{\pi}{a}\right)^4 \frac{[D_{11}m^4 + 2(D_{12} + 2D_{66})m^2 n^2 + D_{22}n^4]}{[I_0 + I_2 \left(\frac{\pi}{a}\right)^2 (m^2 + n^2)]} \quad (5.7.7)$$

When the rotatory inertia I_2 is not zero, it is not simple to find the lowest natural frequency (fundamental frequency). The rotary inertia has the effect of reducing the frequency for any m and n .

When the rotary inertia I_2 is neglected, the frequency of a rectangular specially orthotropic laminate reduces to

$$\omega_{mn}^2 = \frac{\pi^4}{I_0 b^4} \left[D_{11}m^4 \left(\frac{b}{a}\right)^4 + 2(D_{12} + 2D_{66})m^2 n^2 \left(\frac{b}{a}\right)^2 + D_{22}n^4 \right] \quad (5.7.8)$$

and for a square plate we have

$$\omega_{mn}^2 = \frac{\pi^4}{I_0 b^4} [D_{11}m^4 + 2(D_{12} + 2D_{66})m^2 n^2 + D_{22}n^4] \quad (5.7.9)$$

The fundamental frequency occurs at $m = n = 1$:

$$\omega_{11}^2 = \frac{\pi^4}{I_0 b^4} \left[D_{11} \left(\frac{b}{a}\right)^4 + 2(D_{12} + 2D_{66}) \left(\frac{b}{a}\right)^2 + D_{22} \right] \quad (5.7.10)$$

For a rectangular isotropic plate, when the rotary inertia is neglected, the frequency equation (5.7.8) becomes

$$\omega_{mn}^2 = \frac{D\pi^4}{I_0 b^4} \left[m^4 \left(\frac{b}{a} \right)^4 + 2m^2 n^2 \left(\frac{b}{a} \right)^2 + n^4 \right] = \frac{D\pi^4}{I_0 b^4} \left[m^2 \left(\frac{b}{a} \right)^2 + n^2 \right]^2 \quad (5.7.11)$$

and the fundamental frequency is given by

$$\omega_{11} = \frac{\pi^2}{b^2} \sqrt{\frac{D}{I_0}} \left[\left(\frac{b}{a} \right)^2 + 1 \right] \quad (5.7.12)$$

Nondimensionalized frequencies, $\bar{\omega}_{mn} = \omega_{mn}(b^2/\pi^2)\sqrt{\rho h/D_{22}}$, of specially orthotropic square laminates are presented in Table 5.7.1 for modulus ratios $E_1/E_2 = 10, 20$ ($G_{12} = G_{13} = 0.5E_2$, $G_{23} = 0.2E_2$, $\nu_{12} = 0.25$). The results presented in Table 5.7.1 are for $m, n = 1, 2, 3$, and for the case in which the rotary inertia is neglected. The first four frequencies for an orthotropic (0°) plate correspond to the modes, $(m, n) = (1,1), (1,2), (1,3)$, and $(2,1)$, whereas for symmetric cross-ply plates the first four frequencies are provided by the modes: $(m, n) = (1,1), (1,2), (2,1)$, and $(1,3)$. Table 5.7.2 contains nondimensionalized fundamental frequencies of symmetric $(0/90)_s$ laminates for various aspect ratios and modulus ratios. The fundamental frequency increases with modular ratio. The effect of including rotary inertia is to decrease the frequency of vibration, and the effect is negligible for this case. Figure 5.7.1 shows a plot of nondimensionalized fundamental frequency $\bar{\omega}_{11}$ as a function of plate aspect ratio for symmetric $(0/90)_s$ graphite-epoxy laminate ($E_1/E_2 = 40$, $G_{12} = G_{13} = 0.5E_2$, $\nu_{12} = 0.25$).

Table 5.7.1: Nondimensionalized fundamental frequencies of symmetric cross-ply laminates according to the classical plate theory ($\bar{\omega}_{mn} = \omega_{mn}(b^2/\pi^2)\sqrt{\rho h/D_{22}}$).

$\frac{E_1}{E_2}$	m	n	0°	$(0^\circ/90^\circ)_s$
10	1	1	3.672	2.519
	1	2	5.996	4.986
	1	3	10.648	9.783
	2	1	13.075	8.515
	2	2	14.690	10.077
	2	3	18.181	13.783
	3	1	28.868	18.704
	3	2	30.258	19.911
	3	3	33.053	22.674
20	1	1	4.847	2.638
	1	2	6.781	4.917
	1	3	11.111	9.637
	2	1	18.193	9.354
	2	2	19.388	10.554
	2	3	22.153	13.826
	3	1	40.539	20.752
	3	2	41.542	21.578
	3	3	43.623	23.746

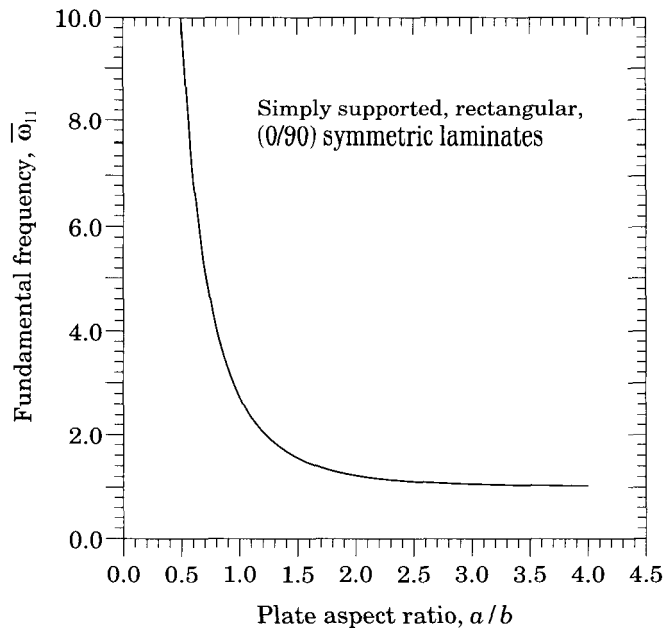


Figure 5.7.1: Nondimensionalized fundamental frequency $\bar{\omega}_{11}$ as a function of plate aspect ratio a/b for symmetric $(0/90)_s$ laminate.

Table 5.7.2: Nondimensionalized fundamental frequencies $\bar{\omega}_{11}$ of symmetric cross-ply laminates $(0/90)_s$ according to the classical plate theory.

a/b	Without Rotary Inertia				With Rotary Inertia			
	$\frac{E_1}{E_2} = 10$	20	30	40	10	20	30	40
0.5	8.515	9.355	9.716	9.917	8.513	9.353	9.714	9.916
1.0	2.519	2.638	2.691	2.721	2.519	2.638	2.691	2.721
1.5	1.531	1.536	1.538	1.539	1.531	1.536	1.538	1.539
2.0	1.246	1.229	1.221	1.216	1.246	1.229	1.221	1.216
2.5	1.138	1.119	1.110	1.105	1.138	1.119	1.110	1.105
3.0	1.087	1.071	1.063	1.059	1.087	1.071	1.063	1.059

5.8 Buckling and Vibration of Plates with Two Parallel Edges Simply Supported

5.8.1 Introduction

The Lévy method can be used to determine natural frequencies and critical buckling loads of rectangular laminates for which two (parallel) opposite edges are simply supported and the other two edges have any boundary conditions, as described in Section 5.3 for bending analysis. For other combinations of fixed, hinged, and free boundary conditions on the edges of rectangular plates, one may use the Ritz method with the approximation functions suggested in Section 5.4.3.

Consider a rectangular laminate with in-plane dimensions a and b and total thickness h . The laminate coordinate system (x, y, z) is taken such that $-a/2 \leq x \leq a/2$, $0 \leq y \leq b$, $-h/2 \leq z \leq h/2$ (see Figure 5.8.1). Here we assume that the edges $y = 0, b$ are simply supported, and the other two edges each have simply supported, clamped, or free boundary conditions. The equation governing buckling under in-plane normal forces and natural vibration of a specially orthotropic laminated plate is given by Eq. (5.1.1):

$$\begin{aligned} D_{11} \frac{\partial^4 w_0}{\partial x^4} + 2(D_{12} + 2D_{66}) \frac{\partial^4 w_0}{\partial x^2 \partial y^2} + D_{22} \frac{\partial^4 w_0}{\partial y^4} \\ - \hat{N}_{xx} \frac{\partial^2 w_0}{\partial x^2} - \hat{N}_{yy} \frac{\partial^2 w_0}{\partial y^2} + I_0 \ddot{w}_0 - I_2 \left(\frac{\partial^2 \ddot{w}_0}{\partial x^2} + \frac{\partial^2 \ddot{w}_0}{\partial y^2} \right) = 0 \end{aligned} \quad (5.8.1)$$

Recall that in the Lévy method the partial differential equation (5.8.1) is reduced to an ordinary differential equation in x by assuming solution in the form of a single Fourier series

$$w_0(x, y) = W_n(x) \sin \beta y, \quad \beta = \frac{n\pi}{b} \quad (5.8.2)$$

which satisfies the simply supported boundary conditions

$$w_0 = 0, \quad M_{xx} = - \left(D_{11} \frac{\partial^2 w_0}{\partial x^2} + D_{12} \frac{\partial^2 w_0}{\partial y^2} \right) = 0 \quad (5.8.3)$$

on edges $y = 0, b$. The ordinary differential equations obtained in the Lévy method can be solved either by direct integration or by means of the state-space approach. We discuss both procedures in the following sections.

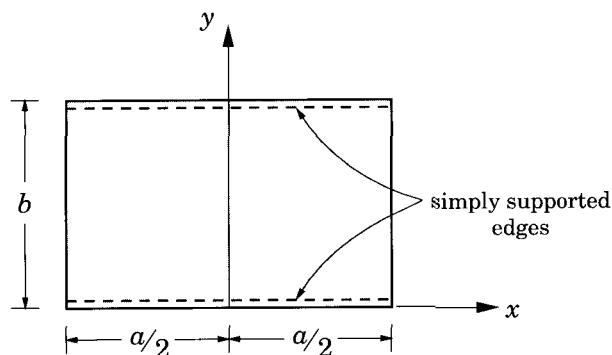


Figure 5.8.1: Geometry and coordinate system of a rectangular plate used in the Lévy method.

5.8.2 Buckling by Direct Integration

Here we consider buckling under uniaxial compressive forces

$$\hat{N}_{xx} = 0, \quad \hat{N}_{yy} = -N_{yy}^0 \quad (5.8.4)$$

Substituting (5.8.2) and (5.8.4) into the governing equation (5.8.1) with the inertia terms zero, for any y , we obtain

$$D_{11} \frac{d^4 W_n}{dx^4} - 2(D_{12} + 2D_{66})\beta^2 \frac{d^2 W_n}{dx^2} + D_{22}\beta^4 W_n - N_{yy}^0 \beta^2 W_n = 0 \quad (5.8.5)$$

We assume the general solution of Eq. (5.8.5) in the form

$$W_n(x) = A_n \cosh \lambda_1 x + B_n \sinh \lambda_1 x + C_n \cos \lambda_2 x + D_n \sin \lambda_2 x \quad (5.8.6)$$

where λ_i are the roots of the characteristic equation

$$D_{11}\lambda^4 - 2(D_{12} + 2D_{66})\beta^2\lambda^2 + D_{22}\beta^4 - N_{yy}^0\beta^2\lambda = 0 \quad (5.8.7)$$

and they are given by

$$\begin{aligned} (\lambda_1)^2 &= \frac{\beta^2}{D_{11}} \left[\sqrt{(D_{12} + 2D_{66})^2 + D_{11}(\tilde{N}_{yy}^0 - D_{22})} + (D_{12} + 2D_{66}) \right] \\ (\lambda_2)^2 &= \frac{\beta^2}{D_{11}} \left[\sqrt{(D_{12} + 2D_{66})^2 + D_{11}(\tilde{N}_{yy}^0 - D_{22})} - (D_{12} + 2D_{66}) \right] \end{aligned} \quad (5.8.8)$$

where $\tilde{N}_{yy}^0 = N_{yy}^0/\beta^2$. The constants A_n, B_n, C_n , and D_n must be determined using the boundary conditions at $x = 0, a$.

For clamped boundary conditions on edges $x = 0, a$, for example, we require

$$W_n = 0, \quad \frac{dW_n}{dx} = 0 \quad (5.8.9)$$

which yield the eigenvalue problem

$$\begin{bmatrix} 1 & 0 & 1 & 0 \\ 0 & \lambda_1 & 0 & \lambda_2 \\ \cosh \lambda_1 a & \sinh \lambda_1 a & \cos \lambda_2 a & \sin \lambda_2 a \\ \lambda_1 \sinh \lambda_1 a & \lambda_1 \cosh \lambda_1 a & -\lambda_2 \sin \lambda_2 a & \lambda_2 \cos \lambda_2 a \end{bmatrix} \begin{Bmatrix} A_n \\ B_n \\ C_n \\ D_n \end{Bmatrix} = \begin{Bmatrix} 0 \\ 0 \\ 0 \\ 0 \end{Bmatrix} \quad (5.8.10)$$

For a nontrivial solution, $A_n \neq 0, B_n \neq 0, C_n \neq 0$, and $D_n \neq 0$, we set the determinant of the coefficient matrix in (5.8.10) to zero. We have [cf. Eq. (4.2.58)]

$$2\lambda_1\lambda_2(1 - \cosh \lambda_1 a \cos \lambda_2 a) + (\lambda_1^2 - \lambda_2^2)\sin \lambda_1 a \sinh \lambda_2 a = 0 \quad (5.8.11)$$

Since λ_1 and λ_2 contain the buckling load N_{yy}^0 , Eq. (5.8.11) can be used, in theory, to determine the critical buckling load of the plate. However, the complexity of (5.8.11) makes it less useful in readily computing the buckling loads.

5.8.3 Vibration by Direct Integration

Here we consider natural vibration of a specially orthotropic plate. For periodic motion, we assume that

$$w_0(x, y, t) = \bar{w}_0(x, y)e^{i\omega t} \quad (5.8.12)$$

where $i = \sqrt{-1}$ and ω is the frequency of natural vibration. Then the amplitude of vibration \bar{w}_0 is approximated as in Eq. (5.8.2). Substituting (5.8.2) and (5.8.12) into the governing equation (5.8.1), with the in-plane forces zero, for any y and t we obtain

$$D_{11} \frac{d^4 W_n}{dx^4} + [I_2 \omega^2 - 2(D_{12} + 2D_{66})\beta^2] \frac{d^2 W_n}{dx^2} - [\omega^2 (I_0 + I_2\beta^2) - D_{22}\beta^4] W_n = 0 \quad (5.8.13)$$

or

$$p \frac{d^4 W_n}{dx^4} + q \frac{d^2 W_n}{dx^2} - r W_n = 0 \quad (5.8.14a)$$

where

$$p = D_{11}, \quad q = I_2 \omega^2 - 2(D_{12} + 2D_{66})\beta^2, \quad r = \omega^2 (I_0 + I_2\beta^2) - D_{22}\beta^4 \quad (5.8.14b)$$

Equation (5.8.14a) is of the same form as Eq. (4.2.44), and the procedure described in Section 4.2.4 can be used to determine the natural frequencies for various boundary conditions on edges $x = 0, a$.

5.8.4 Buckling and Vibration by the State-Space Approach

As explained in Section 5.3, the governing differential equation in (5.8.1) can be reduced, with Eq. (5.8.2), to a system of a first-order matrix differential equation

$$\{Z'\} = [T]\{Z\} \quad (5.8.15)$$

where

$$\{Z\} = \begin{Bmatrix} W_m \\ W'_m \\ W''_m \\ W'''_m \\ W_m \end{Bmatrix}, \quad [T] = \begin{bmatrix} 0 & 1 & 0 & 0 \\ 0 & 0 & 1 & 0 \\ 0 & 0 & 0 & 1 \\ C_1 & 0 & C_2 & 0 \end{bmatrix} \quad (5.8.16)$$

$\hat{N}_{xx} = -N_{xx}^0$, $\hat{N}_{yy} = -N_{yy}^0$, and

$$C_1 = -\frac{(\beta^4 D_{22} - \beta^2 \hat{N}_{yy})}{D_{11}}, \quad C_2 = \frac{[2\beta^2(D_{12} + 2D_{66}) - \hat{N}_{xx}]}{D_{11}} \quad (5.8.17)$$

for buckling analysis and

$$C_1 = -\frac{(\beta^4 D_{22} - \hat{I}_0 \omega_m^2)}{D_{11}}, \quad C_2 = \frac{[2\beta^2(D_{12} + 2D_{66}) - I_2 \omega_m^2]}{D_{11}} \quad (5.8.18)$$

for free vibration analysis. Here ω_m denotes the frequency of vibration of the m th mode, $\hat{I}_0 = I_0 + \beta^2 I_2$, and $i = \sqrt{-1}$.

The solution of Eq. (5.8.15) is given by

$$\mathbf{Z}(x) = e^{\mathbf{A}x} \mathbf{K} \quad (5.8.19)$$

and the vector \mathbf{K} of constants is to be determined from the boundary conditions. Substitution of Eq. (5.8.19) into the set of boundary conditions (expressed in terms of Z_i) results in a homogeneous system of equations

$$[M]\{K\} = \{0\} \quad (5.8.20)$$

For a nontrivial solution, the determinant of the coefficient matrix in (5.8.20) should be zero:

$$|M_{ij}| = 0 \quad (5.8.21)$$

The roots of the above equation are the squares of the frequencies of natural vibration, or, in the case of buckling, they denote the buckling loads.

The Lévy type solution procedure is used to evaluate the natural frequencies and critical buckling loads under uniaxial compression of specially orthotropic rectangular laminates. The lamina material properties used are

$$E_1/E_2 = 40, \quad G_{12} = G_{13} = 0.6E_2, \quad \nu_{12} = 0.25$$

Numerical results for the nondimensionalized fundamental frequencies and critical buckling loads under uniaxial compression

$$\bar{\omega} = \omega \left(\frac{a^2}{h} \right) \sqrt{\rho/E_2}, \quad \bar{N} = N_{xx}^0 b^2 / (E_2 h^3)$$

of square, symmetric, cross-ply laminates are presented in Table 5.8.1 for various ratios of principal moduli of the material. Note that the nondimensionalized frequencies and buckling loads are the same for any odd number of layers $n = 3, 5, 7, \dots$ (with the total thickness of all laminates being the same). Table 5.8.2 contains numerical results for various boundary conditions (see [16]). As before, the notation SF, for example, is used to indicate that edge $x = a/2$ is simply supported (S) and edge $x = -a/2$ is free (F).

Table 5.8.1: Nondimensionalized fundamental frequencies and critical buckling loads under uniaxial compression of simply supported symmetric cross-ply square plates as a function of the modulus ratio.

Laminate	$E_1/E_2 = 3$	10	20	30	40
Fundamental Frequencies, $\bar{\omega} = \omega \left(\frac{a^2}{h} \right) \sqrt{\rho/E_2}$					
(0/90/0) _n	7.5357	10.650	13.948	16.605	18.891
(0/90/90/0)	7.5357	10.650	13.948	16.605	18.891
Uniaxial Critical Buckling Loads, $\bar{N} = N_{xx}^0 b^2 / E_2 h^3$					
(0/90/0) _n	5.754	11.492	19.712	27.936	36.160
(0/90/90/0)	5.754	11.492	19.712	27.936	36.160

Table 5.8.2: Nondimensionalized fundamental frequencies and critical buckling loads under uniaxial compression of symmetric cross-ply ($0^\circ/90^\circ/0^\circ$) square plates for various boundary conditions and modulus ratios.

$\frac{E_1}{E_2}$	SS	SC	CC	FF	FS	FC
Fundamental Frequencies, $\bar{\omega} = \omega \left(\frac{a^2}{h} \right) \sqrt{\rho/E_2}$						
10	10.650	15.199	21.118	3.294	4.088	5.419
20	13.948	20.610	29.166	3.721	4.443	6.515
30	16.605	24.870	35.431	4.106	4.770	7.445
40(1)*	18.891	28.501	40.743	4.457	5.076	8.269
40(2)	26.938	34.533	45.233	17.827	18.473	19.789
40(3)	46.208	51.192	59.023	40.113	40.761	41.505
Biaxial Critical Buckling Loads, $\bar{N} = N_{xx}^0 b^2 / E_2 h^3$						
10	5.746	9.353(2)	13.468(2)	1.123	1.661	3.202
20	9.591(2)†	14.026(2)	21.709(3)	1.420	1.978	4.683
30	12.147(2)	18.703(2)	28.081(3)	1.722	2.288	6.142
40	14.704(2)	23.381(2)	34.454(3)	2.025	2.596	7.595

* Denotes the mode number m .

† Mode m in which the lowest buckling load occurs (otherwise, $m = 1$).

5.9 Transient Analysis

5.9.1 Preliminary Comments

In this section we will develop transient solutions to specially orthotropic plates. Recall that in the static bending analysis of plates we developed the analytical solutions using the Navier method, the Lévy method, and the Ritz method. The same methods can also be used to approximate the spatial variations of the transient solutions of plates. The resulting ordinary differential equations in time can be solved exactly when possible or numerically using a time-integration method. Here we consider simply supported plates to illustrate these ideas (see Reddy [21]).

5.9.2 Spatial Variation of the Solution

The equation of motion governing bending deflection w_0 of a specially orthotropic plate, assuming no applied in-plane and thermal forces, is [see Eq. (5.1.1)]

$$\begin{aligned} -\left[D_{11} \frac{\partial^4 w_0}{\partial x^4} + 2(D_{12} + 2D_{66}) \frac{\partial^4 w_0}{\partial x^2 \partial y^2} + D_{22} \frac{\partial^4 w_0}{\partial y^4} \right] + q(x, y, t) \\ = I_0 \ddot{w}_0 - I_2 \left(\frac{\partial^2 \ddot{w}_0}{\partial x^2} + \frac{\partial^2 \ddot{w}_0}{\partial y^2} \right) \end{aligned} \quad (5.9.1)$$

Suppose that the plate is simply supported with the boundary conditions

$$w_0(x, 0, t) = 0, \quad w_0(x, b, t) = 0, \quad w_0(0, y, t) = 0, \quad w_0(a, y, t) = 0 \quad \text{for } t \geq 0$$

$$M_{xx}(0, y, t) = 0, \quad M_{xx}(a, y, t) = 0, \quad M_{yy}(x, 0, t) = 0, \quad M_{yy}(x, b, t) = 0 \quad \text{for } t \geq 0 \quad (5.9.2)$$

and assume that the initial conditions are

$$w_0(x, y, 0) = d_0(x, y), \quad \frac{\partial w_0}{\partial t}(x, y, 0) = v_0(x, y) \quad \text{for all } x \text{ and } y \quad (5.9.3)$$

where d_0 and v_0 are the initial displacement and velocity, respectively.

We assume the following expansion of the transverse deflection to satisfy the boundary conditions (5.9.2) for any time $t \geq 0$

$$w_0(x, y, t) = \sum_{n=1}^{\infty} \sum_{m=1}^{\infty} W_{mn}(t) \sin \alpha x \sin \beta y \quad (5.9.4)$$

where $\alpha = (m\pi/a)$ and $\beta = (n\pi/b)$. Similarly, we assume that the transverse load, initial displacement, and initial velocity can be expanded as

$$q(x, y, t) = \sum_{n=1}^{\infty} \sum_{m=1}^{\infty} Q_{mn}(t) \sin \alpha x \sin \beta y \quad (5.9.5)$$

$$d_0(x, y) = \sum_{n=1}^{\infty} \sum_{m=1}^{\infty} D_{mn} \sin \alpha x \sin \beta y \quad (5.9.6)$$

$$v_0(x, y) = \sum_{n=1}^{\infty} \sum_{m=1}^{\infty} V_{mn} \sin \alpha x \sin \beta y \quad (5.9.7)$$

where, for example, Q_{mn} are given by

$$Q_{mn}(t) = \frac{4}{ab} \int_0^b \int_0^a q(x, y, t) \sin \alpha x \sin \beta y dx dy \quad (5.9.8)$$

Substituting the expansions (5.9.4) and (5.9.5) into Eq. (5.9.1), we obtain

$$\begin{aligned} & \sum_{n=1}^{\infty} \sum_{m=1}^{\infty} \left\{ W_{mn} [D_{11}\alpha^4 + 2(D_{12} + 2D_{66})\alpha^2\beta^2 + D_{22}\beta^4] \right. \\ & \quad \left. + [I_0 + I_2(\alpha^2 + \beta^2)] \ddot{W}_{mn} - Q_{mn} \right\} \sin \alpha x \sin \beta y = 0 \end{aligned} \quad (5.9.9)$$

Since the above expression must hold for all x and y , it follows that

$$\begin{aligned} & W_{mn} [D_{11}\alpha^4 + 2(D_{12} + 2D_{66})\alpha^2\beta^2 + D_{22}\beta^4] \\ & + [I_0 + I_2(\alpha^2 + \beta^2)] \ddot{W}_{mn} - Q_{mn} = 0 \end{aligned} \quad (5.9.10a)$$

or

$$K_{mn} W_{mn}(t) + M_{mn} \ddot{W}_{mn} = Q_{mn}(t) \quad (5.9.10b)$$

where

$$\begin{aligned} K_{mn} &= D_{11}\alpha^4 + 2(D_{12} + 2D_{66})\alpha^2\beta^2 + D_{22}\beta^4 \\ M_{mn} &= I_0 + I_2(\alpha^2 + \beta^2) \end{aligned} \quad (5.9.10c)$$

5.9.3 Time Integration

The ordinary differential equation (5.9.10a) can be solved either exactly or numerically. The numerical time integration methods will be discussed in the subsequent chapters. To solve it exactly, we first write Eq. (5.9.10a) in the form

$$\frac{d^2W_{mn}}{dt^2} + \left(\frac{K_{mn}}{M_{mn}} \right) W_{mn} = \frac{1}{M_{mn}} Q_{mn}(t) \equiv \hat{Q}_{mn}(t) \quad (5.9.11)$$

The solution of Eq. (5.9.11) is given by

$$W_{mn}(t) = C_1 e^{\lambda_1 t} + C_2 e^{\lambda_2 t} + W_{mn}^p(t) \quad (5.9.12)$$

where C_1 and C_2 are constants to be determined using the initial conditions, $W_{mn}^p(t)$ is the particular solution

$$W_{mn}^p(t) = \int_0^t \frac{r_1(\tau)r_2(t) - r_1(t)r_2(\tau)}{r_1(\tau)\dot{r}_2(\tau) - \dot{r}_1(\tau)r_2(\tau)} \hat{Q}_{mn}(\tau) d\tau \quad (5.9.13a)$$

with $r_1(t) = e^{\lambda_1 t}$ and $r_2(t) = e^{\lambda_2 t}$, and λ_1 and λ_2 are the roots of the equation

$$\lambda^2 + \frac{K_{mn}}{M_{mn}} = 0; \quad \lambda_1 = -i\mu, \quad \lambda_2 = i\mu, \quad i = \sqrt{-1}, \quad \mu = \sqrt{\frac{K_{mn}}{M_{mn}}} \quad (5.9.13b)$$

The solution becomes

$$W_{mn}(t) = A \cos \mu t + B \sin \mu t + W_{mn}^p(t) \quad (5.9.14a)$$

$$W_{mn}^p(t) = \frac{1}{2i\mu} \left(e^{i\mu t} \int_0^t e^{-i\mu\tau} \hat{Q}_{mn}(\tau) d\tau - e^{-i\mu t} \int_0^t e^{i\mu\tau} \hat{Q}_{mn}(\tau) d\tau \right) \quad (5.9.14b)$$

Once the load distribution, both spatially and with time, is known, the solution can be determined from Eq. (5.9.14a).

For a step loading, $Q_{mn}(t) = Q_{mn}^0 H(t)$, where $H(t)$ denotes the Heaviside step function, Eq. (5.9.14a) takes the form

$$W_{mn}(t) = A \cos \mu t + B \sin \mu t + \frac{1}{K_{mn}} Q_{mn}^0 \quad (5.9.15a)$$

Using the initial conditions (5.9.3), we obtain

$$A = D_{mn} - \frac{1}{K_{mn}} Q_{mn}^0, \quad B = \frac{V_{mn}}{\mu} \quad (5.9.15b)$$

Thus the final solution (5.9.4) is given by

$$w_0(x, y, t) = \sum_{n=1}^{\infty} \sum_{m=1}^{\infty} \left[D_{mn} \cos \mu t + \frac{V_{mn}}{\mu} \sin \mu t + \frac{Q_{mn}^0}{K_{mn}} (1 - \cos \mu t) \right] \sin \alpha x \sin \beta y \quad (5.9.16)$$

The coefficients Q_{mn}^0 are given in Table 5.2.1 for various types of distributions. The same holds for D_{mn} and V_{mn} .

It should be noted that the procedure outlined above is valid irrespective of how one arrives at Eq. (5.9.10b); e.g., Eq. (5.9.10b) could have been obtained using the Ritz method or other methods. The exact solution of the differential equation (5.9.10b) can also be obtained using the Laplace transform method. Once the solution w_0 is known, stresses can be computed using Eqs. (5.2.13).

Figure 5.9.1 contains plots of the nondimensionalized center deflection $\bar{w} = w_0(E_2 h^3/a^4 q_0)$ as a function of time for a simply supported (SS-1) symmetric cross-ply (0/90/0) laminate ($h_1 = h_3 = h/4$, $h_2 = h/2$; $E_1/E_2 = 25$, $G_{12} = G_{13} = 0.5E_2$, $\nu_{12} = 0.25$; $a = b = 25$ cm, $h = 5$ cm) under a step loading that is sinusoidally distributed (SSL) or uniformly distributed (UDL) over the plate surface. It is assumed that the plate motion ensues from rest, i.e., $d_0 = 0$ and $v_0 = 0$. The solution is plotted to show one complete wavelength. The dashed curve corresponds to the solution when the rotary inertia is neglected. The rotary inertia has the effect of increasing the wavelength slightly. Figure 5.9.2 contains plots of nondimensionalized center normal stress $\bar{\sigma}_{xx} = \sigma_{xx}(h^2/a^2 q_0)$ as a function of time for the same laminates. Note that the stress variation for the uniformly distributed load case is not as smooth as for the sinusoidally distributed load case.

5.10 Closure

In this chapter analytical and Ritz solutions for bending, buckling, natural vibration, and transient response of specially orthotropic plates are presented. In most cases, the numerical determination of actual solutions require evaluation of a series solution, solution of a transcendental equation, or determination of eigenvalues (in the state-space approach). Thus, even the “exact” solutions become approximate because of the truncation of an infinite series or round-off errors in the solution of nonlinear equations. The analytical solutions developed herein serve to help one understand, at least qualitatively, the behavior of laminated plates.

Problems

- 5.1** Determine the displacement field of a simply supported plate strip under a concentrated (line) load F_0 at the center using the Navier solution method.
- 5.2** Derive the Navier solution of a simply supported rectangular plate under the following temperature distribution

$$T(x, y, z) = T_0(x, y) + zT_1(x, y)$$

where T_0 and T_1 are known functions of x and y only, which can be expanded in double Fourier series in the same way as the mechanical loading $q(x, y)$.

- 5.3** Derive the expressions for transverse shear stresses from 3-D equilibrium equations when the plate is subjected to the temperature distribution of the form given in Problem 5.2. Assume that T_0 and T_1 can be expanded in double sine series.
- 5.4** Determine the constants A_n, B_n, C_n , and D_n in the Lévy solution (5.3.15) of a specially orthotropic rectangular plate with simply supported edges at $y = 0, b$ and $x = a$, and clamped at $x = 0$. Assume uniformly distributed transverse load.

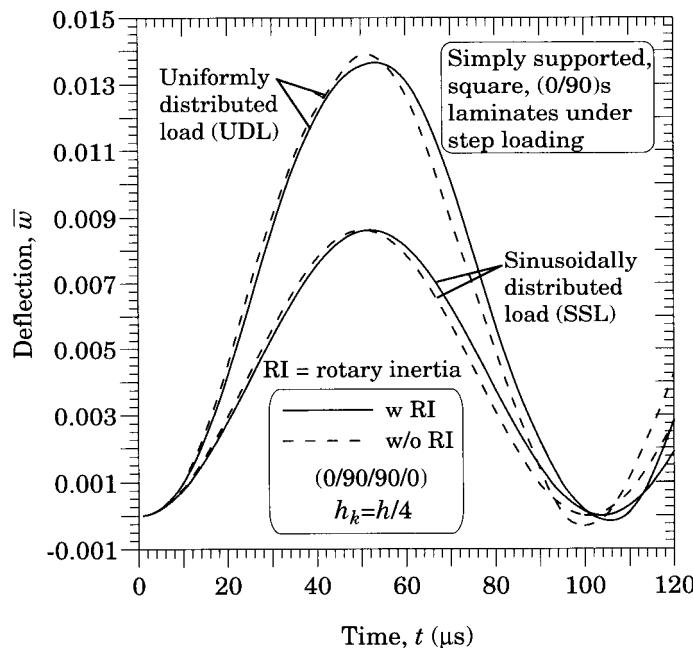


Figure 5.9.1: Nondimensionalized maximum transverse deflection (\bar{w}) versus time for a simply supported symmetric cross-ply $(0/90)_s$ laminate.

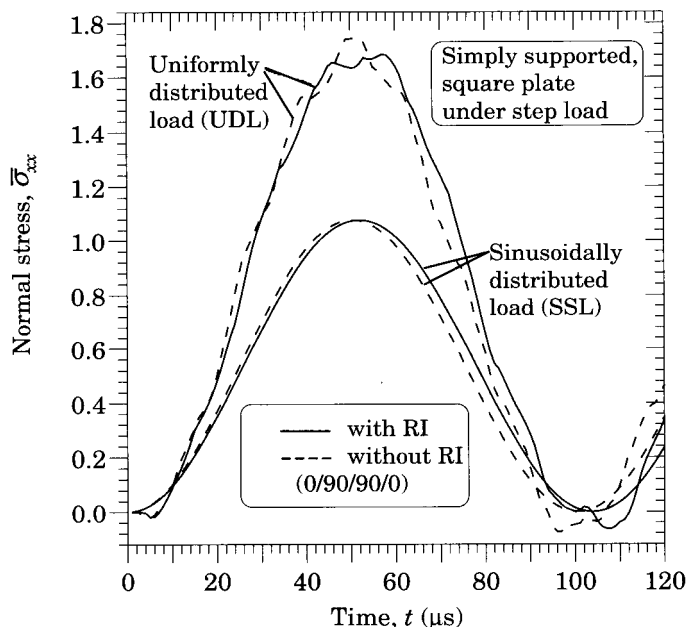


Figure 5.9.2: Nondimensionalized maximum normal stress ($\bar{\sigma}_{xx}$) versus time for a simply supported symmetric cross-ply $(0/90)_s$ laminate.

- 5.5** Determine the constants A_n, B_n, C_n , and D_n in the Lévy solution (5.3.15) of a specially orthotropic rectangular plate with simply supported edges at $y = 0, b$, clamped at $x = 0$, and free at $x = a$. Assume uniformly distributed transverse load. The boundary conditions for the free edge are

$$M_{xx} = 0, \quad V_x \equiv Q_x + \frac{\partial M_{xy}}{\partial y} = \frac{\partial M_{xx}}{\partial x} + 2 \frac{\partial M_{xy}}{\partial y} = 0$$

These boundary conditions can be expressed in terms of the transverse deflection as

$$D_{11} \frac{\partial^2 w_0}{\partial x^2} + D_{12} \frac{\partial^2 w_0}{\partial y^2} = 0, \quad D_{11} \frac{\partial^3 w_0}{\partial x^3} + (D_{12} + 2D_{66}) \frac{\partial^3 w_0}{\partial y^2 \partial x} = 0$$

- 5.6** Determine the constants A_n, B_n, C_n , and D_n in the Lévy solution (5.3.15) of a specially orthotropic rectangular plate with simply supported edges at $y = 0, b$ and $x = a$, and free at $x = 0$. Assume uniformly distributed transverse load.
- 5.7** Use the following one-parameter Ritz approximation to determine the deflection of a simply supported rectangular plate:

$$w_0(x, y) \approx c_1 x(a - x)y(b - y)$$

Ans: The parameter c_1 is given by $c_1 = \frac{q_0 a^2 b^2}{36R_{11}}$ with

$$R_{11} = 2 \left[\frac{1}{15} D_{11} b^4 + \frac{1}{9} (D_{12} + 2D_{66}) a^2 b^2 + \frac{1}{15} D_{22} a^4 \right]$$

- 5.8** Show that the one-parameter Galerkin solution with the algebraic functions in Eq. (5.4.6) is also given by Eq. (5.4.11).
- 5.9** Use one-parameter Ritz approximation of the form

$$w_0(x, y) \approx c_{11} \left(1 - \cos \frac{2\pi x}{a} \right) \left(1 - \cos \frac{2\pi y}{b} \right)$$

to determine the deflection of a rectangular plate with clamped edges and subjected to uniformly distributed transverse load.

- 5.10** Verify the result in Eq. (5.4.14).
5.11 Verify the result in Eq. (5.6.16).
5.12 Determine the critical buckling load of a rectangular orthotropic plate simply supported on edges $y = 0, b$ and clamped on edges $x = 0, a$ using the one-parameter Ritz approximation of the form

$$w_0(x, y) = c_{11} \left(1 - \cos \frac{2\pi x}{a} \right) \sin \frac{n\pi y}{b}$$

- 5.13** Determine the critical buckling load of a rectangular orthotropic plate simply supported on edges $y = 0, b$ and $x = 0$, and clamped on edge $x = a$ using the one-parameter Ritz approximation of the form

$$w_0(x, y) = c_{11} \left(\frac{x}{a} \right) \left(1 - \frac{x}{a} \right)^2 \sin \frac{n\pi y}{b}$$

- 5.14** Determine the transient response of simply supported specially orthotropic plate under transverse loading (a) $q(x, y, t) = q_0 H(t - t_0)$ and (b) $q(x, y, t) = q_0 \delta(t - t_0)$, where $H(t)$ denotes the Heaviside step function and $\delta(t)$ is the Dirac delta function.
5.15 Solve Eq. (5.9.10) using the Laplace transform method.

References for Additional Reading

1. Reddy, J. N., *Energy Principles and Variational Methods in Applied Mechanics*, Second Edition, John Wiley, New York (2002).
2. Reddy, J. N. (Ed.), *Mechanics of Composite Materials. Selected Works of Nicholas J. Pagano*, Kluwer, The Netherlands (1994).
3. Reddy, J. N., *Theory and Analysis of Elastic Plates*, Taylor & Francis, Philadelphia, PA (1999).
4. Whitney, J. M., *Structural Analysis of Laminated Anisotropic Plates*, Technomic, Lancaster, PA (1987).
5. Szilard, R., *Theory and Analysis of Plates, Classical and Numerical Methods*, Prentice-Hall, Englewood Cliffs, NJ (1974).
6. Timoshenko, S. P. and Woinowsky-Krieger, S., *Theory of Plates and Shells*, McGraw-Hill, New York (1959).
7. Lekhnitskii, S. G., *Anisotropic Plates*, Translated from Russian by S. W. Tsai and T. Cheron, Gordon and Breach, Newark, NJ (1968).
8. Hearman, R. F. S., "The Frequency of Flexural Vibration of Rectangular Orthotropic Plates with Clamped or Supported Edges," *Journal of Applied Mechanics*, **26**(4), 537–540 (1959).
9. Young, D., "Vibrations of Rectangular Plates by the Ritz Method," *Journal of Applied Mechanics*, **17**, 448–453 (1950).
10. Pipes, L. A. and Harvill, L. R., *Applied Mathematics for Engineers and Physicists*, Third Edition, McGraw-Hill, New York (1970).
11. Franklin, J. N., *Matrix Theory*, Prentice-Hall, Englewood Cliffs, NJ (1968).
12. Goldberg, J. L. and Schwartz, A. J., *Systems of Ordinary Differential Equations, An Introduction*, Harper and Row, New York (1972).
13. Reddy, J. N., Khdeir, A. A., and Librescu, L., "Lévy Type Solutions for Symmetrically Laminated Rectangular Plates Using First-Order Shear Deformation Theory," *Journal of Applied Mechanics*, **54**, 740–742 (1987).
14. Khdeir, A. A., Reddy, J. N., and Librescu, L., "Analytical Solution of a Refined Shear Deformation Theory for Rectangular Composite Plates," *International Journal of Solids and Structures*, **23**, 1447–1463 (1987).
15. Khdeir, A. A. and Librescu, L., "Analysis of Symmetric Cross-Ply Laminated Elastic Plates Using a Higher-Order Theory: Part I: Stress and Displacement," *Composite Structures*, **9**, 189–213 (1988).
16. Khdeir, A. A. and Librescu, L., "Analysis of Symmetric Cross-Ply Laminated Elastic Plates Using a Higher-Order Theory: Part II: Buckling and Free Vibration," *Composite Structures*, **9**, 259–277 (1988).
17. Khdeir, A. A., "Free Vibration and Buckling of Symmetric Cross-Ply Laminated Plates by an Exact Method," *Journal of Sound and Vibration*, **126**(3), 447–461 (1988).
18. Wang, J. T.-S., "On the Solution of Plates of Composite Materials," *Journal of Composite Materials*, **3**, 590–592 (1969).
19. Ashton, J. E. and Waddoups, M. E., "Analysis of Anisotropic Plates," *Journal of Composite Materials*, **3**, 148–165 (1969).
20. Ashton, J. E., "Analysis of Anisotropic Plates II," *Journal of Composite Materials*, **3**, 470–479 (1969).
21. Reddy, J. N., "On the Solutions to Forced Motions of Rectangular Composite Plates," *Journal of Applied Mechanics*, **49**, 403–408 (1982).
22. Timoshenko, S. P. and Gere, J. P., *Theory of Elastic Stability*, Second Edition, McGraw-Hill, New York (1959).

Analytical Solutions of Rectangular Laminated Plates Using CLPT

6.1 Governing Equations in Terms of Displacements

In this chapter analytical solutions of antisymmetric cross-ply and angle-ply laminated plates based on the classical laminated plate theory (CLPT) are developed. The Navier method, the Lévy method with the state-space approach, and the Ritz method are used, depending on the boundary conditions. In all cases considered in this chapter, the von Kármán nonlinear terms in the strain-displacement relations are omitted. Before we begin with the derivation of the exact solutions, it is useful to express the governing equations in terms of the generalized displacements of the theory.

The linear equations of motion of the classical laminated plate theory (CLPT) can be obtained from Eqs. (3.3.45)–(3.3.47) by setting the nonlinear terms to zero:

$$\begin{aligned} A_{11} \frac{\partial^2 u_0}{\partial x^2} + 2A_{16} \frac{\partial^2 u_0}{\partial x \partial y} + A_{66} \frac{\partial^2 u_0}{\partial y^2} + A_{16} \frac{\partial^2 v_0}{\partial x^2} + (A_{12} + A_{66}) \frac{\partial^2 v_0}{\partial x \partial y} + A_{26} \frac{\partial^2 v_0}{\partial y^2} \\ - \left[B_{11} \frac{\partial^3 w_0}{\partial x^3} + 3B_{16} \frac{\partial^3 w_0}{\partial x^2 \partial y} + (B_{12} + 2B_{66}) \frac{\partial^3 w_0}{\partial x \partial y^2} + B_{26} \frac{\partial^3 w_0}{\partial y^3} \right] \\ - \left(\frac{\partial N_{xx}^T}{\partial x} + \frac{\partial N_{xy}^T}{\partial y} \right) = I_0 \ddot{u}_0 - I_1 \frac{\partial \ddot{w}_0}{\partial x} \end{aligned} \quad (6.1.1)$$

$$\begin{aligned} A_{16} \frac{\partial^2 u_0}{\partial x^2} + (A_{12} + A_{66}) \frac{\partial^2 u_0}{\partial x \partial y} + A_{26} \frac{\partial^2 u_0}{\partial y^2} + A_{66} \frac{\partial^2 v_0}{\partial x^2} + 2A_{26} \frac{\partial^2 v_0}{\partial x \partial y} + A_{22} \frac{\partial^2 v_0}{\partial y^2} \\ - \left[B_{16} \frac{\partial^3 w_0}{\partial x^3} + (B_{12} + 2B_{66}) \frac{\partial^3 w_0}{\partial x^2 \partial y} + 3B_{26} \frac{\partial^3 w_0}{\partial x \partial y^2} + B_{22} \frac{\partial^3 w_0}{\partial y^3} \right] \\ - \left(\frac{\partial N_{xy}^T}{\partial x} + \frac{\partial N_{yy}^T}{\partial y} \right) = I_0 \ddot{v}_0 - I_1 \frac{\partial \ddot{w}_0}{\partial y} \end{aligned} \quad (6.1.2)$$

$$\begin{aligned} B_{11} \frac{\partial^3 u_0}{\partial x^3} + 3B_{16} \frac{\partial^3 u_0}{\partial x^2 \partial y} + (B_{12} + 2B_{66}) \frac{\partial^3 u_0}{\partial x \partial y^2} + B_{26} \frac{\partial^3 u_0}{\partial y^3} \\ + B_{16} \frac{\partial^3 v_0}{\partial x^3} + (B_{12} + 2B_{66}) \frac{\partial^3 v_0}{\partial x^2 \partial y} + 3B_{26} \frac{\partial^3 v_0}{\partial x \partial y^2} + B_{22} \frac{\partial^3 v_0}{\partial y^3} \\ - \left[D_{11} \frac{\partial^4 w_0}{\partial x^4} + 4D_{16} \frac{\partial^4 w_0}{\partial x^3 \partial y} + 2(D_{12} + 2D_{66}) \frac{\partial^4 w_0}{\partial x^2 \partial y^2} + 4D_{26} \frac{\partial^4 w_0}{\partial x \partial y^3} + D_{22} \frac{\partial^4 w_0}{\partial y^4} \right] \end{aligned}$$

$$\begin{aligned}
& - \left(\frac{\partial^2 M_{xx}^T}{\partial x^2} + 2 \frac{\partial^2 M_{xy}^T}{\partial x \partial y} + \frac{\partial^2 M_{yy}^T}{\partial y^2} \right) + \hat{N}_{xx} \frac{\partial^2 w_0}{\partial x^2} + 2 \hat{N}_{xy} \frac{\partial^2 w_0}{\partial x \partial y} + \hat{N}_{yy} \frac{\partial^2 w_0}{\partial y^2} \\
& + q = I_1 \left(\frac{\partial \ddot{u}_0}{\partial x} + \frac{\partial \ddot{v}_0}{\partial y} \right) + I_0 \ddot{w}_0 - I_2 \left(\frac{\partial^2 \ddot{w}_0}{\partial x^2} + \frac{\partial^2 \ddot{w}_0}{\partial y^2} \right)
\end{aligned} \quad (6.1.3)$$

where N^T and M^T denote thermal resultants defined in Eq. (3.3.41), and \hat{N}_{xx} , \hat{N}_{xy} , and \hat{N}_{yy} denote the applied edge forces (see Figure 6.1.1).

Equations (6.1.1)–(6.1.3) can be cast in differential operator form as¹

$$\begin{bmatrix} c_{11} & c_{12} & c_{13} \\ c_{12} & c_{22} & c_{23} \\ c_{13} & c_{23} & c_{33} \end{bmatrix} \begin{Bmatrix} u_0 \\ v_0 \\ w_0 \end{Bmatrix} + \begin{bmatrix} m_{11} & 0 & m_{13} \\ 0 & m_{22} & m_{23} \\ m_{13} & m_{23} & m_{33} \end{bmatrix} \begin{Bmatrix} \ddot{u}_0 \\ \ddot{v}_0 \\ \ddot{w}_0 \end{Bmatrix} = \begin{Bmatrix} 0 \\ 0 \\ q \end{Bmatrix} + \begin{Bmatrix} f_1^T \\ f_2^T \\ f_3^T \end{Bmatrix} \quad (6.1.4)$$

where coefficients c_{ij} are defined by

$$\begin{aligned}
c_{11} &= A_{11}d_x^2 + 2A_{16}d_x d_y + A_{66}d_y^2 \\
c_{12} &= A_{16}d_x^2 + (A_{12} + A_{66})d_x d_y + A_{26}d_y^2 \\
c_{13} &= -[B_{11}d_x^3 + 3B_{16}d_x^2 d_y + (B_{12} + 2B_{66})d_x d_y^2 + B_{26}d_y^3] \\
c_{22} &= A_{66}d_x^2 + 2A_{26}d_x d_y + A_{22}d_y^2 \\
c_{23} &= -[B_{16}d_x^3 + (B_{12} + 2B_{66})d_x^2 d_y + 3B_{26}d_x d_y^2 + B_{22}d_y^3] \\
c_{33} &= D_{11}d_x^4 + 4D_{16}d_x^3 d_y + 2(D_{12} + 2D_{66})d_x^2 d_y^2 + 4D_{26}d_x d_y^3 + D_{22}d_y^4 \\
&\quad - [\hat{N}_{xx}d_x^2 + 2\hat{N}_{xy}d_x d_y + \hat{N}_{yy}d_y^2]
\end{aligned} \quad (6.1.5a)$$

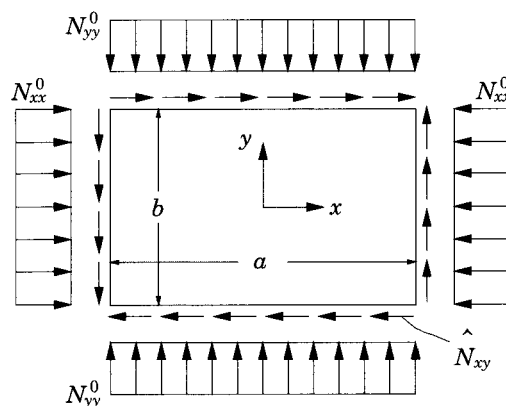


Figure 6.1.1: A plate with applied edge forces ($\hat{N}_{xx} = -N_{xx}^0$, $\hat{N}_{yy} = -N_{yy}^0$).

¹ In order to make the coefficient matrices $[C]$ and $[M]$ symmetric, the third equation is multiplied with a negative sign.

coefficients m_{ij} and f_i^T are defined by

$$\begin{aligned} m_{11} &= -I_0 d_t^2, \quad m_{13} = I_1 d_x d_t^2, \quad m_{22} = -I_0 d_t^2 \\ m_{23} &= I_1 d_y d_t^2, \quad m_{33} = I_0 d_t^2 - I_2 d_t^2(d_x^2 + d_y^2) \end{aligned} \quad (6.1.5b)$$

$$\begin{aligned} f_1^T &= \frac{\partial N_{xx}^T}{\partial x} + \frac{\partial N_{xy}^T}{\partial y} \\ f_2^T &= \frac{\partial N_{xy}^T}{\partial x} + \frac{\partial N_{yy}^T}{\partial y} \\ f_3^T &= -\left(\frac{\partial^2 M_{xx}^T}{\partial x^2} + 2 \frac{\partial^2 M_{xy}^T}{\partial y \partial x} + \frac{\partial^2 M_{yy}^T}{\partial y^2} \right) \end{aligned} \quad (6.1.5c)$$

and d_x^i , d_y^i , and d_t^i denote the differential operators

$$d_x^i = \frac{\partial^i}{\partial x^i}, \quad d_y^i = \frac{\partial^i}{\partial y^i}, \quad d_t^i = \frac{\partial^i}{\partial t^i} \quad (i = 1, 2, 3, 4) \quad (6.1.5d)$$

Note that the thermal forces and moments, $(N_{xx}^T, N_{yy}^T, N_{xy}^T)$ and $(M_{xx}^T, M_{yy}^T, M_{xy}^T)$, are known in terms of the temperature distribution and material coefficients as defined in Eqs. (3.3.41a,b).

6.2 Admissible Boundary Conditions for the Navier Solutions

In the Navier method the generalized displacements are expanded in a double trigonometric series in terms of unknown parameters (see Section 5.2.2). The choice of the functions in the series is restricted to those which satisfy the boundary conditions of the problem. Substitution of the displacement expansions into the governing equations should result in a unique, invertible, set of algebraic equations among the parameters of the expansion. Otherwise, the Navier solution cannot be developed for the problem.

The Navier solutions can be developed for rectangular laminates with two sets of simply supported boundary conditions. Even for these boundary conditions, not all laminates permit the Navier solution. We will determine which lamination schemes permit such solutions. The geometry, laminate coordinate system, and the two types of simply supported boundary conditions are shown in Figure 6.2.1. The two types of boundary conditions are given below.

Simply Supported (SS-1): The displacement boundary conditions are

$$\begin{aligned} u(x, 0, 0, t) &= 0, \quad u(x, b, 0, t) = 0, \quad v(0, y, 0, t) = 0, \quad v(a, y, 0, t) = 0 \\ w(x, 0, 0, t) &= 0, \quad w(x, b, 0, t) = 0, \quad w(0, y, 0, t) = 0, \quad w(a, y, 0, t) = 0 \\ \left. \frac{\partial u}{\partial z} \right|_{(x, 0, 0, t)} &= 0, \quad \left. \frac{\partial u}{\partial z} \right|_{(x, b, 0, t)} = 0, \quad \left. \frac{\partial v}{\partial z} \right|_{(0, y, 0, t)} = 0, \quad \left. \frac{\partial v}{\partial z} \right|_{(a, y, 0, t)} = 0 \end{aligned} \quad (6.2.1)$$

The boundary conditions associated with stress components (for a plate theory) are

$$\begin{aligned}
 & \int_{-\frac{h}{2}}^{\frac{h}{2}} \sigma_{xx}(0, y, z, t) dz = 0, \quad \int_{-\frac{h}{2}}^{\frac{h}{2}} \sigma_{xx}(a, y, z, t) dz = 0 \\
 & \int_{-\frac{h}{2}}^{\frac{h}{2}} \sigma_{yy}(x, 0, z, t) dz = 0, \quad \int_{-\frac{h}{2}}^{\frac{h}{2}} \sigma_{yy}(x, b, z, t) dz = 0 \\
 & \int_{-\frac{h}{2}}^{\frac{h}{2}} z\sigma_{xx}(0, y, z, t) dz = 0, \quad \int_{-\frac{h}{2}}^{\frac{h}{2}} z\sigma_{xx}(a, y, z, t) dz = 0 \\
 & \int_{-\frac{h}{2}}^{\frac{h}{2}} z\sigma_{yy}(x, 0, z, t) dz = 0, \quad \int_{-\frac{h}{2}}^{\frac{h}{2}} z\sigma_{yy}(x, b, z, t) dz = 0 \quad (6.2.2)
 \end{aligned}$$

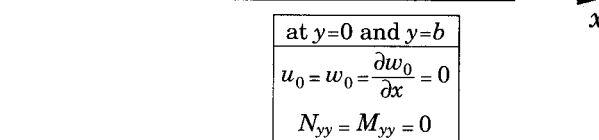
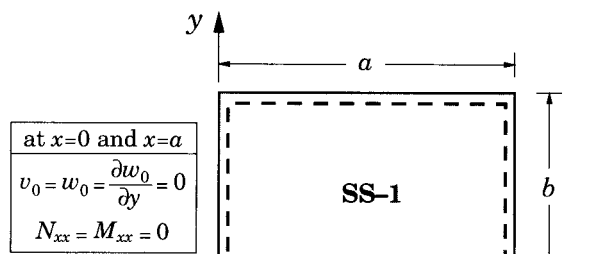


Figure 6.2.1: Types of simply supported boundary conditions, SS-1 and SS-2, used in the analytical solutions of rectangular laminated plates.

Simply Supported-2 (SS-2): The displacement boundary conditions are

$$\begin{aligned} u(0, y, 0, t) &= 0, \quad u(a, y, 0, t) = 0, \quad v(x, 0, 0, t) = 0, \quad v(x, b, 0, t) = 0 \\ w(x, 0, 0, t) &= 0, \quad w(x, b, 0, t) = 0, \quad w(0, y, 0, t) = 0, \quad w(a, y, 0, t) = 0 \\ \frac{\partial u}{\partial z} \Big|_{(x,0,0,t)} &= 0, \quad \frac{\partial u}{\partial z} \Big|_{(x,b,0,t)} = 0, \quad \frac{\partial v}{\partial z} \Big|_{(0,y,0,t)} = 0, \quad \frac{\partial v}{\partial z} \Big|_{(a,y,0,t)} = 0 \end{aligned} \quad (6.2.3)$$

The boundary conditions associated with stress components are

$$\begin{aligned} \int_{-\frac{h}{2}}^{\frac{h}{2}} \sigma_{xy}(0, y, z, t) dz &= 0, & \int_{-\frac{h}{2}}^{\frac{h}{2}} \sigma_{xy}(a, y, z, t) dz &= 0 \\ \int_{-\frac{h}{2}}^{\frac{h}{2}} \sigma_{xy}(x, 0, z, t) dz &= 0, & \int_{-\frac{h}{2}}^{\frac{h}{2}} \sigma_{xy}(x, b, z, t) dz &= 0 \\ \int_{-\frac{h}{2}}^{\frac{h}{2}} z\sigma_{xx}(0, y, z, t) dz &= 0, & \int_{-\frac{h}{2}}^{\frac{h}{2}} z\sigma_{xx}(a, y, z, t) dz &= 0 \\ \int_{-\frac{h}{2}}^{\frac{h}{2}} z\sigma_{yy}(x, 0, z, t) dz &= 0, & \int_{-\frac{h}{2}}^{\frac{h}{2}} z\sigma_{yy}(x, b, z, t) dz &= 0 \end{aligned} \quad (6.2.4)$$

In Eqs. (6.2.1)–(6.2.4), a and b denote the in-plane dimensions along the x and y directions of a rectangular laminate. The origin of the coordinate system is taken at the lower left corner of the midplane, as shown in Figure 6.2.1.

As will be shown in the following sections, the Navier solutions using SS-1 boundary conditions can be obtained only for laminates whose stiffnesses $A_{16}, A_{26}, B_{16}, B_{26}, D_{16}, D_{26}$, and A_{45} are zero. Thus, the Navier solutions for the SS-1 boundary conditions can be developed for laminates with a single generally orthotropic layer, symmetrically laminated plates with multiple specially orthotropic layers, and antisymmetric cross-ply laminated plates. Similarly, the Navier solutions using SS-2 boundary conditions can be obtained only for laminates whose stiffnesses $A_{16}, A_{26}, B_{11}, B_{12}, B_{22}, B_{66}, D_{16}, D_{26}$, and A_{45} are zero, i.e., for laminates with a single generally orthotropic layer, symmetrically laminated plates with multiple specially orthotropic layers, and antisymmetric angle-ply laminated plates.

6.3 Navier Solutions of Antisymmetric Cross-Ply Laminates

6.3.1 Boundary Conditions

The stress boundary conditions in Eqs. (6.2.2) imply, in view of Eq. (3.3.2), the following SS-1 boundary conditions on the displacements and stress resultants of the classical laminate theory:

$$\begin{aligned} u_0(x, 0, t) &= 0, \quad u_0(x, b, t) = 0, \quad v_0(0, y, t) = 0, \quad v_0(a, y, t) = 0 \\ w_0(x, 0, t) &= 0, \quad w_0(x, b, t) = 0, \quad w_0(0, y, t) = 0, \quad w_0(a, y, t) = 0 \\ \frac{\partial w_0}{\partial x} \Big|_{(x,0,t)} &= 0, \quad \frac{\partial w_0}{\partial x} \Big|_{(x,b,t)} = 0, \quad \frac{\partial w_0}{\partial y} \Big|_{(0,y,t)} = 0, \quad \frac{\partial w_0}{\partial y} \Big|_{(a,y,t)} = 0 \end{aligned} \quad (6.3.1)$$

$$\begin{aligned} N_{xx}(0, y, t) &= 0, \quad N_{xx}(a, y, t) = 0, \quad N_{yy}(x, 0, t) = 0, \quad N_{yy}(x, b, t) = 0 \\ M_{xx}(0, y, t) &= 0, \quad M_{xx}(a, y, t) = 0, \quad M_{yy}(x, 0, t) = 0, \quad M_{yy}(x, b, t) = 0 \end{aligned} \quad (6.3.2)$$

The displacement boundary conditions of SS-1 in (6.3.1) are satisfied by assuming the following form of the displacements

$$u_0(x, y, t) = \sum_{n=1}^{\infty} \sum_{m=1}^{\infty} U_{mn}(t) \cos \alpha x \sin \beta y \quad (6.3.3a)$$

$$v_0(x, y, t) = \sum_{n=1}^{\infty} \sum_{m=1}^{\infty} V_{mn}(t) \sin \alpha x \cos \beta y \quad (6.3.3b)$$

$$w_0(x, y, t) = \sum_{n=1}^{\infty} \sum_{m=1}^{\infty} W_{mn}(t) \sin \alpha x \sin \beta y \quad (6.3.3c)$$

where $\alpha = m\pi/a$ and $\beta = n\pi/b$ and (U_{mn}, V_{mn}, W_{mn}) are coefficients to be determined. To see if the boundary conditions (6.3.2) on the stress resultants are also satisfied, we substitute expansions (6.3.3) into the expressions for N_{xx} , N_{yy} , N_{xy} , M_{xx} , M_{yy} , and M_{xy} given in Eqs. (3.3.43) and (3.3.44):

$$\begin{aligned} N_{xx} &= A_{11} \frac{\partial u_0}{\partial x} + A_{12} \frac{\partial v_0}{\partial y} + A_{16} \left(\frac{\partial u_0}{\partial y} + \frac{\partial v_0}{\partial x} \right) \\ &\quad - B_{11} \frac{\partial^2 w_0}{\partial x^2} - B_{12} \frac{\partial^2 w_0}{\partial y^2} - 2B_{16} \frac{\partial^2 w_0}{\partial x \partial y} - N_{xx}^T \\ &= \sum_{n=1}^{\infty} \sum_{m=1}^{\infty} \left[-\alpha A_{11} U_{mn} - \beta A_{12} V_{mn} + (B_{11}\alpha^2 + B_{12}\beta^2) W_{mn} \right] f(x, y) \\ &\quad + \sum_{n=1}^{\infty} \sum_{m=1}^{\infty} [A_{16} (\beta U_{mn} + \alpha V_{mn}) - 2\alpha\beta B_{16} W_{mn}] g(x, y) - N_{xx}^T \end{aligned} \quad (6.3.4a)$$

$$\begin{aligned} N_{yy} &= A_{12} \frac{\partial u_0}{\partial x} + A_{22} \frac{\partial v_0}{\partial y} + A_{26} \left(\frac{\partial u_0}{\partial y} + \frac{\partial v_0}{\partial x} \right) \\ &\quad - B_{12} \frac{\partial^2 w_0}{\partial x^2} - B_{22} \frac{\partial^2 w_0}{\partial y^2} - 2B_{26} \frac{\partial^2 w_0}{\partial x \partial y} - N_{yy}^T \\ &= \sum_{n=1}^{\infty} \sum_{m=1}^{\infty} \left[-\alpha A_{12} U_{mn} - \beta A_{22} V_{mn} + (B_{12}\alpha^2 + B_{22}\beta^2) W_{mn} \right] f(x, y) \\ &\quad + \sum_{n=1}^{\infty} \sum_{m=1}^{\infty} [A_{26} (\beta U_{mn} + \alpha V_{mn}) - 2\alpha\beta B_{26} W_{mn}] g(x, y) - N_{yy}^T \end{aligned} \quad (6.3.4b)$$

$$\begin{aligned} N_{xy} &= A_{16} \frac{\partial u_0}{\partial x} + A_{26} \frac{\partial v_0}{\partial y} + A_{66} \left(\frac{\partial u_0}{\partial y} + \frac{\partial v_0}{\partial x} \right) \\ &\quad - B_{16} \frac{\partial^2 w_0}{\partial x^2} - B_{26} \frac{\partial^2 w_0}{\partial y^2} - 2B_{66} \frac{\partial^2 w_0}{\partial x \partial y} - N_{xy}^T \\ &= \sum_{n=1}^{\infty} \sum_{m=1}^{\infty} \left[-\alpha A_{16} U_{mn} - \beta A_{26} V_{mn} + (B_{16}\alpha^2 + B_{26}\beta^2) W_{mn} \right] f(x, y) \\ &\quad + \sum_{n=1}^{\infty} \sum_{m=1}^{\infty} [A_{66} (\beta U_{mn} + \alpha V_{mn}) - 2\alpha\beta B_{66} W_{mn}] g(x, y) - N_{xy}^T \end{aligned} \quad (6.3.4c)$$

$$\begin{aligned}
M_{xx} &= B_{11} \frac{\partial u_0}{\partial x} + B_{12} \frac{\partial v_0}{\partial y} + B_{16} \left(\frac{\partial u_0}{\partial y} + \frac{\partial v_0}{\partial x} \right) \\
&\quad - D_{11} \frac{\partial^2 w_0}{\partial x^2} - D_{12} \frac{\partial^2 w_0}{\partial y^2} - 2D_{16} \frac{\partial^2 w_0}{\partial x \partial y} - M_{xx}^T \\
&= \sum_{n=1}^{\infty} \sum_{m=1}^{\infty} \left[-\alpha B_{11} U_{mn} - \beta B_{12} V_{mn} + (D_{11}\alpha^2 + D_{12}\beta^2) W_{mn} \right] f(x, y) \\
&\quad + \sum_{n=1}^{\infty} \sum_{m=1}^{\infty} [B_{16} (\beta U_{mn} + \alpha V_{mn}) - 2\alpha\beta D_{16} W_{mn}] g(x, y) - M_{xx}^T \quad (6.3.5a)
\end{aligned}$$

$$\begin{aligned}
M_{yy} &= B_{12} \frac{\partial u_0}{\partial x} + B_{22} \frac{\partial v_0}{\partial y} + B_{26} \left(\frac{\partial u_0}{\partial y} + \frac{\partial v_0}{\partial x} \right) \\
&\quad - D_{12} \frac{\partial^2 w_0}{\partial x^2} - D_{22} \frac{\partial^2 w_0}{\partial y^2} - 2D_{26} \frac{\partial^2 w_0}{\partial x \partial y} - M_{yy}^T \\
&= \sum_{n=1}^{\infty} \sum_{m=1}^{\infty} \left[-\alpha B_{12} U_{mn} - \beta B_{22} V_{mn} + (D_{12}\alpha^2 + D_{22}\beta^2) W_{mn} \right] f(x, y) \\
&\quad + \sum_{n=1}^{\infty} \sum_{m=1}^{\infty} [B_{26} (\beta U_{mn} + \alpha V_{mn}) - 2\alpha\beta D_{26} W_{mn}] g(x, y) - M_{yy}^T \quad (6.3.5b)
\end{aligned}$$

$$\begin{aligned}
M_{xy} &= B_{16} \frac{\partial u_0}{\partial x} + B_{26} \frac{\partial v_0}{\partial y} + B_{66} \left(\frac{\partial u_0}{\partial y} + \frac{\partial v_0}{\partial x} \right) \\
&\quad - D_{16} \frac{\partial^2 w_0}{\partial x^2} - D_{26} \frac{\partial^2 w_0}{\partial y^2} - 2D_{66} \frac{\partial^2 w_0}{\partial x \partial y} - M_{xy}^T \\
&= \sum_{n=1}^{\infty} \sum_{m=1}^{\infty} \left[-\alpha B_{16} U_{mn} - \beta B_{26} V_{mn} + (D_{16}\alpha^2 + D_{26}\beta^2) W_{mn} \right] f(x, y) \\
&\quad + \sum_{n=1}^{\infty} \sum_{m=1}^{\infty} [B_{66} (\beta U_{mn} + \alpha V_{mn}) - 2\alpha\beta D_{66} W_{mn}] g(x, y) - M_{xy}^T \quad (6.3.5c)
\end{aligned}$$

where

$$f(x, y) = \sin \alpha x \sin \beta y, \quad g(x, y) = \cos \alpha x \cos \beta y \quad (6.3.6)$$

Note that the boundary conditions in Eq. (6.3.2) on the stress and moment resultants N_{xx} , N_{yy} , M_{xx} , and M_{yy} can be satisfied only if the laminate stiffnesses A_{16} , A_{26} , B_{16} , B_{26} , D_{16} , D_{26} are zero (because $g(x, y) \neq 0$ for $x = 0, a$ or $y = 0, b$); in addition, the thermal force and moment resultants must satisfy the boundary conditions in Eq. (6.3.2). Thus, the Navier solutions for rectangular laminated plates with SS-1 boundary conditions may exist only when the laminate stacking sequences are such that

$$A_{16} = A_{26} = B_{16} = B_{26} = D_{16} = D_{26} = 0 \quad (6.3.7a)$$

$$N_{xx}^T(0, y, t) = N_{xx}^T(a, y, t) = N_{yy}^T(x, 0, t) = N_{yy}^T(x, b, t) = 0 \quad (6.3.7b)$$

$$M_{xx}^T(0, y, t) = M_{xx}^T(a, y, t) = M_{yy}^T(x, 0, t) = M_{yy}^T(x, b, t) = 0 \quad (6.3.7c)$$

From Section 5.2.2, it follows that plates with a single generally orthotropic layer, symmetrically laminated plates with multiple specially orthotropic layers, and antisymmetric cross-ply laminated plates, which include the former cases as special cases, admit the Navier solutions for the SS-1 boundary conditions. Although the Navier solutions cannot be developed for general laminates, i.e., with no restrictions on laminate stiffnesses, approximate or numerical solutions may be constructed, as shown later in this chapter or in subsequent chapters.

6.3.2 Solution

Substitution of Eqs. (6.3.3) and (6.3.7) into Eqs. (6.1.1)–(6.1.3) yields

$$\begin{aligned} \sum_{n=1}^{\infty} \sum_{m=1}^{\infty} & \left[- (A_{11}\alpha^2 + A_{66}\beta^2) U_{mn} - (A_{12} + A_{66}) \alpha\beta V_{mn} \right. \\ & \left. + (B_{11}\alpha^3 + \tilde{B}_{12}\alpha\beta^2) W_{mn} - I_0 \ddot{U}_{mn} + I_1 \alpha \ddot{W}_{mn} \right] \cos \alpha x \sin \beta y \\ & = \left(\frac{\partial N_{xx}^T}{\partial x} + \frac{\partial N_{xy}^T}{\partial y} \right) \end{aligned} \quad (6.3.8a)$$

$$\begin{aligned} \sum_{n=1}^{\infty} \sum_{m=1}^{\infty} & \left[- (A_{12} + A_{66}) \alpha\beta U_{mn} - (A_{66}\alpha^2 + A_{22}\beta^2) V_{mn} \right. \\ & \left. + (\tilde{B}_{12}\alpha^2\beta + B_{22}\beta^3) W_{mn} - I_0 \ddot{V}_{mn} + I_1 \beta \ddot{W}_{mn} \right] \sin \alpha x \cos \beta y \\ & = \left(\frac{\partial N_{xy}^T}{\partial x} + \frac{\partial N_{yy}^T}{\partial y} \right) \end{aligned} \quad (6.3.8b)$$

$$\begin{aligned} \sum_{n=1}^{\infty} \sum_{m=1}^{\infty} & \left[(B_{11}\alpha^3 + \tilde{B}_{12}\alpha\beta^2) U_{mn} + (\tilde{B}_{12}\alpha^2\beta + B_{22}\beta^3) V_{mn} \right. \\ & - (D_{11}\alpha^4 + 2\tilde{D}_{12}\alpha^2\beta^2 + D_{22}\beta^4) W_{mn} \\ & - (\alpha^2 \hat{N}_{xx} + \beta^2 \hat{N}_{yy}) W_{mn} \\ & \left. + I_1 \alpha \ddot{U}_{mn} + I_1 \beta \ddot{V}_{mn} - (I_0 + I_2(\alpha^2 + \beta^2)) \ddot{W}_{mn} \right] \sin \alpha x \sin \beta y \\ & = \left(\frac{\partial^2 M_{xx}^T}{\partial x^2} + 2 \frac{\partial^2 M_{xy}^T}{\partial x \partial y} + \frac{\partial^2 M_{yy}^T}{\partial y^2} \right) - q(x, y) \end{aligned} \quad (6.3.8c)$$

where

$$\tilde{B}_{12} = B_{12} + 2B_{66}, \quad \tilde{D}_{12} = D_{12} + 2D_{66} \quad (6.3.9)$$

Note that the edge shear force \hat{N}_{xy} is necessarily zero (otherwise, the Navier solution does not exist). In addition, for the class of lamination schemes admissible here, inertia I_1 must be zero.

An examination of Eqs. (6.3.8) shows that the mechanical force q and thermal forces and moments of Eqs. (6.3.8a-c) should also be expanded in the same form as

their counterparts on the left side of the equality in Eqs. (6.3.8a-c). For example, the left side of Eq. (6.3.8c) has the form

$$\sum_{n=1}^{\infty} \sum_{m=1}^{\infty} C_{mn}^3 \sin \alpha x \sin \beta y, \quad \alpha = \frac{m\pi}{a}, \quad \beta = \frac{n\pi}{b}$$

where C_{mn}^3 is the expression in the square bracket of Eq. (6.3.8c). Hence, the right side of Eq. (6.3.8c), which consists of the transverse load and thermal moments, should also be expanded in double sine series. Thus, $q(x, y, t)$ must be expanded as

$$q(x, y, t) = \sum_{n=1}^{\infty} \sum_{m=1}^{\infty} Q_{mn}(t) \sin \alpha x \sin \beta y \quad (6.3.10a)$$

$$Q_{mn}(t) = \frac{4}{ab} \int_0^a \int_0^b q(x, y, t) \sin \alpha x \sin \beta y \, dx dy \quad (6.3.10b)$$

Since the thermal moments M_{xx}^T , M_{xy}^T , and M_{yy}^T are defined in terms of the same temperature increment $\Delta T(x, y, t)$ but they enter Eq. (6.3.8c) with different derivatives, it is expected that not all of them will contribute to the solution. If the temperature increment is expanded as

$$\Delta T(x, y, z, t) = \sum_{n=1}^{\infty} \sum_{m=1}^{\infty} T_{mn}(z, t) \sin \alpha x \sin \beta y \quad (6.3.11a)$$

$$T_{mn}(z, t) = \frac{4}{ab} \int_0^a \int_0^b \Delta T(x, y, z, t) \sin \alpha x \sin \beta y \, dx dy \quad (6.3.11b)$$

then we have from Eq. (3.3.41a,b)

$$\begin{Bmatrix} N_{xx}^T \\ N_{yy}^T \\ N_{xy}^T \end{Bmatrix} = \sum_{n=1}^{\infty} \sum_{m=1}^{\infty} \begin{Bmatrix} N_{mn}^1(t) \\ N_{mn}^2(t) \\ N_{mn}^6(t) \end{Bmatrix} \sin \alpha x \sin \beta y \quad (6.3.12a)$$

$$\begin{Bmatrix} M_{xx}^T \\ M_{yy}^T \\ M_{xy}^T \end{Bmatrix} = \sum_{n=1}^{\infty} \sum_{m=1}^{\infty} \begin{Bmatrix} M_{mn}^1(t) \\ M_{mn}^2(t) \\ M_{mn}^6(t) \end{Bmatrix} \sin \alpha x \sin \beta y \quad (6.3.12b)$$

$$\{N_{mn}(t)\} = \sum_{k=1}^N \int_{z_k}^{z_{k+1}} [\bar{Q}]^{(k)} \{\bar{\alpha}\}^{(k)} T_{mn}(z, t) \, dz \quad (6.3.13a)$$

$$\{M_{mn}(t)\} = \sum_{k=1}^N \int_{z_k}^{z_{k+1}} [\bar{Q}]^{(k)} \{\bar{\alpha}\}^{(k)} T_{mn}(z, t) z \, dz \quad (6.3.13b)$$

Thus we have

$$\begin{aligned} f_1^T &= \frac{\partial N_{xx}^T}{\partial x} + \frac{\partial N_{xy}^T}{\partial y} \\ &= \sum_{n=1}^{\infty} \sum_{m=1}^{\infty} [\alpha N_{mn}^1(t) \cos \alpha x \sin \beta y + \beta N_{mn}^6(t) \sin \alpha x \cos \beta y] \end{aligned} \quad (6.3.14a)$$

$$\begin{aligned} f_2^T &= \frac{\partial N_{xy}^T}{\partial x} + \frac{\partial N_{yy}^T}{\partial y} \\ &= \sum_{n=1}^{\infty} \sum_{m=1}^{\infty} \left[\alpha N_{mn}^6(t) \cos \alpha x \sin \beta y + \beta N_{mn}^2(t) \sin \alpha x \cos \beta y \right] \quad (6.3.14b) \end{aligned}$$

$$\begin{aligned} f_3^T &= \frac{\partial^2 M_{xx}^T}{\partial x^2} + 2 \frac{\partial^2 M_{xy}^T}{\partial y \partial x} + \frac{\partial^2 M_{yy}^T}{\partial y^2} \\ &= \sum_{n=1}^{\infty} \sum_{m=1}^{\infty} \left[-(\alpha^2 M_{mn}^1(t) + \beta^2 M_{mn}^2(t)) \sin \alpha x \sin \beta y \right. \\ &\quad \left. + 2\alpha\beta M_{mn}^6(t) \cos \alpha x \cos \beta y \right] \quad (6.3.14c) \end{aligned}$$

This particular expansion of temperature distribution necessarily requires that N_{mn}^6 and M_{mn}^6 be zero because they must be of the form [see Eqs. (6.3.8a-c)]

$$\begin{aligned} f_1^T &= \sum_{n=1}^{\infty} \sum_{m=1}^{\infty} f_{mn}^1(t) \cos \alpha x \sin \beta y \\ f_2^T &= \sum_{n=1}^{\infty} \sum_{m=1}^{\infty} f_{mn}^2(t) \sin \alpha x \cos \beta y \\ f_3^T &= \sum_{n=1}^{\infty} \sum_{m=1}^{\infty} f_{mn}^3(t) \sin \alpha x \sin \beta y \quad (6.3.15) \end{aligned}$$

This requirement places a restriction on the lamination scheme in order for the Navier solution to exist in the presence of temperature changes. The lamination scheme must be such that

$$\sum_{k=1}^N \int_{z_k}^{z_{k+1}} [\bar{Q}]^{(k)} \{\bar{\alpha}\}^{(k)} T_{mn}(z, t) dz = \begin{Bmatrix} N_{mn}^1 \\ N_{mn}^2 \\ 0 \end{Bmatrix} \quad (6.3.16a)$$

$$\sum_{k=1}^N \int_{z_k}^{z_{k+1}} [\bar{Q}]^{(k)} \{\bar{\alpha}\}^{(k)} T_{mn}(z, t) z dz = \begin{Bmatrix} M_{mn}^1 \\ M_{mn}^2 \\ 0 \end{Bmatrix} \quad (6.3.16b)$$

For single-layer plates with a generally orthotropic layer, symmetrically laminated plates with multiple specially orthotropic layers, and antisymmetric cross-ply laminated plates, the conditions in Eq. (6.3.16a,b) are automatically satisfied. In order to include N_{mn}^6 and M_{mn}^6 , the temperature distribution should be expanded in a double cosine series. Then N_{mn}^1 , N_{mn}^2 , M_{mn}^1 , and M_{mn}^2 must be zero.

Substituting the expansions (6.3.10a) and (6.3.14) with $N_{mn}^6 = M_{mn}^6 = 0$ into Eq. (6.3.8), we obtain expressions of the form

$$\begin{aligned} \sum_{n=1}^{\infty} \sum_{m=1}^{\infty} a_{mn}(t) \cos \alpha x \sin \beta y &= 0 \\ \sum_{n=1}^{\infty} \sum_{m=1}^{\infty} b_{mn}(t) \sin \alpha x \cos \beta y &= 0 \\ \sum_{n=1}^{\infty} \sum_{m=1}^{\infty} c_{mn}(t) \sin \alpha x \sin \beta y &= 0 \quad (6.3.17) \end{aligned}$$

where a_{mn} , b_{mn} , and c_{mn} are coefficients whose explicit form will be given shortly. Since Eqs. (6.3.17) must hold for any m, n, x , and y , it follows that $a_{mn} = 0$, $b_{mn} = 0$, and $c_{mn} = 0$ for every m and n . The explicit forms of the coefficients a_{mn} , b_{mn} , and c_{mn} are given by

$$\begin{aligned} a_{mn} \equiv & - \left(A_{11}\alpha^2 + A_{66}\beta^2 \right) U_{mn} - (A_{12} + A_{66})\alpha\beta V_{mn} \\ & + \left(B_{11}\alpha^3 + \tilde{B}_{12}\alpha\beta^2 \right) W_{mn} - \alpha N_{mn}^1 - I_0 \ddot{U}_{mn} + I_1 \alpha \ddot{W}_{mn} = 0 \end{aligned} \quad (6.3.18a)$$

$$\begin{aligned} b_{mn} \equiv & - (A_{12} + A_{66})\alpha\beta U_{mn} - \left(A_{66}\alpha^2 + A_{22}\beta^2 \right) V_{mn} \\ & + \left(\tilde{B}_{12}\alpha^2\beta + B_{22}\beta^3 \right) W_{mn} - \beta N_{mn}^2 - I_0 \ddot{V}_{mn} + I_1 \beta \ddot{W}_{mn} = 0 \end{aligned} \quad (6.3.18b)$$

$$\begin{aligned} c_{mn} \equiv & \left(B_{11}\alpha^3 + \tilde{B}_{12}\alpha\beta^2 \right) U_{mn} + \left(\tilde{B}_{12}\alpha^2\beta + B_{22}\beta^3 \right) V_{mn} \\ & - \left(D_{11}\alpha^4 + 2\tilde{D}_{12}\alpha^2\beta^2 + D_{22}\beta^4 \right) W_{mn} + Q_{mn} \\ & + \alpha^2 M_{mn}^1 + \beta^2 M_{mn}^2 - \left(\alpha^2 \hat{N}_{xx} + \beta^2 \hat{N}_{yy} \right) W_{mn} \\ & + I_1 \alpha \ddot{U}_{mn} + I_1 \beta \ddot{V}_{mn} - \left(I_0 + I_2(\alpha^2 + \beta^2) \right) \ddot{W}_{mn} = 0 \end{aligned} \quad (6.3.18c)$$

or in matrix form

$$\begin{aligned} \begin{bmatrix} \hat{c}_{11} & \hat{c}_{12} & \hat{c}_{13} \\ \hat{c}_{12} & \hat{c}_{22} & \hat{c}_{23} \\ \hat{c}_{13} & \hat{c}_{23} & \hat{c}_{33} + \tilde{s}_{33} \end{bmatrix} \begin{Bmatrix} U_{mn} \\ V_{mn} \\ W_{mn} \end{Bmatrix} & + \begin{bmatrix} \hat{m}_{11} & 0 & -I_1\alpha \\ 0 & \hat{m}_{22} & -I_1\beta \\ -I_1\alpha & -I_1\beta & \hat{m}_{33} \end{bmatrix} \begin{Bmatrix} \ddot{U}_{mn} \\ \ddot{V}_{mn} \\ \ddot{W}_{mn} \end{Bmatrix} \\ & = \begin{Bmatrix} 0 \\ 0 \\ Q_{mn} \end{Bmatrix} + \begin{Bmatrix} -\alpha N_{mn}^1 \\ -\beta N_{mn}^2 \\ \alpha^2 M_{mn}^1 + \beta^2 M_{mn}^2 \end{Bmatrix} \end{aligned} \quad (6.3.19)$$

where \hat{c}_{ij} and \hat{m}_{ij} are

$$\begin{aligned} \hat{c}_{11} &= (A_{11}\alpha^2 + A_{66}\beta^2) \\ \hat{c}_{12} &= (A_{12} + A_{66})\alpha\beta \\ \hat{c}_{13} &= -B_{11}\alpha^3 - (B_{12} + 2B_{66})\alpha\beta^2 \\ \hat{c}_{22} &= (A_{66}\alpha^2 + A_{22}\beta^2) \\ \hat{c}_{23} &= -(B_{12} + 2B_{66})\alpha^2\beta - B_{22}\beta^3 \\ \hat{c}_{33} &= D_{11}\alpha^4 + 2(D_{12} + 2D_{66})\alpha^2\beta^2 + D_{22}\beta^4 \\ \hat{m}_{11} &= \hat{m}_{22} = I_0 \\ \hat{m}_{33} &= (I_0 + I_2(\alpha^2 + \beta^2)) \\ \tilde{s}_{33} &= \alpha^2 \hat{N}_{xx} + \beta^2 \hat{N}_{yy} \end{aligned} \quad (6.3.20)$$

and $\alpha = m\pi/a$ and $\beta = n\pi/b$.

Equations (6.3.19) provide three second-order differential equations in time among the three variables U_{mn} , V_{mn} , and W_{mn} for any fixed values of m and n . For transient (i.e., time dependent) response, the differential equations in time can be solved either exactly or approximately.

6.3.3 Bending

The static solution can be obtained by solving the algebraic equations resulting from Eqs. (6.3.19) by setting the time derivative terms to zero:

$$\begin{bmatrix} \hat{c}_{11} & \hat{c}_{12} & \hat{c}_{13} \\ \hat{c}_{12} & \hat{c}_{22} & \hat{c}_{23} \\ \hat{c}_{13} & \hat{c}_{23} & \hat{c}_{33} + \tilde{s}_{33} \end{bmatrix} \begin{Bmatrix} U_{mn} \\ V_{mn} \\ W_{mn} \end{Bmatrix} = \begin{Bmatrix} 0 \\ 0 \\ Q_{mn} \end{Bmatrix} + \begin{Bmatrix} -\alpha N_{mn}^1 \\ -\beta N_{mn}^2 \\ \alpha^2 M_{mn}^1 + \beta^2 M_{mn}^2 \end{Bmatrix} \quad (6.3.21)$$

which can be solved for the coefficients U_{mn} , V_{mn} , and W_{mn} in terms of the coefficients Q_{mn} , N_{mn}^1 , N_{mn}^2 , M_{mn}^1 , and M_{mn}^2 . Then the final solution is given by Eqs. (6.3.3a-c).

Equations (6.3.21) can be solved using Cramer's rule or by the method of *static condensation*. The latter allows the elimination of a selected set of variables and retains a desired set of variables. The method is useful in later discussions of this book, and therefore it is described here. First, the column of unknowns is subdivided into two parts, $\{\Delta^1\}$ and $\{\Delta^2\}$, according to what is to be eliminated and what is to be retained. Suppose that we wish to eliminate the coefficients associated with the in-plane displacements and retain those associated with the transverse deflection. Then Eq. (6.3.21) can be written as

$$\begin{bmatrix} [K^{11}] & [K^{12}] \\ [K^{12}]^T & [K^{22}] \end{bmatrix} \begin{Bmatrix} \{\Delta^1\} \\ \{\Delta^2\} \end{Bmatrix} = \begin{Bmatrix} \{F^1\} \\ \{F^2\} \end{Bmatrix} \quad (6.3.22)$$

where

$$\{\Delta^1\} = \begin{Bmatrix} U_{mn} \\ V_{mn} \end{Bmatrix}, \quad \{\Delta^2\} = W_{mn} \quad (6.3.23a)$$

$$[K^{11}] = \begin{bmatrix} \hat{c}_{11} & \hat{c}_{12} \\ \hat{c}_{12} & \hat{c}_{22} \end{bmatrix}, \quad [K^{12}] = \begin{bmatrix} \hat{c}_{13} \\ \hat{c}_{23} \end{bmatrix}, \quad [K^{22}] = \hat{c}_{33} + \tilde{s}_{33}$$

$$\{F^1\} = \begin{Bmatrix} -\alpha N_{mn}^1 \\ -\beta N_{mn}^2 \end{Bmatrix}, \quad \{F^2\} = Q_{mn} + \alpha^2 M_{mn}^1 + \beta^2 M_{mn}^2 \quad (6.3.23b)$$

Equation (6.3.22) represents a pair of two matrix equations:

$$[K^{11}]\{\Delta^1\} + [K^{12}]\{\Delta^2\} = \{F^1\}, \quad [K^{12}]^T\{\Delta^1\} + [K^{22}]\{\Delta^2\} = \{F^2\} \quad (6.3.24a, b)$$

Solving Eq. (6.3.24a) for $\{\Delta^1\}$, which is to be eliminated, we obtain

$$\{\Delta^1\} = [K^{11}]^{-1} (\{F^1\} - [K^{12}]\{\Delta^2\}) \quad (6.3.25)$$

Then substituting the result into (6.3.24b), we obtain

$$([K^{22}] - [K^{12}]^T[K^{11}]^{-1}[K^{12}])\{\Delta^2\} = \{F^2\} - [K^{12}]^T[K^{11}]^{-1}\{F^1\} \quad (6.3.26a)$$

or

$$[\hat{K}^{22}]\{\Delta^2\} = \{\hat{F}^2\} \quad (6.3.26b)$$

where

$$\begin{aligned} \hat{K}^{22} &= [K^{22}] - [K^{12}]^T [K^{11}]^{-1} [K^{12}] \\ \{\hat{F}^2\} &= \{F^2\} - [K^{12}]^T [K^{11}]^{-1} \{F^1\} \end{aligned} \quad (6.3.26c)$$

This procedure of eliminating (or condensing out) a subset of unknowns is known in structural mechanics as the method of *static condensation*. The calculation involves solving for $\{\Delta^2\}$ first, and then, if desired, solving for $\{\Delta^1\}$ next using Eq. (6.3.25).

Using the definitions (6.3.23) in (6.3.26) we obtain (when $\tilde{s}_{33} = 0$)

$$\begin{aligned} W_{mn} &= \frac{1}{a_{mn}} \left[Q_{mn} + \alpha^2 M_{mn}^1 + \beta^2 M_{mn}^2 - \frac{a_1}{a_0} (\alpha N_{mn}^1) - \frac{a_2}{a_0} (\beta N_{mn}^2) \right] \\ U_{mn} &= \frac{1}{a_0} \left[a_1 W_{mn} - \alpha N_{mn}^1 \hat{c}_{22} + \beta N_{mn}^2 \hat{c}_{12} \right] \\ V_{mn} &= \frac{1}{a_0} \left[a_2 W_{mn} + \alpha N_{mn}^1 \hat{c}_{12} - \beta N_{mn}^2 \hat{c}_{11} \right] \end{aligned} \quad (6.3.27a)$$

where

$$\begin{aligned} a_{mn} &= \hat{c}_{33} + \hat{c}_{13} \frac{a_1}{a_0} + \hat{c}_{23} \frac{a_2}{a_0} \\ a_0 &= \hat{c}_{11} \hat{c}_{22} - \hat{c}_{12} \hat{c}_{21} \\ a_1 &= \hat{c}_{12} \hat{c}_{23} - \hat{c}_{13} \hat{c}_{22} \\ a_2 &= \hat{c}_{13} \hat{c}_{12} - \hat{c}_{11} \hat{c}_{23} \end{aligned} \quad (6.3.27b)$$

Solution of Eq. (6.3.27a) for each $m, n = 1, 2, \dots$ gives (U_{mn}, V_{mn}, W_{mn}) , which can then be used to compute the solution (u_0, v_0, w_0) from Eq. (6.3.3). If there are no thermal loads, the solution becomes

$$W_{mn} = \frac{Q_{mn}}{a_{mn}}, \quad U_{mn} = \frac{a_1 Q_{mn}}{a_0 a_{mn}}, \quad V_{mn} = \frac{a_2 Q_{mn}}{a_0 a_{mn}} \quad (6.3.28)$$

Note that for antisymmetric cross-ply laminates, $B_{66} = 0$ and the coefficients in Eq. (6.3.27a) can be simplified.

6.3.4 Determination of Stresses

The in-plane stresses in each layer of a laminate are calculated from constitutive relations in Eq. (3.3.12a). Accounting for only mechanical and thermal effects, we obtain

$$\begin{aligned} \left\{ \begin{array}{l} \sigma_{xx} \\ \sigma_{yy} \\ \sigma_{xy} \end{array} \right\}^{(k)} &= \left[\begin{array}{ccc} \bar{Q}_{11} & \bar{Q}_{12} & \bar{Q}_{16} \\ \bar{Q}_{12} & \bar{Q}_{22} & \bar{Q}_{26} \\ \bar{Q}_{16} & \bar{Q}_{26} & \bar{Q}_{66} \end{array} \right]^{(k)} \left(\left\{ \begin{array}{l} \varepsilon_{xx} \\ \varepsilon_{yy} \\ 2\varepsilon_{xy} \end{array} \right\} - \left\{ \begin{array}{l} \alpha_{xx} \\ \alpha_{yy} \\ 2\alpha_{xy} \end{array} \right\} \Delta T \right) \\ &= \left[\begin{array}{ccc} \bar{Q}_{11} & \bar{Q}_{12} & \bar{Q}_{16} \\ \bar{Q}_{12} & \bar{Q}_{22} & \bar{Q}_{26} \\ \bar{Q}_{16} & \bar{Q}_{26} & \bar{Q}_{66} \end{array} \right]^k \left\{ \begin{array}{l} \varepsilon_{xx}^0 - \alpha_{xx} T_0 \\ \varepsilon_{yy}^0 - \alpha_{yy} T_0 \\ 2(\varepsilon_{xy}^0 - \alpha_{xy} T_0) \end{array} \right\} \\ &+ z \left[\begin{array}{ccc} \bar{Q}_{11} & \bar{Q}_{12} & \bar{Q}_{16} \\ \bar{Q}_{12} & \bar{Q}_{22} & \bar{Q}_{26} \\ \bar{Q}_{16} & \bar{Q}_{26} & \bar{Q}_{66} \end{array} \right]^k \left\{ \begin{array}{l} \varepsilon_{xx}^1 - \alpha_{xx} T_1 \\ \varepsilon_{yy}^1 - \alpha_{yy} T_1 \\ 2(\varepsilon_{xy}^1 - \alpha_{xy} T_1) \end{array} \right\} \end{aligned} \quad (6.3.29a)$$

where temperature increment ΔT is assumed to be of the form

$$\Delta T(x, y, z, t) = \sum_{m=1}^{\infty} \sum_{n=1}^{\infty} (T_{mn}^0 + zT_{mn}^1) \sin \alpha x \sin \beta y \quad (6.3.29b)$$

The in-plane stresses of a simply supported (SS-1) cross-ply laminate (i.e., when $\bar{Q}_{16} = \bar{Q}_{26} = 0$ and $\alpha_{xy} = 0$) are then given by

$$\begin{Bmatrix} \sigma_{xx} \\ \sigma_{yy} \\ \sigma_{xy} \end{Bmatrix}^{(k)} = \sum_{m=1}^{\infty} \sum_{n=1}^{\infty} \begin{bmatrix} \bar{Q}_{11} & \bar{Q}_{12} & 0 \\ \bar{Q}_{12} & \bar{Q}_{22} & 0 \\ 0 & 0 & \bar{Q}_{66} \end{bmatrix}^{(k)} \begin{Bmatrix} (R_{mn}^{xx} + zS_{mn}^{xx}) \sin \alpha x \sin \beta y \\ (R_{mn}^{yy} + zS_{mn}^{yy}) \sin \alpha x \sin \beta y \\ (R_{mn}^{xy} + zS_{mn}^{xy}) \cos \alpha x \cos \beta y \end{Bmatrix} \quad (6.3.30a)$$

$$\begin{Bmatrix} R_{mn}^{xx} \\ R_{mn}^{yy} \\ R_{mn}^{xy} \end{Bmatrix} = \begin{Bmatrix} -\alpha U_{mn} - \alpha_{xx} T_{mn}^0 \\ -\beta V_{mn} - \alpha_{yy} T_{mn}^0 \\ \beta U_{mn} + \alpha V_{mn} \end{Bmatrix}, \quad \begin{Bmatrix} S_{mn}^{xx} \\ S_{mn}^{yy} \\ S_{mn}^{xy} \end{Bmatrix} = \begin{Bmatrix} \alpha^2 W_{mn} - \alpha_{xx} T_{mn}^1 \\ \beta^2 W_{mn} - \alpha_{yy} T_{mn}^1 \\ -2\alpha\beta W_{mn} \end{Bmatrix} \quad (6.3.30b)$$

The maximum normal stresses occur at $(x, y, z) = (a/2, b/2, -h/2)$, and the shear stress is maximum at $(x, y, z) = (a, b, -h/2)$.

The transverse stresses in a laminate can be determined using the 3-D equilibrium equations [see Eqs. (5.2.14)] for any $z_k \leq z \leq z_{k+1}$

$$\begin{aligned} \sigma_{xz}^{(k)} &= - \int_{z_k}^z \left(\frac{\partial \sigma_{xx}^{(k)}}{\partial x} + \frac{\partial \sigma_{xy}^{(k)}}{\partial y} \right) dz + C_1^{(k)}(x, y) \\ \sigma_{yz}^{(k)} &= - \int_{z_k}^z \left(\frac{\partial \sigma_{xy}^{(k)}}{\partial x} + \frac{\partial \sigma_{yy}^{(k)}}{\partial y} \right) dz + C_2^{(k)}(x, y) \\ \sigma_{zz}^{(k)} &= - \int_{z_k}^z \left(\frac{\partial \sigma_{xz}^{(k)}}{\partial x} + \frac{\partial \sigma_{yz}^{(k)}}{\partial y} \right) dz + C_3^{(k)}(x, y) \end{aligned} \quad (6.3.31)$$

where $\sigma_{xx}^{(k)}$, $\sigma_{xy}^{(k)}$, and $\sigma_{yy}^{(k)}$ are known from Eq. (6.3.29), and $C_i^{(k)}$ are functions to be determined using the boundary conditions

$$\sigma_{xz}(x, y, -h/2) = \sigma_{yz}(x, y, -h/2) = \sigma_{zz}(x, y, -h/2) = 0 \quad (6.3.32)$$

and continuity of stresses at layer interfaces:

$$\begin{aligned} \sigma_{xz}^{(k)}(x, y, z_{k+1}) &= \sigma_{xz}^{(k+1)}(x, y, z_{k+1}) \\ \sigma_{yz}^{(k)}(x, y, z_{k+1}) &= \sigma_{yz}^{(k+1)}(x, y, z_{k+1}) \\ \sigma_{zz}^{(k)}(x, y, z_{k+1}) &= \sigma_{zz}^{(k+1)}(x, y, z_{k+1}) \end{aligned} \quad (6.3.33)$$

Substituting for the in-plane stresses from Eq. (6.3.30) into Eq. (6.3.31) and integrating with respect to z , we obtain

$$\begin{Bmatrix} \sigma_{xz} \\ \sigma_{yz} \end{Bmatrix}^{(k)} = (z - z_k) \begin{Bmatrix} A_{xz} \\ A_{yz} \end{Bmatrix}^{(k)} + \left(\frac{z^2 - z_k^2}{2} \right) \begin{Bmatrix} B_{xz} \\ B_{yz} \end{Bmatrix}^{(k)} + \begin{Bmatrix} C_1 \\ C_2 \end{Bmatrix}^{(k)} \quad (6.3.34a)$$

where

$$\begin{aligned}
A_{xz}^{(k)} &= - \left[Q_{11}^{(k)}(\varepsilon_{xx}^0 - \alpha_{xx}T_0)_{,x} + Q_{12}^{(k)}(\varepsilon_{yy}^0 - \alpha_{yy}T_0)_{,x} + 2Q_{16}^{(k)}(\varepsilon_{xy}^0 - \alpha_{xy}T_0)_{,x} \right. \\
&\quad \left. + Q_{16}^{(k)}(\varepsilon_{xx}^0 - \alpha_{xx}T_0)_{,y} + Q_{26}^{(k)}(\varepsilon_{yy}^0 - \alpha_{yy}T_0)_{,y} + 2Q_{66}^{(k)}(\varepsilon_{xy}^0 - \alpha_{xy}T_0)_{,y} \right] \\
B_{xz}^{(k)} &= - \left[Q_{11}^{(k)}(\varepsilon_{xx}^1 - \alpha_{xx}T_1)_{,x} + Q_{12}^{(k)}(\varepsilon_{yy}^1 - \alpha_{yy}T_1)_{,x} + 2Q_{16}^{(k)}(\varepsilon_{xy}^1 - \alpha_{xy}T_1)_{,x} \right. \\
&\quad \left. + Q_{16}^{(k)}(\varepsilon_{xx}^1 - \alpha_{xx}T_1)_{,y} + Q_{26}^{(k)}(\varepsilon_{yy}^1 - \alpha_{yy}T_1)_{,y} + 2Q_{66}^{(k)}(\varepsilon_{xy}^1 - \alpha_{xy}T_1)_{,y} \right] \\
A_{yz}^{(k)} &= - \left[Q_{16}^{(k)}(\varepsilon_{xx}^0 - \alpha_{xx}T_0)_{,x} + Q_{26}^{(k)}(\varepsilon_{yy}^0 - \alpha_{yy}T_0)_{,x} + 2Q_{66}^{(k)}(\varepsilon_{xy}^0 - \alpha_{xy}T_0)_{,x} \right. \\
&\quad \left. + Q_{12}^{(k)}(\varepsilon_{xx}^0 - \alpha_{xx}T_0)_{,y} + Q_{22}^{(k)}(\varepsilon_{yy}^0 - \alpha_{yy}T_0)_{,y} + 2Q_{26}^{(k)}(\varepsilon_{xy}^0 - \alpha_{xy}T_0)_{,y} \right] \\
B_{yz}^{(k)} &= - \left[Q_{16}^{(k)}(\varepsilon_{xx}^1 - \alpha_{xx}T_1)_{,x} + Q_{26}^{(k)}(\varepsilon_{yy}^1 - \alpha_{yy}T_1)_{,x} + 2Q_{66}^{(k)}(\varepsilon_{xy}^1 - \alpha_{xy}T_1)_{,x} \right. \\
&\quad \left. + Q_{12}^{(k)}(\varepsilon_{xx}^1 - \alpha_{xx}T_1)_{,y} + Q_{22}^{(k)}(\varepsilon_{yy}^1 - \alpha_{yy}T_1)_{,y} + 2Q_{26}^{(k)}(\varepsilon_{xy}^1 - \alpha_{xy}T_1)_{,y} \right]
\end{aligned} \tag{6.3.34b}$$

and a comma followed by x or y denotes differentiation. The boundary conditions (6.3.32) yield $C_1^{(1)} = C_2^{(1)} = 0$. The interface continuity conditions (6.3.33) result in

$$C_1^{(k+1)} = \sigma_{xz}^{(k)}(x, y, z_{k+1}), \quad C_2^{(k+1)} = \sigma_{yz}^{(k)}(x, y, z_{k+1}) \tag{6.3.35}$$

for $k = 1, 2, \dots, n$, where n denotes the number of layers.

Substitution of the displacement and temperature expansions from Eqs. (6.3.3a-c) and (6.3.14a-c) into Eq. (6.3.34b) yields the following expressions for interlaminar transverse shear stresses:

$$\begin{aligned}
\sigma_{xz}^{(k)}(x, y, z) &= \sum_{m=1}^{\infty} \sum_{n=1}^{\infty} \left[(z - z_k) \mathcal{A}_{mn}^{(k)} + \frac{1}{2}(z^2 - z_k^2) \mathcal{B}_{mn}^{(k)} \right] \cos \alpha x \sin \beta y \\
&\quad + \sigma_{xz}^{(k-1)}(x, y, z_k) \\
\sigma_{yz}^{(k)}(x, y, z) &= \sum_{m=1}^{\infty} \sum_{n=1}^{\infty} \left[(z - z_k) \mathcal{C}_{mn}^{(k)} + \frac{1}{2}(z^2 - z_k^2) \mathcal{D}_{mn}^{(k)} \right] \sin \alpha x \cos \beta y \\
&\quad + \sigma_{yz}^{(k-1)}(x, y, z_k)
\end{aligned} \tag{6.3.36a}$$

where $\sigma_{xz}^{(0)}(x, y, z_1) = 0$, $\sigma_{yz}^{(0)}(x, y, z_1) = 0$ and

$$\begin{aligned}
\mathcal{A}_{mn}^{(k)} &= \left(\alpha^2 \bar{Q}_{11}^{(k)} + \beta^2 \bar{Q}_{66}^{(k)} \right) U_{mn} + \alpha \beta \left(\bar{Q}_{12}^{(k)} + \bar{Q}_{66}^{(k)} \right) V_{mn} \\
&\quad + \alpha (\bar{Q}_{11} \alpha_{xx} + \bar{Q}_{12} \alpha_{yy}) T_{mn}^0
\end{aligned}$$

$$\begin{aligned}
\mathcal{B}_{mn}^{(k)} &= - \left[\alpha^3 \bar{Q}_{11}^{(k)} + \alpha \beta^2 \left(\bar{Q}_{12}^{(k)} + 2 \bar{Q}_{66}^{(k)} \right) \right] W_{mn} \\
&\quad + \alpha (\bar{Q}_{11} \alpha_{xx} + \bar{Q}_{12} \alpha_{yy}) T_{mn}^1 \\
\mathcal{C}_{mn}^{(k)} &= \alpha \beta \left(\bar{Q}_{12}^{(k)} + \bar{Q}_{66}^{(k)} \right) U_{mn} + \left(\alpha^2 \bar{Q}_{66}^{(k)} + \beta^2 \bar{Q}_{22}^{(k)} \right) V_{mn} \\
&\quad + \beta (\bar{Q}_{12} \alpha_{xx} + \bar{Q}_{22} \alpha_{yy}) T_{mn}^0 \\
\mathcal{D}_{mn}^{(k)} &= - \left[\alpha^2 \beta \left(\bar{Q}_{12}^{(k)} + 2 \bar{Q}_{66}^{(k)} \right) + \beta^3 \bar{Q}_{22}^{(k)} \right] W_{mn} \\
&\quad + \beta (\bar{Q}_{12} \alpha_{xx} + \bar{Q}_{22} \alpha_{yy}) T_{mn}^1
\end{aligned} \tag{6.3.36b}$$

The maximum of σ_{xz} occurs at $(x, y, z) = (0, b/2, 0)$, and the maximum of σ_{yz} occurs at $(x, y, z) = (a/2, 0, 0)$.

The transverse normal stress is given by

$$\begin{aligned}
\sigma_{zz}^{(k)}(x, y, z) &= - \sum_{m=1}^{\infty} \sum_{n=1}^{\infty} \left[\left(\frac{z^2}{2} - zz_k \right) (\alpha \mathcal{A}_{mn}^{(k)} + \beta \mathcal{C}_{mn}^{(k)}) \right. \\
&\quad \left. + \left(\frac{z^3}{6} - \frac{zz_k^2}{2} \right) (\alpha \mathcal{B}_{mn}^{(k)} + \beta \mathcal{D}_{mn}^{(k)}) + \mathcal{E}_{mn}^{(k)} \right] \\
&\quad \times \sin \alpha x \sin \beta y
\end{aligned} \tag{6.3.37}$$

where the functions $\mathcal{E}_{mn}^{(k)}$ are determined using the boundary and interface continuity conditions. We obtain

$$\begin{aligned}
\mathcal{E}_{mn}^{(1)} &= -\frac{h^2}{4} (\alpha \mathcal{A}_{mn}^{(1)} + \beta \mathcal{C}_{mn}^{(1)}) + \frac{h^3}{24} (\alpha \mathcal{B}_{mn}^{(1)} + \beta \mathcal{D}_{mn}^{(1)}) \\
\mathcal{E}_{mn}^{(k+1)} &= \mathcal{E}_{mn}^{(k)} - z_{k+1} \left(\frac{z_{k+1}}{2} - z_k \right) (\alpha \mathcal{A}_{mn}^{(k)} + \beta \mathcal{C}_{mn}^{(k)}) \\
&\quad - z_{k+1} \left(\frac{z_{k+1}^2}{6} - \frac{z_k^2}{2} \right) (\alpha \mathcal{B}_{mn}^{(k)} + \beta \mathcal{D}_{mn}^{(k)}) \\
&\quad - \frac{z_{k+1}^2}{2} (\alpha \mathcal{A}_{mn}^{(k+1)} + \beta \mathcal{C}_{mn}^{(k+1)}) \\
&\quad - \frac{z_{k+1}^3}{3} (\alpha \mathcal{B}_{mn}^{(k+1)} + \beta \mathcal{D}_{mn}^{(k+1)})
\end{aligned} \tag{6.3.38}$$

for $k = 1, 2, \dots, n$.

The bending moments can be calculated from Eqs. (6.3.5a-c)

$$\begin{aligned}
\begin{Bmatrix} M_{xx} \\ M_{yy} \\ M_{xy} \end{Bmatrix} &= \sum_{m=1}^{\infty} \sum_{n=1}^{\infty} \begin{bmatrix} B_{11} & B_{12} & 0 \\ B_{12} & B_{22} & 0 \\ 0 & 0 & B_{66} \end{bmatrix} \begin{Bmatrix} R_{mn}^{xx} \sin \alpha x \sin \beta y \\ R_{mn}^{yy} \sin \alpha x \sin \beta y \\ R_{mn}^{xy} \cos \alpha x \cos \beta y \end{Bmatrix} \\
&\quad + \sum_{m=1}^{\infty} \sum_{n=1}^{\infty} \begin{bmatrix} D_{11} & D_{12} & 0 \\ D_{12} & D_{22} & 0 \\ 0 & 0 & D_{66} \end{bmatrix} \begin{Bmatrix} S_{mn}^{xx} \sin \alpha x \sin \beta y \\ S_{mn}^{yy} \sin \alpha x \sin \beta y \\ S_{mn}^{xy} \cos \alpha x \cos \beta y \end{Bmatrix}
\end{aligned} \tag{6.3.39}$$

For the definitions of R 's and S 's, see Eq. (6.3.30b). The maximum values of M_{xx} and M_{yy} occur at $(x, y) = (a/2, b/2)$, and the maximum of M_{xy} occurs at $(x, y) = (0, 0)$.

The following nondimensionalizations are used in presenting the numerical results:

$$\bar{w} = w_0(a/2, b/2) \left(\frac{E_2 h^3}{a^4 q_0} \right); \quad \bar{\sigma}_{xx} = \sigma_{xx}(a/2, b/2, z) \left(\frac{h^2}{a^2 q_0} \right) \quad (6.3.40a)$$

$$\bar{\sigma}_{yy} = \sigma_{yy}(a/2, b/2, z) \left(\frac{h^2}{a^2 q_0} \right); \quad \bar{\sigma}_{xy} = \sigma_{xy}(a, b, z) \left(\frac{h^2}{a^2 q_0} \right) \quad (6.3.40b)$$

Tables 6.3.1 and 6.3.2 contain nondimensionalized deflections and stresses for antisymmetric cross-ply laminates (all B_{ij} , except for $B_{11} = -B_{22}$, are zero, and $A_{16} = A_{26} = D_{16} = D_{26} = 0$) under various types of mechanical loads. For comparison, results of symmetric laminates are also included. From these results it is clear that, for the same laminate thickness, antisymmetric cross-ply laminates with four or more layers are more desirable than two-layer laminates due to the reduction in deflections as well as stresses. The difference between two-layer and four- or eight-layer laminates is due to the bending-stretching coupling coefficients B_{ij} , which are dominant in the case of two layers. As the number of layers increase, the B_{ij} decrease and the laminate essentially behaves like a specially orthotropic plate.

The effect of stacking sequence on nondimensionalized maximum deflection $\bar{w} \times 10^2$ and in-plane normal stress $-\bar{\sigma}_{xx}(a/2, b/2, -h/2)$ of $(0/90)_k$ and $(0/90)_{ks}$ laminates under uniformly distributed transverse load can be seen from the results presented in Table 6.3.3. The following notation is used: $(0/90)_2 = (0/90/0/90)$ and $(0/90)_{2s} = (0/90/0/90)_s$. The material properties used are $G_{12} = G_{13} = 0.5E_2$, $G_{23} = 0.2E_2$, and $\nu_{12} = 0.25$, and the series is evaluated using $m, n = 1, 3, \dots, 30$.

Table 6.3.1: Transverse deflections and stresses in composite laminates subjected to sinusoidally distributed transverse load ($E_1/E_2 = 25$, $G_{12} = G_{13} = 0.5E_2$, $G_{23} = 0.2E_2$, $\nu_{12} = 0.25$).

Laminate	$(b/a = 1)^*$				$(b/a = 3)^{\dagger}$			
	$\bar{w} \times 10^2$	$\bar{\sigma}_{xx}$	$\bar{\sigma}_{yy}$	$\bar{\sigma}_{xy}$	$\bar{w} \times 10^2$	$\bar{\sigma}_{xx}$	$-\bar{\sigma}_{yy}$	$\bar{\sigma}_{xy}$
0	0.4312	0.5387	0.0267	0.0213	0.4859	0.6016	0.0087	0.0080
(0/90/0)	0.4312	0.5387	0.0267	0.0213	0.5034	0.6233	0.0090	0.0083
(0/90)	1.0636	0.0843	0.7157	0.0525	2.4628	1.6411	0.2065	0.0417
(0/90) ₂	0.5065	0.0357	0.4868	0.0250	1.0850	1.0332	0.1267	0.0181
(0/90) ₄	0.4479	0.0296	0.4950	0.0221	0.9519	1.0425	0.1269	0.0158

* $\bar{\sigma}_{xx}(a/2, b/2, h/2)$, $\bar{\sigma}_{yy}(a/2, b/2, h/2)$, and $\bar{\sigma}_{xy}(a, b, -h/2) = -\bar{\sigma}_{xy}(a, b, h/2)$. For square antisymmetric cross-ply laminates, we have

$$\sigma_{xx}(a/2, b/2, \pm h/2) = \mp \sigma_{yy}(a/2, b/2, \mp h/2).$$

† $\bar{\sigma}_{xx}(a/2, b/2, -h/2)$, $\bar{\sigma}_{yy}(a/2, b/2, h/2)$, and $\bar{\sigma}_{xy}(a, b, -h/2)$.

Table 6.3.2: Transverse deflections and stresses in square laminates subjected to uniformly distributed transverse load (UDL) or central point load (CPL) ($E_1/E_2 = 25$, $G_{12} = G_{13} = 0.5E_2$, $G_{23} = 0.2E_2$, $\nu_{12} = 0.25$; $m, n = 1, 3, \dots, 20$ are used to evaluate the series). See the foot note (*) of Table 6.3.1 for stress locations.

Laminate	UDL				CPL			
	$\bar{w} \times 10^2$	$\bar{\sigma}_{xx}$	$\bar{\sigma}_{yy}$	$\bar{\sigma}_{xy}$	$\bar{w} \times 10^2$	$\bar{\sigma}_{xx}$	$\bar{\sigma}_{yy}$	$\bar{\sigma}_{xy}$
(0/90)	1.6955	0.1268	1.0761	0.0933	4.6664	0.8019	6.8217	0.1932
(90/0)	1.6955	1.0761	0.1268	0.0933	4.6664	6.8217	0.8019	0.1932
(0/90) ₂	0.8085	0.0541	0.7367	0.0442	2.2105	0.3298	4.4952	0.0932
(0/90) ₄	0.7150	0.0449	0.7496	0.0391	1.9536	0.2728	4.5553	0.0825

Table 6.3.3: Effect of lamination scheme on the deflections $\bar{w} \times 10^2$ (first row) and stresses $\bar{\sigma}_{xx}$ (second row) in square laminates subjected to uniformly distributed load (UDL).

k	[(0/90) _k] [*]					[(0/90) _{ks}] [†]				
	$\frac{E_1}{E_2} = 5$	10	15	20	25	$\frac{E_1}{E_2} = 5$	10	15	20	25
1	3.071	2.529	2.169	1.902	1.695	2.273	1.435	1.047	0.824	0.680
	0.503	0.714	0.867	0.984	1.076	0.569	0.704	0.765	0.801	0.824
2	2.440	1.620	1.214	0.971	0.809	2.282	1.445	1.057	0.833	0.687
	0.500	0.619	0.678	0.713	0.737	0.568	0.704	0.767	0.803	0.827
4	2.321	1.487	1.094	0.865	0.715	2.283	1.447	1.058	0.834	0.688
	0.523	0.641	0.697	0.729	0.750	0.565	0.700	0.763	0.799	0.823

* $-\sigma_{xx}(z = -h/2) = \sigma_{yy}(z = h/2)$. † $-\sigma_{xx}(z = -h/2) = \sigma_{xx}(z = h/2)$.

For the $(0/90)_k$ (antisymmetric cross-ply) laminates, both heterogeneity and anisotropy ratio influence the deflections, which decrease as the number of layers is increased. For $(0^\circ/90^\circ)_{ks}$ laminates, heterogeneity has little effect on deflections and stresses. The anisotropy ratio affects deflections and stresses; deflections decrease and stresses increase with increasing value of E_1/E_2 . Also, for antisymmetric laminates the deflections decrease and stresses increase with the number of layers for a fixed anisotropy ratio.

Figures 6.3.1 through 6.3.4 show the effect of bending-stretching coupling and plate aspect ratio on the transverse deflection $\bar{w} = w_0 E_2 h^3 / (q_0 b^4)$ and normal stresses $\bar{\sigma} = [h^2 / (q_0 b^2)] \sigma(a/2, b/2, z_0)$ for a fixed $z = z_0$. The material properties used are $E_1/E_2 = 25$, $G_{12} = G_{13} = 0.5E_2$, and $\nu_{12} = 0.25$. The magnitude of deflections and stresses of symmetric laminates $(0/90/90/0)$ are about two to three times that of antisymmetric $(0/90/0/90)$ laminates for $a/b > 1$. For the uniformly distributed load there corresponds an aspect ratio, around $a/b = 2.25$ for $(0/90)_2$ and $a/b = 3.5$ for $(0/90)_s$, for which the deflection is the maximum of all aspect ratios.

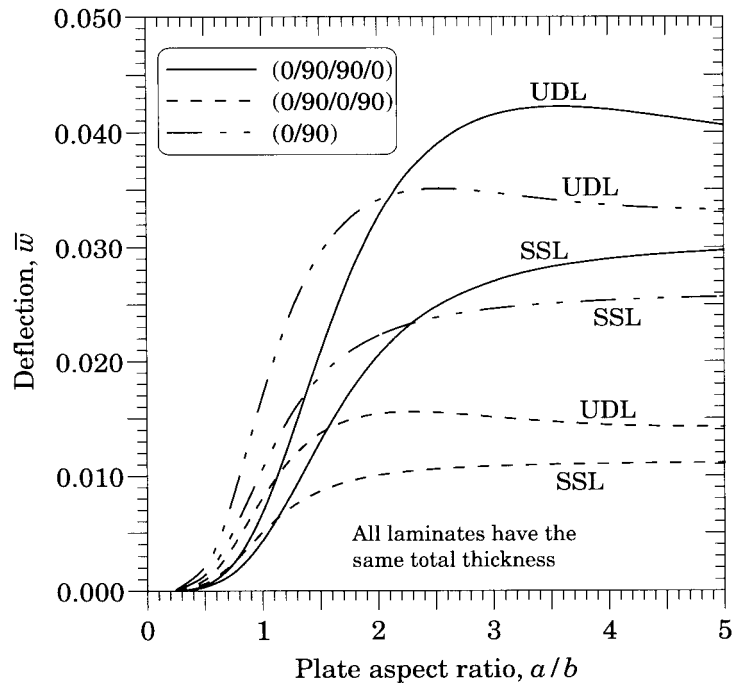


Figure 6.3.1: Nondimensionalized center transverse deflection (\bar{w}) versus plate aspect ratio (a/b) of simply supported (SS-1) laminates.

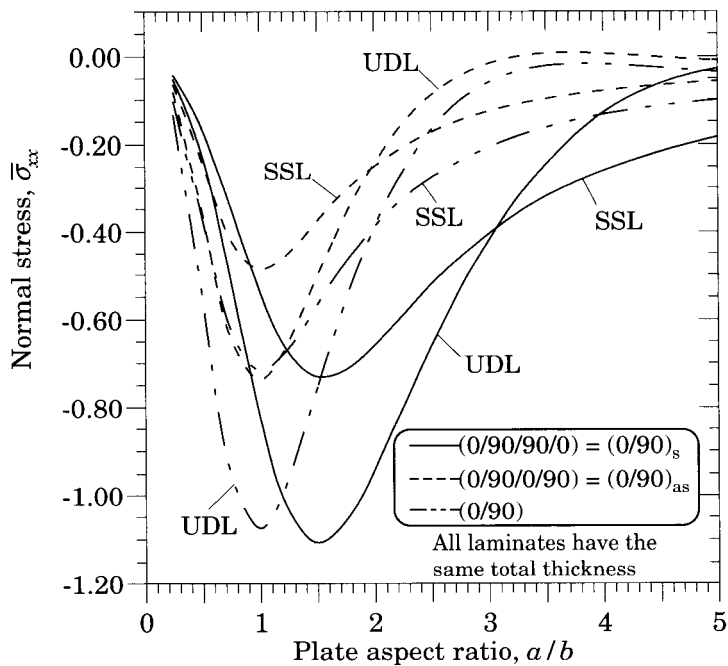


Figure 6.3.2: Nondimensionalized normal stress ($\bar{\sigma}_{xx}(a/2, b/2, -h/2)$) versus plate aspect ratio (a/b) for simply supported (SS-1) laminates.

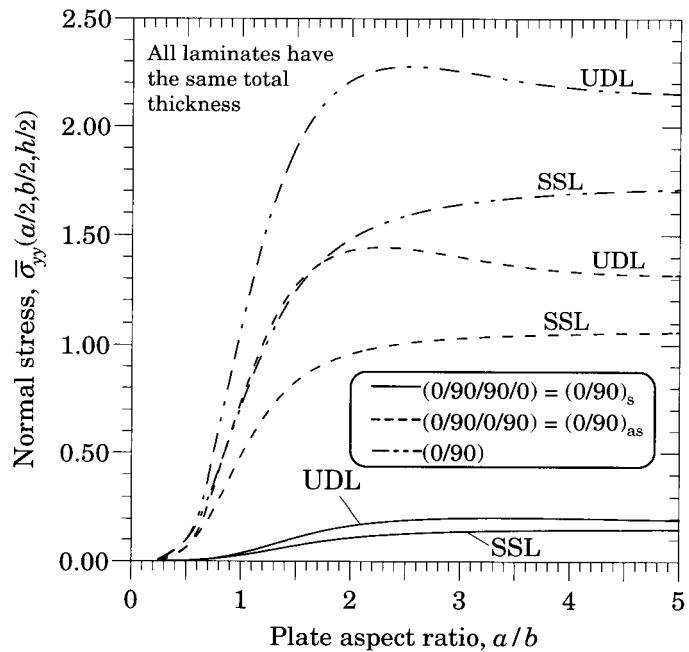


Figure 6.3.3: Nondimensionalized normal stress ($\bar{\sigma}_{yy}(a/2, b/2, h/2)$) versus plate aspect ratio (a/b) of simply supported (SS-1) laminates.

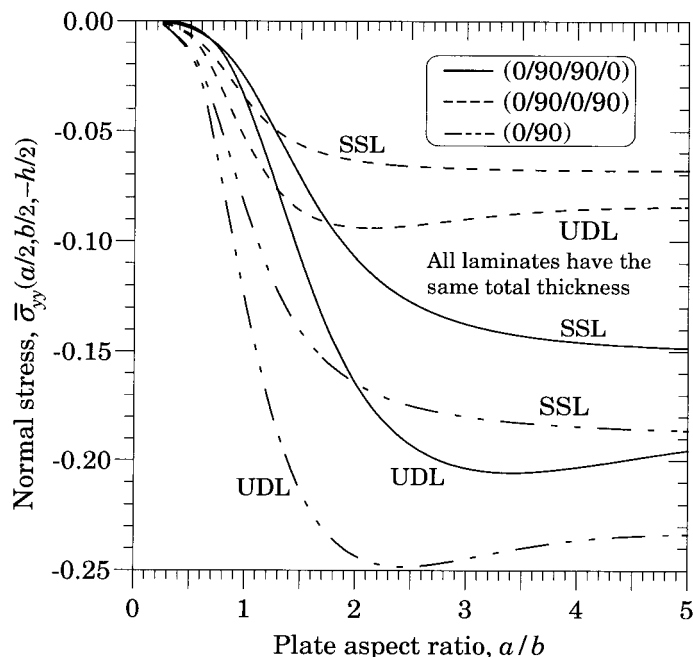


Figure 6.3.4: Nondimensionalized normal stress ($\bar{\sigma}_{yy}(a/2, b/2, -h/2)$) versus plate aspect ratio (a/b) for simply supported (SS-1) laminates.

The effect of coupling is to increase the deflections and stresses. The coupling coefficients B_{ij} decrease in magnitude (hence the effect of coupling decreases) with the increase in the number of layers (for the same total thickness of the plate) in antisymmetric cross-ply laminates. The nondimensionalized center deflection $\bar{w} = w_0 E_2 h^3 / (q_0 b^4)$ versus the aspect ratio a/b is shown in Figure 6.3.5 for $(0/90)_k$ ($k = 1, 2, 3, 4$) laminates under sinusoidal transverse loading ($E_1 = 25E_2$, $G_{12} = G_{13} = 0.5E_2$, $G_{23} = 0.2E_2$, $\nu_{12} = 0.25$). The nondimensionalized deflections of the six-layer and eight-layer plates approach the limiting case of an orthotropic plate.

The dependence of the coupling effect on the modulus ratio is illustrated in Figure 6.3.6, where the maximum nondimensionalized deflection is plotted against the modulus ratio E_1/E_2 ($G_{12} = G_{13} = 0.5E_2$, and $\nu_{12} = 0.25$) for the sinusoidal load. The solution rapidly approaches that of an orthotropic plate for increasing number of layers.

Figures 6.3.7 and 6.3.8 show the distribution of the nondimensionalized maximum normal stress and transverse shear stress

$$\bar{\sigma}_{xx} = \sigma_{xx}(a/2, b/2, z)(h^2/q_0 b^2), \quad \bar{\sigma}_{xz} = \sigma_{xz}(a, b/2, z)(h/q_0 b)$$

computed using the 3-D equilibrium equations, through the thickness of two-layer and eight-layer antisymmetric cross-ply laminates under sinusoidal loading ($a/b = 1$, $a/h = 100$, $E_1 = 25E_2$, $G_{12} = G_{13} = 0.5E_2$, $\nu_{12} = 0.25$). The two-layer plates experience larger stresses than eight-layer plates, and the stress concentration is reduced in the latter. Thus, the effect of the bending-stretching coupling present in two-layer plates on stresses is to increase the magnitude of stresses.

6.3.5 Buckling

For buckling analysis, we assume that the only applied loads are the in-plane forces

$$\hat{N}_{xx} = -N_0, \quad \hat{N}_{yy} = -kN_0, \quad k = \frac{\hat{N}_{yy}}{\hat{N}_{xx}} \quad (6.3.41)$$

and all other mechanical and thermal loads are zero. From Eq. (6.3.19) we have the eigenvalue problem

$$\begin{bmatrix} \hat{c}_{11} & \hat{c}_{12} & \hat{c}_{13} \\ \hat{c}_{12} & \hat{c}_{22} & \hat{c}_{23} \\ \hat{c}_{13} & \hat{c}_{23} & \hat{c}_{33} - N_0(\alpha^2 + k\beta^2) \end{bmatrix} \begin{Bmatrix} U_{mn} \\ V_{mn} \\ W_{mn} \end{Bmatrix} = \begin{Bmatrix} 0 \\ 0 \\ 0 \end{Bmatrix} \quad (6.3.42)$$

where \hat{c}_{ij} are the coefficients defined in Eq. (6.3.20). For a nontrivial solution, $U_{mn} \neq 0$, $V_{mn} \neq 0$, and $W_{mn} \neq 0$, the determinant of the coefficient matrix in (6.3.42) should be zero:

$$\begin{vmatrix} \hat{c}_{11} & \hat{c}_{12} & \hat{c}_{13} \\ \hat{c}_{12} & \hat{c}_{22} & \hat{c}_{23} \\ \hat{c}_{13} & \hat{c}_{23} & \hat{c}_{33} - N_0(\alpha^2 + k\beta^2) \end{vmatrix} = 0 \quad (6.3.43)$$

or

$$N_0 = \frac{d_{mn}}{a_0(\alpha^2 + k\beta^2)}, \quad \alpha = \frac{m\pi}{a}, \quad \beta = \frac{n\pi}{b} \quad (6.3.44a)$$

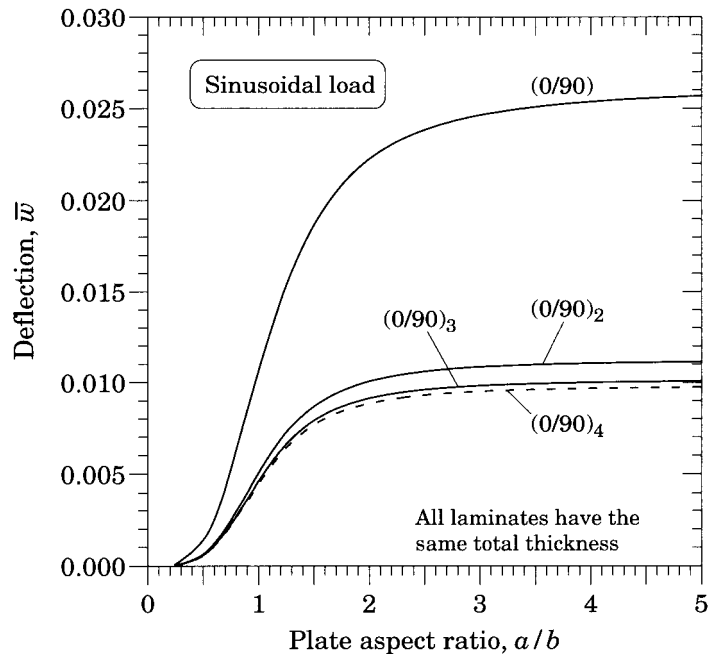


Figure 6.3.5: Nondimensionalized center transverse deflection versus aspect ratio for simply supported cross-ply laminates.

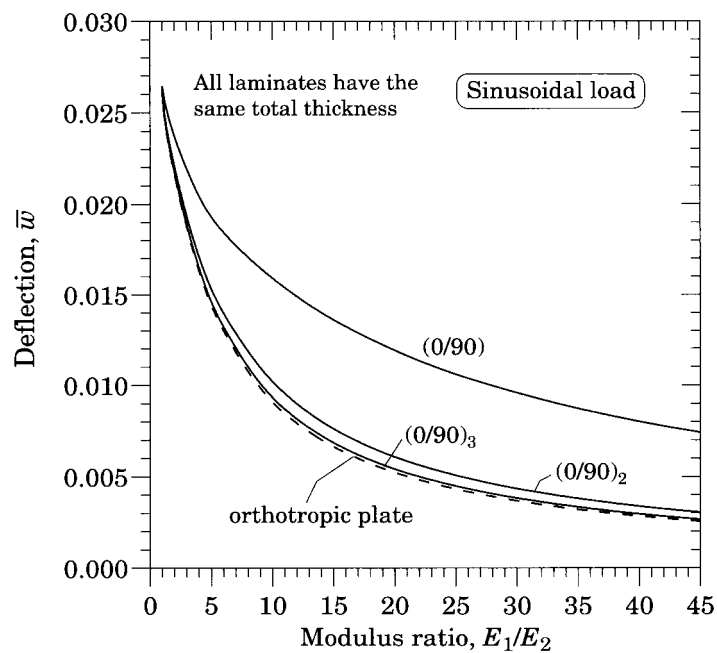


Figure 6.3.6: Nondimensionalized center transverse deflection versus modulus ratio for simply supported cross-ply laminates.

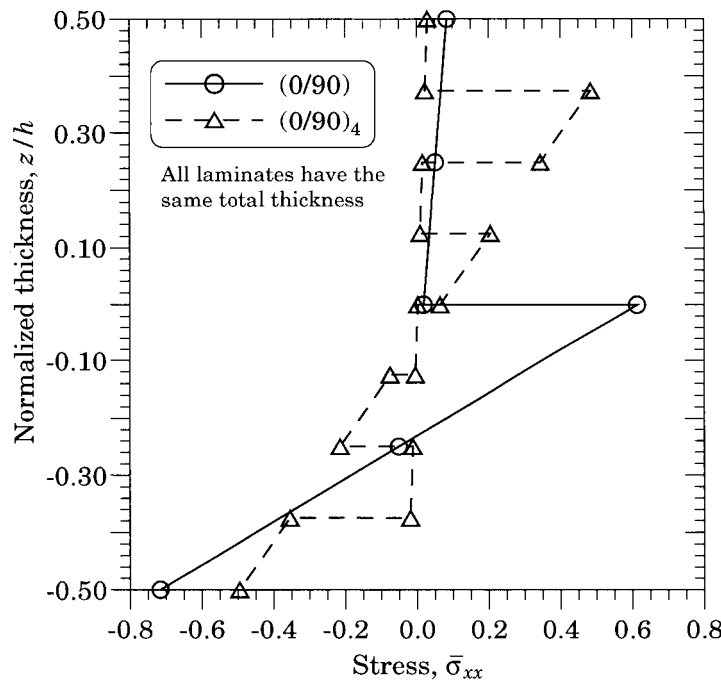


Figure 6.3.7: Nondimensionalized maximum normal stress ($\bar{\sigma}_{xx}$) versus plate thickness (z/h) for simply supported cross-ply laminates (SSL).

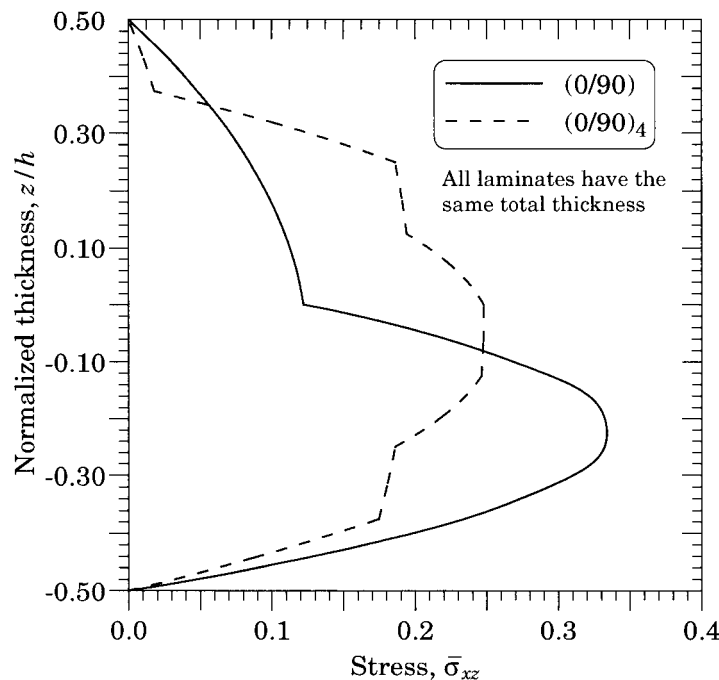


Figure 6.3.8: Nondimensionalized maximum shear stress ($\bar{\sigma}_{xz}$ obtained from equilibrium) versus plate thickness (z/h) for simply supported cross-ply laminates (SSL).

where

$$d_{mn} = \begin{vmatrix} \hat{c}_{11} & \hat{c}_{12} & \hat{c}_{13} \\ \hat{c}_{12} & \hat{c}_{22} & \hat{c}_{23} \\ \hat{c}_{13} & \hat{c}_{23} & \hat{c}_{33} \end{vmatrix}, \quad a_0 = \hat{c}_{11}\hat{c}_{22} - \hat{c}_{12}\hat{c}_{12} \quad (6.3.44b)$$

Alternatively, using the static condensation procedure described in Eqs. (6.3.22)–(6.3.26), we obtain

$$\left[\hat{c}_{33} - N_0 (\alpha^2 + k\beta^2) - \frac{\hat{c}_{13}\hat{c}_{22} - \hat{c}_{23}\hat{c}_{12}}{\hat{c}_{11}\hat{c}_{22} - \hat{c}_{12}\hat{c}_{12}} \hat{c}_{13} - \frac{\hat{c}_{11}\hat{c}_{23} - \hat{c}_{12}\hat{c}_{13}}{\hat{c}_{11}\hat{c}_{22} - \hat{c}_{12}\hat{c}_{12}} \hat{c}_{23} \right] W_{mn} = 0$$

Since $W_{mn} \neq 0$, we obtain

$$N_0 = \frac{1}{\alpha^2 + k\beta^2} \left(\hat{c}_{33} - \frac{\hat{c}_{13}\hat{c}_{22} - \hat{c}_{23}\hat{c}_{12}}{\hat{c}_{11}\hat{c}_{22} - \hat{c}_{12}\hat{c}_{12}} \hat{c}_{13} - \frac{\hat{c}_{11}\hat{c}_{23} - \hat{c}_{12}\hat{c}_{13}}{\hat{c}_{11}\hat{c}_{22} - \hat{c}_{12}\hat{c}_{12}} \hat{c}_{23} \right) \quad (6.3.45)$$

Clearly, for each pair of m and n , there is a unique value of N_0 . The critical buckling load is the smallest of all $N_0 = N_0(m, n)$:

$$N_{cr} = \min_{1 \leq m, n \leq \infty} \{N_0(m, n)\} \quad (6.3.46)$$

Since \hat{c}_{ij} depend on m and n , $N_0(m, n)$ is a complicated function of both m and n and no simple conclusions can be drawn about the mode (m, n) at buckling.

Antisymmetric cross-ply laminates have special stiffness characteristics given in Eq. (6.3.7a). Hence the buckling load for antisymmetric cross-ply laminates is given by Eq. (6.3.44a) or (6.3.45) with coefficients \hat{c}_{ij} from Eq. (6.3.20).

For specially orthotropic plates, neither shear-twist coupling nor bending-extension coupling exists ($\hat{c}_{13} = \hat{c}_{23} = 0$), and therefore U_{mn} and V_{mn} are zero prior to onset of buckling. Therefore, we have (cf. Eq. (5.5.5a))

$$N_0 = \frac{\hat{c}_{33}}{(\alpha^2 + k\beta^2)} \quad (6.3.47a)$$

$$\hat{c}_{33} = D_{11}\alpha^4 + 2(D_{12} + 2D_{66})\alpha^2\beta^2 + D_{22}\beta^4, \quad \alpha = \frac{n\pi}{a}, \quad \beta = \frac{m\pi}{b} \quad (6.3.47b)$$

Table 6.3.4 shows the effect of stacking sequence, plate aspect ratio, and modulus ratio on nondimensionalized critical buckling loads $\bar{N} = N_{cr}(b^2/\pi^2 D_{22})$ of rectangular laminates under uniform compression ($k = 0$) as well as biaxial compression ($k = 1$). The following material properties were used: *material 1*: $E_1/E_2 = 25$, $G_{12} = G_{13} = 0.5E_2$, $\nu_{12} = 0.25$; and *material 2*: $E_1/E_2 = 40$, $G_{12} = G_{13} = 0.5E_2$, $\nu_{12} = 0.25$. In all cases (also see Figures 6.3.9 through 6.3.11) the critical buckling mode is $(m, n) = (1, 1)$, except for the antisymmetric cross-ply laminate, with aspect ratio $a/b = 1.5$, in uniform compression. In the latter case, the mode is $(2, 1)$. The nondimensionalized buckling load increases for symmetric laminates whereas it decreases for antisymmetric laminates as the modulus ratio increases.

Table 6.3.4: Effect of lamination scheme, aspect ratio, and modulus ratio on the nondimensionalized buckling loads \bar{N} of rectangular laminates under uniform compression and biaxial compression (material 1).

$\frac{a}{b}$	$(0/90)_{as} \equiv (0^\circ/90^\circ/0^\circ/90^\circ)$					$(0/90)_s \equiv (0^\circ/90^\circ/90^\circ/0^\circ)$				
	$\frac{E_1}{E_2} = 5$	10	20	25	40	$\frac{E_1}{E_2} = 5$	10	20	25	40
Uniaxial compression ($k = 0$)										
0.5	4.705	4.157	3.828	3.757	3.647	13.900	18.126	21.878	22.874	24.590
1.0	2.643	2.189	1.923	1.866	1.778	5.650	6.347	6.961	7.124	7.404
1.5	2.955	2.487	2.211	2.152	2.061	5.233	5.277	5.310	5.318	15.332
Biaxial compression ($k = 1$)										
0.5	3.764	3.325	3.062	3.005	2.917	11.120	12.694	13.922	14.248	14.766
1.0	1.322	1.095	0.962	0.933	0.889	2.825	3.174	3.481	3.562	3.702
1.5	1.009	0.860	0.773	0.754	0.725	1.610	1.624	1.634	1.636	1.641

The mode number is $(m, n) = (1, 1)$ for all cases, except for the following: (a) $(0^\circ/90^\circ)_2$, $a/b = 1.5$ and $k = 0$: mode is $(2,1)$; (b) $(0^\circ/90^\circ)_s$, $a/b = 0.5$ and $k = 1$: modes are $(1,1)$, $(1,2)$, $(1,2)$, $(1,2)$, and $(1,3)$ for modulus ratios 5, 10, 20, 25, and 40, respectively.

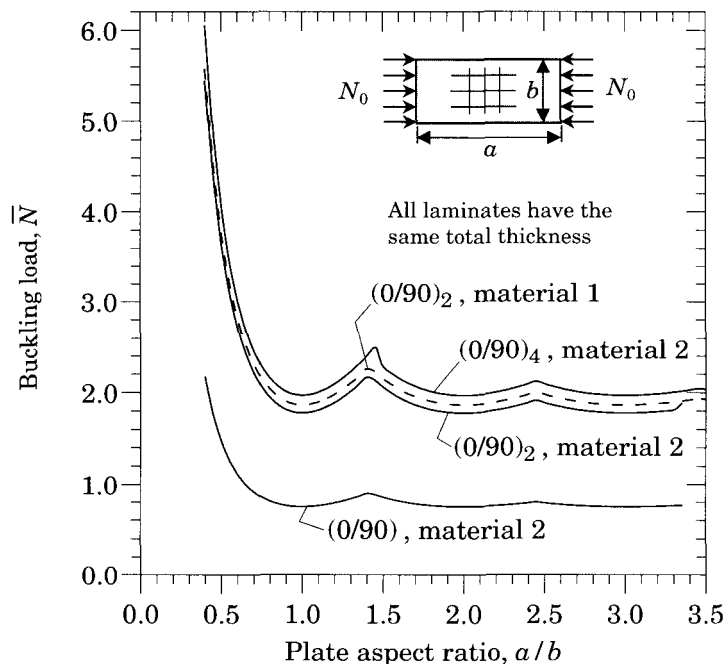


Figure 6.3.9: Nondimensionalized buckling (\bar{N}) load versus plate aspect ratio (a/b) for simply supported (SS-1) antisymmetric cross-ply laminates $(0/90)_n$ under uniaxial compression.

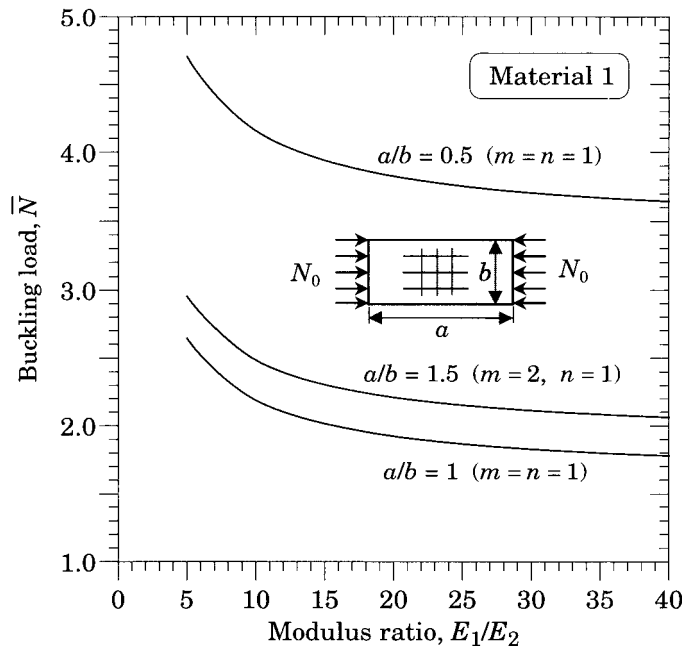


Figure 6.3.10: Nondimensionalized buckling load (\bar{N}) versus modulus ratio (E_1/E_2) for antisymmetric cross-ply laminates $(0/90)_2$ under uniaxial compression.

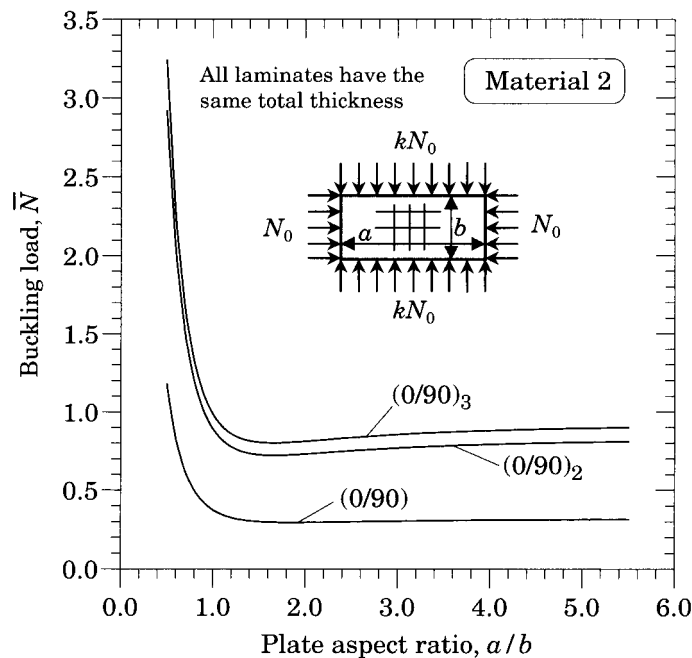


Figure 6.3.11: Nondimensionalized biaxial buckling load (\bar{N}) versus plate aspect ratio (a/b) for antisymmetric cross-ply laminates $(0/90)_n$ ($n = 1, 2, 3$) under biaxial compression ($k = 1$).

6.3.6 Vibration

For free vibration, all applied loads and the in-plane forces are set to zero, and we assume a periodic solution of the form

$$U_{mn}(t) = U_{mn}^0 e^{i\omega t}, \quad V_{mn}(t) = V_{mn}^0 e^{i\omega t}, \quad W_{mn}(t) = W_{mn}^0 e^{i\omega t} \quad (6.3.48)$$

where $i = \sqrt{-1}$ and ω is the frequency of natural vibration. Then Eq. (6.3.19) reduces to the eigenvalue problem

$$\left(\begin{bmatrix} \hat{c}_{11} & \hat{c}_{12} & \hat{c}_{13} \\ \hat{c}_{12} & \hat{c}_{22} & \hat{c}_{23} \\ \hat{c}_{13} & \hat{c}_{23} & \hat{c}_{33} \end{bmatrix} - \omega^2 \begin{bmatrix} \hat{m}_{11} & 0 & 0 \\ 0 & \hat{m}_{22} & 0 \\ 0 & 0 & \hat{m}_{33} \end{bmatrix} \right) \begin{Bmatrix} U_{mn}^0 \\ V_{mn}^0 \\ W_{mn}^0 \end{Bmatrix} = \begin{Bmatrix} 0 \\ 0 \\ 0 \end{Bmatrix} \quad (6.3.49)$$

For a nontrivial solution, $U_{mn}^0 \neq 0$, $V_{mn}^0 \neq 0$, $W_{mn}^0 \neq 0$, the determinant of the coefficient matrix in (6.3.49) should be zero, which yields the characteristic polynomial

$$-p\lambda^3 + q\lambda^2 - r\lambda + s = 0 \quad (6.3.50)$$

where $\lambda = \omega^2$ is the eigenvalue and

$$\begin{aligned} p &= \begin{vmatrix} \hat{m}_{11} & 0 & 0 \\ 0 & \hat{m}_{22} & 0 \\ 0 & 0 & \hat{m}_{33} \end{vmatrix}, \quad s = \begin{vmatrix} \hat{c}_{11} & \hat{c}_{12} & \hat{c}_{13} \\ \hat{c}_{12} & \hat{c}_{22} & \hat{c}_{23} \\ \hat{c}_{13} & \hat{c}_{23} & \hat{c}_{33} \end{vmatrix} \\ q &= \begin{vmatrix} \hat{c}_{11} & 0 & 0 \\ \hat{c}_{12} & \hat{m}_{22} & 0 \\ \hat{c}_{13} & 0 & \hat{m}_{33} \end{vmatrix} + \begin{vmatrix} \hat{m}_{11} & \hat{c}_{12} & 0 \\ 0 & \hat{c}_{22} & 0 \\ 0 & \hat{c}_{23} & \hat{m}_{33} \end{vmatrix} + \begin{vmatrix} \hat{m}_{11} & 0 & \hat{c}_{13} \\ 0 & \hat{m}_{22} & \hat{c}_{23} \\ 0 & 0 & \hat{c}_{33} \end{vmatrix} \\ r &= \begin{vmatrix} \hat{c}_{11} & \hat{c}_{12} & 0 \\ \hat{c}_{12} & \hat{c}_{22} & 0 \\ \hat{c}_{13} & \hat{c}_{23} & \hat{m}_{33} \end{vmatrix} + \begin{vmatrix} \hat{c}_{11} & 0 & \hat{c}_{13} \\ \hat{c}_{12} & \hat{m}_{22} & \hat{c}_{23} \\ \hat{c}_{13} & 0 & \hat{c}_{33} \end{vmatrix} + \begin{vmatrix} \hat{m}_{11} & \hat{c}_{12} & \hat{c}_{13} \\ 0 & \hat{c}_{22} & \hat{c}_{23} \\ 0 & \hat{c}_{23} & \hat{c}_{33} \end{vmatrix} \end{aligned} \quad (6.3.51)$$

The real positive roots of this cubic equation give the square of the natural frequency ω_{mn} associated with mode (m, n) . The smallest of the frequencies is called the *fundamental frequency*. In general, ω_{11} is not the fundamental frequency; the smallest frequency might occur for values other than $m = n = 1$.

If the in-plane inertias are neglected (i.e., $\hat{m}_{11} = \hat{m}_{22} = 0$), and irrespective of whether the rotary inertia is zero, Eq. (6.3.50) takes the same form as Eq. (6.3.43) with $N_0(\alpha^2 + k\beta^2)$ replaced by $\omega^2 \hat{m}_{33}$. Hence, from Eq. (6.3.43) we have

$$\omega^2 = \frac{1}{\hat{m}_{33}} \left(\hat{c}_{33} - \frac{\hat{c}_{13}\hat{c}_{22} - \hat{c}_{23}\hat{c}_{12}}{\hat{c}_{11}\hat{c}_{22} - \hat{c}_{12}\hat{c}_{12}} \hat{c}_{13} - \frac{\hat{c}_{11}\hat{c}_{23} - \hat{c}_{12}\hat{c}_{13}}{\hat{c}_{11}\hat{c}_{22} - \hat{c}_{12}\hat{c}_{12}} \hat{c}_{23} \right) \quad (6.3.52)$$

Note that if the in-plane inertias are not neglected, the eigenvalue problem cannot be simplified to a single equation even if the rotary inertia is zero.

Nondimensionalized frequencies, $\bar{\omega}_{mn} = \omega_{mn}(b^2/\pi^2)\sqrt{\rho h/D_{22}}$, of specially orthotropic and antisymmetric cross-ply square laminates are presented in Table 6.3.5 for modulus ratios $E_1/E_2=10$ and 20 ($G_{12} = G_{13} = 0.5E_2$, $G_{23} = 0.2E_2$, $\nu_{12} = 0.25$). All layers are of equal thickness. Results are presented for $m, n = 1, 2, 3$, and

for the case in which the rotary inertia is neglected. The fundamental frequency increases with modular ratio. As noted earlier, the effect of including rotary inertia is to decrease the frequency of vibration. Note that the first four frequencies for an orthotropic (0°) plate correspond to the modes, $(m, n)=(1,1)$, $(1,2)$, $(1,3)$, and $(2,1)$, whereas for antisymmetric cross-ply plates they are $(m, n)=(1,1)$, $(1,2)$, $(2,1)$, and $(2,2)$. For symmetric cross-ply plates the first four frequencies are provided by the modes: $(m, n)=(1,1)$, $(1,2)$, $(2,1)$, and $(1,3)$. Also, we note that $\omega_{mn} = \omega_{nm}$ for antisymmetric laminates.

Table 6.3.5: Nondimensionalized frequencies $\bar{\omega}$ of cross-ply laminates according to the classical plate theory.

<i>m</i>	<i>n</i>	(0)	(0/90)	(0/90) ₂	(0/90) ₄	(0/90) _s
$E_1/E_2 = 10$						
1	1	3.672	1.183	1.479	1.545	2.519
1	2	5.996	3.174	4.077	4.274	4.986
1	3	10.648	6.666	8.698	9.136	9.783
2	1	13.075	3.174	4.077	4.274	8.515
2	2	14.690	4.733	5.918	6.179	10.077
2	3	18.181	7.927	10.034	10.494	13.783
3	1	28.868	6.666	8.698	9.136	18.704
3	2	30.258	7.927	10.034	10.494	19.911
3	3	33.053	10.650	13.317	13.904	22.674
$E_1/E_2 = 20$						
1	1	4.847	0.990	1.386	1.469	2.638
1	2	6.781	2.719	3.913	4.158	4.917
1	3	11.111	5.789	8.456	8.998	9.637
2	1	18.193	2.719	3.913	4.158	9.354
2	2	19.388	3.959	5.547	5.877	10.554
2	3	22.153	6.702	9.507	10.088	13.826
3	1	40.539	5.789	8.456	8.998	20.752
3	2	41.542	6.193	9.507	10.088	21.578
3	3	43.623	8.908	12.481	13.224	23.746

Figure 6.3.12 shows a plot of fundamental frequency $\bar{\omega}$ versus aspect ratio a/b for symmetric $(0/90)_s$ cross-ply and antisymmetric $(0/90)_2$ cross-ply laminates. The material properties used are $E_1/E_2 = 40$, $G_{12} = G_{13} = 0.6E_2$, and $\nu_{12} = 0.25$. Figure 6.3.13 shows the effect of coupling between bending and extension on the fundamental frequencies of antisymmetric cross-ply laminates. The material properties used are $E_1/E_2 = 25$, $G_{12} = G_{13} = 0.5E_2$, and $\nu_{12} = 0.25$. With an increase in the number of layers, the frequencies approach those of the orthotropic plate. The bending-stretching coupling has the effect of lowering the vibration frequencies. For example, the two-layer plate has vibration frequencies about 40 percent lower than those of eight-layer antisymmetric laminate or orthotropic plate with the same total thickness.

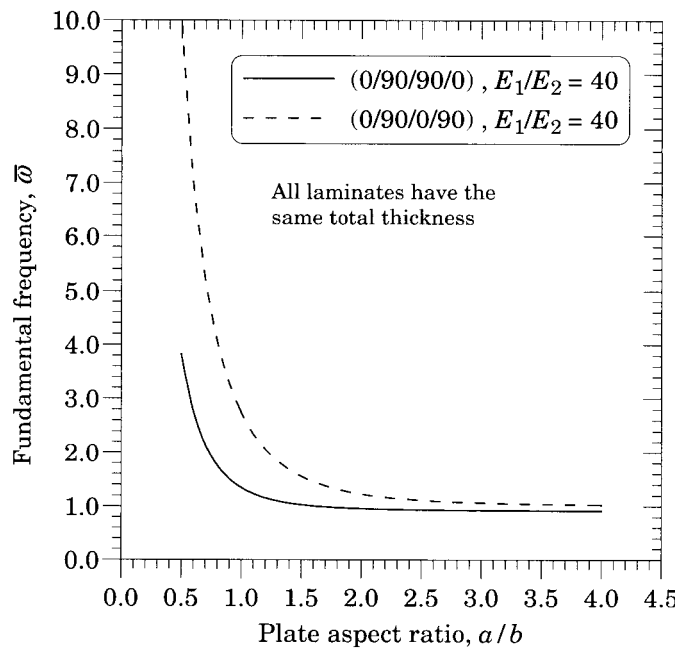


Figure 6.3.12: Nondimensionalized fundamental frequency ($\bar{\omega}$) versus plate aspect ratio (a/b) for cross-ply laminates.

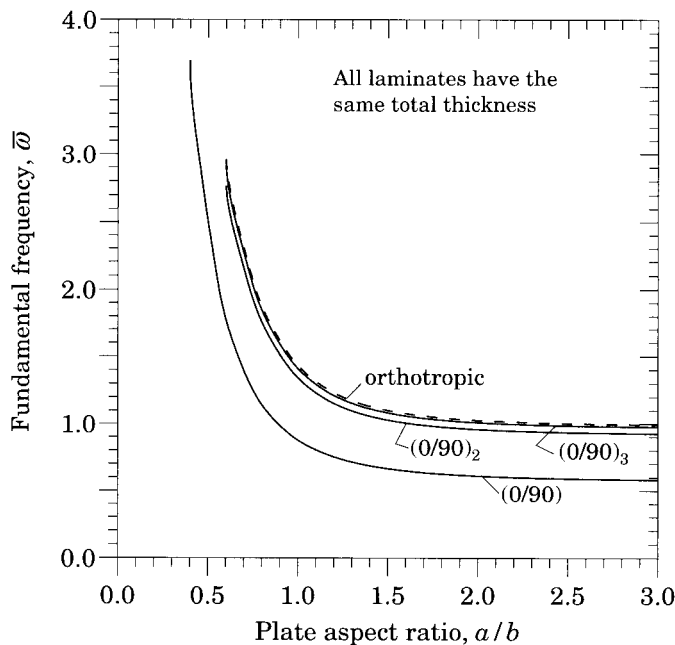


Figure 6.3.13: Nondimensionalized fundamental frequency ($\bar{\omega}$) versus plate aspect ratio (a/b) for antisymmetric cross-ply laminates.

6.4 Navier Solutions of Antisymmetric Angle-Ply Laminates

6.4.1 Boundary Conditions

The SS-2 boundary conditions in Eqs. (6.2.7) imply the following conditions on the generalized displacements and stress resultants of the classical laminate theory:

$$\begin{aligned} u_0(0, y, t) &= 0, & u_0(a, y, t) &= 0, & v_0(x, 0, t) &= 0, & v_0(x, b, t) &= 0 \\ w_0(x, 0, t) &= 0, & w_0(x, b, t) &= 0, & w_0(0, y, t) &= 0, & w_0(a, y, t) &= 0 \\ \frac{\partial w_0}{\partial x} \Big|_{(x,0,t)} &= 0, & \frac{\partial w_0}{\partial x} \Big|_{(x,b,t)} &= 0, & \frac{\partial w_0}{\partial y} \Big|_{(0,y,t)} &= 0, & \frac{\partial w_0}{\partial y} \Big|_{(a,y,t)} &= 0 \end{aligned} \quad (6.4.1a)$$

$$\begin{aligned} N_{xy}(0, y, t) &= 0, & N_{xy}(a, y, t) &= 0, & N_{xy}(x, 0, t) &= 0, & N_{xy}(x, b, t) &= 0 \\ M_{xx}(0, y, t) &= 0, & M_{xx}(a, y, t) &= 0, & M_{yy}(x, 0, t) &= 0, & M_{yy}(x, b, t) &= 0 \end{aligned} \quad (6.4.1b)$$

The displacement boundary conditions in (6.4.1a) are satisfied by assuming the following form of the displacements

$$u_0(x, y, t) = \sum_{n=1}^{\infty} \sum_{m=1}^{\infty} U_{mn}(t) \sin \alpha x \cos \beta y \quad (6.4.2a)$$

$$v_0(x, y, t) = \sum_{n=1}^{\infty} \sum_{m=1}^{\infty} V_{mn}(t) \cos \alpha x \sin \beta y \quad (6.4.2b)$$

$$w_0(x, y, t) = \sum_{n=1}^{\infty} \sum_{m=1}^{\infty} W_{mn}(t) \sin \alpha x \sin \beta y \quad (6.4.2c)$$

where $\alpha = (m\pi/a)$ and $\beta = (n\pi/b)$. Substituting the expansions (6.4.2) into the expressions for N_{xx} , N_{yy} , N_{xy} , M_{xx} , M_{yy} , and M_{xy} , we obtain

$$\begin{aligned} N_{xx} &= A_{11} \frac{\partial u_0}{\partial x} + A_{12} \frac{\partial v_0}{\partial y} + A_{16} \left(\frac{\partial u_0}{\partial y} + \frac{\partial v_0}{\partial x} \right) \\ &\quad - B_{11} \frac{\partial^2 w_0}{\partial x^2} - B_{12} \frac{\partial^2 w_0}{\partial y^2} - 2B_{16} \frac{\partial^2 w_0}{\partial x \partial y} \\ &= \sum_{n=1}^{\infty} \sum_{m=1}^{\infty} (\alpha A_{11} U_{mn} + \beta A_{12} V_{mn} - 2B_{16} \alpha \beta W_{mn}) \cos \alpha x \cos \beta y \\ &\quad + \sum_{n=1}^{\infty} \sum_{m=1}^{\infty} \left[-A_{16} (\beta U_{mn} + \alpha V_{mn}) + (B_{11} \alpha^2 + B_{12} \beta^2) W_{mn} \right] \sin \alpha x \sin \beta y \\ N_{yy} &= A_{12} \frac{\partial u_0}{\partial x} + A_{22} \frac{\partial v_0}{\partial y} + A_{26} \left(\frac{\partial u_0}{\partial y} + \frac{\partial v_0}{\partial x} \right) \\ &\quad - B_{12} \frac{\partial^2 w_0}{\partial x^2} - B_{22} \frac{\partial^2 w_0}{\partial y^2} - 2B_{26} \frac{\partial^2 w_0}{\partial x \partial y} \\ &= \sum_{n=1}^{\infty} \sum_{m=1}^{\infty} (\alpha A_{12} U_{mn} + \beta A_{22} V_{mn} - 2B_{26} \alpha \beta W_{mn}) \cos \alpha x \cos \beta y \end{aligned}$$

$$\begin{aligned}
& + \sum_{n=1}^{\infty} \sum_{m=1}^{\infty} \left[-A_{26} (\beta U_{mn} + \alpha V_{mn}) + (B_{12}\alpha^2 + B_{22}\beta^2) W_{mn} \right] \sin \alpha x \sin \beta y \\
N_{xy} & = A_{16} \frac{\partial u_0}{\partial x} + A_{26} \frac{\partial v_0}{\partial y} + A_{66} \left(\frac{\partial u_0}{\partial y} + \frac{\partial v_0}{\partial x} \right) \\
& - B_{16} \frac{\partial^2 w_0}{\partial x^2} - B_{26} \frac{\partial^2 w_0}{\partial y^2} - 2B_{66} \frac{\partial^2 w_0}{\partial x \partial y} \\
& = \sum_{n=1}^{\infty} \sum_{m=1}^{\infty} [\alpha A_{16} U_{mn} + \beta A_{26} V_{mn} - 2\alpha\beta B_{66} W_{mn}] \cos \alpha x \cos \beta y \\
& + \sum_{n=1}^{\infty} \sum_{m=1}^{\infty} \left[-A_{66} (\beta U_{mn} + \alpha V_{mn}) + (B_{16}\alpha^2 + B_{26}\beta^2) W_{mn} \right] \sin \alpha x \sin \beta y \\
M_{xx} & = B_{11} \frac{\partial u_0}{\partial x} + B_{12} \frac{\partial v_0}{\partial y} + B_{16} \left(\frac{\partial u_0}{\partial y} + \frac{\partial v_0}{\partial x} \right) \\
& - D_{11} \frac{\partial^2 w_0}{\partial x^2} - D_{12} \frac{\partial^2 w_0}{\partial y^2} - 2D_{16} \frac{\partial^2 w_0}{\partial x \partial y} \\
& = \sum_{n=1}^{\infty} \sum_{m=1}^{\infty} [\alpha B_{11} U_{mn} + \beta B_{12} V_{mn} - 2\alpha\beta D_{16} W_{mn}] \cos \alpha x \cos \beta y \\
& + \sum_{n=1}^{\infty} \sum_{m=1}^{\infty} \left[-B_{16} (\beta U_{mn} + \alpha V_{mn}) + (D_{11}\alpha^2 + D_{12}\beta^2) W_{mn} \right] \sin \alpha x \sin \beta y \\
M_{yy} & = B_{12} \frac{\partial u_0}{\partial x} + B_{22} \frac{\partial v_0}{\partial y} + B_{26} \left(\frac{\partial u_0}{\partial y} + \frac{\partial v_0}{\partial x} \right) \\
& - D_{12} \frac{\partial^2 w_0}{\partial x^2} - D_{22} \frac{\partial^2 w_0}{\partial y^2} - 2D_{26} \frac{\partial^2 w_0}{\partial x \partial y} \\
& = \sum_{n=1}^{\infty} \sum_{m=1}^{\infty} [\alpha B_{12} U_{mn} + \beta B_{22} V_{mn} - 2\alpha\beta D_{26} W_{mn}] \cos \alpha x \cos \beta y \\
& + \sum_{n=1}^{\infty} \sum_{m=1}^{\infty} \left[-B_{26} (\beta U_{mn} + \alpha V_{mn}) + (D_{12}\alpha^2 + D_{22}\beta^2) W_{mn} \right] \sin \alpha x \sin \beta y \\
M_{xy} & = B_{16} \frac{\partial u_0}{\partial x} + B_{26} \frac{\partial v_0}{\partial y} + B_{66} \left(\frac{\partial u_0}{\partial y} + \frac{\partial v_0}{\partial x} \right) \\
& - D_{16} \frac{\partial^2 w_0}{\partial x^2} - D_{26} \frac{\partial^2 w_0}{\partial y^2} - 2D_{66} \frac{\partial^2 w_0}{\partial x \partial y} \\
& = \sum_{n=1}^{\infty} \sum_{m=1}^{\infty} [\alpha B_{16} U_{mn} + \beta B_{26} V_{mn} - 2\alpha\beta D_{66} W_{mn}] \cos \alpha x \cos \beta y \\
& + \sum_{n=1}^{\infty} \sum_{m=1}^{\infty} \left[-B_{66} (\beta U_{mn} + \alpha V_{mn}) + (D_{16}\alpha^2 + D_{26}\beta^2) W_{mn} \right] \sin \alpha x \sin \beta y
\end{aligned} \tag{6.4.3}$$

Note that the boundary conditions in (6.4.1b) on the stress resultants N_{xy} , M_{xx} , and M_{yy} can be satisfied only if the laminate stiffnesses A_{16} , A_{26} , B_{11} , B_{12} , B_{22} , B_{66} , D_{16} , and D_{26} are zero. Thus, the Navier solutions for rectangular laminated plates with

SS-2 boundary conditions exist only when the stacking sequences are such that

$$A_{16} = A_{26} = B_{11} = B_{12} = B_{22} = B_{66} = D_{16} = D_{26} = 0 \quad (6.4.4)$$

In addition, for dynamic problems, we must have $I_1 = 0$. Thus plates with a single generally orthotropic layer, symmetrically laminated plates with multiple specially orthotropic layers, and antisymmetric angle-ply laminated plates admit the Navier solutions for the SS-2 boundary conditions.

6.4.2 Solution

Substitution of Eq. (6.4.2) into Eqs. (6.2.1)–(6.2.3) yields

$$\sum_{n=1}^{\infty} \sum_{m=1}^{\infty} \left[- (A_{11}\alpha^2 + A_{66}\beta^2) U_{mn} - (A_{12} + A_{66}) \alpha\beta V_{mn} + (3B_{16}\alpha^2\beta + B_{26}\beta^3) W_{mn} - I_0 \ddot{U}_{mn} \right] \sin \alpha x \cos \beta y = \left(\frac{\partial N_{xx}^T}{\partial x} + \frac{\partial N_{xy}^T}{\partial y} \right) \quad (6.4.5a)$$

$$\sum_{n=1}^{\infty} \sum_{m=1}^{\infty} \left[- (A_{12} + A_{66}) \alpha\beta U_{mn} - (A_{66}\alpha^2 + A_{22}\beta^2) V_{mn} + (B_{16}\alpha^3 + 3B_{26}\alpha\beta^2) W_{mn} - I_0 \ddot{V}_{mn} \right] \cos \alpha x \sin \beta y = \left(\frac{\partial N_{xy}^T}{\partial x} + \frac{\partial N_{yy}^T}{\partial y} \right) \quad (6.4.5b)$$

$$\begin{aligned} & \sum_{n=1}^{\infty} \sum_{m=1}^{\infty} \left[(3B_{16}\alpha^2\beta + B_{26}\beta^3) U_{mn} + (B_{16}\alpha^3 + 3B_{26}\alpha\beta^2) V_{mn} \right. \\ & \quad \left. - (D_{11}\alpha^4 + 2(D_{12} + 2D_{66})\alpha^2\beta^2 + D_{22}\beta^4) W_{mn} \right. \\ & \quad \left. - (\alpha^2 \hat{N}_{xx} + \beta^2 \hat{N}_{yy}) W_{mn} - (I_0 + I_2(\alpha^2 + \beta^2)) \ddot{W}_{mn} \right] \sin \alpha x \sin \beta y \\ & = \left(\frac{\partial^2 M_{xx}^T}{\partial x^2} + 2 \frac{\partial^2 M_{xy}^T}{\partial x \partial y} + \frac{\partial^2 M_{yy}^T}{\partial y^2} \right) - q(x, y) \end{aligned} \quad (6.4.5c)$$

Note that the edge shear force \hat{N}_{xy} is necessarily zero. In addition, inertia I_1 is zero. If the transverse load and thermal resultants are expanded as before [see Eqs. (6.3.10)–(6.3.13)], then it follows from Eq. (6.3.14) that N_{mn}^1 , N_{mn}^2 , and M_{mn}^6 must be zero. If the temperature field is expanded in double cosine series, N_{mn}^6 , M_{mn}^1 , and M_{mn}^2 must be zero.

Equations (6.4.5) can be expressed in matrix form as

$$\begin{aligned} & \begin{bmatrix} \hat{c}_{11} & \hat{c}_{12} & \hat{c}_{13} \\ \hat{c}_{12} & \hat{c}_{22} & \hat{c}_{23} \\ \hat{c}_{13} & \hat{c}_{23} & \hat{c}_{33} + \tilde{s}_{33} \end{bmatrix} \begin{Bmatrix} U_{mn} \\ V_{mn} \\ W_{mn} \end{Bmatrix} + \begin{bmatrix} \hat{m}_{11} & 0 & 0 \\ 0 & \hat{m}_{22} & 0 \\ 0 & 0 & \hat{m}_{33} \end{bmatrix} \begin{Bmatrix} \ddot{U}_{mn} \\ \ddot{V}_{mn} \\ \ddot{W}_{mn} \end{Bmatrix} \\ & = \begin{Bmatrix} 0 \\ 0 \\ Q_{mn} \end{Bmatrix} + \begin{Bmatrix} -\beta N_{mn}^6 \\ -\alpha N_{mn}^6 \\ \alpha^2 M_{mn}^1 + \beta^2 M_{mn}^2 \end{Bmatrix} \text{ or } \begin{Bmatrix} \alpha N_{mn}^1 \\ \beta N_{mn}^2 \\ -2\alpha\beta M_{mn}^6 \end{Bmatrix} \end{aligned} \quad (6.4.6)$$

where

$$\begin{aligned}\hat{c}_{11} &= A_{11}\alpha^2 + A_{66}\beta^2 \\ \hat{c}_{12} &= (A_{12} + A_{66})\alpha\beta \\ \hat{c}_{13} &= -(3B_{16}\alpha^2 + B_{26}\beta^2)\beta \\ \hat{c}_{22} &= A_{66}\alpha^2 + A_{22}\beta^2 \\ \hat{c}_{23} &= -(B_{16}\alpha^2 + 3B_{26}\beta^2)\alpha \\ \hat{c}_{33} &= D_{11}\alpha^4 + 2(D_{12} + 2D_{66})\alpha^2\beta^2 + D_{22}\beta^4\end{aligned}\quad (6.4.7a)$$

$$\tilde{s}_{33} = \alpha^2 \hat{N}_{xx} + \beta^2 \hat{N}_{yy} \quad (6.4.7b)$$

$$\begin{aligned}\hat{m}_{11} &= \hat{m}_{22} = I_0 \\ \hat{m}_{33} &= I_0 + I_2(\alpha^2 + \beta^2)\end{aligned}\quad (6.4.7c)$$

and $\alpha = m\pi/a$ and $\beta = n\pi/b$. The second column of thermal forces in Eq. (6.4.6) are valid for the case in which the temperature field is expanded in double cosine series.

6.4.3 Bending

The static solution can be obtained by setting the time derivative terms in Eq. (6.4.6) to zero:

$$\begin{bmatrix} \hat{c}_{11} & \hat{c}_{12} & \hat{c}_{13} \\ \hat{c}_{12} & \hat{c}_{22} & \hat{c}_{23} \\ \hat{c}_{13} & \hat{c}_{23} & \hat{c}_{33} + \tilde{s}_{33} \end{bmatrix} \begin{Bmatrix} U_{mn} \\ V_{mn} \\ W_{mn} \end{Bmatrix} = \begin{Bmatrix} 0 \\ 0 \\ Q_{mn} \end{Bmatrix} + \begin{Bmatrix} -\alpha N_{mn}^6 \\ -\beta N_{mn}^6 \\ \alpha^2 M_{mn}^1 + \beta^2 M_{mn}^2 \end{Bmatrix} \quad (6.4.8)$$

Using the static condensation procedure presented in Eqs. (6.3.22)–(6.3.26), we can determine the solution to Eq. (6.4.8) (when $\tilde{s}_{33} = 0$) as

$$\begin{aligned}W_{mn} &= \frac{1}{a_{mn}} \left[Q_{mn} + \alpha^2 M_{mn}^1 + \beta^2 M_{mn}^2 - \left(\frac{a_1}{a_0} \alpha + \frac{a_2}{a_0} \beta \right) N_{mn}^6 \right] \\ U_{mn} &= \frac{1}{a_0} \left[a_1 W_{mn} - (\alpha \hat{c}_{22} - \beta \hat{c}_{12}) N_{mn}^6 \right] \\ V_{mn} &= \frac{1}{a_0} \left[a_2 W_{mn} + (\alpha \hat{c}_{12} - \beta \hat{c}_{11}) N_{mn}^6 \right]\end{aligned}\quad (6.4.9a)$$

where

$$\begin{aligned}a_{mn} &= \hat{c}_{33} + \hat{c}_{13} \frac{a_1}{a_0} + \hat{c}_{23} \frac{a_2}{a_0}, \quad a_0 = \hat{c}_{11} \hat{c}_{22} - \hat{c}_{12} \hat{c}_{12} \\ a_1 &= \hat{c}_{12} \hat{c}_{23} - \hat{c}_{13} \hat{c}_{22}, \quad a_2 = \hat{c}_{13} \hat{c}_{12} - \hat{c}_{11} \hat{c}_{23}\end{aligned}\quad (6.4.9b)$$

Solution of Eq. (6.4.9a) for each $m, n = 1, 2, \dots$ gives (U_{mn}, V_{mn}, W_{mn}) , which can then be used to compute the solution (u_0, v_0, w_0) from Eq. (6.4.2a-c). If there are no thermal loads, the solution becomes

$$W_{mn} = \frac{Q_{mn}}{a_{mn}}, \quad U_{mn} = \frac{a_1 Q_{mn}}{a_0 a_{mn}}, \quad V_{mn} = \frac{a_2 Q_{mn}}{a_0 a_{mn}} \quad (6.4.9c)$$

6.4.4 Determination of Stresses

The stresses in each layer of an antisymmetric angle-ply laminate can be calculated from [see Eq. (6.3.29)]

$$\begin{Bmatrix} \sigma_{xx} \\ \sigma_{yy} \\ \sigma_{xy} \end{Bmatrix}^{(k)} = \begin{bmatrix} \bar{Q}_{11} & \bar{Q}_{12} & \bar{Q}_{16} \\ \bar{Q}_{12} & \bar{Q}_{22} & \bar{Q}_{26} \\ \bar{Q}_{16} & \bar{Q}_{26} & \bar{Q}_{66} \end{bmatrix}^{(k)} \left(\begin{Bmatrix} \varepsilon_{xx} \\ \varepsilon_{yy} \\ 2\varepsilon_{xy} \end{Bmatrix} - \begin{Bmatrix} \alpha_{xx} \\ \alpha_{yy} \\ 2\alpha_{xy} \end{Bmatrix} \Delta T \right) \quad (6.4.10)$$

$$\begin{aligned} \left(\begin{Bmatrix} \varepsilon_{xx} \\ \varepsilon_{yy} \\ 2\varepsilon_{xy} \end{Bmatrix} - \begin{Bmatrix} \alpha_{xx} \\ \alpha_{yy} \\ 2\alpha_{xy} \end{Bmatrix} \Delta T \right) &= \sum_{m=1}^{\infty} \sum_{n=1}^{\infty} \left\{ \begin{array}{l} \alpha U_{mn} g_{mn} - \alpha_{xx} T_{mn}^0 f_{mn} \\ \beta V_{mn} g_{mn} - \alpha_{yy} T_{mn}^0 f_{mn} \\ -(\beta U_{mn} + \alpha V_{mn} + 2\alpha_{xy} T_{mn}^0) f_{mn} \end{array} \right\} \\ &\quad + \sum_{m=1}^{\infty} \sum_{n=1}^{\infty} z \left\{ \begin{array}{l} (\alpha^2 W_{mn} - \alpha_{xx} T_{mn}^1) f_{mn} \\ (\beta^2 W_{mn} - \alpha_{yy} T_{mn}^1) f_{mn} \\ -2\alpha\beta W_{mn} g_{mn} - 2\alpha_{xy} T_{mn}^1 f_{mn} \end{array} \right\} \end{aligned} \quad (6.4.11a)$$

$$f_{mn} = \sin \alpha x \sin \beta y, \quad g_{mn} = \cos \alpha x \cos \beta y \quad (6.4.11b)$$

Note that the in-plane stresses in angle-ply laminates will have nonzero contributions from \bar{Q}_{66} . Also, the maxima of $(\sigma_{xx}, \sigma_{yy})$ occur at $(a/2, b/2)$, and they have contributions from $\varepsilon_{xy}^0, \varepsilon_{xx}^1$, and ε_{yy}^1 . The values of shear stress σ_{xy} at $(0, 0)$ and $(a/2, b/2)$ may be comparable, and relative maximum depends on the specific laminate construction.

The transverse stresses are determined as described in Section 6.3.4. For the isothermal case, we obtain

$$\begin{aligned} \sigma_{xz}^{(k)}(x, y, z) &= \sum_{m=1}^{\infty} \sum_{n=1}^{\infty} \left[(z - z_k) \bar{A}_{mn}^{(k)} + \frac{1}{2}(z^2 - z_k^2) \bar{B}_{mn}^{(k)} \right] + \sigma_{xz}^{(k-1)}(x, y, z_k) \\ \sigma_{yz}^{(k)}(x, y, z) &= \sum_{m=1}^{\infty} \sum_{n=1}^{\infty} \left[(z - z_k) \bar{C}_{mn}^{(k)} + \frac{1}{2}(z^2 - z_k^2) \bar{D}_{mn}^{(k)} \right] + \sigma_{yz}^{(k-1)}(x, y, z_k) \end{aligned} \quad (6.4.12a)$$

$$\sigma_{xz}^{(0)}(x, y, z_1) = 0, \quad \sigma_{yz}^{(0)}(x, y, z_1) = 0 \quad (6.4.12b)$$

where

$$\begin{aligned} \bar{A}_{mn}^{(k)} &= \left[\left(\alpha^2 \bar{Q}_{11}^{(k)} + \beta^2 \bar{Q}_{66}^{(k)} \right) U_{mn} + \alpha\beta \left(\bar{Q}_{12}^{(k)} + \bar{Q}_{66}^{(k)} \right) V_{mn} \right] \sin \alpha x \cos \beta y \\ &\quad + \left[2\alpha\beta \bar{Q}_{16}^{(k)} U_{mn} + \left(\alpha^2 \bar{Q}_{16}^{(k)} + \beta^2 \bar{Q}_{26}^{(k)} \right) V_{mn} \right] \cos \alpha x \sin \beta y \\ \bar{B}_{mn}^{(k)} &= - \left[\alpha^3 \bar{Q}_{11}^{(k)} + \alpha\beta^2 \left(\bar{Q}_{12}^{(k)} + 2\bar{Q}_{66}^{(k)} \right) \right] W_{mn} \cos \alpha x \sin \beta y \\ &\quad - \left(3\bar{Q}_{16}^{(k)} \alpha^2 \beta + \bar{Q}_{26}^{(k)} \beta^3 \right) W_{mn} \sin \alpha x \cos \beta y \\ \bar{C}_{mn}^{(k)} &= \left[\left(\alpha^2 \bar{Q}_{16}^{(k)} + \beta^2 \bar{Q}_{26}^{(k)} \right) U_{mn} + 2\alpha\beta \bar{Q}_{26}^{(k)} V_{mn} \right] \sin \alpha x \cos \beta y \\ &\quad + \left[\alpha\beta \left(\bar{Q}_{12}^{(k)} + \bar{Q}_{66}^{(k)} \right) U_{mn} + \left(\alpha^2 \bar{Q}_{66}^{(k)} + \beta^2 \bar{Q}_{22}^{(k)} \right) V_{mn} \right] \cos \alpha x \sin \beta y \\ \bar{D}_{mn}^{(k)} &= - \left(\bar{Q}_{16}^{(k)} \alpha^3 + 3\bar{Q}_{26}^{(k)} \alpha\beta^2 \right) W_{mn} \cos \alpha x \sin \beta y \\ &\quad - \left[\alpha^2 \beta \left(\bar{Q}_{12}^{(k)} + 2\bar{Q}_{66}^{(k)} \right) + \beta^3 \bar{Q}_{22}^{(k)} \right] W_{mn} \sin \alpha x \cos \beta y \end{aligned} \quad (6.4.12c)$$

The maxima of σ_{xz} and σ_{yz} occur at $(x, y) = (0, b/2)$ and $(x, y) = (a/2, 0)$, respectively, although their values at $(x, y) = (a/2, 0)$ and $(x, y) = (0, b/2)$, respectively, are not zero. The location of the maximum value through the thickness depends on the lamination scheme.

The bending moments in an antisymmetric angle-ply laminate can be calculated from Eq. (6.4.3), and it is given by the expression

$$\begin{Bmatrix} M_{xx} \\ M_{yy} \\ M_{xy} \end{Bmatrix} = \sum_{m=1}^{\infty} \sum_{n=1}^{\infty} \begin{bmatrix} 0 & 0 & B_{16} \\ 0 & 0 & B_{26} \\ B_{16} & B_{26} & 0 \end{bmatrix} \begin{Bmatrix} \alpha U_{mn} \cos \alpha x \cos \beta y \\ \beta V_{mn} \cos \alpha x \cos \beta y \\ -(\beta U_{mn} + \alpha V_{mn}) \sin \alpha x \sin \beta y \end{Bmatrix} \\ + \sum_{m=1}^{\infty} \sum_{n=1}^{\infty} \begin{bmatrix} D_{11} & D_{12} & 0 \\ D_{12} & D_{22} & 0 \\ 0 & 0 & D_{66} \end{bmatrix} \begin{Bmatrix} \alpha^2 W_{mn} \sin \alpha x \sin \beta y \\ \beta^2 W_{mn} \sin \alpha x \sin \beta y \\ -2\alpha\beta W_{mn} \cos \alpha x \cos \beta y \end{Bmatrix} \quad (6.4.13)$$

Note that the locations of the maximum values of M_{xx} , M_{yy} , and M_{xy} cannot be determined in the general case. However, when the coupling coefficients are zero, maximum values of M_{xx} and M_{yy} occur at $(x, y) = (a/2, b/2)$, and the maximum of M_{xy} occurs at $(x, y) = (0, 0)$.

The effect of bending-extension coupling and the dependence of the coupling on the modulus ratio can be seen from the deflections $\bar{w} = w_0(E_2 h^3/q_0 b^4)$ and stresses $\bar{\sigma}_{xx} = \sigma_{xx}(a/2, b/2, h/2)(h^2/q_0 b^2)$ presented in Table 6.4.1 for antisymmetric angle-ply laminates $(-45/45)_k$ for $k = 1, 2$, and 4 , and subjected to sinusoidal load (first line) and uniformly distributed load (second line). All laminates are of the same total thickness, and the layer properties are: E_1/E_2 varied, $G_{12} = G_{13} = 0.5E_2$, $G_{23} = 0.2E_2$, $\nu_{12} = 0.25$. The series for uniform load is evaluated using $m, n = 1, 3, \dots, 21$ terms. Note that with increasing number of layers the laminate solution does not tend towards the orthotropic plate solution.

Table 6.4.1: Effect of lamination scheme on the transverse deflections \bar{w} and stresses $\bar{\sigma}_{xx}$ in square angle-ply laminates $(-45/45)_k$.

Laminate	$\bar{w} \times 10^2$					Load					$\bar{\sigma}_{xx}$					
	$\frac{E_1}{E_2} = 1$	10	20	30	40	$\frac{E_1}{E_2} = 1$	10	20	30	40	$\frac{E_1}{E_2} = 1$	10	20	30	40	
0°	2.639	0.908	0.523	0.367	0.283	SSL	0.174	0.462	0.524	0.549	0.563	4.172	1.412	0.795	0.548	0.415
	4.172	1.412	0.795	0.548	0.415	UDL	0.251	0.693	0.772	0.795	0.801					
1†	2.887	1.117	0.757	0.577	0.467	SSL	0.190	0.217	0.242	0.256	0.265	4.577	1.759	1.190	0.906	0.732
	4.577	1.759	1.190	0.906	0.732	UDL	0.278	0.308	0.340	0.358	0.370					
2	2.887	0.636	0.345	0.237	0.181	SSL	0.190	0.153	0.147	0.145	0.144	4.577	0.999	0.542	0.372	0.283
	4.577	0.999	0.542	0.372	0.283	UDL	0.278	0.214	0.205	0.201	0.199					
4	2.887	0.574	0.304	0.207	0.157	SSL	0.190	0.151	0.146	0.144	0.143	4.577	0.902	0.477	0.324	0.245
	4.577	0.902	0.477	0.324	0.245	UDL	0.278	0.211	0.202	0.199	0.197					

† Denotes k in the laminate $(-45/45)_k$.

Figure 6.4.1 contains a plot of the nondimensionalized deflection \bar{w} versus plate aspect ratio for simply supported (SS-2) antisymmetric angle-ply laminates $(-45/45)_k$ under sinusoidal load. Figure 6.4.2 contains \bar{w} as a function of the lamination angle θ for square laminates $(-\theta/\theta)_k$ under sinusoidal load. The material properties used are $E_1/E_2 = 25$, $G_{12} = G_{13} = 0.5E_2$, and $\nu_{12} = 0.25$. Clearly, the bending-extension coupling is quite significant for two-layered plates, but the coupling decreases very rapidly as the number of layers is increased. Lastly, nondimensionalized transverse deflections as a function of the modulus ratio for square laminates under sinusoidal transverse load are presented in Figure 6.4.3. The effect of coupling is significant for all modulus ratios except for those close to unity.

Figures 6.4.4 and 6.4.5 show the plots of nondimensionalized transverse shear stresses $\bar{\sigma}_{xz}(0, b/2, z) = \bar{\sigma}_{yz}(a/2, 0, z)$ and $\bar{\sigma}_{xz}(a/2, 0, z) = \bar{\sigma}_{yz}(0, b/2, z)$, respectively, for two-layer and eight-layer antisymmetric angle-ply laminates $(-45/45/-45/\dots)$ under sinusoidally distributed transverse load ($a/b = 1$, $E_1 = 25E_2$, $G_{12} = G_{13} = 0.5E_2$, $\nu_{12} = 0.25$). Unlike in antisymmetric cross-ply laminates, the stress $\bar{\sigma}_{xz}$ is not zero at $(x, y) = (a/2, 0)$, although small in magnitude compared to that at $(x, y) = (0, b/2)$. Note that through-thickness variations are significantly altered when the number of layers are increased (for the same total laminate thickness). The parabolic type variation shown in Figure 6.4.4 is consistent with that of an orthotropic plate.

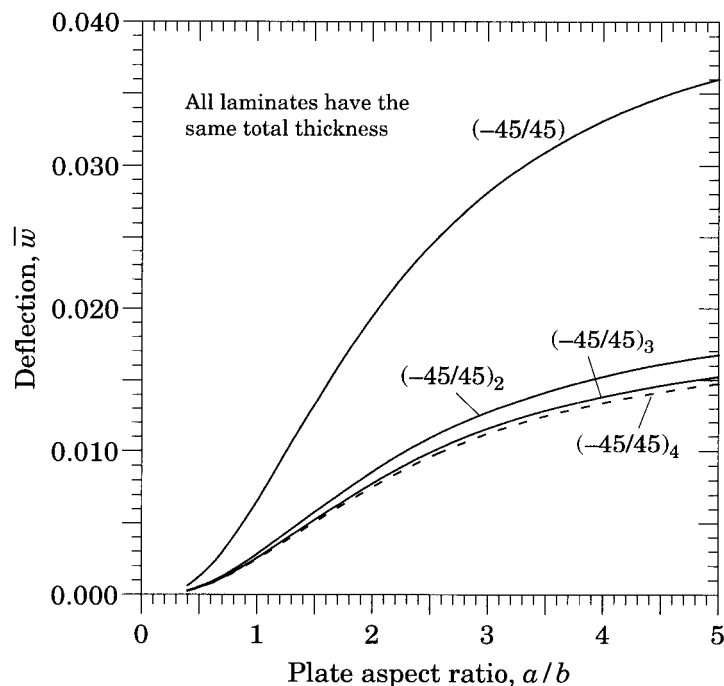


Figure 6.4.1: Nondimensionalized maximum transverse deflection (\bar{w}) versus plate aspect ratio (a/b) for antisymmetric angle-ply $(-45/45)_n$ ($n = 1, 2, 3, 4$) laminates under sinusoidal load.

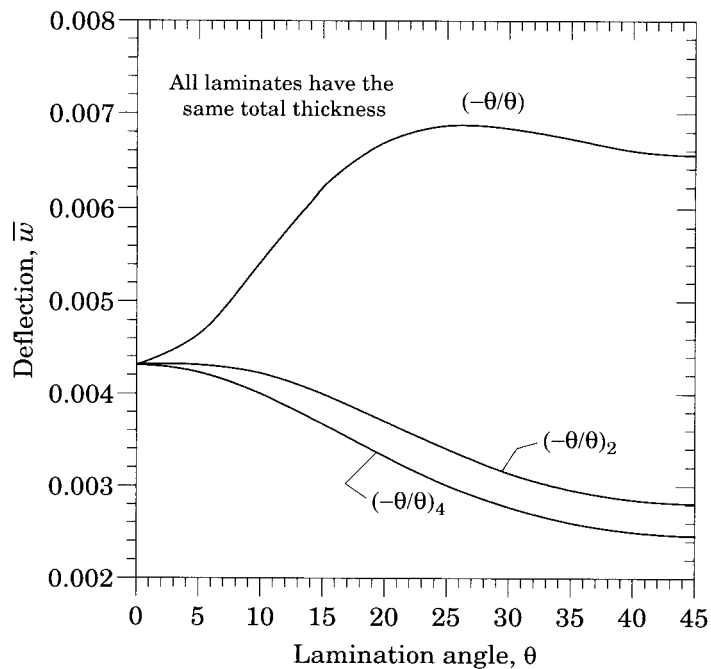


Figure 6.4.2: Nondimensionalized maximum transverse deflection (\bar{w}) versus lamination angle (θ) for antisymmetric angle-ply $(-\theta/\theta)_n$ ($n = 1, 2, 4$) laminates under sinusoidal load.

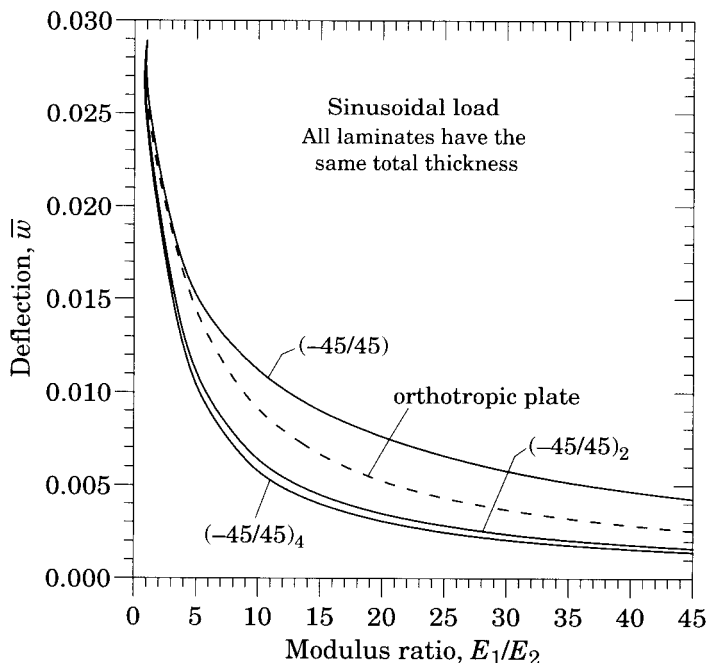


Figure 6.4.3: Nondimensionalized maximum transverse deflection (\bar{w}) versus modulus ratio (E_1/E_2) for antisymmetric angle-ply $(-45/45)_n$ ($n = 1, 2, 4$) laminates under sinusoidal load.

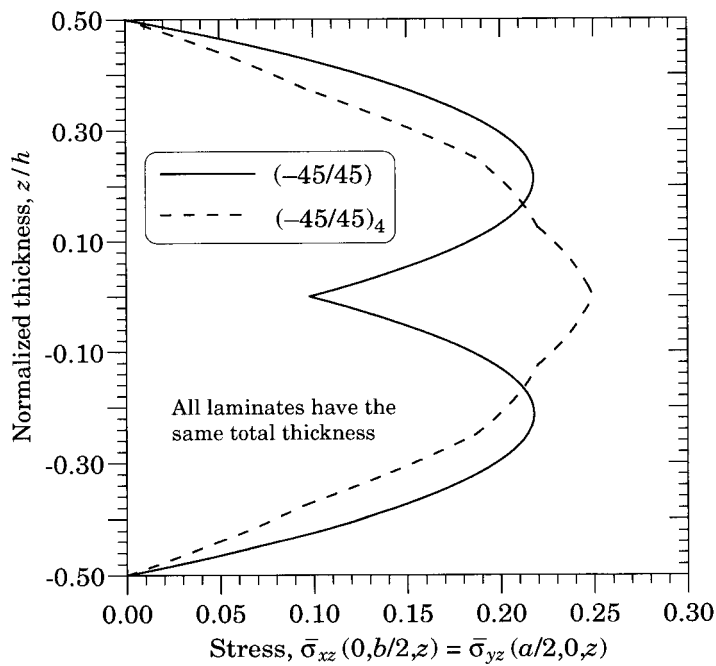


Figure 6.4.4: Variation of the nondimensionalized maximum transverse shear stresses through the thickness of antisymmetric angle-ply $(-45/45)_n$ laminates.

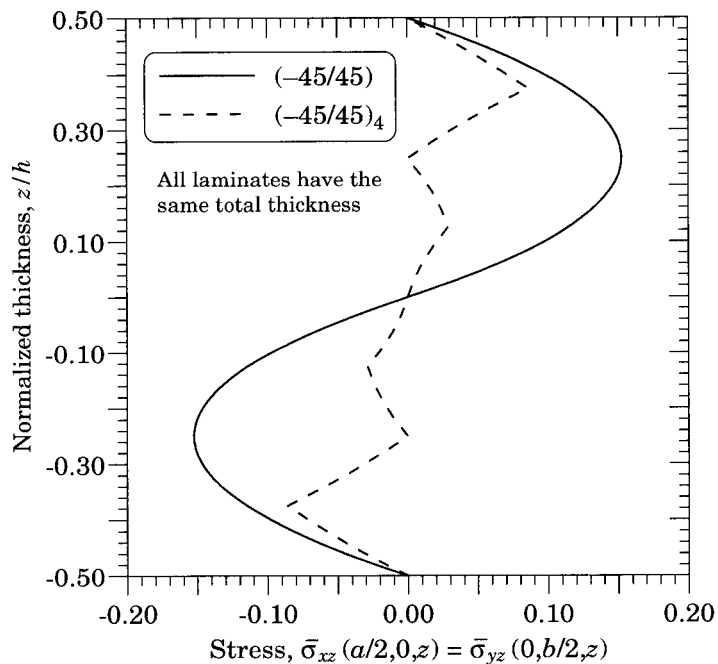


Figure 6.4.5: Variation of the nondimensionalized maximum transverse shear stresses through the thickness of antisymmetric angle-ply $(-45/45)_n$ laminates.

6.4.5 Buckling

For buckling analysis, we assume that the only applied loads are the in-plane forces and all other mechanical and thermal loads are zero:

$$\hat{N}_{xx} = -N_0, \quad \hat{N}_{yy} = -kN_0, \quad k = \frac{\hat{N}_{yy}}{\hat{N}_{xx}} \quad (6.4.14)$$

From Eq. (6.4.6) we have

$$\begin{bmatrix} \hat{c}_{11} & \hat{c}_{12} & \hat{c}_{13} \\ \hat{c}_{12} & \hat{c}_{22} & \hat{c}_{23} \\ \hat{c}_{13} & \hat{c}_{23} & \hat{c}_{33} - N_0(\alpha^2 + k\beta^2) \end{bmatrix} \begin{Bmatrix} U_{mn} \\ V_{mn} \\ W_{mn} \end{Bmatrix} = \begin{Bmatrix} 0 \\ 0 \\ 0 \end{Bmatrix} \quad (6.4.15)$$

where \hat{c}_{ij} are the coefficients defined in Eq. (6.4.7a). Setting the determinant of the coefficient matrix in (6.4.15) to zero, we obtain

$$\begin{aligned} N_0 &= \frac{1}{\alpha^2 + k\beta^2} \left(\hat{c}_{33} - \frac{\hat{c}_{13}\hat{c}_{22} - \hat{c}_{23}\hat{c}_{12}}{\hat{c}_{11}\hat{c}_{22} - \hat{c}_{12}\hat{c}_{12}} \hat{c}_{13} - \frac{\hat{c}_{11}\hat{c}_{23} - \hat{c}_{12}\hat{c}_{13}}{\hat{c}_{11}\hat{c}_{22} - \hat{c}_{12}\hat{c}_{12}} \hat{c}_{23} \right) \\ &= \frac{1}{\alpha^2 + k\beta^2} \left(\hat{c}_{33} + \frac{2\hat{c}_{12}\hat{c}_{23}\hat{c}_{13} - \hat{c}_{22}\hat{c}_{13}^2 - \hat{c}_{11}\hat{c}_{23}^2}{\hat{c}_{11}\hat{c}_{22} - \hat{c}_{12}^2} \right) \end{aligned} \quad (6.4.16)$$

Clearly, for each pair of m and n , there is a unique value of N_0 . The critical buckling load is the smallest of all $N_0 = N_0(m, n)$. Since \hat{c}_{ij} depend on m and n , $N_0(m, n)$ is a complicated function of both m and n and no conclusions can be drawn about the mode (m, n) at buckling.

For specially orthotropic laminates (i.e., a plate made up of a single specially orthotropic layer or a laminate consisting of specially orthotropic layers that are symmetrically arranged about the laminate middle surface), the only nonzero stiffnesses are $A_{11}, A_{12}, A_{22}, A_{66}, D_{11}, D_{12}, D_{22}$, and D_{66} . Thus, neither shear or twist coupling nor bending-extension coupling exists. For biaxial compressive in-plane loading, the buckling load is given by Eq. (6.3.45). The *specially orthotropic solution* for antisymmetric angle-ply laminates is the one that corresponds to the case in which $A_{16}, A_{26}, B_{16}, B_{26}, D_{16}$, and D_{26} are zero.

Table 6.4.2 contains nondimensionalized buckling loads ($\bar{N} = N_{cr}b^2/E_2h^3$) of antisymmetric angle-ply laminates under uniaxial and biaxial in-plane compressive loads. The material properties used for a typical lamina are $G_{12} = 0.5E_2$, and $\nu_{12} = 0.25$. The buckling mode is (1,1), except for uniaxial compression with aspect ratio equal to 1.5.

Plots of nondimensionalized critical buckling loads versus plate aspect ratio (a/b) for simply supported (SS-2) angle-ply laminates (45/-45) _{k} under uniaxial compressive in-plane loads are presented in Figure 6.4.6 for $E_1/E_2 = 40$, $G_{12} = G_{13} = 0.5E_2$, and $\nu_{12} = 0.25$. The buckling mode associated with the critical buckling load is $(m, n) = (1, 1)$ for $a/b \leq 1.4$, $(m, n) = (2, 1)$ for $1.5 \leq a/b \leq 2.4$, $(m, n) = (3, 1)$ for $2.5 \leq a/b \leq 3.4$, $(m, n) = (4, 1)$ for $3.5 \leq a/b \leq 4.4$, and $(m, n) = (5, 1)$ for $4.5 \leq a/b \leq 5$. The effect of bending-stretching coupling is the most for two-layer laminates, and the orthotropic solution is rapidly approached as the number of plies is increased.

Table 6.4.2: Effect of coupling, plate aspect ratio, and modulus ratio on the nondimensionalized critical buckling load, $\bar{N} = N_{cr} \frac{b^2}{E_2 h^3}$, of rectangular laminates under uniform compression and biaxial compression (E_1/E_2 varied, $G_{12} = G_{13} = 0.5E_2$, $\nu_{12} = 0.25$).

$\frac{a}{b}$	(45/-45)				(45/-45) ₄			
	10 [†]	20	25	40	10	20	25	40
Uniaxial compression ($k = 0$)								
0.5	12.633	18.140	20.825	28.809	23.746	43.841	53.888	84.020
1.0	9.060	13.373	15.475	21.713	17.637	33.320	41.166	64.685
1.5*	9.603	23.963	16.285	22.779	18.565	34.909	43.091	67.607
Biaxial compression ($k = 1$)								
0.5	11.893	14.518	16.660	23.045	18.999	35.076	43.110	67.222
1.0	4.530	6.692	7.738	10.856	8.813	16.660	20.578	32.343
1.5	3.129	9.021	5.270	7.353	6.001	11.251	13.877	21.743

[†] Modulus ratio.

* Mode is (2,1) for this row ($a/b = 1.5$); for all other cases, the mode is (1,1).

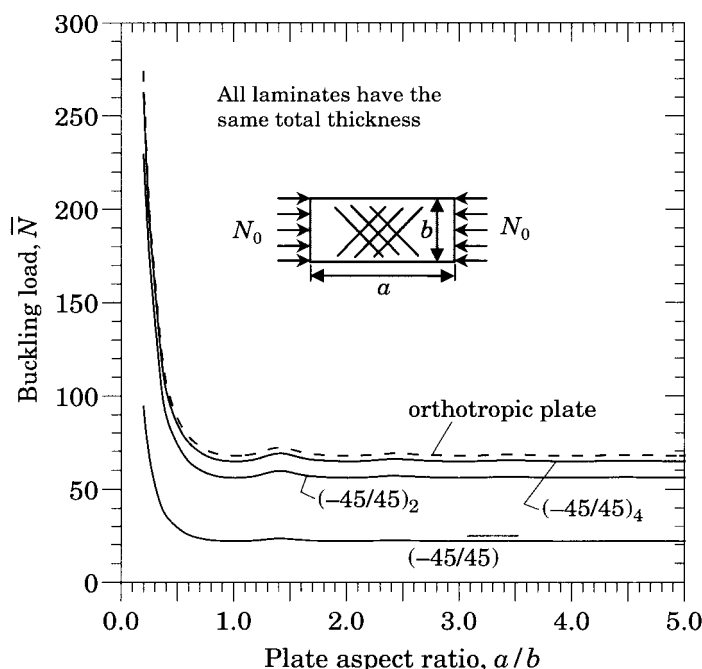


Figure 6.4.6: Nondimensionalized buckling load ($\bar{N} = N_{cr} \frac{b^2}{E_2 h^3}$) versus plate aspect ratio (a/b) of antisymmetric angle-ply laminates under uniaxial compressive edge load.

Nondimensionalized critical buckling loads versus the lamination angle for uniaxial compression ($k = 0$) and biaxial compression ($k = 1$) antisymmetric angle-ply square laminates are shown in Figures 6.4.7 and 6.4.8, respectively, for $E_1 = 40E_2$, $G_{12} = 0.5E_2$, and $\nu_{12} = 0.25$. The plots shown in Figure 6.4.8 are symmetric about $\theta = 45^\circ$. Note that, once again, the bending-stretching coupling severely reduces the buckling load for the two-layer plate. The effect is negligible for eight or more layers. The buckling load is the maximum for $\theta = 45^\circ$.

6.4.6 Vibration

For free vibration Eq. (6.4.6) reduces to the eigenvalue problem

$$\left(\begin{bmatrix} \hat{c}_{11} & \hat{c}_{12} & \hat{c}_{13} \\ \hat{c}_{12} & \hat{c}_{22} & \hat{c}_{23} \\ \hat{c}_{13} & \hat{c}_{23} & \hat{c}_{33} \end{bmatrix} - \omega^2 \begin{bmatrix} \hat{m}_{11} & 0 & 0 \\ 0 & \hat{m}_{22} & 0 \\ 0 & 0 & \hat{m}_{33} \end{bmatrix} \right) \begin{Bmatrix} U_{mn}^0 \\ V_{mn}^0 \\ W_{mn}^0 \end{Bmatrix} = \begin{Bmatrix} 0 \\ 0 \\ 0 \end{Bmatrix} \quad (6.4.17)$$

where \hat{c}_{ij} and \hat{m}_{ij} are defined in Eq. (6.4.7). Setting the determinant of the coefficient matrix in (6.4.17) to zero, we obtain the cubic characteristic polynomial

$$-p\lambda^3 + q\lambda^2 - r\lambda + s = 0 \quad (6.4.18)$$

in the eigenvalue $\lambda = \omega^2$, where

$$\begin{aligned} p &= \begin{vmatrix} \hat{m}_{11} & 0 & 0 \\ 0 & \hat{m}_{22} & 0 \\ 0 & 0 & \hat{m}_{33} \end{vmatrix}, \quad s = \begin{vmatrix} \hat{c}_{11} & \hat{c}_{12} & \hat{c}_{13} \\ \hat{c}_{12} & \hat{c}_{22} & \hat{c}_{23} \\ \hat{c}_{13} & \hat{c}_{23} & \hat{c}_{33} \end{vmatrix} \\ q &= \begin{vmatrix} \hat{c}_{11} & 0 & 0 \\ \hat{c}_{12} & \hat{m}_{22} & 0 \\ \hat{c}_{13} & 0 & \hat{m}_{33} \end{vmatrix} + \begin{vmatrix} \hat{m}_{11} & \hat{c}_{12} & 0 \\ \hat{0} & \hat{c}_{22} & 0 \\ 0 & \hat{c}_{23} & \hat{m}_{33} \end{vmatrix} + \begin{vmatrix} \hat{m}_{11} & 0 & \hat{c}_{13} \\ \hat{0} & \hat{m}_{22} & \hat{c}_{23} \\ 0 & 0 & \hat{c}_{33} \end{vmatrix} \\ r &= \begin{vmatrix} \hat{c}_{11} & \hat{c}_{12} & 0 \\ \hat{c}_{12} & \hat{c}_{22} & 0 \\ \hat{c}_{13} & \hat{c}_{23} & \hat{m}_{33} \end{vmatrix} + \begin{vmatrix} \hat{c}_{11} & \hat{0} & \hat{c}_{13} \\ \hat{c}_{12} & \hat{m}_{22} & \hat{c}_{23} \\ \hat{c}_{13} & 0 & \hat{c}_{33} \end{vmatrix} + \begin{vmatrix} \hat{m}_{11} & \hat{c}_{12} & \hat{c}_{13} \\ \hat{0} & \hat{c}_{22} & \hat{c}_{23} \\ 0 & \hat{c}_{23} & \hat{c}_{33} \end{vmatrix} \end{aligned} \quad (6.4.19)$$

If the in-plane inertias are neglected (i.e., $\hat{m}_{11} = \hat{m}_{22} = 0$), Eq. (6.4.17) yields

$$\omega^2 = \frac{1}{\hat{m}_{33}} \left(\hat{c}_{33} - \frac{\hat{c}_{13}\hat{c}_{22} - \hat{c}_{23}\hat{c}_{12}}{\hat{c}_{11}\hat{c}_{22} - \hat{c}_{12}\hat{c}_{12}} \hat{c}_{13} - \frac{\hat{c}_{11}\hat{c}_{23} - \hat{c}_{12}\hat{c}_{13}}{\hat{c}_{11}\hat{c}_{22} - \hat{c}_{12}\hat{c}_{12}} \hat{c}_{23} \right) \quad (6.4.20)$$

Note that ω is a function of the mode numbers (m, n) because the coefficients \hat{c}_{ij} depend on m and n , as shown in Eq. (6.4.7a).

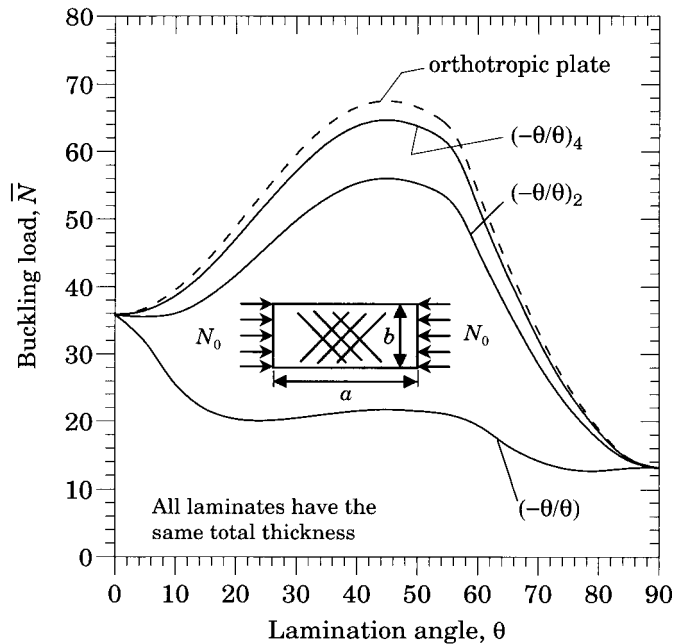


Figure 6.4.7: Nondimensionalized buckling load (\bar{N}) versus lamination angle (θ) of antisymmetric angle-ply square laminates under uniaxial compressive edge load ($k = 0$).

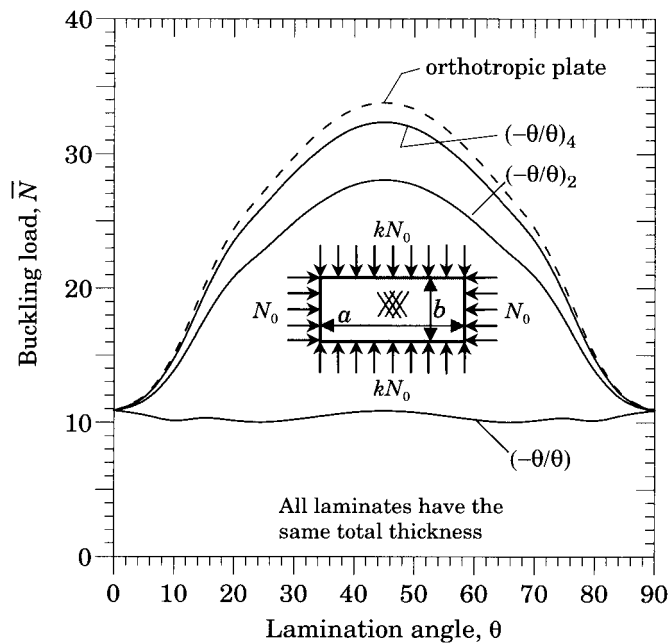


Figure 6.4.8: Nondimensionalized buckling load (\bar{N}) versus lamination angle (θ) of antisymmetric angle-ply square laminates under biaxial compressive edge loads ($k = 1$).

Nondimensionalized fundamental frequencies $\bar{\omega} = \omega(b^2/\pi^2)\sqrt{\rho h/D_{22}}$ of graphite-epoxy composites with $E_1/E_2 = 40$, $G_{12}/E_2 = 0.5$, $\nu_{12} = 0.25$ and $a/b = 1$ are shown as a function of lamination angle in Figure 6.4.9. The bending-stretching coupling due to the presence of B_{16} and B_{26} has the effect of lowering the frequencies. The coupling is the maximum for two-layer plates, and it rapidly decreases with increasing number of layers. At $\theta = 45^\circ$, the fundamental frequency of the two-layer plate is about 40 percent lower than that of the eight-layer laminate. The same conclusions hold for results presented in Figures 6.4.10 and 6.4.11. The effect of coupling is significant for all modulus ratios, and the difference between the two-layer solution and orthotropic solution increases with modulus ratio.

6.5 The Lévy Solutions

6.5.1 Introduction

The Lévy method can be used to solve the governing equations of various plate theories for rectangular laminates for which two (parallel) opposite edges are simply supported and the other two edges can have any boundary conditions. Here we describe the Lévy solution procedure for cross-ply and antisymmetric angle-ply laminates using the classical laminate plate theory (CLPT). However, details are presented for only cross-ply laminates.

Consider a rectangular laminate which has an even number of orthotropic layers with principal material directions alternating at 0° and 90° to the laminate axes (i.e., antisymmetric cross-ply laminate). The planar dimensions are taken to be a and b , and the total thickness h . The laminate coordinate system (x, y, z) is taken

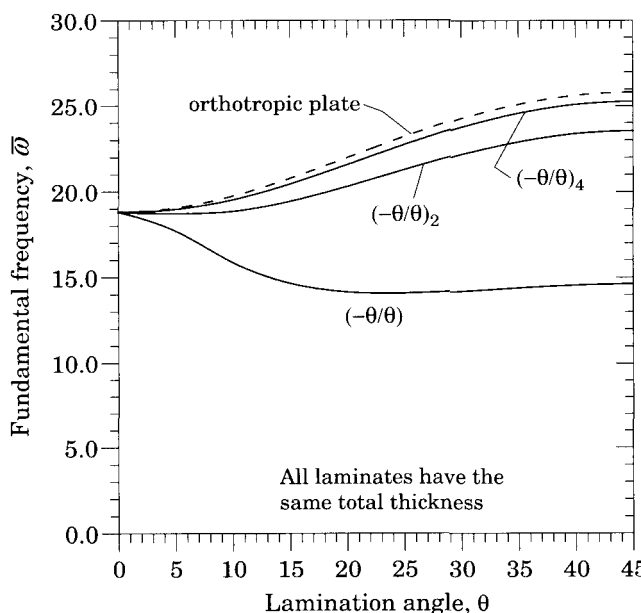


Figure 6.4.9: Nondimensionalized fundamental frequency versus lamination angle (θ) of antisymmetric angle-ply square laminates.

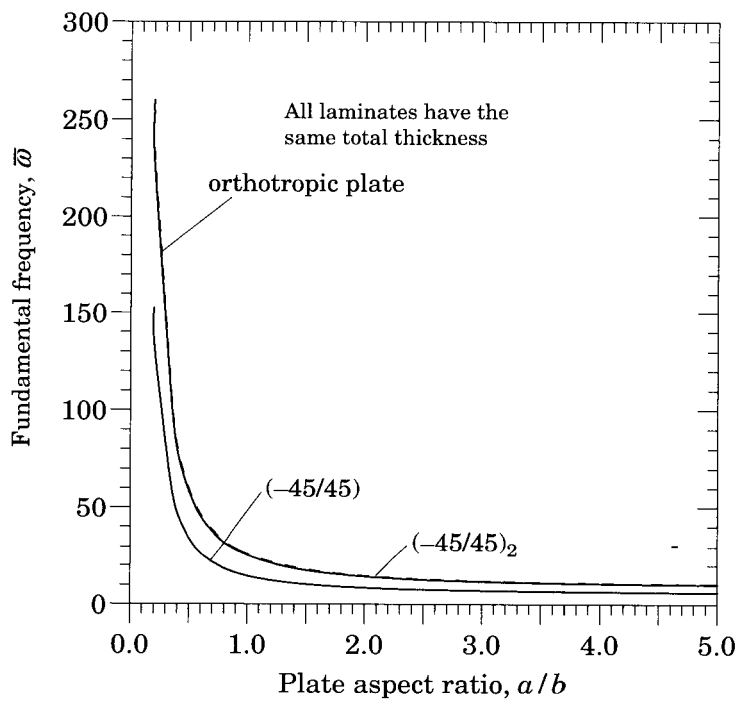


Figure 6.4.10: Nondimensionalized fundamental frequency ($\bar{\omega}$) versus plate aspect ratio (a/b) of antisymmetric angle-ply laminates.

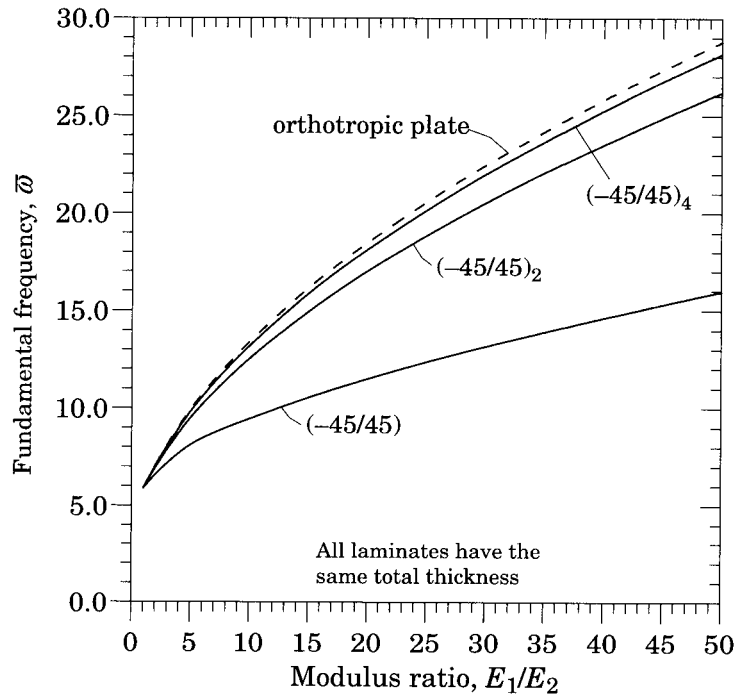


Figure 6.4.11: Nondimensionalized fundamental frequency ($\bar{\omega}$) versus modulus ratio E_1/E_2 of antisymmetric angle-ply square laminates.

such that to be a and b , and the total thickness h . The laminate coordinate system (x, y, z) is taken such that $-a/2 \leq x \leq a/2, 0 \leq y \leq b, -h/2 \leq z \leq h/2$, as shown in Figure 6.5.1. Here we assume that the edges $y = 0, b$ are simply supported, and the other two edges can each have arbitrary boundary conditions (e.g., simply supported, clamped, or free). The type of the boundary conditions for the classical laminate plate theory were derived in Section 5.3 [see Eq. (3.3.34)]. Note that only one quantity in each of the following pairs should be specified on the boundary:

$$(u_n, N_{nn}), (u_s, N_{ns}), (w_0, V_n), (\frac{\partial w_0}{\partial n}, M_{nn}) \quad (6.5.1)$$

where n refers to the normal and s to the tangential directions at the boundary point.

The simply supported boundary conditions on edges $y = 0, b$ ($n = \mp y, s = \mp x, u_n = v_0, u_s = u_0$, etc.) are expressed as follows:

$$u_0 = 0, N_{yy} = 0, w_0 = 0, M_{yy} = 0 \quad (6.5.2)$$

One of the following three types of boundary conditions may be used on the remaining two edges, $x = \mp \frac{a}{2}$ ($n = \mp x$ and $s = \mp y$):

Simply supported (S):

$$N_{xx} = 0, v_0 = 0, w_0 = 0, M_{xx} = 0 \quad (6.5.3)$$

Clamped (C):

$$u_0 = 0, v_0 = 0, w_0 = 0, \frac{\partial w_0}{\partial x} = 0 \quad (6.5.4)$$

Free (F):

$$N_{xx} = 0, N_{xy} = 0, V_x \equiv \frac{\partial M_{xx}}{\partial x} + 2 \frac{\partial M_{xy}}{\partial y} = 0, M_{xx} = 0 \quad (6.5.5)$$

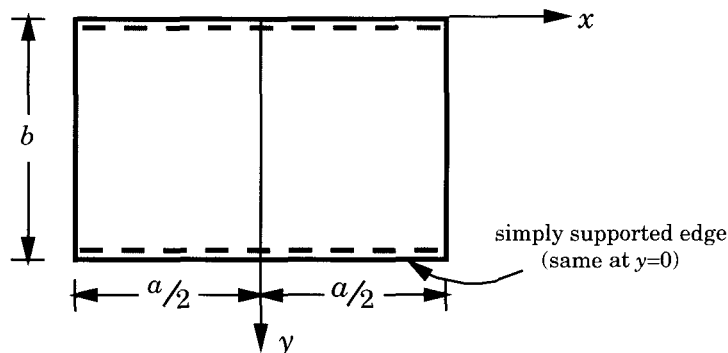


Figure 6.5.1: The coordinate system used in the Lévy solution.

The basic idea of the Lévy method is to seek a solution that satisfies the boundary conditions along the simply supported edges exactly, and thereby reduce the two-dimensional problem to a one-dimensional problem with respect to the coordinate x . This results in ordinary differential equations in x , which involve usually second- or higher-order derivatives of the unknown coefficients of the displacement expansion. These ordinary differential equations are then solved using the so-called *state-space approach* (see Brogan [2] or Franklin [3]).

For the case of antisymmetric cross-ply laminates, we have

$$B_{16} = B_{26} = A_{16} = A_{26} = D_{16} = D_{26} = 0 \quad (6.5.6)$$

Consequently, from Eqs. (6.2.1)–(6.2.3), we have the following equations of motion of the classical laminate theory for the isothermal case:

$$\begin{aligned} & A_{11} \frac{\partial^2 u_0}{\partial x^2} + A_{66} \frac{\partial^2 u_0}{\partial y^2} + (A_{12} + A_{66}) \frac{\partial^2 v_0}{\partial x \partial y} \\ & - \left[B_{11} \frac{\partial^3 w_0}{\partial x^3} + (B_{12} + 2B_{66}) \frac{\partial^3 w_0}{\partial x \partial y^2} \right] = I_0 \ddot{u}_0 - I_1 \frac{\partial \ddot{w}_0}{\partial x} \end{aligned} \quad (6.5.7)$$

$$\begin{aligned} & (A_{12} + A_{66}) \frac{\partial^2 u_0}{\partial x \partial y} + A_{66} \frac{\partial^2 v_0}{\partial x^2} + A_{22} \frac{\partial^2 v_0}{\partial y^2} \\ & - \left[(B_{12} + 2B_{66}) \frac{\partial^3 w_0}{\partial x^2 \partial y} + B_{22} \frac{\partial^3 w_0}{\partial y^3} \right] = I_0 \ddot{v}_0 - I_1 \frac{\partial \ddot{w}_0}{\partial y} \end{aligned} \quad (6.5.8)$$

$$\begin{aligned} & B_{11} \frac{\partial^3 u_0}{\partial x^3} + (B_{12} + 2B_{66}) \left(\frac{\partial^3 u_0}{\partial x \partial y^2} + \frac{\partial^3 v_0}{\partial x^2 \partial y} \right) + B_{22} \frac{\partial^3 v_0}{\partial y^3} \\ & - \left[D_{11} \frac{\partial^4 w_0}{\partial x^4} + 2(D_{12} + 2D_{66}) \frac{\partial^4 w_0}{\partial x^2 \partial y^2} + D_{22} \frac{\partial^4 w_0}{\partial y^4} \right] \\ & + \hat{N}_{xx} \frac{\partial^2 w_0}{\partial x^2} + 2\hat{N}_{xy} \frac{\partial^2 w_0}{\partial x \partial y} + \hat{N}_{yy} \frac{\partial^2 w_0}{\partial y^2} + q \\ & = I_1 \left(\frac{\partial \ddot{u}_0}{\partial x} + \frac{\partial \ddot{v}_0}{\partial y} \right) + I_0 \ddot{w}_0 - I_2 \left(\frac{\partial^2 \ddot{w}_0}{\partial x^2} + \frac{\partial^2 \ddot{w}_0}{\partial y^2} \right) \end{aligned} \quad (6.5.9)$$

6.5.2 Solution Procedure

In the Lévy type procedure, we assume the following representation of the displacements:

$$\begin{aligned} u_0(x, y, t) &= \sum_{m=1}^{\infty} U_m(x, t) \sin \beta y \\ v_0(x, y, t) &= \sum_{m=1}^{\infty} V_m(x, t) \cos \beta y \\ w_0(x, y, t) &= \sum_{m=1}^{\infty} W_m(x, t) \sin \beta y \end{aligned} \quad (6.5.10a)$$

where $\beta = (m\pi/b)$. The transverse load is expanded as

$$q(x, y, t) = \sum_{m=1}^{\infty} Q_m(x, t) \sin \beta y \quad (6.5.10b)$$

where (U_m, V_m, W_m) , and Q_m denote amplitudes of (u_0, v_0, w_0) , and q , respectively. These expansions satisfy the simply supported (SS-1) boundary conditions (6.5.2) on edges $y = 0, b$.

The stress resultants derived from the displacement field (6.5.10a) are given by

$$\begin{aligned} N_{xx} &= \sum_{m=1}^{\infty} \left(A_{11}U'_m - \beta A_{12}V_m + \beta^2 B_{12}W_m - B_{11}W''_m \right) \sin \beta y \\ N_{yy} &= \sum_{m=1}^{\infty} \left(A_{12}U'_m - \beta A_{22}V_m + \beta^2 B_{22}W_m - B_{12}W''_m \right) \sin \beta y \\ N_{xy} &= \sum_{m=1}^{\infty} \left(\beta A_{66}U_m + A_{66}V'_m - 2\beta B_{66}W'_m \right) \cos \beta y \\ M_{xx} &= \sum_{m=1}^{\infty} \left(B_{11}U'_m - \beta B_{12}V_m + \beta^2 D_{12}W_m - D_{11}W''_m \right) \sin \beta y \\ M_{yy} &= \sum_{m=1}^{\infty} \left(B_{12}U'_m - \beta B_{22}V_m + \beta^2 D_{22}W_m - D_{12}W''_m \right) \sin \beta y \\ M_{xy} &= \sum_{m=1}^{\infty} \left(\beta B_{66}U_m + B_{66}V'_m - 2\beta D_{66}W'_m \right) \cos \beta y \\ \frac{\partial M_{xx}}{\partial x} &= \sum_{m=1}^{\infty} \left(B_{11}U''_m - \beta B_{12}V'_m + \beta^2 D_{12}W'_m - D_{11}W'''_m \right) \sin \beta y \\ \frac{\partial M_{xy}}{\partial y} &= \sum_{m=1}^{\infty} \left(-\beta^2 B_{66}U_m - \beta B_{66}V'_m + 2\beta^2 D_{66}W'_m \right) \sin \beta y \\ \frac{\partial M_{yy}}{\partial y} &= \sum_{m=1}^{\infty} \left(\beta B_{12}U'_m - \beta^2 B_{22}V_m - \beta D_{12}W''_m + \beta^3 D_{22}W_m \right) \cos \beta y \\ \frac{\partial M_{xy}}{\partial x} &= \sum_{m=1}^{\infty} \left(\beta B_{66}U'_m + B_{66}V''_m - 2\beta D_{66}W''_m \right) \cos \beta y \end{aligned} \quad (6.5.11)$$

The boundary conditions in (6.5.3)–(6.5.5) on edges $x = \mp a/2$ require that (U_m, V_m, W_m) and their derivatives with respect to x satisfy the following boundary conditions:

Simply supported ($A_{11}D_{11} - B_{11}^2 \neq 0$):

$$U'_m = 0, \quad V_m = 0, \quad W_m = 0, \quad W''_m = 0 \quad (6.5.12)$$

Clamped:

$$U_m = 0, \quad V_m = 0, \quad W_m = 0, \quad W'_m = 0 \quad (6.5.13)$$

Free:

$$A_{11}U'_m - \beta A_{12}V_m + \beta^2 B_{12}W_m - B_{11}W''_m = 0 \quad (6.5.14a)$$

$$\beta A_{66}U_m + A_{66}V'_m - 2\beta B_{66}W'_m = 0 \quad (6.5.14b)$$

$$\begin{aligned} -2\beta^2 B_{66}U_m + B_{11}U''_m - \beta(B_{12} + 2B_{66})V'_m \\ + \beta^2(D_{12} + 4D_{66})W'_m - D_{11}W'''_m = 0 \end{aligned} \quad (6.5.14c)$$

$$B_{11}U'_m - \beta B_{12}V_m + \beta^2 D_{12}W_m - D_{11}W''_m = 0 \quad (6.5.14d)$$

Substituting Eq. (6.5.10) into Eqs. (6.5.7)–(6.5.9), expressing the results in terms of the highest derivatives U''_m , V''_m , and W'''_m , and substituting for U''_m and V''_m into the expression for W'''_m , we obtain (when $\hat{N}_{xy} = 0$)

$$U''_m = C_1U_m + C_2V'_m - C_3W'_m + C_4W'''_m + D_1\ddot{U}_m - D_2\ddot{W}'_m \quad (6.5.15a)$$

$$V''_m = -C_5U'_m + C_6V_m - C_7W_m + C_8W''_m + D_3\ddot{V}_m - D_4\ddot{W}_m \quad (6.5.15b)$$

$$\begin{aligned} W'''_m = C_9U'_m + C_{10}V_m + C_{11}W_m + C_{12}W''_m + C_0Q_m \\ + D_5\ddot{U}'_m + D_6\ddot{V}_m + D_7\ddot{W}_m + D_8\ddot{W}''_m \end{aligned} \quad (6.5.15c)$$

The coefficients C_i appearing in Eqs. (6.5.15) are

$$\begin{aligned} C_1 &= \frac{e_2}{e_1}, \quad C_2 = \frac{e_3}{e_1}, \quad C_3 = \frac{e_4}{e_1}, \quad C_4 = \frac{e_5}{e_1} \\ C_5 &= \frac{e_3}{e_6}, \quad C_6 = \frac{e_7}{e_6}, \quad C_7 = \frac{e_8}{e_6}, \quad C_8 = \frac{e_9}{e_6} \\ C_9 &= [-e_4 + e_5C_1 + (e_9 - e_5C_2)C_5]C_0 \\ C_{10} &= [e_8 - (e_9 - e_5C_2)]C_0, \quad C_0 = (e_{13})^{-1} \\ C_{11} &= [-e_{11} - (e_9 - e_5C_2)C_7]C_0 \\ C_{12} &= [e_{12} - e_5C_3 - (e_9 - e_5C_2)C_8]C_0 \\ D_1 &= \frac{d_1}{e_1}, \quad D_2 = \frac{d_2}{e_1}, \quad D_3 = \frac{d_1}{e_6}, \quad D_4 = \frac{d_3}{e_6} \\ D_5 &= (e_5D_1 - d_2)C_0, \quad D_6 = [d_3 + (e_5C_2 - e_9)D_3]C_0 \\ D_7 &= [-d_4 + (e_9 - e_5C_2)D_4]C_0, \quad D_8 = (d_5 - e_5D_2)C_0 \end{aligned} \quad (6.5.16a)$$

where

$$\begin{aligned} e_1 &= A_{11}, \quad e_2 = \beta^2 A_{66}, \quad e_3 = \beta(A_{12} + A_{66}), \quad e_4 = \beta^2(B_{12} + 2B_{66}), \quad e_5 = B_{11} \\ e_6 &= A_{66}, \quad e_7 = \beta^2 A_{22}, \quad e_8 = \beta^3 B_{22}, \quad e_9 = \beta(B_{12} + 2B_{66}), \quad e_{10} = D_{11} \\ e_{11} &= (\beta^4 D_{22} + \beta^2 \hat{N}_{yy}), \quad e_{12} = 2\beta^2(D_{12} + 2D_{66}) + \hat{N}_{xx}, \quad e_{13} = e_{10} - e_5C_4 \\ d_1 &= I_0, \quad d_2 = I_1, \quad d_3 = I_1\beta, \quad d_4 = I_0 + \beta^2 I_2, \quad d_5 = I_2 \end{aligned} \quad (6.5.16b)$$

The linear system of ordinary differential equations in (6.5.15) with constant coefficients can be expressed in the form of a single, first-order, matrix differential equation

$$\{Z'\} = [T]\{Z\} + \{F\} \quad (6.5.17)$$

where

$$\{Z\} = \begin{Bmatrix} U_m \\ U'_m \\ V_m \\ V'_m \\ W_m \\ W'_m \\ W''_m \\ W'''_m \end{Bmatrix}, \quad \{F\} = \begin{Bmatrix} 0 \\ D_1 \ddot{U}_m - D_2 \ddot{W}'_m \\ 0 \\ D_3 \ddot{V}_m - D_4 \ddot{W}_m \\ 0 \\ 0 \\ 0 \\ \hat{Q}_m \end{Bmatrix} \quad (6.5.18a)$$

$$[T] = \begin{bmatrix} 0 & 1 & 0 & 0 & 0 & 0 & 0 & 0 \\ C_1 & 0 & 0 & C_2 & 0 & -C_3 & 0 & C_4 \\ 0 & 0 & 0 & 1 & 0 & 0 & 0 & 0 \\ 0 & -C_5 & C_6 & 0 & -C_7 & 0 & C_8 & 0 \\ 0 & 0 & 0 & 0 & 0 & 1 & 0 & 0 \\ 0 & 0 & 0 & 0 & 0 & 0 & 1 & 0 \\ 0 & 0 & 0 & 0 & 0 & 0 & 0 & 1 \\ 0 & C_9 & C_{10} & 0 & C_{11} & 0 & C_{12} & 0 \end{bmatrix} \quad (6.5.18b)$$

and

$$\hat{Q}_m = C_0 Q_m + D_5 \ddot{U}'_m + D_6 \ddot{V}_m + D_7 \ddot{W}_m + D_8 \ddot{W}''_m \quad (6.5.18c)$$

Next, we discuss the solution of Eq. (6.5.17) separately for bending, vibration, and buckling problems. In each case, we solve Eq. (6.5.17) or its special cases.

Bending

In the case of static bending, all variables are independent of time. Equations (6.5.17) and (6.5.18) hold with

$$\hat{Q}_m = C_0 Q_m \quad (6.5.19)$$

In addition, \hat{N}_{xx} and \hat{N}_{yy} appearing in the definition of the coefficients e_{12} and e_{11} are assumed to be zero.

The solution of Eq. (6.5.17), $\mathbf{Z}' = \mathbf{T}\mathbf{Z} + \mathbf{F}$, when \mathbf{T} is independent of x , is given by (see Franklin [3], Chapter 3)

$$\mathbf{Z}(x) = e^{\mathbf{T}x} \left(\mathbf{K} + \int_0^x e^{-\mathbf{T}\xi} \mathbf{F}(\xi) d\xi \right) \quad (6.5.20a)$$

where $e^{\mathbf{T}x}$ represents the matrix product

$$e^{\mathbf{T}x} = [E] \begin{bmatrix} e^{\lambda_1 x} & & \mathbf{0} \\ & e^{\lambda_2 x} & \\ & \ddots & \\ \mathbf{0} & & e^{\lambda_8 x} \end{bmatrix} [E]^{-1} \quad (6.5.20b)$$

$[E]$ denotes the matrix of distinct eigenvectors of the matrix $[T]$, $[E]^{-1}$ denotes its inverse, λ_i ($i = 1, 2, 3, \dots, 8$) are the eigenvalues associated with matrix $[T]$, and \mathbf{K} is a vector of constants to be determined from the boundary conditions (6.5.12)–(6.5.14).

Substitution of Eq. (6.5.20a) into any combination of boundary conditions (6.5.12)–(6.5.14) on edges $x = \mp a/2$ yields a nonhomogeneous system of equations

$$[M]\{K\} = \{R\} \quad (6.5.21)$$

which can be solved for the vector $\{K\}$. For example, consider the case in which the edge $x = -a/2$ is clamped and the edge $x = a/2$ is free. For uniformly distributed load (static bending case), the solution (6.5.20) can be written as

$$\begin{aligned} \{Z\} &= [E] \begin{bmatrix} e^{\lambda_1 x} & \mathbf{0} \\ e^{\lambda_2 x} & \ddots \\ \mathbf{0} & e^{\lambda_8 x} \end{bmatrix} [E]^{-1} \{K\} + [E] \begin{bmatrix} -\frac{1}{\lambda_1} & \mathbf{0} \\ -\frac{1}{\lambda_2} & \ddots \\ \mathbf{0} & -\frac{1}{\lambda_8} \end{bmatrix} [E]^{-1} \{F\} \\ &\equiv [G(x)]\{K\} + \{H(x)\} \end{aligned} \quad (6.5.22)$$

Now the components of the matrix $[M]$ and vector $\{R\}$ in Eq. (6.5.21) can be defined in terms of the coefficients G_{ij} and H_i , evaluated at $x = -a/2$ and $x = a/2$, as described below.

The *clamped* boundary condition at $x = -a/2$ requires [see Eq. (6.5.13)] that

$$M_{1j} = G_{1j}(-a/2), \quad M_{2j} = G_{3j}(-a/2), \quad M_{3j} = G_{5j}(-a/2), \quad M_{4j} = G_{6j}(-a/2) \quad (6.5.23a)$$

The *free* boundary condition at $x = a/2$ requires [see Eqs. (6.5.14a-c)] that

$$\begin{aligned} M_{5j} &= A_{11}G_{2j}(a/2) - \beta A_{12}G_{3j}(a/2) + \beta^2 B_{12}G_{5j}(a/2) - B_{11}G_{7j}(a/2) \\ M_{6j} &= \beta A_{66}G_{1j}(a/2) + A_{66}G_{4j}(a/2) - 2\beta B_{66}G_{6j}(a/2) \\ M_{7j} &= \hat{C}_1G_{1j}(a/2) + \hat{C}_2G_{4j}(a/2) + \hat{C}_3G_{6j}(a/2) + \hat{C}_4G_{8j}(a/2) \\ M_{8j} &= B_{11}G_{2j}(a/2) - \beta B_{12}G_{3j}(a/2) + \beta^2 D_{12}G_{5j}(a/2) - D_{11}G_{7j}(a/2) \end{aligned} \quad (6.5.23b)$$

$$\begin{aligned} \hat{C}_1 &= C_1B_{11} - \beta^2 B_{66}, \quad \hat{C}_2 = C_2B_{11} - \beta(B_{12} + B_{66}) \\ \hat{C}_3 &= -C_3B_{11} + \beta^2(D_{12} + 2D_{66}), \quad \hat{C}_4 = C_4B_{11} - D_{11} \end{aligned} \quad (6.5.23c)$$

Similarly, the coefficients R_i are defined by

$$\begin{aligned} R_1 &= -H_1(-a/2), \quad R_2 = -H_3(-a/2), \quad R_3 = -H_5(-a/2), \quad R_4 = -H_6(-a/2) \\ R_5 &= A_{11}H_2(a/2) - \beta A_{12}H_3(a/2) + \beta^2 B_{12}H_5(a/2) - B_{11}H_7(a/2) \\ R_6 &= \beta A_{66}H_1(a/2) + A_{66}H_4(a/2) - 2\beta B_{66}H_6(a/2) \\ R_7 &= \hat{C}_1H_1(a/2) + \hat{C}_2H_4(a/2) + \hat{C}_3H_6(a/2) + \hat{C}_4H_8(a/2) \\ R_8 &= B_{11}H_2(a/2) - \beta B_{12}H_3(a/2) + \beta^2 D_{12}H_5(a/2) - D_{11}H_7(a/2) \end{aligned} \quad (6.5.24)$$

Natural Vibration

In the case of natural vibration, the applied mechanical loads ($Q_m, \hat{N}_{xx}, \hat{N}_{yy}$) are assumed to be zero, and the solution is of the form

$$\begin{aligned} u(x, y, t) &= U_m(x) \sin \beta y e^{i\omega_m t} \\ v(x, y, t) &= V_m(x) \cos \beta y e^{i\omega_m t} \\ w(x, y, t) &= W_m(x) \sin \beta y e^{i\omega_m t} \end{aligned} \quad (6.5.25)$$

where ω_m denotes the frequency of vibration of the m th mode, and $i = \sqrt{-1}$. Equation (6.5.15) becomes

$$\{Z'(x)\} = [A]\{Z(x)\} \quad (6.5.26a)$$

with

$$[A] = \begin{bmatrix} 0 & 1 & 0 & 0 & 0 & 0 & 0 & 0 \\ \hat{C}_1 & 0 & 0 & C_2 & 0 & -\hat{C}_3 & 0 & C_4 \\ 0 & 0 & 0 & 1 & 0 & 0 & 0 & 0 \\ 0 & -C_5 & \hat{C}_6 & 0 & -\hat{C}_7 & 0 & C_8 & 0 \\ 0 & 0 & 0 & 0 & 0 & 1 & 0 & 0 \\ 0 & 0 & 0 & 0 & 0 & 0 & 1 & 0 \\ 0 & 0 & 0 & 0 & 0 & 0 & 0 & 1 \\ 0 & \hat{C}_9 & \hat{C}_{10} & 0 & \hat{C}_{11} & 0 & \hat{C}_{12} & 0 \end{bmatrix} \quad (6.5.26b)$$

where

$$\begin{aligned} \hat{C}_1 &= C_1 - D_1\omega^2, & \hat{C}_3 &= C_3 - D_2\omega^2, & \hat{C}_6 &= C_6 - D_3\omega^2 \\ \hat{C}_7 &= C_7 - D_4\omega^2, & \hat{C}_9 &= C_9 - D_5\omega^2, & \hat{C}_{10} &= C_{10} - D_6\omega^2 \\ \hat{C}_{11} &= C_{11} - D_7\omega^2, & \hat{C}_{12} &= C_{12} - D_8\omega^2 \end{aligned} \quad (6.5.26c)$$

The solution of Eq. (26a) is given by

$$\mathbf{Z}(x) = e^{\mathbf{A}x} \mathbf{K} \quad (6.5.27)$$

and the vector \mathbf{K} of constants is determined from the boundary conditions. Substitution of Eq. (6.5.27) into the set of boundary conditions results in a homogeneous system of equations

$$[M]\{K\} = \{0\} \quad (6.5.28)$$

For a nontrivial solution, the determinant of the coefficient matrix in (6.5.28) should be zero:

$$|M_{ij}| = 0 \quad (6.5.29)$$

The roots of the above equation are (the squares of) the frequencies of natural vibration.

Buckling

In the case of buckling, the applied mechanical load Q_m is zero, and \hat{N}_{xx} and \hat{N}_{yy} are determined. The solution is assumed to be of the form

$$\begin{aligned} u(x, y) &= U_m(x) \sin \beta y \\ v(x, y) &= V_m(x) \cos \beta y \\ w(x, y) &= W_m(x) \sin \beta y \end{aligned} \quad (6.5.30)$$

The operator equation for this case is

$$\{Z'(x)\} = [T]\{Z\} \quad (6.5.31)$$

where $[T]$ is the matrix defined in Eq. (6.5.18b). Note that the buckling loads enter the matrix through the coefficients C_{11} and C_{12} , which contain e_{11} and e_{12} , respectively [see Eqs. (6.5.16a) and (6.5.16b)]. The solution of Eq. (6.5.31) is given by

$$\mathbf{Z}(x) = e^{\mathbf{T}x} \mathbf{K} \quad (6.5.32)$$

and the vector \mathbf{K} of constants is determined from the boundary conditions. Substitution of Eq. (32) into the set of boundary conditions results in a homogeneous system of equations

$$[M]\{K\} = \{0\} \quad (6.5.33)$$

For a nontrivial solution, the determinant of the coefficient matrix in (6.5.33) should be zero. The roots of this equation are the buckling loads, \hat{N}_{xx} and \hat{N}_{yy} .

Computational Issues

Some comments are in order on the numerical solution of Eq. (6.5.22). Due to the sparse nature of matrix $[T]$ or $[A]$, the matrix $[M]$ appearing in Eqs. (6.5.21), (6.5.28), and (6.5.33) is often ill-conditioned and results in computer overflow or underflow. This can be overcome (see, for example, Nosier and Reddy [4]) by rewriting Eq. (6.5.22) as

$$\begin{aligned} \{Z(x)\} &= [E] \begin{bmatrix} e^{\lambda_1 x} & & \mathbf{0} \\ & e^{\lambda_2 x} & \\ & \ddots & \\ \mathbf{0} & & e^{\lambda_8 x} \end{bmatrix} [E]^{-1}\{K\} + e^{\mathbf{T}x} \int_0^x e^{-\mathbf{T}\xi} \{F\} d\xi \\ &= [E] \begin{bmatrix} e^{\lambda_1 x} & & \mathbf{0} \\ & e^{\lambda_2 x} & \\ & \ddots & \\ \mathbf{0} & & e^{\lambda_8 x} \end{bmatrix} \{\hat{K}\} + e^{\mathbf{T}x} \int_0^x e^{-\mathbf{T}\xi} \{F\} d\xi \quad (6.5.34a) \end{aligned}$$

and

$$[\hat{M}]\{\hat{K}\} + \{F\} = \{0\}, \quad \{\hat{K}\} = [E]^{-1}\{K\} \quad (6.5.34b)$$

The matrix $[\hat{M}]$ is not ill-conditioned and therefore can be easily inverted to solve for $\{\hat{K}\}$ and $\{K\} = [E]\{\hat{K}\}$. It should be noted that, while $\{K\}$ and $[M]$ are real-valued, $\{\hat{K}\}$ and $[\hat{M}]$ are complex-valued arrays.

Another source of difficulty in the numerical evaluation of the eigenvalues of the matrix $[T]$ or $[A]$ is due to the fact their diagonals have zero entries. This can be circumvented by adding a nonzero constant to all diagonal elements (i.e., add $-c[I]$). The eigenvalues of the original matrix $[T]$ or $[A]$ are obtained from the eigenvalues of the modified matrix by subtracting the same nonzero constant. The eigenvectors in both cases are the same.

6.5.3 Antisymmetric Cross-Ply Laminates

Here we present numerical results obtained with the Lévy method and the state-space solution approach. Khdeir and his colleagues developed solutions for static and dynamic (natural vibration as well as transient response) analyses and buckling

of rectangular composite laminates with various lamination schemes and boundary conditions. The reader may consult the papers cited in the bibliography for detailed derivations and additional numerical results.

The notation used for rectangular laminates with different boundary conditions on edges $x = \pm a/2$ is as follows (see Figure 6.5.1). The notation SF, for example, is used to denote a plate for which edge $x = -a/2$ is simply supported (S) and edge $x = a/2$ is free (F). Since edges $y = 0, b$ are always simply supported, we also use the notation SSSF to denote SF. Thus SS is used in place of SSSS, SC in place of SSSC, CC in place of SSCC, and so on.

Bending

The following lamina properties, typical of graphite-epoxy material, are used in all numerical examples presented here:

$$E_1/E_2 = 25, \quad G_{12} = G_{13} = 0.5E_2, \quad G_{23} = 0.2E_2, \quad \nu_{12} = 0.25 \quad (6.5.35)$$

The loading, in all cases, is assumed to be sinusoidal

$$q(x, y) = q_0 \cos \alpha x \sin \beta y \quad (6.5.36)$$

where $\alpha = (m\pi/a)$ and $\beta = (n\pi/b)$.

In the tables and figures, the results for deflections and stresses are presented in the following nondimensional form:

$$\bar{w} = w_0(0, b/2) \frac{E_2 h^3}{b^4 q_0} \times 10^2 \quad (6.5.37a)$$

$$\bar{\sigma}_{xx} = -\sigma_{xx}(0, \frac{b}{2}, -\frac{h}{2}) \frac{h^2}{b^2 q_0} \times 10, \quad \bar{\sigma}_{yy} = \sigma_{yy}(0, \frac{b}{2}, \frac{h}{2}) \frac{h^2}{b^2 q_0} \times 10 \quad (6.5.37b)$$

where h is the total thickness of the laminate and q_0 is the intensity of the distributed transverse load. For the coordinate system used in the nondimensionalization, one should refer to Figure 6.5.1.

Figures 6.5.2 and 6.5.3 contain plots of \bar{w} versus E_1/E_2 for two-layer antisymmetric rectangular ($b/a = 2$) laminates ($G_{12} = G_{13} = 0.5E_2$, $\nu_{12} = 0.25$) under various boundary conditions on edges $x = \pm a/2$, showing the effect of material orthotropy on the deflections. The degree of orthotropy has less influence on the deflections for large ratios of E_1 to E_2 . Table 6.5.1 contains numerical results of deflections and stresses for two- and ten-layer laminates.

Numerical results for deflections and stresses of cross-ply laminates subjected to sinusoidal distribution of temperature

$$T(x, y, z) = zT_1(x, y) = z\bar{T}_1 \cos \alpha x \sin \beta y \quad (6.5.38)$$

are presented in Table 6.5.2. The material properties used are the same as those in Eq. (6.5.35), with $\alpha_2 = 3\alpha_1$. The following nondimensionalizations are used:

$$\bar{w} = w_0(0, b/2) \frac{1}{\alpha_1 \bar{T}_1 b^2} \times 10 \quad (6.5.39a)$$

$$\bar{\sigma}_{xx} = \sigma_{xx}(0, \frac{b}{2}, -\frac{h}{2}) \frac{1}{\alpha_1 \bar{T}_1 b E_2} \times 10 \quad (6.5.39b)$$

$$\bar{\sigma}_{yy} = -\sigma_{yy}(0, \frac{b}{2}, \frac{h}{2}) \frac{1}{\alpha_1 \bar{T}_1 b E_2} \times 10 \quad (6.5.39c)$$

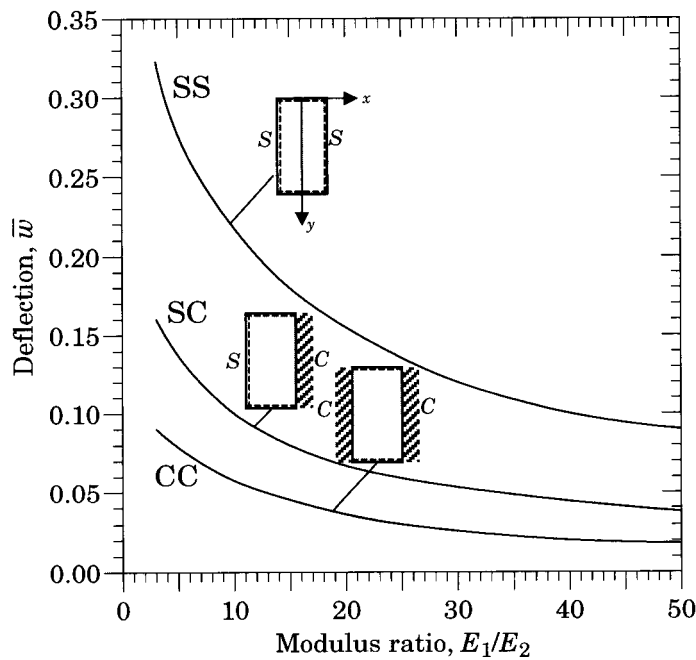


Figure 6.5.2: Nondimensionalized maximum transverse deflection (\bar{w}) versus modulus ratio (E_1/E_2) for antisymmetric cross-ply (0/90) laminates ($b/a = 2$) subjected to sinusoidal load.

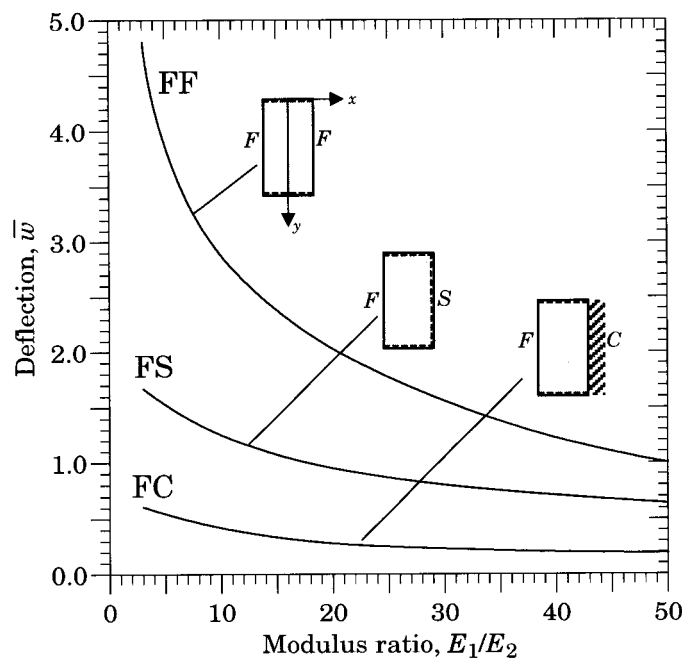


Figure 6.5.3: Nondimensionalized maximum transverse deflection (\bar{w}) versus modulus ratio (E_1/E_2) for antisymmetric cross-ply (0/90) laminates ($b/a = 2$) subjected to sinusoidal load.

Table 6.5.1: Nondimensionalized center deflections (\bar{w}) and in-plane normal stresses ($\bar{\sigma}_{xx}$ and $\bar{\sigma}_{yy}$) of antisymmetric cross-ply square plates subjected to sinusoidal distribution of transverse load and for various boundary conditions.

No. of Layers	Variable	SS	SC	CC	FF	FS	FC
2	\bar{w}	1.064	0.664	0.429	1.777	1.471	0.980
	$\bar{\sigma}_{xx}$	7.157	5.660	4.800	2.403	4.442	3.042
	$\bar{\sigma}_{yy}$	7.157	4.483	2.914	11.849	9.837	6.560
10	\bar{w}	0.442	0.266	0.167	0.665	0.579	0.380
	$\bar{\sigma}_{xx}$	5.009	3.829	3.167	1.725	2.986	1.865
	$\bar{\sigma}_{yy}$	5.009	3.025	1.911	7.480	6.531	4.284

Table 6.5.2: Nondimensionalized center deflections (\bar{w}) and in-plane normal stresses ($\bar{\sigma}_{xx}$ and $\bar{\sigma}_{yy}$) of cross-ply square plates subjected to sinusoidal distribution of temperature distribution and for various boundary conditions.

Laminate	Variable	SS	SC	CC	FF	FS
0	\bar{w}	1.0312	0.4543	0.2443	2.2935	1.6067
(0/90)	\bar{w}	1.1504	0.7183	0.4681	1.2639	1.2152
	$\bar{\sigma}_{yy}$	0.6148	5.1916	8.8393	2.1091	1.4684
(0/90) ₅	\bar{w}	1.0331	0.6222	0.3914	1.0681	1.0546
(0/90/0)	\bar{w}	1.0312	0.4635	0.2512	1.6645	1.3800
	$\bar{\sigma}_{xx}$	0.0526	11.1264	15.2675	1.4489	0.8217

Vibration and Stability

The Lévy type solution procedure is used to evaluate the natural frequencies and critical buckling loads of antisymmetric cross-ply rectangular laminates. The following material properties are used in the analysis (material 2):

$$E_1/E_2 = 40, \quad G_{12} = G_{13} = 0.6E_2, \quad G_{23} = 0.5E_2, \quad \nu_{12} = 0.25 \quad (6.5.40)$$

Numerical results for the nondimensionalized fundamental frequencies of square, antisymmetric, cross-ply laminates (0/90/0/...) are presented in Table 6.5.3 for various boundary conditions, number of layers, and ratio of principal moduli of the material. The fundamental frequencies increase with increasing orthotropy E_1/E_2 as well as number of layers. Similar results for critical buckling loads are also presented in the same table. Results for fundamental frequencies and buckling loads are presented for various boundary conditions and aspect ratios in Table 6.5.4. The natural frequencies increase with an increase in the aspect ratio as well as the number of layers.

Table 6.5.3: Effect of degree of orthotropy of the individual layers on the dimensionless fundamental frequency, $\bar{\omega} = \omega(b^2/h)\sqrt{\rho/E_2}$, and critical buckling loads, $\bar{N} = N_{xx}(b^2/E_2 h^3)$ ($k = 0$), of simply supported antisymmetric square laminates (E_1/E_2 = varied, $G_{12} = G_{13} = 0.6E_2$, $G_{23} = 0.5E_2$, $\nu_{12} = 0.25$).

No. of Layers	E_1/E_2				
	3	10	20	30	40
Natural Frequencies (ω_{11}) [†]					
2	6.977	8.031	9.204	10.227	11.154
	7.034	8.097	9.278	10.310	11.244
4	7.353	9.987	12.826	15.141	17.145
	7.413	10.068	12.931	15.264	17.285
8	7.443	10.422	13.589	16.147	18.352
	7.505	10.507	13.701	16.279	18.502
10	7.455	10.473	13.678	16.264	18.492
	7.516	10.559	13.790	16.397	18.643
Critical Buckling Loads ($k = 0$)					
2	5.034	6.703	8.816	10.891	12.957
4	5.574	10.295	16.988	23.675	30.359
8	5.709	11.192	19.031	26.870	34.710
10	5.725	11.300	19.277	27.254	35.232

[†] Fundamental frequencies obtained with (first row) and without (second row) rotary inertia. When rotary inertia is included, the nondimensionalized frequencies depend on the ratio a/h ; the frequencies are reported for $a/h = 10$.

Table 6.5.4: Dimensionless fundamental frequencies, $\bar{\omega} = \omega(b^2/h)\sqrt{\rho/E_2}$, and uniaxial critical buckling loads, $\bar{N} = N_{xx}(b^2/E_2 h^3)$, of antisymmetric cross-ply plates with various boundary conditions ($E_1 = 40E_2$, $G_{12} = G_{13} = 0.6E_2$, $G_{23} = 0.5E_2$, $\nu_{12} = 0.25$).

No. of Layers	b/a	FF	FS	FC	SS	SC	CC
Natural Frequencies (ω_{11}) [†]							
2	1	7.267	7.636	8.228	11.154	14.223	18.543
10	1	12.680	12.906	13.779	18.492	23.971	31.709
2	2	7.267	8.677	13.915	30.468	45.554	64.832
10	2	12.680	13.569	22.876	52.292	79.371	113.80
2	3	7.267	10.153	25.769	63.325	96.451	137.71
10	3	12.680	14.606	43.616	111.58	159.65	159.95
Critical Buckling Loads ($k = 0$)							
2	1	5.425	6.003	6.968	12.957	21.116	31.280
10	1	16.426	17.023	19.389	35.232	59.288	89.770

[†] Frequencies with rotary inertia included ($a/h = 10$).

6.5.4 Antisymmetric Angle-Ply Laminates

The Lévy solutions in conjunction with the state-space approach can also be obtained for antisymmetric angle-ply laminated plates. In this section numerical results of bending, free vibration, and in-plane compressive buckling of rectangular laminates are presented (see Khdeir [18]).

Bending

Nondimensionalized deflections, $\bar{w} = w_0(0, b/2)E_2 h^3/q_0 b^4 \times 10^2$, of square, antisymmetric angle-ply laminates (45/-45/45/-45) for various boundary conditions and uniformly distributed load of intensity q_0 are presented in Table 6.5.5. The material properties used are the same as those presented in Eq. (6.5.40). As one might expect, plates with a combination of free and simply supported boundary conditions deflect the most and those with simply supported and clamped boundary conditions deflect the least. Table 6.5.6 contains results for two- and ten-layer antisymmetric angle-ply laminates as a function of the lamination angle and for different boundary conditions. The material properties used in this case are

$$\begin{aligned} E_1 &= 19.2 \times 10^6 \text{ psi (132.38 GPa)}, & E_2 &= 1.56 \times 10^6 \text{ psi (10.76 GPa)}, & \nu_{12} &= 0.24 \\ G_{12} &= G_{13} = 0.82 \times 10^6 \text{ psi (5.65 GPa)}, & G_{23} &= 0.523 \times 10^6 \text{ psi (3.61 GPa)} \end{aligned} \quad (6.5.41)$$

It is clear that the bending-stretching coupling is the most significant for two-layer laminates, and its effect is to make the laminate more flexible and hence deflects more than the ten-layer plates, for which the coupling is negligible.

Table 6.5.5: Effect of orthotropy on dimensionless deflections \bar{w} of a (45/-45/45/-45) square laminated plate.

E_1/E_2	SS	SC	CC	FF	FS	FC
2	3.2142	2.2144	1.5308	10.470	6.2336	4.4460
10	1.0000	0.7467	0.5578	5.5710	2.3451	1.7473
20	0.5418	0.4120	0.3133	3.6574	1.3432	1.0104
30	0.3718	0.2847	0.2179	2.7376	0.9433	0.7121

Table 6.5.6: Effect of ply angle (θ) and number of layers (n) on dimensionless deflection \bar{w} of a square plate [$(\theta/-\theta/\theta/\dots/-\theta)$; material properties are as given in Eq. (6.5.41)].

θ	n	SS	SC	CC	FF	FS	FC
30	2	1.6185	1.2996	1.0352	4.3732	2.6983	2.2162
	10	0.8187	0.6898	0.5786	2.2621	1.3936	1.1913
45	2	1.5807	1.1675	0.8628	7.8765	3.5696	2.6432
	10	0.7391	0.5590	0.4229	4.7291	1.8069	1.3554
60	2	1.6184	1.0218	0.6657	12.3713	4.7491	2.8627
	10	0.8187	0.5188	0.3364	10.3035	2.7365	1.6391

Vibration and Buckling

Numerical results for nondimensionalized frequencies, $\bar{\omega} = \omega \frac{b^2}{h} \sqrt{\rho/E_2}$, and dimensionless uniaxial buckling loads, $\bar{N} = N_{xx} \frac{a^2}{E_2 h^3}$, are presented for various laminates in Tables 6.5.7 through 6.5.13. The material used in all these cases is assumed to be a high modulus graphite epoxy with the properties listed in Eq. (6.5.40):

$$E_1/E_2 = 40, G_{12} = G_{13} = 0.6E_2, G_{23} = 0.5E_2, \nu_{12} = 0.25$$

The fundamental frequencies presented are for the case in which rotary inertia is neglected. The parametric effects of the lamination angle, plate aspect ratio, and boundary conditions on frequencies and buckling loads can be seen from the results presented in these tables.

Table 6.5.7: Effect of in-plane orthotropy ratio on dimensionless fundamental frequency $\bar{\omega}$ of a (45/-45/45/-45) square laminated plate.

E_1/E_2	SS	SC	CC	FF	FS	FC
2	7.02	8.39	10.24	3.44	4.24	4.62
10	12.54	14.43	16.90	4.65	6.78	7.38
20	17.02	19.43	22.53	5.72	8.92	9.70
30	20.53	23.37	27.00	6.60	10.62	11.55
40	23.53	26.73	30.83	7.37	12.08	13.14

Table 6.5.8: Effect of ply angle (θ) and number of layers (n) on dimensionless fundamental frequency $\bar{\omega}$ of a square laminate ($\theta/-\theta/\theta/\dots/-\theta$).

θ	n	SS	SC	CC	FF	FS	FC
30	2	14.24	15.44	17.00	7.58	9.35	9.69
	10	23.95	25.59	27.58	12.37	15.38	15.84
45	2	14.64	16.75	19.48	5.12	7.79	8.48
	10	25.47	28.91	33.32	7.89	13.03	14.17
60	2	14.24	17.74	22.31	3.47	6.26	7.54
	10	23.95	29.86	37.62	4.32	9.92	11.96

Table 6.5.9: Effect of aspect ratio dimensionless fundamental frequency $\bar{\omega} = \omega \frac{a^2}{h} \sqrt{\rho/E_2}$ of a (45/-45/45/-45) square laminated plate.

a/b	SS	SC	CC	FF	FS	FC
1	23.57	26.73	30.83	7.37	12.08	13.14
2	53.74	69.75	90.73	6.32	19.80	25.47
3	98.87	138.20	189.13	5.61	28.39	42.95

Table 6.5.10: Dimensionless frequency $\bar{\omega}_m$ for various mode numbers (m) of (45/-45/45/-45) square laminated plate.

m	SS	SC	CC	FF	FS	FC
1	23.53	26.73	30.83	7.37	12.08	13.14
2	53.74	56.10	58.88	31.89	37.32	37.91
3	98.87	100.70	102.76	73.58	79.12	79.48
4	160.35	161.82	163.43	132.42	137.92	138.16
5	238.72	239.93	241.25	208.39	213.78	213.95

Table 6.5.11: Effect of plate aspect ratio (a/b) and number of layers (n) on uniaxial buckling load of simply supported angle-ply (45/-45/45/...) laminates; $\bar{N} = N_{xx}(b^2/\pi^2 D_{22})$.

a/b	mode	$n = 2$	$n = 4$	$n = 6$	$n = 8$
0.5	(1,1)	3.2071	8.0934	8.9980	9.3150
1.0	(1,1)	2.4014	6.2045	6.9088	7.1552
1.5	(2,1)	2.5231	6.4901	7.2247	7.4819
2.0	(2,1)	2.4014	6.2045	6.9088	7.1552
2.5	(3,1)	2.4495	6.3173	7.0336	7.2843
3.0	(3,1)	2.4014	6.2045	6.9088	7.1552

Table 6.5.12: Effect of in-plane orthotropy ratio on dimensionless uniaxial buckling loads $\bar{N} = N_{cr}b^2/E_2h^3$ of a (45/-45/45/-45) square laminated plate.

E_1/E_2	SS	SC	CC	FF	FS	FC
2	4.988	7.126	9.512	1.199	1.819	2.166
10	15.923	21.106	26.278	2.190	4.660	5.521
20	29.333	38.234	46.823	3.313	8.054	9.532
30	42.715	55.321	67.320	4.415	11.421	13.513
40	56.088	72.396	87.803	5.509	14.780	17.484

Table 6.5.13: Effect of ply angle (θ) and number of layers (n) on dimensionless uniaxial buckling loads $\bar{N} = N_{cr}b^2/E_2h^3$ of a square plate [$(\theta/-\theta/\theta/\dots/-\theta)$].

θ	n	SS	SC	CC	FF	FS	FC
30	2	20.543	24.158	29.269	5.822	8.857	9.520
	10	58.135	66.322	77.065	15.499	23.972	25.412
45	2	21.709	28.423	34.963	2.654	6.150	7.283
	10	65.714	84.707	102.596	6.300	17.189	20.332
60	2	19.564	23.834	29.547	1.221	3.975	5.756
	10	52.945	64.103	79.619	1.889	9.977	14.501

6.6 Analysis of Midplane Symmetric Laminates

6.6.1 Introduction

In the previous sections of this chapter we considered analytical solutions of bending, vibration, and buckling of antisymmetric cross-ply and angle-ply rectangular laminates. In these laminates, in general, the bending-stretching coupling stiffnesses B_{ij} were not zero, but the bending-twisting coupling stiffnesses D_{16} and D_{26} were zero. In this section we consider laminates that are symmetric in *both* geometry and material properties about the middle plane. In such symmetric laminates, we have $B_{ij} = 0$ and D_{16} and D_{26} are not zero. The specially orthotropic plates considered in Chapter 5 are a special case of symmetric laminates. Laminates containing multiple generally orthotropic layers (i.e., orthotropic layers whose principal material axes are not parallel to the plate axes) that are symmetrically placed about the midplane fall into the class of symmetric laminates.

An example of symmetric laminates is provided by the class of *regular symmetric angle-ply laminates*, $(\theta/-\theta/\theta)$, $0 \leq \theta \leq 90$ with equal thickness layers. The regular symmetric angle-ply laminates should contain an odd number of plies. A more general example of symmetric angle-ply laminate is provided by $(30/-60/15/-60/30)$ with thicknesses $h_1 = h_5, h_2 = h_4$, and the midplane of the plate coincides with the midplane of the 15° ply. For symmetric angle-ply laminates the coupling terms A_{16}, A_{26}, D_{16} , and D_{26} are proportional to $1/N$, where N is the total number of layers in the laminate. Thus the coupling stiffnesses are the largest when $N = 3$ for symmetric angle-ply laminates, and they decrease with increasing N .

The symmetric angle-ply laminates, with $B_{ij} = 0$ and small A_{16}, A_{26}, D_{16} , and D_{26} , offer both analysis simplifications and practical advantages over more general laminates. For example, symmetric angle-ply laminates offer more shear stiffness than cross-ply laminates. Even when A_{16}, A_{26}, D_{16} , and D_{26} are small, they influence the laminate behavior significantly.

6.6.2 Governing Equations

The governing equations of motion of symmetric laminates according to the classical laminate theory can be obtained from (3.3.45)–(3.3.47) by setting $B_{ij} = 0$ and $I_1 = 0$. For linear analysis, we obtain

$$\begin{aligned} A_{11} \frac{\partial^2 u_0}{\partial x^2} + A_{12} \frac{\partial^2 v_0}{\partial x \partial y} + A_{16} \left(\frac{\partial^2 u_0}{\partial x \partial y} + \frac{\partial^2 v_0}{\partial x^2} + \frac{\partial^2 u_0}{\partial x \partial y} \right) + A_{26} \frac{\partial^2 v_0}{\partial y^2} \\ + A_{66} \left(\frac{\partial^2 u_0}{\partial y^2} + \frac{\partial^2 v_0}{\partial x \partial y} \right) - \left(\frac{\partial N_{xx}^T}{\partial x} + \frac{\partial N_{xy}^T}{\partial y} \right) = I_0 \frac{\partial^2 u_0}{\partial t^2} \end{aligned} \quad (6.6.1)$$

$$\begin{aligned} A_{16} \frac{\partial^2 u_0}{\partial x^2} + A_{26} \left(\frac{\partial^2 v_0}{\partial x \partial y} + \frac{\partial^2 u_0}{\partial y^2} + \frac{\partial^2 v_0}{\partial x \partial y} \right) + A_{66} \left(\frac{\partial^2 u_0}{\partial x \partial y} + \frac{\partial^2 v_0}{\partial x^2} \right) \\ + A_{12} \frac{\partial^2 u_0}{\partial x \partial y} + A_{22} \frac{\partial^2 v_0}{\partial y^2} - \left(\frac{\partial N_{xy}^T}{\partial x} + \frac{\partial N_{yy}^T}{\partial y} \right) = I_0 \frac{\partial^2 v_0}{\partial t^2} \end{aligned} \quad (6.6.2)$$

$$\begin{aligned}
& - D_{11} \frac{\partial^4 w_0}{\partial x^4} - 2(D_{12} + 2D_{66}) \frac{\partial^4 w_0}{\partial x^2 \partial y^2} - D_{22} \frac{\partial^4 w_0}{\partial y^4} - 4D_{16} \frac{\partial^4 w_0}{\partial x^3 \partial y} \\
& - 4D_{26} \frac{\partial^4 w_0}{\partial x \partial y^3} - \left(\frac{\partial^2 M_{xx}^T}{\partial x^2} + 2 \frac{\partial^2 M_{xy}^T}{\partial y \partial x} + \frac{\partial^2 M_{yy}^T}{\partial y^2} \right) + q \\
& + \frac{\partial}{\partial x} \left(\hat{N}_{xx} \frac{\partial w_0}{\partial x} + \hat{N}_{xy} \frac{\partial w_0}{\partial y} \right) + \frac{\partial}{\partial y} \left(\hat{N}_{xy} \frac{\partial w_0}{\partial x} + \hat{N}_{yy} \frac{\partial w_0}{\partial y} \right) \\
& = I_0 \frac{\partial^2 w_0}{\partial t^2} - I_2 \frac{\partial^2}{\partial t^2} \left(\frac{\partial^2 w_0}{\partial x^2} + \frac{\partial^2 w_0}{\partial y^2} \right)
\end{aligned} \tag{6.6.3}$$

where \hat{N}_{xx} , \hat{N}_{yy} , and \hat{N}_{xy} are the applied edge forces.

Clearly the first two equations governing (u_0, v_0) are uncoupled from the third equation governing w_0 . In the absence of any in-plane loads, the first two equations yield zero in-plane displacements everywhere. Because of the presence of the bending-twisting coupling stiffnesses, the Navier solutions of Eq. (6.6.3) cannot be developed, forcing us to use the Ritz, Galerkin, or the finite element method. In the following sections we discuss the Ritz solutions for symmetrically laminated plates.

6.6.3 Weak Forms

We can use the Ritz method to determine an approximate solution to the bending, buckling, and natural vibrations of symmetric laminates. The weak form or the statement of the principle of minimum total potential energy for bending, buckling, and natural vibration problems is given below. For bending, the virtual work done to applied edge forces and moments should be added to the expression

$$\begin{aligned}
0 = \int_0^b \int_0^a & \left\{ D_{11} \frac{\partial^2 w_0}{\partial x^2} \frac{\partial^2 \delta w_0}{\partial x^2} + D_{12} \left(\frac{\partial^2 w_0}{\partial y^2} \frac{\partial^2 \delta w_0}{\partial x^2} + \frac{\partial^2 w_0}{\partial x^2} \frac{\partial^2 \delta w_0}{\partial y^2} \right) \right. \\
& + D_{22} \frac{\partial^2 w_0}{\partial y^2} \frac{\partial^2 \delta w_0}{\partial y^2} + 4D_{66} \frac{\partial^2 w_0}{\partial x \partial y} \frac{\partial^2 \delta w_0}{\partial x \partial y} \\
& + 2D_{16} \left(\frac{\partial^2 w_0}{\partial x \partial y} \frac{\partial^2 \delta w_0}{\partial x^2} + \frac{\partial^2 w_0}{\partial x^2} \frac{\partial^2 \delta w_0}{\partial x \partial y} \right) \\
& + 2D_{26} \left(\frac{\partial^2 w_0}{\partial x \partial y} \frac{\partial^2 \delta w_0}{\partial y^2} + \frac{\partial^2 w_0}{\partial y^2} \frac{\partial^2 \delta w_0}{\partial x \partial y} \right) - q \delta w_0 \\
& + \hat{N}_{xx} \frac{\partial w_0}{\partial x} \frac{\partial \delta w_0}{\partial x} + \hat{N}_{xy} \left(\frac{\partial w_0}{\partial y} \frac{\partial \delta w_0}{\partial x} + \frac{\partial w_0}{\partial x} \frac{\partial \delta w_0}{\partial y} \right) + \hat{N}_{yy} \frac{\partial w_0}{\partial y} \frac{\partial \delta w_0}{\partial y} \\
& \left. - \omega^2 \left[I_0 w_0 \delta w_0 + I_2 \left(\frac{\partial w_0}{\partial x} \frac{\partial \delta w_0}{\partial x} + \frac{\partial w_0}{\partial y} \frac{\partial \delta w_0}{\partial y} \right) \right] \right\} dx dy
\end{aligned} \tag{6.6.4}$$

where ω denotes the frequency of natural vibration. For bending we set all terms involving the in-plane edge forces and frequency of vibration to zero. We set $q = 0$ and $\omega = 0$ for buckling analysis, and $q = 0$ and $\hat{N}_{xx} = \hat{N}_{yy} = \hat{N}_{xy} = 0$ for natural vibration.

6.6.4 The Ritz Solution

We begin with the Ritz approximation of the form

$$w_0(x, y) \approx W_{MN}(x, y) = \sum_{i=1}^M \sum_{j=1}^N c_{ij} \varphi_{ij}(x, y) \quad (6.6.5)$$

where

$$\varphi_{ij}(x, y) = X_i(x)Y_j(y) \quad (6.6.6)$$

and X_i and Y_j denote any admissible approximation functions for the problem. The choice is dictated by the essential (or geometric) boundary conditions of the problem. Substitution of Eq. (6.6.5) into Eq. (6.6.4) results in the following equations:

$$\begin{aligned} 0 &= \sum_{i=1}^M \sum_{j=1}^N \left\{ \int_0^b \int_0^a \left[D_{11} \frac{d^2 X_i}{dx^2} Y_j \frac{d^2 X_p}{dx^2} Y_q + 4D_{66} \frac{dX_i}{dx} \frac{dY_j}{dy} \frac{dX_p}{dx} \frac{dY_q}{dy} \right. \right. \\ &\quad + D_{12} \left(X_i \frac{d^2 Y_j}{dy^2} \frac{d^2 X_p}{dx^2} Y_q + \frac{d^2 X_i}{dx^2} Y_j X_p \frac{d^2 Y_q}{dy^2} \right) \\ &\quad + D_{22} X_i \frac{d^2 Y_j}{dy^2} X_p \frac{d^2 Y_q}{dy^2} \\ &\quad + 2D_{16} \left(\frac{dX_i}{dx} \frac{dY_j}{dy} \frac{d^2 X_p}{dx^2} Y_q + \frac{d^2 X_i}{dx^2} Y_j \frac{dX_p}{dx} \frac{dY_q}{dy} \right) \\ &\quad \left. \left. + 2D_{26} \left(\frac{dX_i}{dx} \frac{dY_j}{dy} X_p \frac{d^2 Y_q}{dy^2} + X_i \frac{d^2 Y_j}{dy^2} \frac{dX_p}{dx} \frac{dY_q}{dy} \right) \right] dx dy \right\} c_{ij} \\ &- \sum_{i=1}^M \sum_{j=1}^N \left\{ \int_0^b \int_0^a \left[\hat{N}_{xx}^0 \frac{dX_i}{dx} Y_j \frac{dX_p}{dx} Y_q + \hat{N}_{yy} X_i \frac{dY_j}{dy} X_p \frac{dY_q}{dy} \right. \right. \\ &\quad \left. \left. + 2\hat{N}_{xy}^0 \left(X_i \frac{dY_j}{dy} \frac{dX_p}{dx} Y_q + \frac{dX_i}{dx} Y_j X_p \frac{dY_q}{dy} \right) \right] dx dy \right\} c_{ij} \\ &- \sum_{i=1}^M \sum_{j=1}^N \left\{ \int_0^b \int_0^a \omega^2 \left[I_0 X_i Y_j X_p Y_q + I_2 \left(\frac{dX_i}{dx} Y_j \frac{dX_p}{dx} Y_q \right. \right. \right. \\ &\quad \left. \left. \left. + X_i \frac{dY_j}{dy} X_p \frac{dY_q}{dy} \right) \right] dx dy \right\} c_{ij} - \int_0^b \int_0^a q X_p Y_q dx dy \quad (6.6.7) \end{aligned}$$

for $p = 1, 2, \dots, M$ and $q = 1, 2, \dots, N$.

6.6.5 Simply Supported Plates

Recall from Eq. (5.2.4) that the choice of the double sine series

$$\varphi_{ij}(x, y) = X_i(x)Y_j(y) \equiv \sin \frac{i\pi x}{a} \sin \frac{j\pi y}{b} \quad (6.6.8)$$

satisfies the simply supported (SS-1) boundary conditions. Substituting (6.6.8) into (6.6.7) we obtain

$$\begin{aligned}
0 = & \sum_{i=1}^M \sum_{j=1}^N \left[\int_0^b \int_0^a \left(A_{ijpq} \sin \alpha_i x \sin \beta_j y \sin \alpha_p x \sin \beta_q y \right. \right. \\
& + B_{ijpq} \cos \alpha_i x \cos \beta_j y \cos \alpha_p x \cos \beta_q y \\
& - C_{ijpq} \cos \alpha_i x \cos \beta_j y \sin \alpha_p x \sin \beta_q y \\
& \left. \left. - D_{ijpq} \sin \alpha_i x \sin \beta_j y \cos \alpha_p x \cos \beta_q y \right) dx dy \right] c_{ij} \\
& - \int_0^b \int_0^a q(x, y) \sin \alpha_p x \sin \beta_q y dx dy \\
& - \sum_{i=1}^M \sum_{j=1}^N \left\{ \int_0^b \int_0^a \left[\hat{N}_{xx}^0 \cos \alpha_i x \sin \beta_j y \cos \alpha_p x \sin \beta_q y \right. \right. \\
& + \hat{N}_{yy}^0 \sin \alpha_i x \cos \beta_j y \sin \alpha_p x \cos \beta_q y \\
& + 2\hat{N}_{xy}^0 (\sin \alpha_i x \cos \beta_j y \cos \alpha_p x \sin \beta_q y \\
& \left. \left. + \cos \alpha_i x \sin \beta_j y \sin \alpha_p x \cos \beta_q y) \right] dx dy \right\} c_{ij} \\
& - \sum_{i=1}^M \sum_{j=1}^N \left\{ \int_0^b \int_0^a \omega^2 [I_0 \sin \alpha_i x \sin \beta_j y \sin \alpha_p x \sin \beta_q y \right. \\
& + I_2 (\cos \alpha_i x \sin \beta_j y \cos \alpha_p x \sin \beta_q y \\
& \left. + \sin \alpha_i x \cos \beta_j y \sin \alpha_p x \cos \beta_q y)] dx dy \right\} c_{ij} \quad (6.6.9)
\end{aligned}$$

where $\alpha_i = \frac{i\pi}{a}$, $\beta_j = \frac{j\pi}{b}$, and

$$\begin{aligned}
A_{ijpq} &= D_{11}\alpha_i^2 \alpha_p^2 + D_{12}(\beta_j^2 \alpha_p^2 + \alpha_i^2 \beta_q^2) + D_{22}\beta_j^2 \beta_q^2 \\
B_{ijpq} &= 4D_{66}\alpha_i \beta_j \alpha_p \beta_q \\
C_{ijpq} &= 2(D_{16}\alpha_i \beta_j \alpha_p^2 + D_{26}\alpha_i \beta_j \beta_q^2) \\
D_{ijpq} &= 2(D_{16}\alpha_i^2 \alpha_p \beta_q + D_{26}\beta_j^2 \alpha_p \beta_q) \quad (6.6.10)
\end{aligned}$$

Suppose that the load $q(x, y)$ is also expanded in double sine series

$$q(x, y) = \sum_{i=1}^M \sum_{j=1}^N Q_{ij} \sin \alpha_i x \sin \beta_j y \quad (6.6.11)$$

In view of the integral identities

$$\int_0^a \sin \alpha_i x \sin \alpha_j x dx = \begin{cases} 0, & i \neq j \\ \frac{a}{2}, & i = j \end{cases} \quad (6.6.12a)$$

$$\int_0^a \cos \alpha_i x \cos \alpha_j x dx = \begin{cases} 0, & i \neq j \\ \frac{a}{2}, & i = j \end{cases} \quad (6.6.12b)$$

$$\int_0^a \cos \alpha_i x \sin \alpha_j x dx = \begin{cases} 0, & i = j \text{ and } i + j \text{ even} \\ \frac{2j}{j^2 - i^2}, & i \neq j \text{ and } i + j \text{ odd} \end{cases} \quad (6.6.12c)$$

Eq. (6.6.9) can be simplified. In particular, when $D_{16} = D_{26} = 0$, Eq. (6.6.9) gives the Navier solutions presented in Chapter 5. When D_{16} and D_{26} are nonzero, the one-term Ritz solution does not exist for a general symmetric laminate, because the solution does not contain the stiffness terms D_{16} and D_{26} due to the vanishing of the integrals. Thus the double sine series solution is incomplete, and it can only give an approximate solution to the symmetrically laminated plates when many terms in the series are used.

As reported by Ashton and Whitney [5], for a square plate with $D_{22} = 0.1D_{11}$, $D_{12} + 2D_{66} = 1.5D_{11}$, and $D_{16} = D_{26} = -0.5D_{11}$, the maximum deflection under uniformly distributed load, obtained with $M = N = 7$ in the series, is

$$w_0(a/2, a/2) = 0.00425 \frac{q_0 a^4}{D_{11}} \quad (6.6.13)$$

For the same case, when D_{16} and D_{26} are neglected the maximum deflection is

$$w_0(a/2, a/2) = 0.00324 \frac{q_0 a^4}{D_{11}} \quad (6.6.14)$$

Thus, the deflection is underpredicted by 23.76% when the bending-twisting coupling is neglected.

Similarly, it is found that the orthotropic plate solutions for buckling loads and natural frequencies of vibration are overpredicted in comparison to the solutions obtained with the bending-twisting coupling in place. In general, the task of computing the Ritz solutions is algebraically complicated, and many terms have to be included to obtain accurate results.

6.6.6 Other Boundary Conditions

Equation (6.6.7) is also valid for other boundary conditions. Only the choice of the approximation functions X_i and Y_j is different for different boundary conditions. As discussed in Section 5.4.3, the eigenfunctions of the Euler–Bernoulli beams can be used for these functions (see Eq. (4.2.46a) and Table 4.2.3; also see [22,23]). For example, for a symmetric laminate with all edges clamped, we can use the eigenfunctions of a beam with both ends clamped:

$$\begin{aligned} X_i(x) &= \sin \lambda_i x - \sinh \lambda_i x + \alpha_i (\cosh \lambda_i x - \cos \lambda_i x) \\ Y_j(y) &= \sin \lambda_j y - \sinh \lambda_j y + \alpha_j (\cosh \lambda_j y - \cos \lambda_j y) \end{aligned} \quad (6.6.15)$$

for $i = 1, 2, \dots, M$; $j = 1, 2, \dots, N$. The parameters λ_i are the roots of the characteristic equation

$$\cos \lambda_i a \cosh \lambda_i a - 1 = 0 \quad (6.6.16)$$

and

$$\alpha_i = \frac{\sinh \lambda_i a - \sin \lambda_i a}{\cosh \lambda_i a - \cos \lambda_i a} = \frac{\cosh \lambda_i a - \cos \lambda_i a}{\sinh \lambda_i a + \sin \lambda_i a} \quad (6.6.17)$$

We will not consider the topic of solving symmetrically laminated plates for bending deflections, buckling loads, and vibration frequencies by the Ritz method further in this book. Interested readers may consult [19–23].

6.7 Transient Analysis

6.7.1 Preliminary Comments

Here we discuss the procedures to determine the transient response of composite laminates. The equations of motion can be solved using analytical solution methods, such as the state-space approach (see Khdeir and Reddy [24–26]). Here we discuss a method which takes advantage of the static solution form for spatial variation and which uses a numerical method to solve the resulting differential equations in time (see Reddy [27]).

As described in Section 5.9, there are two major steps in the solution process: (1) assume a spatial variation of the displacements and reduce the governing partial differential equations to a set of ordinary differential equations in time, and (2) solve the ordinary differential equations exactly if possible or numerically. The first step is amply illustrated in the preceding sections of this chapter. For example, the Navier solution method can be used to determine the spatial variation of the transient solution. The only difference is that the coefficients of the double Fourier series are assumed to be functions of time. Thus a typical dependent variable $\phi(x, y, t)$ is expanded as [see Eq. (6.3.3)]

$$\phi(x, y, t) = \sum_{m=1}^{\infty} \sum_{n=1}^{\infty} T_{mn}(t) F_{mn}(x, y)$$

where F_{mn} are suitable functions that satisfy the boundary conditions and T_{mn} are coefficients to be determined such that $\phi(x, y, t)$ satisfies its governing equation. The choice of a *separable* solution form as above implies that the general spatial variation is independent of time, and its amplitude may vary with time.

6.7.2 Equations of Motion

For simply supported cross-ply and antisymmetric angle-ply laminates, the Navier solution method can be used to reduce the governing equations of motion to differential equations in time. These are given by Eq. (6.3.19) for antisymmetric cross-ply laminates and by Eq. (6.4.6) for antisymmetric angle-ply laminates. In the absence of thermal effects and applied in-plane forces, these equations are of the form

$$\begin{bmatrix} \hat{c}_{11} & \hat{c}_{12} & \hat{c}_{13} \\ \hat{c}_{12} & \hat{c}_{22} & \hat{c}_{23} \\ \hat{c}_{13} & \hat{c}_{23} & \hat{c}_{33} \end{bmatrix} \begin{Bmatrix} U_{mn} \\ V_{mn} \\ W_{mn} \end{Bmatrix} + \begin{bmatrix} \hat{m}_{11} & 0 & 0 \\ 0 & \hat{m}_{22} & 0 \\ 0 & 0 & \hat{m}_{33} \end{bmatrix} \begin{Bmatrix} \ddot{U}_{mn} \\ \ddot{V}_{mn} \\ \ddot{W}_{mn} \end{Bmatrix} = \begin{Bmatrix} 0 \\ 0 \\ Q_{mn} \end{Bmatrix} \quad (6.7.1)$$

or

$$[M]\{\ddot{\Delta}\} + [K]\{\Delta\} = \{F\} \quad (6.7.2)$$

where the superposed dot denotes differentiation with respect to time, and

$$\{\Delta\} = \begin{Bmatrix} U_{mn} \\ V_{mn} \\ W_{mn} \end{Bmatrix}, \quad \{F\} = \begin{Bmatrix} 0 \\ 0 \\ Q_{mn} \end{Bmatrix} \quad (6.7.3)$$

The coefficients \hat{c}_{ij} and \hat{m}_{ij} of Eq. (6.7.1) are defined in Eqs. (6.3.20) and (6.4.7), respectively, for the two classes of laminates.

Equation (6.7.1) is subjected to the initial conditions

$$u_0(x, y, 0) = d_0^1(x, y), \quad v_0(x, y, 0) = d_0^2(x, y), \quad w_0(x, y, 0) = d_0^3(x, y) \quad (6.7.4a)$$

$$\dot{u}_0(x, y, 0) = v_0^1(x, y), \quad \dot{v}_0(x, y, 0) = v_0^2(x, y), \quad \dot{w}_0(x, y, 0) = v_0^3(x, y) \quad (6.7.4b)$$

We assume that the functions d^i and v^i ($i = 1, 2, 3$) can also be expanded in the double Fourier series in the same way as the corresponding displacements. Then we have

$$\Delta_{mn}^1 = U_{mn}(0) = D_{mn}^1, \quad \Delta_{mn}^2 = V_{mn}(0) = D_{mn}^2, \quad \Delta_{mn}^3 = W_{mn}(0) = D_{mn}^3$$

$$\dot{\Delta}_{mn}^1 = \dot{U}_{mn}(0) = V_{mn}^1, \quad \dot{\Delta}_{mn}^2 = \dot{V}_{mn}(0) = V_{mn}^2, \quad \dot{\Delta}_{mn}^3 = \dot{W}_{mn}(0) = V_{mn}^3 \quad (6.7.5)$$

where D_{mn}^i and V_{mn}^i are the coefficients in the Fourier expansion of the i th initial displacement and velocity, respectively.

6.7.3 Numerical Time Integration

The set of three equations in (6.7.2), for any fixed m and n , can be solved exactly using either the Laplace transform method or the modal analysis methods. Both methods are algebraically complicated and require the determination of eigenvalues and eigenfunctions, as in the state-space method. Therefore we will not attempt them here. Alternatively, we seek numerical solutions to Eq. (6.7.2) using the well-known family of Newmark's integration schemes for second-order differential equations (see Reddy [27]). In this numerical integration method, the time derivatives are approximated using difference approximations (or truncated Taylor's series), and therefore solution is obtained only for discrete times and not as a continuous function of time.

In the Newmark method, the function (of time) and its first derivative are approximated using Taylor's series and only terms up to the second derivative are included:

$$\begin{aligned} \{\Delta(t_{s+1})\} &= \{\Delta(t_s)\} + \delta t_s \{\dot{\Delta}(t_s)\} + \frac{1}{2}(\delta t_s)^2 \{\ddot{\Delta}(t_{s+\gamma})\} \\ \{\dot{\Delta}(t_{s+1})\} &= \{\dot{\Delta}(t_s)\} + \delta t_s \{\ddot{\Delta}(t_{s+\alpha})\} \\ \{\ddot{\Delta}(t_{s+\alpha})\} &= (1 - \alpha)\{\ddot{\Delta}(t_s)\} + \alpha\{\ddot{\Delta}(t_{s+1})\}, \quad 0 \leq \alpha \leq 1 \end{aligned} \quad (6.7.6)$$

where δt is the time increment, $\delta t_s = t_{s+1} - t_s$, and t_s is the current time and t_{s+1} is the next time at which we seek the solution. We assume that the solution at time

t_s is known. Substituting the third equation into the first two in Eq. (6.7.6) and solving for $\{\ddot{\Delta}\}$, we obtain

$$\begin{aligned}\{\dot{\Delta}\}_{s+1} &= \{\dot{\Delta}\}_s + a_1\{\ddot{\Delta}\}_s + a_2\{\ddot{\Delta}\}_{s+1} \\ \{\ddot{\Delta}\}_{s+1} &= a_3(\{\Delta\}_{s+1} - \{\Delta\}_s) - a_4\{\dot{\Delta}\}_s - a_5\{\ddot{\Delta}\}_s\end{aligned}\quad (6.7.7)$$

where

$$a_1 = (1 - \alpha)\delta t_s, \quad a_2 = \alpha\delta t_s, \quad a_3 = \frac{2}{\gamma(\delta t_s)^2}, \quad a_4 = a_3\delta t_s, \quad a_5 = \frac{(1 - \gamma)}{\gamma} \quad (6.7.8)$$

and $\{\cdot\}_s$, for example, denotes the value of the enclosed vector at time t_s .

The parameters α and γ are selected such that the error introduced in the approximation (6.7.6) does not grow unboundedly as the scheme is applied at each time step to determine the solution at the next time. When the error introduced is bounded (hence the solution is bounded), such schemes are said to be numerically *stable* schemes. Sometimes, there is a restriction on the size of the time step that would make the error remain bounded. In such cases, the scheme is said to be *conditionally stable*. All schemes for which $\gamma \geq \alpha \geq 1/2$ are unconditionally stable. Schemes for which $\gamma < \alpha$ and $\alpha \geq 0.5$ are conditionally stable, and the stability condition is

$$\delta t \leq \delta t_{cr} \equiv \frac{1}{\sqrt{2\omega_{max}}} (\alpha - \gamma)^{-\frac{1}{2}} \quad (6.7.9)$$

where ω_{max} denotes the maximum frequency of the discrete eigenvalue problem associate with Eq. (6.7.2):

$$([K] - \omega^2[M])\{\Delta\} = \{0\} \quad (6.7.10)$$

The critical time step can also be expressed in terms of the *period of vibration*, $T = 2\pi/\omega$. It should be noted that the frequencies of vibration for different modes, axial, bending, torsional, and shear modes, are different. The critical time step for the element is the smallest of the critical time steps calculated using the maximum frequency of each mode of vibration.

The Newmark family contains several well-known schemes as special cases. The following choices of α and γ define some of the widely used schemes:

$$\begin{aligned}\alpha &= \frac{1}{2}, \quad \gamma = \frac{1}{2}, \quad \text{the constant-average acceleration method (stable)} \\ \alpha &= \frac{1}{2}, \quad \gamma = \frac{1}{3}, \quad \text{the linear acceleration method (conditionally stable)} \\ \alpha &= \frac{1}{2}, \quad \gamma = \frac{1}{6}, \quad \text{the Fox-Goodwin scheme (conditionally stable)} \\ \alpha &= \frac{1}{2}, \quad \gamma = 0, \quad \text{the central difference method (conditionally stable)} \\ \alpha &= \frac{3}{2}, \quad \gamma = \frac{8}{5}, \quad \text{the Galerkin method (stable)} \\ \alpha &= \frac{3}{2}, \quad \gamma = 2, \quad \text{the backward difference method (stable)}\end{aligned}\quad (6.7.11)$$

Premultiplying the second equation in (6.7.7) with $[M]_{s+1}$ and using Eq. (6.7.2) at $t = t_{s+1}$ to replace $[M]_{s+1}\{\ddot{\Delta}\}_{s+1}$, we obtain

$$[\hat{K}]\{\Delta\}_{s+1} = \{\hat{F}\} \quad (6.7.12)$$

$$\begin{aligned} [\hat{K}] &= [K]_{s+1} + a_3[M]_{s+1} \\ \{\hat{F}\} &= \{F\}_{s+1} + [M]_{s+1} \left(a_3\{\Delta\}_s + a_4\{\dot{\Delta}\}_s + a_5\{\ddot{\Delta}\}_s \right) \end{aligned} \quad (6.7.13)$$

An alternative form of Eq. (6.7.12) is given by

$$[\bar{K}]\{\ddot{\Delta}\}_{s+1} = \{\bar{F}\} \quad (6.7.14a)$$

where

$$\begin{aligned} [\bar{K}] &= [M]_{s+1} + \frac{1}{a_3}[K]_{s+1} \\ \{\bar{F}\} &= \{F\}_{s+1} - [K]_{s+1} \left(\{\Delta\}_s + \frac{a_4}{a_3}\{\dot{\Delta}\}_s + \frac{a_5}{a_3}\{\ddot{\Delta}\}_s \right) \end{aligned} \quad (6.7.14b)$$

where a_3 , a_4 , and a_5 are defined in Eq. (6.7.8) in terms of the time step δt and the parameters α and γ . Note that for the central difference scheme ($\gamma = 0$), it is necessary to use Eq. (6.7.14a).

Equation (6.7.12) or (6.7.14a) represents a system of algebraic equations among the (discrete) values of $\{\Delta(t)\}$ at time $t = t_{s+1}$ in terms of known values at time $t = t_s$. Thus the values $\Delta_1(t) = U_{mn}(t)$, $\Delta_2(t) = V_{mn}(t)$, and $\Delta_3(t) = W_{mn}(t)$ are determined at time $t = t_1, t_2, \dots, t_s, \dots$ by a repeated solution (or marching in time) of Eq. (6.7.12). At the first time step (i.e., $s = 0$), the values $\{\Delta\}_0 = \{\Delta(0)\}$ and $\{\dot{\Delta}\}_0 = \{\dot{\Delta}(0)\}$ are known from the initial conditions (6.7.5) of the problem. However, $\{\ddot{\Delta}\}_0 = \{\ddot{\Delta}(0)\}$ is not known at time $t = 0$. Thus, the Newmark method is not a self-starting scheme. Although Eq. (6.7.2) is not valid for $t = 0$, it is used to determine $\{\ddot{\Delta}\}_0$ at $t = 0$:

$$\{\ddot{\Delta}\}_0 = [M]^{-1} \{ \{F\} - [K]\{\Delta\}_0 \} \quad (6.7.15)$$

The transient solution, for example, for the transverse deflection at time t_s , $s > 0$, is given by ($W_{mn}(t_s) = \Delta_{mn}^3(t_s)$)

$$w_0(x, y, t_s) = \sum_{m=1}^{\infty} \sum_{n=1}^{\infty} W_{mn}(t_s) \sin \frac{m\pi x}{a} \sin \frac{n\pi y}{b} \quad (6.7.16)$$

6.7.4 Numerical Results

Several examples of applications of the methodology described in this section are presented here. In all of the numerical examples, zero initial conditions were

assumed. The following data (in dimensional form) were used in all of the computations:

$$\begin{aligned} a = b &= 25 \text{ cm}, h = 1 \text{ cm } (a/b = 1, a/h = 25) \\ \rho &= 8 \times 10^{-6} \text{ N}\cdot\text{s}^2/\text{cm}^4, E_2 = 2.1 \times 10^6 \text{ N/cm}^2 \\ E_1 &= 25E_2, G_{12} = G_{13} = 0.5E_2, \nu_{12} = 0.25 \end{aligned} \quad (6.7.17)$$

The values of α and γ in the Newmark integration scheme are taken to be 0.5, which correspond to constant-average acceleration method.

The effect of the time step on the accuracy of the solution was investigated using a simply supported antisymmetric cross-ply (0/90) laminate under uniformly distributed step loading. Table 6.7.1 shows the nondimensionalized center transverse deflection, $\bar{w} = w_0(E_2h^3/q_0a^4) \times 10^2$, at selective times for three different time steps: $\delta t = 5, 20$, and $50\mu\text{s}$ ($\mu\text{s} = 10^{-6}\text{s}$). The effect of larger time step is to reduce the amplitude and increase the period. Plots of the nondimensionalized center deflection versus time for the same problem are shown in Figure 6.7.1. For all time steps below $10\mu\text{s}$, the difference is not noticeable on the graphs. In all the following examples, $\delta t = 5\mu\text{s}$ is used.

Table 6.7.1 Nondimensionalized center transverse deflections (\bar{w}) in simply supported (SS-1) cross-ply (0/90) laminates subjected to uniformly distributed transverse load ($h = 1\text{cm}$, $E_1/E_2 = 25$, $E_2 = 2.1 \times 10^6 \text{ N/cm}^2$, $G_{12} = G_{13} = 0.5E_2$, $G_{23} = 0.2E_2$, $\nu_{12} = 0.25$).

δt^\dagger	$t = 100^\dagger$	200	300	400	500	600	700	800	900
5	0.452	1.655	2.931	3.451	2.880	1.628	0.460	-0.003	0.511
20	0.372	1.568	2.862	3.404	2.943	1.796	0.530	-0.051	0.467
50	0.271	1.379	2.603	3.372	3.095	2.061	0.774	0.043	0.274

[†] Denotes time in microseconds (μs).

Figures 6.7.2 through 6.7.5 contain nondimensionalized transverse deflections and normal and shear stresses in two-layer and eight-layer antisymmetric cross-ply (0/90/0/...) square plates under suddenly applied transverse load. The nondimensionalizations used are the same as listed in Eq. (6.3.39), except that the nondimensionalized deflection plotted in the figures is $\bar{w} = w_0(E_2h^3/q_0a^4) \times 10^2$ (note the multiplicative factor). The normal stress $\bar{\sigma}_{xx} = \sigma_{xx}(h^2/q_0b^2)$ presented in Figure 6.7.4 is computed at $z = -h/2$, which is larger than that at $z = h/2$ (see Figure 6.7.3). The effect of coupling on the transient response can be seen from the two-layer and eight-layer results. It has the effect of increasing the amplitude as well as the period. The maximum deflections and stresses for the static case are summarized next.

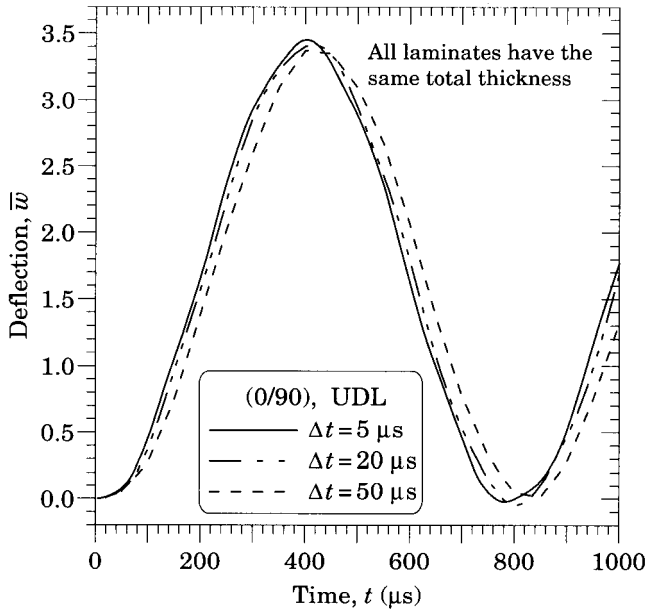


Figure 6.7.1: Nondimensionalized center transverse deflection (\bar{w}) versus time (t) for simply supported (SS-1) antisymmetric cross-ply (0/90) laminates subjected to uniformly distributed step loading; see Eq. (6.7.14) for the data.

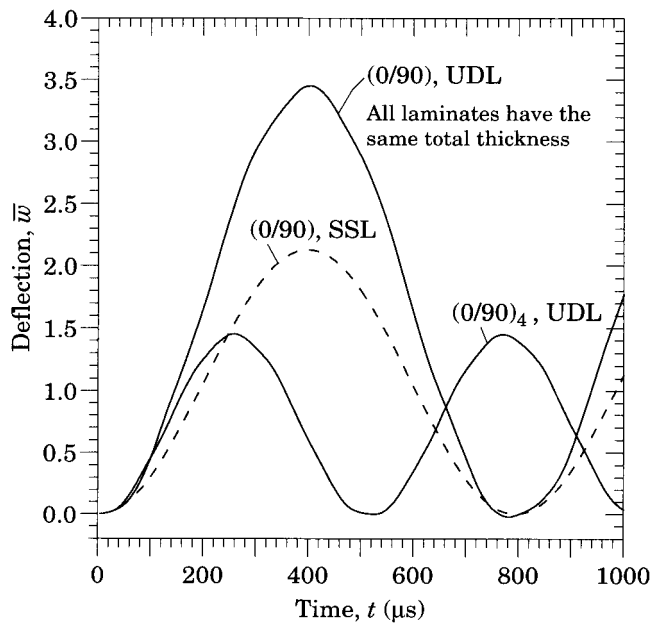


Figure 6.7.2: Nondimensionalized center transverse deflection (\bar{w}) versus time (t) for simply supported (SS-1) two-layer and eight-layer antisymmetric cross-ply laminates.

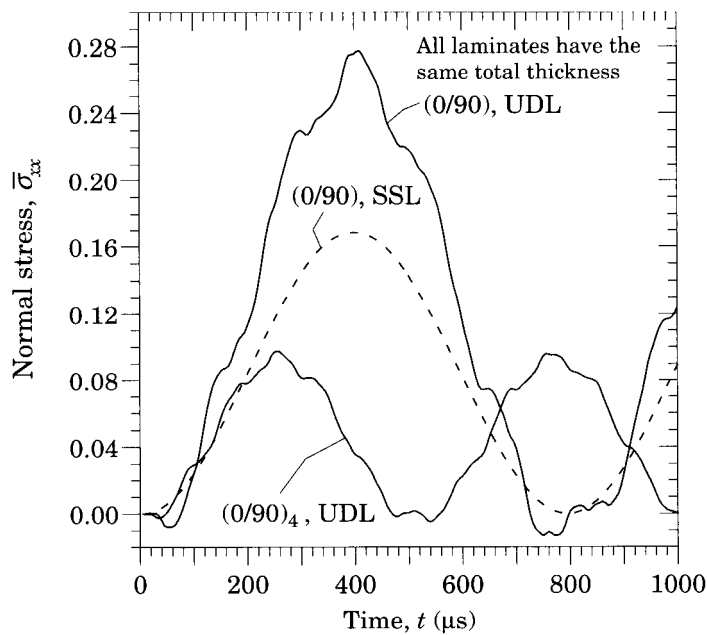


Figure 6.7.3: Nondimensionalized normal stress ($\bar{\sigma}_{xx}$) versus time (t) for simply supported (SS-1) two-layer and eight-layer antisymmetric cross-ply (0/90) laminates.

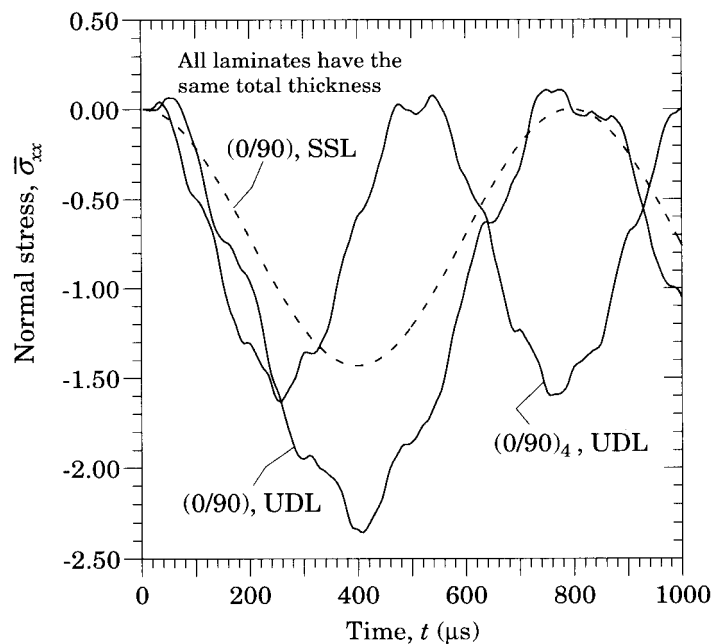


Figure 6.7.4: Nondimensionalized normal stress ($\bar{\sigma}_{xx}$ at the bottom of the laminate) versus time (t) for simply supported (SS-1) two-layer and eight-layer antisymmetric cross-ply (0/90) laminates.

Laminate (0/90), SSL:

$$\begin{aligned}\bar{w} &= 1.064, \quad \bar{\sigma}_{xx}(a/2, b/2, h/2) = 0.084 \\ \bar{\sigma}_{xx}(a/2, b/2, -h/2) &= -0.716, \quad \bar{\sigma}_{xy}(a, b, -h/2) = 0.053\end{aligned}\quad (6.7.18)$$

Laminate (0/90), UDL:

$$\begin{aligned}\bar{w} &= 1.695, \quad \bar{\sigma}_{xx}(a/2, b/2, h/2) = 0.127 \\ \bar{\sigma}_{xx}(a/2, b/2, -h/2) &= -1.076, \quad \bar{\sigma}_{xy}(a, b, -h/2) = 0.093\end{aligned}\quad (6.7.19)$$

Laminate (0/90/0/···), UDL:

$$\begin{aligned}\bar{w} &= 0.715, \quad \bar{\sigma}_{xx}(a/2, b/2, h/2) = 0.045 \\ \bar{\sigma}_{xx}(a/2, b/2, -h/2) &= -0.749, \quad \bar{\sigma}_{xy}(a, b, -h/2) = 0.039\end{aligned}\quad (6.7.20)$$

Note that the maximum transient transverse deflection of (0/90) laminate under UDL, which occurs at $t = 400 \mu s$, is 2.035 times that of the static deflection. Similarly, the stresses are also about 2.035 times that of the static stresses.

Figures 6.7.6 through 6.7.8 contain nondimensionalized transverse deflections and shear and normal stresses in two-layer and eight-layer antisymmetric angle-ply (0/90/0/···) square plates under suddenly applied transverse load. The same observations made for cross-ply laminates also apply for angle-ply plates. The angle-ply plates, for the same material and geometric dimensions, have smaller maximum deflections, stresses, and periods of oscillation. The maximum static deflections and stresses are given below.

Laminate (-45/45), UDL:

$$\bar{w} = 1.028, \quad \bar{\sigma}_{xx}(a/2, b/2, h/2) = 0.351, \quad \bar{\sigma}_{xy}(a, b, -h/2) = 0.442 \quad (6.7.21)$$

Laminate (-45/45/-45/···), UDL:

$$\bar{w} = 0.386, \quad \bar{\sigma}_{xx}(a/2, b/2, h/2) = 0.201, \quad \bar{\sigma}_{xy}(a, b, -h/2) = 0.264 \quad (6.7.22)$$

The maximum transient deflection for the two-layer plate is 2.114 and it occurs at $t = 305 \mu s$; it is about 2.056 times that of the static deflection. In the case of eight-layer laminate, the maximum transient deflection is 0.7988 and it occurs at $t = 190 \mu s$; it is 2.7 times that of the static deflection.

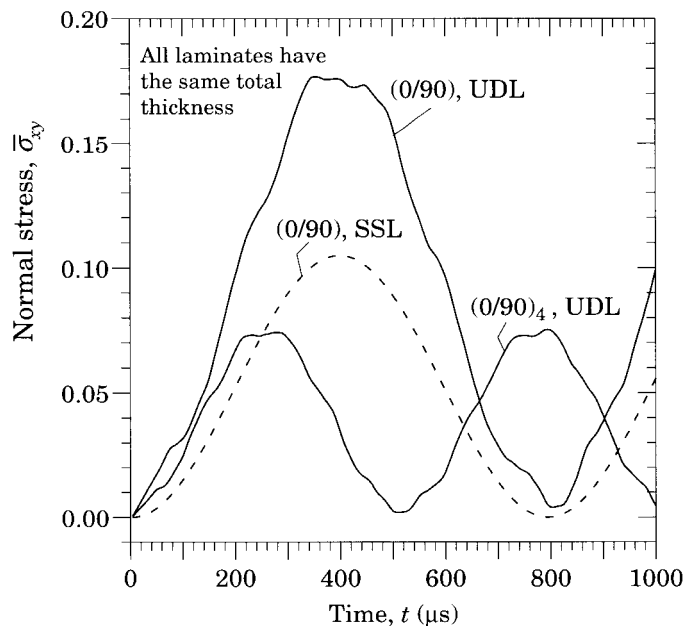


Figure 6.7.5: Nondimensionalized shear stress ($\bar{\sigma}_{xy}$) versus time (t) for simply supported (SS-1) two-layer and eight-layer antisymmetric cross-ply (0/90) laminates.

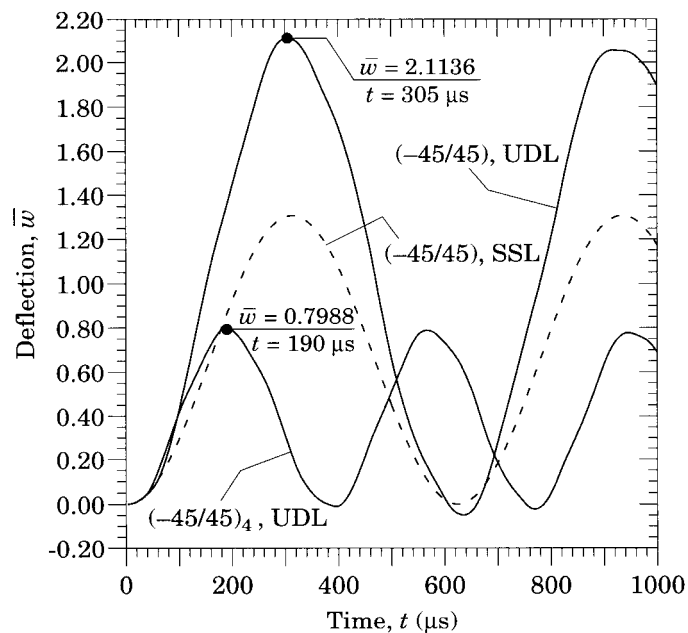


Figure 6.7.6: Nondimensionalized center transverse deflection (\bar{w}) versus time (t) for simply supported (SS-2) two-layer and eight-layer antisymmetric angle-ply (-45/45)_n laminates.

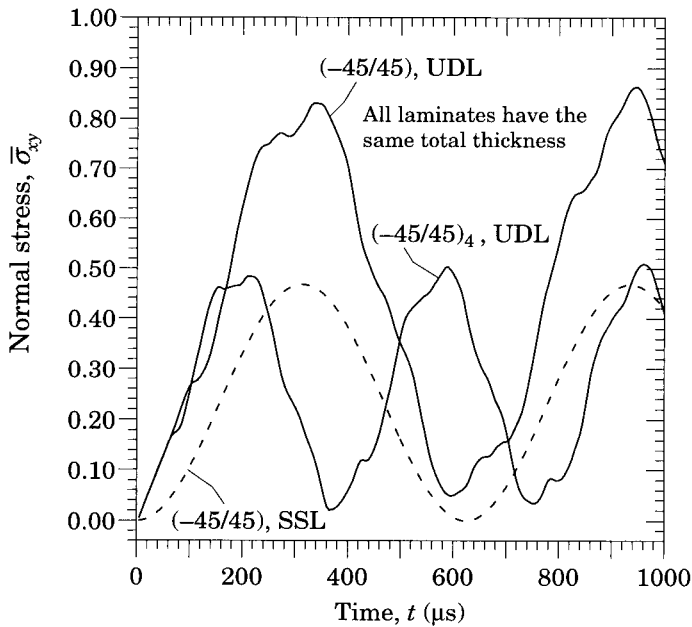


Figure 6.7.7: Nondimensionalized shear stress ($\bar{\sigma}_{xy}$) versus time (t) for simply supported (SS-2) two-layer and eight-layer antisymmetric angle-ply $(-45/45)_n$ laminates.

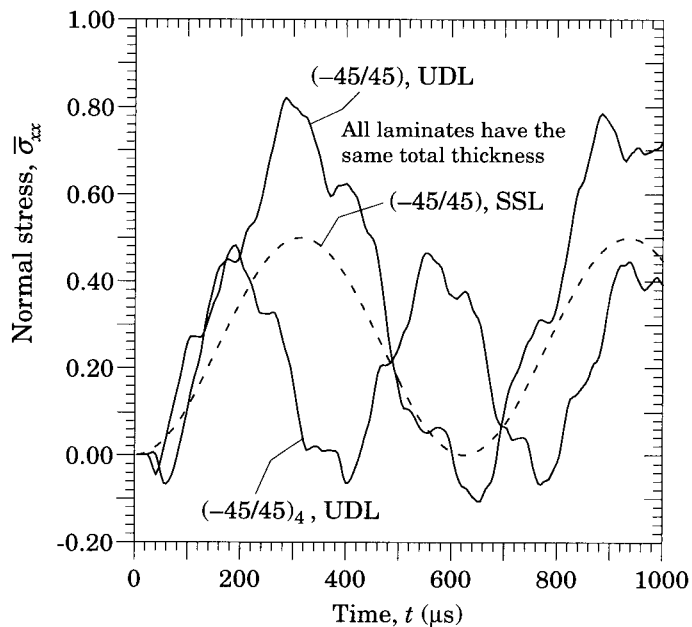


Figure 6.7.8: Nondimensionalized normal stress ($\bar{\sigma}_{xx}$) versus time (t) for simply supported (SS-2) two-layer and eight-layer antisymmetric angle-ply $(-45/45)_n$ laminates.

6.8 Summary

In this chapter analytical solutions for bending, buckling under in-plane compressive loads, and natural vibration of rectangular laminates with various boundary conditions were presented based on the classical laminate theory. The Navier solutions were developed for two classes of laminates: antisymmetric cross-ply laminates and antisymmetric angle-ply laminates, each for a specific type of simply supported boundary conditions, SS-1 and SS-2, respectively. The Lévy solutions with the state-space approach were developed for these classes of laminates when two opposite edges are simply supported with the other two edges having a variety of boundary conditions of choice. A discussion of symmetrically laminated plates, which are characterized by nonzero bending-twisting coupling terms, is also presented. For such laminates, one must use approximate methods, such as the Ritz method or the finite element method because the Navier solutions do not exist for symmetric laminates. The Ritz solutions for symmetric laminates are discussed in some detail. Lastly, a transient solution procedure for antisymmetric cross-ply and angle-ply laminates is presented. In this procedure, the solutions are assumed to be products of functions of spatial coordinates (x, y) only and functions of time t only (i.e., separation of variables). The spatial functions are the same as those used in the static case, and the time variation is determined using the Newmark time integration scheme.

Numerical results were presented for static bending, buckling, natural vibration, and transient response of antisymmetric cross-ply and angle-ply laminates. The presence of bending-extensional coupling in a laminate generally reduces the effective stiffnesses and hence increases deflections and reduces buckling loads and natural frequencies. The coupling also increases the period of oscillation in the transient problems. The coupling is the most significant in two-layer laminates, and it decreases gradually as the number of layers is increased for fixed total thickness.

The presence of twist-curvature coupling in a laminate also has the effect of increasing deflections, decreasing buckling loads, and decreasing natural frequencies. The coupling dies out as the number of layers is increased for fixed total thickness.

The effects of bending-stretching coupling and twist-curvature coupling on deflections, buckling loads, and natural frequencies of general laminates, for example, unsymmetric laminates, can only be assessed by specific studies. Such laminates can be analyzed only with approximate methods of analysis.

In general, the bending-twisting coupling in symmetrically laminated plates has the effect of increasing deflections and decreasing buckling loads and natural frequencies of vibration. Analysis of such laminates by the Ritz method is characterized by slow convergence.

Problems

- 6.1** Verify Eq. (6.2.4) by casting Eqs. (6.2.1)–(6.2.3) in operator form.
- 6.2** Verify Eq. (6.3.19) by substituting expansions (6.3.3) into Eqs. (6.2.1)–(6.2.3) and assuming that conditions in Eqs. (6.3.7) hold.
- 6.3** Verify the solution in Eq. (6.3.27).

- 6.4** Derive the expressions for transverse shear stresses from 3-D equations of equilibrium for the case of isothermal, antisymmetric cross-ply laminates.
- 6.5** Derive the expressions for transverse shear stresses from 3-D equations of equilibrium for the nonisothermal case of antisymmetric angle-ply laminates when the temperature distribution is of the form

$$\Delta T(x, y, z) = T_0(x, y) + zT_1(x, y)$$

Assume that both T_0 and T_1 can be expanded in double sine series (similar to the mechanical load).

- 6.6** Verify Eq. (6.4.6) by substituting expansions (6.4.2) into Eqs. (6.2.1)–(6.2.3) and assuming that conditions in Eqs. (6.4.4) hold.
- 6.7** Verify the solution in Eq. (6.4.9).
- 6.8** Verify the expressions in Eq. (6.5.11) by substituting expansions (6.5.10) into the definitions of the resultants in Eqs. (3.3.43) and (3.3.44).
- 6.9** Verify Eqs. (6.5.15).
- 6.10** Consider antisymmetric angle-ply rectangular laminates with edges $x = 0$ and $x = a$ simply supported and the other two edges, $y = \pm b/2$, having arbitrary boundary conditions. Assume solution of the form

$$\begin{aligned} u_0(x, y, t) &= \sum_{m=1}^{\infty} U_m(y) \sin \alpha x \\ v_0(x, y, t) &= \sum_{m=1}^{\infty} V_m(y) \cos \alpha x \\ w_0(x, y, t) &= \sum_{m=1}^{\infty} W_m(y) \sin \alpha x \end{aligned} \quad (1)$$

and load expansion in the form

$$q(x, y) = \sum_{m=1}^{\infty} Q_m(y) \sin \alpha x \quad (2)$$

where $\alpha = m\pi/a$. Show that the equations of equilibrium of the classical laminated plate theory for such laminates (without any applied in-plane loading) can be reduced to the following ordinary differential equations

$$\begin{aligned} U''_m &= C_1 U_m + C_2 V'_m + C_3 W'_m + C_4 W'''_m \\ V''_m &= C_5 U'_m + C_6 V_m + C_7 W_m + C_8 W''_m \\ W''''_m &= C_9 U'_m + C_{10} V_m + C_{11} W_m + C_{12} W''_m + C_{13} Q_m \end{aligned} \quad (3)$$

where the primes indicate differentiation with respect to y , and the coefficients C_i are defined as

$$\begin{aligned} C_1 &= -e_1/e_2, \quad C_2 = -e_3/e_2, \quad C_3 = -e_4/e_2, \quad C_4 = -e_5/e_2 \\ C_5 &= -e_6/e_8, \quad C_6 = -e_7/e_8, \quad C_7 = -e_9/e_8, \quad C_8 = -e_{10}/e_8 \\ C_9 &= \left(e_{14} - \frac{e_1 e_{16}}{e_2} - \frac{e_6 e_{17}}{e_8} + \frac{e_3 e_6 e_{16}}{e_2 e_8} \right) \left(\frac{e_5 e_{16}}{e_2} - e_{13} \right)^{-1} \\ C_{10} &= \left(e_{15} - \frac{e_7 e_{17}}{e_8} + \frac{e_3 e_7 e_{16}}{e_2 e_8} \right) \left(\frac{e_5 e_{16}}{e_2} - e_{13} \right)^{-1} \\ C_{11} &= \left(e_{11} - \frac{e_9 e_{17}}{e_8} + \frac{e_3 e_9 e_{16}}{e_2 e_8} \right) \left(\frac{e_5 e_{16}}{e_2} - e_{13} \right)^{-1} \\ C_{12} &= \left(e_{12} - \frac{e_4 e_{16}}{e_2} - \frac{e_{10} e_{17}}{e_8} + \frac{e_3 e_{10} e_{16}}{e_2 e_8} \right) \left(\frac{e_5 e_{16}}{e_2} - e_{13} \right)^{-1} \\ C_{13} &= \left(e_{13} - \frac{e_5 e_{16}}{e_2} \right)^{-1} \end{aligned} \quad (4)$$

and the coefficients e_i are defined as

$$\begin{aligned} e_1 &= -\alpha^2 A_{11}, \quad e_2 = A_{66}, \quad e_3 = -\alpha(A_{12} + A_{66}), \quad e_4 = 3\alpha^2 B_{16} \\ e_5 &= -B_{26}, \quad e_6 = -e_3, \quad e_7 = -\alpha^2 A_{66}, \quad e_8 = A_{22} \\ e_9 &= \alpha^3 B_{16}, \quad e_{10} = -3\alpha B_{26}, \quad e_{11} = \alpha^4 D_{11}, \quad e_{12} = -2\alpha^2(D_{12} + 2D_{66}) \\ e_{13} &= D_{22}, \quad e_{14} = e_4, \quad e_{15} = -e_9, \quad e_{16} = e_5, \quad e_{17} = -e_{10} \end{aligned} \quad (5)$$

- 6.11** Repeat Exercise 6.10 for the case of biaxial buckling. All definitions in Problem 6.10 hold with exception of e_{11} and e_{12} , which are modified as

$$\begin{aligned} e_{11} &= \alpha^4 D_{11} - \alpha^2 N_{xx}^0 \\ e_{12} &= -2\alpha^2(D_{12} + 2D_{66}) + N_{yy}^0 \end{aligned}$$

where N_{xx}^0 and N_{yy}^0 are the in-plane compressive forces.

- 6.12** Repeat Exercise 6.10 for the case of free vibration. All definitions in Exercise 6.10 hold with exception of e_{11} , which is modified as (when $I_2 = 0$)

$$e_{11} = \alpha^4 D_{11} - I_0 \omega_m^2, \quad I_0 = \int_{-h/2}^{h/2} \rho^{(m)} dz$$

where ω_m is the frequency of vibration associated with mode m .

- 6.13** Defining the state vector $\mathbf{Z}(\mathbf{y})$ as

$$\begin{aligned} Z_1 &= U_m, \quad Z_2 = U'_m, \quad Z_3 = V_m, \quad Z_4 = V'_m \\ Z_5 &= W_m, \quad Z_6 = W'_m, \quad Z_7 = W''_m, \quad Z_8 = W'''_m \end{aligned} \quad (1)$$

express Eqs. (3) of Problem 6.10 as a first-order matrix equation of the form

$$\mathbf{Z}' = \mathbf{T}\mathbf{Z} + \mathbf{F} \quad (2)$$

where the matrix \mathbf{T} and the column vector \mathbf{F} are given by

$$\mathbf{T} = \begin{bmatrix} 0 & 1 & 0 & 0 & 0 & 0 & 0 & 0 \\ C_1 & 0 & 0 & C_2 & 0 & C_3 & 0 & C_4 \\ 0 & 0 & 0 & 1 & 0 & 0 & 0 & 0 \\ 0 & C_5 & C_6 & 0 & C_7 & 0 & C_8 & 0 \\ 0 & 0 & 0 & 0 & 0 & 1 & 0 & 0 \\ 0 & 0 & 0 & 0 & 0 & 0 & 1 & 0 \\ 0 & 0 & 0 & 0 & 0 & 0 & 0 & 1 \\ 0 & C_9 & C_{10} & 0 & C_{11} & 0 & C_{12} & 0 \end{bmatrix} \quad (3)$$

$$\mathbf{F} = \{0, 0, 0, 0, 0, 0, 0, C_{13} Q_m\}^T \quad (4)$$

- 6.14** Consider a symmetrically laminated rectangular plate under the transverse load $q(x, y)$. The governing equation for static bending analysis is given by

$$\begin{aligned} D_{11} \frac{\partial^4 w_0}{\partial x^4} + 4D_{16} \frac{\partial^4 w_0}{\partial x^3 \partial y} + 2(D_{12} + 2D_{66}) \frac{\partial^4 w_0}{\partial x^2 \partial y^2} \\ + D_{22} \frac{\partial^4 w_0}{\partial y^4} + 4D_{26} \frac{\partial^4 w_0}{\partial x \partial y^3} = q \end{aligned}$$

The weak form (or the virtual work statement) of the same equation is given by Eq. (6.6.4), without the in-plane force and inertial terms. Show that the Ritz solution of the form

$$w_0(x, y) \approx \sum_{i=1}^N c_i \phi_i(x, y) \quad (1)$$

requires the solution of the algebraic equation

$$[R]\{c\} = \{q\} \quad (2)$$

where

$$\begin{aligned} R_{ij} &= \int_0^b \int_0^a \left[D_{11} \frac{\partial^2 \phi_i}{\partial x^2} \frac{\partial^2 \phi_j}{\partial x^2} + D_{12} \left(\frac{\partial^2 \phi_i}{\partial y^2} \frac{\partial^2 \phi_j}{\partial x^2} + \frac{\partial^2 \phi_i}{\partial x^2} \frac{\partial^2 \phi_j}{\partial y^2} \right) \right. \\ &\quad + 4D_{66} \frac{\partial^2 \phi_i}{\partial x \partial y} \frac{\partial^2 \phi_j}{\partial x \partial y} + D_{22} \frac{\partial^2 \phi_i}{\partial y^2} \frac{\partial^2 \phi_j}{\partial y^2} \\ &\quad + 2D_{16} \left(\frac{\partial^2 \phi_i}{\partial x^2} \frac{\partial^2 \phi_j}{\partial x \partial y} + \frac{\partial^2 \phi_i}{\partial x \partial y} \frac{\partial^2 \phi_j}{\partial x^2} \right) \\ &\quad \left. + 2D_{26} \left(\frac{\partial^2 \phi_i}{\partial y^2} \frac{\partial^2 \phi_j}{\partial x \partial y} + \frac{\partial^2 \phi_i}{\partial x \partial y} \frac{\partial^2 \phi_j}{\partial y^2} \right) \right] dx dy \\ q_i &= \int_0^b \int_0^a q(x, y) \phi_i \, dx dy \end{aligned} \quad (3)$$

- 6.15** Consider a symmetrically laminated rectangular plate with simply supported edges. The boundary conditions are given by

$$w_0(x, 0) = 0, \quad w_0(x, b) = 0, \quad w_0(0, y) = 0, \quad w_0(a, y) = 0$$

$$M_{xx}(0, y) = 0, \quad M_{xx}(a, y) = 0, \quad M_{yy}(x, 0) = 0, \quad M_{yy}(x, b) = 0$$

where the bending moments are related to the transverse deflection by the equations

$$\begin{aligned} M_{xx} &= - \left(D_{11} \frac{\partial^2 w_0}{\partial x^2} + 2D_{16} \frac{\partial^2 w_0}{\partial x \partial y} + D_{12} \frac{\partial^2 w_0}{\partial y^2} \right) \\ M_{yy} &= - \left(D_{12} \frac{\partial^2 w_0}{\partial x^2} + 2D_{26} \frac{\partial^2 w_0}{\partial x \partial y} + D_{22} \frac{\partial^2 w_0}{\partial y^2} \right) \end{aligned}$$

Find a two-parameter Ritz approximation using algebraic polynomials. Note that the one-parameter approximation, $w_0(x, y) \approx c_1 xy(a - x)(b - y)$ does not give a solution for the case in which D_{16} and D_{26} are not zero.

Ans: For the approximation of the form

$$w_0(x, y) \approx c_1 xy(a - x)(b - y) + c_2 x^2 y^2 (a - x)(b - y)$$

the Ritz coefficients are given by

$$\begin{aligned} R_{11} &= 2 \left[D_{11} \frac{ab^5}{15} + 2(D_{12} + 2D_{66}) \frac{a^3 b^3}{9} + D_{22} \frac{a^5 b}{15} \right] \\ R_{12} &= \left[D_{11} \frac{a^2 b^7}{60} + 2(D_{12} + 2D_{66}) \frac{a^4 b^4}{36} + D_{22} \frac{a^7 b^2}{60} - 2D_{16} \frac{a^3 b^5}{60} - 2D_{26} \frac{a^5 b^3}{60} \right] \\ R_{22} &= 4 \left[D_{11} \frac{a^3 b^7}{105} + 2(D_{12} + 2D_{66}) \frac{a^5 b^5}{225} + D_{22} \frac{a^7 b^3}{105} + D_{16} \frac{a^4 b^6}{10} + D_{26} \frac{a^6 b^4}{10} \right] \\ q_1 &= q_0 \frac{a^3 b^3}{36}, \quad q_2 = q_0 \frac{a^7 b^7}{(105)(105)} \end{aligned}$$

References for Additional Reading

1. Reddy, J. N., *Energy Principles and Variational Methods in Applied Mechanics*, Second Edition, John Wiley, New York (2002).
2. Brogan, W. L., *Modern Control Theory*, Prentice-Hall, Englewood Cliffs, NJ (1985).
3. Franklin, J. N., *Matrix Theory*, Prentice-Hall, Englewood Cliffs, NJ (1968).
4. Nosier, A. and Reddy, J. N., "Vibration and Stability Analyses of Cross-Ply Laminated Circular Cylindrical Shells," *Journal of Sound and Vibration*, **157** (1), 139–159 (1992).
5. Ashton, J. E. and Whitney, J. M., *Theory of Laminated Plates*, Technomic, Stamford, CT (1970).
6. Reddy, J. N. (ed.), *Mechanics of Composite Materials. Selected Works of Nicholas J. Pagano*, Kluwer, The Netherlands (1994).
7. Pagano, N. J., "Exact Solutions for Rectangular Bidirectional Composites and Sandwich Plates," *Journal of Composite Materials*, **4**(1), 20–34 (1970).
8. Pagano, N. J., and Hatfield, S. J., "Elastic Behavior of Multilayered Bidirectional Composites," *AIAA Journal*, **10**(7), 931–933 (1972).
9. Reddy, J. N. and Chao, W. C., "A Comparison of Closed Form and Finite Element Solutions of Thick Laminated Anisotropic Rectangular Plates," *Nuclear Engineering and Design*, **64**, 153–167 (1981).
10. Reddy, J. N., Khdeir, A. A., and Librescu, L., "Lévy Type Solutions for Symmetrically Laminated Rectangular Plates Using First-Order Shear Deformation Theory," *Journal of Applied Mechanics*, **54**, 740–742 (1987).
11. Khdeir, A. A., Reddy, J. N., and Librescu, L., "Analytical Solution of a Refined Shear Deformation Theory for Rectangular Composite Plates," *International Journal of Solids and Structures*, **23**, 1447–1463 (1987).
12. Khdeir, A. A. and Librescu, L., "Analysis of Symmetric Cross-Ply Laminated Elastic Plates Using a Higher-Order Theory: Part I: Stress and Displacement," *Composite Structures*, **9**, 189–213 (1988).
13. Khdeir, A. A. and Librescu, L., "Analysis of Symmetric Cross-Ply Laminated Elastic Plates Using a Higher-Order Theory: Part II: Buckling and Free Vibration," *Composite Structures*, **9**, 259–277 (1988).
14. Reddy, J. N. and Khdeir, A. A., "Buckling and Vibration of Laminated Composite Plates Using Various Plate Theories," *AIAA Journal*, **27**(12), 1808–1817 (1989).
15. Khdeir, A. A., "Free Vibration of Antisymmetric Angle-Ply Laminated Plates Including Various Boundary Conditions," *Journal of Sound and Vibration*, **122**(2), 377–388 (1988).
16. Khdeir, A. A., "Free Vibration and Buckling of Unsymmetric Cross-Ply Laminated Plates," *Journal of Sound and Vibration*, **128** (3), 377–395 (1989).
17. Khdeir, A. A., "An Exact Approach to the Elastic State of Stress of Shear Deformable Antisymmetric Angle-Ply Laminated Plates," *Composite Structures*, **11**, 245–258 (1989).
18. Khdeir, A. A., "Comparison Between Shear Deformable and Kirchhoff Theories for Bending, Buckling, and Vibration of Antisymmetric Angle-Ply Laminated Plates," *Composite Structures*, **13**, 159–172 (1989).
19. Ashton, J. E. and Waddoups, M. E., "Analysis of Anisotropic Plates," *Journal of Composite Materials*, **3**, 148–165 (1969).
20. Ashton, J. E., "Analysis of Anisotropic Plates II," *Journal of Composite Materials*, **3**, 470–479 (1969).
21. Lekhnitskii, S. G., *Anisotropic Plates*, Translated from Russian by S. W. Tsai and T. Cheron, Gordon and Breach, Newark, NJ (1968).

22. Hearman, R. F. S., "The Frequency of Flexural Vibration of Rectangular Orthotropic Plates with Clamped or Supported Edges," *Journal of Applied Mechanics*, **26**(4), 537–540 (1959).
23. Young, D. and Felgar, F. P., *Tables of Characteristic Functions Representing the Normal Modes of Vibration of a Beam*, University of Texas, Publication No. 4913 (1949).
24. Khdeir A. A., and Reddy, J. N. "Exact Solutions for the Transient Response of Symmetric Cross-Ply Laminates Using a Higher-Order Plate Theory," *Composites Science and Technology*, **34**, 205–224 (1989).
25. Khdeir A. A., and Reddy, J. N. "On the Forced Motions of Antisymmetric Cross-Ply Laminates," *International Journal of Mechanical Sciences*, **31**, 499–510 (1989).
26. Khdeir A. A., and Reddy, J. N. "Dynamic Response of Antisymmetric Angle-Ply Laminated Plates Subjected to Arbitrary Loading," *Journal of Sound and Vibration*, **126**, 437–445 (1988).
27. Reddy, J. N., "On the Solutions to Forced Motions of Rectangular Composite Plates," *Journal of Applied Mechanics*, **49**, 403–408 (1982).
28. Khdeir, A. A. and Reddy, J. N., "Analytical Solutions of Refined Plate Theories of Cross-Ply Composite Laminates," *Journal of Pressure Vessel Technology*, **113**(4), 570–578 (1991).

Analytical Solutions of Rectangular Laminated Plates Using FSDT

7.1 Introduction

The classical laminate plate theory is based on the Kirchhoff assumptions, in which transverse normal and shear stresses are neglected. Although such stresses can be postcomputed through 3-D elasticity equilibrium equations, they are not always accurate. The equilibrium-derived transverse stress field is sufficiently accurate for homogeneous and thin plates; they are not accurate when plates are relatively thick (i.e., $a/h < 20$). In the first-order shear deformation theory (FSDT), a constant state of transverse shear stresses is accounted for, and often the transverse normal stress is neglected. The FSDT allows the computation of interlaminar shear stresses through constitutive equations, which is quite simpler than deriving them through equilibrium equations. It should be noted that the interlaminar stresses derived from constitutive equations do not match, in general, those derived from equilibrium equations. In fact, the transverse shear stresses derived from the equilibrium equations are quadratic through lamina thickness, as was shown in Chapter 6 for CLPT, whereas those computed from constitutive equations are constant.

The more significant difference between the classical and first-order theories is the effect of including transverse shear deformation on the predicted deflections, frequencies, and buckling loads. As noted in Chapter 6, the classical laminate theory underpredicts deflections and overpredicts frequencies as well as buckling loads with plate side-to-thickness ratios of the order of 20 or less. For this reason alone it is necessary to use the first-order theory in the analysis of relatively thick laminated plates. In this chapter, we develop analytical solutions of rectangular laminates using the first-order shear deformation theory. The primary objective is to bring out the effect of shear deformation on deflections, stresses, frequencies, and buckling loads.

To discuss the Navier and other solutions, the equations of motion of the first-order plate theory, Eqs. (3.4.23) through (3.4.27), are expressed in terms of the generalized displacements (u_0, v_0, w_0, ϕ_x and ϕ_y) as

$$\begin{aligned} \frac{\partial}{\partial x} \left[A_{11} \frac{\partial u_0}{\partial x} + A_{12} \frac{\partial v_0}{\partial y} + A_{16} \left(\frac{\partial u_0}{\partial y} + \frac{\partial v_0}{\partial x} \right) + B_{11} \frac{\partial \phi_x}{\partial x} + B_{12} \frac{\partial \phi_y}{\partial y} \right. \\ \left. + B_{16} \left(\frac{\partial \phi_x}{\partial y} + \frac{\partial \phi_y}{\partial x} \right) \right] + \frac{\partial}{\partial y} \left[A_{16} \frac{\partial u_0}{\partial x} + A_{26} \frac{\partial v_0}{\partial y} \right. \\ \left. + A_{66} \left(\frac{\partial u_0}{\partial y} + \frac{\partial v_0}{\partial x} \right) + B_{16} \frac{\partial \phi_x}{\partial x} + B_{26} \frac{\partial \phi_y}{\partial y} + B_{66} \left(\frac{\partial \phi_x}{\partial y} + \frac{\partial \phi_y}{\partial x} \right) \right] \end{aligned}$$

$$-\left(\frac{\partial N_{xx}^T}{\partial x} + \frac{\partial N_{xy}^T}{\partial y}\right) = I_0 \frac{\partial^2 u_0}{\partial t^2} + I_1 \frac{\partial^2 \phi_x}{\partial t^2} \quad (7.1.1)$$

$$\begin{aligned} & \frac{\partial}{\partial x} \left[A_{16} \frac{\partial u_0}{\partial x} + A_{26} \frac{\partial v_0}{\partial y} + A_{66} \left(\frac{\partial u_0}{\partial y} + \frac{\partial v_0}{\partial x} \right) + B_{16} \frac{\partial \phi_x}{\partial x} + B_{26} \frac{\partial \phi_y}{\partial y} \right. \\ & \quad \left. + B_{66} \left(\frac{\partial \phi_x}{\partial y} + \frac{\partial \phi_y}{\partial x} \right) \right] + \frac{\partial}{\partial y} \left[A_{12} \frac{\partial u_0}{\partial x} + A_{22} \frac{\partial v_0}{\partial y} \right. \\ & \quad \left. + A_{26} \left(\frac{\partial u_0}{\partial y} + \frac{\partial v_0}{\partial x} \right) + B_{12} \frac{\partial \phi_x}{\partial x} + B_{22} \frac{\partial \phi_y}{\partial y} + B_{26} \left(\frac{\partial \phi_x}{\partial y} + \frac{\partial \phi_y}{\partial x} \right) \right] \\ & - \left(\frac{\partial N_{xy}^T}{\partial x} + \frac{\partial N_{yy}^T}{\partial y} \right) = I_0 \frac{\partial^2 v_0}{\partial t^2} + I_1 \frac{\partial^2 \phi_y}{\partial t^2} \end{aligned} \quad (7.1.2)$$

$$\begin{aligned} & \frac{\partial}{\partial x} \left[K A_{45} \left(\frac{\partial w_0}{\partial y} + \phi_y \right) + K A_{55} \left(\frac{\partial w_0}{\partial x} + \phi_x \right) \right] \\ & + \frac{\partial}{\partial y} \left[K A_{44} \left(\frac{\partial w_0}{\partial y} + \phi_y \right) + K A_{45} \left(\frac{\partial w_0}{\partial x} + \phi_x \right) \right] \\ & + \hat{N}_{xx} \frac{\partial^2 w_0}{\partial x^2} + 2 \hat{N}_{xy} \frac{\partial^2 w_0}{\partial x \partial y} + \hat{N}_{yy} \frac{\partial^2 w_0}{\partial y^2} + q = I_0 \frac{\partial^2 w_0}{\partial t^2} \end{aligned} \quad (7.1.3)$$

$$\begin{aligned} & \frac{\partial}{\partial x} \left[B_{11} \frac{\partial u_0}{\partial x} + B_{12} \frac{\partial v_0}{\partial y} + B_{16} \left(\frac{\partial u_0}{\partial y} + \frac{\partial v_0}{\partial x} \right) + D_{11} \frac{\partial \phi_x}{\partial x} + D_{12} \frac{\partial \phi_y}{\partial y} \right. \\ & \quad \left. + D_{16} \left(\frac{\partial \phi_x}{\partial y} + \frac{\partial \phi_y}{\partial x} \right) \right] + \frac{\partial}{\partial y} \left[B_{16} \frac{\partial u_0}{\partial x} + B_{26} \frac{\partial v_0}{\partial y} \right. \\ & \quad \left. + B_{66} \left(\frac{\partial u_0}{\partial y} + \frac{\partial v_0}{\partial x} \right) + D_{16} \frac{\partial \phi_x}{\partial x} + D_{26} \frac{\partial \phi_y}{\partial y} + D_{66} \left(\frac{\partial \phi_x}{\partial y} + \frac{\partial \phi_y}{\partial x} \right) \right] \\ & - \left[K A_{45} \left(\frac{\partial w_0}{\partial y} + \phi_y \right) + K A_{55} \left(\frac{\partial w_0}{\partial x} + \phi_x \right) \right] \\ & - \left(\frac{\partial M_{xx}^T}{\partial x} + \frac{\partial M_{xy}^T}{\partial y} \right) = I_2 \frac{\partial^2 \phi_x}{\partial t^2} + I_1 \frac{\partial^2 u_0}{\partial t^2} \end{aligned} \quad (7.1.4)$$

$$\begin{aligned} & \frac{\partial}{\partial x} \left[B_{16} \frac{\partial u_0}{\partial x} + B_{26} \frac{\partial v_0}{\partial y} + B_{66} \left(\frac{\partial u_0}{\partial y} + \frac{\partial v_0}{\partial x} \right) + D_{16} \frac{\partial \phi_x}{\partial x} \right. \\ & \quad \left. + D_{26} \frac{\partial \phi_y}{\partial y} + D_{66} \left(\frac{\partial \phi_x}{\partial y} + \frac{\partial \phi_y}{\partial x} \right) \right] + \frac{\partial}{\partial y} \left[B_{12} \frac{\partial u_0}{\partial x} + B_{22} \frac{\partial v_0}{\partial y} \right. \\ & \quad \left. + B_{26} \left(\frac{\partial u_0}{\partial y} + \frac{\partial v_0}{\partial x} \right) + D_{12} \frac{\partial \phi_x}{\partial y} + D_{22} \frac{\partial \phi_y}{\partial y} + D_{26} \left(\frac{\partial \phi_x}{\partial y} + \frac{\partial \phi_y}{\partial x} \right) \right] \\ & - \left[K A_{44} \left(\frac{\partial w_0}{\partial y} + \phi_y \right) + K A_{45} \left(\frac{\partial w_0}{\partial x} + \phi_x \right) \right] \\ & - \left(\frac{\partial M_{xy}^T}{\partial x} + \frac{\partial M_{yy}^T}{\partial y} \right) = I_2 \frac{\partial^2 \phi_y}{\partial t^2} + I_1 \frac{\partial^2 v_0}{\partial t^2} \end{aligned} \quad (7.1.5)$$

where the thermal resultants, $(N_{xx}^T, N_{yy}^T, N_{xy}^T)$ and $(M_{xx}^T, M_{yy}^T, M_{xy}^T)$, are defined in Eqs. (3.3.41a,b).

7.2 Simply Supported Antisymmetric Cross-Ply Laminated Plates

7.2.1 Solution for the General Case

The SS-1 boundary conditions for the first-order shear deformation plate theory (FSDT) are (Figure 7.2.1):

$$\begin{aligned} u_0(x, 0, t) &= 0, & u_0(x, b, t) &= 0, & v_0(0, y, t) &= 0, & v_0(a, y, t) &= 0 \\ w_0(x, 0, t) &= 0, & w_0(x, b, t) &= 0, & w_0(0, y, t) &= 0, & w_0(a, y, t) &= 0 \\ \phi_x(x, 0, t) &= 0, & \phi_x(x, b, t) &= 0, & \phi_y(0, y, t) &= 0, & \phi_y(a, y, t) &= 0 \end{aligned} \quad (7.2.1a)$$

$$\begin{aligned} N_{xx}(0, y, t) &= 0, & N_{xx}(a, y, t) &= 0, & N_{yy}(x, 0, t) &= 0, & N_{yy}(x, b, t) &= 0 \\ M_{xx}(0, y, t) &= 0, & M_{xx}(a, y, t) &= 0, & M_{yy}(x, 0, t) &= 0, & M_{yy}(x, b, t) &= 0 \end{aligned} \quad (7.2.1b)$$

The boundary conditions in (7.2.1b) are satisfied by the following expansions

$$u_0(x, y, t) = \sum_{n=1}^{\infty} \sum_{m=1}^{\infty} U_{mn}(t) \cos \alpha x \sin \beta y \quad (7.2.2a)$$

$$v_0(x, y, t) = \sum_{n=1}^{\infty} \sum_{m=1}^{\infty} V_{mn}(t) \sin \alpha x \cos \beta y \quad (7.2.2b)$$

$$w_0(x, y, t) = \sum_{n=1}^{\infty} \sum_{m=1}^{\infty} W_{mn}(t) \sin \alpha x \sin \beta y \quad (7.2.3)$$

$$\phi_x(x, y, t) = \sum_{n=1}^{\infty} \sum_{m=1}^{\infty} X_{mn}(t) \cos \alpha x \sin \beta y \quad (7.2.4a)$$

$$\phi_y(x, y, t) = \sum_{n=1}^{\infty} \sum_{m=1}^{\infty} Y_{mn}(t) \sin \alpha x \cos \beta y \quad (7.2.4b)$$

where $\alpha = m\pi/a$ and $\beta = n\pi/b$.

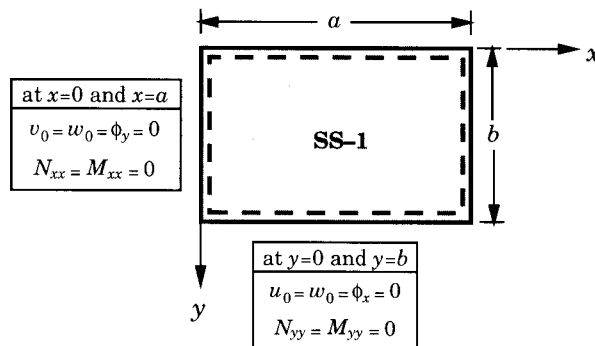


Figure 7.2.1: The simply supported boundary conditions for antisymmetric cross-ply laminates using the first-order shear deformation theory (SS-1).

The mechanical and thermal loads are also expanded in double Fourier sine series

$$q(x, y, t) = \sum_{n=1}^{\infty} \sum_{m=1}^{\infty} Q_{mn}(t) \sin \alpha x \sin \beta y \quad (7.2.5a)$$

$$\Delta T(x, y, z, t) = \sum_{n=1}^{\infty} \sum_{m=1}^{\infty} T_{mn}(z, t) \sin \alpha x \sin \beta y \quad (7.2.5b)$$

where

$$Q_{mn}(t) = \frac{4}{ab} \int_0^a \int_0^b q(x, y, t) \sin \alpha x \sin \beta y dx dy \quad (7.2.6a)$$

$$T_{mn}(z, t) = \frac{4}{ab} \int_0^a \int_0^b \Delta T(x, y, z, t) \sin \alpha x \sin \beta y dx dy \quad (7.2.6b)$$

Substitution of Eqs. (7.2.2)–(7.2.5) into Eqs. (7.1.1)–(7.1.5) will show that the Navier solution exists only if

$$A_{16} = 0, \quad A_{26} = 0, \quad A_{45} = 0, \quad B_{16} = 0, \quad B_{26} = 0, \quad D_{16} = 0, \quad D_{26} = 0, \quad I_1 = 0$$

i.e., for the same laminates as those for the classical laminate theory. For such laminates the coefficients $(U_{mn}, V_{mn}, W_{mn}, X_{mn}, Y_{mn})$ of the Navier solution can be calculated from

$$\begin{bmatrix} \hat{s}_{11} & \hat{s}_{12} & 0 & \hat{s}_{14} & \hat{s}_{15} \\ \hat{s}_{12} & \hat{s}_{22} & 0 & \hat{s}_{24} & \hat{s}_{25} \\ 0 & 0 & \hat{s}_{33} + \tilde{s}_{33} & \hat{s}_{34} & \hat{s}_{35} \\ \hat{s}_{14} & \hat{s}_{24} & \hat{s}_{34} & \hat{s}_{44} & \hat{s}_{45} \\ \hat{s}_{15} & \hat{s}_{25} & \hat{s}_{35} & \hat{s}_{45} & \hat{s}_{55} \end{bmatrix} \begin{Bmatrix} U_{mn} \\ V_{mn} \\ W_{mn} \\ X_{mn} \\ Y_{mn} \end{Bmatrix} + \begin{bmatrix} \hat{m}_{11} & 0 & 0 & 0 & 0 \\ 0 & \hat{m}_{22} & 0 & 0 & 0 \\ 0 & 0 & \hat{m}_{33} & 0 & 0 \\ 0 & 0 & 0 & \hat{m}_{44} & 0 \\ 0 & 0 & 0 & 0 & \hat{m}_{55} \end{bmatrix} \begin{Bmatrix} \ddot{U}_{mn} \\ \ddot{V}_{mn} \\ \ddot{W}_{mn} \\ \ddot{X}_{mn} \\ \ddot{Y}_{mn} \end{Bmatrix} = \begin{Bmatrix} 0 \\ 0 \\ Q_{mn} \\ 0 \\ 0 \end{Bmatrix} - \begin{Bmatrix} \alpha N_{mn}^1 \\ \beta N_{mn}^2 \\ 0 \\ \alpha M_{mn}^1 \\ \beta M_{mn}^2 \end{Bmatrix} \quad (7.2.7a)$$

where \hat{s}_{ij} and \hat{m}_{ij}

$$\begin{aligned} \hat{s}_{11} &= (A_{11}\alpha^2 + A_{66}\beta^2), & \hat{s}_{12} &= (A_{12} + A_{66})\alpha\beta \\ \hat{s}_{14} &= (B_{11}\alpha^2 + B_{66}\beta^2), & \hat{s}_{15} &= (B_{12} + B_{66})\alpha\beta \\ \hat{s}_{22} &= (A_{66}\alpha^2 + A_{22}\beta^2), & \hat{s}_{24} &= \hat{s}_{15} \\ \hat{s}_{25} &= (B_{66}\alpha^2 + B_{22}\beta^2), & \hat{s}_{33} &= K(A_{55}\alpha^2 + A_{44}\beta^2) \\ \tilde{s}_{33} &= \hat{N}_{xx}\alpha^2 + \hat{N}_{yy}\beta^2 \\ \hat{s}_{34} &= KA_{55}\alpha, & \hat{s}_{35} &= KA_{44}\beta, & \hat{s}_{44} &= (D_{11}\alpha^2 + D_{66}\beta^2 + KA_{55}) \\ \hat{s}_{45} &= (D_{12} + D_{66})\alpha\beta, & \hat{s}_{55} &= (D_{66}\alpha^2 + D_{22}\beta^2 + KA_{44}) \end{aligned} \quad (7.2.7b)$$

$$\hat{m}_{11} = I_0, \quad \hat{m}_{22} = I_0, \quad \hat{m}_{33} = I_0, \quad \hat{m}_{44} = I_2, \quad \hat{m}_{55} = I_2 \quad (7.2.7c)$$

where the thermal coefficients $N_{mn}^1, N_{mn}^2, M_{mn}^1$, and M_{mn}^2 are defined in Eqs. (6.3.13a,b).

7.2.2 Bending

The static solution can be obtained from Eqs. (7.2.7) by setting the time derivative terms and edge forces to zero:

$$\begin{bmatrix} \hat{s}_{11} & \hat{s}_{12} & 0 & \hat{s}_{14} & \hat{s}_{15} \\ \hat{s}_{12} & \hat{s}_{22} & 0 & \hat{s}_{24} & \hat{s}_{25} \\ 0 & 0 & \hat{s}_{33} & \hat{s}_{34} & \hat{s}_{35} \\ \hat{s}_{14} & \hat{s}_{24} & \hat{s}_{34} & \hat{s}_{44} & \hat{s}_{45} \\ \hat{s}_{15} & \hat{s}_{25} & \hat{s}_{35} & \hat{s}_{45} & \hat{s}_{55} \end{bmatrix} \begin{Bmatrix} U_{mn} \\ V_{mn} \\ W_{mn} \\ X_{mn} \\ Y_{mn} \end{Bmatrix} = \begin{Bmatrix} 0 \\ 0 \\ Q_{mn} \\ 0 \\ 0 \end{Bmatrix} - \begin{Bmatrix} \alpha N_{mn}^1 \\ \beta N_{mn}^2 \\ 0 \\ \alpha M_{mn}^1 \\ \beta M_{mn}^2 \end{Bmatrix} \quad (7.2.8)$$

Solution of Eq. (7.2.8) for each $m, n = 1, 2, \dots$ gives $(U_{mn}, V_{mn}, W_{mn}, X_{mn}, Y_{mn})$, which can then be used to compute the solution $(u_0, v_0, w_0, \phi_x, \phi_y)$ from Eqs. (7.2.2)–(7.2.4). Antisymmetric cross-ply laminates have the following additional stiffness characteristics [see Eqs. (3.5.29a,b)]:

$$B_{12} = 0, \quad B_{22} = -B_{11}, \quad B_{66} = 0 \quad (7.2.9)$$

Hence, the matrix coefficients in Eq. (7.2.7b) can be simplified.

The stresses in each layer can be computed using the constitutive equations (see Section 6.3.4). The in-plane stresses of a simply supported (SS-1) cross-ply laminated plate (i.e., when $\bar{Q}_{16} = \bar{Q}_{26} = \bar{Q}_{45} = 0$ and $\alpha_{xy} = 0$) are then given by

$$\begin{Bmatrix} \sigma_{xx} \\ \sigma_{yy} \\ \sigma_{xy} \end{Bmatrix}^{(k)} = \sum_{m=1}^{\infty} \sum_{n=1}^{\infty} \begin{bmatrix} \bar{Q}_{11} & \bar{Q}_{12} & 0 \\ \bar{Q}_{12} & \bar{Q}_{22} & 0 \\ 0 & 0 & \bar{Q}_{66} \end{bmatrix}^{(k)} \begin{Bmatrix} (R_{mn}^{xx} + zS_{mn}^{xx}) \sin \alpha x \sin \beta y \\ (R_{mn}^{yy} + zS_{mn}^{yy}) \sin \alpha x \sin \beta y \\ (R_{mn}^{xy} + zS_{mn}^{xy}) \cos \alpha x \cos \beta y \end{Bmatrix} \quad (7.2.10a)$$

where

$$\begin{Bmatrix} R_{mn}^{xx} \\ R_{mn}^{yy} \\ R_{mn}^{xy} \end{Bmatrix} = \begin{Bmatrix} -\alpha U_{mn} - \alpha_{xx} T_{mn}^0 \\ -\beta V_{mn} - \alpha_{yy} T_{mn}^0 \\ \beta U_{mn} + \alpha V_{mn} \end{Bmatrix}, \quad \begin{Bmatrix} S_{mn}^{xx} \\ S_{mn}^{yy} \\ S_{mn}^{xy} \end{Bmatrix} = \begin{Bmatrix} -\alpha X_{mn} - \alpha_{xx} T_{mn}^1 \\ -\beta Y_{mn} - \alpha_{yy} T_{mn}^1 \\ \beta X_{mn} + \alpha Y_{mn} \end{Bmatrix} \quad (7.2.10b)$$

where temperature increment ΔT is assumed to be of the form

$$\Delta T(x, y, z, t) = \sum_{m=1}^{\infty} \sum_{n=1}^{\infty} (T_{mn}^0 + zT_{mn}^1) \sin \alpha x \sin \beta y \quad (7.2.10c)$$

The transverse shear stresses from the constitutive equations are given by

$$\begin{Bmatrix} \sigma_{yz} \\ \sigma_{xz} \end{Bmatrix}^{(k)} = \sum_{m=1}^{\infty} \sum_{n=1}^{\infty} \begin{bmatrix} \bar{Q}_{44} & 0 \\ 0 & \bar{Q}_{55} \end{bmatrix}^{(k)} \begin{Bmatrix} (Y_{mn} + \beta W_{mn}) \sin \alpha x \cos \beta y \\ (X_{mn} + \alpha W_{mn}) \cos \alpha x \sin \beta y \end{Bmatrix} \quad (7.2.11)$$

Note that the stresses are layerwise constant through the thickness.

The bending moments are calculated from

$$\begin{Bmatrix} M_{xx} \\ M_{yy} \\ M_{xy} \end{Bmatrix} = \sum_{m=1}^{\infty} \sum_{n=1}^{\infty} \begin{bmatrix} B_{11} & B_{12} & 0 \\ B_{12} & B_{22} & 0 \\ 0 & 0 & B_{66} \end{bmatrix} \begin{Bmatrix} -\alpha U_{mn} \sin \alpha x \sin \beta y \\ -\beta V_{mn} \sin \alpha x \sin \beta y \\ (\beta U_{mn} + \alpha V_{mn}) \cos \alpha x \cos \beta y \end{Bmatrix} \\ + \sum_{m=1}^{\infty} \sum_{n=1}^{\infty} \begin{bmatrix} D_{11} & D_{12} & 0 \\ D_{12} & D_{22} & 0 \\ 0 & 0 & D_{66} \end{bmatrix} \begin{Bmatrix} -\alpha X_{mn} \sin \alpha x \sin \beta y \\ -\beta Y_{mn} \sin \alpha x \sin \beta y \\ (\alpha Y_{mn} + \beta X_{mn}) \cos \alpha x \cos \beta y \end{Bmatrix} \quad (7.2.12)$$

As discussed in Chapter 6, the transverse stresses can also be determined using the equilibrium equations of 3-D elasticity. Following the procedure outlined in Eqs. (6.3.31)–(6.3.37), we obtain

$$\begin{aligned}\sigma_{xz}^{(k)}(x, y, z) &= \sum_{m=1}^{\infty} \sum_{n=1}^{\infty} \left[(z - z_k) \mathcal{A}_{mn}^{(k)} + \frac{1}{2} (z^2 - z_k^2) \mathcal{B}_{mn}^{(k)} \right] \cos \alpha x \sin \beta y \\ &\quad + \sigma_{xz}^{(k-1)}(x, y, z_k) \\ \sigma_{yz}^{(k)}(x, y, z) &= \sum_{m=1}^{\infty} \sum_{n=1}^{\infty} \left[(z - z_k) \mathcal{C}_{mn}^{(k)} + \frac{1}{2} (z^2 - z_k^2) \mathcal{D}_{mn}^{(k)} \right] \sin \alpha x \cos \beta y \\ &\quad + \sigma_{yz}^{(k-1)}(x, y, z_k)\end{aligned}\quad (7.2.13a)$$

where $\sigma_{xz}^{(0)}(x, y, z_1) = \sigma_{yz}^{(0)}(x, y, z_1) = 0$, and

$$\begin{aligned}\mathcal{A}_{mn}^{(k)} &= \left[(\alpha^2 \bar{Q}_{11}^{(k)} + \beta^2 \bar{Q}_{66}^{(k)}) U_{mn} + \alpha \beta (\bar{Q}_{12}^{(k)} + \bar{Q}_{66}^{(k)}) V_{mn} \right] \\ \mathcal{B}_{mn}^{(k)} &= \left[(\alpha^2 \bar{Q}_{11}^{(k)} + \beta^2 \bar{Q}_{66}^{(k)}) X_{mn} + \alpha \beta (\bar{Q}_{12}^{(k)} + \bar{Q}_{66}^{(k)}) Y_{mn} \right] \\ \mathcal{C}_{mn}^{(k)} &= \left[\alpha \beta (\bar{Q}_{12}^{(k)} + \bar{Q}_{66}^{(k)}) U_{mn} + (\alpha^2 \bar{Q}_{66}^{(k)} + \beta^2 \bar{Q}_{22}^{(k)}) V_{mn} \right] \\ \mathcal{D}_{mn}^{(k)} &= \left[\alpha \beta (\bar{Q}_{12}^{(k)} + \bar{Q}_{66}^{(k)}) X_{mn} + (\alpha^2 \bar{Q}_{66}^{(k)} + \beta^2 \bar{Q}_{22}^{(k)}) Y_{mn} \right]\end{aligned}\quad (7.2.13b)$$

The transverse normal stress can be computed using Eq. (6.3.37) with the coefficients $\mathcal{A}_{mn}^{(k)}$, $\mathcal{B}_{mn}^{(k)}$, $\mathcal{C}_{mn}^{(k)}$, and $\mathcal{D}_{mn}^{(k)}$ defined in Eq. (5.2.13b).

Specially orthotropic plates

Specially orthotropic plates differ from antisymmetric cross-ply laminates in that all B_{ij} are zero. Consequently, $\hat{s}_{14} = 0$, $\hat{s}_{15} = 0$, $\hat{s}_{24} = 0$, and $\hat{s}_{25} = 0$. It is clear from Eq. (7.2.8) that U_{mn} and V_{mn} are uncoupled from (W_{mn}, X_{mn}, Y_{mn}) :

$$\begin{bmatrix} \hat{s}_{11} & \hat{s}_{12} & 0 & 0 & 0 \\ \hat{s}_{12} & \hat{s}_{22} & 0 & 0 & 0 \\ 0 & 0 & \hat{s}_{33} & \hat{s}_{34} & \hat{s}_{35} \\ 0 & 0 & \hat{s}_{34} & \hat{s}_{44} & \hat{s}_{45} \\ 0 & 0 & \hat{s}_{35} & \hat{s}_{45} & \hat{s}_{55} \end{bmatrix} \begin{Bmatrix} U_{mn} \\ V_{mn} \\ W_{mn} \\ X_{mn} \\ Y_{mn} \end{Bmatrix} = \begin{Bmatrix} 0 \\ 0 \\ Q_{mn} \\ 0 \\ 0 \end{Bmatrix} - \begin{Bmatrix} \alpha N_{mn}^1 \\ \beta N_{mn}^2 \\ 0 \\ \alpha M_{mn}^1 \\ \beta M_{mn}^2 \end{Bmatrix}\quad (7.2.14)$$

Decoupling the in-plane displacements from the bending displacements, we have

$$\begin{bmatrix} \hat{s}_{11} & \hat{s}_{12} \\ \hat{s}_{12} & \hat{s}_{22} \end{bmatrix} \begin{Bmatrix} U_{mn} \\ V_{mn} \end{Bmatrix} = - \begin{Bmatrix} \alpha N_{mn}^1 \\ \beta N_{mn}^2 \end{Bmatrix}\quad (7.2.15a)$$

$$\begin{bmatrix} \hat{s}_{33} & \hat{s}_{34} & \hat{s}_{35} \\ \hat{s}_{34} & \hat{s}_{44} & \hat{s}_{45} \\ \hat{s}_{35} & \hat{s}_{45} & \hat{s}_{55} \end{bmatrix} \begin{Bmatrix} W_{mn} \\ X_{mn} \\ Y_{mn} \end{Bmatrix} = \begin{Bmatrix} Q_{mn} \\ 0 \\ 0 \end{Bmatrix} - \begin{Bmatrix} 0 \\ \alpha M_{mn}^1 \\ \beta M_{mn}^2 \end{Bmatrix}\quad (7.2.15b)$$

The solution of Eq. (7.2.15a) is given by

$$\begin{aligned}U_{mn} &= -\frac{1}{a_{mn}} (\hat{s}_{22} \alpha N_{mn}^1 - \hat{s}_{12} \beta N_{mn}^2) \\ V_{mn} &= -\frac{1}{a_{mn}} (\hat{s}_{11} \beta N_{mn}^2 - \hat{s}_{12} \alpha N_{mn}^1)\end{aligned}\quad (7.2.16)$$

where $a_{mn} = \hat{s}_{11}\hat{s}_{22} - \hat{s}_{12}\hat{s}_{12}$. The in-plane deflections are identically zero when the thermal (and in-plane edge) forces are zero.

Equation (7.2.15b) can be solved either directly (by inverting the 3×3 coefficient matrix) or by using the static condensation procedure outlined in Chapter 6 [see Eqs. (6.3.22)–(6.3.26)]. Using the latter, we arrive at

$$\begin{aligned} W_{mn} &= \frac{1}{b_{mn}} \left[Q_{mn} + \frac{\hat{s}_{34}}{b_0} (\alpha M_{mn}^1 \hat{s}_{55} - \beta M_{mn}^2 \hat{s}_{45}) - \frac{\hat{s}_{35}}{b_0} (\alpha M_{mn}^1 \hat{s}_{45} - \beta M_{mn}^2 \hat{s}_{44}) \right] \\ X_{mn} &= \frac{1}{b_0} \left[b_1 W_{mn} - (\alpha M_{mn}^1 \hat{s}_{55} - \beta M_{mn}^2 \hat{s}_{45}) \right] \\ Y_{mn} &= \frac{1}{b_0} \left[b_2 W_{mn} + (\alpha M_{mn}^1 \hat{s}_{45} - \beta M_{mn}^2 \hat{s}_{44}) \right] \end{aligned} \quad (7.2.17a)$$

where

$$\begin{aligned} b_{mn} &= \hat{s}_{33} + \hat{s}_{34} \frac{b_1}{b_0} + \hat{s}_{35} \frac{b_2}{b_0}, \quad b_0 = \hat{s}_{44} \hat{s}_{55} - \hat{s}_{45} \hat{s}_{45} \\ b_1 &= \hat{s}_{45} \hat{s}_{35} - \hat{s}_{34} \hat{s}_{55}, \quad b_2 = \hat{s}_{34} \hat{s}_{45} - \hat{s}_{44} \hat{s}_{35} \end{aligned} \quad (7.2.17b)$$

When the thermal forces are zero, the bending deflections are given by

$$w_0(x, y) = \sum_{n=1}^{\infty} \sum_{m=1}^{\infty} W_{mn} \sin \alpha x \sin \beta y \quad (7.2.18a)$$

$$\phi_x(x, y) = \sum_{n=1}^{\infty} \sum_{m=1}^{\infty} X_{mn} \cos \alpha x \sin \beta y \quad (7.2.18b)$$

$$\phi_y(x, y) = \sum_{n=1}^{\infty} \sum_{m=1}^{\infty} Y_{mn} \sin \alpha x \cos \beta y \quad (7.2.18c)$$

with $\alpha = m\pi/a$, $\beta = n\pi/b$ and

$$W_{mn} = \frac{1}{b_{mn}} Q_{mn}, \quad X_{mn} = \frac{b_1}{b_0 b_{mn}} Q_{mn}, \quad Y_{mn} = \frac{b_2}{b_0 b_{mn}} Q_{mn} \quad (7.2.19)$$

The bending moments are given by

$$M_{xx} = - \sum_{n=1}^{\infty} \sum_{m=1}^{\infty} (D_{11}\alpha X_{mn} + D_{12}\beta Y_{mn}) \sin \alpha x \sin \beta y \quad (7.2.20a)$$

$$M_{yy} = - \sum_{n=1}^{\infty} \sum_{m=1}^{\infty} (D_{12}\alpha X_{mn} + D_{22}\beta Y_{mn}) \sin \alpha x \sin \beta y \quad (7.2.20b)$$

$$M_{xy} = D_{66} \sum_{n=1}^{\infty} \sum_{m=1}^{\infty} (\beta X_{mn} + \alpha Y_{mn}) \cos \alpha x \cos \beta y \quad (7.2.20c)$$

The in-plane stresses are given by

$$\left\{ \begin{array}{l} \sigma_{xx} \\ \sigma_{yy} \\ \sigma_{xy} \end{array} \right\}^{(k)} = -z \sum_{n=1}^{\infty} \sum_{m=1}^{\infty} \left\{ \begin{array}{l} \left(\bar{Q}_{11}^{(k)} \alpha X_{mn} + \bar{Q}_{12}^{(k)} \beta Y_{mn} \right) \sin \alpha x \sin \beta y \\ \left(\bar{Q}_{12}^{(k)} \alpha X_{mn} + \bar{Q}_{22}^{(k)} \beta Y_{mn} \right) \sin \alpha x \sin \beta y \\ -\bar{Q}_{66}^{(k)} (\beta X_{mn} + \alpha Y_{mn}) \cos \alpha x \cos \beta y \end{array} \right\} \quad (7.2.21)$$

and the transverse shear stresses are given by

$$\begin{Bmatrix} \sigma_{yz} \\ \sigma_{xz} \end{Bmatrix}^{(k)} = \sum_{n=1}^{\infty} \sum_{m=1}^{\infty} \begin{Bmatrix} \bar{Q}_{44}^{(k)} (Y_{mn} + \beta W_{mn}) \sin \alpha x \cos \beta y \\ \bar{Q}_{55}^{(k)} (X_{mn} + \alpha W_{mn}) \cos \alpha x \sin \beta y \end{Bmatrix} \quad (7.2.22)$$

The interlaminar stresses, computed using the 3-D stress equilibrium equations, are given by

$$\begin{aligned} \sigma_{xz}^{(k)} &= \left(\frac{z^2 - z_k^2}{2} \right) (T_{11}^{(k)} X_{mn} + T_{12}^{(k)} Y_{mn}) \cos \alpha x \sin \beta y + \sigma_{xz}^{(k-1)}(x, y, z_k) \\ \sigma_{yz}^{(k)} &= \left(\frac{z^2 - z_k^2}{2} \right) (T_{12}^{(k)} X_{mn} + T_{22}^{(k)} Y_{mn}) \sin \alpha x \cos \beta y + \sigma_{yz}^{(k-1)}(x, y, z_k) \\ \sigma_{zz}^{(k)} &= \left[\frac{z_k^3}{3} + \frac{z}{6} (z^2 - 3z_k^2) \right] (T_{31}^{(k)} X_{mn} + T_{32}^{(k)} Y_{mn}) \sin \alpha x \sin \beta y \\ &\quad + \sigma_{zz}^{(k-1)}(x, y, z_k) + (z - z_k) \left(\frac{\partial \sigma_{xz}^{(k)}}{\partial x} + \frac{\partial \sigma_{yz}^{(k)}}{\partial y} \right)_{z_k} \end{aligned} \quad (7.2.23a)$$

where

$$\begin{aligned} T_{11}^{(k)} &= \alpha^2 \bar{Q}_{11}^{(k)} + \beta^2 \bar{Q}_{66}^{(k)}, \quad T_{12}^{(k)} = \alpha \beta (\bar{Q}_{12}^{(k)} + \bar{Q}_{66}^{(k)}), \quad T_{22}^{(k)} = \alpha^2 \bar{Q}_{66}^{(k)} + \beta^2 \bar{Q}_{22}^{(k)} \\ T_{31}^{(k)} &= \alpha^3 \bar{Q}_{11}^{(k)} + \alpha \beta^2 (2\bar{Q}_{66}^{(k)} + \bar{Q}_{12}^{(k)}), \quad T_{32}^{(k)} = \alpha^2 \beta (\bar{Q}_{12}^{(k)} + 2\bar{Q}_{66}^{(k)}) + \beta^3 \bar{Q}_{22}^{(k)} \end{aligned} \quad (7.2.23b)$$

For single-layer plates, Eqs. (7.2.23a) reduce to

$$\begin{aligned} \sigma_{xz} &= -\frac{h^2}{8} \left[1 - \left(\frac{2z}{h} \right)^2 \right] (T_{11} X_{mn} + T_{12} Y_{mn}) \cos \alpha x \sin \beta y \\ \sigma_{yz} &= -\frac{h^2}{8} \left[1 - \left(\frac{2z}{h} \right)^2 \right] (T_{12} X_{mn} + T_{22} Y_{mn}) \sin \alpha x \cos \beta y \\ \sigma_{zz} &= \frac{h^3}{48} \left\{ \left[1 + \left(\frac{2z}{h} \right)^3 \right] - 3 \left[1 + \left(\frac{2z}{h} \right) \right] \right\} (T_{31} X_{mn} + T_{32} Y_{mn}) \sin \alpha x \sin \beta y \end{aligned} \quad (7.2.24)$$

Numerical results for the maximum transverse deflection and stresses of symmetric laminates are discussed next. The following nondimensionalizations are used to present results in graphical and tabular forms:

$$\begin{aligned} \bar{w} &= w_0 \left(\frac{E_2 h^3}{b^4 q_0} \right), \quad \bar{\sigma}_{xx} = \sigma_{xx} \left(\frac{h^2}{b^2 q_0} \right), \quad \bar{\sigma}_{yy} = \sigma_{yy} \left(\frac{h^2}{b^2 q_0} \right) \\ \bar{\sigma}_{xy} &= \sigma_{xy} \left(\frac{h^2}{b^2 q_0} \right), \quad \bar{\sigma}_{xz} = \sigma_{xz} \left(\frac{h}{b q_0} \right), \quad \bar{\sigma}_{yz} = \sigma_{yz} \left(\frac{h}{b q_0} \right) \end{aligned} \quad (7.2.25)$$

Table 7.2.1 contains the maximum nondimensionalized deflections and stresses of simply supported square symmetric laminates (0/90/90/0) and (0/90/0) under

sinusoidally distributed load (SSL) as well as uniformly distributed load (UDL) and for different side-to-thickness ratios ($E_1 = 25E_2$, $G_{12} = G_{13} = 0.5E_2$, $G_{23} = 0.2E_2$, $\nu_{12} = 0.25$, $K = 5/6$). The membrane stresses were evaluated at the following locations: $\bar{\sigma}_{xx}(a/2, b/2, \frac{h}{2})$, $\bar{\sigma}_{yy}(a/2, b/2, \frac{h}{4})$, and $\bar{\sigma}_{xy}(a, b, -\frac{h}{2})$. The transverse shear stresses are calculated using the constitutive equations. For the (0/90/0) laminate, σ_{xz} is evaluated at $(x, y) = (0, b/2)$ in layers 1 and 3, and σ_{yz} is computed at $(x, y) = (a/2, 0)$ in layer 2.

Table 7.2.1: Effect of transverse shear deformation on nondimensionalized maximum transverse deflections and stresses of simply supported (SS-1) symmetric cross-ply square plates.

a/h	Load	$\bar{w} \times 10^2$	$\bar{\sigma}_{xx}$	$\bar{\sigma}_{yy}$	$\bar{\sigma}_{xy}$	$\bar{\sigma}_{xz}$	$\bar{\sigma}_{yz}$
<i>Orthotropic Plate</i> [σ_{yy} is evaluated at $(x, y, z) = (a/2, b/2, h/2)$]							
10	SSL	0.6383	0.5248	0.0338	0.0246	0.3452	0.0367
	UDL	0.9519	0.7706	0.0352	0.0539	0.6147	0.1529
20	SSL	0.4836	0.5350	0.0286	0.0222	0.3501	0.0319
	UDL	0.7262	0.7828	0.0272	0.0487	0.6194	0.1466
100	SSL	0.4333	0.5385	0.0267	0.0213	0.3518	0.0302
	UDL	0.6528	0.7865	0.0245	0.0464	0.6206	0.1449
CLPT	SSL	0.4312	0.5387	0.0267	0.0213	0.4398	0.0377†
	UDL	0.6497	0.7866	0.0244	0.0463	0.7758	0.1811†
<i>Symmetric Laminate, (0/90/90/0)</i>							
10	SSL	0.6627	0.4989	0.3614	0.0241	0.4165	0.1292
	UDL	1.0250	0.7577	0.5006	0.0470	0.7986	0.3499
20	SSL	0.4912	0.5273	0.2956	0.0221	0.4370	0.1087
	UDL	0.7694	0.8045	0.3968	0.0420	0.8305	0.3228
100	SSL	0.4337	0.5382	0.2704	0.0213	0.4448	0.1008
	UDL	0.6833	0.8420	0.3558	0.0396	0.8420	0.3140
CLPT	SSL	0.4312	0.5387	0.2694	0.0213	0.3393	0.1382†
	UDL	0.6796	0.8236	0.3540	0.0395	0.6404	0.4548†
<i>Symmetric Laminate, (0/90/0)</i>							
10	SSL	0.6693	0.5134	0.2536	0.0252	0.4089	0.0914
	UDL	1.0219	0.7719	0.3072	0.0514	0.7548	0.3107
20	SSL	0.4921	0.5318	0.1997	0.0223	0.4205	0.0759
	UDL	0.7572	0.7983	0.2227	0.0453	0.7697	0.2902
100	SSL	0.4337	0.5384	0.1804	0.0213	0.4247	0.0703
	UDL	0.6697	0.8072	0.1925	0.0426	0.7744	0.2842
CLPT	SSL	0.4312	0.5387	0.1796	0.0213	0.3951	0.0823†
	UDL	0.6660	0.8075	0.1912	0.0425	0.7191	0.3791†

† σ_{xz} and σ_{yz} calculated from equilibrium equations (at $z = 0$).

The nondimensionalized quantities in the classical laminate theory are independent of the side-to-thickness ratio. The influence of transverse shear deformation is to increase the transverse deflection. The difference between the deflections predicted by the first-order shear deformation theory and classical plate theory increases with the ratio h/a . For example, for $a/h = 10$ and sinusoidal loading, the classical plate theory underpredicts deflections by as much as about 35%, whereas it is only 12% for $a/h = 20$. Shear deformation has different effects on different stresses.

Table 7.2.2 contains results for cross-ply laminates (0/90/90/0/90/90/0) and (0/90/0/90/0), both laminates of the same total thickness. The material properties used are $E_1 = 25E_2$, $G_{12} = G_{13} = 0.5E_2$, $G_{23} = 0.2E_2$, $\nu_{12} = 0.25$, and $K = 5/6$. The same nondimensionalization as before [see Eq. (7.2.25)] is used except for the following quantities:

$$\bar{\sigma}_{yy} = \sigma_{yy}(a/2, b/2, \frac{h}{3}) \frac{h^2}{b^2 q_0}$$

$$\bar{\sigma}_{xz} = \sigma_{xz}(0, b/2, k = 1, 3, 5) \frac{h}{b q_0}, \quad \bar{\sigma}_{yz} = \sigma_{yz}(a/2, 0, k = 2, 4) \frac{h}{b q_0} \quad (7.2.26)$$

Table 7.2.2: Effect of transverse shear deformation on nondimensionalized maximum transverse deflections and stresses of simply supported (SS-1) symmetric cross-ply square plates.

a/h	Load	\bar{w}	$\bar{\sigma}_{xx}$	$\bar{\sigma}_{yy}$	$\bar{\sigma}_{xy}$	$\bar{\sigma}_{xz}$	$\bar{\sigma}_{yz}$
<i>Symmetric Laminate, (0/90/90/0/90/90/0)</i>							
10	SSL	0.6213	0.5021	0.4107	0.0221	0.3459	0.1998
	UDL	0.9643	0.7605	0.6016	0.0422	0.6927	0.4630
20	SSL	0.4796	0.5276	0.3748	0.0215	0.3617	0.1840
	UDL	0.7575	0.8059	0.5475	0.0396	0.7212	0.4438
100	SSL	0.4332	0.5382	0.3598	0.0213	0.3683	0.1774
	UDL	0.6896	0.8260	0.5241	0.0381	0.7322	0.4365
CLPT	SSL	0.4312	0.5387	0.3591	0.0213	—	—
	UDL	0.6867	0.8270	0.5230	0.0380	—	—
<i>Symmetric Laminate, (0/90/0/90/0)</i>							
10	SSL	0.6277	0.5044	0.3852	0.0226	0.3535	0.1770
	UDL	0.9727	0.7649	0.5525	0.0436	0.6901	0.4410
20	SSL	0.4814	0.5285	0.3416	0.0217	0.3685	0.1591
	UDL	0.7581	0.8080	0.4844	0.0403	0.7166	0.4188
100	SSL	0.4333	0.5383	0.3240	0.0213	0.3746	0.1519
	UDL	0.6874	0.8264	0.4559	0.0386	0.7267	0.4108
CLPT	SSL	0.4312	0.5387	0.3232	0.0213	—	—
	UDL	0.6844	0.8272	0.4546	0.0385	—	—

where k denotes the layer number. The first-order theory results are slightly different from those of the classical plate theory. The influence of transverse shear deformation is less in the case of the laminates presented in Table 7.2.2. Thus, as the number of layers is increased, the effect of transverse shear strains on deflections and stresses decreases. Figure 7.2.2 clearly shows the diminishing effect of transverse shear deformation on deflections, the effect being negligible for side-to-thickness ratios larger than 20.

Table 7.2.3 contains nondimensionalized transverse deflections \bar{w} and stresses $[\bar{\sigma}_{xx}(a/2, b/2, -h/2) = -\bar{\sigma}_{yy}(a/2, b/2, h/2)$ and $\bar{\sigma}_{xz} = \bar{\sigma}_{yz}$] of antisymmetric cross-ply laminates subjected to sinusoidally and uniformly distributed transverse loads. The stresses are nondimensionalized as in Eq. (7.2.25). The locations of the maximum stresses, computed using the constitutive equations, are as follows:

$$\begin{aligned} & \sigma_{xx}(a/2, b/2, -\frac{h}{2}), \sigma_{yy}(a/2, b/2, \frac{h}{2}), \sigma_{xy}(a, b, -\frac{h}{2}) \\ & \sigma_{xz}(0, b/2, k=1), \sigma_{yz}(a/2, 0, k=n) \end{aligned} \quad (7.2.27)$$

Table 7.2.3: Effect of transverse shear deformation on nondimensionalized maximum transverse deflections and stresses of simply supported (SS-1) antisymmetric cross-ply square plates ($h_k = h/n$, $E_1 = 25E_2$, $G_{12} = G_{13} = 0.5E_2$, $G_{23} = 0.2E_2$, $\nu_{12} = 0.25$, $K = 5/6$).

a/h	Load	$\bar{w} \times 10^2$	$\bar{\sigma}_{yy}$	$\bar{\sigma}_{xy}$	$\bar{\sigma}_{xz}$	$\bar{\sigma}_{xz}^\dagger$
<i>Antisymmetric Laminate, (0/90)</i>						
10	SSL	1.2373	0.7157	0.0525	0.2728	0.3322
	UDL	1.9468	1.0715	0.0960	0.5772	0.7250
20	SSL	1.1070	0.7157	0.0525	0.2728	0.3322
	UDL	1.7582	1.0747	0.0943	0.5802	0.7285
100	SSL	1.0653	0.7157	0.0525	0.2728	0.3322
	UDL	1.6980	1.0761	0.0933	0.5813	0.7297
CLPT	SSL	1.0636	0.7157	0.0525	—	0.3322
	UDL	1.6955	1.0761	0.0933	—	0.7297
<i>Antisymmetric Laminate, (0/90)₄</i>						
10	SSL	0.6216	0.4950	0.0221	0.2728	0.2480
	UDL	0.9660	0.7415	0.0420	0.5787	0.5264
20	SSL	0.4913	0.4950	0.0221	0.2728	0.2480
	UDL	0.7776	0.7468	0.0402	0.5839	0.5311
100	SSL	0.4496	0.4950	0.0221	0.2728	0.2480
	UDL	0.7175	0.7494	0.0391	0.5857	0.5328
CLPT	SSL	0.4479	0.4950	0.0221	—	0.2479
	UDL	0.7150	0.7496	0.0391	—	0.5330

[†] Maximum stresses derived from equilibrium. The reported values are at $z = \pm h/4$ for (0/90) laminate, and at $z = 0$ for (0/90)₄ laminate.

We note that the two-layer laminate exhibits quite different behavior, due to bending-extensional coupling, from the eight-layer laminate, and the results for the eight-layer laminate are much the same as those of symmetric laminates in Tables 7.2.1 and 7.2.2.

Figure 7.2.3 shows the effect of transverse shear deformation and bending-extensional coupling on deflections. The eight-layer antisymmetric cross-ply plate behaves much like an orthotropic plate (results are not shown in the figure).

Figures 7.2.4 through 7.2.7 show plots of maximum normal stresses, $\bar{\sigma}_{xx}(a/2, b/2, z)$ and $\bar{\sigma}_{yy}(a/2, b/2, z)$, and maximum transverse shear stresses, $\bar{\sigma}_{xz}(0, b/2, z)$ and $\bar{\sigma}_{yz}(a/2, 0, z)$, through the thickness of simply supported square laminates (0/90/90/0) under sinusoidally distributed transverse load. The material properties used are $E_1 = 25E_2$, $G_{12} = G_{13} = 0.5E_2$, $G_{23} = 0.2E_2$, $\nu_{12} = 0.25$, and $K = 5/6$. The dashed lines correspond to classical plate theory solutions. In Figures 7.2.6 and 7.2.7, stresses computed using the constitutive relations are also included. In the case of $\bar{\sigma}_{xz}$, the equilibrium equations predict a stress variation that is inconsistent with that predicted by constitutive relations; equilibrium equations predict the maximum stress to be at the midplane of the plate, while the constitutive equations predict maximum stress in the outer layers. It turns out that (see Pagano [6]) the constitutive equations yield, qualitatively, the correct stress variation.

Table 7.2.4 contains nondimensionalized deflections, $\bar{w} = w_0/(\alpha_1 T_1 b^2)$, of simply supported plates subjected to the temperature field of the form given in Eq. (7.2.10c). The material properties of orthotropic layers are assumed to be $E_1 = 25E_2$, $G_{12} = G_{13} = 0.5E_2$, $G_{23} = 0.2E_2$, $\nu_{12} = 0.25$, $K = 5/6$, and $\alpha_2 = 3\alpha_3$. The results in the table correspond to $T_0 = 0$ and $T_1 \neq 0$. We note that the effect of shear deformation on thermal deflections is negligible.

7.2.3 Buckling

For buckling analysis, we assume that the only applied loads are the in-plane forces

$$\hat{N}_{xx} = -N_0, \quad \hat{N}_{yy} = -kN_0, \quad k = \frac{\hat{N}_{yy}}{\hat{N}_{xx}} \quad (7.2.28)$$

and all other mechanical and thermal loads are zero. From Eq. (7.2.7) we have

$$\begin{bmatrix} \hat{s}_{11} & \hat{s}_{12} & 0 & \hat{s}_{14} & \hat{s}_{15} \\ \hat{s}_{12} & \hat{s}_{22} & 0 & \hat{s}_{24} & \hat{s}_{25} \\ 0 & 0 & \hat{s}_{33} - N_0 (\alpha^2 + k\beta^2) & \hat{s}_{34} & \hat{s}_{35} \\ \hat{s}_{14} & \hat{s}_{24} & \hat{s}_{34} & \hat{s}_{44} & \hat{s}_{45} \\ \hat{s}_{15} & \hat{s}_{25} & \hat{s}_{35} & \hat{s}_{45} & \hat{s}_{55} \end{bmatrix} \begin{Bmatrix} U_{mn} \\ V_{mn} \\ W_{mn} \\ X_{mn} \\ Y_{mn} \end{Bmatrix} = \begin{Bmatrix} 0 \\ 0 \\ 0 \\ 0 \\ 0 \end{Bmatrix} \quad (7.2.29)$$

Following the condensation of variables procedure to eliminate the in-plane displacements U_{mn} and V_{mn} , we obtain

$$\begin{bmatrix} \hat{s}_{33} - N_0 (\alpha^2 + k\beta^2) & \hat{s}_{34} & \hat{s}_{35} \\ \hat{s}_{34} & \bar{s}_{44} & \bar{s}_{45} \\ \hat{s}_{35} & \bar{s}_{45} & \bar{s}_{55} \end{bmatrix} \begin{Bmatrix} W_{mn} \\ X_{mn} \\ Y_{mn} \end{Bmatrix} = \begin{Bmatrix} 0 \\ 0 \\ 0 \end{Bmatrix} \quad (7.2.30a)$$

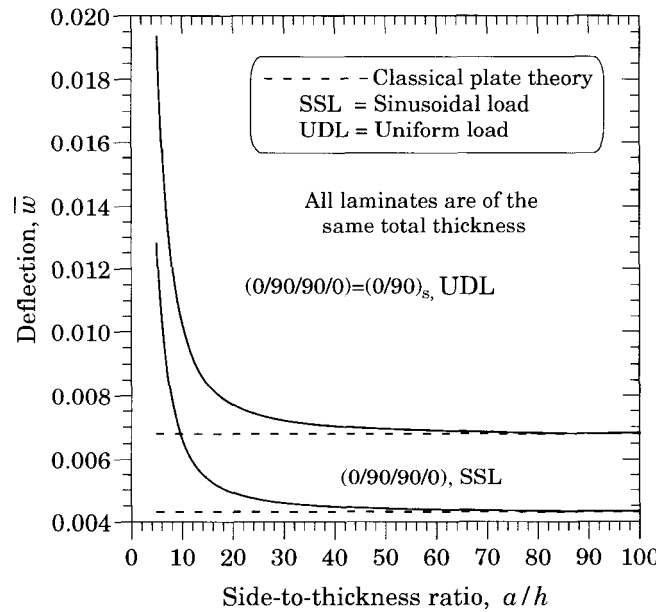


Figure 7.2.2: Center transverse deflection (\bar{w}) versus side-to-thickness ratio for simply supported (SS-1) symmetric cross-ply $(0/90/90/0)$ square laminates subjected to uniformly or sinusoidally distributed transverse load; dashed lines correspond to the classical plate theory (CLPT) solutions.

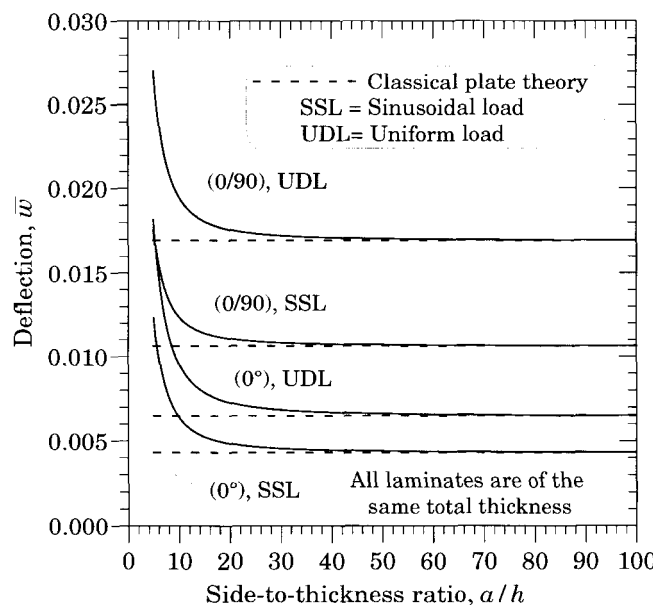


Figure 7.2.3: Center transverse deflection (\bar{w}) versus side-to-thickness ratio for simply supported (SS-1) orthotropic and antisymmetric cross-ply $(0/90)$ laminates under sinusoidally distributed transverse load.

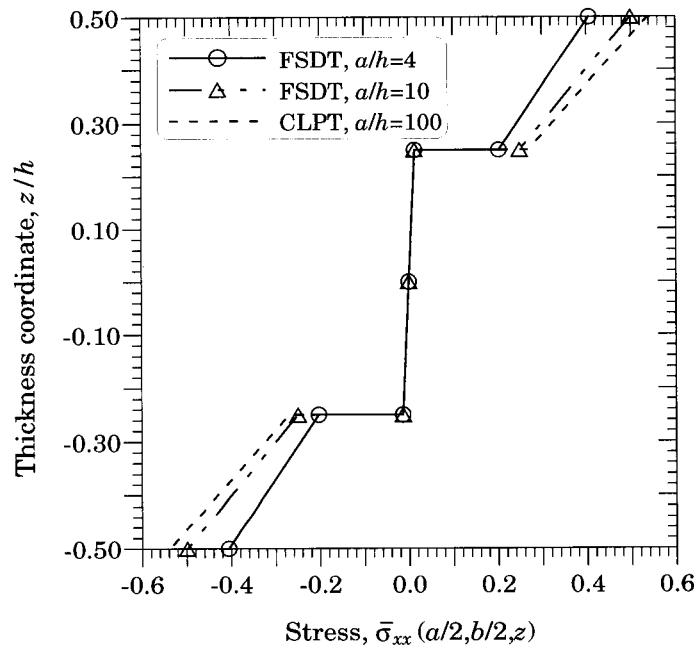


Figure 7.2.4: Nondimensionalized normal stress ($\bar{\sigma}_{xx}$) versus thickness (z/h) for simply supported (SS-1) symmetric cross-ply (0/90/90/0) laminates.

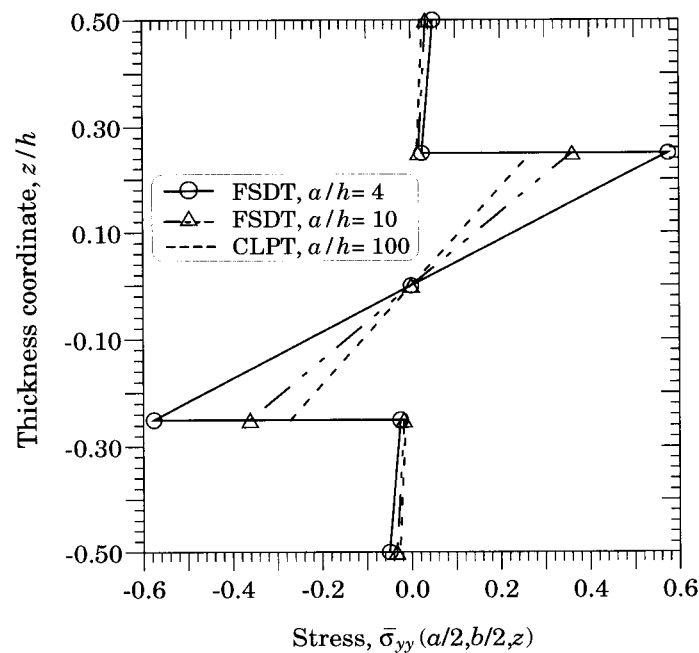


Figure 7.2.5: Nondimensionalized normal stress ($\bar{\sigma}_{yy}$) versus thickness (z/h) for simply supported (SS-1) symmetric cross-ply (0/90/90/0) laminates.

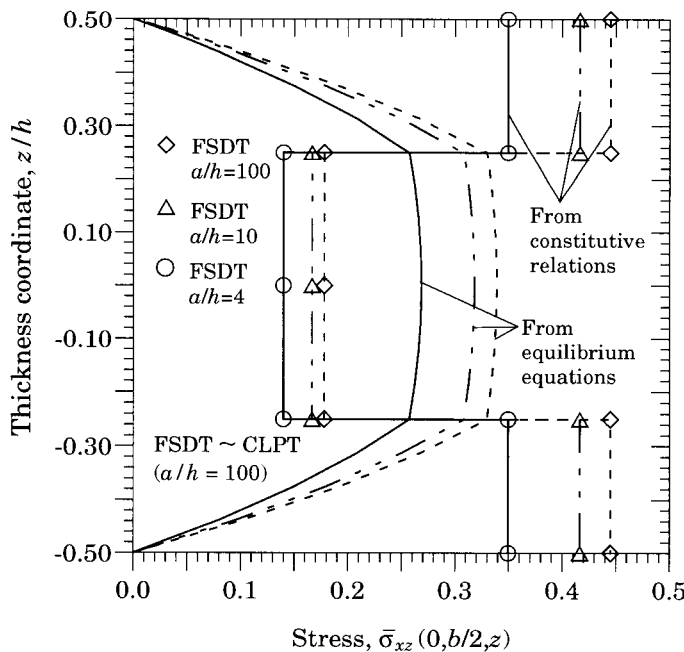


Figure 7.2.6: Nondimensionalized shear stress ($\bar{\sigma}_{xz}$) versus thickness (z/h) for simply supported (SS-1) symmetric cross-ply (0/90/90/0) laminates.

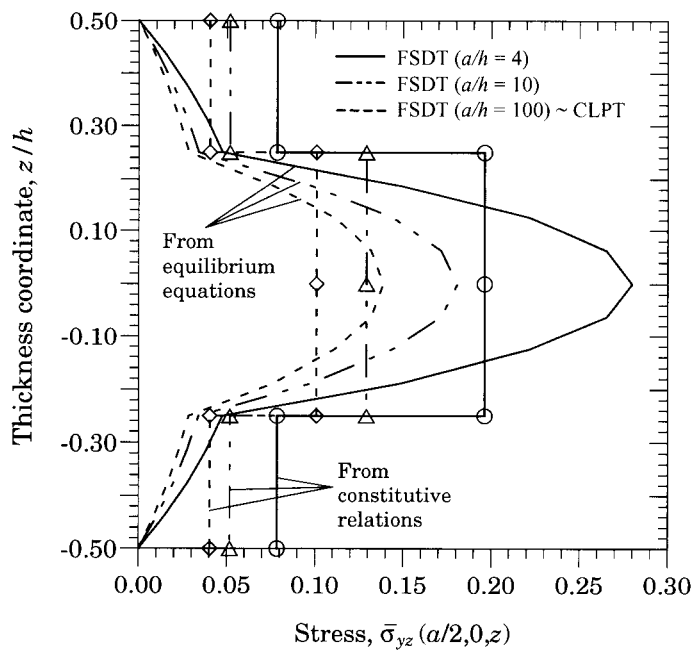


Figure 7.2.7: Nondimensionalized shear stress ($\bar{\sigma}_{yz}$) versus thickness (z/h) for simply supported (SS-1) symmetric cross-ply (0/90/90/0) laminates.

Table 7.2.4: Effect of the aspect ratio and side-to-thickness ratio on the deflection of simply supported (SS-1) plates subjected to temperature field that is uniform in the xy -plane and linearly varying through the thickness ($q_0 = 0, T_0 = 0, T_1 = \text{constant}$).

Load	a/h	$a/b = 1$	$a/b = 1.5$	$a/b = 2$	$a/b = 2.5$	$a/b = 3$
<i>Isotropic</i> [†]						
SSL	10	0.6586	0.9119	1.0537	1.1355	1.1855
UDL	10	0.9575	1.3097	1.4798	1.5582	1.5938
<i>Orthotropic</i>						
SSL	10	1.0440	2.1129	3.0623	3.6394	3.8883
	20	1.0346	2.1128	3.0758	3.6560	3.9002
	100	1.0313	2.1127	3.0804	3.6617	3.9042
CLPT	1.0312	2.1127	3.0806	3.6619	3.9044	
UDL	10	1.4603	3.1321	4.5966	5.4269	5.6987
	20	1.4409	3.1339	4.6243	5.4609	5.7239
	100	1.4334	3.1343	4.6342	5.4729	5.7327
CLPT	1.4331	3.1344	4.6346	5.4734	5.7330	
<i>Laminate, (0/90)</i>						
SSL	10	1.1504	1.4673	1.5186	1.5122	1.4984
	20	1.1504	1.4613	1.5091	1.5026	1.4898
	100	1.1504	1.4592	1.5058	1.4994	1.4869
CLPT	1.1504	1.4591	1.5057	1.4993	1.4868	
UDL	10	1.7213	2.1446	2.1100	1.9862	1.8796
	20	1.7269	2.1394	2.0965	1.9703	1.8649
	100	1.7293	2.1377	2.0918	1.9649	1.8600
CLPT	1.7294	2.1376	2.0916	1.9647	1.8598	
<i>Laminate, (0/90)₄</i>						
SSL	10	1.0343	1.3000	1.3113	1.2781	1.2469
	20	1.0343	1.2837	1.2870	1.2555	1.2280
	100	1.0343	1.2776	1.2783	1.2477	1.2216
CLPT	1.0343	1.2773	1.2779	1.2474	1.2214	
UDL	10	1.5498	1.9026	1.8166	1.6603	1.5334
	20	1.5607	1.8862	1.7816	1.6224	1.5002
	100	1.5661	1.8801	1.7690	1.6091	1.4886
CLPT	1.5664	1.8799	1.7685	1.6085	1.4881	
<i>Laminate, (0/90/90/0)</i>						
SSL	10	1.0421	1.7130	1.9680	1.9807	1.9227
	20	1.0343	1.7339	1.9858	1.9854	1.9193
	100	1.0313	1.7419	1.9923	1.9871	1.9181
CLPT	1.0312	1.7422	1.9925	1.9872	1.9181	
UDL	10	1.5452	2.5733	2.8961	2.8045	2.5921
	20	1.5357	2.6169	2.9352	2.8191	2.5877
	100	1.5318	2.6343	2.9500	2.8243	2.5859
CLPT	1.5316	2.6350	2.9507	2.8245	2.5859	

[†] $\nu = 0.3$; both CLPT and FSDT solutions are the same and independent of a/h .

$$\begin{aligned}
\bar{s}_{44} &= \hat{s}_{44} - \hat{s}_{14} \frac{b_1}{b_0} - \hat{s}_{24} \frac{b_2}{b_0}, \quad \bar{s}_{45} = \hat{s}_{45} - \hat{s}_{15} \frac{b_1}{b_0} - \hat{s}_{25} \frac{b_2}{b_0} \\
\bar{s}_{55} &= \hat{s}_{55} - \hat{s}_{15} \frac{b_3}{b_0} - \hat{s}_{25} \frac{b_4}{b_0}, \quad b_0 = \hat{s}_{11} \hat{s}_{22} - \hat{s}_{12} \hat{s}_{12} \\
b_1 &= \hat{s}_{14} \hat{s}_{22} - \hat{s}_{12} \hat{s}_{24}, \quad b_2 = \hat{s}_{11} \hat{s}_{24} - \hat{s}_{12} \hat{s}_{14} \\
b_3 &= \hat{s}_{15} \hat{s}_{22} - \hat{s}_{12} \hat{s}_{25}, \quad b_4 = \hat{s}_{11} \hat{s}_{25} - \hat{s}_{12} \hat{s}_{15}
\end{aligned} \tag{7.2.30b}$$

Repeating the procedure to eliminate X_{mn} and Y_{mn} , we obtain

$$N_0 = \frac{1}{\alpha^2 + k\beta^2} \left(\hat{s}_{33} - \frac{\hat{s}_{34}\bar{s}_{55} - \hat{s}_{35}\bar{s}_{45}}{\bar{s}_{44}\bar{s}_{55} - \bar{s}_{45}\bar{s}_{45}} \hat{s}_{34} - \frac{\bar{s}_{44}\hat{s}_{35} - \bar{s}_{45}\hat{s}_{34}}{\bar{s}_{44}\bar{s}_{55} - \bar{s}_{45}\bar{s}_{45}} \hat{s}_{35} \right) \tag{7.2.31}$$

Alternatively, we can eliminate X_{mn} and Y_{mn} first and then eliminate U_{mn} and V_{mn} to obtain an expression equivalent to the one given in Eq. (7.2.31); see next section for details.

Specially orthotropic plates

For specially orthotropic plates, we have from Eq. (7.2.30b) $\hat{s}_{14} = \hat{s}_{15} = 0$ and $\hat{s}_{24} = \hat{s}_{25} = 0$; consequently, $b_1 = b_2 = b_3 = b_4 = 0$ and $\bar{s}_{44} = \hat{s}_{44}$, $\bar{s}_{45} = \hat{s}_{45}$, and $\bar{s}_{55} = \hat{s}_{55}$. Equation (7.2.31) takes the form

$$N_0 = \frac{1}{\alpha^2 + k\beta^2} \left(\hat{s}_{33} - \frac{\hat{s}_{34}\hat{s}_{55} - \hat{s}_{35}\hat{s}_{45}}{\hat{s}_{44}\hat{s}_{55} - \hat{s}_{45}\hat{s}_{45}} \hat{s}_{34} - \frac{\hat{s}_{44}\hat{s}_{35} - \hat{s}_{45}\hat{s}_{34}}{\hat{s}_{44}\hat{s}_{55} - \hat{s}_{45}\hat{s}_{45}} \hat{s}_{35} \right) \tag{7.2.32}$$

Using the definitions of \hat{s}_{ij} from Eq. (7.2.7), we can write

$$N_0 = \left(\frac{1}{\alpha^2 + k\beta^2} \right) \left(\frac{K^2 A_{44} A_{55} \hat{c}_{33} + (KA_{55}\alpha^2 + KA_{44}\beta^2) c_1}{c_1 + KA_{44}c_2 + KA_{55}c_3 + K^2 A_{44} A_{55}} \right) \tag{7.2.33a}$$

$$= \left(\frac{1}{\alpha^2 + k\beta^2} \right) \left(\frac{\hat{c}_{33} + \left(\frac{\alpha^2}{KA_{44}} + \frac{\beta^2}{KA_{55}} \right) c_1}{1 + \frac{c_1}{K^2 A_{44} A_{55}} + \frac{c_2}{KA_{55}} + \frac{c_3}{KA_{44}}} \right) \tag{7.2.33b}$$

$$\begin{aligned}
\hat{c}_{33} &= D_{11}\alpha^4 + 2(D_{12} + 2D_{66})\alpha^2\beta^2 + D_{22}\beta^4, \quad c_1 = c_2 c_3 - (c_4)^2 > 0 \\
c_2 &= D_{11}\alpha^2 + D_{66}\beta^2, \quad c_3 = D_{66}\alpha^2 + D_{22}\beta^2, \quad c_4 = (D_{12} + D_{66})\alpha\beta
\end{aligned} \tag{7.2.33c}$$

Clearly, when the effect of transverse shear deformation is neglected, Eq. (7.2.33b) yields the result (6.3.47a) obtained using the classical plate theory. The expression in (7.2.33b) is of the form

$$\frac{\hat{c}_{33} + k_1}{1 + k_2} \quad \text{where} \quad k_1 < k_2 \tag{7.2.34a}$$

from which it follows that

$$\hat{c}_{33} \geq \frac{\hat{c}_{33} + k_1}{1 + k_2} \tag{7.2.34b}$$

indicating that transverse shear deformation has the effect of reducing the buckling load (as long as $\hat{c}_{33} > 1$).

No conclusions can be drawn from the complicated expression of the buckling load concerning its minimum. Hence, a parametric study is carried out to determine the minimum buckling load, which occurs at $m = n = 1$. For an isotropic plate, the critical buckling load becomes

$$N_{cr} = 4D \left(\frac{\pi}{a} \right)^2 \frac{\left[1 + \frac{3(1-\nu^2)\pi^2(h/a)^2}{K} \right]}{\left[1 + \frac{72(1+\nu)(1-\nu^2)\pi^4(h/a)^4}{K^2} + \frac{6(1+\nu)(3-\nu)\pi^2(h/a)^2}{K} \right]} \quad (7.2.35)$$

Table 7.2.5 contains nondimensionalized critical buckling loads of a square orthotropic plate and symmetric square laminates (0/90/0), (0/90/0/90/0), (0/90/0/90/0/90/0), and (0/90/0/90/0/90/0/90/0) under uniaxial and biaxial loadings. In these laminates the 0° layers and 90° layers have the same total thickness. For example, in the case of the nine-layer laminate the individual layer thicknesses are 0.1, 0.125, 0.1, 0.125, 0.1, 0.125, 0.1, 0.125, and 0.1, respectively. The critical buckling loads in all cases occurred in mode (1,1), except for orthotropic plates in biaxial compression, for which the mode is (2,1). For the side-to-thickness ratio of 10, for example, the classical laminate theory overpredicts the critical buckling loads by as much as 48% for orthotropic plates, and the error is less for thin plates.

Figure 7.2.8 shows the effect of transverse shear deformation on critical buckling loads of symmetric (0/90/90/0) laminates under uniaxial and biaxial compression ($a/b = 1$; $E_1/E_2 = 25$, $G_{12} = G_{13} = 0.5E_2$, $G_{23} = 0.2E_2$, $\nu_{12} = 0.25$). The effect of shear deformation is clear from the figure. Figure 7.2.9 shows the effect of transverse shear deformation and bending-extensional coupling on critical buckling loads ($a/b = 1$; $E_1/E_2 = 25$, $G_{12} = G_{13} = 0.5E_2$, $G_{23} = 0.2E_2$, $\nu_{12} = 0.25$). The eight-layer antisymmetric cross-ply plate behaves much like an orthotropic plate. Critical buckling loads of two-layer and eight-layer antisymmetric cross-ply laminated plates under uniaxial and biaxial loading are presented in Table 7.2.6 for modulus ratios $E_1/E_2=10$, 25, and 40. The effect of shear deformation on buckling loads is not as significant as for deflections. Note that the same critical buckling loads are valid for a rectangular laminate with aspect ratio $a/b = 3$, except that the mode at critical buckling is $(m, n) = (3, 1)$.

7.2.4 Vibration

For free vibration, we set the thermal and mechanical loads to zero, and substitute

$$U_{mn}(t) = U_{mn}^0 e^{i\omega t}, \quad V_{mn}(t) = V_{mn}^0 e^{i\omega t}, \quad W_{mn}(t) = W_{mn}^0 e^{i\omega t}, \quad \dots$$

in Eq. (7.2.7) and obtain

$$\left([\hat{S}] - \omega^2 [\hat{M}] \right) \{ \Delta \} = \{ 0 \} \quad (7.2.36a)$$

where

$$[\hat{S}] = \begin{bmatrix} \hat{s}_{11} & \hat{s}_{12} & 0 & \hat{s}_{14} & \hat{s}_{15} \\ \hat{s}_{12} & \hat{s}_{22} & 0 & \hat{s}_{24} & \hat{s}_{25} \\ 0 & 0 & \hat{s}_{33} & \hat{s}_{34} & \hat{s}_{35} \\ \hat{s}_{14} & \hat{s}_{24} & \hat{s}_{34} & \hat{s}_{44} & \hat{s}_{45} \\ \hat{s}_{15} & \hat{s}_{25} & \hat{s}_{35} & \hat{s}_{45} & \hat{s}_{55} \end{bmatrix}, \quad [\hat{M}] = \begin{bmatrix} \hat{m}_{11} & 0 & 0 & 0 & 0 \\ 0 & \hat{m}_{22} & 0 & 0 & 0 \\ 0 & 0 & \hat{m}_{33} & 0 & 0 \\ 0 & 0 & 0 & \hat{m}_{44} & 0 \\ 0 & 0 & 0 & 0 & \hat{m}_{55} \end{bmatrix} \quad (7.2.36b)$$

and $\{\Delta\}^T = \{U_{mn}^0 \ V_{mn}^0 \ W_{mn}^0 \ X_{mn}^0 \ Y_{mn}^0\}$. The coefficients \hat{s}_{ij} and \hat{m}_{ij} are defined in Eqs. (7.2.7b,c).

Table 7.2.5: Effect of shear deformation on nondimensionalized critical buckling loads, $\bar{N} = N_{cr}(a^2/E_2 h^3)$, of simply supported (SS-1) symmetric cross-ply square plates ($E_1 = 25E_2$, $G_{12} = G_{13} = 0.5E_2$, $G_{23} = 0.2E_2$, $\nu_{12} = 0.25$, $K = 5/6$).

a/h	0°	Three-ply	Five-ply	Seven-ply	Nine-ply
<i>Uniaxial Compression (k = 0)</i>					
10	15.874	15.289	16.309	16.535	16.622
20	20.953	20.628	21.125	21.237	21.281
25	21.800	21.568	21.917	21.996	22.027
50	23.046	22.978	23.078	23.101	23.109
100	23.381	23.363	23.389	23.395	23.397
CLPT	23.495	23.495	23.495	23.495	23.495
<i>Biaxial Compression (k = 1)</i>					
10	5.837 [†]	7.644	8.154	8.267	8.311
20	7.555	10.314	10.562	10.619	10.641
25	7.839	10.784	10.958	10.998	11.014
50	8.257	11.489	11.539	11.550	11.555
100	8.369	11.682	11.695	11.698	11.699
CLPT	8.407	11.747	11.747	11.747	11.747

[†] Mode for orthotropic plates in biaxial compression is $(m, n) = (2, 1)$.

Table 7.2.6: Effect of shear deformation on nondimensionalized critical buckling loads, $\bar{N} = N_{cr}(a^2/E_2 h^3)$, of simply supported (SS-1) antisymmetric cross-ply square plates ($G_{12} = G_{13} = 0.5E_2$, $G_{23} = 0.2E_2$, $\nu_{12} = 0.25$, $K = 5/6$).

b/h	$E_1/E_2 = 10$		$E_1/E_2 = 25$		$E_1/E_2 = 40$	
	(0/90)	(0/90) ₄	(0/90)	(0/90) ₄	(0/90)	(0/90) ₄
<i>Uniaxial Compression (k = 0); mode: (1,1)</i>						
10	5.746	9.158	8.189	16.301	10.381	21.631
20	6.205	10.380	9.153	20.623	11.980	29.965
100	6.367	10.843	9.511	22.535	12.601	34.179
CLPT	6.374	10.864	9.526	22.622	12.628	34.381
<i>Biaxial Compression (k = 1); mode: (1,1)</i>						
10	2.873	4.579	4.094	8.150	5.190	10.816
20	3.102	5.190	4.576	10.311	5.990	14.983
100	3.184	5.422	4.755	11.267	6.300	17.090
CLPT	3.187	5.432	4.763	11.311	6.314	17.190

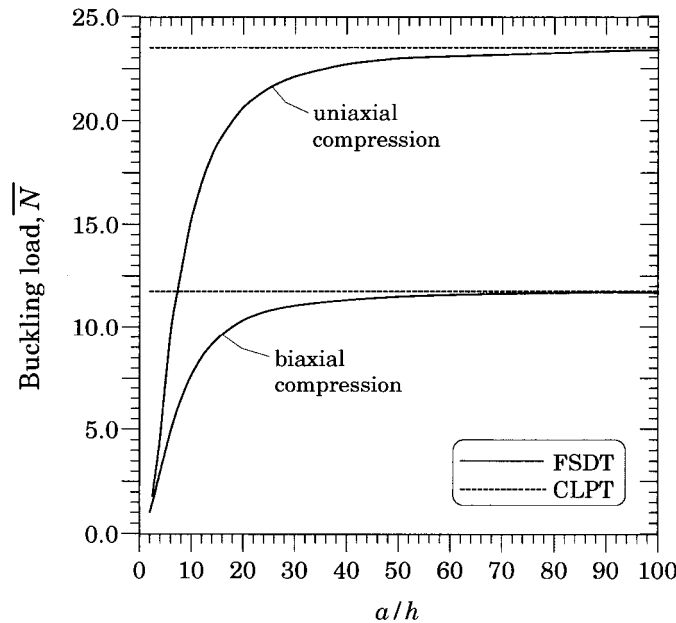


Figure 7.2.8: Nondimensionalized critical buckling load (\bar{N}) versus side-to-thickness ratio (a/h) for simply supported (SS-1) symmetric cross-ply (0/90/90/0) square laminates.

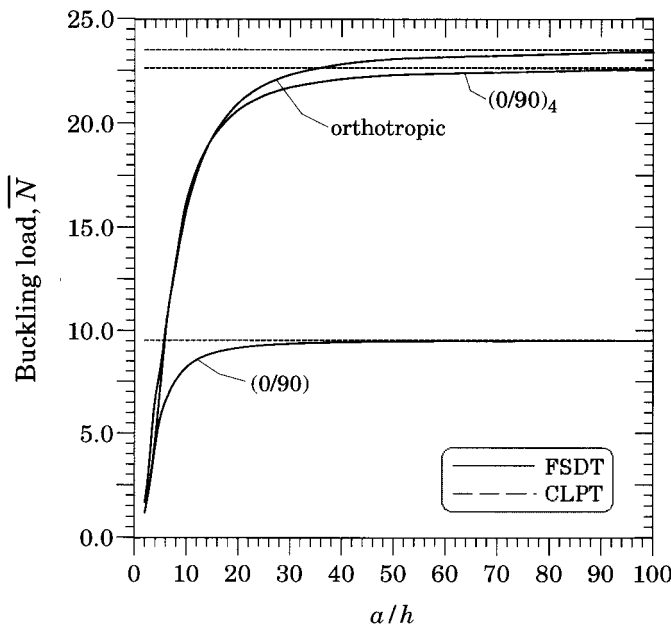


Figure 7.2.9: Nondimensionalized critical buckling load (\bar{N}) versus side-to-thickness ratio (a/h) for simply supported (SS-1) antisymmetric cross-ply (0/90)_n square laminates.

When rotary inertia is omitted, Eq. (7.2.36) can be simplified by eliminating X_{mn} and Y_{mn} (say, using the static condensation method). We obtain the following 3×3 system of eigenvalue problem [cf. Eq. (6.3.49)]:

$$\left(\begin{bmatrix} \bar{s}_{11} & \bar{s}_{12} & \bar{s}_{13} \\ \bar{s}_{12} & \bar{s}_{22} & \bar{s}_{23} \\ \bar{s}_{13} & \bar{s}_{23} & \bar{s}_{33} \end{bmatrix} - \omega^2 \begin{bmatrix} \hat{m}_{11} & 0 & 0 \\ 0 & \hat{m}_{22} & 0 \\ 0 & 0 & \hat{m}_{33} \end{bmatrix} \right) \begin{Bmatrix} U_{mn}^0 \\ V_{mn}^0 \\ W_{mn}^0 \end{Bmatrix} = \begin{Bmatrix} 0 \\ 0 \\ 0 \end{Bmatrix} \quad (7.2.37a)$$

where ($\bar{s}_{ij} = \bar{s}_{ji}$)

$$\begin{aligned} \bar{s}_{11} &= \hat{s}_{11} - (\hat{s}_{14}\hat{s}_{55} - \hat{s}_{15}\hat{s}_{45})\hat{s}_{14}/\hat{s}_{00} - (\hat{s}_{15}\hat{s}_{44} - \hat{s}_{14}\hat{s}_{45})\hat{s}_{15}/\hat{s}_{00} \\ \bar{s}_{12} &= \hat{s}_{12} - (\hat{s}_{24}\hat{s}_{55} - \hat{s}_{25}\hat{s}_{45})\hat{s}_{14}/\hat{s}_{00} - (\hat{s}_{25}\hat{s}_{44} - \hat{s}_{24}\hat{s}_{45})\hat{s}_{15}/\hat{s}_{00} \\ \bar{s}_{13} &= -(\hat{s}_{34}\hat{s}_{55} - \hat{s}_{35}\hat{s}_{45})\hat{s}_{14}/\hat{s}_{00} - (\hat{s}_{35}\hat{s}_{44} - \hat{s}_{34}\hat{s}_{45})\hat{s}_{15}/\hat{s}_{00} \\ \bar{s}_{22} &= \hat{s}_{22} - (\hat{s}_{24}\hat{s}_{55} - \hat{s}_{25}\hat{s}_{45})\hat{s}_{24}/\hat{s}_{00} - (\hat{s}_{25}\hat{s}_{44} - \hat{s}_{24}\hat{s}_{45})\hat{s}_{25}/\hat{s}_{00} \\ \bar{s}_{23} &= \hat{s}_{23} - (\hat{s}_{34}\hat{s}_{55} - \hat{s}_{35}\hat{s}_{45})\hat{s}_{24}/\hat{s}_{00} - (\hat{s}_{35}\hat{s}_{44} - \hat{s}_{34}\hat{s}_{45})\hat{s}_{25}/\hat{s}_{00} \\ \bar{s}_{33} &= \hat{s}_{33} - (\hat{s}_{34}\hat{s}_{55} - \hat{s}_{35}\hat{s}_{45})\hat{s}_{34}/\hat{s}_{00} - (\hat{s}_{35}\hat{s}_{44} - \hat{s}_{34}\hat{s}_{45})\hat{s}_{35}/\hat{s}_{00} \\ \bar{s}_{00} &= \hat{s}_{44}\hat{s}_{55} - \hat{s}_{45}\hat{s}_{45} \end{aligned} \quad (7.2.37b)$$

If the in-plane and rotary inertias are omitted (i.e., $\hat{m}_{11} = \hat{m}_{22} = \hat{m}_{44} = \hat{m}_{55} = 0$), we have [cf. Eq. (6.3.52)]

$$\omega^2 = \frac{1}{\hat{m}_{33}} \left(\bar{s}_{33} - \frac{\bar{s}_{13}\bar{s}_{22} - \bar{s}_{23}\bar{s}_{12}}{\bar{s}_{11}\bar{s}_{22} - \bar{s}_{12}\bar{s}_{12}} \bar{s}_{13} - \frac{\bar{s}_{11}\bar{s}_{23} - \bar{s}_{12}\bar{s}_{13}}{\bar{s}_{11}\bar{s}_{22} - \bar{s}_{12}\bar{s}_{12}} \bar{s}_{23} \right) \quad (7.2.38)$$

If frequencies of in-plane vibration of specially orthotropic laminates or natural frequencies of flexural or in-plane vibration of antisymmetric laminates are required, one must use Eq. (7.2.37a).

Specially orthotropic plates

For specially orthotropic plates, the in-plane displacements are uncoupled from the transverse deflection, and therefore the natural frequencies of vibration are given by Eq. (7.2.37); Eq. (7.2.38) gives the same frequencies of flexural vibration as Eq. (7.2.37a) for this case.

Table 7.2.7 contains frequencies of isotropic plates. Similar results are presented in Tables 7.2.8 and 7.2.9 for symmetric cross-ply laminates. The effect of the shear correction factor is to decrease the frequencies; i.e., the smaller the K , the smaller are the frequencies. The rotary inertia (RI) also has the effect of decreasing frequencies. Figure 7.2.10 shows the effect of transverse shear deformation and rotary inertia on fundamental natural frequencies of orthotropic and symmetric cross-ply (0/90/90/0) square plates with the following lamina properties:

$$E_1/E_2 = 25, \quad G_{12} = G_{13} = 0.5E_2, \quad G_{23} = 0.2E_2, \quad \nu_{12} = 0.25$$

The symmetric cross-ply plate behaves much like an orthotropic plate. The effect of rotary inertia is negligible in FSDT and therefore not shown in the figure.

Table 7.2.7: Effect of shear deformation, rotary inertia, and shear correction coefficient on nondimensionalized natural frequencies of simply supported (SS-1) isotropic square plates ($\bar{\omega} = \omega(a^2/h)\sqrt{\rho/E}$; $\nu = 0.3, a/h = 10$).

<i>m</i>	<i>n</i>	CLPT [†] w/o RI	CLPT with RI	<i>K</i>	FSDT w/o RI	FSDT with RI
1	1	5.973	5.925	2/3	5.773	5.732
				5/6	5.812	5.769
				1.0	5.838	5.794
2	1	14.933	14.635	2/3	13.769	13.568
				5/6	13.980	13.764
				1.0	14.127	13.899
2	2	23.893	23.144	2/3	21.103	20.688
				5/6	21.583	21.121
				1.0	21.922	21.424
3	1	29.867	28.709	2/3	25.682	25.115
				5/6	26.378	25.734
				1.0	26.875	26.171
3	2	38.827	36.904	2/3	32.153	31.357
				5/6	33.213	32.284
				1.0	33.982	32.946
4	1	50.744	47.558	2/3	40.150	39.063
				5/6	41.744	40.436
				1.0	42.919	41.427
3	3	53.760	50.174	2/3	42.051	40.895
				5/6	43.785	42.383
				1.0	45.067	43.461

[†] w/o RI means without rotary inertia.

Table 7.2.8: Effect of shear deformation on dimensionless natural frequencies of simply supported (SS-1) symmetric cross-ply plates ($\bar{\omega} = \omega(a^2/h)\sqrt{\rho/E}$; $E_1 = 25E_2, G_{12} = G_{13} = 0.5E_2, G_{23} = 0.2E_2, \nu_{12} = 0.25, K = 5/6$; rotary inertia is included; the total thickness of all 0° layers and all 90° layers is the same, $h/2$).

<i>a/h</i>	Theory	0°	Three-ply	Five-ply	Seven-ply	Nine-ply
5	FSDT	8.909	8.766	9.215	9.301	9.333
	CLPT	14.750	14.750	14.750	14.750	14.750
10	FSDT	12.452	12.227	12.633	12.720	12.754
	CLPT	15.104	15.104	15.104	15.104	15.104
20	FSDT	14.355	14.244	14.415	14.453	14.468
	CLPT	15.197	15.197	15.197	15.197	15.197
25	FSDT	14.651	14.573	14.690	14.717	14.727
	CLPT	15.208	15.208	15.208	15.208	15.208
50	FSDT	15.077	15.055	15.087	15.095	15.098
	CLPT	15.223	15.223	15.223	15.223	15.223
100	FSDT	15.190	15.184	15.192	15.194	15.195
	CLPT	15.227	15.227	15.227	15.227	15.227

Table 7.2.9: Effect of shear deformation, rotary inertia, and shear correction coefficient on nondimensionalized natural frequencies ($\bar{\omega} = \omega(a^2/h)\sqrt{\rho/E}$) of simply supported (SS-1) symmetric cross-ply (0/90/0) square plates ($h_k = h/3$; $E_1 = 25E_2$, $G_{12} = G_{13} = 0.5E_2$, $G_{23} = 0.2E_2$, $\nu_{12} = 0.25$).

a/h	m	n	CLPT w/o RI	CLPT with RI	FSDT w/o RI	FSDT with RI
10	1	1	15.228	15.104	12.593	12.527 [†]
		2	22.877	22.421	19.440	19.203
		3	40.299	38.738	32.496	31.921
	2	1	56.885	55.751	33.097	32.931
		2	60.911	59.001	36.786	36.362
		4	66.754	62.526	48.837	47.854
	2	3	71.522	67.980	45.484	44.720
					43.212	42.585
100	1	1	15.228	15.227	15.192	15.191
		2	22.877	22.873	22.831	22.827
		3	40.299	40.283	40.190	40.174
	2	1	56.885	56.874	56.330	56.319
		2	60.911	60.891	60.342	60.322
		4	66.754	66.708	66.466	66.421
	2	3	71.522	71.484	70.919	70.882
					70.801	70.764

[†] The first line corresponds to shear correction coefficient of $K = 1.0$ and the second line corresponds to shear correction coefficient of $K = 5/6$.

Figure 7.2.11 shows the effect of transverse shear deformation, bending-extensional coupling, and rotary inertia on fundamental natural frequencies of two-layer and eight-layer antisymmetric cross-ply laminates ($E_1/E_2 = 25$, $G_{12} = G_{13} = 0.5E_2$, $G_{23} = 0.2E_2$, $\nu_{12} = 0.25$). The eight-layer antisymmetric cross-ply plate behaves much like an orthotropic plate. The effect of rotary inertia is negligible in FSDT and therefore not shown in the figure. Table 7.2.10 contains numerical values of fundamental frequencies of antisymmetric cross-ply laminated plates for various modular ratios. Results for both two-layer and eight-layer laminated plates for square and rectangular ($a/b = 3$) geometries are presented.

Table 7.2.10: Effect of shear deformation on nondimensionalized fundamental frequencies of simply supported (SS-1) antisymmetric cross-ply square plates ($G_{12} = G_{13} = 0.5E_2$, $G_{23} = 0.2E_2$, $\nu_{12} = 0.25$, $K = 5/6$).

b/h	Theory	$E_1/E_2 = 10$		$E_1/E_2 = 25$		$E_1/E_2 = 40$	
		(0/90)	(0/90) ₄	(0/90)	(0/90) ₄	(0/90)	(0/90) ₄
<i>Square Plate ($a/b = 1$)</i>							
10	FSDT	7.454	9.450	8.900	12.628	10.027	14.562
	CLPT	7.832	10.268	9.566	14.816	11.011	18.265
20	FSDT	7.802	10.102	9.474	14.241	10.840	17.169
	CLPT	7.906	10.333	9.663	14.910	11.125	18.381
100	FSDT	7.926	10.344	9.687	14.912	11.150	18.365
	CLPT	7.931	10.354	9.695	14.941	11.163	18.419
<i>Rectangular Plate ($a/b = 3$)</i>							
10	FSDT	4.751	6.319	5.952	8.800	6.846	10.269
	CLPT	4.930	6.772	6.324	10.201	7.437	12.738
20	FSDT	4.908	6.592	6.258	9.819	7.313	11.990
	CLPT	4.956	6.796	6.360	10.238	7.480	12.783
100	FSDT	4.962	6.799	6.367	10.231	7.486	12.763
	CLPT	4.964	6.804	6.372	10.249	7.493	12.798

7.3 Simply Supported Antisymmetric Angle-Ply Laminated Plates

7.3.1 Boundary Conditions

The boundary conditions in (6.2.7) imply the following SS-2 boundary conditions on the generalized displacements and resultants of the first-order laminate theory (see Figure 7.3.1):

$$\begin{aligned} u_0(0, y, t) &= 0, & u_0(a, y, t) &= 0, & v_0(x, 0, t) &= 0, & v_0(x, b, t) &= 0 \\ w_0(x, 0, t) &= 0, & w_0(x, b, t) &= 0, & w_0(0, y, t) &= 0, & w_0(a, y, t) &= 0 \\ \phi_x(x, 0, t) &= 0, & \phi_x(x, b, t) &= 0, & \phi_y(0, y, t) &= 0, & \phi_y(a, y, t) &= 0 \end{aligned} \quad (7.3.1a)$$

$$\begin{aligned} N_{xy}(0, y, t) &= 0, & N_{xy}(a, y, t) &= 0, & N_{xy}(x, 0, t) &= 0, & N_{xy}(x, b, t) &= 0 \\ M_{xx}(0, y, t) &= 0, & M_{xx}(a, y, t) &= 0, & M_{yy}(x, 0, t) &= 0, & M_{yy}(x, b, t) &= 0 \end{aligned} \quad (7.3.1b)$$

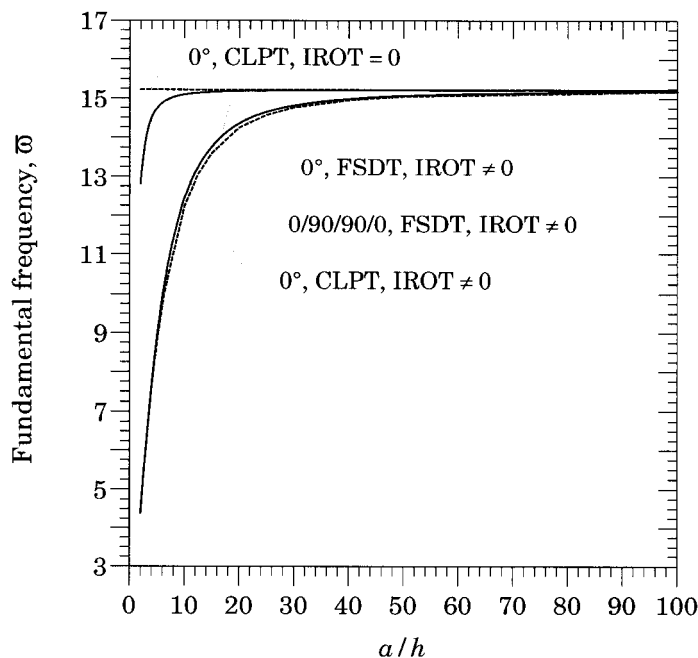


Figure 7.2.10: Nondimensionalized fundamental frequency ($\bar{\omega}$) versus side-to-thickness ratio (a/b) for simply supported (SS-1), orthotropic and symmetric cross-ply (0/90/90/0) laminates.

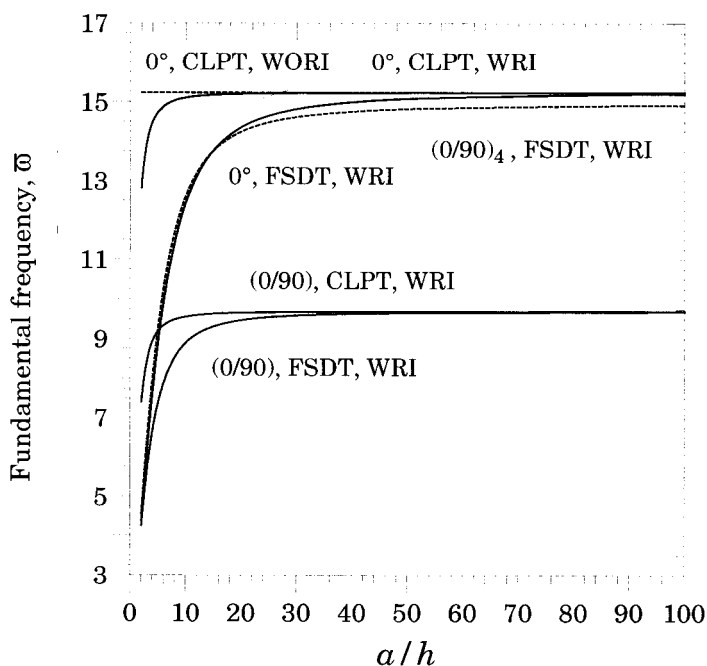


Figure 7.2.11: Nondimensionalized fundamental frequency ($\bar{\omega}$) versus side-to-thickness ratio (a/h) for simply supported (SS-1), antisymmetric cross-ply (0/90) laminates.

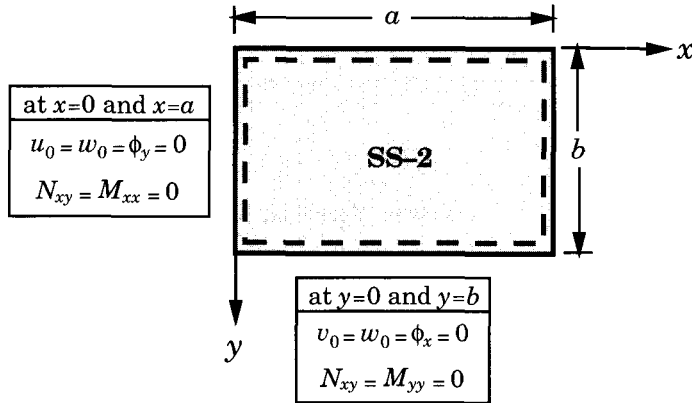


Figure 7.3.1: The simply supported boundary conditions for antisymmetric angle-ply laminates (SS-2).

7.3.2 The Navier Solution

The boundary conditions in (7.3.1) are satisfied by the expansions

$$u_0(x, y, t) = \sum_{n=1}^{\infty} \sum_{m=1}^{\infty} U_{mn}(t) \sin \alpha x \cos \beta y \quad (7.3.2a)$$

$$v_0(x, y, t) = \sum_{n=1}^{\infty} \sum_{m=1}^{\infty} V_{mn}(t) \cos \alpha x \sin \beta y \quad (7.3.2b)$$

$$w_0(x, y, t) = \sum_{n=1}^{\infty} \sum_{m=1}^{\infty} W_{mn}(t) \sin \alpha x \sin \beta y \quad (7.3.3)$$

$$\phi_x(x, y, t) = \sum_{n=1}^{\infty} \sum_{m=1}^{\infty} X_{mn}(t) \cos \alpha x \sin \beta y \quad (7.3.4a)$$

$$\phi_y(x, y, t) = \sum_{n=1}^{\infty} \sum_{m=1}^{\infty} Y_{mn}(t) \sin \alpha x \cos \beta y \quad (7.3.4b)$$

Substitution of Eqs. (7.3.2a,b), (7.3.3), and (7.3.4a,b) into Eqs. (7.1.1)–(7.1.5) shows that the Navier solution exists only if

$$A_{16} = 0, \quad A_{26} = 0, \quad A_{45} = 0, \quad B_{11} = 0, \quad B_{12} = 0, \quad B_{22} = 0, \quad B_{66} = 0$$

$$D_{16} = 0, \quad D_{26} = 0, \quad I_1 = 0 \quad (7.3.5)$$

i.e., for antisymmetric angle-ply laminates [see Eq. (3.5.31)].

The coefficients $U_{mn}, V_{mn}, W_{mn}, X_{mn}, Y_{mn}$ can be determined from the equations

$$\begin{bmatrix} \hat{s}_{11} & \hat{s}_{12} & 0 & \hat{s}_{14} & \hat{s}_{15} \\ \hat{s}_{12} & \hat{s}_{22} & 0 & \hat{s}_{24} & \hat{s}_{25} \\ 0 & 0 & \hat{s}_{33} + \tilde{s}_{33} & \hat{s}_{34} & \hat{s}_{35} \\ \hat{s}_{14} & \hat{s}_{24} & \hat{s}_{34} & \hat{s}_{44} & \hat{s}_{45} \\ \hat{s}_{15} & \hat{s}_{25} & \hat{s}_{35} & \hat{s}_{54} & \hat{s}_{55} \end{bmatrix} \begin{Bmatrix} U_{mn} \\ V_{mn} \\ W_{mn} \\ X_{mn} \\ Y_{mn} \end{Bmatrix} +$$

$$\begin{bmatrix} \hat{m}_{11} & 0 & 0 & 0 & 0 \\ 0 & \hat{m}_{22} & 0 & 0 & 0 \\ 0 & 0 & \hat{m}_{33} & 0 & 0 \\ 0 & 0 & 0 & \hat{m}_{44} & 0 \\ 0 & 0 & 0 & 0 & \hat{m}_{55} \end{bmatrix} \begin{Bmatrix} \ddot{U}_{mn} \\ \ddot{V}_{mn} \\ \ddot{W}_{mn} \\ \ddot{X}_{mn} \\ \ddot{Y}_{mn} \end{Bmatrix} = \begin{Bmatrix} 0 \\ 0 \\ Q_{mn} \\ 0 \\ 0 \end{Bmatrix} + \begin{Bmatrix} -\beta N_{mn}^6 \\ -\alpha N_{mn}^6 \\ 0 \\ -\alpha M_{mn}^1 \\ -\beta M_{mn}^2 \end{Bmatrix} \quad (7.3.6)$$

where

$$\begin{aligned} \hat{s}_{11} &= (A_{11}\alpha^2 + A_{66}\beta^2), & \hat{s}_{12} &= (A_{12} + A_{66})\alpha\beta \\ \hat{s}_{13} &= 0, & \hat{s}_{14} &= 2B_{16}\alpha\beta, & \hat{s}_{15} &= (B_{16}\alpha^2 + B_{26}\beta^2) \\ \hat{s}_{22} &= (A_{66}\alpha^2 + A_{22}\beta^2), & \hat{s}_{23} &= 0 \\ \hat{s}_{24} &= \hat{s}_{15}, & \hat{s}_{25} &= 2B_{26}\alpha\beta \\ \hat{s}_{33} &= K(A_{55}\alpha^2 + A_{44}\beta^2), & \hat{s}_{34} &= KA_{55}\alpha \\ \hat{s}_{35} &= KA_{44}\beta, & \hat{s}_{44} &= (D_{11}\alpha^2 + D_{66}\beta^2 + KA_{55}) \\ \hat{s}_{45} &= (D_{12} + D_{66})\alpha\beta, & \hat{s}_{55} &= (D_{66}\alpha^2 + D_{22}\beta^2 + KA_{44}) \end{aligned} \quad (7.3.7)$$

and the thermal coefficients are defined in Eqs. (6.3.11)–(6.3.16), and \tilde{S}_{ij} and \hat{m}_{ij} are defined in Eqs (7.2.7b,c). Equation (7.3.5) can be specialized for static analysis, buckling under in-plane compressive loads, and natural vibration, as was discussed for antisymmetric cross-ply laminates.

The in-plane stresses in each layer can be computed from the equations

$$\begin{Bmatrix} \sigma_{xx} \\ \sigma_{yy} \\ \sigma_{xy} \end{Bmatrix}^{(k)} = \begin{bmatrix} \bar{Q}_{11} & \bar{Q}_{12} & \bar{Q}_{16} \\ \bar{Q}_{12} & \bar{Q}_{22} & \bar{Q}_{26} \\ \bar{Q}_{16} & \bar{Q}_{26} & \bar{Q}_{66} \end{bmatrix}^{(k)} \left(\begin{Bmatrix} \varepsilon_{xx} \\ \varepsilon_{yy} \\ 2\varepsilon_{xy} \end{Bmatrix} - \begin{Bmatrix} \alpha_{xx} \\ \alpha_{yy} \\ 2\alpha_{xy} \end{Bmatrix} \Delta T \right) \quad (7.3.8)$$

$$\begin{aligned} \left(\begin{Bmatrix} \varepsilon_{xx} \\ \varepsilon_{yy} \\ 2\varepsilon_{xy} \end{Bmatrix} - \begin{Bmatrix} \alpha_{xx} \\ \alpha_{yy} \\ 2\alpha_{xy} \end{Bmatrix} \Delta T \right) &= \sum_{m=1}^{\infty} \sum_{n=1}^{\infty} \left\{ \begin{array}{c} \alpha U_{mn} g_{mn} - \alpha_{xx} T_{mn}^0 f_{mn} \\ \beta V_{mn} g_{mn} - \alpha_{yy} T_{mn}^0 f_{mn} \\ -(\beta U_{mn} + \alpha V_{mn} - 2\alpha_{xy} T_{mn}^0) f_{mn} \end{array} \right\} \\ &\quad - \sum_{m=1}^{\infty} \sum_{n=1}^{\infty} z \left\{ \begin{array}{c} (\alpha X_{mn} + \alpha_{xx} T_{mn}^1) f_{mn} \\ (\beta Y_{mn} + \alpha_{yy} T_{mn}^1) f_{mn} \\ -(\beta X_{mn} + \alpha Y_{mn}) g_{mn} + 2\alpha_{xy} T_{mn}^1 f_{mn} \end{array} \right\} \end{aligned} \quad (7.3.9a)$$

$$f_{mn} = \sin \frac{m\pi x}{a} \sin \frac{n\pi y}{b}, \quad g_{mn} = \cos \frac{m\pi x}{a} \cos \frac{n\pi y}{b} \quad (7.3.9b)$$

The transverse shear stresses from the constitutive equations are given by

$$\begin{Bmatrix} \sigma_{yz} \\ \sigma_{xz} \end{Bmatrix}^{(k)} = \sum_{m=1}^{\infty} \sum_{n=1}^{\infty} \begin{bmatrix} \bar{Q}_{44} & \bar{Q}_{45} \\ \bar{Q}_{45} & \bar{Q}_{55} \end{bmatrix}^{(k)} \left\{ \begin{array}{c} (Y_{mn} + \beta W_{mn}) \sin \alpha x \cos \beta y \\ (X_{mn} + \alpha W_{mn}) \cos \alpha x \sin \beta y \end{array} \right\} \quad (7.3.10)$$

Note that the stresses are layerwise constant through the thickness.

The transverse stresses can also be determined from the equilibrium equations of 3-D elasticity, as discussed before. They are

$$\begin{aligned} \sigma_{xz}^{(k)}(x, y, z) &= \sum_{m=1}^{\infty} \sum_{n=1}^{\infty} \left[(z - z_k) \bar{A}_{mn}^{(k)} + \frac{1}{2}(z^2 - z_k^2) \bar{B}_{mn}^{(k)} \right] + \sigma_{xz}^{(k-1)}(x, y, z_k) \\ \sigma_{yz}^{(k)}(x, y, z) &= \sum_{m=1}^{\infty} \sum_{n=1}^{\infty} \left[(z - z_k) \bar{C}_{mn}^{(k)} + \frac{1}{2}(z^2 - z_k^2) \bar{D}_{mn}^{(k)} \right] + \sigma_{yz}^{(k-1)}(x, y, z_k) \end{aligned} \quad (7.3.11a)$$

where

$$\begin{aligned}
 \bar{A}_{mn}^{(k)} &= \left[\left(\alpha^2 \bar{Q}_{11}^{(k)} + \beta^2 \bar{Q}_{66}^{(k)} \right) U_{mn} + \alpha\beta \left(\bar{Q}_{12}^{(k)} + \bar{Q}_{66}^{(k)} \right) V_{mn} \right] \sin \alpha x \cos \beta y \\
 &\quad + \left[2\alpha\beta \bar{Q}_{16}^{(k)} U_{mn} + \left(\alpha^2 \bar{Q}_{16}^{(k)} + \beta^2 \bar{Q}_{26}^{(k)} \right) V_{mn} \right] \cos \alpha x \sin \beta y \\
 \bar{B}_{mn}^{(k)} &= \left[\left(\alpha^2 \bar{Q}_{11}^{(k)} + \beta^2 \bar{Q}_{66}^{(k)} \right) X_{mn} + \alpha\beta \left(\bar{Q}_{12}^{(k)} + \bar{Q}_{66}^{(k)} \right) Y_{mn} \right] \cos \alpha x \sin \beta y \\
 &\quad + \left[2\alpha\beta \bar{Q}_{16}^{(k)} X_{mn} + \left(\alpha^2 \bar{Q}_{16}^{(k)} + \beta^2 \bar{Q}_{26}^{(k)} \right) Y_{mn} \right] \sin \alpha x \cos \beta y \\
 \bar{C}_{mn}^{(k)} &= \left[\left(\alpha^2 \bar{Q}_{16}^{(k)} + \beta^2 \bar{Q}_{26}^{(k)} \right) U_{mn} + 2\alpha\beta \bar{Q}_{26}^{(k)} V_{mn} \right] \sin \alpha x \cos \beta y \\
 &\quad + \left[\alpha\beta \left(\bar{Q}_{12}^{(k)} + \bar{Q}_{66}^{(k)} \right) U_{mn} + \left(\alpha^2 \bar{Q}_{66}^{(k)} + \beta^2 \bar{Q}_{22}^{(k)} \right) V_{mn} \right] \cos \alpha x \sin \beta y \\
 \bar{D}_{mn}^{(k)} &= \left[\left(\alpha^2 \bar{Q}_{16}^{(k)} + \beta^2 \bar{Q}_{26}^{(k)} \right) X_{mn} + 2\alpha\beta \bar{Q}_{26}^{(k)} Y_{mn} \right] \cos \alpha x \sin \beta y \\
 &\quad + \left[\alpha\beta \left(\bar{Q}_{12}^{(k)} + \bar{Q}_{66}^{(k)} \right) X_{mn} + \left(\alpha^2 \bar{Q}_{66}^{(k)} + \beta^2 \bar{Q}_{22}^{(k)} \right) Y_{mn} \right] \sin \alpha x \cos \beta y
 \end{aligned} \tag{7.3.11b}$$

7.3.3 Bending

Table 7.3.1 contains numerical results of nondimensionalized maximum deflections and stresses of simply supported (SS-2), two-layer and eight-layer antisymmetric angle-ply square laminates, $(-45/45/-45/\dots)$, subjected to sinusoidally and uniformly distributed loads. The nondimensionalizations and locations of maximum quantities are as follows:

$$\begin{aligned}
 \bar{w} &= w_0(a/2, a/2) \frac{E_2 h^3}{b^4 q_0}, & \bar{\sigma}_{xx} &= \sigma_{xx}(a/2, b/2, \frac{h}{2}) \frac{h^2}{b^2 q_0} \\
 \bar{\sigma}_{yy} &= \sigma_{yy}(a/2, b/2, \frac{h}{2}) \frac{h^2}{b^2 q_0}, & \bar{\sigma}_{xy} &= \sigma_{xy}(0, 0, -\frac{h}{2}) \frac{h^2}{b^2 q_0} \\
 \bar{\sigma}_{xz} &= \sigma_{xz}(0, b/2, k) \frac{h}{b q_0}, & \bar{\sigma}_{yz} &= \sigma_{yz}(a/2, 0, k) \frac{h}{b q_0}
 \end{aligned} \tag{7.3.12}$$

where $k = 1, 2, \dots, n$ denotes the ply number. Both constitutive and equilibrium based transverse shear stresses are included in the table. While the deflections are sensitive to the transverse shear deformation, stresses are not. Table 7.3.2 contains the maximum transverse deflection and in-plane normal stress as a function of the modulus ratio of simply supported (SS-2) square, antisymmetric, two-layer $(-45/45)$ and eight-layer $(-45/45/-45/\dots)$ angle-ply laminates ($a/h = 10$) subjected to uniformly distributed load.

Figure 7.3.2 contains plots of the nondimensionalized transverse deflection versus side-to-thickness ratio (a/h) of various angle-ply laminates subjected to uniformly or sinusoidally distributed transverse load ($a/b = 1$; $E_1/E_2 = 25$, $G_{12} = G_{13} = 0.5E_2$, $\nu_{12} = 0.25$, $K = 5/6$). The effect of transverse shear deformation is negligible for all values of a/h greater than 10. For values of a/h less than 10, the effect is quite significant. Figure 7.3.3 contains plots of the nondimensionalized deflection as a function of the lamination angle for two- and eight-layer antisymmetric angle-ply laminates ($a/h = 10$), $(-\theta/\theta/-\theta/\dots)$, subjected to sinusoidally distributed transverse load. The effect of bending-stretching is significant in two-layer laminates.

Table 7.3.1: Effect of transverse shear deformation on nondimensionalized maximum transverse deflections and stresses of simply supported (SS-2) antisymmetric angle-ply square plates ($h_i = h/n, E_1 = 25E_2, G_{12} = G_{13} = 0.5E_2, G_{23} = 0.2E_2, \nu_{12} = 0.25, K = 5/6$).

a/h	Load	$\bar{w} \times 10^2$	$\bar{\sigma}_{xx}$	$\bar{\sigma}_{xy}$	$\bar{\sigma}_{xz}$	$\bar{\sigma}_{xz}^\dagger$
<i>Antisymmetric Laminate, (-45/45)</i>						
10	SSL	0.8284	0.2498	0.2336	0.2728	0.2143
	UDL	1.2792	0.3476	0.4274	0.5072	0.4238
20	SSL	0.6981	0.2498	0.2336	0.2728	0.2143
	UDL	1.0907	0.3496	0.4357	0.5065	0.4205
100	SSL	0.6564	0.2498	0.2336	0.2728	0.2143
	UDL	1.0305	0.3504	0.4417	0.5068	0.4189
CLPT	SSL	0.6547	0.2498	0.2336	—	0.2143
	UDL	1.0280	0.3504	0.4421	—	0.4188
<i>Antisymmetric Laminate, (-45/45)₄</i>						
10	SSL	0.4198	0.1445	0.1384	0.2728	0.2487
	UDL	0.6366	0.1957	0.2463	0.5070	0.4960
20	SSL	0.2896	0.1445	0.1384	0.2728	0.2487
	UDL	0.4483	0.1988	0.2550	0.5050	0.4884
100	SSL	0.2479	0.1445	0.1384	0.2728	0.2487
	UDL	0.3883	0.2005	0.2630	0.5054	0.4841
CLPT	SSL	0.2462	0.1445	0.1384	—	0.2487
	UDL	0.3858	0.2006	0.2637	—	0.4838

† Maximum stress derived from equilibrium. The values reported are at $z = \pm h/4$ for $(-45/45)$ laminate, and at $z = 0$ for the $(-45/45)_4$ laminate; the shear stress derived from constitutive relations will have two values at each interface, and the larger of the two is reported.

Figures 7.3.4 and 7.3.5 contain nondimensionalized maximum transverse shear stress distributions through laminate thickness for an eight-layer antisymmetric angle-ply square laminate $(-45/30/-45/0/0/45/-30/45)$ subjected to uniformly or sinusoidally distributed transverse load. The side-to-thickness ratio is taken to be $a/h = 10$. The material properties used are: $E_1 = 25E_2, G_{12} = G_{13} = 0.5E_2, G_{23} = 0.2E_2, \nu_{12} = 0.25, K = 5/6$. The effect of transverse shear deformation is negligible on the stresses.

7.3.4 Buckling

Table 7.3.3 contains critical buckling loads of uniaxially and biaxially compressed simply supported (SS-1) square, antisymmetric angle-ply laminates for various modulus ratios and two lamination schemes $(-45/45)$ and $(-45/45/-45/\dots)$. Note that for certain modulus ratios, side-to-thickness ratios and lamination schemes, the shear deformation theory predicts buckling modes different from the classical laminate theory. Figures 7.3.6 and 7.3.7 show the influence of shear deformation,

Table 7.3.2: Effect of lamination scheme and shear deformation on the transverse deflections and stresses in square antisymmetric angle-ply laminates subjected to uniformly distributed transverse load ($h_n = h/n$, E_1/E_2 varied, $G_{12} = G_{13} = 0.5E_2$, $G_{23} = 0.2E_2$, $\nu_{12} = 0.25$, $a/h = 10$; $m, n = 1, 3, \dots, 21$ in the series are used to calculate the solutions for uniform load).

Theory	\hat{w}^*					$\bar{\sigma}_{xx}^\dagger$				
	$\frac{E_1}{E_2} = 1$	10	20	30	40	$\frac{E_1}{E_2} = 1$	10	20	30	40
<i>Orthotropic Plate</i>										
FSDT	4.480	1.678	1.089	0.856	0.731	0.255	0.681	0.755	0.780	0.791
CLPT	4.172	1.412	0.795	0.548	0.415	0.251	0.693	0.772	0.795	0.801
<i>Laminate, (-45/45)</i>										
FSDT	4.829	2.010	1.441	1.157	0.983	0.278	0.307	0.338	0.355	0.365
CLPT	4.577	1.759	1.190	0.906	0.732	0.278	0.308	0.340	0.358	0.370
<i>Laminate, (-45/45)₂</i>										
FSDT	4.829	1.251	0.792	0.622	0.534	0.278	0.213	0.201	0.196	0.193
CLPT	4.577	0.999	0.542	0.372	0.283	0.278	0.214	0.205	0.201	0.199
<i>Laminate, (-45/45)₄</i>										
FSDT	4.829	1.153	0.727	0.575	0.496	0.278	0.210	0.198	0.194	0.191
CLPT	4.577	0.902	0.477	0.324	0.245	0.278	0.211	0.203	0.199	0.198

$${}^* \hat{w} = w_0 \frac{E_2 h^3}{q_0 b^4} \times 10^2. \quad {}^\dagger \bar{\sigma}_{xx} = \sigma_{xx} \frac{1}{q_0}.$$

number of composite layers (bending-extensional coupling), and the lamination angle on critical buckling loads of antisymmetric angle-ply square laminates under uniaxial compressive loads ($a/b = 1$, $a/h = 10$, $E_1/E_2 = 25$, $G_{12} = G_{13} = 0.5E_2$, $\nu_{12} = 0.25$). The side-to-thickness ratio for the laminates in Figure 7.3.7 is taken to be $a/h = 10$.

7.3.5 Vibration

Numerical results of nondimensionalized fundamental frequencies of antisymmetric angle-ply laminates $(-45/45/-45/\dots)$ are presented in Table 7.3.4 for two different materials. Numerical results for two-layer $(-45/45)$ and eight-layer $(-45/45)_4$ plates with $E_1/E_2 = 25$, $G_{12} = G_{13} = 0.5E_2$, $G_{23} = 0.2E_2$, $\nu_{12} = 0.25$, and $K = 5/6$ are given as a function of side-to-thickness ratio in Figure 7.3.8 and as a function of lamination angle in Figure 7.3.9. The effect of bending-stretching coupling (i.e., B_{16} and B_{26}), transverse shear deformation (i.e., $\varepsilon_{xz} \neq 0$ and $\varepsilon_{yz} \neq 0$), and rotary inertia is to lower the fundamental frequencies. As the number of layers increases, the coupling decreases. The effect of shear deformation decreases with increasing

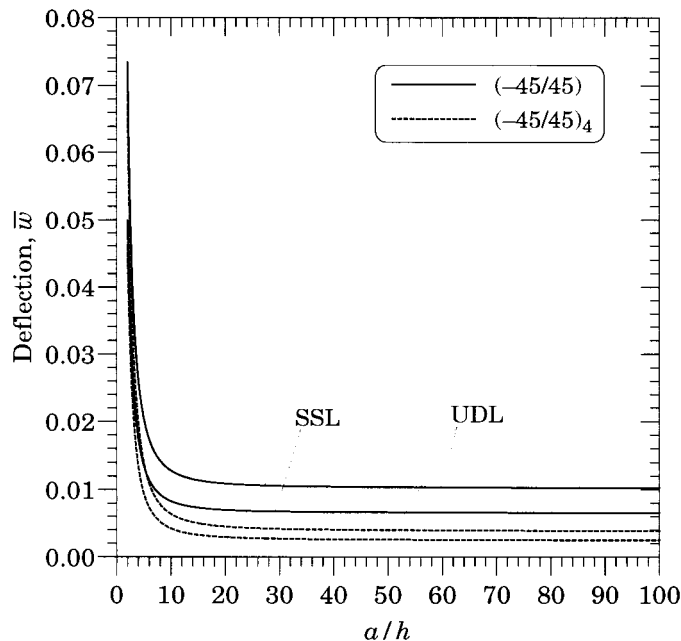


Figure 7.3.2: Center transverse deflection \bar{w} versus side-to-thickness ratio a/h for simply supported (SS-2) antisymmetric angle-ply $(-45/45)_n$ ($n = 1, 4$) square laminates.

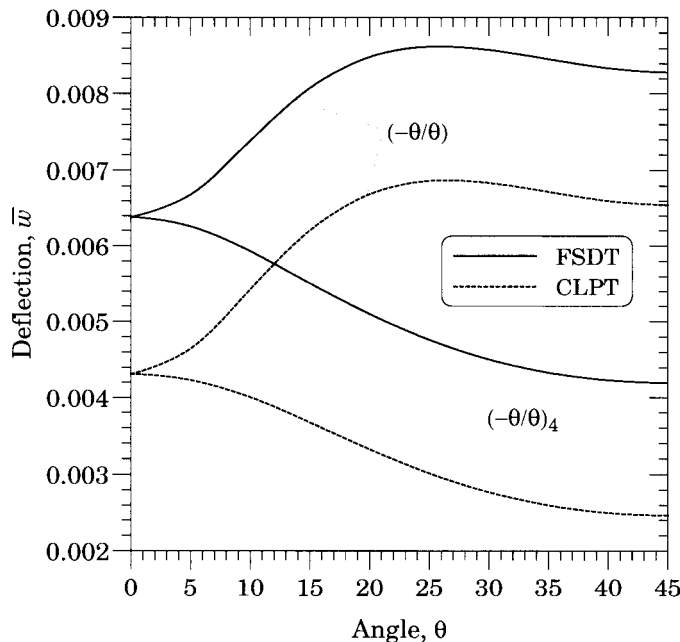


Figure 7.3.3: Center transverse deflection \bar{w} versus lamination angle θ for simply supported (SS-2) antisymmetric angle-ply $(-\theta/\theta)_n$ ($n = 1, 4$) square laminates ($a/h = 10$).

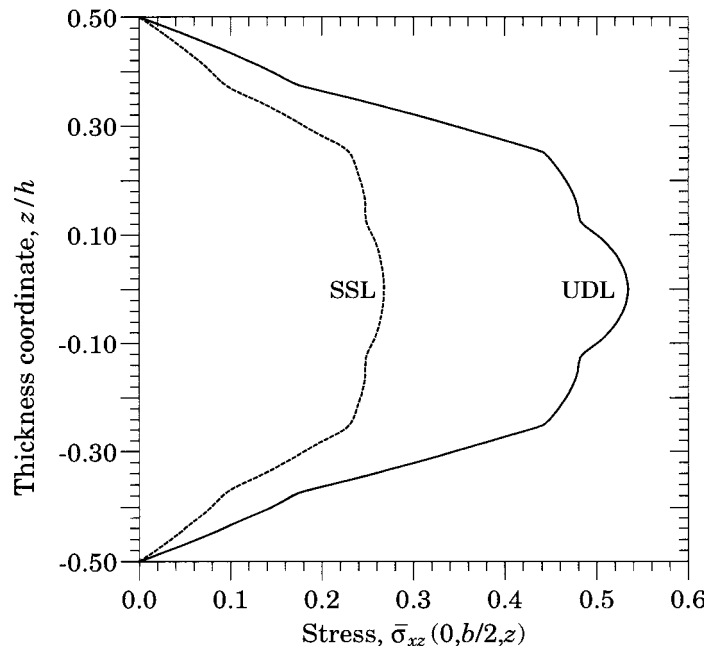


Figure 7.3.4: Distribution of transverse shear stress $\bar{\sigma}_{xz}(0, b/2, z)$ through thickness z/h for simply supported (SS-2) antisymmetric angle-ply ($-45/30/-45/0/0/45/-30/45$) square laminates.

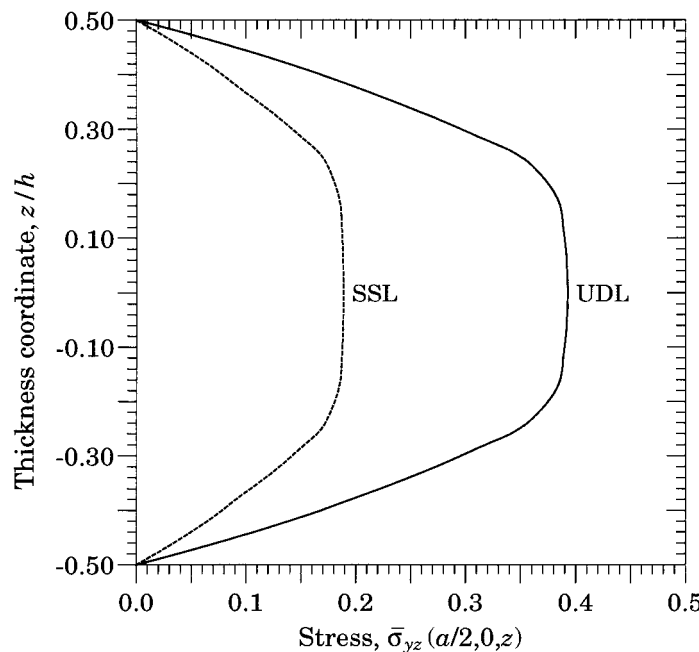


Figure 7.3.5: Distribution of transverse shear stress $\bar{\sigma}_{yz}(a/2, 0, z)$ through thickness z/h for simply supported (SS-2) antisymmetric angle-ply ($-45/30/-45/0/0/45/-30/45$) square laminates ($a/h = 10$).

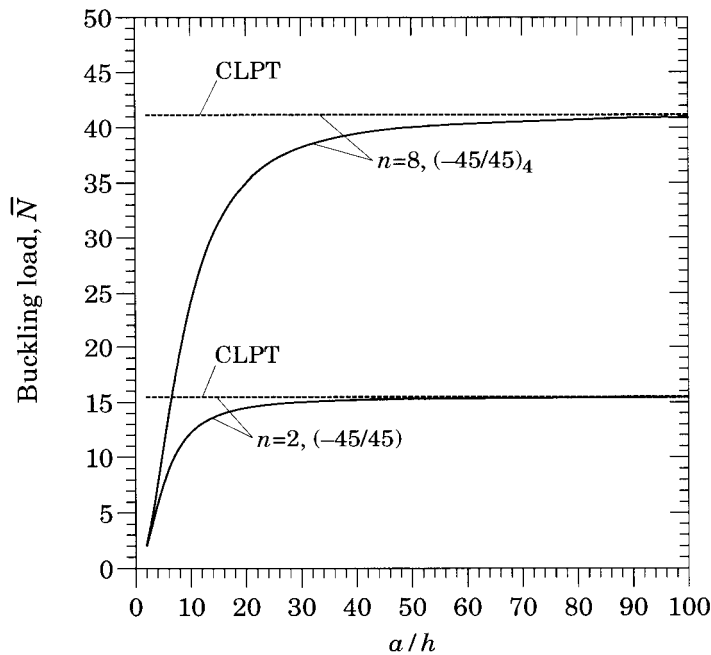


Figure 7.3.6: Critical buckling load (\bar{N}) versus side-to-thickness ratio (a/h) for simply supported (SS-2) antisymmetric angle-ply $(-45/45)_n$ square laminates.

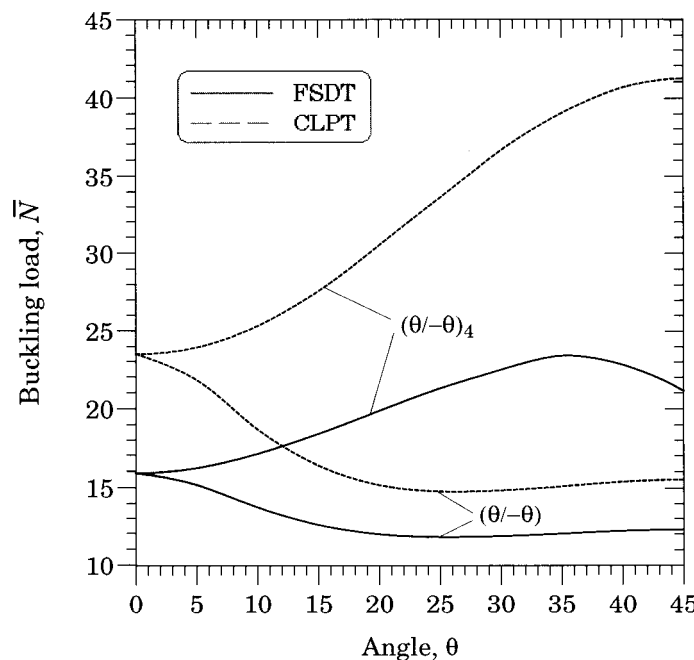


Figure 7.3.7: Critical buckling load (\bar{N}) versus lamination angle (θ) for simply supported (SS-2) antisymmetric angle-ply $(-\theta/\theta)_n$ laminates.

values of a/h . This decrease is slower for eight-layer plates than for two-layer plates. The effect of rotary inertia is negligible in FSDT, whereas it is significant in CLPT only for very thick plates.

Table 7.3.3: Effect of shear deformation on nondimensionalized critical buckling loads, $\bar{N} = N_{cr}(a^2/E_2 h^3)$, of simply supported (SS-2) antisymmetric angle-ply, $(-45/45)_n$, square plates ($G_{12} = G_{13} = 0.5E_2$, $G_{23} = 0.2E_2$, $\nu_{12} = 0.25$, $K = 5/6$).

a/h	$E_1/E_2 = 10$		$E_1/E_2 = 25$		$E_1/E_2 = 40$	
	$n = 2$	$n = 8$	$n = 2$	$n = 8$	$n = 2$	$n = 8$
<i>Uniaxial Compression</i> ($k = 0$); mode: (1,1)						
10	7.847	13.542	12.231	21.082 [†]	15.774 [†]	24.514 [†]
20	8.727	16.397	14.513	34.990	19.861	50.644
100	9.052	17.584	15.435	40.875	21.628	63.974
CLPT	9.066	17.637	15.476	41.163	21.709	64.683
<i>Biaxial Compression</i> ($k = 1$); mode: (1,1)						
10	3.923	6.771	6.115	12.067	7.910	15.336
20	4.364	8.199	7.257	17.495	9.930	25.322
100	4.526	8.792	7.717	20.437	10.810	31.987
CLPT	4.533	8.818	7.738	20.581	10.854	32.341

[†] Mode is (2,1).

Table 7.3.4: Effect of shear deformation on nondimensionalized natural frequencies of simply supported (SS-2) symmetric angle-ply $(-45/45/-45/\dots)$ square plates [$\bar{\omega} = \omega(a^2/h)\sqrt{\rho/E_2}$, $K = 5/6$; rotary inertia is included; mode: (1,1)].

a/h	Theory	Material 1		Material 2	
		$n = 2$	$n = 8$	$n = 2$	$n = 8$
5	FSDT	8.498	10.285	10.799	12.893
	CLPT	11.737	15.708	14.508	17.207
10	FSDT	10.895	15.388	13.629	19.289
	CLPT	12.195	19.986	15.087	25.052
20	FSDT	11.933	18.555	14.815	23.259
	CLPT	12.317	20.113	15.242	25.212
100	FSDT	12.341	20.084	15.274	25.176
	CLPT	12.357	20.154	15.292	26.398

Material 1: $E_1 = 25E_2$, $G_{12} = G_{13} = 0.5E_2$, $G_{23} = 0.2E_2$, $\nu_{12} = 0.25$.

Material 2: $E_1 = 40E_2$, $G_{12} = G_{13} = 0.6E_2$, $G_{23} = 0.5E_2$, $\nu_{12} = 0.25$.

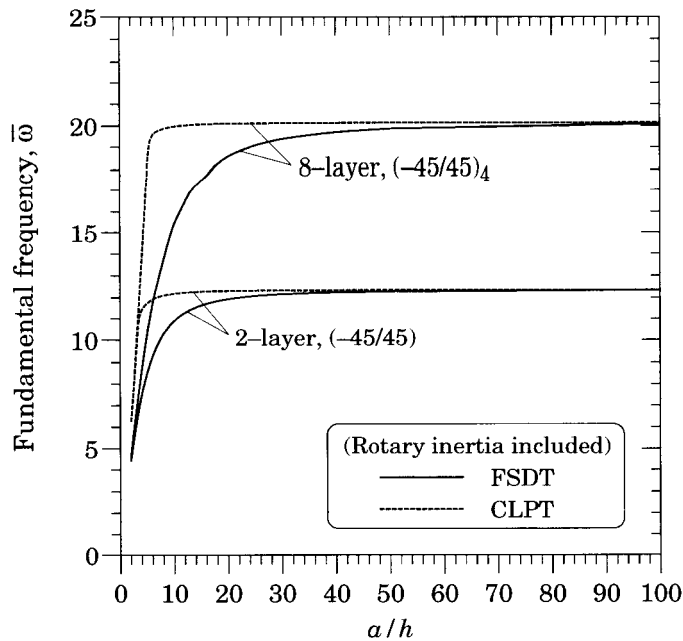


Figure 7.3.8: Nondimensionalized fundamental frequency $\bar{\omega}$ versus side-to-thickness ratio (a/h) for simply supported (SS-2) antisymmetric angle-ply $(-45/45)_n$ square laminates.

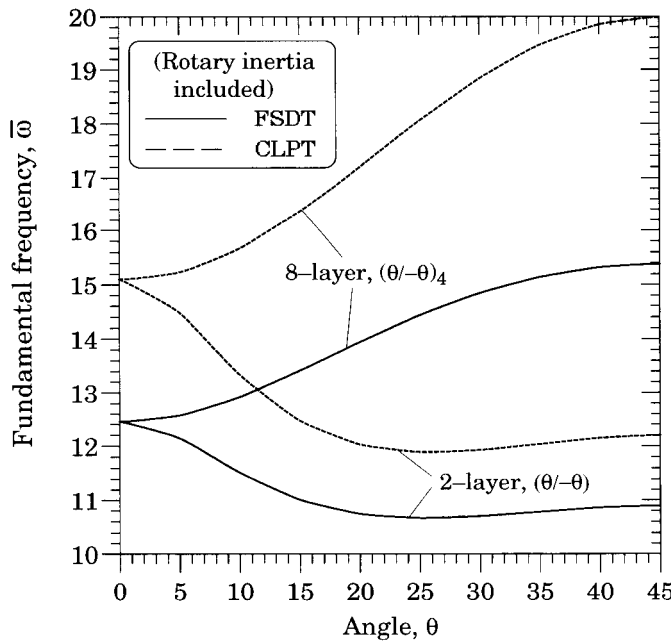


Figure 7.3.9: Nondimensionalized fundamental frequency ($\bar{\omega}$) versus lamination angle (θ) for simply supported (SS-2) antisymmetric angle-ply $(-\theta/\theta)_n$ square laminates.

7.4 Antisymmetric Cross-Ply Laminates with Two Opposite Edges Simply Supported

7.4.1 Introduction

In this section we present the Lévy type solutions for bending, natural vibration, and buckling of antisymmetric cross-ply laminates. In the interest of brevity, the discussion is limited to the bending case. For additional details and for a discussion of the free vibration and buckling analyses, the reader may consult References 8 and 23.

As described earlier, the Lévy solution technique involves choosing a solution form that satisfies the simply supported (SS-1) boundary conditions on two parallel edges of a rectangular laminate, and then the partial differential equations of equilibrium are reduced to ordinary differential equations in the coordinate parallel to the simply supported edges. The ordinary differential equations are then solved using the state-space approach.

Suppose that the edges $y = 0$ and $y = b$ are simply supported (SS-1), while the remaining edges $x = a/2$ and $x = -a/2$ have any combination of free, clamped, and simply supported boundary conditions (see Figure 7.4.1). We now proceed to describe the procedure for bending of cross-ply laminates. For additional details, the reader may consult the references at the end of the chapter.

The equations of equilibrium appropriate for the antisymmetric cross-ply laminated plates, according to the first-order shear deformation plate theory, can be expressed in matrix form as

$$[L]\{\Delta\} = \{F\} \quad (7.4.1)$$

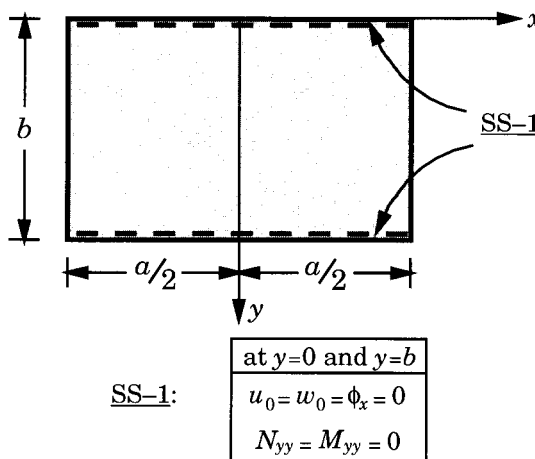


Figure 7.4.1: The coordinate system and boundary conditions used on the simply supported (SS-1) edges for the Lévy solutions of rectangular cross-ply laminates using the first-order shear deformation theory.

where $\{\Delta\}^T = \{u_0, v_0, w_0, \phi_x, \phi_y\}$, $\{F\}^T = \{0, 0, q, 0, 0\}$, and the coefficients $L_{ij} = L_{ji}$ are defined as

$$\begin{aligned} L_{11} &= A_{11}d_x^2 + A_{66}d_y^2, & L_{12} &= (A_{12} + A_{66})d_x d_y, & L_{13} &= 0 \\ L_{14} &= B_{11}d_x^2 + B_{66}d_y^2, & L_{15} &= (B_{12} + B_{66})d_x d_y, & L_{23} &= 0 \\ L_{22} &= A_{66}d_x^2 + A_{22}d_y^2, & L_{25} &= B_{22}d_y^2 + B_{66}d_x^2, & L_{24} &= L_{15} \\ L_{33} &= -KA_{55}d_x^2 - KA_{44}d_y^2, & L_{34} &= -KA_{55}d_x, & L_{35} &= -KA_{44}d_y \\ L_{44} &= -KA_{55} + D_{11}d_x^2 + D_{66}d_y^2, & L_{45} &= (D_{12} + D_{66})d_x d_y \\ L_{55} &= -KA_{44} + D_{22}d_y^2 + D_{66}d_x^2 \end{aligned} \quad (7.4.2)$$

and

$$d_x^i = \frac{\partial^i}{\partial x^i}, \quad d_y^i = \frac{\partial^i}{\partial y^i} \quad (7.4.3)$$

Note that the classical plate theory can be obtained as a special case of the first-order shear deformation theory by setting

$$\phi_x = -\frac{\partial w_0}{\partial x} \quad \text{and} \quad \phi_y = -\frac{\partial w_0}{\partial y} \quad (7.4.4)$$

7.4.2 The Lévy Type Solution

The Lévy method, in conjunction with the state-space concept, can be used to develop analytical solutions of Eq. (7.4.1) when the plate is simply supported on the edges $y = 0, b$ and the remaining edges $x = \pm a/2$ have any boundary conditions. The generalized displacements are expressed as products of undetermined functions and known trigonometric functions so as to satisfy the simply supported boundary conditions at $y = 0, b$ (see Figure 7.4.1):

$$u_0 = w_0 = \phi_x = N_{yy} = M_{yy} = 0 \quad (7.4.5)$$

The displacement field is represented as

$$\begin{Bmatrix} u_0(x, y) \\ v_0(x, y) \\ w_0(x, y) \\ \phi_x(x, y) \\ \phi_y(x, y) \end{Bmatrix} = \sum_{m=1}^{\infty} \begin{Bmatrix} U_m(x) \sin \beta y \\ V_m(x) \cos \beta y \\ W_m(x) \sin \beta y \\ X_m(x) \sin \beta y \\ Y_m(x) \cos \beta y \end{Bmatrix} \quad (7.4.6)$$

where $\beta = m\pi/b$. It can be easily verified that the boundary conditions (7.4.5) are satisfied by the displacement field in (7.4.6). The transverse load is also expanded as

$$q(x, y) = \sum_{m=1}^{\infty} Q_m \sin \frac{m\pi y}{b} \quad (7.4.7)$$

Substitution of the displacement field (7.4.6) into governing equations (7.4.1) results in five ordinary differential equations

$$\begin{aligned} U''_m &= C_1 U_m + C_2 V'_m + C_3 W'_m + C_4 X_m + C_5 Y'_m \\ V''_m &= C_6 U'_m + C_7 V_m + C_8 W_m + C_9 X'_m + C_{10} Y_m \\ W''_m &= C_{11} W_m + C_{12} X'_m + C_{13} Y_m - Q_m/e_{13} \\ X''_m &= C_{14} U_m + C_{15} V'_m + C_{16} W'_m + C_{17} X_m + C_{18} Y'_m \\ Y''_m &= C_{19} U'_m + C_{20} V_m + C_{21} W_m + C_{22} X'_m + C_{23} Y_m \end{aligned} \quad (7.4.8)$$

where the primes denote the derivative with respect to x . The coefficients in Eq. (7.4.8) are given by

$$\begin{aligned} C_1 &= (e_3 e_{21} - e_5 e_{19})/e_0, & C_2 &= (e_3 e_{18} - e_2 e_{19})/e_0 \\ C_3 &= e_3 e_{23}/e_0, & C_4 &= (e_3 e_{22} - e_6 e_{19})/e_0 \\ C_5 &= (e_3 e_{20} - e_4 e_{19})/e_0, & C_6 &= (e_8 e_{27} - e_{10} e_{25})/C_0 \\ C_7 &= (e_{11} e_{27} - e_{10} e_{28})/C_0, & C_8 &= -e_{10} e_{30}/C_0 \\ C_9 &= (e_9 e_{27} - e_{10} e_{26})/C_0, & C_{10} &= (e_{12} e_{27} - e_{10} e_{29})/C_0 \\ C_{11} &= -e_{15}/e_{13}, & C_{12} &= -e_{14}/e_{13} \\ C_{13} &= -e_{16}/e_{13}, & C_{14} &= (e_5 e_{17} - e_1 e_{21})/e_0 \\ C_{15} &= (e_2 e_{17} - e_1 e_{18})/e_0, & C_{16} &= -e_1 e_{23}/e_0 \\ C_{17} &= (e_6 e_{17} - e_1 e_{22})/e_0, & C_{18} &= (e_4 e_{17} - e_1 e_{20})/e_0 \\ C_{19} &= (e_7 e_{25} - e_8 e_{24})/C_0, & C_{20} &= (e_7 e_{28} - e_{11} e_{24})/C_0 \\ C_{21} &= e_7 e_{30}/C_0, & C_{22} &= (e_7 e_{26} - e_9 e_{24})/C_0 \\ C_{23} &= (e_7 e_{29} - e_{12} e_{24})/C_0 & & \\ e_0 &= e_1 e_{19} - e_3 e_{17}, & C_0 &= e_{10} e_{24} - e_7 e_{27} \end{aligned} \quad (7.4.9)$$

$$\begin{aligned} e_1 &= A_{11}, & e_2 &= -\beta(A_{12} + A_{66}), & e_3 &= B_{11} \\ e_4 &= -\beta(B_{12} + B_{66}), & e_5 &= -\beta^2 A_{66}, & e_6 &= -\beta^2 B_{66} \\ e_7 &= A_{66}, & e_8 &= -e_2, & e_9 &= -e_4 \\ e_{10} &= B_{66}, & e_{11} &= -\beta^2 A_{22}, & e_{12} &= -\beta^2 B_{22} \\ e_{13} &= K A_{55}, & e_{14} &= K A_{55}, & e_{15} &= -\beta^2 K A_{44} \\ e_{16} &= -\beta K A_{44}, & e_{17} &= e_3, & e_{18} &= e_4 \\ e_{19} &= D_{11}, & e_{20} &= -\beta(D_{12} + D_{66}), & e_{21} &= -\beta^2 B_{66} \\ e_{22} &= -\beta^2 D_{66} - K A_{55}, & e_{23} &= -e_{14}, & e_{24} &= e_{10} \\ e_{25} &= -e_4, & e_{26} &= -e_{20}, & e_{27} &= D_{66} \\ e_{28} &= -\beta^2 B_{22}, & e_{29} &= -\beta^2 D_{22} - K A_{44}, & e_{30} &= e_{16} \end{aligned} \quad (7.4.10)$$

In order to reduce the system of equations (7.4.8) to a system of first-order equations (i.e., use the state-space approach), the components of the state vector $\mathbf{Z}(x)$ are defined as

$$\begin{aligned} Z_1 &= U_m, & Z_2 &= U'_m, & Z_3 &= V_m, & Z_4 &= V'_m, & Z_5 &= W_m \\ Z_6 &= W'_m, & Z_7 &= X_m, & Z_8 &= X'_m, & Z_9 &= Y_m, & Z_{10} &= Y'_m \end{aligned} \quad (7.4.11)$$

Using the definitions (7.4.11), the systems of equations (7.4.8) may be converted to the form

$$\mathbf{Z}' = \mathbf{T}\mathbf{Z} + \mathbf{r} \quad (7.4.12)$$

where the matrix \mathbf{T} is the 10×10 matrix

$$[T] = \begin{bmatrix} 0 & 1 & 0 & 0 & 0 & 0 & 0 & 0 & 0 & 0 \\ C_1 & 0 & 0 & C_2 & 0 & C_3 & C_4 & 0 & 0 & C_5 \\ 0 & 0 & 0 & 1 & 0 & 0 & 0 & 0 & 0 & 0 \\ 0 & C_6 & C_7 & 0 & C_8 & 0 & 0 & C_9 & C_{10} & 0 \\ 0 & 0 & 0 & 0 & 0 & 1 & 0 & 0 & 0 & 0 \\ 0 & 0 & 0 & 0 & C_{11} & 0 & 0 & C_{12} & C_{13} & 0 \\ 0 & 0 & 0 & 0 & 0 & 0 & 0 & 1 & 0 & 0 \\ C_{14} & 0 & 0 & C_{15} & 0 & C_{16} & C_{17} & 0 & 0 & C_{18} \\ 0 & 0 & 0 & 0 & 0 & 0 & 0 & 0 & 0 & 1 \\ 0 & C_{19} & C_{20} & 0 & C_{21} & 0 & 0 & C_{22} & C_{23} & 0 \end{bmatrix} \quad (7.4.13a)$$

and the load vector \mathbf{r} is defined as

$$\{\mathbf{r}\} = \{0, 0, 0, 0, 0, -Q_m/e_{13}, 0, 0, 0, 0\}^T \quad (7.4.13b)$$

$$Q_m(x) = \frac{2}{b} \int_0^b q(x, y) \sin \frac{m\pi y}{b} dy \quad (7.4.13c)$$

The solution to Eq. (7.4.12) is

$$\mathbf{Z} = e^{Tx} \{ \mathbf{K} + \int_{-a/2}^x e^{-T\zeta} \mathbf{r} d\zeta \} \quad (7.4.14)$$

Here \mathbf{K} denotes constant column vector, which is to be determined from the boundary conditions on edges $x = \pm a/2$. The simply supported (S), clamped (C), and free (F) boundary conditions at the edges $x = \pm a/2$ are

$$\begin{aligned} S : v_0 &= w_0 = \phi_y = N_{xx} = M_{xx} = 0 \\ C : u_0 &= v_0 = w_0 = \phi_x = \phi_y = 0 \\ F : N_{xx} &= M_{xx} = Q_x = N_{xy} = M_{xy} = 0 \end{aligned} \quad (7.4.15)$$

Boundary conditions in (7.4.15) can be used in (7.4.12) to obtain ten equations for the ten constants K_i .

The same procedure can be used to study natural vibration and buckling under in-plane compressive forces. The procedure was discussed earlier for the eigenvalue problems in Chapter 6, and for additional information see [8,9,15–27].

7.4.3 Numerical Examples

Here we present numerical results for a number of example problems of bending, vibration, and buckling of rectangular, cross-ply laminated plates. For the purpose of comparison, the following two sets of lamina properties, typical graphite-epoxy material, are used:

$$\text{Material 1 : } E_1 = 25E_2, G_{12} = G_{13} = 0.5E_2, G_{23} = 0.2E_2, \nu_{12} = 0.25 \quad (7.4.16)$$

$$\text{Material 2 : } E_1 = 40E_2, G_{12} = G_{13} = 0.6E_2, G_{23} = 0.5E_2, \nu_{12} = 0.25 \quad (7.4.17)$$

The shear correction coefficient for the first-order theory is taken to be $K = 5/6$. The notation SC, for example, refers to the boundary conditions used on the edges $x = \pm a/2$, while the other two edges (i.e., $y = 0, b$) are simply supported.

Bending

The loading in all cases considered here is assumed to be sinusoidal

$$q(x, y) = q_0 \cos \frac{\pi x}{a} \sin \frac{\pi y}{b} \quad (7.4.18)$$

In the tables and figures, the results for deflections and stresses are presented using the following nondimensional form (see Khdeir and Reddy [23]):

$$\begin{aligned} \bar{w} &= w_0(0, b/2) \left(\frac{E_2 h^3}{b^4 q_0} \right) \times 10^2, \quad \bar{\sigma}_{xx} = -\sigma_{xx}(0, b/2, -h/2) \left(\frac{h^2}{b^2 q_0} \right) 10 \\ \bar{\sigma}_{yy} &= \sigma_{yy}(0, b/2, h/2) \left(\frac{h^2}{b^2 q_0} \right) 10, \quad \bar{\sigma}_{yz} = \sigma_{yz}(0, 0, 0) \left(\frac{h}{b q_0} \right) 10 \end{aligned} \quad (7.4.19)$$

where h is the total thickness of the laminate.

Figures 7.4.2 and 7.4.3 contain plots of deflections versus side-to-thickness ratio b/h of two-layer and ten-layer antisymmetric (0/90/ \dots)_{even} cross-ply laminates ($a = b/2$) with various boundary conditions (see Khdeir and Reddy [23]). The material properties used are those listed in Eq. (7.4.16) (i.e., material 1). The classical laminate theory always underpredicts deflections because the plate is modeled as infinitely stiff through the thickness. Figures 7.4.4 and 7.4.5 contain plots of \bar{w} vs. E_1/E_2 for the same load, $b/h = 10$, and $a = b/2$. As the degree of orthotropy increases, the difference between the deflections predicted by the classical and the first-order shear deformation theories increases, indicating that the shear deformation effect is more significant in anisotropic plates. Tables 7.4.1 through 7.4.4 contain numerical values of deflections and stresses in square plates obtained using the Lévy method.

Table 7.4.1: Nondimensionalized center deflection (\bar{w}) of antisymmetric cross-ply square plates with various boundary conditions (Material 1).

Layers	$\frac{b}{h}$	Theory	SS	SC	CC	FF	FS	FC
2	5	FSDT	1.758	1.477	1.257	2.777	2.335	1.897
	10	FSDT	1.237	0.883	0.656	2.028	1.687	1.223
		CLPT [†]	1.064	0.664	0.429	1.777	1.471	0.980
10	5	FSDT	1.137	1.045	0.945	1.663	1.460	1.258
	10	FSDT	0.615	0.480	0.385	0.915	0.800	0.612
		CLPT [†]	0.442	0.266	0.167	0.665	0.579	0.380

[†] Results are independent of b/h .

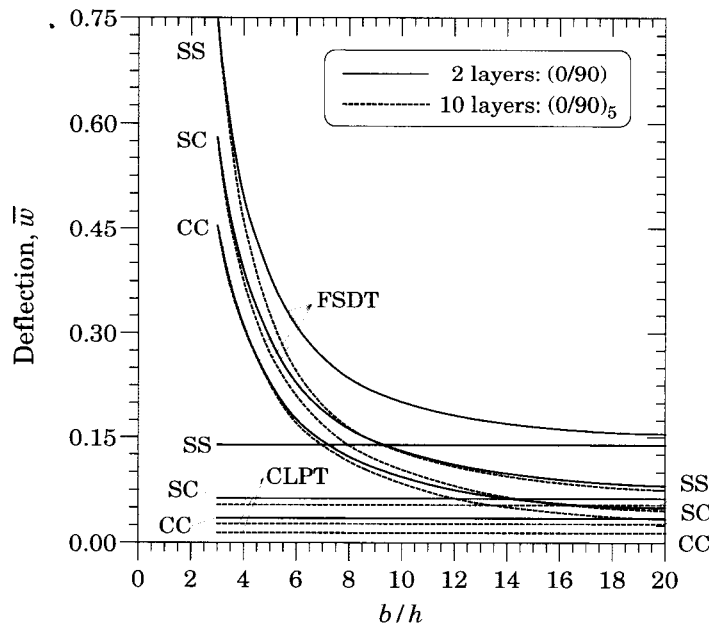


Figure 7.4.2: Nondimensionalized center transverse deflection (\bar{w}) versus side-to-thickness ratio (b/h) for antisymmetric cross-ply $(0/90)_n$ ($n = 1, 5$) laminates (Material 1, $b/a = 2$).

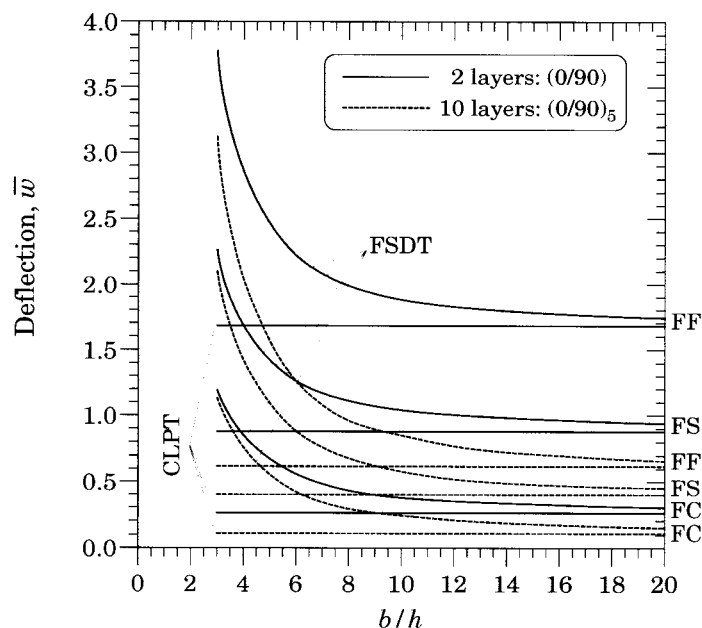


Figure 7.4.3: Nondimensionalized center transverse deflection (\bar{w}) versus side-to-thickness ratio (b/h) for antisymmetric cross-ply $(0/90)_n$ laminates (Material 1, $b/a = 2$).

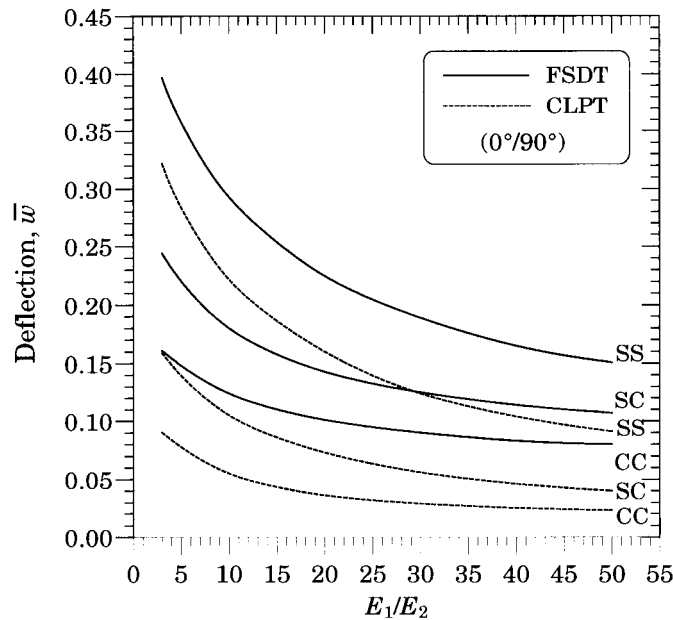


Figure 7.4.4: Nondimensionalized center transverse deflection (\bar{w}) versus modulus ratio (E_1/E_2) for antisymmetric cross-ply (0/90) laminates (Material 1, $b/h = 10$, $b/a = 2$).

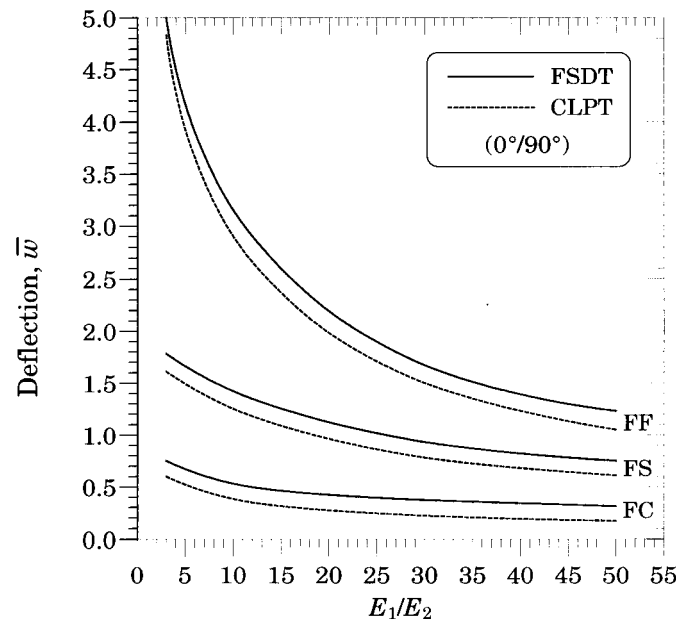


Figure 7.4.5: Nondimensionalized center transverse deflection (\bar{w}) versus modulus ratio (E_1/E_2) for antisymmetric cross-ply (0/90) laminates (Material 1, $b/h = 10$, $b/a = 2$).

Table 7.4.2: Nondimensionalized axial stress ($\bar{\sigma}_{xx}$) of antisymmetric cross-ply square plates with various boundary conditions (Material 1).

Layers	$\frac{b}{h}$	Theory	SS	SC	CC	FF	FS	FC
2	5	FSDT	7.157	5.338	3.911	2.469	4.430	2.434
	10	FSDT	7.157	5.494	4.450	2.442	4.435	2.790
		CLPT [†]	7.157	5.660	4.800	2.403	4.442	3.042
10	5	FSDT	5.009	3.707	2.275	1.712	2.957	1.343
	10	FSDT	5.009	3.642	2.692	1.723	2.968	1.594
		CLPT [†]	5.009	3.829	3.167	1.725	2.986	1.865

Table 7.4.3: Nondimensionalized shear stress ($\bar{\sigma}_{yz}$) of antisymmetric cross-ply square plates with various boundary conditions (Material 1).

Layers	b/h	SS	SC	CC	FF	FS	FC
2	5	2.729	2.297	1.958	3.901	3.390	2.748
	10	2.729	1.993	1.523	3.882	3.383	2.449
10	5	2.729	2.498	2.248	3.883	3.437	2.951
	10	2.729	2.126	1.708	3.853	3.421	2.605

Table 7.4.4: Nondimensionalized axial stress ($\bar{\sigma}_{yy}$) of antisymmetric cross-ply square plates with various boundary conditions (Material 1).

Layers	$\frac{b}{h}$	Theory	SS	SC	CC	FF	FS	FC
2	5	FSDT	7.157	6.034	5.153	11.907	9.848	8.047
	10	FSDT	7.157	5.109	3.799	11.884	9.847	7.150
		CLPT [†]	7.157	4.483	2.914	11.849	9.837	6.560
10	5	FSDT	5.009	4.628	4.212	7.583	6.590	5.706
	10	FSDT	5.009	3.904	3.135	7.533	6.566	5.029
		CLPT [†]	5.009	3.025	1.911	7.480	6.531	4.284

[†] Results are independent of b/h .

Vibration and Buckling

The effect of orthotropy and number of layers (i.e., bending-stretching coupling) on the fundamental frequencies of simply supported, cross-ply, square laminates can be seen from the results presented in Table 7.4.5 (see Reddy and Khdeir [8]). The fundamental frequencies increase with an increase in degree of orthotropy and number of layers (or decrease of coupling). Similar results for critical buckling loads under uniaxial compression are included in Table 7.4.6.

The effect of transverse shear deformation and boundary conditions on the fundamental frequencies of two-layer and ten-layer antisymmetric cross-ply laminates ($a/h = 10$) are examined in Table 7.4.7. The critical buckling loads for the same laminates under uniaxial compression are presented in Table 7.4.8. In all cases, the classical plate theory overpredicts frequencies and buckling loads.

Table 7.4.5: Effect of degree of orthotropy of the individual layers on the dimensionless fundamental frequency of simply supported antisymmetric cross-ply square laminates: $a/h = 5$, $\bar{\omega} = \omega\sqrt{\rho h^2/E_2}$ (Material 2).

Theory	Layers	$E_1/E_2 = 3$	10	20	30	40
FSDT	2	0.24834	0.27757	0.30824	0.33284	0.35333
CLPT		0.27082	0.30968	0.35422	0.39335	0.42884
FSDT	4	0.26017	0.32898	0.38754	0.42479	0.45083
CLPT		0.28676	0.38877	0.49907	0.58900	0.66690
FSDT	6	0.26228	0.33673	0.39771	0.43531	0.46105
CLPT		0.28966	0.40215	0.52234	0.61963	0.70359
FSDT	10	0.26335	0.34053	0.40255	0.44023	0.46577
CLPT		0.29115	0.40888	0.53397	0.63489	0.72184

Table 7.4.6: Effect of degree of orthotropy of the individual layers on the dimensionless critical buckling loads, $N = N_{cr}b^2/(E_2h^3)$, of simply supported (SS-1) antisymmetric cross-ply square laminates ($a/h = 10$) under uniaxial compression (Material 2).

Theory	Layers	$E_1/E_2 = 3$	10	20	30	40
FSDT	2	4.772	6.247	8.042	9.735	11.353
CLPT		5.034	6.703	8.816	10.891	12.957
FSDT	4	5.254	9.255	14.332	18.815	22.806
CLPT		5.574	10.295	16.988	23.675	30.359
FSDT	6	5.343	9.789	15.394	20.280	24.577
CLPT		5.674	10.960	18.502	26.042	33.582
FSDT	10	5.388	10.060	15.927	21.008	25.450
CLPT		5.725	11.300	19.277	27.254	35.232

Table 7.4.7: Effect of number of layers and transverse shear deformation on the dimensionless frequencies $\bar{\omega} = (\omega b^2/h)(\rho/E_2)^{1/2}$ of antisymmetric cross-ply square plates ($a/h = 10$) with various boundary conditions (Material 2).

Layers	Theory	FF	FS	FC	SS	SC	CC
2	FSDT	6.881	7.215	7.741	10.473	12.610	15.152
	CLPT	7.267	7.636	8.228	11.154	14.223	18.543
10	FSDT	10.900	11.079	11.862	15.779	18.044	20.471
	CLPT	12.680	12.906	13.779	18.492	23.971	31.709

Table 7.4.8: Effect of number of layers and transverse shear deformation on dimensionless critical buckling loads, $\bar{N} = N_{cr}b^2/E_2h^3$, of antisymmetric cross-ply square plates ($a/h = 10$) with various boundary conditions (Material 2).

Layers	Theory	FF	FS	FC	SS	SC	CC
2	FSDT	4.851	5.351	6.166	11.353	16.437	20.067
	CLPT	5.425	6.003	6.968	12.957	21.116	31.280
10	FSDT	12.092	12.524	14.358	25.450	32.614	34.837
	CLPT	16.426	17.023	19.389	35.232	59.288	89.770

7.5 Antisymmetric Angle-Ply Laminates with Two Opposite Edges Simply Supported

7.5.1 Introduction

As in the case of classical laminate theory, the Lévy-type solutions of the first-order theory can be developed for bending, buckling, and natural vibrations of antisymmetric angle-ply laminated rectangular plates with two opposite edges simply supported and the remaining ones subjected to a combination of clamped, simply supported, and free boundary conditions. In this section, we present the Lévy solution procedure for natural vibration and buckling analyses.

7.5.2 Governing Equations

Consider a rectangular laminated plate composed of an even number of identical layers having the principal material directions of orthotropy oriented at angles $+\theta$ and $-\theta$ with respect to the x -axis of the laminate (i.e., antisymmetric angle-ply laminates). The laminates exhibit twisting-extensional coupling, and the differential equations (7.1.1)–(7.1.5) associated with the first-order theory take the form

$$\begin{aligned} \frac{\partial}{\partial x} \left[A_{11} \frac{\partial u_0}{\partial x} + A_{12} \frac{\partial v_0}{\partial y} + B_{16} \left(\frac{\partial \phi_x}{\partial y} + \frac{\partial \phi_y}{\partial x} \right) \right] + \\ \frac{\partial}{\partial y} \left[A_{66} \left(\frac{\partial u_0}{\partial y} + \frac{\partial v_0}{\partial x} \right) + B_{16} \frac{\partial \phi_x}{\partial x} + B_{26} \frac{\partial \phi_y}{\partial y} \right] - \\ \left(\frac{\partial N_{xx}^T}{\partial x} + \frac{\partial N_{xy}^T}{\partial y} \right) = I_0 \frac{\partial^2 u_0}{\partial t^2} \end{aligned} \quad (7.5.1)$$

$$\begin{aligned} \frac{\partial}{\partial x} \left[A_{66} \left(\frac{\partial u_0}{\partial y} + \frac{\partial v_0}{\partial x} \right) + B_{16} \frac{\partial \phi_x}{\partial x} + B_{26} \frac{\partial \phi_y}{\partial y} \right] + \\ \frac{\partial}{\partial y} \left[A_{12} \frac{\partial u_0}{\partial x} + A_{22} \frac{\partial v_0}{\partial y} + B_{26} \left(\frac{\partial \phi_x}{\partial y} + \frac{\partial \phi_y}{\partial x} \right) \right] - \\ \left(\frac{\partial N_{xy}^T}{\partial x} + \frac{\partial N_{yy}^T}{\partial y} \right) = I_0 \frac{\partial^2 v_0}{\partial t^2} \end{aligned} \quad (7.5.2)$$

$$\begin{aligned} & \frac{\partial}{\partial x} \left[K A_{55} \left(\frac{\partial w_0}{\partial x} + \phi_x \right) \right] + \frac{\partial}{\partial y} \left[K A_{44} \left(\frac{\partial w_0}{\partial y} + \phi_y \right) \right] \\ & + \hat{N}_{xx} \frac{\partial^2 w_0}{\partial x^2} + 2 \hat{N}_{xy} \frac{\partial^2 w_0}{\partial x \partial y} + \hat{N}_{yy} \frac{\partial^2 w_0}{\partial y^2} + q = I_0 \frac{\partial^2 w_0}{\partial t^2} \end{aligned} \quad (7.5.3)$$

$$\begin{aligned} & \frac{\partial}{\partial x} \left[B_{16} \left(\frac{\partial u_0}{\partial y} + \frac{\partial v_0}{\partial x} \right) + D_{11} \frac{\partial \phi_x}{\partial x} + D_{12} \frac{\partial \phi_y}{\partial y} \right] + \\ & \frac{\partial}{\partial y} \left[B_{16} \frac{\partial u_0}{\partial x} + B_{26} \frac{\partial v_0}{\partial y} + D_{66} \left(\frac{\partial \phi_x}{\partial y} + \frac{\partial \phi_y}{\partial x} \right) \right] - \\ & K A_{55} \left(\frac{\partial w_0}{\partial x} + \phi_x \right) - \left(\frac{\partial M_{xx}^T}{\partial x} + \frac{\partial M_{xy}^T}{\partial y} \right) = I_2 \frac{\partial^2 \phi_x}{\partial t^2} \end{aligned} \quad (7.5.4)$$

$$\begin{aligned} & \frac{\partial}{\partial x} \left[B_{16} \frac{\partial u_0}{\partial x} + B_{26} \frac{\partial v_0}{\partial y} + D_{66} \left(\frac{\partial \phi_x}{\partial y} + \frac{\partial \phi_y}{\partial x} \right) \right] + \\ & \frac{\partial}{\partial y} \left[B_{26} \left(\frac{\partial u_0}{\partial y} + \frac{\partial v_0}{\partial x} \right) + D_{12} \frac{\partial \phi_x}{\partial x} + D_{22} \frac{\partial \phi_y}{\partial y} \right] - \\ & K A_{44} \left(\frac{\partial w_0}{\partial y} + \phi_y \right) - \left(\frac{\partial M_{xy}^T}{\partial x} + \frac{\partial M_{yy}^T}{\partial y} \right) = I_2 \frac{\partial^2 \phi_y}{\partial t^2} \end{aligned} \quad (7.5.5)$$

The following boundary conditions are considered (see Figure 7.5.1):

Simply supported (SS-1) at edges $x = 0, a$:

$$u_0 = w_0 = \phi_y = M_{xx} = N_{xy} = 0 \quad (7.5.6)$$

Simply supported (SS-1) at edges $y = \pm b/2$:

$$v_0 = w_0 = \phi_x = M_{yy} = N_{xy} = 0 \quad (7.5.7)$$

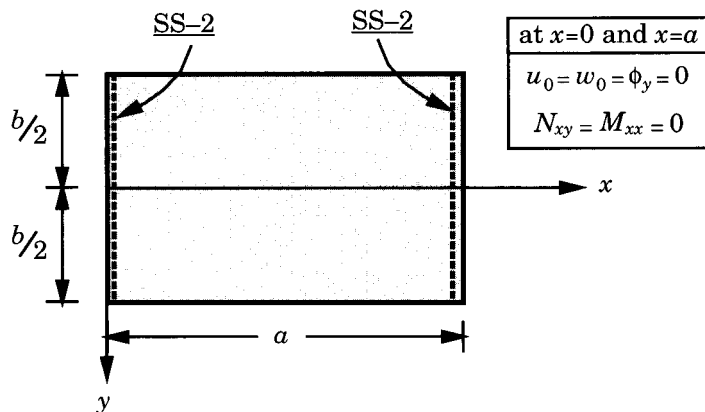


Figure 7.5.1: Boundary conditions used on simply supported edges for the Lévy solutions of rectangular angle-ply laminates (FSDT).

Clamped (C) at edges $y = \pm b/2$:

$$u_0 = v_0 = w_0 = \phi_x = \phi_y = 0 \quad (7.5.8)$$

Free (F) at edges $y = \pm b/2$:

$$M_{yy} = M_{xy} = N_{yy} = N_{xy} = Q_y = 0 \quad (7.5.9)$$

where the stress resultants can be expressed in terms of the generalized displacements are

$$\begin{aligned} N_{xx} &= A_{11} \frac{\partial u_0}{\partial x} + A_{12} \frac{\partial v_0}{\partial y} + B_{16} \left(\frac{\partial \phi_x}{\partial y} + \frac{\partial \phi_y}{\partial x} \right) \\ N_{yy} &= A_{12} \frac{\partial u_0}{\partial x} + A_{22} \frac{\partial v_0}{\partial y} + B_{26} \left(\frac{\partial \phi_x}{\partial y} + \frac{\partial \phi_y}{\partial x} \right) \\ N_{xy} &= A_{66} \left(\frac{\partial u_0}{\partial y} + \frac{\partial v_0}{\partial x} \right) + B_{16} \frac{\partial \phi_x}{\partial x} + B_{26} \frac{\partial \phi_y}{\partial y} \\ M_{xx} &= B_{16} \left(\frac{\partial u_0}{\partial y} + \frac{\partial v_0}{\partial x} \right) + D_{11} \frac{\partial \phi_x}{\partial x} + D_{12} \frac{\partial \phi_y}{\partial y} \\ M_{yy} &= B_{26} \left(\frac{\partial u_0}{\partial y} + \frac{\partial v_0}{\partial x} \right) + D_{12} \frac{\partial \phi_x}{\partial x} + D_{22} \frac{\partial \phi_y}{\partial y} \\ M_{xy} &= B_{16} \frac{\partial u_0}{\partial x} + B_{26} \frac{\partial v_0}{\partial y} + D_{66} \left(\frac{\partial \phi_x}{\partial y} + \frac{\partial \phi_y}{\partial x} \right) \\ Q_x &= K A_{55} \left(\frac{\partial w_0}{\partial x} + \phi_x \right) \\ Q_y &= K A_{44} \left(\frac{\partial w_0}{\partial y} + \phi_y \right) \end{aligned} \quad (7.5.10)$$

7.5.3 The Lévy Solution

Here we present the Lévy type solution procedure in conjunction with the state-space concept to determine the compressive buckling loads of rectangular plates ($a \times b$). The edges $x = 0, a$ are assumed to be simply supported while the remaining edges, $y = \pm b/2$, having an arbitrary set of boundary conditions. The following representation of the displacement field is used:

$$\begin{aligned} u_0(x, y) &= \sum_{m=1}^{\infty} U_m(y) \sin \alpha x \\ v_0(x, y) &= \sum_{m=1}^{\infty} V_m(y) \cos \alpha x \\ w_0(x, y) &= \sum_{m=1}^{\infty} W_m(y) \sin \alpha x \\ \phi_x(x, y) &= \sum_{m=1}^{\infty} X_m(y) \cos \alpha x \\ \phi_y(x, y) &= \sum_{m=1}^{\infty} Y_m(y) \sin \alpha x \end{aligned} \quad (7.5.11)$$

where $\alpha = m\pi/a$. Substitution of Eq. (7.5.11) into Eqs. (7.5.1)–(7.5.5), after setting the inertia terms, q , and \hat{N}_{xy} to zero, yields a system of ordinary differential equations in the y -coordinate. These equations, after some elementary algebraic manipulations, can be expressed as

$$\begin{aligned} U_m'' &= C_1 U_m + C_2 V_m' + C_3 W_m' + C_4 X_m' + C_5 Y_m \\ V_m'' &= C_6 U_m' + C_7 V_m + C_8 W_m + C_9 X_m + C_{10} Y_m' \\ W_m'' &= C_{11} W_m + C_{12} X_m + C_{13} Y_m' \\ X_m'' &= C_{14} U_m' + C_{15} V_m + C_{16} W_m + C_{17} X_m + C_{18} Y_m' \\ Y_m'' &= C_{19} U_m + C_{20} V_m' + C_{21} W_m' + C_{22} X_m' + C_{23} Y_m \end{aligned} \quad (7.5.12a)$$

where the primes indicate differentiation with respect to y , and the constants C_i are defined as

$$\begin{aligned} C_1 &= \alpha^2 \frac{A_{11}D_{22} - B_{16}B_{26}}{A_{66}D_{22} - B_{26}^2}, & C_2 &= \alpha \frac{A_{12}D_{22} + A_{66}D_{22} - 2B_{26}^2}{A_{66}D_{22} - B_{26}^2} \\ C_3 &= -\frac{KA_{44}B_{26}}{A_{66}D_{22} - B_{26}^2}, & C_4 &= \alpha \frac{2B_{16}D_{22} - B_{26}D_{12} - B_{26}D_{66}}{A_{66}D_{22} - B_{26}^2} \\ C_5 &= \frac{\alpha^2 B_{16}D_{22} - \alpha^2 B_{26}D_{66} - B_{26}KA_{44}}{A_{66}D_{22} - B_{26}^2}, & C_6 &= \alpha \frac{2B_{16}B_{26} - A_{12}D_{66} - A_{66}D_{66}}{A_{22}D_{66} - B_{26}^2} \\ C_7 &= \alpha^2 \frac{A_{66}D_{66} - B_{16}B_{26}}{A_{22}D_{66} - B_{26}^2}, & C_8 &= -\frac{\alpha K A_{55}B_{26}}{A_{22}D_{66} - B_{26}^2} \\ C_9 &= \frac{\alpha^2 B_{16}D_{66} - \alpha^2 B_{26}D_{11} - B_{26}KA_{55}}{A_{22}D_{66} - B_{26}^2}, & C_{10} &= \alpha B_{26} \frac{D_{12} - D_{66}}{A_{22}D_{66} - B_{26}^2} \\ C_{11} &= \alpha^2 \frac{KA_{55} + N_{xx}^0}{KA_{44} + N_{yy}^0}, & C_{12} &= \frac{\alpha K A_{55}}{KA_{44} + N_{yy}^0} \\ C_{13} &= -\frac{KA_{44}}{KA_{44} + N_{yy}^0}, & C_{14} &= \alpha \frac{A_{12}B_{26} + A_{66}B_{26} - 2A_{22}B_{16}}{A_{22}D_{66} - B_{26}^2} \\ C_{15} &= \alpha^2 \frac{A_{22}B_{16} - A_{66}B_{26}}{A_{22}D_{66} - B_{26}^2}, & C_{16} &= \frac{\alpha A_{22}KA_{55}}{A_{22}D_{66} - B_{26}^2} \\ C_{17} &= \frac{A_{22}KA_{55} + \alpha^2 A_{22}D_{11} - \alpha^2 B_{16}B_{26}}{A_{22}D_{66} - B_{26}^2}, & C_{18} &= \alpha \frac{2B_{26}^2 - A_{22}D_{12} - A_{22}D_{66}}{A_{22}D_{66} - B_{26}^2} \\ C_{19} &= \alpha^2 \frac{A_{66}B_{16} - A_{11}B_{26}}{A_{66}D_{22} - B_{26}^2}, & C_{20} &= \alpha B_{26} \frac{A_{66} - A_{12}}{A_{66}D_{22} - B_{26}^2} \\ C_{21} &= \frac{KA_{44}A_{66}}{A_{66}D_{22} - B_{26}^2}, & C_{22} &= \alpha \frac{A_{66}D_{12} + A_{66}D_{66} - 2B_{16}B_{26}}{A_{66}D_{22} - B_{26}^2} \\ C_{23} &= \frac{KA_{44}A_{66} + \alpha^2 A_{66}D_{66} - \alpha^2 B_{16}B_{26}}{A_{66}D_{22} - B_{26}^2} \end{aligned} \quad (7.5.12b)$$

Introducing the components of the state vector $\mathbf{Z} = \mathbf{Z}(y)$ as

$$\begin{aligned} Z_1 &= U_m, & Z_2 &= U_m', & Z_3 &= V_m, & Z_4 &= V_m', & Z_5 &= W_m \\ Z_6 &= W_m', & Z_7 &= X_m, & Z_8 &= X_m', & Z_9 &= Y_m, & Z_{10} &= Y_m' \end{aligned} \quad (7.5.13)$$

Eq. (7.5.12a) may be reduced to the matrix form ($\mathbf{Z}' = \mathbf{T}\mathbf{Z}$)

$$\left\{ \frac{d\mathbf{Z}}{dy} \right\} = [\mathbf{T}]\{\mathbf{Z}\} \quad (7.5.14a)$$

$$[\mathbf{T}] = \begin{bmatrix} 0 & 1 & 0 & 0 & 0 & 0 & 0 & 0 & 0 & 0 \\ C_1 & 0 & 0 & C_2 & 0 & C_3 & 0 & C_4 & C_5 & 0 \\ 0 & 0 & 0 & 1 & 0 & 0 & 0 & 0 & 0 & 0 \\ 0 & C_6 & C_7 & 0 & C_8 & 0 & C_9 & 0 & 0 & C_{10} \\ 0 & 0 & 0 & 0 & 0 & 1 & 0 & 0 & 0 & 0 \\ 0 & 0 & 0 & 0 & C_{11} & 0 & C_{12} & 0 & 0 & C_{13} \\ 0 & 0 & 0 & 0 & 0 & 0 & 0 & 1 & 0 & 0 \\ 0 & C_{14} & C_{15} & 0 & C_{16} & 0 & C_{17} & 0 & 0 & C_{18} \\ 0 & 0 & 0 & 0 & 0 & 0 & 0 & 0 & 0 & 1 \\ C_{19} & 0 & 0 & C_{20} & 0 & C_{21} & 0 & C_{22} & C_{23} & 0 \end{bmatrix} \quad (7.5.14b)$$

A formal solution to Eq. (7.5.14a) is given by

$$\mathbf{Z}(y) = e^{\mathbf{T}y} \mathbf{K} \quad (7.5.15)$$

where \mathbf{K} is a constant column vector to be determined using the boundary conditions. In the present case all eigenvalues of matrix $[\mathbf{T}]$ are distinct. In the case of repeated eigenvalues, the Jordan canonical form must be used. Equation (7.5.15) in conjunction with the boundary conditions yields a homogeneous system of equations for the buckling problem

$$\sum_{j=1}^{10} M_{ij} K_j = 0, \quad (i = 1, 2, \dots, 10) \quad (7.5.16)$$

and setting the determinant of $[M]$ to zero

$$|M| = 0 \quad (7.5.17)$$

allows determination of the buckling loads associated with the m th mode for the boundary conditions at $y = \pm b/2$.

The above solution procedure is also valid for the free vibration case, except that the elements of the operator $[\mathbf{T}]$ should be modified to account for the inertia terms. In the case of static analysis, the elements of $[\mathbf{T}]$ are modified by setting the in-plane force terms to zero, and Eq. (7.5.14a) and equations for the determination of the constant vector \mathbf{K} will be modified accordingly, as discussed in Chapter 6.

7.5.4 Numerical Examples

In the examples presented here the two sets of lamina properties given in Eqs. (7.4.16) and (7.4.17) are used. The shear correction coefficient for the first-order theory is taken to be $K = 5/6$. The loading in the case of bending is assumed to be sinusoidal. The deflections and stresses are nondimensionalized as given in Eqs. (7.4.19).

Bending

Table 7.5.1 contains maximum nondimensionalized deflections $\bar{w} \equiv w_0(a/2, 0)E_2h^3 \times 10^2/(a^4q_0)$ of simply supported, two- and sixteen-layer angle-ply ($\theta/-\theta/\theta/-\theta/\dots$) square plates under sinusoidal loading (see Reddy and Chao [10]). The material properties used are those of Material 2 listed in Eq. (7.4.17).

Table 7.5.1: Nondimensionalized deflection \bar{w} as a function of number of layers, angle, and side-to-thickness ratio for simply supported (SS-2) angle-ply square plates under sinusoidally distributed transverse load.

a/h	$\theta = 5^\circ$		$\theta = 30^\circ$		$\theta = 45^\circ$	
	$n = 2$	$n = 16$	$n = 2$	$n = 16$	$n = 2$	$n = 16$
5	9.760	9.256	9.568	6.316	9.088	5.938
	4.883	4.454	6.099	2.872	5.773	2.621
20	3.585	3.172	5.224	2.005	4.944	1.793
25	3.427	3.105	5.119	1.900	4.844	1.693
50	3.215	2.806	4.979	1.761	4.711	1.560
100	3.162	2.754	4.944	1.726	4.678	1.527

Table 7.5.2 contains nondimensionalized deflections \bar{w} of angle-ply laminates subjected to uniformly distributed transverse load, under various boundary conditions (see Khdeir [21]), and with different values of E_1/E_2 (Material 2). Figure 7.5.2 shows the effect of side-to-thickness ratio (a/h) on the nondimensionalized center deflection of a square antisymmetric angle-ply laminate (45/-45/45/-45) under uniformly distributed transverse loading and for various boundary conditions. The material properties used are $E_1 = 19.2 \times 10^6$ psi (132.38 GPa), $E_2 = 1.56 \times 10^6$ psi (10.76 GPa), $G_{12} = G_{13} = 0.82 \times 10^6$ psi (5.65 GPa), $G_{23} = 0.523 \times 10^6$ psi (3.61 GPa), and $\nu_{12} = 0.25$. The effect of the ratio of principal moduli (Material 2) on the nondimensionalized center deflection is shown in Figure 7.5.3 for the same laminate.

Table 7.5.2: Nondimensionalized deflections of simply supported (SS-2), four-layer antisymmetric angle-ply square plates (45/-45/45/-45) under uniformly distributed transverse load (Material 2, $a/h = 10$).

Theory	$\frac{E_1}{E_2}$	SS	SC	CC	FF	FS	FC
FSDT	2	3.375	2.423	1.753	10.735	6.447	4.743
CLPT		3.214	2.214	1.531	10.470	6.234	4.446
FSDT	10	1.160	0.944	0.771	6.049	2.611	2.109
CLPT		1.000	0.747	0.558	5.571	2.345	1.747
FSDT	20	0.701	0.602	0.518	4.284	1.623	1.379
CLPT		0.542	0.412	0.313	3.657	1.343	1.010
FSDT	30	0.531	0.471	0.417	3.422	1.225	1.075
CLPT		0.372	0.285	0.218	2.737	0.943	0.712

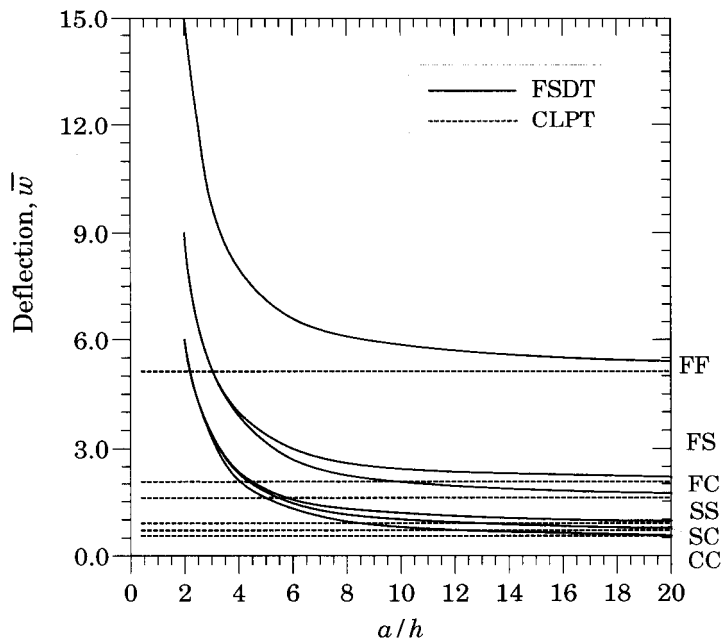


Figure 7.5.2: Nondimensionalized center transverse deflection (\bar{w}) versus side-to-thickness ratio (a/h) for square, antisymmetric angle-ply (45/-45/45/-45) laminates.

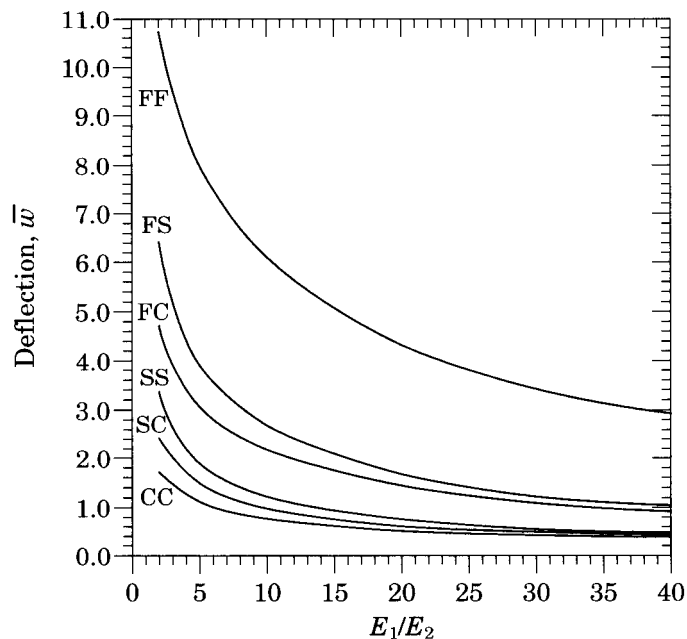


Figure 7.5.3: Nondimensionalized center transverse deflection (\bar{w}) versus modulus ratio (E_1/E_2) for square, antisymmetric angle-ply (45/-45/45/-45) laminates (Material 2, $a/h = 10$).

Vibration and Buckling

The dimensionless frequencies, $\bar{\omega} \equiv \omega(a^2/h)\sqrt{(\rho/E_2)}$, of antisymmetric angle-ply laminates ($\theta/ -\theta/\theta/\dots$), under various boundary conditions and with different values of θ are presented in Table 7.5.3. Figure 7.5.4 shows the effect of side-to-thickness ratio (a/h) and Figure 7.5.5 shows the effect of the ratio of principal moduli on the nondimensionalized fundamental frequencies of a square antisymmetric angle-ply laminate (45/-45/45/-45) for various boundary conditions (see Khdeir [17, 21]). The material properties listed in Eq. (7.4.17) were used. The critical buckling loads, $\bar{N} = N_{cr}a^2/E_2h^3$, for the same laminates under uniaxial compressive load are included in Table 7.5.4.

Table 7.5.3: Effect of ply angle (θ) and number of layers (n) on dimensionless fundamental frequency, $\bar{\omega}$, of antisymmetric angle-ply ($\theta/-\theta/\theta/\dots/-\theta$) square plates (Material 2, $a/h = 10$).

θ°	n	Theory	SS	SC	CC	FF	FS	FC
30	2	FSDT	12.68	13.46	14.41	6.95	8.45	8.65
		CLPT	14.24	15.44	17.00	7.58	9.35	9.69
	10	FSDT	18.51	19.11	19.81	10.11	12.33	12.48
		CLPT	23.95	25.59	27.58	12.37	15.38	15.84
45	2	FSDT	13.04	14.23	15.63	4.76	7.13	7.52
		CLPT	14.64	16.75	19.48	5.12	7.79	8.48
	10	FSDT	19.38	20.27	21.25	6.57	10.60	10.88
		CLPT	25.47	28.91	33.32	7.89	13.03	14.17
60	2	FSDT	12.68	14.52	16.57	3.33	5.87	6.70
		CLPT	14.24	17.74	22.31	3.47	6.26	7.54
	10	FSDT	18.51	19.82	21.21	3.82	8.53	9.22
		CLPT	23.95	29.86	37.62	4.32	9.92	11.96

Table 7.5.4: Effect of ply angle (θ) and number of layers (n) on dimensionless critical buckling load, \bar{N} , of antisymmetric angle-ply ($\theta/-\theta/\theta/\dots/-\theta$) square plates (Material 2, $a/h = 10$).

θ°	n	Theory	SS	SC	CC	FF	FS	FC
30	2	FSDT	16.613	18.718	21.447	4.991	7.372	7.739
		CLPT	20.543	24.158	29.269	5.822	8.857	9.520
	10	FSDT	34.931	37.242	38.920	10.423	15.520	15.899
		CLPT	58.135	66.322	77.065	15.499	23.972	25.412
45	2	FSDT	17.552	19.443	19.957	2.327	5.220	5.824
		CLPT	21.709	28.423	34.963	2.654	6.150	7.283
	10	FSDT	33.173	33.263	33.356	4.401	11.484	12.092
		CLPT	65.714	84.707	102.59	6.300	17.189	20.332
60	2	FSDT	13.863	14.722	15.598	1.136	3.543	4.605
		CLPT	19.564	23.834	29.547	1.221	3.975	5.756
	10	FSDT	23.710	23.759	23.808	1.492	7.432	8.682
		CLPT	52.945	64.103	79.619	1.889	9.977	14.501

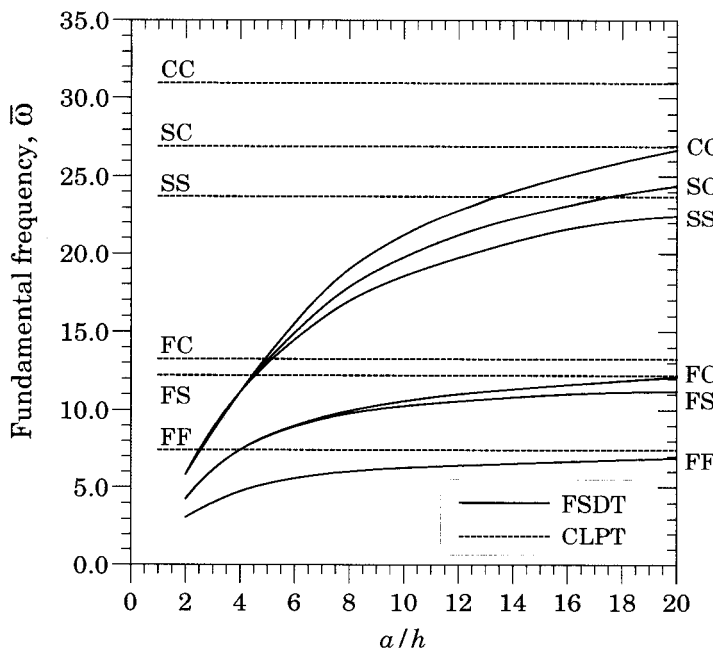


Figure 7.5.4: Nondimensionalized fundamental frequency ($\bar{\omega}$) versus side-to-thickness ratio (a/h) for square, antisymmetric angle-ply (45/-45/45/-45) laminates (Material 2).

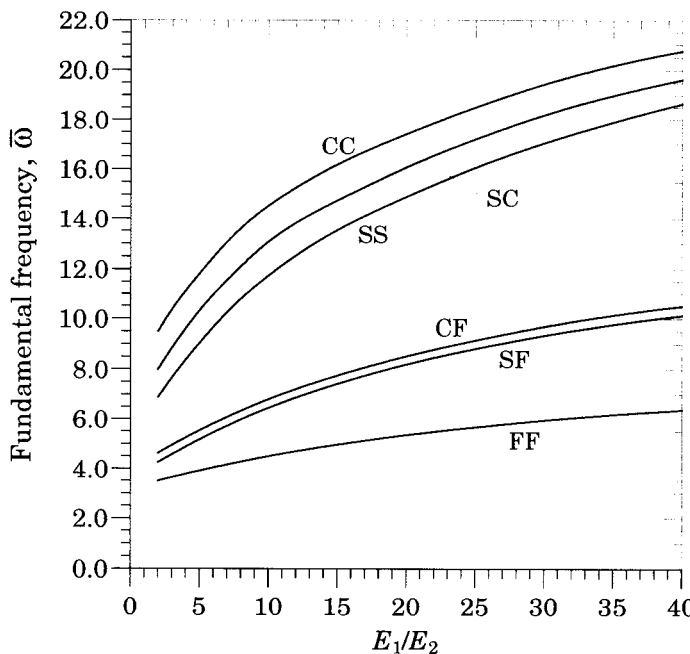


Figure 7.5.5: Nondimensionalized fundamental frequency ($\bar{\omega}$) versus modulus ratio (E_1/E_2) for square, antisymmetric angle-ply (45/-45/45/-45) laminates ($a/h = 10$).

7.6 Transient Solutions

Transient solutions of antisymmetric cross-ply and angle-ply laminates using the first order theory can be developed either by the state-space approach or the combination of the Navier solution procedure and the Newmark time integration scheme as discussed in Section 6.7. The application of the state-space approach to the transient analysis of shear deformable theories can be found in the papers of Khdeir and Reddy [25–27].

The procedure of Section 6.7 is valid here when the coefficient matrices $[M]$ and $[K]$ in Eq. (6.7.2) are replaced with those in Eq. (7.2.7a) for cross-ply laminates and in Eq. (7.3.5) for angle-ply laminates. The solution vector $\{\Delta\}$ consists of the amplitudes of the five generalized displacements, $(u_0, v_0, w_0, \phi_x, \phi_y)$. Here we present numerical results based on this procedure.

Figure 7.6.1 shows plots of nondimensionalized center deflection, $\bar{w} = w_0[E_2 h^3/(q_0 a^4)]^{1/2}$, versus time for antisymmetric cross-ply laminates (0/90) under sinusoidally distributed step loading (see Figure 7.3.1 for the coordinate system used here). The material properties used are

$$\begin{aligned} E_1 &= 25E_2, \quad E_2 = 2.1 \times 10^6 \text{ N/cm}^2, \quad G_{12} = G_{13} = 0.5E_2, \quad G_{23} = 0.2E_2, \quad \nu_{12} = 0.25 \\ \rho &= 8 \times 10^{-6} \text{ N-s}^2/\text{cm}^4, \quad a/b = 1, \quad b = 25 \text{ cm} \end{aligned} \quad (7.6.1)$$

Results obtained with CLPT and FSDT are presented for two values of side-to-thickness ratios, $a/h = 10$ and 25 . The plots in dashed lines correspond to CLPT. The effect of shear deformation is to increase the amplitude and period of the waves. Similar results are presented in Figure 7.6.2 for uniformly distributed step loading. A plot of the deflection under sinusoidal load (obtained with FSDT) is also included for comparison. Figures 7.6.3 and 7.6.4 contain the nondimensionalized center normal stress $\bar{\sigma}_{xx}(a/2, b/2, h/2)$ and shear stress $\bar{\sigma}_{xy}(a, b, -h/2)$ for the uniformly distributed load case ($a/h = 10$). Note that the effect of shear deformation on the amplitude of stresses is negligible; however, it still increases the period. Figures 7.6.5 and 7.6.6 contain plots of nondimensionalized center deflection for two-layer angle-ply (-45/45) laminates under sinusoidally and uniformly distributed step loadings, respectively, for $a/h = 10$. The same material properties as in Eq. (7.6.1) are used. Angle-ply laminates show larger increase in the period due to shear deformation. Figure 7.6.7 show a plot of the maximum in-plane displacement (u_0 or v_0) versus time, while Figures 7.6.8 through 7.6.10 show plots of normal stress at top and bottom of the laminate and shear stress at the bottom of the laminate for the uniform load case. Lastly, Figures 7.6.11 and 7.6.12 show plots of nondimensionalized transverse shear stress $\bar{\sigma}_{xz}$ in two-layer plates (0/90) and (-45/45) under uniformly and sinusoidally distributed transverse loads ($a/h = 10$).

For cross-ply laminates under uniformly distributed load, the ratio of maximum transient deflection to static deflection is found to be $\bar{w}_d/\bar{w}_s = 2.049$ for FSDT, whereas it is 2.017 for CLPT. From this, one may conclude that the effect of transverse shear is greater on dynamic response than static response in the two-layer cross-ply plates. For angle-ply laminates under uniformly distributed load, the ratio of maximum transient deflection to static deflection is found to be 2.041 for FSDT, whereas it is 2.062 for CLPT. This indicates that the effect of transverse shear is less on dynamic response than on static response in the two-layer angle-ply plates. Table 7.6.1 contains the results of transient and static analysis.

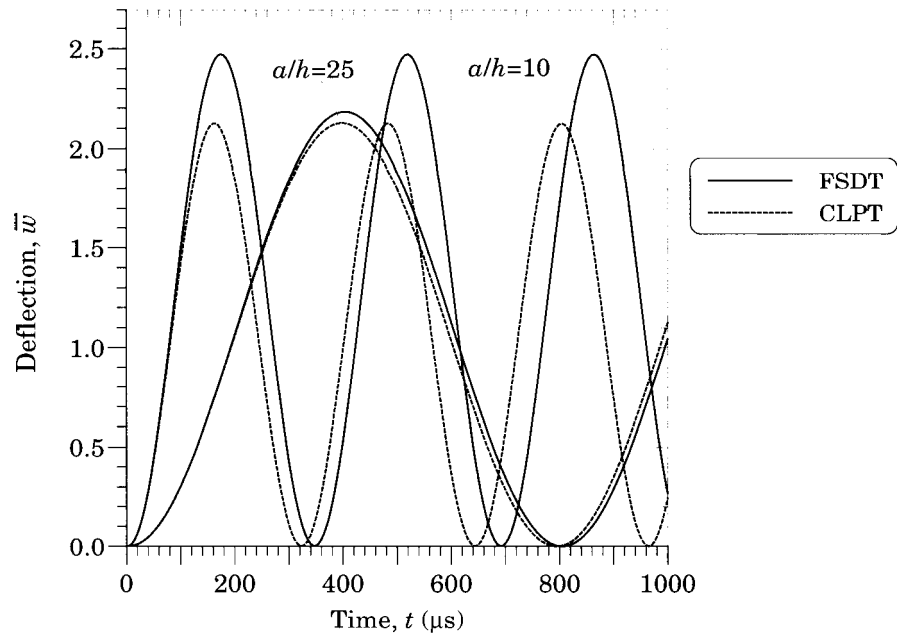


Figure 7.6.1: Nondimensionalized center transverse deflection (\bar{w}) versus time (t) for simply supported (SS-1) antisymmetric cross-ply (0/90) laminates.

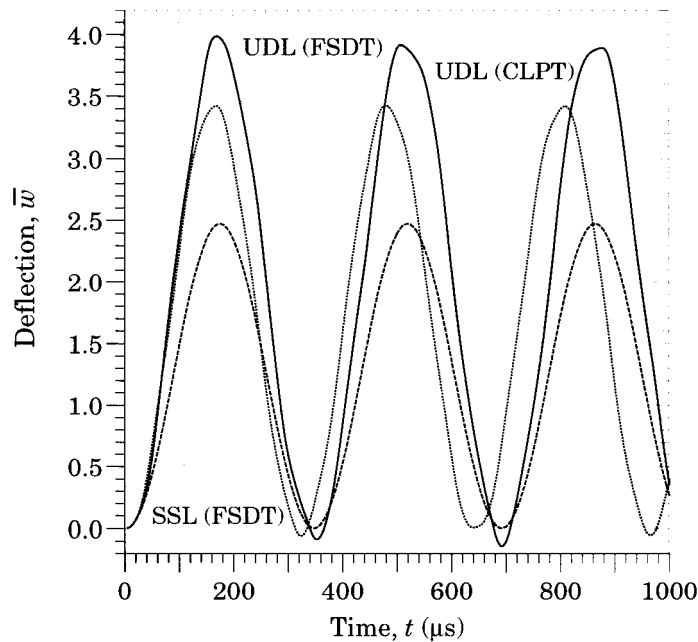


Figure 7.6.2: Nondimensionalized center transverse deflection (\bar{w}) versus time (t) for simply supported (SS-1) antisymmetric cross-ply (0/90) laminates.

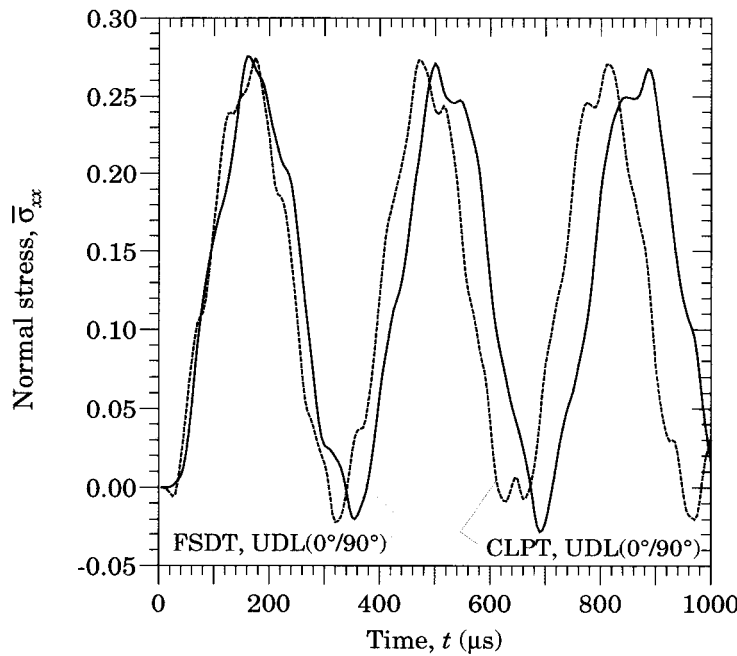


Figure 7.6.3: Nondimensionalized normal stress ($\bar{\sigma}_{xx}$) versus time (t) for simply supported (SS-1) antisymmetric cross-ply ($0/90$) laminates.

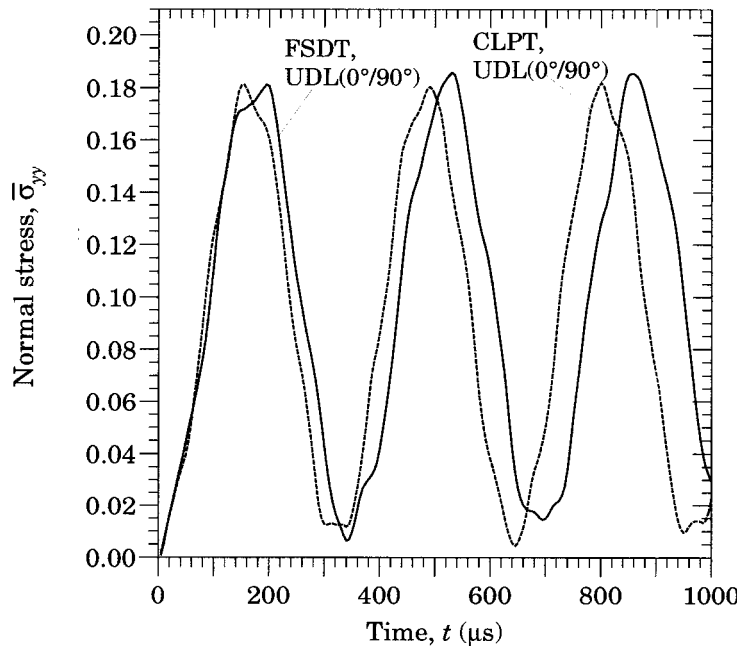


Figure 7.6.4: Nondimensionalized normal stress ($\bar{\sigma}_{yy}$) versus time (t) for simply supported (SS-1) antisymmetric cross-ply ($0/90$) laminates.

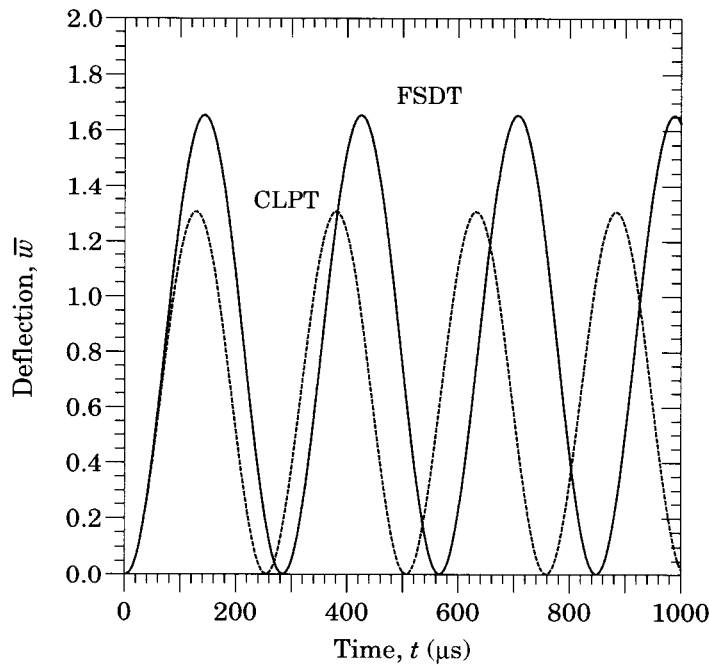


Figure 7.6.5: Nondimensionalized center transverse deflection (\bar{w}) versus time (t) for simply supported (SS-2) antisymmetric angle-ply (-45/45) laminates.

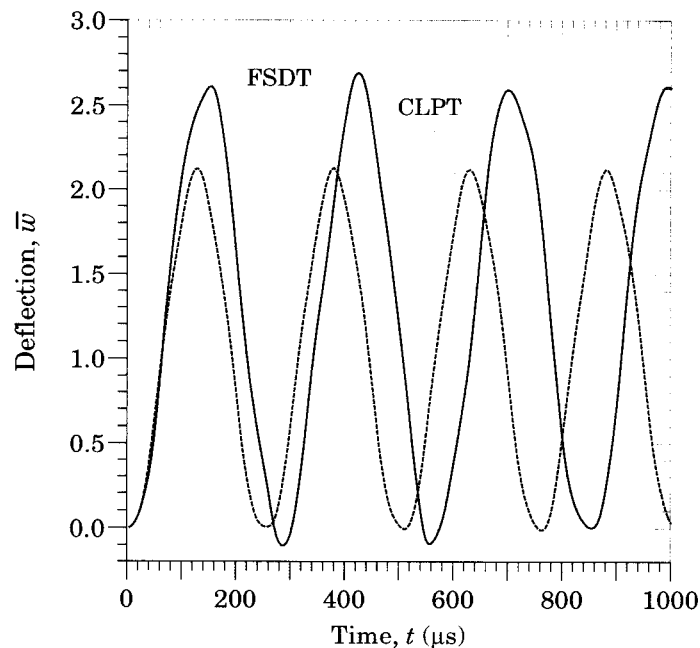


Figure 7.6.6: Nondimensionalized center transverse deflection (\bar{w}) versus time (t) for simply supported (SS-2) antisymmetric angle-ply (-45/45) laminates.

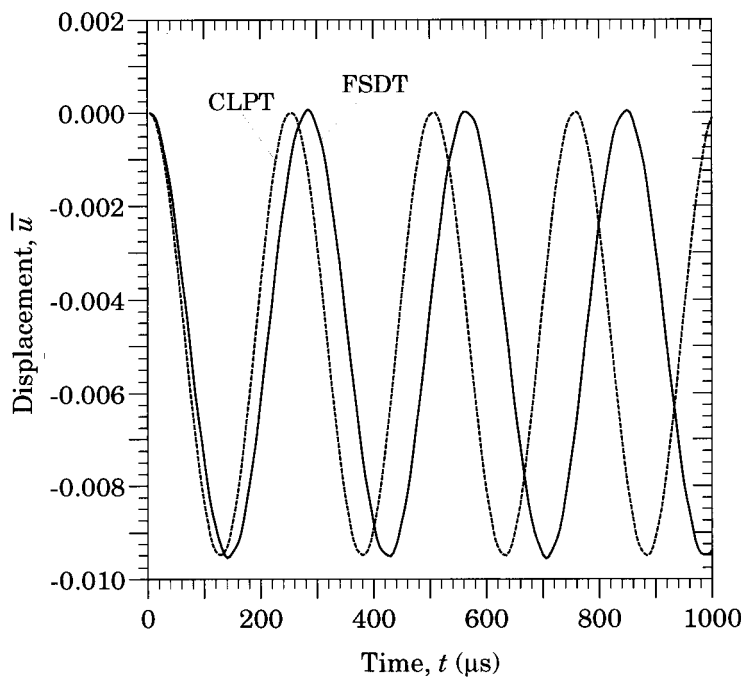


Figure 7.6.7: Nondimensionalized in-plane displacement (\bar{u}) versus time (t) for simply supported (SS-2) antisymmetric angle-ply ($-45/45$) laminates.

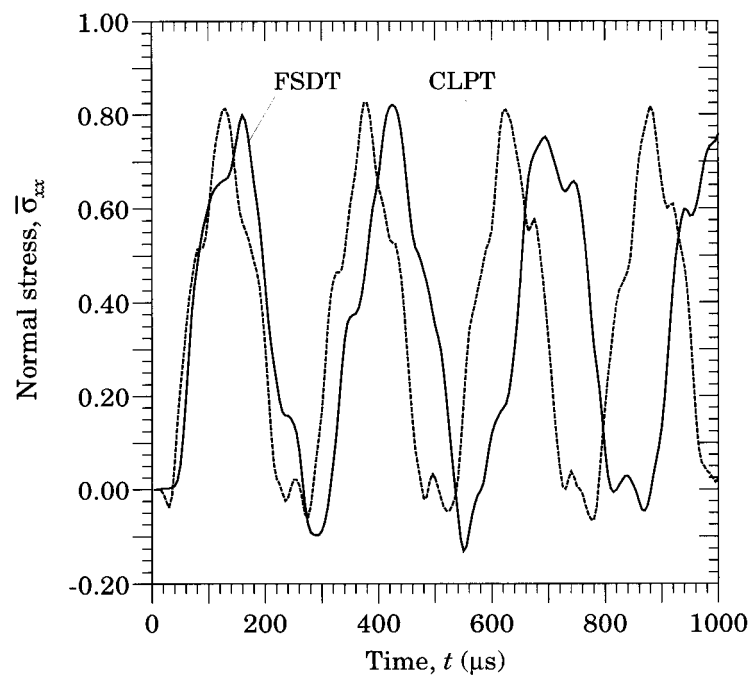


Figure 7.6.8: Nondimensionalized normal stress ($\bar{\sigma}_{xx}$ at the top of the laminate) versus time (t) for simply supported (SS-2) antisymmetric angle-ply ($-45/45$) laminates.

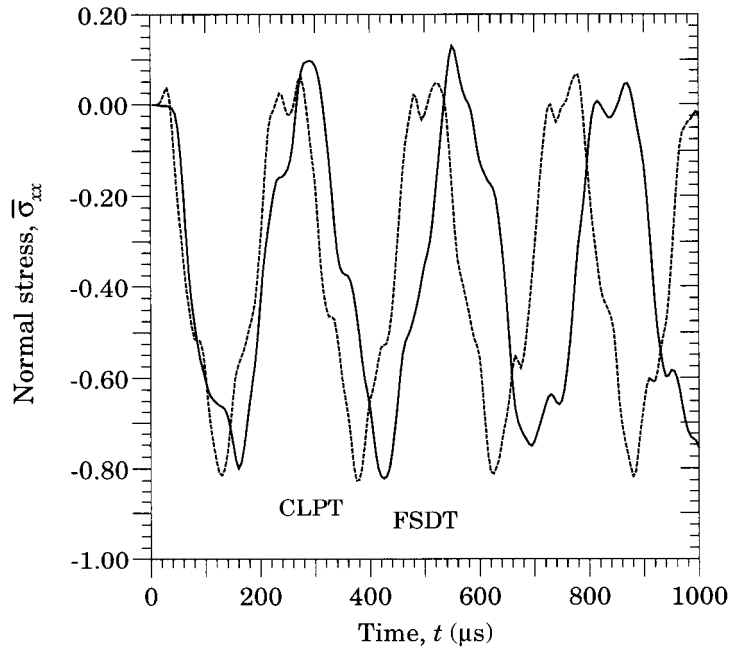


Figure 7.6.9: Nondimensionalized normal stress ($\bar{\sigma}_{xx}$ at the bottom of the laminate) versus time (t) for simply supported (SS-2) antisymmetric angle-ply ($-45/45$) laminates.

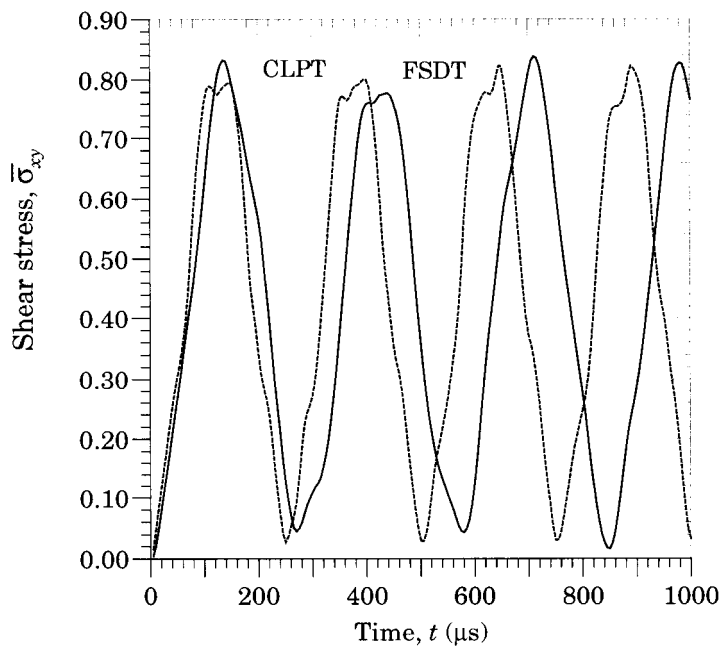


Figure 7.6.10: Nondimensionalized shear stress ($\bar{\sigma}_{xy}$) versus time (t) for simply supported (SS-2) antisymmetric angle-ply ($-45/45$) laminates.

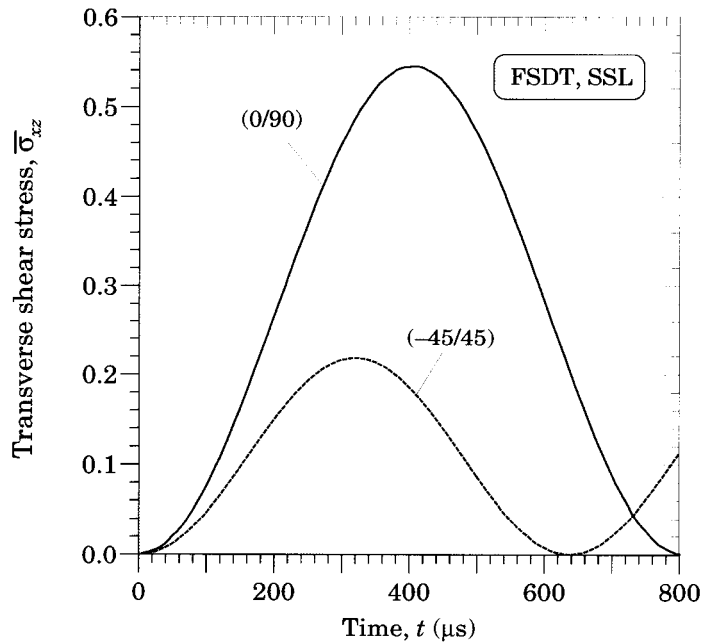


Figure 7.6.11: Nondimensionalized transverse shear stress ($\bar{\sigma}_{xz}$) versus time (t) for simply supported antisymmetric cross-ply (0/90) and angle-ply (-45/45) laminates.

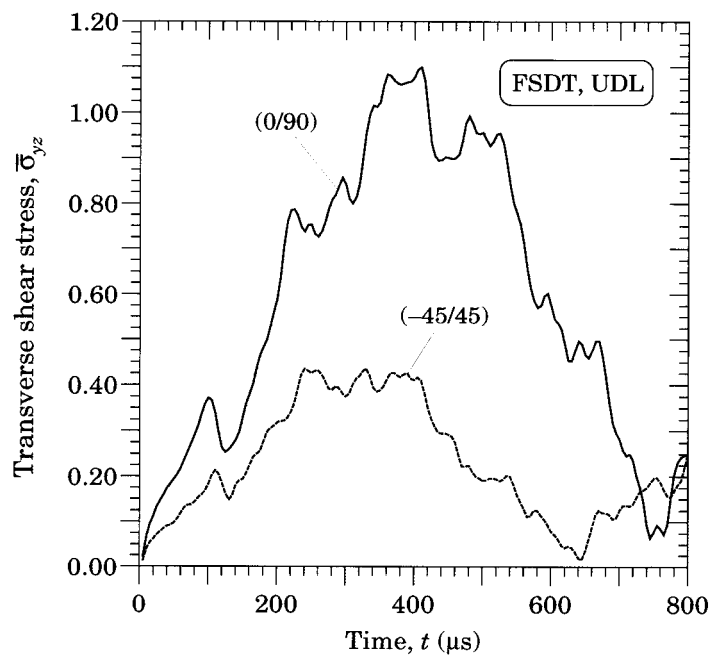


Figure 7.6.12: Nondimensionalized transverse shear stress ($\bar{\sigma}_{xz}$) versus time (t) for simply supported antisymmetric cross-ply (0/90) and angle-ply (-45/45) laminates.

Table 7.6.1: Nondimensionalized deflections and stresses of simply supported cross-ply (0/90) and angle-ply (-45/45) square plates under uniformly distributed transverse load ($E_1/E_2 = 25$, $E_2 = 2.1 \times 10^6$ psi, $G_{12} = G_{13} = 0.5E_2$, $G_{23} = 0.2E_2$, $\nu_{12} = 0.25$, $a/b = 1$, $a = 25$ cm, $a/h = 10$).

Theory	(0/90)			(-45/45)		
	\bar{w}	$\bar{\sigma}_{xx}$	$\bar{\sigma}_{xy}$	\bar{w}	$\bar{\sigma}_{xx}$	$\bar{\sigma}_{xy}$
FSDT [†]	3.990	0.275	0.181	2.611	0.799	0.832
	1.947	0.126	0.096	1.279	0.348	0.427
CLPT	3.421	0.274	0.181	2.120	0.813	0.795
	1.695	0.127	0.093	1.028	0.351	0.442

[†] The first line is the transient solution and the second line is the static solution.

7.7 Vibration Control of Laminated Plates

7.7.1 Preliminary Comments

The study of smart materials and structures has received considerable attentions in recent years. The advantage of incorporating these special types of materials into the structure is that the sensing and actuating mechanism becomes part of the structure so that one can monitor the structural integrity/health of the structure. There are a number of materials that have the capability to be used as a sensor or an actuator or both. Piezoelectric materials, magnetostrictive materials, electrostrictive materials, shape memory alloys, and electrorheological fluids provide examples of such materials. Among these, piezoelectric and magnetostrictive materials have the capability to serve as both sensors and actuators. Piezoelectricity [36] is a phenomenon in which some materials develop polarization upon application of strains. Examples of piezoelectric materials are Rochelle salt, quartz, and lead zirconate titanate or PZT ($Pb(Zr,Ti)O_3$). Piezoelectric materials exhibit a linear relationship between the electric field and strains for low field values (up to 100 V/mm); and they exhibit nonlinear behavior and hysteresis for large electric fields [37]. Furthermore, piezoelectric materials show dielectric aging and hence lack reproducibility of strains; i.e., a drift from zero state of strain is observed under cyclic electric field conditions. Terfenol-D, a magnetostrictive material [38], has the characteristics of being able to produce strains up to 2500 μm and energy density as high as 25000 J/m³ in response to a magnetic field.

There have been a number of studies on vibration control of flexible structures using smart materials (see Section 4.6 for references). Benedou [39] surveyed more than 100 papers and discussed the research trends in piezoelectric finite element modeling. In this section, control of the transient response of laminated composite plates with integrated smart material layers is presented [40,41]. A simple negative velocity feedback control is used to actively control the dynamic response of the structure through a closed-loop control. The effects of material properties, lamination scheme, and placement of the smart material layer on deflection suppression are studied [41].

7.7.2 Theoretical Formulation

The governing equations of motion for FSDT remain the same as before [see Eqs. (3.4.23)–(3.4.27)]. The constitutive relations of the k th lamina take the form [see Eq. (3.3.12a) and (3.4.17a)]

$$\begin{Bmatrix} \sigma_{xx} \\ \sigma_{yy} \\ \sigma_{xy} \end{Bmatrix}^{(k)} = \begin{bmatrix} \bar{Q}_{11} & \bar{Q}_{12} & \bar{Q}_{16} \\ \bar{Q}_{12} & \bar{Q}_{22} & \bar{Q}_{26} \\ \bar{Q}_{16} & \bar{Q}_{26} & \bar{Q}_{66} \end{bmatrix}^{(k)} \begin{Bmatrix} \varepsilon_{xx} \\ \varepsilon_{yy} \\ \gamma_{xy} \end{Bmatrix} - \begin{Bmatrix} \bar{e}_{31} \\ \bar{e}_{32} \\ \bar{e}_{36} \end{Bmatrix}^{(k)} H_z \quad (7.7.1)$$

$$\begin{Bmatrix} \sigma_{yz} \\ \sigma_{xz} \end{Bmatrix}^{(k)} = \begin{bmatrix} \bar{Q}_{44} & \bar{Q}_{45} \\ \bar{Q}_{45} & \bar{Q}_{55} \end{bmatrix}^{(k)} \begin{Bmatrix} \gamma_{yz} \\ \gamma_{xz} \end{Bmatrix} \quad (7.7.2)$$

where $\bar{Q}_{ij}^{(k)}$ are the transformed plane stress-reduced stiffnesses, and $\bar{e}_{ij}^{(k)}$ are the transformed piezoelectric, electrostrictive, or magnetostrictive coupling moduli of k th lamina.

7.7.3 Velocity Feedback Control

Considering velocity proportional closed-loop feedback control, the magnetic field intensity H is expressed in terms of coil current $I(x, y, t)$ as [see Eqs. (4.6.8)–(4.6.10)]

$$H(x, y, t) = k_c c(t) \frac{\partial w_0}{\partial t} \quad (7.7.3)$$

where k_c is the coil constant, which can be expressed in terms of the coil width b_c , coil radius r_c , and number of turns n_c in the coil by

$$k_c = \frac{n_c}{\sqrt{b_c^2 + 4r_c^2}} \quad (7.7.4)$$

and $c(t)$ is the control gain.

In view of the constitutive equations (7.7.1) and (7.7.2), the force and moment resultants are related to the strains by

$$\begin{Bmatrix} \{N\} \\ \{M\} \end{Bmatrix} = \begin{bmatrix} [A] & [B] \\ [B] & [D] \end{bmatrix} \begin{Bmatrix} \{\varepsilon^0\} \\ \{\varepsilon^1\} \end{Bmatrix} - \begin{Bmatrix} \{N\}^M \\ \{M\}^M \end{Bmatrix} \quad (7.7.5a)$$

$$\begin{Bmatrix} Q_y \\ Q_x \end{Bmatrix} = K \begin{bmatrix} A_{44} & A_{45} \\ A_{45} & A_{55} \end{bmatrix} \begin{Bmatrix} \gamma_{yz}^{(0)} \\ \gamma_{xz}^{(0)} \end{Bmatrix} - \begin{Bmatrix} Q_y^M \\ Q_x^M \end{Bmatrix} \quad (7.7.5b)$$

where K is the shear correction factor, and the actuation stress resultants $\{N^M\}$ and $\{M^M\}$ are defined by

$$\begin{aligned} \begin{Bmatrix} N_{xx}^M \\ N_{yy}^M \end{Bmatrix} &= \sum_{k=m, n-m+1} \int_{z_k}^{z_{k+1}} \begin{Bmatrix} \bar{e}_{31} \\ \bar{e}_{32} \end{Bmatrix} H_z dz \\ &= ck_c \sum_{k=m, n-m+1} \int_{z_k}^{z_{k+1}} \begin{Bmatrix} \bar{e}_{31} \\ \bar{e}_{32} \end{Bmatrix} \frac{\partial w_0}{\partial t} dz \end{aligned} \quad (7.7.6)$$

$$\begin{aligned} \begin{Bmatrix} M_{xx}^M \\ M_{yy}^M \end{Bmatrix} &= \sum_{k=m, n-m+1} \int_{z_k}^{z_{k+1}} \begin{Bmatrix} \bar{e}_{31} \\ \bar{e}_{32} \end{Bmatrix} z H_z dz \\ &= ck_c \sum_{k=m, n-m+1} \int_{z_k}^{z_{k+1}} \begin{Bmatrix} \bar{e}_{31} \\ \bar{e}_{32} \end{Bmatrix} \frac{\partial w_0}{\partial t} z dz \equiv \begin{Bmatrix} \mathcal{E}_{31} \\ \mathcal{E}_{32} \end{Bmatrix} \frac{\partial w_0}{\partial t} \end{aligned} \quad (7.7.7)$$

7.7.4 Analytical Solution

For simply supported plates, we can develop the Navier solution. Here we consider the pure bending case (i.e., neglect the in-plane contributions). The equations of motion of the first-order theory can be expressed in terms of the generalized displacements $(u_0, v_0, w_0, \phi_x, \phi_y)$ by substituting for the force and moment resultants in terms of the generalized displacements. For homogeneous laminates, the equations of motion take the form

$$\begin{aligned} KA_{55} \left(\frac{\partial^2 w_0}{\partial x^2} + \frac{\partial \phi_x}{\partial x} \right) + KA_{45} \left(\frac{\partial^2 w_0}{\partial y \partial x} + \frac{\partial \phi_y}{\partial x} \right) + \\ KA_{45} \left(\frac{\partial^2 w_0}{\partial x \partial y} + \frac{\partial \phi_x}{\partial y} \right) + KA_{44} \left(\frac{\partial^2 w_0}{\partial y^2} + \frac{\partial \phi_y}{\partial y} \right) + \\ + q - \left(\frac{\partial Q_x^P}{\partial x} + \frac{\partial Q_y^P}{\partial y} \right) - I_0 \frac{\partial^2 w_0}{\partial t^2} = 0 \end{aligned} \quad (7.7.8)$$

$$\begin{aligned} D_{11} \frac{\partial^2 \phi_x}{\partial x^2} + D_{12} \frac{\partial^2 \phi_y}{\partial y \partial x} + D_{66} \left(\frac{\partial^2 \phi_x}{\partial y^2} + \frac{\partial^2 \phi_y}{\partial y \partial x} \right) \\ - KA_{55} \left(\frac{\partial w_0}{\partial x} + \phi_x \right) - \mathcal{E}_{31} \frac{\partial \dot{w}_0}{\partial x} - I_2 \frac{\partial^2 \phi_x}{\partial t^2} = 0 \end{aligned} \quad (7.7.9)$$

$$\begin{aligned} D_{66} \left(\frac{\partial^2 \phi_x}{\partial x \partial y} + \frac{\partial^2 \phi_y}{\partial x^2} \right) + D_{12} \frac{\partial^2 \phi_x}{\partial x \partial y} + D_{22} \frac{\partial^2 \phi_y}{\partial y^2} \\ - KA_{44} \left(\frac{\partial w_0}{\partial y} + \phi_y \right) - \mathcal{E}_{32} \frac{\partial \dot{w}_0}{\partial x} - I_2 \frac{\partial^2 \phi_y}{\partial t^2} = 0 \end{aligned} \quad (7.7.10)$$

The simply supported boundary conditions for the first-order shear deformation plate theory (FSDT) are

$$\begin{aligned} \phi_x(x, 0, t) = 0, \phi_x(x, b, t) = 0, \phi_y(0, y, t) = 0, \phi_y(a, y, t) = 0 \\ w_0(x, 0, t) = 0, w_0(x, b, t) = 0, w_0(0, y, t) = 0, w_0(a, y, t) = 0 \\ M_{xx}(0, y, t) = 0, M_{xx}(a, y, t) = 0, M_{yy}(x, 0, t) = 0, M_{yy}(x, b, t) = 0 \end{aligned} \quad (7.7.11)$$

The boundary conditions in Eq. (7.7.11) are satisfied by the following expansions

$$\begin{aligned} w_0(x, y, t) &= \sum_{n=1}^{\infty} \sum_{m=1}^{\infty} W_{mn}(t) \sin \alpha x \sin \beta y \\ \phi_x(x, y, t) &= \sum_{n=1}^{\infty} \sum_{m=1}^{\infty} X_{mn}(t) \cos \alpha x \sin \beta y \\ \phi_y(x, y, t) &= \sum_{n=1}^{\infty} \sum_{m=1}^{\infty} Y_{mn}(t) \sin \alpha x \cos \beta y \end{aligned} \quad (7.7.12)$$

The mechanical load and magnetostrictive moments are also expanded in double Fourier sine series as

$$q_0(x, y, t) = \sum_{n=1}^{\infty} \sum_{m=1}^{\infty} Q_{mn}(t) \sin \alpha x \sin \beta y$$

$$\begin{aligned} M_{xx}^M(x, y, t) &= \sum_{n=1}^{\infty} \sum_{m=1}^{\infty} M_{mn}^1(t) \sin \alpha x \sin \beta y \\ M_{yy}^M(x, y, t) &= \sum_{n=1}^{\infty} \sum_{m=1}^{\infty} M_{mn}^2(t) \sin \alpha x \sin \beta y \end{aligned} \quad (7.7.13)$$

where, for example

$$\begin{aligned} Q_{mn}(t) &= \frac{4}{ab} \int_0^a \int_0^b q(x, y, t) \sin \alpha x \sin \beta y \, dx dy \\ M_{mn}^1(t) &= \frac{4}{ab} \int_0^a \int_0^b M_{xx}^M(x, y, t) \sin \alpha x \sin \beta y \, dx dy \\ M_{mn}^2(t) &= \frac{4}{ab} \int_0^a \int_0^b M_{yy}^M(x, y, t) \sin \alpha x \sin \beta y \, dx dy \end{aligned} \quad (7.7.14)$$

Substituting Eq. (7.7.12) into Eqs. (7.7.8)–(7.7.14) we obtain

$$\begin{bmatrix} \hat{S}_{33} & \hat{S}_{34} & \hat{S}_{35} \\ \hat{S}_{43} & \hat{S}_{44} & \hat{S}_{45} \\ \hat{S}_{53} & \hat{S}_{54} & \hat{S}_{55} \end{bmatrix} \begin{Bmatrix} W_{mn} \\ X_{mn} \\ Y_{mn} \end{Bmatrix} + \begin{bmatrix} 0 & 0 & 0 \\ \hat{C}_{43} & 0 & 0 \\ \hat{C}_{53} & 0 & 0 \end{bmatrix} \begin{Bmatrix} \dot{W} \\ \dot{X} \\ \dot{Y} \end{Bmatrix} + \begin{bmatrix} \hat{M}_{33} & 0 & 0 \\ 0 & \hat{M}_{44} & 0 \\ 0 & 0 & \hat{M}_{55} \end{bmatrix} \begin{Bmatrix} \ddot{W} \\ \ddot{X} \\ \ddot{Y} \end{Bmatrix} = \begin{Bmatrix} Q_{mn} \\ 0 \\ 0 \end{Bmatrix} \quad (7.7.15)$$

where $\hat{S}_{ij} = \hat{S}_{ji}$, $\hat{C}_{ij} = \hat{C}_{ji}$ and $\hat{M}_{ij} = \hat{M}_{ji}$ are defined by

$$\begin{aligned} \hat{S}_{33} &= K(2A_{45}\alpha\beta + A_{44}\beta^2 + A_{55}\alpha^2) \\ \hat{S}_{34} &= K(A_{55}\alpha + A_{45}\beta), \quad \hat{S}_{35} = K(A_{45}\alpha + A_{44}\beta) \\ \hat{C}_{33} &= \hat{C}_{34} = \hat{C}_{35} = 0, \quad \hat{M}_{33} = I_0, \quad \hat{M}_{34} = \hat{M}_{35} = 0 \\ \hat{S}_{44} &= D_{11}\alpha^2 + D_{66}\beta^2 + KA_{55}, \quad \hat{S}_{45} = (D_{12} + D_{66})\alpha\beta + KA_{45} \\ \hat{C}_{43} &= \alpha\mathcal{E}_{31}, \quad \hat{C}_{44} = \hat{C}_{45} = 0, \quad \hat{M}_{44} = I_2, \quad \hat{M}_{45} = 0, \quad \hat{M}_{55} = I_2 \\ \hat{S}_{55} &= D_{66}\alpha^2 + D_{22}\beta^2 + KA_{44}, \quad \hat{C}_{53} = \beta\mathcal{E}_{32}, \quad \hat{C}_{54} = \hat{C}_{55} = 0 \end{aligned} \quad (7.7.16)$$

where the magnetostrictive coefficients \mathcal{E}_{31} and \mathcal{E}_{32} are defined in Eq. (7.7.7).

For vibration control, we assume $q = 0$ and seek solution of the ordinary differential equations in Eq. (7.7.15) in the form

$$W_{mn}(t) = W_0 e^{\lambda t}, \quad X_{mn}(t) = X_0 e^{\lambda t}, \quad Y_{mn}(t) = Y_0 e^{\lambda t} \quad (7.7.17)$$

Substituting Eq. (7.7.17) into Eq. (7.7.15), for a non-trivial solution we obtain the result

$$\begin{vmatrix} \bar{S}_{33} & \bar{S}_{34} & \bar{S}_{35} \\ \bar{S}_{43} & \bar{S}_{44} & \bar{S}_{45} \\ \bar{S}_{53} & \bar{S}_{54} & \bar{S}_{55} \end{vmatrix} = 0 \quad (7.7.18)$$

where

$$\bar{S}_{ij} = \hat{S}_{ij} + \lambda \hat{C}_{ij} + \lambda^2 \hat{M}_{ij} \quad (7.7.19)$$

for $i, j = 3, 4, 5$. This equation gives three sets of eigenvalues. The lowest one corresponds to the transverse motion. A typical eigenvalue can be expressed as $\lambda = -\alpha + i\omega_d$, so that the damped transverse deflection is given by

$$w_0(x, y, t) = \frac{1}{\omega_d} e^{-\alpha t} \sin \omega_d t \sin \frac{n\pi x}{a} \sin \frac{n\pi y}{b} \quad (7.7.20)$$

In arriving at the last solution, the following initial conditions are used:

$$\begin{aligned} w_0(x, y, 0) &= 0, \dot{w}_0(x, y, 0) = 1, \phi(x, y, 0)_x = 0 \\ \dot{\phi}_x(x, y, 0) &= 0, \phi_y(x, y, 0) = 0, \dot{\phi}_y(x, y, 0) = 0 \end{aligned} \quad (7.7.21)$$

7.7.5 Numerical Results and Discussion

Numerical results are obtained using the formulation presented above. Numerical studies are carried out to obtain the natural frequencies, magnetostrictive damping coefficients and the vibration suppression time. Various lamination schemes are used to show the influence of the position of the pair of magnetostrictive layers from the neutral axis on the vibration suppression time. Also, a time ratio relation between the thickness of the layers and the distance to the neutral axis of the laminated composite plate is obtained. All values of the composite material and structural constants are tabulated, and damped and undamped frequencies are presented in the form of figures.

The plate is taken to be a unit square of $1\text{m} \times 1\text{m}$. The composite lamina material properties are listed in Table 7.7.1. Magnetostrictive material properties are taken to be

$$E_m = 26.5 \text{ GPa}, \quad \nu_m = 0.0, \quad \rho_m = 9250 \text{ kg}\cdot\text{m}^{-3}, \quad d_k = 1.67^{-8} \text{ mA}^{-1}, \quad c r_c = 10^4 \quad (7.7.22)$$

The numerical values of various material and structural constants (e.g. moment of inertia, magnetostrictive material constants) based on different lamination schemes and material properties (CFRP, graphite-epoxy (Gr-Ep)(AS), glass-epoxy (Gl-Ep), boron-epoxy (Br-Ep)) are listed in Tables 7.7.2 and 7.7.3. Magnetostrictive damping coefficients and natural frequencies for various materials and lamination schemes are also listed in Table 7.7.3.

Table 7.7.1: Material constants of various composite materials.

Material	E_{11} [GPa]	E_{22} [GPa]	G_{13} [GPa]	G_{23} [GPa]	G_{12} [GPa]	ν_{12}	ρ [kg m $^{-3}$]
CFRP	138.6	8.27	4.96	4.96	4.12	0.26	1824
Gr-Ep(AS)	137.9	8.96	7.20	6.21	7.20	0.30	1450
Gl-Ep	53.78	17.93	8.96	3.45	8.96	0.56	1900
Br-Ep	206.9	20.69	6.9	4.14	6.9	0.30	1950

Table 7.7.2: Coefficients for different laminates and materials.

Material	Laminate	$D_{11}(10^3)$ [N m]	$D_{12}(10^3)$ [N m]	$D_{22}(10^3)$ [N m]	$D_{66}(10^3)$ [N m]	$A_{44}(10^7)$ [N/m]	$A_{55}(10^7)$ [N/m]
CFRP	$[\pm 45/\mathbf{m}/0/90]_S$	3.739	2.221	3.215	2.528	6.62	6.62
	$[45/\mathbf{m}/-45/0/90]_S$	3.552	1.816	3.029	2.257	6.62	6.62
	$[\mathbf{m}/\pm 45/0/90]_S$	3.303	1.274	2.78	1.897	6.62	6.62
	$[\mathbf{m}/90_4]_S$	1.432	0.0921	7.015	0.7146	6.62	6.62
	$[\mathbf{m}/0_4]_S$	7.015	0.0921	1.432	0.7146	6.62	6.62
Gr-Ep(AS)	$[\pm 45/\mathbf{m}/0/90]_S$	3.954	2.052	3.435	2.53	7.974	7.974
Gl-Ep	$[\pm 45/\mathbf{m}/0/90]_S$	2.889	1.149	2.729	1.157	7.614	7.614
Br-Ep	$[\pm 45/\mathbf{m}/0/90]_S$	5.73	3.538	4.979	3.751	7.066	7.066

Table 7.7.3: Mass inertia coefficients and parameters α and ω_{dr} .

Material	Laminate	I_0 [kg/m]	$I_2(10^{-4})$ [kg m]	$-\mathcal{E}_{31}$	$-\alpha \pm \omega_{dr}$ (rad s ⁻¹)
CFRP	$[\pm 45/\mathbf{m}/0/90]_S$	33.09	2.461	22.13	6.588 ± 254.823
	$[45/\mathbf{m}/-45/0/90]_S$	33.09	3.352	30.98	9.224 ± 240.724
	$[\mathbf{m}/\pm 45/0/90]_S$	33.09	4.54	39.83	11.861 ± 221.418
	$[\mathbf{m}/90_4]_S$	33.09	4.54	39.83	11.866 ± 187.435
	$[\mathbf{m}/0_4]_S$	33.09	4.54	39.83	11.866 ± 187.435
Gr-Ep(AS)	$[\pm 45/\mathbf{m}/0/90]_S$	30.1	2.196	22.13	7.244 ± 264.443
Gl-Ep	$[\pm 45/\mathbf{m}/0/90]_S$	33.7	2.514	22.13	6.474 ± 187.440
Br-Ep	$[\pm 45/\mathbf{m}/0/90]_S$	34.1	2.55	22.13	6.388 ± 309.992

Figure 7.7.1 shows a comparison of uncontrolled and controlled amplitude of the center deflection of $(\mathbf{m}/\pm 45/0/90)_S$ laminate (\mathbf{m} denotes the magnetostrictive layer). The value of α [see Eq. (7.7.20)] increases when the magnetostrictive layer is located farther away from the neutral axis, indicating faster vibration suppression. This is due to the larger bending moment created by actuating force in the magnetostrictive layers. Figure 7.7.2 contains controlled amplitudes of the center deflection for modes 1 and 2 for $[\pm 45/\mathbf{m}/0/90]_S$ laminate. It can be observed that attenuation favors the higher modes.

7.8 Summary

Analytical solutions for bending, buckling under in-plane compressive loads, natural vibration, and transient response of rectangular laminates with various boundary conditions are presented based on the first-order shear deformation laminate theory. The Navier solutions were developed for two classes of laminates: antisymmetric cross-ply laminates and antisymmetric angle-ply laminates, each for a specific type of simply supported boundary conditions, SS-1 and SS-2, respectively. The Lévy solutions with the state-space approach were developed for these classes of laminates when two opposite edges are simply supported and other two edges having a variety of boundary conditions of choice.

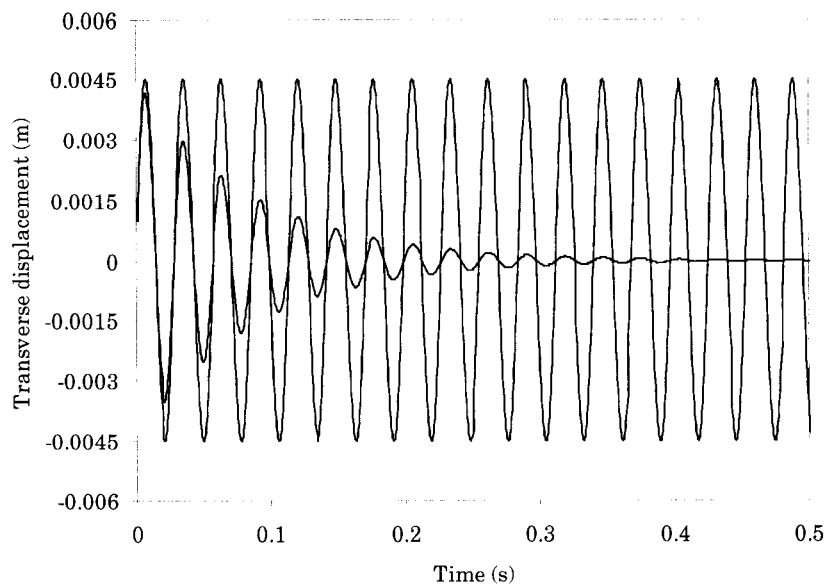


Figure 7.7.1: Comparison of the uncontrolled and controlled center deflection of $(\mathbf{m}/\pm 45/0/90)_s$ laminate.

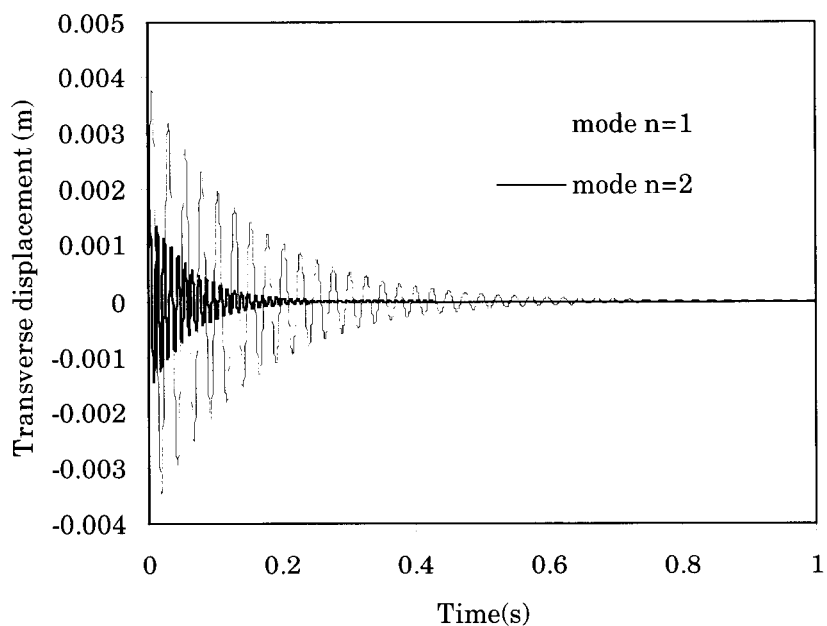


Figure 7.7.2: Comparison of the uncontrolled and controlled center deflection of $(\pm 45/\mathbf{m}/0/90)_s$ laminate.

Numerical results were presented for static bending, buckling, natural vibration, and transient response of antisymmetric cross-ply and angle-ply laminates. The bending-extensional coupling and transverse shear deformation in a laminate generally reduce the effective stiffnesses and hence increase deflections and reduce buckling loads and reduce natural frequencies. The effect of transverse shear deformation on transient response is to increase both amplitude and period of oscillation. The coupling is the most significant in two-layer laminates, and it decreases gradually as the number of layers is increased for fixed total thickness.

Lastly, numerical results are also presented for vibration suppression of simply supported laminated plates with magnetostrictive layers. Additional results can be found in [41].

In a series of papers, relationships between deflections, buckling loads and vibration frequencies predicted by the first-order shear deformation plate theory and the classical plate theory of isotropic plates were presented (see [42–45] and references therein). Extension of these ideas to composite plates has not been done. Analytical solutions for bending, buckling and vibration of stepped laminated plates [46] or laminated plates with internal hinge [47,48] must be carried out for various types of lamination schemes.

Problems

7.1 Show that the solution of Eq. (7.2.15b) is given by

$$\begin{aligned} W_{mn} &= \frac{1}{b_{mn}} (a_1 Q_{mn} - a_2 \alpha M_{mn}^1 - a_3 \beta M_{mn}^2) \\ X_{mn} &= \frac{1}{b_{mn}} (a_2 Q_{mn} - a_4 \alpha M_{mn}^1 - a_5 \beta M_{mn}^2) \\ Y_{mn} &= \frac{1}{b_{mn}} (a_3 Q_{mn} - a_5 \alpha M_{mn}^1 - a_6 \beta M_{mn}^2) \end{aligned} \quad (\text{a})$$

where

$$\begin{aligned} b_{mn} &= \begin{vmatrix} \hat{s}_{33} & \hat{s}_{34} & \hat{s}_{35} \\ \hat{s}_{34} & \hat{s}_{44} & \hat{s}_{45} \\ \hat{s}_{35} & \hat{s}_{45} & \hat{s}_{55} \end{vmatrix} = \hat{s}_{33}a_1 + \hat{s}_{34}a_2 + \hat{s}_{35}a_3 \\ a_1 &= \hat{s}_{44}\hat{s}_{55} - \hat{s}_{45}\hat{s}_{45}, \quad a_2 = \hat{s}_{45}\hat{s}_{35} - \hat{s}_{34}\hat{s}_{55}, \quad a_3 = \hat{s}_{34}\hat{s}_{45} - \hat{s}_{44}\hat{s}_{35} \\ a_4 &= \hat{s}_{33}\hat{s}_{55} - \hat{s}_{35}\hat{s}_{35}, \quad a_5 = \hat{s}_{34}\hat{s}_{35} - \hat{s}_{33}\hat{s}_{45}, \quad a_6 = \hat{s}_{33}\hat{s}_{44} - \hat{s}_{34}\hat{s}_{34} \end{aligned} \quad (\text{b})$$

7.2 Verify the expressions for transverse stresses presented in Eq. (7.2.23).

7.3 Formulate the Lévy type solution procedure for the natural vibration of antisymmetric cross-ply laminates. In particular, show that the operator $[T]$ in Eq. (7.4.13a) holds with

$$\begin{aligned} e_5 &= -\beta^2 A_{66} + I_0 \omega_m^2, \quad e_6 = -\beta^2 B_{66} + I_1 \omega_m^2 \\ e_{11} &= -\beta^2 A_{22} + I_0 \omega_m^2, \quad e_{12} = -\beta^2 B_{22} + I_1 \omega_m^2 \\ e_{15} &= -\beta^2 K A_{44} + I_0 \omega_m^2 \\ e_{21} &= -\beta^2 B_{66} + I_1 \omega_m^2, \quad e_{22} = -\beta^2 D_{66} - K A_{55} + I_2 \omega_m^2 \\ e_{28} &= -\beta^2 B_{22} + I_1 \omega_m^2, \quad e_{29} = -\beta^2 D_{22} - K A_{44} + I_2 \omega_m^2 \end{aligned}$$

7.4 Formulate the Lévy type solution procedure for the buckling of antisymmetric cross-ply laminates under in-plane compressive loads. In particular, show that the operator $[T]$ in Eq. (7.4.13a) holds with

$$e_{13} = K A_{55} + \hat{N}_{xx}, \quad e_{15} = -\beta^2 K A_{44} - \beta^2 \hat{N}_{yy}$$

7.5 Verify the expressions for transverse stresses presented in Eq. (7.3.11).

7.6 Formulate the Lévy type solution procedure for the natural vibration of antisymmetric angle-ply laminates. In particular, show that the operator $[T]$ in Eq. (7.5.14b) holds with

$$\begin{aligned} C_1 &= \frac{\alpha^2 (A_{11}D_{22} - B_{16}B_{26}) - I_0 D_{22}\omega_m^2}{A_{66}D_{22} - B_{26}^2} \\ C_5 &= \frac{\alpha^2 (B_{16}D_{22} - B_{26}D_{66}) - B_{26}K A_{44} + I_2 B_{26}\omega_m^2}{A_{66}D_{22} - B_{26}^2} \\ C_7 &= \frac{\alpha^2 (A_{66}D_{66} - B_{16}B_{26}) - I_0 D_{66}\omega_m^2}{A_{22}D_{66} - B_{26}^2} \\ C_9 &= \frac{\alpha^2 (B_{16}D_{66} - D_{11}B_{26}) - K A_{55}B_{26} + I_2 B_{26}\omega_m^2}{A_{22}D_{66} - B_{26}^2} \\ C_{11} &= \frac{\alpha^2 K A_{55} - I_0 \omega_m^2}{K A_{44}} \\ C_{15} &= \frac{\alpha^2 (A_{22}B_{16} - B_{26}A_{66}) + I_0 B_{26}\omega_m^2}{A_{22}D_{66} - B_{26}^2} \\ C_{17} &= \frac{\alpha^2 (A_{22}D_{11} - B_{16}B_{26}) + A_{22}K A_{55} - I_2 A_{22}\omega_m^2}{A_{22}D_{66} - B_{26}^2} \\ C_{19} &= \frac{\alpha^2 (A_{66}B_{16} - A_{11}B_{26}) + I_0 B_{26}\omega_m^2}{A_{22}D_{66} - B_{26}^2} \\ C_{23} &= \frac{\alpha^2 (A_{66}D_{66} - B_{16}B_{26}) + A_{66}K A_{44} - I_2 A_{66}\omega_m^2}{A_{22}D_{66} - B_{26}^2} \end{aligned}$$

and all other C_i are as defined in Eq. (7.5.12b) with $\hat{N}_{xx} = \hat{N}_{yy} = 0$.

References for Additional Reading

1. Khdeir, A. A., Reddy, J. N., and Librescu, L., "Lévy Type Solutions for Symmetrically Laminated Rectangular Plates Using First-Order Shear Deformation Theory," *Journal of Applied Mechanics*, **54**, 640–642 (1987).
2. Franklin, J. N., *Matrix Theory*, Prentice-Hall, Englewood Cliffs, NJ (1968).
3. Brogan, W. L., *Modern Control Theory*, Prentice-Hall, Englewood Cliffs, NJ (1985).
4. Reddy, J. N., *Energy and Variational Methods in Applied Mechanics*, John Wiley, New York (1984).
5. Reddy, J. N. (ed.), *Mechanics of Composite Materials. Selected Works of Nicholas J. Pagano*, Kluwer, The Netherlands (1994).
6. Pagano, N. J., "Exact Solutions for Rectangular Bidirectional Composites and Sandwich Plates," *Journal of Composite Materials*, **4**(1), 20–34 (1970).
7. Pagano, N. J., and Hatfield, S. J., "Elastic Behavior of Multilayered Bidirectional Composites," *AIAA Journal*, **10**(7), 931–933 (1972).
8. Reddy, J. N. and Khdeir, A. A., "Buckling and Vibration of Laminated Composite Plates Using Various Plate Theories," *AIAA Journal*, **27**(12), 1808–1817 (1989).
9. Nosier, A. and Reddy, J. N., "On Vibration and Buckling of Symmetric Laminated Plates According to Shear Deformation Theories," *Acta Mechanica*, **94**(3,4), 123–170 (1992).
10. Reddy, J. N. and Chao, W. C., "A Comparison of Closed-Form and Finite Element Solutions of Thick Laminated Anisotropic Rectangular Plates," *Nuclear Engineering and Design*, **64**, 153–167 (1981).

11. Reddy, J. N. and Hsu, Y. S., "Effects of Shear Deformation and Anisotropy on the Thermal Bending of Layered Composite Plates," *Journal of Thermal Stresses*, **3**, 475–493 (1980).
12. Khdeir, A. A., Librescu, L., and Reddy, J. N., "Analytical Solution of a Refined Shear Deformation Theory for Rectangular Composite Plates," *International Journal of Solids and Structures*, **23**(10), 1447–1463 (1987).
13. Khdeir, A. A. and Reddy, J. N., "Dynamic Response of Antisymmetric Angle-Ply Laminated Plates Subjected to Arbitrary Loading," *Journal of Sound & Vibration*, **126**(3), 437–445 (1988).
14. Khdeir, A. A. and Librescu, L., "Analysis of Symmetric Cross-Ply Laminated Elastic Plates Using a Higher-Order Theory: Part I—Stress and Displacement," *Composite Structures*, **9**, 189–213 (1988).
15. Khdeir, A. A. and Librescu, L., "Analysis of Symmetric Cross-Ply Laminated Elastic Plates Using a Higher-Order Theory: Part II—Buckling and Free Vibration," *Composite Structures*, **9**, 259–277 (1988).
16. Khdeir, A. A., "Free Vibration and Buckling of Symmetric Cross-Ply Laminated Plates by an Exact Method," *Journal of Sound and Vibration*, **126**(3), 447–461 (1988).
17. Khdeir, A. A., "Free Vibration of Antisymmetric Angle-Ply Laminated Plates Including Various Boundary Conditions," *Journal of Sound and Vibration*, **122**(2), 377–388 (1988).
18. Sun, C. T. and Whitney, J. M., "On Theories for the Dynamic Response of Laminated Plates," *AIAA Journal*, **11**(2), 178–183 (1973).
19. Khdeir, A. A., "Free Vibration and Buckling of Unsymmetric Cross-Ply Laminated Plates Using a Refined Theory," *Journal of Sound and Vibration*, **128**(3), 377–395 (1989).
20. Khdeir, A. A., "An Exact Approach to the Elastic State of Stress of Shear Deformable Antisymmetric Angle-Ply Laminated Plates," *Composite Structures*, **11**, 245–258 (1989).
21. Khdeir, A. A., "Comparison Between Shear Deformable and Kirchhoff Theories for Bending, Buckling and Vibration of Antisymmetric Angle-Ply Laminated Plates," *Composite Structures*, **13**, 159–172 (1989).
22. Khdeir, A. A., "Stability of Antisymmetric Angle-Ply Laminated Plates," *ASCE Journal of Engineering Mechanics*, **115**, 952–962 (1989).
23. Khdeir, A. A. and Reddy, J. N., "Analytical Solutions of Refined Plate Theories of Cross-Ply Composite Laminates," *Journal of Pressure Vessel Technology*, **113**(4), 570–578 (1991).
24. Khdeir, A. A. and Reddy, J. N., "Thermal Stresses and Deflections of Cross-Ply Laminated Plates Using Refined Plate Theories," *Journal of Thermal Stresses*, **14**(4), 419–438 (1991).
25. Khdeir A. A. and Reddy, J. N. "Exact Solutions for the Transient Response of Symmetric Cross-Ply Laminates Using a Higher-Order Plate Theory," *Composites Science and Technology*, **34**, 205–224 (1989).
26. Khdeir A. A. and Reddy, J. N. "On the Forced Motions of Antisymmetric Cross-Ply Laminates," *International Journal of Mechanical Sciences*, **31**, 499–510 (1989).
27. Khdeir A. A. and Reddy, J. N. "Dynamic Response of Antisymmetric Angle-Ply Laminated Plates Subjected to Arbitrary Loading," *Journal of Sound and Vibration*, **126**, 437–445 (1988).
28. Reddy, J. N., "On the Solutions to Forced Motions of Rectangular Composite Plates," *Journal of Applied Mechanics*, **49**, 403–408 (1982).
29. Srinivas, S. and Rao, A. K., "Buckling of Thick Rectangular Plates," *AIAA Journal*, **7**, 1645 (1969).
30. Srinivas, S., Joga Rao, C. V., and Rao, A. K., "An Exact Analysis for Vibration of Simply Supported Homogeneous and Laminated Thick Rectangular Plates," *Journal of Sound and Vibration*, **12**, 187–199 (1970).

31. Srinivas, S., Joga Rao, C. V., and Rao, A. K., "Some Results from an Exact Analysis of Thick Laminates in Vibration and Buckling," *Journal of Applied Mechanics*, **37**, 868–870 (1970).
32. Srinivas, S. and Rao, A. K., "Bending, Vibration, and Buckling of Simply Supported Thick Orthotropic Rectangular Plates and Laminates," *International Journal of Solids and Structures*, **6**, 1463–1481 (1970).
33. Srinivas, S. and Rao, A. K., "A Three-Dimensional Solution for Plates and Laminates," *Journal of Franklin Institute*, **291**, 469–481 (1971).
34. Srinivas, S. and Rao, A. K., "Flexure of Thick Rectangular Plates," *Journal of Applied Mechanics*, **40**, 298–299 (1973).
35. Srinivas, S., "A Refined Analysis of Composite Laminates," *Journal of Sound and Vibration*, **30**, 495–507 (1973).
36. Maugin, G.A., *Continuum Mechanics of Electromagnetic Solids*, North-Holland, Amsterdam, The Netherlands (1988).
37. Uchino, K., "Electrostrictive Actuators: Materials and Applications," *Ceramic Bulletin*, **65**, 647–652 (1986).
38. Goodfriend, M. J., and Shoop, K. M., "Adaptive Characteristics of the Magnetostrictive Alloy, Terfenol-D, for Active Vibration Control," *Journal of Intelligent Material Systems and Structures*, **3**, 245–254 (1992).
39. Benjeddou, A., "Advances in Piezoelectric Finite Element Modeling of Adaptive Structural Elements: A Survey," *Computers and Structures*, **76**, 347–363 (2000).
40. Reddy, J. N., "On Laminated Composite Plates with Integrated Sensors and Actuators," *Engineering Structures*, **21**, 568–593 (1999).
41. Pradhan, S. C., Ng, T. Y., Lam, K. Y., and Reddy, J. N., "Control of Laminated Composite Plates Using Magnetostrictive Layers," *Smart Materials and Structures*, **10**, 1–11 (2001).
42. Wang, C. M., and Reddy, J. N., "Deflection Relationships Between Classical and Third-Order Plate Theories," *Acta Mechanica*, **130**(3-4), 199–208 (1998).
43. Wang, C. M., Reddy, J. N., and Lee, K. H., *Shear Deformation Theories of Beams and Plates. Relationships with Classical Solution*, Elsevier, UK (2000).
44. Wang, C. M., Lim, G. T., Reddy, J. N., and Lee, K. H., "Relationships Between Bending Solutions of Reissner and Mindlin Plate Theories," *Engineering Structures*, **23**, 838–849 (2001).
45. Lim, G. T. and Reddy, J. N., "On Canonical Bending Relationships for Plates," *International Journal of Solids and Structures*, **40**, 3039–3067 (2003).
46. Xiang, Y., and Reddy, J. N., "Buckling and Vibration of Stepped, Symmetric Cross-Ply Laminated Rectangular Plates," *International Journal of Structural Stability and Dynamics*, **1**(3), 385–408 (2001).
47. Gupta, P. R., and Reddy, J. N., "Buckling and Vibration of Orthotropic Plates with an Internal Hinge," *International Journal of Structural Stability and Dynamics*, **2**(4), 457–486 (2002).
48. Xiang, Y., and Reddy, J. N., "Natural Vibration of Rectangular Plates with Internal Line Hinge Using the First-Order Shear Deformation Plate Theory," *Journal of Sound and Vibration*, **263**, 285–297 (2003).

Theory and Analysis of Laminated Shells

8.1 Introduction

In the preceding chapters, we studied the theory and the analysis of flat plates. We now extend the theory to curved plates and surfaces, better known as *shells*. Shells are common structural elements in many engineering structures, including pressure vessels, submarine hulls, ship hulls, wings and fuselages of airplanes, pipes, exteriors of rockets, missiles, automobile tires, concrete roofs, containers of liquids, and many other structures. The theory of laminated shells includes the theories of ordinary shells, flat plates, and curved beams as special cases. Therefore, in the present study, we consider the theory of laminated composite shells.

A number of theories exist for layered anisotropic shells [1–25]. Many of these theories were developed originally for thin shells and are based on the Kirchhoff-Love kinematic hypothesis that straight lines normal to the undeformed midsurface remain straight and normal to the middle surface after deformation. Other shell theories can be found in the works of Naghdi [24,25] and a detailed study of thin isotropic shells can be found in the monographs by Ambartsumyan [1–3], Flügge [6] and Kraus [8]. The first-order shear deformation theory of shells, also known as the Sanders shell theory [26,27], can be found in Kraus [8].

The first analysis that incorporated the bending-stretching coupling (owing to unsymmetric lamination in composites) is due to Ambartsumyan [1–3]. In his analyses, Ambartsumyan assumed that the individual orthotropic layers were oriented such that the principal axes of material symmetry coincided with the principal coordinates of the shell reference surface. Thus, Ambartsumyan's work dealt with what is now known as laminated orthotropic shells, rather than laminated anisotropic shells; in laminated anisotropic shells, the individual layers are, in general, anisotropic, and the principal axes of material symmetry of the individual layers coincide with only one of the principal coordinates of the shell (the thickness normal coordinate).

Dong, Pister, and Taylor [15] formulated a theory of thin shells laminated of anisotropic material that is an extension of the theory developed by Stavsky [28] for laminated anisotropic plates to Donnell's shallow shell theory (see Donnell [17]). Cheng and Ho [29] presented an analysis of laminated anisotropic cylindrical shells using Flügge's shell theory [6]. A shell theory for the unsymmetric deformation of nonhomogeneous, anisotropic, elastic cylindrical shells was derived by Widera and Chung [30] by means of the asymptotic integration of the elasticity equations. For a homogenous, isotropic material, the theory reduces to Donnell's equations.

All of the theories listed above are based on Kirchhoff-Love's hypotheses, in which the transverse shear deformation is neglected. These theories, known as the Love's first-approximation theories (see Love [22]), are expected to yield sufficiently accurate results when (1) the radius-to-thickness ratio is large, (2) the dynamic excitations are within the low-frequency range, and (3) the material anisotropy is not severe. However, the application of such theories to layered anisotropic composite shells could lead to 30% or more errors in deflections, stresses, and frequencies.

The effects of transverse shear deformation and transverse isotropy, as well as thermal expansion through the thickness of cylindrical shells, were considered by Gulati and Essenberg [31] and Zukas and Vinson [32]. Whitney and Sun [33] developed a shear deformation theory for laminated cylindrical shells that includes both transverse shear deformation and transverse normal strain as well as expansional strains. Reddy [34] presented a generalization of the Sanders shell theory [26] to laminated, doubly-curved anisotropic shells. The theory accounts for transverse shear strains and the von Kármán (or Sanders) nonlinear strains. For additional references and applications to composite shells, see Bert [35,36].

Following this introduction, three basic set of equations, namely, the kinetic (equilibrium), kinematic (strain-displacement) and constitutive (Hooke's law), are derived in the next section. In Section 8.3, analytical solutions of the static equations for some cases will be discussed. The finite element models of shells will be considered in Chapters 9 and 10.

8.2 Governing Equations

8.2.1 Geometric Properties of the Shell

Figure 8.2.1a shows a uniform thickness, laminated curved shell, where (ξ_1, ξ_2, ζ) denote the orthogonal curvilinear coordinates such that ξ_1 and ξ_2 curves are the lines of curvature on the middle surface ($\zeta = 0$). The position vector of a point $(\xi_1, \xi_2, 0)$ on the middle surface is denoted by \mathbf{r} , and the position of an arbitrary point (ξ_1, ξ_2, ζ) is denoted by \mathbf{R} (see Figure 8.2.1b). The square of the distance ds between points $(\xi_1, \xi_2, 0)$ and $(\xi_1 + d\xi_1, \xi_2 + d\xi_2, 0)$ is determined by

$$(ds)^2 = d\mathbf{r} \cdot d\mathbf{r} = a_1^2(d\xi_1)^2 + a_2^2(d\xi_2)^2 \quad (8.2.1a)$$

$$d\mathbf{r} = \mathbf{g}_1 d\xi_1 + \mathbf{g}_2 d\xi_2, \quad \mathbf{g}_\alpha = \frac{\partial \mathbf{r}}{\partial \xi_\alpha}, \quad g_{\alpha\beta} = \mathbf{g}_\alpha \cdot \mathbf{g}_\beta \quad (8.2.1b)$$

where the vectors \mathbf{g}_1 and \mathbf{g}_2 are tangent to the ξ_1 and ξ_2 coordinate lines, $g_{\alpha\beta}$ ($\alpha, \beta = 1, 2$) is called the *surface metric tensor* and a_α ($\alpha = 1, 2$) are

$$a_\alpha = \sqrt{g_{\alpha\alpha}}, \quad (\text{no sum on } \alpha) \quad (8.2.2)$$

Note that $\mathbf{g}_1 \cdot \mathbf{g}_2 = 0$ when the lines of principal curvature coincide with the coordinate lines.

The unit vector normal to the middle surface can be determined from

$$\hat{\mathbf{n}} = \frac{\mathbf{g}_1 \times \mathbf{g}_2}{a_1 a_2} \quad (8.2.3)$$

Further, we have the Weingarten–Gauss relations

$$\frac{\partial \hat{\mathbf{n}}}{\partial \xi_\alpha} = \frac{\mathbf{g}_\alpha}{R_\alpha}, \quad (\text{no sum on } \alpha) \quad (\text{theorem of Rodrigues}) \quad (8.2.4)$$

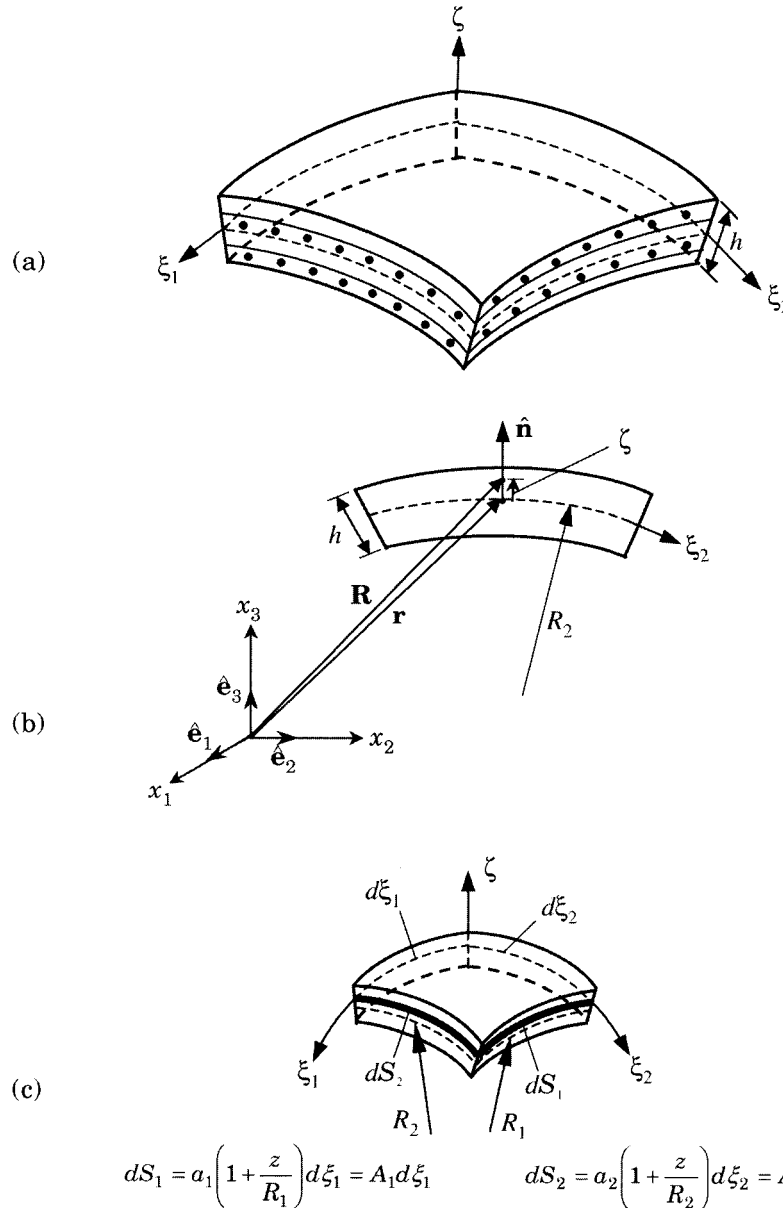


Figure 8.2.1: Geometry of a doubly-curved laminated shell. (a) Shell geometry. (b) Position vectors of points on the midsurface and above the midsurface. (c) A differential element of the shell (dS_1 and dS_2 denote the arc lengths).

$$\frac{\partial}{\partial \xi_2} \left(\frac{a_1}{R_1} \right) = \frac{1}{R_2} \frac{\partial a_1}{\partial \xi_2}, \quad \frac{\partial}{\partial \xi_1} \left(\frac{a_2}{R_2} \right) = \frac{1}{R_1} \frac{\partial a_2}{\partial \xi_1} \quad (\text{Codazzi conditions}) \quad (8.2.5)$$

The values of the principal radii of curvature of the middle surface are denoted by R_1 and R_2 (see Figure 8.2.1c). In general, $\hat{\mathbf{n}}$, R_1 and R_2 are functions of ξ_1 and ξ_2 .

The position vector \mathbf{R} of a point at a distance ζ from the middle surface can be expressed in terms of \mathbf{r} and $\hat{\mathbf{n}}$ by (see Figure 8.2.1b)

$$\mathbf{R} = \mathbf{r} + \zeta \hat{\mathbf{n}} \quad (8.2.6)$$

By differentiation we have

$$\frac{\partial \mathbf{R}}{\partial \xi_\alpha} = \mathbf{g}_\alpha + \zeta \frac{\partial \hat{\mathbf{n}}}{\partial \xi_\alpha} \equiv \mathbf{G}_\alpha \quad (8.2.7)$$

and using Eq. (8.2.4) we obtain

$$\mathbf{G}_\alpha = \frac{\partial \mathbf{R}}{\partial \xi_\alpha} = \left(1 + \frac{\zeta}{R_\alpha} \right) \mathbf{g}_\alpha, \quad (\text{no sum on } \alpha) \quad (8.2.8a)$$

and

$$G_{\alpha\beta} \equiv \mathbf{G}_\alpha \cdot \mathbf{G}_\beta \quad (8.2.8b)$$

Hence, the square of the distance dS between points (ξ_1, ξ_2, ζ) and $(\xi_1 + d\xi_1, \xi_2 + d\xi_2, \zeta + d\zeta)$ is given by

$$(dS)^2 = d\mathbf{R} \cdot d\mathbf{R} = A_1^2(d\xi_1)^2 + A_2^2(d\xi_2)^2 + A_3^2(d\zeta)^2 \quad (8.2.9a)$$

in which

$$d\mathbf{R} = \mathbf{G}_1 d\xi_1 + \mathbf{G}_2 d\xi_2 + \hat{\mathbf{n}} d\zeta, \quad (8.2.9b)$$

and A_1 , A_2 , and A_3 are the Lamé coefficients (see Fig. 8.2.1c)

$$A_1 = a_1 \left(1 + \frac{\zeta}{R_1} \right) = \sqrt{G_{11}}, \quad A_2 = a_2 \left(1 + \frac{\zeta}{R_2} \right) = \sqrt{G_{22}}, \quad A_3 = 1 \quad (8.2.10)$$

Note that vector \mathbf{G}_α is parallel to the vector \mathbf{g}_α . In view of the Codazzi conditions (8.2.5) and Eq. (8.2.10), it can be shown that the following relations between the derivatives of a_α and A_α hold:

$$\frac{1}{A_2} \frac{\partial A_1}{\partial \xi_2} = \frac{1}{a_2} \frac{\partial a_1}{\partial \xi_2}, \quad \frac{1}{A_1} \frac{\partial A_2}{\partial \xi_1} = \frac{1}{a_1} \frac{\partial a_2}{\partial \xi_1} \quad (8.2.11)$$

From Figure 8.2.1c the elements of area of the cross sections are

$$\begin{aligned} dS_1 d\zeta &= A_1 d\xi_1 d\zeta = a_1 \left(1 + \frac{\zeta}{R_1} \right) d\xi_1 d\zeta, \\ dS_2 d\zeta &= A_2 d\xi_2 d\zeta = a_2 \left(1 + \frac{\zeta}{R_2} \right) d\xi_2 d\zeta \end{aligned} \quad (8.2.12)$$

An elemental area of the middle surface ($\zeta = 0$) is determined by (see Figure 8.2.2a)

$$dA_0 = d\mathbf{r}_1 \times d\mathbf{r}_2 \cdot \hat{\mathbf{n}} = \left(\frac{\partial \mathbf{r}}{\partial \xi_1} \times \frac{\partial \mathbf{r}}{\partial \xi_2} \cdot \hat{\mathbf{n}} \right) d\xi_1 d\xi_2 = a_1 a_2 d\xi_1 d\xi_2 \quad (8.2.13)$$

and an elemental area of the surface at ζ is given by (see Figure 8.2.2b)

$$dA_\zeta = d\mathbf{R}_1 \times d\mathbf{R}_2 \cdot \hat{\mathbf{n}} = \left(\frac{\partial \mathbf{R}}{\partial \xi_1} \times \frac{\partial \mathbf{R}}{\partial \xi_2} \cdot \hat{\mathbf{n}} \right) d\xi_1 d\xi_2 = A_1 A_2 d\xi_1 d\xi_2 \quad (8.2.14)$$

The volume of a differential element above the midsurface is given by

$$dV = d\mathbf{R}_1 \times d\mathbf{R}_2 \cdot \hat{\mathbf{n}} d\zeta = dA_\zeta d\zeta = A_1 A_2 d\xi_1 d\xi_2 d\zeta \quad (8.2.15)$$

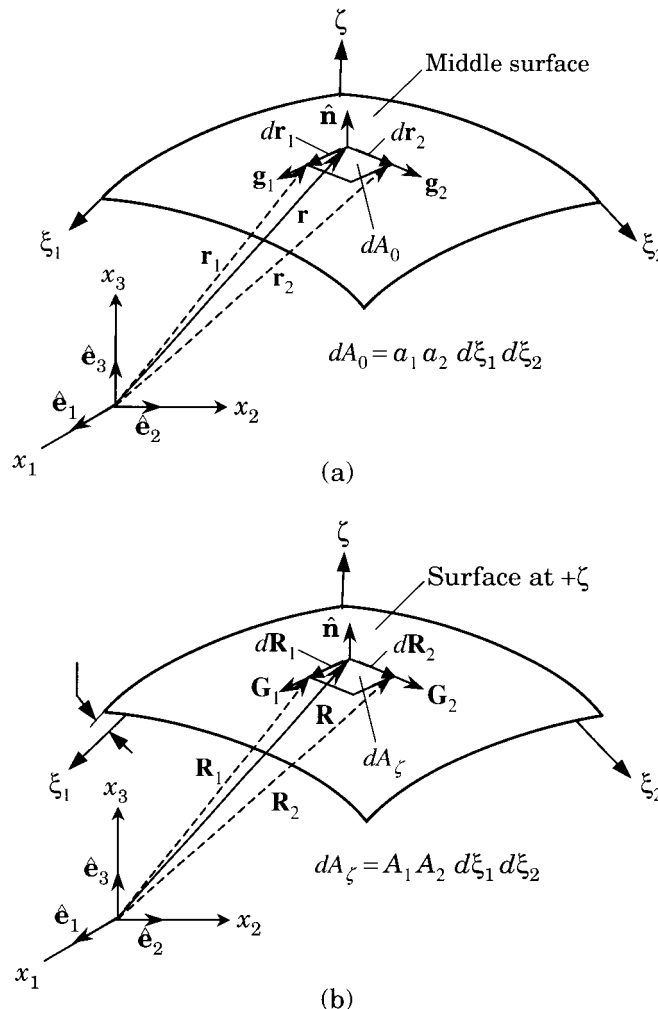


Figure 8.2.2: Surface area elements of a doubly-curved shell. (a) Area element on the midsurface. (b) Area element on a surface at $+\zeta$.

8.2.2 Kinetics of the Shell

Next, we introduce the stress resultants acting on a shell element. The tensile force measured per unit length along a ξ_2 coordinate line on a cross section perpendicular to a ξ_1 coordinate line (see Figure 8.2.1c) is $\sigma_{11} dS_2$. The total tensile force on the differential element in the ξ_1 direction can be computed by integrating over the entire thickness of the shell:

$$\int_{-h/2}^{h/2} \sigma_{11} dS_2 d\zeta = a_2 \left[\int_{-h/2}^{h/2} \sigma_{11} \left(1 + \frac{\zeta}{R_2} \right) d\zeta \right] d\xi_2 \equiv N_{11} a_2 d\xi_2 \quad (8.2.16)$$

where h is the total thickness of the shell, $\zeta = -h/2$ and $\zeta = h/2$ denote the bottom and top surfaces of the shell, and N_{11} is the membrane force per unit length in ξ_1 direction, acting on a surface perpendicular to the ξ_1 -coordinate (see Figure 8.2.3):

$$N_{11} = \int_{-h/2}^{h/2} \sigma_{11} \left(1 + \frac{\zeta}{R_2} \right) d\zeta \quad (8.2.17a)$$

Similarly the moment of the force $\sigma_{11} dS_2$ about the ξ_2 -axis is

$$M_{11} = \int_{-h/2}^{h/2} \zeta \sigma_{11} \left(1 + \frac{\zeta}{R_2} \right) d\zeta \quad (8.2.17b)$$

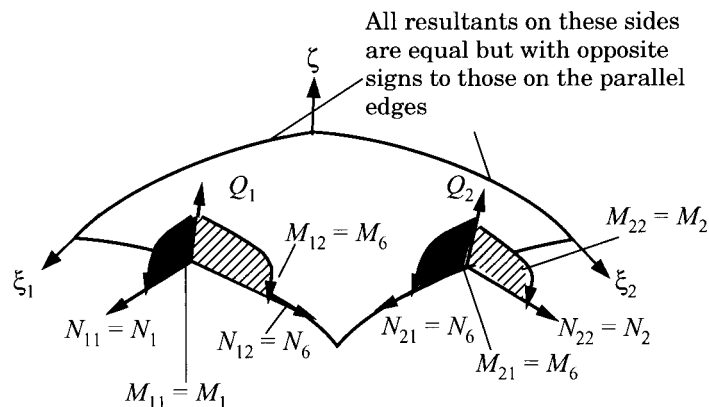


Figure 8.2.3: Stress resultants on a shell element.

Similarly, the remaining stress resultants per unit length (see Figure 8.2.3) can be defined as follows ($\sigma_1 = \sigma_{11}$, $\sigma_2 = \sigma_{22}$, $\sigma_6 = \sigma_{12}$, $\sigma_4 = \sigma_{23}$, $\sigma_5 = \sigma_{13}$):

$$\begin{Bmatrix} N_{11} \\ N_{22} \\ N_{12} \\ N_{21} \\ M_{11} \\ M_{22} \\ M_{12} \\ M_{21} \end{Bmatrix} = \int_{-h/2}^{h/2} \begin{Bmatrix} \sigma_1 \left(1 + \frac{\zeta}{R_2}\right) \\ \sigma_2 \left(1 + \frac{\zeta}{R_1}\right) \\ \sigma_6 \left(1 + \frac{\zeta}{R_2}\right) \\ \sigma_6 \left(1 + \frac{\zeta}{R_1}\right) \\ \zeta \sigma_1 \left(1 + \frac{\zeta}{R_2}\right) \\ \zeta \sigma_2 \left(1 + \frac{\zeta}{R_1}\right) \\ \zeta \sigma_6 \left(1 + \frac{\zeta}{R_2}\right) \\ \zeta \sigma_6 \left(1 + \frac{\zeta}{R_1}\right) \end{Bmatrix} d\zeta \quad (8.2.18)$$

Note that for shells, in general, $N_{\alpha\beta} \neq N_{\beta\alpha}$ and $M_{\alpha\beta} \neq M_{\beta\alpha}$ for $\alpha \neq \beta$ ($\alpha, \beta = 1, 2$). However, for shallow shells, one can neglect ζ/R_1 and ζ/R_2 and obtain $N_{\alpha\beta} = N_{\beta\alpha}$ and $M_{\alpha\beta} = M_{\beta\alpha}$, as in a plate theory. The shear forces Q_i are defined by

$$\begin{Bmatrix} Q_1 \\ Q_2 \end{Bmatrix} = K_s \int_{-h/2}^{h/2} \begin{Bmatrix} \sigma_5 \left(1 + \frac{\zeta}{R_2}\right) \\ \sigma_4 \left(1 + \frac{\zeta}{R_1}\right) \end{Bmatrix} d\zeta \quad (8.2.19)$$

where K_s is the shear correction factor.

8.2.3 Kinematics of the Shell

The linear normal and engineering shear strain components in an orthogonal curvilinear coordinate system are given by (no sum on repeated indices; see [37])

$$\varepsilon_i = \frac{\partial}{\partial \xi_i} \left(\frac{u_i}{A_i} \right) + \frac{1}{A_i} \sum_{k=1}^3 \frac{u_k}{A_k} \frac{\partial A_i}{\partial \xi_k} \quad (8.2.20a)$$

$$\gamma_{ij} = \frac{1}{A_i A_j} \left[A_i^2 \frac{\partial}{\partial \xi_j} \left(\frac{u_i}{A_i} \right) + A_j^2 \frac{\partial}{\partial \xi_i} \left(\frac{u_j}{A_j} \right) \right] \quad (i \neq j) \quad (8.2.20b)$$

where

$$\xi_3 = \zeta, \quad A_1 = a_1 \left(1 + \frac{\zeta}{R_1}\right), \quad A_2 = a_2 \left(1 + \frac{\zeta}{R_2}\right), \quad A_3 = a_3 = 1 \quad (8.2.21)$$

Substituting equation (8.2.21) into (8.2.20a,b) and making use of conditions (8.2.10) and (8.2.11), one obtains

$$\begin{aligned} \varepsilon_1 &= \frac{1}{A_1} \left(\frac{\partial u_1}{\partial \xi_1} + \frac{1}{a_2} \frac{\partial a_1}{\partial \xi_2} u_2 + \frac{a_1}{R_1} u_3 \right) \\ \varepsilon_2 &= \frac{1}{A_2} \left(\frac{\partial u_2}{\partial \xi_2} + \frac{1}{a_1} \frac{\partial a_2}{\partial \xi_1} u_1 + \frac{a_2}{R_2} u_3 \right) \end{aligned}$$

$$\begin{aligned}
\varepsilon_3 &= \frac{\partial u_3}{\partial \zeta} \\
\gamma_{23} &= \frac{1}{A_2} \frac{\partial u_3}{\partial \xi_2} + A_2 \frac{\partial}{\partial \zeta} \left(\frac{u_2}{A_2} \right) \equiv \varepsilon_4 \\
\gamma_{13} &= \frac{1}{A_1} \frac{\partial u_3}{\partial \xi_1} + A_1 \frac{\partial}{\partial \zeta} \left(\frac{u_1}{A_1} \right) \equiv \varepsilon_5 \\
\gamma_{12} &= \frac{A_2}{A_1} \frac{\partial}{\partial \xi_1} \left(\frac{u_2}{A_2} \right) + \frac{A_1}{A_2} \frac{\partial}{\partial \xi_2} \left(\frac{u_1}{A_1} \right) \equiv \varepsilon_6
\end{aligned} \tag{8.2.22}$$

In developing a moderately thick shell theory we make certain assumptions (as we did in the case of plates). They are outlined below [6,8,9,14]:

1. The transverse normal is inextensible (i.e., $\varepsilon_3 \approx 0$).
2. Normals to the reference surface of the shell before deformation remain straight but not necessarily normal after deformation (a relaxed Kirchhoff–Love hypothesis).
3. The shell deflections are small and strains are infinitesimal.
4. The transverse normal stress is negligible so that the plane stress assumption can be invoked.

Consistent with the assumptions of a moderately thick shell theory, we assume the following form of the displacement field:

$$\begin{aligned}
u_1(\xi_1, \xi_2, \zeta, t) &= u_0(\xi_1, \xi_2, t) + \zeta \phi_1(\xi_1, \xi_2, t) \\
u_2(\xi_1, \xi_2, \zeta, t) &= v_0(\xi_1, \xi_2, t) + \zeta \phi_2(\xi_1, \xi_2, t) \\
u_3(\xi_1, \xi_2, \zeta, t) &= w_0(\xi_1, \xi_2, t)
\end{aligned} \tag{8.2.23}$$

in which (u_0, v_0, w_0) are the displacements of a point $(\xi_1, \xi_2, 0)$ on the midsurface of the shell, and (ϕ_1, ϕ_2) are the rotations of a normal to the reference surface.

Substituting the displacement field into the strain-displacement relations (8.2.22), we obtain

$$\begin{aligned}
\varepsilon_1 &= \frac{1}{(1 + \zeta/R_1)} (\varepsilon_1^0 + \zeta \varepsilon_1^1), & \varepsilon_2 &= \frac{1}{(1 + \zeta/R_2)} (\varepsilon_2^0 + \zeta \varepsilon_2^1) \\
\varepsilon_6 &= \frac{1}{(1 + \zeta/R_1)} (\omega_1^0 + \zeta \omega_1^1) + \frac{1}{(1 + \zeta/R_2)} (\omega_2^0 + \zeta \omega_2^1) \\
\varepsilon_4 &= \frac{1}{(1 + \zeta/R_2)} \varepsilon_4^0, & \varepsilon_5 &= \frac{1}{(1 + \zeta/R_1)} \varepsilon_5^0
\end{aligned} \tag{8.2.24}$$

where

$$\begin{aligned}
\varepsilon_1^0 &= \frac{1}{a_1} \left(\frac{\partial u_0}{\partial \xi_1} + \frac{1}{a_2} \frac{\partial a_1}{\partial \xi_2} v_0 + \frac{a_1}{R_1} w_0 \right), & \varepsilon_2^0 &= \frac{1}{a_2} \left(\frac{\partial v_0}{\partial \xi_2} + \frac{1}{a_1} \frac{\partial a_2}{\partial \xi_1} u_0 + \frac{a_2}{R_2} w_0 \right) \\
\varepsilon_4^0 &= \frac{1}{a_2} \left(\frac{\partial w_0}{\partial \xi_2} + a_2 \phi_2 - \frac{a_2}{R_2} v_0 \right), & \varepsilon_5^0 &= \frac{1}{a_1} \left(\frac{\partial w_0}{\partial \xi_1} + a_1 \phi_1 - \frac{a_1}{R_1} u_0 \right) \\
\omega_1^0 &= \frac{1}{a_1} \left(\frac{\partial v_0}{\partial \xi_1} - \frac{1}{a_2} \frac{\partial a_1}{\partial \xi_2} u_0 \right), & \omega_2^0 &= \frac{1}{a_2} \left(\frac{\partial u_0}{\partial \xi_2} - \frac{1}{a_1} \frac{\partial a_2}{\partial \xi_1} v_0 \right)
\end{aligned}$$

$$\begin{aligned}\varepsilon_1^1 &= \frac{1}{a_1} \left(\frac{\partial \phi_1}{\partial \xi_1} + \frac{1}{a_2} \frac{\partial a_1}{\partial \xi_2} \phi_2 \right), & \varepsilon_2^1 &= \frac{1}{a_2} \left(\frac{\partial \phi_2}{\partial \xi_2} + \frac{1}{a_1} \frac{\partial a_2}{\partial \xi_1} \phi_1 \right) \\ \omega_1^1 &= \frac{1}{a_1} \left(\frac{\partial \phi_2}{\partial \xi_1} - \frac{1}{a_2} \frac{\partial a_1}{\partial \xi_2} \phi_1 \right), & \omega_2^1 &= \frac{1}{a_2} \left(\frac{\partial \phi_1}{\partial \xi_2} - \frac{1}{a_1} \frac{\partial a_2}{\partial \xi_1} \phi_2 \right)\end{aligned}\quad (8.2.25)$$

8.2.4 Equations of Motion

The displacement field (8.2.23) can be used to derive the governing equations of the first-order shear deformation theory of shells laminated of orthotropic layers by means of Hamilton's principle (or the dynamic version of the principle of virtual displacements). We have

$$\int_0^T \delta L dt \equiv \int_0^T [\delta K - (\delta U - \delta V)] dt = 0 \quad (8.2.26)$$

where δK denotes the virtual kinetic energy, δU the virtual strain energy, and δV the virtual potential energy due to the applied loads. To write the expressions for these virtual energies, let Ω denote the midsurface and Γ its boundary, with $\Gamma_{1\alpha}$ being the boundary normal to the ξ_α coordinate (and circle on the integral implies that it includes the total boundary of the shell. Then we have

$$\begin{aligned}\delta K &= \int_V \rho (\dot{u}_1 \delta \dot{u}_1 + \dot{u}_2 \delta \dot{u}_2 + \dot{u}_3 \delta \dot{u}_3) dV \\ &= \int_{\Omega} \int_{-h/2}^{h/2} \rho \left[(\dot{u}_0 + \zeta \dot{\phi}_1) (\delta \dot{u}_0 + \zeta \delta \dot{\phi}_1) + (\dot{v}_0 + \zeta \dot{\phi}_2) (\delta \dot{v}_0 + \zeta \delta \dot{\phi}_2) \right. \\ &\quad \left. + \dot{w}_0 \delta \dot{w}_0 \right] A_1 A_2 d\xi_1 d\xi_2 d\zeta \\ &= \int_{\Omega} \left[I_0 (\dot{u}_0 \delta \dot{u}_0 + \dot{v}_0 \delta \dot{v}_0 + \dot{w}_0 \delta \dot{w}_0) + I_1 (\dot{\phi}_1 \delta \dot{u}_0 + \dot{u}_0 \delta \dot{\phi}_1 + \dot{\phi}_2 \delta \dot{v}_0 + \dot{v}_0 \delta \dot{\phi}_2) \right. \\ &\quad \left. + I_2 (\dot{\phi}_1 \delta \dot{\phi}_1 + \dot{\phi}_2 \delta \dot{\phi}_2) \right] a_1 a_2 d\xi_1 d\xi_2 \quad (8.2.27)\end{aligned}$$

$$\begin{aligned}\delta U &= \int_V \sigma_{ij} \delta \varepsilon_{ij} dV = \int_{\Omega} \int_{-h/2}^{h/2} \sigma_{ij} \delta \varepsilon_{ij} A_1 A_2 d\xi_1 d\xi_2 d\zeta \\ &= \int_{\Omega} \left[N_{11} \delta \varepsilon_1^0 + M_{11} \delta \varepsilon_1^1 + N_{22} \delta \varepsilon_2^0 + M_{22} \delta \varepsilon_2^1 + N_{12} \delta \omega_1^0 + M_{12} \delta \omega_1^1 \right. \\ &\quad \left. + N_{21} \delta \omega_2^0 + M_{21} \delta \omega_2^1 + Q_2 \delta \varepsilon_4^0 + Q_1 \delta \varepsilon_5^0 \right] a_1 a_2 d\xi_1 d\xi_2 \quad (8.2.28)\end{aligned}$$

$$\begin{aligned}\delta V &= \int_{\Omega} \left(1 + \frac{h}{2R_1} \right) \left(1 + \frac{h}{2R_2} \right) q \delta w_0 a_1 a_2 d\xi_1 d\xi_2 \\ &\quad + \oint_{\Gamma_2} (\hat{N}_{11} \delta u_0 + \hat{M}_{11} \delta \phi_1 + \hat{N}_{12} \delta v_0 + \hat{M}_{12} \delta \phi_2 + \hat{Q}_1 \delta w_0) a_2 d\xi_2 \\ &\quad + \oint_{\Gamma_1} (\hat{N}_{22} \delta v_0 + \hat{M}_{22} \delta \phi_2 + \hat{N}_{21} \delta u_0 + \hat{M}_{21} \delta \phi_1 + \hat{Q}_2 \delta w_0) a_1 d\xi_1 \quad (8.2.29)\end{aligned}$$

where q is the transverse load on the upper surface ($\zeta = h/2$) of the shell, $(N_{\alpha\beta}, M_{\alpha\beta}, Q_\alpha)$ are the stress resultants defined in Eqs. (8.2.18) and (8.2.19), ρ is the mass density, and I_i are the mass inertias

$$I_i = \int_{-h/2}^{h/2} \rho \left(1 + \frac{\zeta}{R_1}\right) \left(1 + \frac{\zeta}{R_2}\right) (\zeta)^i d\zeta, \quad (i = 0, 1, 2) \quad (8.2.30)$$

A caret () on the stress resultants indicate that they are specified quantities.

To derive the Euler-Lagrange equations (or equations of motions of the shell) from Eq. (8.2.26), we substitute the expressions for δK , δU and δV , and then integrate the expressions by parts (or use the Green-Gauss theorem) to relieve the varied generalized displacements $(\delta u_0, \delta v_0, \delta w_0, \delta \phi_1, \delta \phi_2)$ of any derivatives with respect to ξ_1 , ξ_2 and t :

$$\begin{aligned} 0 = & - \int_0^T \int_{\Omega} \left[(I_0 \ddot{u}_0 + I_1 \ddot{\phi}_1) \delta u_0 + (I_0 \ddot{v}_0 + I_1 \ddot{\phi}_2) \delta v_0 + I_0 \ddot{w}_0 \delta w_0 \right. \\ & \quad \left. + (I_1 \ddot{u}_0 + I_2 \ddot{\phi}_1) \delta \phi_1 + (I_1 \ddot{v}_0 + I_2 \ddot{\phi}_2) \delta \phi_2 \right] a_1 a_2 d\xi_1 d\xi_2 dt \\ & + \int_{\Omega} \left[(I_0 \dot{u}_0 + I_1 \dot{\phi}_1) \delta u_0 + (I_0 \dot{v}_0 + I_1 \dot{\phi}_2) \delta v_0 + I_0 \dot{w}_0 \delta w_0 \right. \\ & \quad \left. + (I_1 \dot{u}_0 + I_2 \dot{\phi}_1) \delta \phi_1 + (I_1 \dot{v}_0 + I_2 \dot{\phi}_2) \delta \phi_2 \right]_0^T a_1 a_2 d\xi_1 d\xi_2 \\ & + \int_0^T \int_{\Omega} \left[(a_2 N_{11})_{,1} \delta u_0 - N_{11} a_{1,2} \delta v_0 - N_{11} \frac{a_1 a_2}{R_1} \delta w_0 \right. \\ & \quad \left. + (a_1 N_{22})_{,2} \delta v_0 - N_{22} a_{2,1} \delta u_0 - N_{22} \frac{a_1 a_2}{R_2} \delta w_0 \right. \\ & \quad \left. + (a_2 N_{12})_{,1} \delta v_0 + N_{12} a_{1,2} \delta u_0 + (a_1 N_{21})_{,2} \delta u_0 + N_{21} a_{2,1} \delta v_0 \right. \\ & \quad \left. + (a_2 M_{11})_{,1} \delta \phi_1 - M_{11} a_{1,2} \delta \phi_2 + (a_1 M_{22})_{,2} \delta \phi_2 - M_{22} a_{2,1} \delta \phi_1 \right. \\ & \quad \left. + (a_2 M_{12})_{,1} \delta \phi_2 + M_{12} a_{1,2} \delta \phi_1 + (a_1 M_{21})_{,2} \delta \phi_1 + M_{21} a_{2,1} \delta \phi_2 \right. \\ & \quad \left. + (a_2 Q_1)_{,1} \delta w_0 - Q_1 a_1 a_2 \delta \phi_1 + Q_1 \frac{a_1 a_2}{R_1} \delta u_0 \right. \\ & \quad \left. + (a_1 Q_2)_{,2} \delta w_0 - Q_2 a_1 a_2 \delta \phi_2 + Q_2 \frac{a_1 a_2}{R_2} \delta v_0 - q a_1 a_2 \right] d\xi_1 d\xi_2 dt \\ & + \int_0^T \oint_{\Gamma_2} \left[(\hat{N}_{11} - N_{11}) \delta u_0 + (\hat{N}_{12} - N_{12}) \delta v_0 + (\hat{M}_{11} - M_{11}) \delta \phi_1 \right. \\ & \quad \left. + (\hat{M}_{12} - M_{12}) \delta \phi_2 + (\hat{Q}_1 - Q_1) \delta w_0 \right] a_2 d\xi_2 \\ & + \int_0^T \oint_{\Gamma_1} \left[(\hat{N}_{21} - N_{21}) \delta u_0 + (\hat{N}_{22} - N_{22}) \delta v_0 + (\hat{M}_{21} - M_{21}) \delta \phi_1 \right. \\ & \quad \left. + (\hat{M}_{22} - M_{22}) \delta \phi_2 + (\hat{Q}_2 - Q_2) \delta w_0 \right] a_1 d\xi_1 \end{aligned} \quad (8.2.31)$$

Noting, by the hypothesis of Hamilton's principle, that the virtual generalized displacements are zero at $t = 0$ and $t = T$, the equations of motion and the natural (or force) boundary conditions are obtained by setting the coefficients of the varied generalized displacements to zero in Ω and on Γ_1 and Γ_2 :

$$\begin{aligned} \frac{\partial}{\partial \xi_1} (a_2 N_{11}) + \frac{\partial}{\partial \xi_2} (a_1 N_{21}) - N_{22} \frac{\partial a_2}{\partial \xi_1} + N_{12} \frac{\partial a_1}{\partial \xi_2} + \frac{a_1 a_2}{R_1} Q_1 \\ = a_1 a_2 \left(I_0 \frac{\partial^2 u_0}{\partial t^2} + I_1 \frac{\partial^2 \phi_1}{\partial t^2} \right) \end{aligned} \quad (8.2.32)$$

$$\begin{aligned} \frac{\partial}{\partial \xi_1} (a_2 N_{12}) + \frac{\partial}{\partial \xi_2} (a_1 N_{22}) - N_{11} \frac{\partial a_1}{\partial \xi_2} + N_{21} \frac{\partial a_2}{\partial \xi_1} + \frac{a_1 a_2}{R_2} Q_2 \\ = a_1 a_2 \left(I_0 \frac{\partial^2 v_0}{\partial t^2} + I_1 \frac{\partial^2 \phi_2}{\partial t^2} \right) \end{aligned} \quad (8.2.33)$$

$$\frac{\partial}{\partial \xi_1} (a_2 Q_1) + \frac{\partial}{\partial \xi_2} (a_1 Q_2) - a_1 a_2 \left(\frac{N_{11}}{R_1} + \frac{N_{22}}{R_2} \right) = q a_1 a_2 + a_1 a_2 I_0 \frac{\partial^2 w_0}{\partial t^2} \quad (8.2.34)$$

$$\begin{aligned} \frac{\partial}{\partial \xi_1} (a_2 M_{11}) + \frac{\partial}{\partial \xi_2} (a_1 M_{21}) - M_{22} \frac{\partial a_2}{\partial \xi_1} + M_{12} \frac{\partial a_1}{\partial \xi_2} - a_1 a_2 Q_1 \\ = a_1 a_2 \left(I_1 \frac{\partial^2 u_0}{\partial t^2} + I_0 \frac{\partial^2 \phi_1}{\partial t^2} \right) \end{aligned} \quad (8.2.35)$$

$$\begin{aligned} \frac{\partial}{\partial \xi_1} (a_2 M_{12}) + \frac{\partial}{\partial \xi_2} (a_1 M_{22}) - M_{11} \frac{\partial a_1}{\partial \xi_2} + M_{21} \frac{\partial a_2}{\partial \xi_1} - a_1 a_2 Q_2 \\ = a_1 a_2 \left(I_1 \frac{\partial^2 v_0}{\partial t^2} + I_0 \frac{\partial^2 \phi_2}{\partial t^2} \right) \end{aligned} \quad (8.2.36)$$

The natural boundary conditions are obvious from the boundary terms in Eq. (8.2.31).

In deriving the equations of motion, we have not assumed that $N_{\alpha\beta} = N_{\beta\alpha}$ and $M_{\alpha\beta} = M_{\beta\alpha}$ for $\alpha \neq \beta$. Vanishing of the moments about the normal to the differential element (see Figure 8.2.1c) yields an additional relation among the twisting moments and surface shear forces:

$$\frac{M_{21}}{R_2} - \frac{M_{12}}{R_1} + N_{21} - N_{12} = 0 \quad (8.2.37)$$

which must be accounted for in the formulation; otherwise, it will lead to inconsistency associated with rigid body rotations (i.e., a rigid body rotation gives a nonvanishing torsion except for flat plates and spherical shells). To account for this discrepancy, we must add the term (see Sanders [28] and Budiansky and Sanders [29])

$$\int_0^T \int_{\Omega} \left(\frac{M_{21}}{R_2} - \frac{M_{12}}{R_1} + N_{21} - N_{12} \right) \delta \phi_n a_1 a_2 d\xi_1 d\xi_2 dt \quad (8.2.38)$$

to the virtual strain energy functional δU . Here ϕ_n denotes the rotation about the transverse normal to the shell surface. This amounts to modifying ω_{α}^0 and ω_{α}^1 in Eq.

(8.2.25) as follows:

$$\begin{aligned}\tilde{\omega}_1^0 &= \frac{1}{a_1} \left(\frac{\partial v_0}{\partial \xi_1} - \frac{1}{a_2} \frac{\partial a_1}{\partial \xi_2} u_0 \right) - \phi_n, & \tilde{\omega}_2^0 &= \frac{1}{a_2} \left(\frac{\partial u_0}{\partial \xi_2} - \frac{1}{a_1} \frac{\partial a_2}{\partial \xi_1} v_0 \right) + \phi_n \\ \tilde{\omega}_1^1 &= \frac{1}{a_1} \left(\frac{\partial \phi_2}{\partial \xi_1} - \frac{1}{a_2} \frac{\partial a_1}{\partial \xi_2} \phi_1 \right) - \frac{\phi_n}{R_1}, & \tilde{\omega}_2^1 &= \frac{1}{a_2} \left(\frac{\partial \phi_1}{\partial \xi_2} - \frac{1}{a_1} \frac{\partial a_2}{\partial \xi_1} \phi_2 \right) + \frac{\phi_n}{R_2}\end{aligned}\quad (8.2.39)$$

The rotation ϕ_n is equal to the normal component of the curl of the displacement vector \mathbf{u}

$$\phi_n \equiv (\nabla \times \mathbf{u}) \cdot \hat{\mathbf{n}} = \frac{1}{2a_1 a_2} [(v_0 a_2)_{,1} - (u_0 a_1)_{,2}] \quad (8.2.40)$$

In view of Eq. (8.2.40), one can show that

$$\tilde{\omega}_1^0 = \tilde{\omega}_2^0 = \frac{1}{2a_1 a_2} \left[a_1 \frac{\partial u_0}{\partial \xi_2} + a_2 \frac{\partial v_0}{\partial \xi_1} - \left(u_0 \frac{\partial a_1}{\partial \xi_2} + v_0 \frac{\partial a_2}{\partial \xi_1} \right) \right] \quad (8.2.41)$$

Use of the modified strain-displacements relations (8.2.39) in Hamilton's principle yields the following equations of motion:

$$\begin{aligned}\frac{\partial}{\partial \xi_1} (a_2 N_{11}) + \frac{\partial}{\partial \xi_2} (a_1 \tilde{N}_{12}) - N_{22} \frac{\partial a_2}{\partial \xi_1} + \tilde{N}_{12} \frac{\partial a_1}{\partial \xi_2} + \frac{a_1 a_2}{R_1} Q_1 \\ + \frac{a_1}{2} \frac{\partial}{\partial \xi_2} \left(\frac{M_{12}}{R_1} - \frac{M_{21}}{R_2} \right) = a_1 a_2 \left(I_0 \frac{\partial^2 u_0}{\partial t^2} + I_1 \frac{\partial^2 \phi_1}{\partial t^2} \right)\end{aligned}\quad (8.2.42)$$

$$\begin{aligned}\frac{\partial}{\partial \xi_1} (a_2 \tilde{N}_{12}) + \frac{\partial}{\partial \xi_2} (a_1 N_{22}) - N_{11} \frac{\partial a_1}{\partial \xi_2} + \tilde{N}_{12} \frac{\partial a_2}{\partial \xi_1} + \frac{a_1 a_2}{R_2} Q_2 \\ + \frac{a_2}{2} \frac{\partial}{\partial \xi_1} \left(\frac{M_{21}}{R_2} - \frac{M_{12}}{R_1} \right) = a_1 a_2 \left(I_0 \frac{\partial^2 v_0}{\partial t^2} + I_1 \frac{\partial^2 \phi_2}{\partial t^2} \right)\end{aligned}\quad (8.2.43)$$

$$\frac{\partial}{\partial \xi_1} (a_2 Q_1) + \frac{\partial}{\partial \xi_2} (a_1 Q_2) - a_1 a_2 \left(\frac{N_{11}}{R_1} + \frac{N_{22}}{R_2} \right) = a_1 a_2 I_0 \frac{\partial^2 w_0}{\partial t^2} \quad (8.2.44)$$

$$\begin{aligned}\frac{\partial}{\partial \xi_1} (a_2 M_{11}) + \frac{\partial}{\partial \xi_2} (a_1 \tilde{M}_{12}) - M_{22} \frac{\partial a_2}{\partial \xi_1} + \tilde{M}_{12} \frac{\partial a_1}{\partial \xi_2} - a_1 a_2 Q_1 \\ = a_1 a_2 \left(I_1 \frac{\partial^2 u_0}{\partial t^2} + I_0 \frac{\partial^2 \phi_1}{\partial t^2} \right)\end{aligned}\quad (8.2.45)$$

$$\begin{aligned}\frac{\partial}{\partial \xi_1} (a_2 \tilde{M}_{12}) + \frac{\partial}{\partial \xi_2} (a_1 M_{22}) - M_{11} \frac{\partial a_1}{\partial \xi_2} + \tilde{M}_{12} \frac{\partial a_2}{\partial \xi_1} - a_1 a_2 Q_2 \\ = a_1 a_2 \left(I_1 \frac{\partial^2 v_0}{\partial t^2} + I_0 \frac{\partial^2 \phi_2}{\partial t^2} \right)\end{aligned}\quad (8.2.46)$$

where

$$\tilde{N}_{12} = \tilde{N}_{21} = \frac{1}{2} (N_{12} + N_{21}), \quad \tilde{M}_{12} = \tilde{M}_{21} = \frac{1}{2} (M_{12} + M_{21}) \quad (8.2.47)$$

8.2.5 Laminate Constitutive Relations

Suppose that the shell is composed of N orthotropic layers of uniform thickness, stacked on each other with the principal material 1 axis of the k th layer is oriented at an angle θ_k from the shell x_1 coordinate in the counterclockwise sense and $x_3^{(k)} = \zeta$. The stress-strain relations of the k th lamina, whether structural layer or actuating/sensing layer, in the shell coordinate system are given as

$$\left\{ \begin{array}{c} \sigma_1 \\ \sigma_2 \\ \sigma_4 \\ \sigma_5 \\ \sigma_6 \end{array} \right\}^{(k)} = \left[\begin{array}{ccccc} \bar{Q}_{11} & \bar{Q}_{12} & 0 & 0 & \bar{Q}_{16} \\ \bar{Q}_{12} & \bar{Q}_{22} & 0 & 0 & \bar{Q}_{26} \\ 0 & 0 & \bar{Q}_{44} & \bar{Q}_{45} & 0 \\ 0 & 0 & \bar{Q}_{45} & \bar{Q}_{55} & 0 \\ \bar{Q}_{16} & \bar{Q}_{26} & 0 & 0 & \bar{Q}_{66} \end{array} \right]^{(k)} \left\{ \begin{array}{c} \varepsilon_1 \\ \varepsilon_2 \\ \varepsilon_4 \\ \varepsilon_5 \\ \varepsilon_6 \end{array} \right\} - \left\{ \begin{array}{c} \bar{e}_{31} \\ \bar{e}_{32} \\ 0 \\ 0 \\ \bar{e}_{36} \end{array} \right\} H_\zeta \quad (8.2.48)$$

where \bar{Q}_{ij} are the transformed stiffnesses, and $Q_{ij}^{(k)}$ are the lamina stiffnesses referred to the principal material coordinates of the k th lamina

$$\begin{aligned} \bar{Q}_{11} &= Q_{11} \cos^4 \theta + 2(Q_{12} + 2Q_{66}) \sin^2 \theta \cos^2 \theta + Q_{22} \sin^4 \theta \\ \bar{Q}_{12} &= (Q_{11} + Q_{22} - 4Q_{66}) \sin^2 \theta \cos^2 \theta + Q_{12}(\sin^4 \theta + \cos^4 \theta) \\ \bar{Q}_{22} &= Q_{11} \sin^4 \theta + 2(Q_{12} + 2Q_{66}) \sin^2 \theta \cos^2 \theta + Q_{22} \cos^4 \theta \\ \bar{Q}_{16} &= (Q_{11} - Q_{12} - 2Q_{66}) \sin \theta \cos^3 \theta + (Q_{12} - Q_{22} + 2Q_{66}) \sin^3 \theta \cos \theta \\ \bar{Q}_{26} &= (Q_{11} - Q_{12} - 2Q_{66}) \sin^3 \theta \cos \theta + (Q_{12} - Q_{22} + 2Q_{66}) \sin \theta \cos^3 \theta \\ \bar{Q}_{66} &= (Q_{11} + Q_{22} - 2Q_{12} - 2Q_{66}) \sin^2 \theta \cos^2 \theta + Q_{66}(\sin^4 \theta + \cos^4 \theta) \\ \bar{Q}_{44} &= Q_{44} \cos^2 \theta + Q_{55} \sin^2 \theta \\ \bar{Q}_{45} &= (Q_{55} - Q_{44}) \cos \theta \sin \theta \\ \bar{Q}_{55} &= Q_{55} \cos^2 \theta + Q_{44} \sin^2 \theta \end{aligned} \quad (8.2.49a)$$

$$Q_{11} = \frac{E_1}{1 - \nu_{12}\nu_{21}}, \quad Q_{12} = \frac{\nu_{12}E_2}{1 - \nu_{12}\nu_{21}}, \quad Q_{22} = \frac{E_2}{1 - \nu_{12}\nu_{21}} \quad (8.2.49b)$$

The superscript k on Q_{ij} , θ , as well as on the engineering constants E_1 , E_2 , ν_{12} and so on, is omitted for brevity. In equation (8.2.48), H_ζ denotes the intensity of the electric or magnetic field and \bar{e}_{ij} are the electro- or magnetostrictive material coefficients

$$\begin{aligned} \bar{e}_{31} &= e_{31} \cos^2 \theta + e_{32} \sin^2 \theta \\ \bar{e}_{32} &= e_{32} \cos^2 \theta + e_{31} \sin^2 \theta \\ \bar{e}_{36} &= (e_{31} - e_{32}) \sin \theta \cos \theta \end{aligned} \quad (8.2.50)$$

Using the lamina constitutive equations, the stress resultants defined in Eqs. (8.2.18) and (8.2.19) can be expressed in terms of the membrane strains ε_α^0 and bending strains ε_α^1 . However, the laminate constitutive equations do not exhibit the symmetry among the stiffnesses (i.e., $A_{ij} \neq A_{ji}$, $B_{ij} \neq B_{ji}$ and $D_{ij} \neq D_{ji}$) primarily due to $N_{\alpha\beta} \neq N_{\beta\alpha}$ and $M_{\alpha\beta} \neq M_{\beta\alpha}$ for $\alpha \neq \beta$.

8.3 Theory of Doubly-Curved Shells

8.3.1 Equations of Motion

If we omit the term z/R in the definition of the stress resultants and assume that $a_{\alpha,\beta} = 0$ ($\alpha, \beta = 1, 2$) (i.e., constant radii of curvatures), the equations can be simplified substantially [14]. For thin shallow shells, we have

$$\left(1 + \frac{\zeta}{R_1}\right) \approx 1, \quad \left(1 + \frac{\zeta}{R_2}\right) \approx 1$$

and we have $N_{12} = N_{21}$ and $M_{12} = M_{21}$. The laminate constitutive relations become

$$\begin{Bmatrix} \{N\} \\ \{M\} \end{Bmatrix} = \begin{bmatrix} [A] & [B] \\ [B] & [D] \end{bmatrix} \begin{Bmatrix} \{\varepsilon^0\} \\ \{\kappa\} \end{Bmatrix} - \begin{Bmatrix} \{N\} \\ \{M\} \end{Bmatrix}^M \quad (8.3.1a)$$

$$\begin{Bmatrix} Q_2 \\ Q_1 \end{Bmatrix} = K_S \begin{bmatrix} A_{44} & A_{45} \\ A_{45} & A_{55} \end{bmatrix} \begin{Bmatrix} \varepsilon_4^0 \\ \varepsilon_5^0 \end{Bmatrix} - \begin{Bmatrix} Q_2^M \\ Q_1^M \end{Bmatrix} \quad (8.3.1b)$$

where the laminate stiffness coefficients (A_{ij}, B_{ij}, D_{ij}) are defined by

$$\begin{aligned} A_{ij} &= \sum_{k=1}^N \bar{Q}_{ij}^{(k)} (\zeta_{k+1} - \zeta_k), \quad i, j = 1, 2, 6 \\ B_{ij} &= \frac{1}{2} \sum_{k=1}^N \bar{Q}_{ij}^{(k)} (\zeta_{k+1}^2 - \zeta_k^2), \quad i, j = 1, 2, 6 \\ D_{ij} &= \frac{1}{3} \sum_{k=1}^N \bar{Q}_{ij}^{(k)} (\zeta_{k+1}^3 - \zeta_k^3), \quad i, j = 1, 2, 6 \\ A_{ij} &= \sum_{k=1}^N \bar{Q}_{ij}^{(k)} (\zeta_{k+1} - \zeta_k), \quad i, j = 4, 5 \end{aligned} \quad (8.3.2)$$

and the strains are given by [see Eqs. (8.2.25) and (8.2.39)]

$$\{\varepsilon^0\} = \begin{Bmatrix} \varepsilon_1^0 \\ \varepsilon_2^0 \\ \varepsilon_6^0 \end{Bmatrix}; \quad \{\varepsilon^1\} = \begin{Bmatrix} \varepsilon_1^1 \\ \varepsilon_2^1 \\ \varepsilon_6^1 \end{Bmatrix} \quad (8.3.3a)$$

and

$$\varepsilon_6^0 = \omega_1^0 + \omega_2^0 = 2\tilde{\omega}_1^0; \quad \varepsilon_6^1 = \omega_1^1 + \omega_2^1 \quad (8.3.3b)$$

and the magnetostrictive stress resultants $\{N^M\}$ and $\{M^M\}$ are defined as

$$\begin{aligned} \begin{Bmatrix} N_1^M \\ N_2^M \end{Bmatrix} &= \sum_{k=m_1, m_2, \dots}^N \int_{\zeta_k}^{\zeta_{k+1}} \begin{Bmatrix} \bar{e}_{31} \\ \bar{e}_{32} \end{Bmatrix} H_\zeta d\zeta \\ &= ck_c \sum_{k=m_1, m_2, \dots}^N \int_{\zeta_k}^{\zeta_{k+1}} \begin{Bmatrix} \bar{e}_{31} \\ \bar{e}_{32} \end{Bmatrix} \frac{\partial w_0}{\partial t} d\zeta \equiv \begin{Bmatrix} \mathcal{A}_{31} \\ \mathcal{A}_{32} \end{Bmatrix} \frac{\partial w_0}{\partial t} \end{aligned} \quad (8.3.4a)$$

$$\begin{aligned} \begin{Bmatrix} M_1^M \\ M_2^M \end{Bmatrix} &= \sum_{k=m_1, m_2, \dots}^N \int_{\zeta_k}^{\zeta_{k+1}} \begin{Bmatrix} \bar{e}_{31} \\ \bar{e}_{32} \end{Bmatrix} \zeta H_\zeta d\zeta \\ &= ck_c \sum_{k=m_1, m_2, \dots}^N \int_{\zeta_k}^{\zeta_{k+1}} \begin{Bmatrix} \bar{e}_{31} \\ \bar{e}_{32} \end{Bmatrix} \frac{\partial w_0}{\partial t} \zeta d\zeta \equiv \begin{Bmatrix} \mathcal{B}_{31} \\ \mathcal{B}_{32} \end{Bmatrix} \frac{\partial w_0}{\partial t} \end{aligned} \quad (8.3.4b)$$

where

$$\mathcal{A}_{ij} = ck_c \sum_{k=m_1, m_2, \dots} \bar{e}_{ij}^{(k)} (\zeta_{k+1} - \zeta_k), \quad i = 3; j = 1, 2 \quad (8.3.5a)$$

$$\mathcal{B}_{ij} = \frac{1}{2} ck_c \sum_{k=m_1, m_2, \dots} \bar{e}_{ij}^{(k)} (\zeta_{k+1}^2 - \zeta_k^2), \quad i = 3; j = 1, 2 \quad (8.3.5b)$$

and m_1, m_2, \dots denote the layer numbers of the magnetostrictive (or any actuating/sensing) layers.

Then equations of motion of the simplified theory in the Cartesian coordinate system ($x_1, x_2, x_3 = \zeta$) (note that $N_{12} = N_{21} = N_6$ and $M_{12} = M_{21} = M_6$) are

$$\frac{\partial N_1}{\partial x_1} + \frac{\partial}{\partial x_2} (N_6 + C_0 M_6) + \frac{Q_1}{R_1} = I_0 \frac{\partial^2 u_0}{\partial t^2} + I_1 \frac{\partial^2 \phi_1}{\partial t^2} \quad (8.3.6)$$

$$\frac{\partial}{\partial x_1} (N_6 - C_0 M_6) + \frac{\partial N_2}{\partial x_2} + \frac{Q_2}{R_2} = I_0 \frac{\partial^2 v_0}{\partial t^2} + I_1 \frac{\partial^2 \phi_2}{\partial t^2} \quad (8.3.7)$$

$$\frac{\partial Q_1}{\partial x_1} + \frac{\partial Q_2}{\partial x_2} - \left(\frac{N_1}{R_1} + \frac{N_2}{R_2} \right) + q = I_1 \frac{\partial^2 w_0}{\partial t^2} \quad (8.3.8)$$

$$\frac{\partial M_1}{\partial x_1} + \frac{\partial M_6}{\partial x_2} - Q_1 = I_2 \frac{\partial^2 \phi_1}{\partial t^2} + I_1 \frac{\partial^2 u_0}{\partial t^2} \quad (8.3.9)$$

$$\frac{\partial M_6}{\partial x_1} + \frac{\partial M_2}{\partial x_2} - Q_2 = I_2 \frac{\partial^2 \phi_2}{\partial t^2} + I_1 \frac{\partial^2 v_0}{\partial t^2} \quad (8.3.10)$$

$$C_0 = \frac{1}{2} \left(\frac{1}{R_1} - \frac{1}{R_2} \right), \quad \frac{1}{\partial x_i} = \frac{1}{\alpha_i} \frac{1}{\partial \xi_i}, \quad (i = 1, 2)$$

$$I_i = \sum_{k=1}^N \int_{\zeta_k}^{\zeta_{k+1}} \rho^{(k)} (\zeta)^i \, d\zeta \quad (i = 0, 1, 2) \quad (8.3.11)$$

and $\rho^{(k)}$ being the density of the k th layer and n is the number of layers in the laminate.

8.3.2 Analytical Solution

Analytical solutions of the equations (8.3.6)–(8.3.10) can be obtained for simply supported cross-ply laminated shells [34]. Towards using the Navier type solution, first we write the equations of motion (8.3.6)–(8.3.10) in terms of displacements ($u_0, v_0, w_0, \phi_1, \phi_2$) by substituting for the force and moment resultants from equations (8.3.1a,b) into Eqs. (8.3.6)–(8.3.10):

$$\begin{aligned} & A_{11} \left(\frac{\partial^2 u_0}{\partial x_1^2} + \frac{1}{R_1} \frac{\partial w_0}{\partial x_1} \right) + A_{12} \left(\frac{\partial^2 v_0}{\partial x_1 \partial x_2} + \frac{1}{R_2} \frac{\partial w_0}{\partial x_1} \right) + A_{16} \left(\frac{\partial^2 v_0}{\partial x_1^2} + \frac{\partial^2 u_0}{\partial x_1 \partial x_2} \right) \\ & + B_{11} \frac{\partial^2 \phi_1}{\partial x_1^2} + B_{12} \frac{\partial^2 \phi_2}{\partial x_1 \partial x_2} + B_{16} \left[\frac{\partial^2 \phi_2}{\partial x_1^2} + \frac{\partial^2 \phi_1}{\partial x_1 \partial x_2} - C_0 \left(\frac{\partial^2 v_0}{\partial x_1^2} - \frac{\partial^2 u_0}{\partial x_1 \partial x_2} \right) \right] \\ & + A_{16} \left(\frac{\partial^2 u_0}{\partial x_1 \partial x_2} + \frac{1}{R_1} \frac{\partial w_0}{\partial x_2} \right) + A_{26} \left(\frac{\partial^2 v_0}{\partial x_2^2} + \frac{1}{R_2} \frac{\partial w_0}{\partial x_2} \right) + A_{66} \left(\frac{\partial^2 v_0}{\partial x_1 \partial x_2} + \frac{\partial^2 u_0}{\partial x_2^2} \right) \end{aligned}$$

$$\begin{aligned}
& + B_{16} \frac{\partial^2 \phi_1}{\partial x_1 \partial x_2} + B_{26} \frac{\partial^2 \phi_2}{\partial x_2^2} + B_{66} \left[\frac{\partial^2 \phi_2}{\partial x_1 \partial x_2} + \frac{\partial^2 \phi_1}{\partial x_2^2} - C_0 \left(\frac{\partial^2 v_0}{\partial x_1 \partial x_2} - \frac{\partial^2 u_0}{\partial x_2^2} \right) \right] \\
& - \mathcal{A}_{31} \frac{\partial^2 w_0}{\partial x_1 \partial t} + \frac{1}{R_1} \left[K_S A_{44} \left(\phi_1 + \frac{\partial w_0}{\partial x_1} - \frac{u_0}{R_1} \right) + K_S A_{45} \left(\phi_2 + \frac{\partial w_0}{\partial x_2} - \frac{v_0}{R_2} \right) \right] \\
& - I_0 \frac{\partial^2 u_0}{\partial t^2} - I_1 \frac{\partial^2 \phi_1}{\partial t^2} = 0
\end{aligned} \tag{8.3.12}$$

$$\begin{aligned}
& A_{12} \left(\frac{\partial^2 u_0}{\partial x_1 \partial x_2} + \frac{1}{R_1} \frac{\partial w_0}{\partial x_2} \right) + A_{22} \left(\frac{\partial^2 v_0}{\partial x_2^2} + \frac{1}{R_2} \frac{\partial w_0}{\partial x_2} \right) + A_{26} \left(\frac{\partial^2 v_0}{\partial x_1 \partial x_2} + \frac{\partial^2 u_0}{\partial x_2^2} \right) \\
& + B_{12} \frac{\partial^2 \phi_1}{\partial x_1 \partial x_2} + B_{22} \frac{\partial^2 \phi_2}{\partial x_2^2} + B_{26} \left[\frac{\partial^2 \phi_2}{\partial x_1 \partial x_2} + \frac{\partial^2 \phi_1}{\partial x_2^2} - C_0 \left(\frac{\partial^2 v_0}{\partial x_1 \partial x_2} - \frac{\partial^2 u_0}{\partial x_2^2} \right) \right] \\
& + A_{16} \left(\frac{\partial^2 u_0}{\partial x_1^2} + \frac{1}{R_1} \frac{\partial w_0}{\partial x_1} \right) + A_{26} \left(\frac{\partial^2 v_0}{\partial x_1 \partial x_2} + \frac{1}{R_2} \frac{\partial w_0}{\partial x_1} \right) + A_{66} \left(\frac{\partial^2 v_0}{\partial x_1^2} + \frac{\partial^2 u_0}{\partial x_1 \partial x_2} \right) \\
& + B_{16} \frac{\partial^2 \phi_1}{\partial x_1^2} + B_{26} \frac{\partial^2 \phi_2}{\partial x_1 \partial x_2} + B_{66} \left[\frac{\partial^2 \phi_2}{\partial x_1^2} + \frac{\partial^2 \phi_1}{\partial x_2 \partial x_1} - C_0 \left(\frac{\partial^2 v_0}{\partial x_1^2} - \frac{\partial^2 u_0}{\partial x_1 \partial x_2} \right) \right] \\
& - \mathcal{A}_{32} \frac{\partial^2 w_0}{\partial x_2 \partial t} + \frac{1}{R_2} \left[K_S A_{45} \left(\phi_1 + \frac{\partial w_0}{\partial x_1} - \frac{u_0}{R_1} \right) + K_S A_{55} \left(\phi_2 + \frac{\partial w_0}{\partial x_2} - \frac{v_0}{R_2} \right) \right] \\
& - I_0 \frac{\partial^2 v_0}{\partial t^2} - I_1 \frac{\partial^2 \phi_2}{\partial t^2} = 0
\end{aligned} \tag{8.3.13}$$

$$\begin{aligned}
& K_S A_{45} \left(\frac{\partial^2 w_0}{\partial x_1 \partial x_2} + \frac{\partial \phi_2}{\partial x_1} - \frac{1}{R_2} \frac{\partial v_0}{\partial x_1} \right) + K_S A_{55} \left(\frac{\partial^2 w_0}{\partial^2 x_1} + \frac{\partial \phi_1}{\partial x_1} - \frac{1}{R_1} \frac{\partial u_0}{\partial x_1} \right) \\
& + K_S A_{44} \left(\frac{\partial^2 w_0}{\partial^2 x_2} + \frac{\partial \phi_2}{\partial x_2} - \frac{1}{R_2} \frac{\partial v_0}{\partial x_2} \right) + K_S A_{45} \left(\frac{\partial^2 w_0}{\partial x_1 \partial x_2} + \frac{\partial \phi_1}{\partial x_2} - \frac{1}{R_1} \frac{\partial u_0}{\partial x_2} \right) \\
& - \frac{1}{R_1} \left\{ A_{11} \left(\frac{\partial u_0}{\partial x_1} + \frac{w_0}{R_1} \right) + A_{12} \left(\frac{\partial v_0}{\partial x_2} + \frac{w_0}{R_2} \right) + A_{16} \left(\frac{\partial v_0}{\partial x_1} + \frac{\partial u_0}{\partial x_2} \right) \right. \\
& \left. + B_{11} \frac{\partial \phi_1}{\partial x_1} + B_{12} \frac{\partial \phi_2}{\partial x_2} + B_{16} \left[\frac{\partial \phi_2}{\partial x_1} + \frac{\partial \phi_1}{\partial x_2} - C_0 \left(\frac{\partial v_0}{\partial x_1} + \frac{\partial u_0}{\partial x_2} \right) \right] - \mathcal{A}_{31} \frac{\partial w_0}{\partial t} \right\} \\
& - \frac{1}{R_2} \left\{ A_{12} \left(\frac{\partial u_0}{\partial x_1} + \frac{w_0}{R_1} \right) + A_{22} \left(\frac{\partial v_0}{\partial x_2} + \frac{w_0}{R_2} \right) + A_{26} \left(\frac{\partial v_0}{\partial x_1} - \frac{\partial u_0}{\partial x_2} \right) \right. \\
& \left. + B_{12} \frac{\partial \phi_1}{\partial x_1} + B_{22} \frac{\partial \phi_2}{\partial x_1} + B_{26} \left[\frac{\partial \phi_2}{\partial x_1} + \frac{\partial \phi_1}{\partial x_2} - C_0 \left(\frac{\partial v_0}{\partial x_1} - \frac{\partial u_0}{\partial x_2} \right) \right] - \mathcal{A}_{32} \frac{\partial w_0}{\partial t} \right\} \\
& + q - I_1 \frac{\partial^2 w_0}{\partial t^2} = 0
\end{aligned} \tag{8.3.14}$$

$$\begin{aligned}
& B_{11} \left(\frac{\partial^2 u_0}{\partial x_1^2} + \frac{1}{R_1} \frac{\partial w_0}{\partial x_1} \right) + B_{12} \left(\frac{\partial^2 v_0}{\partial x_1 \partial x_2} + \frac{1}{R_2} \frac{\partial w_0}{\partial x_1} \right) + B_{16} \left(\frac{\partial^2 v_0}{\partial x_1^2} + \frac{\partial^2 u_0}{\partial x_1 \partial x_2} \right) \\
& + D_{11} \frac{\partial^2 \phi_1}{\partial x_1^2} + D_{12} \frac{\partial^2 \phi_2}{\partial x_1 \partial x_2} + D_{16} \left[\frac{\partial^2 \phi_2}{\partial x_1^2} + \frac{\partial^2 \phi_1}{\partial x_1 \partial x_2} - C_0 \left(\frac{\partial^2 v_0}{\partial x_1^2} - \frac{\partial^2 u_0}{\partial x_1 \partial x_2} \right) \right] \\
& + B_{16} \left(\frac{\partial^2 u_0}{\partial x_1 \partial x_2} + \frac{1}{R_1} \frac{\partial w_0}{\partial x_2} \right) + B_{26} \left(\frac{\partial^2 v_0}{\partial x_2^2} + \frac{1}{R_2} \frac{\partial w_0}{\partial x_2} \right) + B_{66} \left(\frac{\partial^2 v_0}{\partial x_1 \partial x_2} + \frac{\partial^2 u_0}{\partial x_2^2} \right)
\end{aligned}$$

$$\begin{aligned}
& + D_{16} \frac{\partial^2 \phi_1}{\partial x_1 \partial x_2} + D_{26} \frac{\partial^2 \phi_2}{\partial x_2^2} + D_{66} \left[\frac{\partial^2 \phi_2}{\partial x_1 \partial x_2} + \frac{\partial^2 \phi_1}{\partial x_2^2} - C_0 \left(\frac{\partial^2 v_0}{\partial x_1 \partial x_2} - \frac{\partial^2 u_0}{\partial x_2^2} \right) \right] \\
& + K_S A_{45} \left(\frac{\partial w_0}{\partial x_2} + \phi_2 - \frac{v_0}{R_2} \right) + K_S A_{55} \left(\frac{\partial u_3}{\partial x_1} + \phi_1 - \frac{u_0}{R_1} \right) - B_{31} \frac{\partial^2 w_0}{\partial x_1 \partial t} \\
& - I_2 \frac{\partial^2 \phi_1}{\partial t^2} - I_1 \frac{\partial^2 u_0}{\partial t^2} = 0
\end{aligned} \tag{8.3.15}$$

$$\begin{aligned}
& B_{16} \left(\frac{\partial^2 u_0}{\partial x_1^2} + \frac{1}{R_1} \frac{\partial w_0}{\partial x_1} \right) + B_{26} \left(\frac{\partial^2 v_0}{\partial x_1 \partial x_2} + \frac{1}{R_2} \frac{\partial w_0}{\partial x_1} \right) + B_{66} \left(\frac{\partial^2 v_0}{\partial x_1^2} + \frac{\partial^2 u_0}{\partial x_1 \partial x_2} \right) \\
& + D_{16} \frac{\partial^2 \phi_1}{\partial x_1^2} + D_{26} \frac{\partial^2 \phi_2}{\partial x_1 \partial x_2} + D_{66} \left[\frac{\partial^2 \phi_2}{\partial x_1^2} + \frac{\partial^2 \phi_1}{\partial x_1 \partial x_2} - C_0 \left(\frac{\partial^2 v_0}{\partial x_1^2} - \frac{\partial^2 u_0}{\partial x_1 \partial x_2} \right) \right] \\
& + B_{12} \left(\frac{\partial^2 u_0}{\partial x_1 \partial x_2} + \frac{1}{R_1} \frac{\partial w_0}{\partial x_2} \right) + B_{22} \left(\frac{\partial^2 v_0}{\partial x_2^2} + \frac{1}{R_2} \frac{\partial w_0}{\partial x_2} \right) + B_{66} \left(\frac{\partial^2 v_0}{\partial x_1 \partial x_2} + \frac{\partial^2 u_0}{\partial x_2^2} \right) \\
& + D_{12} \frac{\partial^2 \phi_1}{\partial x_1 \partial x_2} + D_{22} \frac{\partial^2 \phi_2}{\partial x_2^2} + D_{26} \left[\frac{\partial^2 \phi_2}{\partial x_1 \partial x_2} + \frac{\partial^2 \phi_1}{\partial x_2^2} - C_0 \left(\frac{\partial^2 v_0}{\partial x_1 \partial x_2} - \frac{\partial^2 u_0}{\partial x_2^2} \right) \right] \\
& + K_S A_{44} \left(\frac{\partial w_0}{\partial x_2} + \phi_2 - \frac{u_2}{R_2} \right) + K_S A_{45} \left(\frac{\partial w_0}{\partial x_1} + \phi_1 - \frac{u_0}{R_1} \right) - B_{32} \frac{\partial^2 u_0}{\partial x_2 \partial t} \\
& - I_2 \frac{\partial^2 \phi_2}{\partial t^2} - I_1 \frac{\partial^2 u_0}{\partial t^2} = 0
\end{aligned} \tag{8.3.16}$$

The simply supported boundary conditions (SS-1) for the first-order shear deformation shell theory are

$$\begin{aligned}
u_1(x_1, 0, t) &= 0, \quad u_1(x_1, b, t) = 0, \quad u_2(0, x_2, t) = 0, \quad u_2(a, x_2, t) = 0 \\
N_1(0, x_2, t) &= 0, \quad N_1(a, x_2, t) = 0, \quad N_2(x_1, 0, t) = 0, \quad N_2(x_1, b, t) = 0 \\
\phi_1(x_1, 0, t) &= 0, \quad \phi_1(x_1, b, t) = 0, \quad \phi_2(0, x_2, t) = 0, \quad \phi_2(a, x_2, t) = 0 \\
u_3(x_1, 0, t) &= 0, \quad u_3(x_2, b, t) = 0, \quad u_3(0, x_2, t) = 0, \quad u_3(a, x_2, t) = 0 \\
M_1(0, x_2, t) &= 0, \quad M_1(a, x_2, t) = 0, \quad M_2(x_1, 0, t) = 0, \quad M_2(x_1, b, t) = 0
\end{aligned} \tag{8.3.17}$$

The simply supported boundary conditions in (8.3.17) are satisfied by the following expansions of the generalized displacement field:

$$\begin{aligned}
u_0(x_1, x_2, t) &= \sum_{n=1}^{\infty} \sum_{m=1}^{\infty} U_{mn}(t) \cos \alpha x_1 \sin \beta x_2 \\
v_0(x_1, x_2, t) &= \sum_{n=1}^{\infty} \sum_{m=1}^{\infty} V_{mn}(t) \sin \alpha x_1 \cos \beta x_2 \\
w_0(x_1, x_2, t) &= \sum_{n=1}^{\infty} \sum_{m=1}^{\infty} W_{mn}(t) \sin \alpha x_1 \sin \beta x_2 \\
\phi_1(x_1, x_2, t) &= \sum_{n=1}^{\infty} \sum_{m=1}^{\infty} X_{mn}(t) \cos \alpha x_1 \sin \beta x_2 \\
\phi_2(x_1, x_2, t) &= \sum_{n=1}^{\infty} \sum_{m=1}^{\infty} Y_{mn}(t) \sin \alpha x_1 \cos \beta x_2
\end{aligned} \tag{8.3.18}$$

Substituting the expansions (8.3.18) into equations (8.3.12)-(8.3.16) yields the equations

$$\begin{aligned} & \left[\begin{array}{ccccc} S_{11} & S_{12} & S_{13} & S_{14} & S_{15} \\ S_{21} & S_{22} & S_{23} & S_{24} & S_{25} \\ S_{31} & S_{32} & S_{33} & S_{34} & S_{35} \\ S_{41} & S_{42} & S_{43} & S_{44} & S_{45} \\ S_{51} & S_{52} & S_{53} & S_{54} & S_{55} \end{array} \right] \left\{ \begin{array}{c} U_{mn} \\ V_{mn} \\ W_{mn} \\ X_{mn} \\ Y_{mn} \end{array} \right\} + \left[\begin{array}{ccccc} 0 & 0 & C_{13} & 0 & 0 \\ 0 & 0 & C_{23} & 0 & 0 \\ 0 & 0 & C_{33} & 0 & 0 \\ 0 & 0 & C_{43} & 0 & 0 \\ 0 & 0 & C_{53} & 0 & 0 \end{array} \right] \left\{ \begin{array}{c} \dot{U}_{mn} \\ \dot{V}_{mn} \\ \dot{W}_{mn} \\ \dot{X}_{mn} \\ \dot{Y}_{mn} \end{array} \right\} \\ & + \left[\begin{array}{ccccc} M_{11} & 0 & 0 & M_{14} & 0 \\ 0 & M_{22} & 0 & 0 & M_{25} \\ 0 & 0 & M_{33} & 0 & 0 \\ M_{41} & 0 & 0 & M_{44} & 0 \\ 0 & M_{52} & 0 & 0 & M_{55} \end{array} \right] \left\{ \begin{array}{c} \ddot{U}_{mn} \\ \ddot{V}_{mn} \\ \ddot{W}_{mn} \\ \ddot{X}_{mn} \\ \ddot{Y}_{mn} \end{array} \right\} = \left\{ \begin{array}{c} 0 \\ 0 \\ Q_{mn} \\ 0 \\ 0 \end{array} \right\} \end{aligned} \quad (8.3.19)$$

where $S_{ij} = S_{ji}$, $C_{ij} = M_{ji}$ ($i, j = 1, 2, \dots, 5$) are defined by (only nonzero elements are given)

$$\begin{aligned} S_{11} &= A_{11}\alpha^2 + (A_{66} + 2C_0B_{66} + C_0^2D_{66})\beta^2 + \frac{K_S A_{55}}{R_1^2} \\ S_{12} &= (A_{12} + A_{66} - C_0^2D_{66})\alpha\beta \\ S_{13} &= -\left[\frac{1}{R_1}(A_{11} + K_S A_{55}) + \frac{A_{12}}{R_2}\right]\alpha \\ S_{14} &= B_{11}\alpha^2 + (B_{66} + C_0D_{66})\beta^2 - \frac{K_S A_{55}}{R_1} \\ S_{15} &= (B_{12} + B_{66} + C_0D_{66})\alpha\beta \\ S_{22} &= (A_{66} - 2C_0B_{66} + C_0^2D_{66})\alpha^2 + A_{22}\beta^2 + \frac{K_S A_{44}}{R_2^2} \\ S_{23} &= -\left(\frac{1}{R_1}A_{12} + \frac{1}{R_2}A_{22} + \frac{K_S A_{44}}{R_2}\right)\beta \\ S_{24} &= (B_{12} + B_{66} - C_0D_{66})\alpha\beta \\ S_{25} &= (B_{66} - C_0D_{66})\alpha^2 + B_{22}\beta^2 - \frac{K_S A_{44}}{R_2} \\ S_{33} &= K_S A_{55}\alpha^2 + K_S A_{44}\beta^2 + \frac{A_{11}}{R_1^2} + \frac{2A_{12}}{R_1 R_2} + \frac{A_{22}}{R_2^2} \\ S_{34} &= -\left(\frac{B_{11}}{R_1} + \frac{B_{12}}{R_2}\right)\alpha, \quad S_{35} = \left[K_S A_{44} - \left(\frac{B_{12}}{R_1} + \frac{B_{22}}{R_2}\right)\right]\beta \\ S_{44} &= D_{11}\alpha^2 + D_{66}\beta^2 + K_S A_{55}, \quad S_{45} = (D_{12} + D_{66})\alpha\beta \\ S_{55} &= D_{66}\alpha^2 + D_{22}\beta^2 + K_S A_{44} \end{aligned} \quad (8.3.20)$$

$$M_{11} = M_{22} = M_{33} = I_0, \quad M_{14} = M_{25} = I_1, \quad M_{44} = M_{55} = I_2 \quad (8.3.21)$$

$$C_{13} = A_{31}\alpha, \quad C_{23} = A_{32}\beta, \quad C_{33} = \frac{A_{32}}{R_2} + \frac{A_{31}}{R_1}$$

$$C_{43} = B_{31}\alpha, \quad C_{53} = B_{32}\beta \quad (8.3.22)$$

and all other $C_{ij} = 0$. Here the magnetostrictive coefficients A_{31} , A_{32} , B_{31} and B_{32} are defined in Eqs. (8.3.5a,b).

Static Analysis

For static analysis, we set the time derivatives terms in Eq. (8.3.19) to zero and solve the resulting equations for the amplitudes U_{mn} , V_{mn} , W_{mn} , X_{mn} and Y_{mn} . The total solution is obtained by substituting the amplitudes into Eq. (8.3.18). As an example consider simply supported cross-ply laminated spherical shell panels ($R_1 = R_2 = R$) under uniformly distributed load of intensity q_0 . The lamina material properties are assumed to be [15,36]

$$E_1 = 25E_2, \quad G_{23} = 0.2E_2, \quad G_{13} = G_{12} = 0.5E_2, \quad \nu_{12} = 0.25 \quad (8.3.23)$$

Table 8.3.1 contains nondimensionalized center deflections, $\bar{w} = 10^3 w_0 E_2 h^3 / (q_0 a^4)$, for various values of radius-to-side (R/a) ratios and two values of side-to-thickness (a/h) ratios (see Figure 8.3.1).

Table 8.3.1: Nondimensional^a center deflection versus radius-to-thickness ratio of spherical shells under uniformly distributed load (19-term Navier solution).

R/a	$0^\circ/90^\circ$		$0^\circ/90^\circ/0^\circ$		$0^\circ/90^\circ/90^\circ/0^\circ$	
	$a/h = 100$	$a/h = 10$	$a/h = 100$	$a/h = 10$	$a/h = 100$	$a/h = 10$
1	0.0718	6.054	0.0718	4.8173	0.0715	4.8366
2	0.2855	12.668	0.2858	8.0210	0.2844	8.0517
3	0.6441	15.739	0.6224	9.1148	0.6246	9.1463
4	1.1412	17.184	1.0443	9.5686	1.0559	9.5999
5	1.7535	19.944	1.5118	9.7937	1.5358	9.8249
10	5.5428	19.065	3.6445	10.110	3.7208	10.141
10^{30}	16.980	19.469	6.6970	10.220	6.8331	10.251

$$^a \bar{w} = [w E_2 h^3 / (q_0 a^4)] 10^3$$

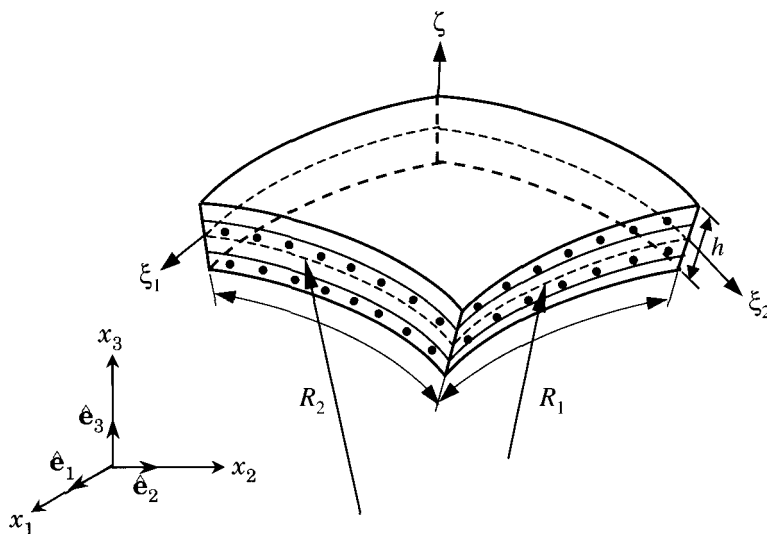


Figure 8.3.1: Geometry of a doubly-curved shell panel.

Natural Vibration

For natural vibration without structural damping, we set all $C_{ij} = 0$ and assume solution of the form

$$\begin{aligned} U_{mn}(t) &= U_{mn}^0 e^{i\omega t}, \quad V_{mn}(t) = V_{mn}^0 e^{i\omega t}, \quad W_{mn}(t) = W_{mn}^0 e^{i\omega t} \\ X_{mn}(t) &= X_{mn}^0 e^{i\omega t}, \quad Y_{mn}(t) = Y_{mn}^0 e^{i\omega t} \end{aligned} \quad (8.3.24)$$

in (8.3.19). Substitution of (8.3.24) in (8.3.19) yields

$$\left(\begin{bmatrix} S_{11} & S_{12} & S_{13} & S_{14} & S_{15} \\ S_{21} & S_{22} & S_{23} & S_{24} & S_{25} \\ S_{31} & S_{32} & S_{33} & S_{34} & S_{35} \\ S_{41} & S_{42} & S_{43} & S_{44} & S_{45} \\ S_{51} & S_{52} & S_{53} & S_{54} & S_{55} \end{bmatrix} - \omega^2 \begin{bmatrix} M_{11} & 0 & 0 & M_{14} & 0 \\ 0 & M_{22} & 0 & 0 & M_{25} \\ 0 & 0 & M_{33} & 0 & 0 \\ M_{41} & 0 & 0 & M_{44} & 0 \\ 0 & M_{52} & 0 & 0 & M_{55} \end{bmatrix} \right) \begin{Bmatrix} U_{mn}^0 \\ V_{mn}^0 \\ W_{mn}^0 \\ X_{mn}^0 \\ Y_{mn}^0 \end{Bmatrix} = \begin{Bmatrix} 0 \\ 0 \\ 0 \\ 0 \\ 0 \end{Bmatrix} \quad (8.3.25)$$

which is an eigenvalue problem. For nontrivial solution, the determinant of the matrix in the parenthesis is set to zero. This gives values of ω^2 .

Table 8.3.2 contains nondimensionalized fundamental natural frequencies, $\bar{\omega} = \omega(a^2/h)\sqrt{\rho/E_2}$, for cross-ply laminated spherical shell panels [14,34]. Results for three different laminates and two different thickness ($a/h = 10$ and $a/h = 100$) are presented using a shear correction factor of $K_s = 5/6$. The case $R/a = 10^{-30}$ corresponds to a square plate.

Table 8.3.2: Nondimensionalized fundamental frequencies^a ($\bar{\omega} = \omega a^2 \sqrt{\rho/E_2}/h$), versus radius-to-side length ratio of spherical shells ($a/b = 1$, $R_1 = R_2$, and $K_s = 5/6$)

R/a	0°/90°		0°/90°/0°		0°/90°/90°/0°	
	$a/h = 100$	$a/h = 10$	$a/h = 100$	$a/h = 10$	$a/h = 100$	$a/h = 10$
1	125.93	14.481	125.99	16.115	126.33	16.172
2	67.362	10.749	68.075	13.382	68.294	13.447
3	46.002	9.9608	47.265	12.731	47.415	12.795
4	35.228	9.4102	36.971	12.487	37.082	12.552
5	28.825	9.2309	30.993	12.372	31.079	12.437
10	16.706	8.9841	20.347	12.215	20.380	12.280
10^{30}	9.6873	8.8998	15.183	12.162	15.184	12.226

Vibration Control

For vibration control, we assume $q = 0$ and seek solution of the ordinary differential equations in (8.3.20) in the form

$$\begin{aligned} U_{mn}(t) &= U_0 e^{\lambda t}, & V_{mn}(t) &= V_0 e^{\lambda t} \\ W_{mn}(t) &= W_0 e^{\lambda t}, & X_{mn}(t) &= X_0 e^{\lambda t} \\ Y_{mn}(t) &= Y_0 e^{\lambda t} \end{aligned} \quad (8.3.26)$$

Substituting Eq. (8.3.26) into Eq. (8.3.20), we obtain, for a non-trivial solution, the result

$$\begin{vmatrix} \bar{S}_{11} & \bar{S}_{12} & \bar{S}_{13} & \bar{S}_{14} & \bar{S}_{15} \\ \bar{S}_{21} & \bar{S}_{22} & \bar{S}_{23} & \bar{S}_{24} & \bar{S}_{25} \\ \bar{S}_{31} & \bar{S}_{32} & \bar{S}_{33} & \bar{S}_{34} & \bar{S}_{35} \\ \bar{S}_{41} & \bar{S}_{42} & \bar{S}_{43} & \bar{S}_{44} & \bar{S}_{45} \\ \bar{S}_{51} & \bar{S}_{52} & \bar{S}_{53} & \bar{S}_{54} & \bar{S}_{55} \end{vmatrix} = 0 \quad (8.3.27)$$

where

$$\bar{S}_{ij} = S_{ij} + \lambda C_{ij} + \lambda^2 M_{ij} \quad (8.3.28)$$

for $i, j = 1, 2, 3, 4, 5$. This equation gives five sets of eigenvalues. The eigenvalue with the lowest imaginary part corresponds to the transverse motion, $W_{mn}(t)$. The eigenvalues can be written as $\lambda = -\alpha + i\omega_d$, so that the damped motion is given by

$$w_0(x_1, x_2, t) = \frac{1}{\omega_d} e^{-\alpha t} \sin \omega_d t \sin \frac{n\pi x_1}{a} \sin \frac{n\pi x_2}{b} \quad (8.3.29)$$

In arriving at the last solution, the following boundary conditions are used:

$$\begin{aligned} u_0(x_1, x_2, 0) &= 0, & \dot{u}_0(x_1, x_2, 0) &= 0, & v_0(x_1, x_2, 0) &= 0, \\ \dot{v}_0(x_1, x_2, 0) &= 0, & w_0(x_1, x_2, 0) &= 0, & \dot{w}_0(x_1, x_2, 0) &= 1, \\ \phi_1(x_1, x_2, 0) &= 0, & \dot{\phi}_1(x_1, x_2, 0) &= 0, & \phi_2(x_1, x_2, 0) &= 0, \\ \dot{\phi}_2(x_1, x_2, 0) &= 0 \end{aligned} \quad (8.3.30)$$

Numerical results are obtained for various lamination schemes to show the influence of the position of the pair of magnetostrictive layers from the neutral axis on the amplitude suppression time [38,39]. All values of the composite material and structural constants are tabulated and both damped and undamped frequencies are presented in the figures.

The composite lamina material properties were given in Table 7.7.1. Magnetostrictive material properties (for Terfenol-D material) are taken to be [see Eq. (7.7.22)]

$$E_m = 26.5 \text{ GPa}, \quad \nu_m = 0.0, \quad \rho_m = 9250 \text{ kg-m}^{-3}, \quad d_k = 1.67^{-8} \text{ mA}^{-1}, \quad C(t)r_c = 10^4$$

The numerical values of various material and structural constants (e.g., moment of inertia, magnetostrictive material constants) based on different lamination schemes and material properties [CFRP, Graphite-Epoxy (Gr-Ep), Glass-Epoxy (Gl-Ep), Boron-Epoxy (Br-Ep)] are listed in Tables 8.3.3 and 8.3.4. Magnetostrictive damping coefficients and natural frequencies for various materials and lamination schemes are also listed in Table 8.3.4.

Table 8.3.3: Stiffnesses for different laminates and materials.

Material	Laminate	$D_{11}(10^3)$ [N m]	$D_{12}(10^3)$ [N m]	$D_{22}(10^3)$ [N m]	$D_{66}(10^3)$ [N m]	$A_{44}(10^7)$ [N/m]
CFRP	[0/90/0/90/ m] _S	0.768	0.182	0.454	0.348	0.616
	[0/90/0/ m /90] _S	0.776	0.197	0.410	0.375	0.616
	[0/90/ m /0/90] _S	0.687	0.226	0.425	0.430	0.616
	[0/ m /90/0/90] _S	0.710	0.270	0.292	0.512	0.616
	[m /0/90/0/90] _S	0.532	0.329	0.323	0.621	0.616
	[0/0/ m /90/90] _S	0.949	0.226	0.164	0.430	0.616
	[90/90/ m /0/0] _S	0.164	0.226	0.949	0.430	0.616
Gr-Ep	[0/90/ m /0/90] _S	0.687	0.265	0.427	0.640	0.751
Gl-Ep	[0/90/ m /0/90] _S	0.358	0.866	0.278	0.772	0.715
Br-Ep	[0/90/ m /0/90] _S	1.032	0.516	0.659	0.626	0.661

Table 8.3.4: Mass inertias and parameters α and ω_{dr} .

Material	Laminate	I_0 [kg/m]	$I_2(10^{-4})$ [kg m]	$-\mathcal{E}_{31}$	$-\alpha \pm \omega_{dr}$ (rad s ⁻¹)
CFRP	[0/90/0/90/ m] _S	33.092	0.157	0.926	4.63
	[0/90/0/ m /90] _S	33.092	0.187	0.926	13.9
	[0/90/ m /0/90] _S	33.092	0.246	0.926	23.1
	[0/ m /90/0/90] _S	33.092	0.335	0.926	32.4
	[m /0/90/0/90] _S	33.092	0.454	0.926	41.7
	[0/0/ m /90/90] _S	33.092	0.246	0.926	23.1
	[90/90/ m /0/0] _S	33.092	0.246	0.926	23.1
Gr-Ep	[0/90/ m /0/90] _S	30.1	0.220	0.926	23.1
Gl-Ep	[0/90/ m /0/90] _S	33.7	0.251	0.926	23.1
Br-Ep	[0/90/ m /0/90] _S	34.1	0.255	0.926	23.1

The value of α [see Eq. (8.3.29)] increases when the magnetostrictive layer is located farther away from the neutral axis, indicating faster vibration suppression. Figure 8.3.2 shows the uncontrolled and controlled deflection amplitude at the center of the laminate. It is observed from Figure 8.3.3 that [**m**/0/90/0/90]_S \equiv [**m**/(0/90)₂]_S has the maximum vibration suppression. Present results also show that the vibration suppression time decreases very rapidly as mode number increases. Figures 8.3.4 shows a plot of vibration amplitude for mode 5, for a ten-layered [0/90/**m**/0/90]_S laminate. It can be observed that attenuation favors the higher modes. This is clearly seen in Figure 8.3.5, where modes 1 and 2 are superposed and it is obvious that mode 2 attenuates at a significantly faster rate.

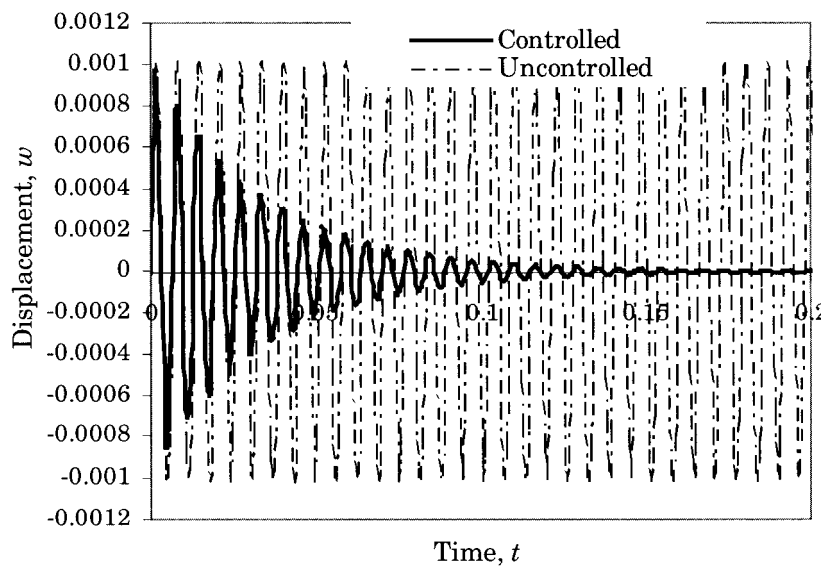


Figure 8.3.2: Comparison of controlled (—) and uncontrolled (----) motion at the midpoint of the shell for the lay-up $[m/0/90/0/90]_s$.

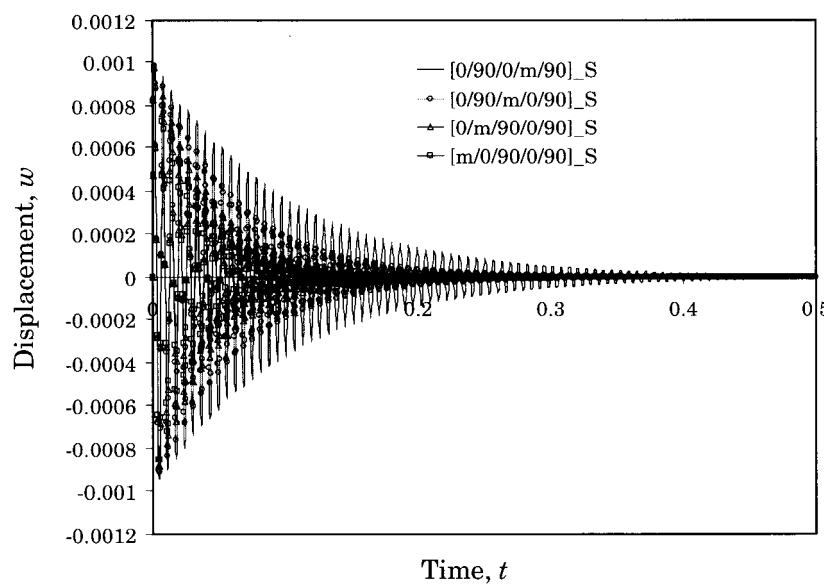


Figure 8.3.3: Controlled motion at the midpoint of the shell for different lamination schemes.

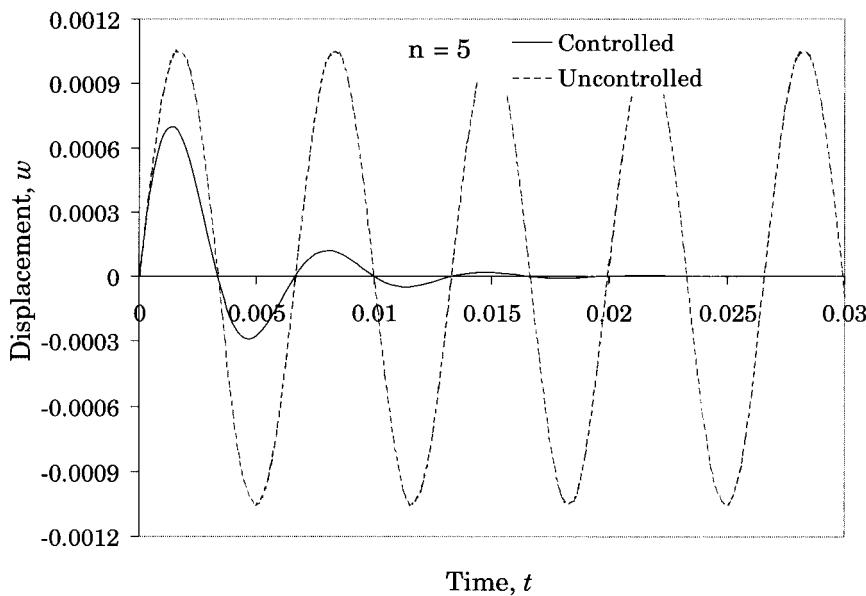


Figure 8.3.4: Comparison of controlled (—) and uncontrolled (----) motion at the midpoint of the shell for the lay-up $[m/0/90/0/90]_S$.

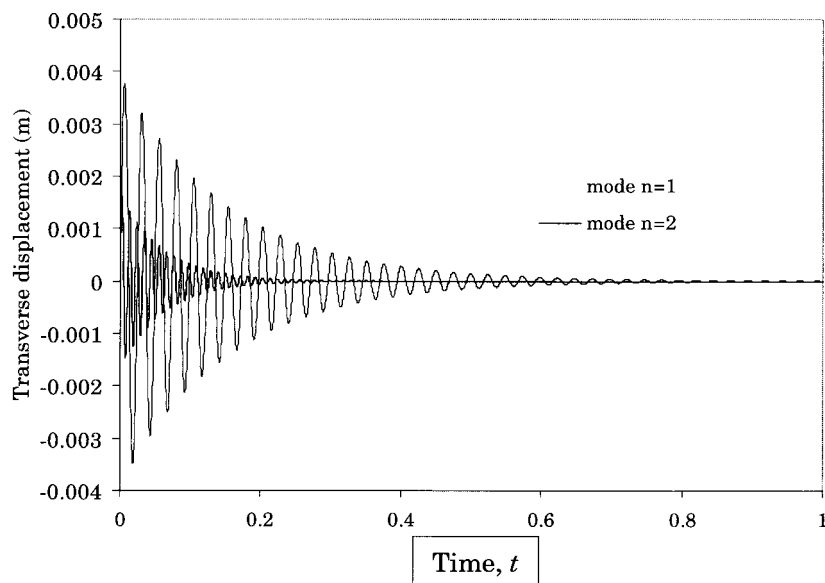


Figure 8.3.5: Comparison of original and controlled motion at the midpoint of the shell for modes $n = 1, 2$ (lay-up $[0/90/m/0/90]_S$).

8.4 Vibration and Buckling of Cross-Ply Laminated Circular Cylindrical Shells

8.4.1 Equations of Motion

The equations of motion of the first-order shear deformation shell theory (FST) of a laminated circular cylindrical shell are (see [14,40,41]; cf. (8.3.6)–(8.3.10) with $C_0 = 0$, $1/R_1 = 0$ and $R_2 = R$):

$$\begin{aligned} \frac{\partial N_1}{\partial x_1} + \frac{\partial N_6}{\partial x_2} &= I_0 \ddot{u}_0 + I_1 \ddot{\phi}_1 \\ \frac{\partial N_6}{\partial x_1} + \frac{\partial N_2}{\partial x_2} + \frac{Q_2}{R} &= I_0 \ddot{u}_0 + I_1 \ddot{\phi}_2 \\ \frac{\partial M_1}{\partial x_1} + \frac{\partial M_6}{\partial x_2} - Q_1 &= I_1 \ddot{u}_0 + I_2 \ddot{\phi}_1 \\ \frac{\partial M_6}{\partial x_1} + \frac{\partial M_2}{\partial x_2} - Q_2 &= I_1 \ddot{v}_0 + I_2 \ddot{\phi}_2 \\ \frac{\partial Q_1}{\partial x_1} + \frac{\partial Q_2}{\partial x_2} - \frac{N_2}{R} - \hat{N} \frac{\partial^2 w_0}{\partial x_1^2} &= I_0 \ddot{w}_0 \end{aligned} \quad (8.4.1)$$

where R is the radius of the cylinder; \hat{N} is the axial compressive load (positive in compression); u_0, v_0 and w_0 are the displacement components along the x_1, x_2 and $x_3 = \zeta$ axes (see Figure 8.4.1); ϕ_1 and ϕ_2 are the rotation functions; a superposed dot indicates differentiation with respect to time t ; and I_i ($i = 0, 1, 2$) are the mass inertia terms defined as

$$I_i = \sum_{k=1}^N \int_{\zeta_{k+1}}^{\zeta_k} \rho^{(k)} \zeta^i \, d\zeta, \quad i = 0, 1, 2 \quad (8.4.2)$$

N is the total number of layers and $\rho^{(k)}$ is the material mass density of the k th layer.

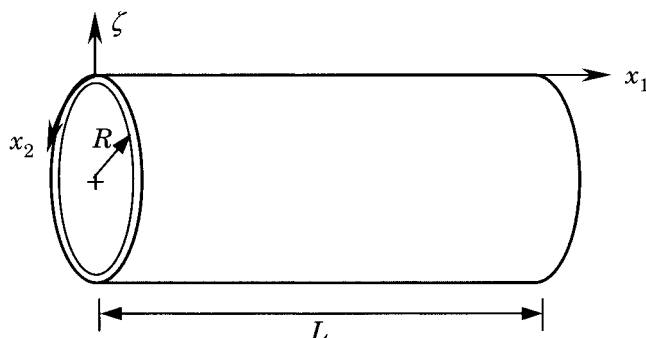


Figure 8.4.1: Laminated shell geometry and coordinate system.

For a general cross-ply laminate (i.e., a laminated shell with stiffnesses $A_{16} = A_{26} = A_{45} = B_{16} = B_{26} = D_{16} = D_{26} = 0$), the stress resultants are given by

$$\begin{aligned} N_1 &= A_{11}\varepsilon_1^0 + A_{12}\varepsilon_2^0 + B_{11}\varepsilon_1^1 + B_{12}\varepsilon_2^1 \\ N_2 &= A_{12}\varepsilon_1^0 + A_{22}\varepsilon_2^0 + B_{12}\varepsilon_1^1 + B_{22}\varepsilon_2^1 \\ M_1 &= B_{11}\varepsilon_1^0 + B_{12}\varepsilon_2^0 + D_{11}\varepsilon_1^1 + D_{12}\varepsilon_2^1 \\ M_2 &= B_{12}\varepsilon_1^0 + B_{22}\varepsilon_2^0 + D_{12}\varepsilon_1^1 + D_{22}\varepsilon_2^1 \\ N_6 &= A_{66}\varepsilon_6^0 + B_{66}\varepsilon_6^1, \quad M_6 = B_{66}\varepsilon_6^0 + D_{66}\varepsilon_6^1 \\ Q_1 &= K_{55}^2 A_{55}\varepsilon_5^0, \quad Q_2 = K_{44}^2 A_{44}\varepsilon_4^0 \end{aligned} \quad (8.4.3)$$

where K_{44}^2 and K_{55}^2 are the shear correction factors, and the strains are defined as

$$\begin{aligned} \varepsilon_1^0 &= \frac{\partial u_0}{\partial x_1}, & \varepsilon_1^1 &= \frac{\partial \phi_1}{\partial x_1} \\ \varepsilon_2^0 &= \frac{\partial v_0}{\partial x_2} + \frac{w_0}{R}, & \varepsilon_2^1 &= \frac{\partial \phi_2}{\partial x_2} \\ \varepsilon_6^0 &= \frac{\partial v_0}{\partial x_1} + \frac{\partial u_0}{\partial x_2}, & \varepsilon_6^1 &= \frac{\partial \phi_2}{\partial x_1} + \frac{\partial \phi_1}{\partial x_2} \\ \varepsilon_4^0 &= \phi_2 + \frac{\partial w_0}{\partial x_2}, & \varepsilon_5^0 &= \phi_1 + \frac{\partial w_0}{\partial x_1} \end{aligned} \quad (8.4.4)$$

The equations of motion of the classical shell theory (CST) are obtained from equations (8.4.1) by setting

$$\phi_1 = -\frac{\partial w_0}{\partial x_1}, \quad \phi_2 = -\frac{\partial w_0}{\partial x_2} \quad (8.4.5)$$

The equations of motion can be expressed in terms of generalized displacements ($u_0, v_0, w_0, \phi_1, \phi_2$) by substituting Eqs. (8.4.4) [and Eq. (8.4.5) in the case of CST] into equations (8.4.3) and the subsequent results into equations (8.4.1):

$$[L]\{\Delta\} = \{0\} \quad (8.4.6)$$

where the coefficients of the linear operator L ($L_{ij} = L_{ji}$) and displacement vector $\{\Delta\}$ for FST and CST are given below.

Classical shell theory (CST): $\{\Delta\} = \{u_0, v_0, w_0\}^T$

$$\begin{aligned} L_{11} &= A_{11} \frac{\partial^2}{\partial x_1^2} + A_{66} \frac{\partial^2}{\partial x_2^2} - I_0 \frac{\partial^2}{\partial t^2}, \quad L_{12} = (A_{12} + A_{66}) \frac{\partial^2}{\partial x_1 \partial x_2} \\ L_{13} &= -B_{11} \frac{\partial^2}{\partial x_1^3} - (B_{12} + 2B_{66}) \frac{\partial^3}{\partial x_1 \partial x_2^2} + \frac{A_{12}}{R} \frac{\partial}{\partial x_1} + I_1 \frac{\partial^3}{\partial x_1 \partial t^2} \\ L_{22} &= A_{66} \frac{\partial^2}{\partial x_1^2} + A_{22} \frac{\partial^2}{\partial x_2^2} - I_0 \frac{\partial^2}{\partial t^2} \\ L_{23} &= -(B_{12} + 2B_{66}) \frac{\partial^3}{\partial x_1^2 \partial x_2} - B_{22} \frac{\partial^3}{\partial x_2^2} + \frac{A_{22}}{R} \frac{\partial}{\partial x_2} + I_1 \frac{\partial^3}{\partial x_2 \partial t^2} \\ L_{33} &= D_{11} \frac{\partial^4}{\partial x_1^4} + 2(D_{12} + 2D_{66}) \frac{\partial^4}{\partial x_1^2 \partial x_2^2} + D_{22} \frac{\partial^4}{\partial x_2^4} + \left(\hat{N} - 2 \frac{B_{12}}{R} \right) \frac{\partial^2}{\partial x_1^2} \\ &\quad + \frac{A_{22}}{R^2} - 2 \frac{B_{22}}{R} \frac{\partial^2}{\partial x_2^2} + I_0 \frac{\partial^2}{\partial t^2} - I_2 \frac{\partial^2}{\partial t^2} \left(\frac{\partial^2}{\partial x_1^2} + \frac{\partial^2}{\partial x_2^2} \right) \end{aligned} \quad (8.4.7)$$

Note that the longitudinal, circumferential and rotary inertia terms are included.

First-order shell theory (FST): $\{\Delta\} = \{u_0, v_0, \phi_1, \phi_2, w_0\}^T$

$$\begin{aligned}
 L_{11} &= A_{11} \frac{\partial^2}{\partial x_1^2} + A_{66} \frac{\partial^2}{\partial x_2^2} - I_0 \frac{\partial^2}{\partial t^2}, & L_{12} &= (A_{12} + A_{66}) \frac{\partial^2}{\partial x_1 \partial x_2} \\
 L_{13} &= B_{11} \frac{\partial^2}{\partial x_1^2} + B_{66} \frac{\partial^2}{\partial x_2^2} - I_1 \frac{\partial^2}{\partial t^2}, & L_{14} &= (B_{12} + B_{66}) \frac{\partial^2}{\partial x_1 \partial x_2} \\
 L_{22} &= A_{66} \frac{\partial^2}{\partial x_1^2} + A_{22} \frac{\partial^2}{\partial x_2^2} - I_0 \frac{\partial^2}{\partial t^2}, & L_{15} &= \frac{A_{12}}{R} \frac{\partial}{\partial x_1} \\
 L_{24} &= B_{66} \frac{\partial^2}{\partial x_1^2} + B_{22} \frac{\partial^2}{\partial x_2^2} - I_1 \frac{\partial^2}{\partial t^2}, & L_{23} &= L_{14} \\
 L_{33} &= -K_{55}^2 A_{55} + D_{11} \frac{\partial^2}{\partial x_1^2} + D_{66} \frac{\partial^2}{\partial x_2^2} - I_2 \frac{\partial^2}{\partial t^2}, & L_{25} &= \frac{A_{22}}{R} \frac{\partial}{\partial x_2} \\
 L_{35} &= \left(\frac{B_{12}}{R} - K_{55}^2 A_{55} \right) \frac{\partial}{\partial x_1}, & L_{34} &= (D_{12} + D_{66}) \frac{\partial^2}{\partial x_1 \partial x_2} \\
 L_{44} &= -K_{44}^2 A_{44} + D_{66} \frac{\partial^2}{\partial x_1^2} + D_{22} \frac{\partial^2}{\partial x_2^2} - I_2 \frac{\partial^2}{\partial t^2}, & L_{45} &= \left(\frac{B_{22}}{R} - K_{44}^2 A_{44} \right) \frac{\partial}{\partial x_2} \\
 L_{55} &= \frac{A_{22}}{R} + (\hat{N} - K_{55}^2 A_{55}) \frac{\partial^2}{\partial x_1^2} - K_{44}^2 A_{44} \frac{\partial^2}{\partial x_2^2} + I_0 \frac{\partial^2}{\partial t^2} & & (8.4.8)
 \end{aligned}$$

8.4.2 Analytical Solution Procedure

Here we discuss the Lévy type solution procedure. For the circular cylindrical shell with arbitrary boundary conditions at $x_1 = \pm L/2$, we assume the following representation for the generalized displacement components:

$$\begin{Bmatrix} u_0 \\ v_0 \\ \phi_1 \\ \phi_2 \\ w_0 \end{Bmatrix} = \begin{Bmatrix} U_m(x_1) \cos \beta_m x_2 \\ V_m(x_1) \sin \beta_m x_2 \\ X_m(x_1) \cos \beta_m x_2 \\ Y_m(x_1) \sin \beta_m x_2 \\ W_m(x_1) \cos \beta_m x_2 \end{Bmatrix} T_m(t), \quad (8.4.9)$$

where $T_m = e^{i\omega_m t}$, ω_m being the natural frequency corresponding to the m th mode, when performing an eigenfrequency analysis (we keep in mind that there are denumerable infinite frequencies for each value of m), $i = \sqrt{-1}$ and $\beta_m = m/R$ ($m = 0, 1, 2, \dots$). Since the solution technique presented for these equations is general, we present only the equations of FST and include the numerical results of CST for the sake of comparison. Substitution of Eq. (8.4.9) into Eq. (8.4.6) results in five (three for CST) coupled ordinary differential equations:

$$\begin{aligned}
 U_m'' &= C_1 U_m + C_2 V_m' + C_3 X_m + C_4 Y_m' + C_5 W_m' \\
 V_m'' &= C_6 U_m' + C_7 V_m + C_8 X_m' + C_9 Y_m + C_{10} W_m \\
 X_m'' &= C_{11} U_m + C_{12} V_m' + C_{13} X_m + C_{14} Y_m' + C_{15} W_m' \\
 Y_m'' &= C_{14} U_m' + C_{17} V_m + C_{18} X_m' + C_{19} Y_m + C_{20} W_m \\
 W_m'' &= C_{21} U_m' + C_{22} V_m + C_{23} X_m' + C_{24} Y_m + C_{25} W_m
 \end{aligned} \quad (8.4.10)$$

where a prime indicates a derivative with respect to x_1 . The coefficients C_j ($j = 1, 2, \dots, 25$) are given for free vibration analysis by

$$\begin{aligned} C_1 &= (e_2 - e_1 e_{14})/e_{26}, & C_2 &= (e_3 - e_1 e_{17})/e_{26}, & C_3 &= (e_4 - e_1 e_{16})/e_{26} \\ C_4 &= (e_5 - e_1 e_{17})/e_{26}, & C_5 &= (e_6 - e_1 e_{18})/e_{26}, & C_6 &= (e_8 - e_7 e_{20})/e_{27} \\ C_7 &= (e_3 - e_7 e_{21})/e_{27}, & C_8 &= (e_{10} - e_7 e_{22})/e_{27}, & C_9 &= (e_{11} - e_7 e_{23})/e_{27} \\ C_{10} &= (e_{12} - e_7 e_{24})/e_{27}, & C_{11} &= (e_{14} - e_{13} e_2)/e_{26}, & C_{12} &= (e_{15} - e_{13} e_3)/e_{26} \\ C_{13} &= (e_{16} - e_{13} e_4)/e_{26}, & C_{14} &= (e_{17} - e_{13} e_5)/e_{26}, & C_{15} &= (e_{18} - e_{13} e_6)/e_{26} \\ C_{16} &= (e_{20} - e_{19} e_8)/e_{27}, & C_{17} &= (e_{21} - e_{19} e_9)/e_{27}, & C_{18} &= (e_{22} - e_{19} e_{10})/e_{27} \\ C_{19} &= (e_{23} - e_{19} e_{11})/e_{27}, & C_{20} &= (e_{24} - e_{19} e_{12})/e_{27}, & C_{21} &= e_{28}/e_{25} \\ C_{22} &= e_{29}/e_{25}, & C_{23} &= e_{30}/e_{25}, & C_{24} &= e_{31}/e_{25}, & C_{25} &= e_{32}/e_{25} \end{aligned} \quad (8.4.11)$$

where

$$\begin{aligned} e_1 &= B_{11}/A_{11}, & e_2 &= (A_{66}\beta_m^2 - \omega_m^2 I_0)/A_{11}, & e_3 &= -\beta_m(A_{12} + A_{66})/A_{11} \\ e_4 &= (B_{66}\beta_m^2 - \omega_m^2 I_1)/A_{11}, & e_5 &= -\beta_m(B_{12} + B_{66})/A_{11}, & e_6 &= -A_{12}/(A_{11}R) \\ e_7 &= B_{66}/A_{66}, & e_8 &= \beta_m(A_{12} + A_{66})/A_{66}, & e_9 &= (A_{22}\beta_m^2 - \omega_m^2 I_0)/A_{66} \\ e_{10} &= \beta_m(B_{12} + B_{66})/A_{66}, & e_{11} &= (B_{22}\beta_m^2 - \omega_m^2 I_1)/A_{66}, & e_{12} &= \beta_m A_{22}/(A_{66}R) \\ e_{13} &= B_{11}/D_{11}, & e_{14} &= (B_{66}\beta_m^2 - \omega_m^2 I_1)/D_{11}, & e_{15} &= -\beta_m(B_{12} + B_{66})/D_{11} \\ e_{16} &= (K_{55}^2 A_{55} + D_{66}\beta_m^2 - \omega_m^2 I_2)/D_{11}, & e_{17} &= -\beta_m(D_{12} + D_{66})/D_{11} \\ e_{18} &= -(B_{12}/R - K_{55}^2 A_{55})/D_{11}, & e_{19} &= B_{66}/D_{66}, & e_{20} &= \beta_m(B_{12} + B_{66})/D_{66} \\ e_{21} &= (B_{22}\beta_m^2 - \omega_m^2 I_1)/D_{66}, & e_{22} &= \beta_m(D_{12} + D_{66})/D_{66} \\ e_{23} &= (K_{44}^2 A_{44} + D_{22}\beta_m^2 - \omega_m^2 I_2)/D_{66}, & e_{24} &= \beta_m(B_{22}/R - K_{44}^2 A_{44})/D_{66} \\ e_{25} &= K_{55}^2 A_{55} - \hat{N}, & e_{26} &= 1 - e_1 e_{13}, & e_{27} &= 1 - e_7 e_{19}, & e_{28} &= A_{12}/R \\ e_{29} &= \beta_m A_{22}/R, & e_{30} &= -K_{55}^2 A_{55} + B_{12}/R, & e_{31} &= \beta_m(-K_{44}^2 A_{44} + B_{22}/R) \\ e_{32} &= K_{44}^2 A_{44}\beta_m^2 - \omega_m^2 I_0 + A_{22}/R^2 \end{aligned} \quad (8.4.12)$$

In the stability analysis, we let $\omega_m \rightarrow 0$ in e_j ($j = 1, 2, \dots, 32$).

With some simple algebraic operations (addition and subtraction), it is made sure that only one unknown variable with its highest derivative appears in equations (8.4.10). This will save the computational time required in the method that we will introduce for solving equations (8.4.10).

There exists a number of ways to solve a system of ordinary differential equations. However, when there are more than three governing equations, as in Eq. (8.4.10), it is more practical to introduce new unknown variables and replace the original system of equations by an equivalent system of first-order equations (to be able to use the state-space approach). We introduce the following variables:

$$\begin{aligned} Z_{1m} &= U_m(x_1), & Z_{2m}(x_1) &= U'_m(x_1) = Z'_{1m}(x_1) \\ Z_{3m} &= V_m(x_1), & Z_{4m}(x_1) &= V'_m(x_1) = Z'_{3m}(x_1) \\ Z_{5m} &= X_m(x_1), & Z_{6m}(x_1) &= X'_m(x_1) = Z'_{5m}(x_1) \\ Z_{7m} &= Y_m(x_1), & Z_{8m}(x_1) &= Y'_m(x_1) = Z'_{9m}(x_1) \\ Z_{9m} &= W_m(x_1), & Z_{10m}(x_1) &= W'_m(x_1) = Z'_{9m}(x_1) \end{aligned} \quad (8.4.13)$$

for $m = 1, 2, \dots$. In view of the definitions in (8.4.13), Eqs. (8.4.10) along with relations in (8.4.13) can be expressed in the form

$$\{Z'\} = [A]\{Z\}, \quad (8.4.14)$$

where

$$\{Z'\} = \{Z'_{1m}, Z'_{2m}, \dots, Z'_{10m}\}^T, \quad \{Z\} = \{Z_{1m}, Z_{2m}, \dots, Z_{10m}\}^T, \quad (8.4.15)$$

and the coefficient matrix $[A]$ is

$$[A] = \begin{bmatrix} 0 & 1 & 0 & 0 & 0 & 0 & 0 & 0 & 0 & 0 \\ C_1 & 0 & 0 & c_2 & C_3 & 0 & 0 & C_4 & 0 & C_5 \\ 0 & 0 & 0 & 1 & 0 & 0 & 0 & 0 & 0 & 0 \\ 0 & C_4 & C_7 & 0 & 0 & C_8 & C_9 & 0 & C_{10} & 0 \\ 0 & 0 & 0 & 0 & 1 & 0 & 0 & 0 & 0 & 0 \\ C_{11} & 0 & C_{12} & C_{13} & 0 & 0 & C_{14} & 0 & C_{15} & 0 \\ 0 & 0 & 0 & 0 & 0 & 0 & 1 & 0 & 0 & 0 \\ 0 & C_{16} & C_{17} & 0 & 0 & C_{18} & C_{19} & 0 & C_{20} & 0 \\ 0 & 0 & 0 & 0 & 0 & 0 & 0 & 0 & 0 & 1 \\ 0 & C_{21} & C_{22} & 0 & 0 & C_{23} & C_{24} & 0 & C_{25} & 0 \end{bmatrix} \quad (8.4.16)$$

A formal solution of Eq. (8.4.14) (see [43,44]) is given as

$$\{Z(x_1)\} = \Psi(x_1)\{D\}, \quad (8.4.17)$$

where $\Psi(x_1)$ is a fundamental matrix, the columns of which consist of ten linearly independent solutions of equations (8.4.10) and $\{D\}$ is an unknown constant vector. Some or all components of this vector, as will be seen later, are in general complex. The non-singular fundamental matrix $\Psi(x_1)$ is not unique. However, all fundamental matrices differ from each other by a multiplicative constant matrix. Since equations (8.4.17) are the solutions of equations (8.4.10) and $\Psi(0)$ is a non-singular constant matrix, a special fundamental matrix $\Phi(x_1)$ (known as the state transition matrix) for Eq. (8.4.10) can be defined from Eq. (8.4.17) such that

$$\{Z(x_1)\} = \Phi(x_1)\{Z(0)\} \quad (8.4.18)$$

are also the solutions of equations (8.4.10), with

$$\Phi(x_1) = \Psi(x_1)\Psi^{-1}(0) \quad \text{and} \quad \{D\} = \Psi^{-1}(0)\{Z(0)\} \quad (8.4.19)$$

Since $[A]$ is a constant matrix, the state transition matrix is given by a matrix exponential function as

$$\Phi(x_1) = e^{[A]x_1} \quad (8.4.20)$$

By imposing the ten boundary conditions at $x_1 = \pm L/2$ on the solution given by Eq. (8.4.17), a homogeneous system of algebraic equations can be found:

$$[M]\{Z(0)\} = \{0\} \quad (8.4.21)$$

For a non-trivial solution of natural frequency or critical buckling load, the determinant of the coefficient matrix $[M]$ must be set to zero

$$|M| = 0 \quad (8.4.22)$$

Since the constant vector $\{Z(0)\}$ is real, the determinant of $[M]$ is also real. Hence, in a trial and error procedure, one can easily find the correct value of natural frequency (in a free vibration problem) or of critical buckling load (in a stability problem) which would make $|M| = 0$. A non-zero compressive (or tensile) edge load can also be included in the free vibration analysis.

Numerous methods are available (e.g., see [43,44]) for determining the matrix exponential, $e^{[A]x_1}$, appearing in equation (8.4.20). However, regardless of any method used, it is found that $|M|$ becomes ill conditioned when the ratio of the characteristic length of the structure to its thickness is near or larger than 20. This is also the case in the Lévy-type eigenfrequency and stability problems of laminated plates and shell panels when shear deformation theories are used.

When the eigenvalues of the coefficient matrix $[A]$ are distinct, the fundamental matrix $\Psi(x_1)$ is given by

$$\Psi(x_1) = [U][Q(x_1)], \quad (8.4.23)$$

where $[Q(x_1)]$ is another fundamental matrix, defined as

$$[Q(x_1)] = \begin{bmatrix} e^{\lambda_1 x_1} & & & 0 \\ & e^{\lambda_2 x_1} & & \\ & & \ddots & \\ 0 & & & e^{\lambda_{10} x_1} \end{bmatrix} \quad (8.4.24)$$

and $[U]$ is a modal matrix that transforms $[A]$ into a diagonal form (i.e., the j th column of $[U]$ constitutes the eigenvectors of $[A]$ corresponding to the j th eigenvalue of $[A]$). In Eq. (8.4.20), λ_j ($j = 1, 2, \dots, 10$) are the distinct eigenvalues of $[A]$, which in general can be real and complex. We note that the eigenvalues of $[A]$ are the same as the roots of the auxiliary equation of (8.4.19). These eigenvalues in most eigenfrequency and stability problems of plates and shells are distinct. The axisymmetric buckling problem and axisymmetric eigenfrequency problem (when all inertia forces, except the radial inertia force, are neglected) of a cylindrical shell are two examples where two of the eigenvalues, as will be seen, are identical. When the eigenvalues are repeated, Eq. (8.4.24) is no longer valid and a Jordan canonical form of $[A]$ must be used [42,43].

Substituting Eq. (8.4.23) into Eqs. (8.4.19) yields

$$\Phi(x_1) = [U][Q(x_1)][U]^{-1} \quad (8.4.25)$$

and

$$\{D\} = [U]^{-1}\{Z(0)\} \quad (8.4.26)$$

Equations (8.4.18) and (8.4.25) were used in [40]. However, due to the occurrence of an ill-conditioned determinant $|M|$ in Eq. (8.4.22), Nosier and Reddy [41] proposed the following approach. Instead of imposing the boundary conditions on equations

(8.4.18), impose the boundary conditions on equations (8.4.17), which have a simpler form. This way we come up with a set of homogeneous algebraic equations of the form

$$[K]\{D\} = \{0\}. \quad (8.4.27)$$

For a non-trivial solution of Eq. (8.4.27) to exist, the determinant of the generally complex coefficient matrix $[K]$ must vanish. Since, in general, $[K]$ can be complex, it may be computationally more convenient to substitute Eq. (8.4.26) into Eq. (8.4.27) to obtain

$$[K][U]^{-1}\{Z(0)\} = \{0\} \quad (8.4.28a)$$

and set the coefficient matrix in equation (8.4.28a) to zero:

$$|([K][U]^{-1})| = 0 \quad (8.4.28b)$$

In this way the determinant in equation (8.4.28b) will always be a real number. However, it will have the same computational problem as $|M|$ in Eq. (8.4.22). The key point in overcoming this difficulty is to rewrite Eq. (8.4.28b) as

$$|K|/|U| = 0; \quad (8.4.29)$$

that is, to evaluate the determinants of $[K]$ and $[U]$ separately, rather than evaluating the determinant of $([K][U]^{-1})$. It should also be noted that, in this way, the inverse of $[U]$ is never needed. For very thin shells (or long shells), computer overflow and underflow may occur when we evaluate the elements of the coefficient matrix $[K]$. This problem is addressed in detail in [41]. However, it should be kept in mind that the determinant of $[K]$ never becomes ill conditioned. In summary, after assuming a trial value for natural frequency (in free vibration analysis) or for buckling load (in stability analysis) for a particular m , we will impose the ten boundary conditions at $x_1 = \pm L/2$ on Eq. (8.4.17), derive Eq. (8.4.27) and check whether Eq. (8.4.29) is satisfied. It should be remembered that $|U|$ appearing in Eq. (8.4.29) is never zero, since the eigenvectors in $[U]$ are independent of each other.

A remark must be made concerning the computation of eigenvalues and eigenvectors of the coefficient matrix $[A]$. Since the diagonal elements of $[A]$ are all zero, during the computation of eigenvalues and eigenvectors computer overflow or underflow may occur. To resolve this problem, we can subtract a non-zero constant number from the diagonal elements of $[A]$ and compute the eigenvalues and eigenvectors of the new matrix. The eigenvalues of $[A]$ can then be obtained by adding the same number to each eigenvalue of the new matrix. The eigenvectors of $[A]$ will be identical to those of the new matrix (see page 52 of [43]).

8.4.3 Boundary Conditions

A combination of boundary conditions may be assumed to exist at the edges of the shell. Here we classify these boundary conditions for the FST according to [41]:

Simply supported

- S1: $w_0 = M_1 = \phi_2 = N_1 = N_6 = 0$, S2: $w_0 = M_1 = \phi_2 = u_0 = N_6 = 0$
- S3: $w_0 = M_1 = \phi_2 = N_1 = v_0 = 0$, S4: $w_0 = M_1 = \phi_2 = u_0 = v_0 = 0$ (8.4.30)

Clamped

$$\begin{aligned} \text{C1: } w_0 &= \phi_1 = \phi_2 = N_1 = N_6 = 0, & \text{C2: } w_0 &= \phi_1 = \phi_2 = u_0 = N_6 = 0 \\ \text{C3: } w_0 &= \phi_1 = \phi_2 = N_1 = v_0 = 0, & \text{C4: } w_0 &= \phi_1 = \phi_2 = u_0 = v_0 = 0 \end{aligned} \quad (8.4.31)$$

Free edge

$$\text{F: } N_1 = N_4 = M_1 = M_4 = Q_1 - \hat{N} \frac{\partial w_0}{\partial x_1} = 0 \quad (8.4.32)$$

The boundary type S3 is referred to as a shear diaphragm by Leissa [44]. Similar boundary conditions may also be classified for the CST (see [41]).

In the above discussion it was assumed that $m \neq 0$ (non-axisymmetric case). For axisymmetric mode (i.e., when $m = 0$) we have $v_0 = \phi_2 = 0$, and Eqs. (8.4.9) and (8.4.10) become

$$(u_0, \phi_1, w_0) = (U_0, X_0, W_0)T_0(t) \quad (8.4.33)$$

and

$$\begin{aligned} U_0'' &= \bar{C}_1 U_0 + \bar{C}_3 X_0 + \bar{C}_3 W_0' \\ X_0'' &= \bar{C}_4 U_0 + \bar{C}_5 X_0 + \bar{C}_4 W_0' \\ W_0'' &= \bar{C}_7 U_0' + \bar{C}_8 X_0' + \bar{C}_9 W_0 \end{aligned} \quad (8.4.34)$$

where $T_0(t) = e^{i\omega_0 t}$ for free vibration and $T_0(t) = 1$ for stability problems. The coefficients \bar{C}_j ($j = 1, 2, \dots, 9$) appearing in Eq. (8.4.34) are

$$\begin{aligned} \bar{C}_1 &= (e_2 - e_1 e_6)/e_{13}, & \bar{C}_2 &= (e_3 - e_1 e_7)/e_{13}, & \bar{C}_3 &= (e_4 - e_1 e_8)/e_{13} \\ \bar{C}_4 &= (e_6 - e_5 e_2)/e_{13}, & \bar{C}_5 &= (e_7 - e_5 e_3)/e_{13}, & \bar{C}_6 &= (e_8 - e_5 e_4)/e_{13} \\ \bar{C}_7 &= e_9/e_{12}, & \bar{C}_8 &= e_{10}, & \bar{C}_9 &= e_{11}/e_{12} \end{aligned} \quad (8.4.35a)$$

where

$$\begin{aligned} e_1 &= B_{11}/A_{11}, & e_2 &= I_0 \omega_0^2/A_{11}, & e_3 &= -I_1 \omega_0^2/A_{11}, & e_4 &= -A_{12}/(R A_{11}) \\ e_5 &= B_{11}/D_{11}, & e_6 &= -I_1 \omega_0^2/D_{11}, & e_7 &= (K_{55}^2 A_{55} - I_2 \omega_0^2)/D_{11} \\ e_8 &= (K_{55}^2 A_{55} - B_{12}/R)/D_{11}, & e_9 &= A_{12}/R, & e_{10} &= B_{12}/R - K_{55}^2 A_{55} \\ e_{11} &= A_{22}/R^2 - I_0 \omega_0^2, & e_{12} &= K_{55}^2 A_{55} - \hat{N}, & e_{13} &= 1 - e_1 e_5 \end{aligned} \quad (8.4.35b)$$

In the stability problem, we let $\omega_0 \rightarrow 0$ in e_j ($j = 1, 2, \dots, 13$). In the vibration problem, when only the radial inertia is included, we will have

$$e_2 = e_3 = e_6 = 0, \quad e_7 = K_{55}^2 A_{55}/D_{11}$$

For additional details and discussion, the reader may consult [41].

8.4.4 Numerical Results

Numerical results are presented here for an orthotropic material with the following properties [42]:

$$E_1/E_2 = 10, \quad G_{13} = G_{12} = 0.6E_2, \quad G_{23} = 0.5E_2, \quad \nu_{12} = 0.25 \quad (8.4.36)$$

and for an isotropic material with Poisson ratio $\nu = 0.25$. It is assumed that $K_{44}^2 = K_{55}^2 = K_s = 5/6$ and the total thickness h of the shell is equal to 1 in. in all the numerical examples. Furthermore, all layers are assumed to be of equal thickness.

The effect of altering the lamination scheme on the fundamental frequency of a cross-ply shell with various boundary conditions is shown in Table 8.4.1 (a number in parentheses denotes the circumferential mode number m). Note that in a (90/0) laminated shell, the fibers of the outside layer are in the circumferential direction and those of the inside layer are along the longitudinal axis of the shell. It is observed that, except for the S4-F case, the fundamental frequency for a (90/0) laminated shell is slightly smaller than that of a (0/90) laminated shell. However, an analysis based on a more accurate theory, known as the generalized layerwise shell theory [45] (also see Chapter 12), indicates that this exception for boundary type S4-F does not occur.

Table 8.4.1: The effects of lamination and various boundary conditions on the dimensionless fundamental frequency ω_m of a shell; $R/h = 60$, $L/R = 1$, $\hat{N} = 0$ and $\bar{\omega}_m = \omega_m(L^2/10h)\sqrt{\rho/E_2}$.

Laminate	Theory	F-F	S3-F	C4-F	S3-S3	S3-C4	C4-C4
(0/90)	FST	0.4096 (3)	0.4579 (3)	1.7158 (5)	2.8497 (6)	3.0291 (6)	3.2659 (6)
	CST	0.4098 (3)	0.4585 (3)	1.7193 (5)	2.8535 (6)	3.0358 (6)	3.2762 (6)
(90/0)	FST	0.4071 (3)	0.4542 (3)	1.7200 (5)	2.7747 (6)	2.9745 (6)	3.2424 (6)
	CST	0.4076 (3)	0.4545 (3)	1.7233 (5)	2.7788 (6)	2.9805 (6)	3.2508 (6)

The numerical results indicate that, unless the shell is extremely short, the minimum axisymmetric frequency is always quite larger than the fundamental frequency of cross-ply and isotropic shells. This is particularly true for cross-ply shells as can be seen from Table 8.4.2, where the results are tabulated for cases C1-C1 through C4-C4. It should be noted that the effect of imposing various in-

Table 8.4.2: Comparison of the dimensionless fundamental frequency with dimensionless minimum axisymmetric frequency of a shell according to FST: $R/h = 60$, $L/R = 1$, $\hat{N}=0$ and $\bar{\omega}_m = \omega_m(L^2/10h)\sqrt{\rho/E_2}$.

Laminate	C1 C1	C2 C2	C3 C3	C4 C4
(0/90)	3.0836 (6)	3.2007 (6)	3.1133 (6)	3.2659 (6)
	14.1068 (0)	14.1198 (0)	14.1068 (0)	14.1198 (0)
	14.1140 (0)	14.1239 (0)	14.1140 (0)	14.1239 (0)
Isotropic	1.9928 (6)	2.1882 (5)	2.0196 (6)	1.2090 (6)
	6.0155 (0)	6.1657 (0)	6.0155 (0)	6.1657 (0)
	6.0155 (0)	6.1657 (0)	6.0155 (0)	6.1657 (0)
	6.0368 (0)	6.1685 (0)	6.0368 (0)	6.1685 (0)

plane boundary conditions is more severe for isotropic shells than cross-ply shells. In Table 8.4.2, two minimum axisymmetric frequencies are presented. The second number, which is slightly larger than the first one, corresponds to the case when only the radial force is included. For additional discussion, see [41].

The influence of various simply supported boundary conditions on the critical buckling load of laminated and isotropic shells can be studied with the help of Table 8.4.3. As in the frequency problem, it is seen that various in-plane boundary conditions have more severe influence on the critical buckling load of isotropic shells. Also, the minimum axisymmetric buckling load in isotropic shells is relatively larger than the critical buckling load in cross-ply shells. Indeed, the actual computations indicate that only for extremely short cross-ply shells the axisymmetric buckling load will be the actual critical load. It should be noted that the bending-extension coupling induced by the lamination asymmetry substantially decreases the buckling loads. However, for antisymmetric cross-ply shells, the effect of the coupling dies out rapidly as the number of layers is increased, as can be seen from the results of Table 8.4.4. Note that we have not generated any numerical results for unsymmetric cross-ply shells. Furthermore, for antisymmetric cross-ply shells we have $B_{12} = B_{66} = 0$, $B_{22} = -B_{11}$, $A_{22} = A_{11}$ and $D_{22} = D_{11}$.

Table 8.4.3: The effects of various simply supported conditions on the dimensionless critical buckling load \bar{N} of cross-ply shells [$\bar{N} = \hat{N}L^2/(100h^3E_2)$] and an isotropic shell [$\bar{N} = \hat{N}L^2/(10h^3E)$]; $R/h = 40$ and $L/R = 2$.

Laminate	Theory	S1–S1	S2–S2	S3–S3	S4–S4
(90/0)	FST	1.5451 (4) 3.6512 (0)	1.5793 (4) 3.6637 (0)	1.8479 (6) 3.6512 (0)	1.8849 (6) 3.6637 (0)
	CST	1.5705 (4) 3.7693 (0)	1.6081 (4) 3.7839 (0)	1.8663 (6) 3.7693 (0)	1.9044 (6) 3.7839 (0)
(0/90/0)	FST	1.8234 (4) 5.5233 (0)	1.8266 (5) 5.5233 (0)	2.0372 (6) 5.5233 (0)	2.0959 (6) 5.5233 (0)
	CST	1.8396 (5) 5.7739 (0)	1.8430 (5) 5.7739 (0)	2.0507 (6) 5.7739 (0)	2.1095 (6) 5.7739 (0)
Isotropic	FST	4.7535 (1) 9.5074 (0)	4.7560 (1) 9.5128 (0)	9.4428 (3) 9.5074 (0)	9.4440 (3) 9.5128 (0)
	CST	4.8062 (1) 9.5923 (0)	4.8090 (1) 9.5977 (0)	9.5548 (4) 9.5923 (0)	9.5492 (3) 9.5977 (0)

Table 8.4.4: The influences of lamination and boundary conditions on the dimensionless critical buckling load \bar{N} of a shell according to FST: $R/h = 80$, $L/R = 1$ and $\bar{N} = \hat{N}L^2/(10h^3E_2)$.

Lamination	F-F	S3-F	C4-F	S3-S3	C4-C4
(90/0)	1.6372 (5)	2.1895 (4)	5.2273 (8)	9.3966 (9)	9.8950 (8)
(0/90)	1.6329 (5)	2.1753 (4)	5.2542 (8)	9.3325 (8)	9.8394 (8)
(90/0/90/00)	2.4524 (5)	3.4898 (4)	6.2835 (7)	11.6085 (7)	12.5659 (8)
(0/90/0/90)	2.4486 (5)	3.4775 (4)	6.2953 (7)	11.6417 (7)	12.5078
(90/0/90/0/90/0)	2.5988 (5)	3.7177 (4)	6.4610 (7)	11.9466 (7)	12.9768 (7)
(0/90/0/90/0/90)	2.5961	3.7089 (4)	6.4691 (7)	11.9688 (7)	12.9381 (7)
(90/0/.../100 layers)	2.7138 (5)	3.8941 (4)	6.6030 (7)	12.2219 (7)	13.2932 (7)
(0/90/.../100 layers)	2.7136 (5)	3.8936 (4)	6.6035 (7)	12.2233 (7)	13.2909 (7)

Problems

8.1 Verify the strain-displacement relations in (8.2.22).

8.2 Verify the strain-displacement relations in (8.2.24).

8.3 Show that the equations of motion associated with a cylindrical shell of radius R are

$$\frac{\partial N_x}{\partial x} + \frac{1}{R} \frac{\partial}{\partial \theta} \left(N_{x\theta} - \frac{1}{2R} M_{x\theta} \right) = I_0 \frac{\partial^2 u_0}{\partial t^2} + I_1 \frac{\partial^2 \phi_x}{\partial t^2} \quad (1)$$

$$\frac{\partial}{\partial x} \left(N_{x\theta} + \frac{1}{2R} M_{x\theta} \right) + \frac{1}{R} \frac{\partial N_\theta}{\partial \theta} + \frac{Q_\theta}{R} = I_0 \frac{\partial^2 v_0}{\partial t^2} + I_1 \frac{\partial^2 \phi_\theta}{\partial t^2} \quad (2)$$

$$\frac{\partial Q_x}{\partial x} + \frac{1}{R} \frac{\partial Q_\theta}{\partial \theta} - \frac{N_\theta}{R} + q = I_1 \frac{\partial^2 w_0}{\partial t^2} \quad (3)$$

$$\frac{\partial M_x}{\partial x} + \frac{1}{R} \frac{\partial M_{x\theta}}{\partial \theta} - Q_x = I_2 \frac{\partial^2 \phi_x}{\partial t^2} + I_1 \frac{\partial^2 u_0}{\partial t^2} \quad (4)$$

$$\frac{\partial M_{x\theta}}{\partial x} + \frac{1}{R} \frac{\partial M_\theta}{\partial \theta} - Q_\theta = I_2 \frac{\partial^2 \phi_\theta}{\partial t^2} + I_1 \frac{\partial^2 v_0}{\partial t^2} \quad (5)$$

where $x_1 = x$, $x_2 = R\theta$, $R_1 = \infty$, and $R_2 = R$.

References for Additional Reading

1. Ambartsumyan, S. A., "Calculation of Laminated Anisotropic Shells," *Izvestiia Akademii Nauk Armenskoi SSR, Ser. Fiz. Mat. Est. Tekh. Nauk.*, **6**(3), p.15 (1953).
2. Ambartsumyan, S. A., *Theory of Anisotropic Shells*, NASA Report TT F-118 (1964).
3. Ambartsumyan, S. A., *Theory of Anisotropic Shells*, Moscow (1961); English translation, NASA-TT-F-118 (1964).
4. Kuhn, P., *Stresses in Aircraft and Shell Structures*, McGraw-Hill, New York (1956).
5. Novozhilov, V. V., *The Theory of Thin Shells*, Noordhoff, Gröningen (1959).
6. Flügge, W., *Stresses in Shells*, Springer-Verlag, Berlin (1960).
7. Vlasov, V. Z., *General Theory of Shells and Its Applications in Engineering*, (Translation of *Obshchaya teoriya obolochek i yeye prilozheniya v tekhnike*), NASA TT F-99, National Aeronautical and Space Administration, Washington, D.C. (1964).
8. Kraus, H., *Thin Elastic Shells*, John Wiley, New York (1967).
9. Dym, C. L., *Introduction to the Theory of Shells*, Pergamon, New York (1974).

10. Librescu, L., *Elastostatics and Kinetics of Anisotropic and Heterogeneous Shell-Type Structures*, Noordhoff, Leyden, The Netherlands (1975).
11. Timoshenko, S. and Woinowsky-Krieger, S., *Theory of Plates and Shells*, McGraw-Hill, New York (1959).
12. Heyman, J., *Equilibrium of Shell Structures*, Oxford University Press, UK (1977).
13. Dikeman, M., *Theory of Thin Elastic Shells*, Pitman, Boston, MA (1982).
14. Reddy, J. N., *Energy and Variational Methods in Applied Mechanics*, (First Edition) John Wiley, New York (1984).
15. Dong, S. B., Pister, K. S., and Taylor, R. L., "On the Theory of Laminated Anisotropic Shells and Plates," *Journal of Aerospace Sciences*, **29**, 969–975 (1962).
16. Dong, S. B. and Tso, K. W., "On a Laminated Orthotropic Shell Theory Including Transverse Shear Deformation," *Journal of Applied Mechanics*, **39**, 1091–1096 (1972).
17. Donnell, L. N., "Stability of Thin Walled Tubes in Torsion," NASA Report (1933).
18. Green, A. E., "On the Linear Theory of Thin Elastic Shells," *Proceedings of the Royal Society, Series A*, **266** (1962).
19. Hsu, T. M. and Wang, J. T. S., "A Theory of Laminated Cylindrical Shells Consisting of Layers of Orthotropic Laminae," *AIAA Journal*, **8**(12), P. 2141 (1970).
20. Koiter, W. T., "Foundations and Basic Equations of Shell Theory. A Survey of Recent Progress," *Theory of Shells*, F. I. Niordson (Ed.), IUTAM Symposium, Copenhagen, pp. 93–105 (1967).
21. Logan, D. L. and Widera, G. E. O., "Refined Theories for Nonhomogeneous Anisotropic Cylindrical Shells: Part II-Application," *Journal of the Engineering Mechanics Division*, **106**(EM6), 1075–1090 (1980).
22. Love, A. E. H., "On the Small Free Vibrations and Deformations of the Elastic Shells," *Philosophical Transactions of the Royal Society* (London), Ser. A, **17**, 491–546 (1888).
23. Morley, L. S. D., "An Improvement of Donnell's Approximation of Thin-Walled Circular Cylinders," *Quarterly Journal of Mechanics and Applied Mathematics*, **8**, 169–176 (1959).
24. Naghdi, P. M., "A Survey of Recent Progress in the Theory of Elastic Shells," *Applied Mechanics Reviews*, **9**(9), 365–368 (1956).
25. Naghdi, P. M., "Foundations of Elastic Shell Theory," *Progress in Solid Mechanics*, **4**, I. N. Sneddon and R. Hill (Eds.), North-Holland, Amsterdam, The Netherlands, P. 1 (1963).
26. Sanders Jr., J. L., "An Improved First Approximation Theory for Thin Shells," NASA TR-R24 (1959).
27. Budiansky, B. and Sanders, J. L., "On the 'Best' First Order Linear Shell Theory," *Progress in Applied Mechanics, The Prager Anniversary Volume*, Macmillan, New York, 129–140 (1963).
28. Stavsky, Y., "Thermoelasticity of Heterogeneous Aeolotropic Plates," *Journal of Engineering Mechanics Division*, EM2, 89–105 (1963).
29. Cheng, S. and Ho, B. P. C., "Stability of Heterogeneous Aeolotropic Cylindrical Shells Under Combined Loading," *AIAA Journal*, **1**(4), 892–898 (1963).
30. Widera, O. E. and Chung, S. W., "A Theory for Non-Homogeneous Anisotropic Cylindrical Shells," *Z. Angew Math. Physik*, **21**, 3787–399 (1970).
31. Gulati, S. T. and Essenber, F., "Effects of Anisotropy in Axisymmetric Cylindrical Shells," *Journal of Applied Mechanics*, **34**, 659–666 (1967).
32. Zukas, J. A. and Vinson, J. R., "Laminated Transversely Isotropic Cylindrical Shells," *Journal of Applied Mechanics*, 400–407 (1971).

33. Whitney, J. M. and Sun, C. T., "A Refined Theory for Laminated Anisotropic, Cylindrical Shells," *Journal of Applied Mechanics*, **41**, 471–476 (1974).
34. Reddy, J. N., "Exact Solutions of Moderately Thick Laminated Shells," *Jurnal of Engineering Mechanics*, **110**(5), 794–809 (1984).
35. Bert, C. W., "Dynamics of Composite and Sandwich Panels - Parts I and II," (corrected title), *Shock & Vibration Digest*, **8**(10), 37–48, 1976; **8**(11), 15–24 (1976).
36. Bert, C. W., "Analysis of Shells," *Structural Design and Analysis, Part I*, C. C. Chamis (Ed.), Vol. 7 of *Composite Materials*, L. J. Broutman and R. H. Krock (Eds.) Academic Press, New York, 207–258 (1974).
37. Saada, A. S., *Elasticity: Theory and Applications*, Second Edition, Krieger, Boca Raton, FL (1993).
38. Cheng, Z.-Q. and Reddy, J. N., "Asymptotic Theory for Laminated Piezoelectric Circular Cylindrical Shells," *AIAA Journal*, **40**(9), 553–558 (2002).
39. Pradhan, S. C., Li, H., Reddy, J. N., "Vibration Control of Composite Shells Using Embedded Actuating Layers," (to appear).
40. Khdeir, A. A., Reddy, J. N., and Frederick, D., "A study of Bending, Vibration and Buckling of Cross-Ply Circular Cylindrical Shells with Various Shell Theories," *International Journal of Engineering Science*, **27**, 1337–1351 (1989).
41. Nosier, A. and Reddy, J. N., "Vibration and Stability Analyses of Cross-Ply Laminated Circular Cylindrical Shells," *Journal of Sound and Vibration*, **157**(1), 139–159 (1992).
42. Ogata, K., *State Space Analysis of Control Systems*, Prentice-Hall, Englewood Cliffs, NJ (1967).
43. Gopal, M., *Modern Control System Theory*, Wiley Eastern, New York (1984).
44. Leissa, A. W., *Vibration of Shells*, NASA SP-288, NASA, Washington, DC (1973).
45. Barbero, E. J. and Reddy, J. N., "General Two-Dimensional Theory of Laminated Cylindrical Shells," *AIAA Journal*, **28**, 544–553 (1990).

Linear Finite Element Analysis of Composite Plates and Shells

9.1 Introduction

In Chapters 4 through 8, the Navier, Lévy, and variational (Ritz) solutions to the equations of composite beams, plates and shells were presented for simple geometries. However, exact analytical or variational solutions to these problems cannot be developed when complex geometries, arbitrary boundary conditions, or nonlinearities are involved. Therefore, one must resort to approximate methods of analysis that are capable of solving such problems.

The *finite element method* is a powerful computational technique for the solution of differential and integral equations that arise in various fields of engineering and applied science. The method is a generalization of the classical variational (i.e., Ritz) and weighted-residual (e.g., Galerkin, least-squares, collocation, etc.) methods [1–5]. Since most real-world problems are defined on domains that are geometrically complex and may have different types of boundary conditions on different portions of the boundary of the domain, it is difficult to generate approximation functions required in the traditional variational methods. The basic idea of the finite element method is to view a given domain as an assemblage of simple geometric shapes, called *finite elements*, for which it is possible to systematically generate the approximation functions needed in the solution of differential equations by any of the variational and weighted-residual methods. The ability to represent domains with irregular geometries by a collection of finite elements makes the method a valuable practical tool for the solution of boundary, initial, and eigenvalue problems arising in various fields of engineering. The approximation functions are often constructed using ideas from interpolation theory, and hence they are also called *interpolation functions*. Thus the finite element method is a piecewise (or element wise) application of the variational and weighted-residual methods. For a given differential equation, it is possible to develop different finite element approximations (or *finite element models*), depending on the choice of a particular variational or weighted-residual method. For a detailed introduction to the finite element method, the reader is advised to consult References 1–5.

The major steps in the finite element analysis of a typical problem are (see Reddy [1,2])

1. Discretization of the domain into a set of finite elements (*mesh generation*).
2. Weighted-integral or weak formulation of the differential equation over a typical finite element (subdomain).
3. Development of the finite element model of the problem using its weighted-integral or weak form. The finite element model consists of a set of algebraic equations among the unknown parameters of the element.
4. Assembly of finite elements to obtain the global system (i.e., for the total problem) of algebraic equations.
5. Imposition of boundary conditions.
6. Solution of equations.
7. Post-computation of solution and quantities of interest.

The above steps of the finite element method make it a modular technique that can be implemented on a computer, independent of the shape of the domain and boundary conditions. In addition, the method allows coupling of various physical problems because finite elements based on different physical problems can be easily generated in the same computer program.

In this chapter, we develop finite element models of the linear equations governing laminated composite plates and shells. The objective is to introduce the reader to the finite element formulations of laminated composite structures. While the coverage is not exhaustive in terms of solving complicated problems, for this is primarily a textbook, it helps the reader in gaining an understanding of the plate and shell finite elements used in the analysis of practical problems.

It is important to note that any numerical or computational method is a means to analyze a practical engineering problem and that analysis is not an end in itself but rather an aid to design. *The value of the theory and analytical solutions presented in the preceding chapters to gain insight into the behavior of simple laminated beam and plate structures is immense in the numerical modeling of complicated problems by the finite element method or any numerical method.* Those who are quick to use a computer rather than *think* about the problem to be analyzed may find it difficult to interpret or explain the computer-generated results. Even to develop proper input data to a computer program requires a good understanding of the underlying theory of the problem as well as the method on which the program is based.

9.2 Finite Element Models of the Classical Plate Theory (CLPT)

9.2.1 Weak Forms

In this section, finite element models of Eqs. (6.1.1)–(6.1.3) governing the motion of laminated plates according to the classical laminate theory are developed. For the sake of brevity, Eqs. (3.3.25), which are expressed in terms of the stress resultants but equivalent to Eqs. (6.1.1)–(6.1.3), are used to develop the weak forms.

Multiplying three equations in (3.3.25) with δu_0 , δv_0 , and δw_0 , respectively, and integrating over the element domain, we obtain

$$0 = \int_{\Omega^e} \delta u_0 \left[-\frac{\partial N_{xx}}{\partial x} - \frac{\partial N_{xy}}{\partial y} + I_0 \frac{\partial^2 u_0}{\partial t^2} - I_1 \frac{\partial^2}{\partial t^2} \left(\frac{\partial w_0}{\partial x} \right) \right] dx dy \quad (9.2.1a)$$

$$0 = \int_{\Omega^e} \delta v_0 \left[-\frac{\partial N_{xy}}{\partial x} - \frac{\partial N_{yy}}{\partial y} + I_0 \frac{\partial^2 v_0}{\partial t^2} - I_1 \frac{\partial^2}{\partial t^2} \left(\frac{\partial w_0}{\partial y} \right) \right] dx dy \quad (9.2.1b)$$

$$\begin{aligned} 0 = \int_{\Omega^e} \delta w_0 & \left[-\frac{\partial^2 M_{xx}}{\partial x^2} - 2 \frac{\partial^2 M_{xy}}{\partial y \partial x} - \frac{\partial^2 M_{yy}}{\partial y^2} - q \right. \\ & - \frac{\partial}{\partial x} \left(\hat{N}_{xx} \frac{\partial w_0}{\partial x} + \hat{N}_{xy} \frac{\partial w_0}{\partial y} \right) - \frac{\partial}{\partial y} \left(\hat{N}_{xy} \frac{\partial w_0}{\partial x} + \hat{N}_{yy} \frac{\partial w_0}{\partial y} \right) \\ & \left. + I_0 \frac{\partial^2 w_0}{\partial t^2} - I_2 \frac{\partial^2}{\partial t^2} \left(\frac{\partial^2 w_0}{\partial x^2} + \frac{\partial^2 w_0}{\partial y^2} \right) + I_1 \frac{\partial^2}{\partial t^2} \left(\frac{\partial u_0}{\partial x} + \frac{\partial v_0}{\partial y} \right) \right] dx dy \end{aligned} \quad (9.2.1c)$$

where \hat{N}_{xx} , \hat{N}_{xy} , and \hat{N}_{yy} are in-plane edge forces. The stress and moment resultants N_{xx} , M_{xx} , etc. are known in terms of the displacements (u_0, v_0, w_0) through Eq. (3.3.40). Note that the virtual displacements $(\delta u_0, \delta v_0, \delta w_0)$ take the role of weight functions in the development of weak forms. Integration by parts to weaken the differentiability of u_0 , v_0 , and w_0 results in the expressions

$$\begin{aligned} 0 = \int_{\Omega^e} & \left[\frac{\partial \delta u_0}{\partial x} N_{xx} + \frac{\partial \delta u_0}{\partial y} N_{xy} + I_0 \delta u_0 \frac{\partial^2 u_0}{\partial t^2} - I_1 \delta u_0 \frac{\partial^2}{\partial t^2} \left(\frac{\partial w_0}{\partial x} \right) \right] dx dy \\ & - \oint_{\Gamma^e} (N_{xx} n_x + N_{xy} n_y) \delta u_0 ds \end{aligned} \quad (9.2.2a)$$

$$\begin{aligned} 0 = \int_{\Omega^e} & \left[\frac{\partial \delta v_0}{\partial x} N_{xy} + \frac{\partial \delta v_0}{\partial y} N_{yy} + I_0 \delta v_0 \frac{\partial^2 v_0}{\partial t^2} - I_1 \delta v_0 \frac{\partial^2}{\partial t^2} \left(\frac{\partial w_0}{\partial y} \right) \right] dx dy \\ & - \oint_{\Gamma^e} (N_{xy} n_x + N_{yy} n_y) \delta v_0 ds \end{aligned} \quad (9.2.2b)$$

$$\begin{aligned} 0 = \int_{\Omega^e} & \left[-\frac{\partial^2 \delta w_0}{\partial x^2} M_{xx} - 2 \frac{\partial^2 \delta w_0}{\partial x \partial y} M_{xy} - \frac{\partial^2 \delta w_0}{\partial y^2} M_{yy} - \delta w_0 q \right. \\ & + \frac{\partial \delta w_0}{\partial x} \left(\hat{N}_{xx} \frac{\partial w_0}{\partial x} + \hat{N}_{xy} \frac{\partial w_0}{\partial y} \right) + \frac{\partial \delta w_0}{\partial y} \left(\hat{N}_{xy} \frac{\partial w_0}{\partial x} + \hat{N}_{yy} \frac{\partial w_0}{\partial y} \right) \\ & + I_0 \delta w_0 \frac{\partial^2 w_0}{\partial t^2} + I_2 \left(\frac{\partial \delta w_0}{\partial x} \frac{\partial^3 w_0}{\partial x \partial t^2} + \frac{\partial \delta w_0}{\partial y} \frac{\partial^3 w_0}{\partial y \partial t^2} \right) \\ & \left. - I_1 \left(\frac{\partial \delta w_0}{\partial x} \frac{\partial^2 u_0}{\partial t^2} + \frac{\partial \delta w_0}{\partial y} \frac{\partial^2 v_0}{\partial t^2} \right) \right] dx dy \\ & - \oint_{\Gamma^e} \left[\left(\frac{\partial M_{xx}}{\partial x} + \frac{\partial M_{xy}}{\partial y} + \hat{N}_{xx} \frac{\partial w_0}{\partial x} + \hat{N}_{xy} \frac{\partial w_0}{\partial y} \right) n_x \right. \\ & \left. + \left(\frac{\partial M_{xy}}{\partial x} + \frac{\partial M_{yy}}{\partial y} + \hat{N}_{xy} \frac{\partial w_0}{\partial x} + \hat{N}_{yy} \frac{\partial w_0}{\partial y} \right) n_y \right] \end{aligned}$$

$$\begin{aligned}
& + \left(I_1 \frac{\partial^2 u_0}{\partial t^2} - I_2 \frac{\partial^3 w_0}{\partial x \partial t^2} \right) n_x + \left(I_1 \frac{\partial^2 v_0}{\partial t^2} - I_2 \frac{\partial^3 w_0}{\partial y \partial t^2} \right) n_y \right] \delta w_0 \, ds \\
& + \oint_{\Gamma^e} \left[\frac{\partial \delta w_0}{\partial x} (M_{xx} n_x + M_{xy} n_y) + \frac{\partial \delta w_0}{\partial y} (M_{xy} n_x + M_{yy} n_y) \right] \, ds
\end{aligned} \tag{9.2.2c}$$

where (n_x, n_y) denote the direction cosines of the unit normal on the element boundary Γ^e . Integration by parts of the inertia terms in the last equation is necessitated by the symmetry considerations of the resulting weak form, which leads to symmetric mass matrix in the finite element model.

We note from the boundary terms in Eq. (9.2.2) that u_0 , v_0 , w_0 , $\partial w_0 / \partial x$, and $\partial w_0 / \partial y$ are the primary variables (or generalized displacements), and

$$\begin{aligned}
p_x &\equiv N_{xx} n_x + N_{xy} n_y, \quad p_y \equiv N_{xy} n_x + N_{yy} n_y \\
T_x &\equiv M_{xx} n_x + M_{xy} n_y, \quad T_y \equiv M_{xy} n_x + M_{yy} n_y \\
Q_n &\equiv \left(\frac{\partial M_{xx}}{\partial x} + \frac{\partial M_{xy}}{\partial y} + \hat{N}_{xx} \frac{\partial w_0}{\partial x} + \hat{N}_{xy} \frac{\partial w_0}{\partial y} + I_1 \frac{\partial^2 u_0}{\partial t^2} - I_2 \frac{\partial^3 w_0}{\partial x \partial t^2} \right) n_x \\
&+ \left(\frac{\partial M_{xy}}{\partial x} + \frac{\partial M_{yy}}{\partial y} + \hat{N}_{xy} \frac{\partial w_0}{\partial x} + \hat{N}_{yy} \frac{\partial w_0}{\partial y} + I_1 \frac{\partial^2 v_0}{\partial t^2} - I_2 \frac{\partial^3 w_0}{\partial y \partial t^2} \right) n_y
\end{aligned} \tag{9.2.3}$$

are the secondary degrees of freedom (or generalized forces). Thus, finite elements based on the classical plate theory require continuity of the transverse deflection and its normal derivative across element boundaries. Also, to satisfy the constant displacement (rigid body mode) and constant strain requirements, the polynomial expansion for w_0 should be a complete quadratic.

9.2.2 Spatial Approximations

First, we note that the stress and moment resultants contain first-order derivatives of (u_0, v_0) and second-order derivatives of w_0 with respect to the coordinates x and y . Second, the primary variables u_0 , v_0 , w_0 , $\partial w_0 / \partial x$, and $\partial w_0 / \partial y$ must be carried as the nodal variables in order to enforce their interelement continuity. Thus, the displacements (u_0, v_0) must be approximated using the Lagrange interpolation functions, whereas w_0 should be approximated using Hermite interpolation functions over an element Ω^e . Let

$$\begin{aligned}
u_0(x, y, t) &\approx \sum_{j=1}^m u_j^e(t) \psi_j^e(x, y) \\
v_0(x, y, t) &\approx \sum_{j=1}^m v_j^e(t) \psi_j^e(x, y) \\
w_0(x, y, t) &\approx \sum_{k=1}^n \Delta_k^e(t) \varphi_k^e(x, y)
\end{aligned} \tag{9.2.4}$$

where (u_j^e, v_j^e) denote the values of (u_0, v_0) at the j th node of the Lagrange elements, Δ_k^e denote the values of w_0 and its derivatives with respect to x and y at the k -th node, and (ψ_j^e, φ_k^e) are the Lagrange and Hermite interpolation functions, respectively.

Lagrange Interpolation Functions

The Lagrange interpolation functions $\psi_i^e(x, y)$ used for the in-plane displacements (u_0, v_0) can be derived as described for the one-dimensional functions (see Reddy [1], Chapter 9). The simplest Lagrange element in two dimensions is the triangular element with nodes at its vertices (see Figure 9.2.1), and its interpolation functions have the form

$$\psi_i^e(x, y) = a_i + b_i x + c_i y \quad (9.2.5a)$$

The functions are linear in x and y , complete, and have nonzero first derivatives with respect to x and y . The linear triangular element (i.e., element with linear variation of the dependent variables) can represent only a constant state of strains:

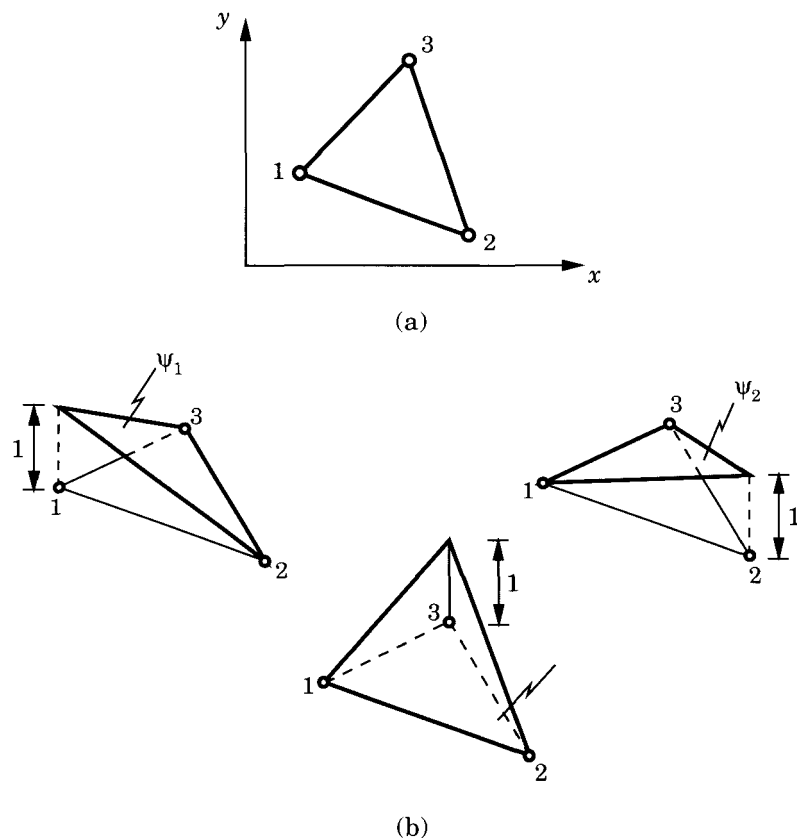


Figure 9.2.1: Linear Lagrange triangular element and its interpolation functions.

$$\begin{aligned}\varepsilon_{xx}^0 &= \sum_{i=1}^3 u_i^e \frac{\partial \psi_i^e}{\partial x} = \sum_{i=1}^3 u_i^e b_i, \quad \varepsilon_{yy}^0 = \sum_{i=1}^3 v_i^e \frac{\partial \psi_i^e}{\partial y} = \sum_{j=1}^3 v_i^e c_i \\ 2\varepsilon_{xy}^0 &= \sum_{i=1}^3 \left(u_i^e \frac{\partial \psi_i^e}{\partial y} + v_i^e \frac{\partial \psi_i^e}{\partial x} \right) = \sum_{i=1}^3 (u_i^e c_i + v_i^e b_i)\end{aligned}\quad (9.2.5b)$$

For this reason the linear triangular element is known as the *constant strain triangle* (CST). A triangular element with quadratic variation of the dependent variables requires six nodes, because a complete quadratic polynomial in two dimensions has six coefficients:

$$\psi_i^e(x, y) = a_i + b_i x + c_i y + d_i x y + e_i x^2 + f_i y^2 \quad (9.2.6a)$$

The three vertex nodes uniquely describe the geometry of the element (as in the linear element), and the other three nodes are placed at the midpoints of the sides (see Figure 9.2.2). The quadratic triangular element represents a state of linear strains:

$$\begin{aligned}\varepsilon_{xx}^0 &= \sum_{i=1}^6 u_i^e (b_i + 2e_i x + d_i y), \quad \varepsilon_{yy}^0 = \sum_{i=1}^6 v_i^e (c_i + d_i x + 2f_i y) \\ 2\varepsilon_{xy}^0 &= \sum_{i=1}^6 [u_i^e (c_i + d_i x + 2f_i y) + v_j^e (b_i + 2e_i x + d_i y)]\end{aligned}\quad (9.2.6b)$$

The interpolation functions for linear and quadratic triangular elements are presented below in terms of the area coordinates, L_i (see Figures 9.2.1 and 9.2.2):

$$\begin{Bmatrix} \psi_1^e \\ \psi_2^e \\ \psi_3^e \end{Bmatrix} = \begin{Bmatrix} L_1 \\ L_2 \\ L_3 \end{Bmatrix}, \quad \begin{Bmatrix} \psi_1^e \\ \psi_2^e \\ \psi_3^e \\ \psi_4^e \\ \psi_5^e \\ \psi_6^e \end{Bmatrix} = \begin{Bmatrix} L_1(2L_1 - 1) \\ L_2(2L_2 - 1) \\ L_3(2L_3 - 1) \\ 4L_1L_2 \\ 4L_2L_3 \\ 4L_3L_1 \end{Bmatrix} \quad (9.2.7a)$$

where L_i are the area coordinates defined within an element

$$L_i = \frac{A_i}{A}, \quad A = \sum_{i=1}^3 A_i \quad (9.2.7b)$$

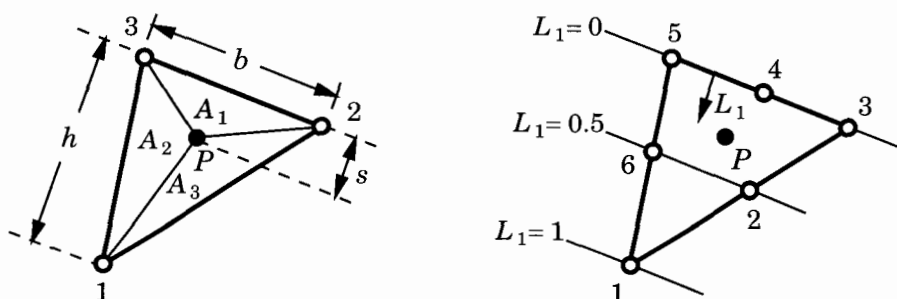


Figure 9.2.2: Quadratic Lagrange triangular element.

The simplest rectangular element has four nodes at vertices (see Figure 9.2.3), which define the geometry. The interpolation functions for this element have the form

$$\psi_i^e(x, y) = a_i + b_i x + c_i y + d_i x y \quad (9.2.8a)$$

The strains in the linear rectangular element are partially linear (i.e., at least linear in one coordinate)

$$\begin{aligned} \varepsilon_{xx}^0 &= \sum_{i=1}^4 u_i^e (b_i + d_i y), \quad \varepsilon_{yy}^0 = \sum_{j=1}^4 v_j^e (c_j + d_j x) \\ 2\varepsilon_{xy}^0 &= \sum_{i=1}^4 [u_i^e (c_i + d_i x) + v_i^e (b_i + d_i y)] \end{aligned} \quad (9.2.8b)$$

Note that the shear strain is represented as a bilinear function of the coordinates.

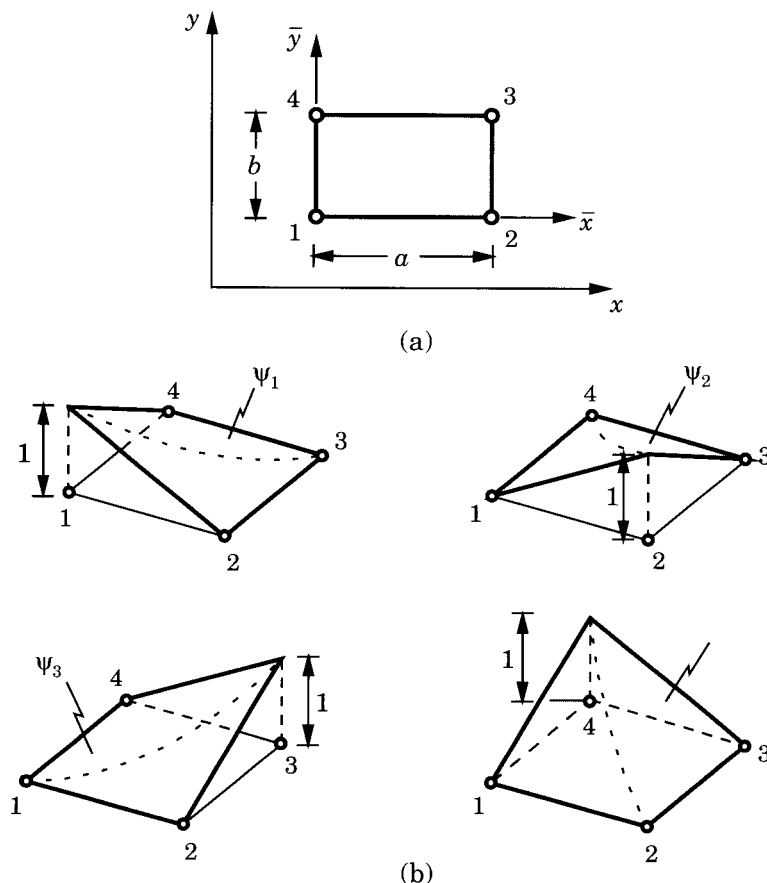


Figure 9.2.3: Linear Lagrange rectangular element and its interpolation functions.

A rectangular element with a complete quadratic polynomial representation

$$\begin{aligned}\psi_i^e(x, y) = & a_i + b_i x + c_i y + d_i x y + e_i x^2 + f_i y^2 + g_i x^2 y \\ & + h_i x y^2 + k_i x^2 y^2\end{aligned}\quad (9.2.9a)$$

contains nine parameters and hence nine nodes (see Figure 9.2.4). In these elements the strains are represented at least as bilinear:

$$\begin{aligned}\varepsilon_{xx}^0 &= \sum_{i=1}^9 u_i^e (b_i + 2e_i x + d_i y + 2g_i x y + h_i y^2 + 2k_i x y^2) \\ \varepsilon_{yy}^0 &= \sum_{j=1}^9 v_j^e (c_j + d_j x + 2f_j y + 2h_j x y + g_j x^2 + 2k_j x^2 y)\end{aligned}\quad (9.2.9b)$$

and the shear strain is represented as a bi-quadratic function of the coordinates.

The linear and quadratic Lagrange interpolation functions of rectangular elements are given below in terms of the element coordinates (ξ, η) , called the *natural coordinates*.

$$\left\{ \begin{array}{l} \psi_1^e \\ \psi_2^e \\ \psi_3^e \\ \psi_4^e \end{array} \right\} = \frac{1}{4} \left\{ \begin{array}{l} (1-\xi)(1-\eta) \\ (1+\xi)(1-\eta) \\ (1+\xi)(1+\eta) \\ (1-\xi)(1+\eta) \end{array} \right\} \quad (9.2.10)$$

$$\left\{ \begin{array}{l} \psi_1^e \\ \psi_2^e \\ \psi_3^e \\ \psi_4^e \\ \psi_5^e \\ \psi_6^e \\ \psi_7^e \\ \psi_8^e \\ \psi_9^e \end{array} \right\} = \frac{1}{4} \left\{ \begin{array}{l} (1-\xi)(1-\eta)(-\xi-\eta-1) + (1-\xi^2)(1-\eta^2) \\ (1+\xi)(1-\eta)(\xi-\eta-1) + (1-\xi^2)(1-\eta^2) \\ (1+\xi)(1+\eta)(\xi+\eta-1) + (1-\xi^2)(1-\eta^2) \\ (1-\xi)(1+\eta)(-\xi+\eta-1) + (1-\xi^2)(1-\eta^2) \\ 2(1-\xi^2)(1-\eta) - (1-\xi^2)(1-\eta^2) \\ 2(1+\xi)(1-\eta^2) - (1-\xi^2)(1-\eta^2) \\ 2(1-\xi^2)(1+\eta) - (1-\xi^2)(1-\eta^2) \\ 2(1-\xi)(1-\eta^2) - (1-\xi^2)(1-\eta^2) \\ 4(1-\xi^2)(1-\eta^2) \end{array} \right\} \quad (9.2.11)$$

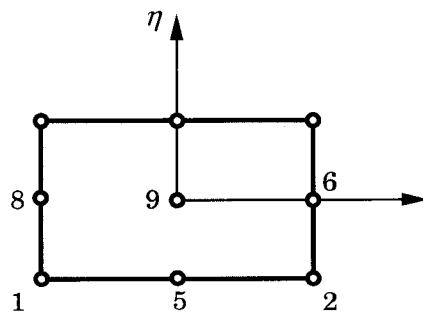


Figure 9.2.4: Nine-node quadratic Lagrange rectangular element.

The *serendipity* family of Lagrange elements are those elements which have no interior nodes. Serendipity elements have fewer nodes compared to the higher-order Lagrange elements. The interpolation functions of the serendipity elements are not complete, and they cannot be obtained using tensor products of one-dimensional Lagrange interpolation functions. Instead, an alternative procedure must be employed, as discussed in Reference 1. The interpolation functions for the quadratic serendipity element are given in Eq. (9.2.12) below (also see Figure 9.2.5). Although the interpolation functions are not complete because the last term in Eq. (9.2.9a) is omitted, the serendipity elements have proven to be very effective in most practical applications (*serendipity*!).

$$\left\{ \begin{array}{l} \psi_1^e \\ \psi_2^e \\ \psi_3^e \\ \psi_4^e \\ \psi_5^e \\ \psi_6^e \\ \psi_7^e \\ \psi_8^e \end{array} \right\} = \frac{1}{4} \left\{ \begin{array}{l} (1-\xi)(1-\eta)(-\xi-\eta-1) \\ (1+\xi)(1-\eta)(\xi-\eta-1) \\ (1+\xi)(1+\eta)(\xi+\eta-1) \\ (1-\xi)(1+\eta)(-\xi+\eta-1) \\ 2(1-\xi^2)(1-\eta) \\ 2(1+\xi)(1-\eta^2) \\ 2(1-\xi^2)(1+\eta) \\ 2(1-\xi)(1-\eta^2) \end{array} \right\} \quad (9.2.12)$$

Hermite Interpolation Functions

There exists a vast literature on triangular and rectangular plate bending finite elements of isotropic or orthotropic plates based on the classical plate theory (e.g., see References 6–27). Here we discuss triangular and rectangular C^1 plate bending elements.

There are two kinds of C^1 plate bending elements. A *conforming element* is one in which the interelement continuity of w_0 , $\partial w_0/\partial x$, and $\partial w_0/\partial y$ (or $\partial w_0/\partial n$) is satisfied, and a *nonconforming element* is one in which the continuity of the normal slope, $\partial w_0/\partial n$, is not satisfied.

An effective nonconforming triangular element (the BCIZ triangle) was developed by Bazeley, Cheung, Irons, and Zienkiewicz [7], and it consists of three degrees of freedom ($w_0, -\partial w_0/\partial y, \partial w_0/\partial x$) at the three vertex nodes (see Figure 9.2.6). The interpolation functions for the linear triangular element can be expressed in terms

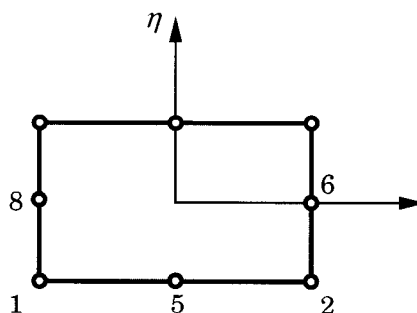


Figure 9.2.5: Eight-node quadratic serendipity rectangular element.

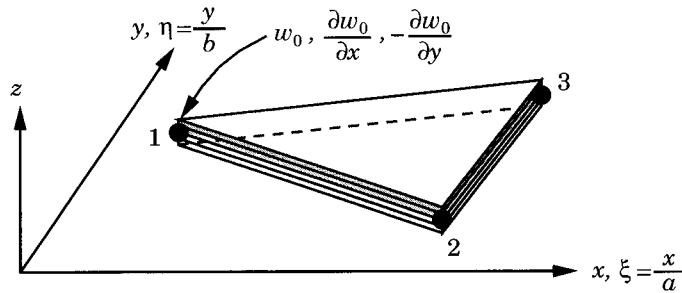


Figure 9.2.6: A nonconforming triangular element with three degrees of freedom ($w_0, \partial w_0 / \partial x, \partial w_0 / \partial y$) per node.

of the area coordinates as

$$\left\{ \begin{array}{l} \varphi_1^e \\ \varphi_2^e \\ \varphi_3^e \\ \varphi_4^e \\ \varphi_5^e \\ \varphi_6^e \\ \varphi_7^e \\ \varphi_8^e \\ \varphi_9^e \end{array} \right\} = \left\{ \begin{array}{l} L_1 + L_1^2 L_2 + L_1^2 L_3 - L_1 L_2^2 - L_1 L_3^2 \\ x_{31}(L_3 L_1^2 - f) - x_{12}(L_1^2 L_2 + f) \\ y_{31}(L_3 L_1^2 + f) - y_{12}(L_1^2 L_2 + f) \\ L_2 + L_2^2 L_3 + L_2^2 L_1 - L_2 L_3^2 - L_2 L_1^2 \\ x_{12}(L_1 L_2^2 - f) - x_{23}(L_2^2 L_3 + f) \\ y_{12}(L_1 L_2^2 + f) - y_{23}(L_2^2 L_3 + f) \\ L_3 + L_3^2 L_1 + L_3^2 L_2 - L_3 L_1^2 - L_3 L_2^2 \\ x_{23}(L_2 L_3^2 - f) - x_{31}(L_3^2 L_1 + f) \\ y_{23}(L_2 L_3^2 + f) - y_{31}(L_3^2 L_1 + f) \end{array} \right\} \quad (9.2.13)$$

where $f = 0.5L_1 L_2 L_3$, $x_{ij} = x_i - x_j$, and $y_{ij} = y_i - y_j$, (x_i, y_i) being the global coordinates of the i th node.

A conforming triangular element due to Clough and Tocher [22] is an assemblage of three triangles as shown in Figure 9.2.7. The normal slope continuity is enforced at the midside nodes between the subtriangles. In each subtriangle, the transverse deflection is represented by the polynomial ($i = 1, 2, 3$)

$$w_0^i(x, y) = a_1^i + a_2^i \xi + a_3^i \eta + a_4^i \xi^2 + a_5^i \xi \eta + a_6^i \eta^2 + a_7^i \xi^3 + a_8^i \xi \eta^2 + a_9^i \eta^3 \quad (9.2.14)$$

where (ξ, η) are the local coordinates, as shown in the Figure 9.2.7. The thirty coefficients are reduced to nine, three ($w_0, \partial w_0 / \partial x, \partial w_0 / \partial y$) at each vertex of the triangle, by equating the variables from the vertices of each subtriangle at the common points and normal slope between the midside points of subtriangles.

A nonconforming rectangular element has w_0 , θ_x , and θ_y as the nodal variables (see Figure 9.2.8). The element was developed by Melosh [18] and Zienkiewicz and Cheung [19]. The normal slope varies cubically along an edge whereas there are only two values of $\partial w_0 / \partial n$ available on the edge. Therefore, the cubic polynomial for the normal derivative of w_0 is not the same on the edge common to two elements. The interpolation functions for this element can be expressed compactly as

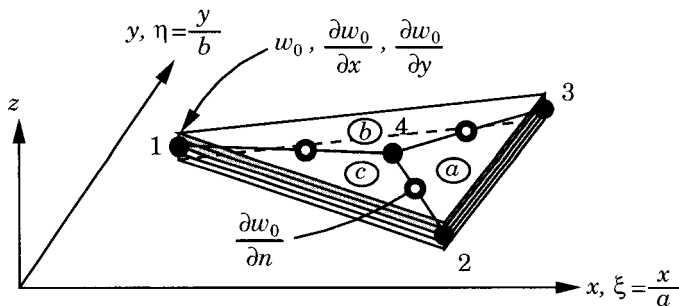


Figure 9.2.7: A conforming triangular element with three degrees of freedom.

$$\begin{aligned}\varphi_i^e &= g_{i1} \quad (i = 1, 4, 7, 10); \quad \varphi_i^e = g_{i2} \quad (i = 2, 5, 8, 11) \\ \varphi_i^e &= g_{i3} \quad (i = 3, 6, 9, 12)\end{aligned}\quad (9.2.15a)$$

where

$$\begin{aligned}g_{i1} &= \frac{1}{8}(1 + \xi_0)(1 + \eta_0)(2 + \xi_0 + \eta_0 - \xi^2 - \eta^2) \\ g_{i2} &= \frac{1}{8}\xi_i(\xi_0 - 1)(1 + \eta_0)(1 + \xi_0)^2 \\ g_{i3} &= \frac{1}{8}\eta_i(\eta_0 - 1)(1 + \xi_0)(1 + \eta_0)^2 \\ \xi &= (x - x_c)/2, \quad \eta = (y - y_c)/b, \quad \xi_0 = \xi\xi_i, \quad \eta_0 = \eta\eta_i\end{aligned}\quad (9.2.15b)$$

where $2a$ and $2b$ are the sides of the rectangle, and (x_c, y_c) are the global coordinates of the center of the rectangle.

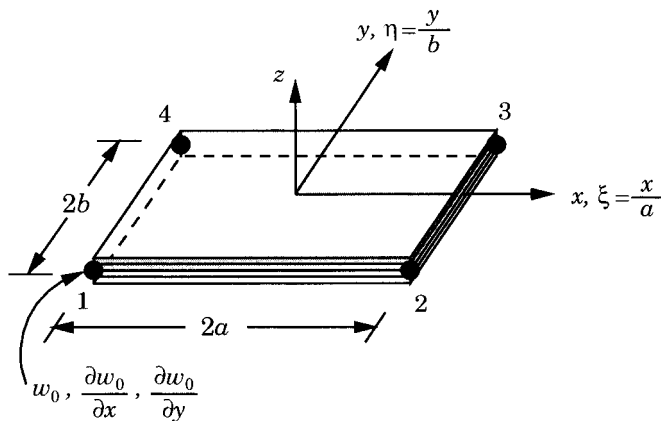


Figure 9.2.8: A nonconforming rectangular element with three degrees of freedom ($w_0, \partial w_0 / \partial x, \partial w_0 / \partial y$) per node.

A conforming rectangular element with w_0 , $\partial w_0/\partial x$, $\partial w_0/\partial y$, and $\partial^2 w_0/\partial x \partial y$ as the nodal variables was developed by Bogner, Fox, and Schmidt [20]. The interpolation functions for this element (see Figure 9.2.9) are

$$\begin{aligned}\varphi_i^e &= g_{i1} \quad (i = 1, 5, 9, 13); \quad \varphi_i^e = g_{i2} \quad (i = 2, 6, 10, 14) \\ \varphi_i^e &= g_{i3} \quad (i = 3, 7, 11, 15); \quad \varphi_i^e = g_{i4} \quad (i = 4, 8, 12, 16)\end{aligned}\quad (9.2.16a)$$

where

$$\begin{aligned}g_{i1} &= \frac{1}{16}(\xi + \xi_i)^2(\xi_0 - 2)(\eta + \eta_i)^2(\eta_0 - 2) \\ g_{i2} &= \frac{1}{16}\xi_i(\xi + \xi_i)^2(1 - \xi_0)(\eta + \eta_i)^2(\eta_0 - 2) \\ g_{i3} &= \frac{1}{16}\eta_i(\xi + \xi_i)^2(\xi_0 - 2)(\eta + \eta_i)^2(1 - \eta_0) \\ g_{i4} &= \frac{1}{16}\xi_i\eta_i(\xi + \xi_i)^2(1 - \xi_0)(\eta + \eta_i)^2(1 - \eta_0)\end{aligned}\quad (9.2.16b)$$

In this book we will use the Lagrange linear rectangular element for in-plane displacements and the conforming and nonconforming rectangular elements for bending deflections to present numerical results. The combined conforming element has a total of six degrees of freedom per node, whereas the nonconforming element has a total of five degrees of freedom per node. For the conforming rectangular element ($m = 4$ and $n = 12$) the total number of nodal degrees of freedom per element is 24, and for the nonconforming element the total number of degrees of freedom per element is 12.

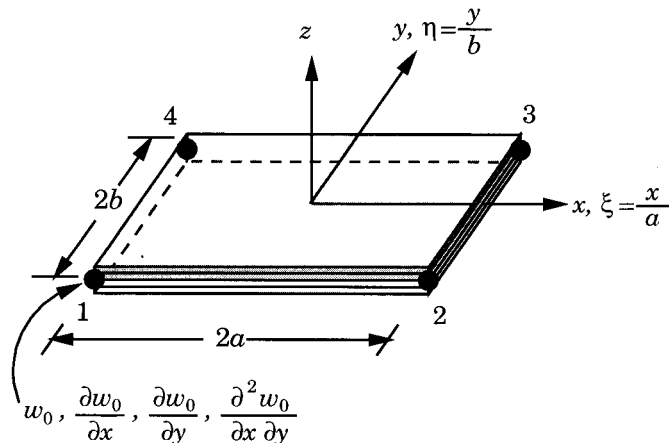


Figure 9.2.9: A conforming rectangular element with four degrees of freedom ($w_0, \partial w_0/\partial x, \partial w_0/\partial y, \partial^2 w_0/\partial x \partial y$) per node.

9.2.3 Semidiscrete Finite Element Model

Substituting approximations (9.2.4) for the displacements and the i th interpolation function for the virtual displacement ($\delta u_0 \sim \psi_i, \delta v_0 \sim \psi_i, \delta w_0 \sim \varphi_i$) into the weak forms, we obtain the i th equation associated with each weak form

$$\begin{aligned} 0 &= \sum_{j=1}^m \left(K_{ij}^{11} u_j^e + K_{ij}^{12} v_j^e + M_{ij}^{11} \ddot{u}_j^e \right) + \sum_{k=1}^n \left(K_{ik}^{13} \Delta_k^e + M_{ik}^{13} \ddot{\Delta}_k^e \right) - F_i^1 - F_i^{T1} \\ 0 &= \sum_{j=1}^m \left(K_{ij}^{21} u_j^e + K_{ij}^{22} v_j^e + M_{ij}^{22} \ddot{v}_j^e \right) + \sum_{k=1}^n \left(K_{ik}^{23} \Delta_k^e + M_{ik}^{23} \ddot{\Delta}_k^e \right) - F_i^2 - F_i^{T2} \\ 0 &= \sum_{j=1}^m \left(K_{kj}^{31} u_j^e + K_{kj}^{32} v_j^e + M_{kj}^{31} \ddot{u}_j^e + M_{kj}^{32} \ddot{v}_j^e \right) \\ &\quad + \sum_{\ell=1}^n \left[\left(K_{k\ell}^{33} + G_{k\ell}^e \right) \Delta_\ell^e + M_{k\ell}^{33} \ddot{\Delta}_\ell^e \right] - F_k^3 - F_k^{T3} \end{aligned} \quad (9.2.17)$$

where $i = 1, 2, \dots, m; k = 1, 2, \dots, n$. The coefficients of the stiffness matrix $K_{ij}^{\alpha\beta} = K_{ji}^{\beta\alpha}$, mass matrix $M_{ij}^{\alpha\beta} = M_{ji}^{\beta\alpha}$ (symmetric), and force vectors F_i^α and $F_i^{T\alpha}$ are defined as follows:

$$\begin{aligned} K_{ij}^{11} &= A_{11} S_{ij}^{xx} + A_{16} \left(S_{ij}^{xy} + S_{ij}^{yx} \right) + A_{66} S_{ij}^{yy} \\ K_{ij}^{12} &= A_{12} S_{ij}^{xy} + A_{16} S_{ij}^{xx} + A_{26} S_{ij}^{yy} + A_{66} S_{ij}^{yx} \\ K_{ij}^{22} &= A_{66} S_{ij}^{xx} + A_{26} \left(S_{ij}^{xy} + S_{ij}^{yx} \right) + A_{22} S_{ij}^{yy} \\ K_{ik}^{13} &= -B_{11} R_{ik}^{xxx} - B_{12} R_{ik}^{xxy} - 2B_{26} R_{ik}^{xxy} - B_{16} R_{ik}^{yxx} - B_{26} R_{ik}^{yyy} - 2B_{66} R_{ik}^{xyx} \\ K_{ik}^{23} &= -B_{16} R_{ik}^{xxx} - B_{26} R_{ik}^{xxy} - 2B_{66} R_{ik}^{xxy} - B_{12} R_{ik}^{yxx} - B_{22} R_{ik}^{yyy} - 2B_{26} R_{ik}^{xyx} \\ K_{k\ell}^{33} &= D_{11} T_{k\ell}^{xxxx} + D_{12} (T_{k\ell}^{xxyy} + T_{k\ell}^{yyxx}) + 2D_{16} (T_{k\ell}^{xxyy} + T_{k\ell}^{xyxx}) \\ &\quad + 2D_{26} (T_{k\ell}^{xyyy} + T_{k\ell}^{yyxy}) + 4D_{66} T_{k\ell}^{xyxy} + D_{22} T_{k\ell}^{yyyy} \\ G_{ij}^e &= \int_{\Omega^e} \left[\hat{N}_{xx} \hat{S}_{ij}^{xx} + \hat{N}_{xy} \left(\hat{S}_{ij}^{xy} + \hat{S}_{ij}^{yx} \right) + \hat{N}_{yy} \hat{S}_{ij}^{yy} \right] dx dy \\ M_{ij}^{11} &= \int_{\Omega^e} I_0 \psi_i^e \psi_j^e dx dy, & M_{ik}^{13} &= - \int_{\Omega^e} I_1 \psi_i^e \frac{\partial \varphi_k^e}{\partial x} dx dy \\ M_{ij}^{22} &= \int_{\Omega^e} I_0 \psi_i^e \psi_j^e dx dy, & M_{ik}^{23} &= - \int_{\Omega^e} I_1 \psi_i^e \frac{\partial \varphi_k^e}{\partial y} dx dy \\ M_{k\ell}^{33} &= \int_{\Omega^e} \left[I_0 \varphi_k^e \varphi_\ell^e + I_2 \left(\frac{\partial \varphi_k^e}{\partial x} \frac{\partial \varphi_\ell^e}{\partial x} + \frac{\partial \varphi_k^e}{\partial y} \frac{\partial \varphi_\ell^e}{\partial y} \right) \right] ds \\ F_i^1 &= \oint_{\Gamma_e} p_x \psi_i^e ds, & F_i^2 &= \int_{\Gamma_e} p_y \psi_i^e ds \\ F_k^3 &= \int_{\Omega^e} q \varphi_k^e dx dy + \oint_{\Gamma_e} \left(Q_n \varphi_k^e + T_x \frac{\partial \varphi_k^e}{\partial x} + T_y \frac{\partial \varphi_k^e}{\partial y} \right) ds \\ F_i^{T1} &= \int_{\Omega^e} \left(\frac{\partial \psi_i^e}{\partial x} N_{xx}^T + \frac{\partial \psi_i^e}{\partial y} N_{xy}^T \right) dx dy, & F_i^{T2} &= \int_{\Omega^e} \left(\frac{\partial \psi_i^e}{\partial x} N_{xy}^T + \frac{\partial \psi_i^e}{\partial y} N_{yy}^T \right) dx dy \\ F_k^{T3} &= \int_{\Omega^e} \left(\frac{\partial^2 \varphi_k^e}{\partial x^2} M_{xx}^T + 2 \frac{\partial^2 \varphi_k^e}{\partial x \partial y} M_{xy}^T + \frac{\partial^2 \varphi_k^e}{\partial y^2} M_{yy}^T \right) dx dy \end{aligned} \quad (9.2.18a)$$

where N_{xx}^T , M_{xx}^T , etc. are the thermal force and moment resultants [see Eq. (3.3.41)], and

$$\begin{aligned} S_{ij}^{\xi\eta} &= \int_{\Omega^e} \frac{\partial \psi_i^e}{\partial \xi} \frac{\partial \psi_j^e}{\partial \eta} dx dy, & \hat{S}_{k\ell}^{\xi\eta} &= \int_{\Omega^e} \frac{\partial \varphi_k^e}{\partial \xi} \frac{\partial \varphi_\ell^e}{\partial \eta} dx dy \\ R_{ik}^{\xi\eta\zeta} &= \int_{\Omega^e} \frac{\partial \psi_i^e}{\partial \xi} \frac{\partial^2 \varphi_k^e}{\partial \eta \partial \zeta} dx dy, & T_{k\ell}^{\xi\eta\zeta\mu} &= \int_{\Omega^e} \frac{\partial^2 \varphi_k^e}{\partial \xi \partial \eta} \frac{\partial^2 \varphi_\ell^e}{\partial \zeta \partial \mu} dx dy \end{aligned} \quad (9.2.18b)$$

and ξ, η, ζ , and μ can be equal to x or y . In matrix notation, Eq. (9.2.17) can be expressed as

$$\begin{aligned} &\left[\begin{array}{ccc} [K^{11}] & [K^{12}] & [K^{13}] \\ [K^{12}]^T & [K^{22}] & [K^{23}] \\ [K^{13}]^T & [K^{23}]^T & [K^{33}] \end{array} \right] \left\{ \begin{array}{c} \{u^e\} \\ \{v^e\} \\ \{\Delta^e\} \end{array} \right\} + \left[\begin{array}{ccc} [0] & [0] & [0] \\ [0] & [0] & [0] \\ [0] & [0] & [G] \end{array} \right] \left\{ \begin{array}{c} \{u^e\} \\ \{v^e\} \\ \{\Delta^e\} \end{array} \right\} \\ &+ \left[\begin{array}{ccc} [M^{11}] & [0] & [M^{13}] \\ [0] & [M^{22}] & [M^{23}] \\ [M^{13}]^T & [M^{23}]^T & [M^{33}] \end{array} \right] \left\{ \begin{array}{c} \{\dot{u}^e\} \\ \{\dot{v}^e\} \\ \{\ddot{\Delta}^e\} \end{array} \right\} = \left\{ \begin{array}{c} \{F^1\} + \{F^{T1}\} \\ \{F^2\} + \{F^{T2}\} \\ \{F^3\} + \{F^{T3}\} \end{array} \right\} \end{aligned} \quad (9.2.19)$$

This completes the finite element model development of the classical laminate theory. The finite element model in Eq. (9.2.17) or (9.2.19) is called a *displacement finite element model* because it is based on equations of motion expressed in terms of the displacements, and the generalized displacements are the primary nodal degrees of freedom.

It should be noted that the contributions of the internal forces defined in Eq. (9.2.3) to the force vector will cancel when element equations are assembled. They will remain in the force vector only when the element boundary coincides with the boundary of the domain being modeled (see Reddy [1], pp. 313–318). Of course, the contributions of the applied loads (i.e., $q(x, y)$ and $\Delta T(x, y)$) to a node will add up from elements connected at the node and remain as a part of the force vector.

9.2.4 Fully Discretized Finite Element Models

Static Bending

In the case of static bending under applied mechanical and thermal loads, Eq. (9.2.19) reduces to

$$\left[\begin{array}{ccc} [K^{11}] & [K^{12}] & [K^{13}] \\ [K^{12}]^T & [K^{22}] & [K^{23}] \\ [K^{13}]^T & [K^{23}]^T & [K^{33}] + [G] \end{array} \right] \left\{ \begin{array}{c} \{u^e\} \\ \{v^e\} \\ \{\Delta^e\} \end{array} \right\} = \left\{ \begin{array}{c} \{F^1\} + \{F^{T1}\} \\ \{F^2\} + \{F^{T2}\} \\ \{F^3\} + \{F^{T3}\} \end{array} \right\} \quad (9.2.20)$$

where it is understood that all time-derivative terms are zero.

Buckling

In the case of buckling under applied in-plane compressive and shear edge loads, Eq. (9.2.19) reduces to

$$\left(\left[\begin{array}{ccc} [K^{11}] & [K^{12}] & [K^{13}] \\ [K^{12}]^T & [K^{22}] & [K^{23}] \\ [K^{13}]^T & [K^{23}]^T & [K^{33}] \end{array} \right] - \lambda \left[\begin{array}{ccc} [0] & [0] & [0] \\ [0] & [0] & [0] \\ [0] & [0] & [\bar{G}] \end{array} \right] \right) \left\{ \begin{array}{c} \{u^e\} \\ \{v^e\} \\ \{\Delta^e\} \end{array} \right\} = \left\{ \begin{array}{c} \{F^1\} \\ \{F^2\} \\ \{\bar{F}^3\} \end{array} \right\} \quad (9.2.21)$$

where

$$\begin{aligned}\lambda &= -\hat{N}_{xx}/\hat{N}_{xx}^0 = -\hat{N}_{yy}/\hat{N}_{yy}^0 = -\hat{N}_{xy}/\hat{N}_{xy}^0 \\ \bar{G}_{ij}^e &= \int_{\Omega^e} \left[\hat{N}_{xx}^0 S_{ij}^{xx} + \hat{N}_{xy}^0 (S_{ij}^{xy} + S_{ij}^{yx}) + \hat{N}_{yy}^0 S_{ij}^{yy} \right] dx dy \\ \bar{F}_k^3 &= \oint_{\Gamma^e} \left(Q_n \varphi_k^e + T_x \frac{\partial \varphi_k^e}{\partial x} + T_y \frac{\partial \varphi_k^e}{\partial y} \right) ds\end{aligned}\quad (9.2.22)$$

and all time-derivative terms are zero.

Natural Vibration

In the case of natural vibration, the response of the plate is assumed to be periodic

$$\{u\} = \{u^0\} e^{i\omega t}, \quad \{v\} = \{v^0\} e^{i\omega t}, \quad \{\Delta\} = \{\Delta^0\} e^{i\omega t}, \quad i = \sqrt{-1} \quad (9.2.23)$$

where $\{\Delta^0\}$ is the vector of amplitudes (independent of time) and ω is the frequency of natural vibration of the system. Substitution of Eq. (9.2.23) into Eq. (9.2.19) yields

$$\begin{aligned}&\left(\begin{bmatrix} [K^{11}] & [K^{12}] & [K^{13}] \\ [K^{12}]^T & [K^{22}] & [K^{23}] \\ [K^{13}]^T & [K^{23}]^T & [K^{33}] \end{bmatrix} - \omega^2 \begin{bmatrix} [M^{11}] & [0] & [M^{13}] \\ [0] & [M^{22}] & [M^{23}] \\ [M^{13}]^T & [M^{23}]^T & [M^{33}] \end{bmatrix} \right) \begin{Bmatrix} \{u^e\} \\ \{v^e\} \\ \{\Delta^e\} \end{Bmatrix} \\ &= \begin{Bmatrix} \{F^1\} \\ \{F^2\} \\ \{\bar{F}^3\} \end{Bmatrix}\end{aligned}\quad (9.2.24)$$

Transient Analysis

For transient analysis, Eq. (9.2.19) can be written symbolically as

$$[K^e]\{\bar{\Delta}^e\} + [M^e]\{\ddot{\Delta}^e\} = \{F^e\} \quad (9.2.25)$$

where $[K^e]$ (which may contain $[G^e]$) and $[M^e]$ are the stiffness and mass matrices appearing in Eq. (9.2.19), and

$$\{\bar{\Delta}^e\} = \begin{Bmatrix} \{u^e\} \\ \{v^e\} \\ \{\Delta^e\} \end{Bmatrix} \quad (9.2.26)$$

Equation (9.2.25) represents a set of ordinary differential equations in time. To fully discretize them (i.e., reduce them to algebraic equations), we must approximate the time derivatives. Here we discuss the Newmark time integration scheme [1,2,28] for a more general equation than that in (9.2.25).

Consider matrix equation of the form

$$[M^e]\{\ddot{\Delta}^e\} + [C^e]\{\dot{\Delta}^e\} + [K^e]\{\Delta^e\} = \{F^e\} \quad (9.2.27)$$

where $[C^e]$ denotes the damping matrix (due to structural damping and/or velocity proportional feedback control), $[M^e]$ the mass matrix, and $[K^e]$ the stiffness matrix. The global displacement vector $\{\Delta\}$ is subject to the initial conditions

$$\{\Delta(0)\} = \{\Delta\}_0, \quad \{\dot{\Delta}(0)\} = \{\dot{\Delta}\}_0 \quad (9.2.28)$$

In the Newmark method [28], the function and its time derivatives are approximated according to

$$\{\Delta\}_{s+1} = \{\Delta\}_s + \delta t \{\dot{\Delta}\}_s + \frac{1}{2}(\delta t)^2 \{\ddot{\Delta}\}_{s+\gamma} \quad (9.2.29a)$$

$$\{\dot{\Delta}\}_{s+1} = \{\dot{\Delta}\}_s + \{\ddot{\Delta}\}_{s+\alpha} \delta t \quad (9.2.29b)$$

$$\{\ddot{\Delta}\}_{s+\alpha} = (1 - \alpha) \{\ddot{\Delta}\}_s + \alpha \{\ddot{\Delta}\}_{s+1} \quad (9.2.29c)$$

and α and γ are parameters that determine the stability and accuracy of the scheme, and δt is the time step. For $\alpha = 0.5$, the following values of γ define various well-known schemes:

$$\gamma = \begin{cases} \frac{1}{2}, & \text{the constant-average acceleration method (stable)} \\ \frac{1}{3}, & \text{the linear acceleration method (conditionally stable)} \\ 0, & \text{the central difference method (conditionally stable)} \\ \frac{8}{5}, & \text{the Galerkin method (stable)} \\ 2, & \text{the backward difference method (stable)} \end{cases} \quad (9.2.30)$$

The set of ordinary differential equations in (9.2.27) can be reduced, with the help of Eqs. (9.2.29a-c), to a set of algebraic equations relating $\{\Delta\}_{s+1}$ to $\{\Delta\}_s$. We have

$$[\hat{K}]_{s+1} \{\Delta\}_{s+1} = \{\hat{F}\}_{s,s+1} \quad (9.2.31)$$

where

$$\begin{aligned} [\hat{K}]_{s+1} &= [K]_{s+1} + a_3[M]_{s+1} + a_6[C]_{s+1} \\ \{\hat{F}\}_{s,s+1} &= \{F\}_{s+1} + [M]_{s+1}\{A\}_s + [C]_{s+1}\{B\}_s \\ \{A\}_s &= a_3\{\Delta\}_s + a_4\{\dot{\Delta}\}_s + a_5\{\ddot{\Delta}\}_s \\ \{B\}_s &= a_6\{\Delta\}_s + a_7\{\dot{\Delta}\}_s + a_8\{\ddot{\Delta}\}_s \end{aligned} \quad (9.2.32)$$

and a_i , $i = 1, 2, \dots, 8$, are defined as ($\gamma = 2\beta$)

$$\begin{aligned} a_1 &= \alpha \delta t, \quad a_2 = (1 - \alpha) \delta t, \quad a_3 = \frac{1}{\beta(\delta t)^2}, \quad a_4 = a_3 \delta t \\ a_5 &= \frac{1}{\gamma} - 1, \quad a_6 = \frac{\alpha}{\beta \delta t}, \quad a_7 = \frac{\alpha}{\beta} - 1, \quad a_8 = \delta t \left(\frac{\alpha}{\gamma} - 1 \right) \end{aligned} \quad (9.2.33)$$

Note that in Newmark's scheme the calculation of $[\hat{K}]$ and $\{\hat{F}\}$ requires knowledge of the initial conditions $\{\Delta\}_0$, $\{\dot{\Delta}\}_0$, and $\{\ddot{\Delta}\}_0$. In practice, one does not know $\{\ddot{\Delta}\}_0$. As an approximation, it can be calculated from the assembled system

of equations associated with (9.2.31) using initial conditions on $\{\Delta\}$, $\{\dot{\Delta}\}$, and $\{F\}$ (often $\{F\}$ is assumed to be zero at $t = 0$):

$$\{\ddot{\Delta}\}_0 = [M]^{-1} (\{F\}_0 - [K]\{\Delta\}_0 - [C]\{\dot{\Delta}\}) \quad (9.2.34)$$

At the end of each time step, the new velocity vector $\{\dot{\Delta}\}_{s+1}$ and acceleration vector $\{\ddot{\Delta}\}_{s+1}$ are computed using the equations

$$\begin{aligned} \{\ddot{\Delta}\}_{s+1} &= a_3(\{\Delta\}_{s+1} - \{\Delta\}_s) - a_4\{\dot{\Delta}\}_s - a_5\{\ddot{\Delta}\}_s \\ \{\dot{\Delta}\}_{s+1} &= \{\dot{\Delta}\}_s + a_2\{\ddot{\Delta}\}_s + a_1\{\ddot{\Delta}\}_{s+1} \end{aligned} \quad (9.2.35)$$

where a_1 and a_2 are defined in Eq. (9.2.33).

Returning to Eq. (9.2.25), the fully discretized system is given by

$$[\hat{K}^e]_{s+1}\{\bar{\Delta}^e\}_{s+1} = \{\hat{F}^e\} \quad (9.2.36a)$$

$$\begin{aligned} [\hat{K}^e]_{s+1} &= ([K^e]_{s+1} + [G^e]_{s+1}) + a_3[M^e]_{s+1} \\ \{\hat{F}^e\} &= \{F^e\}_{s+1} + [M^e]_{s+1}\{A^e\} \\ \{A^e\} &= (a_3\{\bar{\Delta}^e\}_s + a_4\{\dot{\bar{\Delta}}^e\}_s + a_5\{\ddot{\bar{\Delta}}^e\}_s) \end{aligned} \quad (9.2.36b)$$

9.2.5 Quadrilateral Elements and Numerical Integration

Introduction

An accurate representation of irregular domains (i.e., domains with curved boundaries) can be accomplished by the use of refined meshes and/or irregularly shaped elements. For example, a nonrectangular region cannot be represented using all rectangular elements; however, it can be represented by triangular and quadrilateral elements. However, it is easy to derive the interpolation functions for a rectangular element, and it is easier to evaluate integrals over rectangular geometries than over irregular geometries. Therefore, it is practical to use quadrilateral elements with straight or curved sides but have a means to generate interpolation functions and evaluate their integrals over the quadrilateral elements. A coordinate transformation between the coordinates (x, y) used in the formulation of the problem, called *global coordinates*, and the element coordinates (\bar{x}, \bar{y}) used to derive the interpolation functions of rectangular elements is introduced for this purpose. The transformation of the geometry and the variable coefficients of the differential equation from the problem coordinates (x, y) to the local coordinates (\bar{x}, \bar{y}) results in algebraically complex expressions, and they preclude analytical (i.e., exact) evaluation of the integrals. Therefore, numerical integration is used to evaluate such complicated expressions.

While the element coordinate system, also called a *local coordinate system*, can be any convenient system that permits easy construction of the interpolation functions, it is useful to select one that is also convenient in the numerical evaluation of the integrals. Numerical integration schemes, such as the Gauss-Legendre numerical

integration scheme, require the integral to be evaluated on a specific domain or with respect to a specific coordinate system. Gauss quadrature, for example, requires the integral to be expressed over a square region $\hat{\Omega}$ of dimension 2×2 and the coordinate system (ξ, η) be such that $-1 \leq (\xi, \eta) \leq 1$. The coordinates (ξ, η) are called *normalized* or *natural coordinates*. Thus, the transformation between (x, y) and (ξ, η) of a given integral expression defined over a quadrilateral element Ω^e to one on the domain $\hat{\Omega}$ facilitates the use of Gauss–Legendre quadrature to evaluate integrals. The element $\hat{\Omega}$ is called a *master element* (see Reddy [1], Chapter 9).

Coordinate Transformations

The transformation between Ω^e and $\hat{\Omega}$ is accomplished by a coordinate transformation of the form

$$x = \sum_{j=1}^m x_j^e \hat{\psi}_j^e(\xi, \eta), \quad y = \sum_{j=1}^n y_j^e \hat{\psi}_j^e(\xi, \eta) \quad (9.2.37)$$

while a typical dependent variable $u(x, y)$ is approximated by

$$u(x, y) = \sum_{j=1}^n u_j^e \hat{\psi}_j^e(x, y) = \sum_{j=1}^n u_j^e \hat{\psi}_j^e(x(\xi, \eta), y(\xi, \eta)) \quad (9.2.38)$$

where $\hat{\psi}_j^e$ denote the interpolation functions of the master element $\hat{\Omega}$ and ψ_j^e are interpolation functions of a typical element Ω^e over which u is approximated. Although the Lagrange interpolation of the geometry is implied by Eqs. (9.2.27) and (9.2.28), one can also use Hermite interpolation of the geometry and/or the solution as required. The transformation (9.2.27) maps a point (x, y) in a typical element Ω^e of the mesh to a point (ξ, η) in the master element $\hat{\Omega}$, and vice versa if the Jacobian of the transformation is positive-definite. The positive-definite requirement of the Jacobian dictates admissible geometries of elements in a mesh (see Reddy [1], pp. 421–448).

The interpolation functions ψ_j^e used for the approximation of the dependent variable are, in general, different from $\hat{\psi}_j^e$ used in the approximation of the geometry. Depending on the relative degree of approximations used for the geometry and the dependent variable(s), the finite element formulations are classified into three categories.

1. *Superparametric* ($m > n$): The polynomial degree of approximation used for the geometry is of higher order than that used for the dependent variable.
2. *Isoparametric* ($m = n$): Equal degree of approximation is used for both geometry and dependent variables.
3. *Subparametric* ($m < n$): Higher-order approximation of the dependent variable is used.

For example, in the finite element analysis of the Euler–Bernoulli beams, we may use linear Lagrange interpolation of the geometry

$$x = \sum_{j=1}^2 x_j \hat{\psi}_j(\xi) \quad (9.2.39)$$

whereas the Hermite cubic interpolation is used to approximate the transverse deflection

$$w_0(x) = \sum_{j=1}^4 \Delta_j^e \varphi_j(x(\xi)) \quad (9.2.40)$$

Then we say that subparametric formulation is used for the transverse deflection w_0 . In the Timoshenko beam element we can use the same degree of interpolation for both geometry and dependent variables. Then we say that isoparametric formulation is used for the transverse deflection w_0 and rotation ϕ_x .

An example of the coordinate transformation in one dimension is provided by the linear transformation, which maps straight lines into straight lines

$$x = \sum_{i=1}^2 x_i^e \hat{\psi}_i(\xi), \quad \hat{\psi}_1(\xi) = \frac{1}{2}(1 - \xi), \quad \hat{\psi}_2(\xi) = \frac{1}{2}(1 + \xi) \quad (9.2.41a)$$

where $x_1^e = x_e$ and $x_2^e = x_{e+1}$, x_i^e being the global coordinate of the i th node of the e th element, and x_I denotes the global coordinate of the I th global node of the mesh. The transformation (9.2.41a) can be expressed directly in terms of x and ξ :

$$x = x_e + \frac{h_e}{2}(1 + \xi) \quad (9.2.41b)$$

where $h_e = x_{e+1} - x_e$ is the element length. Note that the Lagrange and Hermite interpolation functions defined in Eqs. (9.2.39) and (9.2.40), respectively, can be written in terms of the natural coordinate ξ with the help of the linear coordinate transformation (9.2.41):

$$\psi_1 = \frac{1}{2}(1 - \xi), \quad \psi_2 = \frac{1}{2}(1 + \xi) \quad (9.2.42)$$

$$\begin{aligned} \varphi_1 &= \frac{1}{4}(2 - 3\xi^2 + \xi^3), & \varphi_2 &= -\frac{h_e}{8}(1 - \xi)(1 - \xi^2) \\ \varphi_3 &= \frac{1}{4}(2 + 3\xi^2 - \xi^3), & \varphi_4 &= \frac{h_e}{8}(1 + \xi)(1 - \xi^2) \end{aligned} \quad (9.2.43)$$

It should be noted that, once the approximations of geometry and solution are selected, the coordinate transformations have the sole purpose of numerically evaluating the integrals inside the computer program. *No transformation of the physical domain or the solution is involved in the finite element analysis.* The resulting algebraic equations of the finite element formulation are always among the nodal values of the physical domain and the nodal values are referred to the global coordinate system. Different elements of the finite element mesh can be generated from the same master element by assigning the global coordinates of the elements. Master elements of different order interpolation define different transformations and hence different collections of finite element meshes. Thus, with the help of an appropriate master element, any given element of a mesh can be generated. However, the transformations of a master element should be such that there exist no spurious gaps between elements and no element overlaps occur.

Numerical Integration: the Gauss Quadrature

Recall that a finite element model is a system of algebraic equations among the nodal values of the primary variables (generalized displacements) and secondary variables (generalized forces). The coefficients of these algebraic equations contain integrals of the physical parameters (e.g., material properties) and functions used for the approximation of the primary variables. The integral expressions are, in general, complicated algebraically due to the spatial variation of the parameters or coordinate transformations. Therefore, numerical integration methods, known as numerical quadratures, are used to evaluate them. Here we discuss the Gauss quadrature, which is the most widely used method for master elements of rectangular or prismatic geometries.

We illustrate the essential elements of the Gauss quadrature by considering the following representative integral expression

$$K_{ij}^e = \int_{\Omega^e} \left[a(x, y) \frac{\partial \psi_i^e}{\partial x} \frac{\partial \psi_j^e}{\partial x} + b(x, y) \left(\frac{\partial \psi_i^e}{\partial x} \frac{\partial \psi_j^e}{\partial y} + \frac{\partial \psi_i^e}{\partial y} \frac{\partial \psi_j^e}{\partial x} \right) \right. \\ \left. + c(x, y) \frac{\partial \psi_i^e}{\partial y} \frac{\partial \psi_j^e}{\partial y} + d(x, y) \psi_i^e \psi_j^e \right] dx dy \quad (9.2.44)$$

We wish to transform the integral from Ω^e to the master element $\hat{\Omega} = \{(\xi, \eta) : -1 \leq \xi \leq 1, -1 \leq \eta \leq 1\}$ so that the Gauss quadrature can be used. Note that the integrand contains not only $\psi_i^e(x, y)$, but also their derivatives with respect to the global coordinates (x, y) . The functions $\psi_i^e(x, y)$ can be easily expressed in terms of the local coordinates ξ and η by means of the transformation in Eq. (9.2.37), as was shown for one-dimensional Lagrange and Hermite functions in Eqs. (9.2.42) and (9.2.43). We must first develop relations $\partial \psi_i^e / \partial x$ and $\partial \psi_i^e / \partial y$ to $\partial \psi_i^e / \partial \xi$ and $\partial \psi_i^e / \partial \eta$ using the transformation (9.2.37).

By the chain rule of partial differentiation, we have

$$\begin{Bmatrix} \frac{\partial \psi_i^e}{\partial \xi} \\ \frac{\partial \psi_i^e}{\partial \eta} \end{Bmatrix} = \begin{bmatrix} \frac{\partial x}{\partial \xi} & \frac{\partial y}{\partial \xi} \\ \frac{\partial x}{\partial \eta} & \frac{\partial y}{\partial \eta} \end{bmatrix}^e \begin{Bmatrix} \frac{\partial \psi_i^e}{\partial x} \\ \frac{\partial \psi_i^e}{\partial y} \end{Bmatrix} \quad (9.2.45)$$

which gives the relation between the derivatives of ψ_i^e with respect to the global and local coordinates. The coefficient matrix in Eq. (9.2.45) is called the *Jacobian matrix* of the transformation (9.2.37)

$$[J]^e = \begin{bmatrix} \frac{\partial x}{\partial \xi} & \frac{\partial y}{\partial \xi} \\ \frac{\partial x}{\partial \eta} & \frac{\partial y}{\partial \eta} \end{bmatrix}^e \quad (9.2.46)$$

and its determinant \mathcal{J} is called the *Jacobian*, which must be greater than zero in order to invert Eq. (9.2.45). Negative nonzero values of \mathcal{J} imply that a right-hand coordinate system is transformed to a left-hand coordinate system, which should be avoided. Inverting Eq. (9.2.45), we obtain

$$\begin{Bmatrix} \frac{\partial \psi_i^e}{\partial x} \\ \frac{\partial \psi_i^e}{\partial y} \end{Bmatrix} = [J]^{-1} \begin{Bmatrix} \frac{\partial \psi_i^e}{\partial \xi} \\ \frac{\partial \psi_i^e}{\partial \eta} \end{Bmatrix} \quad (9.2.47)$$

This requires the Jacobian matrix $[\mathcal{J}]$ be nonsingular. The Jacobian can be determined using the transformation (9.2.37) in Eq. (9.2.46). We have

$$\begin{aligned} [J] &= \begin{bmatrix} \frac{\partial x}{\partial \xi} & \frac{\partial y}{\partial \xi} \\ \frac{\partial x}{\partial \eta} & \frac{\partial y}{\partial \eta} \end{bmatrix} = \begin{bmatrix} \sum_{i=1}^m x_i \frac{\partial \hat{\psi}_i}{\partial \xi} & \sum_{i=1}^m y_i \frac{\partial \hat{\psi}_i}{\partial \xi} \\ \sum_{i=1}^m x_i \frac{\partial \hat{\psi}_i}{\partial \eta} & \sum_{i=1}^m y_i \frac{\partial \hat{\psi}_i}{\partial \eta} \end{bmatrix} \\ &= \begin{bmatrix} \frac{\partial \hat{\psi}_1}{\partial \xi} & \frac{\partial \hat{\psi}_2}{\partial \xi} & \dots & \frac{\partial \hat{\psi}_m}{\partial \xi} \\ \frac{\partial \hat{\psi}_1}{\partial \eta} & \frac{\partial \hat{\psi}_2}{\partial \eta} & \dots & \frac{\partial \hat{\psi}_m}{\partial \eta} \end{bmatrix} \begin{bmatrix} x_1 & y_1 \\ x_2 & y_2 \\ \vdots & \vdots \\ x_m & y_m \end{bmatrix} \end{aligned} \quad (9.2.48)$$

Thus, given the global coordinates (x_j, y_j) of element nodes and the interpolation functions $\hat{\psi}_j^e$ used for geometry, the Jacobian matrix can be evaluated using Eq. (9.2.48). Note that $\hat{\psi}_j^e$ are different, in general, from ψ_j^e used in the approximation of the dependent variables. The Jacobian is given by

$$\mathcal{J} = J_{11}J_{22} - J_{12}J_{21} \quad (9.2.49)$$

We have from Eq. (9.2.47)

$$\left\{ \begin{array}{c} \frac{\partial \psi_i^e}{\partial x} \\ \frac{\partial \psi_i^e}{\partial y} \end{array} \right\} = [J]^{-1} \left\{ \begin{array}{c} \frac{\partial \psi_i^e}{\partial \xi} \\ \frac{\partial \psi_i^e}{\partial \eta} \end{array} \right\} \equiv [J^*] \left\{ \begin{array}{c} \frac{\partial \psi_i^e}{\partial \xi} \\ \frac{\partial \psi_i^e}{\partial \eta} \end{array} \right\} \quad (9.2.40a)$$

where

$$J_{11}^* = \frac{J_{22}}{\mathcal{J}}, \quad J_{12}^* = -\frac{J_{12}}{\mathcal{J}}, \quad J_{22}^* = \frac{J_{11}}{\mathcal{J}}, \quad J_{21}^* = -\frac{J_{21}}{\mathcal{J}} \quad (9.2.50b)$$

Returning the integral in Eq. (9.2.44), we can write it now in terms of the natural coordinates as

$$\begin{aligned} K_{ij}^e &= \int_{\hat{\Omega}} \left\{ a(\xi, \eta) \left(J_{11}^* \frac{\partial \psi_i^e}{\partial \xi} + J_{12}^* \frac{\partial \psi_i^e}{\partial \eta} \right) \left(J_{11}^* \frac{\partial \psi_j^e}{\partial \xi} + J_{12}^* \frac{\partial \psi_j^e}{\partial \eta} \right) \right. \\ &\quad + b(\xi, \eta) \left[\left(J_{11}^* \frac{\partial \psi_i^e}{\partial \xi} + J_{12}^* \frac{\partial \psi_i^e}{\partial \eta} \right) \left(J_{21}^* \frac{\partial \psi_j^e}{\partial \xi} + J_{22}^* \frac{\partial \psi_j^e}{\partial \eta} \right) \right. \\ &\quad + \left. \left(J_{21}^* \frac{\partial \psi_i^e}{\partial \xi} + J_{22}^* \frac{\partial \psi_i^e}{\partial \eta} \right) \left(J_{11}^* \frac{\partial \psi_j^e}{\partial \xi} + J_{12}^* \frac{\partial \psi_j^e}{\partial \eta} \right) \right] \\ &\quad + c(\xi, \eta) \left(J_{21}^* \frac{\partial \psi_j^e}{\partial \xi} + J_{22}^* \frac{\partial \psi_j^e}{\partial \eta} \right) \left(J_{21}^* \frac{\partial \psi_j^e}{\partial \xi} + J_{22}^* \frac{\partial \psi_j^e}{\partial \eta} \right) \\ &\quad \left. + d(\xi, \eta) \psi_i^e \psi_j^e \right\} \mathcal{J} d\xi d\eta \equiv \int_{\hat{\Omega}} F_{ij}^e(\xi, \eta) d\xi d\eta \end{aligned} \quad (9.2.51)$$

where the element area $dA = dx dy$ in element Ω^e is transformed to $dA \equiv dx dy = \mathcal{J} d\xi d\eta$ in the master element $\hat{\Omega}$.

Using the Gauss quadrature formulas for integrals defined over a rectangular master element $\hat{\Omega}$, which are the same as those for the one-dimensional quadrature, we obtain

$$\begin{aligned} \int_{\hat{\Omega}} F_{ij}(\xi, \eta) d\xi d\eta &= \int_{-1}^1 \left[\int_{-1}^1 F_{ij}(\xi, \eta) d\eta \right] d\xi \approx \int_{-1}^1 \left[\sum_{J=1}^N F_{ij}(\xi, \eta_J) W_J \right] d\xi \\ &\approx \sum_{I=1}^M \sum_{J=1}^N F_{ij}(\xi_I, \eta_J) W_I W_J \end{aligned} \quad (9.2.52)$$

where M and N denote the number of Gauss quadrature points in the ξ and η directions, (ξ_I, η_J) denote the Gauss points, and W_I and W_J denote the corresponding Gauss weights. Table 9.2.1 contains Gauss point locations and associated weights for $N = 1, 2, \dots, 5$. For Gauss point locations and weights for $N > 5$, see [29].

Table 9.2.1: Weights and points for the Gauss-Legendre quadrature in one coordinate direction.

$$\int_{\hat{\Omega}} F_{ij}^e(\xi, \eta) d\xi d\eta \approx \sum_{I=1}^M \sum_{J=1}^N F_{ij}^e(\xi_I, \eta_J) W_I W_J$$

N or M	Points ξ_I or η_J	Weights W_I or W_J
1	0.0000000000	2.0000000000
2	± 0.5773502692	1.0000000000
3	0.0000000000 ± 0.7745966692	0.8888888889 0.5555555555
4	± 0.3399810435 ± 0.8611363116	0.6521451548 0.3478548451
5	0.0000000000 ± 0.5384693101 ± 0.9061798459	0.5688888889 0.4786286705 0.2369268850
6	± 0.2386191861 ± 0.6612093865 ± 0.9324695142	0.4679139346 0.3607615730 0.1713244924

The selection of the number of Gauss points required to evaluate the integrals accurately is based on the following rule: a polynomial of degree p is integrated exactly employing $N = \text{int}[\frac{1}{2}(p+1)]$; that is, the smallest integer greater than $\frac{1}{2}(p+1)$. In most cases, the interpolation functions are of the same degree in both ξ and η , and therefore one has $M = N$. When the integrand is of different degree in ξ and η , the number of Gauss points is selected on the basis of the largest-degree polynomial in one of the coordinates. The minimum allowable quadrature rule is one that computes the mass of the element exactly when the density is constant.

Table 9.2.2 contains information on the selection of the integration order and the location of the Gauss points for linear, quadratic, and cubic elements. The maximum degree of the polynomial refers to the degree of the highest polynomial in ξ or η that is present in the integrand of the element matrices of the type in Eq. (9.2.42). Note that the polynomial degree of coefficients as well as J_{ij}^* and \mathcal{J} should be accounted for in determining the total polynomial degree of the integrand. Of course, the coefficients a , b , and c and \mathcal{J}_{ij}^* in general may not be polynomials. In those cases, their functional variations must be approximated by a suitable polynomial in order to determine the polynomial degree of the integrand. The $N \times N$ Gauss point locations are given by the *tensor product* of one-dimensional Gauss points ξ_I .

Table 9.2.2: Selection of the integration order and location of the Gauss points for linear, quadratic, and cubic quadrilateral elements (nodes not shown).

Element Type	Maximum Polynomial Degree	Order of Integration ($r \times r$)	Order of the Residual	Location of Integration Points [†] in Master Element
Linear ($r = 2$)	2	(2 \times 2)	$O(h^4)$	
Quadratic ($r = 3$)	4	(3 \times 3)	$O(h^6)$	
Cubic ($r = 4$)	6	(4 \times 4)	$O(h^8)$	

[†]See Table 9.2.1 for the integration points and weights for each coordinate direction.

9.2.6 Post-Computation of Stresses

Once the generalized displacements at the nodes are determined, Eq.(9.2.4) can be used to determine the strains using the strain-displacement relations (3.3.10). For the case of small strains, displacements and rotations, the membrane strains at any point (x, y, z) in a typical element Ω^e can be computed from the equations

$$\begin{aligned} \left\{ \begin{array}{c} \varepsilon_{xx} \\ \varepsilon_{yy} \\ 2\varepsilon_{xy} \end{array} \right\}^e &= \left\{ \begin{array}{c} \frac{\partial u_0}{\partial x} \\ \frac{\partial v_0}{\partial y} \\ \frac{\partial u_0}{\partial y} + \frac{\partial v_0}{\partial x} \end{array} \right\}^e - z \left\{ \begin{array}{c} \frac{\partial^2 w_0}{\partial x^2} \\ \frac{\partial^2 w_0}{\partial y^2} \\ 2\frac{\partial^2 w_0}{\partial x \partial y} \end{array} \right\}^e \\ &= \sum_{j=1}^m \left\{ \begin{array}{c} u_j \frac{\partial \psi_j}{\partial x} \\ v_j \frac{\partial \psi_j}{\partial y} \\ u_j \frac{\partial \psi_j}{\partial y} + v_j \frac{\partial \psi_j}{\partial x} \end{array} \right\}^e - z \sum_{k=1}^n \Delta_k^e \left\{ \begin{array}{c} \frac{\partial^2 \varphi_k}{\partial x^2} \\ \frac{\partial^2 \varphi_k}{\partial y^2} \\ 2\frac{\partial^2 \varphi_k}{\partial x \partial y} \end{array} \right\}^e \quad (9.2.53) \end{aligned}$$

Recall that only (u_0, v_0) and $(w_0, \partial w_0 / \partial x, \partial w_0 / \partial y)$ are continuous across element interfaces; the first derivatives of the in-plane displacements and the second derivatives of the transverse deflection are, in general, not continuous across element interfaces. In particular, the values of any strain component computed from different elements connected at a node are different.

The stresses at any point in the plate can be computed from the constitutive equations of a lamina, as given in Eq. (6.3.29a). Since the strains are discontinuous, the stresses are also discontinuous across element interfaces, including nodes. It was shown by Barlow [30,31] that stresses computed at the Gauss points associated with the Gauss rule used to evaluate the stiffness matrix of an element are the most accurate.

9.2.7 Numerical Results

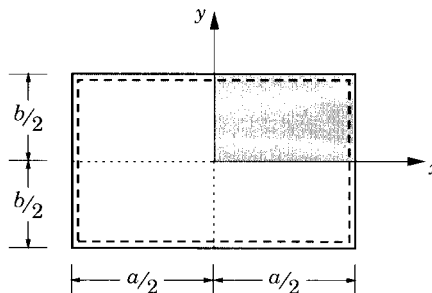
Here we use the conforming (C) and nonconforming (NC) rectangular finite elements to analyze laminated plates for bending and natural vibration. Additional numerical results will be presented in Section 9.3. Note should be made of the fact that the finite element model developed herein is not restricted to any particular lamination scheme, geometry, boundary conditions, or loading. Additional results are presented in Section 9.3.5.

The notation $m \times n$ mesh denotes m subdivisions along the x -axis and n subdivisions along the y -axis with the same type of elements. Solution symmetries available in a problem should be taken advantage of to identify the computational domain because they reduce computational effort. For example, a 2×2 mesh in a quadrant of the plate is the same as 4×4 mesh in the total plate, and the results obtained with the two meshes would be identical, within the round-off errors of the computation, if the solution exhibits biaxial symmetry. A solution is symmetric about a line only if (a) the geometry, including boundary conditions, (b) the material properties, and (c) the loading are symmetric about the line. The boundary conditions along a line of symmetry should be correctly identified and imposed in the finite element model. When one is not sure of the solution symmetry, it is advised that the whole plate be modeled.

Bending Analyses

For antisymmetric cross-ply and angle-ply rectangular laminates with their respective simply supported boundary conditions, a quadrant of the plate may be used as the computational domain of the finite element analysis. The boundary conditions along the symmetry lines for the cross-ply and angle-ply laminates are different, as shown in Figure 9.2.10. The symmetry boundary conditions can be identified from the Navier solutions for each case. When one is doubtful of the boundary conditions along the lines of symmetry, it is safe to use the full plate model. In the case of conforming element, it is necessary that the cross-derivative $\partial w_0 / \partial x \partial y$ be also set to zero at the center of the plate when a quarter-plate model is used. Otherwise, the results will be less accurate.

Table 9.2.3 shows a comparison of finite element solutions with the analytical solutions of simply supported orthotropic and two-layer cross-ply and angle-ply ($-45/45$) square laminates under a uniformly distributed transverse load. In all cases, a quadrant of the plate was used in the finite element analysis. The stresses in the finite element analysis were computed at the Gauss points nearest to the locations at which the stresses were evaluated analytically. For the nonconforming and conforming rectangular plate elements used here, the strains and stresses are computed using the one-point Gauss rule, i.e., at the center of the element. Stresses σ_{xx} and σ_{yy} are computed at $(5a/8, 5b/8)$, $(9a/16, 9b/16)$, and $(17a/32, 17b/32)$ for uniform meshes 2×2 , 4×4 , and 8×8 , respectively; the origin of the coordinate system is taken at the center of the laminate (see Figure 9.2.10); σ_{xy} is computed for the same meshes at $(3a/8, 3b/8)$, $(7a/16, 7b/16)$, and $(15a/32, 15b/32)$.



Theory	B.C.	$x = 0$	$y = 0$
FSDT	SS-1	$u_0 = 0$ $\phi_x = 0$	$v_0 = 0$ $\phi_y = 0$
	SS-2	$v_0 = 0$ $\phi_x = 0$	$u_0 = 0$ $\phi_y = 0$
CLPT	SS-1	$u_0 = 0$ $\frac{\partial w_0}{\partial x} = 0$	$v_0 = 0$ $\frac{\partial w_0}{\partial y} = 0$
	SS-2	$v_0 = 0$ $\frac{\partial w_0}{\partial x} = 0$	$u_0 = 0$ $\frac{\partial w_0}{\partial y} = 0$

Figure 9.2.10: Symmetry boundary conditions for antisymmetric cross-ply and angle-ply laminates.

Table 9.2.3: A comparison of the maximum transverse deflections and stresses[†] of simply supported square plates under uniformly distributed transverse load ($h_n = h/n$, $E_1/E_2 = 25$, $G_{12} = G_{13} = 0.5E_2$, $G_{23} = 0.2E_2$, $\nu_{12} = 0.25$; CLPT solutions).

Variable	Nonconforming			Conforming			Analytical solution
	2 × 2	4 × 4	8 × 8	2 × 2	4 × 4	8 × 8	
Orthotropic Plate (SS-1)							
\bar{w}	0.7082	0.6635	0.6531	0.7532	0.6651	0.6517	0.6497
$\bar{\sigma}_{xx}$	0.7148	0.7709	0.7828	0.5772	0.7388	0.7759	0.7866
$\bar{\sigma}_{yy}$	0.0296	0.0253	0.0246	0.0283	0.0249	0.0246	0.0244
$\bar{\sigma}_{xy}$	0.0337	0.0421	0.0444	0.0369	0.0416	0.0448	0.0463
Cross-Ply (0/90) Plate (SS-1)							
\bar{w}	1.7937	1.7203	1.7017	1.7004	1.6909	1.6935	1.6955
$\bar{\sigma}_{xx}$	0.1109	0.1230	0.1259	0.1056	0.1215	0.1255	0.1268
$\bar{\sigma}_{yy}$	0.9436	1.0440	1.0683	0.8819	1.0263	1.0637	1.0761
$\bar{\sigma}_{xy}$	0.0751	0.0872	0.0914	0.0704	0.0853	0.0908	0.0933
Angle-Ply (-45/45) Plate (SS-2)							
\bar{w}	1.0524	1.0341	1.0296	1.0111	1.0222	1.0264	1.0280
$\bar{\sigma}_{xx} = \bar{\sigma}_{yy}$	0.2600	0.3279	0.3449	0.2639	0.3303	0.3445	0.3504
$\bar{\sigma}_{xy}$	0.3935	0.4264	0.4376	0.3852	0.4206	0.4356	0.4421
Angle-Ply (-45/45)₄ Plate (SS-2)							
\bar{w}	0.4045	0.3905	0.3870	0.3948	0.3870	0.3859	0.3858
$\bar{\sigma}_{xx} = \bar{\sigma}_{yy}$	0.1500	0.1880	0.1975	0.1406	0.1867	0.1973	0.2006
$\bar{\sigma}_{xy}$	0.2501	0.2612	0.2636	0.2495	0.2590	0.2627	0.2637

[†] The stresses are computed at the center of each finite element.

The conforming element ($\partial^2 w_0 / \partial x \partial y = 0$ at the center of the plate) yields slightly better solutions than the nonconforming element, and both elements show good convergence. However, convergence of the displacements is always faster than stresses for the displacement-based finite elements, and the rate of convergence of stresses is two orders less than that of displacements for the CLPT-based element. Since the stresses in the finite element analysis are computed at locations different from the analytical solutions, they are expected to be different. Mesh refinement not only improves the accuracy of the solution, but the Gauss point locations also get closer to the node point locations (but never become the nodal locations), resulting in better agreement with the true solution.

It is clear from the results presented in Table 9.2.3 that the convergence of the finite element results to the analytical solutions is very good. The slower convergence of stresses in two-layer angle-ply plates compared to the eight-layer laminate is due to the presence of bending stretching-coupling. Recall that in angle-ply laminates the analytical solution for stresses is the sum of two parts: one is a double sine series and the other is double cosine series. They are mutually exclusive at points $(a/2, b/2)$ and $(0, 0)$; however, the parts add up at the Gauss

points (0.46875,0.46875) and (0.03125,0.03125). For example, the analytical results of stresses for the (-45/45) laminate are $\bar{\sigma}_{xx} = 0.3486$ and $\bar{\sigma}_{xy} = 0.4312$ at the Gauss points (0.46875,0.46875) and (0.03125,0.03125), respectively, which shows better agreement between the analytical and finite element stress values.

The effect of the simply supported SS-1 ($u_s = w_0 = \theta_s = 0$) and SS-2 ($u_n = w_0 = \theta_s = 0$) and clamped ($u_n = u_s = w_0 = \theta_n = \theta_s = 0$) boundary conditions on two-layer cross-ply and angle-ply laminates is investigated using full plate models and 8×8 uniform mesh of conforming elements (no boundary condition on the cross-derivative was imposed) and the results are presented in Table 9.2.4. Recall that cross-ply laminates admit the Navier solutions for the SS-1 boundary conditions whereas antisymmetric angle-ply laminates admit for the SS-2 boundary conditions. Analytical solutions (i.e., Navier or Lévy type solutions) are not available for cross-ply laminates with SS-2, antisymmetric angle-ply laminates with SS-1, and any laminate for clamped (CC) boundary conditions. The locations of maximum stresses are indicated below for various cases.

Cross-Ply SS-1 and SS-2 [$\sigma_{xx}(x_0, y_0, -h/2) = -\sigma_{yy}(x_0, y_0, h/2)$]:

$$\sigma_{yy}(0.5625a, 0.5625a, h/2) ; \quad \sigma_{xy}(0.9375a, 0.9375a, -h/2)$$

Cross-Ply Clamped [$\sigma_{xx}(x_0, y_0, -h/2) = -\sigma_{yy}(y_0, x_0, h/2)$]:

$$-\sigma_{yy}(0.4375a, 0.0625a, h/2) ; \quad \sigma_{xy}(0.8125a, 0.8125a, -h/2)$$

Angle-Ply [$\sigma_{xx}(x_0, y_0, h/2) = \sigma_{yy}(x_0, y_0, h/2)$]:

$$\text{SS-1: } \sigma_{yy}(0.6875a, 0.3125a, h/2) ; \quad \sigma_{xy}(0.8125a, 0.1875a, -h/2)$$

$$\text{SS-2: } \sigma_{yy}(0.8125a, 0.1875a, h/2) ; \quad -\sigma_{xy}(0.9375a, 0.9375a, h/2)$$

$$\text{Clamped: } -\sigma_{xx}(0.0625a, 0.4375a, h/2) ; \quad -\sigma_{xy}(0.0625a, 0.6875a, h/2)$$

Table 9.2.4: Maximum transverse deflections and stresses[†] of square laminates under uniformly distributed transverse load and for different boundary conditions ($h_n = h/n$, $E_1/E_2 = 25$, $G_{12} = G_{13} = 0.5E_2$, $G_{23} = 0.2E_2$, $\nu_{12} = 0.25$).

Variable	(0/90)			(-45/45)		
	SS-1	SS-2	CC	SS-1	SS-2	CC
\bar{w}	1.6839	0.8957	0.3814	0.6773	1.0208	0.3891
$\bar{\sigma}_{yy}$	1.0469	0.8939	0.5699	0.3392	0.3659	0.2202
$\bar{\sigma}_{xy}$	0.0851	0.0361	0.0181	0.3341	0.4201	0.1772

[†] The stresses are computed at the center of each finite element; 8×8 uniform mesh of conforming elements is used in the full plate.

From the results (see Table 9.2.4) it is clear that SS-2 boundary conditions make the cross-ply laminate stiffer because they restrain the bidirectional composite from having normal in-plane displacements ($u_n = 0$). Similarly, SS-1 boundary conditions make the antisymmetric angle-ply stiffer by restraining the in-plane tangential displacements ($u_s = 0$). The clamped boundary conditions make both plates quite stiff compared to the simply supported boundary conditions.

A comparison of finite element solutions with the analytical solutions of antisymmetric cross-ply and angle-ply laminates under sinusoidal loading is presented in Table 9.2.5. The finite element solutions are obtained using 8×8 uniform mesh of conforming elements in the full plate. The stresses are computed at the Gauss points and the locations of the stresses are indicated in the footnote of the table.

Table 9.2.5: A comparison of finite element (second row) and analytical (first row) solutions of antisymmetric cross-ply and angle-ply square plates subjected to sinusoidal distribution of transverse load and for various boundary conditions ($h_n = h/n$, $E_1/E_2 = 25$, $G_{12} = G_{13} = 0.5E_2$, $G_{23} = 0.2E_2$, $\nu_{12} = 0.25$; n = number of layers).

n	Variable	SS	SC	CC	FF	FS	FC
Cross-Ply Laminates (0/90/0···)							
2	\bar{w}	1.064	0.664	0.429	1.777	1.471	0.980
		1.055	0.652	0.415	1.761	1.445	0.966
	$\bar{\sigma}_{xx}$	7.157	5.660	4.800	2.403	4.442	3.042
		6.888 ^a	5.859 ^a	4.457 ^a	2.262 ^a	4.562 ^a	3.150 ^a
	$\bar{\sigma}_{yy}$	7.157	4.483	2.914	11.849	9.837	6.560
		6.888 ^a	4.496 ^a	2.722 ^a	11.516 ^a	10.029 ^b	7.142 ^a
10	\bar{w}	0.442	0.266	0.167	0.665	0.579	0.380
		0.442	0.266	0.168	0.665	0.579	0.381
	$\bar{\sigma}_{xx}$	5.009	3.829	3.167	1.725	2.986	1.865
		4.791 ^a	3.953 ^a	2.904 ^a	1.615 ^a	2.999 ^a	1.925 ^a
	$\bar{\sigma}_{yy}$	5.009	3.025	1.911	7.480	6.531	4.284
		4.791 ^a	3.046 ^a	1.811 ^a	7.258 ^a	6.711 ^b	4.694 ^a
Angle-Ply Laminates (-45/45/-45···) (FEM only)							
2	\bar{w}	0.649	0.497	0.384	3.026	1.319	0.981
	$\bar{\sigma}_{xx}$	0.652 ^c	0.554 ^c	0.375 ^d	0.698 ^f	1.043 ^c	0.733 ^g
	$\bar{\sigma}_{yy}$	0.652 ^c	0.554 ^c	0.374 ^d	0.830 ^f	1.043 ^c	0.745 ^g
10	\bar{w}	0.243	0.191	0.429	1.426	0.524	0.397
	$\bar{\sigma}_{xx}$	0.188 ^c	0.163 ^c	0.116 ^e	0.357 ^f	0.318 ^c	0.249 ^g
	$\bar{\sigma}_{yy}$	0.188 ^c	0.163 ^c	0.115 ^e	0.427 ^f	0.317 ^c	0.254 ^g

a : (0.4375, 0.4375); *b* : (0.5625, 0.5625); *c* : (0.0625, 0.0625); *d* : (0.9375, 0.8125);

e : (0.3125, 0.3125); *f* : (0.1875, 0.9375); *g* : (0.8125, 0.6875).

Natural Vibration

The finite element solutions are compared with the analytical solutions of antisymmetric cross-ply and angle-ply laminates in Table 9.2.6. In all cases, a quarter-plate model with appropriate symmetry boundary conditions was used in the finite element analysis. The finite element solutions show convergence to the analytical solutions with mesh refinements.

Table 9.2.6: A comparison of the natural frequencies,[†] $\bar{\omega} = \omega(b^2/h)\sqrt{\rho/E_2}$ of simply supported square plates ($h_n = h/n$, $E_1/E_2 = 40$, $G_{12} = G_{13} = 0.6E_2$, $G_{23} = 0.5E_2$, $\nu_{12} = 0.25$, $a/h = 10$).

n^\ddagger	Nonconforming		Conforming		Analytical solution
	2×2	4×4	2×2	4×4	
Cross-Ply (0/90/0/...) Plates (SS-1)					
2	10.882	11.080	11.215	11.186	11.154
4	16.461	16.960	16.745	17.101	17.145
8	17.559	18.140	17.795	18.279	18.352
Angle-Ply (-45/45/-45/...) Plates (SS-2)					
2	14.360	14.413	14.659	14.504	14.439
4	22.821	23.168	23.168	23.294	23.304
8	23.699	24.888	24.883	25.024	25.052

[†] The rotary inertia is included. [‡] n = Number of layers in the laminate.

9.3 Finite Element Models of Shear Deformation Plate Theory (FSDT)

9.3.1 Weak Forms

Following the procedure described in Section 9.2.1, we can develop the weak forms of the equations governing the first-order shear deformation plate theory. We consider the linear equations of motion of FSDT from Eqs. (5.4.13), which are in terms of the stress resultants but equivalent to Eqs. (9.1.1) through (9.1.5). The generalized displacements of FSDT are $(u_0, v_0, w_0, \phi_x, \phi_y)$. The weak forms of the five equations in (5.4.13) are obtained by multiplying them with $\delta u_0, \delta v_0, \delta w_0, \delta \phi_x$, and $\delta \phi_y$, respectively, and integrating over the element domain. We obtain

$$0 = \int_{\Omega^e} \left(\frac{\partial \delta u_0}{\partial x} N_{xx} + \frac{\partial \delta u_0}{\partial y} N_{xy} + I_0 \delta u_0 \frac{\partial^2 u_0}{\partial t^2} + I_1 \delta u_0 \frac{\partial^2 \phi_x}{\partial t^2} \right) dx dy - \oint_{\Gamma^e} P_x \delta u_0 ds \quad (9.3.1a)$$

$$0 = \int_{\Omega^e} \left(\frac{\partial \delta v_0}{\partial x} N_{xy} + \frac{\partial \delta v_0}{\partial y} N_{yy} + I_0 \delta v_0 \frac{\partial^2 v_0}{\partial t^2} + I_1 \delta v_0 \frac{\partial^2 \phi_y}{\partial t^2} \right) dx dy - \oint_{\Gamma^e} P_y \delta v_0 ds \quad (9.3.1b)$$

$$\begin{aligned}
0 = & \int_{\Omega^e} \left[\frac{\partial \delta w_0}{\partial x} Q_x + \frac{\partial \delta w_0}{\partial y} Q_y - \delta w_0 q + I_0 \delta w_0 \frac{\partial^2 w_0}{\partial t^2} \right. \\
& \left. + \frac{\partial \delta w_0}{\partial x} \left(\hat{N}_{xx} \frac{\partial w_0}{\partial x} + \hat{N}_{xy} \frac{\partial w_0}{\partial y} \right) + \frac{\partial \delta w_0}{\partial y} \left(\hat{N}_{xy} \frac{\partial w_0}{\partial x} + \hat{N}_{yy} \frac{\partial w_0}{\partial y} \right) \right] dx dy \\
& - \oint_{\Gamma^e} \left[\left(Q_x + \hat{N}_{xx} \frac{\partial w_0}{\partial x} + \hat{N}_{xy} \frac{\partial w_0}{\partial y} \right) n_x + \left(Q_y + \hat{N}_{xy} \frac{\partial w_0}{\partial x} + \hat{N}_{yy} \frac{\partial w_0}{\partial y} \right) n_y \right] \delta w_0 ds
\end{aligned} \tag{9.3.1c}$$

$$\begin{aligned}
0 = & \int_{\Omega^e} \left(\frac{\partial \delta \phi_x}{\partial x} M_{xx} + \frac{\partial \delta \phi_x}{\partial y} M_{xy} + \delta \phi_x Q_x + I_2 \delta \phi_x \frac{\partial^2 \phi_x}{\partial t^2} + I_1 \delta \phi_x \frac{\partial^2 u_0}{\partial t^2} \right) dx dy \\
& - \oint_{\Gamma^e} T_x \delta \phi_x ds
\end{aligned} \tag{9.3.1d}$$

$$\begin{aligned}
0 = & \int_{\Omega^e} \left(\frac{\partial \delta \phi_y}{\partial x} M_{xy} + \frac{\partial \delta \phi_y}{\partial y} M_{yy} + \delta \phi_y Q_y + I_2 \delta \phi_y \frac{\partial^2 \phi_y}{\partial t^2} + I_1 \delta \phi_y \frac{\partial^2 v_0}{\partial t^2} \right) dx dy \\
& - \oint_{\Gamma^e} T_y \delta \phi_y ds
\end{aligned} \tag{9.3.1e}$$

We note from the boundary terms in Eq. (9.3.1a-e) that $(u_0, v_0, w_0, \phi_x, \phi_y)$ are the primary variables (or generalized displacements). Unlike in the classical plate theory, the rotations (ϕ_x, ϕ_y) are independent of w_0 . Note also that no derivatives of w_0 are in the list of the primary variables. The secondary variables are

$$\begin{aligned}
P_x &\equiv N_{xx} n_x + N_{xy} n_y, \quad P_y \equiv N_{xy} n_x + N_{yy} n_y \\
T_x &\equiv M_{xx} n_x + M_{xy} n_y, \quad T_y \equiv M_{xy} n_x + M_{yy} n_y \\
Q_n &\equiv \left(Q_x + \hat{N}_{xx} \frac{\partial w_0}{\partial x} + \hat{N}_{xy} \frac{\partial w_0}{\partial y} \right) n_x \\
&\quad + \left(Q_y + \hat{N}_{xy} \frac{\partial w_0}{\partial x} + \hat{N}_{yy} \frac{\partial w_0}{\partial y} \right) n_y
\end{aligned} \tag{9.3.2}$$

9.3.2 Finite Element Model

The weak forms of the first-order theory contain, at the most, only the first derivatives of the dependent variables $(u_0, v_0, w_0, \phi_x, \phi_y)$. Therefore, they can all be approximated using the Lagrange interpolation functions. In principle, the sets (u_0, v_0) , w_0 , and (ϕ_x, ϕ_y) can be approximated with differing degrees of functions. For simplicity, we use the same interpolation for all variables. Let

$$u_0(x, y, t) = \sum_{j=1}^m u_j(t) \psi_j^e(x, y) \tag{9.3.3a}$$

$$v_0(x, y, t) = \sum_{j=1}^m v_j(t) \psi_j^e(x, y) \tag{9.3.3b}$$

$$w_0(x, y, t) = \sum_{j=1}^n w_j(t) \psi_j^e(x, y) \quad (9.3.4)$$

$$\phi_x(x, y, t) = \sum_{j=1}^p S_j^1(t) \psi_j^e(x, y) \quad (9.3.5a)$$

$$\phi_y(x, y, t) = \sum_{j=1}^p S_j^2(t) \psi_j^e(x, y) \quad (9.3.5b)$$

where ψ_j^e are Lagrange interpolation functions. In general, (u_0, v_0) , w_0 , and (ϕ_x, ϕ_y) may be interpolated with different degree of interpolation. One can use linear, quadratic, or higher-order interpolations of these sets.

Substituting Eqs. (9.3.3)–(9.3.5) for $(u_0, v_0, w_0, \phi_x, \phi_y)$ into the weak forms in Eq. (9.3.1), we obtain the semidiscrete finite element model of the first-order theory:

$$\left(\begin{bmatrix} [K^{11}] & [K^{12}] & [K^{13}] & [K^{14}] & [K^{15}] \\ [K^{12}]^T & [K^{22}] & [K^{23}] & [K^{24}] & [K^{25}] \\ [K^{13}]^T & [K^{23}]^T & [K^{33}] & [K^{34}] & [K^{35}] \\ [K^{14}]^T & [K^{24}]^T & [K^{34}]^T & [K^{44}] & [K^{45}] \\ [K^{15}]^T & [K^{25}]^T & [K^{35}]^T & [K^{45}]^T & [K^{55}] \end{bmatrix} + \begin{bmatrix} [0] & [0] & [0] & [0] & [0] \\ [0] & [0] & [0] & [0] & [0] \\ [0] & [0] & [G] & [0] & [0] \\ [0] & [0] & [0] & [0] & [0] \\ [0] & [0] & [0] & [0] & [0] \end{bmatrix} \right) \begin{Bmatrix} \{u^e\} \\ \{v^e\} \\ \{w^e\} \\ \{S^1\} \\ \{S^2\} \end{Bmatrix} \\ + \begin{bmatrix} I_0[M] & [0] & [0] & I_1[M] & [0] \\ [0] & I_0[M] & [0] & [0] & I_1[M] \\ [0] & [0] & I_0[M] & [0] & [0] \\ I_1[M] & [0] & [0] & I_2[M] & [0] \\ [0] & I_1[M] & [0] & [0] & I_2[M] \end{bmatrix} \begin{Bmatrix} \{\ddot{u}^e\} \\ \{\ddot{v}^e\} \\ \{\ddot{w}^e\} \\ \{\ddot{S}^1\} \\ \{\ddot{S}^2\} \end{Bmatrix} = \begin{Bmatrix} \{F^1\} - \{F^{T1}\} \\ \{F^2\} - \{F^{T2}\} \\ \{F^3\} \\ \{F^4\} - \{F^{T4}\} \\ \{F^5\} - \{F^{T5}\} \end{Bmatrix} \quad (9.3.6a)$$

or

$$[K^e]\{\Delta^e\} + [M^e]\{\ddot{\Delta}^e\} = \{F^e\} \quad (9.3.6b)$$

where the coefficients of the submatrices $[K^{\alpha\beta}]$ and $[M^{\alpha\beta}]$ and vectors $\{F^\alpha\}$ are defined for ($\alpha, \beta = 1, 2, \dots, 5$) by the expressions

$$\begin{aligned} K_{ij}^{1\alpha} &= \int_{\Omega^e} \left(\frac{\partial \psi_i^e}{\partial x} N_{1j}^\alpha + \frac{\partial \psi_i^e}{\partial y} N_{6j}^\alpha \right) dx dy \\ K_{ij}^{2\alpha} &= \int_{\Omega^e} \left(\frac{\partial \psi_i^e}{\partial x} N_{6j}^\alpha + \frac{\partial \psi_i^e}{\partial y} N_{2j}^\alpha \right) dx dy \\ K_{ij}^{3\alpha} &= \int_{\Omega^e} \left(\frac{\partial \psi_i^e}{\partial x} Q_{1j}^\alpha + \frac{\partial \psi_i^e}{\partial y} Q_{2j}^\alpha \right) dx dy \\ K_{ij}^{4\alpha} &= \int_{\Omega^e} \left(\frac{\partial \psi_i^e}{\partial x} M_{1j}^\alpha + \frac{\partial \psi_i^e}{\partial y} M_{6j}^\alpha + \psi_i^e Q_{1j}^\alpha \right) dx dy \\ K_{ij}^{5\alpha} &= \int_{\Omega^e} \left(\frac{\partial \psi_i^e}{\partial x} M_{6j}^\alpha + \frac{\partial \psi_i^e}{\partial y} M_{2j}^\alpha + \psi_i^e Q_{2j}^\alpha \right) dx dy \\ G_{ij} &= \int_{\Omega^e} \left[\hat{N}_{xx} \frac{\partial \psi_i^e}{\partial x} \frac{\partial \psi_j^e}{\partial y} + \hat{N}_{xy} \left(\frac{\partial \psi_i^e}{\partial x} \frac{\partial \psi_j^e}{\partial y} + \frac{\partial \psi_i^e}{\partial y} \frac{\partial \psi_j^e}{\partial x} \right) + \hat{N}_{yy} \frac{\partial \psi_i^e}{\partial y} \frac{\partial \psi_j^e}{\partial y} \right] dx dy \\ M_{ij} &= \int_{\Omega^e} \psi_i^e \psi_j^e dx dy \end{aligned} \quad (9.3.7)$$

The coefficients N_{Ij}^α , M_{Ij}^α , and Q_{Ij}^α for $\alpha = 1, 2, \dots, 5$ and $I = 1, 2, 6$ are given by

$$\begin{aligned}
N_{1j}^1 &= A_{11} \frac{\partial \psi_j^e}{\partial x} + A_{16} \frac{\partial \psi_j^e}{\partial y}, \quad N_{1j}^2 = A_{12} \frac{\partial \psi_j^e}{\partial y} + A_{16} \frac{\partial \psi_j^e}{\partial x} \\
N_{1j}^4 &= B_{11} \frac{\partial \psi_j^e}{\partial x} + B_{16} \frac{\partial \psi_j^e}{\partial y}, \quad N_{1j}^5 = B_{12} \frac{\partial \psi_j^e}{\partial y} + B_{16} \frac{\partial \psi_j^e}{\partial x} \\
N_{2j}^1 &= A_{12} \frac{\partial \psi_j^e}{\partial x} + A_{26} \frac{\partial \psi_j^e}{\partial y}, \quad N_{2j}^2 = A_{22} \frac{\partial \psi_j^e}{\partial y} + A_{26} \frac{\partial \psi_j^e}{\partial x} \\
N_{2j}^4 &= B_{12} \frac{\partial \psi_j^e}{\partial x} + B_{26} \frac{\partial \psi_j^e}{\partial y}, \quad N_{2j}^5 = B_{22} \frac{\partial \psi_j^e}{\partial y} + B_{26} \frac{\partial \psi_j^e}{\partial x} \\
N_{6j}^1 &= A_{16} \frac{\partial \psi_j^e}{\partial x} + A_{66} \frac{\partial \psi_j^e}{\partial y}, \quad N_{6j}^2 = A_{26} \frac{\partial \psi_j^e}{\partial y} + A_{66} \frac{\partial \psi_j^e}{\partial x} \\
N_{6j}^4 &= B_{16} \frac{\partial \psi_j^e}{\partial x} + B_{66} \frac{\partial \psi_j^e}{\partial y}, \quad N_{6j}^5 = B_{26} \frac{\partial \psi_j^e}{\partial y} + B_{66} \frac{\partial \psi_j^e}{\partial x} \\
M_{1j}^1 &= B_{11} \frac{\partial \psi_j^e}{\partial x} + B_{16} \frac{\partial \psi_j^e}{\partial y}, \quad M_{1j}^2 = B_{12} \frac{\partial \psi_j^e}{\partial y} + B_{16} \frac{\partial \psi_j^e}{\partial x} \\
M_{1j}^4 &= D_{11} \frac{\partial \psi_j^e}{\partial x} + D_{16} \frac{\partial \psi_j^e}{\partial y}, \quad M_{1j}^5 = D_{12} \frac{\partial \psi_j^e}{\partial y} + D_{16} \frac{\partial \psi_j^e}{\partial x} \\
M_{2j}^1 &= B_{12} \frac{\partial \psi_j^e}{\partial x} + B_{26} \frac{\partial \psi_j^e}{\partial y}, \quad M_{2j}^2 = B_{22} \frac{\partial \psi_j^e}{\partial y} + B_{26} \frac{\partial \psi_j^e}{\partial x} \\
M_{2j}^4 &= D_{12} \frac{\partial \psi_j^e}{\partial x} + D_{26} \frac{\partial \psi_j^e}{\partial y}, \quad M_{2j}^5 = D_{22} \frac{\partial \psi_j^e}{\partial y} + D_{26} \frac{\partial \psi_j^e}{\partial x} \\
M_{6j}^1 &= B_{16} \frac{\partial \psi_j^e}{\partial x} + B_{66} \frac{\partial \psi_j^e}{\partial y}, \quad M_{6j}^2 = B_{26} \frac{\partial \psi_j^e}{\partial y} + B_{66} \frac{\partial \psi_j^e}{\partial x} \\
M_{6j}^4 &= D_{16} \frac{\partial \psi_j^e}{\partial x} + D_{66} \frac{\partial \psi_j^e}{\partial y}, \quad M_{6j}^5 = D_{26} \frac{\partial \psi_j^e}{\partial y} + D_{66} \frac{\partial \psi_j^e}{\partial x} \\
N_{1j}^3 &= N_{2j}^3 = N_{6j}^3 = M_{1j}^3 = M_{2j}^3 = M_{6j}^3 = 0 \\
Q_{1j}^3 &= A_{55} \frac{\partial \psi_j}{\partial x} + A_{45} \frac{\partial \psi_j}{\partial y}, \quad Q_{2j}^3 = A_{45} \frac{\partial \psi_j}{\partial x} + A_{44} \frac{\partial \psi_j}{\partial y} \\
Q_{1j}^4 &= A_{55} \psi_j, \quad Q_{1j}^5 = Q_{2j}^4 = A_{45} \psi_j, \quad Q_{2j}^5 = A_{44} \psi_j
\end{aligned} \tag{9.3.8a}$$

$$\begin{aligned}
F_i^1 &= \oint_{\Gamma_e} P_x \psi_i^e \, dx dy, \quad F_i^2 = \oint_{\Gamma_e} P_y \psi_i^e \, dx dy \\
F_i^3 &= \int_{\Omega^e} q \psi_i^e \, dx dy + \oint_{\Gamma_e} Q_n \psi_i^e \, ds \\
F_i^4 &= \oint_{\Gamma_e} T_x \psi_i^e \, dx dy, \quad F_i^5 = \oint_{\Gamma_e} T_y \psi_i^e \, dx dy
\end{aligned}$$

$$\begin{aligned}
 F_i^{T1} &= \oint_{\Gamma_e} \left(\frac{\partial \psi_i^e}{\partial x} N_{xx}^T + \frac{\partial \psi_i^e}{\partial y} N_{xy}^T \right) dx dy \\
 F_i^{T2} &= \oint_{\Gamma_e} \left(\frac{\partial \psi_i^e}{\partial x} N_{xy}^T + \frac{\partial \psi_i^e}{\partial y} N_{yy}^T \right) dx dy \\
 F_i^{T4} &= \oint_{\Gamma_e} \left(\frac{\partial \psi_i^e}{\partial x} M_{xx}^T + \frac{\partial \psi_i^e}{\partial y} M_{xy}^T \right) dx dy \\
 F_i^{T5} &= \oint_{\Gamma_e} \left(\frac{\partial \psi_i^e}{\partial x} M_{xy}^T + \frac{\partial \psi_i^e}{\partial y} M_{yy}^T \right) dx dy
 \end{aligned} \tag{9.3.8b}$$

where N_{xx}^T , M_{xx}^T , etc. are the thermal force and moment resultants.

The displacement-based C^0 plate bending element of Eq. (9.3.6) is often referred to in the finite element literature as the *Mindlin plate element* due to the fact that it is based on the so-called Mindlin plate theory, which is labeled in this book as the first-order shear deformation plate theory. Any of the Lagrange interpolation functions presented in Eqs. (9.2.10), (9.2.11), and (9.2.12) may be used to approximate the displacement field $(u_0, v_0, w_0, \phi_x, \phi_y)$. When the bilinear rectangular element is used for all generalized displacements, the element stiffness matrices are of the order 20×20 ; and for the nine-node quadratic element they are 45×45 (see Figure 9.3.1).

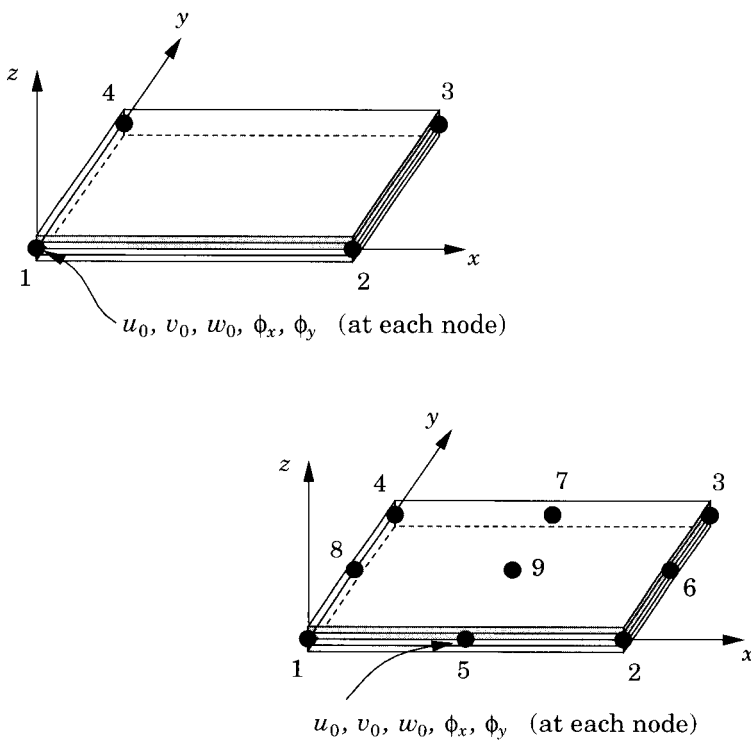


Figure 9.3.1: Linear and quadratic Lagrange rectangular elements for the first-order shear deformation theory.

Equation (9.3.6) can be simplified for static bending, buckling, natural vibration, and transient analyses, as described in Eqs. (9.2.20)–(9.2.24). The simplifications are obvious and therefore are not repeated for the FSDT element. However, numerical results for bending, buckling, natural vibration, and transient response will be discussed.

9.3.3 Penalty Function Formulation and Shear Locking

A finite element model equivalent to that in Eq. (9.3.6) can also be derived using the penalty function approach (see Reddy [32,33]) applied to the classical plate theory. For the sake of simplicity in discussion, consider the weak form of the classical plate theory without membrane strains, nonlinearity, and inertia terms [see Eq. (3.3.19)]:

$$0 = \int_{\Omega_0} \left(M_{xx} \delta \varepsilon_{xx}^{(1)} + M_{yy} \delta \varepsilon_{yy}^{(1)} + M_{xy} \delta \gamma_{xy}^{(1)} - q \delta w_0 \right) dx dy \quad (9.3.9)$$

Next assume, again for the sake of simplicity, that the plate under consideration is orthotropic. Using the plate constitutive equations (3.3.44), we rewrite the weak form (9.3.9) in terms of the generalized displacements

$$\begin{aligned} 0 &= \int_{\Omega_0} \left[\left(D_{11} \frac{\partial^2 w_0}{\partial x^2} + D_{12} \frac{\partial^2 w_0}{\partial y^2} \right) \frac{\partial^2 \delta w_0}{\partial x^2} + \left(D_{12} \frac{\partial^2 w_0}{\partial x^2} + D_{22} \frac{\partial^2 w_0}{\partial y^2} \right) \frac{\partial^2 \delta w_0}{\partial y^2} \right. \\ &\quad \left. + 4D_{66} \frac{\partial^2 w_0}{\partial x \partial y} \frac{\partial^2 \delta w_0}{\partial x \partial y} - q \delta w_0 \right] dx dy \\ &= \delta \int_{\Omega_0} \frac{1}{2} \left[D_{11} \left(\frac{\partial^2 w_0}{\partial x^2} \right)^2 + 2D_{12} \frac{\partial^2 w_0}{\partial x^2} \frac{\partial^2 w_0}{\partial y^2} + D_{22} \left(\frac{\partial^2 w_0}{\partial y^2} \right)^2 \right. \\ &\quad \left. + 4D_{66} \left(\frac{\partial^2 w_0}{\partial x \partial y} \right)^2 - q w_0 \right] dx dy \equiv \delta \Pi_0(w_0) \end{aligned} \quad (9.3.10)$$

where Π_0 denotes the total potential energy functional

$$\begin{aligned} \Pi_0(w_0) &= \int_{\Omega_0} \frac{1}{2} \left[D_{11} \left(\frac{\partial^2 w_0}{\partial x^2} \right)^2 + 2D_{12} \frac{\partial^2 w_0}{\partial x^2} \frac{\partial^2 w_0}{\partial y^2} + D_{22} \left(\frac{\partial^2 w_0}{\partial y^2} \right)^2 \right. \\ &\quad \left. + 4D_{66} \left(\frac{\partial^2 w_0}{\partial x \partial y} \right)^2 - q w_0 \right] dx dy \end{aligned} \quad (9.3.11)$$

Equation (9.3.10) is a statement of the principle of the minimum potential energy, which is a special case of the principle of virtual displacements when the material of plate is assumed to obey Hooke's law. Introduce the variables θ_x and θ_y such that

$$\frac{\partial w_0}{\partial x} - \theta_x = 0, \quad \frac{\partial w_0}{\partial y} - \theta_y = 0 \quad (9.3.12)$$

Then the potential energy functional takes the form

$$\begin{aligned}\Pi(w_0, \theta_x, \theta_y) = \int_{\Omega_0} \frac{1}{2} & \left[D_{11} \left(\frac{\partial \theta_x}{\partial x} \right)^2 + 2D_{12} \frac{\partial \theta_x}{\partial x} \frac{\partial \theta_y}{\partial y} + D_{22} \left(\frac{\partial \theta_y}{\partial y} \right)^2 \right. \\ & \left. + D_{66} \left(\frac{\partial \theta_x}{\partial y} + \frac{\partial \theta_y}{\partial x} \right)^2 - qw_0 \right] dx dy \quad (9.3.13)\end{aligned}$$

The difference between $\Pi_0(w_0)$ and $\Pi(w_0, \theta_x, \theta_y)$ is that the latter contains at the most only the first derivatives of the dependent variables, and therefore will require C^0 -interpolation in the finite element model. However, the potential energy functional $\Pi(w_0, \theta_x, \theta_y)$ in Eq. (9.3.13) does not include the fact that the dependent variables θ_x and θ_y are related to w_0 by Eqs. (9.3.12). Therefore, the principle of the minimum potential energy must be stated as one of minimizing the functional $\Pi(w_0, \theta_x, \theta_y)$ subjected to the (constraint) conditions in Eq. (9.3.12): minimize

$$\Pi(w_0, \theta_x, \theta_y) \quad (9.3.14a)$$

subjected to the constraints

$$\frac{\partial w_0}{\partial x} - \theta_x = 0, \quad \frac{\partial w_0}{\partial y} - \theta_y = 0 \quad (9.3.14b)$$

The constrained minimization problem (9.3.14) can be solved either using the Lagrange multiplier method or the penalty function method. In the Lagrange multiplier method we assume that there exist *Lagrange multipliers* λ_1 and λ_2 such that the constrained minimization problem is equivalent to $\delta\Pi_L(w_0, \theta_x, \theta_y, \lambda_1, \lambda_2) = 0$, where

$$\Pi_L \equiv \Pi(w_0, \theta_x, \theta_y) + \int_{\Omega_0} \left[\lambda_1 \left(\frac{\partial w_0}{\partial x} - \theta_x \right) + \lambda_2 \left(\frac{\partial w_0}{\partial y} - \theta_y \right) \right] dx dy \quad (9.3.15)$$

The weak form, $\delta\Pi_L = 0$, can be used to construct a finite element model with C^0 -interpolation of all dependent unknowns: $w_0, \theta_x, \theta_y, \lambda_1$, and λ_2 . The Lagrange multipliers can be shown to have the meaning of shear forces $\lambda_1 \sim Q_x$ and $\lambda_2 \sim Q_y$. The finite element model based on the functional Π_L is called a *mixed finite element model*, because displacements are mixed with forces as element degrees of freedom.

In the penalty function method the constrained problem is posed as one of minimizing the functional $\Pi_p(w_0, \theta_x, \theta_y)$

$$\Pi_p \equiv \Pi(w_0, \theta_x, \theta_y) + \frac{1}{2} \int_{\Omega_0} \left[\gamma_1 \left(\frac{\partial w_0}{\partial x} - \theta_x \right)^2 + \gamma_2 \left(\frac{\partial w_0}{\partial y} - \theta_y \right)^2 \right] dx dy \quad (9.3.16)$$

where γ_1 and γ_2 are called the *penalty parameters*, which are preselected positive functions of (x, y) . In the penalty function method, the square of the error in each constraint is minimized along with the original functional, and the penalty parameters represent weights with which the constraints are minimized relative to the original functional. Thus, in the penalty function method the constraints are

satisfied only approximately and the minimum character of the problem is penalized. The larger the values of the penalty parameters, the smaller the error in satisfying the constraint conditions. A desirable aspect of the penalty function method is that no new variables are introduced in addition to those in the original functional and the constraint equations.

At this juncture we should remind ourselves that the problem we are trying to formulate is the classical plate bending. A finite element model based on the penalty functional (9.3.16) is expected to give an approximate solution to the classical plate theory for sufficiently large values of the penalty parameters. However, there are computational problems, namely shear locking, arising from the finite element implementation of the model based on (9.3.16). Before we embark on the discussion of shear locking, it is useful to note the similarity between the functional Π_p and that of the first-order shear deformation plate theory.

The total potential energy functional for the first-order theory, omitting membrane effects and the von Kármán nonlinearity, and assuming orthotropic material behavior, can be derived from Eq. (3.4.9):

$$0 = \int_{\Omega_0} \left(M_{xx} \delta \varepsilon_{xx}^{(1)} + M_{yy} \delta \varepsilon_{yy}^{(1)} + M_{xy} \delta \gamma_{xy}^{(1)} + Q_x \delta \gamma_{xz}^{(0)} + Q_y \delta \gamma_{yz}^{(0)} - q \delta w_0 \right) dx dy \quad (9.3.17)$$

Using the plate constitutive equations (3.4.21) and (3.4.22), we rewrite the weak form (9.3.17) in terms of the generalized displacements

$$\begin{aligned} 0 = \int_{\Omega_0} & \left[\left(D_{11} \frac{\partial \phi_x}{\partial x} + D_{12} \frac{\partial \phi_y}{\partial y} \right) \frac{\partial \delta \phi_x}{\partial x} + \left(D_{12} \frac{\partial \phi_x}{\partial x} + D_{22} \frac{\partial \phi_y}{\partial y} \right) \frac{\partial \delta \phi_y}{\partial y} \right. \\ & + 2D_{66} \left(\frac{\partial \phi_x}{\partial y} + \frac{\partial \phi_y}{\partial x} \right) \left(\frac{\partial \delta \phi_x}{\partial y} + \frac{\partial \delta \phi_y}{\partial x} \right) - q \delta w_0 \\ & \left. + A_{55} \left(\frac{\partial w_0}{\partial x} + \phi_x \right) \left(\frac{\partial \delta w_0}{\partial x} + \delta \phi_x \right) + A_{44} \left(\frac{\partial w_0}{\partial y} + \phi_y \right) \left(\frac{\partial \delta w_0}{\partial y} + \delta \phi_y \right) \right] dx dy \end{aligned} \quad (9.3.18)$$

which is the first variation of the functional

$$\begin{aligned} \bar{\Pi}(w_0, \phi_x, \phi_y) = \int_{\Omega_0} & \frac{1}{2} \left[D_{11} \left(\frac{\partial \phi_x}{\partial x} \right)^2 + 2D_{12} \frac{\partial \phi_x}{\partial x} \frac{\partial \phi_y}{\partial y} + D_{22} \left(\frac{\partial \phi_y}{\partial y} \right)^2 \right. \\ & + D_{66} \left(\frac{\partial \phi_x}{\partial y} + \frac{\partial \phi_y}{\partial x} \right)^2 + A_{55} \left(\frac{\partial w_0}{\partial x} + \phi_x \right)^2 \\ & \left. + A_{44} \left(\frac{\partial w_0}{\partial y} + \phi_y \right)^2 - q w_0 \right] dx dy \end{aligned} \quad (9.3.19)$$

We note the similarity between the functionals Π_p of (9.3.16) and $\bar{\Pi}$ in (9.3.19). They are the same with the following correspondence

$$\theta_x \sim -\phi_x, \quad \theta_y \sim -\phi_y, \quad \gamma_1 \sim A_{55}, \quad \gamma_2 \sim A_{44} \quad (9.3.20)$$

Thus, for a particular choice of the penalty parameters, we recover the first-order shear deformation theory from the penalty formulation of the classical plate theory;

for large values of the penalty parameters, the classical plate theory is recovered. Indeed, use of the functional in (9.3.19) is more appropriate because it naturally gives rise to the classical plate theory as the plate thickness is reduced in relation to the plate in-plane dimensions. This is due to the fact that D_{ij} are proportional to h^3 whereas A_{ij} are proportional to h . Thus the penalty parameters are of the order h^{-2} . When $a/h = 100$, the penalty parameters A_{ij} are 10^4 times larger than D_{ij} , and hence the constraints (9.3.12) are satisfied accurately; i.e., the classical plate theory is realized.

The C^0 -plate bending elements based on the first-order shear deformation plate theory are among the simplest available in the literature. They are expected, in theory, to give the thin plate theory solution when the side-to-thickness ratio a/h is very large ($a/h \geq 100$). Unfortunately, when lower-order (quadratic or less) equal interpolation of the transverse deflection and rotations is used, the elements do not accurately represent the bending behavior as the side-to-thickness ratio of the element becomes large (i.e., thin plate limit). For thin plates, the shearing strains ε_{xz} and ε_{yz} are required to vanish, and the plate elements based on the first-order theory become excessively stiff, yielding displacements that are too small compared to the true solution. This type of behavior is known as *shear locking*. There are a number of papers on the subject of shear locking and elements developed to alleviate the problem (see [32–57]).

Shear locking is due to the inability of shear deformable elements to accurately model the bending within an element under a state of zero transverse shearing strain. When thin plates are analyzed by the shear deformable elements, the energy due to transverse shear strains must vanish. Numerically this is equivalent to requiring the product of the shear stiffness matrix and the displacement vector be zero. Therefore, in order to obtain a nontrivial solution, the shear stiffness matrix must be singular. One way to achieve the singularity of the transverse shear stiffness matrix is to use an order of numerical integration lower than is necessary to evaluate the integrals exactly. Thus, *reduced integration* of transverse shear stiffnesses (i.e., all coefficients in $K_{ij}^{\alpha\beta}$ that contain A_{44} , A_{45} , and A_{55}) is necessary. Higher-order elements or refined meshes of lower-order elements experience relatively less locking, but sometimes at the expense of rate of convergence.

In this chapter only rectangular or quadrilateral elements based on the first-order shear deformation theory are used. Equal interpolation of all generalized displacements is employed. Stiffness coefficients associated with the transverse shear deformation (i.e., terms containing A_{44} , A_{45} , and A_{55}) are evaluated using reduced integration, and full integration is used for all other stiffness coefficients, mass coefficients, and force components.

With the suggested Gauss rule, highly distorted elements tend to have slower rates of convergence but they give sufficiently accurate results. Of course, one should avoid using highly distorted elements; most commercial codes issue warning messages when the element is highly distorted (e.g., see Chapter 9, pp. 439–448, of the textbook by Reddy [1] for a discussion of modeling considerations).

9.3.4 Post-Computation of Stresses

Here we discuss the evaluation of stresses from the known displacement expansions. Once the nodal values of generalized displacements ($u_0, v_0, w_0, \phi_x, \phi_y$) have been obtained by solving the assembled equations of a problem, the strains are evaluated in each element by differentiating the displacement expansions [see Eqs. (9.3.3)–(9.3.5)]. Since only the displacements and not their derivatives are continuous across the element boundaries in the C^0 finite element formulations, strain continuity across the boundaries is not ensured. That is, along a boundary common to two elements, the strains and hence stresses take different values on the two sides of the interface. However, strains and hence stresses are continuous within an element. Here we give the equations for the computation of stresses in an element. We assume that there are no temperature effects.

As noted earlier, the strains and stresses are the most accurate if they are computed at the $(N - 1) \times (N - 1)$ Gauss points, where $N \times N$ is the exact Gauss quadrature rule used to evaluate the bending stiffness coefficients. For example, the linear rectangular plate bending element of the first-order theory requires 2×2 integration to evaluate the bending stiffnesses exactly. Then the one-point integration should be used to evaluate the transverse shear stiffness coefficients, strains, and stresses. Similarly, for a quadratic rectangular element the reduced integration rule is the 2×2 Gauss rule.

Since the displacements in the finite element models are referred to the global coordinates (x, y, z) , the stresses are computed at the Barlow points (i.e., reduced integration points) in the global coordinates using the constitutive relations

$$\left\{ \begin{array}{c} \sigma_{xx} \\ \sigma_{yy} \\ \sigma_{xy} \\ \sigma_{xz} \\ \sigma_{yz} \end{array} \right\}^{(k)} = \left[\begin{array}{ccccc} \bar{Q}_{11} & \bar{Q}_{12} & \bar{Q}_{16} & 0 & 0 \\ \bar{Q}_{12} & \bar{Q}_{22} & \bar{Q}_{26} & 0 & 0 \\ \bar{Q}_{16} & \bar{Q}_{26} & \bar{Q}_{66} & 0 & 0 \\ 0 & 0 & 0 & \bar{Q}_{55} & \bar{Q}_{45} \\ 0 & 0 & 0 & \bar{Q}_{45} & \bar{Q}_{44} \end{array} \right]^{(k)} \left\{ \begin{array}{c} \varepsilon_{xx} \\ \varepsilon_{yy} \\ \gamma_{xy} \\ \gamma_{xz} \\ \gamma_{yz} \end{array} \right\} \quad (9.3.21)$$

where

$$\left\{ \begin{array}{c} \varepsilon_{xx} \\ \varepsilon_{yy} \\ \gamma_{yz} \\ \gamma_{xz} \\ \gamma_{xy} \end{array} \right\} = \left\{ \begin{array}{c} \frac{\partial u_0}{\partial x} \\ \frac{\partial v_0}{\partial y} \\ \frac{\partial w_0}{\partial y} + \phi_y \\ \frac{\partial w_0}{\partial x} + \phi_x \\ \frac{\partial u_0}{\partial y} + \frac{\partial v_0}{\partial x} \end{array} \right\} + z \left\{ \begin{array}{c} \frac{\partial \phi_x}{\partial x} \\ \frac{\partial \phi_y}{\partial y} \\ 0 \\ 0 \\ \frac{\partial \phi_x}{\partial y} + \frac{\partial \phi_y}{\partial x} \end{array} \right\} \quad (9.3.22)$$

If stresses and strains are required in the lamina principal material coordinates, for example, to check for failures, the strains and stresses of Eqs. (9.3.21) and (9.3.22) should be transformed to material coordinates associated with each layer using the transformation relations (2.3.14) and (2.3.10). Alternatively, the strains can be transformed using Eq. (2.3.14)

$$\left\{ \begin{array}{c} \varepsilon_1 \\ \varepsilon_2 \\ \varepsilon_4 \\ \varepsilon_5 \\ \varepsilon_6 \end{array} \right\}^{(k)} = [R]^{(k)} \left\{ \begin{array}{c} \varepsilon_{xx} \\ \varepsilon_{yy} \\ \gamma_{yz} \\ \gamma_{xz} \\ \gamma_{xy} \end{array} \right\} \quad (9.3.23a)$$

$$[R]^{(k)} = \begin{bmatrix} \cos^2 \theta_k & \sin^2 \theta_k & 0 & 0 & \sin \theta_k \cos \theta_k \\ \sin^2 \theta_k & \cos^2 \theta_k & 0 & 0 & -\sin \theta_k \cos \theta_k \\ 0 & 0 & \cos \theta_k & -\sin \theta_k & 0 \\ 0 & 0 & \sin \theta_k & \cos \theta_k & 0 \\ -2 \sin \theta_k \cos \theta_k & 2 \sin \theta_k \cos \theta_k & 0 & 0 & \cos^2 \theta_k - \sin^2 \theta_k \end{bmatrix} \quad (9.3.23b)$$

and then the lamina constitutive equations are used to compute the stresses:

$$\left\{ \begin{array}{c} \sigma_1 \\ \sigma_2 \\ \sigma_4 \\ \sigma_5 \\ \sigma_6 \end{array} \right\}^{(k)} = \left[\begin{array}{ccccc} Q_{11} & Q_{12} & 0 & 0 & 0 \\ Q_{12} & Q_{22} & 0 & 0 & 0 \\ 0 & 0 & Q_{44} & 0 & 0 \\ 0 & 0 & 0 & Q_{55} & 0 \\ 0 & 0 & 0 & 0 & Q_{66} \end{array} \right] \left\{ \begin{array}{c} \varepsilon_1 \\ \varepsilon_2 \\ \varepsilon_4 \\ \varepsilon_5 \\ \varepsilon_6 \end{array} \right\}^{(k)} \quad (9.3.24)$$

9.3.5 Bending Analysis

First the effect of integration rule and the convergence characteristics of the C^0 finite element model based on equal interpolation is investigated using a simply supported (SS-1) cross-ply square laminate under sinusoidally distributed transverse load [58]. The laminate consists of three plies (0/90/0) of thicknesses $h/4$, $h/2$, and $h/4$, where h denotes the total laminate thickness; it is equivalent to (0/90/90/0) laminate with equal thickness plies. For this problem, we have developed closed-form solutions in Chapters 5 and 7, and Pagano [59,60] developed the 3-D elasticity solution for the problem. Also see [61–77] for analytical solutions for bending, vibration, and stability of shear deformation plate theories. The material properties used are those typical of graphite-epoxy material (*Material 1*)

$$E_1 = 25E_2, \quad G_{12} = G_{13} = 0.5E_2, \quad G_{23} = 0.2E_2, \quad \nu_{12} = 0.25, \quad K_s = 5/6 \quad (9.3.25)$$

The transverse load in all cases is assumed to be (sinusoidal on the whole plate)

$$q(x, y) = q_0 \cos \frac{\pi x}{a} \cos \frac{\pi y}{b} \quad (9.3.26)$$

where the origin of the coordinate system (x, y) is taken at the center of the plate, $-a/2 \leq x \leq a/2$, $-a/2 \leq y \leq a/2$, and $-h/2 \leq z \leq h/2$.

The following nondimensionalizations of the quantities are used:

$$\begin{aligned} \bar{w} &= w_0(0, 0) \frac{E_2 h^3}{b^4 q_0}, \quad \bar{\sigma}_{xx} = \sigma_{xx}(0, 0, \frac{h}{2}) \frac{h^2}{b^2 q_0} = -\sigma_{xx}(0, 0, -\frac{h}{2}) \frac{h^2}{b^2 q_0} \\ \bar{\sigma}_{yy} &= \sigma_{yy}(0, 0, \frac{h}{4}) \frac{h^2}{b^2 q_0} = -\sigma_{yy}(0, 0, -\frac{h}{4}) \frac{h^2}{b^2 q_0} \\ \bar{\sigma}_{xy} &= \sigma_{xy}(\frac{a}{2}, \frac{b}{2}, -\frac{h}{2}) \frac{h^2}{b^2 q_0} = -\sigma_{xy}(\frac{a}{2}, \frac{b}{2}, \frac{h}{2}) \frac{h^2}{b^2 q_0} \\ \bar{\sigma}_{xz} &= \sigma_{xz}(\frac{a}{2}, 0, k=1, 3) \frac{h}{b q_0}, \quad \bar{\sigma}_{yz} = \sigma_{yz}(0, \frac{b}{2}, k=2) \frac{h}{b q_0} \end{aligned} \quad (9.3.27)$$

As noted earlier, the stresses in the finite element analysis are computed at the reduced Gauss points, irrespective of the Gauss rule used for the evaluation of the element stiffness coefficients. The Gauss point locations differ for each mesh used. The Gauss point coordinates A and B are shown in Table 9.3.1. The finite element solutions (FES) are compared with the 3-D elasticity solution (ELS) and the closed-form solutions (CFS) in Table 9.3.2 for three side-to-thickness ratios $a/h = 10, 20$, and 100 . The notation nL stands for $n \times n$ uniform mesh of linear rectangular elements, $nQ8$ for $n \times n$ uniform mesh of eight-node quadratic elements, and $nQ9$ for $n \times n$ uniform mesh of nine-node quadratic elements in a quarter plate. The stresses in FEM are evaluated at the Gauss points as indicated below:

$$\begin{aligned} \sigma_{xx}(A, A, \frac{h}{2}), \quad \sigma_{yy}(A, A, \frac{h}{4}), \quad \sigma_{xy}(B, B, -\frac{h}{2}) \\ \sigma_{xz}(B, A) \text{ in layers 1 and 3}, \quad \sigma_{yz}(A, B) \text{ in layer 2} \end{aligned} \quad (9.3.28)$$

Table 9.3.1: The Gauss point locations at which the stresses are computed.

Coordinate	2L	4L	8L	2Q8/2Q9	4Q8/4Q9
A	$0.125a$	$0.0625a$	$0.03125a$	$0.05283a$	$0.02642a$
B	$0.375a$	$0.4375a$	$0.46875a$	$0.44717a$	$0.47358a$

Table 9.3.2: Effect of reduced integration on the nondimensionalized maximum deflections \bar{w} and stresses $\bar{\sigma}$ of simply supported (SS-1) cross-ply (0/90/90/0) square plates under sinusoidal load (see [58]).

a/h	Source	$\bar{w} \times 10^2$	$\bar{\sigma}_{xx}$	$\bar{\sigma}_{yy}$	$\bar{\sigma}_{xy}$	$\bar{\sigma}_{xz}$	$\bar{\sigma}_{yz}$
Finite Element Solutions [†]							
10	2L-F	0.5901	0.3339	0.2454	0.0163	0.316	0.125
	2L-R	0.6508	0.3799	0.2838	0.0187	0.335	0.107
	2L-S	0.6655	0.3796	0.2882	0.0189	0.353	0.114
	4L-F	0.6427	0.4512	0.3280	0.0219	0.389	0.129
	4L-R	0.6599	0.4668	0.3406	0.0227	0.395	0.123
	4L-S	0.6632	0.4667	0.3419	0.0227	0.400	0.125
	2Q8-F	0.6605	0.4831	0.3492	0.0234	0.404	0.126
	2Q8-R	0.6615	0.4842	0.3509	0.0234	0.404	0.126
	2Q8-S	0.6613	0.4844	0.3509	0.0233	0.405	0.126
	2Q9-F	0.6551	0.4790	0.3400	0.0231	0.399	0.126
	2Q9-R	0.6633	0.4841	0.3508	0.0234	0.404	0.125
	2Q9-S	0.6631	0.4844	0.3509	0.0233	0.404	0.126
	8L-S	0.6628	0.4907	0.3565	0.0238	0.412	0.128
	4Q8-S	0.6626	0.4954	0.3589	0.0240	0.414	0.128
	4Q8-S	0.6627	0.4954	0.3589	0.0240	0.414	0.128
Analytical Solutions							
10	CFS	0.6627	0.4989	0.3614	0.0241	0.416 (0.318)	0.129 (0.181) [‡]
	ELS	0.7370	0.5590	0.4010	0.0276	0.301	0.196

(table is continued on the next page)

(table is continued from the previous page)

a/h	Source	$\bar{w} \times 10^2$	$\bar{\sigma}_{xx}$	$\bar{\sigma}_{yy}$	$\bar{\sigma}_{xy}$	$\bar{\sigma}_{xz}$	$\bar{\sigma}_{yz}$
Finite Element Solutions							
20	2L-F	0.3236	0.2645	0.1491	0.0111	0.303	0.139
	2L-R	0.4712	0.4036	0.2289	0.0170	0.353	0.089
	2L-S	0.4760	0.4043	0.2308	0.0171	0.373	0.094
	4L-F	0.4346	0.4365	0.2451	0.0183	0.395	0.123
	4L-R	0.4863	0.4940	0.2777	0.0207	0.415	0.103
	4L-S	0.4874	0.4942	0.2782	0.0207	0.420	0.105
	2Q8-F	0.4876	0.5082	0.2828	0.0214	0.424	0.106
	2Q8-R	0.4901	0.5117	0.2870	0.0214	0.424	0.106
	2Q8-S	0.4901	0.5120	0.2870	0.0214	0.424	0.106
	2Q9-F	0.4891	0.5083	0.2829	0.0214	0.424	0.106
	2Q9-R	0.4915	0.5118	0.2870	0.0213	0.424	0.106
	2Q9-S	0.4915	0.5120	0.2870	0.0213	0.424	0.105
	8L-S	0.4902	0.5189	0.2912	0.0218	0.433	0.108
	4Q8-S	0.4911	0.5236	0.2936	0.0219	0.434	0.108
	4Q9-S	0.4912	0.5236	0.2936	0.0219	0.434	0.108
Analytical Solutions							
20	CFS	0.4912	0.5273	0.2956	0.0221	0.437 (0.333)	0.109 (0.150)
	ELS	0.5128	0.5430	0.3080	0.0230	0.328	0.156
Finite Element Solutions							
100	2L-F	0.0315	0.0299	0.0151	0.0012	0.230	0.211
	2L-R	0.4107	0.4129	0.2076	0.0164	0.360	0.082
	2L-S	0.4120	0.4140	0.2082	0.0164	0.381	0.086
	4L-F	0.1034	0.1203	0.0604	0.0048	0.298	0.221
	4L-R	0.4281	0.5045	0.2535	0.0200	0.422	0.098
	4L-S	0.4284	0.5048	0.2537	0.0207	0.428	0.097
	2Q8-F	0.4143	0.4900	0.2435	0.0199	0.430	0.100
	2Q8-R	0.4319	0.5214	0.2621	0.0206	0.435	0.102
	2Q8-S	0.4319	0.5214	0.2620	0.0206	0.433	0.102
	2Q9-F	0.4193	0.4946	0.2420	0.0201	0.431	0.098
	2Q9-R	0.4339	0.5224	0.2625	0.0207	0.432	0.098
	2Q9-S	0.4339	0.5224	0.2550	0.0206	0.430	0.097
	8L-S	0.4324	0.5297	0.2662	0.0210	0.441	0.100
	4Q8-S	0.4336	0.5344	0.2685	0.0212	0.441	0.100
	4Q9-S	0.4337	0.5344	0.2685	0.0212	0.441	0.100
Analytical Solutions							
100	CFS	0.4337	0.5382	0.2704	0.0213	0.445 (0.339)	0.101 (0.139)
	ELS	0.4347	0.5390	0.2710	0.0214	0.339	0.139
	CLPT*	0.4313	0.5387	0.2667	0.0213	(0.339)	(0.138)

[†] F = full integration; R = reduced integration; S = selective integration.[‡] The values of transverse shear stresses in parentheses are obtained using the 3-D equilibrium equations.* The CLPT solution is independent of side-to-thickness ratio, a/h .

An examination of the numerical results presented in Table 9.3.2 shows that the FSDT finite element with equal interpolation of all generalized displacements does not experience shear locking for thick plates even when full integration rule is used. Shear locking is evident when the element is used to model thin plates ($a/h \geq 100$) with full integration rule (F). Also, higher-order elements show less locking but with slower convergence. The element behaves uniformly well for thin and thick plates when the reduced (R) or selectively reduced integration (S) rule is used. The finite element results are in excellent agreement with the closed-form solutions of the first-order shear deformation theory. The displacements converge faster than stresses, which is expected because the rate of convergence of gradients of the solution is one order less than the rate of convergence of the solution.

Nondimensionalized maximum deflections and stresses in five-layer ($h_1 = h_3 = h_5 = h/6$, $h_2 = h_4 = h/4$) cross-ply (0/90/0/90/0) square laminates under sinusoidally distributed transverse load are compared in Table 9.3.3. The finite element results were obtained with 4×4 mesh of eight-node quadratic elements in a quarter plate are in excellent agreement with the closed-form solutions. Although the first-order shear deformation theory underpredicts deflections for small values of a/h , the stresses are in good agreement with those predicted by the 3-D elasticity theory; the error is relatively more for the five-layer case compared to the three-layer case shown in Table 9.3.2.

Table 9.3.3: Comparison of nondimensionalized maximum deflections and stresses of simply supported (SS-1) five-layer (0/90/0/90/0) square plates under sinusoidal loading ($E_1 = 25E_2$, $G_{12} = G_{13} = 0.5E_2$, $G_{23} = 0.2E_2$, $\nu_{12} = 0.25$, $K = 5/6$).

a/h	Source	$\bar{w} \times 10^2$	$\bar{\sigma}_{xx}$	$\bar{\sigma}_{yy}$	$\bar{\sigma}_{xy}$	$\bar{\sigma}_{xz}$	$\bar{\sigma}_{yz}$
4	ELS	1.8505	0.685	0.633	0.0384	0.238	0.229
	CFS	1.5623	0.4369	0.5026	0.0235	0.3054 (0.2267)	0.2403 (0.2809)
	FEM	1.5620	0.4339	0.4991	0.0233	0.3033	0.2281
10	ELS	0.6771	0.545	0.430	0.0247	0.258	0.223
	CFS	0.6213	0.5021	0.4107	0.0221	0.3459 (0.2559)	0.1998 (0.2324)
	FEM	0.6212	0.4986	0.4078	0.0219	0.3435	0.1984
20	ELS	0.4938	0.539	0.380	0.0222	0.268	0.212
	CFS	0.4796	0.5276	0.3748	0.0215	0.3617 (0.2673)	0.1840 (0.2135)
	FEM	0.4796	0.5239	0.3722	0.0214	0.3592	0.1827
100	ELS	0.4338	0.539	0.360	0.0213	0.272	0.205
	CFS	0.4332	0.5382	0.3598	0.0213	0.3683 (0.2720)	0.1774 (0.2056)
	FEM	0.4331	0.5345	0.3573	0.0211	0.3655	0.1761
	CLPT	0.4313	0.5387	0.3591	0.0213	(0.2722)	(0.2052) [†]

[†] Stresses computed from 3-D equilibrium equations.

Table 9.3.4 shows a comparison of the elasticity solution of Pagano [60], with the closed-form and finite element solutions of a three-layer cross-ply (0/90/0) square plate under sinusoidally distributed transverse load. The layers are of equal thickness, with the material properties listed in Eq. (9.3.25). The same locations and nondimensionalizations as given in Eqs. (9.3.26) and (9.3.27) are used. The finite element results obtained with 4×4 mesh of eight-node quadratic elements in a quarter plate are in excellent agreement with the closed-form solutions.

While the classical laminate plate theory underpredicts deflections for small values of a/h , the stresses predicted are in general agreement with the first-order shear deformation theory and elasticity theory. Also, the transverse shear stresses predicted through equilibrium equations, for the laminates studied so far, are very close to those predicted by the elasticity theory.

Table 9.3.4: Comparison of nondimensionalized maximum deflections and stresses of simply supported (SS-1) three-ply (0/90/0) square plates subjected to sinusoidal loading ($h_i = h/3$, $E_1 = 25E_2$, $G_{12} = G_{13} = 0.5E_2$, $G_{23} = 0.2E_2$, $\nu_{12} = 0.25$, $K = 5/6$).

a/h	Source		$\bar{w} \times 10^2$	$\bar{\sigma}_{xx}$	$\bar{\sigma}_{yy}$	$\bar{\sigma}_{xy}$	$\bar{\sigma}_{xz}$	$\bar{\sigma}_{yz}$
10	ELS		—	0.590	0.288	0.029	0.357	0.123
	CFS		0.6693	0.5134	0.2536	0.0252	0.4089 (0.3806)	0.0915 (0.1108) [†]
	FEM	4Q8-S	0.6692	0.5098	0.2518	0.0250	0.4060	0.0908
20	ELS		—	0.552	0.210	0.0234	0.385	0.094
	CFS		0.4921	0.5318	0.1997	0.0223	0.4205 (0.3912)	0.0759 (0.0901)
	FEM	4Q8-S	0.4921	0.5281	0.1983	0.0222	0.4176	0.0754
100	ELS		—	0.539	0.181	0.0213	0.395	0.083
	CFS		0.4337	0.5384	0.1804	0.0213	0.4247 (0.3950)	0.0703 (0.0827)
	FEM	4Q8-S	0.4336	0.5346	0.1791	0.0212	0.4215	0.0699
	CLPT		0.4313	0.5387	0.1796	0.0213	(0.3951)	(0.0823)

[†] Values computed from equilibrium equations.

Next, we consider a sandwich plate subjected to sinusoidally distributed transverse loading. The face sheets (i.e., layers 1 and 3) are assumed to be orthotropic with the following material properties:

$$E_1 = 25E_2, E_2 = 10^6 \text{ psi}, G_{12} = G_{13} = 0.5E_2, G_{23} = 0.2E_2, \nu_{12} = 0.25 \quad (9.3.29)$$

and the core material is transversely isotropic and is characterized by the following material properties:

$$E_1 = E_2 = 10^6 \text{ psi}, G_{13} = G_{23} = 0.06 \times 10^6 \text{ psi}, \nu_{12} = 0.25$$

$$G_{12} = \frac{E_1}{2(1 + \nu_{12})} = 0.016 \times 10^6 \text{ psi} \quad (9.3.30)$$

Each face sheet is assumed to be one-tenth of the total thickness of the sandwich plate ($a = b$). The finite element results obtained with 4×4 mesh of eight-node quadratic elements with reduced integration (4Q8-R) are compared with the closed form solution and elasticity solution of Pagano [60] in Table 9.3.5. The stresses are nondimensionalized as before, and their locations with respect to a coordinate system whose origin is at the center of the plate are as follows:

$$\sigma_{xx}(0, 0, \frac{h}{2}), \sigma_{yy}(0, 0, \frac{h}{2}), \sigma_{xy}(a/2, b/2, -\frac{h}{2}), \sigma_{xz}(0, b/2, 0), \sigma_{yz}(a/2, 0, 0) \quad (9.3.31)$$

The results indicate that the effect of shear deformation on deflections is significant in sandwich plates even at large values of a/h . The equilibrium-derived transverse shear stresses are surprisingly close to those predicted by the elasticity theory for $a/h \geq 10$, while those computed from constitutive equations are considerably underestimated for small side-to-thickness ratios. The transverse shear stress component σ_{yz} is significantly overestimated by CLPT. Figures 9.3.2 and 9.3.3 show the variation of the transverse shear stresses through the thickness of the sandwich plates for side-to-thickness ratios $a/h = 2, 10$, and 100 .

Table 9.3.5: Comparison of nondimensionalized maximum deflections and stresses in a simply supported (SS-1) sandwich plate subjected to sinusoidally varying transverse load ($h_1 = h_3 = 0.1h$, $h_2 = 0.8h$, $K = 5/6$).

a/h	Source	$\bar{w} \times 10^2$	$\bar{\sigma}_{xx}$	$\bar{\sigma}_{yy}$	$\bar{\sigma}_{xy}$	$\bar{\sigma}_{xz}$	$\bar{\sigma}_{yz}$
4	ELS	—	1.556	0.2595	0.1481	0.239	0.1072
	CFS	4.7666	0.8918	0.1562	0.0907	0.1229	0.0537
	FEM	4.7663	0.8856	0.1551	0.0901	0.1221	(0.0746)
10	ELS	—	1.153	0.1104	0.0717	0.300	0.0527
	CFS	1.5604	1.0457	0.0798	0.0552	0.1374	0.0293
	FEM	1.5603	1.0384	0.0792	0.0548	0.1365	(0.0408)
20	ELS	—	1.110	0.0700	0.0511	0.317	0.0361
	CFS	1.0524	1.0831	0.0612	0.0466	0.1409	0.0234
	FEM	1.0523	1.0755	0.0608	0.0462	0.1399	(0.0325)
100	ELS	—	1.098	0.0550	0.0437	0.324	0.0297
	CFS	0.8852	1.0964	0.0546	0.0435	0.1422	0.0213
	FEM	0.8851	1.0887	0.0542	0.0432	0.1412	(0.0296)
	CPT	0.8782	1.0970	0.0543	0.0433	(0.3243)	0.0161

† Values computed from equilibrium equations.

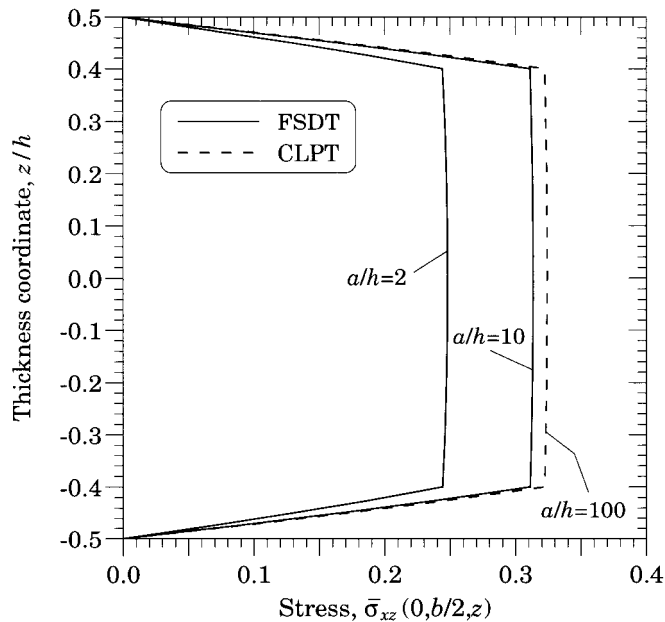


Figure 9.3.2: Distribution of transverse shear stress σ_{xz} through the thickness of a simply supported (SS-1) sandwich plate under sinusoidally distributed transverse load.

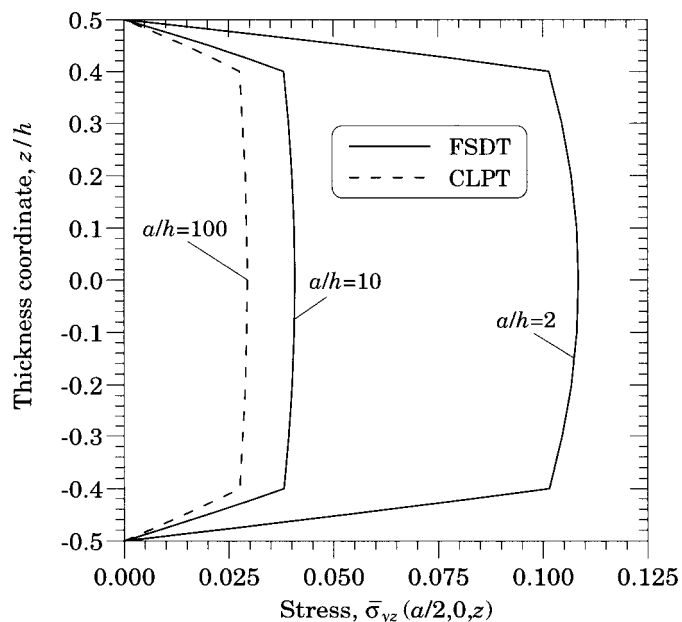


Figure 9.3.3: Distribution of transverse shear stress σ_{yz} through the thickness of a simply supported (SS-1) sandwich plate under sinusoidally distributed transverse load.

The same sandwich plate as discussed above is analyzed for simply supported and clamped boundary conditions when uniformly distributed load is used. Once again a quarter plate model is used with 4×4 mesh of quadratic FSDT elements and 8×8 mesh of CLPT conforming cubic elements. The results are presented in Table 9.3.6. The effect of shear deformation on the deflections is even more significant in clamped plates than in simply supported plates.

Table 9.3.6: Nondimensionalized maximum deflections and stresses in a square sandwich plate with simply supported (SS-1) and clamped boundary conditions ($h_1 = h_3 = 0.1h$, $h_2 = 0.8h$, $K = 5/6$).

a/h	Source	$\bar{w} \times 10^2$	$\bar{\sigma}_{xx}$	$\bar{\sigma}_{yy}$	$\bar{\sigma}_{xy}$	$\bar{\sigma}_{xz}$	$\bar{\sigma}_{yz}$
Simply supported plate under uniformly distributed load							
10	4Q8-R	2.3370	1.5430	0.0883	0.1136	0.2396	0.0991
50	4Q8-R	1.3671	1.5964	0.0526	0.0916	0.2433	0.0881
100	4Q8-R	1.3359	1.5978	0.0514	0.0906	0.2394	0.0880
CLPT	8CC-F [‡]	1.3296	1.5830	0.0509	0.0906	—	—
Clamped plate under uniformly distributed load							
10	4Q9-R [†]	1.2654	0.5018	0.0550	0.0120	0.2318	0.1445
50	4Q9-R	0.3111	0.5356	0.0108	0.0039	0.2406	0.1160
100	4Q9-R	0.2785	0.5347	0.0094	0.0030	0.2400	0.1148
CLPT	8CC-F [‡]	0.2951	0.5401	0.0145	0.0605	—	—

[†] The 4Q9-S element gives the same results as 4Q9-R.

[‡] 8×8 mesh of conforming cubic elements with full integration for stiffness coefficient evaluation and one-point Gauss rule for stresses.

Table 9.3.7 shows maximum nondimensionalized deflections for angle-ply ($\theta/-\theta/\theta/-\theta, \dots$) square plates under sinusoidal load for $\theta = 5^\circ, 30^\circ$, and 45° . The material properties of an individual layer are assumed to be (*Material 2*)

$$E_1 = 40E_2, G_{12} = G_{13} = 0.6E_2, G_{23} = 0.5E_2, \nu_{12} = 0.25 \quad (9.3.32)$$

The finite element results obtained with a 4×4 mesh of nine-node elements in a quadrant are identical to the closed-form solutions (CFS) for all angles and side-to-thickness ratios, when the correct symmetry boundary conditions (SS-1) are used. Figure 9.3.4 shows the effect of side-to-thickness ratio, number of layers, and the lamination angle on the nondimensionalized maximum deflection of simply supported (SS-1) antisymmetric angle-ply plates. The figure also shows the effect of using incorrect boundary conditions along the lines of symmetry; the symmetry conditions of SS-1 (see Figure 9.2.10) were used to obtain solutions of the two- and sixteen-layer laminates. It is clear from the results that when the lamination angle is small or the number of layers is large, the error due to the incorrect symmetry boundary conditions is small. This is expected because for very small lamination angle, the laminate is close to being a cross-ply laminate, and when the number of layers is large ($n \geq 8$), the laminate behaves like an orthotropic plate, for which the SS-1 boundary conditions are valid.

Table 9.3.7: Nondimensionalized deflections, $\bar{w} \times 10^2$, as a function of number of layers, angle, and side-to-thickness ratio for simply supported (SS-2) angle-ply square plates under sinusoidally distributed transverse load ($h_n = h/n$, $E_1 = 40E_2$, $G_{12} = G_{13} = 0.6E_2$, $G_{23} = 0.5E_2$, $\nu_{12} = 0.25$, $K = 5/6$, n = Number of layers in the laminate).

a/h	Source	$\theta = 5^\circ$		$\theta = 30^\circ$		$\theta = 45^\circ$	
		$n = 2$	$n = 10$	$n = 2$	$n = 10$	$n = 2$	$n = 10$
2	CFS	3.7849	3.6899	3.3330	2.9934	3.2300	2.9175
	FEM	3.7853	3.6903	3.3334	2.9937	3.2303	2.9178
4	CFS	1.3165	1.2611	1.2155	0.8904	1.1576	0.8450
	FEM	1.3166	1.2612	1.2156	0.8905	1.1576	0.8451
10	CFS	0.4883	0.4463	0.6099	0.2901	0.5773	0.2647
	FEM	0.4883	0.4464	0.6099	0.2901	0.5773	0.2647
20	CFS	0.3586	0.3181	0.5224	0.2033	0.4944	0.1818
	FEM	0.3586	0.3181	0.5224	0.2033	0.4944	0.1818
50	CFS	0.3216	0.2815	0.4979	0.1789	0.4712	0.1586
	FEM	0.3216	0.2815	0.4979	0.1789	0.4712	0.1586
100	CFS	0.3162	0.2763	0.4944	0.1755	0.4678	0.1553
	FEM	0.3162	0.2763	0.4944	0.1755	0.4678	0.1553
	CLPT	0.3145	0.2745	0.4932	0.1745	0.4667	0.1542

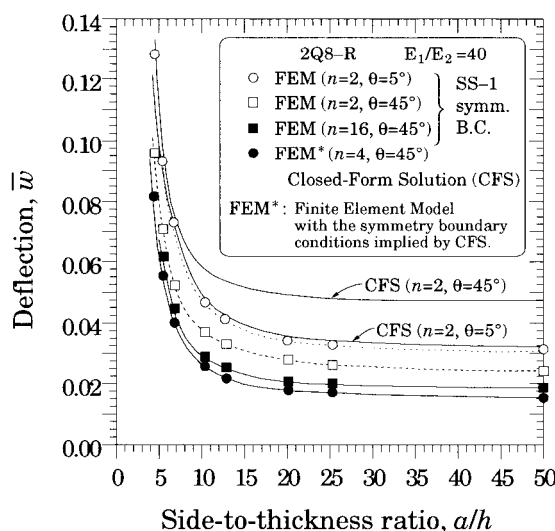


Figure 9.3.4: Effect of transverse shear deformation, lamination angle, number of layers, and symmetry boundary conditions on the deflections of simply supported (SS-1) antisymmetric angle-ply laminates under sinusoidal load.

The stresses obtained with the same mesh as above for ten-layer antisymmetric angle-ply laminates are presented in Table 9.3.8. The stresses in the finite element analysis as well as in the closed-form solution are evaluated at the Gauss points:

$$(\bar{\sigma}_{xx}, \bar{\sigma}_{yy}) = (\sigma_{xx}, \sigma_{yy})(x_c, y_c, \frac{h}{2}) \frac{h^2}{b^2 q_0} , \quad \bar{\sigma}_{xy} = \sigma_{xy}(x_s, y_s, -\frac{h}{2}) \frac{h^2}{b^2 q_0}$$

$$x_c = y_c = 0.47358a, \quad x_s = y_s = 0.02642a \quad (9.3.33)$$

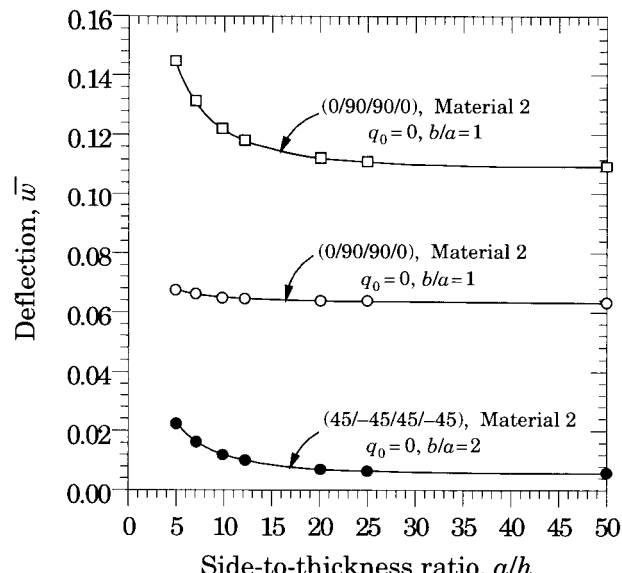
The finite element stresses (second row) are in excellent agreement with the closed-form solution (first row). For $\theta = 45^\circ$ it is found that the stresses are independent of side-to-thickness ratio.

Next, results for thermal bending are presented (see [61,62]). Figure 9.3.5 shows the effect of side-to-thickness ratio a/h on the nondimensionalized deflections and stresses of cross-ply and angle-ply plates subjected to temperature distribution that is linear through the thickness and varies sinusoidally in the plane of the plate ($q = 0, T_0 = 0, T_1 \neq 0$). The deflection and stresses are amplified to show the effect of thickness-shear strain. Clearly, the effect of shear deformation on thermal deflections and stresses is not as significant as in mechanically loaded plates.

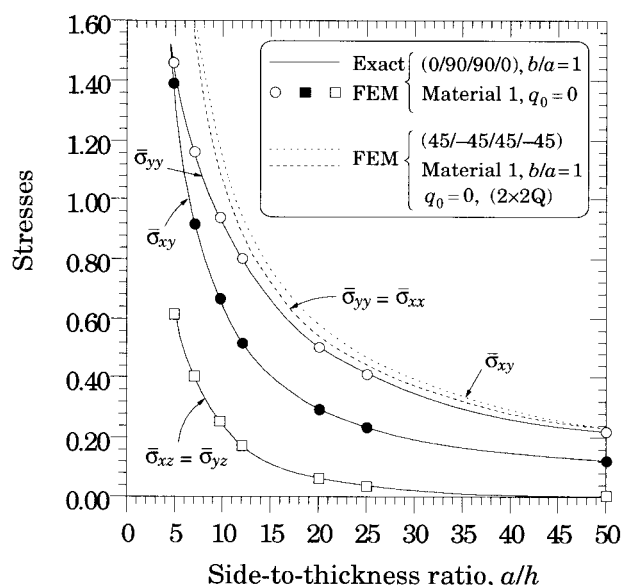
Table 9.3.8: Nondimensionalized stresses for simply supported (SS-2) angle-ply $(-\theta/\theta/-\theta/\dots)$ square plates under sinusoidal transverse load ($h_n = h/n, n = 10, E_1 = 40E_2, G_{12} = G_{13} = 0.6E_2, G_{23} = 0.5E_2, \nu_{12} = 0.25, K = 5/6, 4Q9-R, n = \text{number of layers}$).

a/h	$\theta = 5^\circ$			$\theta = 30^\circ$			$\theta^\dagger = 45^\circ$	
	$\bar{\sigma}_{xx}$	$\bar{\sigma}_{yy}$	$\bar{\sigma}_{xy}$	$\bar{\sigma}_{xx}$	$\bar{\sigma}_{yy}$	$\bar{\sigma}_{xy}$	$\bar{\sigma}_{xx}$	$\bar{\sigma}_{xy}$
2	0.3324	0.0964	0.0850	0.1530	0.0786	0.1688	0.1430	0.1392
	0.3280	0.0957	0.0846	0.1500	0.0774	0.1689	0.1421	0.1401
4	0.4423	0.0551	0.0511	0.2011	0.0890	0.1425	0.1430	0.1392
	0.4379	0.0547	0.0510	0.1982	0.0822	0.1423	0.1421	0.1401
10	0.5146	0.0279	0.0289	0.2328	0.0865	0.1252	0.1430	0.1392
	0.5103	0.0277	0.0290	0.2298	0.0854	0.1252	0.1421	0.1401
20	0.5286	0.0227	0.0246	0.2389	0.0871	0.1218	0.1430	0.1392
	0.5243	0.0225	0.0247	0.2359	0.0860	0.1219	0.1421	0.1401
50	0.5327	0.0211	0.0233	0.2407	0.0873	0.1208	0.1430	0.1392
	0.5284	0.0210	0.0234	0.2377	0.0862	0.1209	0.1421	0.1401
100	0.5333	0.0209	0.0231	0.2410	0.0873	0.1207	0.1430	0.1392
	0.5290	0.0207	0.0233	0.2380	0.0862	0.1208	0.1421	0.1401
CLPT	0.5290	0.0207	0.0233	0.2411	0.0873	0.1206	0.1440	0.1402

[†] The stresses are independent of side-to-thickness ratio.



(a) Center deflections



(b) Stresses at the Gauss points

Figure 9.3.5: Effect of shear deformation on the nondimensionalized (a) deflections and (b) stresses of simply supported antisymmetric cross-ply and angle-ply laminates subjected to thermal loading.

Lastly, numerical results for transverse deflections and stresses of rectangular plates for a variety of boundary conditions are presented. The analytical results reported were obtained using the Lévy method with state-space approach (see Sections 7.4 and 7.5, and References 63–76). For the finite element analysis, a 4×4 mesh is used for the classical plate theory, while 2×2 mesh of nine-node quadratic elements is used for the first-order theory when a quadrant of a plate is analyzed (for SS, CC, and FF boundary conditions), and equivalent 8×4 and 4×2 meshes were used for the half-plate models (in the case of SC, FS, and FC boundary conditions). The notation SC, for example, refers to simply supported boundary condition on the edge $x = -a/2$ and clamped boundary condition on the edge $x = a/2$, while the remaining two edges, $y = 0, b$, are simply supported. In all cases a sinusoidally varying transverse load is used, and the material properties of each lamina are assumed to be those of graphite-epoxy material with the properties listed in Eq. (9.3.25). The deflections and stresses are nondimensionalized as follows:

$$\bar{w} = w_0(0, \frac{b}{2}) \times \frac{E_2 h^3}{b^4 q_0}, \quad \bar{\sigma}_{xx} = \sigma_{xx}(0, \frac{b}{2}, -\frac{h}{2}) \frac{h^2}{b^2 q_0} \times 10$$

$$\bar{\sigma}_{yy} = \sigma_{yy}(0, \frac{b}{2}, \frac{h}{2}) \frac{h^2}{b^2 q_0} \times 10, \quad \bar{\sigma}_{yz} = \sigma_{yz}(0, 0, 0) \frac{h}{b q_0} \times 10 \quad (9.3.34)$$

Tables 9.3.9 through 9.3.11 contain numerical values of deflections and stresses of antisymmetric cross-ply square plates ($0/90/0/\dots$) with various boundary conditions and sinusoidally distributed transverse load. The analytical (first row) and finite element solutions (second row) are presented. In all cases the finite element results are in good agreement with the analytical solutions.

Table 9.3.9: Nondimensionalized center deflections $\bar{w} \times 10^2$ of antisymmetric, two-layer and ten-layer cross-ply square plates ($0/90$)_k.

k	$\frac{a}{h}$	Theory	SS	SC	CC	FF	FS	FC
1	5	FSDT	1.758	1.477	1.257	2.777	2.335	1.897
		CLPT	1.759	1.478	1.257	2.776	2.334	1.897 [†]
	10	FSDT	1.064	0.664	0.429	1.777	1.471	0.980
		CLPT	1.043	0.648	0.417	1.786	1.465	0.977
5	10	FSDT	1.237	0.883	0.656	2.028	1.687	1.223
		CLPT	1.238	0.883	0.657	2.027	1.687	1.223
		FSDT	1.064	0.664	0.429	1.777	1.471	0.980
		CLPT	1.043	0.648	0.417	1.786	1.465	0.977
	5	FSDT	1.137	1.045	0.945	1.663	1.460	1.258
		CLPT	1.137	1.045	0.945	1.662	1.460	1.258
		FSDT	0.442	0.266	0.167	0.665	0.579	0.380
		CLPT	0.444	0.266	0.169	0.686	0.593	0.391
	10	FSDT	0.615	0.480	0.385	0.915	0.800	0.612
		CLPT	0.616	0.480	0.386	0.914	0.800	0.612
		FSDT	0.442	0.266	0.167	0.665	0.579	0.380
		CLPT	0.444	0.266	0.169	0.686	0.593	0.391

[†] The second row corresponds to finite element results.

Table 9.3.10: Nondimensionalized stress ($\bar{\sigma}_{xx}$) of antisymmetric cross-ply square plates ($0/90/0/\dots$); n denotes the total number of layers.

n	$\frac{a}{h}$	Theory	SS	SC	CC	FF	FS	FC
2	5	FSDT	7.157 6.948	5.338 5.465	3.911 3.707	2.469 2.359	4.430 4.479	2.434 2.542
		CLPT	7.157	5.660	4.800	2.403	4.442	3.042
			6.659	5.782	4.348	2.034	4.288	2.991
		FSDT	7.157 6.948	5.494 5.668	4.450 4.222	2.442 2.331	4.435 4.491	2.790 2.895
	10	CLPT	7.157	5.660	4.800	2.403	4.442	3.042
			6.659	5.782	4.348	2.034	4.288	2.991
		FSDT	5.009 4.864	3.707 3.755	2.275 2.154	1.712 1.639	2.957 2.993	1.343 1.427
		CLPT	5.009	3.829	3.167	1.725	2.986	1.865
10	5		4.611	3.911	2.798	1.324	2.806	1.700
		FSDT	5.009 4.863	3.642 3.754	2.692 2.550	1.723 1.648	2.968 3.010	1.594 1.674
		CLPT	5.009 4.611	3.829 3.911	3.167 2.798	1.725 1.324	2.986 2.806	1.865 1.700

Table 9.3.11: Nondimensionalized stress ($\bar{\sigma}_{yy}$) of antisymmetric cross-ply ($0/90/0/\dots$) square plates; n denotes the total number of layers.

n	$\frac{a}{h}$	Theory	SS	SC	CC	FF	FS	FC
2	5	FSDT	7.157 6.948	6.034 5.914	5.153 4.990	11.907 11.675	9.848 9.140	8.047 8.367
		CLPT	7.157	4.483	2.914	11.849	9.837	6.560
			6.659	4.393	2.615	11.614	8.878	7.181
		FSDT	7.157 6.948	5.109 5.082	3.799 3.661	11.884 11.654	9.847 9.120	7.150 7.610
	10	CLPT	7.157	4.483	2.914	11.849	9.837	6.560
			6.659	4.393	2.615	11.614	8.878	7.181
		FSDT	5.009 4.864	4.628 4.511	4.212 4.086	7.583 7.429	6.590 6.141	5.706 5.844
		CLPT	5.009	3.025	1.911	7.480	6.531	4.284
10	5		4.611	2.942	1.694	7.395	5.935	4.782
		FSDT	5.009 4.863	3.904 3.852	3.135 3.031	7.533 7.384	6.566 6.097	5.029 5.279
		CLPT	5.009 4.611	3.025 2.942	1.911 1.694	7.480 7.395	6.531 5.935	4.284 4.782

Table 9.3.12 contains nondimensionalized deflections of angle-ply laminates subjected to uniformly distributed transverse load under various boundary conditions and with different values of E_1/E_2 ($G_{12} = G_{13} = 0.6E_2$, $G_{23} = 0.5E_2$, $\nu_{12} = 0.25$). The results were obtained using the Lévy method with state-space approach discussed in Section 7.5.

Table 9.3.12: Nondimensionalized deflections $\bar{w} \equiv w_0(0, b/2)E_2 h^3 \times 10^2 / (a^4 q_0)$ of simply supported (SS-2), four-layer antisymmetric angle-ply square plates [(45/-45/45/-45), $a/h = 10$].

Theory	$\frac{E_1}{E_2}$	SS	SC	CC	FF	FS	FC
FSDT	2	3.3749	2.4227	1.7530	10.7347	6.4469	4.7427
CLPT		3.2142	2.2144	1.6308	10.4702	6.2336	4.4460
FSDT	10	1.1598	0.9443	0.7708	6.0487	2.6109	2.1091
CLPT		1.000	0.7457	0.5578	5.5710	2.3451	1.7473
FSDT	20	0.7013	0.6024	0.5180	4.2843	1.6234	1.3787
CLPT		0.5418	0.4120	0.3133	3.6574	1.3432	1.0104
FSDT	30	0.5312	0.4706	0.4170	3.2417	1.2252	1.0749
CLPT		0.3718	0.2847	0.2179	2.7376	0.9433	0.7121

As noted in Section 6.6, the midplane symmetric plates are characterized by nonzero bending-twisting coupling coefficients D_{16} and D_{26} . Figure 9.3.6 contains plots of the nondimensionalized center deflection versus side-to-thickness ratio for three-layer (-45/45/-45) simply supported (SS-1) and clamped, square, symmetric laminates under uniformly distributed transverse load ($E_1 = 25E_2$, $G_{12} = G_{13} = 0.5E_2$, $G_{23} = 0.2E_2$, $\nu_{12} = 0.25$, $K = 5/6$, $a/h = 10$). The finite element results are obtained using 4×4 mesh of nine-node elements (*i.e.*, 4Q9-R). The solution obtained with omitting D_{16} and D_{26} is also shown in the figure. The bending-twisting coupling has the effect of increasing deflections. Also, the effect of shear deformation is more in the clamped plate than in the simply supported plate. Figure 9.3.7 shows the nondimensionalized center deflections obtained by the CLPT and FSDT ($a/h = 10$) as functions of the lamination angle for simply supported (SS-2) symmetric three-layer ($-\theta/\theta/-\theta$) plates under uniformly distributed load. The plots are symmetric about 45° .

Table 9.3.13: Effects of side-to-thickness ratio, integration, and type of element on the nondimensionalized fundamental frequency $\bar{\omega} = \omega(a^2/h)\sqrt{\rho/E_2}$ of simply supported (SS-1) cross-ply (0/90/90/0)square plates.

a/h	Serendipity Element			Lagrange Element			CFS
	F	R	S	F	R	S	
2	5.502	5.503	5.501	5.502	5.503	5.501	5.500
10	15.174	15.179	15.159	15.182	15.193	15.172	15.143
100	19.171	18.841	18.808	19.225	18.883	18.933	18.836

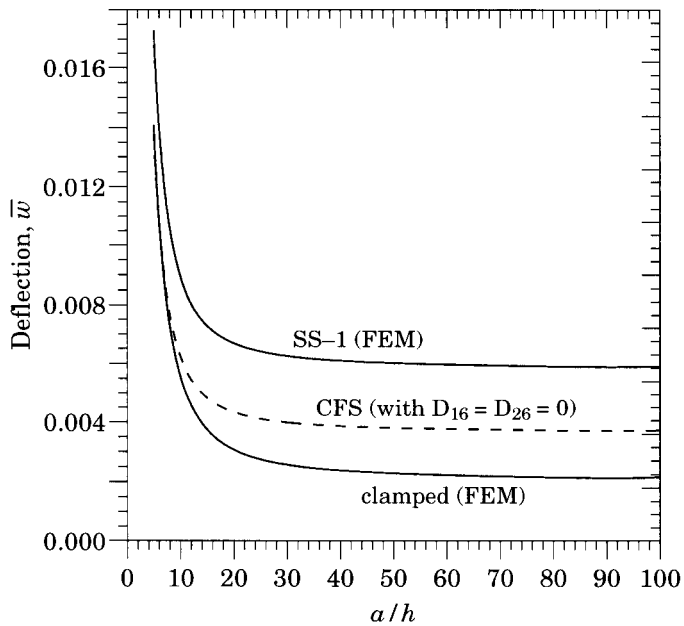


Figure 9.3.6: Nondimensionalized deflection versus side-to-thickness ratio for three-layer $(-45/45/-45)$, simply supported (SS-1) and clamped symmetric plates under uniform loading.

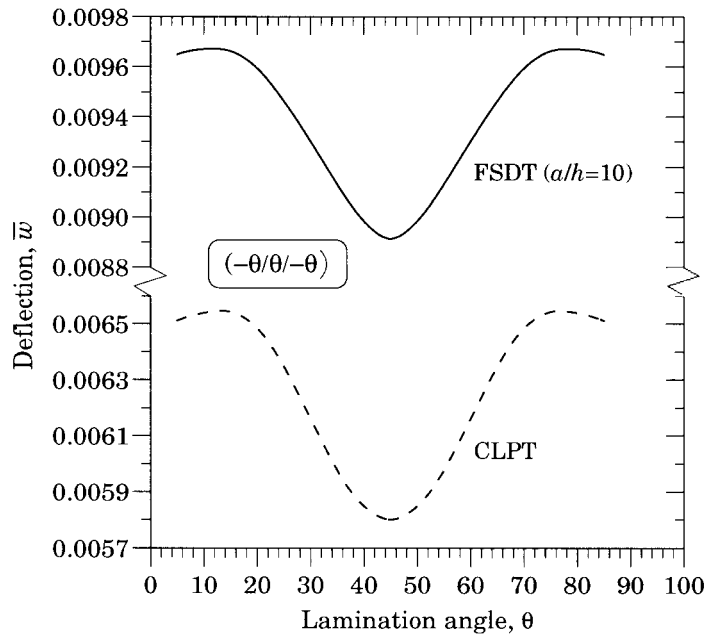


Figure 9.3.7: Nondimensionalized deflection versus lamination angle for simply supported (SS-1) symmetric three-layer $(-\theta/\theta/-\theta)$ plates under uniformly distributed load.

9.3.6 Vibration Analysis

The effect of reduced integration and the use of eight-node and nine-node elements on the accuracy of the natural frequencies are studied using three-layer cross-ply (0/90/0) laminate used to obtain the results in Table 9.3.2. A 2×2 mesh in a quarter plate is used to obtain the results [58,77]. Effects of side-to-thickness ratio, integration, and type of element on the nondimensionalized fundamental frequency $\bar{\omega}$ of simply supported (SS-1) cross-ply (0/90/90/0) square plates (Material 2; rotary inertia included) are presented in Table 9.3.13. From the results obtained, it is clear that both full (F) and selective (S) integrations give good results for thick plates ($a/h \leq 10$), whereas reduced integration (R) gives the best results for thin plates ($a/h \geq 100$). However, the reduced integration and selective integration rules both give good results for a wide range of side-to-thickness ratios.

Table 9.3.14 contains the lowest six natural frequencies of two- and four-layer cross-ply and angle-ply laminates with clamped edges. While the first two fundamental frequencies are very close, the higher frequencies are quite different for these laminates.

Table 9.3.14: The lowest six nondimensionalized frequencies of cross-ply and angle-ply square plates with clamped boundary conditions ($\bar{\omega} = \omega(a^2/h)\sqrt{\rho/E_2}$; $h_i = h/n$, $a/h = 10$, Material 2, 2Q8-R in full plate).

Laminate	a/h	ω_1	ω_2	ω_3	ω_4	ω_5	ω_6
(0/90)	2	5.900	10.137 [†]	14.750 [†]	18.123	18.245	20.759
	10	19.567	43.702 [†]	128.43 [†]	98.578	98.658	141.47
	100	25.677	244.77 [†]	967.21 [†]	1454.2 [†]	1625.5	1687.1 [†]
$(0/90)_2$	2	6.001	10.374 [†]	23.477 [†]	27.019	27.181	34.240 [†]
	10	24.368	47.200 [†]	101.35	101.69	141.23 [†]	157.31
	100	40.506	259.23 [†]	968.04	968.06	1455.6 [†]	1627.2
$(-45/45)$	2	5.883	10.106 [†]	14.75 [†]	19.101	20.129	20.826
	10	18.979	41.482 [†]	96.584	98.336	128.43 [†]	160.64
	100	24.420	241.00 [†]	966.94	967.16	1454.5 [†]	1943.9
$(-45/45)_2$	2	5.992	10.359 [†]	20.830	21.081	23.479 [†]	31.771
	10	23.834	45.720 [†]	99.174	101.37	141.26 [†]	185.49
	100	38.201	249.30 [†]	967.32	967.92	1455.8 [†]	1947.0

[†] Occur in pairs.

Figure 9.3.8a shows the effect of side-to-thickness ratio on the nondimensionalized fundamental frequencies, $\bar{\omega} = \omega(a^2/h)\sqrt{\rho h/E_2}$, of cross-ply plates ($a/h = 10$, $E_1/E_2 = 25$, $G_{12} = G_{13} = 0.5E_2$, $G_{23} = 0.2E_2$, $\nu_{12} = 0.25$, $K = 5/6$). Similar results are presented for angle-ply plates in Figure 9.3.8b, which also contains a plot of the fundamental natural frequency versus the lamination angle for four-layer antisymmetric angle-ply laminates. The dashed line in Figure 9.3.8b corresponds to the case in which the SS-1 (incorrect) symmetry boundary conditions were used.

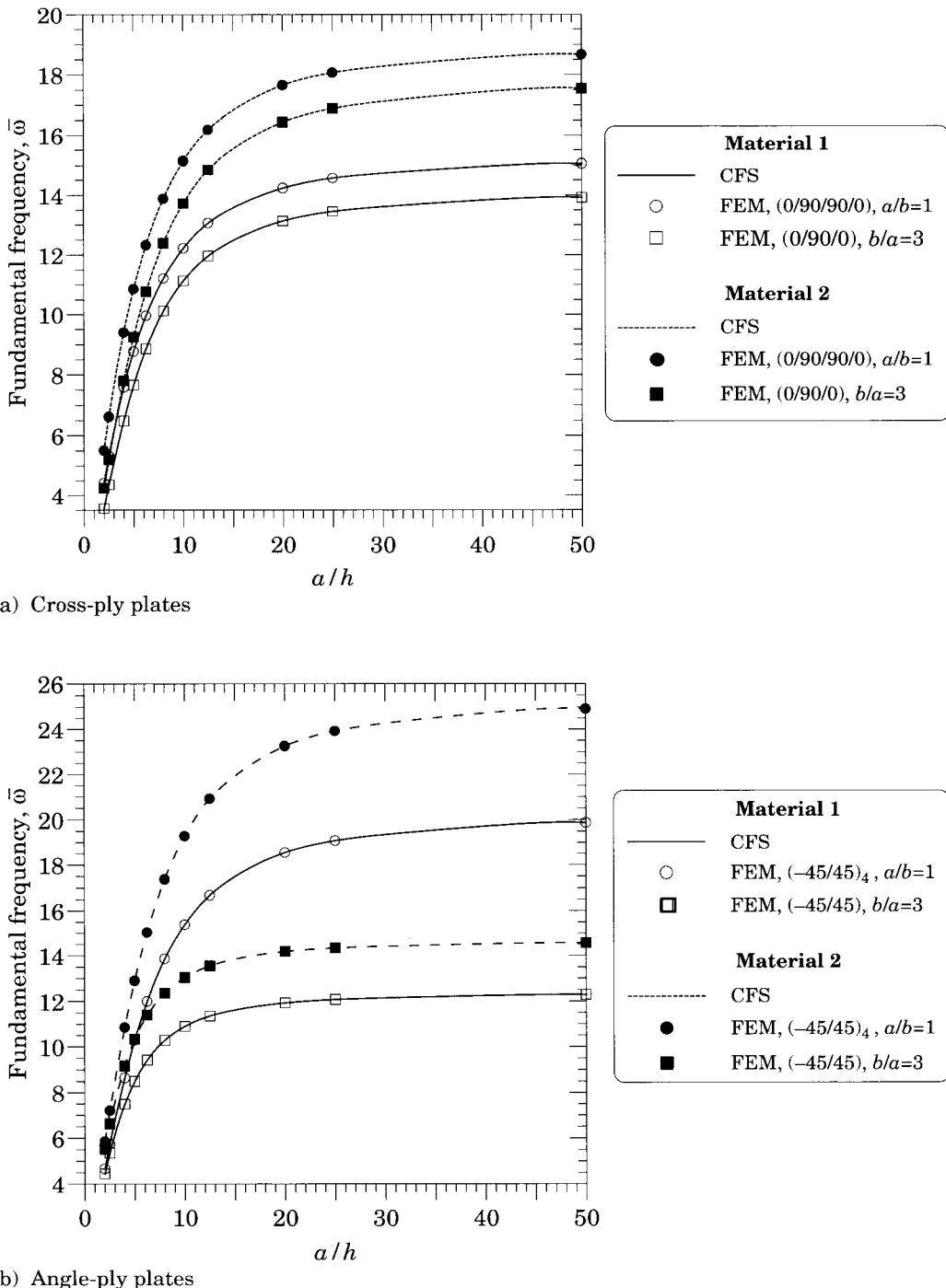


Figure 9.3.8: Nondimensionalized fundamental frequency versus side-to-thickness ratio of simply supported antisymmetric (a) cross-ply (SS-1) and (b) angle-ply (SS-2) plates.

9.3.7 Transient Analysis

Here we present results of transient analysis obtained using the shear deformable finite element. For additional results, the reader may consult References 78–80. The nine-node quadratic element with selective integration rule is used in the examples discussed here. In all cases initial conditions were assumed to be zero. The constant-average-acceleration scheme ($\alpha = \gamma = 0.5$) of Newmark is used for time integration.

Simply supported (SS-1) antisymmetric cross-ply square plates (0/90)_n under suddenly applied sinusoidally (SSL) or uniformly (UDL) distributed transverse step load are analyzed. The boundary conditions for a quadrant are (see Figure 9.2.10):

$$\begin{aligned} x = 0 : \quad u_0 &= \phi_x = 0; \quad x = a/2 : \quad v_0 = w_0 = \phi_y = 0 \\ y = 0 : \quad v_0 &= \phi_y = 0; \quad y = a/2 : \quad u_0 = w_0 = \phi_x = 0 \end{aligned} \quad (9.3.35)$$

The finite element results were obtained using a 2×2 mesh of nine-node quadratic FSDT finite elements in a quadrant. The following geometric and material properties were used:

$$a = b = 25 \text{ cm}, \quad h = 5 \text{ cm}, \quad q_0 = 10 \text{ N/cm}^2, \quad \Delta t = 5 \mu\text{s} \quad (9.3.36)$$

$$\begin{aligned} \rho &= 8 \times 10^{-6} \text{ N-s}^2/\text{cm}^4, \quad E_1 = 25E_2 \text{ N/cm}^2, \quad E_2 = 2.1 \times 10^6 \text{ N/cm}^2 \\ G_{12} &= G_{13} = 0.5E_2 \text{ N/cm}^2, \quad G_{23} = 0.2E_2 \text{ N/cm}^2 \end{aligned} \quad (9.3.37)$$

The following nondimensionalizations are used:

$$\begin{aligned} \bar{w} &= w_0 \left(\frac{a}{2}, \frac{a}{2} \right) \frac{E_2 h^3}{b^4 q_0} \times 10^2, \quad \bar{\sigma}_{xx} = \sigma_{xx} \left(\frac{a}{2}, \frac{b}{2}, \frac{h}{2} \right) \frac{h^2}{b^2 q_0} \\ \bar{\sigma}_{yy} &= \sigma_{yy} \left(\frac{a}{2}, \frac{b}{2}, \frac{h}{2} \right) \frac{h^2}{b^2 q_0}, \quad \bar{\sigma}_{xy} = \sigma_{xy} \left(0, 0, -\frac{h}{2} \right) \frac{h^2}{b^2 q_0} \end{aligned} \quad (9.3.38)$$

We note that

$$\begin{aligned} \sigma_{xx} \left(\frac{a}{2}, \frac{b}{2}, \frac{h}{2} \right) &= -\sigma_{yy} \left(\frac{a}{2}, \frac{b}{2}, -\frac{h}{2} \right) \\ \sigma_{yy} \left(\frac{a}{2}, \frac{b}{2}, \frac{h}{2} \right) &= -\sigma_{xx} \left(\frac{a}{2}, \frac{b}{2}, -\frac{h}{2} \right) \\ \sigma_{xy} \left(\frac{a}{2}, \frac{b}{2}, -\frac{h}{2} \right) &= -\sigma_{xy} \left(\frac{a}{2}, \frac{b}{2}, \frac{h}{2} \right) \end{aligned} \quad (9.3.39)$$

Table 9.3.15 contains nondimensionalized center deflection and stresses for (0/90) laminate under sinusoidal load. The finite element results are compared with the closed-form solutions (CFS) developed in Section 6.7 (also see Reddy [78]). The results are in good agreement with the analytical solutions.

Figures 9.3.9 through 9.3.12 show plots of center deflection \bar{w} and maximum stresses $\bar{\sigma}_{xx}$, $\bar{\sigma}_{yy}$, and $\bar{\sigma}_{xy}$ of two-layer and eight-layer antisymmetric cross-ply square plates under suddenly applied sinusoidally or uniformly distributed transverse step load. The geometry and material properties are the same as listed in Eqs. (9.3.36) and (9.3.37). The finite element results are in excellent agreement with the analytical solutions of the first-order shear deformation plate theory.

Table 9.3.15: Comparison of transverse deflection and stresses obtained by the finite element method with closed-form solution of two-layer cross-ply square plate under suddenly applied sinusoidal load.

Time (μs)	\bar{w}		$\bar{\sigma}_{xx}$		$\bar{\sigma}_{xy}$	
	CFS [†]	FES	CFS	FES	CFS	FES
10	0.0514	0.0515	0.0080	0.0077	0.0058	0.0056
20	0.2486	0.2489	0.0777	0.0754	0.0525	0.0507
40	1.0152	1.0165	0.4962	0.4819	0.3073	0.2978
60	2.0523	2.0544	0.9679	0.9400	0.6039	0.5849
80	2.9782	2.9807	1.4649	1.4224	0.9075	0.8790
100	3.4784	3.4802	1.6724	1.6233	1.0404	1.0073
120	3.3620	3.3621	1.6544	1.6052	1.0251	0.9922
140	2.6836	2.6818	1.2807	1.2416	0.7979	0.7715
160	1.6705	1.6674	0.8195	0.7936	0.5080	0.4907
180	0.6952	0.6921	0.2997	0.2892	0.1902	0.1829
200	0.0902	0.0889	0.0394	0.0375	0.0248	0.0236

[†] Closed-form solution with Newmark's scheme for time integration.

9.4 Finite Element Analysis of Shells

9.4.1 Weak Forms

The displacement finite element model of the equations governing doubly-curved shells, Eqs. (8.3.6)–(8.3.10), can be derived in a manner similar to that of plates. In fact, the finite element model of doubly-curved shells is identical to that of FSDT with additional terms in the stiffness coefficients (see pages 465–468 of Reddy [89]). For the sake of completeness, the main equations are presented here.

We begin with the weak forms of Eqs. (8.3.6)–(8.3.10) ($x_1 = x$ and $x_2 = y$):

$$0 = \int_{\Omega^e} \left[\frac{\partial \delta u_0}{\partial x} N_1 + \frac{\partial \delta u_0}{\partial y} (N_6 + C_0 M_6) - \delta u_0 \frac{Q_1}{R_1} + I_0 \delta u_0 \frac{\partial^2 u_0}{\partial t^2} + I_1 \delta u_0 \frac{\partial^2 \phi_1}{\partial t^2} \right] dx dy - \oint_{\Gamma^e} P_1 \delta u_0 ds \quad (9.4.1a)$$

$$0 = \int_{\Omega^e} \left[\frac{\partial \delta v_0}{\partial x} (N_6 - C_0 M_6) + \frac{\partial \delta v_0}{\partial y} N_2 - \delta v_0 \frac{Q_2}{R_2} + I_0 \delta v_0 \frac{\partial^2 v_0}{\partial t^2} + I_1 \delta v_0 \frac{\partial^2 \phi_2}{\partial t^2} \right] dx dy - \oint_{\Gamma^e} P_2 \delta v_0 ds \quad (9.4.1b)$$

$$0 = \int_{\Omega^e} \left[\frac{\partial \delta w_0}{\partial x} Q_1 + \frac{\partial \delta w_0}{\partial y} Q_2 + \delta w_0 \left(\frac{N_1}{R_1} + \frac{N_2}{R_2} \right) - \delta w_0 q + I_0 \delta w_0 \frac{\partial^2 w_0}{\partial t^2} + \frac{\partial \delta w_0}{\partial x} \left(\hat{N}_1 \frac{\partial w_0}{\partial x} + \hat{N}_6 \frac{\partial w_0}{\partial y} \right) + \frac{\partial \delta w_0}{\partial y} \left(\hat{N}_6 \frac{\partial w_0}{\partial x} + \hat{N}_2 \frac{\partial w_0}{\partial y} \right) \right] dx dy - \oint_{\Gamma^e} V_n \delta w_0 ds \quad (9.4.1c)$$

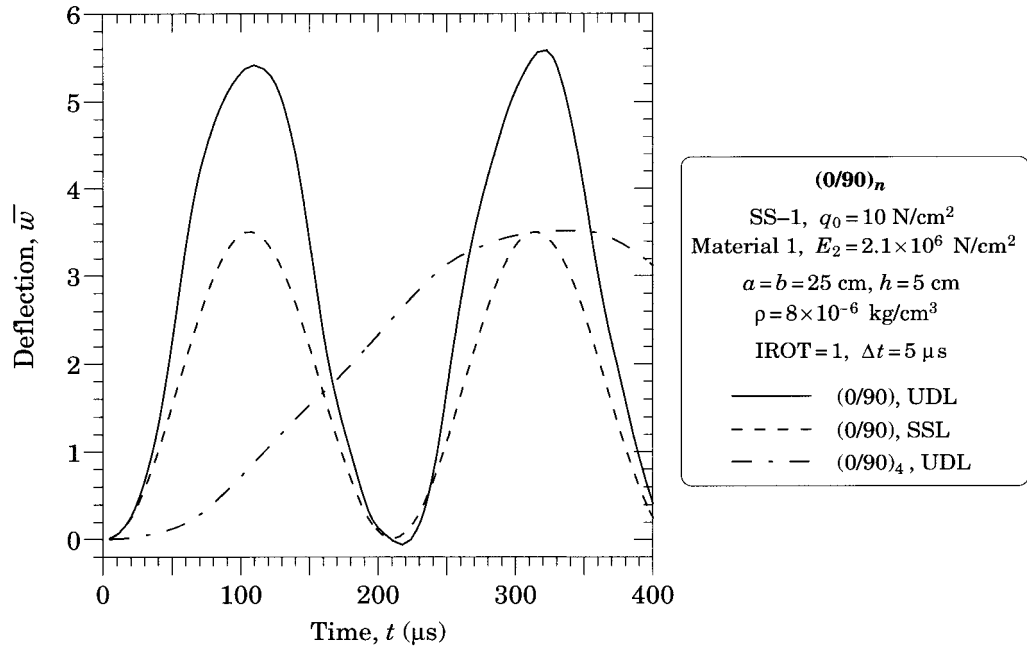


Figure 9.3.9: Plots of center deflection \bar{w} versus time for simply supported (SS-1) two-layer and eight-layer cross-ply square plates under sinusoidal or uniform step loading.

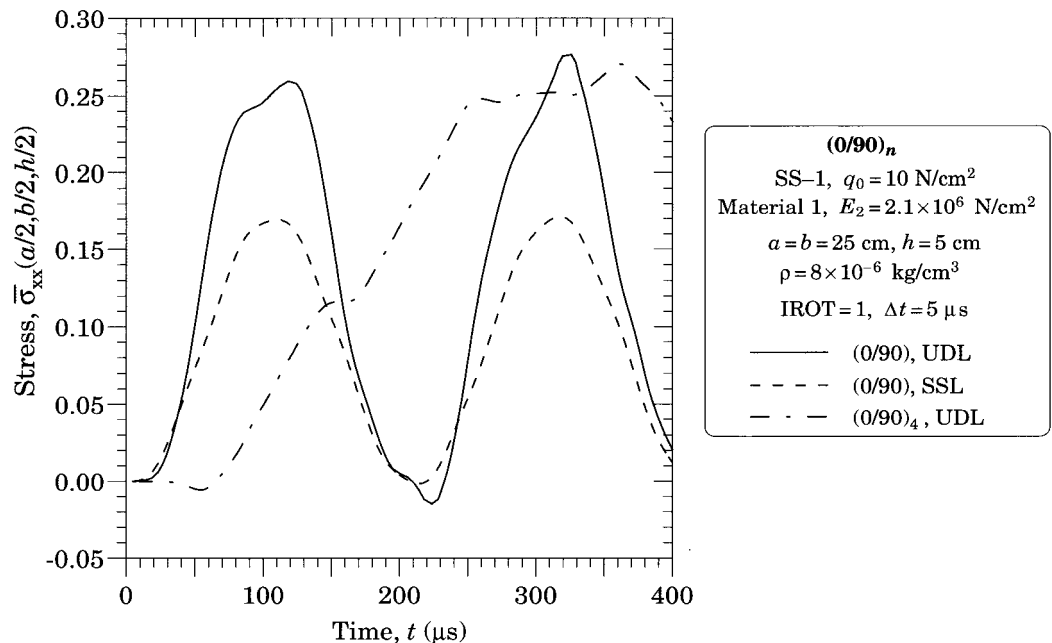


Figure 9.3.10: Plots of center normal stress $\bar{\sigma}_{xx}$ versus time for simply supported (SS-1) two-layer and eight-layer cross-ply square plates under sinusoidal or uniform step loading.

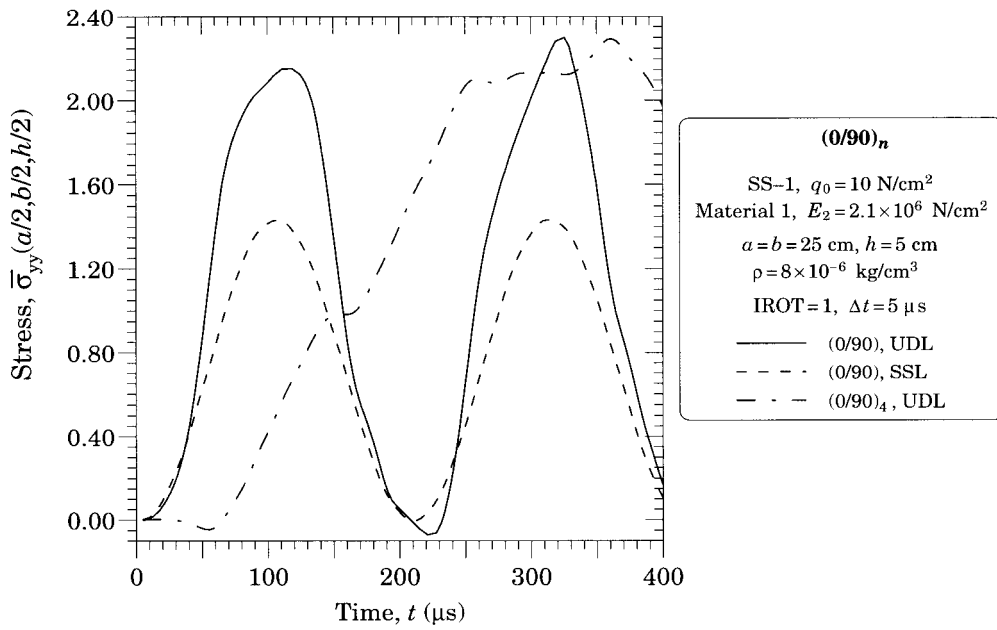


Figure 9.3.11: Plots of center normal stress $\bar{\sigma}_{yy}$ versus time for simply supported (SS-1) two-layer and eight-layer cross-ply square plates under sinusoidal or uniform step loading.

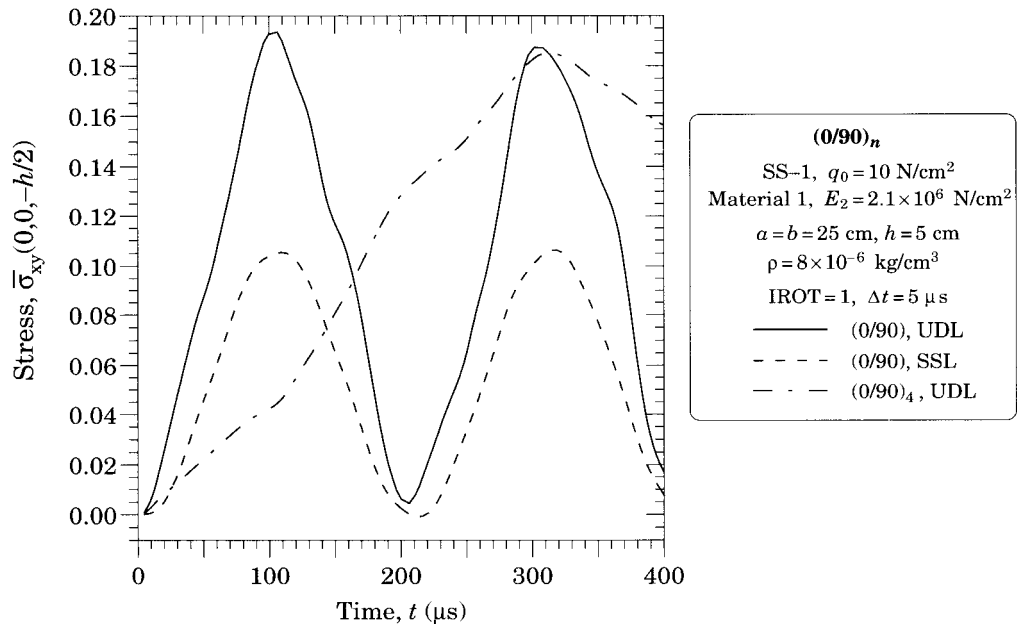


Figure 9.3.12: Plots of center normal stress $\bar{\sigma}_{xy}$ versus time for simply supported (SS-1) two-layer and eight-layer cross-ply square plates under sinusoidal or uniform step loading.

$$0 = \int_{\Omega^e} \left(\frac{\partial \delta \phi_1}{\partial x} M_1 + \frac{\partial \delta \phi_1}{\partial y} M_6 + \delta \phi_1 Q_1 + I_2 \delta \phi_1 \frac{\partial^2 \phi_1}{\partial t^2} + I_1 \delta \phi_1 \frac{\partial^2 u_0}{\partial t^2} \right) dx dy \\ - \oint_{\Gamma^e} T_1 \delta \phi_1 ds \quad (9.4.1d)$$

$$0 = \int_{\Omega^e} \left(\frac{\partial \delta \phi_2}{\partial x} M_6 + \frac{\partial \delta \phi_2}{\partial y} M_2 + \delta \phi_2 Q_2 + I_2 \delta \phi_2 \frac{\partial^2 \phi_2}{\partial t^2} + I_1 \delta \phi_2 \frac{\partial^2 v_0}{\partial t^2} \right) dx dy \\ - \oint_{\Gamma^e} T_2 \delta \phi_2 ds \quad (9.4.1e)$$

where $C_0 = 0.5(1/R_1 - 1/R_2)$ and the stress resultants N_i , M_i and Q_i are defined by Eqs. (8.3.1a,b). We note from the boundary terms in Eq. (9.4.1a-e) that $(u_0, v_0, w_0, \phi_1, \phi_2)$ are the primary variables. Therefore, we can use the C^0 interpolation of the displacements. The secondary variables are

$$\begin{aligned} P_1 &\equiv N_1 n_1 + (N_6 + C_0 M_6) n_2, & P_2 &\equiv (N_6 - C_0 M_6) n_1 + N_2 n_2 \\ T_2 &\equiv M_1 n_1 + M_6 n_2, & T_2 &\equiv M_6 n_1 + M_2 n_2 \\ V_n &\equiv \left(Q_1 + \hat{N}_1 \frac{\partial w_0}{\partial x} + \hat{N}_6 \frac{\partial w_0}{\partial y} \right) n_1 + \left(Q_2 + \hat{N}_6 \frac{\partial w_0}{\partial x} + \hat{N}_2 \frac{\partial w_0}{\partial y} \right) n_2 \end{aligned} \quad (9.4.2)$$

where $(\hat{N}_1, \hat{N}_2, \hat{N}_6)$ are the applied surface loads that are introduced to study the buckling problem. Note that in the case of shells, surface displacements are coupled to the transverse displacement even for linear analysis of isotropic shells.

9.4.2 Finite Element Model

Using interpolation of the form

$$u_0(x, y, t) = \sum_{j=1}^m u_j(t) \psi_j^e(x, y) \quad (9.4.3a)$$

$$v_0(x, y, t) = \sum_{j=1}^m v_j(t) \psi_j^e(x, y) \quad (9.4.3b)$$

$$w_0(x, y, t) = \sum_{j=1}^n w_j(t) \psi_j^e(x, y) \quad (9.4.4)$$

$$\phi_1(x, y, t) = \sum_{j=1}^p S_j^1(t) \psi_j^e(x, y) \quad (9.4.5a)$$

$$\phi_2(x, y, t) = \sum_{j=1}^p S_j^2(t) \psi_j^e(x, y) \quad (9.4.5b)$$

where ψ_j^e are Lagrange interpolation functions. In the present study equal interpolation ($m = n = p$) of five displacements, with $p = 1, 2, \dots$ is used. Note that the finite element model developed here for doubly-curved shells contains the FSDT plate element as a special case (set $C_0 = 0$, $1/R_1 = 0$ and $1/R_2 = 0$).

Substituting Eqs. (9.4.3)–(9.4.5) for $(u_0, v_0, w_0, \phi_1, \phi_2)$ into the weak forms in Eq. (9.4.1a-e), we obtain the semidiscrete finite element model of the first-order shear deformation shell theory:

$$\left(\begin{bmatrix} [K^{11}] & [K^{12}] & [K^{13}] & [K^{14}] & [K^{15}] \\ [K^{12}]^T & [K^{22}] & [K^{23}] & [K^{24}] & [K^{25}] \\ [K^{13}]^T & [K^{23}]^T & [K^{33}] & [K^{34}] & [K^{35}] \\ [K^{14}]^T & [K^{24}]^T & [K^{34}]^T & [K^{44}] & [K^{45}] \\ [K^{15}]^T & [K^{25}]^T & [K^{35}]^T & [K^{45}]^T & [K^{55}] \end{bmatrix} + \begin{bmatrix} [0] & [0] & [0] & [0] & [0] \\ [0] & [0] & [0] & [0] & [0] \\ [0] & [0] & [G] & [0] & [0] \\ [0] & [0] & [0] & [0] & [0] \\ [0] & [0] & [0] & [0] & [0] \end{bmatrix} \right) \begin{Bmatrix} \{u^e\} \\ \{v^e\} \\ \{w^e\} \\ \{S^1\} \\ \{S^2\} \end{Bmatrix} \\ + \begin{bmatrix} I_0[M] & [0] & [0] & I_1[M] & [0] \\ [0] & I_0[M] & [0] & [0] & I_1[M] \\ [0] & [0] & I_0[M] & [0] & [0] \\ I_1[M] & [0] & [0] & I_2[M] & [0] \\ [0] & I_1[M] & [0] & [0] & I_2[M] \end{bmatrix} \begin{Bmatrix} \{\ddot{u}^e\} \\ \{\ddot{v}^e\} \\ \{\ddot{w}^e\} \\ \{\ddot{S}^1\} \\ \{\ddot{S}^2\} \end{Bmatrix} = \begin{Bmatrix} \{F^1\} - \{F^{T1}\} \\ \{F^2\} - \{F^{T2}\} \\ \{F^3\} \\ \{F^4\} - \{F^{T4}\} \\ \{F^5\} - \{F^{T5}\} \end{Bmatrix} \quad (9.4.6)$$

where the coefficients of the submatrices $[M^{\alpha\beta}]$ and G_{ij} are the same as those defined for $(\alpha, \beta = 1, 2, \dots, 5)$ by the expressions in (9.3.7). The stiffness coefficients $[K^{\alpha\beta}]$ are defined as follows:

$$\begin{aligned} K_{ij}^{1\alpha} &= \int_{\Omega^e} \left[\frac{\partial \psi_i^e}{\partial x} N_{1j}^\alpha + \frac{\partial \psi_i^e}{\partial y} (N_{6j}^\alpha + C_0 M_{6j}^\alpha) - \psi_i^e \frac{Q_{1j}^\alpha}{R_1} \right] dx dy \\ K_{ij}^{2\alpha} &= \int_{\Omega^e} \left[\frac{\partial \psi_i^e}{\partial x} (N_{6j}^\alpha - C_0 M_{6j}^\alpha) + \frac{\partial \psi_i^e}{\partial y} N_{2j}^\alpha - \psi_i^e \frac{Q_{2j}^\alpha}{R_2} \right] dx dy \\ K_{ij}^{3\alpha} &= \int_{\Omega^e} \left[\frac{\partial \psi_i^e}{\partial x} Q_{1j}^\alpha + \frac{\partial \psi_i^e}{\partial y} Q_{2j}^\alpha + \psi_i^e \left(\frac{N_{1j}^\alpha}{R_1} + \frac{N_{2j}^\alpha}{R_2} \right) \right] dx dy \\ K_{ij}^{4\alpha} &= \int_{\Omega^e} \left(\frac{\partial \psi_i^e}{\partial x} M_{1j}^\alpha + \frac{\partial \psi_i^e}{\partial y} M_{6j}^\alpha + \psi_i^e Q_{1j}^\alpha \right) dx dy \\ K_{ij}^{5\alpha} &= \int_{\Omega^e} \left(\frac{\partial \psi_i^e}{\partial x} M_{6j}^\alpha + \frac{\partial \psi_i^e}{\partial y} M_{2j}^\alpha + \psi_i^e Q_{2j}^\alpha \right) dx dy \end{aligned} \quad (9.4.7)$$

and the nonzero coefficients N_{Ij}^α , M_{Ij}^α , and Q_{Ij}^α for $\alpha = 1, 2, \dots, 5$ and $I = 1, 2, 6$ are given by

$$\begin{aligned} N_{1j}^1 &= A_{11} \frac{\partial \psi_j^e}{\partial x} + A_{16} \frac{\partial \psi_j^e}{\partial y}, \quad N_{1j}^2 = A_{12} \frac{\partial \psi_j^e}{\partial y} + A_{16} \frac{\partial \psi_j^e}{\partial x} \\ N_{1j}^4 &= B_{11} \frac{\partial \psi_j^e}{\partial x} + B_{16} \frac{\partial \psi_j^e}{\partial y}, \quad N_{1j}^5 = B_{12} \frac{\partial \psi_j^e}{\partial y} + B_{16} \frac{\partial \psi_j^e}{\partial x} \\ N_{2j}^1 &= A_{12} \frac{\partial \psi_j^e}{\partial x} + A_{26} \frac{\partial \psi_j^e}{\partial y}, \quad N_{2j}^2 = A_{22} \frac{\partial \psi_j^e}{\partial y} + A_{26} \frac{\partial \psi_j^e}{\partial x} \\ N_{2j}^4 &= B_{12} \frac{\partial \psi_j^e}{\partial x} + B_{26} \frac{\partial \psi_j^e}{\partial y}, \quad N_{2j}^5 = B_{22} \frac{\partial \psi_j^e}{\partial y} + B_{26} \frac{\partial \psi_j^e}{\partial x} \\ N_{6j}^1 &= A_{16} \frac{\partial \psi_j^e}{\partial x} + A_{66} \frac{\partial \psi_j^e}{\partial y}, \quad N_{6j}^2 = A_{26} \frac{\partial \psi_j^e}{\partial y} + A_{66} \frac{\partial \psi_j^e}{\partial x} \end{aligned}$$

$$\begin{aligned}
N_{6j}^4 &= B_{16} \frac{\partial \psi_j^e}{\partial x} + B_{66} \frac{\partial \psi_j^e}{\partial y}, \quad N_{6j}^5 = B_{26} \frac{\partial \psi_j^e}{\partial y} + B_{66} \frac{\partial \psi_j^e}{\partial x} \\
M_{1j}^1 &= B_{11} \frac{\partial \psi_j^e}{\partial x} + B_{16} \frac{\partial \psi_j^e}{\partial y}, \quad M_{1j}^2 = B_{12} \frac{\partial \psi_j^e}{\partial y} + B_{16} \frac{\partial \psi_j^e}{\partial x} \\
M_{1j}^4 &= D_{11} \frac{\partial \psi_j^e}{\partial x} + D_{16} \frac{\partial \psi_j^e}{\partial y}, \quad M_{1j}^5 = D_{12} \frac{\partial \psi_j^e}{\partial y} + D_{16} \frac{\partial \psi_j^e}{\partial x} \\
M_{2j}^1 &= B_{12} \frac{\partial \psi_j^e}{\partial x} + B_{26} \frac{\partial \psi_j^e}{\partial y}, \quad M_{2j}^2 = B_{22} \frac{\partial \psi_j^e}{\partial y} + B_{26} \frac{\partial \psi_j^e}{\partial x} \\
M_{2j}^4 &= D_{12} \frac{\partial \psi_j^e}{\partial x} + D_{26} \frac{\partial \psi_j^e}{\partial y}, \quad M_{2j}^5 = D_{22} \frac{\partial \psi_j^e}{\partial y} + D_{26} \frac{\partial \psi_j^e}{\partial x} \\
M_{6j}^1 &= B_{16} \frac{\partial \psi_j^e}{\partial x} + B_{66} \frac{\partial \psi_j^e}{\partial y}, \quad M_{6j}^2 = B_{26} \frac{\partial \psi_j^e}{\partial y} + B_{66} \frac{\partial \psi_j^e}{\partial x} \\
M_{6j}^4 &= D_{16} \frac{\partial \psi_j^e}{\partial x} + D_{66} \frac{\partial \psi_j^e}{\partial y}, \quad M_{6j}^5 = D_{26} \frac{\partial \psi_j^e}{\partial y} + D_{66} \frac{\partial \psi_j^e}{\partial x} \\
N_{1j}^3 &= \left(\frac{A_{11}}{R_1} + \frac{A_{12}}{R_2} \right) \psi_j^e, \quad N_{2j}^3 = \left(\frac{A_{12}}{R_1} + \frac{A_{22}}{R_2} \right) \psi_j^e, \quad N_{6j}^3 = \left(\frac{A_{16}}{R_1} + \frac{A_{26}}{R_2} \right) \psi_j^e
\end{aligned} \tag{9.4.8a}$$

$$\begin{aligned}
Q_{1j}^1 &= -\frac{A_{55}}{R_1} \psi_j^e, \quad Q_{1j}^2 = -\frac{A_{45}}{R_2} \psi_j^e \\
Q_{1j}^3 &= A_{55} \frac{\partial \psi_j}{\partial x} + A_{45} \frac{\partial \psi_j}{\partial y}, \quad Q_{2j}^3 = A_{45} \frac{\partial \psi_j}{\partial x} + A_{44} \frac{\partial \psi_j}{\partial y} \\
Q_{1j}^4 &= A_{55} \psi_j, \quad Q_{1j}^5 = Q_{2j}^4 = A_{45} \psi_j, \quad Q_{2j}^5 = A_{44} \psi_j \\
Q_{2j}^1 &= -\frac{A_{45}}{R_1} \psi_j^e, \quad Q_{2j}^2 = -\frac{A_{44}}{R_2} \psi_j^e
\end{aligned} \tag{9.4.8b}$$

$$\begin{aligned}
F_i^1 &= \oint_{\Gamma_e} P_1 \psi_i^e \, dx dy, \quad F_i^2 = \oint_{\Gamma_e} P_2 \psi_i^e \, dx dy \\
F_i^3 &= \int_{\Omega_e} q \psi_i^e \, dx dy + \oint_{\Gamma_e} Q_n \psi_i^e \, ds \\
F_i^4 &= \oint_{\Gamma_e} T_1 \psi_i^e \, dx dy, \quad F_i^5 = \oint_{\Gamma_e} T_2 \psi_i^e \, dx dy \\
F_i^{T1} &= \oint_{\Gamma_e} \left[\frac{\partial \psi_i^e}{\partial x} N_1^T + \frac{\partial \psi_i^e}{\partial y} (N_6^T + C_0 M_6^T) \right] \, dx dy \\
F_i^{T2} &= \oint_{\Gamma_e} \left[\frac{\partial \psi_i^e}{\partial x} (N_6^T - C_0 M_6^T) + \frac{\partial \psi_i^e}{\partial y} N_2^T \right] \, dx dy \\
F_i^{T4} &= \oint_{\Gamma_e} \left(\frac{\partial \psi_i^e}{\partial x} M_1^T + \frac{\partial \psi_i^e}{\partial y} M_6^T \right) \, dx dy \\
F_i^{T5} &= \oint_{\Gamma_e} \left(\frac{\partial \psi_i^e}{\partial x} M_6^T + \frac{\partial \psi_i^e}{\partial y} M_2^T \right) \, dx dy
\end{aligned} \tag{9.4.8c}$$

where N_1^T, M_1^T , etc. are the thermal force and moment resultants.

9.4.3 Numerical Results

Here we present numerical results for a number of problems, isotropic as well as composite shells (mostly cylindrical shells). In all examples presented here we set $C_0 = 0$. The results are compared, when available, with those reported in the literature. Quadrilateral elements with selective integration rule to evaluate the stiffness coefficients (full integration for bending terms and reduced integration for bending-membrane coupling terms and transverse shear terms) are used. See Chapter 10 for a discussion of the so-called membrane locking.

Clamped cylindrical shell

Consider the deformation of a cylindrical shell with internal pressure [89]. The shell is clamped at its ends (see Figure 9.4.1). The geometric and material parameters used are

$$R_1 = 10^{30} \left(\frac{1}{R_1} \approx 0 \right), \quad R_2 = R = 20 \text{ in.}, \quad a = 20 \text{ in.}, \quad h = 1 \text{ in.} \quad (9.4.9a)$$

$$\begin{aligned} E_1 &= 7.5 \times 10^6 \text{ psi}, \quad E_2 = 2 \times 10^6 \text{ psi}, \quad G_{12} = 1.25 \times 10^6 \text{ psi} \\ G_{13} &= G_{23} = 0.625 \times 10^6 \text{ psi}, \quad \nu_{12} = 0.25 \end{aligned} \quad (9.4.9b)$$

The pressure is taken to be $p_0 = (6.41/\pi)$ ksi. The numerical results obtained using 4×4 mesh of four-node (linear) quadrilateral elements ($4 \times 4Q4$) and 2×2 mesh of nine-node (quadratic) quadrilateral elements ($2 \times 2Q9$) in an octant ($u_0 = \phi_1 = 0$ at $x_1 = 0$; $v_0 = \phi_2 = 0$ at $x_2 = 0, \pi R/2$; and $u_0 = v_0 = w_0 = \phi_1 = \phi_2 = 0$ at $x_1 = a/2$) of the shell are presented in Table 9.4.1. The reference solutions by Rao [90] and Timoshenko and Woinowsky-Krieger [91] did not account for the transverse shear strains.

Table 9.4.1: Maximum radial deflection (w_0 in.) of a clamped cylindrical shell with internal pressure.

Laminate	Present Solutions		Ref. [90]	Ref. [91]
	$4 \times 4Q4$	$2 \times 2Q9$		
0	0.3754	0.3727	0.3666	0.367
0/90	0.1870	0.1803	--	--

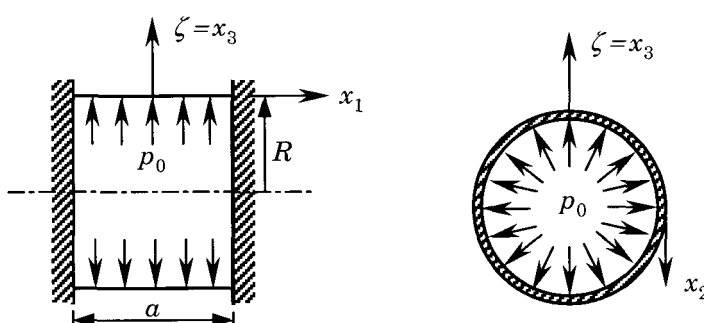


Figure 9.4.1: Clamped cylindrical shell with internal pressure.

Doubly-curved shell panel

Next, we consider a spherical shell panel ($R_1 = R_2 = R$) under central point load [89]. The shell panel is simply supported at edges (see Figure 9.4.2). The geometric and material parameters used are

$$R_1 = R_2 = R = 96 \text{ in.}, \quad a = b = 32 \text{ in.}, \quad h = 0.1 \text{ in.} \quad (9.4.10a)$$

$$E_1 = 25E_2, \quad E_2 = 10^6 \text{ psi}, \quad G_{12} = G_{13} = 0.5E_2, \quad G_{23} = 0.2E_2, \quad \nu_{12} = 0.25 \quad (9.4.10b)$$

The point load is taken to be $F_0 = 100$ lbs. The numerical results obtained using various meshes of linear and quadratic elements in a quadrant of the shell are presented in Table 9.4.2. The finite element solution converges with refinement of the mesh to the series solution of Vlasov [92], who did not consider transverse shear strains in his analysis.

Table 9.4.2: Maximum radial deflection ($-w_0 \times 10$ in.) of a simply supported spherical shell panel under central point load.

Laminate	Present Solutions					Ref. [90]	Ref. [92]
	4 × 4Q4 Uniform	2 × 2Q9 Uniform	4 × 4Q9 Uniform	4 × 4Q9 Nonuniform			
Isotropic	0.3506	0.3726	0.3904	0.3935	0.3866	0.3956	—
Orthotropic	0.9373	1.0349	—	1.2644	—	—	—
0/90	—	1.0217	—	1.2376	—	—	—
45/-45	—	0.5504	—	—	—	—	—

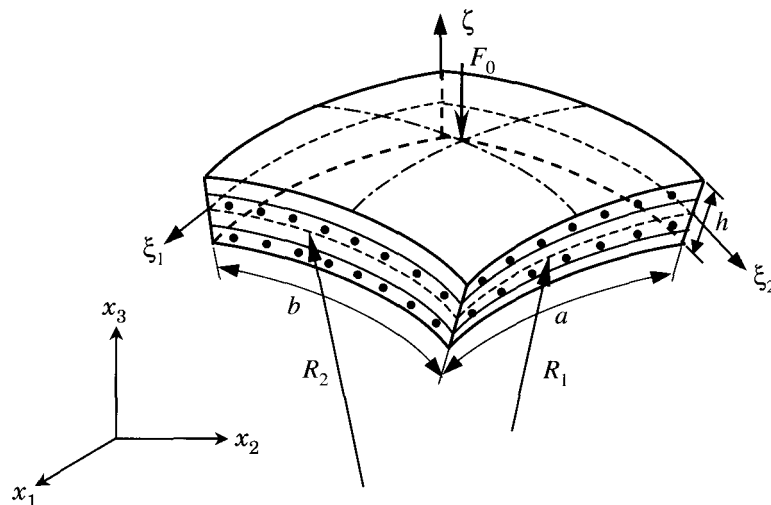


Figure 9.4.2: Simply supported spherical shell panel under central point load.

The remaining example problems of this chapter are analyzed using various p levels [see Eq. (9.4.3)–(9.4.5)]. With 5 degrees of freedom at each node, the number of degrees of freedom per element for different p values is as follows:

Element type	p level	DoF per element
Q4	1	20
Q9	2	45
Q25	4	125
Q49	6	245
Q81	8	405

The numerical integration rule (Gauss quadrature) used is $I \times J \times K$, where K denotes the number of Gauss points (i.e., $K \times K$ Gauss rule) used to evaluate the transverse shear terms (i.e., those containing A_{44} , A_{45} or A_{44}), J denotes the number of Gauss points to evaluate the bending-membrane coupling terms (which are zero for the linear analysis of plates), and I denotes the number of Gauss points used to evaluate all remaining terms in the stiffness matrix. “Full integration” means using a Gauss rule that evaluates an integral exactly. “Reduced integration” rule is one in which one point less than that in the full integration rule is used. One may use full integration for all terms, reduced integration for all terms, or selective integration where reduced integration for transverse shear and coupling terms and full integration for all other terms in the stiffness matrix. The values of I , J and K used in the present study for different p levels and integration rules are listed below.

p level	Full integration	Selective integration	Reduced integration
1	$2 \times 2 \times 2$	$2 \times 1 \times 1$	$1 \times 1 \times 1$
2	$3 \times 3 \times 3$	$3 \times 2 \times 2$	$2 \times 2 \times 2$
4	$5 \times 5 \times 5$	$5 \times 4 \times 4$	$4 \times 4 \times 4$
6	$7 \times 7 \times 7$	$7 \times 6 \times 6$	$6 \times 6 \times 6$
8	$9 \times 9 \times 9$	$9 \times 8 \times 8$	$8 \times 8 \times 8$

Clamped cylindrical shell panel

First we consider an isotropic cylindrical shell panel with the following geometric and material parameters and subjected to uniformly distributed transverse (normal to the surface) load q (see Figure 9.4.3):

$$\alpha = 0.1 \text{ rad.}, \quad R = 100 \text{ in.}, \quad a = 20 \text{ in.}, \quad h = 0.125 \text{ in.} \quad (9.4.11a)$$

$$E = 0.45 \times 10^6 \text{ psi}, \quad \nu = 0.3, \quad q = 0.04 \text{ psi} \quad (9.4.11b)$$

Two sets of uniform meshes, one with 81 nodes (405 DoF) and the other with 289 nodes (1,445 DoF), are used in a quadrant of the shell with different p levels. For example, for $p = 1$ the mesh is 8×8 Q4, for $p = 2$ the mesh is 4×4 Q9, and for $p = 8$ the mesh is 1×1 Q81 – all meshes have a total of 81 nodes. Doubling the above

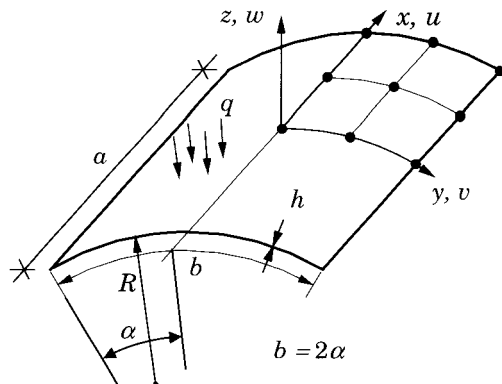


Figure 9.4.3: Clamped cylindrical shell panel under uniform transverse load.

meshes will have 289 nodes. The vertical displacement at the center of the shell obtained with various meshes and integration rules are presented in Table 9.4.3. The results obtained with selective and reduced integrations are in close agreement with those of Palazotto and Dennis [93] and Brebbia and Connor [94].

Table 9.4.3: Vertical deflection ($-w_A \times 10^2$ in.)[†] at the center of the clamped cylindrical panel under uniform transverse load.

p level	Mesh of 81 nodes			Mesh of 289 nodes		
	Full integ.	Selective integ.	Reduced integ.	Full integ.	Selective integ.	Reduced integ.
1	0.3378	1.1562	1.1577	0.7456	1.1401	1.1404
2	1.1721	1.1351	1.1352	1.1427	1.1349	1.1349
4	1.1347	1.1349	1.1349	1.1349	1.1349	1.1349
8	1.1349	1.1348	1.1348	1.1348	1.1349	1.1349

[†] Palazotto and Dennis [93] reported -1.144×10^{-2} in., while Brebbia and Connor [94] reported a value of -1.1×10^{-2} in.

Barrel vault

This is a well-known benchmark problem, known as the Scordelis–Lo roof [95]. A solution to this problem was first discussed by Cantin and Clough [96] (who used $\nu = 0.3$). The problem consists of a cylindrical roof with rigid supports at edges $x = \pm a/2$ while edges at $y = \pm b/2$ are free. The shell is assumed to deform under its own weight (i.e., q acts vertically down, not perpendicular to the surface of the shell). The geometric and material data of the problem is (see Figure 9.4.4)

$$\alpha = 40^\circ \text{ (0.698 rad.)}, \quad R = 300 \text{ in.}, \quad a = 600 \text{ in.}, \quad h = 3 \text{ in.} \quad (9.4.12)$$

$$E = 3 \times 10^6 \text{ psi}, \quad \nu = 0.0, \quad q_y = q \sin \frac{y}{R}, \quad q_z = -q \cos \frac{y}{R}, \quad q = 0.625 \text{ psi}$$

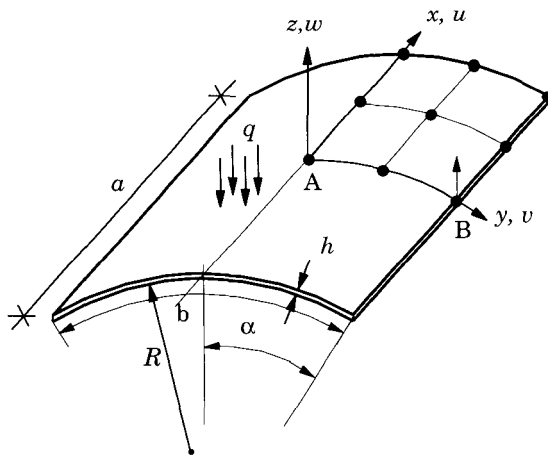


Figure 9.4.4: A cylindrical shell roof under its own weight.

The boundary conditions on the computational domain are

$$\begin{aligned} \text{At } x = 0 : \quad & u_0 = \phi_1 = 0, \quad \text{At } x = a/2 : \quad v_0 = w_0 = \phi_2 = 0 \\ \text{At } y = 0 : \quad & v_0 = \phi_2 = 0, \quad \text{At } y = b/2 : \quad \text{Free} \end{aligned} \quad (9.4.13)$$

Two sets of uniform meshes, one with 289 nodes (1,445 DoF) and the other with 1,089 nodes (5,445 DoF), are used in a quadrant of the shell with different p levels. The displacement at $y = \pm b/2$ (middle of the free edge) of the shell, obtained with various meshes and integration rules, are presented in Table 9.4.4. To avoid shear and membrane locking one must use at least a mesh of $4 \times 4Q25$ ($p = 4$). The results obtained with selective and reduced integrations are in close agreement with those reported by Simo, Fox and Rifai [97].

Table 9.4.4: Vertical deflection ($-w_B$ in.)[†] at the center of the free edge of a cylindrical roof panel under its own weight.

p level	Mesh of 289 nodes			Mesh of 1,089 nodes		
	Full integ.	Selective integ.	Reduced integ.	Full integ.	Selective integ.	Reduced integ.
1	0.9002	3.2681	3.6434	1.8387	3.5415	3.6431
2	3.6170	3.6393	3.6430	3.6367	3.6425	3.6428
4	3.6374	3.6430	3.6430	3.6399	3.6428	3.6428
8	3.6392	3.6429	3.6429	3.6419	3.6429	3.6429

[†] Simo, Fox and Rifai [97] reported $w_{\text{ref}} = -3.6288$ in. for deep shells.

Figure 9.4.5 shows the variation of the vertical deflections $w_0(0, y)$ and $u_0(300, y)$ as a function of $x_2 = y$, while Figure 9.4.6 shows the convergence of the vertical displacement w_B for $p = 1, 2, 4, 8$. Figure 9.4.5 also contains the results of Zienkiewicz [98].

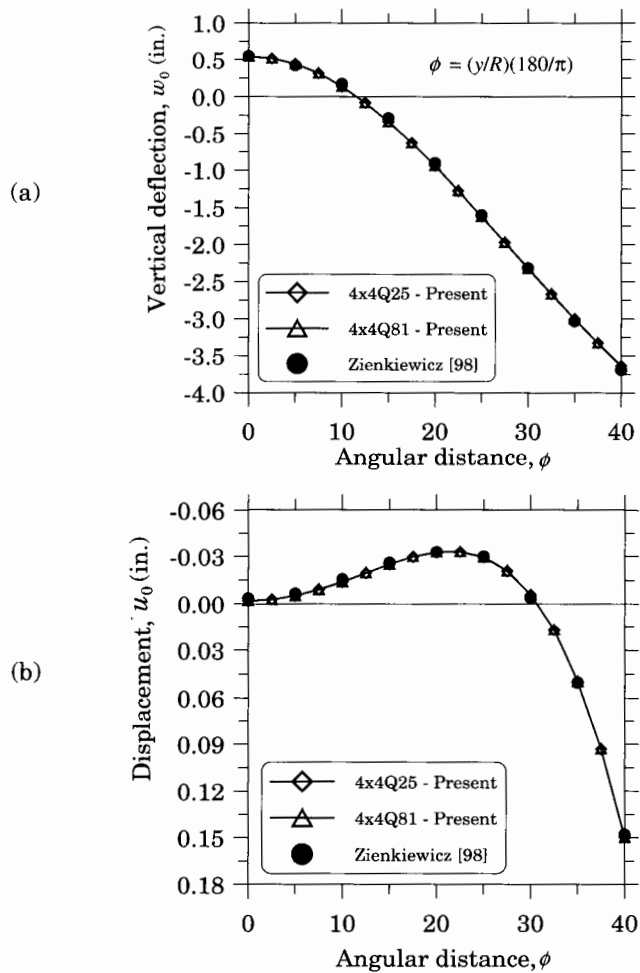


Figure 9.4.5: (a) Vertical deflection $w_0(0, y)$. (b) Displacement $u_0(300, y)$.

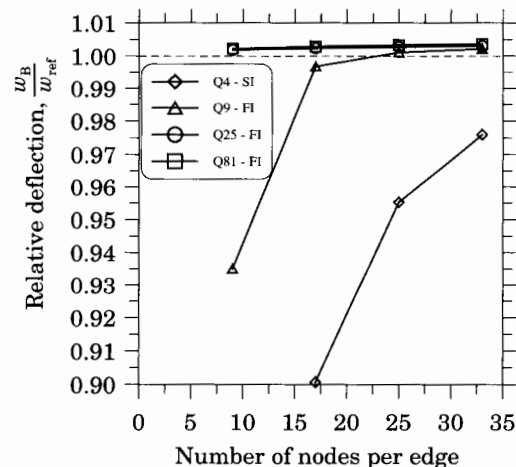


Figure 9.4.6: Convergence of the relative vertical deflection, w_B/w_{ref} .

The barrel vault problem is also analyzed when the shell is laminated of a composite material. The data of the problem is $\alpha = 40^\circ$, $R = 300$ in., $a = 600$ in. and

$$E_1 = 25E_2, \quad G_{12} = G_{13} = 0.5E_2, \quad G_{23} = 0.2E_2, \quad \nu_{12} = 0.25 \quad (9.4.14a)$$

The full panel is modeled with 4×4 Q81 mesh and boundary conditions $v_0 = w_0 = \phi_2 = 0$ at $x = \pm a/2$. In addition, u_0 is set to zero at $x = y = 0$ to eliminate the rigid body mode. The following dimensionless quantities are presented in Table 9.4.5:

$$\bar{w} = 10w_B \frac{E_1 h^3}{qR^4}, \quad \bar{\sigma}_{xx} = \sigma_{xx}(0, 0, -\frac{h}{2}) \frac{10h^2}{qR^2}, \quad \bar{\sigma}_{yy} = \sigma_{xx}(0, 0, \frac{h}{2}) \frac{10h^2}{qR^2} \quad (9.4.14b)$$

Table 9.4.5 contains the nondimensionalized deflection and normal stresses for two-layer and ten-layer antisymmetric cross-ply ($0/90/0/90/\dots$) and angle-ply ($-45/45/-45/\dots$) laminated shells for different radius-to-thickness ratio, $S = R/h$.

Table 9.4.5: Maximum transverse deflections and stresses of cross-ply and angle-ply laminated cylindrical shell roof under its own weight.

Layers	$S = R/h$	Cross-ply laminates			Angle-ply laminates		
		\bar{w}	$\bar{\sigma}_{xx}$	$\bar{\sigma}_{yy}$	\bar{w}	$\bar{\sigma}_{xx}$	$\bar{\sigma}_{yy}$
2	20	12.1529	1.0036	-9.1915	20.0913	5.6676	-1.7034
	50	5.4211	0.7577	-8.7572	7.2105	4.2838	-3.1827
	100	3.1191	-0.4476	-5.3055	4.7959	2.9433	-3.0257
10	20	8.7239	-1.6420	-5.6938	16.7332	3.7232	0.1132
	50	3.1358	0.8313	-6.6390	4.3687	3.2165	-1.6501
	100	1.8877	0.1773	-5.4245	2.4243	2.4786	-1.9317

Pinched cylinder

This is another well-known benchmark problem [99–101]. The circular cylinder with *rigid* end diaphragms is subjected to a point load at the center on opposite sides of the cylinder, as shown in Figure 9.4.7. The geometric and material data of the problem is

$$\begin{aligned} \alpha &= \frac{\pi}{2} \text{ rad.}, \quad R = 300 \text{ in.}, \quad a = 600 \text{ in.}, \quad h = 3 \text{ in.} \\ E &= 3 \times 10^6 \text{ psi}, \quad \nu_{12} = 0.3 \end{aligned} \quad (9.4.15)$$

The boundary conditions used are:

$$\begin{aligned} \text{At } x = 0 : \quad u_0 &= \phi_1 = 0, \quad \text{At } x = a/2 : \quad v_0 = w_0 = \phi_2 = 0 \\ \text{At } y = 0, b/2 : \quad v_0 &= \phi_2 = 0 \end{aligned} \quad (9.4.16)$$

Three different meshes with 81 nodes, 289 nodes and 1,089 nodes (with different p values) are used in the octant of the cylinder. Table 9.4.6 contains radial displacement at the point of load application. The solution of Flügge [99] is based on classical shell theory. It is clear that the problem requires a high p level to overcome shear and membrane locking. Figure 9.4.8 shows the convergence characteristics of the problem.

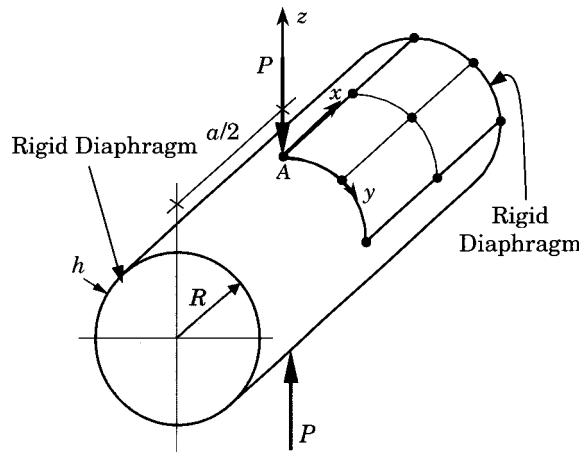


Figure 9.4.7: Geometry of the pinched circular cylinder problem.

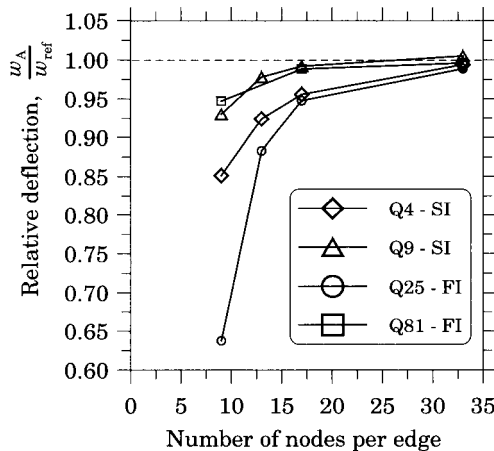


Figure 9.4.8: Convergence of the relative radial deflection, w_A/w_{ref} .

Table 9.4.6: Radial displacement ($-w_A \times 10^5$)[†] at node 1 of the pinched circular cylinder problem.

p level	Mesh of 81 nodes			Mesh of 289 nodes			Mesh of 1,089 nodes		
	Full	Selec.	Reduc.	Full	Selec.	Reduc.	Full	Selec.	Reduc.
1	0.1282	1.5784	1.8453	0.2785	1.7724	1.8600	0.6017	1.8432	1.8690
2	0.4184	1.7247	1.8451	1.2238	1.8395	1.8596	1.6844	1.8636	1.8677
4	1.1814	1.8108	1.8438	1.7574	1.8510	1.8586	1.8335	1.8648	1.8667
8	1.7562	1.8309	1.8415	1.8325	1.8548	1.8579	1.8471	1.8653	1.8661

[†] The analytical solution of Flügge [99] is -1.8248×10^{-5} in.; Cho and Roh [100] reported the value $w_{\text{ref}} = -1.8541 \times 10^{-5}$ in.

The pinched circular cylinder problem is also analyzed when the shell is laminated of a composite material. The data of the problem is $\alpha = 45^\circ$, $R = 300$ in., $a = 600$ in. and the lamina material properties used are the same as those in Eq. (9.4.14b). The following nondimensionlization is used:

$$\begin{aligned}\bar{w} &= 10w_0\left(\frac{a}{2}, \frac{b}{2}\right) \frac{E_1 h^3}{PR^2}, \quad \bar{u} = 10u_0\left(a, \frac{b}{2}\right) \frac{E_1 h^2}{PR} \\ \bar{\sigma}_{xx} &= \sigma_{xx}\left(\frac{a}{2}, \frac{b}{2}, -\frac{h}{2}\right) \frac{10h^2}{P} \quad \bar{\sigma}_{yy} = \sigma_{yy}\left(\frac{b}{2}, \frac{b}{2}, \frac{h}{2}\right) \frac{10h^2}{P}\end{aligned}\quad (9.4.17)$$

The boundary conditions used are:

$$\text{Angle-Ply : } x = 0, a : v_0 = w_0 = \phi_2 = 0; \quad y = 0, b : v_0 = \phi_2 = 0 \quad (9.4.16a)$$

$$\text{Cross-Ply : } x = 0, a : v_0 = w_0 = \phi_2 = 0; \quad y = 0, b : u_0 = \phi_2 = 0$$

$$x = \frac{a}{2}, y = \frac{b}{2} : u_0 = 0 \quad (9.4.16b)$$

Table 9.4.7 contains the nondimensionalized deflections and normal stresses for two-layer and ten-layer antisymmetric cross-ply (0/90/0/90/ \dots) and angle-ply ($-45/45/-45/\dots$) laminated shells for different radius-to-thickness ratio, $S = R/h$. The results were obtained using 4×4 Q81 mesh in half cylinder and full integration [and boundary conditions given in Eq. (9.4.16)]. If the same mesh and boundary conditions as those used for the cross-ply laminated cylinder to analyze the angle-ply laminated cylinder, we would obtain erroneous results.

Table 9.4.7: Displacements and normal stresses at point A of the laminated pinched circular cylinder problem.

Layers	$S = R/h$	Cross-Ply				Angle-Ply			
		$-\bar{w}$	$-\bar{u}$	$\bar{\sigma}_{xx}$	$-\bar{\sigma}_{yy}$	$-\bar{w}$	$-\bar{u}$	$\bar{\sigma}_{xx}$	$-\bar{\sigma}_{yy}$
2	20	6.0742	1.9536	73.364	82.045	5.2275	5.5368	35.089	42.256
	50	2.3756	1.4257	59.438	67.737	2.2283	4.8263	29.964	35.201
	100	1.2450	1.1712	44.853	55.209	1.3065	4.4498	24.650	29.386
10	20	4.2118	0.9106	53.866	64.446	3.6457	3.7541	23.301	30.027
	50	1.4527	0.7383	45.643	52.575	1.2986	3.1528	20.615	24.593
	100	0.7405	0.6721	36.927	42.616	0.7373	2.9870	17.691	20.897

Simply supported cylindrical panel

The last example of the section deals with the bending of a cross-ply laminated circular cylindrical panel of length a , angle 2α and radius R . The panel is simply supported at all its edges, and subjected to distributed transverse load q , as shown in Figure 9.4.9. The geometric and material parameters of the problem are

$$\begin{aligned}\alpha &= \pi/8 \text{ rad.}, \quad R = 1, \quad a = 4, \quad q(x, y) = q_0 \sin \frac{\pi x}{a} \sin \frac{\pi y}{b} \\ E_1 &= 25E_2, \quad G_{12} = G_{13} = 0.5E_2, \quad G_{23} = 0.2E_2, \quad \nu_{12} = 0.25\end{aligned}\quad (9.4.18a)$$

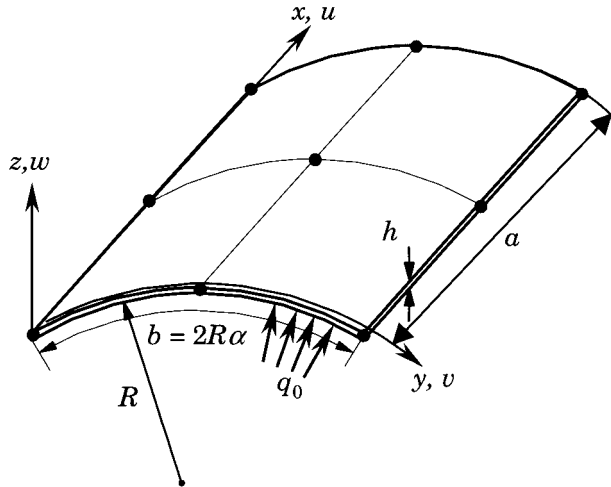


Figure 9.4.9: Geometry of the simply supported circular cylindrical panel.

The boundary conditions used for the panel are:

$$\text{At } x = 0, a : \quad v_0 = w_0 = \phi_2 = 0, \quad \text{At } y = 0, b : \quad u_0 = w_0 = \phi_1 = 0 \quad (9.4.18b)$$

A mesh of 4×4 Q25 is used in the full panel and the stiffness coefficients were evaluated using full integration. Table 9.4.8 contains the maximum displacement [$\bar{w} = w_0(a/2, b/2, 0)(10E_1/q_0S^3)$, $S = R/h$] at the center of the panel, and various stresses [$\bar{\sigma}_{\alpha\beta} = \sigma_{\alpha\beta}(10/q_0S^2)$] for different radius-to-thickness ratios. The present results are compared with the 3-D analytical solutions of Varadan and Bhaskar [102] and closed-form solution developed by Cheng, et al. [103] using the third-order shell theory (see Chapter 11) for (90/0/90) and (0/90) laminates. They are in good agreement with each other.

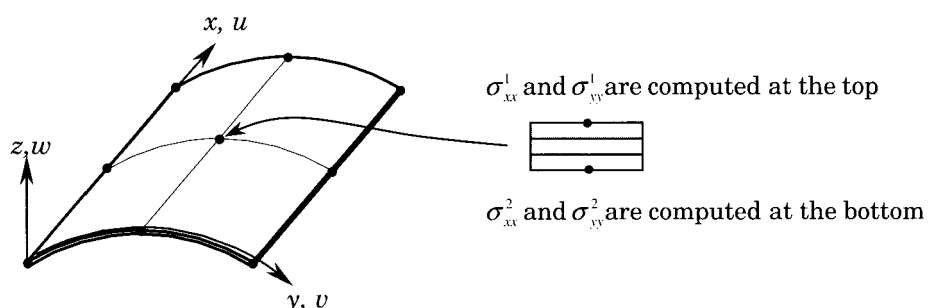
9.5 Summary

In this chapter, linear finite element models of the classical and first-order shear deformation plate theories and the Sanders shell theory for doubly-curved shells are developed. The finite element models developed herein are general in that they can be used for any lamination scheme, geometry, and boundary conditions. Numerical examples of bending, buckling, natural vibration, and transient response of rectangular plates and bending of doubly-curved (mostly cylindrical) shells are presented in tabular and graphical forms. The Sanders shell theory accounts for transverse shear strains in much the same way as the first-order shear deformation plate theory. For additional details, the reader may consult the references listed at the end of the chapter.

Table 9.4.8: Displacements and stresses in simply supported, cross-ply laminated circular cylindrical panel under sinusoidally distributed load.

Variable [†]	$S = R/h$	(90/0/90)			(0/90)		
		Ref. [102]	Ref. [103]	Present	Ref. [102]	Ref. [103]	Present
\bar{w}	50	0.5495	0.5486	0.5458	2.2420	2.2372	2.2586
	100	0.4715	0.4711	0.4718	1.3670	1.3666	1.3720
	500	0.1027	0.1027	0.1028	0.1005	0.1005	0.1006
$\bar{\sigma}_{xx}^1$	50	0.0712	0.0710	0.0711	0.2189	0.2187	0.2211
	100	0.0838	0.0837	0.0841	0.1871	0.1871	0.1882
	500	0.0559	0.0559	0.0560	0.0449	0.0449	0.0451
$\bar{\sigma}_{xx}^2$	50	-0.0225	-0.0217	-0.0214	1.6100	1.6051	1.6169
	100	0.0018	0.0020	0.0021	2.3000	2.2979	2.3036
	500	0.0379	0.0379	0.0380	0.9436	0.9436	0.9438
$\bar{\sigma}_{yy}^1$	50	3.9300	3.9265	3.9489	8.9370	8.9543	9.0939
	100	3.5070	3.5048	3.5338	5.5600	5.5643	5.6366
	500	0.7895	0.7897	0.8048	0.4345	0.4346	0.4489
$\bar{\sigma}_{yy}^2$	50	-3.9870	-3.9870	-3.9555	-0.9670	-0.9615	-0.9601
	100	-3.5070	-3.5063	-3.4972	-0.5759	-0.5750	-0.5740
	500	-0.7542	-0.7545	-0.7492	-0.0339	-0.0339	-0.0342
$\bar{\sigma}_{xy}^1$	50	0.0118	0.0123	0.0114	0.0784	0.0784	0.0767
	100	0.0478	0.0480	0.0474	0.1819	0.1819	0.1813
	500	0.0766	0.0766	0.0765	0.0925	0.0925	0.0924
$\bar{\sigma}_{xy}^2$	50	0.0760	0.0764	0.0765	0.3449	0.3444	0.3501
	100	0.1038	0.1039	0.1045	0.3452	0.3414	0.3480
	500	0.0889	0.0889	0.0890	0.1045	0.1045	0.1047

† $\bar{w}(a/2, b/2)$; $\bar{\sigma}_{xx}^1 = \bar{\sigma}_{xx}(a/2, b/2, h/2)$; $\bar{\sigma}_{xx}^2 = \bar{\sigma}_{xx}(a/2, b/2, -h/2)$; $\bar{\sigma}_{yy}^1 = \bar{\sigma}_{yy}(a/2, b/2, h/2)$; $\bar{\sigma}_{yy}^2 = \bar{\sigma}_{yy}(a/2, b/2, -h/2)$; $\bar{\sigma}_{xy}^1 = \bar{\sigma}_{xy}(0, 0, h/2)$; and $\bar{\sigma}_{xy}^2 = \bar{\sigma}_{xy}(0, 0, -h/2)$



Problems

- 9.1** The equation of motion governing the bending of *symmetrically laminated beams* according to the classical laminate theory is given by (see Chapter 4)

$$\frac{\partial^2}{\partial x^2} \left(E_{xx}^b I_{yy} \frac{\partial^2 w_0}{\partial x^2} \right) - b \hat{N}_{xx} \frac{\partial^2 w_0}{\partial x^2} - \hat{q} + \hat{I}_0 \frac{\partial^2 w_0}{\partial t^2} - \hat{I}_2 \frac{\partial^4 w_0}{\partial x^2 \partial t^2} = 0 \quad (1)$$

where \hat{N}_{xx} is the axial load and

$$\hat{q} = bq, \quad \hat{I}_0 = bI_0, \quad \hat{I}_2 = bI_2 \quad (2)$$

and b is the width of the beam, $q(x, t)$ is the distributed transverse load, and I_0 and I_2 are mass inertias

$$I_0 = \int_{-\frac{h}{2}}^{\frac{h}{2}} \rho \, dz, \quad I_2 = \int_{-\frac{h}{2}}^{\frac{h}{2}} \rho z^2 \, dz \quad (3)$$

Develop the weak form and finite element model of Eq. (1).

- 9.2** (a) Derive finite element interpolation functions using w_0 , $\theta = -dw_0/dx$, and d^2w_0/dx^2 as the nodal variables of an element with two (end) nodes, with a total of six degrees of freedom per element. Note that you must select a complete polynomial containing six parameters

$$w_0(x) = c_1 + c_2x + c_3x^2 + c_4x^3 + c_5x^4 + c_6x^5$$

and derive the Hermite interpolation functions.

- (b) Use the finite element approximation to compute the stiffness matrix $[K^e]$ derived in Problem 9.1.

- 9.3** Derive finite element Hermite interpolation functions using w_0 and $\theta = -dw_0/dx$ as the nodal variables of an element with three nodes (two end nodes and the middle node), with a total of six degrees of freedom per element. As in Problem 9.2, you must select a complete polynomial containing six parameters and derive the Hermite interpolation functions.

- 9.4** The equations of motion governing symmetrically laminated beams according to the first-order shear deformation (i.e., the Timoshenko) beam theory are

$$KG_{xz}^b bh \left(\frac{\partial^2 w_0}{\partial x^2} + \frac{\partial \phi_x}{\partial x} \right) + b \hat{N}_{xz} \frac{\partial^2 w_0}{\partial x^2} + \hat{q} = \hat{I}_0 \frac{\partial^2 w_0}{\partial t^2} \quad (1)$$

$$E_{xx}^b I_{yy} \frac{\partial^2 \phi_x}{\partial x^2} - KG_{xz}^b bh \left(\frac{\partial w_0}{\partial x} + \phi_x \right) = \hat{I}_2 \frac{\partial^2 \phi_x}{\partial t^2} \quad (2)$$

where

$$\hat{q} = bq, \quad \hat{I}_0 = bI_0, \quad \hat{I}_2 = bI_2 \quad (3)$$

Construct weak forms of Eqs. (1) and (2) over the typical finite element, assume interpolation of the primary variables, and develop the finite element model.

- 9.5** Consider the following set of equations governing the classical plate theory:

$$q = - \left(\frac{\partial^2 M_{xx}}{\partial x^2} + 2 \frac{\partial^2 M_{xy}}{\partial x \partial y} + \frac{\partial^2 M_{yy}}{\partial y^2} \right) \quad (1)$$

$$M_{xx} = - \left(D_{11} \frac{\partial^2 w_0}{\partial x^2} + D_{12} \frac{\partial^2 w_0}{\partial y^2} \right) \quad (2)$$

$$M_{yy} = - \left(D_{12} \frac{\partial^2 w_0}{\partial x^2} + D_{22} \frac{\partial^2 w_0}{\partial y^2} \right) \quad (3)$$

$$M_{xy} = -2D_{66} \frac{\partial^2 w_0}{\partial x \partial y} \quad (4)$$

where D_{ij} are the bending stiffnesses of a specially orthotropic plate (see Chapter 5)

$$D_{ij} = Q_{ij} \frac{h^3}{12}, \quad (i = 1, 2, 6) \quad (5)$$

Rewrite Eqs. (1)–(4) in an alternative form (curvatures in terms of the moments) such that $(w_0, M_{xx}, M_{xy}, M_{yy})$ are the independent variables, develop the weak form of the equations and develop a mixed finite element model of the equations.

- 9.6** A simplified mixed model can be derived by eliminating the twisting moment M_{xy} from equations (1)–(4) of Problem 9.5. We can write the resulting equations as

$$q = - \left(\frac{\partial^2 M_{xx}}{\partial x^2} - 4D_{66} \frac{\partial^4 w_0}{\partial x^2 \partial y^2} + \frac{\partial^2 M_{yy}}{\partial y^2} \right) \quad (1)$$

$$\frac{\partial^2 w_0}{\partial x^2} = - (\bar{D}_{22} M_{xx} + \bar{D}_{12} M_{yy}) \quad (2)$$

$$\frac{\partial^2 w_0}{\partial y^2} = - (\bar{D}_{12} M_{xx} + \bar{D}_{11} M_{yy}) \quad (3)$$

where h denotes the plate thickness and

$$\bar{D}_{ij} = \frac{D_{ij}}{D_0}, \quad D_0 = D_{11}D_{22} - D_{12}^2 \quad (4)$$

Develop the weak forms of the equations and associated finite element model.

References for Additional Reading

1. Reddy, J. N., *An Introduction to the Finite Element Method*, Second Edition, McGraw-Hill, New York (1993).
2. Reddy, J. N., *Energy Principles and Variational Methods in Applied Mechanics*, Second Edition, John Wiley, New York (2002).
3. Burnett, D. S., *Finite Element Analysis*, Addison-Wesley, Reading, MA (1987).
4. Zienkiewicz, O. C. and Taylor, R. L., *The Finite Element Method, Vol. 1: Linear Problems*, McGraw-Hill, New York (1989).
5. Hughes, T. J. R., *The Finite Element Method, Linear Static and Dynamic Finite Element Analysis*, Prentice-Hall, Englewood Cliffs, NJ (1987).
6. Hrabok, M. M. and Hrudey, T. M., "A Review and Catalog of Plate Bending Finite Elements," *Computers and Structures* **19**(3), 479–495 (1984).
7. Bazeley, G. P., Cheung, Y. K., Irons, B. M., and Zienkiewicz, O. C., "Triangular Elements in Plate Bending – Conforming and Non-Conforming Solutions," *Proceedings of the Conference on Matrix Methods in Structural Mechanics*, AFFDL-TR-66-80, Air Force Institute of Technology, Wright-Patterson Air Force Base, Ohio, 547–576 (1965).
8. Fraeijis de Veubeke, B., "A Conforming Finite Element for Plate Bending," *International Journal of Solids and Structures*, **4**(1), 95–108 (1968).
9. Argyris, J. H., Fried, I., and Scharpf, D. W., "The TUBA Family of Plate Bending Elements for the Matrix Displacement Method," *Journal of the Royal Aeronautical Society*, **72**, 701–709 (1969).
10. Bell, K., "A Refined Triangular Plate Bending Finite Element," *International Journal for Numerical Methods in Engineering*, **1**, 101–122 (1969).
11. Irons, B. M., "A Conforming Quartic Triangular Element for Plate Bending," *International Journal for Numerical Methods in Engineering*, **1**, 29–45 (1969).

12. Stricklin, J. A., Haisler, W., Tisdale, P., and Gunderson, R., "A Rapidly Converging Triangular Plate Element," *AIAA Journal*, **7**(1), 180–181 (1969).
13. Batoz, J. L., Bathe, K. J., and Ho, L. W., "A Study of Three-Node Triangular Plate Bending Elements," *International Journal for Numerical Methods in Engineering*, **15**(12), 1771–1812 (1980).
14. Batoz, J. L., "An Explicit Formulation for an Efficient Triangular Plate Bending Element," *International Journal for Numerical Methods in Engineering*, **18**(7), 1077–1089 (1985).
15. Batoz, J. L. and Tahar, M. B., "Evaluation of a New Quadrilateral Thin Plate Bending Element," *International Journal for Numerical Methods in Engineering*, **18**, 1655–1677 (1982).
16. Jeyachandrabose, C. and Kirkhope, J., "An Alternative Formulation for DKT Plate Bending Element," *International Journal for Numerical Methods in Engineering*, **21**(7), 1289–1293 (1985).
17. Hellan, K., "Analysis of Plates in Flexure by a Simplified Finite Element Method," *Acta Polytechnica Scandinavica*, Civil Engineering Series 46, Trondheim (1967).
18. Melosh, R. J., "Basis of Derivation of Matrices for the Direct Stiffness Method," *AIAA Journal*, **1**, 1631–1637 (1963).
19. Zienkiewicz, O. C. and Cheung, Y. K., "The Finite Element Method for Analysis of Elastic Isotropic and Orthotropic Slabs," *Proceeding of the Institute of Civil Engineers*, London, UK, **28**, 471–488 (1964).
20. Bogner, F. K., Fox, R. L., and Schmidt, Jr. L. A., "The Generation of Inter-Element-Compatible Stiffness and Mass Matrices by the Use of Interpolation Formulas," *Proceedings of the Conference on Matrix Methods in Structural Mechanics*, AFFDL-TR-66-80, Air Force Institute of Technology, Wright-Patterson Air Force Base, Ohio, 397–443 (1965).
21. Anderson, R. G., Irons, B. M., and Zienkiewicz, O. C., "Vibration and Stability of Plates Using Finite Elements," *International Journal of Solids and Structures*, **4**(10), 1031–1055 (1968).
22. Clough, R. W., and Tocher, J. L., "Finite Element Stiffness Matrices for Analysis of Plate Bending," *Proceedings of the Conference on Matrix Methods in Structural Mechanics*, AFFDL-TR-66-80, Air Force Institute of Technology, Wright-Patterson Air Force Base, Ohio, 515–545 (1965).
23. Clough, R. W. and Felippa, C. A., "A Refined Quadrilateral Element for Analysis of Plate Bending," *Proceedings of the Second Conference on Matrix Methods in Structural Mechanics*, AFFDL-TR-66-80, Air Force Institute of Technology, Wright-Patterson Air Force Base, Ohio, 399–440 (1968).
24. Ahmad, S., Irons, B. M., and Zienkiewicz, O. C., "Analysis of Thick and Thin Shell Structures by Curved Finite Elements," *International Journal for Numerical Methods in Engineering*, **13**(4), 575–586 (1971).
25. Morley, L. S. D., "A Triangular Equilibrium Element with Linearly Varying Bending Moments for Plate Bending Problems," Technical Note, *Journal of the Aeronautical Society*, **71** (1967).
26. Morley, L. S. D., "The Triangular Equilibrium Element in the Solution of Plate Bending Problems," *Journal of the Aeronautical Society*, **72** (1968).
27. Morley, L. S. D., "The Constant-Moment Plate Bending Element," *Journal of Strain Analysis*, **6**(1), 20–24 (1971).
28. Newmark, N. M., "A Method for Computation of Structural Dynamics," *Journal of Engineering Mechanics*, **85**, 67–94 (1959).
29. Carnahan, B., Luther, L. A., and Wilkes, J. O., *Applied Numerical Methods*, John Wiley & Sons, New York, 1969.
30. Barlow, J., "Optimal Stress Location in Finite Element Models," *International Journal for Numerical Methods in Engineering*, **10**, 243–251 (1976).

31. Barlow, J., "More on Optimal Stress Points — Reduced Integration Element Distortions and Error Estimation," *International Journal for Numerical Methods in Engineering*, **28**, 1486–1504 (1989).
32. Reddy, J. N., "Simple Finite Elements with Relaxed Continuity for Non-Linear Analysis of Plates," *Proceedings of the Third International Conference in Australia on Finite Element Methods*, University of New South Wales, Sydney (1979).
33. Reddy, J. N., "A Penalty Plate-Bending Element for the Analysis of Laminated Anisotropic Composite Plates," *International Journal for Numerical Methods in Engineering*, **15**(8), 1187–1206 (1980).
34. Averill, R. C. and Reddy, J. N., "Behavior of Plate Elements Based on the First-Order Shear Deformation Theory," *Engineering Computations*, **7**, 57–74 (1990).
35. Reddy, J. N. and Averill, R. C., "Advances in the Modeling of Laminated Plates," *Computing Systems in Engineering*, **2**(5/6), 541–555 (1991).
36. Belytschko, T. and Tsay, C. S., "A Stabilization Procedure for the Quadrilateral Plate Bending Element with One-point Quadrature," *International Journal for Numerical Methods in Engineering*, **19** 405–420 (1983).
37. Park, K. C. and Flagg, D. L., "A Symbolic Fourier Synthesis of a One-point Integrated Quadrilateral Plate Element," *Computer Methods in Applied Mechanics and Engineering*, **48**(2), 203–236 (1985).
38. Belytschko, T., Ong, J. S.-J., and Liu, W. K., "A Consistent Control of Spurious Singular Modes in the 9-node Lagrange Element for the Laplace and Mindlin Plate Equation," *Computer Methods in Applied Mechanics and Engineering*, **44**, 269–295 (1984).
39. Crisfield, M. A., "A Quadratic Mindlin Element Using Shear Constraints," *Computers and Structures*, **18**, 833–852 (1984).
40. Huang, H. C. and Hinton, E., "A Nine-Node Lagrangian Plate Element with Enhanced Shear Interpolation," *Engineering Computations*, **1**, 369–379 (1984).
41. Tessler, A. and Dong, S. B., "On a Hierarchy of Conforming Timoshenko Beam Elements," *Computers and Structures* **14**, 335–344 (1981).
42. Zienkiewicz, O. C., Too, J. J. M., and Taylor, R. L., "Reduced Integration Technique in General Analysis of Plates and Shells," *International Journal for Numerical Methods in Engineering*, **3**, 275–290 (1971).
43. Hughes, T. J. R. and Cohen, M., "The 'Heterosis' Finite Element for Plate Bending," *Computers and Structures*, **9**(5), 445–450 (1978).
44. Hinton, E. and Huang, H. C., "A Family of Quadrilateral Mindlin Plate Elements with Substitute Shear Strain Fields," *Computers and Structures* **23**(3), 409–431 (1986).
45. Hughes, T. J. R., Taylor, R. L., and Kanoknukulchai, W., "A Simple and Efficient Element for Plate Bending," *International Journal for Numerical Methods in Engineering*, **11**(10), 1529–1543 (1977).
46. Pugh, E. D. L., Hinton, E., and Zienkiewicz, O. C., "A Study of Quadrilateral Plate Bending Elements with 'Reduced' Integration," *International Journal for Numerical Methods in Engineering*, **12**(7), 1059–1079 (1978).
47. Malkus, D. S. and Hughes, T. J. R., "Mixed Finite Element Methods—Reduced and Selective Integration Techniques: A Unification of Concepts," *Computer Methods in Applied Mechanics and Engineering*, **15**(1), 63–81 (1978).
48. Hughes, T. J. R., Cohen, M., and Haroun, M., "Reduced and Selective Integration Techniques in the Finite Element Analysis of Plates," *Nuclear Engineering and Design*, **46**, 203–222 (1981).
49. Belytschko, T., Tsay, C. S., and Liu, W. K., "Stabilization Matrix for the Bilinear Mindlin Plate Element," *Computer Methods in Applied Mechanics and Engineering*, **29**, 313–327 (1981).

50. Hughes, T. J. R. and Tezduyar, T. E., "Finite Elements Based Upon Mindlin Plate Theory with Particular Reference to the Four-Node Bilinear Isoparametric Element," *Journal of Applied Mechanics*, **48**(3), 587–596 (1981).
51. Spilker, R. L. and Munir, N. I., "The Hybrid-Stress Model for Thin Plates," *International Journal for Numerical Methods in Engineering*, **15**(8), 1239–1260 (1980).
52. Spilker, R. L. and Munir, N. I., "A Serendipity Cubic-Displacement Hybrid-Stress Element for Thin and Moderately Thick Plates," *International Journal for Numerical Methods in Engineering*, **15**(8), 1261–1278 (1980).
53. Spilker, R. L. and Munir, N. I., "A Hybrid-Stress Quadratic Serendipity Displacement Mindlin Plate Bending Element," *Computers and Structures*, **12**, 11–21 (1980).
54. Crisfield, M. A., "A Four-Noded Plate Bending Element Using Shear Constraints; A Modified Version of Lyons' Element," *Computer Methods in Applied Mechanics and Engineering*, **38**, 93–120 (1983).
55. Tessler, A. and Hughes, T. J. R., "An Improved Treatment of Transverse Shear in the Mindlin-Type Four-Node Quadrilateral Element," *Computer Methods in Applied Mechanics and Engineering*, **39**, 311–335 (1983).
56. Tessler, A. and Hughes, T. J. R., "Three-Node Mindlin Plate Element with Improved Transverse Shear," *Computer Methods in Applied Mechanics and Engineering*, **50**, 71–101 (1985).
57. Bathe, K. J. and Dvorkin, E. N., "A Four-Node Plate Bending Element Based on Mindlin/Reissner Plate Theory and Mixed Interpolation," *International Journal for Numerical Methods in Engineering*, **21**, 367–383 (1985).
58. Reddy, J. N. and Chao, W. C., "A Comparison of Closed-Form and Finite Element Solutions of Thick Laminated Anisotropic Rectangular Plates," *Nuclear Engineering and Design*, **64**, 153–167 (1981).
59. Pagano, N. J., "Exact Solutions for Composite Laminates in Cylindrical Bending," *Journal of Composite Materials*, **3**, 398–411 (1967).
60. Pagano, N. J., "Exact Solutions for Rectangular Bidirectional Composites and Sandwich Plates," *Journal of Composite Materials*, **4**, 20–34 (1970).
61. Reddy, J. N. and Hsu, Y. S., "Effects of Shear Deformation and Anisotropy on the Thermal Bending of Layered Composite Plates," *Journal of Thermal Stresses*, **3**, 475–493 (1980).
62. Khdeir, A. A. and Reddy, J. N., "Thermal Stresses and Deflections of Cross-Ply Laminated Plates Using Refined Plate Theories," *Journal of Thermal Stresses*, **14**(4), 419–438 (1991).
63. Reddy, J. N. and Khdeir, A. A., "Buckling and Vibration of Laminated Composite Plates Using Various Plate Theories," *AIAA Journal*, **27** (12), 1808–1817 (1989).
64. Nosier, A. and Reddy, J. N., "On Vibration and Buckling of Symmetric Laminated Plates According to Shear Deformation Theories," *Acta Mechanica*, **94** (3–4), 123–170 (1992).
65. Khdeir, A. A., Librescu, L., and Reddy, J. N., "Analytical Solution of a Refined Shear Deformation Theory for Rectangular Composite Plates," *International Journal of Solids and Structures*, **23**(10), 1447–1463 (1987).
66. Khdeir, A. A. and Reddy, J. N., "Dynamic Response of Antisymmetric Angle-Ply Laminated Plates Subjected to Arbitrary Loading," *Journal of Sound and Vibration*, **126**(3), 437–445 (1988).
67. Khdeir, A. A. and Librescu, L., "Analysis of Symmetric Cross-Ply Laminated Elastic Plates Using a Higher-Order Theory: Part I—Stress and Displacement," *Composite Structures*, **9**, 189–213 (1988).
68. Khdeir, A. A. and Librescu, L., "Analysis of Symmetric Cross-Ply Laminated Elastic Plates Using a Higher-Order Theory: Part II—Buckling and Free Vibration," *Composite Structures*, **9**, 259–277 (1988).

69. Khdeir, A. A., "Free Vibration and Buckling of Symmetric Cross-Ply Laminated Plates by an Exact Method," *Journal of Sound and Vibration*, **126**(3), 447–461 (1988).
70. Khdeir, A. A., "Free Vibration of Antisymmetric Angle-Ply Laminated Plates Including Various Boundary Conditions," *Journal of Sound and Vibration*, **122**(2), 377–388 (1988).
71. Khdeir, A. A., "Free Vibration and Buckling of Unsymmetric Cross-Ply Laminated Plates Using a Refined Theory," *Journal of Sound and Vibration*, **128**(3), 377–395 (1989).
72. Khdeir, A. A. and Reddy, J. N., "Exact Solutions for the Transient Response of Symmetric Cross-Ply Laminates Using a Higher-Order Plate Theory," *Composite Science and Technology*, **34**, 205–224 (1989).
73. Khdeir, A. A., "An Exact Approach to the Elastic State of Stress of Shear Deformable Antisymmetric Angle-Ply Laminated Plates," *Composite Structures*, **11**, 245–258 (1989).
74. Khdeir, A. A., "Comparison Between Shear Deformable and Kirchhoff Theories for Bending, Buckling and Vibration of Antisymmetric Angle-Ply Laminated Plates," *Composite Structures*, **13**, 159–172 (1989).
75. Khdeir, A. A., "Stability of Antisymmetric Angle-Ply Laminated Plates," *ASCE Journal of Engineering Mechanics*, **115**, 952–962 (1989).
76. Khdeir, A. A. and Reddy, J. N., "Analytical Solutions of Refined Plate Theories of Cross-Ply Composite Laminates," *Journal of Pressure Vessel Technology*, **113**(4), 570–578 (1991).
77. Reddy, J. N., "Free Vibration of Antisymmetric, Angle-Ply Laminated Plates Including Transverse Shear Deformation by the Finite Element Method," *Journal of Sound and Vibration*, **66**(4), 565–576 (1979).
78. Reddy, J. N., "On the Solutions to Forced Motions of Rectangular Composite Plates," *Journal of Applied Mechanics*, **49**, 403–408 (1982).
79. Reddy, J. N., "Dynamic (Transient) Analysis of Layered Anisotropic Composite-Material Plates," *International Journal for Numerical Methods in Engineering*, **19**, 237–255 (1983).
80. Reddy, J. N., "Geometrically Nonlinear Transient Analysis of Laminated Composite Plates," *AIAA Journal*, **21**(4), 621–629 (1983).
81. Maugin, G. A., *Continuum Mechanics of Electromagnetic Solids*, North-Holland, Amsterdam, The Netherlands (1988).
82. Uchino, K., "Electrostrictive Actuators: Materials and Applications," *Ceramic Bulletin*, **65**, 647–652 (1986).
83. Goodfriend, M. J. and Shoop, K. M., "Adaptive Characteristics of the Magnetostrictive Alloy, Terfenol-D, for Active Vibration Control," *Journal of Intelligent Material Systems and Structures*, **3**, 245–254 (1992).
84. Benjeddou, A., "Advances in Piezoelectric Finite Element Modeling of Adaptive Structural Elements: A Survey," *Computers & Structures*, **76**, 347–363 (2000).
85. Lam, K. Y., Peng, X. Q., Liu, G. R., and Reddy, J. N., "A Finite-Element Model for Piezoelectric Composite Laminates," *Smart Materials and Structures*, **6**(5), 583–591 (1997).
86. Reddy, J. N., "On Laminated Composite Plates with Integrated Sensors and Actuators," *Engineering Structures*, **21**, 568–593 (1999).
87. Pradhan, S. C., Ng, T. Y., Lam, K. Y., and Reddy, J. N., "Control of Laminated Composite Plates Using Magnetostrictive Layers," *Smart Materials and Structures*, **10**, 1–11 (2001).
88. Reddy, J. N. and Cheng, Z.-Q., "Deformations of Piezothermoelastic Laminates with Internal Electrodes," *ZAMM*, **81**(5), 347–359 (2001).
89. Reddy, J. N., *Energy and Variational Methods in Applied Mechanics*, John Wiley & Sons, New York (1984).
90. Rao, K. P., "A Rectangular Laminated Anisotropic Shallow Thin Shell Finite Element," *Computer Methods in Applied Mechanics and Engineering*, **15**, 13–33 (1978).

91. Timoshenko, S. and Woinowsky-Krieger, S., *Theory of Plates and Shells*, McGraw-Hill, New York (1959).
92. Vlasov, V. Z., *General Theory of Shells and Its Applications in Engineering*, (Translation of *Obshchaya teoriya obolochek i yeye prilozheniya v tekhnike*), NASA TT F-99, National Aeronautics and Space Administration, Washington, D.C. (1964).
93. Palazotto, A. N. and Dennis, S. T., *Nonlinear Analysis of Shell Structures*, AIAA Education Series, Washington, D.C. (1992).
94. Brebbia, C. and Connor, J., "Geometrically Nonlinear Finite Element Analysis," *Journal of Engineering Mechanics*, 463-483 (1969).
95. Scordelis, A. C. and Lo, K. S., "Computer Analysis of Cylindrical Shells," *Journal of American Concrete Institute*, 538-560 (1964).
96. Cantin, G. and Clough, R. W., "A Curved Cylindrical Shell Finite Element," *AIAA Journal*, 6, 1057 (1968).
97. Simo, J. C., Fox, D. D., and Rifai, M. S., "On a Stress Resultant Geometrically Exact Shell Model. Part II: The Linear Theory," *Computer Methods in Applied Mechanics and Engineering* 73, 53-92 (1989).
98. Zienkiewicz, O. C., *The Finite Element Method*, McGraw-Hill, New York (1977).
99. Flügge, W., *Stresses in Shells*, Second Edition, Springer-Verlag, Berlin, Germany (1973).
100. Cho, M. and Roh, H. Y., "Development of Geometrically Exact New Elements Based on General Curvilinear Coordinates," *International Journal for Numerical Methods in Engineering*, 56, 81-115 (2003).
101. Kreja, I., Schmidt, R., and Reddy, J. N., "Finite Elements Based on a First-order Shear Deformation Moderate Rotation Theory with Applications to the Analysis of Composite Structures," *International Journal of Non-Linear Mechanics*, 32(6), 1123-1142 (1997).
102. Varadan, T. K. and Bhaskar, K., "Bending of Laminated Orthotropic Cylindrical Shells - An Elasticity Approach," *Composite Structures*, 17, 141-156 (1991).
103. Cheng, Z. Q., He, L. H., and Kitipornchai, S., "Influence of Imperfect Interfaces on Bending and Vibration of Laminated Composite Shells," *International Journal of Solids and Structures*, 37, 2127-2150 (2000).

10

Nonlinear Analysis of Composite Plates and Shells

10.1 Introduction

The nonlinear partial differential equations governing composite laminates of arbitrary geometries and boundary conditions cannot be solved exactly. Approximate analytical solutions to the large-deflection theory (in von Kármán's sense) of laminated composite plates were obtained by many (see, for example, [1–12]). In most of these studies the effects of shear deformation and rotary inertia were neglected, and only rectangular or cylindrical geometries were considered. The latter restriction is a direct result of the methods of analysis used; i.e., Ritz method, Galerkin method, perturbation method, and the double series method cannot be applied to plates of complicated geometries. For example, the classical variational methods (e.g., the Ritz and Galerkin methods) are limited to simple geometries because of the difficulty in constructing the approximation functions for complicated geometries. The use of numerical methods facilitates the solution of such problems. Among the numerical methods available for the solution of nonlinear differential equations defined over arbitrary domains, the finite element method is the most practical and robust computational technique.

Historically, two distinct approaches have been followed in developing nonlinear finite element models of laminated structures. The first approach is based on a laminate theory, in which the 3-D elasticity equations are reduced to 2-D equations through certain kinematic assumptions and homogenization through the thickness, as described in Chapter 3. In the nonlinear formulation based on small strains and moderate rotations, the geometry of the structure is assumed to remain unchanged during the loading, and the geometric nonlinearity in the form of the von Kármán strains is included. We shall term the elements based on such assumptions the *laminated elements* (see [13–20]).

The second approach is based on the 3-D continuum formulation, where any kinematic assumptions are directly introduced through the spatial finite element approximations. Full nonlinear strains or only the von Kármán nonlinear strains are included as desired, and the equations are derived in an incremental form directly. The formulation accounts for geometric changes that occurred during the previous increment of loading. Thus, the geometry is updated between load increments. Finite elements based on this formulation are called *continuum elements* (see [21,23,26–32]).

There are two incremental continuum formulations that are used to determine the deformation and stress states in continuum problems (see Bathe, et al. [26] and Reddy [32]): (1) the *total Lagrangian formulation* and (2) the *updated Lagrangian formulation*. In these formulations, the configuration (i.e., geometry) of the structure for the current load increment is determined from a previously known configuration. In the total Lagrangian formulation, all of the quantities are referred to a fixed, often the undeformed, configuration, and changes in the displacement and stress fields are determined with respect to the reference configuration. The strain and stress measures used in this approach are the Green–Lagrange strain tensor and 2nd Piola–Kirchhoff stress tensor. In the updated Lagrangian formulation, the geometry of the structure from the previous increment is updated using the deformation computed in the current increment, and the updated configuration is used as the reference configuration for the next increment. A direct consequence of this is that differentiations and integrations are performed with respect to this reference configuration. The stress and strain measures used in this approach are the Cauchy stresses and the infinitesimal (Almansi) strains.

The major objective of this chapter is to study the geometrically nonlinear behavior of laminated plates and shells. Towards this objective we develop the displacement finite element models of the classical laminated plate theory (CLPT) and the first-order shear deformation plate theory (FSDT) when the von Kármán nonlinear strains are accounted for, i.e., develop nonlinear laminated plate elements. Alternative finite element models to the displacement model, i.e., mixed and hybrid finite element models, can be found in [33–42]. Then a formulation of the continuum shell element is presented. For additional discussion of the continuum finite elements, one may consult [21,23,26–32]. The shear deformable nonlinear finite element models presented herein are used to study nonlinear bending, transient behavior, and postbuckling of laminated structures. Additional details and numerical examples may be found in [17,19–25,32].

10.2 Classical Plate Theory

10.2.1 Governing Equations

The equations of motion of the classical theory of laminated plates are given by [see Eq. (3.3.25)]

$$-\left(\frac{\partial N_{xx}}{\partial x} + \frac{\partial N_{xy}}{\partial y}\right) + I_0 \frac{\partial^2 u_0}{\partial t^2} - I_1 \frac{\partial^2}{\partial t^2} \left(\frac{\partial w_0}{\partial x}\right) = 0 \quad (10.2.1)$$

$$-\left(\frac{\partial N_{xy}}{\partial x} + \frac{\partial N_{yy}}{\partial y}\right) + I_0 \frac{\partial^2 v_0}{\partial t^2} - I_1 \frac{\partial^2}{\partial t^2} \left(\frac{\partial w_0}{\partial y}\right) = 0 \quad (10.2.2)$$

$$\begin{aligned} & -\left(\frac{\partial^2 M_{xx}}{\partial x^2} + 2\frac{\partial^2 M_{xy}}{\partial y \partial x} + \frac{\partial^2 M_{yy}}{\partial y^2}\right) - \mathcal{N}(u_0, v_0, w_0) - q + I_0 \frac{\partial^2 w_0}{\partial t^2} \\ & - I_2 \frac{\partial^2}{\partial t^2} \left(\frac{\partial^2 w_0}{\partial x^2} + \frac{\partial^2 w_0}{\partial y^2}\right) + I_1 \frac{\partial^2}{\partial t^2} \left(\frac{\partial u_0}{\partial x} + \frac{\partial v_0}{\partial y}\right) = 0 \end{aligned} \quad (10.2.3)$$

where the nonlinear expression \mathcal{N} and the mass moments of inertia I_i are defined

by

$$\mathcal{N}(u_0, v_0, w_0) = \frac{\partial}{\partial x} \left(N_{xx} \frac{\partial w_0}{\partial x} + N_{xy} \frac{\partial w_0}{\partial y} \right) + \frac{\partial}{\partial y} \left(N_{xy} \frac{\partial w_0}{\partial x} + N_{yy} \frac{\partial w_0}{\partial y} \right) \quad (10.2.4a)$$

$$\begin{Bmatrix} I_0 \\ I_1 \\ I_2 \end{Bmatrix} = \int_{-\frac{h}{2}}^{\frac{h}{2}} \begin{Bmatrix} 1 \\ z \\ z^2 \end{Bmatrix} \rho_0 \ dz \quad (10.2.4b)$$

and the stress resultants (N_{xx}, N_{yy}, N_{xy}) and (M_{xx}, M_{yy}, M_{xy}) are defined by

$$\begin{aligned} \begin{Bmatrix} N_{xx} \\ N_{yy} \\ N_{xy} \end{Bmatrix} &= \begin{bmatrix} A_{11} & A_{12} & A_{16} \\ A_{12} & A_{22} & A_{26} \\ A_{16} & A_{26} & A_{66} \end{bmatrix} \begin{Bmatrix} \frac{\partial u_0}{\partial x} + \frac{1}{2} \left(\frac{\partial w_0}{\partial x} \right)^2 \\ \frac{\partial v_0}{\partial y} + \frac{1}{2} \left(\frac{\partial w_0}{\partial y} \right)^2 \\ \frac{\partial u_0}{\partial y} + \frac{\partial v_0}{\partial x} + \frac{\partial w_0}{\partial x} \frac{\partial w_0}{\partial y} \end{Bmatrix} \\ &+ \begin{bmatrix} B_{11} & B_{12} & B_{16} \\ B_{12} & B_{22} & B_{26} \\ B_{16} & B_{26} & B_{66} \end{bmatrix} \begin{Bmatrix} -\frac{\partial^2 w_0}{\partial x^2} \\ -\frac{\partial^2 w_0}{\partial y^2} \\ -2 \frac{\partial^2 w_0}{\partial x \partial y} \end{Bmatrix} - \begin{Bmatrix} N_{xx}^T \\ N_{yy}^T \\ N_{xy}^T \end{Bmatrix} - \begin{Bmatrix} N_{xx}^P \\ N_{yy}^P \\ N_{xy}^P \end{Bmatrix} \quad (10.2.5) \end{aligned}$$

$$\begin{aligned} \begin{Bmatrix} M_{xx} \\ M_{yy} \\ M_{xy} \end{Bmatrix} &= \begin{bmatrix} B_{11} & B_{12} & B_{16} \\ B_{12} & B_{22} & B_{26} \\ B_{16} & B_{26} & B_{66} \end{bmatrix} \begin{Bmatrix} \frac{\partial u_0}{\partial x} + \frac{1}{2} \left(\frac{\partial w_0}{\partial x} \right)^2 \\ \frac{\partial v_0}{\partial y} + \frac{1}{2} \left(\frac{\partial w_0}{\partial y} \right)^2 \\ \frac{\partial u_0}{\partial y} + \frac{\partial v_0}{\partial x} + \frac{\partial w_0}{\partial x} \frac{\partial w_0}{\partial y} \end{Bmatrix} \\ &+ \begin{bmatrix} D_{11} & D_{12} & D_{16} \\ D_{12} & D_{22} & D_{26} \\ D_{16} & D_{26} & D_{66} \end{bmatrix} \begin{Bmatrix} -\frac{\partial^2 w_0}{\partial x^2} \\ -\frac{\partial^2 w_0}{\partial y^2} \\ -2 \frac{\partial^2 w_0}{\partial x \partial y} \end{Bmatrix} - \begin{Bmatrix} M_{xx}^T \\ M_{yy}^T \\ M_{xy}^T \end{Bmatrix} - \begin{Bmatrix} M_{xx}^P \\ M_{yy}^P \\ M_{xy}^P \end{Bmatrix} \quad (10.2.6) \end{aligned}$$

where $\{N^T\}$ and $\{M^T\}$ are thermal force resultants

$$\{N^T\} = \sum_{k=1}^N \int_{z_k}^{z_{k+1}} [\bar{Q}]^{(k)} \{\bar{\alpha}\}^{(k)} \Delta T \ dz \quad (10.2.7a)$$

$$\{M^T\} = \sum_{k=1}^N \int_{z_k}^{z_{k+1}} [\bar{Q}]^{(k)} \{\bar{\alpha}\}^{(k)} \Delta T \ z \ dz \quad (10.2.7b)$$

and $\{N^P\}$ and $\{M^P\}$ are the piezoelectric (or other actuation field) resultants

$$\{N^P\} = \sum_{k=1}^N \int_{z_k}^{z_{k+1}} [\bar{e}]^{(k)} \{E\}^{(k)} \ dz \quad (10.2.8a)$$

$$\{M^P\} = \sum_{k=1}^N \int_{z_k}^{z_{k+1}} [\bar{e}]^{(k)} \{E\}^{(k)} \ z \ dz \quad (10.2.8b)$$

10.2.2 Virtual Work Statement

The stress resultants (N 's and M 's) in (10.2.1)–(10.2.3), in general, are related to the displacement gradients, temperature increment, and electric/magnetic (or any

actuation) field by Eqs. (10.2.6). Therefore, the equations of motion (10.2.1)–(10.2.3) can be expressed in terms of displacements (u_0, v_0, w_0) by substituting for the stress resultants from Eqs. (10.2.5) and (10.2.6). Then the weak forms of (10.2.1)–(10.2.3) over a typical laminated plate finite element Ω^e are given by (here only the thermal stress resultants are included)

$$\begin{aligned}
0 = & \int_{\Omega^e} \left(\frac{\partial \delta u_0}{\partial x} \left\{ A_{11} \left[\frac{\partial u_0}{\partial x} + \frac{1}{2} \left(\frac{\partial w_0}{\partial x} \right)^2 \right] + A_{12} \left[\frac{\partial v_0}{\partial y} + \frac{1}{2} \left(\frac{\partial w_0}{\partial y} \right)^2 \right] \right. \right. \\
& + A_{16} \left[\frac{\partial u_0}{\partial y} + \frac{\partial v_0}{\partial x} + \frac{\partial w_0}{\partial x} \frac{\partial w_0}{\partial y} \right] - B_{11} \frac{\partial^2 w_0}{\partial x^2} - B_{12} \frac{\partial^2 w_0}{\partial y^2} - 2B_{16} \frac{\partial^2 w_0}{\partial x \partial y} \} \\
& + \frac{\partial \delta u_0}{\partial y} \left\{ A_{16} \left[\frac{\partial u_0}{\partial x} + \frac{1}{2} \left(\frac{\partial w_0}{\partial x} \right)^2 \right] + A_{26} \left[\frac{\partial v_0}{\partial y} + \frac{1}{2} \left(\frac{\partial w_0}{\partial y} \right)^2 \right] \right. \\
& + A_{66} \left[\frac{\partial u_0}{\partial y} + \frac{\partial v_0}{\partial x} + \frac{\partial w_0}{\partial x} \frac{\partial w_0}{\partial y} \right] - B_{16} \frac{\partial^2 w_0}{\partial x^2} - B_{26} \frac{\partial^2 w_0}{\partial y^2} - 2B_{66} \frac{\partial^2 w_0}{\partial x \partial y} \} \\
& \left. \left. - \frac{\partial \delta u_0}{\partial x} N_{xx}^T - \frac{\partial \delta u_0}{\partial y} N_{xy}^T \right) dx dy - \oint_{\Gamma^e} N_n \delta u_{0n} ds \right. \\
& \left. + \int_{\Omega^e} \left(I_0 \frac{\partial^2 u_0}{\partial t^2} - I_1 \frac{\partial^3 w_0}{\partial t^2 \partial x} \right) \delta u_0 dx dy \right) \quad (10.2.9a)
\end{aligned}$$

$$\begin{aligned}
0 = & \int_{\Omega^e} \left(\frac{\partial \delta v_0}{\partial y} \left\{ A_{12} \left[\frac{\partial u_0}{\partial x} + \frac{1}{2} \left(\frac{\partial w_0}{\partial x} \right)^2 \right] + A_{22} \left[\frac{\partial v_0}{\partial y} + \frac{1}{2} \left(\frac{\partial w_0}{\partial y} \right)^2 \right] \right. \right. \\
& + A_{26} \left[\frac{\partial u_0}{\partial y} + \frac{\partial v_0}{\partial x} + \frac{\partial w_0}{\partial x} \frac{\partial w_0}{\partial y} \right] - B_{12} \frac{\partial^2 w_0}{\partial x^2} - B_{22} \frac{\partial^2 w_0}{\partial y^2} - 2B_{26} \frac{\partial^2 w_0}{\partial x \partial y} \} \\
& + \frac{\partial \delta v_0}{\partial x} \left\{ A_{16} \left[\frac{\partial u_0}{\partial x} + \frac{1}{2} \left(\frac{\partial w_0}{\partial x} \right)^2 \right] + A_{26} \left[\frac{\partial v_0}{\partial y} + \frac{1}{2} \left(\frac{\partial w_0}{\partial y} \right)^2 \right] \right. \\
& + A_{66} \left[\frac{\partial u_0}{\partial y} + \frac{\partial v_0}{\partial x} + \frac{\partial w_0}{\partial x} \frac{\partial w_0}{\partial y} \right] - B_{16} \frac{\partial^2 w_0}{\partial x^2} - B_{26} \frac{\partial^2 w_0}{\partial y^2} - 2B_{66} \frac{\partial^2 w_0}{\partial x \partial y} \} \\
& \left. \left. - \frac{\partial \delta v_0}{\partial x} N_{xy}^T - \frac{\partial \delta v_0}{\partial y} N_{yy}^T \right) dx dy - \oint_{\Gamma^e} N_s \delta u_{0s} ds \right. \\
& \left. + \int_{\Omega^e} \left(I_0 \frac{\partial^2 v_0}{\partial t^2} - I_1 \frac{\partial^3 w_0}{\partial t^2 \partial y} \right) \delta v_0 dx dy \right) \quad (10.2.9b)
\end{aligned}$$

$$\begin{aligned}
0 = & \int_{\Omega^e} \left\{ \frac{\partial \delta w_0}{\partial x} \left[\frac{\partial w_0}{\partial x} \left\{ A_{11} \left[\frac{\partial u_0}{\partial x} + \frac{1}{2} \left(\frac{\partial w_0}{\partial x} \right)^2 \right] + A_{12} \left[\frac{\partial v_0}{\partial y} + \frac{1}{2} \left(\frac{\partial w_0}{\partial y} \right)^2 \right] \right. \right. \right. \right. \\
& + A_{16} \left[\frac{\partial u_0}{\partial y} + \frac{\partial v_0}{\partial x} + \frac{\partial w_0}{\partial x} \frac{\partial w_0}{\partial y} \right] - B_{11} \frac{\partial^2 w_0}{\partial x^2} - B_{12} \frac{\partial^2 w_0}{\partial y^2} - 2B_{16} \frac{\partial^2 w_0}{\partial x \partial y} \} \\
& + \frac{\partial w_0}{\partial y} \left\{ A_{16} \left[\frac{\partial u_0}{\partial x} + \frac{1}{2} \left(\frac{\partial w_0}{\partial x} \right)^2 \right] + A_{26} \left[\frac{\partial v_0}{\partial y} + \frac{1}{2} \left(\frac{\partial w_0}{\partial y} \right)^2 \right] \right. \\
& + A_{66} \left[\frac{\partial u_0}{\partial y} + \frac{\partial v_0}{\partial x} + \frac{\partial w_0}{\partial x} \frac{\partial w_0}{\partial y} \right] - B_{16} \frac{\partial^2 w_0}{\partial x^2} - B_{26} \frac{\partial^2 w_0}{\partial y^2} - 2B_{66} \frac{\partial^2 w_0}{\partial x \partial y} \} \right\}
\end{aligned}$$

$$\begin{aligned}
& + \frac{\partial \delta w_0}{\partial y} \left[\frac{\partial w_0}{\partial y} \left\{ A_{12} \left[\frac{\partial u_0}{\partial x} + \frac{1}{2} \left(\frac{\partial w_0}{\partial x} \right)^2 \right] + A_{22} \left[\frac{\partial v_0}{\partial y} + \frac{1}{2} \left(\frac{\partial w_0}{\partial y} \right)^2 \right] \right. \right. \\
& + A_{26} \left[\frac{\partial u_0}{\partial y} + \frac{\partial v_0}{\partial x} + \frac{\partial w_0}{\partial x} \frac{\partial w_0}{\partial y} \right] - B_{12} \frac{\partial^2 w_0}{\partial x^2} - B_{22} \frac{\partial^2 w_0}{\partial y^2} - 2B_{26} \frac{\partial^2 w_0}{\partial x \partial y} \Big\} \\
& + \frac{\partial w_0}{\partial x} \left\{ A_{16} \left[\frac{\partial u_0}{\partial x} + \frac{1}{2} \left(\frac{\partial w_0}{\partial x} \right)^2 \right] + A_{26} \left[\frac{\partial v_0}{\partial y} + \frac{1}{2} \left(\frac{\partial w_0}{\partial y} \right)^2 \right] \right. \\
& + A_{66} \left[\frac{\partial u_0}{\partial y} + \frac{\partial v_0}{\partial x} + \frac{\partial w_0}{\partial x} \frac{\partial w_0}{\partial y} \right] - B_{16} \frac{\partial^2 w_0}{\partial x^2} - B_{26} \frac{\partial^2 w_0}{\partial y^2} - 2B_{66} \frac{\partial^2 w_0}{\partial x \partial y} \Big\} \\
& - \frac{\partial^2 \delta w_0}{\partial x^2} \left\{ B_{11} \left[\frac{\partial u_0}{\partial x} + \frac{1}{2} \left(\frac{\partial w_0}{\partial x} \right)^2 \right] + B_{12} \left[\frac{\partial v_0}{\partial y} + \frac{1}{2} \left(\frac{\partial w_0}{\partial y} \right)^2 \right] \right. \\
& + B_{16} \left[\frac{\partial u_0}{\partial y} + \frac{\partial v_0}{\partial x} + \frac{\partial w_0}{\partial x} \frac{\partial w_0}{\partial y} \right] - \left(D_{11} \frac{\partial^2 w_0}{\partial x^2} + D_{12} \frac{\partial^2 w_0}{\partial y^2} + 2D_{16} \frac{\partial^2 w_0}{\partial x \partial y} \right) \Big\} \\
& - \frac{\partial^2 \delta w_0}{\partial y^2} \left\{ B_{12} \left[\frac{\partial u_0}{\partial x} + \frac{1}{2} \left(\frac{\partial w_0}{\partial x} \right)^2 \right] + B_{22} \left[\frac{\partial v_0}{\partial y} + \frac{1}{2} \left(\frac{\partial w_0}{\partial y} \right)^2 \right] \right. \\
& + B_{26} \left[\frac{\partial u_0}{\partial y} + \frac{\partial v_0}{\partial x} + \frac{\partial w_0}{\partial x} \frac{\partial w_0}{\partial y} \right] - \left(D_{12} \frac{\partial^2 w_0}{\partial x^2} + D_{22} \frac{\partial^2 w_0}{\partial y^2} + 2D_{26} \frac{\partial^2 w_0}{\partial x \partial y} \right) \Big\} \\
& - 2 \frac{\partial^2 \delta w_0}{\partial x \partial y} \left\{ B_{16} \left[\frac{\partial u_0}{\partial x} + \frac{1}{2} \left(\frac{\partial w_0}{\partial x} \right)^2 \right] + B_{26} \left[\frac{\partial v_0}{\partial y} + \frac{1}{2} \left(\frac{\partial w_0}{\partial y} \right)^2 \right] \right. \\
& + B_{66} \left[\frac{\partial u_0}{\partial y} + \frac{\partial v_0}{\partial x} + \frac{\partial w_0}{\partial x} \frac{\partial w_0}{\partial y} \right] - \left(D_{16} \frac{\partial^2 w_0}{\partial x^2} + D_{26} \frac{\partial^2 w_0}{\partial y^2} + 2D_{66} \frac{\partial^2 w_0}{\partial x \partial y} \right) \Big\} \\
& - \delta w_0 q + \frac{\partial^2 \delta w_0}{\partial x^2} M_{xx}^T + \frac{\partial^2 \delta w_0}{\partial y^2} M_{yy}^T + 2 \frac{\partial^2 \delta w_0}{\partial x \partial y} M_{xy}^T \\
& - \left[\frac{\partial \delta w_0}{\partial x} \left(N_{xx}^T \frac{\partial w_0}{\partial x} + N_{xy}^T \frac{\partial w_0}{\partial y} \right) + \frac{\partial \delta w_0}{\partial y} \left(N_{xy}^T \frac{\partial w_0}{\partial x} + N_{yy}^T \frac{\partial w_0}{\partial y} \right) \right] \delta w_0 \Big\} dx dy \\
& + \int_{\Omega^e} \left[I_0 \frac{\partial^2 w_0}{\partial t^2} + I_2 \left(\frac{\partial^3 w_0}{\partial t^2 \partial x} \frac{\partial w_0}{\partial x} + \frac{\partial^3 w_0}{\partial t^2 \partial y} \frac{\partial w_0}{\partial y} \right) \right. \\
& \left. - I_1 \left(\frac{\partial^2 u_0}{\partial t^2} \frac{\partial w_0}{\partial x} + \frac{\partial^2 v_0}{\partial t^2} \frac{\partial w_0}{\partial y} \right) \right] dx dy - \oint_{\Gamma^e} \left(V_n \delta w_0 - M_n \frac{\partial \delta w_0}{\partial n} \right) ds \quad (10.2.9c)
\end{aligned}$$

where

$$\begin{aligned}
N_n &= N_{xx} n_x + N_{xy} n_y, \quad N_s = N_{xy} n_x + N_{yy} n_y \\
V_n &= Q_n + \frac{\partial M_{ns}}{\partial s} + \mathcal{P} \\
M_n &= M_{xx} n_x + M_{xy} n_y, \quad M_s = M_{xy} n_x + M_{yy} n_y \\
\mathcal{P} &= \left(N_{xx} \frac{\partial w_0}{\partial x} + N_{xy} \frac{\partial w_0}{\partial y} \right) n_x + \left(N_{xy} \frac{\partial w_0}{\partial x} + N_{yy} \frac{\partial w_0}{\partial y} \right) n_y \quad (10.2.10)
\end{aligned}$$

and (n_x, n_y) denote the direction cosines of the unit normal on the element boundary Γ^e .

10.2.3 Finite Element Model

Assume finite element approximation of the form

$$u_0(x, y) = \sum_{j=1}^m u_j^e \psi_j^e(x, y), \quad v_0(x, y) = \sum_{j=1}^m v_j^e \psi_j^e(x, y), \quad w_0(x, y) = \sum_{j=1}^n \Delta_j^e \varphi_j^e(x, y) \quad (10.2.11)$$

where ψ_j^e are the Lagrange interpolation functions, Δ_j^e are the values of w_0 and its derivatives at the nodes, and φ_j^e are the interpolation functions, the specific form of which will depend on the geometry of the element and the nodal degrees of freedom interpolated. Substituting approximations (10.2.11) into Eq. (10.2.9), we obtain

$$\begin{aligned} \begin{bmatrix} [K^{11}] & [K^{12}] & [K^{13}] \\ [K^{21}] & [K^{22}] & [K^{23}] \\ [K^{31}] & [K^{32}] & [K^{33}] \end{bmatrix} \begin{Bmatrix} \{u\} \\ \{v\} \\ \{\Delta\} \end{Bmatrix} + \begin{bmatrix} [M^{11}] & [0] & [M^{13}] \\ [0] & [M^{22}] & [M^{23}] \\ [M^{13}]^T & [M^{23}]^T & [M^{33}] \end{bmatrix} \begin{Bmatrix} \{\ddot{u}\} \\ \{\ddot{v}\} \\ \{\ddot{\Delta}\} \end{Bmatrix} \\ = \begin{Bmatrix} \{F^1\} \\ \{F^2\} \\ \{F^3\} \end{Bmatrix} + \begin{Bmatrix} \{F^{1T}\} \\ \{F^{2T}\} \\ \{F^{3T}\} \end{Bmatrix} \end{aligned} \quad (10.2.12)$$

or, in compact form

$$[K^e]\{\bar{\Delta}^e\} + [M^e]\{\ddot{\bar{\Delta}}^e\} = \{F^e\} \quad (10.2.13)$$

The nonzero elements of the stiffness matrix $[K^e]$ and mass matrix $[M^e] = [M^e]^T$ and force vectors $\{F\}$ and $\{F^T\}$ are defined as follows:

$$\begin{aligned} K_{ij}^{11} &= \int_{\Omega^e} \left[A_{11} \frac{\partial \psi_i^e}{\partial x} \frac{\partial \psi_j^e}{\partial x} + A_{66} \frac{\partial \psi_i^e}{\partial y} \frac{\partial \psi_j^e}{\partial y} + A_{16} \left(\frac{\partial \psi_i^e}{\partial x} \frac{\partial \psi_j^e}{\partial y} + \frac{\partial \psi_i^e}{\partial y} \frac{\partial \psi_j^e}{\partial x} \right) \right] dx dy \\ K_{ij}^{12} &= \int_{\Omega^e} \left(A_{12} \frac{\partial \psi_i^e}{\partial x} \frac{\partial \psi_j^e}{\partial y} + A_{66} \frac{\partial \psi_i^e}{\partial y} \frac{\partial \psi_j^e}{\partial x} + A_{26} \frac{\partial \psi_i^e}{\partial y} \frac{\partial \psi_j^e}{\partial y} + A_{16} \frac{\partial \psi_i^e}{\partial x} \frac{\partial \psi_j^e}{\partial x} \right) dx dy = K_{ji}^{21} \\ K_{ij}^{13} &= - \int_{\Omega^e} \left[\frac{\partial \psi_i^e}{\partial x} \left(B_{11} \frac{\partial^2 \varphi_j^e}{\partial x^2} + B_{12} \frac{\partial^2 \varphi_j^e}{\partial y^2} + 2B_{16} \frac{\partial^2 \varphi_j^e}{\partial x \partial y} \right) \right. \\ &\quad \left. + \frac{\partial \psi_i^e}{\partial y} \left(B_{16} \frac{\partial^2 \varphi_j^e}{\partial x^2} + B_{26} \frac{\partial^2 \varphi_j^e}{\partial y^2} + 2B_{66} \frac{\partial^2 \varphi_j^e}{\partial x \partial y} \right) \right] dx dy \\ &\quad + \frac{1}{2} \int_{\Omega^e} \left\{ \frac{\partial \psi_i^e}{\partial x} \left[A_{11} \frac{\partial w_0}{\partial x} \frac{\partial \varphi_j^e}{\partial x} + A_{12} \frac{\partial w_0}{\partial y} \frac{\partial \varphi_j^e}{\partial y} + A_{16} \left(\frac{\partial w_0}{\partial x} \frac{\partial \varphi_j^e}{\partial y} + \frac{\partial w_0}{\partial y} \frac{\partial \varphi_j^e}{\partial x} \right) \right] \right. \\ &\quad \left. + \frac{\partial \psi_i^e}{\partial y} \left[A_{16} \frac{\partial w_0}{\partial x} \frac{\partial \varphi_j^e}{\partial x} + A_{26} \frac{\partial w_0}{\partial y} \frac{\partial \varphi_j^e}{\partial y} + A_{66} \left(\frac{\partial w_0}{\partial x} \frac{\partial \varphi_j^e}{\partial y} + \frac{\partial w_0}{\partial y} \frac{\partial \varphi_j^e}{\partial x} \right) \right] \right\} dx dy \\ K_{ij}^{22} &= \int_{\Omega^e} \left[A_{22} \frac{\partial \psi_i^e}{\partial y} \frac{\partial \psi_j^e}{\partial y} + A_{66} \frac{\partial \psi_i^e}{\partial x} \frac{\partial \psi_j^e}{\partial x} + A_{26} \left(\frac{\partial \psi_i^e}{\partial x} \frac{\partial \psi_j^e}{\partial y} + \frac{\partial \psi_i^e}{\partial y} \frac{\partial \psi_j^e}{\partial x} \right) \right] dx dy \\ K_{ij}^{23} &= - \int_{\Omega^e} \left\{ \frac{\partial \psi_i^e}{\partial y} \left(B_{12} \frac{\partial^2 \varphi_j^e}{\partial x^2} + B_{22} \frac{\partial^2 \varphi_j^e}{\partial y^2} + 2B_{26} \frac{\partial^2 \varphi_j^e}{\partial x \partial y} \right) \right. \\ &\quad \left. + \frac{\partial \psi_i^e}{\partial x} \left(B_{16} \frac{\partial^2 \varphi_j^e}{\partial x^2} + B_{26} \frac{\partial^2 \varphi_j^e}{\partial y^2} + 2B_{66} \frac{\partial^2 \varphi_j^e}{\partial x \partial y} \right) \right\} dx dy \end{aligned}$$

$$\begin{aligned}
& + \frac{1}{2} \int_{\Omega^e} \left\{ \frac{\partial \psi_i^e}{\partial y} \left[A_{12} \frac{\partial w_0}{\partial x} \frac{\partial \varphi_j^e}{\partial x} + A_{22} \frac{\partial w_0}{\partial y} \frac{\partial \varphi_j^e}{\partial y} + A_{26} \left(\frac{\partial w_0}{\partial x} \frac{\partial \varphi_j^e}{\partial y} + \frac{\partial w_0}{\partial y} \frac{\partial \varphi_j^e}{\partial x} \right) \right] \right. \\
& \quad \left. + \frac{\partial \psi_i^e}{\partial x} \left[A_{16} \frac{\partial w_0}{\partial x} \frac{\partial \varphi_j^e}{\partial x} + A_{26} \frac{\partial w_0}{\partial y} \frac{\partial \varphi_j^e}{\partial y} + A_{66} \left(\frac{\partial w_0}{\partial x} \frac{\partial \varphi_j^e}{\partial y} + \frac{\partial w_0}{\partial y} \frac{\partial \varphi_j^e}{\partial x} \right) \right] \right\} dx dy \\
K_{ij}^{31} = & - \int_{\Omega^e} \left[\frac{\partial \psi_j^e}{\partial x} \left(B_{11} \frac{\partial^2 \varphi_i^e}{\partial x^2} + B_{12} \frac{\partial^2 \varphi_i^e}{\partial y^2} + 2B_{16} \frac{\partial^2 \varphi_i^e}{\partial x \partial y} \right) \right. \\
& \quad \left. + \frac{\partial \psi_j^e}{\partial y} \left(B_{16} \frac{\partial^2 \varphi_i^e}{\partial x^2} + B_{26} \frac{\partial^2 \varphi_i^e}{\partial y^2} + 2B_{66} \frac{\partial^2 \varphi_i^e}{\partial x \partial y} \right) \right] dx dy \\
& + \int_{\Omega^e} \left\{ \frac{\partial \psi_j^e}{\partial x} \left[A_{11} \frac{\partial w_0}{\partial x} \frac{\partial \varphi_i^e}{\partial x} + A_{12} \frac{\partial w_0}{\partial y} \frac{\partial \varphi_i^e}{\partial y} + A_{16} \left(\frac{\partial w_0}{\partial x} \frac{\partial \varphi_i^e}{\partial y} + \frac{\partial w_0}{\partial y} \frac{\partial \varphi_i^e}{\partial x} \right) \right] \right. \\
& \quad \left. + \frac{\partial \psi_j^e}{\partial y} \left[A_{16} \frac{\partial w_0}{\partial x} \frac{\partial \varphi_i^e}{\partial x} + A_{26} \frac{\partial w_0}{\partial y} \frac{\partial \varphi_i^e}{\partial y} + A_{66} \left(\frac{\partial w_0}{\partial x} \frac{\partial \varphi_i^e}{\partial y} + \frac{\partial w_0}{\partial y} \frac{\partial \varphi_i^e}{\partial x} \right) \right] \right\} dx dy \\
K_{ij}^{32} = & - \int_{\Omega^e} \left\{ \frac{\partial \psi_j^e}{\partial y} \left(B_{12} \frac{\partial^2 \varphi_i^e}{\partial x^2} + B_{22} \frac{\partial^2 \varphi_i^e}{\partial y^2} + 2B_{26} \frac{\partial^2 \varphi_i^e}{\partial x \partial y} \right) \right. \\
& \quad \left. + \frac{\partial \psi_j^e}{\partial x} \left(B_{16} \frac{\partial^2 \varphi_i^e}{\partial x^2} + B_{26} \frac{\partial^2 \varphi_i^e}{\partial y^2} + 2B_{66} \frac{\partial^2 \varphi_i^e}{\partial x \partial y} \right) \right\} dx dy \\
& + \int_{\Omega^e} \left\{ \frac{\partial \psi_j^e}{\partial y} \left[A_{12} \frac{\partial w_0}{\partial x} \frac{\partial \varphi_i^e}{\partial x} + A_{22} \frac{\partial w_0}{\partial y} \frac{\partial \varphi_i^e}{\partial y} + A_{26} \left(\frac{\partial w_0}{\partial x} \frac{\partial \varphi_i^e}{\partial y} + \frac{\partial w_0}{\partial y} \frac{\partial \varphi_i^e}{\partial x} \right) \right] \right. \\
& \quad \left. + \frac{\partial \psi_j^e}{\partial x} \left[A_{16} \frac{\partial w_0}{\partial x} \frac{\partial \varphi_i^e}{\partial x} + A_{26} \frac{\partial w_0}{\partial y} \frac{\partial \varphi_i^e}{\partial y} + A_{66} \left(\frac{\partial w_0}{\partial x} \frac{\partial \varphi_i^e}{\partial y} + \frac{\partial w_0}{\partial y} \frac{\partial \varphi_i^e}{\partial x} \right) \right] \right\} dx dy \\
K_{ij}^{33} = & \int_{\Omega^e} \left[\frac{\partial^2 \varphi_i^e}{\partial x^2} \left(D_{11} \frac{\partial^2 \varphi_j^e}{\partial x^2} + D_{12} \frac{\partial^2 \varphi_j^e}{\partial y^2} + 2D_{16} \frac{\partial^2 \varphi_j^e}{\partial x \partial y} \right) \right. \\
& \quad \left. + \frac{\partial^2 \varphi_i^e}{\partial y^2} \left(D_{12} \frac{\partial^2 \varphi_j^e}{\partial x^2} + D_{22} \frac{\partial^2 \varphi_j^e}{\partial y^2} + 2D_{26} \frac{\partial^2 \varphi_j^e}{\partial x \partial y} \right) \right. \\
& \quad \left. + 2 \frac{\partial^2 \varphi_i^e}{\partial x \partial y} \left(D_{16} \frac{\partial^2 \varphi_j^e}{\partial x^2} + D_{26} \frac{\partial^2 \varphi_j^e}{\partial y^2} + 2D_{66} \frac{\partial^2 \varphi_j^e}{\partial x \partial y} \right) \right] dx dy \\
& + \frac{1}{2} \int_{\Omega^e} \left\{ \left[A_{11} \left(\frac{\partial w_0}{\partial x} \right)^2 + A_{12} \left(\frac{\partial w_0}{\partial y} \right)^2 + 2A_{16} \frac{\partial w_0}{\partial x} \frac{\partial w_0}{\partial y} \right] \frac{\partial \varphi_i^e}{\partial x} \frac{\partial \varphi_j^e}{\partial x} \right. \\
& \quad \left. + \left[A_{16} \left(\frac{\partial w_0}{\partial x} \right)^2 + A_{26} \left(\frac{\partial w_0}{\partial y} \right)^2 + 2A_{66} \frac{\partial w_0}{\partial x} \frac{\partial w_0}{\partial y} \right] \left(\frac{\partial \varphi_i^e}{\partial x} \frac{\partial \varphi_j^e}{\partial y} + \frac{\partial \varphi_j^e}{\partial x} \frac{\partial \varphi_i^e}{\partial y} \right) \right. \\
& \quad \left. + \left[A_{12} \left(\frac{\partial w_0}{\partial x} \right)^2 + A_{22} \left(\frac{\partial w_0}{\partial y} \right)^2 + 2A_{26} \frac{\partial w_0}{\partial x} \frac{\partial w_0}{\partial y} \right] \frac{\partial \varphi_i^e}{\partial y} \frac{\partial \varphi_j^e}{\partial y} \right\} dx dy \\
& - \int_{\Omega^e} \left\{ \frac{\partial \varphi_i^e}{\partial x} \left[\frac{\partial w_0}{\partial x} \left(B_{11} \frac{\partial^2 \varphi_j^e}{\partial x^2} + B_{12} \frac{\partial^2 \varphi_j^e}{\partial y^2} + 2B_{16} \frac{\partial^2 \varphi_j^e}{\partial x \partial y} \right) \right. \right. \\
& \quad \left. \left. + \frac{\partial w_0}{\partial y} \left(B_{16} \frac{\partial^2 \varphi_j^e}{\partial x^2} + B_{26} \frac{\partial^2 \varphi_j^e}{\partial y^2} + 2B_{66} \frac{\partial^2 \varphi_j^e}{\partial x \partial y} \right) \right] \right\}
\end{aligned}$$

$$\begin{aligned}
& + \frac{\partial \varphi_i^e}{\partial y} \left[\frac{\partial w_0}{\partial y} \left(B_{12} \frac{\partial^2 \varphi_j^e}{\partial x^2} + B_{22} \frac{\partial^2 \varphi_j^e}{\partial y^2} + 2B_{26} \frac{\partial^2 \varphi_j^e}{\partial x \partial y} \right) \right. \\
& \quad \left. + \frac{\partial w_0}{\partial x} \left(B_{16} \frac{\partial^2 \varphi_j^e}{\partial x^2} + B_{26} \frac{\partial^2 \varphi_j^e}{\partial y^2} + 2B_{66} \frac{\partial^2 \varphi_j^e}{\partial x \partial y} \right) \right] \Big\} dx dy \\
& - \frac{1}{2} \int_{\Omega^e} \left\{ \frac{\partial^2 \varphi_i^e}{\partial x^2} \left[B_{11} \frac{\partial w_0}{\partial x} \frac{\partial \varphi_j^e}{\partial x} + B_{12} \frac{\partial w_0}{\partial y} \frac{\partial \varphi_j^e}{\partial y} + B_{16} \left(\frac{\partial w_0}{\partial y} \frac{\partial \varphi_j^e}{\partial x} + \frac{\partial w_0}{\partial x} \frac{\partial \varphi_j^e}{\partial y} \right) \right] \right. \\
& \quad \left. + \frac{\partial^2 \varphi_i^e}{\partial y^2} \left[B_{12} \frac{\partial w_0}{\partial x} \frac{\partial \varphi_j^e}{\partial x} + B_{22} \frac{\partial w_0}{\partial y} \frac{\partial \varphi_j^e}{\partial y} + B_{26} \left(\frac{\partial w_0}{\partial y} \frac{\partial \varphi_j^e}{\partial x} + \frac{\partial w_0}{\partial x} \frac{\partial \varphi_j^e}{\partial y} \right) \right] \right. \\
& \quad \left. + 2 \frac{\partial^2 \varphi_i^e}{\partial x \partial y} \left[B_{16} \frac{\partial w_0}{\partial x} \frac{\partial \varphi_j^e}{\partial x} + B_{26} \frac{\partial w_0}{\partial y} \frac{\partial \varphi_j^e}{\partial y} + B_{66} \left(\frac{\partial w_0}{\partial y} \frac{\partial \varphi_j^e}{\partial x} + \frac{\partial w_0}{\partial x} \frac{\partial \varphi_j^e}{\partial y} \right) \right] \right\} dx dy
\end{aligned} \tag{10.2.14}$$

$$\begin{aligned}
M_{ij}^{11} &= \int_{\Omega^e} I_0 \psi_i^e \psi_j^e dx dy, \quad M_{ij}^{13} = - \int_{\Omega^e} I_1 \psi_i^e \frac{\partial \varphi_j^e}{\partial x} dx dy \\
M_{ij}^{22} &= \int_{\Omega^e} I_0 \psi_i^e \psi_j^e dx dy, \quad M_{ij}^{23} = - \int_{\Omega^e} I_1 \psi_i^e \frac{\partial \varphi_j^e}{\partial y} dx dy \\
M_{ij}^{33} &= \int_{\Omega^e} \left[I_0 \varphi_i^e \varphi_j^e + I_2 \left(\frac{\partial \varphi_i^e}{\partial x} \frac{\partial \varphi_j^e}{\partial x} + \frac{\partial \varphi_i^e}{\partial y} \frac{\partial \varphi_j^e}{\partial y} \right) \right] dx dy \\
F_i^1 &= \oint_{\Gamma^e} N_n \psi_i^e ds, \quad F_i^2 = \oint_{\Gamma^e} N_s \psi_i^e ds \\
F_i^3 &= \int_{\Omega^e} q \varphi_i^e dx dy + \oint_{\Gamma^e} \left(V_n \varphi_i^e - M_n \frac{\partial \varphi_i^e}{\partial n} \right) ds \\
F_i^{1T} &= \int_{\Omega^e} \left(N_{xx}^T \frac{\partial \psi_i^e}{\partial x} + N_{xy}^T \frac{\partial \psi_i^e}{\partial y} \right) dx dy, \quad F_i^{2T} = \int_{\Omega^e} \left(N_{xy}^T \frac{\partial \psi_i^e}{\partial x} + N_{yy}^T \frac{\partial \psi_i^e}{\partial y} \right) dx dy \\
F_i^{3T} &= - \int_{\Omega^e} \left(\frac{\partial^2 \varphi_i^e}{\partial x^2} M_{xx}^T + 2 \frac{\partial^2 \varphi_i^e}{\partial x \partial y} M_{xy}^T + \frac{\partial^2 \varphi_i^e}{\partial y^2} M_{yy}^T \right) dx dy \\
& + \int_{\Omega^e} \left[\frac{\partial \varphi_i^e}{\partial x} \left(N_{xx}^T \frac{\partial w_0}{\partial x} + N_{xy}^T \frac{\partial w_0}{\partial y} \right) + \frac{\partial \varphi_i^e}{\partial y} \left(N_{xy}^T \frac{\partial w_0}{\partial x} + N_{yy}^T \frac{\partial w_0}{\partial y} \right) \right] dx dy
\end{aligned} \tag{10.2.15}$$

where N_{xx}^T, M_{xx}^T , etc. are the thermal (or hygrothermal and/or actuation) forces and moments defined in Eqs. (10.2.7a,b).

The plate bending elements discussed in Chapter 9 for the classical plate theory can be used here with a choice of Lagrange interpolation of the in-plane displacements (u_0, v_0) . For example, linear interpolation of (u_0, v_0) and Hermite cubic interpolation of w_0 will have 20 element degrees of freedom for nonconforming rectangular element and 25 degrees of freedom for conforming rectangular element.

This completes the development of the nonlinear displacement finite element model of the classical plate theory in the rectangular Cartesian coordinate system. Equation (10.2.13) can be reduced to a set of nonlinear algebraic equations by means of the Newmark time integration scheme, as shown in Section 6.7. A discussion of iterative methods for the solution of the nonlinear algebraic equations resulting from (10.2.13) is presented in Section 10.4 (also, see Reddy [32]).

10.3 First-Order Shear Deformation Plate Theory

10.3.1 Governing Equations

The equations of motion of the first-order shear deformation plate theory are given by

$$-\left(\frac{\partial N_{xx}}{\partial x} + \frac{\partial N_{xy}}{\partial y}\right) + I_0 \frac{\partial^2 u_0}{\partial t^2} + I_1 \frac{\partial^2 \phi_x}{\partial t^2} = 0 \quad (10.3.1)$$

$$-\left(\frac{\partial N_{xy}}{\partial x} + \frac{\partial N_{yy}}{\partial y}\right) + I_0 \frac{\partial^2 v_0}{\partial t^2} + I_1 \frac{\partial^2 \phi_y}{\partial t^2} = 0 \quad (10.3.2)$$

$$-\left(\frac{\partial Q_x}{\partial x} + \frac{\partial Q_y}{\partial y}\right) - \mathcal{N}(u_0, v_0, w_0) - q + I_0 \frac{\partial^2 w_0}{\partial t^2} = 0 \quad (10.3.3)$$

$$-\left(\frac{\partial M_{xx}}{\partial x} + \frac{\partial M_{xy}}{\partial y}\right) + Q_x + I_2 \frac{\partial^2 \phi_x}{\partial t^2} + I_1 \frac{\partial^2 u_0}{\partial t^2} = 0 \quad (10.3.4)$$

$$-\left(\frac{\partial M_{xy}}{\partial x} + \frac{\partial M_{yy}}{\partial y}\right) + Q_y + I_2 \frac{\partial^2 \phi_y}{\partial t^2} + I_1 \frac{\partial^2 v_0}{\partial t^2} = 0 \quad (10.3.5)$$

where \mathcal{N} and I_i are defined by Eq. (10.2.4a,b), and the stress resultants are given by

$$\begin{Bmatrix} N_{xx} \\ N_{yy} \\ N_{xy} \end{Bmatrix} = \begin{bmatrix} A_{11} & A_{12} & A_{16} \\ A_{12} & A_{22} & A_{26} \\ A_{16} & A_{26} & A_{66} \end{bmatrix} \begin{Bmatrix} \frac{\partial u_0}{\partial x} + \frac{1}{2} \left(\frac{\partial w_0}{\partial x} \right)^2 \\ \frac{\partial v_0}{\partial y} + \frac{1}{2} \left(\frac{\partial w_0}{\partial y} \right)^2 \\ \frac{\partial u_0}{\partial y} + \frac{\partial v_0}{\partial x} + \frac{\partial w_0}{\partial x} \frac{\partial w_0}{\partial y} \end{Bmatrix} + \begin{bmatrix} B_{11} & B_{12} & B_{16} \\ B_{12} & B_{22} & B_{26} \\ B_{16} & B_{26} & B_{66} \end{bmatrix} \begin{Bmatrix} \frac{\partial \phi_x}{\partial x} \\ \frac{\partial \phi_y}{\partial y} \\ \frac{\partial \phi_x}{\partial y} + \frac{\partial \phi_y}{\partial x} \end{Bmatrix} - \begin{Bmatrix} N_{xx}^T \\ N_{yy}^T \\ N_{xy}^T \end{Bmatrix} - \begin{Bmatrix} N_{xx}^P \\ N_{yy}^P \\ N_{xy}^P \end{Bmatrix} \quad (10.3.6a)$$

$$\begin{Bmatrix} M_{xx} \\ M_{yy} \\ M_{xy} \end{Bmatrix} = \begin{bmatrix} B_{11} & B_{12} & B_{16} \\ B_{12} & B_{22} & B_{26} \\ B_{16} & B_{26} & B_{66} \end{bmatrix} \begin{Bmatrix} \frac{\partial u_0}{\partial x} + \frac{1}{2} \left(\frac{\partial w_0}{\partial x} \right)^2 \\ \frac{\partial v_0}{\partial y} + \frac{1}{2} \left(\frac{\partial w_0}{\partial y} \right)^2 \\ \frac{\partial u_0}{\partial y} + \frac{\partial v_0}{\partial x} + \frac{\partial w_0}{\partial x} \frac{\partial w_0}{\partial y} \end{Bmatrix} + \begin{bmatrix} D_{11} & D_{12} & D_{16} \\ D_{12} & D_{22} & D_{26} \\ D_{16} & D_{26} & D_{66} \end{bmatrix} \begin{Bmatrix} \frac{\partial \phi_x}{\partial x} \\ \frac{\partial \phi_y}{\partial y} \\ \frac{\partial \phi_x}{\partial y} + \frac{\partial \phi_y}{\partial x} \end{Bmatrix} - \begin{Bmatrix} M_{xx}^T \\ M_{yy}^T \\ M_{xy}^T \end{Bmatrix} - \begin{Bmatrix} M_{xx}^P \\ M_{yy}^P \\ M_{xy}^P \end{Bmatrix} \quad (10.3.6b)$$

$$\begin{Bmatrix} Q_y \\ Q_x \end{Bmatrix} = K_s \begin{bmatrix} A_{44} & A_{45} \\ A_{45} & A_{55} \end{bmatrix} \begin{Bmatrix} \frac{\partial w_0}{\partial y} + \phi_y \\ \frac{\partial w_0}{\partial x} + \phi_x \end{Bmatrix} - \begin{Bmatrix} Q_y^P \\ Q_x^P \end{Bmatrix} \quad (10.3.6c)$$

$$\begin{Bmatrix} Q_x^P \\ Q_y^P \end{Bmatrix} = \sum_{k=1}^N \int_{z_k}^{z_{k+1}} \begin{bmatrix} \bar{e}_{14} & \bar{e}_{24} & 0 \\ \bar{e}_{15} & \bar{e}_{25} & 0 \end{bmatrix}^{(k)} \begin{Bmatrix} \mathcal{E}_x \\ \mathcal{E}_y \\ \mathcal{E}_z \end{Bmatrix}^{(k)} dz \quad (10.3.7)$$

and the shear stiffnesses (A_{44}, A_{55}, A_{45}) are defined by

$$(A_{44}, A_{45}, A_{55}) = \sum_{k=1}^N (\bar{Q}_{44}^{(k)}, \bar{Q}_{45}^{(k)}, \bar{Q}_{55}^{(k)}) (z_{k+1} - z_k) \quad (10.3.8a)$$

10.3.2 Virtual Work Statements

The weak forms of the equations of motion associated with the first-order shear deformation plate theory are

$$\begin{aligned}
 0 = & \int_{\Omega^e} \left(\frac{\partial \delta u_0}{\partial x} \left\{ A_{11} \left[\frac{\partial u_0}{\partial x} + \frac{1}{2} \left(\frac{\partial w_0}{\partial x} \right)^2 \right] + A_{12} \left[\frac{\partial v_0}{\partial y} + \frac{1}{2} \left(\frac{\partial w_0}{\partial y} \right)^2 \right] \right. \right. \\
 & + A_{16} \left[\frac{\partial u_0}{\partial y} + \frac{\partial v_0}{\partial x} + \frac{\partial w_0}{\partial x} \frac{\partial w_0}{\partial y} \right] + B_{11} \frac{\partial \phi_x}{\partial x} + B_{12} \frac{\partial \phi_y}{\partial y} + B_{16} \left(\frac{\partial \phi_x}{\partial y} + \frac{\partial \phi_y}{\partial x} \right) \left. \right\} \\
 & + \frac{\partial \delta u_0}{\partial y} \left\{ A_{16} \left[\frac{\partial u_0}{\partial x} + \frac{1}{2} \left(\frac{\partial w_0}{\partial x} \right)^2 \right] + A_{26} \left[\frac{\partial v_0}{\partial y} + \frac{1}{2} \left(\frac{\partial w_0}{\partial y} \right)^2 \right] \right. \\
 & + A_{66} \left[\frac{\partial u_0}{\partial y} + \frac{\partial v_0}{\partial x} + \frac{\partial w_0}{\partial x} \frac{\partial w_0}{\partial y} \right] + B_{16} \frac{\partial \phi_x}{\partial x} + B_{26} \frac{\partial \phi_y}{\partial y} + B_{66} \left(\frac{\partial \phi_x}{\partial y} + \frac{\partial \phi_y}{\partial x} \right) \left. \right\} \\
 & - \int_{\Omega^e} \left(\frac{\partial \delta u_0}{\partial x} N_{xx}^T + \frac{\partial \delta u_0}{\partial y} N_{xy}^T \right) dx dy - \oint_{\Gamma^e} N_n \delta u_{0n} ds \\
 & + \int_{\Omega^e} \left(I_0 \frac{\partial^2 u_0}{\partial t^2} + I_1 \frac{\partial^2 \phi_x}{\partial t^2} \right) \delta u_0 dx dy
 \end{aligned} \tag{10.3.9a}$$

$$\begin{aligned}
 0 = & \int_{\Omega^e} \left(\frac{\partial \delta v_0}{\partial y} \left\{ A_{12} \left[\frac{\partial u_0}{\partial x} + \frac{1}{2} \left(\frac{\partial w_0}{\partial x} \right)^2 \right] + A_{22} \left[\frac{\partial v_0}{\partial y} + \frac{1}{2} \left(\frac{\partial w_0}{\partial y} \right)^2 \right] \right. \right. \\
 & + A_{26} \left[\frac{\partial u_0}{\partial y} + \frac{\partial v_0}{\partial x} + \frac{\partial w_0}{\partial x} \frac{\partial w_0}{\partial y} \right] + B_{12} \frac{\partial \phi_x}{\partial x} + B_{22} \frac{\partial \phi_y}{\partial y} + B_{26} \left(\frac{\partial \phi_x}{\partial y} + \frac{\partial \phi_y}{\partial x} \right) \left. \right\} \\
 & + \frac{\partial \delta v_0}{\partial x} \left\{ A_{16} \left[\frac{\partial u_0}{\partial x} + \frac{1}{2} \left(\frac{\partial w_0}{\partial x} \right)^2 \right] + A_{26} \left[\frac{\partial v_0}{\partial y} + \frac{1}{2} \left(\frac{\partial w_0}{\partial y} \right)^2 \right] \right. \\
 & + A_{66} \left[\frac{\partial u_0}{\partial y} + \frac{\partial v_0}{\partial x} + \frac{\partial w_0}{\partial x} \frac{\partial w_0}{\partial y} \right] + B_{16} \frac{\partial \phi_x}{\partial x} + B_{26} \frac{\partial \phi_y}{\partial y} + B_{66} \left(\frac{\partial \phi_x}{\partial y} + \frac{\partial \phi_y}{\partial x} \right) \left. \right\} \\
 & - \int_{\Omega^e} \left(\frac{\partial \delta v_0}{\partial x} N_{xy}^T + \frac{\partial \delta v_0}{\partial y} N_{yy}^T \right) dx dy - \oint_{\Gamma^e} N_s \delta u_{0s} ds \\
 & + \int_{\Omega^e} \left(I_0 \frac{\partial^2 v_0}{\partial t^2} + I_1 \frac{\partial^2 \phi_y}{\partial t^2} \right) \delta v_0 dx dy
 \end{aligned} \tag{10.3.9b}$$

$$\begin{aligned}
 0 = & K_s \int_{\Omega^e} \left\{ \frac{\partial \delta w_0}{\partial x} \left[A_{55} \left(\frac{\partial w_0}{\partial x} + \phi_x \right) + A_{45} \left(\frac{\partial w_0}{\partial y} + \phi_y \right) \right] \right. \\
 & + \frac{\partial \delta w_0}{\partial y} \left[A_{45} \left(\frac{\partial w_0}{\partial x} + \phi_x \right) + A_{44} \left(\frac{\partial w_0}{\partial y} + \phi_y \right) \right] \left. \right\} dx dy \\
 & + \int_{\Omega^e} \left\{ \frac{\partial \delta w_0}{\partial x} \left[\frac{\partial w_0}{\partial x} \left\{ A_{11} \left[\frac{\partial u_0}{\partial x} + \frac{1}{2} \left(\frac{\partial w_0}{\partial x} \right)^2 \right] + A_{12} \left[\frac{\partial v_0}{\partial y} + \frac{1}{2} \left(\frac{\partial w_0}{\partial y} \right)^2 \right] \right. \right. \right. \\
 & + A_{16} \left[\frac{\partial u_0}{\partial y} + \frac{\partial v_0}{\partial x} + \frac{\partial w_0}{\partial x} \frac{\partial w_0}{\partial y} \right] + B_{11} \frac{\partial \phi_x}{\partial x} + B_{12} \frac{\partial \phi_y}{\partial y} + B_{16} \left(\frac{\partial \phi_x}{\partial y} + \frac{\partial \phi_y}{\partial x} \right) \left. \right\} \\
 & + \frac{\partial w_0}{\partial y} \left\{ A_{16} \left[\frac{\partial u_0}{\partial x} + \frac{1}{2} \left(\frac{\partial w_0}{\partial x} \right)^2 \right] + A_{26} \left[\frac{\partial v_0}{\partial y} + \frac{1}{2} \left(\frac{\partial w_0}{\partial y} \right)^2 \right] \right. \\
 & + A_{66} \left[\frac{\partial u_0}{\partial y} + \frac{\partial v_0}{\partial x} + \frac{\partial w_0}{\partial x} \frac{\partial w_0}{\partial y} \right] + B_{16} \frac{\partial \phi_x}{\partial x} + B_{26} \frac{\partial \phi_y}{\partial y} + B_{66} \left(\frac{\partial \phi_x}{\partial y} + \frac{\partial \phi_y}{\partial x} \right) \left. \right\}
 \end{aligned}$$

$$\begin{aligned}
& + \frac{\partial \delta w_0}{\partial y} \left\{ \frac{\partial w_0}{\partial y} \left\{ A_{12} \left[\frac{\partial u_0}{\partial x} + \frac{1}{2} \left(\frac{\partial w_0}{\partial x} \right)^2 \right] + A_{22} \left[\frac{\partial v_0}{\partial y} + \frac{1}{2} \left(\frac{\partial w_0}{\partial y} \right)^2 \right] \right. \right. \\
& + A_{26} \left[\frac{\partial u_0}{\partial y} + \frac{\partial v_0}{\partial x} + \frac{\partial w_0}{\partial x} \frac{\partial w_0}{\partial y} \right] + B_{12} \frac{\partial \phi_x}{\partial x} + B_{22} \frac{\partial \phi_y}{\partial y} + B_{26} \left(\frac{\partial \phi_x}{\partial y} + \frac{\partial \phi_y}{\partial x} \right) \left. \right\} \\
& + \frac{\partial w_0}{\partial x} \left\{ A_{16} \left[\frac{\partial u_0}{\partial x} + \frac{1}{2} \left(\frac{\partial w_0}{\partial x} \right)^2 \right] + A_{26} \left[\frac{\partial v_0}{\partial y} + \frac{1}{2} \left(\frac{\partial w_0}{\partial y} \right)^2 \right] \right. \\
& + A_{66} \left[\frac{\partial u_0}{\partial y} + \frac{\partial v_0}{\partial x} + \frac{\partial w_0}{\partial x} \frac{\partial w_0}{\partial y} \right] + B_{16} \frac{\partial \phi_x}{\partial x} + B_{26} \frac{\partial \phi_y}{\partial y} + B_{66} \left(\frac{\partial \phi_x}{\partial y} + \frac{\partial \phi_y}{\partial x} \right) \left. \right\} \\
& - \left[\frac{\partial \delta w_0}{\partial x} \left(N_{xx}^T \frac{\partial w_0}{\partial x} + N_{xy}^T \frac{\partial w_0}{\partial y} \right) + \frac{\partial \delta w_0}{\partial y} \left(N_{xy}^T \frac{\partial w_0}{\partial x} + N_{yy}^T \frac{\partial w_0}{\partial y} \right) \right] \\
& - \delta w_0 q \Big\} dx dy - \oint_{\Gamma^e} V_n \delta w_0 ds + \int_{\Omega^e} I_0 \frac{\partial^2 w_0}{\partial t^2} \delta w_0 dx dy \quad (10.3.9c)
\end{aligned}$$

$$\begin{aligned}
0 = & \int_{\Omega^e} \left(\frac{\partial \delta \phi_x}{\partial x} \left\{ B_{11} \left[\frac{\partial u_0}{\partial x} + \frac{1}{2} \left(\frac{\partial w_0}{\partial x} \right)^2 \right] + B_{12} \left[\frac{\partial v_0}{\partial y} + \frac{1}{2} \left(\frac{\partial w_0}{\partial y} \right)^2 \right] \right. \right. \\
& + B_{16} \left[\frac{\partial u_0}{\partial y} + \frac{\partial v_0}{\partial x} + \frac{\partial w_0}{\partial x} \frac{\partial w_0}{\partial y} \right] + D_{11} \frac{\partial \phi_x}{\partial x} + D_{12} \frac{\partial \phi_y}{\partial y} + D_{16} \left(\frac{\partial \phi_x}{\partial y} + \frac{\partial \phi_y}{\partial x} \right) \left. \right\} \\
& + \frac{\partial \delta \phi_x}{\partial y} \left\{ B_{16} \left[\frac{\partial u_0}{\partial x} + \frac{1}{2} \left(\frac{\partial w_0}{\partial x} \right)^2 \right] + B_{26} \left[\frac{\partial v_0}{\partial y} + \frac{1}{2} \left(\frac{\partial w_0}{\partial y} \right)^2 \right] \right. \\
& + B_{66} \left[\frac{\partial u_0}{\partial y} + \frac{\partial v_0}{\partial x} + \frac{\partial w_0}{\partial x} \frac{\partial w_0}{\partial y} \right] + D_{16} \frac{\partial \phi_x}{\partial x} + D_{26} \frac{\partial \phi_y}{\partial y} + D_{66} \left(\frac{\partial \phi_x}{\partial y} + \frac{\partial \phi_y}{\partial x} \right) \left. \right\} \\
& + K_s \delta \phi_x \left[A_{55} \left(\phi_x + \frac{\partial w_0}{\partial x} \right) + A_{45} \left(\phi_y + \frac{\partial w_0}{\partial y} \right) \right] \Big) dx dy \\
& - \int_{\Omega^e} \left(\frac{\partial \delta \phi_x}{\partial x} M_{xx}^T + \frac{\partial \delta \phi_x}{\partial y} M_{xy}^T \right) dx dy - \oint_{\Gamma^e} M_n \delta \phi_n ds \\
& + \int_{\Omega^e} \left(I_2 \frac{\partial^2 \phi_x}{\partial t^2} + I_1 \frac{\partial^2 u_0}{\partial t^2} \right) \delta \phi_x dx dy \quad (10.3.9d)
\end{aligned}$$

$$\begin{aligned}
0 = & \int_{\Omega^e} \left(\frac{\partial \delta \phi_y}{\partial y} \left\{ B_{12} \left[\frac{\partial u_0}{\partial x} + \frac{1}{2} \left(\frac{\partial w_0}{\partial x} \right)^2 \right] + B_{22} \left[\frac{\partial v_0}{\partial y} + \frac{1}{2} \left(\frac{\partial w_0}{\partial y} \right)^2 \right] \right. \right. \\
& + B_{26} \left[\frac{\partial u_0}{\partial y} + \frac{\partial v_0}{\partial x} + \frac{\partial w_0}{\partial x} \frac{\partial w_0}{\partial y} \right] + D_{12} \frac{\partial \phi_x}{\partial x} + D_{22} \frac{\partial \phi_y}{\partial y} + D_{26} \left(\frac{\partial \phi_x}{\partial y} + \frac{\partial \phi_y}{\partial x} \right) \left. \right\} \\
& + \frac{\partial \delta \phi_y}{\partial x} \left\{ B_{16} \left[\frac{\partial u_0}{\partial x} + \frac{1}{2} \left(\frac{\partial w_0}{\partial x} \right)^2 \right] + B_{26} \left[\frac{\partial v_0}{\partial y} + \frac{1}{2} \left(\frac{\partial w_0}{\partial y} \right)^2 \right] \right. \\
& + B_{66} \left[\frac{\partial u_0}{\partial y} + \frac{\partial v_0}{\partial x} + \frac{\partial w_0}{\partial x} \frac{\partial w_0}{\partial y} \right] + D_{16} \frac{\partial \phi_x}{\partial x} + D_{26} \frac{\partial \phi_y}{\partial y} + D_{66} \left(\frac{\partial \phi_x}{\partial y} + \frac{\partial \phi_y}{\partial x} \right) \left. \right\} \\
& + K_s \delta \phi_y \left[A_{45} \left(\phi_x + \frac{\partial w_0}{\partial x} \right) + A_{44} \left(\phi_y + \frac{\partial w_0}{\partial y} \right) \right] \Big) dx dy \\
& - \int_{\Omega^e} \left(\frac{\partial \delta \phi_y}{\partial x} M_{xy}^T + \frac{\partial \delta \phi_y}{\partial y} M_{yy}^T \right) dx dy - \oint_{\Gamma^e} M_s \delta \phi_s ds
\end{aligned}$$

$$+ \int_{\Omega^e} \left(I_2 \frac{\partial^2 \phi_y}{\partial t^2} + I_1 \frac{\partial^2 v_0}{\partial t^2} \right) \delta \phi_y \, dx dy \quad (10.3.9e)$$

where the secondary variables of the formulation as

$$N_n \equiv N_{xx}n_x + N_{xy}n_y, \quad N_s \equiv N_{xy}n_x + N_{yy}n_y \quad (10.3.10a)$$

$$M_n \equiv M_{xx}n_x + M_{xy}n_y, \quad M_s \equiv M_{xy}n_x + M_{yy}n_y \quad (10.3.10b)$$

$$\begin{aligned} V_n &\equiv \left(Q_x + N_{xx} \frac{\partial w_0}{\partial x} + N_{xy} \frac{\partial w_0}{\partial y} \right) n_x \\ &+ \left(Q_y + N_{xy} \frac{\partial w_0}{\partial x} + N_{yy} \frac{\partial w_0}{\partial y} \right) n_y \end{aligned} \quad (10.3.10c)$$

10.3.3 Finite Element Model

The virtual work statements in Eqs. (10.3.9a-e) contain at the most only the first derivatives of the dependent variables ($u_0, v_0, w_0, \phi_x, \phi_y$). Therefore, they can all be approximated using the Lagrange interpolation functions. In principle, (u_0, v_0) , w_0 , and (ϕ_x, ϕ_y) can be approximated with differing degrees of functions. Let

$$u_0(x, y) = \sum_{j=1}^m u_j \psi_j^{(1)}(x, y), \quad v_0(x, y) = \sum_{j=1}^m v_j \psi_j^{(1)}(x, y) \quad (10.3.11)$$

$$w_0(x, y) = \sum_{j=1}^n w_j \psi_j^{(2)}(x, y) \quad (10.3.12)$$

$$\phi_x(x, y) = \sum_{j=1}^p S_j^1 \psi_j^{(3)}(x, y), \quad \phi_y(x, y) = \sum_{j=1}^p S_j^2 \psi_j^{(3)}(x, y) \quad (10.3.13)$$

where $\psi_j^{(\alpha)}$ ($\alpha = 1, 2, 3$) are Lagrange interpolation functions. One can use linear, quadratic, or higher-order interpolations of these variables.

Substituting Eqs. (10.3.11)-(10.3.13) for $(u_0, v_0, w_0, \phi_x, \phi_y)$ into Eqs. (10.3.9a-e), we obtain the following finite element model:

$$\begin{aligned} \left\{ \begin{array}{l} \{F^1\} \\ \{F^2\} \\ \{F^3\} \\ \{F^4\} \\ \{F^5\} \end{array} \right\} + \left\{ \begin{array}{l} \{F^{1T}\} \\ \{F^{2T}\} \\ \{0\} \\ \{F^{4T}\} \\ \{F^{5T}\} \end{array} \right\} &= \left[\begin{array}{ccccc} [K^{11}] & [K^{12}] & [K^{13}] & [K^{14}] & [K^{15}] \\ [K^{21}] & [K^{22}] & [K^{23}] & [K^{24}] & [K^{25}] \\ [K^{31}] & [K^{32}] & [K^{33}] & [K^{34}] & [K^{35}] \\ [K^{41}] & [K^{42}] & [K^{43}] & [K^{44}] & [K^{45}] \\ [K^{51}] & [K^{52}] & [K^{53}] & [K^{54}] & [K^{55}] \end{array} \right] \left\{ \begin{array}{l} \{u^e\} \\ \{v^e\} \\ \{w^e\} \\ \{S^1\} \\ \{S^2\} \end{array} \right\} \\ &+ \left[\begin{array}{ccccc} [M^{11}] & [0] & [0] & [M^{14}] & [0] \\ [0] & [M^{22}] & [0] & [0] & [M^{25}] \\ [0] & [0] & [M^{33}] & [0] & [0] \\ [M^{14}]^T & [0] & [0] & [M^{44}] & [0] \\ [0] & [M^{25}]^T & [0] & [0] & [M^{55}] \end{array} \right] \left\{ \begin{array}{l} \{\ddot{u}^e\} \\ \{\ddot{v}^e\} \\ \{\ddot{w}^e\} \\ \{\ddot{S}^1\} \\ \{\ddot{S}^2\} \end{array} \right\} \end{aligned} \quad (10.3.14)$$

or, in compact matrix form

$$[K^e]\{\Delta^e\} + [M^e]\{\ddot{\Delta}^e\} = \{F^e\} \quad (10.3.15)$$

where the coefficients of the submatrices $[K^{\alpha\beta}]$, $[M^{\alpha\beta}]$ and vectors $\{F^\alpha\}$ and $\{F^{\alpha T}\}$ are defined for ($\alpha, \beta = 1, 2, 3, 4, 5$) by the expressions

$$\begin{aligned}
 K_{ij}^{11} &= \int_{\Omega^e} \left[A_{11} \frac{\partial \psi_i^{(1)}}{\partial x} \frac{\partial \psi_j^{(1)}}{\partial x} + A_{66} \frac{\partial \psi_i^{(1)}}{\partial y} \frac{\partial \psi_j^{(1)}}{\partial y} \right. \\
 &\quad \left. + A_{16} \left(\frac{\partial \psi_i^{(1)}}{\partial x} \frac{\partial \psi_j^{(1)}}{\partial y} + \frac{\partial \psi_i^{(1)}}{\partial y} \frac{\partial \psi_j^{(1)}}{\partial x} \right) \right] dx dy \\
 K_{ij}^{12} &= \int_{\Omega^e} \left[A_{12} \frac{\partial \psi_i^{(1)}}{\partial x} \frac{\partial \psi_j^{(1)}}{\partial y} + A_{66} \frac{\partial \psi_i^{(1)}}{\partial y} \frac{\partial \psi_j^{(1)}}{\partial x} + A_{26} \frac{\partial \psi_i^{(1)}}{\partial y} \frac{\partial \psi_j^{(1)}}{\partial y} \right. \\
 &\quad \left. + A_{16} \frac{\partial \psi_i^{(1)}}{\partial x} \frac{\partial \psi_j^{(1)}}{\partial x} \right] dx dy = K_{ji}^{21} \\
 K_{ij}^{13} &= \frac{1}{2} \int_{\Omega^e} \left\{ \frac{\partial \psi_i^{(1)}}{\partial x} \left[A_{11} \frac{\partial w_0}{\partial x} \frac{\partial \psi_j^{(2)}}{\partial x} + A_{12} \frac{\partial w_0}{\partial y} \frac{\partial \psi_j^{(2)}}{\partial y} \right. \right. \\
 &\quad \left. + A_{16} \left(\frac{\partial w_0}{\partial x} \frac{\partial \psi_j^{(2)}}{\partial y} + \frac{\partial w_0}{\partial y} \frac{\partial \psi_j^{(2)}}{\partial x} \right) \right] \\
 &\quad \left. + \frac{\partial \psi_i^{(1)}}{\partial y} \left[A_{16} \frac{\partial w_0}{\partial x} \frac{\partial \psi_j^{(2)}}{\partial x} + A_{26} \frac{\partial w_0}{\partial y} \frac{\partial \psi_j^{(2)}}{\partial y} \right. \right. \\
 &\quad \left. + A_{66} \left(\frac{\partial w_0}{\partial x} \frac{\partial \psi_j^{(2)}}{\partial y} + \frac{\partial w_0}{\partial y} \frac{\partial \psi_j^{(2)}}{\partial x} \right) \right] \right\} dx dy \\
 K_{ij}^{14} &= \int_{\Omega^e} \left[\frac{\partial \psi_i^{(1)}}{\partial x} \left(B_{11} \frac{\partial \psi_j^{(3)}}{\partial x} + B_{16} \frac{\partial \psi_j^{(3)}}{\partial y} \right) \right. \\
 &\quad \left. + \frac{\partial \psi_i^{(1)}}{\partial y} \left(B_{16} \frac{\partial \psi_j^{(3)}}{\partial x} + B_{66} \frac{\partial \psi_j^{(3)}}{\partial y} \right) \right] dx dy = K_{ji}^{41} \\
 K_{ij}^{15} &= \int_{\Omega^e} \left[\frac{\partial \psi_i^{(1)}}{\partial x} \left(B_{16} \frac{\partial \psi_j^{(3)}}{\partial x} + B_{12} \frac{\partial \psi_j^{(3)}}{\partial y} \right) \right. \\
 &\quad \left. + \frac{\partial \psi_i^{(1)}}{\partial y} \left(B_{66} \frac{\partial \psi_j^{(3)}}{\partial x} + B_{26} \frac{\partial \psi_j^{(3)}}{\partial y} \right) \right] dx dy = K_{ji}^{51} \\
 K_{ij}^{22} &= \int_{\Omega^e} \left[A_{22} \frac{\partial \psi_i^{(1)}}{\partial y} \frac{\partial \psi_j^{(1)}}{\partial y} + A_{66} \frac{\partial \psi_i^{(1)}}{\partial x} \frac{\partial \psi_j^{(1)}}{\partial x} \right. \\
 &\quad \left. + A_{26} \left(\frac{\partial \psi_i^{(1)}}{\partial x} \frac{\partial \psi_j^{(1)}}{\partial y} + \frac{\partial \psi_i^{(1)}}{\partial y} \frac{\partial \psi_j^{(1)}}{\partial x} \right) \right] dx dy \\
 K_{ij}^{23} &= \frac{1}{2} \int_{\Omega^e} \left\{ \frac{\partial \psi_i^{(1)}}{\partial y} \left[A_{12} \frac{\partial w_0}{\partial x} \frac{\partial \psi_j^{(2)}}{\partial x} + A_{22} \frac{\partial w_0}{\partial y} \frac{\partial \psi_j^{(2)}}{\partial y} \right. \right.
 \end{aligned}$$

$$\begin{aligned}
& + A_{26} \left(\frac{\partial w_0}{\partial x} \frac{\partial \psi_j^{(2)}}{\partial y} + \frac{\partial w_0}{\partial y} \frac{\partial \psi_j^{(2)}}{\partial x} \right) \Big] \\
& + \frac{\partial \psi_i^{(1)}}{\partial x} \left[A_{16} \frac{\partial w_0}{\partial x} \frac{\partial \psi_j^{(2)}}{\partial x} + A_{26} \frac{\partial w_0}{\partial y} \frac{\partial \psi_j^{(2)}}{\partial y} \right. \\
& \left. + A_{66} \left(\frac{\partial w_0}{\partial x} \frac{\partial \psi_j^{(2)}}{\partial y} + \frac{\partial w_0}{\partial y} \frac{\partial \psi_j^{(2)}}{\partial x} \right) \right] \Big\} dx dy \\
K_{ij}^{24} &= \int_{\Omega^e} \left[\frac{\partial \psi_i^{(1)}}{\partial y} \left(B_{12} \frac{\partial \psi_j^{(3)}}{\partial x} + B_{26} \frac{\partial \psi_j^{(3)}}{\partial y} \right) \right. \\
& \left. + \frac{\partial \psi_i^{(1)}}{\partial x} \left(B_{16} \frac{\partial \psi_j^{(3)}}{\partial x} + B_{66} \frac{\partial \psi_j^{(3)}}{\partial y} \right) \right] dx dy = K_{ji}^{42} \\
K_{ij}^{25} &= \int_{\Omega^e} \left[\frac{\partial \psi_i^{(1)}}{\partial y} \left(B_{26} \frac{\partial \psi_j^{(3)}}{\partial x} + B_{22} \frac{\partial \psi_j^{(3)}}{\partial y} \right) \right. \\
& \left. + \frac{\partial \psi_i^{(1)}}{\partial x} \left(B_{66} \frac{\partial \psi_j^{(3)}}{\partial x} + B_{26} \frac{\partial \psi_j^{(3)}}{\partial y} \right) \right] dx dy = K_{ji}^{52} \\
K_{ij}^{31} &= \int_{\Omega^e} \left\{ \frac{\partial \psi_j^{(2)}}{\partial x} \left[A_{11} \frac{\partial w_0}{\partial x} \frac{\partial \psi_i^{(1)}}{\partial x} + A_{12} \frac{\partial w_0}{\partial y} \frac{\partial \psi_i^{(1)}}{\partial y} \right. \right. \\
& \left. + A_{16} \left(\frac{\partial w_0}{\partial x} \frac{\partial \psi_i^{(1)}}{\partial y} + \frac{\partial w_0}{\partial y} \frac{\partial \psi_i^{(1)}}{\partial x} \right) \right] \\
& + \frac{\partial \psi_j^{(2)}}{\partial y} \left[A_{16} \frac{\partial w_0}{\partial x} \frac{\partial \psi_i^{(1)}}{\partial x} + A_{26} \frac{\partial w_0}{\partial y} \frac{\partial \psi_i^{(1)}}{\partial y} \right. \\
& \left. + A_{66} \left(\frac{\partial w_0}{\partial x} \frac{\partial \psi_i^{(1)}}{\partial y} + \frac{\partial w_0}{\partial y} \frac{\partial \psi_i^{(1)}}{\partial x} \right) \right] \Big\} dx dy \\
K_{ij}^{32} &= \int_{\Omega^e} \left\{ \frac{\partial \psi_j^{(2)}}{\partial y} \left[A_{12} \frac{\partial w_0}{\partial x} \frac{\partial \psi_i^{(1)}}{\partial x} + A_{22} \frac{\partial w_0}{\partial y} \frac{\partial \psi_i^{(1)}}{\partial y} \right. \right. \\
& \left. + A_{26} \left(\frac{\partial w_0}{\partial x} \frac{\partial \psi_i^{(1)}}{\partial y} + \frac{\partial w_0}{\partial y} \frac{\partial \psi_i^{(1)}}{\partial x} \right) \right] \\
& + \frac{\partial \psi_j^{(2)}}{\partial x} \left[A_{16} \frac{\partial w_0}{\partial x} \frac{\partial \psi_i^{(1)}}{\partial x} + A_{26} \frac{\partial w_0}{\partial y} \frac{\partial \psi_i^{(1)}}{\partial y} \right. \\
& \left. + A_{66} \left(\frac{\partial w_0}{\partial x} \frac{\partial \psi_i^{(1)}}{\partial y} + \frac{\partial w_0}{\partial y} \frac{\partial \psi_i^{(1)}}{\partial x} \right) \right] \Big\} dx dy \\
K_{ij}^{33} &= K_s \int_{\Omega^e} \left[\frac{\partial \psi_i^{(2)}}{\partial x} \left(A_{55} \frac{\partial \psi_j^{(2)}}{\partial x} + A_{45} \frac{\partial \psi_j^{(2)}}{\partial y} \right) \right]
\end{aligned}$$

$$\begin{aligned}
& + \frac{\partial \psi_i^{(2)}}{\partial y} \left(A_{45} \frac{\partial \psi_j^{(2)}}{\partial x} + A_{44} \frac{\partial \psi_j^{(2)}}{\partial y} \right) \Big] dx dy \\
& + \frac{1}{2} \int_{\Omega^e} \left\{ \left[A_{11} \left(\frac{\partial w_0}{\partial x} \right)^2 + A_{12} \left(\frac{\partial w_0}{\partial y} \right)^2 + 2A_{16} \frac{\partial w_0}{\partial x} \frac{\partial w_0}{\partial y} \right] \frac{\partial \psi_i^{(2)}}{\partial x} \frac{\partial \psi_j^{(2)}}{\partial x} \right. \\
& + \left[A_{16} \left(\frac{\partial w_0}{\partial x} \right)^2 + A_{26} \left(\frac{\partial w_0}{\partial y} \right)^2 + 2A_{66} \frac{\partial w_0}{\partial x} \frac{\partial w_0}{\partial y} \right] \\
& \quad \left(\frac{\partial \psi_i^{(2)}}{\partial x} \frac{\partial \psi_j^{(2)}}{\partial y} + \frac{\partial \psi_j^{(2)}}{\partial x} \frac{\partial \psi_i^{(2)}}{\partial y} \right) \\
& \left. + \left[A_{12} \left(\frac{\partial w_0}{\partial x} \right)^2 + A_{22} \left(\frac{\partial w_0}{\partial y} \right)^2 + 2A_{26} \frac{\partial w_0}{\partial x} \frac{\partial w_0}{\partial y} \right] \frac{\partial \psi_i^{(2)}}{\partial y} \frac{\partial \psi_j^{(2)}}{\partial y} \right\} dx dy \\
K_{ij}^{34} &= K_s \int_{\Omega^e} \left(A_{55} \frac{\partial \psi_i^{(2)}}{\partial x} \psi_j^{(3)} + A_{45} \frac{\partial \psi_i^{(2)}}{\partial y} \psi_j^{(3)} \right) dx dy \\
& + \int_{\Omega^e} \frac{\partial \psi_i^{(2)}}{\partial x} \left[\frac{\partial w_0}{\partial x} \left(B_{11} \frac{\partial \psi_j^{(3)}}{\partial x} + B_{16} \frac{\partial \psi_j^{(3)}}{\partial y} \right) \right. \\
& \quad \left. + \frac{\partial w_0}{\partial y} \left(B_{16} \frac{\partial \psi_j^{(3)}}{\partial x} + B_{66} \frac{\partial \psi_j^{(3)}}{\partial y} \right) \right] \\
& + \frac{\partial \psi_i^{(2)}}{\partial y} \left[\frac{\partial w_0}{\partial y} \left(B_{12} \frac{\partial \psi_j^{(3)}}{\partial x} + B_{26} \frac{\partial \psi_j^{(3)}}{\partial y} \right) \right. \\
& \quad \left. + \frac{\partial w_0}{\partial x} \left(B_{16} \frac{\partial \psi_j^{(3)}}{\partial x} + B_{66} \frac{\partial \psi_j^{(3)}}{\partial y} \right) \right] \Big\} dx dy \\
K_{ij}^{35} &= K_s \int_{\Omega^e} \left(A_{45} \frac{\partial \psi_i^{(2)}}{\partial x} \psi_j^{(3)} + A_{44} \frac{\partial \psi_i^{(2)}}{\partial y} \psi_j^{(3)} \right) dx dy \\
& + \int_{\Omega^e} \frac{\partial \psi_i^{(2)}}{\partial x} \left[\frac{\partial w_0}{\partial x} \left(B_{12} \frac{\partial \psi_j^{(3)}}{\partial y} + B_{16} \frac{\partial \psi_j^{(3)}}{\partial x} \right) \right. \\
& \quad \left. + \frac{\partial w_0}{\partial y} \left(B_{26} \frac{\partial \psi_j^{(3)}}{\partial y} + B_{66} \frac{\partial \psi_j^{(3)}}{\partial x} \right) \right] \\
& + \frac{\partial \psi_i^{(2)}}{\partial y} \left[\frac{\partial w_0}{\partial y} \left(B_{22} \frac{\partial \psi_j^{(3)}}{\partial y} + B_{26} \frac{\partial \psi_j^{(3)}}{\partial x} \right) \right. \\
& \quad \left. + \frac{\partial w_0}{\partial x} \left(B_{26} \frac{\partial \psi_j^{(3)}}{\partial y} + B_{66} \frac{\partial \psi_j^{(3)}}{\partial x} \right) \right] \Big\} dx dy \\
K_{ij}^{43} &= K_s \int_{\Omega^e} \left(A_{55} \frac{\partial \psi_j^{(2)}}{\partial x} \psi_i^{(3)} + A_{45} \frac{\partial \psi_j^{(2)}}{\partial y} \psi_i^{(3)} \right) dx dy
\end{aligned}$$

$$\begin{aligned}
& + \frac{1}{2} \int_{\Omega^e} \frac{\partial \psi_j^{(2)}}{\partial x} \left[\frac{\partial w_0}{\partial x} \left(B_{11} \frac{\partial \psi_i^{(3)}}{\partial x} + B_{16} \frac{\partial \psi_i^{(3)}}{\partial y} \right) \right. \\
& \quad \left. + \frac{\partial w_0}{\partial y} \left(B_{16} \frac{\partial \psi_i^{(3)}}{\partial x} + B_{66} \frac{\partial \psi_i^{(3)}}{\partial y} \right) \right] \\
& \quad + \frac{\partial \psi_j^{(2)}}{\partial y} \left[\frac{\partial w_0}{\partial y} \left(B_{12} \frac{\partial \psi_i^{(3)}}{\partial x} + B_{26} \frac{\partial \psi_i^{(3)}}{\partial y} \right) \right. \\
& \quad \left. + \frac{\partial w_0}{\partial x} \left(B_{16} \frac{\partial \psi_i^{(3)}}{\partial x} + B_{66} \frac{\partial \psi_i^{(3)}}{\partial y} \right) \right] \Big\} dx dy \\
K_{ij}^{44} &= \int_{\Omega^e} \left[\frac{\partial \psi_i^{(3)}}{\partial x} \left(D_{11} \frac{\partial \psi_j^{(3)}}{\partial x} + D_{16} \frac{\partial \psi_j^{(3)}}{\partial y} \right) \right. \\
& \quad \left. + \frac{\partial \psi_i^{(3)}}{\partial y} \left(D_{16} \frac{\partial \psi_j^{(3)}}{\partial x} + D_{66} \frac{\partial \psi_j^{(3)}}{\partial y} \right) + K_s A_{55} \psi_i^{(3)} \psi_j^{(3)} \right] dx dy \\
K_{ij}^{45} &= \int_{\Omega^e} \left[\frac{\partial \psi_i^{(3)}}{\partial x} \left(D_{16} \frac{\partial \psi_j^{(3)}}{\partial x} + D_{12} \frac{\partial \psi_j^{(3)}}{\partial y} \right) \right. \\
& \quad \left. + \frac{\partial \psi_i^{(3)}}{\partial y} \left(D_{66} \frac{\partial \psi_j^{(3)}}{\partial x} + D_{26} \frac{\partial \psi_j^{(3)}}{\partial y} \right) + K_s A_{45} \psi_i^{(3)} \psi_j^{(3)} \right] dx dy = K_{ji}^{54} \\
K_{ij}^{53} &= K_s \int_{\Omega^e} \left(A_{45} \frac{\partial \psi_j^{(2)}}{\partial x} \psi_i^{(3)} + A_{44} \frac{\partial \psi_j^{(2)}}{\partial y} \psi_i^{(3)} \right) dx dy \\
& \quad + \frac{1}{2} \int_{\Omega^e} \frac{\partial \psi_j^{(2)}}{\partial x} \left[\frac{\partial w_0}{\partial x} \left(B_{12} \frac{\partial \psi_i^{(3)}}{\partial y} + B_{16} \frac{\partial \psi_i^{(3)}}{\partial x} \right) \right. \\
& \quad \left. + \frac{\partial w_0}{\partial y} \left(B_{26} \frac{\partial \psi_i^{(3)}}{\partial y} + B_{66} \frac{\partial \psi_i^{(3)}}{\partial x} \right) \right] \\
& \quad + \frac{\partial \psi_j^{(2)}}{\partial y} \left[\frac{\partial w_0}{\partial y} \left(B_{22} \frac{\partial \psi_i^{(3)}}{\partial y} + B_{26} \frac{\partial \psi_i^{(3)}}{\partial x} \right) \right. \\
& \quad \left. + \frac{\partial w_0}{\partial x} \left(B_{26} \frac{\partial \psi_i^{(3)}}{\partial y} + B_{66} \frac{\partial \psi_i^{(3)}}{\partial x} \right) \right] \Big\} dx dy \\
K_{ij}^{55} &= \int_{\Omega^e} \left[\frac{\partial \psi_i^{(3)}}{\partial x} \left(D_{66} \frac{\partial \psi_j^{(3)}}{\partial x} + D_{26} \frac{\partial \psi_j^{(3)}}{\partial y} \right) \right. \\
& \quad \left. + \frac{\partial \psi_j^{(3)}}{\partial y} \left(D_{26} \frac{\partial \psi_i^{(3)}}{\partial x} + D_{22} \frac{\partial \psi_i^{(3)}}{\partial y} \right) + K_s A_{44} \psi_i^{(3)} \psi_j^{(3)} \right] dx dy \\
M_{ij}^{11} &= \int_{\Omega^e} I_0 \psi_i^{(1)} \psi_j^{(1)} dx dy, \quad M_{ij}^{14} = - \int_{\Omega^e} I_1 \psi_i^{(1)} \psi_j^{(3)} dx dy \\
M_{ij}^{22} &= \int_{\Omega^e} I_0 \psi_i^{(1)} \psi_j^{(1)} dx dy, \quad M_{ij}^{25} = - \int_{\Omega^e} I_1 \psi_i^{(1)} \psi_j^{(3)} dx dy
\end{aligned}$$

$$\begin{aligned}
M_{ij}^{33} &= \int_{\Omega^e} I_0 \psi_i^{(2)} \psi_j^{(2)} \, dx dy \\
M_{ij}^{44} &= \int_{\Omega^e} I_2 \psi_i^{(3)} \psi_j^{(3)} \, dx dy, \quad M_{ij}^{55} = - \int_{\Omega^e} I_2 \psi_i^{(3)} \psi_j^{(3)} \, dx dy \\
F_i^1 &= \oint_{\Gamma^e} N_n \psi_i^{(1)} \, ds, \quad F_i^2 = \oint_{\Gamma^e} N_s \psi_i^{(1)} \, ds \\
F_i^3 &= \int_{\Omega^e} q \psi_i^{(2)} \, dx dy + \oint_{\Gamma^e} V_n \psi_i^{(2)} \, ds, \\
F_i^4 &= \oint_{\Gamma^e} M_n \psi_i^{(3)} \, ds, \quad F_i^5 = \oint_{\Gamma^e} M_s \psi_i^{(3)} \, ds \\
F_i^{1T} &= \int_{\Omega^e} \left(N_{xx}^T \frac{\partial \psi_i^{(1)}}{\partial x} + N_{xy}^T \frac{\partial \psi_i^{(1)}}{\partial y} \right) \, dx dy \\
F_i^{2T} &= \int_{\Omega^e} \left(N_{xy}^T \frac{\partial \psi_i^{(1)}}{\partial x} + N_{yy}^T \frac{\partial \psi_i^{(1)}}{\partial y} \right) \, dx dy \\
F_i^{3T} &= \int_{\Omega^e} \left[\frac{\partial \psi_i^{(2)}}{\partial x} \left(N_{xx}^T \frac{\partial w_0}{\partial x} + N_{xy}^T \frac{\partial w_0}{\partial y} \right) + \frac{\partial \psi_i^{(2)}}{\partial y} \left(N_{xy}^T \frac{\partial w_0}{\partial x} + N_{yy}^T \frac{\partial w_0}{\partial y} \right) \right] \, dx dy \\
F_i^{4T} &= \int_{\Omega^e} \left(\frac{\partial \psi_i^{(3)}}{\partial x} M_{xx}^T + \frac{\partial \psi_i^{(3)}}{\partial y} M_{xy}^T \right) \, dx dy \\
F_i^{5T} &= \int_{\Omega^e} \left(\frac{\partial \psi_i^{(3)}}{\partial x} M_{xy}^T + \frac{\partial \psi_i^{(3)}}{\partial y} M_{yy}^T \right) \, dx dy
\end{aligned} \tag{10.3.16}$$

where N_{xx}^T , N_{yy}^T and N_{xy}^T are thermal forces and M_{xx}^T , M_{yy}^T and M_{xy}^T are the thermal moments. When the bilinear rectangular element is used for all generalized displacements (u_0 , v_0 , w_0 , ϕ_x , ϕ_y), the element stiffness matrices are of the order 20×20 , and for the nine-node quadratic element they are 45×45 (see Figure 9.3.1).

10.4 Time Approximation and the Newton–Raphson Method

10.4.1 Time Approximations

Here we discuss the solution of equations of the form in (10.2.13) and (10.3.15). Equation (10.3.15), when generalized to include damping (structural or otherwise), has the form [32]

$$[M]\{\ddot{\Delta}\} + [C]\{\dot{\Delta}\} + [K]\{\Delta\} = \{F\} \tag{10.4.1}$$

The fully discretized equations using Newmark's scheme are

$$[\hat{K}(\{\Delta\}_{s+1})]\{\Delta\}_{s+1} = \{\hat{F}\}_{s,s+1} \tag{10.4.2}$$

where

$$\begin{aligned}
\hat{K}(\{\Delta\}_{s+1}) &= [K(\{\Delta\}_{s+1})] + a_3[M]_{s+1} + a_6[C]_{s+1} \\
\{\hat{F}\}_{s,s+1} &= \{F\}_{s+1} + [M]_{s+1}\{A\}_s + [C]_{s+1}\{B\}_s \\
\{A\}_s &= a_3\{\Delta\}_s + a_4\{\dot{\Delta}\}_s + a_5\{\ddot{\Delta}\}_s \\
\{B\}_s &= a_6\{\Delta\}_s + a_7\{\dot{\Delta}\}_s + a_8\{\ddot{\Delta}\}_s
\end{aligned} \tag{10.4.3a}$$

and a_i are defined as ($\gamma = 2\beta$)

$$\begin{aligned} a_1 &= \alpha\Delta t, & a_2 &= (1 - \alpha)\Delta t, & a_3 &= \frac{1}{\beta(\Delta t)^2}, & a_4 &= a_3\Delta t, \\ a_5 &= \frac{1}{\gamma} - 1, & a_6 &= \frac{\alpha}{\beta\Delta t}, & a_7 &= \frac{\alpha}{\beta} - 1, & a_8 &= \Delta t \left(\frac{\alpha}{\gamma} - 1 \right) \end{aligned} \quad (10.4.3b)$$

In Eqs. (2.4.2) and (2.4.3a), the notation $(\cdot)_s$ indicates that the enclosed quantity is evaluated at time t_s .

The new velocity vector $\{\dot{\Delta}\}_{s+1}$ and acceleration vector $\{\ddot{\Delta}\}_{s+1}$ at the end of each time step are computed using the equations

$$\{\ddot{\Delta}\}_{s+1} = a_3(\{\Delta\}_{s+1} - \{\Delta\}_s) - a_4\{\dot{\Delta}\} - a_5\{\ddot{\Delta}\}_s \quad (10.4.4a)$$

$$\{\dot{\Delta}\}_{s+1} = \{\dot{\Delta}\}_s + a_2\{\ddot{\Delta}\}_s + a_1\{\ddot{\Delta}\}_{s+1} \quad (10.4.4b)$$

10.4.2 The Newton–Raphson Method

Equation (10.4.2) represents a system of nonlinear algebraic equations at time t_{s+1} . These equations must be solved using an iterative method. Here we discuss the Newton–Raphson iteration method, which is based on Taylor's series (see [32, 43–47]).

The Newton–Raphson iterative method is based on Taylor's series expansion of the nonlinear algebraic equation (10.4.2) about the known solution. Suppose that Eq. (10.4.2) is to be solved for the generalized displacement vector $\{\Delta\}_{s+1}$ at time t_{s+1} . Due to the fact that the coefficient matrix $[\hat{K}(\{\Delta\}_{s+1})]$ depends on the unknown solution, the equations are solved iteratively. To formulate the equations to be solved at the $r + 1$ st iteration by the Newton–Raphson method, we assume that the solution at the r th iteration, $\{\Delta\}_{s+1}^r$, is known. Then define

$$\{R\}(\{\Delta\}_{s+1}) \equiv [\hat{K}(\{\Delta\}_{s+1})]\{\Delta\}_{s+1} - \{\hat{F}\}_{s,s+1} = 0 \quad (10.4.5)$$

where $\{R\}$ is called the *residual*, which is a nonlinear function of the unknown solution $\{\Delta\}_{s+1}$. Expanding $\{R\}$ in Taylor's series about $\{\Delta\}_{s+1}^r$, we obtain

$$\begin{aligned} \{0\} &= \{R\}(\{\Delta\}_{s+1}) = \{R\}_{s+1}^r + \left[\frac{\partial\{R\}}{\partial\{\Delta\}} \right]_{s+1}^r \left(\{\Delta\}_{s+1}^{r+1} - \{\Delta\}_{s+1}^r \right) \\ &\quad + \frac{1}{2!} \left[\frac{\partial^2\{R\}}{\partial\{\Delta\}\partial\{\Delta\}} \right]_{s+1}^r \left(\{\Delta\}_{s+1}^{r+1} - \{\Delta\}_{s+1}^r \right)^2 + \dots \end{aligned} \quad (10.4.6a)$$

$$0 = \{R\}_{s+1}^r + \left([\hat{K}^T(\{\Delta\}_{s+1}^r)] \right) \{\delta\Delta\} + O(\{\delta\Delta\}^2) \quad (10.4.6b)$$

where $O(\cdot)$ denotes the higher-order terms in $\{\delta\Delta\}$, and $[\hat{K}^T]$ is known as the *tangent stiffness matrix* (or geometric stiffness matrix)

$$[\hat{K}^T(\{\Delta\}_{s+1}^r)] \equiv \left[\frac{\partial\{R\}}{\partial\{\Delta\}} \right]_{s+1}^r, \quad \{R\}_{s+1}^r = [\hat{K}(\{\Delta\}_{s+1}^r)]\{\Delta\}_{s+1}^r - \{\hat{F}\}_{s,s+1} \quad (10.4.7)$$

Equations (10.4.5)–(10.4.7) are also applicable to a typical finite element. In other words, the coefficient matrix in Eq. (10.4.7) can be assembled after the element tangent stiffness matrices and force residual vectors are computed. The assembled equations are then solved for the incremental displacement vector after imposing the boundary and initial conditions of the problem [see Eq. (10.4.6b)]

$$\{\delta\Delta\} = -[\hat{K}^T(\{\Delta\}_{s+1}^r)]^{-1}\{R\}_{s+1}^r \quad (10.4.8)$$

The total displacement vector is obtained from

$$\{\Delta\}_{s+1}^{r+1} = \{\Delta\}_{s+1}^r + \{\delta\Delta\} \quad (10.4.9)$$

Note that the element tangent stiffness matrix is evaluated using the latest known solution, while the residual vector contains contributions from the latest known solution in computing element $[\hat{K}(\{\Delta\}_{s+1}^r)]\{\Delta\}_{s+1}^r$ and previous time step solution in computing element $\{\hat{F}\}_{s,s+1}$. After assembly and imposition of the boundary conditions, the linearized system of equations are solved for $\{\delta\Delta\}$.

At the beginning of the iteration i.e., $r = 0$, we assume that $\{\Delta\}^0 = \{0\}$ so that the solution at the first iteration is the linear solution, because the nonlinear stiffness matrix reduces to the linear one. The iteration process is continued [i.e., Eq. (10.4.8) is solved in each iteration] until the difference between $\{\Delta\}_{s+1}^r$ and $\{\Delta\}_{s+1}^{r+1}$ reduces to a preselected error tolerance. The *error criterion* is of the form (for the sake of brevity the subscript ‘ $(s+1)$ ’ on the quantities is omitted)

$$\sqrt{\frac{\sum_{I=1}^N |\Delta_I^{r+1} - \Delta_I^r|^2}{\sum_{I=1}^N |\Delta_I^{r+1}|^2}} < \epsilon \quad (\text{say } 10^{-3}) \quad (10.4.10)$$

where N is the total number of nodal generalized displacements in the finite element mesh, and ϵ is the error tolerance. The velocity and acceleration vectors are updated using Eqs. (10.4.4a,b) only after convergence is reached for a given time step.

In the Newton–Raphson method the global tangent stiffness matrix and residual vector must be updated using the latest available solution $\{\Delta\}_{s+1}^r$ before Eq. (10.4.8) is solved. If the tangent stiffness matrix is kept constant for a preselected number of iterations but the residual vector is updated during each iteration, the method is known as the *modified Newton–Raphson method*. The approach often takes more iterations to obtain convergence. The Newton–Raphson method fails to trace the nonlinear equilibrium path through the limit points where the tangent matrix $[K_T]$ becomes singular and the iteration procedure diverges. Riks [44] and Wempner [47] suggested a procedure to predict the nonlinear equilibrium path through limit points. The method, known as the *Riks–Wempner method* provides the Newton–Raphson method and its modifications with a technique to control progress along the equilibrium path. The theoretical development of this method and its modification can be found in [32,43–46].

10.4.3 Tangent Stiffness Coefficients for CLPT

The Newton-Raphson iterative method involves solving equations of the form

$$\begin{bmatrix} [T^{11}] & [T^{12}] & [T^{13}] \\ [T^{21}] & [T^{22}] & [T^{23}] \\ [T^{31}] & [T^{32}] & [T^{33}] \end{bmatrix} \begin{Bmatrix} \{\delta\Delta^1\} \\ \{\delta\Delta^2\} \\ \{\delta\Delta^3\} \end{Bmatrix} = - \begin{Bmatrix} \{R^1\} \\ \{R^2\} \\ \{R^3\} \end{Bmatrix} \quad (10.4.11a)$$

where

$$\Delta_i^1 = u_i, \quad \Delta_i^2 = v_i, \quad \Delta_i^3 = \bar{\Delta}_i \quad (10.4.11b)$$

the coefficients of the submatrices $[T^{\alpha\beta}]$ are defined by

$$T_{ij}^{\alpha\beta} = \frac{\partial R_i^\alpha}{\partial \Delta_j^\beta} \quad (10.4.12)$$

the components of the residual vector $\{R^\alpha\}$ are

$$R_i^\alpha = \sum_{\gamma=1}^3 \sum_{k=1}^{n*} K_{ik}^{\alpha\gamma} \Delta_k^\gamma - F_i^\alpha \quad (10.4.13)$$

and $n*$ denotes n or m , depending on the nodal degree of freedom. Thus, we have

$$\begin{aligned} T_{ij}^{\alpha\beta} &= \frac{\partial}{\partial \Delta_j^\beta} \left(\sum_{\gamma=1}^3 \sum_{k=1}^{n*} K_{ik}^{\alpha\gamma} \Delta_k^\gamma - F_i^\alpha \right) \\ &= \sum_{\gamma=1}^3 \sum_{k=1}^{n*} \frac{\partial K_{ik}^{\alpha\gamma}}{\partial \Delta_j^\beta} \Delta_k^\gamma + K_{ij}^{\alpha\beta} \end{aligned} \quad (10.4.14)$$

The only coefficients that depend on the solution are K_{ij}^{13} , K_{ij}^{23} , K_{ij}^{31} , K_{ij}^{32} , and K_{ij}^{33} , and they are functions of only $\Delta_i^3 = \bar{\Delta}_i$. Hence, derivatives of all stiffness coefficients with respect to $\Delta^1 = u_j$ and $\Delta^2 = v_j$ are zero.

Thus, we have

$$\begin{aligned} T_{ij}^{11} &= \sum_{\gamma=1}^3 \sum_{k=1}^{n*} \frac{\partial K_{ik}^{1\gamma}}{\partial u_j} \Delta_k^\gamma + K_{ij}^{11} = K_{ij}^{11}, \quad T_{ij}^{12} = \sum_{\gamma=1}^3 \sum_{k=1}^{n*} \frac{\partial K_{ik}^{1\gamma}}{\partial v_j} \Delta_k^\gamma + K_{ij}^{12} = K_{ij}^{12} \\ T_{ij}^{21} &= \sum_{\gamma=1}^3 \sum_{k=1}^{n*} \frac{\partial K_{ik}^{2\gamma}}{\partial u_j} \Delta_k^\gamma + K_{ij}^{21} = K_{ij}^{21}, \quad T_{ij}^{22} = \sum_{\gamma=1}^3 \sum_{k=1}^{n*} \frac{\partial K_{ik}^{2\gamma}}{\partial v_j} \Delta_k^\gamma + K_{ij}^{22} = K_{ij}^{22} \\ T_{ij}^{31} &= \sum_{\gamma=1}^3 \sum_{k=1}^{n*} \frac{\partial K_{ik}^{3\gamma}}{\partial u_j} \Delta_k^\gamma + K_{ij}^{31} = K_{ij}^{31}, \quad T_{ij}^{32} = \sum_{\gamma=1}^3 \sum_{k=1}^{n*} \frac{\partial K_{ik}^{3\gamma}}{\partial v_j} \Delta_k^\gamma + K_{ij}^{32} = K_{ij}^{32} \\ T_{ij}^{13} &= \sum_{\gamma=1}^3 \sum_{k=1}^{n*} \frac{\partial K_{ik}^{1\gamma}}{\partial \bar{\Delta}_j^3} \Delta_k^\gamma + K_{ij}^{13} = \sum_{k=1}^n \frac{\partial K_{ik}^{13}}{\partial \bar{\Delta}_j^3} \bar{\Delta}_k^3 + K_{ij}^{13} \\ T_{ij}^{23} &= \sum_{\gamma=1}^3 \sum_{k=1}^{n*} \frac{\partial K_{ik}^{2\gamma}}{\partial \bar{\Delta}_j^3} \Delta_k^\gamma + K_{ij}^{23} = \sum_{k=1}^n \frac{\partial K_{ik}^{23}}{\partial \bar{\Delta}_j^3} \bar{\Delta}_k^3 + K_{ij}^{23} \\ T_{ij}^{33} &= \sum_{\gamma=1}^3 \sum_{k=1}^{n*} \frac{\partial K_{ik}^{3\gamma}}{\partial \bar{\Delta}_j^3} \Delta_k^\gamma - \frac{\partial F_i^{3T}}{\partial \bar{\Delta}_j^3} + K_{ij}^{33} \\ &= \sum_{k=1}^n \left(\frac{\partial K_{ik}^{31}}{\partial \bar{\Delta}_j^3} u_k + \frac{\partial K_{ik}^{32}}{\partial \bar{\Delta}_j^3} v_k + \frac{\partial K_{ik}^{33}}{\partial \bar{\Delta}_j^3} \bar{\Delta}_k^3 \right) - \frac{\partial F_i^{3T}}{\partial \bar{\Delta}_j^3} + K_{ij}^{33} \end{aligned} \quad (10.4.15)$$

Thus, we must compute the following derivatives of the element stiffness coefficients (only the nonzero parts are shown in the calculation):

$$\begin{aligned} \sum_{k=1}^n \frac{\partial K_{ik}^{13}}{\partial \bar{\Delta}_j^3} \bar{\Delta}_k^3 &= \frac{1}{2} \sum_{k=1}^n \bar{\Delta}_k^3 \frac{\partial}{\partial \bar{\Delta}_j^3} \left[\int_{\Omega^e} \left\{ \frac{\partial \psi_i^e}{\partial x} \left[A_{11} \frac{\partial w_0}{\partial x} \frac{\partial \varphi_k^e}{\partial x} + A_{12} \frac{\partial w_0}{\partial y} \frac{\partial \varphi_k^e}{\partial y} \right. \right. \right. \\ &\quad \left. \left. \left. + A_{16} \left(\frac{\partial w_0}{\partial x} \frac{\partial \varphi_k^e}{\partial y} + \frac{\partial w_0}{\partial y} \frac{\partial \varphi_k^e}{\partial x} \right) \right] \right. \\ &\quad \left. \left. + \frac{\partial \psi_i^e}{\partial y} \left[A_{16} \frac{\partial w_0}{\partial x} \frac{\partial \varphi_k^e}{\partial x} + A_{26} \frac{\partial w_0}{\partial y} \frac{\partial \varphi_k^e}{\partial y} \right. \right. \right. \\ &\quad \left. \left. \left. + A_{66} \left(\frac{\partial w_0}{\partial x} \frac{\partial \varphi_k^e}{\partial y} + \frac{\partial w_0}{\partial y} \frac{\partial \varphi_k^e}{\partial x} \right) \right] \right\} dx dy \right] \\ &= \frac{1}{2} \int_{\Omega^e} \left\{ \frac{\partial \psi_i^e}{\partial x} \left[A_{11} \frac{\partial w_0}{\partial x} \frac{\partial \varphi_j^e}{\partial x} + A_{12} \frac{\partial w_0}{\partial y} \frac{\partial \varphi_j^e}{\partial y} \right. \right. \\ &\quad \left. \left. + A_{16} \left(\frac{\partial w_0}{\partial x} \frac{\partial \varphi_j^e}{\partial y} + \frac{\partial w_0}{\partial y} \frac{\partial \varphi_j^e}{\partial x} \right) \right] \right. \\ &\quad \left. \left. + \frac{\partial \psi_i^e}{\partial y} \left[A_{16} \frac{\partial w_0}{\partial x} \frac{\partial \varphi_j^e}{\partial x} + A_{26} \frac{\partial w_0}{\partial y} \frac{\partial \varphi_j^e}{\partial y} \right. \right. \right. \\ &\quad \left. \left. \left. + A_{66} \left(\frac{\partial w_0}{\partial x} \frac{\partial \varphi_j^e}{\partial y} + \frac{\partial w_0}{\partial y} \frac{\partial \varphi_j^e}{\partial x} \right) \right] \right\} dx dy \quad (10.4.16) \end{aligned}$$

$$\begin{aligned} \sum_{k=1}^n \frac{\partial K_{ik}^{23}}{\partial \bar{\Delta}_j^3} \bar{\Delta}_k^3 &= \frac{1}{2} \sum_{k=1}^n \bar{\Delta}_k^3 \frac{\partial}{\partial \bar{\Delta}_j^3} \left[\int_{\Omega^e} \left\{ \frac{\partial \psi_i^e}{\partial y} \left[A_{12} \frac{\partial w_0}{\partial x} \frac{\partial \varphi_k^e}{\partial x} + A_{22} \frac{\partial w_0}{\partial y} \frac{\partial \varphi_k^e}{\partial y} \right. \right. \right. \\ &\quad \left. \left. \left. + A_{26} \left(\frac{\partial w_0}{\partial x} \frac{\partial \varphi_k^e}{\partial y} + \frac{\partial w_0}{\partial y} \frac{\partial \varphi_k^e}{\partial x} \right) \right] \right. \\ &\quad \left. \left. + \frac{\partial \psi_i^e}{\partial x} \left[A_{16} \frac{\partial w_0}{\partial x} \frac{\partial \varphi_k^e}{\partial x} + A_{26} \frac{\partial w_0}{\partial y} \frac{\partial \varphi_k^e}{\partial y} \right. \right. \right. \\ &\quad \left. \left. \left. + A_{66} \left(\frac{\partial w_0}{\partial x} \frac{\partial \varphi_k^e}{\partial y} + \frac{\partial w_0}{\partial y} \frac{\partial \varphi_k^e}{\partial x} \right) \right] \right\} dx dy \right] \\ &= \frac{1}{2} \int_{\Omega^e} \left\{ \frac{\partial \psi_i^e}{\partial y} \left[A_{12} \frac{\partial w_0}{\partial x} \frac{\partial \varphi_j^e}{\partial x} + A_{22} \frac{\partial w_0}{\partial y} \frac{\partial \varphi_j^e}{\partial y} \right. \right. \\ &\quad \left. \left. + A_{26} \left(\frac{\partial w_0}{\partial x} \frac{\partial \varphi_j^e}{\partial y} + \frac{\partial w_0}{\partial y} \frac{\partial \varphi_j^e}{\partial x} \right) \right] \right. \\ &\quad \left. \left. + \frac{\partial \psi_i^e}{\partial x} \left[A_{16} \frac{\partial w_0}{\partial x} \frac{\partial \varphi_j^e}{\partial x} + A_{26} \frac{\partial w_0}{\partial y} \frac{\partial \varphi_j^e}{\partial y} \right. \right. \right. \\ &\quad \left. \left. \left. + A_{66} \left(\frac{\partial w_0}{\partial x} \frac{\partial \varphi_j^e}{\partial y} + \frac{\partial w_0}{\partial y} \frac{\partial \varphi_j^e}{\partial x} \right) \right] \right\} dx dy \quad (10.4.17) \end{aligned}$$

$$\begin{aligned} \sum_{k=1}^n u_k \frac{\partial K_{ik}^{31}}{\partial \bar{\Delta}_j^3} &= \sum_{k=1}^n u_k \frac{\partial}{\partial \bar{\Delta}_j^3} \left[\int_{\Omega^e} \left\{ \frac{\partial \psi_k^e}{\partial x} \left[A_{11} \frac{\partial w_0}{\partial x} \frac{\partial \varphi_i^e}{\partial x} + A_{12} \frac{\partial w_0}{\partial y} \frac{\partial \varphi_i^e}{\partial y} \right. \right. \right. \\ &\quad \left. \left. \left. + A_{16} \left(\frac{\partial w_0}{\partial x} \frac{\partial \varphi_i^e}{\partial y} + \frac{\partial w_0}{\partial y} \frac{\partial \varphi_i^e}{\partial x} \right) \right] \right\} dx dy \right] \end{aligned}$$

$$\begin{aligned}
& + \frac{\partial \psi_k^e}{\partial y} \left[A_{16} \frac{\partial w_0}{\partial x} \frac{\partial \varphi_i^e}{\partial x} + A_{26} \frac{\partial w_0}{\partial y} \frac{\partial \varphi_i^e}{\partial y} \right. \\
& \quad \left. + A_{66} \left(\frac{\partial w_0}{\partial x} \frac{\partial \varphi_i^e}{\partial y} + \frac{\partial w_0}{\partial y} \frac{\partial \varphi_i^e}{\partial x} \right) \right] \} dx dy \\
= & \int_{\Omega^e} \left\{ \frac{\partial u}{\partial x} \left[A_{11} \frac{\partial \varphi_i^e}{\partial x} \frac{\partial \varphi_j^e}{\partial x} + A_{12} \frac{\partial \varphi_i^e}{\partial y} \frac{\partial \varphi_j^e}{\partial y} \right. \right. \\
& \quad \left. + A_{16} \left(\frac{\partial \varphi_i^e}{\partial y} \frac{\partial \varphi_j^e}{\partial x} + \frac{\partial \varphi_i^e}{\partial x} \frac{\partial \varphi_j^e}{\partial y} \right) \right] \\
& \quad + \frac{\partial u}{\partial y} \left[A_{16} \frac{\partial \varphi_i^e}{\partial x} \frac{\partial \varphi_j^e}{\partial x} + A_{26} \frac{\partial \varphi_i^e}{\partial y} \frac{\partial \varphi_j^e}{\partial y} \right. \\
& \quad \left. + A_{66} \left(\frac{\partial \varphi_i^e}{\partial y} \frac{\partial \varphi_j^e}{\partial x} + \frac{\partial \varphi_i^e}{\partial x} \frac{\partial \varphi_j^e}{\partial y} \right) \right] \} dx dy \quad (10.4.18)
\end{aligned}$$

$$\begin{aligned}
\sum_{k=1}^n v_k \frac{\partial K_{ik}^{32}}{\partial \bar{\Delta}_j^3} = & \sum_{k=1}^n v_k \frac{\partial}{\partial \bar{\Delta}_j^3} \left[\int_{\Omega^e} \left\{ \frac{\partial \psi_k^e}{\partial y} \left[A_{12} \frac{\partial w_0}{\partial x} \frac{\partial \varphi_i^e}{\partial x} + A_{22} \frac{\partial w_0}{\partial y} \frac{\partial \varphi_i^e}{\partial y} \right. \right. \right. \\
& \quad \left. \left. + A_{26} \left(\frac{\partial w_0}{\partial x} \frac{\partial \varphi_i^e}{\partial y} + \frac{\partial w_0}{\partial y} \frac{\partial \varphi_i^e}{\partial x} \right) \right] \right. \\
& \quad \left. + \frac{\partial \psi_k^e}{\partial x} \left[A_{16} \frac{\partial w_0}{\partial x} \frac{\partial \varphi_i^e}{\partial x} + A_{26} \frac{\partial w_0}{\partial y} \frac{\partial \varphi_i^e}{\partial y} \right. \right. \\
& \quad \left. \left. + A_{66} \left(\frac{\partial w_0}{\partial x} \frac{\partial \varphi_i^e}{\partial y} + \frac{\partial w_0}{\partial y} \frac{\partial \varphi_i^e}{\partial x} \right) \right] \right\} dx dy \right] \\
= & \int_{\Omega^e} \left\{ \frac{\partial v}{\partial y} \left[A_{12} \frac{\partial \varphi_i^e}{\partial x} \frac{\partial \varphi_j^e}{\partial x} + A_{22} \frac{\partial \varphi_i^e}{\partial y} \frac{\partial \varphi_j^e}{\partial y} \right. \right. \\
& \quad \left. + A_{26} \left(\frac{\partial \varphi_i^e}{\partial y} \frac{\partial \varphi_j^e}{\partial x} + \frac{\partial \varphi_i^e}{\partial x} \frac{\partial \varphi_j^e}{\partial y} \right) \right] \\
& \quad + \frac{\partial v}{\partial x} \left[A_{16} \frac{\partial \varphi_i^e}{\partial x} \frac{\partial \varphi_j^e}{\partial x} + A_{26} \frac{\partial \varphi_i^e}{\partial y} \frac{\partial \varphi_j^e}{\partial y} \right. \\
& \quad \left. + A_{66} \left(\frac{\partial \varphi_i^e}{\partial y} \frac{\partial \varphi_j^e}{\partial x} + \frac{\partial \varphi_i^e}{\partial x} \frac{\partial \varphi_j^e}{\partial y} \right) \right] \} dx dy \quad (10.4.19)
\end{aligned}$$

$$\begin{aligned}
\sum_{k=1}^n w_k \frac{\partial K_{ik}^{33}}{\partial \bar{\Delta}_j^3} = & \sum_{k=1}^n \bar{\Delta}_k^3 \frac{\partial}{\partial \bar{\Delta}_j^3} \left[\frac{1}{2} \int_{\Omega^e} \left\{ \left[A_{11} \left(\frac{\partial w_0}{\partial x} \right)^2 + A_{12} \left(\frac{\partial w_0}{\partial y} \right)^2 \right. \right. \right. \\
& \quad \left. + 2A_{16} \frac{\partial w_0}{\partial x} \frac{\partial w_0}{\partial y} \right] \frac{\partial \varphi_i^e}{\partial x} \frac{\partial \varphi_k^e}{\partial x} + \left[A_{16} \left(\frac{\partial w_0}{\partial x} \right)^2 + A_{26} \left(\frac{\partial w_0}{\partial y} \right)^2 \right. \\
& \quad \left. + 2A_{66} \frac{\partial w_0}{\partial x} \frac{\partial w_0}{\partial y} \right] \left(\frac{\partial \varphi_i^e}{\partial x} \frac{\partial \varphi_k^e}{\partial y} + \frac{\partial \varphi_k^e}{\partial x} \frac{\partial \varphi_i^e}{\partial y} \right) \\
& \quad \left. + \left[A_{12} \left(\frac{\partial w_0}{\partial x} \right)^2 + A_{22} \left(\frac{\partial w_0}{\partial y} \right)^2 + 2A_{26} \frac{\partial w_0}{\partial x} \frac{\partial w_0}{\partial y} \right] \frac{\partial \varphi_i^e}{\partial y} \frac{\partial \varphi_k^e}{\partial y} \right\} dx dy \right] \\
& - \int_{\Omega^e} \left\{ \frac{\partial \varphi_i^e}{\partial x} \left[\frac{\partial w_0}{\partial x} \left(B_{11} \frac{\partial^2 \varphi_k^e}{\partial x^2} + B_{12} \frac{\partial^2 \varphi_k^e}{\partial y^2} + 2B_{16} \frac{\partial^2 \varphi_k^e}{\partial x \partial y} \right) \right. \right. \\
& \quad \left. \left. + \frac{\partial w_0}{\partial y} \left(B_{21} \frac{\partial^2 \varphi_k^e}{\partial x \partial y} + B_{22} \frac{\partial^2 \varphi_k^e}{\partial y^2} + 2B_{26} \frac{\partial^2 \varphi_k^e}{\partial x^2} \right) \right] \right\} dx dy
\end{aligned}$$

$$\begin{aligned}
& + \frac{\partial w_0}{\partial y} \left(B_{16} \frac{\partial^2 \varphi_k^e}{\partial x^2} + B_{26} \frac{\partial^2 \varphi_k^e}{\partial y^2} + 2B_{66} \frac{\partial^2 \varphi_k^e}{\partial x \partial y} \right) \Big] \\
& + \frac{\partial \varphi_i^e}{\partial y} \left[\frac{\partial w_0}{\partial y} \left(B_{12} \frac{\partial^2 \varphi_k^e}{\partial x^2} + B_{22} \frac{\partial^2 \varphi_k^e}{\partial y^2} + 2B_{26} \frac{\partial^2 \varphi_k^e}{\partial x \partial y} \right) \right. \\
& \left. + \frac{\partial w_0}{\partial x} \left(B_{16} \frac{\partial^2 \varphi_k^e}{\partial x^2} + B_{26} \frac{\partial^2 \varphi_k^e}{\partial y^2} + 2B_{66} \frac{\partial^2 \varphi_k^e}{\partial x \partial y} \right) \right] \Big\} dx dy \\
- \frac{1}{2} \int_{\Omega^e} & \left\{ \frac{\partial^2 \varphi_i^e}{\partial x^2} \left[B_{11} \frac{\partial w_0}{\partial x} \frac{\partial \varphi_k^e}{\partial x} + B_{12} \frac{\partial w_0}{\partial y} \frac{\partial \varphi_k^e}{\partial y} \right. \right. \\
& + B_{16} \left(\frac{\partial w_0}{\partial y} \frac{\partial \varphi_k^e}{\partial x} + \frac{\partial w_0}{\partial x} \frac{\partial \varphi_k^e}{\partial y} \right) \Big] \\
& + \frac{\partial^2 \varphi_i^e}{\partial y^2} \left[B_{12} \frac{\partial w_0}{\partial x} \frac{\partial \varphi_k^e}{\partial x} + B_{22} \frac{\partial w_0}{\partial y} \frac{\partial \varphi_k^e}{\partial y} \right. \\
& \left. + B_{26} \left(\frac{\partial w_0}{\partial y} \frac{\partial \varphi_k^e}{\partial x} + \frac{\partial w_0}{\partial x} \frac{\partial \varphi_k^e}{\partial y} \right) \right] \\
& + 2 \frac{\partial^2 \varphi_i^e}{\partial x \partial y} \left[B_{16} \frac{\partial w_0}{\partial x} \frac{\partial \varphi_k^e}{\partial x} \right. \\
& \left. + B_{26} \frac{\partial w_0}{\partial y} \frac{\partial \varphi_k^e}{\partial y} + B_{66} \left(\frac{\partial w_0}{\partial y} \frac{\partial \varphi_k^e}{\partial x} + \frac{\partial w_0}{\partial x} \frac{\partial \varphi_k^e}{\partial y} \right) \right] \Big\} dx dy \\
= \int_{\Omega^e} & \left\{ \left[A_{11} \left(\frac{\partial w_0}{\partial x} \right)^2 + 2A_{16} \frac{\partial w_0}{\partial x} \frac{\partial w_0}{\partial y} + A_{66} \left(\frac{\partial w_0}{\partial y} \right)^2 \right] \frac{\partial \varphi_i^e}{\partial x} \frac{\partial \varphi_j^e}{\partial x} \right. \\
& + \left[A_{66} \left(\frac{\partial w_0}{\partial x} \right)^2 + 2A_{26} \frac{\partial w_0}{\partial x} \frac{\partial w_0}{\partial y} + A_{22} \left(\frac{\partial w_0}{\partial y} \right)^2 \right] \frac{\partial \varphi_i^e}{\partial y} \frac{\partial \varphi_j^e}{\partial y} \\
& \left. + \left[A_{16} \left(\frac{\partial w_0}{\partial x} \right)^2 + (A_{12} + A_{66}) \frac{\partial w_0}{\partial x} \frac{\partial w_0}{\partial y} + A_{26} \left(\frac{\partial w_0}{\partial y} \right)^2 \right] \right. \\
& \left. \left(\frac{\partial \varphi_i^e}{\partial x} \frac{\partial \varphi_j^e}{\partial y} + \frac{\partial \varphi_i^e}{\partial y} \frac{\partial \varphi_j^e}{\partial x} \right) \right. \\
& - \int_{\Omega^e} \left[\left(B_{11} \frac{\partial^2 w_0}{\partial x^2} + B_{12} \frac{\partial^2 w_0}{\partial y^2} + 2B_{16} \frac{\partial^2 w_0}{\partial x \partial y} \right) \frac{\partial \varphi_i^e}{\partial x} \frac{\partial \varphi_j^e}{\partial x} \right. \\
& + \left(B_{16} \frac{\partial^2 w_0}{\partial x^2} + B_{26} \frac{\partial^2 w_0}{\partial y^2} + 2B_{66} \frac{\partial^2 w_0}{\partial x \partial y} \right) \\
& \left. \left(\frac{\partial \varphi_i^e}{\partial x} \frac{\partial \varphi_j^e}{\partial y} + \frac{\partial \varphi_i^e}{\partial y} \frac{\partial \varphi_j^e}{\partial x} \right) \right. \\
& + \left(B_{12} \frac{\partial^2 w_0}{\partial x^2} + B_{22} \frac{\partial^2 w_0}{\partial y^2} + 2B_{26} \frac{\partial^2 w_0}{\partial x \partial y} \right) \frac{\partial \varphi_i^e}{\partial y} \frac{\partial \varphi_j^e}{\partial y} \Big] dx dy \\
- \frac{1}{2} \int_{\Omega^e} & \left\{ \frac{\partial^2 \varphi_i^e}{\partial x^2} \left[B_{11} \frac{\partial w_0}{\partial x} \frac{\partial \varphi_j^e}{\partial x} + B_{12} \frac{\partial w_0}{\partial y} \frac{\partial \varphi_j^e}{\partial y} \right. \right. \\
& \left. \left. + B_{16} \frac{\partial w_0}{\partial y} \frac{\partial \varphi_j^e}{\partial x} + B_{26} \frac{\partial w_0}{\partial x} \frac{\partial \varphi_j^e}{\partial y} \right] \right\} dx dy
\end{aligned}$$

$$\begin{aligned}
& + B_{16} \left(\frac{\partial w_0}{\partial y} \frac{\partial \varphi_j^e}{\partial x} + \frac{\partial w_0}{\partial x} \frac{\partial \varphi_j^e}{\partial y} \right) \Big] \\
& + \frac{\partial^2 \varphi_i^e}{\partial y^2} \left[B_{12} \frac{\partial w_0}{\partial x} \frac{\partial \varphi_j^e}{\partial x} + B_{22} \frac{\partial w_0}{\partial y} \frac{\partial \varphi_j^e}{\partial y} \right. \\
& \quad \left. + B_{26} \left(\frac{\partial w_0}{\partial y} \frac{\partial \varphi_j^e}{\partial x} + \frac{\partial w_0}{\partial x} \frac{\partial \varphi_j^e}{\partial y} \right) \right] \\
& + 2 \frac{\partial^2 \varphi_i^e}{\partial x \partial y} \left[B_{16} \frac{\partial w_0}{\partial x} \frac{\partial \varphi_j^e}{\partial x} + B_{26} \frac{\partial w_0}{\partial y} \frac{\partial \varphi_j^e}{\partial y} \right. \\
& \quad \left. + B_{66} \left(\frac{\partial w_0}{\partial y} \frac{\partial \varphi_j^e}{\partial x} + \frac{\partial w_0}{\partial x} \frac{\partial \varphi_j^e}{\partial y} \right) \right] \Big\} dx dy
\end{aligned} \tag{10.4.20}$$

$$\frac{\partial F_i^{3T}}{\partial \Delta_j^3} = \int_{\Omega^e} \left[\frac{\partial \varphi_i^e}{\partial x} \left(N_{xx}^T \frac{\partial \varphi_j^e}{\partial x} + N_{xy}^T \frac{\partial \varphi_j^e}{\partial y} \right) + \frac{\partial \varphi_i^e}{\partial y} \left(N_{xy}^T \frac{\partial \varphi_j^e}{\partial x} + N_{yy}^T \frac{\partial \varphi_j^e}{\partial y} \right) \right] dx dy \tag{10.4.21}$$

Note that T_{ij}^{33} is given by combining the expressions in Eqs. (10.4.18)–(10.4.21) and K_{ij}^{33} . One may find that the tangent stiffness matrix is symmetric. This completes the finite element model development of the classical plate theory.

10.4.4 Tangent Stiffness Coefficients for FSDT

Since the source of nonlinearity in the classical and first-order shear deformation plate theories is the same, the nonlinear parts of the tangent stiffness coefficients derived for the classical plate theory are also applicable to the first-order theory. For the sake of completeness, they are presented here again.

The coefficients of the submatrices $[T^{\alpha\beta}]$ ($\alpha, \beta = 1, 2, \dots, 5$) are defined by

$$T_{ij}^{\alpha\beta} = \frac{\partial R_i^\alpha}{\partial \Delta_j^\beta} \tag{10.4.22}$$

where the components of the residual vector $\{R^\alpha\}$ are given by

$$R_i^\alpha = \sum_{\gamma=1}^5 \sum_{k=1}^{n*} K_{ik}^{\alpha\gamma} \Delta_k^\gamma - F_i^\alpha \tag{10.4.23a}$$

$$\Delta_i^1 = u_i, \quad \Delta_i^2 = v_i, \quad \Delta_i^3 = w_i, \quad \Delta_i^4 = S_i^1, \quad \Delta_i^5 = S_i^2 \tag{10.4.23b}$$

and $n*$ denotes n , m , or p , depending on the nodal degree of freedom. Thus, we have

$$\begin{aligned}
T_{ij}^{\alpha\beta} &= \frac{\partial}{\partial \Delta_j^\beta} \left(\sum_{\gamma=1}^5 \sum_{k=1}^{n*} K_{ik}^{\alpha\gamma} \Delta_k^\gamma - F_i^\alpha \right) \\
&= \sum_{\gamma=1}^5 \sum_{k=1}^{n*} \frac{\partial K_{ik}^{\alpha\gamma}}{\partial \Delta_j^\beta} \Delta_k^\gamma + K_{ij}^{\alpha\beta}
\end{aligned} \tag{10.4.24}$$

It should be noted that only coefficients that depend on the solution are K_{ij}^{13} , K_{ij}^{23} , K_{ij}^{31} , K_{ij}^{32} , and K_{ij}^{33} . Since they are functions of only w_0 (or functions of w_j), derivatives of all stiffness coefficients with respect to u_j , v_j , S_j^1 , and S_j^2 are zero. Thus, we have

$$\begin{aligned}
T_{ij}^{11} &= \sum_{\gamma=1}^5 \sum_{k=1}^{n*} \frac{\partial K_{ik}^{1\gamma}}{\partial u_j} \Delta_k^\gamma + K_{ij}^{11} = K_{ij}^{11}, \quad T_{ij}^{12} = \sum_{\gamma=1}^5 \sum_{k=1}^{n*} \frac{\partial K_{ik}^{1\gamma}}{\partial v_j} \Delta_k^\gamma + K_{ij}^{12} = K_{ij}^{12} \\
T_{ij}^{13} &= \sum_{\gamma=1}^5 \sum_{k=1}^{n*} \frac{\partial K_{ik}^{1\gamma}}{\partial w_j} \Delta_k^\gamma + K_{ij}^{13} = \sum_{k=1}^n \frac{\partial K_{ik}^{13}}{\partial w_j} w_k + K_{ij}^{13} \\
&= \frac{1}{2} \int_{\Omega^e} \left\{ \frac{\partial \psi_i^{(1)}}{\partial x} \left[A_{11} \frac{\partial w_0}{\partial x} \frac{\partial \psi_j^{(2)}}{\partial x} + A_{12} \frac{\partial w_0}{\partial y} \frac{\partial \psi_j^{(2)}}{\partial y} \right. \right. \\
&\quad \left. \left. + A_{16} \left(\frac{\partial w_0}{\partial x} \frac{\partial \psi_j^{(2)}}{\partial y} + \frac{\partial w_0}{\partial y} \frac{\partial \psi_j^{(2)}}{\partial x} \right) \right] \right. \\
&\quad \left. + \frac{\partial \psi_i^{(1)}}{\partial y} \left[A_{16} \frac{\partial w_0}{\partial x} \frac{\partial \psi_j^{(2)}}{\partial x} + A_{26} \frac{\partial w_0}{\partial y} \frac{\partial \psi_j^{(2)}}{\partial y} \right. \right. \\
&\quad \left. \left. + A_{66} \left(\frac{\partial w_0}{\partial x} \frac{\partial \psi_j^{(2)}}{\partial y} + \frac{\partial w_0}{\partial y} \frac{\partial \psi_j^{(2)}}{\partial x} \right) \right] \right\} dx dy + K_{ij}^{13} \\
&= K_{ij}^{13} + K_{ij}^{13} = 2K_{ij}^{13} (= T_{ji}^{31}) \\
T_{ij}^{14} &= \sum_{\gamma=1}^5 \sum_{k=1}^{n*} \frac{\partial K_{ik}^{1\gamma}}{\partial S_j^1} \Delta_k^\gamma + K_{ij}^{14} = K_{ij}^{14}, \quad T_{ij}^{15} = \sum_{\gamma=1}^5 \sum_{k=1}^{n*} \frac{\partial K_{ik}^{1\gamma}}{\partial S_j^2} \Delta_k^\gamma + K_{ij}^{15} = K_{ij}^{15} \\
T_{ij}^{21} &= \sum_{\gamma=1}^5 \sum_{k=1}^{n*} \frac{\partial K_{ik}^{2\gamma}}{\partial u_j} \Delta_k^\gamma + K_{ij}^{21} = K_{ij}^{21}, \quad T_{ij}^{22} = \sum_{\gamma=1}^5 \sum_{k=1}^{n*} \frac{\partial K_{ik}^{2\gamma}}{\partial v_j} \Delta_k^\gamma + K_{ij}^{22} = K_{ij}^{22} \\
T_{ij}^{23} &= \sum_{\gamma=1}^5 \sum_{k=1}^{n*} \frac{\partial K_{ik}^{2\gamma}}{\partial w_j} \Delta_k^\gamma + K_{ij}^{23} = \sum_{k=1}^n \frac{\partial K_{ik}^{23}}{\partial w_j} w_k + K_{ij}^{23} \\
&= \frac{1}{2} \int_{\Omega^e} \left\{ \frac{\partial \psi_i^{(1)}}{\partial y} \left[A_{12} \frac{\partial w_0}{\partial x} \frac{\partial \psi_j^{(2)}}{\partial x} + A_{22} \frac{\partial w_0}{\partial y} \frac{\partial \psi_j^{(2)}}{\partial y} \right. \right. \\
&\quad \left. \left. + A_{26} \left(\frac{\partial w_0}{\partial x} \frac{\partial \psi_j^{(2)}}{\partial y} + \frac{\partial w_0}{\partial y} \frac{\partial \psi_j^{(2)}}{\partial x} \right) \right] \right. \\
&\quad \left. + \frac{\partial \psi_i^{(1)}}{\partial x} \left[A_{16} \frac{\partial w_0}{\partial x} \frac{\partial \psi_j^{(2)}}{\partial x} + A_{26} \frac{\partial w_0}{\partial y} \frac{\partial \psi_j^{(2)}}{\partial y} \right. \right. \\
&\quad \left. \left. + A_{66} \left(\frac{\partial w_0}{\partial x} \frac{\partial \psi_j^{(2)}}{\partial y} + \frac{\partial w_0}{\partial y} \frac{\partial \psi_j^{(2)}}{\partial x} \right) \right] \right\} dx dy + K_{ij}^{23} \\
&= K_{ij}^{23} + K_{ij}^{23} = 2K_{ij}^{23} (= T_{ji}^{32}) \\
T_{ij}^{24} &= \sum_{\gamma=1}^5 \sum_{k=1}^{n*} \frac{\partial K_{ik}^{2\gamma}}{\partial S_j^1} \Delta_k^\gamma + K_{ij}^{24} = K_{ij}^{24}, \quad T_{ij}^{25} = \sum_{\gamma=1}^5 \sum_{k=1}^{n*} \frac{\partial K_{ik}^{2\gamma}}{\partial S_j^2} \Delta_k^\gamma + K_{ij}^{25} = K_{ij}^{25}
\end{aligned}$$

$$\begin{aligned}
T_{ij}^{31} &= \sum_{\gamma=1}^5 \sum_{k=1}^{n^*} \frac{\partial K_{ik}^{3\gamma}}{\partial u_j} \Delta_k^\gamma + K_{ij}^{31} = K_{ij}^{31}, \quad T_{ij}^{32} = \sum_{\gamma=1}^5 \sum_{k=1}^{n^*} \frac{\partial K_{ik}^{3\gamma}}{\partial v_j} \Delta_k^\gamma + K_{ij}^{32} = K_{ij}^{32} \\
T_{ij}^{33} &= \sum_{\gamma=1}^5 \sum_{k=1}^{n^*} \frac{\partial K_{ik}^{3\gamma}}{\partial w_j} \Delta_k^\gamma - \frac{\partial F_i^{3T}}{\partial w_j} + K_{ij}^{33} \\
&= \sum_{k=1}^{n^*} \left(\frac{\partial K_{ik}^{31}}{\partial w_j} u_k + \frac{\partial K_{ik}^{32}}{\partial w_j} v_k + \frac{\partial K_{ik}^{33}}{\partial w_j} w_k + \frac{\partial K_{ik}^{34}}{\partial w_j} S_k^1 + \frac{\partial K_{ik}^{35}}{\partial w_j} S_k^2 \right) \\
&\quad - \frac{\partial F_i^{3T}}{\partial w_j} + K_{ij}^{33} \\
&= \int_{\Omega^e} \left\{ \frac{\partial u_0}{\partial x} \left[A_{11} \frac{\partial \psi_j^{(2)}}{\partial x} \frac{\partial \psi_i^{(2)}}{\partial x} + A_{12} \frac{\partial \psi_j^{(2)}}{\partial y} \frac{\partial \psi_i^{(2)}}{\partial y} \right. \right. \\
&\quad \left. \left. + A_{16} \left(\frac{\partial \psi_j^{(2)}}{\partial x} \frac{\partial \psi_i^{(2)}}{\partial y} + \frac{\partial \psi_j^{(2)}}{\partial y} \frac{\partial \psi_i^{(2)}}{\partial x} \right) \right] \right. \\
&\quad \left. + \frac{\partial u_0}{\partial y} \left[A_{16} \frac{\partial \psi_j^{(2)}}{\partial x} \frac{\partial \psi_i^{(2)}}{\partial x} + A_{26} \frac{\partial \psi_j^{(2)}}{\partial y} \frac{\partial \psi_i^{(2)}}{\partial y} \right. \right. \\
&\quad \left. \left. + A_{66} \left(\frac{\partial \psi_j^{(2)}}{\partial x} \frac{\partial \psi_i^{(2)}}{\partial y} + \frac{\partial \psi_j^{(2)}}{\partial y} \frac{\partial \psi_i^{(2)}}{\partial x} \right) \right] \right\} dx dy \\
&+ \int_{\Omega^e} \left\{ \frac{\partial v_0}{\partial y} \left[A_{12} \frac{\partial \psi_j^{(2)}}{\partial x} \frac{\partial \psi_i^{(2)}}{\partial x} + A_{22} \frac{\partial \psi_j^{(2)}}{\partial y} \frac{\partial \psi_i^{(2)}}{\partial y} \right. \right. \\
&\quad \left. \left. + A_{26} \left(\frac{\partial \psi_j^{(2)}}{\partial x} \frac{\partial \psi_i^{(2)}}{\partial y} + \frac{\partial \psi_j^{(2)}}{\partial y} \frac{\partial \psi_i^{(2)}}{\partial x} \right) \right] \right. \\
&\quad \left. + \frac{\partial v_0}{\partial x} \left[A_{16} \frac{\partial \psi_j^{(2)}}{\partial x} \frac{\partial \psi_i^{(2)}}{\partial x} + A_{26} \frac{\partial \psi_j^{(2)}}{\partial y} \frac{\partial \psi_i^{(2)}}{\partial y} \right. \right. \\
&\quad \left. \left. + A_{66} \left(\frac{\partial \psi_j^{(2)}}{\partial x} \frac{\partial \psi_i^{(2)}}{\partial y} + \frac{\partial \psi_j^{(2)}}{\partial y} \frac{\partial \psi_i^{(2)}}{\partial x} \right) \right] \right\} dx dy \\
&+ \int_{\Omega^e} \left\{ \left[A_{11} \frac{\partial w_0}{\partial x} \frac{\partial \psi_j^{(2)}}{\partial x} + A_{12} \frac{\partial w_0}{\partial y} \frac{\partial \psi_j^{(2)}}{\partial y} \right. \right. \\
&\quad \left. \left. + A_{16} \left(\frac{\partial w_0}{\partial x} \frac{\partial \psi_j^{(2)}}{\partial y} + \frac{\partial w_0}{\partial y} \frac{\partial \psi_j^{(2)}}{\partial x} \right) \right] \frac{\partial \psi_i^{(2)}}{\partial x} \frac{\partial w_0}{\partial x} \right. \\
&\quad \left. + \left[A_{16} \frac{\partial w_0}{\partial x} \frac{\partial \psi_j^{(2)}}{\partial x} + A_{26} \frac{\partial w_0}{\partial y} \frac{\partial \psi_j^{(2)}}{\partial y} \right. \right. \\
&\quad \left. \left. + A_{66} \left(\frac{\partial w_0}{\partial x} \frac{\partial \psi_j^{(2)}}{\partial y} + \frac{\partial w_0}{\partial y} \frac{\partial \psi_j^{(2)}}{\partial x} \right) \right] \left(\frac{\partial \psi_i^{(2)}}{\partial x} \frac{\partial w_0}{\partial y} + \frac{\partial w_0}{\partial x} \frac{\partial \psi_i^{(2)}}{\partial y} \right) \right\}
\end{aligned}$$

$$\begin{aligned}
& + \left[A_{12} \frac{\partial w_0}{\partial x} \frac{\partial \psi_j^{(2)}}{\partial x} + A_{22} \frac{\partial w_0}{\partial y} \frac{\partial \psi_j^{(2)}}{\partial y} \right. \\
& \quad \left. + A_{26} \left(\frac{\partial w_0}{\partial x} \frac{\partial \psi_j^{(2)}}{\partial y} + \frac{\partial w_0}{\partial y} \frac{\partial \psi_j^{(2)}}{\partial x} \right) \right] \frac{\partial \psi_i^{(2)}}{\partial y} \frac{\partial w_0}{\partial y} \Big\} dx dy \\
& + \int_{\Omega^e} \frac{\partial \psi_i^{(2)}}{\partial x} \left[\frac{\partial \psi_j^{(2)}}{\partial x} \left(B_{11} \frac{\partial \phi_x}{\partial x} + B_{16} \frac{\partial \phi_x}{\partial y} \right) \right. \\
& \quad \left. + \frac{\partial \psi_j^{(2)}}{\partial y} \left(B_{16} \frac{\partial \phi_x}{\partial x} + B_{66} \frac{\partial \phi_x}{\partial y} \right) \right] \\
& \quad + \frac{\partial \psi_i^{(2)}}{\partial y} \left[\frac{\partial \psi_j^{(2)}}{\partial y} \left(B_{12} \frac{\partial \phi_x}{\partial x} + B_{26} \frac{\partial \phi_x}{\partial y} \right) \right. \\
& \quad \left. + \frac{\partial \psi_j^{(2)}}{\partial x} \left(B_{16} \frac{\partial \phi_x}{\partial x} + B_{66} \frac{\partial \phi_x}{\partial y} \right) \right] \Big\} dx dy \\
& + \int_{\Omega^e} \frac{\partial \psi_i^{(2)}}{\partial x} \left[\frac{\partial \psi_j^{(2)}}{\partial x} \left(B_{12} \frac{\partial \phi_y}{\partial y} + B_{16} \frac{\partial \phi_y}{\partial x} \right) \right. \\
& \quad \left. + \frac{\partial \psi_j^{(2)}}{\partial y} \left(B_{26} \frac{\partial \phi_y}{\partial y} + B_{66} \frac{\partial \phi_y}{\partial x} \right) \right] \\
& \quad + \frac{\partial \psi_i^{(2)}}{\partial y} \left[\frac{\partial \psi_j^{(2)}}{\partial y} \left(B_{22} \frac{\partial \phi_y}{\partial y} + B_{26} \frac{\partial \phi_y}{\partial x} \right) \right. \\
& \quad \left. + \frac{\partial \psi_j^{(2)}}{\partial x} \left(B_{26} \frac{\partial \phi_y}{\partial y} + B_{66} \frac{\partial \phi_y}{\partial x} \right) \right] \\
& \quad - \frac{\partial \psi_i^{(2)}}{\partial x} \left(N_{xx}^T \frac{\partial \psi_j^{(2)}}{\partial x} + N_{xy}^T \frac{\partial \psi_j^{(2)}}{\partial y} \right) \\
& \quad - \frac{\partial \psi_i^{(2)}}{\partial y} \left(N_{xy}^T \frac{\partial \psi_j^{(2)}}{\partial x} + N_{yy}^T \frac{\partial \psi_j^{(2)}}{\partial y} \right) \Big\} dx dy + K_{ij}^{33} \\
T_{ij}^{34} & = \sum_{\gamma=1}^5 \sum_{k=1}^{n*} \frac{\partial K_{ik}^{3\gamma}}{\partial S_j^1} \Delta_k^\gamma + K_{ij}^{34} = K_{ij}^{34}, \quad T_{ij}^{35} = \sum_{\gamma=1}^5 \sum_{k=1}^{n*} \frac{\partial K_{ik}^{3\gamma}}{\partial S_j^2} \Delta_k^\gamma + K_{ij}^{35} = K_{ij}^{35} \\
T_{ij}^{41} & = \sum_{\gamma=1}^5 \sum_{k=1}^{n*} \frac{\partial K_{ik}^{4\gamma}}{\partial u_j} \Delta_k^\gamma + K_{ij}^{41} = K_{ij}^{41}, \quad T_{ij}^{42} = \sum_{\gamma=1}^5 \sum_{k=1}^{n*} \frac{\partial K_{ik}^{4\gamma}}{\partial v_j} \Delta_k^\gamma + K_{ij}^{42} = K_{ij}^{42} \\
T_{ij}^{43} & = \sum_{\gamma=1}^5 \sum_{k=1}^{n*} \frac{\partial K_{ik}^{4\gamma}}{\partial w_j} \Delta_k^\gamma + K_{ij}^{43} = \sum_{k=1}^n \frac{\partial K_{ik}^{43}}{\partial w_j} \Delta_k^3 + K_{ij}^{43} \\
& = \frac{1}{2} \int_{\Omega^e} \frac{\partial w_0}{\partial x} \left[\frac{\partial \psi_j^{(2)}}{\partial x} \left(B_{11} \frac{\partial \psi_i^{(3)}}{\partial x} + B_{16} \frac{\partial \psi_i^{(3)}}{\partial y} \right) \right. \\
& \quad \left. + \frac{\partial \psi_j^{(2)}}{\partial y} \left(B_{16} \frac{\partial \psi_i^{(3)}}{\partial x} + B_{66} \frac{\partial \psi_i^{(3)}}{\partial y} \right) \right]
\end{aligned}$$

$$\begin{aligned}
& + \frac{\partial w_0}{\partial y} \left[\frac{\partial \psi_j^{(2)}}{\partial y} \left(B_{12} \frac{\partial \psi_i^{(3)}}{\partial x} + B_{26} \frac{\partial \psi_i^{(3)}}{\partial y} \right) \right. \\
& \quad \left. + \frac{\partial \psi_j^{(2)}}{\partial x} \left(B_{16} \frac{\partial \psi_i^{(3)}}{\partial x} + B_{66} \frac{\partial \psi_i^{(3)}}{\partial y} \right) \right] \} dx dy + K_{ij}^{43} \\
T_{ij}^{44} &= \sum_{\gamma=1}^5 \sum_{k=1}^{n*} \frac{\partial K_{ik}^{4\gamma}}{\partial S_j^1} \Delta_k^\gamma + K_{ij}^{44} = K_{ij}^{44}, \quad T_{ij}^{45} = \sum_{\gamma=1}^5 \sum_{k=1}^{n*} \frac{\partial K_{ik}^{4\gamma}}{\partial S_j^2} \Delta_k^\gamma + K_{ij}^{45} = K_{ij}^{45} \\
T_{ij}^{53} &= \sum_{\gamma=1}^5 \sum_{k=1}^{n*} \frac{\partial K_{ik}^{5\gamma}}{\partial w_j} \Delta_k^\gamma + K_{ij}^{53} \\
&= \frac{1}{2} \int_{\Omega^e} \frac{\partial w_0}{\partial x} \left[\frac{\partial \psi_j^{(2)}}{\partial x} \left(B_{12} \frac{\partial \psi_i^{(3)}}{\partial y} + B_{16} \frac{\partial \psi_i^{(3)}}{\partial x} \right) \right. \\
& \quad \left. + \frac{\partial \psi_j^{(2)}}{\partial y} \left(B_{26} \frac{\partial \psi_i^{(3)}}{\partial y} + B_{66} \frac{\partial \psi_i^{(3)}}{\partial x} \right) \right] \\
&+ \frac{\partial w_0}{\partial y} \left[\frac{\partial \psi_j^{(2)}}{\partial y} \left(B_{22} \frac{\partial \psi_i^{(3)}}{\partial y} + B_{26} \frac{\partial \psi_i^{(3)}}{\partial x} \right) \right. \\
& \quad \left. + \frac{\partial \psi_j^{(2)}}{\partial x} \left(B_{26} \frac{\partial \psi_i^{(3)}}{\partial y} + B_{66} \frac{\partial \psi_i^{(3)}}{\partial x} \right) \right] \} dx dy + K_{ij}^{53} \\
T_{ij}^{54} &= \sum_{\gamma=1}^5 \sum_{k=1}^{n*} \frac{\partial K_{ik}^{5\gamma}}{\partial S_j^1} \Delta_k^\gamma + K_{ij}^{54} = K_{ij}^{54}, \quad T_{ij}^{55} = \sum_{\gamma=1}^5 \sum_{k=1}^{n*} \frac{\partial K_{ik}^{5\gamma}}{\partial S_j^2} \Delta_k^\gamma + K_{ij}^{55} = K_{ij}^{55}
\end{aligned} \tag{10.4.25}$$

Clearly, the tangent stiffness matrix is symmetric.

10.4.5 Membrane Locking

Recall that when lower order (quadratic or less) equal interpolation of the generalized displacements is used, the FSDT elements become excessively stiff in the thin plate limit, yielding displacements that are too small compared to the true solution. This type of behavior is known as shear locking (see Reddy [32] and references therein). As discussed earlier, shear locking is avoided by using selective integration: full integration to evaluate all linear stiffness coefficients and reduced integration to evaluate the transverse shear stiffnesses (i.e., all coefficients in $K_{ij}^{\alpha\beta}$ that contain A_{44} , A_{45} , and A_{55}).

Another type of locking, known as the *membrane locking*, occurs in plates and shells due to the inconsistency of approximation of the in-plane displacements (u_0, v_0) and the transverse displacement w_0 . The membrane locking can be explained by considering, for simplicity, the Timoshenko beam finite element (see Problem 10.12). When the element is used to analyze pure bending deformation, it should experience no axial (or membrane) strain:

$$\varepsilon_{xx}^0 \equiv \frac{du_0}{dx} + \frac{1}{2} \left(\frac{dw_0}{dx} \right)^2 = 0 \quad (\text{for pure bending}) \tag{10.4.26}$$

In order that the above constraint be satisfied for independent approximations of u_0 and w_0 , the term should cancel the second term in Eq. (10.4.26). This in turn requires that

$$\text{degree of polynomial of } \frac{du_0}{dx} \sim \text{degree of polynomial of } \left(\frac{dw_0}{dx} \right)^2 \quad (10.4.27)$$

If both variables are approximated with sufficiently higher-order polynomials, the coefficients in the polynomials get adjusted to satisfy the constraint (10.4.26). Also, when both u_0 and w_0 are approximated using linear polynomials, the correspondence (10.4.27), hence constraint (10.4.26), is automatically satisfied; however, when quadratic interpolation of both u_0 and w_0 is used, then $\frac{du_0}{dx}$ is linear and $(\frac{dw_0}{dx})^2$ is quadratic and there is no possibility of canceling the coefficient in quadratic term. If u_0 is interpolated with cubic polynomials and w_0 is interpolated with quadratic polynomials, we have

$$\frac{du_0}{dx} \text{ (quadratic)} \sim \left(\frac{dw_0}{dx} \right)^2 \text{ (quadratic)} \quad (10.4.28)$$

Thus the constraint (10.4.26) is again satisfied. In summary, the element does not experience membrane locking for the following two cases:

- (1) u_0 is linear and w is linear
- (2) u_0 is cubic and w_0 is quadratic

and it experiences locking when both u_0 and w_0 are interpolated using quadratic polynomials.

Since quadratic approximation of u_0 and w_0 is common in practice, it is necessary to find a way to avoid membrane locking of the element. It is found that, for this case, the membrane locking can be avoided by using selective integrations of the terms of the form in ε_{xx} . For example, consider the coefficient $(K_{ij}^{22})^{tan}$ (see Problem 10.14):

$$(K_{ij}^{22})^{tan} = \int_{x_A}^{x_B} E_{xx}^b A \left[\frac{du_0}{dx} + \frac{3}{2} \left(\frac{dw_0}{dx} \right)^2 \right] \frac{d\psi_i}{dx} \frac{d\psi_j}{dx} dx \quad (10.4.29)$$

For quadratic interpolation of u_0 and w_0 , the first term is a cubic ($p = 3$) polynomial and the second term is a fourth-order ($p = 4$) polynomial. Thus the exact evaluation of the first term requires $NGP = (p+1)/2 = 2$ and the second term requires $NGP = [(p+1)/2] = 3$, where NGP denotes the number of Gauss points. Thus, for constant $E_{xx}^b A$, three-point Gauss quadrature yields exact values of both integrals. However, the two-point Gauss rule would yield an exact value for the first term

$$\int_{x_A}^{x_B} \frac{du_0}{dx} \frac{d\psi_i}{dx} \frac{d\psi_j}{dx} dx$$

and at the same time the second term

$$\int_{x_A}^{x_B} \left(\frac{dw_0}{dx} \right)^2 \frac{d\psi_i}{dx} \frac{d\psi_j}{dx} dx$$

is approximated as the same degree polynomial as the first term. This amounts to using an interpolation for w_0 that satisfies the constraint $\varepsilon_{xx}^0 = 0$.

The discussion presented above for the Timoshenko beam element also applies to membrane locking in CLPT and FSDT plate elements. Of course, if the mesh of quadratic elements is sufficiently refined, the membrane locking disappears.

10.5 Numerical Examples of Plates

10.5.1 Preliminary Comments

Here we present some numerical examples of laminated plates and shells using the nonlinear shear deformable laminated plate finite element presented in Section 10.2. A shear correction coefficient $K = 5/6$ is used here.

The problems presented here illustrate certain features characteristic to composite laminates. These include:

- (1) the effect of geometric nonlinearity on static deflections,
- (2) the use of biaxial symmetry boundary conditions in quarter plate models of rectangular laminates,
- (3) postbuckling response of laminates under in-plane compression,
- (4) nonlinear transient response of composite laminates, and
- (5) postbuckling and progressive failure analysis of composite panels subjected to in-plane compression.

All of the problems are selected from the author's publications, and additional examples can be found in the references cited at the end of the chapter (in particular, see Reddy [32]).

10.5.2 Isotropic and Orthotropic Plates

In this section several examples of isotropic and orthotropic plates with various edge conditions are presented to illustrate the use of the CLPT and FSDT elements in the geometrically nonlinear (in the von Kármán sense). The effect of the integration rule to evaluate the nonlinear and transverse shear stiffness coefficients is investigated in the first example. Unless stated otherwise, a uniform mesh of 4×4 nine-node quadratic elements is used in a quarter plate for the FSDT. For this choice of mesh, full integration (F) is to use 3×3 Gauss rule, and reduced integration (R) is to use 2×2 Gauss rule. Stresses are calculated at the center of the element. The shear correction coefficient is taken to be $K_s = 5/6$. A tolerance of $\epsilon = 10^{-2}$ is used for convergence in the Newton–Raphson iteration scheme to check for convergence of the nodal displacements.

Example 10.5.1: _____

Consider an isotropic, square plate with

$$a = b = 10 \text{ in.}, \quad h = 1 \text{ in.}, \quad E = 7.8 \times 10^6 \text{ psi}, \quad \nu = 0.3 \quad (10.5.1)$$

Two types of simply supported boundary conditions are studied. The displacement boundary conditions used for SS-1 and SS-3 are

$$\text{SS-1:} \quad \text{At } x = a/2 : \quad v_0 = w_0 = \phi_y = 0$$

$$\text{At } y = b/2 : \quad u_0 = w_0 = \phi_x = 0 \quad (10.5.2)$$

$$\text{SS-3:} \quad u_0 = v_0 = w_0 = 0 \quad \text{on simply supported edges} \quad (10.5.3)$$

Uniformly distributed load of intensity q_0 is used. The boundary conditions along the symmetry lines for both cases are given by

$$\text{At } x = 0 : \quad u_0 = \phi_x = 0; \quad \text{At } y = 0 : \quad v_0 = \phi_y = 0 \quad (\text{symm. lines}) \quad (10.5.4)$$

It is clear that SS-3 provides more edge restraint than SS-1 and therefore should produce lower transverse deflections.

Using the load parameter, $\bar{P} \equiv q_0 a^4 / Eh^4$, the incremental load vector is chosen to be

$$\{\Delta P\} = \{6.25, 6.25, 12.5, 25.0, 25.0, \dots, 25.0\}$$

Table 10.5.1 contains the deflections $w_0(0,0)$ and normal stresses $\bar{\sigma}_{xx} = \sigma_{xx}(a^2/Eh^2)$ at the center of the first element for various integration rules (also see Figure 10.5.1). The number of iterations taken for convergence are listed in parenthesis. The linear FSDT plate solution for load $q_0 = 4875\text{psi}$ (or $\bar{P} = 6.25$) is $w_0 = 0.2917\text{in.}$ for SS-1 and $w_0 = 0.3151\text{in.}$ for SS-3. As discussed earlier, the $4 \times 4Q9$ meshes are not sensitive to shear or membrane locking, and therefore the results obtained with various integration rules are essentially the same.

Table 10.5.1: Center deflection \bar{w} and stresses $\bar{\sigma}_{xx}$ of simply supported (SS-1 and SS-3) plates under uniformly distributed load.

\bar{P}	SS-3			SS-1		
	R-R*	F-R	F-F	R-R	F-R	F-F
Deflections, $w_0(0,0)$						
6.25	0.2790 (3)	0.2790 (4)	0.2780 (3)	0.2813 (3)	0.2813 (3)	0.2812 (3)
12.5	0.4630 (3)	0.4630 (3)	0.4619 (3)	0.5186 (3)	0.5186 (3)	0.5185 (3)
25.0	0.6911 (3)	0.6911 (3)	0.6902 (3)	0.8673 (4)	0.8673 (4)	0.8672 (4)
50.0	0.9575 (3)	0.9575 (3)	0.9570 (3)	1.3149 (4)	1.3149 (4)	1.3147 (4)
75.0	1.1333 (3)	1.1333 (3)	1.1330 (3)	1.6241 (3)	1.6239 (3)	1.6237 (3)
100.0	1.2688 (3)	1.2688 (3)	1.2686 (3)	1.8687 (3)	1.8683 (3)	1.8679 (3)
125.0	1.3809 (2)	1.3809 (2)	1.3808 (2)	2.0758 (2)	2.0751 (2)	2.0746 (2)
150.0	1.4774 (2)	1.4774 (2)	1.4774 (2)	2.2567 (2)	2.2556 (2)	2.2549 (2)
175.0	1.5628 (2)	1.5629 (2)	1.5629 (2)	2.4194 (2)	2.4177 (2)	2.4168 (2)
200.0	1.6398 (2)	1.6399 (2)	1.6399 (2)	2.5681 (2)	2.5657 (2)	2.5645 (2)
Normal stresses, $\bar{\sigma}_{xx}(0.3125, 0.3125, h/2)$						
6.25	1.861	1.861	1.856	1.779	1.779	1.780
12.5	3.305	3.305	3.300	3.396	3.396	3.398
25.0	5.319	5.320	5.317	5.882	5.882	5.885
50.0	8.001	8.002	8.001	9.159	9.162	9.165
75.0	9.983	9.984	9.983	11.458	11.462	11.465
100.0	11.633	11.634	11.634	13.299	13.307	13.308
125.0	13.084	13.085	13.085	14.878	14.890	14.889
150.0	14.396	14.398	14.398	16.278	16.293	16.290
175.0	15.608	15.610	15.610	17.553	17.572	17.567
200.0	16.741	16.743	16.743	18.733	18.755	18.748

* The first letter refers to the integration rule used for the nonlinear terms while the second letter refers to the integration rule used for the shear terms.

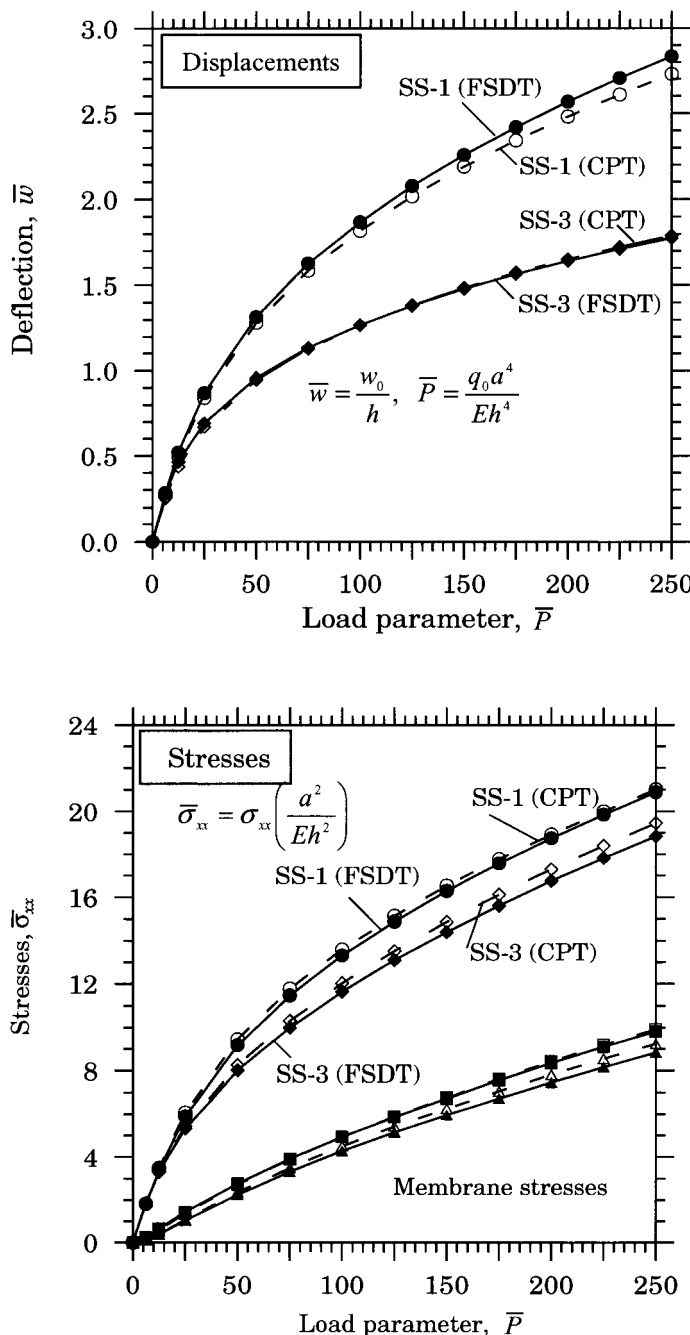


Figure 10.5.1: Plots of center deflection w_0 versus load \bar{P} and center normal stress $\bar{\sigma}_{xx}$ versus load \bar{P} for isotropic ($\nu = 0.3$), simply supported square plates under uniformly distributed load (4 × 4Q9 for FSDT and 8 × 8C for CPT).

Example 10.5.2:

Orthotropic plates with

$$\begin{aligned} a = b &= 12 \text{ in.}, \quad h = 0.138 \text{ in.}, \quad E_1 = 3 \times 10^6 \text{ psi}, \quad E_2 = 1.28 \times 10^6 \text{ psi} \\ G_{12} = G_{13} &= G_{23} = 0.37 \times 10^6 \text{ psi}, \quad \nu_{12} = 0.32 \end{aligned} \quad (10.5.5)$$

and subjected to uniformly distributed transverse load (i.e., $q = q_0 = \text{constant}$) are analyzed. A uniform mesh of 4×4 Q9 elements with reduced integration is used in a quadrant. The incremental load vector is chosen to be

$$\{\Delta P\} = \{0.05, 0.05, 0.1, 0.2, 0.2, \dots, 0.2\}$$

Twelve load steps are used, and a tolerance of $\epsilon = 0.01$ is used for convergence.

Table 10.5.2 contains the center deflection and total normal stress as a function of the load for SS-1 and SS-3 boundary conditions. The linear FSDT solution for load $q_0 = 0.05$ is $w_0 = 0.01132$ for SS-1 and $w_0 = 0.01140$ for SS-3. Plots of load q_0 (psi) vs. center deflection w_0 (in.) and q_0 versus normal stress (total as well as membrane) $\bar{\sigma}_{xx} = \sigma_{xx}(a^2/E_2 h^2)$ are shown in Figure 10.5.2 for SS-1 and SS-3 plates. The figures also show the results obtained using 8×8 mesh of conforming CPT elements.

Table 10.5.2: Center deflection w_0 and normal stress $\bar{\sigma}_{xx}$ for simply supported orthotropic square plates under uniformly distributed load (4×4 Q9).

q_0	SS-1			SS-3		
	CPT w_0	FSDT w_0	FSDT $\bar{\sigma}_{xx}$	CPT w_0	FSDT w_0	FSDT $\bar{\sigma}_{xx}$
0.05	0.0113 (2)	0.0113	1.034	0.0112	0.0113	1.056
0.10	0.0224 (2)	0.0224	2.070	0.0217	0.0218	2.116
0.20	0.0438 (3)	0.0439	4.092	0.0395	0.0397	4.058
0.40	0.0812 (3)	0.0815	7.716	0.0648	0.0650	7.103
0.60	0.1116 (3)	0.1122	10.702	0.0823	0.0824	9.406
0.80	0.1367 (3)	0.1377	13.169	0.0957	0.0959	11.284
1.00	0.1581 (2)	0.1594	15.255	0.1068	0.1069	12.894
1.20	0.1767 (2)	0.1783	17.050	0.1162	0.1162	14.316
1.40	0.1932 (2)	0.1951	18.631	0.1245	0.1244	15.602
1.60	0.2081 (2)	0.2103	20.044	0.1318	0.1318	16.783
1.80	0.2217 (2)	0.2241	21.324	0.1385	0.1384	17.880
2.00	0.2343 (2)	0.2370	22.495	0.1447	0.1445	18.909

Example 10.5.3:

Here, we analyze an orthotropic plate with clamped edges; i.e., all generalized displacements are set to zero on the boundary. The boundary conditions of a clamped edge are taken to be

$$u_0 = v_0 = w_0 = \phi_x = \phi_y = 0 \quad (10.5.6)$$

The geometric and material parameters used are the same as those listed in Eq. (10.5.5). A uniformly distributed load of intensity q_0 is used.

The linear solution for load $q_0 = 0.5$ is $w_0 = 0.0301$. Table 10.5.3 contains center deflections and stresses for the problem (see [36-38]). Figure 10.5.3 contains plots of load versus center deflection of an isotropic plate ($h = 0.138$ in., $E = 1.28 \times 10^6$ psi, and $\nu = 0.3$); the CPT deflections were obtained using 8×8 mesh of the non-conforming elements and the FSDT deflections were obtained with 4×4 Q9 mesh (mesh of nine-node Lagrange elements).

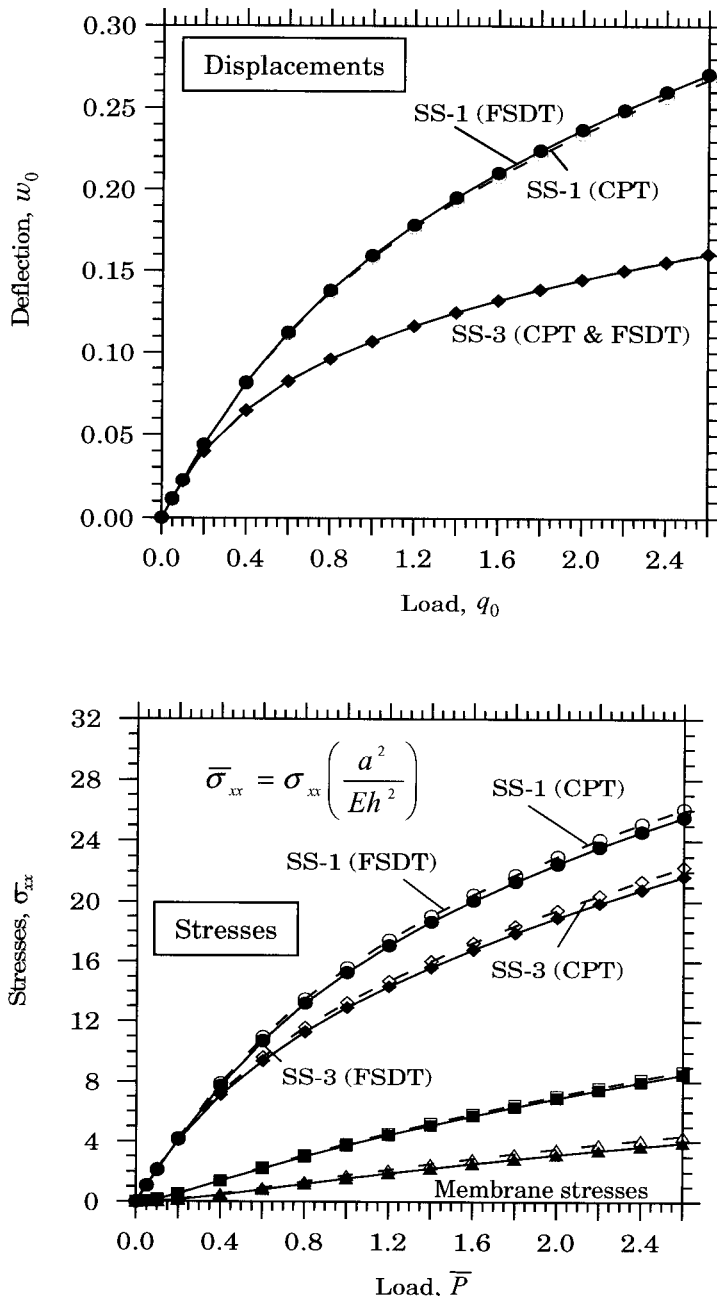


Figure 10.5.2: Center deflection $w_0(0,0)$ and stresses $\bar{\sigma}_{xx}$ as functions of the load q_0 for simply supported, orthotropic, square plates under uniformly distributed load.

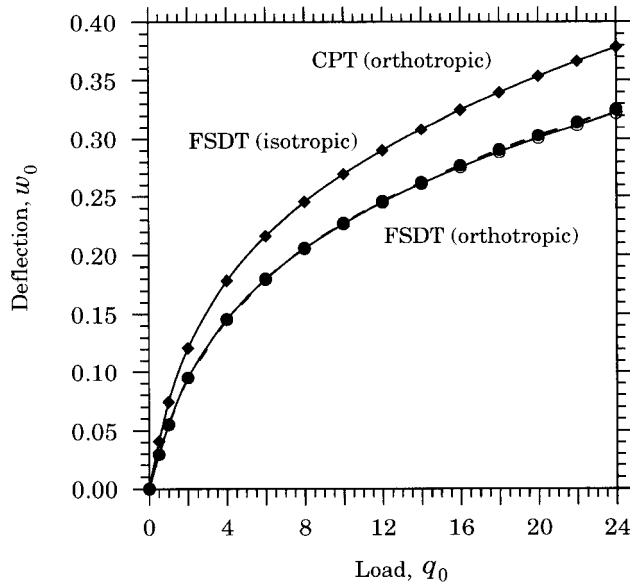


Figure 10.5.3: Nonlinear center deflection w_0 versus load parameter q_0 for clamped, orthotropic, square plates under uniform load.

Table 10.5.3: Center deflection w_0 and normal stress $\bar{\sigma}_{xx}$ for clamped orthotropic square plates under uniformly distributed load (4 × 4Q9).

q_0	w_0	$\bar{\sigma}_{xx}$	q_0	w_0	$\bar{\sigma}_{xx}$
0.5	0.0294 (3)	4.317	12.0	0.2450 (2)	46.001
1.0	0.0552 (3)	8.467	14.0	0.2610 (2)	49.851
2.0	0.0948 (3)	15.309	16.0	0.2754 (2)	53.431
4.0	0.1456 (3)	24.811	18.0	0.2886 (2)	56.800
6.0	0.1795 (3)	31.599	20.0	0.3006 (2)	59.998
8.0	0.2054 (3)	37.078	22.0	0.3119 (2)	63.053
10.0	0.2268 (2)	41.793	24.0	0.3224 (2)	65.986

10.5.3 Laminated Composite Plates

In this section examples of laminated plates with various laminations schemes and edge conditions are presented. Unless stated otherwise, all example problems are analyzed using the FSDT element.

Example 10.5.4:

This example is concerned with the nonlinear bending of a square, simply-supported (SS-1), orthotropic plate (see Figure 10.5.4 for the geometry and boundary conditions) made of high modulus glass-epoxy fiber-reinforced material

$$E_1 = 25E_2, \quad E_2 = \times 10^6, \quad G_{12} = G_{13} = 0.5E_2, \quad G_{23} = 0.2E_2, \quad \nu_{12} = 0.25 \quad (10.5.7)$$

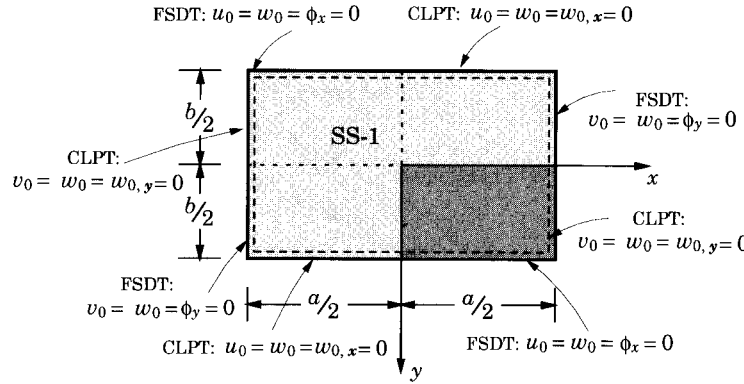


Figure 10.5.4: Geometric boundary conditions for SS-1 type simply supported rectangular plates.

and subjected to sinusoidal or uniform load. Uniform meshes of 8×8 CPT nonconforming elements and 4×4 nine-node quadratic FSDT elements in a quarter plate. The linear deflections predicted by the CPT and FSDT elements for $\bar{P} \equiv (q_0 a^4 / E_2 h^4) = 10$ and plate side-to-thickness ratio of $a/h = 10$ are $\hat{w} \equiv w_0(0,0)(E_2 h^3 / q_0 a^4) = 0.0653$ and $\hat{w} = 0.0952$. These values coincide with the analytical solutions (see Reddy [40]). Table 10.5.4 contains results of the nonlinear analysis for $a/h = 10$ (also see Figure 10.5.5). The following nondimensionalizations are used:

$$\begin{aligned}\bar{w} &= \frac{w_0}{h}, & \bar{\sigma}_{xx} &= \sigma_{xx}(A, A, h/2) \frac{h^2}{E_2 a^2}, & \bar{\sigma}_{yy} &= \sigma_{yy}(A, A, h/2) \frac{h^2}{E_2 a^2} \\ \bar{\sigma}_{xy} &= \sigma_{xy}(B, B, -h/2) \frac{h^2}{E_2 a^2}, & \bar{\sigma}_{xz} &= \sigma_{xz}(B, A) \frac{h}{E_2 a}, & \bar{\sigma}_{yz} &= \sigma_{yz}(A, B) \frac{h}{q_0 a} \quad (10.5.8)\end{aligned}$$

where $A = 0.0625a$ and $B = 0.4375a$.

Table 10.5.4: Nondimensionalized maximum transverse deflections and stresses of simply supported (SS-1) square plates.

\bar{P}	\bar{w}	$\bar{\sigma}_{xx}$	$\bar{\sigma}_{yy}$	$\bar{\sigma}_{xy}$	$-\bar{\sigma}_{xz}$	$-\bar{\sigma}_{yz}$
10	0.0951	7.453	0.3771	0.4800	0.0540	0.0092
20	0.1895	14.852	0.7827	0.9845	0.1077	0.0183
30	0.2826	22.146	1.2117	1.5113	0.1608	0.0275
40	0.3738	29.291	1.6590	2.0583	0.2130	0.0366
50	0.4627	36.253	2.1198	2.6229	0.2641	0.0456
60	0.5491	43.010	2.5900	3.2026	0.3139	0.0546
70	0.6328	49.546	3.0660	3.7952	0.3624	0.0635
80	0.7136	55.856	3.5450	4.3985	0.4096	0.0722
90	0.7917	61.940	4.0248	5.0106	0.4554	0.0808
100	0.8670	67.802	4.5037	5.6300	0.4998	0.0893
110	0.9397	73.450	4.9804	6.2551	0.5430	0.0977
120	1.0099	78.893	5.4540	6.8849	0.5849	0.1058
130	1.0776	84.141	5.9239	7.5184	0.6256	0.1138
140	1.1431	89.205	6.3894	8.1548	0.6653	0.1217

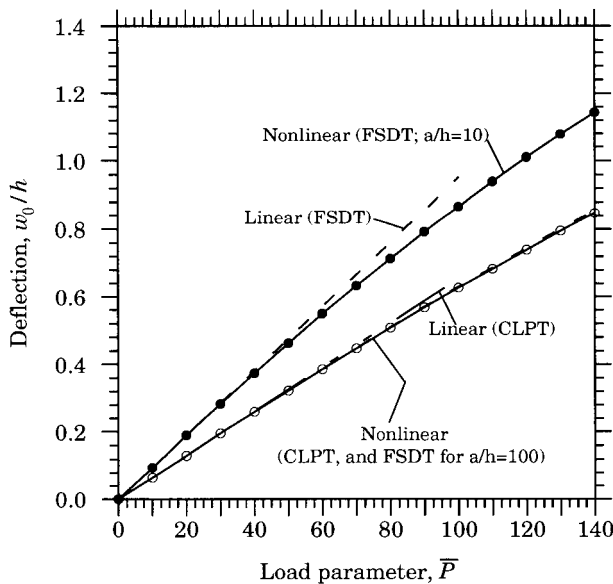


Figure 10.5.5: Nonlinear center deflection w_0 versus load parameter q_0 for simply supported (SS-1), orthotropic, square plates under uniform load.

Example 10.5.5:

This example is concerned with the nonlinear bending of a square, symmetric cross-ply (0/90/90/0) laminated plate made of layer properties, $E_1 = 1.8282 \times 10^6$, $E_2 = 1.8315 \times 10^6$, $G_{12} = G_{13} = G_{23} = 0.3125 \times 10^6$, $\nu_{12} = 0.2395$. The geometric parameters used are: $a = b = 12$ in and $h = 0.096$ in (each layer of 0.024 in. thick). A mesh of 4×4 Q9 FSDT elements in a quarter plate is used. Results for both clamped and SS-3 boundary conditions under uniform load are obtained. A load increment of $\Delta q_0 = 0.2$ psi is used. The maximum linear deflection for the clamped case is $w_0(0, 0) = 0.04102$ in and for SS-3 it is $w_0(0, 0) = 0.07611$ in. Table 10.5.5 and Figure 10.5.6 contain nondimensionalized deflections and stresses for the plate. The stresses are nondimensionalized as in Eq. (10.5.8).

Table 10.5.5: Maximum transverse deflections of clamped and simply supported (SS-3) cross-ply (0/90/90/0) square plates under uniform load.

q_0	Clamped Plate				Simply Supported Plate			
	$10w_0$	$\bar{\sigma}_{yy}$	$\bar{\sigma}_{xy}$	$10\bar{\sigma}_{xz}$	$10w_0$	$\bar{\sigma}_{yy}$	$\bar{\sigma}_{xy}$	$10^2\bar{\sigma}_{xz}$
0.2	0.3773	-1.2751	0.2540	0.0965	0.7324	-0.4254	1.4812	0.0265
0.4	0.6504	-1.5699	0.4903	0.1843	0.9946	0.3911	2.1387	0.0658
0.6	0.8489	-1.4175	0.7049	0.2647	1.1677	1.2271	2.6145	0.0987
0.8	1.0039	-1.0753	0.9031	0.3396	1.3012	2.0315	3.0012	0.1263
1.0	1.1316	-0.6444	1.0890	0.4103	1.4116	2.8012	3.3326	0.1499
1.2	1.2406	-0.1693	1.2651	0.4779	1.5067	3.5386	3.6249	0.1702
1.4	1.3362	0.3279	1.4331	0.5426	1.5908	4.2481	3.8881	0.1879
1.6	1.4216	0.8356	1.5944	0.6049	1.6667	4.9331	4.1284	0.2036
1.8	1.4991	1.3472	1.7499	0.6652	1.7360	5.5965	4.3503	0.2175
2.0	1.5701	1.8588	1.9003	0.7236	1.8001	6.2408	4.5567	0.2301
2.2	1.6359	2.3682	2.0461	0.7804	1.8597	6.8680	4.7501	0.2414
2.4	1.6972	2.8739	2.1878	0.8358	1.9156	7.4798	4.9322	0.2516

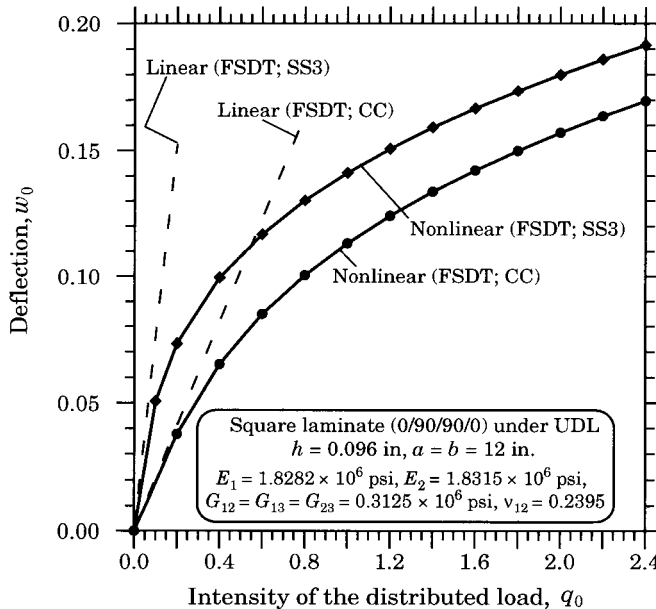


Figure 10.5.6: Load-deflection curves for symmetric cross-ply (0/90/90/0) laminates.

Example 10.5.6:

Here we consider nonlinear bending of square, antisymmetric, cross-ply (0/90/0/90...) laminated plates made of material

$$E_1 = 40 \times 10^6, \quad E_2 = 10^6, \quad G_{12} = G_{13} = 0.6E_2, \quad G_{23} = 0.5E_2, \quad v_{12} = 0.25 \quad (10.5.9)$$

The geometric parameters used are: $a = b = 12$ in and total thickness $h = 0.3$ in. Again, uniform mesh of 4×4 Q9 FSDT elements in a quarter plate is used. Results for clamped boundary conditions under uniform load are obtained. A load increment of $\Delta q_0 = 200$ psi is used. The maximum linear deflection for two layers (0/90) is $w_0(0,0) = 0.22683$ in, and for six layers (0/90/0/90/0/90) it is $w_0(0,0) = 0.08669$ in. Table 10.5.6 contains results of the nonlinear analysis (also see Figure 10.5.7). Note that the six-layer laminate is relatively stiffer than the two-layer laminate (for the same total thickness of the laminates).

10.5.4 Effect of Symmetry Boundary Conditions on Nonlinear Response

As discussed in Chapters 5, 6, and 7, the Navier solutions of the linear theories can be developed for antisymmetric cross-ply plates with SS-1 boundary conditions and antisymmetric angle-ply laminates with the SS-2 boundary conditions. The Navier solutions can be used to determine the conditions on deflections and forces along the lines of biaxial symmetry, i.e., along the lines $x = a/2$ and $y = b/2$ of a rectangular plate of dimension $a \times b$ and with the origin of the (x,y) coordinate system being at the lower left corner of the plate. If the symmetry conditions implied by the Navier solutions are used in the linear finite element analysis of a quarter plate, as was

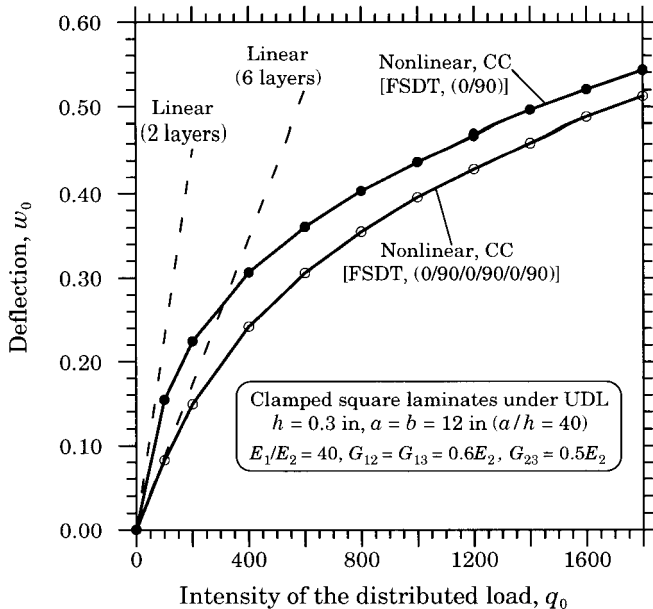


Figure 10.5.7: Load-deflection curves for clamped, antisymmetric cross-ply (0/90/0/90 \cdots) laminated square plates under uniform load.

Table 10.5.6: Maximum deflections of two-layer and six-layer cross-ply (0/90/0/90 \cdots) square plates under uniform load.

q_0	(0°/90°)				(0/90/0/90/0/90)		
	w_0	$\bar{\sigma}_{xx}$	$\bar{\sigma}_{yy}$	w_0	$\bar{\sigma}_{xx}$	$\bar{\sigma}_{yy}$	
100	0.1541	82.63	-0.3807	0.0826	-28.40	-1.423	
200	0.2243	130.03	9.3434	0.1491	-40.12	-2.200	
400	0.3063	195.00	1.1977	0.2419	-37.73	-2.644	
600	0.3609	245.53	2.2529	0.3095	-22.49	-2.482	
800	0.4032	289.35	3.2416	0.3552	-2.96	-2.092	
1,000	0.4385	329.07	4.1747	0.3957	18.19	-1.599	
1,200	0.4690	365.89	5.0614	0.4303	39.91	-1.055	
1,400	0.4961	400.54	5.9104	0.4607	61.74	-0.486	
1,600	0.5206	433.46	6.7275	0.4879	83.47	0.095	
1,800	0.5431	464.97	7.5173	0.5126	104.99	0.680	

done in Chapter 9, one obtains correct full plate solutions. When quarter-plate models with the geometric boundary conditions implied by the Navier solutions on the lines of symmetry are used in the nonlinear finite element analysis, results do not agree, in general, with those of the corresponding full-plate models (see Reddy [51]).

To illustrate this point, a two-layer, antisymmetric angle-ply (45/-45) square laminate ($a = 1000$ mm, $h = 2$ mm), under uniform transverse load is considered.

The following layer properties are used:

$$\begin{aligned} E_1 &= 250 \text{ GPa}, \quad E_2 = 20 \text{ GPa}, \quad G_{12} = G_{13} = 10 \text{ GPa} \\ G_{23} &= 4 \text{ GPa}, \quad \nu_{12} = \nu_{13} = 0.25 \end{aligned} \quad (10.5.10)$$

The load-deflection curves obtained from the quarter-plate and full-plate analyses are shown in Figure 10.5.8. Meshes of 2×2 and 4×4 nine-node quadratic elements based on the first-order shear deformation plate theory are used to model the quarter and full plates, respectively. The following boundary conditions along the lines of symmetry were used:

$$\begin{aligned} \text{at } x = a/2 : \quad v_0 &= \phi_x = 0 ; \quad N_{xx} = M_{xy} = 0 \\ \text{at } y = b/2 : \quad u_0 &= \phi_y = 0 ; \quad N_{yy} = M_{xy} = 0 \end{aligned} \quad (10.5.11)$$

where the coordinate system is fixed at the lower left corner of the laminate.

Note that the force boundary conditions are included in the finite element model in an integral sense. It is clear from the results that the use of a quarter-plate model with the symmetry conditions (10.5.11) yields larger deflections than those obtained from the full-plate model. The discrepancy increases with the intensity of the transverse load. This discrepancy can be explained in the light of the symmetry conditions (10.5.11) used to model the quarter plate. As noted earlier, the symmetry

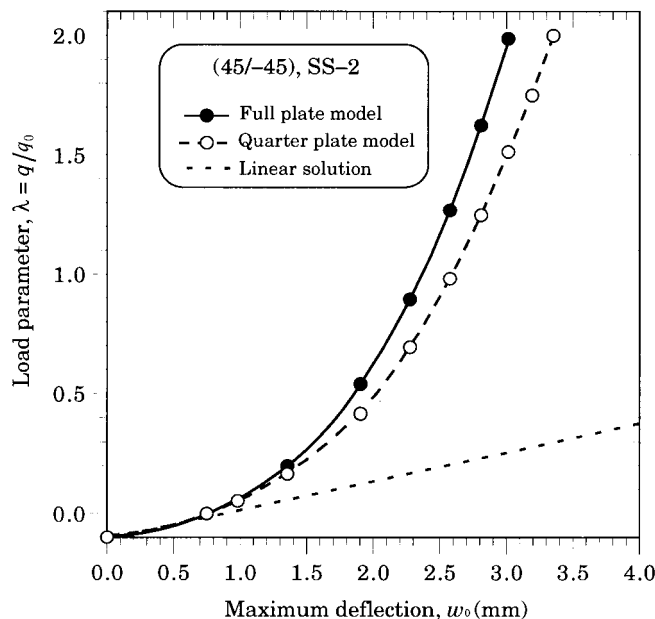


Figure 10.5.8: Load-deflection curves (λ vs. w_0) for full-plate and quarter-plate models of simply supported (SS-2) antisymmetric angle-ply (45/-45) laminates.

conditions are derived from the Navier solution for the linear theory. For the angle-ply case, the assumed solution is of the form [see Eqs. (7.3.2)]

$$\begin{aligned} u_0 &= \sum_{m,n=1}^{\infty} U_{mn} \sin \frac{m\pi x}{a} \cos \frac{n\pi y}{b}, \quad v_0 = \sum_{m,n=1}^{\infty} V_{mn} \cos \frac{m\pi x}{a} \sin \frac{n\pi y}{b} \\ w_0 &= \sum_{m,n=1}^{\infty} W_{mn} \sin \frac{m\pi x}{a} \sin \frac{n\pi y}{b} \\ \phi_x &= \sum_{m,n=1}^{\infty} S_{mn}^1 \cos \frac{m\pi x}{a} \sin \frac{n\pi y}{b}, \quad \phi_y = \sum_{m,n=1}^{\infty} S_{mn}^2 \sin \frac{m\pi x}{a} \cos \frac{n\pi y}{b} \end{aligned} \quad (10.5.12)$$

The resultant forces N_{xx} and N_{yy} and moment M_{xy} are given by (note that $A_{16} = A_{26} = A_{45} = 0$, $B_{11} = B_{12} = B_{22} = B_{66} = 0$, and $D_{16} = D_{26} = 0$)

$$\begin{aligned} N_{xx} &= A_{11} \left[\frac{\partial u_0}{\partial x} + \frac{1}{2} \left(\frac{\partial w_0}{\partial x} \right)^2 \right] + A_{12} \left[\frac{\partial v_0}{\partial y} + \left(\frac{\partial w_0}{\partial y} \right)^2 \right] \\ &\quad + B_{16} \left(\frac{\partial \phi_x}{\partial y} + \frac{\partial \phi_y}{\partial x} \right) \end{aligned} \quad (10.5.13a)$$

$$\begin{aligned} N_{yy} &= A_{12} \left[\frac{\partial u_0}{\partial x} + \frac{1}{2} \left(\frac{\partial w_0}{\partial x} \right)^2 \right] + A_{22} \left[\frac{\partial v_0}{\partial y} + \left(\frac{\partial w_0}{\partial y} \right)^2 \right] \\ &\quad + B_{26} \left(\frac{\partial \phi_x}{\partial y} + \frac{\partial \phi_y}{\partial x} \right) \end{aligned} \quad (10.5.13b)$$

$$\begin{aligned} M_{xy} &= B_{16} \left[\frac{\partial u_0}{\partial x} + \frac{1}{2} \left(\frac{\partial w_0}{\partial x} \right)^2 \right] + B_{26} \left[\frac{\partial v_0}{\partial y} + \left(\frac{\partial w_0}{\partial y} \right)^2 \right] \\ &\quad + D_{66} \left(\frac{\partial \phi_x}{\partial y} + \frac{\partial \phi_y}{\partial x} \right) \end{aligned} \quad (10.5.13c)$$

The expressions in Eqs. (10.5.13a-c), for the nonlinear case, indicate that the force boundary conditions in (10.5.11) are *not* satisfied. For example, N_{xx} and N_{yy} have the form

$$\begin{aligned} N_{xx}(a/2, y) &\approx A_{12} \frac{n^2 \pi^2 W_{mn}^2}{2b^2} \cos^2 \frac{n\pi y}{b} \neq 0 \\ N_{yy}(x, b/2) &\approx A_{12} \frac{m^2 \pi^2 W_{mn}^2}{2a^2} \cos^2 \frac{m\pi x}{a} \neq 0 \end{aligned} \quad (10.5.14)$$

When a quarter plate model is used without specifying u_0 on line $x = a/2$ and v_0 on line $y = b/2$, in the finite element analysis it is implied that the natural boundary conditions $N_{xx} = 0$ on $x = a/2$ and $N_{yy} = 0$ on $y = b/2$ are specified. The quarter-plate model with zero in-plane forces $N_{xx}(a/2, y)$ and $N_{yy}(x, b/2)$ simulates the plate as more flexible than the full-plate model, in which the in-plane forces are not taken to be zero on the lines of symmetry.

For antisymmetric cross-ply laminates, a quarter-plate model with the symmetry conditions implied by the Navier solution gives the same solution as the full-plate

model for both linear and nonlinear theories. This is due to the fact that the zero force boundary conditions are satisfied in an integral sense for cross-ply laminates.

10.5.5 Nonlinear Response Under In-Plane Compressive Loads

Another interesting characteristic of composite laminates is their behavior under compressive loads. Most often the critical buckling loads are determined through an eigenvalue analysis. The critical buckling loads can also be determined from geometric nonlinear analysis, where the critical buckling load is taken to be the so-called limit load.

First we consider an angle-ply (45/-45) laminate with the following geometric parameters and material properties:

$$\begin{aligned} a = b &= 1,000 \text{ mm}, \quad h = 2 \text{ mm} \\ E_1 &= 40E_2, \quad E_2 = 6.25 \text{ GPa}, \quad G_{12} = G_{13} = 0.82E_2, \quad G_{23} = 0.52E_2 \\ \nu_{12} &= \nu_{13} = 0.24, \quad \nu_{23} = 0.49 \end{aligned} \quad (10.5.15)$$

For SS-2 type simply supported boundary conditions, the uniaxial buckling load can be determined analytically (see Chapter 7). Here we use 4×4 mesh of nine-node elements in the full plate to determine the critical buckling load, and the same mesh is used to determine the nonlinear response under applied in-plane compressive load $N_{yy} = \lambda_0 N_{yy}^0$, where λ_0 is the critical buckling load determined from the eigenvalue analysis. Figure 10.5.9 contains a plot of the maximum out-of-plane deflection w_0 (mm) versus load parameter λ ($N_{yy}^0 = 10.85$ N/m). It is clear the load-deflection curve exhibits a limit point, which is the same as the critical buckling load determined from the eigenvalue analysis.

Next we consider antisymmetric cross-ply laminates. The geometry and materials properties used are the same as those used for the angle-ply laminate. The SS-1 type simply supported boundary conditions and 2×2 mesh of nine-node elements in a quarter plate are used to determine the critical buckling loads N_0 by eigenvalue analysis and load-deflection curves in the nonlinear analysis under in-plane load $N_{yy} = \lambda_0 N_{yy}^0$ ($N_{yy}^0 = 6.25$ N/m). Figure 10.5.10 contains load-deflection curves for two-, four-, six-, and eight-layer laminates. The critical buckling loads are indicated on the load-deflection curves for comparison. Unlike the angle-ply laminates, the cross-ply laminates do not exhibit clear limit-load behavior.

10.5.6 Nonlinear Response of Antisymmetric Cross-Ply Laminated Plate Strips

Unlike isotropic metallic plates, composite plates exhibit quite different nonlinear behavior. For example, the geometric nonlinear effects could be very significant even at small loads and deflections, depending on the lamination scheme and boundary conditions (see [24,25,52]). To illustrate the point we analyze an antisymmetric cross-ply square laminate (90/0) with two opposite edges pinned ($u_0 = 0$) or hinged ($u_0 \neq 0$) and the other two edges free, and subjected to uniformly distributed transverse load.

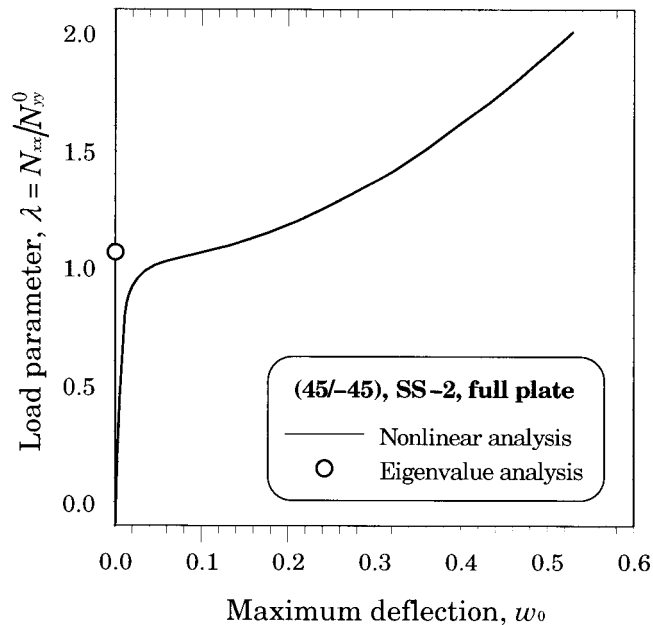


Figure 10.5.9: Load-deflection curves (λ vs. w_0) of a simply supported (SS-2) two-layer antisymmetric angle-ply (45/-45) laminate under uniformly distributed in-plane compressive edge load.

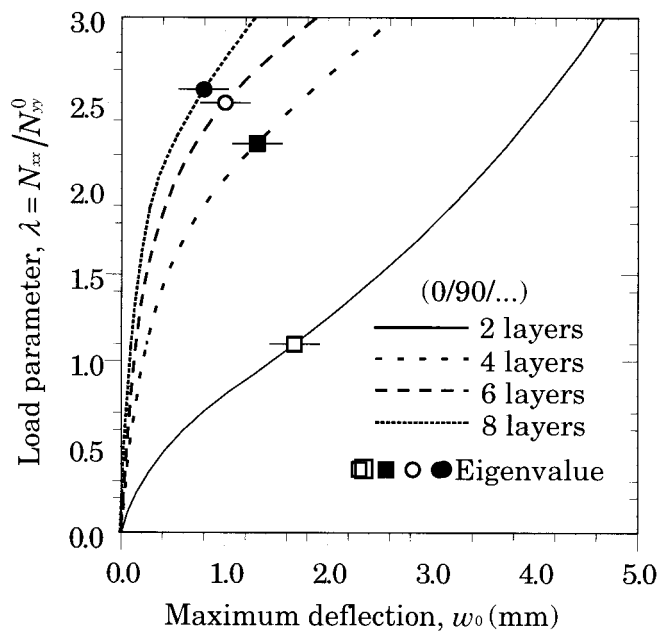


Figure 10.5.10: Load-deflection curves (λ vs. w_0) of a simply supported (SS-1) antisymmetric cross-ply (0/90/ \dots) laminate under uniformly distributed in-plane compressive edge load.

The geometry, finite element mesh, and boundary conditions for the pinned-pinned and hinged-hinged cases are shown in Figure 10.5.11. The material properties and geometric parameters used are

$$\begin{aligned} E_1 &= 20 \text{ msi}, \quad E_2 = 1.4 \text{ msi}, \quad \nu_{12} = 0.3, \quad G_{12} = G_{13} = G_{23} = 0.7 \text{ msi} \\ a &= 9 \text{ in.}, \quad b = 1.5 \text{ in.}, \quad h = 0.4 \text{ in.} \end{aligned} \quad (10.5.16)$$

The results of the nonlinear analysis are presented in Table 10.5.7. For hinged-hinged boundary conditions, the plate strip is essentially in pure bending and hence the axial force $N_{xx} = 0$. Therefore, the solution is independent of the sign of the applied load. For a pinned plate strip, the axial force N_{xx} is not zero; it is

$$N_{xx} = A_{11} \left[\frac{du_0}{dx} + \frac{1}{2} \left(\frac{dw_0}{dx} \right)^2 \right] + B_{11} \frac{d\phi_x}{dx}, \quad B_{11} < 0 \quad (10.5.17)$$

For small values of the positive load, the expression containing the A_{11} coefficient is small compared to the expression containing the B_{11} coefficient, which is negative for $0 < x < 4.5$. Hence, N_{xx} is compressive and increases the transverse deflection — analogous to the transverse deflection of a plate strip under an axial compressive load and a transverse load. Thus, the nonlinear solution is larger than the linear solution for small values of the load. As the load is increased, the A_{11} expression becomes larger than the B_{11} expression, and N_{xx} becomes positive. This stiffens the structure and the nonlinear solution becomes smaller than the linear solution. The load deflection curves for the first few load steps are shown in Figure 10.5.12. For a negative load, $B_{11} \frac{d\phi_x}{dx}$ is positive, and the two terms in N_{xx} add up; this yields a larger axial force and therefore a stiffer structure than for the positive load case. Therefore the deflection is lower than that for the case of positive load.

Table 10.5.7: Transverse deflections, w_0/h , of cylindrical bending of a (90/0) laminate under uniformly distributed transverse load.

Load P_0	Pinned			Hinged	
	Linear*	Nonlinear*	Nonlinear†	Case 1*	Case 2†
0.005	-0.235	-0.159	0.475	-0.429	0.429
0.01	-0.470	-0.255	0.673	-0.858	0.858
0.02	-0.940	-0.386	0.847	-1.710	1.710
0.03	-1.41	-0.480	0.954	-2.550	2.55
0.04	-1.88	-0.555	1.034	-3.370	3.37
0.05	-2.35	-0.618	1.100	-4.190	4.19
0.10	-4.70	-0.845	1.327	-7.920	7.92
0.25	-11.75	-1.233	1.705	-16.16	16.17
0.50	-23.50	-1.609	2.075	-24.82	24.82
0.75	-35.25	-1.870	2.332	-30.87	30.87
1.0	-47.00	-2.078	2.532	-35.69	35.69
2.0	-94.00	-2.665	3.117	-49.56	49.56
3.0	-141.00	-3.075	3.525	-59.65	59.65
4.0	-188.00	-3.402	3.850	-68.00	68.00
5.0	-235.00	-3.675	4.125	-75.33	75.33

*For negative load values. † For positive load values.

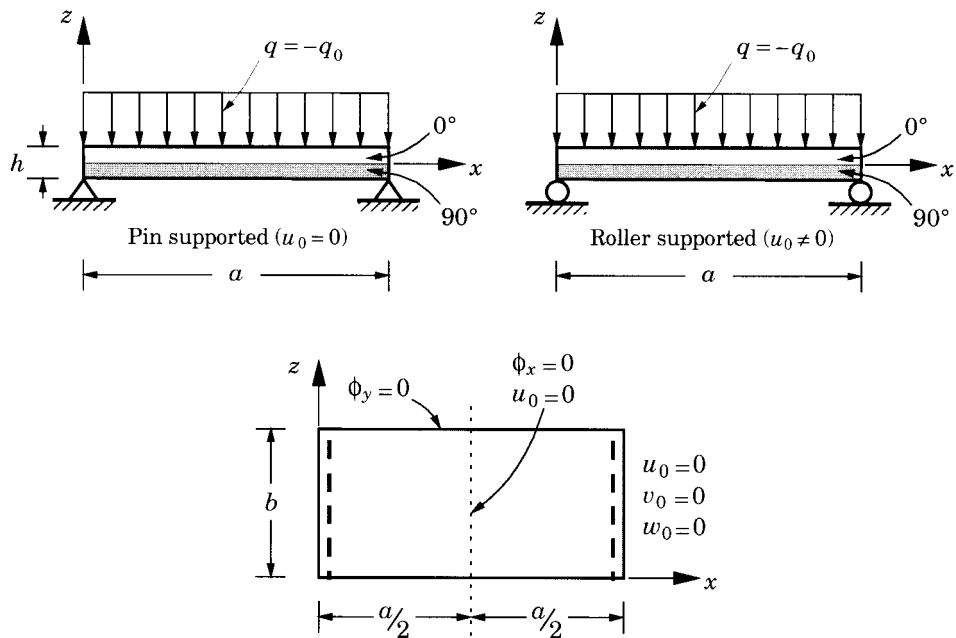


Figure 10.5.11: Geometry, loading, and boundary conditions used for cylindrical bending of a cross-ply plate strip.

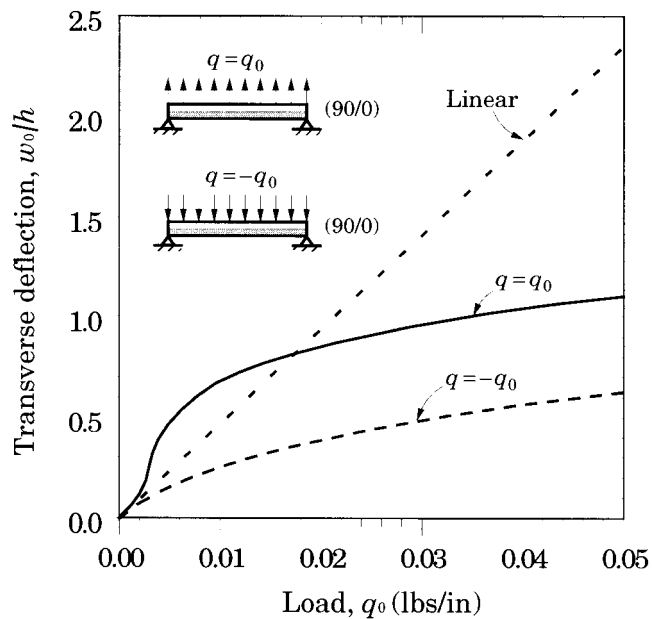


Figure 10.5.12: Load-deflection curves (q_0 vs. w_0) for cylindrical bending of a cross-ply (90/0) plate strip with pinned-pinned edges.

10.5.7 Transient Analysis of Composite Plates

Nonlinear transient response of laminated composite plates was reported by Reddy [20]. Here we present a few examples from this paper. For additional examples, the reader may consult [20]. In all examples discussed here, suddenly applied transverse step loads are considered, and the initial conditions are taken to be zero. In the nonlinear transient analysis, there are three loops. The iterative loop for convergence of the solution is the innermost, followed by loops on time increments and the load increments.

The first example involves a simply supported isotropic square plate subjected to suddenly applied uniformly distributed transverse load. The following geometric, material, and load parameters were used:

$$\begin{aligned} a = b &= 243.8 \text{ cm}, \quad h = 0.635 \text{ cm}, \quad \rho = 2.547 \times 10^{-6} \text{ N}\cdot\text{s}^2/\text{cm}^4 \\ E_1 = E_2 &= 7.031 \times 10^5 \text{ N/cm}^2, \quad \nu_{12} = 0.25 \\ q_0 &= 4.882 \times 10^{-4} \text{ N/cm}^2, \quad \Delta t = 0.005 \text{ s} \end{aligned} \quad (10.5.18)$$

Figure 10.5.13 shows the center deflection w_0 as a function of time for four different values of the load and two different time steps. The amplitude increases while the period of response decreases with an increase in the intensity of load. Load versus the maximum deflection is also shown in the figure. This problem may serve as a reference for verification of the geometric nonlinear option of a finite element program.

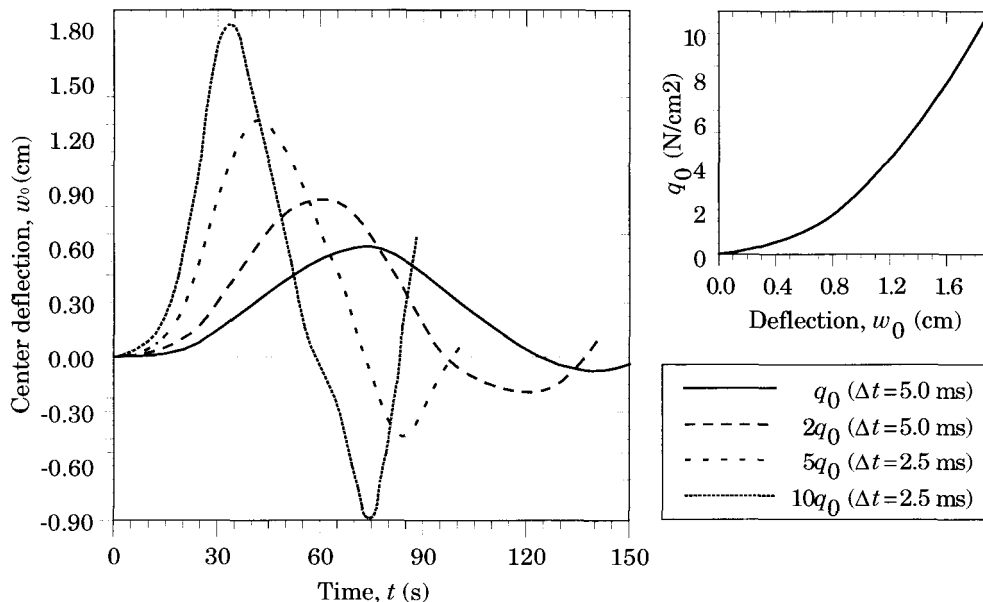


Figure 10.5.13: Center deflection versus time for nonlinear transient analysis of an isotropic, simply supported, square plate.

Next, we consider nonlinear transient analysis of simply supported cross-ply (0/90) and angle-ply (45/-45) plates. Figure 10.5.14 contains plots of center deflections ($\bar{w} = w_0 \times 10^3$ and $\dot{w} = w_0 \times 10^2$) of simply supported (SS-1) cross-ply laminated rectangular plate ($a = \sqrt{2}$, $b = 1$, $h = 0.2$, $\rho = 1.0$, in English units of inches and pounds) under uniformly distributed transverse patch loading of intensity $q_0 = 10^{-2}$ over the area $0 \leq (x, y) \leq 0.2$. The material properties were assumed to be

$$E_1 = 25E_2, \quad G_{12} = G_{13} = 0.5E_2, \quad G_{23} = 0.2E_2, \quad \nu_{12} = 0.25 \quad (10.5.19)$$

A time step of $\Delta t = 0.1$ was used. A nonuniform 4×4 mesh of nine-node quadratic elements in quarter plate was used. Figure 10.5.14 contains results of both five and three degrees of freedom models. The three degrees of freedom element models the plate stiffer than the five degrees of freedom element.

Figure 10.5.15 contains plots of center deflection versus time for simply supported (SS-2), square ($a = b = 243.8$ cm, $h = 0.635$ cm, $\rho = 2.547 \times 10^{-6}$ Ns²/cm⁴), angle-ply (45/-45) plates under uniformly distributed pressure loading ($q_0 = 50 \times 10^{-4}$ N/cm²). The material properties in Eq. (10.5.19) were used. The effect of geometric nonlinearity is obvious from the figure.

10.6 Functionally Graded Plates

10.6.1. Background

While laminated composite materials provide the design flexibility to achieve desirable stiffness and strength through the choice of lamination scheme, the anisotropic constitution of laminated composite structures often results in stress concentrations near material and geometric discontinuities that can lead to damage in the form of delamination, matrix cracking, and adhesive bond separation. Functionally gradient materials (FGM) are a class of composites that have a *continuous* variation of material properties from one surface to another and thus alleviate the stress concentrations found in laminated composites. The gradation in properties of the material reduces thermal stresses, residual stresses, and stress concentration factors. The gradual variation results in a very efficient material tailored to suit the needs of the structure and therefore is called a functionally graded material. They are typically manufactured from isotropic components such as metals and ceramics since they are mainly used as thermal barrier structures in environments with severe thermal gradients (e.g., thermoelectric devices for energy conversion, semiconductor industry). In such applications the ceramic provides heat and corrosion resistance; meanwhile the metal provides the strength and toughness.

Thin-walled members, i.e., plates and shells, used in reactor vessels, turbines and other machine parts are susceptible to failure from buckling, large amplitude deflections, or excessive stresses induced by thermal or combined thermomechanical loading. The main applications of functionally gradient materials have been in high temperature environments, including thermal shock – a situation that arises when a body is subjected to a high transient heating or cooling in a short time period. References 54–69 provide a background and insights into thermomechanical and transient analysis of FGM structures. A brief review of the work carried out in [54,69] for plates is presented here.

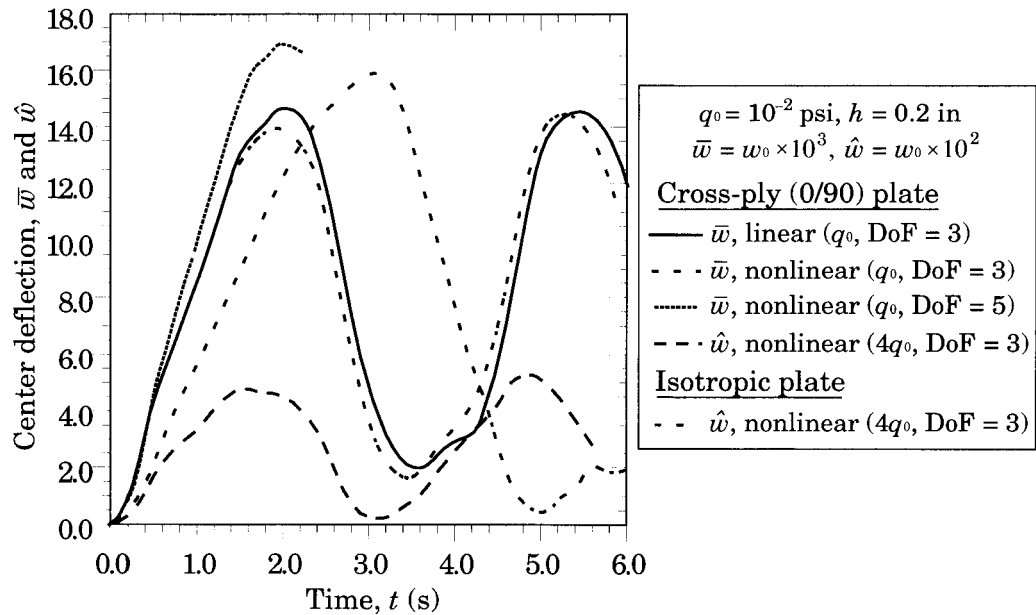


Figure 10.5.14: Center deflection versus time for nonlinear transient analysis of a simply supported (SS-1) cross-ply (0/90) plate.

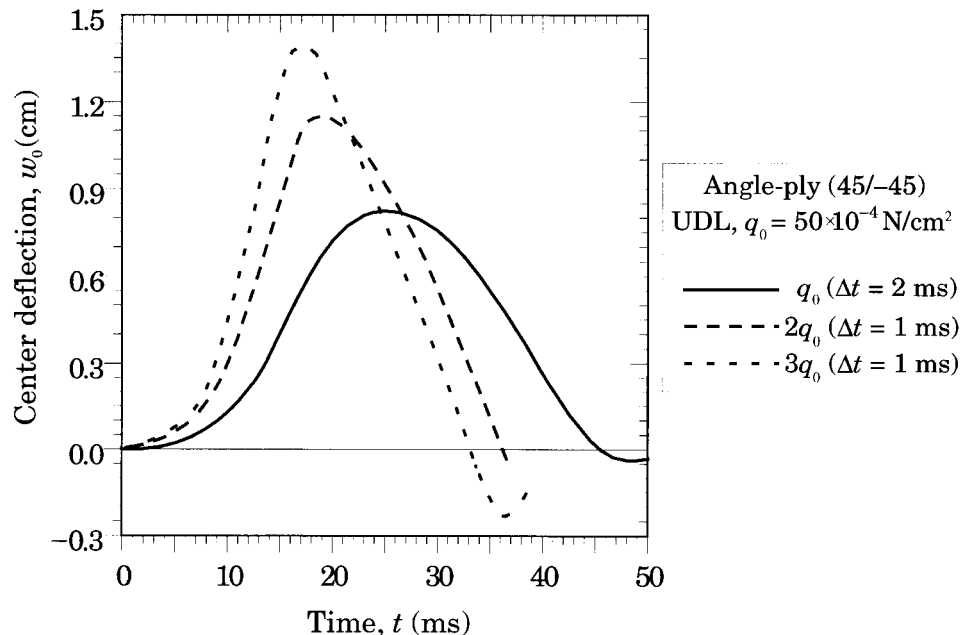


Figure 10.5.15: Center deflection versus time for nonlinear transient analysis of a simply supported (SS-2) angle-ply (45/-45) square plate under suddenly applied uniformly distributed transverse load.

10.6.2 Theoretical Formulation

Consider a plate of total thickness h and made of an isotropic but inhomogeneous material through the thickness of the plate. Further, we restrict the formulation to linear elastic material behavior, small strains and displacements, and to the case in which the temperature field is known.

Suppose that a typical material property P is varied through the plate thickness according to the expressions (a power law)

$$P(z) = (P_t - P_b)V + P_b, \quad V = \left(\frac{z}{h} + \frac{1}{2} \right)^n \quad (10.6.1)$$

where P_t and P_b denote the property of the top and bottom faces of the plate, respectively, and n is a parameter that dictates the material variation profile through the thickness. Here we assume that moduli E and G , density ρ , thermal coefficient of expansion α , and thermal conductivity k vary according to Eq. (10.6.1), while ν is assumed to be a constant. We take $P_t = P_c$ and $P_b = P_m$ as the properties of the ceramic and metal, respectively. The metal content in the plate increases as the value of n increases. The value of $n = 0$ represents a fully ceramic plate. The above power law assumption reflects a simple rule of mixtures used to obtain the effective properties of the ceramic-metal plate.

The through-thickness functionally graded plate is an inhomogeneous (through the thickness) isotropic plate, exhibiting bending stretching coupling (i.e., not all $B_{ij} = 0$). Hence, the governing equations of motion as well as the finite element models derived for the CLPT and FSDT are valid for the FGM plates. However, the temperature distribution through the thickness must be calculated by solving the equation

$$-\frac{d}{dz} \left(k(z) \frac{dT}{dz} \right) = 0 \quad (10.6.2a)$$

$$T\left(-\frac{h}{2}\right) = T_m, \quad T\left(\frac{h}{2}\right) = T_c \quad (10.6.2b)$$

The temperature field $T(z)$ is then used in computing the thermal forces and moments

$$\{N^T\} = \int_{-\frac{h}{2}}^{\frac{h}{2}} \{\beta\} T(z) dz, \quad \{M^T\} = \int_{-\frac{h}{2}}^{\frac{h}{2}} \{\beta\} T(z) z dz \quad (10.6.3a)$$

$$\{\beta\} = [Q]\{\alpha\} = \begin{Bmatrix} (Q_{11}(z) + Q_{12}(z)) \alpha(z) \\ (Q_{12}(z) + Q_{22}(z)) \alpha(z) \\ 0 \end{Bmatrix} \quad (10.6.3b)$$

The plate stiffnesses are given by

$$(A_{ij}, B_{ij}, D_{ij}) = \int_{-\frac{h}{2}}^{\frac{h}{2}} Q_{ij}(z) (1, z, z^2) dz \quad (i, j = 1, 2, 6) \quad (10.6.4a)$$

$$A_{ij} = \int_{-\frac{h}{2}}^{\frac{h}{2}} Q_{ij}(z) dz \quad (i, j = 4, 5) \quad (10.6.4b)$$

$$(I_0, I_1, I_2) = \int_{-\frac{h}{2}}^{\frac{h}{2}} \left[(\rho_c - \rho_m) \left(\frac{2z + h}{2h} \right)^n + \rho_m \right] (1, z, z^2) dz \quad (10.6.4c)$$

$$Q_{11} = Q_{22} = \frac{E(z)}{1 - \nu^2}, \quad Q_{12} = Q_{21} = \frac{\nu E(z)}{1 - \nu^2}$$

$$Q_{44} = Q_{55} = Q_{66} = \frac{E}{2(1 + \nu)} \quad (10.6.4d)$$

where quantities with subscripts, ‘*m*’ and ‘*c*’ correspond to the metal and ceramic, respectively. The modulus *E* and the thermal coefficient of expansion α , and the elastic coefficients Q_{ij} , vary through the plate thickness according to Eqs. (10.6.1a,b).

10.6.3 Thermomechanical Coupling

The finite element model associated with Eq. (10.6.2a) is of the form (see Reddy [32])

$$\begin{aligned} [K^T]\{T\} &= \{Q\}, \quad K_{ij}^T = \int_{z_b}^{z_t} k(z) \frac{d\psi_i}{dz} \frac{d\psi_j}{dz} dz, \\ Q_i &= \psi_i(z_t) \left(k \frac{dT}{dz} \right)_{z=z_t} + \psi_i(z_b) \left(-k \frac{dT}{dz} \right)_{z=z_b} \end{aligned} \quad (10.6.5)$$

Due to the dependence of the conductivity *k* on *z*, the temperature distribution through the thickness of a FGM plate, for the boundary conditions given in (10.6.2b), is a nonlinear function of *z*.

Next, we wish to examine the contribution of the temperature field to the nonlinear finite element equations. The thermal contributions to the finite element equations associated with the five generalized displacements are:

$$\begin{aligned} \delta u_0 : \quad & \int_{\Omega_e} \left(N_{xx}^T \frac{\partial \psi_i^{(1)}}{\partial x} + N_{xy}^T \frac{\partial \psi_i^{(1)}}{\partial y} \right) dx dy \\ \delta v_0 : \quad & \int_{\Omega_e} \left(N_{xy}^T \frac{\partial \psi_i^{(1)}}{\partial x} + N_{yy}^T \frac{\partial \psi_i^{(1)}}{\partial y} \right) dx dy \\ \delta w_0 : \quad & \sum_{j=1}^n \left\{ \int_{\Omega_e} \left[N_{xx}^T \frac{\partial \psi_i^{(2)}}{\partial x} \frac{\partial \psi_j^{(2)}}{\partial x} + N_{yy}^T \frac{\partial \psi_i^{(2)}}{\partial y} \frac{\partial \psi_j^{(2)}}{\partial y} \right. \right. \\ & \quad \left. \left. + N_{xy}^T \left(\frac{\partial \psi_i^{(2)}}{\partial x} \frac{\partial \psi_j^{(2)}}{\partial y} + \frac{\partial \psi_i^{(2)}}{\partial y} \frac{\partial \psi_j^{(2)}}{\partial x} \right) \right] dx dy \right\} w_j \\ \delta \phi_x : \quad & \int_{\Omega_e} \left(M_{xx}^T \frac{\partial \psi_i^{(3)}}{\partial x} + M_{xy}^T \frac{\partial \psi_i^{(3)}}{\partial y} \right) dx dy \\ \delta \phi_y : \quad & \int_{\Omega_e} \left(M_{xy}^T \frac{\partial \psi_i^{(3)}}{\partial x} + M_{yy}^T \frac{\partial \psi_i^{(3)}}{\partial y} \right) dx dy \end{aligned} \quad (10.6.6)$$

The thermal contribution associated with δw_0 is nonlinear in w_0 . For the purpose of computational efficiency, this term is included in the stiffness matrix. Therefore,

The K^{33} term of the stiffness matrix can be expressed as (superscript 2 on ψ_i is omitted for simplicity)

$$K_{ij}^{33} = \int_{\Omega_e} \left[N_{xx}^T \frac{\partial \psi_i}{\partial x} \frac{\partial \psi_j}{\partial x} + N_{yy}^T \frac{\partial \psi_i}{\partial y} \frac{\partial \psi_j}{\partial y} + N_{xy}^T \left(\frac{\partial \psi_i}{\partial x} \frac{\partial \psi_j}{\partial y} + \frac{\partial \psi_i}{\partial y} \frac{\partial \psi_j}{\partial x} \right) \right] dx dy \quad (10.6.7)$$

10.6.4 Numerical Results

Numerical results are presented for ceramic-metal FGM plates. The metal is taken to be aluminum and the ceramic used is zirconia. The properties for the two materials are listed below.

Aluminum

$$E = 70 \text{ GPa}; \quad \nu = 0.3, \quad \rho = 2,707 \text{ Kg/m}^3, \quad k = 204 \text{ W/mK}, \quad \alpha = 23 \times 10^{-6} \text{ }^\circ\text{C}$$

Zirconia

$$E = 151 \text{ GPa}; \quad \nu = 0.3, \quad \rho = 3,000 \text{ Kg/m}^3, \quad k = 2.09 \text{ W/mK}, \quad \alpha = 10 \times 10^{-6} \text{ }^\circ\text{C}$$

The plate considered is a square plate with side $a = 0.2$ m and thickness $h = 0.01$ m. The boundary conditions considered are all sides simply supported (SS-1). Because of the biaxial symmetry of the problem, the computational domain is taken to be the positive quadrant. A regular mesh of 4×4 four-node elements is used. In order to avoid membrane and shear locking, reduced integration is used in the numerical evaluation of the nonlinear and the shear terms of the stiffness matrix (see Reddy [32]).

The nondimensionalized quantities used in reporting the results are: center deflection, $\bar{w} = w_0/h$ and load parameter $P = q_0 a^4 / (E_m h^4)$. First, bending of FGM plates under transverse mechanical load is investigated. Figures 10.6.1 and 10.6.2 contain plots of nondimensionalized deflection \bar{w} versus the load parameter P for simply supported plates for various values of the power-law index n under distributed transverse load. As expected, the deflection response of FGM plates is intermediate, both for linear and nonlinear response, to that of the ceramic (stiffer) and metal (softer) plates. Note that the value of power-law index $n = 0$ corresponds to the ceramic plate and $n \rightarrow \infty$ corresponds to the metal plate. One may note that the nonlinear deflections are smaller than the linear ones, showing the stiffening effect due to the development of in-plane forces that make the plate stiffer with increasing load.

Next, bending under applied temperature field is studied. The metal surface is exposed to 20°C and the ceramic surface is exposed to fixed but different temperatures. The melting point of pure aluminum is 600°C and that of zirconia is 2600°C . Thus, using 0 to 600°C for aluminum plate is not realistic (the modulus and other properties of aluminum will change long before its temperature reaches 600°C), but the purpose is to establish the bounds for the FGM analysis. Also, aluminum reacts with oxygen and forms aluminum oxide, whose melting point is about 1900°C . Typical property variations as well as the temperature variations through the thickness for various values of n are shown in Figure 10.6.3 and 10.6.4, respectively.

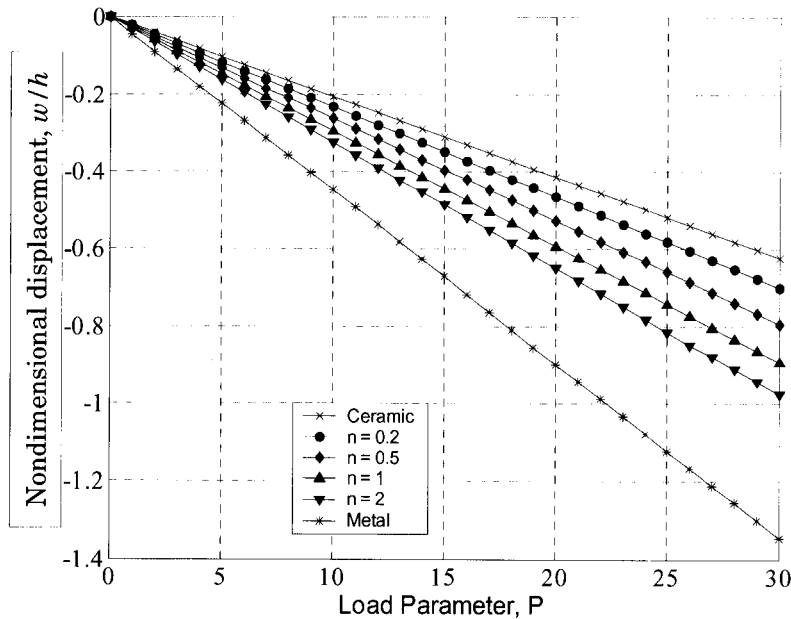


Figure 10.6.1: Nondimensionalized center deflection for a simply supported aluminum-zirconia FGM plate for various values of volume fraction exponent (mechanical load and linear analysis).

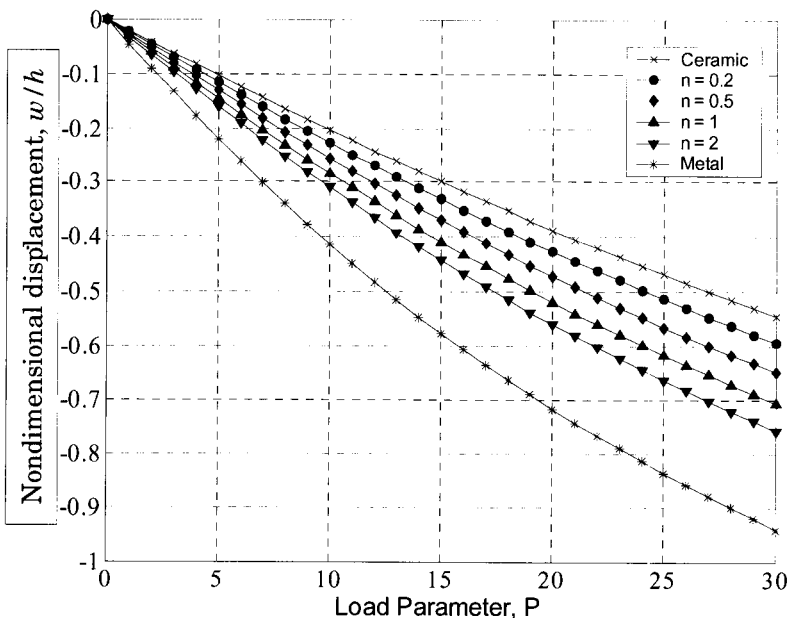


Figure 10.6.2: Nondimensionalized center deflection for a simply supported aluminum-zirconia FGM plate for various values of volume fraction exponent (mechanical load and nonlinear analysis).

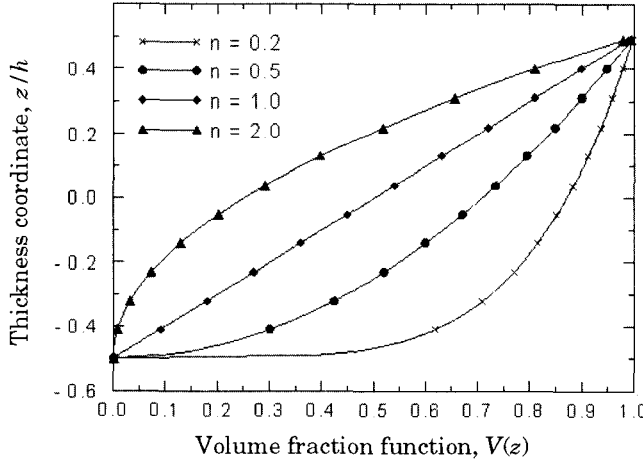


Figure 10.6.3: Variation of the material property.

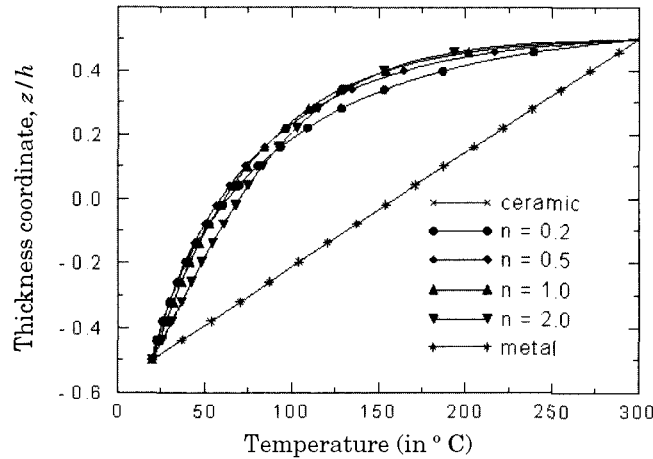


Figure 10.6.4: Variation of the temperature through the plate thickness.

Plots of the nondimensionalized deflection as a function of the temperature of the ceramic surface are presented in Figures 10.6.5 and 10.6.6 for linear and nonlinear analysis, respectively. The intermediate behavior observed for mechanical loads is not present in the thermal load case, linear or nonlinear analysis. The FGM plates experience less transverse deflections due to the thermal forces than their monolithic counterparts. This is due to the fact that the thermal resultants (i.e., thermal forces as well as bending moments) that develop in FGM plates are smaller than those of the monolithic plates. Another interesting observation is that the nonlinear deflections are larger than the linear deflections under thermal loads (for FGM as well as for monolithic plates). This is again due to the fact that the in-plane forces developed due to the geometric nonlinearity are negated by the thermal forces and moments [see Eq. (10.6.7)], making the overall plate stiffness reduced.

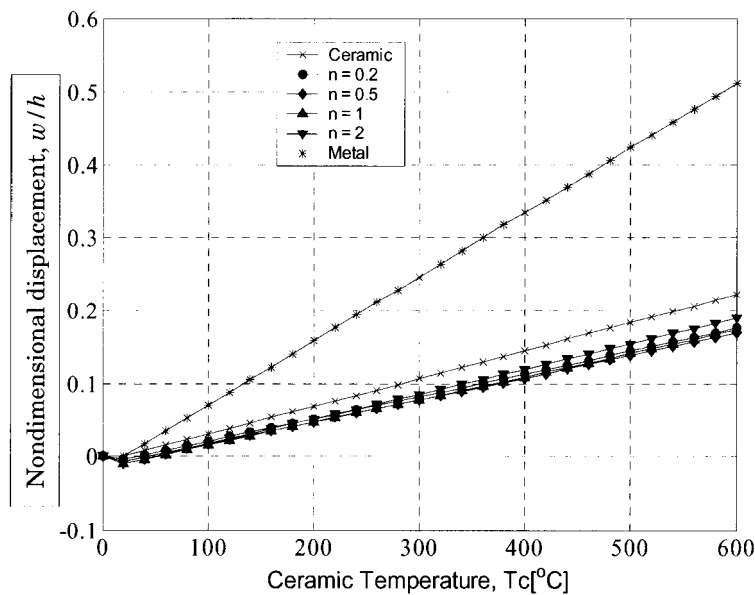


Figure 10.6.5: Nondimensionalized center deflection for a simple supported aluminum-zirconia FGM plate for various values of volume fraction exponent (thermal load and linear analysis).

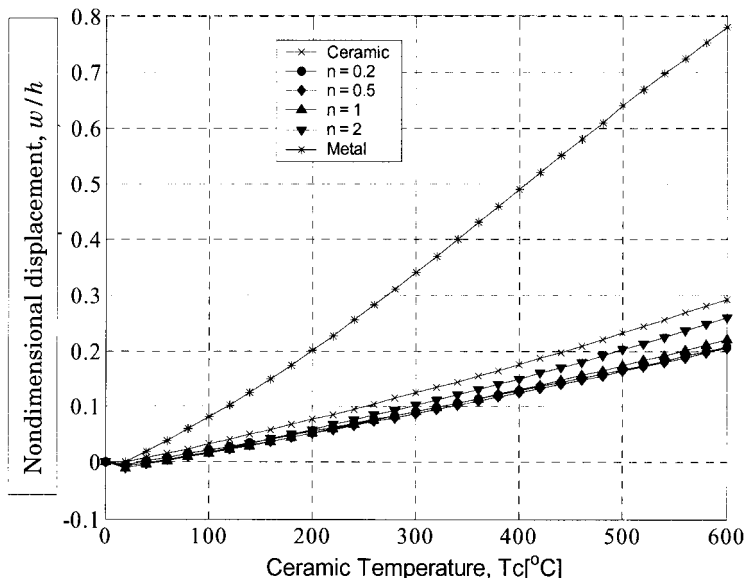


Figure 10.6.6: Nondimensionalized center deflection for a simple supported aluminum-zirconia FGM plate for various values of volume fraction exponent (thermal load and nonlinear analysis).

10.7 Finite Element Models of Laminated Shell Theory

10.7.1 Governing Equations

The finite element model of the laminated shallow shell theory with the von Kármán (or Sanders [70]) nonlinear strains can be developed in the same way as for the plate element. Here we present a brief development of the finite element model [71].

The equations of motion of the first-order shear deformation shell theory (see Chapter 8) are summarized here for the case $C_0 = 0$ (see Figure 10.7.1 for the coordinate system used):

$$-\left(\frac{\partial N_{xx}}{\partial x} + \frac{\partial N_{xy}}{\partial y}\right) - \frac{Q_x}{R_1} + I_0 \frac{\partial^2 u_0}{\partial t^2} + I_1 \frac{\partial^2 \phi_x}{\partial t^2} = 0 \quad (10.7.1)$$

$$-\left(\frac{\partial N_{xy}}{\partial x} + \frac{\partial N_{yy}}{\partial y}\right) - \frac{Q_y}{R_2} + I_0 \frac{\partial^2 v_0}{\partial t^2} + I_1 \frac{\partial^2 \phi_y}{\partial t^2} = 0 \quad (10.7.2)$$

$$-\left(\frac{\partial Q_x}{\partial x} + \frac{\partial Q_y}{\partial y}\right) + \frac{N_{xx}}{R_1} + \frac{N_{yy}}{R_2} - \mathcal{N}(u_0, v_0, w_0) - q + I_0 \frac{\partial^2 w_0}{\partial t^2} = 0 \quad (10.7.3)$$

$$-\left(\frac{\partial M_{xx}}{\partial x} + \frac{\partial M_{xy}}{\partial y}\right) + Q_x + I_2 \frac{\partial^2 \phi_x}{\partial t^2} + I_1 \frac{\partial^2 u_0}{\partial t^2} = 0 \quad (10.7.4)$$

$$-\left(\frac{\partial M_{xy}}{\partial x} + \frac{\partial M_{yy}}{\partial y}\right) + Q_y + I_2 \frac{\partial^2 \phi_y}{\partial t^2} + I_1 \frac{\partial^2 v_0}{\partial t^2} = 0 \quad (10.7.5)$$

where

$$I_i = \sum_{k=1}^N \int_{z_k}^{z_{k+1}} \rho^{(k)} \zeta^i \, d\zeta \quad (10.7.6)$$

ρ being the mass density, and

$$\mathcal{N}(u_0, v_0, w_0) = \frac{\partial}{\partial x} \left(N_{xx} \frac{\partial w_0}{\partial x} + N_{xy} \frac{\partial w_0}{\partial y} \right) + \frac{\partial}{\partial y} \left(N_{xy} \frac{\partial w_0}{\partial x} + N_{yy} \frac{\partial w_0}{\partial y} \right) \quad (10.7.7)$$

is the nonlinear contribution to the equilibrium equations due to the von Kármán nonlinear strains.

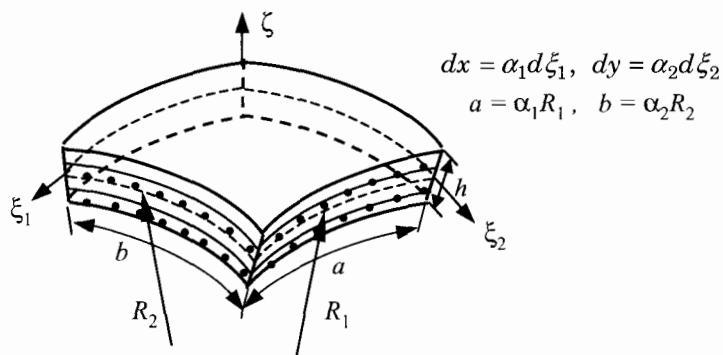


Figure 10.7.1: Geometry and coordinate system of a doubly curved shell.

It should be noted that the nonlinear strain-displacement equations of the Sanders nonlinear shell theory [70] are modified here for shallow shells by omitting the nonlinear terms of the form

$$\left(\frac{u_0}{R_1}\right)^2, \quad \left(\frac{v_0}{R_2}\right)^2, \quad \frac{u_0}{R_1} \frac{v_0}{R_2}, \quad \frac{\partial w_0}{\partial y} \frac{u_0}{R_1}, \quad \frac{\partial w_0}{\partial x} \frac{v_0}{R_2}$$

Otherwise, the governing equations in Eqs. (10.7.1)–(10.7.4) will contain additional nonlinear terms (see Reddy [32]).

The stress resultants are related to the strains (in the absence of thermal and other influences)

$$\begin{Bmatrix} N_{xx} \\ N_{yy} \\ N_{xy} \end{Bmatrix} = \begin{bmatrix} A_{11} & A_{12} & A_{16} \\ A_{12} & A_{22} & A_{26} \\ A_{16} & A_{26} & A_{66} \end{bmatrix} \begin{Bmatrix} \frac{\partial u_0}{\partial x} + \frac{w_0}{R_1} + \frac{1}{2} \left(\frac{\partial w_0}{\partial x} \right)^2 \\ \frac{\partial v_0}{\partial y} + \frac{w_0}{R_2} + \frac{1}{2} \left(\frac{\partial w_0}{\partial y} \right)^2 \\ \frac{\partial u_0}{\partial y} + \frac{\partial v_0}{\partial x} + \frac{\partial w_0}{\partial x} \frac{\partial w_0}{\partial y} \end{Bmatrix} \\ + \begin{bmatrix} B_{11} & B_{12} & B_{16} \\ B_{12} & B_{22} & B_{26} \\ B_{16} & B_{26} & B_{66} \end{bmatrix} \begin{Bmatrix} \frac{\partial \phi_x}{\partial x} \\ \frac{\partial \phi_y}{\partial y} \\ \frac{\partial \phi_x}{\partial y} + \frac{\partial \phi_y}{\partial x} \end{Bmatrix} \quad (10.7.8a)$$

$$\begin{Bmatrix} M_{xx} \\ M_{yy} \\ M_{xy} \end{Bmatrix} = \begin{bmatrix} B_{11} & B_{12} & B_{16} \\ B_{12} & B_{22} & B_{26} \\ B_{16} & B_{26} & B_{66} \end{bmatrix} \begin{Bmatrix} \frac{\partial u_0}{\partial x} + \frac{w_0}{R_1} + \frac{1}{2} \left(\frac{\partial w_0}{\partial x} \right)^2 \\ \frac{\partial v_0}{\partial y} + \frac{w_0}{R_2} + \frac{1}{2} \left(\frac{\partial w_0}{\partial y} \right)^2 \\ \frac{\partial u_0}{\partial y} + \frac{\partial v_0}{\partial x} + \frac{\partial w_0}{\partial x} \frac{\partial w_0}{\partial y} \end{Bmatrix} \\ + \begin{bmatrix} D_{11} & D_{12} & D_{16} \\ D_{12} & D_{22} & D_{26} \\ D_{16} & D_{26} & D_{66} \end{bmatrix} \begin{Bmatrix} \frac{\partial \phi_x}{\partial x} \\ \frac{\partial \phi_y}{\partial y} \\ \frac{\partial \phi_x}{\partial y} + \frac{\partial \phi_y}{\partial x} \end{Bmatrix} \quad (10.7.8b)$$

$$\begin{Bmatrix} Q_y \\ Q_x \end{Bmatrix} = K_s \begin{bmatrix} A_{44} & A_{45} \\ A_{45} & A_{55} \end{bmatrix} \begin{Bmatrix} \frac{\partial w_0}{\partial y} + \phi_y - \frac{v_0}{R_2} \\ \frac{\partial w_0}{\partial x} + \phi_x - \frac{u_0}{R_1} \end{Bmatrix} \quad (10.7.8c)$$

10.7.2 Finite Element Model

The weak forms of Eqs. (10.7.1)–(10.7.5) were presented in Eqs. (9.4.1a-e), with the understanding that $x_1 = x$, $x_2 = y$ and $N_1 = N_{xx}$, etc., and \hat{N}_i replaced by N_{xx}, N_{yy}, N_{xy}). The finite element model is of the form

$$\begin{Bmatrix} \{F^1\} \\ \{F^2\} \\ \{F^3\} \\ \{F^4\} \\ \{F^5\} \end{Bmatrix} = \begin{bmatrix} [K^{11}] & [K^{12}] & [K^{13}] & [K^{14}] & [K^{15}] \\ [K^{21}] & [K^{22}] & [K^{23}] & [K^{24}] & [K^{25}] \\ [K^{31}] & [K^{32}] & [K^{33}] & [K^{34}] & [K^{35}] \\ [K^{41}] & [K^{42}] & [K^{43}] & [K^{44}] & [K^{45}] \\ [K^{51}] & [K^{52}] & [K^{53}] & [K^{54}] & [K^{55}] \end{bmatrix} \begin{Bmatrix} \{u^e\} \\ \{v^e\} \\ \{w^e\} \\ \{S^1\} \\ \{S^2\} \end{Bmatrix} + \\ + \begin{bmatrix} [M^{11}] & [0] & [0] & [M^{14}] & [0] \\ [0] & [M^{22}] & [0] & [0] & [M^{25}] \\ [0] & [0] & [M^{33}] & [0] & [0] \\ [M^{14}]^T & [0] & [0] & [M^{44}] & [0] \\ [0] & [M^{25}]^T & [0] & [0] & [M^{55}] \end{bmatrix} \begin{Bmatrix} \{\ddot{u}^e\} \\ \{\ddot{v}^e\} \\ \{\ddot{w}^e\} \\ \{\ddot{S}^1\} \\ \{\ddot{S}^2\} \end{Bmatrix} \quad (10.7.9)$$

where the linear stiffness coefficients, mass coefficients and force coefficients are as defined in Eqs. (9.4.7) and (9.4.8a-c). Since all of the linear stiffness coefficients are already defined in Eq. (9.4.7), only the stiffness coefficients that contain nonlinear terms are given here. Note that K_{ij}^{33} are the only ones that have additional nonlinear terms when compared to the plate element:

$$K_{ij}^{13} = \frac{1}{2} \int_{\Omega^e} \left\{ \frac{\partial \psi_i^{(1)}}{\partial x} \left[A_{11} \frac{\partial w_0}{\partial x} \frac{\partial \psi_j^{(2)}}{\partial x} + A_{12} \frac{\partial w_0}{\partial y} \frac{\partial \psi_j^{(2)}}{\partial y} \right. \right. \\ \left. \left. + A_{16} \left(\frac{\partial w_0}{\partial x} \frac{\partial \psi_j^{(2)}}{\partial y} + \frac{\partial w_0}{\partial y} \frac{\partial \psi_j^{(2)}}{\partial x} \right) \right] \right. \\ \left. + \frac{\partial \psi_i^{(1)}}{\partial y} \left[A_{16} \frac{\partial w_0}{\partial x} \frac{\partial \psi_j^{(2)}}{\partial x} + A_{26} \frac{\partial w_0}{\partial y} \frac{\partial \psi_j^{(2)}}{\partial y} \right. \right. \\ \left. \left. + A_{66} \left(\frac{\partial w_0}{\partial x} \frac{\partial \psi_j^{(2)}}{\partial y} + \frac{\partial w_0}{\partial y} \frac{\partial \psi_j^{(2)}}{\partial x} \right) \right] \right. \\ \left. + \left[\left(\frac{A_{11}}{R_1} + \frac{A_{12}}{R_2} \right) \frac{\partial \psi_i^{(1)}}{\partial x} + \left(\frac{A_{16}}{R_1} + \frac{A_{26}}{R_2} \right) \frac{\partial \psi_i^{(1)}}{\partial y} \right] \psi_j^{(2)} \right. \\ \left. - \frac{K_s}{R_1} \psi_i^{(1)} \left(A_{45} \frac{\partial \psi_j^{(2)}}{\partial y} + A_{55} \frac{\partial \psi_j^{(2)}}{\partial x} \right) \right\} dx dy \quad (10.7.10a)$$

$$K_{ij}^{23} = \frac{1}{2} \int_{\Omega^e} \left\{ \frac{\partial \psi_i^{(1)}}{\partial y} \left[A_{12} \frac{\partial w_0}{\partial x} \frac{\partial \psi_j^{(2)}}{\partial x} + A_{22} \frac{\partial w_0}{\partial y} \frac{\partial \psi_j^{(2)}}{\partial y} \right. \right. \\ \left. \left. + A_{26} \left(\frac{\partial w_0}{\partial x} \frac{\partial \psi_j^{(2)}}{\partial y} + \frac{\partial w_0}{\partial y} \frac{\partial \psi_j^{(2)}}{\partial x} \right) \right] \right. \\ \left. + \frac{\partial \psi_i^{(1)}}{\partial x} \left[A_{16} \frac{\partial w_0}{\partial x} \frac{\partial \psi_j^{(2)}}{\partial x} + A_{26} \frac{\partial w_0}{\partial y} \frac{\partial \psi_j^{(2)}}{\partial y} \right. \right. \\ \left. \left. + A_{66} \left(\frac{\partial w_0}{\partial x} \frac{\partial \psi_j^{(2)}}{\partial y} + \frac{\partial w_0}{\partial y} \frac{\partial \psi_j^{(2)}}{\partial x} \right) \right] \right. \\ \left. + \left[\left(\frac{A_{16}}{R_1} + \frac{A_{26}}{R_2} \right) \frac{\partial \psi_i^{(1)}}{\partial x} + \left(\frac{A_{12}}{R_1} + \frac{A_{22}}{R_2} \right) \frac{\partial \psi_i^{(1)}}{\partial y} \right] \psi_j^{(2)} \right. \\ \left. - \frac{K_s}{R_2} \psi_i^{(1)} \left(A_{44} \frac{\partial \psi_j^{(2)}}{\partial y} + A_{45} \frac{\partial \psi_j^{(2)}}{\partial x} \right) \right\} dx dy \quad (10.7.10b)$$

$$K_{ij}^{31} = \int_{\Omega^e} \left\{ \frac{\partial \psi_j^{(2)}}{\partial x} \left[A_{11} \frac{\partial w_0}{\partial x} \frac{\partial \psi_i^{(1)}}{\partial x} + A_{12} \frac{\partial w_0}{\partial y} \frac{\partial \psi_i^{(1)}}{\partial y} \right. \right. \\ \left. \left. + A_{16} \left(\frac{\partial w_0}{\partial x} \frac{\partial \psi_i^{(1)}}{\partial y} + \frac{\partial w_0}{\partial y} \frac{\partial \psi_i^{(1)}}{\partial x} \right) \right] \right\}$$

$$\begin{aligned}
& + \frac{\partial \psi_j^{(2)}}{\partial y} \left[A_{16} \frac{\partial w_0}{\partial x} \frac{\partial \psi_i^{(1)}}{\partial x} + A_{26} \frac{\partial w_0}{\partial y} \frac{\partial \psi_i^{(1)}}{\partial y} \right. \\
& + A_{66} \left(\frac{\partial w_0}{\partial x} \frac{\partial \psi_i^{(1)}}{\partial y} + \frac{\partial w_0}{\partial y} \frac{\partial \psi_i^{(1)}}{\partial x} \right) \left. \right] \\
& + \psi_i^{(2)} \left[\frac{1}{R_1} \left(A_{11} \frac{\partial \psi_j^{(1)}}{\partial x} + A_{16} \frac{\partial \psi_j^{(1)}}{\partial y} \right) \right. \\
& + \frac{1}{R_2} \left(A_{12} \frac{\partial \psi_j^{(1)}}{\partial x} + A_{26} \frac{\partial \psi_j^{(1)}}{\partial y} \right) \left. \right] \\
& - \frac{K_s}{R_1} \left(A_{55} \frac{\partial \psi_i^{(2)}}{\partial x} + A_{45} \frac{\partial \psi_i^{(2)}}{\partial y} \right) \psi_j^{(1)} \Big\} dx dy
\end{aligned} \tag{10.7.10c}$$

$$\begin{aligned}
K_{ij}^{32} = \int_{\Omega^e} & \left\{ \frac{\partial \psi_j^{(2)}}{\partial y} \left[A_{12} \frac{\partial w_0}{\partial x} \frac{\partial \psi_i^{(1)}}{\partial x} + A_{22} \frac{\partial w_0}{\partial y} \frac{\partial \psi_i^{(1)}}{\partial y} \right. \right. \\
& + A_{26} \left(\frac{\partial w_0}{\partial x} \frac{\partial \psi_i^{(1)}}{\partial y} + \frac{\partial w_0}{\partial y} \frac{\partial \psi_i^{(1)}}{\partial x} \right) \left. \right] \\
& + \frac{\partial \psi_j^{(2)}}{\partial x} \left[A_{16} \frac{\partial w_0}{\partial x} \frac{\partial \psi_i^{(1)}}{\partial x} + A_{26} \frac{\partial w_0}{\partial y} \frac{\partial \psi_i^{(1)}}{\partial y} \right. \\
& + A_{66} \left(\frac{\partial w_0}{\partial x} \frac{\partial \psi_i^{(1)}}{\partial y} + \frac{\partial w_0}{\partial y} \frac{\partial \psi_i^{(1)}}{\partial x} \right) \left. \right] \\
& + \psi_i^{(2)} \left[\frac{1}{R_1} \left(A_{12} \frac{\partial \psi_j^{(1)}}{\partial y} + A_{16} \frac{\partial \psi_j^{(1)}}{\partial x} \right) \right. \\
& + \frac{1}{R_2} \left(A_{22} \frac{\partial \psi_j^{(1)}}{\partial y} + A_{26} \frac{\partial \psi_j^{(1)}}{\partial x} \right) \left. \right] \\
& - \frac{K_s}{R_2} \left(A_{45} \frac{\partial \psi_i^{(2)}}{\partial x} + A_{44} \frac{\partial \psi_i^{(2)}}{\partial y} \right) \psi_j^{(1)} \Big\} dx dy
\end{aligned} \tag{10.7.10d}$$

$$\begin{aligned}
K_{ij}^{33} = K_s \int_{\Omega^e} & \left[\frac{\partial \psi_i^{(2)}}{\partial x} \left(A_{55} \frac{\partial \psi_j^{(2)}}{\partial x} + A_{45} \frac{\partial \psi_j^{(2)}}{\partial y} \right) \right. \\
& + \frac{\partial \psi_i^{(2)}}{\partial y} \left(A_{45} \frac{\partial \psi_j^{(2)}}{\partial x} + A_{44} \frac{\partial \psi_j^{(2)}}{\partial y} \right) \Big] dx dy \\
& + \frac{1}{2} \int_{\Omega^e} \left\{ \left[A_{11} \left(\frac{\partial w_0}{\partial x} \right)^2 + A_{12} \left(\frac{\partial w_0}{\partial y} \right)^2 \right. \right. \\
& \left. \left. + 2A_{16} \frac{\partial w_0}{\partial x} \frac{\partial w_0}{\partial y} \right] \frac{\partial \psi_i^{(2)}}{\partial x} \frac{\partial \psi_j^{(2)}}{\partial x} \right\}
\end{aligned}$$

$$\begin{aligned}
& + \left[A_{16} \left(\frac{\partial w_0}{\partial x} \right)^2 + A_{26} \left(\frac{\partial w_0}{\partial y} \right)^2 + 2A_{66} \frac{\partial w_0}{\partial x} \frac{\partial w_0}{\partial y} \right] \\
& \quad \left(\frac{\partial \psi_i^{(2)}}{\partial x} \frac{\partial \psi_j^{(2)}}{\partial y} + \frac{\partial \psi_j^{(2)}}{\partial x} \frac{\partial \psi_i^{(2)}}{\partial y} \right) \\
& + \left[A_{12} \left(\frac{\partial w_0}{\partial x} \right)^2 + A_{22} \left(\frac{\partial w_0}{\partial y} \right)^2 + 2A_{26} \frac{\partial w_0}{\partial x} \frac{\partial w_0}{\partial y} \right] \frac{\partial \psi_i^{(2)}}{\partial y} \frac{\partial \psi_j^{(2)}}{\partial y} \\
& + \left[\frac{1}{R_1} \left(\frac{A_{11}}{R_1} + \frac{A_{12}}{R_2} \right) + \frac{1}{R_2} \left(\frac{A_{12}}{R_1} + \frac{A_{22}}{R_2} \right) \right] \psi_i^{(2)} \psi_j^{(2)} \\
& + \left[\frac{\partial w_0}{\partial x} \left(\frac{A_{11}}{R_1} + \frac{A_{12}}{R_2} \right) + \frac{\partial w_0}{\partial y} \left(\frac{A_{16}}{R_1} + \frac{A_{26}}{R_2} \right) \right] \frac{\partial \psi_i^{(2)}}{\partial x} \psi_j^{(2)} \\
& + \left[\frac{\partial w_0}{\partial x} \left(\frac{A_{16}}{R_1} + \frac{A_{26}}{R_2} \right) + \frac{\partial w_0}{\partial y} \left(\frac{A_{12}}{R_1} + \frac{A_{22}}{R_2} \right) \right] \frac{\partial \psi_i^{(2)}}{\partial y} \psi_j^{(2)} \Big\} dx dy
\end{aligned} \tag{10.7.10d}$$

The tangent stiffness coefficients can be computed as in the case of plates.

10.7.3 Numerical Examples

Here we present two numerical examples. The following boundary conditions are used:

SS-1: At $x = a$: $u_0 = w_0 = \phi_y = 0$; At $y = b$: $v_0 = w_0 = \phi_x = 0$

CC-1: $v_0 = u_0 = w_0 = \phi_x = \phi_y = 0$ along the clamped edges

Along the symmetry lines the normal surface displacement and normal rotation are set to zero (for the cross-ply laminates discussed here). The following two sets of material properties of a lamina are used (labeled as Material 1 and Material 2, respectively):

$$E_1 = 25 \times 10^6, \quad E_2 = 10^6, \quad G_{12} = G_{13} = 0.5E_2, \quad G_{23} = 0.2E_2, \quad \nu_{12} = 0.25$$

$$E_1 = 40 \times 10^6, \quad E_2 = 10^6, \quad G_{12} = G_{13} = 0.6E_2, \quad G_{23} = 0.5E_2, \quad \nu_{12} = 0.25$$

The first example is concerned with the bending of a simply supported (SS-1), nine-layer (0/90/90/ \dots), spherical panel under uniform transverse load, q_0 . The geometric parameters used are: $a = b = 50$ in., $R = 10^3$ in., and $h = 1$ in. Figure 10.7.2 contains the load-deflection response of the shells for the two sets of material properties.

The second example consists of a clamped (CC-1), two-layer (0/90), cylindrical shell panel under uniform load q_0 . Material properties used are those of Material 1. Figure 10.7.3 contains the center deflection w_0 , normal stress σ_{yy} and transverse shear stress σ_{xz} as functions of the load q_0 .

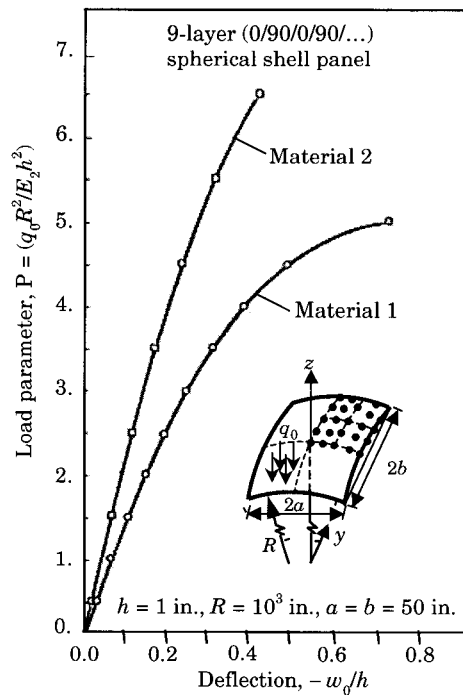


Figure 10.7.2: Center deflection versus load parameter for simply supported cross-ply (0/90/90/...) laminated spherical shell panel under uniform load.

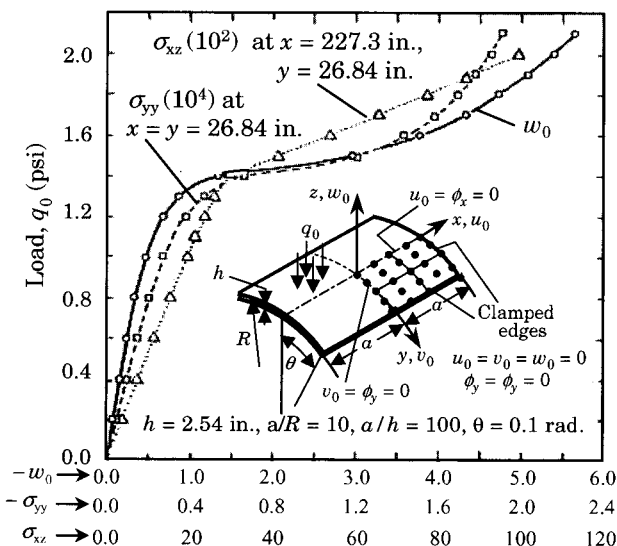


Figure 10.7.3: Center deflection, normal stress and transverse shear stress versus load for clamped cross-ply (0/90) laminated cylindrical shell panel under uniform load.

10.8 Continuum Shell Finite Element

10.8.1 Introduction

The plate and shell finite elements developed in Chapter 9 and previous sections of this chapter were based on laminated plate and shell theories. Such theories are limited to geometrically linear analyses and nonlinear analysis with small strains and moderate rotations. The finite element model to be developed in this section is based on 3-D elasticity equations, and the geometry and the displacement fields of the structure are directly discretized by imposing certain geometric and static constraints to satisfy the assumptions of a shell theory (see [21,23–32,72-80]). The development presented here is based on the material in Chapter 9 of the author’s nonlinear finite element book [32].

Consider the motion of a body in a fixed Cartesian coordinate system, and assume that the body may experience large displacements and rotations. It is difficult to determine the final configuration of a deformed body subjected to loads with large magnitude. A practical way of determining the final configuration \mathcal{C} from a known initial configuration \mathcal{C}_0 is to assume that the total load is applied in increments so that the body occupies several intermediate configurations, \mathcal{C}_i ($i = 1, 2, \dots$), prior to occupying the final configuration. The magnitude of load increments should be such that the computational method used is capable of predicting the deformed configuration at each load step. In the determination of an intermediate configuration \mathcal{C}_i , the Lagrangian description of motion can use any of the previously known configurations $\mathcal{C}_0, \mathcal{C}_1, \dots$, and \mathcal{C}_{i-1} as the reference configuration. If the initial configuration is used as the reference configuration with respect to which all quantities are measured, it is called the *total Lagrangian description*. If the latest known configuration \mathcal{C}_{i-1} is used as the reference configuration, it is called the *updated Lagrangian description*.

Here we use the total Lagrangian description to formulate the governing equations of a continuum. We consider three equilibrium configurations of the body, namely, $\mathcal{C}_0, \mathcal{C}_1$, and \mathcal{C}_2 , which correspond to three different loads (see Figure 10.8.1). The three configurations of the body can be thought of as the initial undeformed configuration \mathcal{C}_0 , the last known deformed configuration \mathcal{C}_1 , and the current deformed configuration \mathcal{C}_2 to be determined. It is assumed that all variables, such as the displacements, strains, and stresses are known up to the \mathcal{C}_1 configuration. We wish to develop a formulation for determining the displacement field of the body in the current deformed configuration \mathcal{C}_2 . It is assumed that the deformation of the body from \mathcal{C}_1 to \mathcal{C}_2 due to an increment in the load is small, and the accumulated deformation of the body from \mathcal{C}_0 to \mathcal{C}_1 can be arbitrarily large but continuous (i.e., neighborhoods move into neighborhoods).

The notation used for positions, displacements, strains, stresses, etc. is that used by Bathe [31]. A left superscript on a quantity denotes the configuration in which the quantity occurs, and a left subscript denotes the configuration with respect to which the quantity is measured. Thus ${}_j^i Q$ indicates that the quantity Q occurs in configuration \mathcal{C}_i but measured in configuration \mathcal{C}_j . When the quantity under consideration is measured in the same configuration in which it occurs, the left subscript may not be used. The left superscript will be omitted on incremental quantities that occur between configurations \mathcal{C}_1 and \mathcal{C}_2 . For example, the total

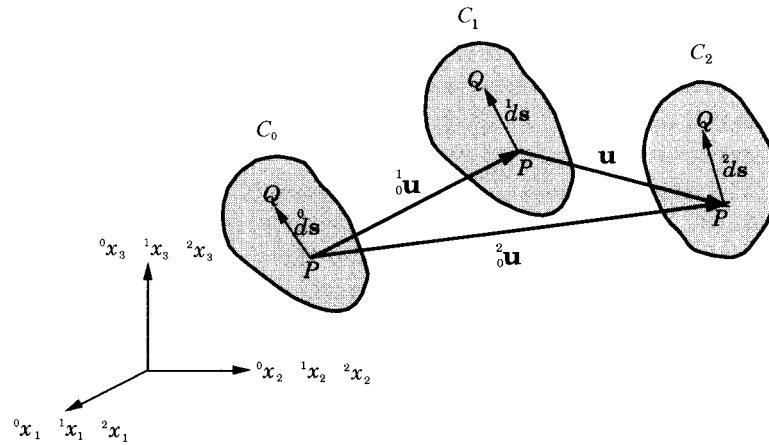


Figure 10.8.1: Three different equilibrium configurations of a body.

displacements of the particle X in the two configurations \mathcal{C}_1 and \mathcal{C}_2 can be written as

$$\begin{aligned} {}^1_0\mathbf{u} &= {}^1\mathbf{x} - {}^0\mathbf{x} \quad \text{or} \quad {}^1_0u_i = {}^1x_i - {}^0x_i \quad (i = 1, 2, 3) \\ {}^2_0\mathbf{u} &= {}^2\mathbf{x} - {}^0\mathbf{x} \quad \text{or} \quad {}^2_0u_i = {}^2x_i - {}^0x_i \quad (i = 1, 2, 3) \end{aligned}$$

and the displacement increment of the point from \mathcal{C}_1 to \mathcal{C}_2 is

$$\mathbf{u} = {}^2_0\mathbf{u} - {}^1_0\mathbf{u} \quad \text{or} \quad u_i = {}^2_0u_i - {}^1_0u_i \quad (i = 1, 2, 3)$$

10.8.2 Incremental Equations of Motion

The principle of virtual displacements requires that the sum of the external virtual work done on a body and the internal virtual work stored in the body should be equal to zero:

$$\delta W \equiv \int_{^2V} {}^2\sigma : \delta({}^2\mathbf{e}) \, d^2V - \delta {}^2R = 0 \quad (10.8.1a)$$

$$= \int_{^2V} {}^2\sigma_{ij} \delta({}^2e_{ij}) \, d^2V - \delta {}^2R = 0 \quad (10.8.1b)$$

where $\delta {}^2R$ denotes the virtual work done by applied forces

$$\delta {}^2R = \int_{^2V} {}^2\mathbf{f} \cdot \delta \mathbf{u} \, d^2V + \int_{^2S} {}^2\mathbf{t} \cdot \delta \mathbf{u} \, d^2S \quad (10.8.2a)$$

$$= \int_{^2V} {}^2f_i \delta u_i \, d^2V + \int_{^2S} {}^2t_i \delta u_i \, d^2S \quad (10.8.2b)$$

and d^2S denotes the surface element and ${}^2\mathbf{f}$ is the body force vector (measured per unit volume), ${}^2\sigma$ is the Cauchy stress tensor, ${}^2e_{ij}$ is the infinitesimal strain tensor

$${}^2e_{ij} = \frac{1}{2} \left(\frac{\partial u_i}{\partial {}^2x_j} + \frac{\partial u_j}{\partial {}^2x_i} \right) \quad (10.8.2c)$$

and ${}^2\mathbf{t}$ is the boundary stress vector (measured per unit surface area) in configuration \mathcal{C}_2 . The variational symbol ‘ δ ’ is understood to operate on unknown displacement variables (2u_i and u_i).

Equation (10.8.1a) cannot be solved directly since the configuration \mathcal{C}_2 is unknown. This is an important difference compared with the linear analysis in which we assume that the displacements are infinitesimally small so that the configuration of the body does not change. In a large deformation analysis special attention must be given to the fact that the configuration of the body is changing continuously. This change in configuration can be dealt with by defining appropriate stress and strain measures. The stress and strain measures that we shall use are the 2nd Piola–Kirchhoff stress tensor \mathbf{S} and the Green–Lagrange strain tensor \mathbf{E} , which are “energetically conjugate” to each other (see [32]).

In the total Lagrangian formulation, all quantities are measured with respect to the initial configuration \mathcal{C}_0 . Hence, the virtual work statement in Eq. (10.8.1a) must be expressed in terms of quantities referred to the reference configuration. We use the following identities [31,32]:

$$\int_{{}^2V} {}^2\sigma_{ij} \delta({}^2e_{ij}) d^2V = \int_{{}^0V} {}^2S_{ij} \delta({}^2E_{ij}) d^0V \quad (10.8.3)$$

$$\int_{{}^2V} {}^2f_i \delta u_i d^2V = \int_{{}^0V} {}^2f_i \delta u_i d^0V \quad (10.8.4)$$

$$\int_{{}^2S} {}^2t_i \delta u_i d^2S = \int_{{}^0S} {}^2t_i \delta u_i d^0S \quad (10.8.5)$$

where 2f_i and 2t_i are the body force and boundary traction components referred to the configuration \mathcal{C}_0 . Using Eqs. (10.8.3)–(10.8.5) in Eq. (10.8.1b) we arrive at

$$\int_{{}^0V} {}^2S_{ij} \delta({}^2E_{ij}) d^0V - \delta({}^2R) = 0 \quad (10.8.6)$$

where

$$\delta({}^2R) = \int_{{}^0V} {}^2f_i \delta u_i d^0V + \int_{{}^0S} {}^2t_i \delta u_i d^0S \quad (10.8.7)$$

Next, we simplify the virtual work statement (10.8.6). First, we note that (see Eqs. (9.3.15) and (9.3.16) of [32])

$$\begin{aligned} \delta({}^2E_{ij}) &= \delta({}^1E_{ij}) + \delta({}^0\varepsilon_{ij}) = \delta({}^0\varepsilon_{ij}) \\ &= \delta({}^0e_{ij}) + \delta({}^0\eta_{ij}) \end{aligned} \quad (10.8.8)$$

where $\delta({}^1E_{ij}) = 0$ because it is not a function of the unknown displacements.

The virtual strains are given by

$$\delta(0e_{ij}) = \frac{1}{2} \left(\frac{\partial \delta u_i}{\partial {}^0x_j} + \frac{\partial \delta u_j}{\partial {}^0x_i} + \frac{\partial \delta u_k}{\partial {}^0x_i} \frac{\partial {}^1u_k}{\partial {}^0x_j} + \frac{\partial {}^1u_k}{\partial {}^0x_i} \frac{\partial \delta u_k}{\partial {}^0x_j} \right) \quad (10.8.9)$$

$$\delta(0\eta_{ij}) = \frac{1}{2} \left(\frac{\partial \delta u_k}{\partial {}^0x_i} \frac{\partial u_k}{\partial {}^0x_j} + \frac{\partial u_k}{\partial {}^0x_i} \frac{\partial \delta u_k}{\partial {}^0x_j} \right) \quad (10.8.10)$$

Substituting Eqs. (10.8.8) for $\delta({}^2E_{ij})$ and using the decomposition

$${}^2S_{ij} = {}^1S_{ij} + {}_0S_{ij}$$

for ${}^2S_{ij}$ into Eq. (10.8.6), we arrive at the expression

$$\begin{aligned} 0 &= \int_{{}^0V} {}^2S_{ij} \delta({}^2E_{ij}) d{}^0V - \delta({}^2R) \\ &= \int_{{}^0V} \left({}^1S_{ij} + {}_0S_{ij} \right) \delta({}^0\varepsilon_{ij}) d{}^0V - \delta({}^2R) \\ &= \int_{{}^0V} \left\{ {}_0S_{ij} \delta({}^0\varepsilon_{ij}) + {}^1S_{ij} [\delta({}^0e_{ij}) + \delta({}^0\eta_{ij})] \right\} d{}^0V - \delta({}^2R) \\ &= \int_{{}^0V} {}_0S_{ij} \delta({}^0\varepsilon_{ij}) d{}^0V + \int_{{}^0V} {}^1S_{ij} \delta({}^0\eta_{ij}) d{}^0V + \delta({}^1R) - \delta({}^2R) \end{aligned} \quad (10.8.11)$$

where $\delta({}^1R)$ is the virtual internal energy (in moving the actual internal forces through virtual displacements) stored in the body at configuration \mathcal{C}_1

$$\delta({}^1R) = \int_{{}^0V} {}^1S_{ij} \delta({}^0e_{ij}) d{}^0V \quad (10.8.12)$$

Since the body is in equilibrium at configuration \mathcal{C}_1 , by the principle of virtual work applied to configuration \mathcal{C}_1 we have

$$0 = \int_{{}^0V} {}^1S_{ij} \delta({}^0e_{ij}) d{}^0V - \int_{{}^0V} {}^1f_i \delta u_i d{}^0V - \int_{{}^0S} {}^1t_i \delta u_i d{}^0S \quad (10.8.13)$$

and therefore

$$\delta({}^1R) = \int_{{}^0V} {}^1f_i \delta u_i d{}^0V + \int_{{}^0S} {}^1t_i \delta u_i d{}^0S \quad (10.8.14)$$

We need only to replace ${}_0S_{ij}$ in terms of the strains and ultimately the displacement increments using an appropriate constitutive relation.

The first term of Eq. (10.8.11) represents the change in the virtual strain energy due to the virtual incremental displacements u_i between configurations \mathcal{C}_1 and \mathcal{C}_2 . The second term represents the virtual work done by forces due to initial stresses ${}^1S_{ij}$. The last two terms together denote the change in the virtual work done by applied body forces and surface tractions in moving from \mathcal{C}_1 to \mathcal{C}_2 . This is primarily due to the geometric changes that take place between the two configurations. Equation (10.8.11) represents the statement of virtual work for the incremental

deformation between the configurations \mathcal{C}_1 to \mathcal{C}_2 , and no approximations are made in arriving at it.

For dynamic analysis, the principle of virtual displacements (10.8.11) can be written as [32]

$$\begin{aligned} \int_{\text{o}V} {}^0\rho {}^2\ddot{u}_i \delta({}^2u_i) d^0V + \int_{\text{o}V} {}^0C_{ijrs} {}_0e_{rs} \delta {}_0e_{ij} d^0V + \int_{\text{o}V} {}^1_0S_{ij} \delta {}_0\eta_{ij} d^0V \\ = {}^2R - \int_{\text{o}V} {}^1_0S_{ij} \delta {}_0e_{ij} d^0V \end{aligned} \quad (10.8.15)$$

where $\delta({}^2u_i) = \delta u_i$.

10.8.3 Continuum Finite Element Model

Equation (10.8.15) can be used to develop the nonlinear displacement finite element model for any continuum. The basic step in deriving the finite element equations for a shell element is the selection of proper interpolation functions for the displacement field and geometry. In the case of beam and shell elements, the approximation for the geometry is chosen such that the beam or shell kinematic hypotheses are realized. First we derive the finite element model of a continuum and then specialize it to shells [24–26].

It is important that the coordinates and displacements are interpolated using the same interpolation functions (isoparametric formulation) so that the displacement compatibility across element boundaries can be preserved in all configurations. Let

$${}^0x_i = \sum_{k=1}^n \psi_k {}^0x_i^k, \quad {}^1x_i = \sum_{k=1}^n \psi_k {}^1x_i^k, \quad {}^2x_i = \sum_{k=1}^n \psi_k {}^2x_i^k \quad (10.8.16)$$

$${}^1u_i = \sum_{k=1}^n \psi_k {}^1u_i^k, \quad u_i = \sum_{k=1}^n \psi_k u_i^k \quad (i = 1, 2, 3) \quad (10.8.17)$$

where the right superscript k indicates the quantity at nodal point k , ψ_k is the interpolation function corresponding to nodal point k , and n is the number of element nodal points.

Substitution of Eqs. (10.8.16) and (10.8.17) in Eq. (10.8.15) yields the finite element model of a 3-D continuum

$${}^1_0[M]\{{}^{\ddot{\Delta}}e\} + ({}^1_0[K_L] + {}^1_0[K_{NL}])\{\Delta^e\} = {}^2\{R\} - {}^1_0\{F\} \quad (10.8.18)$$

where $\{\Delta^e\}$ is the vector of nodal incremental displacements from time t to time $t+\Delta t$ in an element, and ${}^1_0[M]\{{}^{\ddot{\Delta}}e\}$, ${}^1_0[K_L]\{\Delta^e\}$, ${}^1_0[K_{NL}]\{\Delta^e\}$, and ${}^1_0\{F\}$ are obtained by evaluating the integrals, respectively:

$$\begin{aligned} \int_{\text{o}V} {}^0\rho {}^2\ddot{u}_i \delta {}^2u_i d^0V, \quad \int_{\text{o}V} {}^0C_{ijrs} {}_0e_{rs} \delta {}_0e_{ij} d^0V \\ \int_{\text{o}V} {}^1_0S_{ij} \delta {}_0\eta_{ij} d^0V, \quad \int_{\text{o}V} {}^1_0S_{ij} \delta {}_0e_{ij} d^0V \end{aligned}$$

Various matrices are defined by

$${}^1_0[K_L] = \int_{0A} {}^1_0[B_L]^T {}_0[C] {}^1_0[B_L] d^0V \quad (10.8.19a)$$

$${}^1_0[K_{NL}] = \int_{0V} {}^1_0[B_{NL}]^T {}_0[S] {}^1_0[B_{NL}] d^0V \quad (10.8.19b)$$

$${}^1_0[M] = \int_{0V} {}^0\rho {}^1[H]^T {}^1[H] d^0V \quad (10.8.19c)$$

$${}^1_0\{F\} = \int_{0V} {}^1_0[B_L]^T {}^1\{\hat{S}\} d^0V \quad (10.8.19d)$$

In the above equations, ${}^1_0[B_L]$ and ${}^1_0[B_{NL}]$ are the linear and nonlinear strain-displacement transformation matrices, ${}_0[C]$ is the incremental stress-strain material property matrix, ${}_0[S]$ is a matrix of 2nd Piola-Kirchhoff stress components, ${}^1_0\{\hat{S}\}$ is a vector of these stresses, and ${}^1[H]$ is the incremental displacement interpolation matrix. All matrix elements correspond to the configuration at time t and are defined with respect to the configuration at time $t = 0$. It is important to note that Eq. (10.8.18) is only an approximation to the actual solution to be determined in each time step. Therefore, it may be necessary to iterate in each time step until Eq. (10.8.15), with inertia terms, is satisfied to a required tolerance.

The finite element equations (10.8.18) are second-order differential equations in time. In order to obtain numerical solutions at each time step, Eq. (10.8.18) needs to be converted to algebraic equations using a time approximation scheme, as explained in previous sections. We have

$${}^1_0[\hat{K}]\{\Delta\} = {}^2\{\hat{R}\} \quad (10.8.20)$$

where $\{\Delta\}$ is the vector of nodal incremental displacements at time t , $\{\Delta\} = {}^{t+\Delta t}\{\Delta\} - {}^t\{\Delta\}$, and

$${}^1_0[\hat{K}] = a_3 {}^1_0[M] + {}^1_0[K_L] + {}^1_0[K_{NL}] \quad (10.8.21a)$$

$${}^2\{\hat{R}\} = {}^2\{R\} - {}^1_0\{F\} + {}^1_0[M] \left(a_3 {}^t\{\Delta\} + a_4 {}^t\{\dot{\Delta}\} + a_5 {}^t\{\ddot{\Delta}\} \right) \quad (10.8.21b)$$

$$a_3 = \frac{1}{\beta(\Delta t)^2}, \quad a_4 = a_3 \Delta t, \quad a_5 = \frac{1}{2\beta} - 1 \quad (10.8.22)$$

Once Eq. (10.8.20) is solved for $\{\Delta\}$ at time $t + \Delta t$, the acceleration and velocity vectors are obtained using

$$\begin{aligned} {}^{t+\Delta t}\{\ddot{\Delta}\} &= a_3\{\Delta\} - a_4 {}^t\{\dot{\Delta}\} - a_5 {}^t\{\ddot{\Delta}\} \\ {}^{t+\Delta t}\{\dot{\Delta}\} &= {}^t\{\dot{\Delta}\} + a_1 {}^{t+\Delta t}\{\dot{\Delta}\} + a_2 {}^t\{\ddot{\Delta}\} \end{aligned} \quad (10.8.23)$$

where $a_1 = \alpha \Delta t$ and $a_2 = (1 - \alpha) \Delta t$.

The finite element equations (10.8.20) are solved, after assembly and imposition of boundary conditions, iteratively at each time step until Eq. (10.8.15) is satisfied within a required tolerance. The Newton-Raphson method with Riks-Wempner algorithm (see Reddy [32]) is used in the present study.

10.8.4 Shell Finite Element

The FSDT shell finite element can be deduced from the 3-D continuum element by imposing two kinematic constraints: (1) straight line normal to the midsurface of the shell before deformation remains straight but not normal after deformation; (2) the transverse normal components of stress are ignored in the development. However, the shell element admits arbitrarily large displacements and rotations but small strains since the shell thickness is assumed not to change and the normal is not allowed to distort [31,32,78,79].

Consider the solid 3-D element shown in Figure 10.8.2. Let (ξ, η) be the curvilinear coordinates in the middle surface of the shell and ζ be the coordinate in the thickness direction. The coordinates (ξ, η, ζ) are normalized such that they vary between -1 and $+1$. The coordinates of a typical point in the element can be written as

$$x_i = \sum_{k=1}^n \psi_k(\xi, \eta) \left[\frac{1+\zeta}{2} (x_i^k)_{\text{top}} + \frac{1-\zeta}{2} (x_i^k)_{\text{bottom}} \right] \quad (10.8.24)$$

where n is the number of nodes in the element, and $\psi_k(\xi, \eta)$ is the finite element interpolation function associated with node k . If $\psi_k(\xi, \eta)$ are derived as interpolation functions of a parent element, square or triangular in plane, then compatibility is achieved at the interfaces of curved space shell elements.

Define

$$V_{3i}^k = (x_i^k)_{\text{top}} - (x_i^k)_{\text{bottom}}, \quad \hat{\mathbf{e}}_3^k = \mathbf{V}_3^k / |\mathbf{V}_3^k| \quad (10.8.25)$$

where \mathbf{V}_3^k is the vector connecting the upper and lower points of the normal at node k . Equation (10.8.24) can be rewritten as

$$x_i = \sum_{k=1}^n \psi_k(\xi, \eta) \left[(x_i^k)_{\text{mid}} + \frac{\zeta}{2} V_{3i}^k \right] = \sum_{k=1}^n \psi_k(\xi, \eta) \left[(x_i^k)_{\text{mid}} + \frac{\zeta}{2} h_k e_{3i}^k \right] \quad (10.8.26)$$

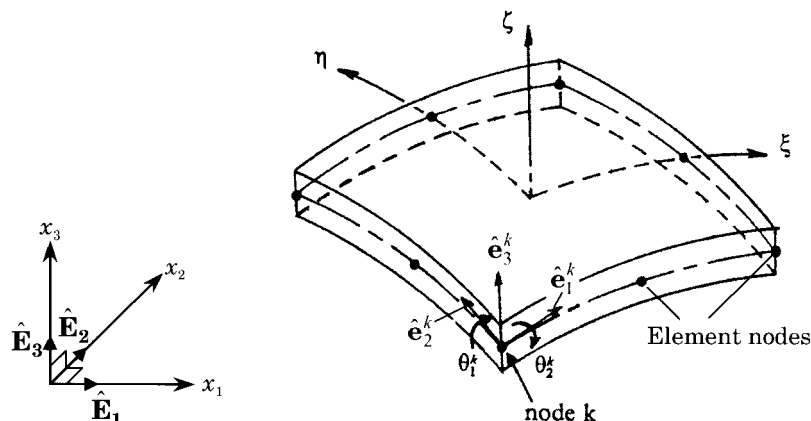


Figure 10.8.2: Geometry and coordinate system of a shell element.

where $h_k = |\mathbf{V}_3^k|$ is the thickness of the shell element at node k . Hence, the coordinates of any point in the element at time t are interpolated by the expression

$${}^1x_i = \sum_{k=1}^n \psi_k(\xi, \eta) \left[{}^1x_i^k + \frac{\zeta}{2} h_k {}^1e_{3i}^k \right] \quad (10.8.27)$$

The displacements and the displacement increments are interpolated by

$${}^1u_i = {}^1x_i - {}^0x_1 = \sum_{k=1}^n \psi_k(\xi, \eta) \left[{}^1u_i^k + \frac{\zeta}{2} h_k \left({}^1e_{3i}^k - {}^0e_{3i}^k \right) \right] \quad (10.8.28)$$

$$u_i = {}^2u_i - {}^1u_i = \sum_{k=1}^n \psi_k(\xi, \eta) \left[u_i^k + \frac{\zeta}{2} h_k \left({}^2e_{3i}^k - {}^1e_{3i}^k \right) \right] \quad (10.8.29)$$

Here ${}^1u_i^k$ and u_i^k denote, respectively, the displacement and incremental displacement components in the x_i -direction at the k th node and time t . For small rotation $d\Omega$ at each node, we have

$$d\Omega = \theta_2^k {}^1\hat{\mathbf{e}}_1^k + \theta_1^k {}^1\hat{\mathbf{e}}_2^k + \theta_3^k {}^1\hat{\mathbf{e}}_3^k \quad (10.8.30)$$

the increment of vector ${}^1\hat{\mathbf{e}}_3^k$ can be written as

$$\Delta {}^1\hat{\mathbf{e}}_3^k = {}^2\hat{\mathbf{e}}_3^k - {}^1\hat{\mathbf{e}}_3^k = d\Omega \times {}^1\hat{\mathbf{e}}_3^k = \theta_1^k {}^1\hat{\mathbf{e}}_1^k - \theta_2^k {}^1\hat{\mathbf{e}}_2^k \quad (10.8.31)$$

Then Eq. (10.8.29) becomes

$$u_i = \sum_{k=1}^n \psi_k(\xi, \eta) \left[u_i^k + \frac{\zeta}{2} h_k \left(\theta_1^k {}^1e_{1i}^k - \theta_2^k {}^1e_{2i}^k \right) \right] \quad (i = 1, 2, 3) \quad (10.8.32)$$

The unit vectors ${}^1\hat{\mathbf{e}}_1^k$ and ${}^1\hat{\mathbf{e}}_2^k$ at node k can be obtained from the relations

$${}^1\hat{\mathbf{e}}_1^k = \frac{\hat{\mathbf{E}}_2 \times {}^1\hat{\mathbf{e}}_3^k}{|\hat{\mathbf{E}}_2 \times {}^1\hat{\mathbf{e}}_3^k|}, \quad {}^1\hat{\mathbf{e}}_2^k = {}^1\hat{\mathbf{e}}_3^k \times {}^1\hat{\mathbf{e}}_1^k \quad (10.8.33)$$

where $\hat{\mathbf{E}}_i$ are the unit vectors of the stationary global coordinate system (${}^0x_1, {}^0x_2, {}^0x_3$). Equation (10.8.35) can be written in matrix form as

$$\{u\} = \{u_1 \ u_2 \ u_3\}^T = {}^1[H]_{3 \times 5n} \{\Delta^e\}_{5n \times 1} \quad (10.8.34)$$

where $\{\Delta^e\} = \{u_i^k \ \theta_1^k \ \theta_2^k\}^T$, ($i = 1, 2, 3$, $k = 1, 2, \dots, n$, and n is the number of nodes) is the vector of nodal incremental displacements (five per node), and ${}^1[H]$ is the incremental displacement interpolation matrix

$${}^1[H]_{3 \times 5n} = \begin{bmatrix} \dots & \psi_k & 0 & 0 & \frac{1}{2}\psi_k\zeta h_k {}^1e_{11}^k & -\frac{1}{2}\psi_k\zeta h_k {}^1e_{21}^k & \dots \\ \dots & 0 & \psi_k & 0 & \frac{1}{2}\psi_k\zeta h_k {}^1e_{12}^k & -\frac{1}{2}\psi_k\zeta h_k {}^1e_{22}^k & \dots \\ \dots & 0 & 0 & \psi_k & \frac{1}{2}\psi_k\zeta h_k {}^1e_{13}^k & -\frac{1}{2}\psi_k\zeta h_k {}^1e_{23}^k & \dots \end{bmatrix} \quad (10.8.35)$$

For each time step or iteration step one can find 3 unit vectors at each node from Eqs. (10.8.31) and (10.8.33).

The linear strain increments $\{0e\} = \{0e_{11} \ 0e_{22} \ 0e_{33} \ 2_0e_{12} \ 2_0e_{13} \ 2_0e_{23}\}^T$ can be expressed as

$$\{0e\} = {}^1[A]\{0u\} \quad (10.8.36a)$$

where $\{0u\}$ is the vector of derivatives of increment displacements,

$$\{0u\} = \{0u_{1,1} \ 0u_{1,2} \ 0u_{1,3} \ 0u_{2,1} \ 0u_{2,2} \ 0u_{2,3} \ 0u_{3,1} \ 0u_{3,2} \ 0u_{3,3}\}^T$$

$${}^1[A]_{6 \times 9} = \begin{bmatrix} 1 + {}^1_0u_{1,1} & 0 & 0 & {}^1_0u_{2,1} & 0 & 0 \\ 0 & {}^1_0u_{1,2} & 0 & 0 & 1 + {}^1_0u_{2,2} & 0 \\ 0 & 0 & {}^1_0u_{1,3} & 0 & 0 & {}^1_0u_{2,3} \\ {}^1_0u_{1,2} & 1 + {}^1_0u_{1,1} & 0 & 1 + {}^1_0u_{2,2} & {}^1_0u_{3,1} & 0 \\ {}^1_0u_{1,3} & 0 & 1 + {}^1_0u_{1,1} & {}^1_0u_{2,3} & 0 & {}^1_0u_{2,1} \\ 0 & {}^1_0u_{1,3} & {}^1_0u_{1,2} & 0 & {}^1_0u_{2,3} & 1 + {}^1_0u_{2,2} \\ & & & & & \\ & & {}^1_0u_{3,1} & 0 & 0 & 0 \\ & & 0 & {}^1_0u_{3,2} & 0 & 0 \\ & & 0 & 0 & 1 + {}^1_0u_{3,3} & 0 \\ & & {}^1_0u_{3,2} & {}^1_0u_{3,1} & 0 & 0 \\ & & 1 + {}^1_0u_{3,3} & 0 & {}^1_0u_{3,1} & 0 \\ & & 0 & 1 + {}^1_0u_{3,3} & {}^1_0u_{3,2} & 0 \end{bmatrix} \quad (10.8.36b)$$

and ${}_0u_{i,j} = \partial u_i / \partial {}^0x_j$. The vectors $\{0u\}$ and $\{0e\}$ are related to the displacement increments at nodes by

$$\begin{aligned} \{0u\} &= [N] \{u\} = [N] {}^1[H]\{\Delta^e\} \\ \{0e\} &= {}^1[A]\{0u\} = {}^1[A][N] {}^1[H]\{\Delta^e\} \equiv {}^1[B_L]\{\Delta^e\} \\ {}^1[B_L] &= {}^1[A][N] {}^1[H] \end{aligned} \quad (10.8.37a)$$

where $[N]^T$ is the operator of differentials

$$[N]^T = \begin{bmatrix} \partial/\partial {}^0x_1 & \partial/\partial {}^0x_2 & \partial/\partial {}^0x_3 & 0 & 0 & 0 \\ 0 & 0 & 0 & \partial/\partial {}^0x_1 & \partial/\partial {}^0x_2 & \partial/\partial {}^0x_3 \\ 0 & 0 & 0 & 0 & 0 & 0 \\ & & & 0 & 0 & 0 \\ & & & 0 & 0 & 0 \\ \partial/\partial {}^0x_1 & \partial/\partial {}^0x_2 & \partial/\partial {}^0x_3 & & & \end{bmatrix} \quad (10.8.37b)$$

The components of ${}^1[A]$ include ${}_0^1u_{i,j}$. From Eq. (10.8.28) the global displacements are related to the natural curvilinear coordinates (ξ, η) and the linear coordinate ζ . Hence the derivatives of these displacements ${}_0^1u_{i,j}$ with respect to the global coordinates 0x_1 , 0x_2 and 0x_3 are obtained through the relation

$$[{}^1u_{i,j}] = \left[\begin{array}{ccc} \frac{\partial {}^1u_1}{\partial {}^0x_1} & \frac{\partial {}^1u_2}{\partial {}^0x_1} & \frac{\partial {}^1u_3}{\partial {}^0x_1} \\ \frac{\partial {}^1u_1}{\partial {}^0x_2} & \frac{\partial {}^1u_2}{\partial {}^0x_2} & \frac{\partial {}^1u_3}{\partial {}^0x_2} \\ \frac{\partial {}^1u_1}{\partial {}^0x_3} & \frac{\partial {}^1u_2}{\partial {}^0x_3} & \frac{\partial {}^1u_3}{\partial {}^0x_3} \end{array} \right] = {}^0[J]^{-1} \left[\begin{array}{ccc} \frac{\partial {}^1u_1}{\partial \xi} & \frac{\partial {}^1u_2}{\partial \xi} & \frac{\partial {}^1u_3}{\partial \xi} \\ \frac{\partial {}^1u_1}{\partial \eta} & \frac{\partial {}^1u_2}{\partial \eta} & \frac{\partial {}^1u_3}{\partial \eta} \\ \frac{\partial {}^1u_1}{\partial \zeta} & \frac{\partial {}^1u_2}{\partial \zeta} & \frac{\partial {}^1u_3}{\partial \zeta} \end{array} \right] \quad (10.8.38)$$

The Jacobian matrix ${}^0[J]$ is defined as

$${}^0[J] = \begin{bmatrix} \frac{\partial {}^0x_1}{\partial \xi} & \frac{\partial {}^0x_2}{\partial \xi} & \frac{\partial {}^0x_3}{\partial \xi} \\ \frac{\partial {}^0x_1}{\partial \eta} & \frac{\partial {}^0x_2}{\partial \eta} & \frac{\partial {}^0x_3}{\partial \eta} \\ \frac{\partial {}^0x_1}{\partial \zeta} & \frac{\partial {}^0x_2}{\partial \zeta} & \frac{\partial {}^0x_3}{\partial \zeta} \end{bmatrix} \quad (10.8.39)$$

and is computed from the coordinate definition of Eq. (10.8.27). The derivatives of displacements 1u_i with respect to the coordinates ξ, η and ζ can be computed from Eq. (10.8.28). In the evaluations of element matrices in Eqs (10.8.6a-d), the integrands of ${}^1[B_L]$, ${}^0[C]$, ${}^1[B_{NL}]$, ${}^1[S]$, ${}^1[H]$ and ${}^1\{\hat{S}\}$ should be expressed in the same coordinate system, namely the global coordinate system (${}^0x_1, {}^0x_2, {}^0x_3$) or the local curvilinear system (x'_1, x'_2, x'_3).

The number of stress and strain components are reduced to five since we neglect the transverse normal components of stress and strain. Hence, the global derivatives of displacements, $[{}^1u_{i,j}]$ which are obtained in Eq. (10.8.26), are transformed to the local derivatives of the local displacements along the orthogonal coordinates by the following relation

$$\begin{bmatrix} \frac{\partial {}^1u'_1}{\partial x'_1} & \frac{\partial {}^1u'_2}{\partial x'_1} & \frac{\partial {}^1u'_3}{\partial x'_1} \\ \frac{\partial {}^1u'_1}{\partial x'_2} & \frac{\partial {}^1u'_2}{\partial x'_2} & \frac{\partial {}^1u'_3}{\partial x'_2} \\ \frac{\partial {}^1u'_1}{\partial x'_3} & \frac{\partial {}^1u'_2}{\partial x'_3} & \frac{\partial {}^1u'_3}{\partial x'_3} \end{bmatrix} = [\theta]_{3 \times 3}^T [{}^1u_{i,j}] [\theta]_{3 \times 3} \quad (10.8.40)$$

where $[\theta]^T$ is the transformation matrix between the local coordinate system (x'_1, x'_2, x'_3) and the global coordinate system (${}^0x_1, {}^0x_2, {}^0x_3$). The transformation matrix $[\theta]$ is obtained by interpolating the three orthogonal unit vectors (${}^1\hat{\mathbf{e}}_1, {}^1\hat{\mathbf{e}}_2, {}^1\hat{\mathbf{e}}_3$) at each node:

$$[\theta] = \begin{bmatrix} \sum_{k=1}^n \psi_k {}^1e_{11}^k & \sum_{k=1}^n \psi_k {}^1e_{21}^k & \sum_{k=1}^n \psi_k {}^1e_{31}^k \\ \sum_{k=1}^n \psi_k {}^1e_{12}^k & \sum_{k=1}^n \psi_k {}^1e_{22}^k & \sum_{k=1}^n \psi_k {}^1e_{32}^k \\ \sum_{k=1}^n \psi_k {}^1e_{13}^k & \sum_{k=1}^n \psi_k {}^1e_{23}^k & \sum_{k=1}^n \psi_k {}^1e_{33}^k \end{bmatrix} \quad (10.8.41)$$

Since the element matrices are evaluated using numerical integration, the transformation must be performed at each integration point during the numerical integration.

In order to obtain ${}^1[B_L]$, the vector of derivatives of incremental displacements $\{u_0\}$ needs to be evaluated. Equations (10.8.38) and (10.8.40) can be used again except that 1u_i are replaced by u_i and the interpolation equation for u_i , Eq. (10.8.41), is applied.

Next we discuss the matrix of material stiffness. For a shell element composed of orthotropic material layers, with the principal material coordinates (x_1, x_2, x_3) oriented arbitrarily with respect to the shell coordinate system ($x'_1, x'_2, x'_3 = x_3$). For a k th lamina of a laminated composite shell, the matrix of material stiffnesses is given by

$${}^0[C']_{(k)} = \begin{bmatrix} C'_{11} & C'_{12} & C'_{16} & 0 & 0 \\ C'_{12} & C'_{22} & C'_{26} & 0 & 0 \\ C'_{16} & C'_{26} & C'_{66} & 0 & 0 \\ 0 & 0 & 0 & C'_{44} & C'_{45} \\ 0 & 0 & 0 & C'_{45} & C'_{55} \end{bmatrix} \quad (10.8.42)$$

where

$$\begin{aligned}
 C'_{11} &= m^4 Q_{11} + 2m^2 n^2 (Q_{12} + 2Q_{66}) + n^4 Q_{22} \\
 C'_{12} &= m^2 n^2 (Q_{11} + Q_{22} - 4Q_{66}) + (m^4 + n^4) Q_{12} \\
 C'_{16} &= mn[m^2 Q_{11} - n^2 Q_{22} - (m^2 - n^2)(Q_{12} + 2Q_{66})] \\
 C'_{22} &= n^4 Q_{11} + 2m^2 n^2 (Q_{12} + 2Q_{66}) + m^4 Q_{22} \\
 C'_{26} &= mn[n^2 Q_{11} - m^2 Q_{22} + (m^2 - n^2)(Q_{12} + 2Q_{66})] \\
 C'_{66} &= m^2 n^2 (Q_{11} + Q_{22} - 2Q_{12}) + (m^2 - n^2)^2 Q_{66} \\
 C'_{44} &= m^2 Q_{44} + n^2 Q_{55}, \quad C'_{45} = mn(Q_{55} - Q_{44}) \\
 C'_{55} &= m^2 Q_{55} + n^2 Q_{44} \\
 m &= \cos \theta_{(k)}, \quad n = \sin \theta_{(k)}
 \end{aligned} \tag{10.8.43}$$

where Q_{ij} are the surface stress-reduced stiffnesses of the k th orthotropic lamina in the material coordinate system. The Q_{ij} can be expressed in terms of engineering constants of a lamina

$$\begin{aligned}
 Q_{11} &= \frac{E_1}{1 - \nu_{12}\nu_{21}}, \quad Q_{12} = \frac{\nu_{12}E_2}{1 - \nu_{12}\nu_{21}}, \quad Q_{22} = \frac{E_2}{1 - n\nu_{12}\nu_{21}} \\
 Q_{44} &= G_{23}, \quad Q_{55} = G_{13}, \quad Q_{66} = G_{12}
 \end{aligned} \tag{10.8.44}$$

where E_i is the modulus in the x_i direction, G_{ij} ($i \neq j$) are the shear moduli in the x_i - x_j surface, and ν_{ij} are the associated Poisson's ratios.

To evaluate element matrices in Eqs. (10.8.19a-d), we employ the Gauss quadrature. Since we are dealing with laminated composite structures, integration through the thickness involves individual lamina. One way is to use Gauss quadrature through the thickness direction. Since the constitutive relation ${}_0[C]$ is different from layer to layer and is not a continuous function in the thickness direction, the integration should be performed separately for each layer. This increases the computational time as the number of layers is increased. An alternative way is to perform explicit integration through the thickness and reduce the problem to a 2-D one. The Jacobian matrix, in general, is a function of (ξ, η, ζ) . The terms in ζ may be neglected provided the thickness to curvature ratios are small. Thus the Jacobian matrix ${}^0[J]$ becomes independent of ζ and explicit integration can be employed. If ζ terms are retained in ${}^0[J]$, Gauss points through the thickness should be added. In the present study we assume that the Jacobian matrix is independent of ζ in the evaluation of element matrices and the internal nodal force vector.

Since the explicit integration is performed through the thickness, the expression for

$$\left[\frac{\partial^1 u'_i}{\partial x'_j} \right], \quad {}^1[A'], \quad \{{}_0 u'\}, \quad {}^1[H], \quad {}^1[B'], \quad \{{}_0 \varepsilon'_{ij}\}$$

is now expressed in an explicit form in terms of ζ . Hence, we can use exact integration through the thickness and use the Gauss quadrature to perform numerical integration on the midsurface of the shell element.

For thin shell structures, in order to avoid "locking" we use the reduced integration scheme to evaluate the stiffness coefficients associated with the transverse

shear deformation. Hence we split the constitutive matrix ${}_0[C']$ into two parts, one without transverse shear moduli ${}_0[C']_B$, and the other with only transverse shear moduli ${}_0[C']_S$. Full integration is used to evaluate the stiffness coefficients containing ${}_0[C']_B$, and reduced integration is used for those containing ${}_0[C']_S$.

If a shell element is subjected to a distributed load (such as the weight or pressure), the corresponding load vector ${}^2\{R\}$ from Eq. (10.8.19a-d) is given by

$${}^2\{R\}_{5n \times 1} = \int {}^0_A [H]^T \begin{Bmatrix} {}^2P_1 \\ {}^2P_2 \\ {}^2P_3 \end{Bmatrix} d {}^0 A \quad (10.8.45)$$

where 2P_i is the component of distributed load in the 0x_i direction at time $t + \Delta t$, 0A is the area of upper, middle or bottom surface of the shell element depending on the position on the position of the loading and the loading is assumed deformation-independent.

Substituting ${}^1[H]$ into Eq. (10.8.45) yields

$$\begin{aligned} {}^2\{R\}_{5n \times 1} &= \int {}^0_A \begin{bmatrix} \dots & \dots & \dots \\ \psi_k & 0 & 0 \\ 0 & \psi_k & 0 \\ 0 & 0 & \psi_k \\ \frac{1}{2}\zeta\psi_k h_k^{-1}e_{11}^k & \frac{1}{2}\zeta\psi_k h_k^{-1}e_{12}^k & -\frac{1}{2}\zeta\psi_k h_k^{-1}e_{13}^k \\ -\frac{1}{2}\zeta\psi_k h_k^{-1}e_{21}^k & \frac{1}{2}\zeta\psi_k h_k^{-1}e_{22}^k & -\frac{1}{2}\zeta\psi_k h_k^{-1}e_{23}^k \\ \dots & \dots & \dots \end{bmatrix} \begin{Bmatrix} {}^2P_1 \\ {}^2P_2 \\ {}^2P_3 \end{Bmatrix} d {}^0 A \\ &= \sum_{r=1}^{NGP} \sum_{s=1}^{NGP} \begin{Bmatrix} \dots \\ \psi_k {}^2P_1 \\ \psi_k {}^2P_2 \\ \psi_k {}^2P_3 \\ \frac{1}{2}\zeta\psi_k h_k \sum_{i=1}^3 {}^2P_i {}^1e_{1i}^k \\ -\frac{1}{2}\zeta\psi_k h_k \sum_{i=1}^3 {}^2P_i {}^1e_{2i}^k \\ \dots \end{Bmatrix} W_{\xi_r} W_{\eta_s} |{}^0J|_{(\xi_r, \eta_s)} \frac{2}{h} \quad (10.8.46) \end{aligned}$$

where $h = \sum_{k=1}^{NPE} \psi_k(\xi, \eta) h_k$ is the shell thickness at each Gauss point, and W is the weight at each Gauss point, and $|{}^0J|$ is the determinant of the Jacobian matrix in Eq. (10.8.39) at each Gauss point. Here the ζ terms are retained in Jacobian matrix and let ζ equal to 1, -1 or 0, respectively, when the distributed loading is at the top, bottom or middle surface.

10.8.5 Numerical Examples

A number of numerical examples of laminated plates and shells are presented. Only static bending problems of plates and shells are included. The Riks-Wempner method is employed for tracing the nonlinear load-deflection path (see Appendix 1 of [32]). For most of the problems the reduced/selective integration scheme is used to evaluate the element stiffness coefficients. The following three sets of boundary conditions are used in the numerical examples presented here (see Figure 10.8.3).

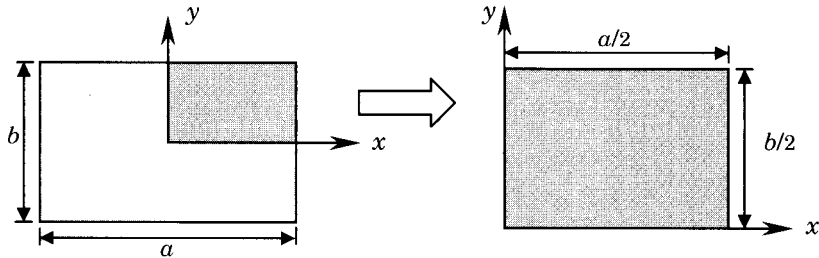


Figure 10.8.3: Geometry and coordinate system for a plate or shell panel.

$$\begin{aligned} \text{BC1: } & v_0 = w_0 = \phi_y = 0 \text{ at } x = a/2 \\ & u_0 = w_0 = \phi_x = 0 \text{ at } y = b/2 \\ & u_0 = \phi_x = 0 \text{ at } x = 0; \quad v_0 = \phi_y = 0 \text{ at } y = 0 \end{aligned} \quad (10.8.47)$$

$$\begin{aligned} \text{BC2: } & u_0 = w_0 = \phi_y = 0 \text{ at } x = a/2 \\ & v_0 = w_0 = \phi_x = 0 \text{ at } y = b/2 \\ & v_0 = \phi_x = 0 \text{ at } x = 0; \quad u_0 = \phi_y = 0 \text{ at } y = 0 \end{aligned} \quad (10.8.48)$$

$$\begin{aligned} \text{BC3: } & u_0 = w_0 = \phi_y = 0 \text{ at } x = a/2 \\ & v_0 = w_0 = \phi_x = 0 \text{ at } y = b/2 \\ & u_0 = \phi_x = 0 \text{ at } x = 0; \quad v_0 = \phi_y = 0 \text{ at } y = 0 \end{aligned} \quad (10.8.49)$$

Orthotropic plate under uniform load

Here we consider a simply supported, orthotropic, square plate under uniform transverse load q_0 . The geometry and material parameters used are

$$\begin{aligned} a = b = 12 \text{ in.}, \quad h = 0.138 \text{ in.}, \quad E_1 = 3 \times 10^6 \text{ psi}, \quad E_2 = 1.28 \times 10^6 \text{ psi} \\ G_{12} = G_{13} = G_{23} = 0.37 \times 10^6 \text{ psi}, \quad \nu_{12} = 0.25 \end{aligned} \quad (10.8.50)$$

A quarter of the plate with BC1 boundary and symmetry conditions is modeled with the $2 \times 2Q9$ mesh of continuum shell elements. The present results shown in Figure 10.8.4 are in good agreement with the experimental results of Zaghloul and Kennedy [8].

Simply supported spherical shell panel under point load

A simply supported isotropic spherical shell panel under central point load is analyzed for its large displacement response using $4 \times 4Q4$ and $2 \times 2Q9$ meshes in a quarter of the shell. The geometric and material parameters of the shell are shown in Figure 10.8.5. Figure 10.8.6 shows the response, including the post-buckling range (calculated using the modified Riks-Wempner method). The figure also includes the results of Bathe and Ho [53].

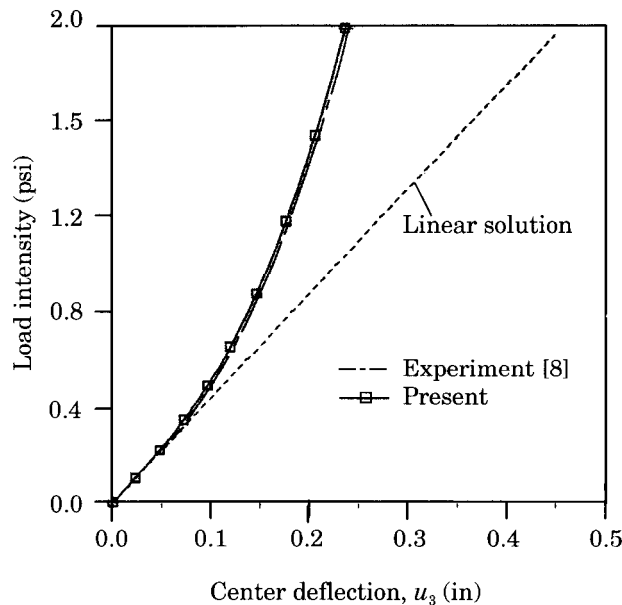
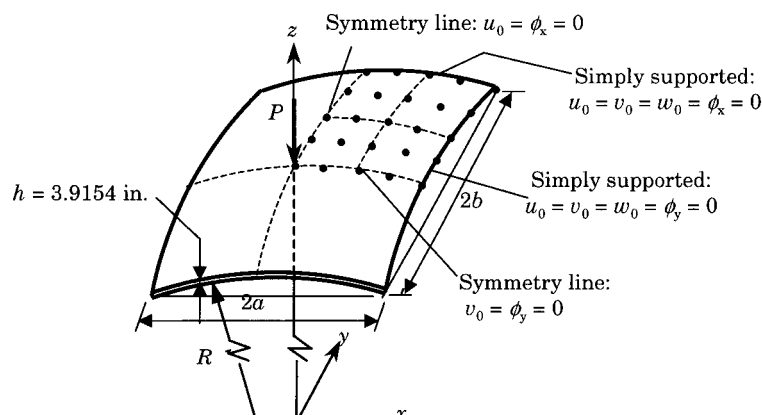


Figure 10.8.4: Maximum deflection versus the load magnitude for a simply supported orthotropic plate.



$$E = 10^4 \text{ psi}, v = 0.3, R = 100 \text{ in.}, a = b = 30.9017 \text{ in.}$$

Figure 10.8.5: Geometry and boundary conditions of the spherical shell panel analyzed.

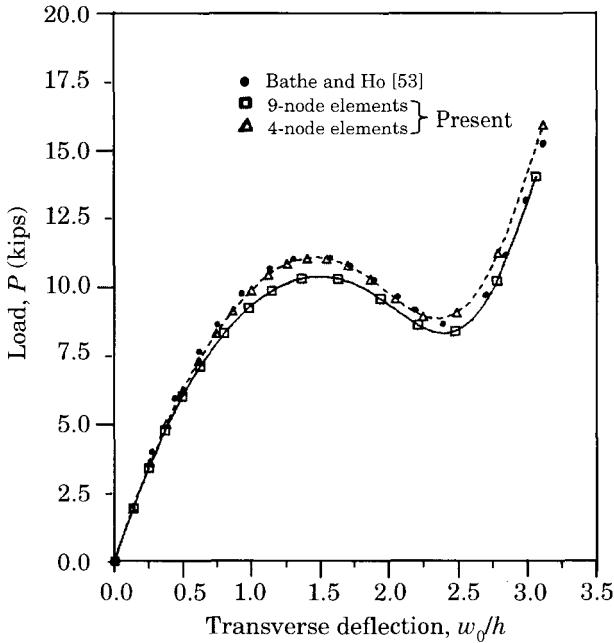


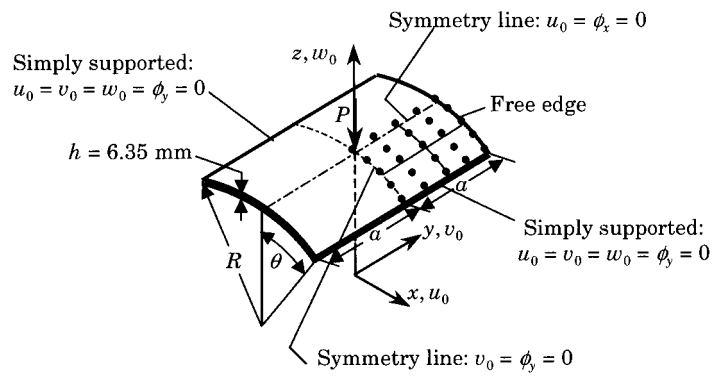
Figure 10.8.6: Load-deflection curves for a simply supported spherical shell panel under central point load (see Figure 10.8.5 for the geometry and boundary conditions).

Isotropic cylindrical shell panel under point load

An isotropic shallow cylindrical shell panel hinged along the longitudinal edges and free at the curved boundaries and subjected to a point load is analyzed (see Figure 10.8.7a). A quadrant of the shell is modeled with 2×2 Q9 mesh of continuum shell elements. The structure exhibits snap-through as well as snap-back phenomena, as shown in 10.8.7b. The solution obtained by Crisfield [46] is also shown in Figure 10.8.7b to be compared with the present results.

Simply supported composite spherical shell panel under uniform load

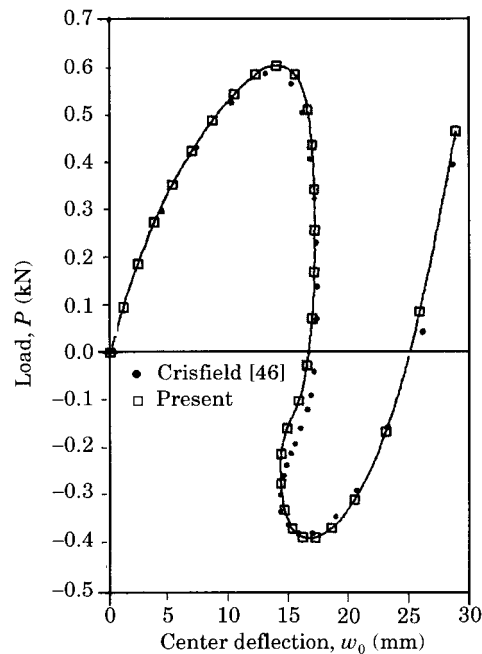
A simply supported laminated spherical shell panel under uniform load was analyzed for its large displacement response with 2×2 Q9 mesh of continuum shell elements in a quadrant of the shell. The geometry and material parameters used are: $a = b = 50$ in., $h = 1$ in., $R = 1,000$ in., $E_1 = 25E_2$, $E_2 = 10^6$ psi, $G_{12} = G_{13} = 0.5E_2$, $G_{23} = 0.2E_2$ psi, $\nu_{12} = 0.25$. The effect of edge boundary conditions and symmetry conditions on the nonlinear response is investigated using BC1 and BC3. The effect of slight difference in the boundary conditions is very significant on the deflection response, as shown in Figures 10.8.8a and 10.8.8b for two-layer cross-ply (0/90) and (-45/45) angle-ply laminates, respectively.



$$E = 3103 \text{ N/mm}^2, v = 0.3$$

$$R = 2540 \text{ mm}, a = 254 \text{ mm}, \theta = 0.1$$

(a)



(b)

Figure 10.8.7: Geometrically nonlinear response of a shallow cylindrical shell. (a) Geometry and finite element mesh. (b) Load-deflection curves.

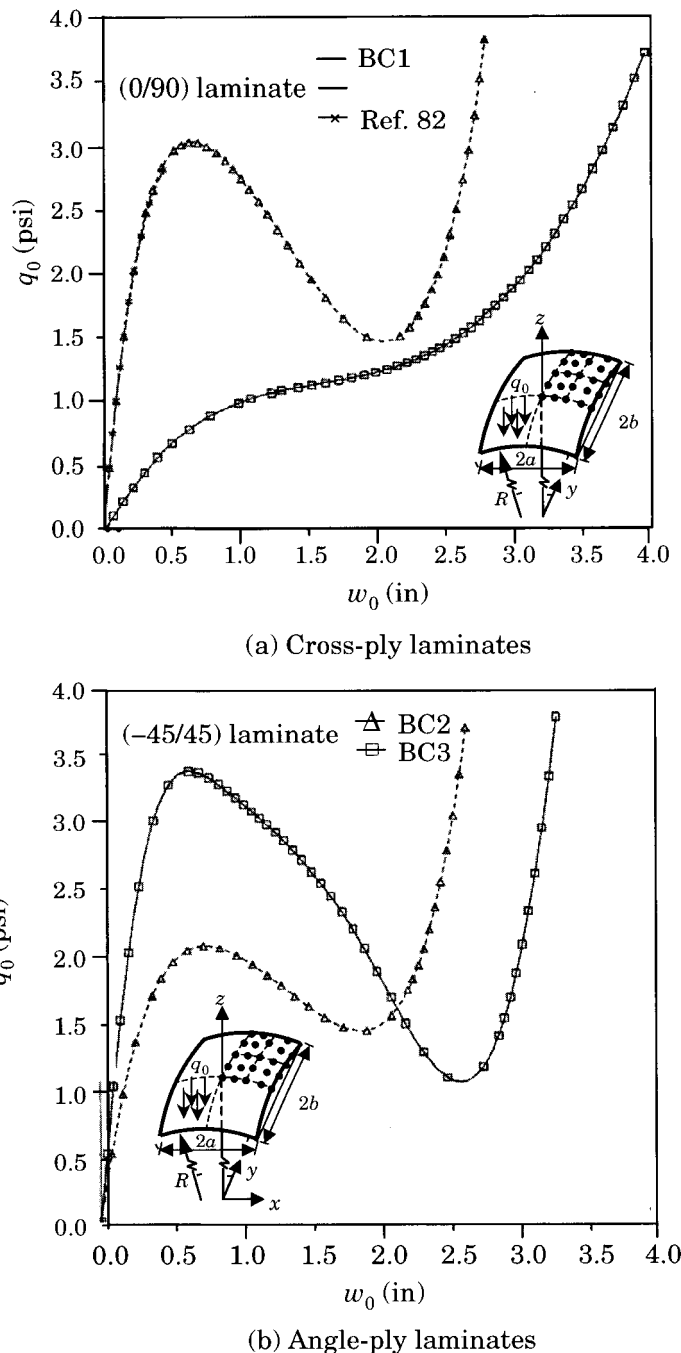


Figure 10.8.8: Geometrically nonlinear response of a shallow cylindrical shell. (a) Load-deflection curves for (0/90) laminates. (b) Load-deflection curves for (-45/45) laminates.

Nine-layer cross-ply (0/90/0/90/...) simply supported spherical shell panel

A cross-ply spherical shell laminated of nine graphite-epoxy material layers with the material properties

$$E_1 = 40E_2, \quad E_2 = 10^6 \text{ psi}, \quad G_{12} = G_{13} = 0.6E_2, \quad G_{23} = 0.5E_2, \quad \nu_{12} = 0.25$$

and subjected to uniform transverse load. The same geometry as that in the last problem ($a = b = 50$ in., $h = 1$ in., $R = 1,000$ in.) is used. A quadrant of the shell was modeled using 2×2 Q9 mesh of continuum shell elements and simply supported (BC1) boundary conditions. The load-deflection curve obtained with the modified Riks-Wempner method is compared with that obtained by Noor and Hartley [75] in Figure 10.8.9. Note that the laminated shell exhibits softening first and then stiffening and does not have a limit point. This response is similar to that in Figure 10.8.7b with the same boundary conditions.

10.8.6 Closure

This completes the nonlinear finite element analysis of laminated plates and shells using continuum shell element. Additional examples involving stiffened shells can be found in [21,23,78,79].

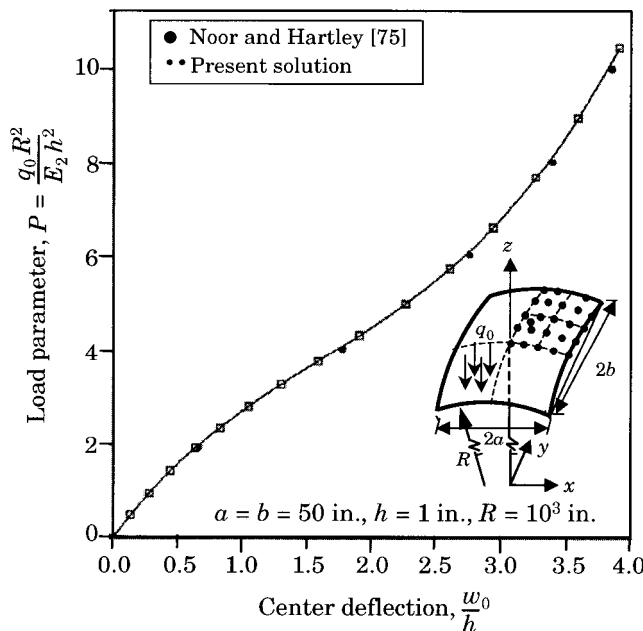


Figure 10.8.9: Load-deflection response of a simply supported (BC1), nine-layer (0/90/0/90/...), laminated spherical shell panel under uniform load.

10.9 Postbuckling Response and Progressive Failure of Composite Panels in Compression

10.9.1 Preliminary Comments

The classical lamination theory, in which the transverse shear effects are neglected, is often used to analyze laminated composite structures. Because of low moduli and strengths in transverse directions compared to that of in-plane directions, composite laminates may fail due to transverse stresses. Indeed, it is found that composite laminates loaded in compression fail due to high interlaminar stresses (see [83,84]). Therefore, shear deformable plate and shell elements are needed to provide information regarding the through-thickness strength of composite structures. Insight gained by using these elements may aid in the characterization of failure modes of composite panels.

In this section we present a case study of the postbuckling response of two graphite-epoxy panels loaded in axial compression. The study makes comparisons between the experimentally obtained and analytically determined postbuckling response of composite panels (see Engelstad, Reddy, and Knight [84]).

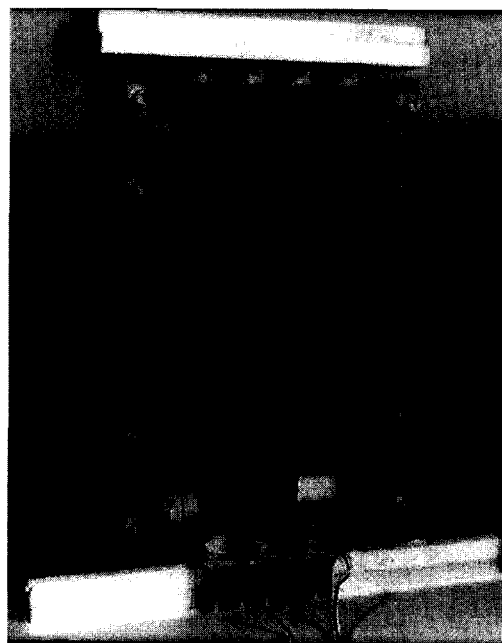
10.9.2 Experimental Study

The postbuckling and failure characteristics of flat, rectangular graphite-epoxy panels, with and without holes, and loaded in axial compression have been examined in an experimental study by Starnes and Rouse [83]. The panels were fabricated from commercially available unidirectional Thorne 300 graphite-fiber tapes pre-impregnated with 450°K cure Narmco 5208 thermosetting epoxy resin. Typical lamina properties for this graphite-epoxy system are

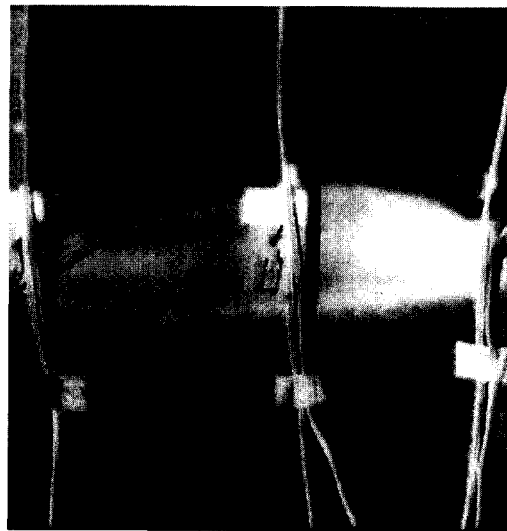
$$E_1 = 131.0 \text{ GPa (19,000 ksi)}, \quad E_2 = 12.0 \text{ GPa (1,890 ksi)} \\ G_{12} = 6.4 \text{ GPa (930 ksi)}, \quad \nu_{12} = 0.38, \quad h_k = 0.14 \text{ mm (0.0055 in.)} \quad (10.9.1)$$

where h_k denotes ply thickness. Each panel was loaded in axial compression using a 1.33 MN (300 kips) capacity hydraulic testing machine. The loaded ends of the panels were clamped by fixtures during testing and the unloaded edges were simply supported by knife-edge restraints to prevent the panels from buckling as wide columns. A typical panel mounted in the support fixture is shown in Figure 10.9.1a. Most panels exhibited postbuckling strength and failed along a nodal line of the buckling mode in a transverse shear failure mode, as shown in Figure 10.9.1b (see [83]). However, a different failure mode was observed for some of the 24-ply panels with holes. These panels failed along a transverse line passing through the hole, and failed soon after buckling.

Here we analyze two panels, denoted C4 and H4 (see Figure 10.9.2) in [83]. The finite element results are compared with the experimental results of Starnes and Rouse [83]. Panel C4 is 50.8 cm by 17.8 cm (20.0 in. long and 7.0 in. wide), 24-ply laminate, ($\pm 45/0_2/\pm 45/0_2/\pm 45/0/90_s$) (orthotropic). Panel C4 was observed in the test to buckle into two longitudinal half-waves and one transverse half-wave. The second panel, Panel H4, is a 50.8 cm by 14.0 cm (20.0 in. long by 5.5 in. wide) 24-ply laminate ($\pm 45/0/90_{3s}$) (quasi-isotropic). A 1.91 cm diameter (0.75 in. diameter) hole is located 19.1 cm (7.5 in.) from one of the loaded edges and along



(a) Typical panel with test fixture



(b) A transverse shear failure mode

Figure 10.9.1: (a) Typical panel with test fixture (load frame). (b) Failure mode (from Starnes and Rouse [83]).

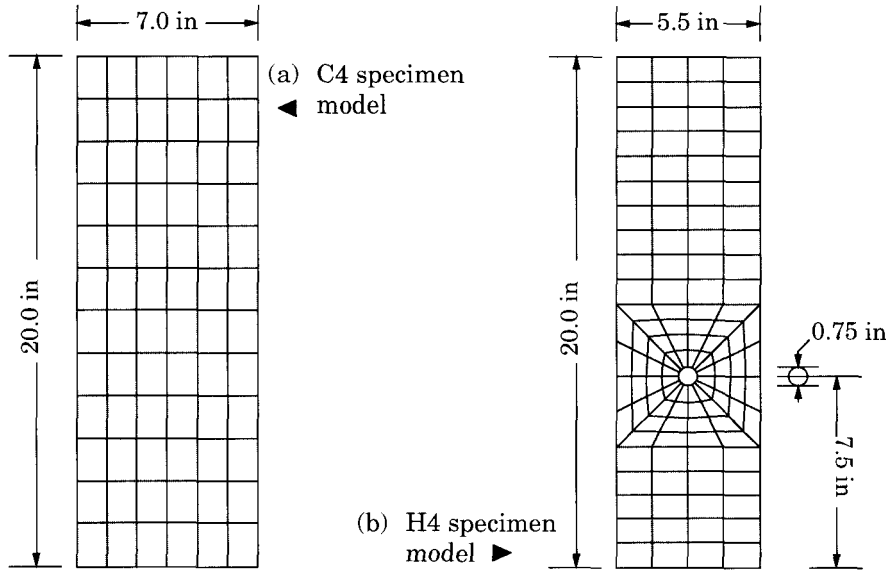


Figure 10.9.2: Geometry and finite elements meshes of the C4 and H4 composite panels used in the postbuckling study.

the panel centerline. Panel H4 was observed in the test to buckle into four longitudinal half-waves and one transverse half-wave with the hole located near the buckle crest of the second longitudinal half-wave.

10.9.3 Finite Element Models

Finite element models of such panels were developed in Section 10.8, which are based on continuum formulation of a laminated shell, and it is denoted here as the nine-node Chao–Reddy element [21], 9CR. The final incremental equations of equilibrium for an element are of the form [see Eqs. (10.8.21) and (10.8.22)]

$$([K_L] + [K_{NL}])\{\delta\Delta\} = \{R\} - \{F\} \quad (10.9.2)$$

where $\{\delta\Delta\}$ is the vector of incremental nodal displacements, $([K_L], [K_{NL}])$ are the linear and nonlinear parts of the stiffness matrix, and $\{F\}$ is the force vector [see Eqs. (10.8.19a,b,d)]:

$$\begin{aligned} [K_L] &= \int_{\Omega^e} [B_L]^T [C] [B_L] dv \\ [K_{NL}] &= \int_{\Omega^e} [B_{NL}] [S] [B_{NL}] dv \\ \{F\} &= \int_{\Omega^e} [B_L] \{\hat{S}\} dv \end{aligned} \quad (10.9.3)$$

In these equations, $[B_L]$ and $[B_{NL}]$ are linear and nonlinear strain-displacement transformation matrices, $[C]$ is the constitutive elasticity matrix, $[S]$ and $\{\hat{S}\}$ are the matrix and vector of second Piola–Kirchhoff stresses, and $\{R\}$ is the external load vector. All matrix elements refer to the deformed state and are measured with respect to the original undeformed configuration.

To evaluate the integrals in Eq. (10.9.3), we use Gauss quadrature in the surface directions of the shell, but explicit integration in the thickness direction. Thus the thickness direction integration for matrices $[K_L]$ and $[K_{NL}]$ gives the following laminate stiffnesses:

$$\begin{aligned}[A] &= \sum_{k=1}^P [C']_k (\zeta_{k+1} - \zeta_k) \\[B] &= \frac{1}{2} \sum_{k=1}^P [C']_k (\zeta_{k+1}^2 - \zeta_k^2) \\[D] &= \frac{1}{3} \sum_{k=1}^P [C']_k (\zeta_{k+1}^3 - \zeta_k^3)\end{aligned}\quad (10.9.4)$$

Here ζ_k is the thickness coordinate of the bottom of the k th lamina, P is the number of laminae, $[C']_k$ is the constitutive matrix for the k th lamina in the principal material coordinates, which has the form [see Eqs. (10.8.43) and (10.8.44)]

$$[C'] = f([Q], \theta) \quad (10.9.5)$$

where Q_{ij} are the plane stress-reduced elastic coefficients in the material coordinates and θ is the fiber orientation angle.

The finite element model used in Reference 84 consisted of six elements per buckle half-wave in each direction. Hence, the finite element model of Panel C4 consists of 12 nine-node quadrilateral elements along the panel length. Figure 10.9.2a shows the model used for the C4 specimen. The finite element model of Panel H4 is different, due to the presence of the hole. This model has four “rings” of elements around the hole with each ring subdivided into 16 elements, as shown in Figure 10.9.2b. The total numbers of nine-node quadrilateral elements in the finite element models of Panels C4 and H4 are 72 and 124, respectively.

In order to proceed beyond the critical buckling point in the analysis of each panel, an initial geometric imperfection, typically the same shape as the first linear buckling mode, was assumed in the finite element analysis. The amplitude of each mode was selected to be 1–5% of the total laminate thickness. This allows efficient progress past the critical buckling point, but does not affect the results in the postbuckling range.

10.9.4 Failure Analysis

The maximum stress and Tsai–Wu failure criteria are used (see [13,14,85–88]). In the *maximum stress criterion*, failure is assumed to occur if any one of the following conditions are satisfied:

$$\sigma_1 \geq X_T, \quad \sigma_4 \geq R, \quad \sigma_2 \geq Y_T, \quad \sigma_5 \geq S, \quad \sigma_3 \geq Z_T, \quad \sigma_6 \geq T \quad (10.9.6)$$

where $(\sigma_1, \sigma_2, \sigma_3)$ are the normal stress components, $(\sigma_4, \sigma_5, \sigma_6)$ are shear stress components, (X_T, Y_T, Z_T) are the lamina normal strengths in tension (T) along the (1, 2, 3) directions, and (R, S, T) are the shear strengths in the (23, 13, 12) planes, respectively. When $(\sigma_1, \sigma_2, \sigma_3)$ are compressive, they should be compared with (X_C, Y_C, Z_C) , which are normal strengths in compression (C) along the (1, 2, 3) principal material directions, respectively.

The *Tsai-Wu criterion* is given by

$$\mathcal{F} \equiv \sum_{i=1}^6 F_i \sigma_i + \sum_{i=1}^6 \sum_{j=1}^6 F_{ij} \sigma_i \sigma_j \geq 1 \quad (10.9.7)$$

$$\begin{aligned} F_1 &= \frac{1}{X_T} - \frac{1}{X_C}, \quad F_2 = \frac{1}{Y_T} - \frac{1}{Y_C}, \quad F_3 = \frac{1}{Z_T} - \frac{1}{Z_C} \\ F_{11} &= \frac{1}{X_T X_C}, \quad F_{22} = \frac{1}{Y_T Y_C}, \quad F_{33} = \frac{1}{Z_T Z_C} \\ F_{44} &= \frac{1}{R^2}, \quad F_{55} = \frac{1}{S^2}, \quad F_{66} = \frac{1}{T^2}, \quad F_{12} = -\frac{1}{2} \frac{1}{\sqrt{X_T X_C Y_T Y_C}} \\ F_{13} &= -\frac{1}{2} \frac{1}{\sqrt{X_T X_C Z_T Z_C}}, \quad F_{23} = -\frac{1}{2} \frac{1}{\sqrt{Y_T Y_C Z_T Z_C}} \end{aligned} \quad (10.9.8)$$

where σ_i denote the stress components referred to the principal material coordinates.

In reality, laminate failure occurs due to propagation of damage as the load is increased. To model this effect, a progressive failure approach is used in the nonlinear finite element analysis. At each load step, Gauss point stresses are used in the selected failure criterion. If failure occurred at a Gauss point, a modification of the lamina properties was made at that Gauss point, which results in reduced stiffnesses [A], [B], and [D] of the laminate. For example, for the maximum stress criterion, if the σ_1 stress exceeds the longitudinal tensile strength X_T , then the longitudinal modulus E_1 at that point is reduced to zero. For the Tsai-Wu criterion, if failure occurs, then the following expressions are used to determine the failure mode:

$$\begin{aligned} H_1 &= F_1 \sigma_1 + F_{11} \sigma_1^2, \quad H_2 = F_2 \sigma_2 + F_{22} \sigma_2^2 \\ H_4 &= F_{44} \sigma_4^2, \quad H_5 = F_{55} \sigma_5^2, \quad H_6 = F_{66} \sigma_6^2 \end{aligned} \quad (10.9.9)$$

The largest H_i term is selected as the dominant failure mode and the corresponding modulus is reduced to zero. Thus H_1 corresponds to the modulus E_1 , H_2 to E_2 , H_4 to G_{23} , H_5 to G_{13} , and H_6 to G_{12} . As a consequence of this reduction, engineering material properties are updated as failure progresses. An outline of the steps used in the analysis is given below.

1. After nonlinear iterative displacement convergence is achieved, calculate stresses in the global (x, y, z) coordinates at the middle of each layer at each Gauss point.
2. Transform the stresses to the principal material coordinates.
3. Compute the failure index, \mathcal{F} .
4. If failure occurs (i.e., $\mathcal{F} \geq 1$),
 - (a) identify the maximum value of H_i ,

- (b) reduce the appropriate lamina moduli at that Gauss point, and
 - (c) recompute laminate stiffnesses and restart the nonlinear analysis at the same load step (i.e., return to Step 1).
5. If no failure occurs, proceed to the next load step.

The end shortening of the panel is monitored as in a compression test. The failure load is defined to be that load for which the panel undergoes large end shortening for small increments of load.

10.9.5 Results for Panel C4

Comparison between test results from Reference 83 and finite element results from Reference 84 for Panel C4 are shown in Figure 10.9.3. The figure shows (a) end shortening u_0 , normalized by the analytical end shortening u_{cr} at buckling (Figure 10.9.3a); (b) out-of-plane deflection w_0 near a point of maximum deflection, normalized by the panel thickness h (Figure 10.9.3b); and (c) the longitudinal surface strains e near a point of maximum out-of-plane deflection, normalized by the analytical buckling strain e_{cr} . These are all shown as functions of the applied load P , normalized by the theoretical buckling load P_{cr} . These experimental and finite element results agree well up to failure of the panel. The postbuckling response exhibits large out-of-plane deflections (nearly three times the panel thickness; see Figure 10.9.3b) and high longitudinal strains from front and back surfaces (nearly three times the analytical buckling strain; see Figure 10.9.3c).

Figure 10.9.4a contains a contour plot of the out-of-plane deflections generated from the finite element analysis at an applied load of $2.1P_{cr}$. Figure 10.9.4b contains a photograph of the Moiré fringe pattern from Reference 83 corresponding to the out-of-plane deflections observed during the testing of Panel C4 at the same load. These results indicate that the out-of-plane deflections from both test and analysis have the same pattern over the entire panel. Both patterns indicate two longitudinal half-waves with a buckling-mode nodal line at panel midlength. Stress distributions in each layer of the laminate were calculated using the nonlinear finite element results in order to determine the failure loads. The stresses were determined using the constitutive relations for both the in-plane and transverse components. In addition, the transverse shear stress distributions were also obtained by integrating the equilibrium equations, wherein the in-plane stresses were computed using the constitutive relations.

Figure 10.9.5 shows the distribution of the maximum σ_{xz} stress through the thickness direction z , normalized by the laminate thickness h for $P = 2.1 P_{cr}$. It is clear that the 0° layers carry the largest transverse shear load. Figure 10.9.6 contains the distribution of the normal stress σ_{xx} in the third layer of the laminate (a 0° ply) at panel midlength for three values of the applied load. At the buckling load, the normal stress is nearly uniform across the panel. Although σ_{xx} is large, the largest value is well below the material allowable values: $X_T = 1400$ MPa (203 ksi) in tension and $X_C = 1138$ MPa (165 ksi) in compression. The contour plot of σ_{xx} over the entire panel in this 0° ply for an applied load of $2.1P_{cr}$ indicates (not shown here; see [84]) that high compressive axial stresses occur along the longitudinal edges of the panel.

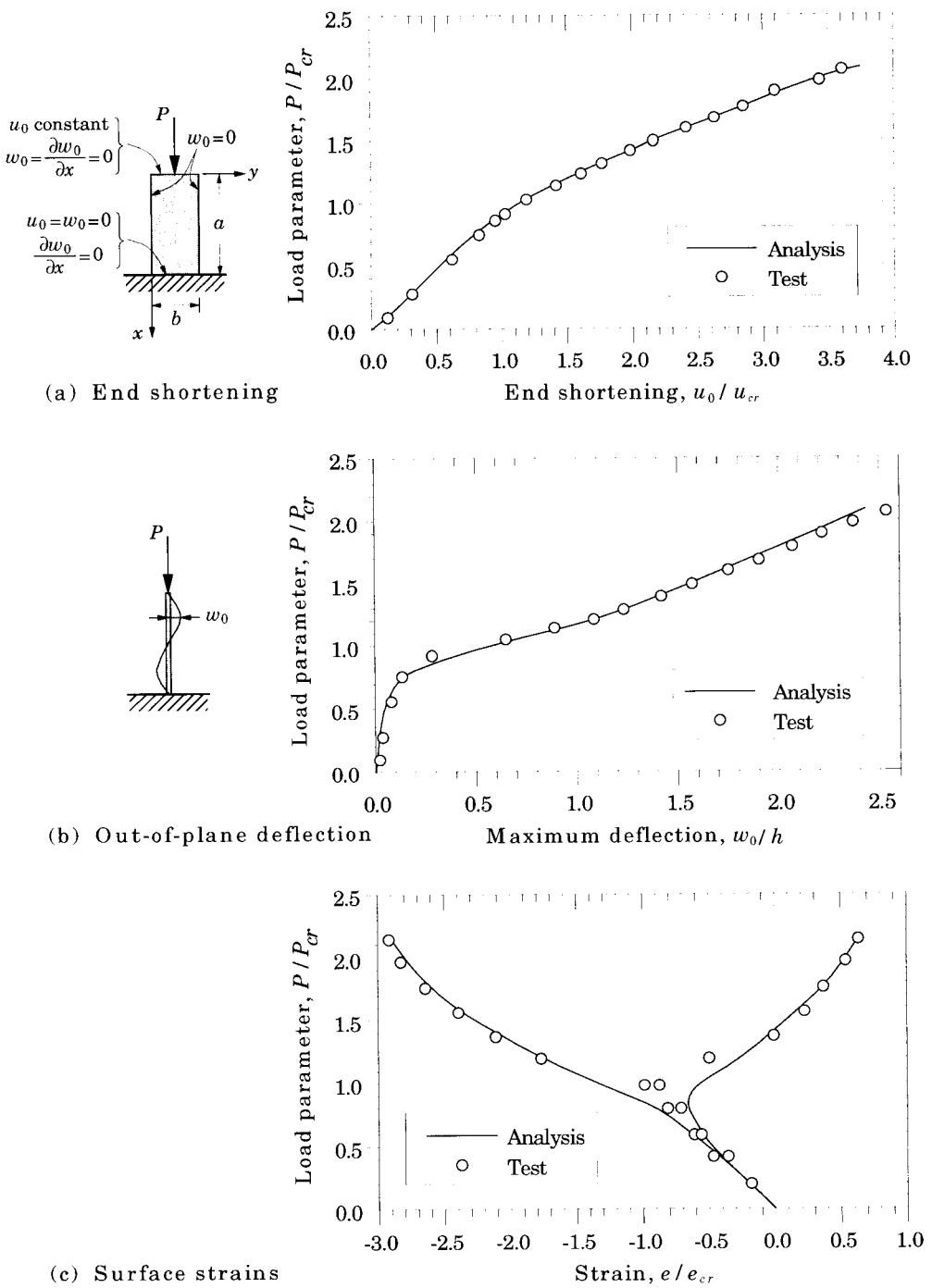


Figure 10.9.3: Postbuckling response characteristics of panel C4.

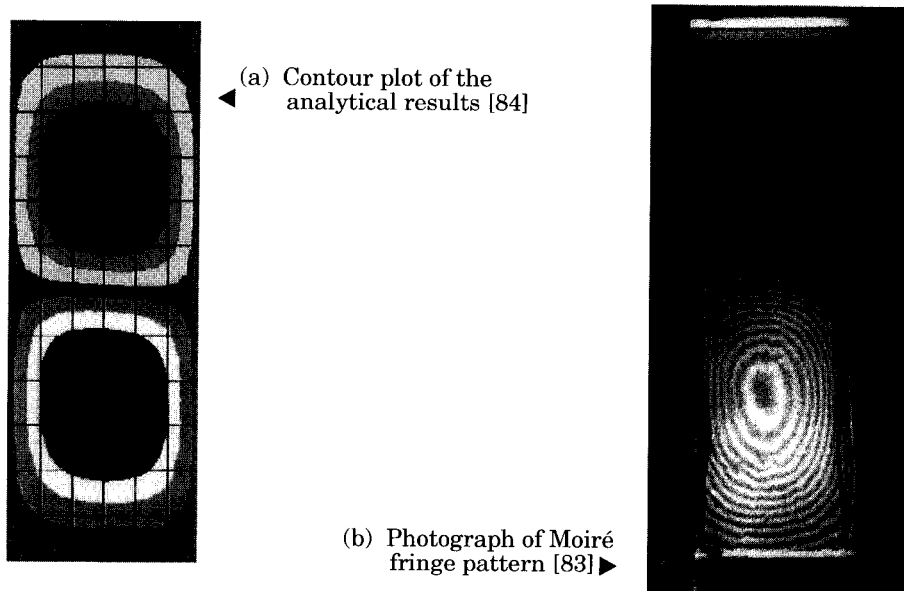


Figure 10.9.4: Comparison of experimental (Moiré) and analytical out-of-plane deflection patterns for panel C4.

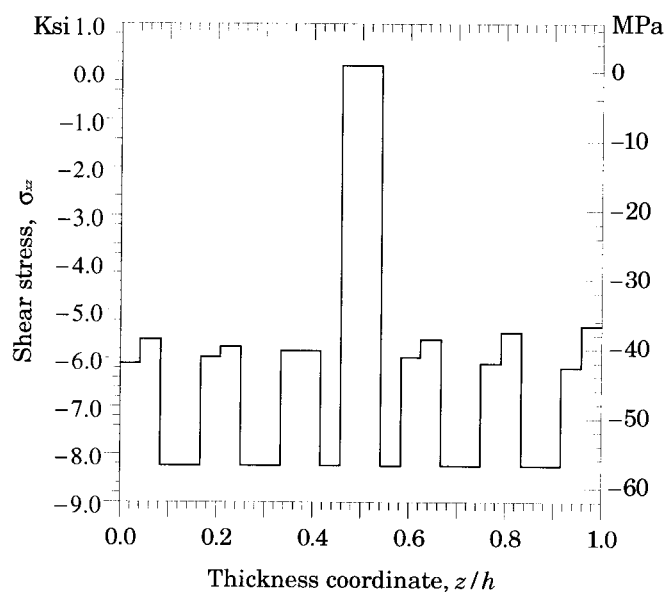


Figure 10.9.5: Transverse shear stress, σ_{xz} , distribution through the thickness of panel C4.

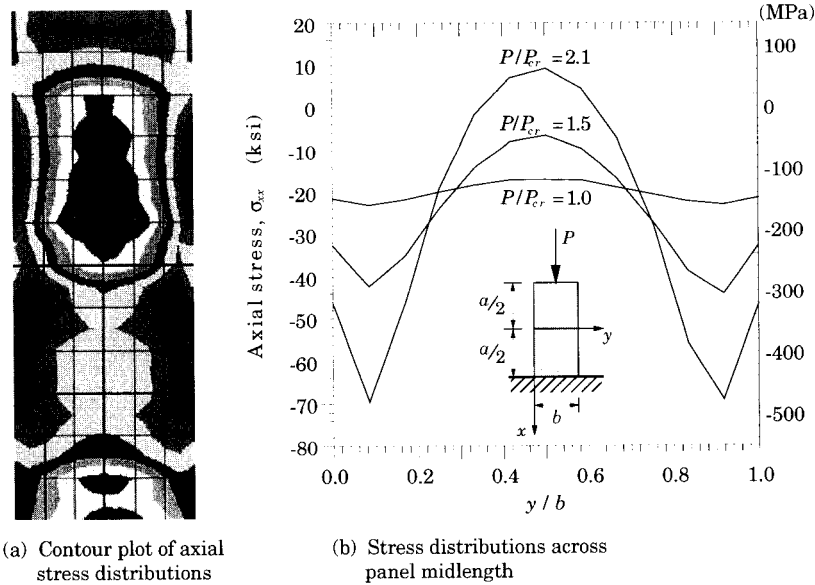


Figure 10.9.6: Axial stress, σ_{xx} , distributions in the third layer from the surface (0° ply) of panel C4.

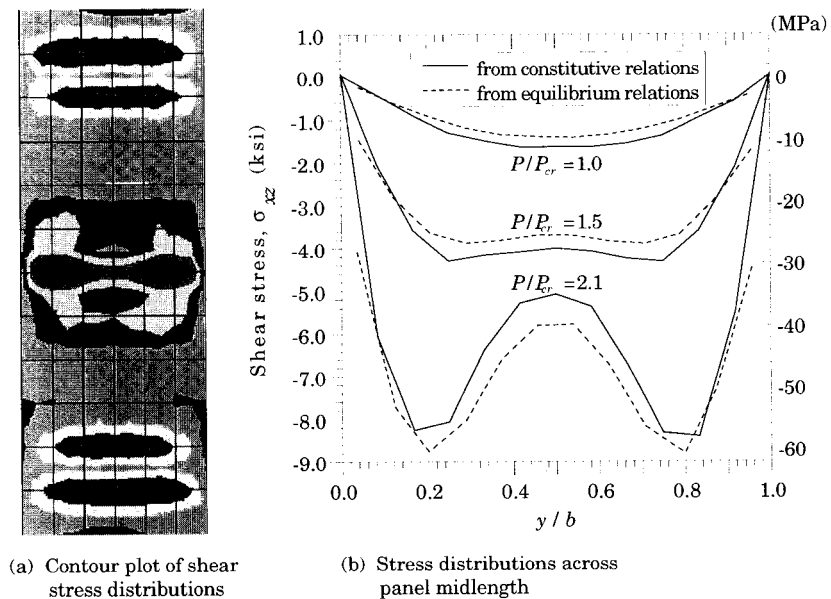


Figure 10.9.7: Transverse shear stress, σ_{xz} , distributions in the third layer from the surface (0° ply) of panel C4.

Figure 10.9.7 shows the distribution of the transverse shear stress in the third layer of the laminate (a 0° ply) at panel midlength for three values of the applied load. The solid curves represent the transverse shear stress distributions obtained using the constitutive relations, and the dashed curves denote the transverse shearing stress distributions obtained from the equilibrium equations. Both methods give very similar results. At the buckling load, the peak transverse shear stress occurs near the center of the panel. After buckling, the transverse shear stresses σ_{xz} redistribute towards the edges of the panel. The peak values of the transverse shear stress σ_{xz} approach the material allowable value of $S = T = 62$ MPa (9 ksi) for $P = 2.1P_{cr}$, indicating the panel failure due to transverse shear stress. A contour plot (not shown here) of the distribution of the transverse shear stress σ_{xz} over the entire panel in this 0° ply for an applied load of $P = 2.1P_{cr}$ indicates that high transverse shear stresses occur along the buckling-mode nodal line.

This failure mode can be further explained through a close examination of the Green–Lagrange strain component

$$\varepsilon_{xz} = \frac{1}{2} \left(\frac{\partial u}{\partial z} + \frac{\partial w}{\partial x} + \frac{\partial u}{\partial x} \frac{\partial u}{\partial z} + \frac{\partial v}{\partial x} \frac{\partial v}{\partial z} + \frac{\partial w}{\partial x} \frac{\partial w}{\partial z} \right) \quad (10.9.10)$$

in conjunction with the displacement field of the first-order shear deformation theory

$$\begin{aligned} u(x, y, z) &= u_0(x, y) + z\phi_x \\ v(x, y, z) &= v_0(x, y) + z\phi_y \\ w(x, y, z) &= w_0(x, y) \end{aligned} \quad (10.9.11)$$

Substituting of the displacements from Eq. (10.9.11) into the strain in Eq. (10.9.10) and noting that ϕ_y is zero along a buckling-mode nodal line, we obtain

$$\varepsilon_{xz} = \frac{1}{2} \left(\phi_x + \frac{\partial w_0}{\partial x} + \frac{\partial u_0}{\partial x} \phi_x \right) \quad (10.9.12)$$

The quantity $\frac{\partial w_0}{\partial x}$ (out-of-plane deflection gradient) is largest along a buckling-mode nodal line and the quantity $\frac{\partial u_0}{\partial x}$ (related to the membrane strain) is largest along the panel edges. A similar examination of the other transverse shearing strain ε_{yz} leads to the conclusion that the transverse shearing strain ε_{xz} is the dominant one.

Figures 10.9.8a and 10.9.8b present the progressive failure results for Panel C4, using the maximum stress and Tsai–Wu failure criteria, respectively. In addition to the strengths already mentioned, the other allowables used are transverse tensile strength, $X_T = 80.9$ MPa (11.7 ksi); transverse compressive strength, $X_C = 189.0$ MPa (27.4 ksi); and in-plane shear strength, $T = 69.0$ MPa (10.0 ksi). At some point in the analysis a dramatic change in slope indicates an inability of the panel to support additional load. This location is identified as the failure load. Figures 10.9.8a and 10.9.8b show that the Tsai–Wu criterion estimates the experimental failure more closely than the maximum stress criterion. This is attributed to the presence of stress interaction terms in the Tsai–Wu criterion failure index.

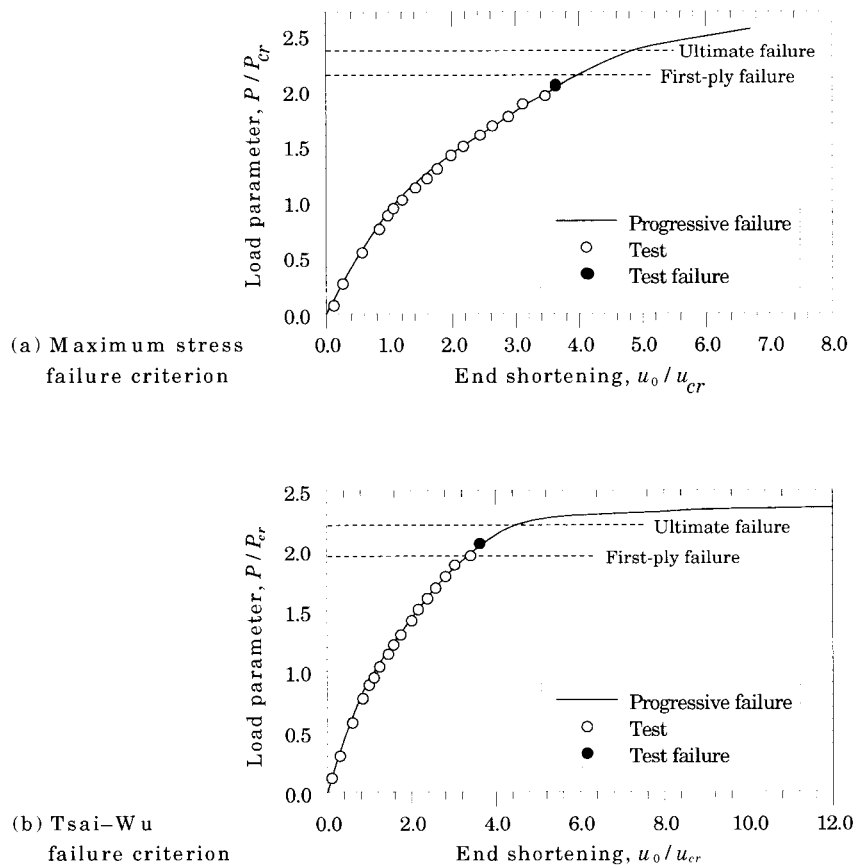


Figure 10.9.8: Progressive failure results of panel C4.

10.9.6 Results for Panel H4

Panel H4 was analyzed to investigate deformation and failure of a panel with a hole. An imperfection of 1% of panel thickness times mode 1 was used to proceed into the postbuckling range. Figure 10.9.9a contains a comparison of end shortening obtained numerically and experimentally. Figures 10.9.9b and 10.9.9c show the longitudinal surface strains e (both top and bottom surfaces) across the panel at the hole for a load of $0.90P_{cr}$ and $1.39P_{cr}$, respectively. These results are in good agreement with experimental results from Reference 83.

It should be noted that if uniformly reduced or selectively reduced integration were used in the analysis of this panel, it would predict spurious modes. These occur because of zero energy modes, and lack of restraint of the model around the hole. Element distortion around the hole could be another contributing factor. It is necessary to use full integration to alleviate this problem, and the mesh should be sufficiently refined so that element locking effects are negligible.

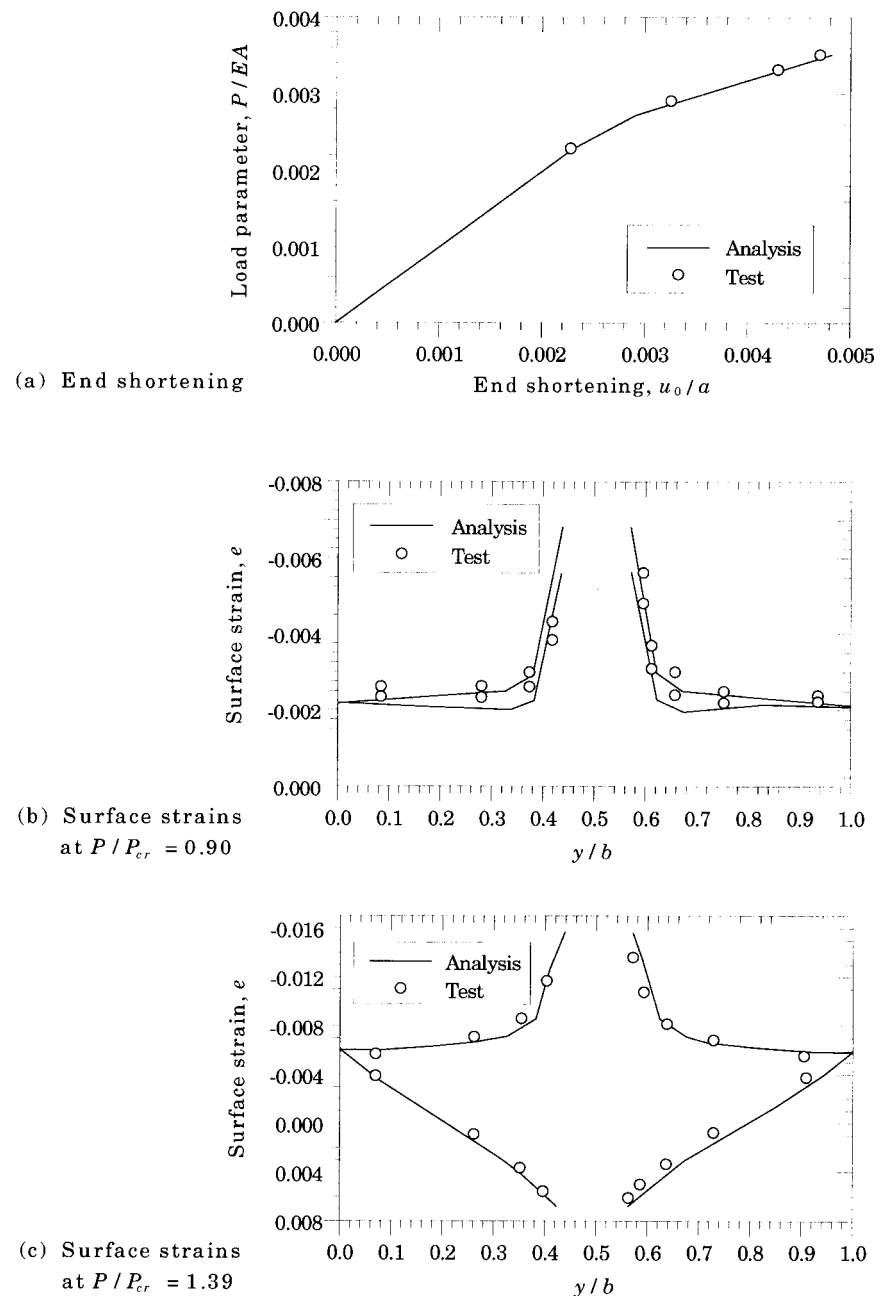


Figure 10.9.9: Postbuckling response characteristics of panel H4.

For panel H4, once again, a transverse shear mechanism develops along nodal lines away from the hole. However, the peak stress approaches only 48.3 MPa (7.0 ksi) at the experimental failure load. At this load the in-plane shear stress approaches its allowable around the hole. Simultaneous first-ply failure occurs due to σ_{xy} and σ_{xx} components around the hole edge. Thus the failure mode is not a dominant transverse shear mode as for Panels C4 and C10, but a more complex interacting mode with a dominant in-plane shear component. Progressive failure results are shown in Figures 10.9.10a and 10.9.10b. The Tsai-Wu criterion is, once again, in better agreement with experimental results.

We close this section with a comment that the case study presented in this section brings out the importance of interlaminar stresses. References 13 and 84 contain additional results of postbuckling and progressive failures.

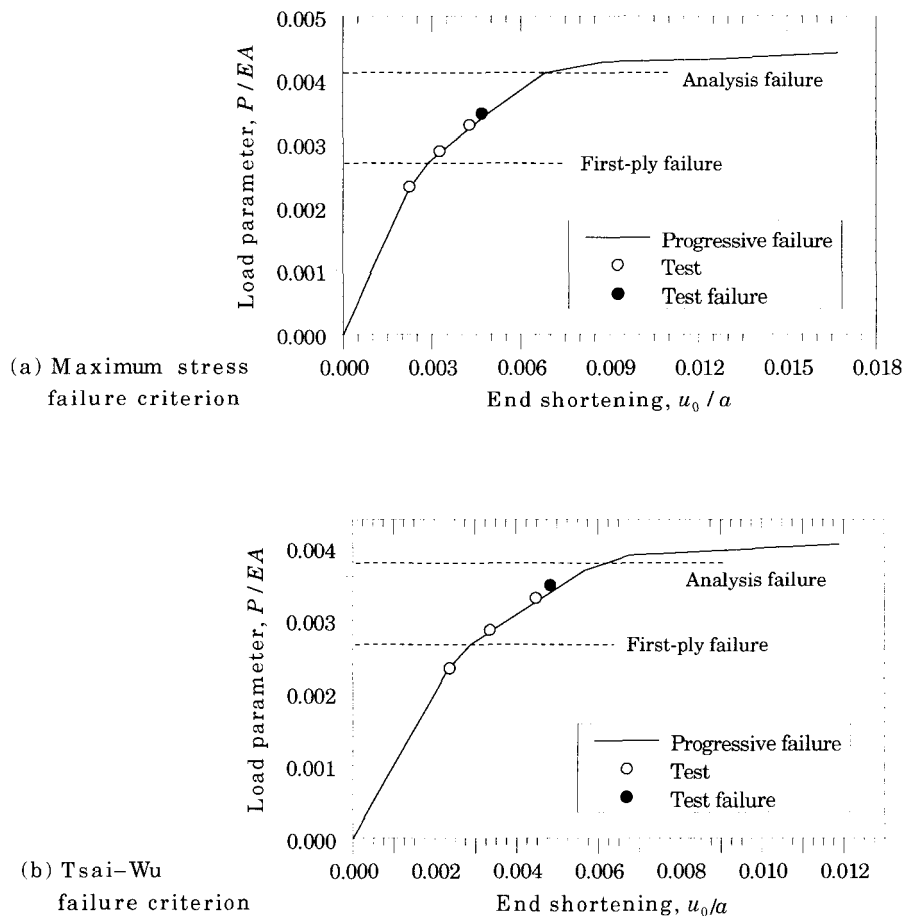


Figure 10.9.10: Progressive failure results of panel H4.

10.10 Closure

The objective of the chapter was to introduce the concept of geometric nonlinearity, develop finite element models of the von Kármán nonlinear plate and shell theories, present the continuum shell finite element, and study the influence of geometric nonlinearity on bending, transient and buckling response and ultimate failure of laminated plates and shells. In particular, the von Kármán nonlinear formulations of laminated plates using the classical and first-order shear deformation theories of plates and Sanders theory of shells are developed. The development of continuum shell element is also presented. The Newton–Raphson iterative method of solution is discussed, and the tangent stiffness matrix coefficients of the FSDT element are derived. Numerical results of the nonlinear analysis using the FSDT plate and shell elements as well as continuum shell element are presented to illustrate the influence of symmetry boundary conditions on the nonlinear response, effect of the geometric nonlinearity on the response of antisymmetric cross-ply plate strips, nonlinear transient response of laminated plates, and postbuckling response and progressive failure analysis of laminated panels under compressive load. For studies on damage and failures in composites, the reader may consult [13,92–110].

Problems

- 10.1** Consider the nonlinear differential equation

$$-\frac{d}{dx} \left(u \frac{du}{dx} \right) = f(x), \quad 0 < x < 1 \quad (1a)$$

$$\frac{du}{dx}(0) = 0, \quad u(1) = \sqrt{2} \quad (1b)$$

Show that the finite element model is given by

$$[K^e]\{u^e\} = \{F^e\} \quad (2a)$$

$$K_{ij}^e = \int_{x_A}^{x_B} u \frac{d\psi_i}{dx} \frac{d\psi_j}{dx} dx, \quad F_i^e = P_i^e + \int_{x_A}^{x_B} f \psi_i dx \quad (2b)$$

- 10.2** Compute the tangent coefficient matrix for the finite element model of Problem 10.1. Note that in an iterative solution of the problem, the initial guess for u should be *nonzero*. Explain why.
- 10.3** Consider the displacement field of the Euler–Bernoulli beam theory (see Example 1.4.1):

$$u_1(x, z) = u_0(x) - z \frac{dw_0}{dx}, \quad u_2 = 0, \quad u_3(x, z) = w_0(x) \quad (1)$$

Show that the von Kármán nonlinear strains are given by

$$\varepsilon_{xx} = \frac{du_0}{dx} + \frac{1}{2} \left(\frac{dw_0}{dx} \right)^2 - z \frac{d^2 w_0}{dx^2} \quad (2)$$

and that the total potential energy associated with a laminated beam is

$$\begin{aligned} \Pi(u_0, w_0) = & \int_0^L \left\{ \frac{E_{xx}^b A}{2} \left[\frac{du_0}{dx} + \frac{1}{2} \left(\frac{dw_0}{dx} \right)^2 \right]^2 + \frac{E_{xx}^b I_{yy}}{2} \left(\frac{d^2 w_0}{dx^2} \right)^2 \right\} dx \\ & - \int_0^L \hat{q} w_0 dx \end{aligned} \quad (3)$$

where $\hat{q} = qb$ is the distributed transverse load, b is the width, and $A = bh$ is the area of cross section of the beam.

- 10.4** Show that the Euler–Lagrange equations associated with the displacement field of Problem 10.3 are

$$-\frac{dN_{xx}}{dx} = 0, \quad -\frac{d^2M_{xx}}{dx^2} - \frac{d}{dx} \left(N_{xx} \frac{dw_0}{dx} \right) - q = 0 \quad (1)$$

where N_{xx} and M_{xx} are the force and moment resultants

$$N_{xx} = \int_A \sigma_{xx} dx, \quad M_{xx} = \int_A \sigma_{xx} z dx \quad (2)$$

Show that the force and moment resultants for symmetrically laminated beams can be expressed in terms of the displacements as

$$N_{xx} = E_{xx}^b A \left[\frac{du_0}{dx} + \frac{1}{2} \left(\frac{dw_0}{dx} \right)^2 \right], \quad M_{xx} = -E_{xx}^b I_{yy} \frac{d^2w_0}{dx^2} \quad (3)$$

- 10.5** Use the equations of equilibrium of Problem 10.4 to derive the following weak forms for a beam finite element, $x_A < x < x_B$:

$$0 = \int_{x_A}^{x_B} E_{xx}^b A \frac{d\delta u_0}{dx} \left[\frac{du_0}{dx} + \frac{1}{2} \left(\frac{dw_0}{dx} \right)^2 \right] dx \\ - P_1 \delta u_0(x_A) - P_2 \delta u_0(x_B) \quad (1)$$

$$0 = \int_{x_A}^{x_B} \left\{ E_{xx}^b I_{yy} \frac{d^2 w_0}{dx^2} \frac{d^2 \delta w_0}{dx^2} + E_{xx}^b A \frac{d\delta w_0}{dx} \frac{dw_0}{dx} \left[\frac{du_0}{dx} + \frac{1}{2} \left(\frac{dw_0}{dx} \right)^2 \right] \right\} dx \\ - \int_{x_A}^{x_B} q \delta w_0 dx - \bar{Q}_1 w_0(x_A) - \bar{Q}_3 w_0(x_B) - \bar{Q}_2 \theta(x_A) - \bar{Q}_4 \theta(x_B) \quad (2)$$

Define the secondary variables P_i and \bar{Q}_i in terms of the displacements.

- 10.6** Develop the nonlinear finite element model of a laminated beam using the weak forms given in Problem 10.5. Assume finite element interpolation of u_0 and w_0 in the form

$$u_0(x) = \sum_{j=1}^2 u_j \psi_j(x), \quad w_0(x) = \sum_{j=1}^4 \bar{\Delta}_j \varphi_j(x) \quad (1)$$

$$\bar{\Delta}_1 = w_1, \quad \bar{\Delta}_2 = \theta_1, \quad \bar{\Delta}_3 = w_2, \quad \bar{\Delta}_4 = \theta_2 \quad (2)$$

and ψ_j are the linear Lagrange interpolation functions, φ_j are the Hermite cubic interpolation functions, and $\theta = -\frac{dw_0}{dx}$. In particular, show that

$$0 = \sum_{j=1}^2 K_{ij}^{11} u_j + \sum_{j=1}^4 K_{ij}^{12} \bar{\Delta}_j - F_i^1 \quad (i = 1, 2) \quad (3a)$$

$$0 = \sum_{j=1}^2 K_{ij}^{21} u_j + \sum_{j=1}^4 K_{ij}^{22} \bar{\Delta}_j - F_i^2 \quad (i = 1, 2, 3, 4) \quad (3b)$$

$$K_{ij}^{11} = \int_{x_A}^{x_B} E_{xx}^b A \frac{d\psi_i}{dx} \frac{d\psi_j}{dx} dx$$

$$K_{ij}^{12} = \int_{x_A}^{x_B} \frac{1}{2} E_{xx}^b A \frac{dw_0}{dx} \frac{d\psi_i}{dx} \frac{d\varphi_j}{dx} dx$$

$$\begin{aligned}
K_{ij}^{21} &= \int_{x_A}^{x_B} E_{xx}^b A \frac{dw_0}{dx} \frac{d\varphi_i}{dx} \frac{d\psi_j}{dx} dx \\
K_{ij}^{22} &= \int_{x_A}^{x_B} E_{xx}^b A \frac{1}{2} \left(\frac{dw_0}{dx} \right)^2 \frac{d\varphi_i}{dx} \frac{d\varphi_j}{dx} dx \\
&\quad + \int_{x_A}^{x_B} E_{xx}^b A \frac{d^2\varphi_i}{dx^2} \frac{d^2\varphi_j}{dx^2} dx \\
F_i^1 &= P_i, \quad F_i^2 = \int_{x_A}^{x_B} q\psi_i dx + \bar{Q}_i
\end{aligned} \tag{4}$$

Note: $[K^{12}]^T \neq [K^{21}]$; hence, the element stiffness matrix is unsymmetric. Equations (3a,b) can be written in matrix form as

$$\begin{bmatrix} [K^{11}] & [K^{12}] \\ [K^{21}] & [K^{22}] \end{bmatrix} \begin{Bmatrix} \{u\} \\ \{\bar{\Delta}\} \end{Bmatrix} = \begin{Bmatrix} \{F^1\} \\ \{F^2\} \end{Bmatrix} \tag{5}$$

10.7 Use matrix notation

$$\begin{Bmatrix} u_0 \\ w_0 \end{Bmatrix} = \begin{Bmatrix} \sum_{j=1}^2 u_j \psi_j \\ \sum_{j=1}^4 \bar{\Delta}_j \varphi_j \end{Bmatrix} = \begin{bmatrix} \psi_1 & 0 & 0 & \psi_2 & 0 & 0 \\ 0 & \varphi_1 & \varphi_2 & 0 & \varphi_3 & \varphi_4 \end{bmatrix} \begin{Bmatrix} u_1 \\ \bar{\Delta}_1 \\ \bar{\Delta}_2 \\ u_2 \\ \bar{\Delta}_3 \\ \bar{\Delta}_4 \end{Bmatrix} \equiv [\Psi] \{\Delta\} \tag{1}$$

$$\begin{Bmatrix} \frac{du_0}{dx} + \frac{1}{2} \left(\frac{dw_0}{dx} \right)^2 \\ \frac{d^2w_0}{dx^2} \end{Bmatrix} = \begin{Bmatrix} \frac{du_0}{dx} \\ \frac{d^2w_0}{dx^2} \end{Bmatrix} + \begin{Bmatrix} \frac{1}{2} \left(\frac{dw_0}{dx} \right)^2 \\ 0 \end{Bmatrix} \tag{2a}$$

$$\begin{Bmatrix} \frac{du_0}{dx} \\ \frac{d^2w_0}{dx^2} \end{Bmatrix} = \begin{bmatrix} \psi'_1 & 0 & 0 & \psi'_2 & 0 & 0 \\ 0 & \varphi''_1 & \varphi''_2 & 0 & \varphi''_3 & \varphi''_4 \end{bmatrix} \{\Delta\} \equiv [B_L] \{\Delta\} \tag{2b}$$

$$\begin{aligned}
\begin{Bmatrix} \frac{1}{2} \left(\frac{dw_0}{dx} \right)^2 \\ 0 \end{Bmatrix} &= \frac{1}{2} \frac{dw_0}{dx} \begin{bmatrix} 0 & \varphi'_1 & \varphi'_2 & 0 & \varphi'_3 & \varphi'_4 \end{bmatrix} \{\Delta\} \\
&= \frac{1}{2} [B_N] \{\Delta\}
\end{aligned} \tag{2c}$$

$$\varphi'_i \equiv \frac{d\varphi_i}{dx}, \quad \varphi''_i \equiv \frac{d^2\varphi_i}{dx^2}$$

and express the total potential energy functional for an element as

$$\begin{aligned}
\Pi^e(\{\Delta\}) &= \int_{x_A}^{x_B} \frac{1}{2} \left(([B_L] + \frac{1}{2} [B_N]) \{\Delta\} \right)^T [D] ([B_L] + \frac{1}{2} [B_N]) \{\Delta\} dx \\
&\quad - \int_{x_A}^{x_B} ([\Psi] \{\Delta\})^T \begin{Bmatrix} 0 \\ q \end{Bmatrix} dx - \{\Delta\}^T \{Q\}
\end{aligned} \tag{3}$$

$$\begin{aligned}
\Pi^e(\{\Delta\}) &= \frac{1}{2} \{\Delta\}^T \left\{ \left(\int_{x_A}^{x_B} [B_L]^T [D] [B_L] dx \right) + \frac{1}{2} \left(\int_{x_A}^{x_B} [B_L]^T [D] [B_N] dx \right) \right. \\
&\quad \left. - \{\Delta\}^T \left(\int_{x_A}^{x_B} [\Psi]^T \begin{Bmatrix} 0 \\ q \end{Bmatrix} dx + \{Q\} \right) \right\}
\end{aligned} \tag{4}$$

$$[D] = \begin{bmatrix} E_{xx}^b A & 0 \\ 0 & E_{xx}^b I_{yy} \end{bmatrix}, \quad \{Q\} = \begin{Bmatrix} P_1 \\ \bar{Q}_1 \\ \bar{Q}_2 \\ P_2 \\ \bar{Q}_3 \\ Q_4 \\ Q_5 \\ Q_6 \end{Bmatrix} = \begin{Bmatrix} Q_1 \\ Q_2 \\ Q_3 \\ Q_4 \\ Q_5 \\ Q_6 \end{Bmatrix} \quad (4)$$

10.8 Use the principle of the minimum total potential energy and show that

$$\{0\} = ([K_L] + [K_{NL}] + [K_N]) \{\Delta\} - \{F\} \quad (5a)$$

where

$$\begin{aligned} [K_L] &= \int_{x_A}^{x_B} [B_L]^T [D] [B_L] dx \\ [K_{NL}] &= \frac{1}{2} \int_{x_A}^{x_B} [B_L]^T [D] [B_N] dx + \int_{x_A}^{x_B} [B_N]^T [D] [B_L] dx \\ [K_N] &= \frac{1}{2} \int_{x_A}^{x_B} [B_N]^T [D] [B_N] dx \\ \{F\} &= \int_{x_A}^{x_B} [\Psi]^T \begin{Bmatrix} 0 \\ q \end{Bmatrix} dx + \{Q\} \end{aligned} \quad (5b)$$

10.9 Show that the tangent stiffness matrix of the Euler–Bernoulli beam element is

$$[K]^{tan} = \frac{\partial^2}{\partial \{\Delta\}^2} (\Pi(\{\Delta\})) \quad (1a)$$

where

$$\begin{aligned} [K]^{tan} &= [K] + \frac{\partial}{\partial \{\Delta\}} [K] \\ &= [K] + \frac{1}{2} \int_{x_A}^{x_B} [B_L]^T [D] [B_N] dx + \int_{x_A}^{x_B} [B_N]^T [D] [B_N] dx \\ &= [K_L] + [\hat{K}_{NL}] + \frac{3}{2} [K_N] \end{aligned} \quad (1b)$$

and

$$\hat{K}_{NL} = K_{NL} + \frac{1}{2} \int_{x_A}^{x_B} [B_L]^T [D] [B_N] dx \quad (1c)$$

10.10 Beginning with the displacement field

$$u_1(x, z) = u_0(x) + z\phi_x(x), \quad u_2(x, z) = 0, \quad u_3(x, z) = w_0(x) \quad (1)$$

show that the equations governing the Timoshenko beam theory (see Example 1.4.3) with the von Kármán nonlinearity are given by

$$\begin{aligned} -\frac{dN_{xx}}{dx} &= 0, \quad -\frac{dM_{xx}}{dx} + Q_x = 0 \\ -\frac{d}{dx} \left(N_{xx} \frac{dw_0}{dx} \right) - \frac{dQ_x}{dx} - q &= 0 \end{aligned} \quad (2)$$

where N_{xx} , Q_x and M_{xx} are the force and moment resultants

$$N_{xx} = \int_A \sigma_{xx} dx, \quad Q_x = \int_A \sigma_{xz} dx, \quad M_{xx} = \int_A \sigma_{xx} z dx \quad (3)$$

Show that the force and moment resultants can be expressed in terms of the displacements as

$$\begin{aligned} N_{xx} &= E_{xx}^b A \left[\frac{du_0}{dx} + \frac{1}{2} \left(\frac{dw_0}{dx} \right)^2 \right] \\ M_{xx} &= E_{xx}^b I_{yy} \frac{d\phi_x}{dx} \\ Q_x &= K G_{xz}^b A \left(\phi_x + \frac{dw_0}{dx} \right) \end{aligned} \quad (4)$$

- 10.11** Show that the weak forms of the Timoshenko beam theory with the von Kármán nonlinearity are given by

$$\begin{aligned} 0 &= \int_{x_A}^{x_B} E_{xx}^b A \frac{d\delta u_0}{dx} \left[\frac{du_0}{dx} + \frac{1}{2} \left(\frac{dw_0}{dx} \right)^2 \right] dx \\ &\quad - P_1 \delta u_0(x_A) - P_2 \delta u_0(x_B) \end{aligned} \quad (1)$$

$$\begin{aligned} 0 &= \int_{x_A}^{x_B} \left(\frac{d\delta w_0}{dx} N_{xx} \frac{dw_0}{dx} + \frac{d\delta w_0}{dx} Q_x - \delta w_0 q \right) dx \\ &\quad - Q_1 \delta w_0(x_A) - Q_3 \delta w_0(x_B) \end{aligned} \quad (2)$$

$$\begin{aligned} 0 &= \int_{x_A}^{x_B} \left[E_{xx}^b I_{yy} \frac{d\delta \phi_x}{dx} \frac{d\phi_x}{dx} + G_{xz}^b A K \delta \phi_x \left(\phi_x + \frac{dw_0}{dx} \right) \right] dx \\ &\quad - Q_2 \delta \phi_x(x_A) - Q_4 \delta \phi_x(x_B) \end{aligned} \quad (3)$$

- 10.12** Assume that the generalized displacements (u_0, w_0, ϕ_x) of the Timoshenko beam theory are approximated by

$$u_0 = \sum_{i=1}^m u_i \psi_i^1, \quad w_0 = \sum_{i=1}^n w_i \psi_i^2, \quad \phi_x = \sum_{i=1}^p S_i \psi_i^3 \quad (1)$$

and show that the finite element model is of the form

$$\begin{bmatrix} [K^{11}] & [K^{12}] & [K^{13}] \\ [K^{21}] & [K^{22}] & [K^{23}] \\ [K^{31}] & [K^{32}] & [K^{33}] \end{bmatrix} \begin{Bmatrix} \{u\} \\ \{w\} \\ \{S\} \end{Bmatrix} = \begin{Bmatrix} \{F^1\} \\ \{F^2\} \\ \{F^3\} \end{Bmatrix} \quad (2)$$

$$\begin{aligned} K_{ij}^{11} &= \int_{x_A}^{x_B} E_{xx}^b A \frac{d\psi_i^1}{dx} \frac{d\psi_j^1}{dx} dx, \quad K_{ij}^{12} = \frac{1}{2} \int_{x_A}^{x_B} E_{xx}^b A \left(\frac{dw_0}{dx} \right) \frac{d\psi_i^1}{dx} \frac{d\psi_j^2}{dx} dx \\ K_{ij}^{22} &= \frac{1}{2} \int_{x_A}^{x_B} E_{xx}^b A \left(\frac{dw_0}{dx} \right)^2 \frac{d\psi_i^1}{dx} \frac{d\psi_j^2}{dx} dx + \int_{x_A}^{x_B} G_{xz}^b A K \frac{d\psi_i^2}{dx} \frac{d\psi_j^2}{dx} dx \\ K_{ij}^{23} &= \int_{x_A}^{x_B} G_{xz}^b A K \frac{d\psi_i^2}{dx} \psi_i^3 \psi_j^3 dx \\ K_{ij}^{33} &= \int_{x_A}^{x_B} E_{xx}^b I_{yy} \frac{d\psi_i^3}{dx} \frac{d\psi_j^3}{dx} dx + \int_{x_A}^{x_B} G_{xz}^b A K \psi_i^3 \psi_j^3 dx \\ K_{ij}^{13} &= 0, \quad K_{ij}^{21} = 2K_{ji}^{12}, \quad K_{ij}^{32} = K_{ji}^{23} \end{aligned} \quad (3)$$

- 10.13** Evaluate the direct stiffness coefficients $[K^{\alpha\beta}]$ ($\alpha, \beta = 1, 2, 3$) of the nonlinear Timoshenko beam finite element assuming linear but equal interpolation of u_0, w_0 , and ϕ_x .

- 10.14** Compute the tangent stiffness matrix coefficients associated with the nonlinear Timoshenko beam finite element. *Ans:* The tangent stiffness coefficients are

$$\begin{aligned} (K_{ij}^{11})^{tan} &= \int_{x_A}^{x_B} E_{xx}^b A \frac{d\psi_i}{dx} \frac{d\psi_j}{dx} dx \\ (K_{ij}^{12})^{tan} &= \int_{x_A}^{x_B} E_{xx}^b A \left(\frac{dw_0}{dx} \right) \frac{d\psi_i}{dx} \frac{d\psi_j}{dx} dx = 2K_{ij}^{12} \\ (K_{ij}^{13})^{tan} &= K_{ij}^{13} = 0 \\ (K_{ij}^{21})^{tan} &= \int_{x_A}^{x_B} E_{xx}^b A \frac{dw_0}{dx} \frac{d\psi_i}{dx} \frac{d\psi_j}{dx} dx = K_{ij}^{21} \\ (K_{ij}^{22})^{tan} &= \int_{x_A}^{x_B} \left\{ E_{xx}^b A \left[\frac{du_0}{dx} + \frac{3}{2} \left(\frac{dw_0}{dx} \right)^2 \right] \frac{d\psi_i}{dx} \frac{d\psi_j}{dx} \right. \\ &\quad \left. + KG_{xz}^b A \frac{d\psi_i}{dx} \frac{d\psi_j}{dx} \right\} dx \\ (K_{ij}^{23})^{tan} &= K_{ij}^{23}, \quad (K_{ij}^{31})^{tan} = K_{ij}^{31} \\ (K_{ij}^{32})^{tan} &= K_{ij}^{32}, \quad (K_{ij}^{33})^{tan} = K_{ij}^{33} \end{aligned}$$

- 10.15** Compute the tangent stiffness coefficients for the shell finite element of Section 10.7.

- 10.16** The nonlinear strain-displacement relations associated with the displacement field in Eq. (8.2.23) according to the Sanders' [70] nonlinear shell theory are

$$\{\varepsilon\} = \{\varepsilon^0\} + \zeta\{\varepsilon^1\} \quad (\text{a})$$

where

$$\begin{Bmatrix} \varepsilon_{xx}^0 \\ \varepsilon_{yy}^0 \\ \gamma_{xy}^0 \\ \gamma_{xz}^0 \\ \gamma_{yz}^0 \end{Bmatrix} = \begin{Bmatrix} \frac{\partial u_0}{\partial x} + \frac{w_0}{R_1} + \frac{1}{2} \left(\frac{\partial w_0}{\partial x} - \frac{u_0}{R_1} \right)^2 \\ \frac{\partial v_0}{\partial y} + \frac{w_0}{R_2} + \frac{1}{2} \left(\frac{\partial w_0}{\partial y} - \frac{v_0}{R_2} \right)^2 \\ \frac{\partial u_0}{\partial y} + \frac{\partial v_0}{\partial x} + \left(\frac{\partial w_0}{\partial x} - \frac{u_0}{R_1} \right) \left(\frac{\partial w_0}{\partial y} - \frac{v_0}{R_2} \right) \\ \frac{\partial w_0}{\partial x} - \frac{u_0}{R_1} + \phi_x \\ \frac{\partial w_0}{\partial y} - \frac{v_0}{R_2} + \phi_y \end{Bmatrix}, \quad \begin{Bmatrix} \varepsilon_{xx}^1 \\ \varepsilon_{yy}^1 \\ \gamma_{xy}^1 \\ \gamma_{xz}^1 \\ \gamma_{yz}^1 \end{Bmatrix} = \begin{Bmatrix} \frac{\partial \phi_x}{\partial x} \\ \frac{\partial \phi_y}{\partial y} \\ \frac{\partial \phi_x}{\partial y} + \frac{\partial \phi_y}{\partial x} \\ 0 \\ 0 \end{Bmatrix} \quad (\text{b})$$

and $dx = \alpha_1 d\xi_1$, $dy = \alpha_2 d\xi_2$, and $dz = d\zeta$. Derive the equations of motion of Sanders nonlinear shell theory.

- 10.17** Derive the finite element model associated with the governing equations developed in Problem 10.16. In particular, show that the finite element model is of the form

$$\begin{aligned} K_{ij}^{1\alpha} &= \int_{\Omega^e} \left(\frac{\partial \psi_i^e}{\partial x} N_{1j}^\alpha + \frac{\partial \psi_i^e}{\partial y} N_{6j}^\alpha - \psi_i^e \frac{Q_{1j}^\alpha + N_{1j}^\alpha}{R_1} \right) dx dy \\ K_{ij}^{2\alpha} &= \int_{\Omega^e} \left(\frac{\partial \psi_i^e}{\partial x} N_{6j}^\alpha + \frac{\partial \psi_i^e}{\partial y} N_{2j}^\alpha - \psi_i^e \frac{Q_{2j}^\alpha + N_{2j}^\alpha}{R_2} \right) dx dy \\ K_{ij}^{3\alpha} &= \int_{\Omega^e} \left[\frac{\partial \psi_i^e}{\partial x} Q_{1j}^\alpha + \frac{\partial \psi_i^e}{\partial y} Q_{2j}^\alpha + \psi_i^e \left(\frac{N_{1j}^\alpha}{R_1} + \frac{N_{2j}^\alpha}{R_2} \right) \right] dx dy \\ K_{ij}^{4\alpha} &= \int_{\Omega^e} \left(\frac{\partial \psi_i^e}{\partial x} M_{1j}^\alpha + \frac{\partial \psi_i^e}{\partial y} M_{6j}^\alpha + \psi_i^e Q_{1j}^\alpha \right) dx dy \\ K_{ij}^{5\alpha} &= \int_{\Omega^e} \left(\frac{\partial \psi_i^e}{\partial x} M_{6j}^\alpha + \frac{\partial \psi_i^e}{\partial y} M_{2j}^\alpha + \psi_i^e Q_{2j}^\alpha \right) dx dy \end{aligned} \quad (6.10.7)$$

for $\alpha = 1, 2, \dots, 5$, and define the coefficients N_{Ij}^α , M_{Ij}^α , and Q_{Ij}^α for $\alpha = 1, 2, \dots, 5$ and $I = 1, 2, 6$.

References for Additional Reading

1. Khot, N. S., "Buckling and Postbuckling Behavior of Composite Cylindrical Shells Under Axial Compression," *AIAA Journal*, **8**, 229–235 (1970).
2. Khot, N. S., Venkayya, V. B., and Berke, L., "Buckling and Postbuckling of Initially Imperfect Orthotropic Cylindrical Shells Under Axial Compression and Internal Pressure," in *Instability of Continuous Systems*, IUTAM Symposium, Leipholz, H. (ed.), Springer-Verlag, Berlin, 392–398 (1971).
3. Bennett, J. A., "Nonlinear Vibration of Simply Supported Angle-Ply Laminated Plates," *AIAA Journal*, **9**, 1997–2003 (1971).
4. Bert, C. W., "Nonlinear Vibration of a Rectangular Plate Arbitrarily Laminated of Anisotropic Material," *Journal of Applied Mechanics*, **40**, 452–458 (1973).
5. Chandra, R. and Raju, B. B., "Large Amplitude Flexural Vibration of Cross Ply Laminated Composite Plates," *Fibre Science and Technology*, **8**, 243–263 (1975).
6. Chandra, R., "Large Deflection Vibration of Cross-Ply Laminated Plates with Certain Edge Conditions," *Journal of Sound and Vibration*, **47**(4), 509–514 (1976).
7. Zaghloul, S. A. and Kennedy, J. B., "Nonlinear Analysis of Unsymmetrically Laminated Plates," *Journal of Engineering Mechanics Division, ASCE*, **101**(EM3), 169–185 (1975).
8. Zaghloul, S. A. and Kennedy, J. B., "Nonlinear Behavior of Symmetrically Laminated Plates," *Journal of Applied Mechanics*, **42**, 234–236 (1975).
9. Chia, C. Y. and Prabhakara, M. K., "Large Deflection of Unsymmetric Cross-Ply and Angle-Ply Plates," *Journal of Mechanical Engineering Science*, **18**(4), 179–183 (1976).
10. Iu, V. P. and Chia, C. Y., "Effect of Transverse Shear on Nonlinear Vibration and Post-Buckling of Antisymmetric Cross-Ply Imperfect Cylindrical Shells," *International Journal of Solids and Structures*, **30**, 705–718 (1988).
11. Reddy, J. N. and Savoia, M., "The Layerwise Shell Theory for Post-Buckling of Circular Cylindrical Shells," *AIAA Journal*, **30**, 2148–2154 (1992).
12. Savoia, M. and Reddy, J. N., "Post-Buckling Behavior of Stiffened Cross-Ply Cylindrical Shells," *Journal of Applied Mechanics*, **61**, 998–1000 (1994).
13. Ochoa, O. O. and Reddy, J. N., *Finite Element Analysis of Composite Laminates*, Kluwer, The Netherlands (1992).
14. Reddy, J. N. and Miravete, A., *Practical Analysis of Composite Laminates*, CRC Press, Boca Raton, FL (1995).
15. Noor, A. K. and Hartley, S. J., "Effect of Shear Deformation and Anisotropy on the Non-Linear Response of Composite Plates," *Developments in Composite Materials - 1*, G. Holister (Ed), Applied Science Publishers, Barking, UK, 55–56 (1977).
16. Reddy, J. N., "Simple Finite Elements with Relaxed Continuity for Nonlinear Analysis of Plates," *Proceedings of the Third International Conference on Finite Element Methods, Australia*, 265–281, (1979).
17. Reddy, J. N. and Chao, W. C., "Large Deflection and Large Amplitude Free Vibrations of Laminated Composite-Material Plates," *Symposium on Computational Methods in Nonlinear Structural and Solid Mechanics*, Washington, D.C. (1980).
18. Chang, T. Y. and Sawamiphakdi, K., "Large Deformation Analysis of Laminated Shells by Finite Element Method," *Computers and Structures*, **13**, 331–340 (1981).
19. Reddy, J. N., "Analysis of Layered Composite Plates Accounting for Large Deflections and Transverse Shear Strains," in *Recent Advances in Nonlinear Computational Mechanics*, E. Hinton et al. (Eds.), 155–202 (1982).
20. Reddy, J. N., "Geometrically Nonlinear Transient Analysis of Laminated Composite Plates," *AIAA Journal*, **21**(4), 621–629 (1983).

21. Chao, W. C. and Reddy, J. N., "Analysis of Laminated Composite Shells Using a Degenerated 3-D Element," *International Journal for Numerical Methods in Engineering*, **20**, 1991–2007 (1984).
22. Putcha, N. S. and Reddy, J. N., "A Refined Mixed Shear Flexible Finite Element for the Nonlinear Analysis of Laminated Plates," *Computers and Structures*, **22**(2), 529–538 (1986).
23. Liao, C. L. and Reddy, J. N., "Continuum-Based Stiffened Composite Shell Element for Geometrically Nonlinear Analysis," *AIAA Journal*, **27**(1), 95–101 (1989).
24. Reddy, J. N., "On Refined Computational Models of Composite Laminates," *International Journal for Numerical Methods in Engineering*, **27**, 361–382 (1989).
25. Barbero, E. J. and Reddy, J. N., "Nonlinear Analysis of Composite Laminates Using a Generalized Laminate Plate Theory," *AIAA Journal*, **28**(11), 1987–1994 (1990).
26. Bathe, K. J., Ramm, E., and Wilson, E. L., "Finite Element Formulations for Large Deformation Dynamic Analysis," *International Journal for Numerical Methods in Engineering*, **9**, 353–386 (1975).
27. Horrigmoe, G. and Bergan, P. G., "Incremental Variational Principle and Finite Element Models for Nonlinear Problems," *Computer Methods in Applied Mechanics and Engineering*, **7**, 201–217 (1976).
28. Wunderlich, W., "Incremental Formulations for Geometrically Nonlinear Problems," in *Formulations and Algorithms in Finite Element Analysis*, K. J. Bathe et al. (Eds.), MIT Press, Boston, MA, 193–239 (1977).
29. Ramm, E., "A Plate/Shell Element for Large Deflections and Rotations," in *Formulations and Computational Algorithms in Finite Element Analysis*, K. J. Bathe et al. (Eds.), MIT Press, Boston, MA (1977).
30. Stricklin, J. A., Von Riesemann, W. A., Tillerson, J. R., and Haisler, W. E., "Static Geometrical and Material Nonlinear Analysis," *Advances in Computer Methods in Structural Mechanics and Design*, J. T. Oden et al. (Eds.), University of Alabama in Huntsville, Huntsville, AL, 301–324 (1972).
31. Bathe, K. J., *Finite Element Procedures*, Prentice-Hall, Englewood Cliffs, NJ (1996).
32. Reddy, J. N., *An Introduction to Nonlinear Finite Element Analysis*, Oxford University Press, Oxford, UK (2004).
33. Pian, T. H. H. and Boland, P., "Formulation of Large Deflection Shell Analysis by Assumed Stress Finite Element Method," in *Formulations and Computational Algorithms in Finite Element Analysis*, K. J. Bathe, et al. (Eds.), MIT Press, Boston, MA (1977).
34. Lee, S. W. and Pian, T. H. H., "Improvement of Plate and Shell Finite Elements by Mixed Formulations," *AIAA Journal*, **16**, 29–34 (1978).
35. Spilker, R. L. and Munir, N. I., "The Hybrid-Stress Model for Thin Plates," *International Journal for Numerical Methods in Engineering*, **15**, 1239–1260 (1980).
36. Bathe, K. J., Dvorkin, E. N., and Ho, L. W., "On Discrete-Kirchhoff and Isoparametric Shell Elements for Nonlinear Analysis – An Assessment," *Computers and Structures*, **16**, 89–98 (1983).
37. Putcha, N. S. and Reddy, J. N., "A Mixed Finite Element for the Analysis of Laminated Plates," in *Advances in Aerospace Structures, Materials and Dynamics*, U. Yuceoglu et al. (Eds.), ASME AD-06, 31–39 (1983).
38. Putcha, N. S. and Reddy, J. N., "Stability and Natural Vibration Analysis of Laminated Plates by Using a Mixed Element Based on a Refined Plate Theory," *Journal of Sound and Vibration*, **104**(2), 285–300 (1986).
39. Reddy, J. N., "On Mixed Finite-Element Formulations of a Higher-Order Theory of Composite Laminates," *Finite Element Methods for Plate and Shell Structures*, T. J. R. Hughes and E. Hinton (Eds.), Pineridge Press, UK, 31–57 (1986).

40. Park, K. C. and Stanley, G. M., "A Curved C^0 Shell Element Based on Assumed Natural-Coordinate Strains," *Journal of Applied Mechanics*, **53**, 278–290 (1986).
41. Reddy, J. N. and Heyliger, P. R., "A Mixed Updated Lagrangian Formulation for Plane Elastic Problems," *Journal of Composites Technology and Research*, **9**(4), 131–140 (1987).
42. Liao, C. L. and Reddy, J. N., "Analysis of Anisotropic, Stiffened Composite Laminates Using a Continuum-Based Shell Element," *Computers and Structures*, **34**(6), 805–815 (1990).
43. Batoz, J. L. and Dhatt, G., "Incremental Displacement Algorithms for Nonlinear Problems," *International Journal for Numerical Methods in Engineering*, **14**, 1262–1266 (1979).
44. Riks, E., "An Incremental Approach to the Solution of Snapping and Buckling Problem," *International Journal of Solids and Structures*, **15**, 529–551 (1979).
45. Ramm, E., "Strategies for Tracing the Nonlinear Response Near Limit Points," *Nonlinear Finite Element Analysis in Structural Mechanics*, W. Wunderlich et al. (Eds.), Springer-Verlag, Berlin, 63–89 (1981).
46. Crisfield, M. A., "A Fast Incremental/Iterative Solution Procedure That Handles Snap-Through," *Computers and Structures*, **13**, 55–62 (1981).
47. Wempner, G. A., "Discrete Approximations Related to Nonlinear Theories of Solids," *International Journal of Solids and Structures*, **7**, 1581–1599 (1971).
48. Lévy, S., "Bending of Rectangular Plates with Large Deflections," Report No. 737, NACA (1942).
49. Wang, C. T., "Bending of Rectangular Plates with Large Deflections," Report No. 1462, NACA (1948).
50. Yamaki, N., "Influence of Large Amplitudes on Flexural Vibrations of Elastic Plates," *ZAMM*, **41**, 501–510 (1967).
51. Reddy, J. N., "A Note on Symmetry Considerations in the Transient Response of Unsymmetrically Laminated Anisotropic Plates," *International Journal for Numerical Methods in Engineering*, **20**, 175–194 (1984).
52. Sun, C. T. and Chin, H., "Analysis of Asymmetric Composite Laminates," *AIAA Journal*, **26**(6), 714–718 (1988).
53. Bathe, K. J. and Ho, L. W., "A Simple Effective Element for the Analysis of General Shell Structures," *Computers and Structures*, **13**, 673–681 (1981).
54. Praveen, G. N. and Reddy, J. N., "Nonlinear Transient Thermoelastic Analysis of Functionally Graded Ceramic-Metal Plates," *International Journal of Solids and Structures*, **35**(33), 4457–4476 (1998).
55. Gong, S. W., Lam, K. Y., and Reddy, J. N., "The Elastic Response of Functionally Graded Cylindrical Shells to Low Velocity Impact," *International Journal of Impact Engineering*, **22**(4), 397–417 (1999).
56. Praveen, G. N., Chin, C. D., and Reddy, J. N., "Thermoelastic Analysis of a Functionally Graded Ceramic-Metal Cylinder," *Journal of Engineering Mechanics*, **125**(11), 1259–1267 (1999).
57. Loy, C. T., Lam, K. Y., and Reddy, J. N., "Vibration of Functionally Graded Cylindrical Shells," *International Journal of Mechanical Sciences*, **41**(3), 309–324 (1999).
58. Reddy, J. N., Wang, C. M., and Kitipornchai, S., "Axisymmetric Bending of Functionally Graded Circular and Annular Plates," *European Journal of Mechanics*, **18**, 185–199 (1999).
59. Reddy, J. N., "Analysis of Functionally Graded Plates," *International Journal for Numerical Methods in Engineering* **47**, 663–684 (2000).
60. Pradhan, S. C., Loy, C. T., Lam, K. Y., and Reddy, J. N., "Vibration Characteristics of Functionally Graded Cylindrical Shells Under Various Boundary Conditions," *Applied Acoustics*, **61**, 111–129 (2000).

61. Reddy, J. N. and Cheng, Z. -Q., "Three-Dimensional Solution of Smart Functionally Graded Plates," *Journal of Applied Mechanics*, **68**, 234–241 (2001).
62. Reddy, J. N. and Cheng, Z. -Q., "Three-Dimensional Thermomechanical Deformations of Functionally Graded Rectangular Plates," *European Journal of Mechanics, A/Solids*, **20**(5), 841–860 (2001).
63. Reddy, J. N. and Cheng, Z. -Q., "Frequency Correspondence Between Membranes and Functionally Graded Spherical Shallow Shells of Polygonal Planform," *International Journal of Mechanical Sciences*, **44**(5), 967–985 (2002).
64. Ng, T. Y., Lam, K. Y., Liew, K. M., and Reddy, J. N., "Dynamic Stability Analysis of Functionally Graded Cylindrical Shells Under Periodic Axial Loading," *International Journal of Solids and Structures*, **38**, 1295–1309 (2001).
65. Woo, J. and Meguid S. A., "Nonlinear Analysis of Functionally Graded Plates and Shallow Shells," *International Journal of Solids and Structures*, **38**, 7409–7421 (2001).
66. Shen, H.-S., "Nonlinear Bending Response of Functionally Graded Plates Subjected to Transverse Loads and in Thermal Environments," *International Journal of Mechanical Sciences*, **44**, 561–584 (2002).
67. Shen, H.-S., "Postbuckling Analysis of Axially-loaded Functionally Graded Cylindrical Shells in Thermal Environments," *Composite Science and Technology*, **62**, 977–987 (2002).
68. Yang, J. and Shen, H.-S., "Vibration Characteristics and Transient Response of Shear-Deformable Functionally Graded Plates in Thermal Environments," *Journal of Sound and Vibration*, **255**(3), 579–602 (2002).
69. Aliaga, W. and Reddy, J. N., "Nonlinear Thermoelastic Analysis of Functionally Graded Plates Using the Third-Order Shear Deformation Theory," *International Journal of Computational Engineering Science* (to appear).
70. Sanders Jr., J. L., "Nonlinear Theories for Thin Shells," *Quarterly of Applied Mathematics*, **21**(1), 21–36 (1963).
71. Reddy, J. N. and Chandrashekara, K., "Nonlinear Analysis of Laminated Shells Including Transverse Shear Strains," *AIAA Journal*, **23**(3), 440–441 (1985).
72. Rao, K. P., "A Rectangular Laminated Anisotropic Shallow Thin Shell Finite Element," *Computer Methods in Applied Mechanics and Engineering*, **15**, 13–33 (1978).
73. Bathe, K. J., and Bolourchi, S., "A Geometric and Material Nonlinear Plate and Shell Element," *Computers and Structures*, **11**, 23–48 (1980).
74. Bathe, J. J., Ramm, E., and Wilson, E. L., "Finite Element Formulations for Large Deformation Dynamic Analysis," *International Journal for Numerical Methods in Engineering*, **9**, 353–386 (1975).
75. Noor, A. K. and Hartley, S. J., "Nonlinear Shell Analysis via Mixed Isoparametric Elements," *Computers and Structures*, **7**, 615–626 (1977).
76. Kreja, I., Schmidt, R., and Reddy, J. N., "Finite Elements Based on a First-Order Shear Deformation Moderate Rotation Shell Theory with Application to the Analysis of Composite Structures," *International Journal of Non-Linear Mechanics*, **32**(6), 1123–1142 (1997).
77. Stanley, G. M. and Felippa, C. A., "Computational Procedures for Postbuckling for Composite Shells" in *Finite Element Methods for Nonlinear Problems*, P. G. Bergan, K. J. Bathe, and W. Wunderlich (Eds.), 359–385, Springer-Verlag (1986).
78. Liao, C. L., Reddy, J. N., and Engelstad, S. P., "A Solid-Shell Transition Element for Geometrically Nonlinear Analysis of Laminated Composite Structures," *International Journal for Numerical Methods in Engineering*, **26**, 1843–1854 (1988).
79. Liao, C. L. and Reddy, J. N., "A Continuum-Based Stiffened Composite Shell Element for Geometrically Nonlinear Analysis," *AIAA Journal*, **27**(1), 95–101 (1989).

80. Scordelis, A. C. and Lo, K. S., "Computer Analysis of Cylindrical Shells," *ACI Journal*, **61**, 539–561 (1964).
81. Zaghoul, S. A. and Kennedy, J. B., "Nonlinear Behavior of Symmetrically Laminated Plates," *Journal of Applied Mechanics*, **42**, 234–236 (1975).
82. Putcha, N. S. and J. N. Reddy, J. N., "A Refined Mixed Shear Flexible Finite Element for the Nonlinear Analysis of Laminated Plates," *Computers and Structures*, **22**, 529–538 (1986).
83. Starnes, J. H., Jr. and Rouse, M., "Postbuckling and Failure Characteristics of Selected Flat Rectangular Graphite-Epoxy Plates Loaded in Compression," AIAA Paper No. 81-0543 (1981).
84. Engelstad, S. P., Reddy, J. N., and Knight, N. F., Jr., "Postbuckling Response and Failure Prediction of Graphite-Epoxy Plates Loaded in Compression," *AIAA Journal*, **30**(8), 2106–2113 (1992).
85. Tsai, S. W., "A Survey of Macroscopic Failure Criteria for Composite Materials," *Journal of Reinforced Plastics and Composites*, **3**, 40–62 (1984).
86. Hill, R., "A Theory of the Yielding and Plastic Flow of Anisotropic Metals," *Proceedings of the Royal Society, Series A*, **193**, 281–297 (1948).
87. Wu, E. M., "Phenomenological Anisotropic Failure Criterion," *Composite Materials*, **2**, 353–431 (1974).
88. Azzi, V. D. and Tsai, S. W., "Anisotropic Strength of Composites," *Experimental Mechanics*, **5**, 283–288 (1965).
89. Knight, N. F., Jr., "Factors Influencing Nonlinear Static Response Prediction and Test-Analysis Correlation for Composite Panels," *Composite Structures*, **29**, 13–25 (1994).
90. Theocaris, P. S., "Positive and Negative Failure-Shears in Orthotropic Materials," *Journal of Reinforced Plastics and Composites*, **11**, 32–55 (1992).
91. Joo, J. W. and Sun, C. T., "A Failure Criterion for Laminates Governed by Free Edge Interlaminar Shear Stress," *Journal of Composite Materials*, **26**(10), 1510–1512 (1992).
92. Reddy, Y. S. N. and Reddy, J. N., "Linear and Non-Linear failure analysis of Composite Laminates with Transverse shear," *Composites Science and Technology*, **44**, 227–255 (1992).
93. Reddy, Y. S. N., Reddy, J. N., and Dakshina Moorthy, C. M., "Nonlinear Progressive Failure Analysis of Laminated Composite Plates," *International Journal of Non-Linear Mechanics*, **30**(5), 629–649 (1995).
94. Praveen, G. N. and Reddy, J. N., "Transverse Matrix Cracks in Cross-Ply Laminates: Stress Transfer, Stiffness Reduction and Crack Opening Profiles," *Acta Mechanica*, **130**(3-4), 227–248 (1998).
95. Soni, S. R., "A Comparative Study of Failure Envelops in Composite Laminates," *Journal of Reinforced Plastics and Composites*, **2**, 34–42 (1983).
96. Turvey, G. J., "An Initial Flexure Failure Analysis of Symmetrically Laminated Cross-Ply Rectangular Plates," *International Journal of Solids and Structures*, **16**, 451–463 (1980).
97. Turvey, G. J., "Flexural Failure Analysis of Angle-Ply Laminates of GFRP and CFRP," *Journal of Strain Analysis*, **15**, 43–49 (1980).
98. Jamison, R. D., "The Role of Microdamage in Tensile Failure of Graphite/Epoxy Laminates," *Composites Science and Technology*, **24**, 83–99 (1985).
99. Chang, F. K. and Chang, K. Y., "A Progressive Damage Model for Laminated Composites containing Stress Concentrations," *Journal of Composite Materials*, **21**, 834–855 (1987).
100. Reddy, J. N. and Pandey, A. K., "A first-Ply Failure Analysis of Composite Laminates," *Computers and Structures*, **25**, 371–393 (1987).
101. Dvorak, G. J. and Laws, N., "Analysis of Progressive Matrix Cracking in Composite Laminates II. First Ply Failure," *Journal of Composite Materials*, **21**, 309–329 (1987).

102. Turvey, G. J., "Effects of Shear Deformation on the Onset of Flexural Failure in Symmetric Cross-Ply Laminated Rectangular Plates," *Composite Structures*, **4**, I. H. Marshall (Ed.), Elsevier, London, UK, 141–146 (1987).
103. Ochoa, O. O. and Engblom, J. J., "Analysis of Progressive Failure in Composites," *Composites Science and Technology*, **28**, 87–102 (1987).
104. Turvey, G. J. and Osman, M. Y., "Exact and Approximate Linear and Nonlinear Initial Failure Analysis of Laminated Mindlin Plates in Flexure," *Composite Structures*, **5**, I. H. Marshall (Ed.), Elsevier, London, UK, 133–371 (1989).
105. Tan, S. C., "A Progressive Failure Model for Composite Laminates Containing Openings," *Journal of Composite Materials*, **25**, 556–577 (1991).
106. Marshall, D. B., Cox, B. N. and Evans, A. G., "The Mechanics of Matrix Cracking in Brittle-Matrix Fiber Composites," *Acta Metallurgica*, **33**(11), 2013–2021 (1985).
107. Ladeveze, P. and Le Dantec, E., "Damage Modelling of the Elementary Ply for Laminated Composites," *Composites Science and Technology*, **43**, 257–267 (1992).
108. Chen, F., Hiltner, A., and Baer, E., "Damage and Failure Mechanisms of Continuous Glass Fiber Reinforced Polyphenylene Sulfide," *Journal of Composite Materials*, **26**(15), 2289–2306 (1992).
109. Talreja, R. (Ed.), *Damage Mechanics of Composite Materials*, Vol. 9, Composite Materials Series edited by R. B. Pipes, Elsevier, Amsterdam, The Netherlands (1994).
110. Hashagen, F., *Numerical Analysis of Failure Mechanisms in Fibre Metal Laminates*, Ph. D. Dissertation, Delft University Press, Delft, The Netherlands (1998).

Third-Order Theory of Laminated Composite Plates and Shells

11.1 Introduction

The classical laminate plate theory and the first-order shear deformation theory are the simplest equivalent single-layer theories, and they adequately describe the kinematic behavior of most laminates. Higher-order theories can represent the kinematics better, may not require shear correction factors, and can yield more accurate interlaminar stress distributions. However, they involve higher-order stress resultants that are difficult to interpret physically and require considerably more computational effort. Therefore, such theories should be used only when necessary.

In principle, it is possible to expand the displacement field in terms of the thickness coordinate up to any desired degree. However, due to the algebraic complexity and computational effort involved with higher-order theories in return for marginal gain in accuracy, theories higher than third order have not been attempted. The reason for expanding the displacements up to the cubic term in the thickness coordinate is to have quadratic variation of the transverse shear strains and transverse shear stresses through each layer. This avoids the need for shear correction coefficients used in the first-order theory.

There are many papers on third-order theories (see [1–32]) and their applications [33–52]. Although many of them seem to differ from each other on the surface, the displacement fields of these theories are related (see Reddy [49]). Here we present the original third-order shear deformation laminate theory of Reddy [25,26] that contains other lower-order laminate theories, including the classical laminate theory and first-order shear deformation laminate theory as special cases. Analytical as well as finite element results of this third-order theory are developed and numerical results are compared with those of the classical and first-order theories.

11.2 A Third-Order Plate Theory

11.2.1 Displacement Field

The third-order plate theory to be developed is based on the same assumptions as the classical and first-order plate theories, except that we relax the assumption on the straightness and normality of a transverse normal after deformation by expanding the displacements (u, v, w) as cubic functions of the thickness coordinate. Figure 11.2.1 shows the kinematics of deformation of a transverse normal on edge $y = 0$.

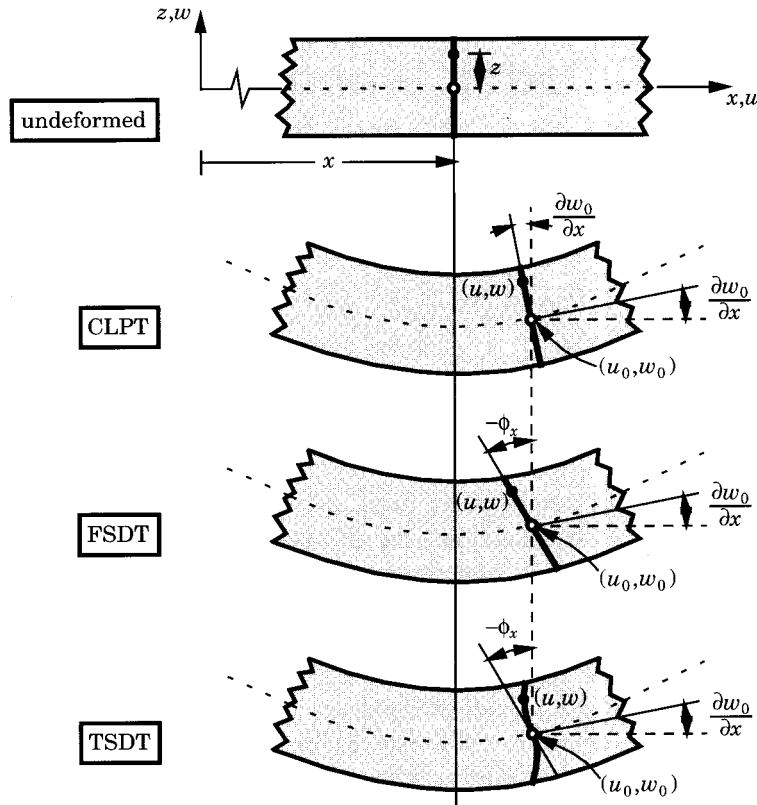


Figure 11.2.1: Deformation of a transverse normal according to the classical, first-order, and third-order plate theories.

Consider the displacement field

$$\begin{aligned} u &= u_0 + z\phi_x + z^2\theta_x + z^3\lambda_x \\ v &= v_0 + z\phi_y + z^2\theta_y + z^3\lambda_y \\ w &= w_0 \end{aligned} \quad (11.2.1)$$

where (ϕ_x, ϕ_y) , (θ_x, θ_y) and (λ_x, λ_y) are functions to be determined. Clearly, we have

$$\begin{aligned} u_0 &= u(x, y, 0, t), & v_0 &= v(x, y, 0, t), & w_0 &= w(x, y, 0, t) \\ \phi_x &= \left(\frac{\partial u}{\partial z} \right)_{z=0}, & \phi_y &= \left(\frac{\partial v}{\partial z} \right)_{z=0}, & 2\theta_x &= \left(\frac{\partial^2 u}{\partial z^2} \right)_{z=0}, \\ 2\theta_y &= \left(\frac{\partial^2 v}{\partial z^2} \right)_{z=0}, & 6\lambda_x &= \left(\frac{\partial^3 u}{\partial z^3} \right)_{z=0}, & 6\lambda_y &= \left(\frac{\partial^3 v}{\partial z^3} \right)_{z=0} \end{aligned} \quad (11.2.2)$$

There are 9 dependent unknowns, and the theory derived using the displacement field (11.2.1) will result in 9 second-order partial differential equations. The weak-form finite element models based on the theory require C^0 -interpolation of all 9 dependent unknowns.

The number of dependent unknowns can be reduced by imposing certain conditions. Suppose that we wish to impose traction-free boundary conditions on the top and bottom faces of the laminate [25,26]:

$$\sigma_{xz}(x, y, \pm h/2, t) = 0, \quad \sigma_{yz}(x, y, \pm h/2, t) = 0 \quad (11.2.3)$$

Expressing the above conditions in terms of strains, we have

$$\begin{aligned} 0 &= \sigma_{xz}(x, y, \pm h/2, t) = Q_{55}\gamma_{xz}(x, y, \pm h/2, t) + Q_{45}\gamma_{yz}(x, y, \pm h/2, t), \\ 0 &= \sigma_{yz}(x, y, \pm h/2, t) = Q_{45}\gamma_{xz}(x, y, \pm h/2, t) + Q_{44}\gamma_{yz}(x, y, \pm h/2, t) \end{aligned}$$

which in turn requires, for arbitrary Q_{ij} ($i, j = 4, 5$),

$$\begin{aligned} 0 &= \gamma_{xz}(x, y, \pm h/2, t) = \phi_x + \frac{\partial w_0}{\partial x} + (2z\theta_x + 3z^2\lambda_x)_{z=\pm h/2} \\ 0 &= \gamma_{yz}(x, y, \pm h/2, t) = \phi_y + \frac{\partial w_0}{\partial y} + (2z\theta_y + 3z^2\lambda_y)_{z=\pm h/2} \end{aligned}$$

Thus we have

$$\begin{aligned} \phi_x + \frac{\partial w_0}{\partial x} + \left(-h\theta_x + \frac{3h^2}{4}\lambda_x \right) &= 0, \quad \phi_x + \frac{\partial w_0}{\partial x} + \left(h\theta_x + \frac{3h^2}{4}\lambda_x \right) = 0 \\ \phi_y + \frac{\partial w_0}{\partial y} + \left(-h\theta_y + \frac{3h^2}{4}\lambda_y \right) &= 0, \quad \phi_y + \frac{\partial w_0}{\partial y} + \left(h\theta_y + \frac{3h^2}{4}\lambda_y \right) = 0 \end{aligned}$$

or

$$\lambda_x = -\frac{4}{3h^2} \left(\phi_x + \frac{\partial w_0}{\partial x} \right), \quad \theta_x = 0; \quad \lambda_y = -\frac{4}{3h^2} \left(\phi_y + \frac{\partial w_0}{\partial y} \right), \quad \theta_y = 0 \quad (11.2.4)$$

The displacement field (11.2.1) now can be expressed in terms of u_0, v_0, w_0, ϕ_x and ϕ_y using the relations in Eq. (11.2.4):

$$\begin{aligned} u(x, y, z, t) &= u_0(x, y, t) + z\phi_x(x, y, t) - \frac{4}{3h^2}z^3 \left(\phi_x + \frac{\partial w_0}{\partial x} \right) \\ v(x, y, z, t) &= v_0(x, y, t) + z\phi_y(x, y, t) - \frac{4}{3h^2}z^3 \left(\phi_y + \frac{\partial w_0}{\partial y} \right) \\ w(x, y, z, t) &= w_0(x, y, t) \end{aligned} \quad (11.2.5)$$

Next, we shall derive a third-order theory [25,26,49] based on the displacement field (11.2.5).

11.2.2 Strains and Stresses

Substitution of the displacements (11.2.5) into the nonlinear strain-displacement relations in Eq. (3.3.7) yields the strains

$$\begin{Bmatrix} \varepsilon_{xx} \\ \varepsilon_{yy} \\ \gamma_{xy} \end{Bmatrix} = \begin{Bmatrix} \varepsilon_{xx}^{(0)} \\ \varepsilon_{yy}^{(0)} \\ \gamma_{xy}^{(0)} \end{Bmatrix} + z \begin{Bmatrix} \varepsilon_{xx}^{(1)} \\ \varepsilon_{yy}^{(1)} \\ \gamma_{xy}^{(1)} \end{Bmatrix} + z^3 \begin{Bmatrix} \varepsilon_{xx}^{(3)} \\ \varepsilon_{yy}^{(3)} \\ \gamma_{xy}^{(3)} \end{Bmatrix} \quad (11.2.6)$$

$$\begin{Bmatrix} \gamma_{yz} \\ \gamma_{xz} \end{Bmatrix} = \begin{Bmatrix} \gamma_{yz}^{(0)} \\ \gamma_{xz}^{(0)} \end{Bmatrix} + z^2 \begin{Bmatrix} \gamma_{yz}^{(2)} \\ \gamma_{xz}^{(2)} \end{Bmatrix} \quad (11.2.7)$$

where ($c_2 = 3c_1$ and $c_1 = 4/3h^2$)

$$\begin{Bmatrix} \varepsilon_{xx}^{(0)} \\ \varepsilon_{yy}^{(0)} \\ \gamma_{xy}^{(0)} \end{Bmatrix} = \begin{Bmatrix} \frac{\partial u_0}{\partial x} + \frac{1}{2} \left(\frac{\partial w_0}{\partial x} \right)^2 \\ \frac{\partial v_0}{\partial y} + \frac{1}{2} \left(\frac{\partial w_0}{\partial y} \right)^2 \\ \frac{\partial u_0}{\partial y} + \frac{\partial v_0}{\partial x} + \frac{\partial w_0}{\partial x} \frac{\partial w_0}{\partial y} \end{Bmatrix} \quad (11.2.8)$$

$$\begin{Bmatrix} \varepsilon_{xx}^{(1)} \\ \varepsilon_{yy}^{(1)} \\ \gamma_{xy}^{(1)} \end{Bmatrix} = \begin{Bmatrix} \frac{\partial \phi_x}{\partial x} \\ \frac{\partial \phi_y}{\partial y} \\ \frac{\partial \phi_x}{\partial y} + \frac{\partial \phi_y}{\partial x} \end{Bmatrix}, \quad \begin{Bmatrix} \gamma_{yz}^{(0)} \\ \gamma_{xz}^{(0)} \end{Bmatrix} = \begin{Bmatrix} \phi_y + \frac{\partial w_0}{\partial y} \\ \phi_x + \frac{\partial w_0}{\partial x} \end{Bmatrix} \quad (11.2.9)$$

$$\begin{Bmatrix} \varepsilon_{xx}^{(3)} \\ \varepsilon_{yy}^{(3)} \\ \gamma_{xy}^{(3)} \end{Bmatrix} = -c_1 \begin{Bmatrix} \frac{\partial \phi_x}{\partial x} + \frac{\partial^2 w_0}{\partial x^2} \\ \frac{\partial \phi_y}{\partial y} + \frac{\partial^2 w_0}{\partial y^2} \\ \frac{\partial \phi_x}{\partial y} + \frac{\partial \phi_y}{\partial x} + 2 \frac{\partial^2 w_0}{\partial x \partial y} \end{Bmatrix}, \quad \begin{Bmatrix} \gamma_{yz}^{(2)} \\ \gamma_{xz}^{(2)} \end{Bmatrix} = -c_2 \begin{Bmatrix} \phi_y + \frac{\partial w_0}{\partial y} \\ \phi_x + \frac{\partial w_0}{\partial x} \end{Bmatrix} \quad (11.2.10)$$

11.2.3 Equations of Motion

The equations of motion of the third-order theory will be derived using the dynamic version of the principle of virtual displacements. The virtual strain energy δU , virtual work done by applied forces δV , and the virtual kinetic energy δK are given by

$$\begin{aligned} \delta U &= \int_{\Omega_0} \left\{ \int_{-\frac{h}{2}}^{\frac{h}{2}} \left[\sigma_{xx} \left(\delta \varepsilon_{xx}^{(0)} + z \delta \varepsilon_{xx}^{(1)} - c_1 z^3 \delta \varepsilon_{xx}^{(3)} \right) \right. \right. \\ &\quad + \sigma_{yy} \left(\delta \varepsilon_{yy}^{(0)} + z \delta \varepsilon_{yy}^{(1)} - c_1 z^3 \delta \varepsilon_{yy}^{(3)} \right) + \sigma_{xy} \left(\delta \gamma_{xy}^{(0)} + z \delta \gamma_{xy}^{(1)} - c_1 z^3 \delta \gamma_{xy}^{(3)} \right) \\ &\quad \left. \left. + \sigma_{xz} \left(\delta \gamma_{xz}^{(0)} + z^2 \delta \gamma_{xz}^{(2)} \right) + \sigma_{yz} \left(\delta \gamma_{yz}^{(0)} + z^2 \delta \gamma_{yz}^{(2)} \right) \right] dz \right\} dx dy \\ &= \int_{\Omega_0} \left(N_{xx} \delta \varepsilon_{xx}^{(0)} + M_{xx} \delta \varepsilon_{xx}^{(1)} - c_1 P_{xx} \delta \varepsilon_{xx}^{(3)} + N_{yy} \delta \varepsilon_{yy}^{(0)} + M_{yy} \delta \varepsilon_{yy}^{(1)} - c_1 P_{yy} \delta \varepsilon_{yy}^{(3)} \right. \\ &\quad + N_{xy} \delta \gamma_{xy}^{(0)} + M_{xy} \delta \gamma_{xy}^{(1)} - c_1 P_{xy} \delta \gamma_{xy}^{(3)} \\ &\quad \left. + Q_x \delta \gamma_{xz}^{(0)} - c_2 R_x \delta \gamma_{xz}^{(0)} + Q_y \delta \gamma_{yz}^{(0)} - c_2 R_y \delta \gamma_{yz}^{(0)} \right) dx dy \quad (11.2.11) \end{aligned}$$

$$\begin{aligned}
\delta V = & - \int_{\Omega_0} \left[q_b(x, y) \delta w(x, y, -\frac{h}{2}) + q_t(x, y) \delta w(x, y, \frac{h}{2}) \right] dx dy \\
& - \int_{\Gamma} \int_{-\frac{h}{2}}^{\frac{h}{2}} \left[\hat{\sigma}_{nn} (\delta u_n + z \delta \phi_n - c_1 z^3 \delta \varphi_n) \right. \\
& \quad \left. + \hat{\sigma}_{ns} (\delta u_s + z \delta \phi_s - c_1 z^3 \delta \varphi_{ns}) + \hat{\sigma}_{nz} \delta w_0 \right] dz d\Gamma \\
= & - \int_{\Omega_0} q \delta w_0 dx dy - \int_{\Gamma} (\hat{N}_{nn} \delta u_n + \hat{M}_{nn} \delta \phi_n - c_1 \hat{P}_{nn} \delta \varphi_n \\
& + \hat{N}_{ns} \delta u_s + \hat{M}_{ns} \delta \phi_s - c_1 \hat{P}_{ns} \delta \varphi_{ns} + \hat{Q}_n \delta w_0) d\Gamma \tag{11.2.12}
\end{aligned}$$

$$\begin{aligned}
\delta K = & \int_{\Omega_0} \int_{-\frac{h}{2}}^{\frac{h}{2}} \rho_0 \left[(\dot{u}_0 + z \dot{\phi}_x - c_1 z^3 \dot{\varphi}_x) (\delta \dot{u}_0 + z \delta \dot{\phi}_x - c_1 z^3 \delta \dot{\varphi}_x) \right. \\
& \quad \left. + (\dot{v}_0 + z \dot{\phi}_y - c_1 z^3 \dot{\varphi}_y) (\delta \dot{v}_0 + z \delta \dot{\phi}_y - c_1 z^3 \delta \dot{\varphi}_y) + \dot{w}_0 \delta \dot{w}_0 \right] dv \\
= & \int_{\Omega_0} \left[(I_0 \dot{u}_0 + I_1 \dot{\phi}_x - c_1 I_3 \dot{\varphi}_x) \delta \dot{u}_0 + (I_1 \dot{u}_0 + I_2 \dot{\phi}_x - c_1 I_4 \dot{\varphi}_x) \delta \dot{\phi}_x \right. \\
& \quad - c_1 (I_3 \dot{u}_0 + I_4 \dot{\phi}_x - c_1 I_6 \dot{\varphi}_x) \delta \dot{\varphi}_x + (I_0 \dot{v}_0 + I_1 \dot{\phi}_y - c_1 I_3 \dot{\varphi}_y) \delta \dot{v}_0 \\
& \quad \left. + (I_1 \dot{v}_0 + I_2 \dot{\phi}_y - c_1 I_4 \dot{\varphi}_y) \delta \dot{\phi}_y - c_1 (I_3 \dot{v}_0 + I_4 \dot{\phi}_y - c_1 I_6 \dot{\varphi}_y) \delta \dot{\varphi}_y \right] dx dy \tag{11.2.13}
\end{aligned}$$

where Ω_0 denotes the midplane of the laminate, and

$$\begin{Bmatrix} N_{\alpha\beta} \\ M_{\alpha\beta} \\ P_{\alpha\beta} \end{Bmatrix} = \int_{-\frac{h}{2}}^{\frac{h}{2}} \sigma_{\alpha\beta} \begin{Bmatrix} 1 \\ z \\ z^3 \end{Bmatrix} dz, \quad \begin{Bmatrix} Q_\alpha \\ R_\alpha \end{Bmatrix} = \int_{-\frac{h}{2}}^{\frac{h}{2}} \sigma_{\alpha z} \begin{Bmatrix} 1 \\ z^2 \end{Bmatrix} dz \tag{11.2.14}$$

$$I_i = \int_{-\frac{h}{2}}^{\frac{h}{2}} \rho_0 (z)^i dz \quad (i = 0, 1, 2, \dots, 6) \tag{11.2.15}$$

In Eq. (11.2.14), α and β take the symbols x and y . The same definitions hold for the stress resultants with a hat, which are specified.

Substituting for δU , δV , and δK from Eqs. (11.2.11)–(11.2.13) into the virtual work statement in Eq. (3.4.5), noting that the virtual strains can be written in terms of the generalized displacements using Eqs. (11.2.7a-c), integrating by parts to relieve the virtual generalized displacements, δu_0 , δv_0 , δw_0 , $\delta \phi_x$, and $\delta \phi_y$ in Ω_0 of any differentiation, and using the fundamental lemma of calculus of variations, we obtain the following Euler–Lagrange equations:

$$\frac{\partial N_{xx}}{\partial x} + \frac{\partial N_{xy}}{\partial y} = I_0 \ddot{u}_0 + J_1 \ddot{\phi}_x - c_1 I_3 \frac{\partial \ddot{w}_0}{\partial x} \tag{11.2.16}$$

$$\frac{\partial N_{xy}}{\partial x} + \frac{\partial N_{yy}}{\partial y} = I_0 \ddot{v}_0 + J_1 \ddot{\phi}_y - c_1 I_3 \frac{\partial \ddot{w}_0}{\partial y} \tag{11.2.17}$$

$$\begin{aligned} \frac{\partial \bar{Q}_x}{\partial x} + \frac{\partial \bar{Q}_y}{\partial y} + \frac{\partial}{\partial x}(N_{xx}\frac{\partial w_0}{\partial x} + N_{xy}\frac{\partial w_0}{\partial y}) + \frac{\partial}{\partial y}(N_{xy}\frac{\partial w_0}{\partial x} + N_{yy}\frac{\partial w_0}{\partial y}) \\ + c_1(\frac{\partial^2 P_{xx}}{\partial x^2} + 2\frac{\partial^2 P_{xy}}{\partial x \partial y} + \frac{\partial^2 P_{yy}}{\partial y^2}) + q = I_0 \ddot{w}_0 - c_1^2 I_6 (\frac{\partial^2 \ddot{w}_0}{\partial x^2} + \frac{\partial^2 \ddot{w}_0}{\partial y^2}) \\ + c_1 \left[I_3 (\frac{\partial \ddot{u}_0}{\partial x} + \frac{\partial \ddot{v}_0}{\partial y}) + J_4 (\frac{\partial \ddot{\phi}_x}{\partial x} + \frac{\partial \ddot{\phi}_y}{\partial y}) \right] \end{aligned} \quad (11.2.18)$$

$$\frac{\partial \bar{M}_{xx}}{\partial x} + \frac{\partial \bar{M}_{xy}}{\partial y} - \bar{Q}_x = J_1 \ddot{u}_0 + K_2 \ddot{\phi}_x - c_1 J_4 \frac{\partial \ddot{w}_0}{\partial x} \quad (11.2.19)$$

$$\frac{\partial \bar{M}_{xy}}{\partial x} + \frac{\partial \bar{M}_{yy}}{\partial y} - \bar{Q}_y = J_1 \ddot{v}_0 + K_2 \ddot{\phi}_y - c_1 J_4 \frac{\partial \ddot{w}_0}{\partial y} \quad (11.2.20)$$

where

$$\bar{M}_{\alpha\beta} = M_{\alpha\beta} - c_1 P_{\alpha\beta} \quad (\alpha, \beta = 1, 2, 6); \quad \bar{Q}_\alpha = Q_\alpha - c_2 R_\alpha \quad (\alpha = 4, 5) \quad (11.2.21)$$

$$I_i = \sum_{k=1}^N \int_{z_k}^{z_{k+1}} \rho^{(k)}(z)^i dz \quad (i = 0, 1, 2, \dots, 6) \quad (11.2.22)$$

$$J_i = I_i - c_1 I_{i+2}, \quad K_2 = I_2 - 2c_1 I_4 + c_1^2 I_6, \quad c_1 = \frac{4}{3h^2}, \quad c_2 = 3c_1 \quad (11.2.23)$$

The primary and secondary variables of the theory are

$$\text{Primary Variables : } u_n, u_s, w_0, \frac{\partial w_0}{\partial n}, \phi_n, \phi_s \quad (11.2.24)$$

$$\text{Secondary Variables : } N_{nn}, N_{ns}, \bar{V}_n, P_{nn}, \bar{M}_{nn}, \bar{M}_{ns} \quad (11.2.25)$$

where

$$\begin{aligned} \bar{V}_n &\equiv c_1 \left[\left(\frac{\partial P_{xx}}{\partial x} + \frac{\partial P_{xy}}{\partial y} \right) n_x + \left(\frac{\partial P_{xy}}{\partial x} + \frac{\partial P_{yy}}{\partial y} \right) n_y \right] \\ &- c_1 \left[\left(I_3 \ddot{u}_0 + J_4 \ddot{\phi}_x - c_1 I_6 \frac{\partial \ddot{w}_0}{\partial x} \right) n_x + \left(I_3 \ddot{v}_0 + J_4 \ddot{\phi}_y - c_1 I_6 \frac{\partial \ddot{w}_0}{\partial y} \right) n_y \right] \\ &+ (\bar{Q}_x n_x + \bar{Q}_y n_y) + \mathcal{P}(w_0) + c_1 \frac{\partial P_{ns}}{\partial s} \end{aligned} \quad (11.2.26)$$

$$\mathcal{P}(w_0) = \left(N_{xx} \frac{\partial w_0}{\partial x} + N_{xy} \frac{\partial w_0}{\partial y} \right) n_x + \left(N_{xy} \frac{\partial w_0}{\partial x} + N_{yy} \frac{\partial w_0}{\partial y} \right) n_y \quad (11.2.27)$$

The stress resultants are related to the strains by the relations

$$\begin{Bmatrix} \{N\} \\ \{M\} \\ \{P\} \end{Bmatrix} = \begin{bmatrix} [A] & [B] & [E] \\ [B] & [D] & [F] \\ [E] & [F] & [H] \end{bmatrix} \begin{Bmatrix} \{\varepsilon^{(0)}\} \\ \{\varepsilon^{(1)}\} \\ \{\varepsilon^{(3)}\} \end{Bmatrix} \quad (11.2.28)$$

$$\begin{Bmatrix} \{Q\} \\ \{R\} \end{Bmatrix} = \begin{bmatrix} [A] & [D] \\ [D] & [F] \end{bmatrix} \begin{Bmatrix} \{\gamma^{(0)}\} \\ \{\gamma^{(2)}\} \end{Bmatrix} \quad (11.2.29)$$

$$(A_{ij}, B_{ij}, D_{ij}, E_{ij}, F_{ij}, H_{ij}) = \sum_{k=1}^N \int_{z_k}^{z_{k+1}} \bar{Q}_{ij}^{(k)} (1, z, z^2, z^3, z^4, z^6) dz \quad (11.2.30a)$$

$$(A_{ij}, D_{ij}, F_{ij}) = \sum_{k=1}^N \int_{z_k}^{z_{k+1}} \bar{Q}_{ij}^{(k)} (1, z^2, z^4) dz \quad (11.2.30b)$$

The stiffnesses in Eq. (11.2.30a) are defined for $i, j = 1, 2, 6$ and those in Eq. (11.2.30b) are defined for $i, j = 4, 5$. Note that the matrices in (11.2.30a) are of the order 3×3 and those in (11.2.30b) are of order 2×2 . The coefficients A_{ij} , B_{ij} , and D_{ij} were given in terms of the layer stiffnesses $\bar{Q}_{ij}^{(k)}$ and layer coordinates z_{k+1} and z_k in Eqs. (3.3.38b) and (3.4.19). Additional stiffness coefficients are defined by

$$\begin{aligned} E_{ij} &= \frac{1}{4} \sum_{k=1}^N \bar{Q}_{ij}^{(k)} \left[(z_{k+1})^4 - (z_k)^4 \right] \\ F_{ij} &= \frac{1}{5} \sum_{k=1}^N \bar{Q}_{ij}^{(k)} \left[(z_{k+1})^5 - (z_k)^5 \right] \\ H_{ij} &= \frac{1}{7} \sum_{k=1}^N \bar{Q}_{ij}^{(k)} \left[(z_{k+1})^7 - (z_k)^7 \right] \end{aligned} \quad (11.2.31)$$

Note that the stiffnesses E_{ij} , F_{ij} and so on of the third-order theory involve fourth or higher powers of the thickness, and, therefore, they are expected to contribute little to thin laminate solutions. Even for moderately thick laminates the contribution can be small.

This completes the development of the Reddy third-order laminate theory. Note that the equations of motion of the first-order theory are obtained from the present third-order theory by setting $c_1 = 0$. However, the classical plate theory can be obtained from this theory only by replacing ϕ_α with $\varphi_\alpha + \partial w_0 / \partial x_\alpha$, which is a differential, not an algebraic relationship. The displacement field in Eq. (11.2.4) contains, as special cases, the displacement fields used by other researchers to derive a third-order plate theory, as shown in Table 11.2.1. Therefore, the third-order plate theories reported in the literature, despite their different looks, are equivalent. Many of these theories were developed for only isotropic plates.

11.3 Higher-Order Laminate Stiffness Characteristics

Since a detailed discussion of the laminate stiffnesses was presented in Section 3.5, a brief discussion is presented here for additional laminate stiffnesses (i.e., E_{ij} , F_{ij} , H_{ij} for $i, j = 1, 2, 6$ and D_{ij} and F_{ij} for $i, j = 4, 5$) introduced in the present third-order theory. A simplified third-order theory may be deduced from the general third-order theory presented here by omitting the higher-order stress resultants (P_{xx}, P_{yy}, P_{xy}) but keeping the higher-order stress resultants (R_x, R_y). The resulting theory is not consistent in energy sense.

We recall that the plane-stress-reduced stiffnesses Q_{ij} in the material coordinate system are given in terms of the engineering constants as

$$\begin{aligned} Q_{11} &= \frac{E_1}{1 - \nu_{12}\nu_{21}}, \quad Q_{12} = \frac{\nu_{12}E_2}{1 - \nu_{12}\nu_{21}}, \quad Q_{22} = \frac{E_2}{1 - \nu_{12}\nu_{21}} \\ Q_{66} &= G_{12}, \quad Q_{44} = G_{23}, \quad Q_{55} = G_{13} \end{aligned} \quad (11.3.1)$$

where the subscript 1 refers to the fiber direction and 2 to the direction transverse to the fiber. The transformed coefficients \bar{Q}_{ij} are related to Q_{ij} by Eq. (8.2.49a).

Table 11.2.1: Relationship of the displacements of other third-order theories to the one in Eq. (11.2.5): $u_\alpha = u_\alpha^0 + z\phi_\alpha - c_1 z^3(\phi_\alpha + u_{3,\alpha}^0)$, $u_3 = u_3^0$.

Reference	Displacement Field and Variables [†]	Relationship with ϕ_α
Schmidt [16]	$u_\alpha = u_\alpha^0 - z u_{3,\alpha}^0 + \frac{3}{2} f(z) \varepsilon_\alpha$	$\varepsilon_\alpha = \frac{2}{3} (\phi_\alpha + u_{3,\alpha}^0)$
Krishna Murty [20]	$u_\alpha = u_\alpha^0 - z u_{3,\alpha}^0 - c_3 f(z) \theta_\alpha$	$\theta_\alpha = -\frac{1}{c_3} (\phi_\alpha + u_{3,\alpha}^0)$
Vlasov [5], Jemielita [14], Levinson [21], Reddy [25,26]	$u_\alpha = u_\alpha^0 + f(z) \psi_\alpha - c_1 z^3 u_{3,\alpha}^0$	$\psi_\alpha = \phi_\alpha$
Murthy [22]	$u_\alpha = u_\alpha^0 + \frac{z}{4} (5\beta_\alpha + u_{3,\alpha}^0) - c_4 z^3 (\beta_\alpha + u_{3,\alpha}^0)$	$\beta_\alpha = \frac{4}{5} \phi_\alpha - \frac{1}{5} u_{3,\alpha}^0$
Reddy [32]	$u_\alpha = u_\alpha^0 + f(z) \hat{\phi}_\alpha - z u_{3,\alpha}^b - c_1 z^3 u_{3,\alpha}^s$	$\hat{\phi}_\alpha = \phi_\alpha + u_{3,\alpha}^b$ $u_3^s + u_3^b = u_3^0$
Bhimaraddi [27], Reddy [49]	$u_\alpha = u_\alpha^0 - z u_{3,\alpha}^0 + f(z) \varphi_\alpha$	$\varphi_\alpha = \phi_\alpha$

[†] $c_1 = \frac{4}{3h^2}$, $c_3 = \frac{3}{4h}$, $c_4 = \frac{5}{3h^2}$, $f(z) = z(1 - c_1 z^2)$.

11.3.1 Single-Layer Plates

Single Isotropic Layer

For a single isotropic layer of material constants E and ν [$G = \frac{E}{2(1+\nu)}$] and thickness h , the nonzero stiffnesses of Eqs. (11.2.30a,b) become

$$B_{ij} = E_{ij} = 0, \quad F_{ij} = \frac{h^5}{80} Q_{ij}, \quad H_{ij} = \frac{h^7}{448} Q_{ij} \quad (11.3.2a)$$

for $i, j = 1, 2, 6$, and

$$D_{ij} = \frac{h^3}{12} Q_{ij}, \quad F_{ij} = \frac{h^5}{80} Q_{ij} \quad (i, j = 4, 5) \quad (11.3.2b)$$

Hence, we have

$$F_{11} = \frac{Eh^5}{80(1-\nu^2)}, \quad F_{12} = \nu F_{11}, \quad F_{22} = F_{11}, \quad F_{66} = \frac{1-\nu}{2} F_{11} \quad (11.3.3a)$$

$$H_{11} = \frac{Eh^7}{448(1-\nu^2)}, \quad H_{12} = \nu H_{11}, \quad H_{22} = H_{11}, \quad H_{66} = \frac{1-\nu}{2} H_{11}$$

$$D_{44} = D_{55} = \frac{Gh^3}{12} = \frac{1-\nu}{2} D_{11}, \quad F_{44} = F_{55} = \frac{Gh^5}{80} = \frac{1-\nu}{2} F_{11} \quad (11.3.3b)$$

The plate constitutive equations (11.2.28) for the third-order theory become

$$\begin{Bmatrix} N_{xx} \\ N_{yy} \\ N_{xy} \end{Bmatrix} = \begin{bmatrix} A_{11} & \nu A_{11} & 0 \\ \nu A_{11} & A_{11} & 0 \\ 0 & 0 & \frac{1-\nu}{2} A_{11} \end{bmatrix} \begin{Bmatrix} \varepsilon_{xx}^{(0)} \\ \varepsilon_{yy}^{(0)} \\ \gamma_{xy}^{(0)} \end{Bmatrix} \quad (11.3.4a)$$

$$\begin{Bmatrix} M_{xx} \\ M_{yy} \\ M_{xy} \end{Bmatrix} = \begin{bmatrix} D_{11} & \nu D_{11} & 0 \\ \nu D_{11} & D_{11} & 0 \\ 0 & 0 & \frac{1-\nu}{2} D_{11} \end{bmatrix} \begin{Bmatrix} \varepsilon_{xx}^{(1)} \\ \varepsilon_{yy}^{(1)} \\ \gamma_{xy}^{(1)} \end{Bmatrix} + \begin{bmatrix} F_{11} & \nu F_{11} & 0 \\ \nu F_{11} & F_{11} & 0 \\ 0 & 0 & \frac{1-\nu}{2} F_{11} \end{bmatrix} \begin{Bmatrix} \varepsilon_{xx}^{(3)} \\ \varepsilon_{yy}^{(3)} \\ \gamma_{xy}^{(3)} \end{Bmatrix} \quad (11.3.4b)$$

$$\begin{Bmatrix} P_{xx} \\ P_{yy} \\ P_{xy} \end{Bmatrix} = \begin{bmatrix} F_{11} & \nu F_{11} & 0 \\ \nu F_{11} & F_{11} & 0 \\ 0 & 0 & \frac{1-\nu}{2} F_{11} \end{bmatrix} \begin{Bmatrix} \varepsilon_{xx}^{(1)} \\ \varepsilon_{yy}^{(1)} \\ \gamma_{xy}^{(1)} \end{Bmatrix} + \begin{bmatrix} H_{11} & \nu H_{11} & 0 \\ \nu H_{11} & H_{11} & 0 \\ 0 & 0 & \frac{1-\nu}{2} H_{11} \end{bmatrix} \begin{Bmatrix} \varepsilon_{xx}^{(3)} \\ \varepsilon_{yy}^{(3)} \\ \gamma_{xy}^{(3)} \end{Bmatrix} \quad (11.3.5)$$

$$\begin{Bmatrix} Q_y \\ Q_x \end{Bmatrix} = \frac{1-\nu}{2} \begin{bmatrix} A_{11} & 0 \\ 0 & A_{11} \end{bmatrix} \begin{Bmatrix} \gamma_{yz}^{(0)} \\ \gamma_{xz}^{(0)} \end{Bmatrix} + \frac{1-\nu}{2} \begin{bmatrix} D_{11} & 0 \\ 0 & D_{11} \end{bmatrix} \begin{Bmatrix} \gamma_{yz}^{(2)} \\ \gamma_{xz}^{(2)} \end{Bmatrix} \quad (11.3.6a)$$

$$\begin{Bmatrix} R_y \\ R_x \end{Bmatrix} = \frac{1-\nu}{2} \begin{bmatrix} D_{11} & 0 \\ 0 & D_{11} \end{bmatrix} \begin{Bmatrix} \gamma_{yz}^{(0)} \\ \gamma_{xz}^{(0)} \end{Bmatrix} + \frac{1-\nu}{2} \begin{bmatrix} F_{11} & 0 \\ 0 & F_{11} \end{bmatrix} \begin{Bmatrix} \gamma_{yz}^{(2)} \\ \gamma_{xz}^{(2)} \end{Bmatrix} \quad (11.3.6b)$$

Single Specially Orthotropic Layer

For a single specially orthotropic layer, the stiffnesses can be expressed in terms of the Q_{ij} and thickness h . The nonzero stiffnesses of Eqs. (11.2.30a,b) become ($B_{ij} = E_{ij} = 0$)

$$D_{11} = \frac{Q_{11}h^3}{12}, \quad D_{12} = \frac{Q_{12}h^3}{12}, \quad D_{22} = \frac{Q_{22}h^3}{12}, \quad D_{66} = \frac{Q_{66}h^3}{12} \quad (11.3.7a)$$

$$F_{11} = \frac{Q_{11}h^5}{80}, \quad F_{12} = \frac{Q_{12}h^5}{80}, \quad F_{22} = \frac{Q_{22}h^5}{80}, \quad F_{66} = \frac{Q_{66}h^5}{80} \quad (11.3.7b)$$

$$H_{11} = \frac{Q_{11}h^7}{448}, \quad H_{12} = \frac{Q_{12}h^7}{448}, \quad H_{22} = \frac{Q_{22}h^7}{448}, \quad H_{66} = \frac{Q_{66}h^7}{448} \quad (11.3.7c)$$

The plate constitutive equations for the higher-order stress resultants become (and similar equations hold for N 's and M 's)

$$\begin{Bmatrix} P_{xx} \\ P_{yy} \\ P_{xy} \end{Bmatrix} = \frac{h^5}{80} \begin{bmatrix} Q_{11} & Q_{12} & 0 \\ Q_{12} & Q_{22} & 0 \\ 0 & 0 & Q_{66} \end{bmatrix} \begin{Bmatrix} \varepsilon_{xx}^{(1)} \\ \varepsilon_{yy}^{(1)} \\ \gamma_{xy}^{(1)} \end{Bmatrix} + \frac{h^7}{448} \begin{bmatrix} Q_{11} & Q_{12} & 0 \\ Q_{12} & Q_{22} & 0 \\ 0 & 0 & Q_{66} \end{bmatrix} \begin{Bmatrix} \varepsilon_{xx}^{(3)} \\ \varepsilon_{yy}^{(3)} \\ \gamma_{xy}^{(3)} \end{Bmatrix} \quad (11.3.8)$$

$$\begin{Bmatrix} R_y \\ R_x \end{Bmatrix} = \frac{h^3}{12} \begin{bmatrix} Q_{44} & 0 \\ 0 & Q_{55} \end{bmatrix} \begin{Bmatrix} \gamma_{yz}^{(0)} \\ \gamma_{xz}^{(0)} \end{Bmatrix} + \frac{h^5}{80} \begin{bmatrix} Q_{44} & 0 \\ 0 & Q_{55} \end{bmatrix} \begin{Bmatrix} \gamma_{yz}^{(2)} \\ \gamma_{xz}^{(2)} \end{Bmatrix} \quad (11.3.9)$$

Single Generally Orthotropic Layer

For a single generally orthotropic layer (i.e., the principal material coordinates do not coincide with those of the plate), the stiffnesses are expressed in terms of the transformed coefficients \bar{Q}_{ij} and thickness h . The plate constitutive equations are

$$\begin{Bmatrix} P_{xx} \\ P_{yy} \\ P_{xy} \end{Bmatrix} = \begin{bmatrix} F_{11} & F_{12} & F_{16} \\ F_{12} & F_{22} & F_{26} \\ F_{16} & F_{26} & F_{66} \end{bmatrix} \begin{Bmatrix} \varepsilon_{xx}^{(1)} \\ \varepsilon_{yy}^{(1)} \\ \gamma_{xy}^{(1)} \end{Bmatrix} + \begin{bmatrix} H_{11} & H_{12} & H_{16} \\ H_{12} & H_{22} & H_{26} \\ H_{16} & H_{26} & H_{66} \end{bmatrix} \begin{Bmatrix} \varepsilon_{xx}^{(3)} \\ \varepsilon_{yy}^{(3)} \\ \gamma_{xy}^{(3)} \end{Bmatrix} \quad (11.3.10)$$

$$\begin{Bmatrix} R_y \\ R_x \end{Bmatrix} = \begin{bmatrix} D_{44} & D_{45} \\ D_{45} & D_{55} \end{bmatrix} \begin{Bmatrix} \gamma_{yz}^{(0)} \\ \gamma_{xz}^{(0)} \end{Bmatrix} + \begin{bmatrix} F_{44} & F_{45} \\ F_{45} & F_{55} \end{bmatrix} \begin{Bmatrix} \gamma_{yz}^{(2)} \\ \gamma_{xz}^{(2)} \end{Bmatrix} \quad (11.3.11)$$

The higher-order thermal stress resultants for this case are given by

$$\begin{Bmatrix} P_{xx}^T \\ P_{yy}^T \\ P_{xy}^T \end{Bmatrix} = \sum_{k=1}^L \int_{z_k}^{z_{k+1}} \begin{bmatrix} \bar{Q}_{11}^k & \bar{Q}_{12}^k & \bar{Q}_{16}^k \\ \bar{Q}_{12}^k & \bar{Q}_{22}^k & \bar{Q}_{26}^k \\ \bar{Q}_{16}^k & \bar{Q}_{26}^k & \bar{Q}_{66}^k \end{bmatrix}^{(k)} \begin{Bmatrix} \alpha_{xx} \\ \alpha_{yy} \\ 2\alpha_{xy} \end{Bmatrix} \Delta T z^3 dz \quad (11.3.12)$$

Single Anisotropic Layer

For a single anisotropic layer, the stiffnesses are expressed in terms of the coefficients C_{ij} and thickness h . The nonzero higher-order stiffnesses are ($B_{ij} = 0$)

$$F_{ij} = \frac{C_{ij} h^5}{80}, \quad H_{ij} = \frac{C_{ij} h^7}{448} \quad (11.3.13)$$

for $i, j = 1, 2, 4, 5$, and 6 [see Eq. (2.4.3a)]. The plate constitutive equations are the same as in Eqs. (11.3.10) and (11.3.11), except that the plate stiffnesses are given by Eq. (11.3.13).

11.3.2 Symmetric Laminates

The force and moment resultants for a symmetric laminate, in general, have the same form as the generally orthotropic single-layer plates [see Eqs. (11.3.10) and (11.3.11)]. For certain special cases of symmetric laminates, the relations between strains and resultants can be further simplified, as explained next.

Symmetric Laminates with Multiple Isotropic Layers

When isotropic layers of possibly different material properties and thicknesses are arranged symmetrically from both a geometric and a material property standpoint, the resulting laminate will have the following laminate constitutive equations for the third-order theories:

$$\begin{Bmatrix} P_{xx} \\ P_{yy} \\ P_{xy} \end{Bmatrix} = \begin{bmatrix} F_{11} & F_{12} & 0 \\ F_{12} & F_{11} & 0 \\ 0 & 0 & F_{66} \end{bmatrix} \begin{Bmatrix} \varepsilon_{xx}^{(1)} \\ \varepsilon_{yy}^{(1)} \\ \gamma_{xy}^{(1)} \end{Bmatrix} + \begin{bmatrix} H_{11} & H_{12} & 0 \\ H_{12} & H_{11} & 0 \\ 0 & 0 & H_{66} \end{bmatrix} \begin{Bmatrix} \varepsilon_{xx}^{(3)} \\ \varepsilon_{yy}^{(3)} \\ \gamma_{xy}^{(3)} \end{Bmatrix} \quad (11.3.14)$$

$$\begin{Bmatrix} R_y \\ R_x \end{Bmatrix} = \begin{bmatrix} D_{44} & 0 \\ 0 & D_{55} \end{bmatrix} \begin{Bmatrix} \gamma_{yz}^{(0)} \\ \gamma_{xz}^{(0)} \end{Bmatrix} + \begin{bmatrix} F_{44} & 0 \\ 0 & F_{55} \end{bmatrix} \begin{Bmatrix} \gamma_{yz}^{(2)} \\ \gamma_{xz}^{(2)} \end{Bmatrix} \quad (11.3.15)$$

where the laminate stiffnesses F_{ij} and H_{ij} are defined by Eqs. (3.5.24) with

$$\bar{Q}_{11}^{(k)} = \bar{Q}_{22}^{(k)} = \frac{E^k}{1 - \nu_k^2}, \quad \bar{Q}_{16}^{(k)} = \bar{Q}_{26}^{(k)} = 0 \quad (11.3.16a)$$

$$\bar{Q}_{12}^{(k)} = \frac{\nu_k E^k}{1 - \nu_k^2}, \quad \bar{Q}_{44}^{(k)} = \bar{Q}_{55}^{(k)} = \bar{Q}_{66}^{(k)} = \frac{E^k}{2(1 + \nu_k)} \quad (11.3.16b)$$

The thermal stress resultants for this case are given by

$$\begin{Bmatrix} P_{xx}^T \\ P_{yy}^T \end{Bmatrix} = \sum_{k=1}^L \int_{z_k}^{z_{k+1}} \begin{bmatrix} \bar{Q}_{11} & \bar{Q}_{12} \\ \bar{Q}_{12} & \bar{Q}_{22} \end{bmatrix}^{(k)} \begin{Bmatrix} \alpha_{xx} \\ \alpha_{yy} \end{Bmatrix}^{(k)} \Delta T z^3 dz \quad (11.3.17)$$

Symmetric Laminates with Multiple Specially Orthotropic Layers

A laminate of multiple specially orthotropic layers that are symmetrically disposed, both from a material and geometric properties standpoint, about the midplane of the laminate do not exhibit coupling between bending and extension. The laminate constitutive equations are again given by Eqs. (11.3.13)–(11.3.16), where the laminate stiffnesses F_{ij} and H_{ij} are defined by Eqs. (11.2.24) with

$$\begin{aligned} \bar{Q}_{11}^{(k)} &= \frac{E_1^k}{1 - \nu_{12}^k \nu_{21}^k}, \quad \bar{Q}_{12}^{(k)} = \frac{\nu_{21}^k E_1^k}{1 - \nu_{12}^k \nu_{21}^k}, \quad \bar{Q}_{22}^{(k)} = \frac{E_2^k}{1 - \nu_{12}^k \nu_{21}^k} \\ \bar{Q}_{16}^{(k)} &= 0, \quad \bar{Q}_{26}^{(k)} = 0, \quad \bar{Q}_{66}^{(k)} = G_{12}^k, \quad \bar{Q}_{44}^{(k)} = G_{23}^k, \quad \bar{Q}_{55}^{(k)} = G_{13}^k \end{aligned} \quad (11.3.18)$$

The thermal stress resultants have the same form as those given in Eq. (11.3.17).

11.3.3 Antisymmetric Laminates

Due to the antisymmetry of the lamination scheme but symmetry of the thicknesses of each pair of layers, this class of antisymmetric laminates have the feature that $F_{16} = F_{26} = H_{16} = H_{26} = 0$. The coupling stiffnesses B_{ij} and E_{ij} are not zero. The relations between the stress resultants and the strains are

$$\begin{aligned} \begin{Bmatrix} P_{xx} \\ P_{yy} \\ P_{xy} \end{Bmatrix} &= \begin{bmatrix} E_{11} & E_{12} & E_{16} \\ E_{12} & E_{22} & E_{26} \\ E_{16} & E_{26} & E_{66} \end{bmatrix} \begin{Bmatrix} \varepsilon_{xx}^{(0)} \\ \varepsilon_{yy}^{(0)} \\ \varepsilon_{xy}^{(0)} \end{Bmatrix} + \begin{bmatrix} F_{11} & F_{12} & 0 \\ F_{12} & F_{22} & 0 \\ 0 & 0 & F_{66} \end{bmatrix} \begin{Bmatrix} \varepsilon_{xx}^{(1)} \\ \varepsilon_{yy}^{(1)} \\ \varepsilon_{xy}^{(1)} \end{Bmatrix} \\ &+ \begin{bmatrix} H_{11} & H_{12} & 0 \\ H_{12} & H_{22} & 0 \\ 0 & 0 & H_{66} \end{bmatrix} \begin{Bmatrix} \varepsilon_{xx}^{(3)} \\ \varepsilon_{yy}^{(3)} \\ \varepsilon_{xy}^{(3)} \end{Bmatrix} \end{aligned} \quad (11.3.19)$$

$$\begin{Bmatrix} R_y \\ R_x \end{Bmatrix} = \begin{bmatrix} D_{44} & 0 \\ 0 & D_{55} \end{bmatrix} \begin{Bmatrix} \varepsilon_{yz}^{(0)} \\ \varepsilon_{xz}^{(0)} \end{Bmatrix} + \begin{bmatrix} F_{44} & 0 \\ 0 & F_{55} \end{bmatrix} \begin{Bmatrix} \varepsilon_{yz}^{(2)} \\ \varepsilon_{xz}^{(2)} \end{Bmatrix} \quad (11.3.20)$$

Antisymmetric Cross-Ply Laminates

For antisymmetric cross-ply laminates the coupling stiffnesses have the following properties:

$$E_{22} = -E_{11}, \text{ and all other } E_{ij} = D_{45} = F_{45} = 0 \quad (11.3.21)$$

For regular antisymmetric cross-ply laminates, the coupling coefficients E_{11} can be shown to approach zero as the number of layers increases.

Antisymmetric Angle-Ply Laminates

For antisymmetric angle-ply laminates the stiffnesses can be simplified as

$$D_{45} = F_{45} = F_{16} = F_{26} = H_{16} = H_{26} = E_{11} = E_{22} = E_{12} = E_{66} = 0 \quad (11.3.22)$$

For a fixed laminate thickness, the stiffnesses E_{16} and E_{26} go to zero as the number of layers in the laminate increases.

This completes the development of the third-order theory of Reddy. In the next section, we develop the Navier solutions of antisymmetric angle-ply and cross-ply laminates. The Lévy solutions are presented in Section 11.5, and finite element models are discussed in Section 11.6.

11.4 The Navier Solutions

11.4.1 Preliminary Comments

The equations of motion of the third-order theory of Reddy presented in Eqs. (11.2.16)–(11.2.20) are very similar in form to the first-order shear deformation theory. In fact, it is possible to develop the Navier solutions of simply supported antisymmetric cross-ply and angle-ply laminates using the third-order theory (see References 25, 26, and 29). For antisymmetric cross-ply laminates the following stiffnesses are zero:

$$\begin{aligned} A_{16} &= A_{26} = A_{45} = B_{16} = B_{26} = D_{16} = D_{26} = I_1 = 0 \\ E_{16} &= E_{26} = F_{16} = F_{26} = H_{16} = H_{26} = D_{45} = F_{45} = I_3 = I_5 = I_7 = 0 \end{aligned} \quad (11.4.1)$$

For antisymmetric angle-ply laminates the following stiffnesses are zero:

$$\begin{aligned} A_{16} &= A_{26} = A_{45} = B_{11} = B_{12} = B_{22} = B_{66} = D_{16} = D_{26} = I_1 = 0 \\ E_{11} &= E_{12} = E_{22} = E_{66} = F_{16} = F_{26} = H_{16} = H_{26} = D_{45} = F_{45} = I_3 = I_5 = I_7 = 0 \end{aligned} \quad (11.4.2)$$

The SS-1 boundary conditions for the third-order shear deformation plate theory are (see Figure 11.4.1):

$$\begin{aligned} u_0(x, 0, t) &= 0, \quad \phi_x(x, 0, t) = 0, \quad u_0(x, b, t) = 0, \quad \phi_x(x, b, t) = 0 \\ v_0(0, y, t) &= 0, \quad \phi_y(0, y, t) = 0, \quad v_0(a, y, t) = 0, \quad \phi_y(a, y, t) = 0 \\ w_0(x, 0, t) &= 0, \quad w_0(x, b, t) = 0, \quad w_0(0, y, t) = 0, \quad w_0(a, y, t) = 0 \end{aligned} \quad (11.4.3a)$$

$$\begin{aligned} N_{xx}(0, y, t) &= 0, \quad N_{xx}(a, y, t) = 0, \quad N_{yy}(x, 0, t) = 0, \quad N_{yy}(x, b, t) = 0 \\ \bar{M}_{xx}(0, y, t) &= 0, \quad \bar{M}_{xx}(a, y, t) = 0, \quad \bar{M}_{yy}(x, 0, t) = 0, \quad \bar{M}_{yy}(x, b, t) = 0 \end{aligned} \quad (11.4.3b)$$

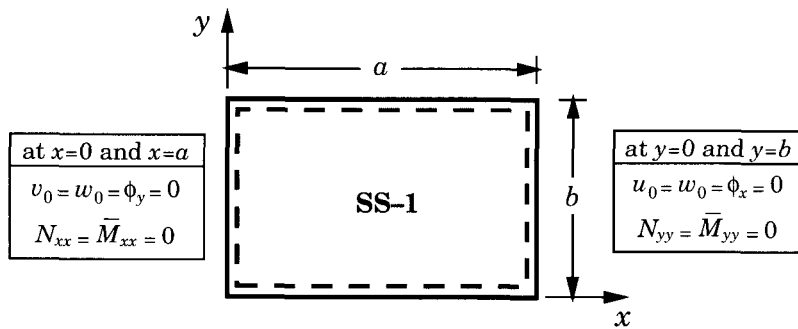


Figure 11.4.1: Simply supported (SS-1) boundary conditions for antisymmetric cross-ply laminates.

The SS-2 boundary conditions for the third-order shear deformation plate theory are (see Figure 11.4.2)

$$\begin{aligned} u_0(0, y, t) &= 0, \quad \phi_x(x, 0, t) = 0, \quad u_0(a, y, t) = 0, \quad \phi_x(x, b, t) = 0 \\ v_0(x, 0, t) &= 0, \quad \phi_y(0, y, t) = 0, \quad v_0(x, b, t) = 0, \quad \phi_y(a, y, t) = 0 \\ w_0(x, 0, t) &= 0, \quad w_0(x, b, t) = 0, \quad w_0(0, y, t) = 0, \quad w_0(a, y, t) = 0 \end{aligned} \quad (11.4.4a)$$

$$\begin{aligned} N_{xy}(0, y, t) &= 0, \quad N_{xy}(a, y, t) = 0, \quad N_{xy}(x, 0, t) = 0, \quad N_{xy}(x, b, t) = 0 \\ \bar{M}_{xx}(0, y, t) &= 0, \quad \bar{M}_{xx}(a, y, t) = 0, \quad \bar{M}_{yy}(x, 0, t) = 0, \quad \bar{M}_{yy}(x, b, t) = 0 \end{aligned} \quad (11.4.4b)$$

In the following sections, we present the Navier solutions of cross-ply laminates for the SS-1 boundary conditions and antisymmetric angle-ply laminates for the SS-2 boundary conditions.

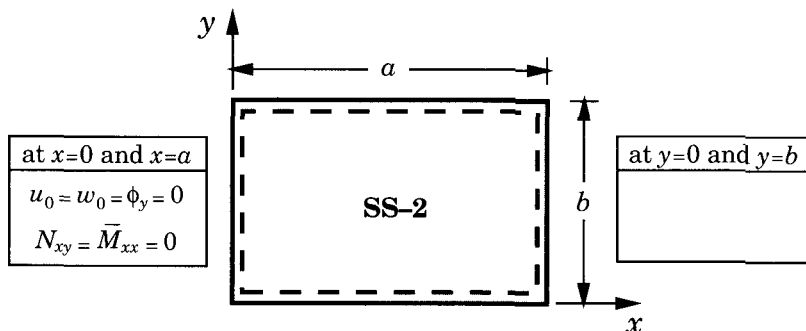


Figure 11.4.2: Simply supported (SS-2) boundary conditions for antisymmetric angle-ply laminates.

11.4.2 Antisymmetric Cross-Ply Laminates

The boundary conditions in (11.4.3a,b) are satisfied by the following expansions:

$$u_0(x, y, t) = \sum_{n=1}^{\infty} \sum_{m=1}^{\infty} U_{mn}(t) \cos \alpha x \sin \beta y \quad (11.4.5a)$$

$$v_0(x, y, t) = \sum_{n=1}^{\infty} \sum_{m=1}^{\infty} V_{mn}(t) \sin \alpha x \cos \beta y \quad (11.4.5b)$$

$$w_0(x, y, t) = \sum_{n=1}^{\infty} \sum_{m=1}^{\infty} W_{mn}(t) \sin \alpha x \sin \beta y \quad (11.4.5c)$$

$$\phi_x(x, y, t) = \sum_{n=1}^{\infty} \sum_{m=1}^{\infty} X_{mn}(t) \cos \alpha x \sin \beta y \quad (11.4.5d)$$

$$\phi_y(x, y, t) = \sum_{n=1}^{\infty} \sum_{m=1}^{\infty} Y_{mn}(t) \sin \alpha x \cos \beta y \quad (11.4.5e)$$

where $\alpha = m\pi/a$ and $\beta = n\pi/b$. The transverse load q is also expanded in double Fourier sine series

$$q(x, y, t) = \sum_{n=1}^{\infty} \sum_{m=1}^{\infty} Q_{mn}(t) \sin \alpha x \sin \beta y \quad (11.4.6a)$$

$$Q_{mn}(t) = \frac{4}{ab} \int_0^a \int_0^b q(x, y, t) \sin \alpha x \sin \beta y \, dx \, dy \quad (11.4.6b)$$

Substitution of Eqs. (11.4.5) and (11.4.6) into Eqs. (11.2.16)–(11.2.20) will show that the Navier solution exists only if the laminate stiffnesses are such that the conditions in Eq. (11.4.1) hold. The coefficients ($U_{mn}, V_{mn}, W_{mn}, X_{mn}, Y_{mn}$) of the Navier solution of cross-ply laminates are governed by

$$[\hat{S}]\{\Delta\} + [\hat{M}]\{\ddot{\Delta}\} = \{F\} \quad (11.4.7a)$$

$$\{\Delta\} = \begin{Bmatrix} U_{mn} \\ V_{mn} \\ W_{mn} \\ X_{mn} \\ Y_{mn} \end{Bmatrix}, \quad \{F\} = \begin{Bmatrix} 0 \\ 0 \\ Q_{mn} \\ 0 \\ 0 \end{Bmatrix} - \begin{Bmatrix} \alpha N_{mn}^1 \\ \beta N_{mn}^2 \\ 0 \\ \alpha \hat{M}_{mn}^1 \\ \beta \hat{M}_{mn}^2 \end{Bmatrix} \quad (11.4.7b)$$

where \hat{s}_{ij} and \hat{m}_{ij} are defined by

$$\begin{aligned} \hat{s}_{11} &= A_{11}\alpha^2 + A_{66}\beta^2, & \hat{s}_{12} &= (A_{12} + A_{66})\alpha\beta \\ \hat{s}_{13} &= -c_1 [E_{11}\alpha^2 + (E_{12} + 2E_{66})\beta^2] \alpha \\ \hat{s}_{14} &= \hat{B}_{11}\alpha^2 + \hat{B}_{66}\beta^2, & \hat{s}_{15} &= (\hat{B}_{12} + \hat{B}_{66})\alpha\beta \\ \hat{s}_{22} &= A_{66}\alpha^2 + A_{22}\beta^2, & \hat{s}_{24} &= \hat{s}_{15} \\ \hat{s}_{23} &= -c_1 [E_{22}\beta^2 + (E_{12} + 2E_{66})\alpha^2] \beta, & \hat{s}_{25} &= \hat{B}_{66}\alpha^2 + \hat{B}_{22}\beta^2 \\ \hat{s}_{33} &= \bar{A}_{55}\alpha^2 + \bar{A}_{44}\beta^2 + c_1^2 [H_{11}\alpha^4 + 2(H_{12} + 2H_{66})\alpha^2\beta^2 + H_{22}\beta^4] \end{aligned}$$

$$\begin{aligned}
\hat{s}_{34} &= \bar{A}_{55}\alpha - c_1 \left[\hat{F}_{11}\alpha^3 + (\hat{F}_{12} + 2\hat{F}_{66})\alpha\beta^2 \right] \\
\hat{s}_{35} &= \bar{A}_{44}\beta - c_1 \left[\hat{F}_{22}\beta^3 + (\hat{F}_{12} + 2\hat{F}_{66})\alpha^2\beta \right] \\
\hat{s}_{44} &= \bar{A}_{55} + \bar{D}_{11}\alpha^2 + \bar{D}_{66}\beta^2, \quad \hat{s}_{45} = (\bar{D}_{12} + \bar{D}_{66})\alpha\beta \\
\hat{s}_{55} &= \bar{A}_{44} + \bar{D}_{66}\alpha^2 + \bar{D}_{22}\beta^2, \quad \tilde{s}_{33} = \hat{N}_{xx}\alpha^2 + \hat{N}_{yy}\beta^2
\end{aligned} \tag{11.4.8a}$$

$$\begin{aligned}
\hat{m}_{11} &= I_0, \quad \hat{m}_{22} = I_0, \quad \hat{m}_{33} = I_0 + c_1^2 I_6 (\alpha^2 + \beta^2), \quad \hat{m}_{34} = -c_1 J_4 \alpha \\
\hat{m}_{35} &= -c_1 J_4 \beta, \quad \hat{m}_{44} = K_2, \quad \hat{m}_{55} = K_2
\end{aligned} \tag{11.4.8b}$$

$$\begin{aligned}
\hat{A}_{ij} &= A_{ij} - c_1 D_{ij}, \quad \hat{B}_{ij} = B_{ij} - c_1 E_{ij}, \quad \hat{D}_{ij} = D_{ij} - c_1 F_{ij} \quad (i, j = 1, 2, 6) \\
\hat{F}_{ij} &= F_{ij} - c_1 H_{ij}, \quad \bar{A}_{ij} = \hat{A}_{ij} - c_1 \hat{D}_{ij} = A_{ij} - 2c_1 D_{ij} + c_1^2 F_{ij} \quad (i, j = 1, 2, 6) \\
\bar{D}_{ij} &= \hat{D}_{ij} - c_1 \hat{F}_{ij} = D_{ij} - 2c_1 F_{ij} + c_1^2 H_{ij} \quad (i, j = 1, 2, 6) \\
\bar{A}_{ij} &= \hat{A}_{ij} - c_2 \hat{D}_{ij} = A_{ij} - 2c_2 D_{ij} + c_2^2 F_{ij} \quad (i, j = 4, 5)
\end{aligned}$$

$$J_i = I_i - c_1 I_{i+2}, \quad K_2 = I_2 - 2c_1 I_4 + c_1^2 I_6, \quad c_1 = \frac{4}{3h^2}, \quad c_2 = 3c_1 \tag{11.4.9}$$

The thermal resultants are defined by [see Eqs. (6.3.11) through (6.3.13)]

$$\left\{ \begin{array}{l} N_{xx}^T \\ N_{yy}^T \\ N_{xy}^T \end{array} \right\} = \sum_{n=1}^{\infty} \sum_{m=1}^{\infty} \left\{ \begin{array}{l} N_{mn}^1(t) \\ N_{mn}^2(t) \\ N_{mn}^6(t) \end{array} \right\} \sin \alpha x \sin \beta y \tag{11.4.10a}$$

$$\left\{ \begin{array}{l} M_{xx}^T \\ M_{yy}^T \\ M_{xy}^T \end{array} \right\} = \sum_{n=1}^{\infty} \sum_{m=1}^{\infty} \left\{ \begin{array}{l} M_{mn}^1(t) \\ M_{mn}^2(t) \\ M_{mn}^6(t) \end{array} \right\} \sin \alpha x \sin \beta y \tag{11.4.10b}$$

$$\left\{ \begin{array}{l} P_{xx}^T \\ P_{yy}^T \\ P_{xy}^T \end{array} \right\} = \sum_{n=1}^{\infty} \sum_{m=1}^{\infty} \left\{ \begin{array}{l} P_{mn}^1(t) \\ P_{mn}^2(t) \\ P_{mn}^6(t) \end{array} \right\} \sin \alpha x \sin \beta y \tag{11.4.10c}$$

$$\{N_{mn}(t)\} = \sum_{k=1}^N \int_{z_k}^{z_{k+1}} [\bar{Q}]^{(k)} \{\bar{\alpha}\}^{(k)} T_{mn}(z, t) dz \tag{11.4.11a}$$

$$\{M_{mn}(t)\} = \sum_{k=1}^N \int_{z_k}^{z_{k+1}} [\bar{Q}]^{(k)} \{\bar{\alpha}\}^{(k)} T_{mn}(z, t) z dz \tag{11.4.11b}$$

$$\{P_{mn}(t)\} = \sum_{k=1}^N \int_{z_k}^{z_{k+1}} [\bar{Q}]^{(k)} \{\bar{\alpha}\}^{(k)} T_{mn}(z, t) z^3 dz \tag{11.4.11c}$$

$$\Delta T(x, y, z, t) = \sum_{m=1}^{\infty} \sum_{n=1}^{\infty} (T_{mn}^0 + z T_{mn}^1) \sin \alpha x \sin \beta y \tag{11.4.12a}$$

$$(T_{mn}^0, T_{mn}^1) = \frac{4}{ab} \int_0^a \int_0^b (T_0, T_1) \sin \alpha x \sin \beta y dx dy \tag{11.4.12b}$$

$$\{\hat{M}_{mn}\} = \{M_{mn}\} - c_1 \{P_{mn}\} \tag{11.4.13}$$

The ordinary differential equations (11.4.7) in time can be solved for transient response using the Newmark integration procedure described in Chapter 7. Equation (11.4.7) can be specialized to static bending analysis, buckling, and natural vibration.

The in-plane stresses in each layer can be computed from the equations [see Eqs. (6.3.29) and (6.3.30)]

$$\begin{Bmatrix} \sigma_{xx} \\ \sigma_{yy} \\ \sigma_{xy} \end{Bmatrix}^{(k)} = \begin{bmatrix} \bar{Q}_{11} & \bar{Q}_{12} & 0 \\ \bar{Q}_{12} & \bar{Q}_{22} & 0 \\ 0 & 0 & \bar{Q}_{66} \end{bmatrix}^{(k)} \left(\begin{Bmatrix} \varepsilon_{xx} \\ \varepsilon_{yy} \\ \gamma_{xy} \end{Bmatrix} - \begin{Bmatrix} \alpha_{xx} \\ \alpha_{yy} \\ 2\alpha_{xy} \end{Bmatrix}^{(k)} \Delta T \right) \quad (11.4.14)$$

where

$$\begin{aligned} \begin{Bmatrix} \varepsilon_{xx} \\ \varepsilon_{yy} \\ \gamma_{xy} \end{Bmatrix} &= \begin{Bmatrix} \varepsilon_{xx}^{(0)} \\ \varepsilon_{yy}^{(0)} \\ \gamma_{xy}^{(0)} \end{Bmatrix} + z \begin{Bmatrix} \varepsilon_{xx}^{(1)} \\ \varepsilon_{yy}^{(1)} \\ \gamma_{xy}^{(1)} \end{Bmatrix} + z^3 \begin{Bmatrix} \varepsilon_{xx}^{(3)} \\ \varepsilon_{yy}^{(3)} \\ \gamma_{xy}^{(3)} \end{Bmatrix} \\ &= \sum_{m=1}^{\infty} \sum_{n=1}^{\infty} \begin{Bmatrix} (R_{mn}^{xx} + zS_{mn}^{xx} + c_1 z^3 T_{mn}^{xx}) \sin \alpha x \sin \beta y \\ (R_{mn}^{yy} + zS_{mn}^{yy} + c_1 z^3 T_{mn}^{yy}) \sin \alpha x \sin \beta y \\ (R_{mn}^{xy} + zS_{mn}^{xy} + c_1 z^3 T_{mn}^{xy}) \cos \alpha x \cos \beta y \end{Bmatrix} \quad (11.4.15a) \end{aligned}$$

$$\begin{aligned} \begin{Bmatrix} R_{mn}^{xx} \\ R_{mn}^{yy} \\ R_{mn}^{xy} \end{Bmatrix} &= \begin{Bmatrix} -\alpha U_{mn} \\ -\beta V_{mn} \\ \beta U_{mn} + \alpha V_{mn} \end{Bmatrix}, \quad \begin{Bmatrix} S_{mn}^{xx} \\ S_{mn}^{yy} \\ S_{mn}^{xy} \end{Bmatrix} = \begin{Bmatrix} -\alpha X_{mn} \\ -\beta Y_{mn} \\ \beta X_{mn} + \alpha Y_{mn} \end{Bmatrix} \\ \begin{Bmatrix} T_{mn}^{xx} \\ T_{mn}^{yy} \\ T_{mn}^{xy} \end{Bmatrix} &= \begin{Bmatrix} \alpha X_{mn} + \alpha^2 W_{mn} \\ \beta Y_{mn} + \beta^2 W_{mn} \\ -(\beta X_{mn} + \alpha Y_{mn} + 2\alpha\beta W_{mn}) \end{Bmatrix} \quad (11.4.15b) \end{aligned}$$

The transverse shear stresses from the constitutive equations are given by

$$\begin{aligned} \begin{Bmatrix} \sigma_{yz} \\ \sigma_{xz} \end{Bmatrix}^{(k)} &= \sum_{m=1}^{\infty} \sum_{n=1}^{\infty} \begin{bmatrix} \bar{Q}_{44} & 0 \\ 0 & \bar{Q}_{55} \end{bmatrix}^{(k)} \left(\begin{Bmatrix} \gamma_{yz}^{(0)} \\ \gamma_{xz}^{(0)} \end{Bmatrix} + z^2 \begin{Bmatrix} \gamma_{yz}^{(2)} \\ \gamma_{xz}^{(2)} \end{Bmatrix} \right) \\ &= (1 - c_2 z^2) \sum_{m=1}^{\infty} \sum_{n=1}^{\infty} \begin{bmatrix} \bar{Q}_{44} & 0 \\ 0 & \bar{Q}_{55} \end{bmatrix}^{(k)} \begin{Bmatrix} (Y_{mn} + \beta W_{mn}) \sin \alpha x \cos \beta y \\ (X_{mn} + \alpha W_{mn}) \cos \alpha x \sin \beta y \end{Bmatrix} \quad (11.4.16) \end{aligned}$$

where $c_2 = 4/h^2$. Note that the transverse shear stresses are layerwise quadratic through the thickness.

The transverse shear stresses can also be determined using the equilibrium equations of 3-D elasticity. In the absence of thermal effects they are given by

$$\begin{aligned} \sigma_{xz}^{(k)}(x, y, z) &= \sum_{m=1}^{\infty} \sum_{n=1}^{\infty} \left[(z - z_k) \mathcal{A}_{mn}^{(k)} + \frac{1}{2} (z^2 - z_k^2) \mathcal{B}_{mn}^{(k)} \right. \\ &\quad \left. + \frac{c_1}{4} (z^4 - z_k^4) \mathcal{E}_{mn}^{(k)} \right] \cos \alpha x \sin \beta y + \sigma_{xz}^{(k-1)}(x, y, z_k) \quad (11.4.17a) \end{aligned}$$

$$\begin{aligned} \sigma_{yz}^{(k)}(x, y, z) &= \sum_{m=1}^{\infty} \sum_{n=1}^{\infty} \left[(z - z_k) \mathcal{C}_{mn}^{(k)} + \frac{1}{2} (z^2 - z_k^2) \mathcal{D}_{mn}^{(k)} \right. \\ &\quad \left. + \frac{c_1}{4} (z^4 - z_k^4) \mathcal{F}_{mn}^{(k)} \right] \sin \alpha x \cos \beta y + \sigma_{yz}^{(k-1)}(x, y, z_k) \quad (11.4.17b) \end{aligned}$$

where

$$\begin{aligned}
 \mathcal{A}_{mn}^{(k)} &= \left[(\alpha^2 \bar{Q}_{11}^{(k)} + \beta^2 \bar{Q}_{66}^{(k)}) U_{mn} + \alpha\beta (\bar{Q}_{12}^{(k)} + \bar{Q}_{66}^{(k)}) V_{mn} \right] \\
 \mathcal{B}_{mn}^{(k)} &= \left[(\alpha^2 \bar{Q}_{11}^{(k)} + \beta^2 \bar{Q}_{66}^{(k)}) X_{mn} + \alpha\beta (\bar{Q}_{12}^{(k)} + \bar{Q}_{66}^{(k)}) Y_{mn} \right] \\
 \mathcal{C}_{mn}^{(k)} &= \left[\alpha\beta (\bar{Q}_{12}^{(k)} + \bar{Q}_{66}^{(k)}) U_{mn} + (\alpha^2 \bar{Q}_{66}^{(k)} + \beta^2 \bar{Q}_{22}^{(k)}) V_{mn} \right] \\
 \mathcal{D}_{mn}^{(k)} &= \left[\alpha\beta (\bar{Q}_{12}^{(k)} + \bar{Q}_{66}^{(k)}) X_{mn} + (\alpha^2 \bar{Q}_{66}^{(k)} + \beta^2 \bar{Q}_{22}^{(k)}) Y_{mn} \right] \\
 \mathcal{E}_{mn}^{(k)} &= - \left[\alpha^3 \bar{Q}_{11}^{(k)} + \alpha\beta^2 (\bar{Q}_{12}^{(k)} + 2\bar{Q}_{66}^{(k)}) \right] W_{mn} - \mathcal{B}_{mn}^{(k)} \\
 \mathcal{F}_{mn}^{(k)} &= - \left[\beta^3 \bar{Q}_{22}^{(k)} + \alpha^2 \beta (\bar{Q}_{12}^{(k)} + 2\bar{Q}_{66}^{(k)}) \right] W_{mn} - \mathcal{D}_{mn}^{(k)}
 \end{aligned} \tag{11.4.18}$$

11.4.3 Antisymmetric Angle-Ply Laminates

The simply supported (SS-2) boundary conditions in (11.4.4a,b) are satisfied by

$$u_0(x, y, t) = \sum_{n=1}^{\infty} \sum_{m=1}^{\infty} U_{mn}(t) \sin \alpha x \cos \beta y \tag{11.4.19a}$$

$$v_0(x, y, t) = \sum_{n=1}^{\infty} \sum_{m=1}^{\infty} V_{mn}(t) \cos \alpha x \sin \beta y \tag{11.4.19b}$$

and (w_0, ϕ_x, ϕ_y) have the same expansions as in Eqs. (11.4.5c-e). Substituting the expansions in Eqs. (11.4.19a,b) into Eqs. (11.2.16)–(11.2.20), we obtain equations of the form in (11.4.7a)

$$[\hat{S}]\{\Delta\} + [\hat{M}]\{\ddot{\Delta}\} = \{F\} \tag{11.4.20}$$

with the following coefficients

$$\begin{aligned}
 \hat{s}_{11} &= A_{11}\alpha^2 + A_{66}\beta^2, \quad \hat{s}_{12} = (A_{12} + A_{66})\alpha\beta \\
 \hat{s}_{13} &= -c_1 (3E_{16}\alpha^2 + E_{26}\beta^2) \beta \\
 \hat{s}_{14} &= 2\hat{B}_{16}\alpha\beta, \quad \hat{s}_{15} = \hat{B}_{16}\alpha^2 + \hat{B}_{26}\beta^2 \\
 \hat{s}_{22} &= A_{66}\alpha^2 + A_{22}\beta^2, \quad \hat{s}_{23} = -c_1 (E_{16}\alpha^2 + 3E_{26}\beta^2) \alpha \\
 \hat{s}_{24} &= \hat{s}_{15}, \quad \hat{s}_{25} = 2\hat{B}_{26}\alpha\beta \\
 \hat{s}_{33} &= \bar{A}_{55}\alpha^2 + \bar{A}_{44}\beta^2 + c_1^2 [H_{11}\alpha^4 + 2(H_{12} + 2H_{66})\alpha^2\beta^2 + H_{22}\beta^4] \\
 \hat{s}_{34} &= \bar{A}_{55}\alpha - c_1 [\hat{F}_{11}\alpha^3 + (\hat{F}_{12} + 2\hat{F}_{66})\alpha\beta^2] \\
 \hat{s}_{35} &= \bar{A}_{44}\beta - c_1 [\hat{F}_{22}\beta^3 + (\hat{F}_{12} + 2\hat{F}_{66})\alpha^2\beta] \\
 \hat{s}_{44} &= \bar{A}_{55} + \bar{D}_{11}\alpha^2 + \bar{D}_{66}\beta^2, \quad \hat{s}_{45} = (\bar{D}_{12} + \bar{D}_{66})\alpha\beta \\
 \hat{s}_{55} &= \bar{A}_{44} + \bar{D}_{66}\alpha^2 + \bar{D}_{22}\beta^2
 \end{aligned} \tag{11.4.21}$$

The mass and coefficients with hat and overbar are the same as those defined in Eqs. (11.4.8) and (11.4.9), and thermal effects are not considered.

The in-plane stresses in each layer can be computed from the equations

$$\begin{Bmatrix} \sigma_{xx} \\ \sigma_{yy} \\ \sigma_{xy} \end{Bmatrix}^{(k)} = \begin{bmatrix} \bar{Q}_{11} & \bar{Q}_{12} & \bar{Q}_{16} \\ \bar{Q}_{12} & \bar{Q}_{22} & \bar{Q}_{26} \\ \bar{Q}_{16} & \bar{Q}_{26} & \bar{Q}_{66} \end{bmatrix}^{(k)} \left(\begin{Bmatrix} \varepsilon_{xx}^{(0)} \\ \varepsilon_{yy}^{(0)} \\ \gamma_{xy}^{(0)} \end{Bmatrix} + z \begin{Bmatrix} \varepsilon_{xx}^{(1)} \\ \varepsilon_{yy}^{(1)} \\ \gamma_{xy}^{(1)} \end{Bmatrix} + z^3 \begin{Bmatrix} \varepsilon_{xx}^{(3)} \\ \varepsilon_{yy}^{(3)} \\ \gamma_{xy}^{(3)} \end{Bmatrix} \right) \quad (11.4.22)$$

$$\begin{Bmatrix} \varepsilon_{xx}^{(0)} \\ \varepsilon_{yy}^{(0)} \\ \gamma_{xy}^{(0)} \end{Bmatrix} = \sum_{m=1}^{\infty} \sum_{n=1}^{\infty} \left\{ \begin{array}{c} \alpha U_{mn} \cos \frac{m\pi x}{a} \cos \frac{n\pi y}{b} \\ \beta V_{mn} \cos \alpha x \cos \beta y \\ -(\beta U_{mn} + \alpha V_{mn}) \sin \alpha x \sin \beta y \end{array} \right\} \quad (11.4.23a)$$

$$\begin{Bmatrix} \varepsilon_{xx}^{(1)} \\ \varepsilon_{yy}^{(1)} \\ \gamma_{xy}^{(1)} \end{Bmatrix} = - \sum_{m=1}^{\infty} \sum_{n=1}^{\infty} \left\{ \begin{array}{c} \alpha X_{mn} \sin \alpha x \sin \beta y \\ \beta Y_{mn} \sin \alpha x \sin \beta y \\ -(\beta X_{mn} + \alpha Y_{mn}) \cos \alpha x \cos \beta y \end{array} \right\} \quad (11.4.23b)$$

$$\begin{Bmatrix} \varepsilon_{xx}^{(3)} \\ \varepsilon_{yy}^{(3)} \\ \gamma_{xy}^{(3)} \end{Bmatrix} = c_1 \sum_{m=1}^{\infty} \sum_{n=1}^{\infty} \left\{ \begin{array}{c} (\alpha X_{mn} + \alpha^2 W_{mn}) \sin \alpha x \sin \beta y \\ (\beta Y_{mn} + \beta^2 W_{mn}) \sin \alpha x \sin \beta y \\ -(\beta X_{mn} + \alpha Y_{mn} + 2\alpha\beta W_{mn}) \cos \alpha x \cos \beta y \end{array} \right\} \quad (11.4.23c)$$

The transverse stresses determined from the equilibrium equations of 3-D elasticity are

$$\begin{aligned} \sigma_{xz}^{(k)}(x, y, z) = & \sum_{m=1}^{\infty} \sum_{n=1}^{\infty} \left[(z - z_k) \bar{A}_{mn}^{(k)} + \frac{1}{2} (z^2 - z_k^2) \bar{B}_{mn}^{(k)} + \frac{c_1}{4} (z^4 - z_k^4) \bar{E}_{mn}^{(k)} \right] \\ & + \sigma_{xz}^{(k-1)}(x, y, z_k) \end{aligned} \quad (11.4.24a)$$

$$\begin{aligned} \sigma_{yz}^{(k)}(x, y, z) = & \sum_{m=1}^{\infty} \sum_{n=1}^{\infty} \left[(z - z_k) \bar{C}_{mn}^{(k)} + \frac{1}{2} (z^2 - z_k^2) \bar{D}_{mn}^{(k)} + \frac{c_1}{4} (z^4 - z_k^4) \bar{F}_{mn}^{(k)} \right] \\ & + \sigma_{yz}^{(k-1)}(x, y, z_k) \end{aligned} \quad (11.4.24b)$$

where

$$\begin{aligned} \bar{A}_{mn}^{(k)} = & \left[\left(\alpha^2 \bar{Q}_{11}^{(k)} + \beta^2 \bar{Q}_{66}^{(k)} \right) U_{mn} + \alpha\beta \left(\bar{Q}_{12}^{(k)} + \bar{Q}_{66}^{(k)} \right) V_{mn} \right] \sin \alpha x \cos \beta y \\ & + \left[2\alpha\beta \bar{Q}_{16}^{(k)} U_{mn} + \left(\alpha^2 \bar{Q}_{16}^{(k)} + \beta^2 \bar{Q}_{26}^{(k)} \right) V_{mn} \right] \cos \alpha x \sin \beta y \end{aligned}$$

$$\begin{aligned} \bar{B}_{mn}^{(k)} = & \left[\left(\alpha^2 \bar{Q}_{11}^{(k)} + \beta^2 \bar{Q}_{66}^{(k)} \right) X_{mn} + \alpha\beta \left(\bar{Q}_{12}^{(k)} + \bar{Q}_{66}^{(k)} \right) Y_{mn} \right] \cos \alpha x \sin \beta y \\ & + \left[2\alpha\beta \bar{Q}_{16}^{(k)} X_{mn} + \left(\alpha^2 \bar{Q}_{16}^{(k)} + \beta^2 \bar{Q}_{26}^{(k)} \right) Y_{mn} \right] \sin \alpha x \cos \beta y \end{aligned}$$

$$\begin{aligned} \bar{C}_{mn}^{(k)} = & \left[\left(\alpha^2 \bar{Q}_{16}^{(k)} + \beta^2 \bar{Q}_{26}^{(k)} \right) U_{mn} + 2\alpha\beta \bar{Q}_{16}^{(k)} V_{mn} \right] \sin \alpha x \cos \beta y \\ & + \left[\alpha\beta \left(\bar{Q}_{12}^{(k)} + \bar{Q}_{66}^{(k)} \right) U_{mn} + \left(\alpha^2 \bar{Q}_{66}^{(k)} + \beta^2 \bar{Q}_{22}^{(k)} \right) V_{mn} \right] \cos \alpha x \sin \beta y \end{aligned}$$

$$\begin{aligned}
\bar{\mathcal{D}}_{mn}^{(k)} &= \left[\left(\alpha^2 \bar{Q}_{16}^{(k)} + \beta^2 \bar{Q}_{66}^{(k)} \right) X_{mn} + 2\alpha\beta \bar{Q}_{26}^{(k)} Y_{mn} \right] \cos \alpha x \sin \beta y \\
&\quad + \left[\alpha\beta \left(\bar{Q}_{12}^{(k)} + \bar{Q}_{66}^{(k)} \right) X_{mn} + \left(\alpha^2 \bar{Q}_{66}^{(k)} + \beta^2 \bar{Q}_{22}^{(k)} \right) Y_{mn} \right] \sin \alpha x \cos \beta y \\
\bar{\mathcal{E}}_{mn}^{(k)} &= - \left[\alpha^3 \bar{Q}_{11}^{(k)} + \alpha\beta^2 \left(\bar{Q}_{12}^{(k)} + 2\bar{Q}_{66}^{(k)} \right) \right] W_{mn} \cos \alpha x \sin \beta y \\
&\quad - \left(3\bar{Q}_{16}^{(k)} \alpha^2 \beta + \bar{Q}_{26}^{(k)} \beta^3 \right) W_{mn} \sin \alpha x \cos \beta y - \bar{\mathcal{B}}_{mn}^{(k)} \\
\bar{\mathcal{F}}_{mn}^{(k)} &= - \left(\bar{Q}_{16}^{(k)} \alpha^3 + 3\bar{Q}_{26}^{(k)} \alpha\beta^2 \right) W_{mn} \cos \alpha x \sin \beta y \\
&\quad - \left[\alpha^2 \beta \left(\bar{Q}_{12}^{(k)} + 2\bar{Q}_{66}^{(k)} \right) + \beta^3 \bar{Q}_{22}^{(k)} \right] W_{mn} \sin \alpha x \cos \beta y - \bar{\mathcal{D}}_{mn}^{(k)} \quad (11.4.25)
\end{aligned}$$

11.4.4 Numerical Results

Bending Analysis

Tables 11.4.1 and 11.4.2 contain nondimensionalized center deflections and stresses obtained with 3-D elasticity theory (ELS), third-order shear deformation plate theory (TSDT), first-order shear deformation theory (FSDT), and classical laminate plate theory (CLPT) for the following two problems (see Reddy [25]):

1. A three-ply (0/90/0) square ($a/b = 1$) laminate with layers of equal thickness and subjected to sinusoidally distributed transverse load.
2. A four-ply (0/90/90/0) square ($a/b = 1$) laminate with layers of equal thickness and subjected to sinusoidally distributed transverse load.

The material properties of a ply are assumed to be

Material 1:

$$\begin{aligned}
E_1 &= 25 \times 10^6 \text{ psi (175 GPa)}, \quad E_2 = 10^6 \text{ psi (7 GPa)} \\
G_{12} &= G_{13} = 0.5 \times 10^6 \text{ psi (3.5 GPa)} \\
G_{23} &= 0.2 \times 10^6 \text{ psi (1.4 GPa)}, \quad \nu_{12} = \nu_{13} = 0.25 \quad (11.4.26)
\end{aligned}$$

The following nondimensionalized quantities are reported in the tables:

$$\begin{aligned}
\bar{w} &= w_0 \left(\frac{a}{2}, \frac{b}{2} \right) \left(\frac{E_2 h^3}{a^4 q_0} \right), \quad \bar{\sigma}_{xx} = \sigma_{xx} \left(\frac{a}{2}, \frac{b}{2}, \frac{h}{2} \right) \left(\frac{h^2}{b^2 q_0} \right) \\
\bar{\sigma}_{yy} &= \sigma_{yy} \left(\frac{a}{2}, \frac{b}{2}, \frac{h}{4} \right) \left(\frac{h^2}{b^2 q_0} \right), \quad \bar{\sigma}_{xy} = \sigma_{xy} \left(0, 0, \frac{h}{2} \right) \left(\frac{h^2}{b^2 q_0} \right) \\
\bar{\sigma}_{yz} &= \sigma_{yz} \left(\frac{a}{2}, 0, 0 \right) \left(\frac{h}{b q_0} \right), \quad \bar{\sigma}_{xz} = \sigma_{xz} \left(0, \frac{b}{2}, 0 \right) \left(\frac{h}{b q_0} \right) \quad (11.4.27)
\end{aligned}$$

The origin of the coordinate system is taken at the lower left corner of the plate.

Table 11.4.1: Nondimensionalized center deflections and stresses in simply supported (SS-1) three-layer (0/90/0) square laminates under sinusoidally distributed transverse load.

FSDT								
a/h	Variable	ELS [†]	TSDT	$K = 1$	$K = \frac{5}{6}$	$K = \frac{3}{4}$	$K = \frac{1}{2}$	CLPT
4	$\bar{w} \times 10^2$	—	1.9218	1.5681	1.7758	1.9122	2.5770	0.4313
	$\bar{\sigma}_{xx}$	0.755	0.7345	0.4475	0.4370	0.4308	0.4065	0.5387
	$(\bar{\sigma}_{yz})^\ddagger$	0.217	0.1832	0.1227	0.1561	0.1793	0.3030	—
10	$\bar{w} \times 10^2$	—	0.7125	0.6306	0.6693	0.6949	0.8210	0.4313
	$\bar{\sigma}_{xx}$	0.590	0.5684	0.5172	0.5134	0.5109	0.4993	0.5387
	$\bar{\sigma}_{yz}$	0.123	0.1033	0.0735	0.0915	0.1039	0.1723	—
100	$\bar{w} \times 10^2$	—	0.4342	0.4333	0.4337	0.4340	0.4353	0.4313
	$\bar{\sigma}_{xx}$	0.552	0.5390	0.5385	0.5384	0.5384	0.5382	0.5387
	$\bar{\sigma}_{yz}$	0.094	0.0750	0.0586	0.0703	0.0782	0.1174	—

[†] 3-D elasticity solution of Pagano [53].[‡] The second line corresponds to stresses computed from 3-D equilibrium equations.**Table 11.4.2:** Nondimensionalized maximum deflections and stresses in simply supported (SS-1) symmetric cross-ply (0/90/90/0) square laminates under sinusoidally distributed transverse load.

a/h	Source	$\bar{w} \times 10^2$	$\bar{\sigma}_{xx}$	$\bar{\sigma}_{yy}$	$\bar{\sigma}_{yz}$	$\bar{\sigma}_{xz}$	$\bar{\sigma}_{xy}$
4	ELS [†]	1.954	0.720	0.663	0.292	0.219	0.0467
	TSDT	1.894	0.665	0.632	0.239	0.206	0.0440
	FSDT	1.710	0.406	0.576	0.196 0.280	0.140 0.269	0.0308
10	ELS	0.743	0.559	0.401	0.196	0.301	0.0275
	TSDT	0.715	0.546	0.389	0.153 0.192	0.264 0.307	0.0268
	FDST	0.663	0.4989	0.361	0.130 0.181	0.167 0.318	0.0241
20	ELS	0.517	0.543	0.308	0.156	0.328	0.0230
	TSDT	0.506	0.539	0.304	0.123 0.154	0.282 0.330	0.0228
	FDST	0.491	0.527	0.296	0.109 0.150	0.175 0.333	0.0221
100	ELS	0.438	0.539	0.276	0.141	0.337	0.0216
	TSDT	0.434	0.539	0.271	0.112 0.139	0.290 0.339	0.0213
	FDST	0.434	0.538	0.270	0.101 0.139	0.178 0.339	0.0213

[†] 3-D elasticity solution of Pagano and Hatfield [54].[‡] Equilibrium-derived stresses.

From the results it is clear that the third-order theory gives more accurate results for deflections and stresses when compared to the first-order shear deformation plate theory with $K = 5/6$. It is known that the shear correction factor K depends on the lamina properties and the stacking sequence. The fact that no shear correction coefficients are needed in the third-order theory makes it more convenient to use. In general, the equilibrium-derived transverse shear stresses compare more favorably with the elasticity solution than those obtained from the constitutive equations for equivalent single-layer theories.

Figure 11.4.3 contains plots of nondimensionalized center deflection, $\bar{w} = w_0(E_2 h^3/q_0 a^4)$, versus side-to-thickness ratio a/h for Problem 2 (a square, symmetric cross-ply laminate (0/90/90/0) under sinusoidally distributed load; Material 1). Compared to the elasticity solution, the third-order theory underpredicts deflection by 3% while the first-order theory underpredicts by about 12.5% for $a/h = 4$; for $a/h = 10$, the errors are 2.4% in TSDT and 11.8% in FSDT. The errors are much less at lower values of a/h .

Figures 11.4.4 and 11.4.5 show distributions of nondimensionalized [$\bar{\sigma} = \sigma(h^2/q_0 a^2)$] maximum normal stresses $\bar{\sigma}_{xx}$ and $\bar{\sigma}_{yy}$ predicted by the classical, first-order, and third-order plate theories through the thickness of a square symmetric cross-ply laminate (0/90/90/0) under sinusoidally distributed load (Material 1; $a/h = 4$ and 10). The third-order theory predicts a cubic variation whereas the classical and first-order theories predict linear variation of the stresses. Plots of constitutively derived and equilibrium-derived transverse shear stresses $\bar{\sigma}_{xz} = \sigma_{xz}(h/q_0 a)$ and $\bar{\sigma}_{yz} = \sigma_{yz}(h/q_0 a)$ are shown as functions of thickness in Figures 11.4.6 and 11.4.7, respectively, for a square, symmetric cross-ply laminate (0/90/90/0) under sinusoidally distributed load (Material 1; $a/h = 10$). The stresses

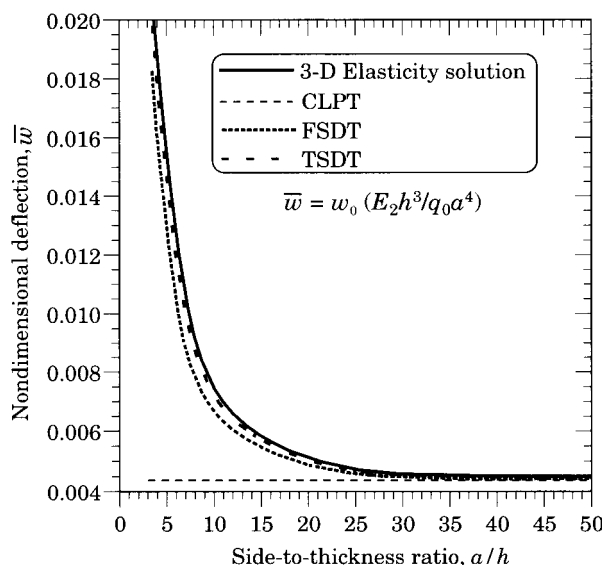


Figure 11.4.3: Plots of nondimensionalized center transverse deflection versus side-to-thickness ratio of a symmetric cross-ply (0/90/90/0) laminate under sinusoidally distributed load (Material 1).

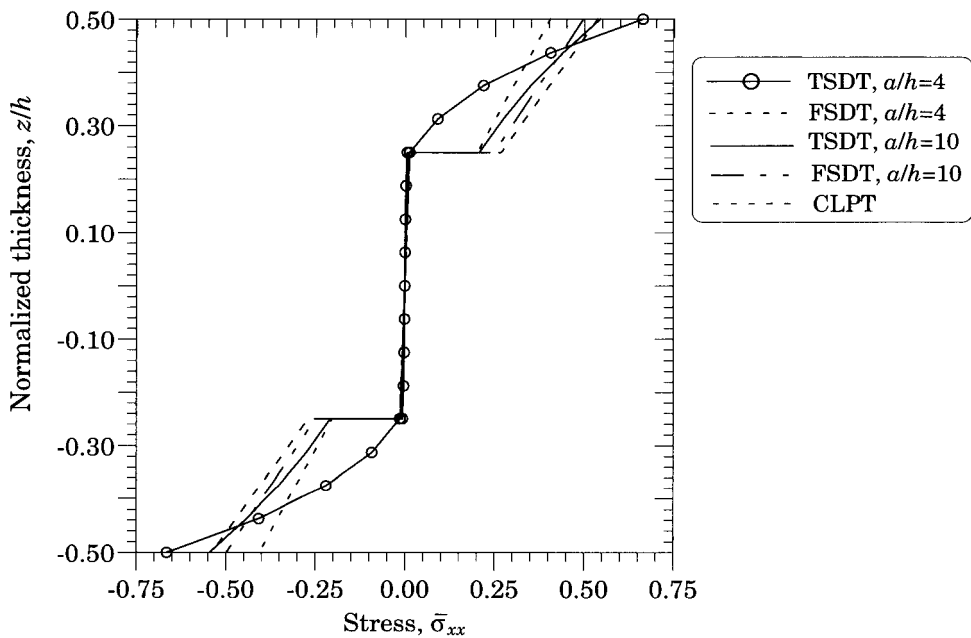


Figure 11.4.4: Comparison of center normal stress $\bar{\sigma}_{xx}$ distributions predicted by the classical, first-order, and third-order plate theories.

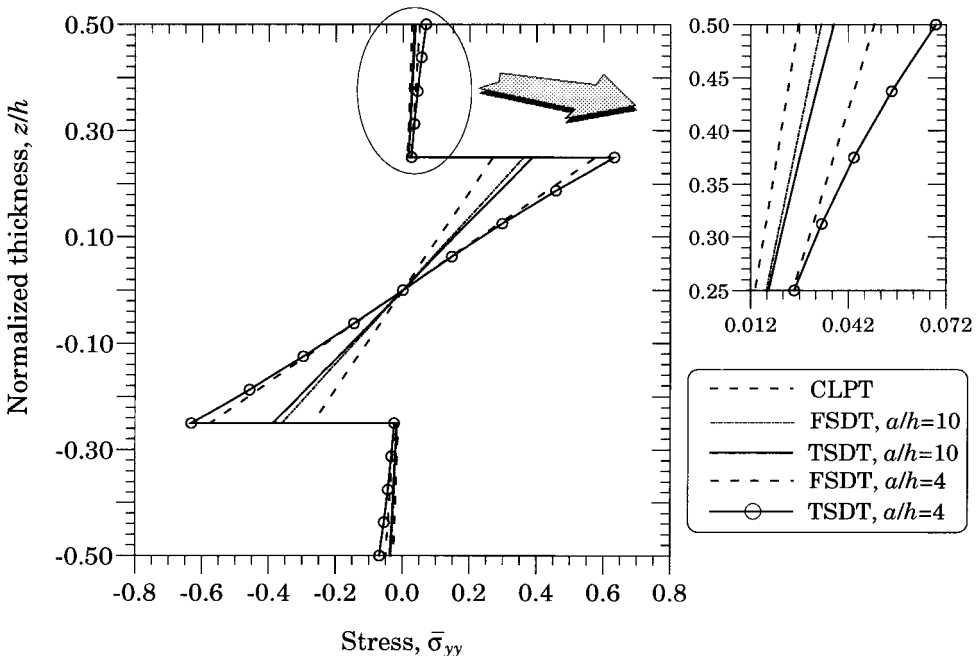


Figure 11.4.5: Comparison of normal stress $\bar{\sigma}_{yy}$ distributions predicted by the classical, first-order, and third-order plate theories.

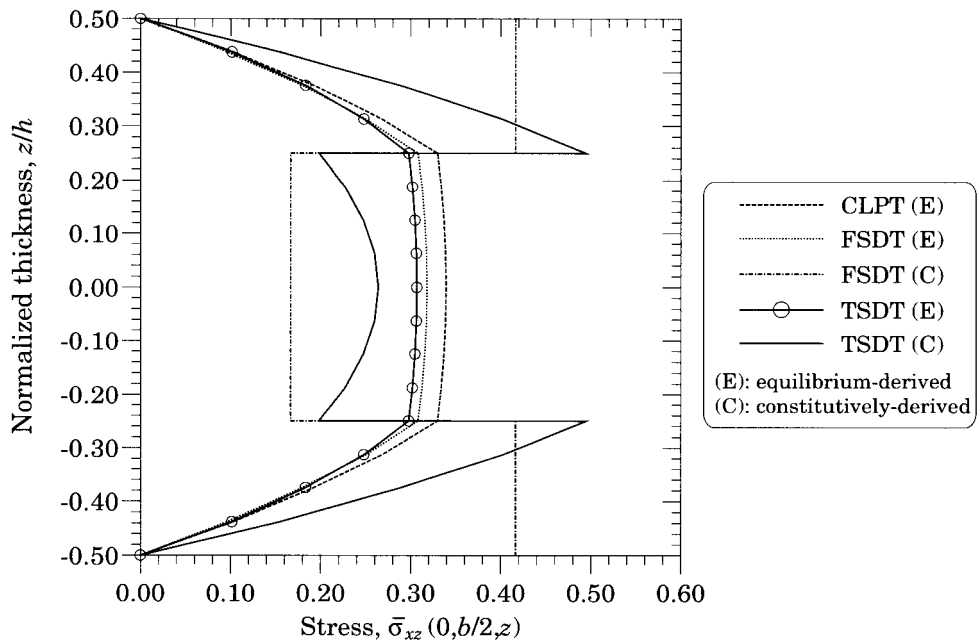


Figure 11.4.6: Plots of constitutively derived (C) and equilibrium-derived (E) transverse shear stresses $\bar{\sigma}_{xz}$ as functions of thickness coordinate.

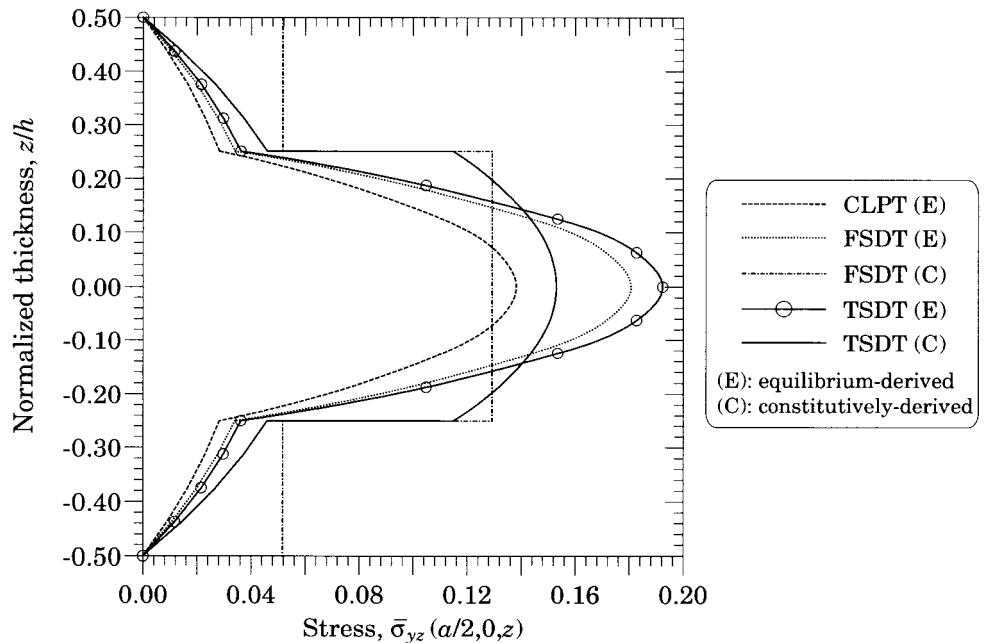


Figure 11.4.7: Plots of constitutively derived (C) and equilibrium-derived (E) transverse shear stresses $\bar{\sigma}_{yz}$ as functions of thickness coordinate.

derived using the equilibrium equations are continuous through thickness because they are made to satisfy the interface continuity conditions (in determining the constants of integration), while the stresses computed using constitutive equations are always discontinuous for all equivalent single-layer theories due to the continuity of the transverse shear strains through thickness of the laminate. The third-order theory correctly satisfies vanishing of transverse shear stresses at the top and bottom of the laminate, because the displacement field in TSDT is derived to satisfy these conditions *a priori*.

Figure 11.4.8 shows the effect of material anisotropy on the deflections of antisymmetric cross-ply $(0/90)_n$ ($n = 1, 3$) square laminates under sinusoidal loading (SS-1) for $a/h = 10$, $G_{12} = G_{13} = 0.5E_2$, $G_{23} = 0.2E_2$, $\nu_{12} = 0.25$, and $a/h = 10$. The results predicted by FSDT and TSDT are very close; it is interesting to note that the first-order theory overpredicts deflections for the two-layer case and underpredicts for the six-layer case when compared to TSDT. As noted earlier, bending-stretching coupling is negligible for laminates with six or more layers; hence the deflections of a two-layer laminate without accounting for the coupling are virtually the same as those obtained for the six-layer laminate (see Table 11.4.3).

The deflections of antisymmetric angle-ply $(45/-45)_n$ ($n = 1, 3$) square laminates under sinusoidal loading are presented in Figure 11.4.9 for various ratios of moduli $\frac{E_1}{E_2}$ ($G_{12} = G_{13} = 0.6E_2$, $G_{23} = 0.5E_2$, $\nu_{12} = 0.25$, $a/h = 10$). The effect of coupling between bending and extension is increasingly more pronounced with an increasing degree of material anisotropy. Even at low modulus ratios, the coupling terms cannot be neglected.

Table 11.4.3: Maximum deflections, $\bar{w} \times 10^2$, of simply supported (SS-1) antisymmetric cross-ply $(0/90/0/90/\dots)$ square plates subjected to sinusoidally distributed transverse load.

$\frac{a}{h}$	$n = 2$		$n = 6$	
	FSDT	TSDT	FSDT	TSDT
4	2.1492	1.9985	1.5473	1.5411
10	1.2373	1.2161	0.6354	0.6382
20	1.1070	1.1018	0.5052	0.5060
50	1.0705	1.0697	0.4687	0.4688
100	1.0653	1.0651	0.4635	0.4635
CLPT	1.0636		0.4618	

Table 11.4.4 contains a comparison of the maximum deflections of two- and six-layer $(\theta/-\theta/\dots)$ antisymmetric angle-ply laminates under sinusoidal loading with different fiber orientations. The following material properties are assumed

Material 2:

$$\frac{E_1}{E_2} = 40, \quad \frac{G_{12}}{E_2} = 0.6, \quad \frac{G_{23}}{E_2} = 0.5, \quad \nu_{12} = \nu_{13} = 0.25 \quad (11.4.28)$$

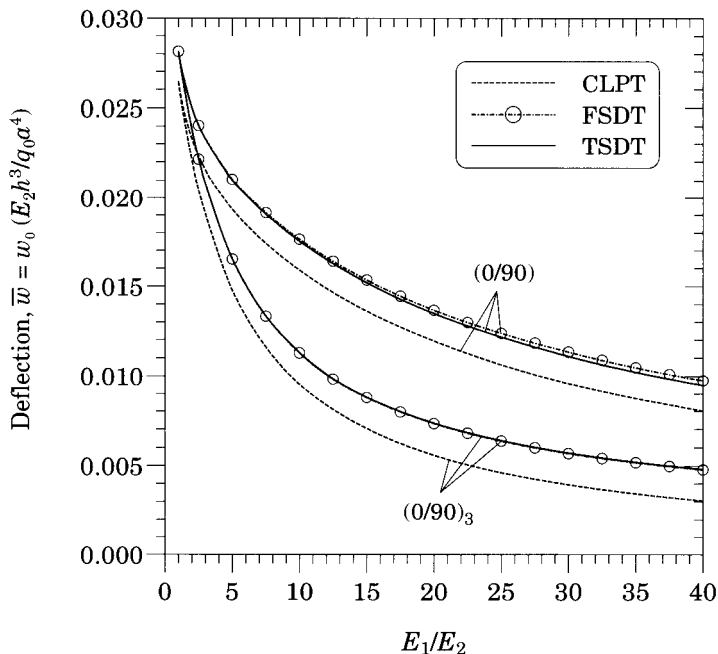


Figure 11.4.8: The effect of material anisotropy on the nondimensionalized deflections \bar{w} of simply supported (SS-1) antisymmetric cross-ply $(0/90)_n$ ($n = 1, 3$) square laminates.

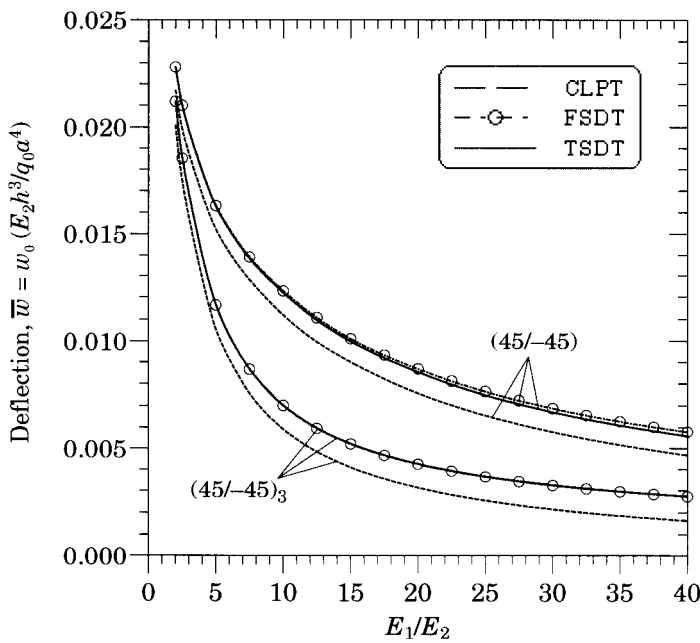


Figure 11.4.9: The effect of material anisotropy on the nondimensionalized deflections \bar{w} of simply supported (SS-2) antisymmetric angle-ply $(45/-45)_n$ ($n = 1, 3$) square laminates.

As in the case of antisymmetric cross-ply plates, the coupling causes a significant reduction of the plate stiffness, with the most critical case being for $\theta = 45^\circ$. This observation can be explained by the fact that the magnitudes of the bending-stretching terms ($B_{16}, B_{26}, E_{16}, E_{26}, \dots$) are the largest at this particular fiber orientation for a given number of layers.

Table 11.4.4: Maximum deflections, $\bar{w} \times 10^2$, of simply supported (SS-2), antisymmetric angle-ply ($\theta/-\theta/\dots$) square plates subjected to sinusoidal loading.

$\frac{a}{h}$	Source	$\theta = 5^\circ$		$\theta = 30^\circ$		$\theta = 45^\circ$	
		$n = 2$	$n = 6$	$n = 2$	$n = 6$	$n = 2$	$n = 6$
4	TSDT	1.2625	1.2282	1.0838	0.8851	1.0203	0.8375
	FSDT	1.3165	1.2647	1.2155	0.8994	1.1576	0.8531
10	TSDT	0.4848	0.4485	0.5916	0.3007	0.5581	0.2745
	FSDT	0.4883	0.4491	0.6099	0.2989	0.5773	0.2728
20	TSDT	0.3579	0.3209	0.5180	0.2127	0.4897	0.1905
	FSDT	0.3586	0.3208	0.5224	0.2121	0.4944	0.1899
50	TSDT	0.3215	0.2842	0.4972	0.1878	0.4704	0.1668
	FSDT	0.3216	0.2841	0.4979	0.1877	0.4712	0.1667
100	TSDT	0.3162	0.2789	0.4942	0.1842	0.4676	0.1634
	FSDT	0.3162	0.2789	0.4944	0.1842	0.4678	0.1633
	CLPT	0.3145	0.2771	0.4932	0.1831	0.4667	0.1622

Natural Vibration

Fundamental frequencies, $\bar{\omega} = \omega_{11}(a^2/h)\sqrt{\rho/E_2}$, of simply supported laminates are presented for the following three cases:

1. Four-layer (0/90/90/0) symmetric cross-ply square plate (SS-1).
2. Two- and six-layer (0/90/...) antisymmetric cross-ply square plates (SS-1).
3. Two- and six-layer ($\theta/-\theta/\dots$) antisymmetric angle-ply square plates (SS-2) with $\theta = 5^\circ, 30^\circ$, and 45° .

The rotary inertias are included in all cases and theories. Table 11.4.5 contains the nondimensionalized fundamental frequencies $\bar{\omega} = \omega(a^2/h)\sqrt{\rho/E_2}$ of the first laminate as a function of modulus ratio E_1/E_2 ($G_{12} = G_{13} = 0.6E_2$, $G_{23} = 0.5E_2$, $\nu_{12} = 0.25$) for $a/h = 5$ and 10 . The fundamental natural frequencies $\bar{\omega}$ of antisymmetric cross-ply laminates (Material 2) as functions of the side-to-thickness are presented in Figure 11.4.10. Table 11.4.6 contains natural frequencies of two-layer and six-layer antisymmetric angle-ply laminates. All these results indicate that there is no significant difference between the predictions of FSDT and TSDT. However, TSDT does not require shear correction factors.

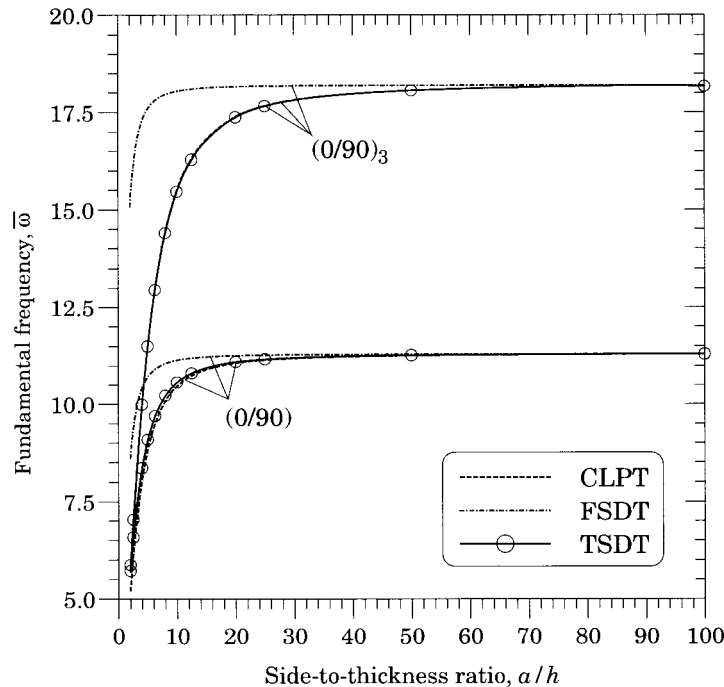


Figure 11.4.10: Plots of nondimensionalized fundamental frequency versus side-to-thickness ratio for cross-ply $(0/90)_n$ ($n = 1, 3$) square laminates.

Table 11.4.5: Nondimensionalized frequencies $\bar{\omega}$ of $(0/90/90/0)$ cross-ply laminates as functions of modulus ratio.

E_1/E_2	a/h	ELS [†]	TSDT	FSDT	CLPT
3	5	6.618	6.560	6.570	7.299
	10	—	7.247	7.243	7.475
10	5	8.210	8.272	8.298	10.316
	10	—	9.853	9.841	10.563
20	5	9.560	9.526	9.567	13.511
	10	—	12.238	12.218	13.835
30	5	10.272	10.272	10.326	16.084
	10	—	13.892	13.864	16.470
40	5	10.752	10.787	10.854	18.299
	10	—	15.143	15.107	18.738

[†] Approximate 3-D solution of Noor [55].

Table 11.4.6: Nondimensionalized fundamental frequencies, $\bar{\omega} = \omega_{11} \frac{a^2}{h} \sqrt{\frac{\rho}{E_2}}$, of simply supported (SS-2), antisymmetric angle-ply ($\theta/-\theta/\dots$) square plates.

$\frac{a}{h}$	Source	$\theta = 5^\circ$		$\theta = 30^\circ$		$\theta = 45^\circ$	
		$n = 2$	$n = 6$	$n = 2$	$n = 6$	$n = 2$	$n = 6$
4	TSDT	8.715	8.859	9.446	10.577	9.759	10.895
	FSDT	8.531	8.737	8.917	10.502	9.161	10.805
	CLPT	14.514	16.563	13.012	21.647	13.506	13.766
10	TSDT	14.230	14.848	12.873	18.170	13.263	19.025
	FSDT	14.179	14.840	12.681	18.226	13.044	19.025
	CLPT	17.500	18.819	14.031	23.165	14.439	24.611
20	TSDT	16.656	17.619	13.849	21.648	14.246	22.877
	FSDT	16.641	17.622	13.790	21.679	14.179	22.913
	CLPT	17.754	18.952	14.187	23.320	14.587	24.773
50	TSDT	17.626	18.753	14.174	23.067	14.572	24.480
	FSDT	17.623	18.754	14.164	23.074	14.561	24.488
	CLPT	17.820	18.989	14.231	23.364	14.630	24.819
100	TSDT	17.780	18.935	14.223	23.295	14.621	24.739
	FSDT	17.780	18.935	14.220	23.297	14.618	24.741
	CLPT	17.830	18.995	14.237	23.371	14.636	24.825

Buckling Analysis

The uniaxial critical buckling loads of a four-layer (0/90/90/0) cross-ply plate (Material 2) with various side-to-thickness ratios are compared in Table 11.4.7. The buckling loads of the same laminate as a function of modulus ratio E_1/E_2 are presented in Table 11.4.8. The results are also compared with approximate 3-D elasticity results obtained by Noor [57]. In Figure 11.4.11, the buckling loads of two-layer and six-layer (0/90/0/...) antisymmetric cross-ply laminates are shown as a function of the side-to-thickness ratio. Table 11.4.9 contains critical buckling loads for the two-layer and six-layer antisymmetric angle-ply laminates. Both TSDT and FSDT give very good results and the difference between them is not very significant.

Table 11.4.7: Nondimensionalized uniaxial buckling loads, $\bar{N} = N_{cr} \frac{a^2}{E_2 h^3}$, of simply supported (SS-1) symmetric cross-ply (0/90/90/0) square plates.

$\frac{a}{h}$	CLPT	FSDT	TSDT
5	36.160	11.575	11.997
10	36.160	23.453	23.340
20	36.160	31.707	31.660
50	36.160	35.356	35.347
100	36.160	35.955	35.953

Table 11.4.8: Effect of material anisotropy on the uniaxial buckling loads, $\bar{N} = N_{cr} \frac{a^2}{E_2 h^3}$, of symmetric cross-ply (0/90/90/0) square plates ($G_{12} = G_{13} = 0.6E_2$, $G_{23} = 0.5E_2$, $\nu_{12} = 0.25$, $a/h = 10$).

E_1/E_2	CLPT	FSDT	TSDT	ELS [57]
3	5.754	5.399	5.114	5.304
10	11.492	9.965	9.777	9.762
20	19.712	15.351	15.298	15.019
30	27.936	19.756	19.957	19.304
40	36.160	23.453	23.340	22.881

Table 11.4.9: Nondimensionalized uniaxial buckling loads, $\bar{N} = N_{cr} \frac{a^2}{E_2 h^3}$, of simply supported (SS-2) antisymmetric angle-ply ($\theta/-\theta/\dots$) square plates.

$\frac{a}{h}$	Source	$\theta = 5^\circ$		$\theta = 30^\circ$		$\theta = 45^\circ$	
		$n = 2$	$n = 6$	$n = 2$	$n = 6$	$n = 2$	$n = 6$
5	TSDT	10.674	11.082	11.547	13.546	10.881	12.169
	FSDT	10.384	10.899	10.586	11.986	9.385	11.297
10	TSDT	20.989	22.592	17.127	33.701	18.154	32.405
	FSDT	20.752	22.562	16.613	33.903	17.552	32.525
20	TSDT	28.308	31.577	19.561	47.643	20.691	53.198
	FSDT	28.259	31.587	19.394	47.779	20.495	53.365
50	TSDT	31.519	35.657	20.379	53.951	21.539	60.760
	FSDT	31.511	35.660	20.350	53.981	21.505	60.798
100	TSDT	32.042	36.332	20.502	54.993	21.666	62.022
	FSDT	32.040	36.333	20.494	55.001	21.658	62.032
	CLPT	32.220	36.563	20.543	55.350	21.709	62.455

11.5 Lévy Solutions of Cross-Ply Laminates

11.5.1 Preliminary Comments

The Lévy type solutions for bending, natural vibration, and buckling of rectangular laminates of cross-ply constructions have been developed for the third-order theory of Reddy (see [34,41,42,44,48,50–52]). Here we present the solutions for static bending of cross-ply laminates (see Khdeir and Reddy [50,51]). For additional results, the reader may consult references at the end of the chapter. For the static case, the governing equations appropriate for the antisymmetric cross-ply laminate construction are given by

$$[L]\{\Delta\} = \{F\} \quad (11.5.1)$$

where

$$\{\Delta\}^T = \{u_0, v_0, w_0, \phi_x, \phi_y\}, \quad \{F\}^T = \{0, 0, q, 0, 0\} \quad (11.5.2a)$$

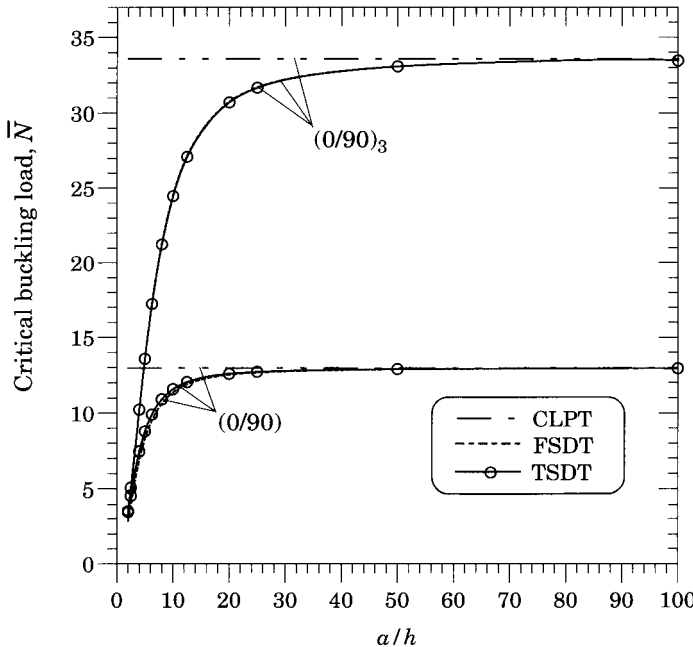


Figure 11.4.11: Critical buckling load [$\bar{N} = N_{cr}(a^2/E_2 h^3)$] versus side-to-thickness ratio for antisymmetric cross-ply $(0/90)_n$ ($n = 1, 3$) square laminates subjected to uniaxial compressive load (Material 2).

$$\begin{aligned}
 L_{11} &= A_{11}d_1^2 + A_{66}d_2^2, \quad L_{12} = (A_{12} + A_{66})d_1d_2 \\
 L_{13} &= -c_1[E_{11}d_1^3 + (E_{12} + 2E_{66})d_1d_2^2] \\
 L_{14} &= \hat{B}_{11}d_1^2 + \hat{B}_{66}d_2^2, \quad L_{15} = (\hat{B}_{12} + \hat{B}_{66})d_1d_2 \\
 L_{22} &= A_{66}d_1^2 + A_{22}d_2^2, \quad L_{23} = -c_1[E_{22}d_2^3 + (E_{12} + 2E_{66})d_1^2d_2] \\
 L_{24} &= L_{15}, \quad L_{25} = \hat{B}_{22}d_2^2 + \hat{B}_{66}d_1^2 \\
 L_{33} &= -\bar{A}_{55}d_1^2 - \bar{A}_{44}d_2^2 + c_1^2 [H_{11}d_1^4 + (2H_{12} + 4H_{66})d_1^2d_2^2 + H_{22}d_2^4] \\
 L_{34} &= (c_2\hat{D}_{55} - \hat{A}_{55})d_1 - c_1 [\hat{F}_{11}d_1^3 + (\hat{F}_{12} + 2\hat{F}_{66})d_1d_2^2] \\
 L_{35} &= (c_2\hat{D}_{44} - \hat{A}_{44})d_2 - c_1 [\hat{F}_{22}d_2^3 + (\hat{F}_{12} + 2\hat{F}_{66})d_1^2d_2] \\
 L_{44} &= -\bar{A}_{55} + \bar{D}_{11}d_1^2 + \bar{D}_{66}d_2^2, \quad L_{45} = (\bar{D}_{12} + \bar{D}_{66})d_1d_2 \\
 L_{55} &= -\bar{A}_{44} + \bar{D}_{22}d_2^2 + \bar{D}_{66}d_1^2
 \end{aligned} \tag{11.5.2b}$$

and

$$d_\alpha^i = \frac{\partial^i}{\partial x_\alpha^i}, \quad x_1 = x \text{ and } x_2 = y \tag{11.5.3}$$

11.5.2 Solution Procedure

A generalized Lévy type solution, in conjunction with the state-space concept can be used to determine bending solutions of cross-ply laminated rectangular plates with two parallel edges simply supported and other two having arbitrary combination of boundary conditions. Suppose that the edges $y = 0, b$ are simply supported, while the remaining ones ($x = \pm a/2$) may have arbitrary combinations of free, clamped, and simply supported edge conditions (see Figure 11.5.1).

The generalized displacements may be expressed as products of undetermined functions and known trigonometric functions so as to identically satisfy the simply supported boundary conditions at $y = 0, b$:

$$u_0 = w_0 = \phi_x = N_{yy} = M_{yy} = P_{yy} = 0 \quad (11.5.4)$$

A sinusoidal distribution of the transverse load is considered

$$q(x, y) = q_0 \cos \frac{\pi x}{a} \sin \frac{\pi y}{b} \quad (11.5.5)$$

The displacement quantities are represented as

$$\begin{Bmatrix} u_0(x, y) \\ v_0(x, y) \\ w_0(x, y) \\ \phi_x(x, y) \\ \phi_y(x, y) \end{Bmatrix} = \begin{Bmatrix} U_m(x) \sin \beta y \\ V_m(x) \cos \beta y \\ W_m(x) \sin \beta y \\ X_m(x) \sin \beta y \\ Y_m(x) \cos \beta y \end{Bmatrix} \quad (11.5.6)$$

where $\beta = m\pi/b$.

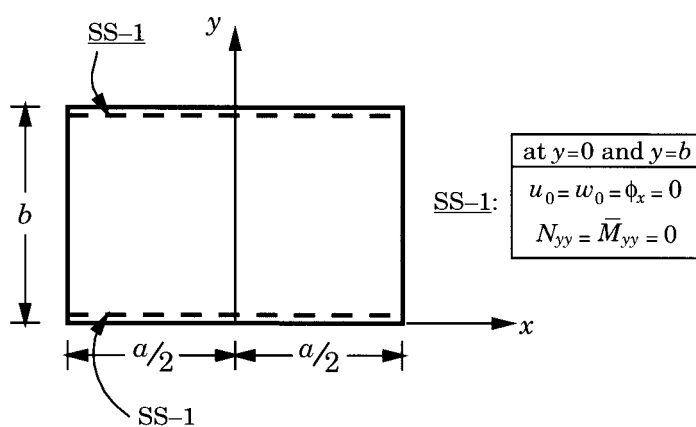


Figure 11.5.1: The coordinate system ($-a/2 \leq x \leq a/2, 0 \leq y \leq b$) and boundary conditions used on the simply supported edges for the Lévy solutions of rectangular cross-ply laminates using the third-order shear deformation theory.

Substitution of (11.5.6) into Eqs. (11.5.1) results in the following five differential equations:

$$\begin{aligned} U''_m &= C_1 U_m + C_2 V'_m + C_3 W'_m + C_4 W'''_m + C_5 X_m + C_6 Y'_m + f_1^T \sin \alpha x \\ V''_m &= C_7 U'_m + C_8 V_m + C_9 W_m + C_{10} W''_m + C_{11} X'_m + C_{12} Y_m + f_2^T \cos \alpha x \\ W''''_m &= C_{13} U'_m + C_{14} V_m + C_{15} W_m + C_{16} W''_m + C_{17} X'_m + C_{18} Y_m + f_3^T \cos \alpha x \\ X''_m &= C_{19} U_m + C_{20} V'_m + C_{21} W'_m + C_{22} W'''_m + C_{23} X_m + C_{24} Y'_m + f_4^T \sin \alpha x \\ Y''_m &= C_{25} U'_m + C_{26} V_m + C_{27} W_m + C_{28} W''_m + C_{29} X'_m + C_{30} Y_m + f_5^T \cos \alpha x \end{aligned} \quad (11.5.7)$$

where primes denote the derivative with respect to x , and the coefficients C_i are defined by

$$\begin{aligned} C_1 &= (e_7 e_{30} - e_3 e_{34})/e_0, \quad C_2 = (e_2 e_{30} - e_3 e_{29})/e_0 \\ C_3 &= (e_6 e_{30} - e_3 e_{33})/e_0, \quad C_4 = (e_5 e_{30} - e_3 e_{32})/e_0 \\ C_5 &= (e_8 e_{30} - e_3 e_{35})/e_0, \quad C_6 = (e_4 e_{30} - e_3 e_{31})/e_0 \\ C_7 &= (e_9 e_{39} - e_{12} e_{36})/C_0, \quad C_8 = (e_{14} e_{39} - e_{12} e_{41})/C_0 \\ C_9 &= (e_{16} e_{39} - e_{12} e_{43})/C_0, \quad C_{10} = (e_{13} e_{39} - e_{12} e_{40})/C_0 \\ C_{11} &= (e_{11} e_{39} - e_{12} e_{38})/C_0 \quad C_{12} = (e_{15} e_{39} - e_{12} e_{42})/C_0 \\ C_{19} &= (e_1 e_{34} - e_7 e_{28})/e_0, \quad C_{20} = (e_1 e_{29} - e_2 e_{28})/e_0 \\ C_{21} &= (e_1 e_{33} - e_6 e_{28})/e_0, \quad C_{22} = (e_1 e_{32} - e_5 e_{28})/e_0 \\ C_{23} &= (e_1 e_{35} - e_8 e_{28})/e_0, \quad C_{24} = (e_1 e_{31} - e_4 e_{28})/e_0 \\ C_{25} &= (e_{10} e_{36} - e_9 e_{37})/C_0, \quad C_{26} = (e_{10} e_{41} - e_{14} e_{37})/C_0 \\ C_{27} &= (e_{10} e_{43} - e_{16} e_{37})/C_0, \quad C_{28} = (e_{10} e_{40} - e_{13} e_{37})/C_0 \\ C_{29} &= (e_{10} e_{38} - e_{11} e_{37})/C_0, \quad C_{30} = (e_{10} e_{42} - e_{15} e_{37})/C_0 \\ C_{13} &= a_0(C_1 e_{21} + C_7 a_1 + C_{25} a_2 + C_{19} e_{23} + e_{26}) \\ C_{14} &= a_0(C_8 a_1 + C_{26} a_2 + e_{27}), \quad C_{15} = a_0(C_9 a_1 + C_{27} a_2 + e_{20}) \\ C_{16} &= a_0(e_{18} + C_3 e_{21} + C_{21} e_{23} + C_{10} a_1 + C_{28} a_2) \\ C_{17} &= a_0(e_{17} + C_5 e_{21} + C_{23} e_{23} + C_{11} a_1 + C_{29} a_2) \\ C_{18} &= a_0(e_{19} + C_{12} a_1 + C_{30} a_2), \quad e_0 = e_3 e_{28} - e_1 e_{30} \\ C_0 &= e_{12} e_{37} - e_{10} e_{39}, \quad a_0 = -1/(C_4 e_{21} + C_{22} e_{23} + e_{25}) \\ a_1 &= C_2 e_{21} + C_{20} e_{23} + e_{22}, \quad a_2 = C_6 e_{21} + C_{24} e_{23} + e_{24} \end{aligned} \quad (11.5.8)$$

where

$$\begin{aligned} e_1 &= A_{11}, \quad e_2 = -\beta(A_{12} + A_{66}), \quad e_3 = \hat{B}_{11} \\ e_4 &= -\beta(\hat{B}_{12} + \hat{B}_{66}), \quad e_5 = -c_1 E_{11} \\ e_6 &= \beta^2 c_1(E_{12} + 2E_{66}), \quad e_7 = -\beta^2 A_{66} \\ e_8 &= -\beta^2 \hat{B}_{66}, \quad e_9 = -e_2, \quad e_{10} = A_{66}, \quad e_{11} = -e_4 \\ e_{12} &= \hat{B}_{66}, \quad e_{13} = -c_1 \beta(E_{12} + 2E_{66}), \quad e_{14} = -\beta^2 A_{22} \\ e_{15} &= -\beta^2 \hat{B}_{22}, \quad e_{16} = c_1 \beta^3 E_{22} \end{aligned}$$

$$\begin{aligned}
e_{17} &= \bar{A}_{55} - c_1 \beta^2 (\hat{F}_{12} + 2\hat{F}_{66}), \quad e_{18} = \bar{A}_{55} + 2c_1^2 \beta^2 (H_{12} + 2H_{66}) \\
e_{19} &= -\beta \bar{A}_{44} + c_1 \beta^3 \hat{F}_{22}, \quad e_{20} = -\beta^2 \bar{A}_{44} - c_1^2 \beta^4 H_{22} \\
e_{21} &= -e_5, \quad e_{22} = e_{13}, \quad e_{23} = c_1 \hat{F}_{11}, \quad e_{24} = -c_1 \beta (\hat{F}_{12} + 2\hat{F}_{66}), \\
e_{25} &= -c_1^2 H_{11}, \quad e_{26} = -e_6, \quad e_{27} = e_{16}, \quad e_{28} = e_3, \quad e_{29} = e_4 \\
e_{30} &= \bar{D}_{11}, \quad e_{31} = -\beta (\bar{D}_{12} + \bar{D}_{66}) \\
e_{32} &= -e_{23}, \quad e_{33} = -e_{17}, \quad e_{34} = e_8, \quad e_{35} = -\bar{A}_{55} - \beta^2 \bar{D}_{66} \\
e_{36} &= -e_4, \quad e_{37} = e_{12}, \quad e_{38} = -e_{31}, \quad e_{39} = \bar{D}_{66} \\
e_{40} &= e_{24}, \quad e_{41} = e_{15}, \quad e_{42} = -\bar{A}_{44} - \beta^2 \bar{D}_{22}, \quad e_{43} = e_{19}
\end{aligned} \tag{11.5.9}$$

The stiffnesses with bars and hats are defined in Eq. (11.4.9). The coefficients f_i^T are associated with thermal effects

$$\begin{aligned}
f_1^T &= \left(\frac{e_{30}}{e_0} g_1 - \frac{e_3}{e_0} g_4 \right), \quad f_2^T = \left(\frac{e_{12}}{c_0} g_5 - \frac{e_{39}}{c_0} g_2 \right) \\
f_4^T &= \left(\frac{e_1}{e_0} g_4 - \frac{e_{28}}{e_0} g_1 \right), \quad f_5^T = \left(\frac{e_{37}}{c_0} g_2 - \frac{e_{10}}{c_0} g_5 \right) \\
f_3^T &= a_0 [a_1 f_2^T + a_2 f_5^T + \alpha (e_{21} f_1^T + e_{23} f_4^T) - g_3 + q_0]
\end{aligned} \tag{11.5.10a}$$

$$\begin{aligned}
g_1 &= \alpha (N_{mn}^1 \bar{T}_0 + M_{mn}^1 \bar{T}_1), \quad g_2 = \beta (N_{mn}^2 \bar{T}_0 + M_{mn}^2 \bar{T}_1) \\
g_3 &= -c_1 (\alpha^2 P_{mn}^1 + \beta^2 P_{mn}^2) \bar{T}_0, \quad g_4 = \alpha (M_{mn}^1 - c_1 P_{mn}^1) \bar{T}_0 \\
g_5 &= \beta (M_{mn}^2 - c_1 P_{mn}^2) \bar{T}_0
\end{aligned} \tag{11.5.10b}$$

In order to reduce the system of equations (11.5.7) to a state-space form, the components of the state vector $\mathbf{Z}(x)$ are defined as follows:

$$\begin{aligned}
Z_1 &= U_m, \quad Z_2 = U'_m, \quad Z_3 = V_m, \quad Z_4 = V'_m, \quad Z_5 = W_m, \quad Z_6 = W'_m, \quad Z_7 = W''_m \\
Z_8 &= W'''_m, \quad Z_9 = X_m, \quad Z_{10} = X'_m, \quad Z_{11} = Y_m, \quad Z_{12} = Y'_m
\end{aligned} \tag{11.5.11}$$

Using the definitions (11.5.11), the systems of equations (11.5.7) may be converted to the first-order differential operator form

$$\mathbf{Z}' = A\mathbf{Z} + \mathbf{r} \tag{11.5.12a}$$

where the matrix $[A]$ is a 12×12 matrix

$$[A] = \begin{bmatrix} 0 & 1 & 0 & 0 & 0 & 0 & 0 & 0 & 0 & 0 & 0 & 0 \\ C_1 & 0 & 0 & C_2 & 0 & C_3 & 0 & C_4 & C_5 & 0 & 0 & C_6 \\ 0 & 0 & 0 & 1 & 0 & 0 & 0 & 0 & 0 & 0 & 0 & 0 \\ 0 & C_7 & C_8 & 0 & C_9 & 0 & C_{10} & 0 & 0 & C_{11} & C_{12} & 0 \\ 0 & 0 & 0 & 0 & 0 & 1 & 0 & 0 & 0 & 0 & 0 & 0 \\ 0 & 0 & 0 & 0 & 0 & 0 & 1 & 0 & 0 & 0 & 0 & 0 \\ 0 & 0 & 0 & 0 & 0 & 0 & 0 & 1 & 0 & 0 & 0 & 0 \\ 0 & C_{13} & C_{14} & 0 & C_{15} & 0 & C_{16} & 0 & 0 & C_{17} & C_{18} & 0 \\ 0 & 0 & 0 & 0 & 0 & 0 & 0 & 0 & 0 & 1 & 0 & 0 \\ C_{19} & 0 & 0 & C_{20} & 0 & C_{21} & 0 & C_{22} & C_{23} & 0 & 0 & C_{24} \\ 0 & 0 & 0 & 0 & 0 & 0 & 0 & 0 & 0 & 0 & 0 & 1 \\ 0 & C_{25} & C_{26} & 0 & C_{27} & 0 & C_{28} & 0 & 0 & C_{29} & C_{30} & 0 \end{bmatrix} \tag{11.5.12b}$$

and the load vector \mathbf{r} is

$$\{\mathbf{r}\} = \{0, f_1^T \sin \alpha x, 0, f_2^T \cos \alpha x, 0, 0, 0, f_3^T \cos \alpha x, 0, f_4^T \sin \alpha x, 0, f_5^T \cos \alpha x\}^T \quad (11.5.13)$$

The solution to Eq. (11.5.12a) is given by

$$\mathbf{Z} = e^{Ax} \left\{ \mathbf{K} + \int_{-a/2}^x e^{-A\zeta} \mathbf{r}(\zeta) d\zeta \right\} \quad (11.5.14)$$

Here \mathbf{K} is a column vector of constants to be determined from the edge conditions, and

$$e^{Ax} = [S] \begin{bmatrix} e^{\lambda_1 x} & \mathbf{0} \\ \mathbf{0} & e^{\lambda_n x} \end{bmatrix} [S]^{-1} \quad (11.5.15)$$

where $n = 12$, λ_i denote the distinct eigenvalues of $[A]$, and $[S]$ denotes the matrix of eigenvectors of $[A]$.

The boundary conditions for simply supported (S), clamped (C), and free (F) at the edges $x = \pm a/2$ are

$$S : v_0 = w_0 = \phi_y = N_{xx} = M_{xx} = P_{xx} = 0 \quad (11.5.16)$$

$$C : u_0 = v_0 = w_0 = \frac{\partial w_0}{\partial x} = \phi_x = \phi_y = 0 \quad (11.5.17)$$

$$F : N_{xx} = N_{xy} = M_{xx} = P_{xx} = M_{xy} - c_1 P_{xy} = 0 \\ Q_x - c_2 R_x + c_1 \left(\frac{\partial P_{xx}}{\partial x} + \frac{\partial P_{xy}}{\partial y} \right) = 0 \quad (11.5.18)$$

where the stress resultants $P_{\alpha\beta}$ and R_α of the third-order theory are defined in Eq. (11.2.14).

11.5.3 Numerical Results

The nondimensionalized center transverse deflections and stresses of two-layer and ten-layer cross-ply laminates under sinusoidally distributed transverse load are presented in Table 11.5.1 for various boundary conditions and side-to-thickness ratio of $a/h = 5$. The nondimensionalized variables used are

$$\bar{w} = w_0(0, b/2) \frac{E_2 h^3}{q_0 b^4} \times 10^2, \quad \bar{\sigma}_{xx} = -\sigma_{xx}(0, \frac{b}{2}, -\frac{h}{2}) \frac{h^2}{q_0 b^2} 10 \\ \bar{\sigma}_{yy} = -\sigma_{yy}(0, \frac{b}{2}, \frac{h}{2}) \frac{h^2}{q_0 b^2} 10, \quad \bar{\sigma}_{yz} = -\sigma_{yz}(0, 0, 0) \frac{h}{q_0 b} 10 \quad (11.5.19)$$

For the thick plates considered in this case, there is a significant difference between the results predicted by TSDT and FSDT; FSDT slightly overpredicts deflections and underpredicts stresses.

Table 11.5.1: Nondimensionalized deflections and stresses of antisymmetric cross-ply square plates for various boundary conditions ($a/h = 5$, $E_1/E_2 = 25$, $G_{12} = G_{13} = 0.5E_2$, $G_{23} = 0.2E_2$, $\nu_{12} = 0.25$).

No. of Layers	Theory	Variable	SS	SC	CC	FF	FS	FC
2	TSDT	\bar{w}	1.667	1.333	1.088	2.624	2.211	1.733
		$\bar{\sigma}_{xx}$	8.385	6.816	5.679	3.171	5.349	3.727
		$\bar{\sigma}_{yy}$	8.385	6.725	5.505	13.551	11.324	8.919
		$\bar{\sigma}_{yz}$	3.155	2.543	2.095	4.457	3.893	3.048
	FSDT	\bar{w}	1.758	1.477	1.257	2.777	2.335	1.897
		$\bar{\sigma}_{xx}$	7.157	5.338	3.911	2.469	4.430	2.434
		$\bar{\sigma}_{yy}$	7.157	6.034	5.153	11.907	9.848	8.047
		$\bar{\sigma}_{yz}$	2.729	2.297	1.958	3.901	3.390	2.748
	CLPT	\bar{w}	1.064	0.664	0.429	1.777	1.471	0.980
		$\bar{\sigma}_{xx}$	7.157	5.660	4.800	2.403	4.442	3.042
		$\bar{\sigma}_{yy}$	7.157	4.483	2.914	11.849	9.837	6.560
10	TSDT	\bar{w}	1.129	1.001	0.879	1.651	1.450	1.214
		$\bar{\sigma}_{xx}$	6.340	5.196	4.025	2.482	3.946	2.608
		$\bar{\sigma}_{yy}$	6.340	5.635	4.963	9.454	8.252	6.934
		$\bar{\sigma}_{yz}$	3.362	2.974	2.601	4.784	4.234	3.535
	FSDT	\bar{w}	1.137	1.045	0.945	1.663	1.460	1.258
		$\bar{\sigma}_{xx}$	5.009	3.707	2.275	1.712	2.957	1.343
		$\bar{\sigma}_{yy}$	5.009	4.628	4.212	7.583	6.590	5.706
		$\bar{\sigma}_{yz}$	2.729	2.498	2.248	3.883	3.437	2.951
	CLPT	\bar{w}	0.442	0.266	0.167	0.665	0.579	0.380
		$\bar{\sigma}_{xx}$	5.009	3.829	3.167	1.725	2.986	1.865
		$\bar{\sigma}_{yy}$	5.009	3.025	1.911	7.480	6.531	4.284

Tables 11.5.2 and 11.5.3 contain deflections and stresses in cross-ply laminates subjected to a sinusoidally distributed temperature field (see [50])

$$T(x, y, z) = z\bar{T}_1 \cos \alpha x \sin \beta y \quad (11.5.20)$$

The following nondimensionalized variables are used:

$$\bar{w} = w_0(0, b/2) \frac{10}{\alpha_1 \bar{T}_1 b^2}, \quad \bar{\sigma}_{xx} = \sigma_{xx}(0, b/2, -h/2) \frac{10}{\alpha_1 \bar{T}_1 E_2 b} \quad (11.5.21)$$

$$\bar{\sigma}_{yy} = -\sigma_{yy}(0, b/2, h/2) \frac{10}{\alpha_1 \bar{T}_1 E_2 b}, \quad \bar{\sigma}_{yz} = \sigma_{yz}(0, b, 0) \frac{10}{\alpha_1 \bar{T}_1 E_2 b} \quad (11.5.22)$$

The difference between the results obtained with TSDT and FSDT is insignificant for side-to-thickness ratios greater than 5.

Additional numerical results based on the Lévy solution technique for TSDT are presented along with the finite element results in Section 11.6.3. For additional results the reader may consult the references at the end of the chapter. In the next section we develop the displacement finite element model of the Reddy third-order theory.

Table 11.5.2: Nondimensionalized center deflections \bar{w} of cross-ply square plates subjected to sinusoidally distributed temperature distribution.

Laminate	b/h	Theory	SS	SC	CC	FF	FS
0	5	TSDT	1.0711	0.7175	0.3663	2.2812	1.5831
		FSDT	1.0721	0.7613	0.3915	2.2894	1.5859
		CLPT	1.0312	0.4543	0.2443	2.2935	1.6067
	10	TSDT	1.0439	0.5587	0.2871	2.2854	1.5931
		FSDT	1.0440	0.5677	0.2912	2.2928	1.5952
		CLPT	1.0312	0.4543	0.2443	2.2935	1.6067
0/90	5	TSDT	1.1430	0.8190	0.5814	1.2652	1.2068
		FSDT	1.1504	0.8547	0.6231	1.2784	1.2170
		CLPT	1.1504	0.7183	0.4681	1.2639	1.2152
	10	TSDT	1.1485	0.7586	0.5164	1.2693	1.2145
		FSDT	1.1504	0.7703	0.5307	1.2736	1.2176
		CLPT	1.1504	0.7183	0.4681	1.2639	1.2152
0/90/0	5	TSDT	1.0874	0.8032	0.4556	1.6687	1.3805
		FSDT	1.0763	0.8155	0.4578	1.6597	1.3698
		CLPT	1.0312	0.4635	0.2512	1.6645	1.3800
	10	TSDT	1.0499	0.6142	0.3275	1.6632	1.3757
		FSDT	1.0460	0.6037	0.3211	1.6640	1.3737
		CLPT	1.0312	0.4635	0.2512	1.6645	1.3800
0/90/... 10 layers	5	TSDT	1.0336	0.7993	0.5623	1.0733	1.0549
		FSDT	1.0331	0.8191	0.5847	1.0736	1.0549
		CLPT	1.0331	0.6222	0.3914	1.0681	1.0546
	10	TSDT	1.0333	0.7101	0.4880	1.0718	1.0556
		FSDT	1.0331	0.7157	0.4949	1.0722	1.0558
		CLPT	1.0331	0.6222	0.3914	1.0681	1.0546

11.6 Finite Element Model of Plates

11.6.1 Introduction

Recall from Eq. (11.2.24) that the primary variables of the third-order theory developed in Section 11.2 are $(u_n, u_s, w_0, w_{0,n} = \partial w_0 / \partial n, \phi_n, \phi_s)$, where (u_n, u_s) denote in-plane normal and tangential displacements, and (ϕ_n, ϕ_s) are the rotations of a transverse line about the in-plane normal and tangent. A displacement finite element model based on Eqs. (11.2.16) through (11.2.20), with $(u_0, v_0, w_0, w_{0,n}, \phi_x, \phi_y)$ as the primary variables, is called a displacement finite element model (see Phan and Reddy [30]), and it requires the Lagrange interpolation of $(u_0, v_0, \phi_x, \phi_y)$ and Hermite interpolation of w_0 . A conforming element will have eight degrees of freedom $(u_0, v_0, w_0, w_{0,x}, w_{0,y}, w_{0,xy}, \phi_x, \phi_y)$ whereas a nonconforming element will have $(u_0, v_0, w_0, w_{0,x}, w_{0,y}, \phi_x, \phi_y)$ seven degrees of freedom per node.

Table 11.5.3: Nondimensionalized thermal stresses of cross-ply square plates subjected to sinusoidally distributed temperature.

Stress	Laminate	b/h	Theory	SS	SC	CC	FF	FS	FC
$\bar{\sigma}_{xx}$	0/90/0	5	TSDT	0.1154	5.9126	14.6976	1.1490	0.6671	3.8065
			FSDT	0.4072	6.8460	15.6783	1.0220	0.7501	4.5545
			CLPT	0.0526	11.1264	15.2675	1.4489	0.8217	6.4107
	10	10	TSDT	0.0372	4.4944	7.5416	0.6291	0.3648	2.6993
			FSDT	0.0847	4.7320	7.7020	0.6103	0.3782	2.8579
			CLPT	0.0263	5.5632	7.6338	0.7245	0.4109	3.2052
$\bar{\sigma}_{yy}$	0/90	5	TSDT	-0.5846	2.6319	5.0886	-1.8754	-1.2598	2.6457
			FSDT	-0.6148	1.7502	3.6323	-1.7733	-1.2190	1.7814
			CLPT	-0.6148	5.1916	8.8393	-2.1091	-1.4684	4.9149
	10	10	TSDT	-0.3036	2.0911	3.6908	-1.0526	-0.7131	2.0023
			FSDT	-0.3074	1.8991	3.3902	-1.0399	-0.7075	1.8168
			CLPT	-0.3074	2.5958	4.4197	-1.0545	-0.7342	2.4575
$\bar{\sigma}_{yz}$	0	5	TSDT	0.1109	0.1981	0.2909	-0.0332	0.0499	0.2332
			FSDT	0.0740	0.1279	0.1921	-0.0229	0.0331	0.1515
	10	10	TSDT	0.0347	0.0702	0.0903	-0.0085	0.0157	0.0784
			FSDT	0.0231	0.0466	0.0601	-0.0058	0.0104	0.0520

Alternatively, one can develop mixed finite element models of Eqs. (11.2.16)–(11.2.20), in which both generalized displacements and stress resultants become the nodal variables and require only Lagrange interpolation of all variables (see Reddy and his colleagues [58–61]). The number of primary degrees of freedom per node vary from eight to eleven depending on the formulation. The C^0 displacement finite element models of third-order theories can be found in the work of Pandya and Kant [61].

Here we present a displacement finite element model of the third-order theory in Eqs. (11.2.16)–(11.2.20). In view of the detailed discussion of finite element models of the classical and first-order theories presented in Chapter 10, only the salient features of the model are discussed here.

11.6.2 Finite Element Model

The Hamilton's principle or the dynamic version of the principle of virtual displacements [or a weak form of Eqs. (11.2.16)–(11.2.20)] of a typical plate finite element is given by

$$\begin{aligned}
 0 = \int_{\Omega^e} & \left\{ N_{xx} \delta u_{0,x} + N_{xy} (\delta u_{0,y} + \delta v_{0,x}) + N_{yy} \delta v_{0,y} + (Q_x - c_2 R_x) \delta w_{0,x} \right. \\
 & + (Q_y - c_2 R_y) \delta w_{0,y} - c_1 (P_x \delta w_{0,xx} + P_y \delta w_{0,yy} + 2P_{xy} \delta w_{0,xy}) - q \delta w_0 \\
 & + (Q_x - c_2 R_x) \delta \phi_x + (M_x - c_1 P_x) \delta \phi_{x,x} + (M_{xy} - c_1 P_{xy}) \delta \phi_{x,y} \\
 & + (Q_y - c_2 R_y) \delta \phi_y + (M_{xy} - c_1 P_{xy}) \delta \phi_{y,x} + (M_{yy} - c_1 P_y) \delta \phi_{y,y} \\
 & \left. + (I_0 \ddot{u}_0 + J_1 \ddot{\phi}_x - c_1 I_3 \ddot{w}_{0,x}) \delta u_0 + (I_0 \ddot{v}_0 + J_1 \ddot{\phi}_y - c_1 I_3 \ddot{w}_{0,y}) \delta v_0 \right\}
 \end{aligned}$$

$$\begin{aligned}
& + \left(J_1 \ddot{u}_0 + K_2 \ddot{\phi}_x - c_1 J_4 \ddot{w}_{0,x} \right) \delta \phi_x + \left(J_1 \ddot{v}_0 + K_2 \ddot{\phi}_y - c_1 J_4 \ddot{w}_{0,y} \right) \delta \phi_y + I_0 \ddot{w}_0 \delta w_0 \\
& + c_1 \left(-I_3 \ddot{u}_0 - J_4 \ddot{\phi}_x + c_1 I_6 \ddot{w}_{0,x} \right) \delta w_{0,x} + c_1 \left(-I_3 \ddot{v}_0 - J_4 \ddot{\phi}_y + c_1 I_6 \ddot{w}_{0,y} \right) \delta w_{0,y} \\
& + \left. \left(\hat{N}_{xx} w_{0,x} + \hat{N}_{xy} w_{0,y} \right) \delta w_{0,x} + \left(\hat{N}_{xy} w_{0,x} + \hat{N}_{yy} w_{0,y} \right) \delta w_{0,y} \right\} dx dy \\
& - \oint_{\Gamma^e} (N_n \delta u_n + N_{nx} \delta u_{ns}) ds - \oint_{\Gamma^e} (\bar{V}_n \delta w_0 + P_{nn} \delta w_{0,n}) ds \\
& - \oint_{\Gamma^e} (M_n \delta \phi_n + M_{ns} \delta \phi_{ns}) ds
\end{aligned} \tag{11.6.1}$$

where a comma followed by x or y denotes differentiation with respect to the coordinates, the superposed dot denotes differentiation with respect to time, and

$$I_i = \sum_{k=1}^N \int_{z_k}^{z_{k+1}} \rho^{(k)}(z)^i dz \quad (i = 0, 1, 2, \dots, 6) \tag{11.6.2}$$

$$c_1 = \frac{4}{3h^2}, \quad c_2 = \frac{4}{h^2}, \quad J_i = I_i - c_1 I_{i+2}, \quad K_2 = I_2 - 2c_1 I_4 + c_1^2 I_6 \tag{11.6.3}$$

The resultants $N_{\alpha\beta}$, $M_{\alpha\beta}$, and so on are defined in Eq. (11.2.14), and they are known in terms of the generalized displacements through relations (11.2.28), (11.2.29) and (11.2.7); $\hat{N}_{\alpha\beta}$ are specified in-plane forces in the stability analysis.

The generalized displacements are approximated over an element Ω^e by the expressions

$$\begin{aligned}
u_0(x, y, t) &= \sum_{i=1}^m u_i^e(t) \psi_i^e(x, y) \\
v_0(x, y, t) &= \sum_{i=1}^m v_i^e(t) \psi_i^e(x, y) \\
w_0(x, y, t) &= \sum_{i=1}^m \Delta_i^e(t) \varphi_i^e(x, y) \\
\phi_x(x, y, t) &= \sum_{i=1}^m X_i^e(t) \psi_i^e(x, y) \\
\phi_y(x, y, t) &= \sum_{i=1}^m Y_i^e(t) \psi_i^e(x, y)
\end{aligned} \tag{11.6.4}$$

where ψ_i^e denote the Lagrange interpolation functions and φ_i^e are the Hermite interpolation functions. Here we chose the same approximation for the in-plane displacements (u_0, v_0) and rotations (ϕ_x, ϕ_y), although one could use different approximations for these two pairs.

Substitution of Eq. (11.6.4) into the weak form (11.6.1) yields the finite element model

$$\begin{bmatrix} [K^{11}] & [K^{12}] & [K^{13}] & [K^{14}] & [K^{15}] \\ [K^{12}]^T & [K^{22}] & [K^{23}] & [K^{24}] & [K^{25}] \\ [K^{13}]^T & [K^{23}]^T & [K^{33}] & [K^{34}] & [K^{35}] \\ [K^{14}]^T & [K^{24}]^T & [K^{34}]^T & [K^{44}] & [K^{45}] \\ [K^{15}]^T & [K^{25}]^T & [K^{35}]^T & [K^{45}]^T & [K^{55}] \end{bmatrix} \begin{Bmatrix} \{u^e\} \\ \{v^e\} \\ \{\Delta^e\} \\ \{X^e\} \\ \{Y^e\} \end{Bmatrix}$$

$$\begin{aligned}
& + \begin{bmatrix} [M^{11}] & [0] & [M^{13}] & [M^{14}] & [0] \\ [0] & [M^{22}] & [M^{23}] & [0] & [M^{25}] \\ [M^{13}]^T & [M^{23}]^T & [M^{33}] & [M^{34}] & [M^{35}] \\ [M^{14}]^T & [0] & [M^{34}]^T & [M^{44}] & [0] \\ [0] & [M^{25}]^T & [M^{35}]^T & [0] & [M^{55}] \end{bmatrix} \begin{Bmatrix} \{\ddot{u}^e\} \\ \{\ddot{v}^e\} \\ \{\ddot{\Delta}^e\} \\ \{\ddot{X}^e\} \\ \{\ddot{Y}^e\} \end{Bmatrix} \\
& + \begin{bmatrix} [0] & [0] & [0] & [0] & [0] \\ [0] & [0] & [0] & [0] & [0] \\ [0] & [0] & [G] & [0] & [0] \\ [0] & [0] & [0] & [0] & [0] \\ [0] & [0] & [0] & [0] & [0] \end{bmatrix} \begin{Bmatrix} \{u^e\} \\ \{v^e\} \\ \{\Delta^e\} \\ \{X^e\} \\ \{Y^e\} \end{Bmatrix} = \begin{Bmatrix} \{F^1\} \\ \{F^2\} \\ \{F^3\} \\ \{F^4\} \\ \{F^5\} \end{Bmatrix} \quad (11.6.5)
\end{aligned}$$

or, in compact form, we can write

$$\sum_{\beta=1}^5 \sum_{j=1}^{n_\beta} \left(K_{ij}^{\alpha\beta} \Delta_j^\beta + M_{ij}^{\alpha\beta} \ddot{\Delta}_j^\beta + S_{ij}^{\alpha\beta} \Delta_j^\beta \right) - F_i^\alpha = 0, \quad i = 1, 2, \dots, n_\alpha \quad (11.6.6)$$

where $\alpha = 1, 2, 3, 4, 5$; $n_1 = n_2 = n_4 = n_5 = 4$ and $n_3 = 16$ for the conforming element. The nodal values Δ_j^β are defined by

$$\Delta_j^1 = u_j, \quad \Delta_j^2 = v_j, \quad \Delta_j^3 = \bar{\Delta}_j, \quad \Delta_j^4 = X_j^1, \quad \Delta_j^5 = Y_j^2 \quad (11.6.7)$$

and the nonzero stiffness, mass, and geometric stiffness coefficients are defined by

$$\begin{aligned}
K_{ij}^{1\alpha} &= \int_{\Omega^e} \left(\frac{\partial \psi_i}{\partial x} N_{1j}^\alpha + \frac{\partial \psi_i}{\partial y} N_{6j}^\alpha \right) dx dy \\
K_{ij}^{2\alpha} &= \int_{\Omega^e} \left(\frac{\partial \psi_i}{\partial x} N_{6j}^\alpha + \frac{\partial \psi_i}{\partial y} N_{2j}^\alpha \right) dx dy \\
K_{ij}^{3\alpha} &= \int_{\Omega^e} \left[\frac{\partial \varphi_i}{\partial x} \hat{Q}_{1j}^\alpha + \frac{\partial \varphi_i}{\partial y} \hat{Q}_{2j}^\alpha - c_1 \left(\frac{\partial^2 \varphi_i}{\partial x^2} P_{1j}^\alpha + 2 \frac{\partial^2 \varphi_i}{\partial x \partial y} P_{6j}^\alpha + \frac{\partial^2 \varphi_i}{\partial y^2} P_{2j}^\alpha \right) \right] dx dy \\
K_{ij}^{4\alpha} &= \int_{\Omega^e} \left(\frac{\partial \psi_i}{\partial x} \hat{M}_{1j}^\alpha + \frac{\partial \psi_i}{\partial y} \hat{M}_{6j}^\alpha + \psi_i \hat{Q}_{1j}^\alpha \right) dx dy \\
K_{ij}^{5\alpha} &= \int_{\Omega^e} \left(\frac{\partial \psi_i}{\partial x} \hat{M}_{6j}^\alpha + \frac{\partial \psi_i}{\partial y} \hat{M}_{2j}^\alpha + \psi_i \hat{Q}_{2j}^\alpha \right) dx dy \quad (11.6.8)
\end{aligned}$$

$$\begin{aligned}
M_{ij}^{11} &= I_0 S_{ij}^0, \quad M_{ij}^{12} = 0, \quad M_{ij}^{13} = -c_1 I_3 S_{ij}^{ox}, \quad M_{ij}^{14} = J_1 S_{ij}^0, \quad M_{ij}^{15} = 0 \\
M_{ij}^{22} &= I_0 S_{ij}^0, \quad M_{ij}^{23} = -c_1 I_3 S_{ij}^{oy}, \quad M_{ij}^{24} = 0, \quad M_{ij}^{25} = J_1 S_{ij}^0 \\
M_{ij}^{33} &= I_0 S_{ij}^1 + c_1^2 I_6 (S_{ij}^{xx} + S_{ij}^{yy}), \quad M_{ij}^{34} = -c_1 J_4 S_{ji}^{ox}, \quad M_{ij}^{35} = -c_1 J_4 S_{ji}^{oy} \\
M_{ij}^{44} &= K_2 S_{ij}^0, \quad M_{ij}^{45} = 0, \quad M_{ij}^{55} = K_2 S_{ij}^0 \quad (11.6.9)
\end{aligned}$$

$$\begin{aligned}
S_{ij}^{33} &= G_{ij} = \hat{N}_{xx} S_{ij}^{xx} + \hat{N}_{xy} (S_{ij}^{xy} + S_{ij}^{yx}) + \hat{N}_{yy} S_{ij}^{yy} \\
F_i^1 &= \oint_{\Gamma^e} (N_{xx} n_x + N_{xy} n_y) \psi_i ds, \quad F_i^2 = \oint_{\Gamma^e} (N_{xy} n_x + N_{yy} n_y) \psi_i ds \\
F_i^4 &= \oint_{\Gamma^e} (M_{xx} n_x + M_{xy} n_y) \psi_i ds, \quad F_i^5 = \oint_{\Gamma^e} (M_{xy} n_x + M_{yy} n_y) \psi_i ds \\
F_i^3 &= \int_{\Omega^e} q \varphi_i dx dy + \oint_{\Gamma^e} \left(\bar{V}_n \varphi_i + P_{nn} \frac{\partial \varphi_i}{\partial n} \right) ds \quad (11.6.10)
\end{aligned}$$

$$\begin{aligned}
S_{ij}^0 &= \int_{\Omega^e} \psi_i \psi_j \, dx dy, & S_{ij}^{0x} &= \int_{\Omega^e} \psi_i \frac{\partial \varphi_j}{\partial x} \, dx dy, & S_{ij}^{0y} &= \int_{\Omega^e} \psi_i \frac{\partial \varphi_j}{\partial y} \, dx dy \\
S_{ij}^1 &= \int_{\Omega^e} \varphi_i \varphi_j \, dx dy, & S_{ij}^{xx} &= \int_{\Omega^e} \frac{\partial \varphi_i}{\partial x} \frac{\partial \varphi_j}{\partial x} \, dx dy, & S_{ij}^{yy} &= \int_{\Omega^e} \frac{\partial \varphi_i}{\partial y} \frac{\partial \varphi_j}{\partial y} \, dx dy
\end{aligned} \tag{11.6.11}$$

In addition, we have

$$\begin{aligned}
N_{1j}^1 &= A_{11} \frac{\partial \psi_j}{\partial x} + A_{16} \frac{\partial \psi_j}{\partial y}, & N_{1j}^2 &= A_{16} \frac{\partial \psi_j}{\partial x} + A_{12} \frac{\partial \psi_j}{\partial y} \\
N_{1j}^3 &= -c_1 \left(E_{11} \frac{\partial^2 \varphi_j}{\partial x^2} + 2E_{16} \frac{\partial^2 \varphi_j}{\partial x \partial y} + E_{12} \frac{\partial^2 \varphi_j}{\partial y^2} \right) \\
N_{1j}^4 &= \hat{B}_{11} \frac{\partial \psi_j}{\partial x} + \hat{B}_{16} \frac{\partial \psi_j}{\partial y}, & N_{1j}^5 &= \hat{B}_{12} \frac{\partial \psi_j}{\partial x} + \hat{B}_{16} \frac{\partial \psi_j}{\partial y} \\
N_{6j}^1 &= A_{16} \frac{\partial \psi_j}{\partial x} + A_{66} \frac{\partial \psi_j}{\partial y}, & N_{6j}^2 &= A_{66} \frac{\partial \psi_j}{\partial x} + A_{26} \frac{\partial \psi_j}{\partial y} \\
N_{6j}^3 &= -c_1 \left(E_{16} \frac{\partial^2 \varphi_j}{\partial x^2} + 2E_{66} \frac{\partial^2 \varphi_j}{\partial x \partial y} + E_{26} \frac{\partial^2 \varphi_j}{\partial y^2} \right) \\
N_{6j}^4 &= \hat{B}_{66} \frac{\partial \psi_j}{\partial x} + \hat{B}_{16} \frac{\partial \psi_j}{\partial y}, & N_{6j}^5 &= \hat{B}_{26} \frac{\partial \psi_j}{\partial x} + \hat{B}_{66} \frac{\partial \psi_j}{\partial y} \\
N_{2j}^1 &= A_{12} \frac{\partial \psi_j}{\partial x} + A_{26} \frac{\partial \psi_j}{\partial y}, & N_{2j}^2 &= A_{26} \frac{\partial \psi_j}{\partial x} + A_{22} \frac{\partial \psi_j}{\partial y} \\
N_{2j}^3 &= -c_1 \left(E_{12} \frac{\partial^2 \varphi_j}{\partial x^2} + 2E_{26} \frac{\partial^2 \varphi_j}{\partial x \partial y} + E_{22} \frac{\partial^2 \varphi_j}{\partial y^2} \right) \\
N_{2j}^4 &= \hat{B}_{12} \frac{\partial \psi_j}{\partial x} + \hat{B}_{26} \frac{\partial \psi_j}{\partial y}, & N_{2j}^5 &= \hat{B}_{26} \frac{\partial \psi_j}{\partial x} + \hat{B}_{22} \frac{\partial \psi_j}{\partial y} \\
\hat{M}_{1j}^1 &= \hat{B}_{11} \frac{\partial \psi_j}{\partial x} + \hat{B}_{16} \frac{\partial \psi_j}{\partial y}, & \hat{M}_{2j}^1 &= \hat{B}_{16} \frac{\partial \psi_j}{\partial x} + \hat{B}_{12} \frac{\partial \psi_j}{\partial y} \\
\hat{M}_{1j}^3 &= -c_1 \left(\hat{F}_{11} \frac{\partial^2 \varphi_j}{\partial x^2} + 2\hat{F}_{16} \frac{\partial^2 \varphi_j}{\partial x \partial y} + \hat{F}_{12} \frac{\partial^2 \varphi_j}{\partial y^2} \right) \\
\hat{M}_{1j}^4 &= \bar{D}_{11} \frac{\partial \psi_j}{\partial x} + \bar{D}_{16} \frac{\partial \psi_j}{\partial y}, & \hat{M}_{1j}^5 &= \bar{D}_{12} \frac{\partial \psi_j}{\partial x} + \bar{D}_{16} \frac{\partial \psi_j}{\partial y} \\
\hat{M}_{6j}^1 &= \hat{B}_{16} \frac{\partial \psi_j}{\partial x} + \hat{B}_{66} \frac{\partial \psi_j}{\partial y}, & \hat{M}_{6j}^2 &= \hat{B}_{66} \frac{\partial \psi_j}{\partial x} + \hat{B}_{26} \frac{\partial \psi_j}{\partial y} \\
\hat{M}_{6j}^3 &= -c_1 \left(\hat{F}_{16} \frac{\partial^2 \varphi_j}{\partial x^2} + 2\hat{F}_{66} \frac{\partial^2 \varphi_j}{\partial x \partial y} + \hat{F}_{26} \frac{\partial^2 \varphi_j}{\partial y^2} \right) \\
\hat{M}_{6j}^4 &= \bar{D}_{16} \frac{\partial \psi_j}{\partial x} + \bar{D}_{66} \frac{\partial \psi_j}{\partial y}, & \hat{M}_{6j}^5 &= \bar{D}_{26} \frac{\partial \psi_j}{\partial x} + \bar{D}_{66} \frac{\partial \psi_j}{\partial y} \\
\hat{M}_{2j}^1 &= \hat{B}_{12} \frac{\partial \psi_j}{\partial x} + \hat{B}_{26} \frac{\partial \psi_j}{\partial y}, & \hat{M}_{2j}^2 &= \hat{B}_{26} \frac{\partial \psi_j}{\partial x} + \hat{B}_{22} \frac{\partial \psi_j}{\partial y} \\
\hat{M}_{2j}^3 &= -c_1 \left(\hat{F}_{12} \frac{\partial^2 \varphi_j}{\partial x^2} + 2\hat{F}_{26} \frac{\partial^2 \varphi_j}{\partial x \partial y} + \hat{F}_{22} \frac{\partial^2 \varphi_j}{\partial y^2} \right) \\
\hat{M}_{2j}^4 &= \bar{D}_{12} \frac{\partial \psi_j}{\partial x} + \bar{D}_{26} \frac{\partial \psi_j}{\partial y}, & \hat{M}_{2j}^5 &= \bar{D}_{22} \frac{\partial \psi_j}{\partial x} + \bar{D}_{26} \frac{\partial \psi_j}{\partial y}
\end{aligned} \tag{11.6.12}$$

$$\begin{aligned}
P_{1j}^1 &= E_{11} \frac{\partial \psi_j}{\partial x} + E_{16} \frac{\partial \psi_j}{\partial y}, \quad P_{1j}^2 = E_{12} \frac{\partial \psi_j}{\partial x} + E_{16} \frac{\partial \psi_j}{\partial y} \\
P_{1j}^3 &= -c_1 \left(H_{11} \frac{\partial^2 \varphi_j}{\partial x^2} + 2H_{16} \frac{\partial^2 \varphi_j}{\partial x \partial y} + H_{12} \frac{\partial^2 \varphi_j}{\partial y^2} \right) \\
P_{1j}^4 &= \hat{F}_{11} \frac{\partial \psi_j}{\partial x} + \hat{F}_{16} \frac{\partial \psi_j}{\partial y}, \quad P_{1j}^5 = \hat{F}_{12} \frac{\partial \psi_j}{\partial x} + \hat{F}_{16} \frac{\partial \psi_j}{\partial y} \\
P_{2j}^1 &= E_{12} \frac{\partial \psi_j}{\partial x} + E_{26} \frac{\partial \psi_j}{\partial y}, \quad P_{2j}^2 = E_{22} \frac{\partial \psi_j}{\partial x} + E_{26} \frac{\partial \psi_j}{\partial y} \\
P_{2j}^3 &= -c_1 \left(H_{21} \frac{\partial^2 \varphi_j}{\partial x^2} + 2H_{26} \frac{\partial^2 \varphi_j}{\partial x \partial y} + H_{22} \frac{\partial^2 \varphi_j}{\partial y^2} \right) \\
P_{2j}^4 &= \hat{F}_{12} \frac{\partial \psi_j}{\partial x} + \hat{F}_{26} \frac{\partial \psi_j}{\partial y}, \quad P_{2j}^5 = \hat{F}_{22} \frac{\partial \psi_j}{\partial x} + \hat{F}_{26} \frac{\partial \psi_j}{\partial y} \\
P_{6j}^1 &= E_{16} \frac{\partial \psi_j}{\partial x} + E_{66} \frac{\partial \psi_j}{\partial y}, \quad P_{6j}^2 = E_{26} \frac{\partial \psi_j}{\partial x} + E_{66} \frac{\partial \psi_j}{\partial y} \\
P_{6j}^3 &= -c_1 \left(H_{16} \frac{\partial^2 \varphi_j}{\partial x^2} + 2H_{66} \frac{\partial^2 \varphi_j}{\partial x \partial y} + H_{26} \frac{\partial^2 \varphi_j}{\partial y^2} \right) \\
P_{6j}^4 &= \hat{F}_{16} \frac{\partial \psi_j}{\partial x} + \hat{F}_{66} \frac{\partial \psi_j}{\partial y}, \quad P_{6j}^5 = \hat{F}_{26} \frac{\partial \psi_j}{\partial x} + \hat{F}_{66} \frac{\partial \psi_j}{\partial y} \\
\hat{Q}_{1j}^3 &= \bar{A}_{55} \frac{\partial \varphi_j}{\partial x} + \bar{A}_{45} \frac{\partial \varphi_j}{\partial y}, \quad \hat{Q}_{2j}^3 = \bar{A}_{45} \frac{\partial \varphi_j}{\partial x} + \bar{A}_{44} \frac{\partial \varphi_j}{\partial y} \\
\hat{Q}_{1j}^4 &= \hat{A}_{55} \psi_j, \quad \hat{Q}_{1j}^5 = \hat{Q}_{2j}^4 = \hat{A}_{45} \psi_j, \quad \hat{Q}_{2j}^5 = \hat{A}_{44} \psi_j
\end{aligned} \tag{11.6.13}$$

$$\begin{aligned}
F_i^1 &= \oint_{\Gamma_e} \psi_i N_n \, ds, \quad F_i^2 = \oint_{\Gamma_e} \psi_i N_{ns} \, ds \\
F_i^4 &= \oint_{\Gamma_e} \psi_i M_n \, ds, \quad F_i^5 = \oint_{\Gamma_e} \psi_i M_{ns} \, ds \\
F_i^3 &= \int_{\Omega^e} q \varphi_i \, dx dy + \oint_{\Gamma_e} \varphi_i Q_n \, ds
\end{aligned} \tag{11.6.14}$$

In obtaining the numerical results presented in the next section, we used linear interpolation of $(u_0, v_0, w_0, \phi_1, \phi_2)$ as well as the geometry

$$x = \sum_{j=1}^n x_j \psi_j, \quad y = \sum_{j=1}^n y_j \psi_j \tag{11.6.15}$$

and Hermite cubic interpolation of w_0 . In the case of the conforming element, the four nodal values associated with w_0 are

$$\bar{\Delta}_1 = w_0, \quad \bar{\Delta}_2 = \frac{\partial w_0}{\partial x}, \quad \bar{\Delta}_3 = \frac{\partial w_0}{\partial y}, \quad \bar{\Delta}_4 = \frac{\partial^2 w_0}{\partial x \partial y} \tag{11.6.16}$$

For the nonconforming element, the cross derivative is omitted. The conforming rectangular element with linear interpolation of the in-plane displacements and rotations has eight degrees of freedom per node. The corresponding nonconforming element has seven degrees of freedom per node.

11.6.3 Numerical Results

For the purpose of comparison, the following lamina properties, typical of graphite-epoxy material, are used in all numerical examples presented here:

Material 1: $E_1 = 25E_2$, $G_{12} = G_{13} = 0.5E_2$, $G_{23} = 0.2E_2$, $\nu_{12} = 0.25$ (11.6.17a)

Material 2: $E_1 = 40E_2$, $G_{12} = G_{13} = 0.6E_2$, $G_{23} = 0.5E_2$, $\nu_{12} = 0.25$ (11.6.17b)

The shear correction coefficients for the first-order theory are taken to be 5/6. The loading, in all cases, is assumed to be sinusoidal (see Figure 11.5.1 for the geometry and coordinate system):

$$q(x, y) = q_0 \cos \frac{\pi x}{a} \sin \frac{\pi y}{b} \quad (11.6.18)$$

The notation SC, for example, refers to the simply supported boundary condition on edge $x = -a/2$ and clamped boundary condition on edge $x = a/2$, while the other two edges (i.e., $y = 0, b$), in all cases, are simply supported.

Bending Results

The results for deflections and stresses are presented in tables using the following nondimensional form (see [51]):

$$\begin{aligned} \bar{w} &= w_0(0, b/2) \frac{E_2 h^3}{q_0 b^4} \times 10^2, \quad \bar{\sigma}_{xx} = -\sigma_{xx}(0, \frac{b}{2}, -\frac{h}{2}) \frac{h^2}{q_0 b^2} 10 \\ \bar{\sigma}_{yy} &= -\sigma_{yy}(0, \frac{b}{2}, \frac{h}{2}) \frac{h^2}{q_0 b^2} 10, \quad \bar{\sigma}_{yz} = -\sigma_{yz}(0, 0, 0) \frac{h}{b q_0} 10 \end{aligned} \quad (11.6.19)$$

where h is the total thickness of the laminate.

Tables 11.6.1 through 11.6.4 contain numerical values of deflections and stresses obtained by the Lévy or the Navier method, and the finite element model (Table 11.6.4 does not include the FEM results). The reduced integration rule is used to evaluate the shear stiffness coefficients. Quarter-plate models with 2×2 mesh are used for SS, CC, and FF boundary conditions, and half-plate models with 4×2 mesh are used for all other boundary conditions. The finite element results are in good agreement with the analytical solutions.

Natural Vibration and Buckling Results

Tables 11.6.5 and 11.6.6 contain nondimensionalized fundamental frequencies and critical buckling loads, respectively, of antisymmetric cross-ply square laminates for various boundary conditions. Both the Lévy and finite element results are presented in the tables. A 2×2 mesh of nine-node quadratic elements is used in FSDT and a 4×4 mesh of conforming elements is used in TSDT. The rotary inertia is accounted for in the vibration analysis. The first-order theory underpredicts fundamental frequencies and critical buckling loads when compared to the third-order theory. Table 11.6.7 contains natural frequencies of a two-layer (0/90) cantilever plate as predicted by various theories. Figures 11.6.1 and 11.6.2 contain a comparison of the finite element (FEM) results with the closed-form solutions (CFS) for antisymmetric angle-ply plates.

Table 11.6.1: Nondimensionalized center deflection (\bar{w}) of antisymmetric cross-ply square plates with various boundary conditions.

<i>N</i>	<i>b/h</i>	Theory	Solution	SS	SC	CC	FF	FS	FC
2	5	TSDT ^a	Exact	1.667	1.333	1.088	2.624	2.211	1.733
		FEM		1.667	1.317	1.068	2.647	2.221	1.728
	10	FSDT ^b	Exact	1.758	1.477	1.257	2.777	2.335	1.897
		FEM		1.759	1.478	1.257	2.776	2.334	1.897
	2	CLPT ^c	Exact	1.064	0.664	0.429	1.777	1.471	0.980
		FEM		1.043	0.648	0.417	1.786	1.465	0.977
	10	TSDT	Exact	1.216	0.848	0.617	1.992	1.658	1.184
		FEM		1.214	0.838	0.605	2.002	1.662	1.180
	10	FSDT	Exact	1.237	0.883	0.656	2.028	1.687	1.223
		FEM		1.238	0.883	0.657	2.027	1.687	1.223
	10	CLPT	Exact	1.064	0.664	0.429	1.777	1.471	0.980
		FEM		1.043	0.648	0.417	1.786	1.465	0.977
10	5	TSDT	Exact	1.129	1.001	0.879	1.651	1.450	1.214
		FEM		1.135	0.995	0.869	1.670	1.461	1.214
	10	FSDT	Exact	1.137	1.045	0.945	1.663	1.460	1.258
		FEM		1.137	1.045	0.945	1.662	1.460	1.258
	10	CLPT	Exact	0.442	0.266	0.167	0.665	0.579	0.380
		FEM		0.444	0.266	0.169	0.686	0.593	0.391
	10	TSDT	Exact	0.616	0.473	0.375	0.916	0.801	0.607
		FEM		0.619	0.471	0.372	0.926	0.808	0.609
	10	FSDT	Exact	0.615	0.480	0.385	0.915	0.800	0.612
		FEM		0.616	0.480	0.386	0.914	0.800	0.612
	10	CLPT	Exact	0.442	0.266	0.167	0.665	0.579	0.380
		FEM		0.444	0.266	0.169	0.686	0.593	0.391

^a Finite element results are obtained using meshes of quadrilateral elements with linear interpolation of $(u_0, v_0, \phi_x, \phi_y)$ and Hermite cubic interpolation of w_0 .

^b Finite element results are obtained using meshes of nine-node quadrilateral elements with equal interpolation of $(u_0, v_0, w_0, \phi_x, \phi_y)$.

^c Finite element results are obtained using meshes of quadrilateral elements with linear interpolation of (u_0, v_0) and Hermite cubic interpolation of w_0 .

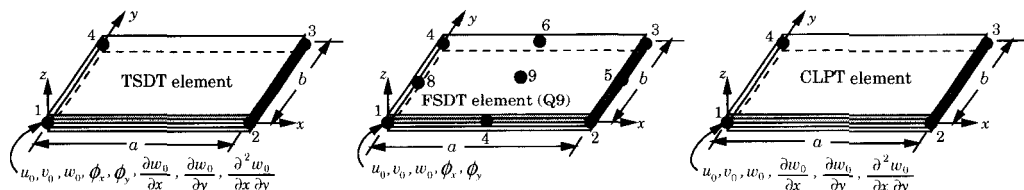


Table 11.6.2: Nondimensionalized axial stress ($\bar{\sigma}_{xx}$) of antisymmetric cross-ply square plates with various boundary conditions (see the foot notes of Table 11.6.1).

N	b/h	Theory	Solution	SS	SC	CC	FF	FS	FC
5	TSDT	Exact	8.385	6.816	5.679	3.171	5.349	3.727	
		FEM	7.669	6.732	5.060	2.722	5.231	3.544	
	FSDT	Exact	7.157	5.338	3.911	2.469	4.430	2.434	
		FEM	6.948	5.465	3.707	2.359	4.479	2.542	
	CLPT	Exact	7.157	5.660	4.800	2.403	4.442	3.042	
		FEM	6.659	5.782	4.348	2.034	4.288	2.991	
2	TSDT	Exact	7.468	5.910	4.952	2.624	4.669	3.158	
		FEM	6.829	5.914	4.346	2.212	4.537	3.054	
	FSDT	Exact	7.157	5.494	4.450	2.442	4.435	2.790	
		FEM	6.948	5.668	4.222	2.331	4.491	2.895	
	CLPT	Exact	7.157	5.660	4.800	2.403	4.442	3.042	
		FEM	6.659	5.782	4.348	2.034	4.288	2.991	
10	TSDT	Exact	6.340	5.196	4.025	2.482	3.946	2.608	
		FEM	5.762	5.047	3.584	2.124	3.855	2.420	
	FSDT	Exact	5.009	3.707	2.275	1.712	2.957	1.343	
		FEM	4.864	3.755	2.154	1.639	2.993	1.427	
	CLPT	Exact	5.009	3.829	3.167	1.725	2.986	1.865	
		FEM	4.611	3.911	2.798	1.324	2.806	1.700	
10	TSDT	Exact	5.346	4.066	3.193	1.924	3.221	1.954	
		FEM	4.842	4.030	2.770	1.597	3.102	1.839	
	FSDT	Exact	5.009	3.642	2.692	1.723	2.968	1.594	
		FEM	4.863	3.754	2.550	1.648	3.010	1.674	
	CPT	Exact	5.009	3.829	3.167	1.725	2.986	1.865	
		FEM	4.611	3.911	2.798	1.324	2.806	1.700	

11.6.4 Closure

We close this section with a few comments on the third-order plate theory. The main merit of the third-order plate theory is that the transverse shear stress distributions are accurately represented through the laminate thickness and thus no shear correction factors are required. However, the accuracy gained over the FSDT in predicting the displacements, buckling loads and fundamental frequencies is not significant. For additional numerical results, one may consult [33–52,63–66].

Table 11.6.3: Nondimensionalized axial stress ($\bar{\sigma}_{yy}$) of antisymmetric cross-ply square plates with various boundary conditions.

<i>N</i>	<i>b/h</i>	Theory	Solution	SS	SC	CC	FF	FS	FC
5	TSDT	Exact	8.385	6.725	5.505	13.551	11.324	8.919	
		FEM	7.669	6.285	4.886	13.142	10.182	9.215	
	FSDT	Exact	7.157	6.034	5.153	11.907	9.848	8.047	
		FEM	6.948	5.914	4.990	11.675	9.140	8.367	
	CLPT	Exact	7.157	4.483	2.914	11.849	9.837	6.560	
		FEM	6.659	4.393	2.615	11.614	8.878	7.181	
2	TSDT	Exact	7.468	5.219	3.803	12.295	10.218	7.314	
		FEM	6.829	4.932	3.345	11.890	9.138	7.725	
	FSDT	Exact	7.157	5.109	3.799	11.884	9.847	7.150	
		FEM	6.948	5.082	3.661	11.654	9.1201	7.610	
10	CLPT	Exact	7.157	4.483	2.914	11.849	9.837	6.560	
		FEM	6.659	4.393	2.615	11.614	8.878	7.181	
	TSDT	Exact	6.340	5.635	4.963	9.454	8.252	6.934	
		FEM	5.762	5.209	4.410	9.113	7.424	6.994	
5	FSDT	Exact	5.009	4.628	4.212	7.583	6.590	5.706	
		FEM	4.864	4.511	4.086	7.429	6.141	5.844	
	CLPT	Exact	5.009	3.025	1.911	7.480	6.531	4.284	
		FEM	4.611	2.942	1.694	7.395	5.935	4.782	
10	TSDT	Exact	5.346	4.110	3.260	8.005	6.987	5.299	
		FEM	4.842	3.817	2.871	7.708	6.246	5.483	
	FSDT	Exact	5.009	3.904	3.135	7.533	6.566	5.029	
		FEM	4.863	3.852	3.031	7.384	6.097	5.279	
	CLPT	Exact	5.009	3.025	1.911	7.480	6.531	4.284	
		FEM	4.611	2.942	1.694	7.395	5.935	4.782	

Table 11.6.4: Nondimensionalized transverse shear ($\bar{\sigma}_{yz}$) of antisymmetric cross-ply square plates with various boundary conditions.

<i>N</i>	<i>b/h</i>	Theory	Solution	SS	SC	CC	FF	FS	FC
2	5	TSDT	Exact	3.155	2.543	2.095	4.457	3.893	3.048
		FSDT	Exact	2.729	2.297	1.958	3.901	3.390	2.748
	10	TSDT	Exact	3.190	2.290	1.725	4.489	3.927	2.805
		FSDT	Exact	2.729	1.993	1.523	3.882	3.383	2.449
10	5	TSDT	Exact	3.362	2.974	2.601	4.784	4.234	3.535
		FSDT	Exact	2.729	2.498	2.248	3.883	3.437	2.951
	10	TSDT	Exact	3.408	2.622	2.083	4.814	4.275	3.225
		FSDT	Exact	2.729	2.126	1.708	3.853	3.421	2.605

Table 11.6.5: Effect of side-to-thickness ratio on the dimensionless frequencies, $\bar{\omega} = \omega(b^2/h)\sqrt{\rho/E_2}$, of antisymmetric cross-ply square plates (Material 2).

N	b/h	Theory	Solution	FF	FS	FC	SS	SC	CC
2	5	TSDT	Exact	6.128	6.387	6.836	9.087	10.393	11.890
			FEM	6.172	6.192	6.648	9.103	10.582	12.053
		FSDT	Exact	5.952	6.213	6.638	8.833	9.822	10.897
			FEM	5.955	6.219	6.646	8.837	9.899	10.906
		CLPT	Exact	7.124	7.450	8.041	10.721	13.627	17.741
			FEM	7.150	7.279	7.802	11.192	15.357	18.694
	10	TSDT	Exact	6.943	7.277	7.810	10.568	12.870	15.709
			FEM	6.915	7.134	7.680	10.594	13.180	15.914
		FSDT	Exact	6.881	7.215	7.741	10.473	12.610	15.152
			FEM	6.886	7.222	7.714	10.480	12.791	15.181
		CLPT	Exact	7.267	7.636	8.228	11.154	14.223	18.543
			FEM	7.262	7.345	7.821	11.383	14.828	19.053
10	5	TSDT	Exact	8.155	8.288	8.966	11.673	12.514	13.568
			FEM	7.989	7.998	8.694	11.664	12.633	13.710
		FSDT	Exact	8.139	8.264	8.919	11.644	12.197	12.923
			FEM	8.143	8.270	8.925	11.647	12.239	12.928
		CLPT	Exact	11.459	11.815	13.618	12.167	23.348	30.855
			FEM	12.156	11.260	11.980	18.624	24.118	31.855
	10	TSDT	Exact	10.893	11.074	11.863	15.771	18.175	20.831
			FEM	10.906	11.088	11.788	15.787	18.214	20.493
		FSDT	Exact	10.900	11.079	11.862	15.779	18.044	20.471
			FEM	10.906	11.088	11.788	15.787	18.214	20.493
		CLPT	Exact	12.680	12.906	13.779	18.492	23.971	31.709
			FEM	12.419	11.283	11.983	18.637	23.991	31.912

Table 11.6.6: Effect of side-to-thickness ratio on the dimensionless critical buckling loads, $\bar{N} = N_{yy}^0 \frac{b^2}{E_2 h^3}$, of antisymmetric cross-ply square plates under uniaxial compression (Material 2).

N	b/h	Theory	Solution	FF	FS	FC	SS	SC	CC
2	5	TSDT	Exact	3.905	4.283	4.908	8.769	10.754	11.490
			FEM	3.979	4.375	5.022	8.985	11.241	12.318
		FSDT	Exact	3.682	4.054	4.632	8.277	9.309	9.757
			FEM	3.719	4.094	4.667	8.328	9.650	9.949
		CLPT	Exact	5.425	6.003	6.968	12.957	21.116	31.280
			FEM	5.616	6.292	7.203	14.520	23.869	37.106
	10	TSDT	Exact	4.940	5.442	6.274	11.562	17.133	21.464
			FEM	5.090	5.621	6.487	12.011	18.257	24.262
		FSDT	Exact	4.851	5.351	6.166	11.353	16.437	20.067
			FEM	4.916	5.420	6.234	11.485	18.338	21.916
		CLPT	Exact	5.425	6.003	6.968	12.957	21.116	31.280
			FEM	5.616	6.292	7.203	14.520	23.869	37.106

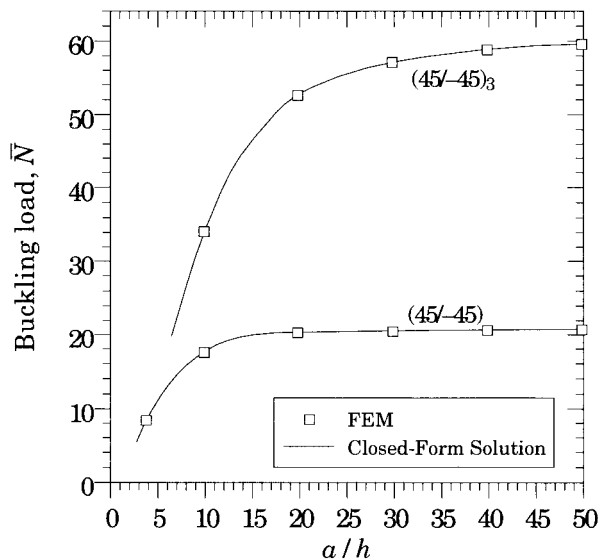
Table continued on the next page

Table continued from the previous page

N	b/h	Theory	Solution	FF	FS	FC	SS	SC	CC
10	5	TSDT	Exact	6.780	7.050	8.221	12.109	12.607	13.254
			FEM	6.802	7.089	8.278	12.224	12.800	13.659
		FSDT	Exact	6.750	7.020	8.143	11.494	11.495	11.628
			FEM	6.791	7.064	8.174	11.172	11.181	11.216
		CLPT	Exact	16.426	17.023	19.389	35.232	59.288	89.770
			FEM	16.457	17.141	19.422	36.384	60.406	90.833
	10	TSDT	Exact	12.077	12.506	14.351	25.423	32.885	35.376
			FEM	12.248	12.699	14.568	25.828	33.662	36.657
		FSDT	Exact	12.092	12.524	14.358	25.450	32.614	34.837
			FEM	12.226	12.661	14.480	25.647	33.970	36.129
		CLPT	Exact	16.426	17.023	19.389	35.232	59.288	89.770
			FEM	16.457	17.141	19.422	36.384	60.406	90.833

Table 11.6.7: Fundamental frequencies, $\bar{\omega} = \omega(b^2/h)\sqrt{\rho/E_2}$, of a cantilever plate (0/90) as predicted by various theories (Material 2).

b/a	CLPT		FSDT		TSDT	
	$b/h = 100$	$b/h = 10$	$b/h = 100$	$b/h = 10$	$b/h = 100$	$b/h = 10$
1	2.6285	2.6250	2.6103	2.5334	2.6378	2.5610
2	10.5138	10.4588	10.4318	9.3501	10.5385	9.5988
3	23.6548	23.3775	23.4354	18.8491	23.6666	19.8325

**Figure 11.6.1:** Nondimensionalized uniaxial critical buckling load versus side-to-thickness ratio for simply supported antisymmetric angle-ply (45/-45)_n ($n = 1, 3$) square plates (Material 2).

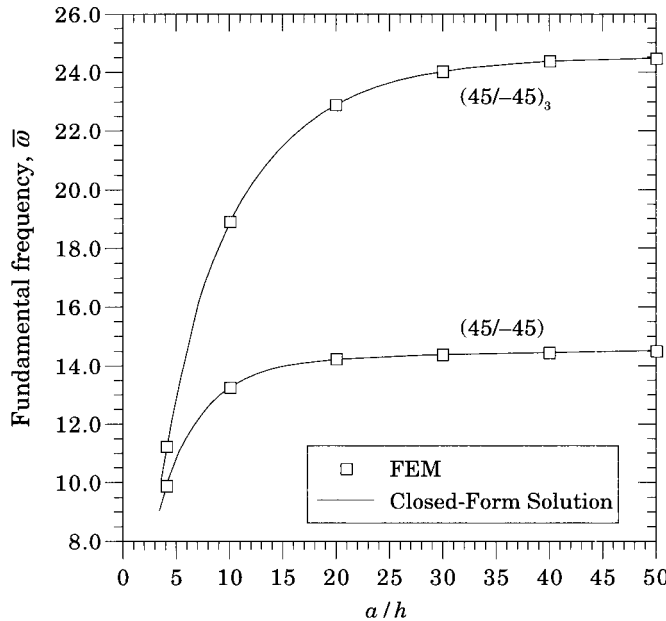


Figure 11.6.2: Nondimensionalized fundamental frequency versus side-to-thickness ratio for simply supported antisymmetric angle-ply $(45/-45)_n$ ($n = 1, 3$) square plates (Material 2).

11.7 Equations of Motion of the Third-Order Theory of Doubly-Curved Shells

Here we present the governing equations of the third-order shell theory. The development is made brief by the fact that we have discussed the geometric and kinematic relations of shells in Chapter 8, and the kinematics of the third-order theory in Section 11.2. We will not present any numerical results of the theory, and the interested readers may consult [67-74].

We begin with the following displacement field (see Reddy and Liu [67]):

$$\begin{aligned} u &= u_0 + \zeta \phi_1 - \zeta^3 \frac{4}{3h^2} \left(\phi_1 + \frac{\partial w_0}{\partial x} \right) \\ v &= v_0 + \zeta \phi_2 - \zeta^3 \frac{4}{3h^2} \left(\phi_2 + \frac{\partial w_0}{\partial y} \right) \\ w &= w_0 \end{aligned} \tag{11.7.1}$$

where (u, v, w) are the displacements along the orthogonal curvilinear coordinates such that the ξ_1 and ξ_2 curves are lines of principal curvature on the midsurface $\zeta = 0$, (u_0, v_0, w_0) are the displacements of a point on the middle surface, ϕ_1 and ϕ_2 are rotations at $\zeta = 0$ of normals to the midsurface with respect to the ξ_2 and ξ_1 -axes, respectively, and (x, y) are the planeform coordinates. The parameters R_1 and R_2 denote the values of the principal radii of curvature of the middle surface. All displacement components $(u_0, v_0, w_0, \phi_1, \phi_2)$ are functions of (x, y, t) .

The strain-displacement relations of the third-order shell theory are

$$\varepsilon_i = \varepsilon_i^0 + \zeta \left(\varepsilon_i^1 + \zeta^2 \varepsilon_i^2 \right) \text{ for } i = 1, 2, 6; \quad \varepsilon_i = \varepsilon_i^0 + \zeta^2 \varepsilon_i^1 \text{ for } i = 4, 5 \quad (11.7.2)$$

where

$$\begin{aligned} \varepsilon_1^0 &= \frac{\partial u_0}{\partial x} + \frac{w_0}{R_1}, & \varepsilon_1^0 &= \frac{\partial \phi_1}{\partial x}, & \varepsilon_4^0 &= \phi_2 + \frac{\partial w_0}{\partial y} - \frac{v_0}{R_2} \\ \varepsilon_2^0 &= \frac{\partial v_0}{\partial y} + \frac{w_0}{R_2}, & \varepsilon_2^0 &= \frac{\partial \phi_2}{\partial y}, & \varepsilon_5^0 &= \phi_1 + \frac{\partial w_0}{\partial x} - \frac{u_0}{R_1} \\ \varepsilon_6^0 &= \frac{\partial v_0}{\partial x} + \frac{\partial u_0}{\partial y}, & \varepsilon_6^1 &= \frac{\partial \phi_2}{\partial x} + \frac{\partial \phi_1}{\partial y} \\ \varepsilon_1^2 &= -c_2 \left(\frac{\partial \phi_1}{\partial x} + \frac{\partial^2 w_0}{\partial x^2} - \frac{1}{R_1} \frac{\partial u_0}{\partial x} \right), & \varepsilon_2^2 &= -c_2 \left(\frac{\partial \phi_2}{\partial y} + \frac{\partial^2 w_0}{\partial y^2} - \frac{1}{R_2} \frac{\partial v_0}{\partial y} \right) \\ \varepsilon_6^2 &= -c_2 \left(\frac{\partial \phi_2}{\partial x} + \frac{\partial \phi_1}{\partial y} + 2 \frac{\partial^2 w_0}{\partial x \partial y} - \frac{1}{R_2} \frac{\partial v_0}{\partial x} - \frac{1}{R_1} \frac{\partial u_0}{\partial y} \right) \\ \varepsilon_4^1 &= -c_1 \left(\phi_2 + \frac{\partial w_0}{\partial y} - \frac{v_0}{R_2} \right), & \varepsilon_5^1 &= -c_1 \left(\phi_1 + \frac{\partial w_0}{\partial x} - \frac{u_0}{R_1} \right) \end{aligned} \quad (11.7.3)$$

and $c_1 = 4/h^2$ and $c_2 = c_1/3$.

Using Hamilton's principle, the equations of motion of the third-order shell theory are obtained as

$$\frac{\partial N_{xx}}{\partial x} + \frac{\partial N_{xy}}{\partial y} + \frac{\bar{Q}_x}{R_1} + \frac{c_1}{R_1} \left(\frac{\partial P_{xx}}{\partial x} + \frac{\partial P_{xy}}{\partial y} \right) = I_0 \ddot{u}_0 + J_1 \ddot{\phi}_x - c_1 I_3 \frac{\partial \ddot{w}_0}{\partial x} \quad (11.7.4)$$

$$\frac{\partial N_{xy}}{\partial x} + \frac{\partial N_{yy}}{\partial y} + \frac{\bar{Q}_y}{R_2} + \frac{c_1}{R_2} \left(\frac{\partial P_{xy}}{\partial x} + \frac{\partial P_{yy}}{\partial y} \right) = I_0 \ddot{v}_0 + J_1 \ddot{\phi}_y - c_1 I_3 \frac{\partial \ddot{w}_0}{\partial y} \quad (11.7.5)$$

$$\begin{aligned} \frac{\partial \bar{Q}_x}{\partial x} + \frac{\partial \bar{Q}_y}{\partial y} + \frac{\partial}{\partial x} (N_{xx} \frac{\partial w_0}{\partial x} + N_{xy} \frac{\partial w_0}{\partial y}) + \frac{\partial}{\partial y} (N_{xy} \frac{\partial w_0}{\partial x} + N_{yy} \frac{\partial w_0}{\partial y}) \\ + c_2 \left(\frac{\partial^2 P_{xx}}{\partial x^2} + \frac{\partial^2 P_{yy}}{\partial y^2} + 2 \frac{\partial^2 P_{xy}}{\partial x \partial y} \right) - \frac{N_{xx}}{R_1} - \frac{N_{yy}}{R_2} + q \\ = I_0 \ddot{w}_0 - c_1^2 I_6 \left(\frac{\partial^2 \ddot{w}_0}{\partial x^2} + \frac{\partial^2 \ddot{w}_0}{\partial y^2} \right) + c_1 \left[I_3 \left(\frac{\partial \ddot{u}_0}{\partial x} + \frac{\partial \ddot{v}_0}{\partial y} \right) + J_4 \left(\frac{\partial \ddot{\phi}_x}{\partial x} + \frac{\partial \ddot{\phi}_y}{\partial y} \right) \right] \end{aligned} \quad (11.7.6)$$

$$\frac{\partial \bar{M}_{xx}}{\partial x} + \frac{\partial \bar{M}_{xy}}{\partial y} - \bar{Q}_x = J_1 \ddot{u}_0 + K_2 \ddot{\phi}_x - c_1 J_4 \frac{\partial \ddot{w}_0}{\partial x} \quad (11.7.7)$$

$$\frac{\partial \bar{M}_{xy}}{\partial x} + \frac{\partial \bar{M}_{yy}}{\partial y} - \bar{Q}_y = J_1 \ddot{v}_0 + K_2 \ddot{\phi}_y - c_1 J_4 \frac{\partial \ddot{w}_0}{\partial y} \quad (11.7.8)$$

where q is the distributed transverse mechanical load, and all other quantities are the same as those defined in Eqs. (11.2.21)–(11.2.23). The displacement finite element model of these equations can be developed using the steps outlined in Section 9.4.2.

Problems

- 11.1** Suppose that the displacements (u, v, w) along the three coordinate axes (x, y, z) in a laminated beam can be expressed as

$$\begin{aligned} u(x, z) &= u_0(x) + z \left[c_0 \frac{dw_0}{dx} + c_1 \phi(x) \right] + c_2 z^2 \psi(x) + c_3 \left(\frac{z}{h} \right)^3 \left(\phi + \frac{dw_0}{dx} \right) \\ v(x, z) &= 0 \\ w(x, z) &= w_0(x) \end{aligned} \quad (1)$$

where (u_0, w_0) denote the displacements of a point $(x, y, 0)$ along the x and z directions, respectively, ϕ denotes the rotation of a transverse normal about the y -axis. Show that the nonzero linear strains are given by

$$\begin{aligned} \varepsilon_{xx} &= \varepsilon_{xx}^{(0)} + z \varepsilon_{xx}^{(1)} + z^2 \varepsilon_{xx}^{(2)} + z^3 \varepsilon_{xx}^{(3)} \\ \gamma_{xz} &= \gamma_{xz}^{(0)} + z \gamma_{xz}^{(1)} + z^2 \gamma_{xz}^{(2)} \end{aligned} \quad (2a)$$

where

$$\begin{aligned} \varepsilon_{xx}^{(0)} &= \frac{du_0}{dx}, \quad \varepsilon_{xx}^{(1)} = c_0 \frac{d^2 w_0}{dx^2} + c_1 \frac{d\phi}{dx}, \quad \varepsilon_{xx}^{(2)} = c_2 \frac{d\psi}{dx}, \quad \varepsilon_{xx}^{(3)} = \frac{c_3}{h^3} \left(\frac{d\phi}{dx} + \frac{d^2 w_0}{dx^2} \right) \\ \gamma_{xz}^{(0)} &= (1 + c_0) \frac{dw_0}{dx} + c_1 \phi, \quad \gamma_{xz}^{(1)} = 2c_2 \psi, \quad \gamma_{xz}^{(2)} = \frac{3c_3}{h^3} \left(\phi + \frac{dw_0}{dx} \right) \end{aligned} \quad (2b)$$

- 11.2** (Continuation of Problem 11.1.) Use the principle of virtual displacements to derive the equations of equilibrium and the natural and essential boundary conditions associated with the displacement field of Exercise 1. In particular show that

$$\begin{aligned} \delta u_0 : \quad & \frac{dN_x}{dx} - p = 0 \\ \delta \phi : \quad & \frac{d}{dx} \left(c_1 M_x \right) + \frac{d}{dx} \left(\frac{c_3}{h^3} P_x \right) - c_1 Q_x - \frac{3c_3}{h^3} S_x = 0 \\ \delta \psi : \quad & \frac{d}{dx} \left(c_2 L_x \right) - 2c_2 R_x = 0 \\ \delta w_0 : \quad & \frac{d^2}{dx^2} \left(c_0 M_x + \frac{c_3}{h^3} P_x \right) - (1 + c_0) \frac{dQ_x}{dx} - \frac{3c_3}{h^3} \frac{dS_x}{dx} - f = 0 \end{aligned} \quad (1)$$

and the boundary conditions involve specifying

$$\begin{aligned} N_x &\text{ or } u \\ c_1 M_x + \frac{c_3}{h^3} P_x &\text{ or } \phi \\ c_2 L_x &\text{ or } \psi \\ -\frac{d}{dx} \left(c_0 M_x + \frac{c_3}{h^3} P_x \right) + (1 + c_0) Q_x + \frac{3c_3}{h^3} S_x &\text{ or } w_0 \\ c_0 M_x + \frac{c_3}{h^3} P_x &\text{ or } \frac{dw_0}{dx} \end{aligned} \quad (2)$$

where

$$N_x = \int_A \sigma_{xx} dA, \quad M_{xx} = \int_A \sigma_{xx} z dA, \quad L_x = \int_A \sigma_{xx} z^2 dA, \quad P_x = \int_A \sigma_{xx} z^3 dA \quad (3)$$

$$Q_x = \int_A \sigma_{xz} dA, \quad R_x = \int_A \sigma_{xz} z dA, \quad S_x = \int_A \sigma_{xz} z^2 dA \quad (4)$$

Note that the displacement field of Problem 11.1, hence the equations of equilibrium (1), contain those of the classical (Euler–Bernoulli) beam theory ($c_0 = -1$, $c_1 = 0$, $c_2 = 0$, $c_3 =$

0), the first-order (Timoshenko) beam theory ($c_0 = 0$, $c_1 = 1$, $c_2 = 0$, $c_3 = 0$), and the third-order (Reddy) beam theory ($c_0 = 0$, $c_1 = 1$, $c_2 = 0$, $c_3 = -4h/3$).

11.3 (Continuation of Problems 11.1 and 11.2) Assume linear elastic constitutive behavior and show that the laminated beam's constitutive equations are given by

$$\begin{Bmatrix} N_x \\ M_x \\ L_x \\ P_x \end{Bmatrix} = \begin{bmatrix} A_{11} & B_{11} & D_{11} & E_{11} \\ B_{11} & D_{11} & E_{11} & F_{11} \\ D_{11} & E_{11} & F_{11} & G_{11} \\ E_{11} & F_{11} & G_{11} & H_{11} \end{bmatrix} \begin{Bmatrix} \varepsilon_{xx}^{(0)} \\ \varepsilon_{xx}^{(1)} \\ \varepsilon_{xx}^{(2)} \\ \varepsilon_{xx}^{(3)} \end{Bmatrix} \quad (1)$$

$$\begin{Bmatrix} Q_x \\ R_x \\ S_x \end{Bmatrix} = \begin{bmatrix} A_{55} & B_{55} & D_{55} \\ B_{55} & D_{55} & E_{55} \\ D_{55} & E_{55} & F_{55} \end{bmatrix} \begin{Bmatrix} \gamma_{xz}^{(0)} \\ \gamma_{xz}^{(1)} \\ \gamma_{xz}^{(2)} \end{Bmatrix} \quad (2)$$

where

$$\begin{aligned} (A_{11}, B_{11}, D_{11}, F_{11}, G_{11}, H_{11}) &= \int_A E_1(1, z, z^2, z^4, z^5, z^6) dA \\ (A_{55}, B_{55}, D_{55}, E_{55}, F_{55}) &= \int_A G_{13}(1, z, z^2, z^3, z^4) dA \end{aligned} \quad (3)$$

- 11.4** Show that for a general laminate composed of multiple isotropic layers, the laminate stiffnesses B_{16} , B_{26} , E_{16} , E_{26} , F_{16} , and F_{26} are zero.
- 11.5** Specialize the equations of Problem 11.2 to the case in which $c_0 = 0$, $c_1 = 1$, $c_2 = 0$ and $c_3 = -4h/3$, and express the equations in terms of the displacements.
- 11.6** Simplify the equations of motion in Eqs. (11.2.16)–(11.2.20) to cylindrical bending of plate strips.
- 11.7** Specialize the equations of motion and boundary conditions of the third-order theory of Reddy (see Section 11.2.3) to static bending of beams. Discuss the consequence of neglecting the higher-order resultant P_{xx} (but not R_x) on the equations and boundary conditions.
- 11.8** Develop the Navier solution of the third-order theory of laminated beams derived in Problem 11.5.

References for Additional Reading

1. Reddy, J. N., and Chandrasekhar, K., "A Review of the Literature on Finite-Element Modeling of Laminated Composite Plates," *Shock and Vibration Digest*, **17**(4), 3–8 (1985).
2. Reddy, J. N., "A Review of Refined Theories of Laminated Composite Plates," *Shock and Vibration Digest*, **22**(7), 3–17 (1990).
3. Basset, A. B., "On the Extension and Flexure of Cylindrical and Spherical Thin Elastic Shells," *Philosophical Transactions of the Royal Society*, (London) Series A, **181**(6), 433–480 (1890).
4. Hildebrand, F. B., Reissner, E., and Thomas, G. B., "Notes on the Foundations of the Theory of Small Displacements of Orthotropic Shells," NACA TN-1833, Washington, D.C. (1949).
5. Vlasov, B. F., "Ob uravnieniakh izgiba plastinok (On equations of bending of plates)," (in Russian), *Doklady Akademii Nauk Azerbeijanskoi SSR*, **3**, 955–959 (1957).
6. Dong, S. B. and Tso, F. K. W., "On a Laminated Orthotropic Shell Theory Including Transverse Shear Deformation," *Journal of Applied Mechanics*, **39**, 1091–1097 (1972).
7. Librescu, L., "The Elasto-Kinetic Problems in the Theory of Anisotropic Shells and Plates, Part II, Plates Theory," *Revue Roumaine des Sciences Techniques Serie de Mecanique Appliquee*, **7**(3) (1969).
8. Sun, C. T., "Theory of Laminated Plates," *Journal of Applied Mechanics*, **38**, 231–238 (1971).
9. Sun, C. T. and Cheng, N. C., "On the Governing Equations for a Laminated Plate," *Journal of Sound and Vibration*, **21**(3), 307–316 (1972).

11. Sun, C. T. and Whitney, J. M., "On Theories for the Dynamic Response of Laminated Plates," *AIAA Journal*, **11**(2), 178–183 (1973).
11. Whitney, J. M. and Sun, C. T., "A Higher Order Theory for Extensional Motion of Laminated Anisotropic Shells and Plates," *Journal of Sound and Vibration*, **30**, 85–97 (1973).
12. Mau, S. T., "A Refined Laminate Plate Theory," *Journal of Applied Mechanics*, **40**, 606–607 (1973).
13. Nelson, R. B. and Lorch, D. R., "A Refined Theory for Laminated Orthotropic Plates," *Journal of Applied Mechanics*, **41**, 177–183 (1974).
14. Jemielita, G., "Techniczna Teoria Płyty Średniej Grubbosci," (Technical Theory of Plates with Moderate Thickness), *Rozprawy Inżynierskie (Engineering Transactions)*, *Polska Akademia Nauk*, **23**(3), 483–499 (1975).
15. Librescu, L., *Elastostatics and Kinetics of Anisotropic and Heterogeneous Shell-Type Structures*, Noordhoff, Leyden, The Netherlands (1975).
16. Schmidt, R., "A Refined Nonlinear Theory for Plates with Transverse Shear Deformation," *Journal of the Industrial Mathematics Society*, **27**(1), 23–38 (1977).
17. Lo, K. H., Christensen, R. M., and Wu, E. M., "A High-Order Theory of Plate Deformation: Part 1: Homogeneous Plates," *Journal of Applied Mechanics*, **44**(4), 663–668 (1977).
18. Lo, K. H., Christensen, R. M., and Wu, E. M., "A High-Order Theory of Plate Deformation, Part 2: Laminated Plates," *Journal of Applied Mechanics*, **44**(4), 669–676 (1977).
19. Lo, K. H., Christensen, R. M., and Wu, E. M., "Stress Solution Determination for High Order Plate Theory," *International Journal of Solids and Structures*, **14**, 665–662 (1978).
20. Krishna Murty, A. V., "Higher Order Theory for Vibration of Thick Plates," *AIAA Journal*, **15**(2), 1823–1824 (1977).
21. Levinson, M., "An Accurate, Simple Theory of the Static and Dynamics of Elastic Plates," *Mechanics Research Communications*, **7**(6), 343–350 (1980).
22. Murthy, M. V. V., "An Improved Transverse Shear Deformation Theory for Laminated Anisotropic Plates," NASA Technical Paper, 1903, 1–37 (1981).
23. Levinson, M. and Cooke, D. W., "Thick Rectangular Plates—I. The Generalized Navier Solution," *International Journal of Mechanical Sciences*, **25**(3), 199–205 (1983).
24. Cooke, D. W. and Levinson, M., "Thick Rectangular Plates—II. The Generalized Lévy Solution," *International Journal of Mechanical Sciences*, **25**(3), 207–215 (1983).
25. Reddy, J. N., "A Simple Higher-Order Theory for Laminated Composite Plates," *Journal of Applied Mechanics*, **51**, 745–752 (1984).
26. Reddy, J. N., "A Refined Nonlinear Theory of Plates with Transverse Shear Deformation," *International Journal of Solids Structures*, **20**(9/10), 881–906 (1984).
27. Bhimaraddi, A. and Stevens, L. K., "A Higher Order Theory for Free Vibration of Orthotropic, Homogeneous and Laminated Rectangular Plates," *Journal of Applied Mechanics*, **51**, 195–198 (1984).
28. Di Sciuva, M., "A Refined Transverse Shear Deformation Theory for Multilayered Anisotropic Plates," *Atti della Accademia delle Scienze di Torino*, **118**, 269–295 (1984).
29. Reddy, J. N. and Phan, N. D., "Stability and Vibration of Isotropic Orthotropic and Laminated Plates According to a Higher-Order Shear Deformation Theory," *Journal of Sound and Vibration*, **98**, 157–170 (1985).
30. Phan, N. D., and Reddy, J. N., "Analysis of Laminated Composite Plates Using a Higher-Order Shear Deformation Theory," *International Journal for Numerical Methods in Engineering*, **21**, 2201–2219 (1985).
31. Krishna Murty, A. V., "Flexure of Composite Plates," *Composite Structures*, **7**(3), 161–177 (1987).
32. Reddy, J. N., "A Small Strain and Moderate Rotation Theory of Laminated Anisotropic Plates," *Journal of Applied Mechanics*, **54**, 623–626 (1987).
33. Khdeir, A. A., Reddy, J. N., and Librescu, L., "Lévy Type Solutions for Symmetrically Laminated Rectangular Plates Using First-Order Shear Deformation Theory," *Journal of Applied Mechanics*, **54**, 640–642 (1987).

34. Khdeir, A. A., Reddy, J. N., and Librescu, L., "Analytical Solution of a Refined Shear Deformation Theory for Rectangular Composite Plates," *International Journal of Solids and Structures*, **23**(10), 1447–1463 (1987).
35. Librescu, L., Khdeir, A. A., and Reddy, J. N., "A Comprehensive Analysis of the State of Elastic Anisotropic Flat Plates Using Refined Theories," *Acta Mechanica*, **70**, 57–81 (1987).
36. Di Sciuva, M., "An Improved Shear-deformation Theory for Moderately Thick Multilayered Anisotropic Shells and Plates," *Journal of Applied Mechanics*, **54**(3), 589–596 (1987).
37. Bhimaraddi, A., "Dynamic Response Orthotropic, Homogeneous, and Laminated Cylindrical Shells," *AIAA Journal*, **27**(11), 1834–1837 (1985).
38. Khdeir, A. A. and Reddy, J. N., "Dynamic Response of Antisymmetric Angle-Ply Laminated Plates Subjected to Arbitrary Loading," *Journal of Sound and Vibration*, **126**(3), 437–445 (1988).
39. Khdeir, A. A., "Free Vibration of Antisymmetric Angle-Ply Laminated Plates Including Various Boundary Conditions," *Journal of Sound and Vibration*, **122**(2), 377–388 (1988).
40. Khdeir, A. A., "Free Vibration and Buckling of Symmetric Cross-Ply Laminated Plates by an Exact Method," *Journal of Sound and Vibration*, **126**(3), 447–461 (1988).
41. Librescu, L. and Khdeir, A. A., "Analysis of Symmetric Cross-Ply Laminated Elastic Plates Using a Higher-Order Theory, Part I. Stress and Displacement," *Composite Structures*, **9**, 189–213 (1988).
42. Khdeir, A. A. and Librescu, L., "Analysis of Symmetric Cross-Ply Laminated Elastic Plates Using a Higher-Order Theory, Part II. Buckling and Free Vibration," *Composite Structures*, **9**, 259–277 (1988).
43. Librescu, L. and Reddy, J. N., "A Few Remarks Concerning Several Refined Theories of Anisotropic Composite Laminated Plates," *International Journal of Engineering Science*, **27**(5), 515–527 (1989).
44. Khdeir, A. A. and Reddy, J. N., "Exact-Solutions for the Transient Response of Symmetric Cross-Ply Laminates Using a Higher-Order Plate Theory," *Composite Science and Technology*, **34**, 205–224 (1989).
45. Khdeir, A. A. and Reddy, J. N., "On the Forced Motions of Antisymmetric Cross-Ply Laminated Plates," *International Journal of Mechanical Sciences*, **31**(7), 499–510 (1989).
46. Khdeir, A. A., "An Exact Approach to the Elastic State of Stress of Shear Deformable Antisymmetric Angle-Ply Laminated Plates," *Composite Structures*, **11**, 245–258 (1989).
47. Khdeir, A. A., "Stability of Antisymmetric Angle-Ply Laminated Plates," *Journal of Engineering Mechanics*, **115**(5), 952–962 (1989).
48. Khdeir, A. A., "Free Vibration and Buckling of Unsymmetric Cross-Ply Laminated Plates Using a Refined Theory," *Journal of Sound and Vibration*, **128**(3), 377–395 (1989).
49. Reddy, J. N., "A General Non-Linear Third-Order Theory of Plates with Moderate Thickness," *International Journal of Non-Linear Mechanics*, **25**(6), 677–686 (1990).
50. Khdeir, A. A. and Reddy, J. N., "Thermal Stresses and Deflections of Cross-Ply Laminated Plates Using Refined Plate Theories," *Journal of Thermal Stresses*, **14**(4), 419–438 (1991).
51. Khdeir, A. A. and Reddy, J. N., "Analytical Solutions of Refined Plate Theories of Cross-Ply Composite Laminates," *Journal of Pressure Vessel Technology*, **113**(4), 570–578 (1991).
52. Nosier, A. and Reddy, J. N., "On Vibration and Buckling of Symmetric Laminated Plates According to Shear Deformation Theories," *Acta Mechanica*, **94**(3,4), 123–170 (1992).
53. Pagano, N. J., "Exact Solutions for Rectangular Bidirectional Composites and Sandwich Plates," *Journal of Composite Materials*, **4**, 20–34 (1970).
54. Pagano, N. J. and Hatfield, S. J., "Elastic Behavior of Multilayered Bidirectional Composites," *AIAA Journal*, **10**, 931–933 (1972).
55. Noor, A. K., "Free Vibrations of Multilayered Composite Plates," *AIAA Journal*, **11**(7), 1038–1039 (1972).
56. Noor, A. K., "Mixed Finite-Difference Scheme for Analysis of Simply Supported Thick Plates," *Computers and Structures*, **3**, 967–982 (1973).

57. Noor, A. K., "Stability of Multilayered Composite Plates," *Fibre Science and Technology*, **8**, 81–88 (1975).
58. Reddy, J. N., "On Mixed Finite-Element Formulations of a Higher-Order Theory of Composite Laminates," *Finite Element Methods for Plate and Shell Structures*, T. J. R. Hughes and E. Hinton (Eds.), Pineridge Press, UK, 31–57 (1986).
59. Putcha, N. S. and Reddy, J. N., "A Mixed Shear Flexible Finite Element for the Analysis of Laminated Plates," *Computer Methods in Applied Mechanics and Engineering*, **44**, 213–227 (1984).
60. Putcha, N. S. and Reddy, J. N., "A Refined Mixed Shear Flexible Finite Element for the Nonlinear Analysis of Laminated Plates," *Computers and Structures*, **22**(4), 529–538 (1986).
61. Pandya, B. N. and Kant, T., "Flexural Analysis of Laminated Composites Using Refined Higher-Order C^0 Plate Bending Element," *Computer Methods in Applied Mechanics and Engineering*, **66**, 173–198 (1988).
62. Reddy, J. N., *An Introduction to the Finite Element Method*, Second Edition, McGraw-Hill, New York (1993).
63. Reddy, J. N. and Khdeir, A. A., "Buckling and Vibration of Laminated Composite Plates Using Various Plate Theories," *AIAA Journal*, **27**(12), 1808–1817 (1989).
64. Nosier, A. and Reddy, "On Vibration and Buckling of Symmetric Laminated Plates According to Shear Deformation Theories," Parts I and II, *Acta Mechanica*, **94** (11), 123–144 and 145–169 (1992).
65. Bose, P., and Reddy, J. N., "Analysis of Composite Plates Using Various Plate Theories, Part 1: Formulation and Analytical Results," *Structural Engineering and Mechanics*, **6**(6), 583–612 (1998).
66. Bose, P., and Reddy, J. N., "Analysis of Composite Plates Using Various Plate Theories, Part 2: Finite Element Model and Numerical Results," *Structural Engineering and Mechanics*, **6**(7), 727–746 (1998).
67. Reddy, J. N. and Liu, C. F., "A Higher-Order Shear Deformation Theory for Laminated Elastic Shells," *International Journal of Engineering Science*, **23**, 319–330 (1985).
68. Reddy, J. N. and Liu, C. F., "A Higher-Order Theory for Geometrically Nonlinear Analysis of Composite Laminates," NASA CR 4656, NASA Langley Research Center, Hampton, VA (1987).
69. Khdeir, A. A., Reddy, J. N., and Frederick, D., "A Study of Bending, Vibration and Buckling of Cross-Ply Circular Cylindrical Shells with Various Shell Theories," *International Journal of Engineering Science*, **27** (11), 1337–1351 (1989).
70. Reddy, J. N. and Khdeir, A. A., "Dynamic Response of Cross-Ply Laminated Shallow Shells According to a Refined Shear Deformation Theory," *Journal of the Acoustical Society of America*, **85**(6), 2423–2431 (1991).
71. Mitchell, J. A. and Reddy, J. N., "A Refined Hybrid Plate Theory for Composite Laminates with Piezoelectric Laminae," *International Journal of Solids and Structures*, **32**(16), 2345–2367 (1995).
72. Reddy, J. N. and Mitchell, J. A., "Refined Nonlinear Theories of Laminated Composite Structures with Piezoelectric Laminae," *Sadhana (Journal of the Indian Academy of Sciences)*, **20**, 721–747 (1995).
73. Wang, C. M. and Reddy, J. N., "Deflection Relationships Between Classical and Third-Order Plate Theories," *Acta Mechanica*, **130**(3-4), 199–208 (1998).
74. Shi, G., Lam, K. Y., Tay, S. T. E., and Reddy, J. N., "Assumed Strain Quadrilateral C^0 Laminated Plate Element Based on Third-Order Shear Deformation Theory," *Structural Engineering Mechanics*, **8**(6), 623–637 (1999).

Layerwise Theory and Variable Kinematic Models

12.1 Introduction

12.1.1 Motivation

The analysis of fiber-reinforced, laminated composite structures presents the analyst with many challenges. Unlike their homogeneous isotropic counterparts, the heterogeneous anisotropic constitution of laminated composite structures often results in the appearance of many unique phenomena that can occur on vastly different geometric scales, i.e., at the global or laminate level, the ply level, or the fiber/matrix level. For example, the global deformation of laminated composite structures is often characterized by complex coupling between the extension, bending, and shearing modes. Further, due to their characteristically low transverse shear stiffness, composite laminates often exhibit significant transverse shear deformation at lower thickness-to-span ratios than do similar homogeneous isotropic plates and shells. At the ply level, laminated composites often exhibit transverse stress concentrations near material and geometric discontinuities (the so-called free edge effect) that can lead to damage in the form of delamination, matrix cracking, and adhesive joint separation. Once significant damage occurs at the ply level, the kinematic and material description of the problem must be changed before further analysis can proceed. At the fiber/matrix level, stress concentrations can cause fiber/matrix separation, radial matrix cracking, and other forms of cumulative damage that degrade the stiffness of individual laminae, thus causing a complex load redistribution.

When the main emphasis of the analysis is to determine the global response of the laminated component, for example, gross deflections, critical buckling loads, fundamental vibration frequencies, and associated mode shapes, such global behavior can often be accurately determined using relatively simple equivalent-single-layer laminate theories (ESL theories), especially for very thin laminates. Two commonly used examples of simple ESL theories are the classical and the first-order shear deformation theories discussed earlier.

As laminated composite materials undergo the transition from secondary structural components to primary critical structural components, the goals of analysis must be broadened to include a highly accurate assessment of localized regions where damage initiation is likely. The simple ESL laminate theories that often prove adequate for modeling secondary structures are of limited value in

modeling primary structures for two reasons. First of all, most primary structural components are considerably thicker than secondary components; thus even the determination of the global response may require a refined laminate theory that accounts for thickness effects. Second, the assessment of localized regions of potential damage initiation begins with an accurate determination of the three-dimensional state of stress and strain at the ply level, regardless of whether damage prediction and assessment is desired at the ply level or at the fiber/matrix level. The simple ESL laminate theories are most often incapable of accurately determining the 3-D stress field at the ply level. Thus the analysis of primary composite structural components may require the use of 3-D elasticity theory or a layerwise laminate theory that contains full 3-D kinematics and constitutive relations.

From the equilibrium of interlaminar forces, it follows that the following continuity conditions hold between the stress fields of adjacent layers at their interface (see Figure 12.1.1):

$$\left\{ \begin{array}{c} \sigma_{xx} \\ \sigma_{yy} \\ \sigma_{xy} \end{array} \right\}^{(k)} \neq \left\{ \begin{array}{c} \sigma_{xx} \\ \sigma_{yy} \\ \sigma_{xy} \end{array} \right\}^{(k+1)}, \quad \left\{ \begin{array}{c} \sigma_{xz} \\ \sigma_{yz} \\ \sigma_{zz} \end{array} \right\}^{(k)} = \left\{ \begin{array}{c} \sigma_{xz} \\ \sigma_{yz} \\ \sigma_{zz} \end{array} \right\}^{(k+1)} \quad (12.1.1)$$

These conditions in turn imply, since $[\bar{Q}^{(k)}] \neq [\bar{Q}^{(k+1)}]$ in general, that the strain fields of adjacent layers satisfy the following conditions:

$$\left\{ \begin{array}{c} \gamma_{xz} \\ \gamma_{yz} \\ \varepsilon_{zz} \end{array} \right\}^{(k)} \neq \left\{ \begin{array}{c} \gamma_{xz} \\ \gamma_{yz} \\ \varepsilon_{zz} \end{array} \right\}^{(k+1)} \quad (12.1.2)$$

In all equivalent single-layer laminate theories based on assumed displacement fields, it is assumed that the displacements are continuous functions of the thickness coordinate. This in turn results in continuous transverse strains, contrary to the requirement (12.1.1). Hence, all stresses in equivalent-single layer theories are discontinuous at layer interfaces. More important, the transverse stresses at the interface of two layers, called *interlaminar stresses*, are discontinuous:

$$\left\{ \begin{array}{c} \sigma_{xz} \\ \sigma_{yz} \\ \sigma_{zz} \end{array} \right\}^{(k)} \neq \left\{ \begin{array}{c} \sigma_{xz} \\ \sigma_{yz} \\ \sigma_{zz} \end{array} \right\}^{(k+1)} \quad (12.1.3)$$

For thin laminates the error introduced due to discontinuous interlaminar stresses can be negligible. However, for thick laminates, the ESL theories can give erroneous results for all stresses, requiring use of layerwise theories.

12.1.2 An Overview of Layerwise Theories

In contrast to the ESL theories, the layerwise theories are developed by assuming that the displacement field exhibits only C^0 -continuity through the laminate thickness. Thus the displacement components are continuous through the laminate thickness but the derivatives of the displacements with respect to the thickness coordinate may be discontinuous at various points through the thickness, thereby allowing for the possibility of continuous transverse stresses at interfaces separating dissimilar materials. Layerwise displacement fields provide a much more kinematically correct representation of the moderate to severe cross-sectional warping associated with the deformation of thick laminates.

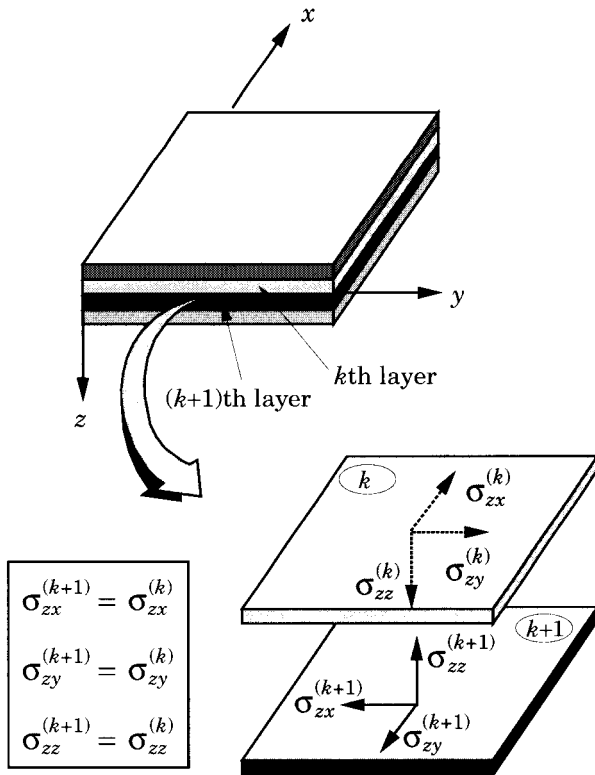


Figure 12.1.1: Equilibrium of interlaminar stresses.

The displacement-based layerwise theories can be subdivided into two classes: (1) the *partial layerwise theories* that use layerwise expansions for the in-plane displacement components but not the transverse displacement component, and (2) the *full layerwise theories* that use layerwise expansions for all three displacement components. Compared to the ESL theories, the partial layerwise theories provide a more realistic description of the kinematics of composite laminates by introducing discrete layer transverse shear effects into the assumed displacement field. The full layerwise theories go one step further by adding both discrete layer transverse shear effects and discrete layer transverse normal effects.

The use of the partial and full layerwise theories for the analysis of thick laminated composite plates is widely accepted. Such theories allow the in-plane displacements to vary in a layerwise manner through the thickness of the laminate. The layerwise theories can represent the zigzag behavior of the in-plane displacements through the thickness. This zigzag behavior is more pronounced for thick laminates where the transverse shear modulus changes abruptly through the thickness and can be seen in the exact 3-D elasticity solutions obtained by Pagano [1,2], Pagano and Hatfield [3], Srinivas and Rao [4,5], Noor [6,7], and Savoia and Reddy [8] for the bending of rectangular laminated plates, and by Varadan and Bhaskar [9] and Ren [10] for the bending of laminated shells.

Whitney [11] used a layerwise quadratic variation of the transverse stresses for improving the gross behavior of laminated plates. This led to a layerwise cubic variation of the in-plane displacements. The use of the necessary continuity conditions resulted in the same number of variables as in the FSDT. However, the equations of equilibrium were taken to be those of the classical lamination theory, and thus they were not consistent in an energy sense. The numerical results obtained for deflections, natural frequencies, and buckling loads were found to be in good agreement with available exact elasticity solutions.

In a series of papers, Swift and Heller [12] studied laminated beams by assuming layerwise constant shear strains and a continuous transverse displacement through the thickness. A similar approach was used by Durocher and Solecki [13] to study transversely isotropic plates with two or three layers. Seide [14], and Choudhuri and Seide [15] extended the work of Swift and Heller to laminated plates (also see [16–20]). The approach involves writing the equilibrium equations for k th lamina in terms of the force and moment resultants

$$\frac{\partial N_{\alpha\beta}^{(k)}}{\partial x_\beta} + \sigma_{\alpha 3}^{(k+1)} - \sigma_{\alpha 3}^{(k)} = 0, \quad \frac{\partial Q_\alpha^{(k)}}{\partial x_\alpha} + \sigma_{33}^{(k+1)} - \sigma_{33}^{(k)} = 0 \quad (12.1.4a)$$

$$\frac{\partial M_{\alpha\beta}^{(k)}}{\partial x_\beta} + \sigma_{\alpha 3}^{(k+1)} z_{k+1} - \sigma_{\alpha 3}^{(k)} z_k - Q_\alpha^k = 0 \quad (12.1.4b)$$

for $k = 1, 2, \dots, N$ and $\alpha, \beta = 1, 2$ ($x_1 = x, x_2 = y, x_3 = z$), where N is the total number of layers, and

$$(N_{\alpha\beta}^{(k)}, M_{\alpha\beta}^{(k)}) = \int_{z_k}^{z_{k+1}} (1, z) \sigma_{\alpha\beta}^{(k)} dz \quad (12.1.5b)$$

$$Q_\alpha^{(k)} = \int_{z_k}^{z_{k+1}} \sigma_{\alpha 3}^{(k)} dz \quad (12.1.5b)$$

$$\sigma_{ij}^{(k)} = \sigma_{ij}(x_\beta, z_k) \quad (12.1.6)$$

Here z_k denotes the z -coordinate of the bottom of the k th layer. Then the continuity of the displacements and transverse stresses at layer interfaces and the traction boundary conditions at the top and bottom of the laminate are used to obtain $2(N + 1) + 1 = 2N + 3$ equations in (u_k, v_k, w) .

Several other layerwise models for laminated plates have been presented by Mau [21], Chou and Carleone [22], Di Sciuva [23–25], Murakami [26], and Ren [27]. Di Sciuva [23–25] used ideas similar to those of [12–15] to formulate a displacement-based theory, called the *zigzag theory* or *discrete-layer theory*. The displacement field is assumed to be of the form

$$\begin{aligned} u_\alpha(x_\beta, x_3, t) &= u_\alpha^0(x_\beta, t) - x_3 u_{3,\alpha}^0(x_\beta, t) + f_{\alpha\gamma}(x_3) \phi_\gamma(x_\beta, t) \\ u_3(x_\beta, x_3, t) &= u_3^0(x_\beta, t) \end{aligned} \quad (12.1.7)$$

where α, β , and γ take the values of 1 and 2, and ($x_1 = x, x_2 = y, x_3 = z$). The functions $f_{\alpha\gamma}$ and ϕ_γ are then determined such that the displacements and transverse stresses are continuous at the layer interfaces. The functions $f_{\alpha\gamma}$ are

shown to depend only on x_3 and the layer stiffnesses. The resulting laminate theory contains only five dependent unknowns (also see Zukas and Vinson [28], and Waltz and Vinson [29]), as in the first-order theory or the third-order theory of Reddy [30]. The layerwise cubic model of Ren [27] required two variables more than the FSDT but it produced results which agreed well with those from exact elasticity. These models demonstrated that layerwise functions are necessary for determining the zigzag thickness distribution of the in-plane displacements.

Using an explicit approximation for the transverse shear stresses within each layer, Hsu and Wang [31] proposed a layerwise model for laminated cylindrical shells consisting of orthotropic layers. The transverse shear stresses satisfied the traction boundary conditions on the top and bottom surfaces, and the equilibrium conditions at the layer interfaces of the shell. Rath and Das [32] extended this model to symmetrically laminated generally orthotropic shells. However, the number of equations increases with the number of layers.

Mau et al. [33] used a layerwise theory in the context of hybrid-stress finite element analysis of thick laminated plates. The theory is based on assumed stresses within each layer, resulting in a large number of variables. Spilker [34,35] used the idea of Mau et al. in developing an eight-node hybrid-stress element. In this model, the higher-order distributions of stresses through the thickness were characterized by as many as 67 stress parameters, and different shear strains are assumed within each layer. Using cubic spline functions to approximate the thickness variation of displacements, Hinrichsen and Palazotto [36] proposed a layerwise finite element model for the nonlinear analysis of thick laminated plates. Use of spline functions or Hermite cubic functions, which include continuity of the derivatives, violates the required discontinuity of the interlaminar strains between layers.

A more direct method of achieving a layerwise displacement field was proposed by Reddy [37], who represented the transverse variation of the displacement components in terms of one-dimensional Lagrangian finite elements. The resulting strain field is kinematically correct in that the in-plane strains are continuous through the thickness while the transverse strains are discontinuous through the thickness, thereby allowing for the possibility of continuous transverse stresses as the number of layers is increased. The layerwise field proposed by Reddy is very general in that any desired number of layers, distribution of layers, and order of interpolation can be achieved simply by specifying a particular mesh of one-dimensional finite elements through the thickness. The theory was extended by Barbero, Reddy, and Teply [38] to laminated composite cylindrical shells. Owen and Li [39,40] used the layerwise displacement idea similar to that of Reddy [37] to develop a continuum shell element (also see [41,42]).

Lee et al. [43,44] presented a partial layerwise model for laminated plates with a layerwise cubic variation of the in-plane displacements. By imposing the continuity of the interlaminar shear stresses, the number of unknowns is reduced to the same number and type of variables as in FSDT. While the numerical results for the maximum in-plane stresses at the free surfaces showed very good agreement with 3-D elasticity solutions for the cylindrical bending of thick symmetric cross-ply laminates, the displacements and stresses at the interfaces were not accurate enough. The theory predicts even more inaccurate results for unsymmetric laminates. The theory was extended to laminated shells by Xavier et al. [45,46].

The displacement-based partial layerwise laminate theories, in which the transverse normal strain is neglected, provide a more realistic description of the kinematics of composite laminates when compared to the ESL theories by introducing discrete layer transverse shear effects into the assumed displacement field. However, these models are not capable of accurately determining interlaminar stresses near discontinuities such as holes or cut-outs, traction free edges, and delamination fronts. In modeling these localized effects, inclusion of the transverse normal strain is important for two reasons. First of all, the transverse normal stress is usually a significant, if not dominant, stress in these regions. Secondly, layerwise models that neglect transverse normal strain do not satisfy traction-free boundary conditions for transverse shear stresses at the laminate edge. Examination of the natural boundary conditions associated with the governing differential equations of a partial layerwise theory reveals that the transverse shear stresses satisfy the traction-free boundary conditions at the laminate edge only in the integral sense and not in the local sense (despite the level of refinement through the thickness). In contrast to the partial layerwise theories, full layerwise theories [37] use layerwise expansions for all three displacement components, and thus include both discrete layer transverse shear effects and discrete layer transverse normal effects.

In this chapter we present the displacement-based full layerwise theory of Reddy, develop its finite element model, and present some numerical results to illustrate the accuracy. It should be noted that the full layerwise finite element model is equivalent to the displacement finite element model of 3-D elasticity. Following the layerwise theory, a variable kinematic model that incorporates both equivalent single-layer theories and layerwise theories is also presented.

12.2 Development of the Theory

12.2.1 Displacement Field

In the layerwise theory of Reddy, the displacements of the k th layer are written as

$$\begin{aligned} u^k(x, y, z, t) &= \sum_{j=1}^m u_j^k(x, y, t) \phi_j^k(z) \\ v^k(x, y, z, t) &= \sum_{j=1}^m v_j^k(x, y, t) \phi_j^k(z) \\ w^k(x, y, z, t) &= \sum_{j=1}^n w_j^k(x, y, t) \psi_j^k(z) \end{aligned} \quad (12.2.1)$$

where u^k , v^k , and w^k represent the total displacement components in the x , y and z directions, respectively, of a material point initially located at (x, y, z) in the undeformed laminate, and $\phi_j^k(z)$ and $\psi_j^k(z)$ are continuous functions of the thickness coordinate z . In general, $\psi^k \neq \phi^k$.

The functions $\phi_j^k(z)$ and $\psi_j^k(z)$ are selected to be layerwise continuous functions. For example, they can be chosen to be the one-dimensional Lagrange interpolation functions of the thickness coordinate, in which case, (u_j^k, v_j^k, w_j^k) denote the values of (u^k, v^k, w^k) at the j th plane (see [37,47–52]). The number of nodes, n , through

the layer thickness define the polynomial degree $p = n + 1$ of $\psi_j^k(z)$, which are defined only within the k th numerical layer (see Figure 12.2.1). The functions $u_j^k(x, y, t)$, $v_j^k(x, y, t)$, and $w_j^k(x, y, t)$ represent the displacement components of all points located on the j th plane (defined by $z = z_j$) in the undeformed laminate.

Since the thickness variation of the displacement components is defined in terms of piecewise Lagrangian interpolation functions, the displacement components will be continuous through the laminate thickness, but the transverse strains will be discontinuous across the interface between adjacent thickness subdivisions. This leaves the possibility that the transverse stresses may be continuous across the interface between layers. Note that the use of piecewise Hermite interpolation through the thickness is kinematically incorrect for general laminates since the transverse strains are forced to be continuous through the thickness.

Any desired degree of displacement variation through the thickness is easily obtained by either adding more one-dimensional finite element subdivisions through the thickness (h -refinement) or using higher order Lagrangian interpolation polynomials (p -refinement) through the thickness. The layerwise concept introduced here is very general in that the number of subdivisions through the thickness can be greater than, equal to, or less than the number of material layers through the thickness and each layer can have linear, quadratic, or higher-order polynomial variations of the displacements. Note that the sublamine concept can be used (i.e., the number of thickness subdivisions is less than the number of material layers); however, each sublamine will be represented as an equivalent, single, homogeneous layer.

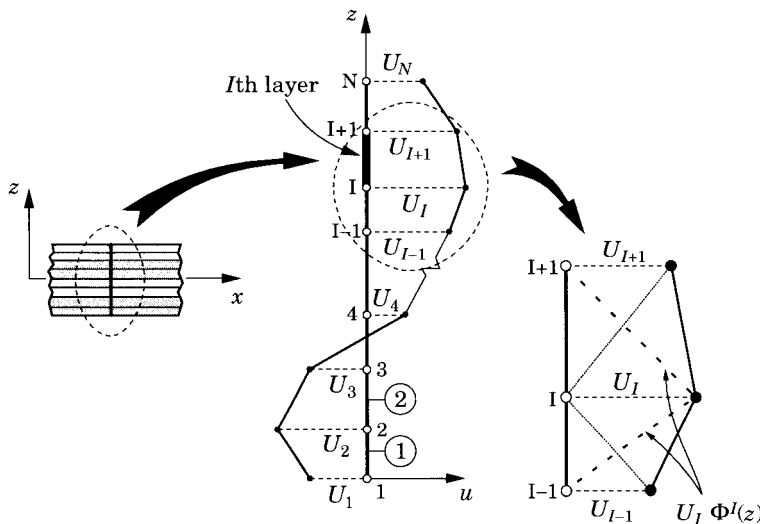


Figure 12.2.1: Displacement representation and the linear approximation functions $\Phi^I(z)$ used in the layerwise theory.

The total displacement field of the laminate can be written as

$$\begin{aligned} u(x, y, z, t) &= \sum_{I=1}^N U_I(x, y, t) \Phi^I(z) \\ v(x, y, z, t) &= \sum_{I=1}^N V_I(x, y, t) \Phi^I(z) \\ w(x, y, z, t) &= \sum_{I=1}^M W_I(x, y, t) \Psi^I(z) \end{aligned} \quad (12.2.2)$$

where (U_I, V_I, W_I) denote the nodal values of (u, v, w) , N is the number of nodes and Φ^I are the *global* interpolation functions (see Figure 12.2.1) for the discretization of the in-plane displacements through thickness, and M is the number of nodes and Ψ^I are the global interpolation functions for discretization of the transverse displacement through thickness. For linear and quadratic variation through each numerical layer these functions are given below [53] (N_e denotes the number of numerical layers through the thickness):

Linear functions ($N = N_e + 1$):

$$\begin{aligned} \Phi^1(z) &= \psi_1^{(1)}(z), \quad z_1 \leq z \leq z_2 \\ \Phi^I(z) &= \begin{cases} \psi_2^{(I-1)}(z), & z_{I-1} \leq z \leq z_I \\ \psi_1^{(I)}(z), & z_I \leq z \leq z_{I+1} \end{cases} \quad (I = 2, 3, \dots, N_e) \\ \Phi^N(z) &= \psi_2^{(N_e)}(z), \quad z_{N-1} \leq z \leq z_N \end{aligned} \quad (12.2.3a)$$

$$\psi_1^{(k)} = 1 - \frac{\bar{z}}{h_k}, \quad \psi_2^{(k)} = \frac{\bar{z}}{h_k}, \quad 0 \leq \bar{z} \leq h_k \quad (12.2.3b)$$

Quadratic functions ($N = 2N_e + 1$):

$$\begin{aligned} \Phi^1(z) &= \psi_1^{(1)}(z), \quad z_1 \leq z \leq z_3 \\ \Phi^{2I}(z) &= \psi_2^{(I)}(z), \quad z_{2I-1} \leq z \leq z_{2I+1} \quad (I = 1, 2, \dots, N_e) \\ \Phi^{2I+1}(z) &= \begin{cases} \psi_3^{(I)}(z), & z_{2I-1} \leq z \leq z_{2I+1} \\ \psi_1^{(I+1)}(z), & z_{2I+1} \leq z \leq z_{2I+3} \end{cases} \quad (I = 1, 2, \dots, N_e - 1) \\ \Phi^N(z) &= \psi_3^{(N_e)}(z), \quad z_{N-1} \leq z \leq z_N \end{aligned} \quad (12.2.4a)$$

$$\begin{aligned} \psi_1^{(k)} &= \left(1 - \frac{z}{h_k}\right) \left(1 - \frac{2z}{h_k}\right), \quad \psi_2^{(k)} = 4 \frac{z}{h_k} \left(1 - \frac{z}{h_k}\right), \quad \psi_3^{(k)} = -\frac{z}{h_k} \left(1 - \frac{2z}{h_k}\right) \\ z_{2k-1} \leq z &\leq z_{2k+1} \end{aligned} \quad (12.2.4b)$$

where h_k is the thickness of the k th layer, $\bar{z} = z - z_t^k$, and z_t^k denotes the z -coordinate of top of the k th numerical layer. Independent approximations for the in-plane and transverse displacements are assumed in order to include the possibility

of inextensibility of transverse normals. The inextensibility of transverse normals can be included by setting $M = 1$ and $\Psi^1 = 1$ for all z .

12.2.2 Strains and Stresses

The von Kármán nonlinear strains associated with the displacement field (12.2.2) are

$$\varepsilon_{xx} = \sum_{I=1}^N \frac{\partial U_I}{\partial x} \Phi^I + \frac{1}{2} \left(\sum_{I=1}^M \frac{\partial W_I}{\partial x} \Psi^I \right) \left(\sum_{J=1}^M \frac{\partial W_J}{\partial x} \Psi^J \right) \quad (12.2.5a)$$

$$\varepsilon_{yy} = \sum_{I=1}^N \frac{\partial V_I}{\partial y} \Phi^I + \frac{1}{2} \left(\sum_{I=1}^M \frac{\partial W_I}{\partial y} \Psi^I \right) \left(\sum_{J=1}^M \frac{\partial W_J}{\partial y} \Psi^J \right) \quad (12.2.5b)$$

$$\gamma_{xy} = \sum_{I=1}^N \left(\frac{\partial U_I}{\partial y} + \frac{\partial V_I}{\partial x} \right) \Phi^I + \left(\sum_{I=1}^M \frac{\partial W_I}{\partial x} \Psi^I \right) \left(\sum_{J=1}^M \frac{\partial W_J}{\partial y} \Psi^J \right) \quad (12.2.5c)$$

$$\varepsilon_{zz} = \sum_{I=1}^M W_I \frac{d\Psi^I}{dz} \quad (12.2.6)$$

$$\gamma_{yz} = \sum_{I=1}^N V_I \frac{d\Phi^I}{dz} + \sum_{I=1}^M \frac{\partial W_I}{\partial y} \Psi^I \quad (12.2.7a)$$

$$\gamma_{xz} = \sum_{I=1}^N U_I \frac{d\Phi^I}{dz} + \sum_{I=1}^M \frac{\partial W_I}{\partial x} \Psi^I \quad (12.2.7b)$$

Note that the strains are discontinuous at the layer interfaces because of the layerwise definition of the functions Φ^I and Ψ^I .

The stresses in the k th layer may be computed from the 3-D stress-strain equations. For the k th (orthotropic) lamina we have [from Eq. (2.3.19)]

$$\begin{Bmatrix} \sigma_{xx} \\ \sigma_{yy} \\ \sigma_{zz} \\ \sigma_{yz} \\ \sigma_{xz} \\ \sigma_{xy} \end{Bmatrix}^{(k)} = \begin{bmatrix} \bar{C}_{11} & \bar{C}_{12} & \bar{C}_{13} & 0 & 0 & \bar{C}_{16} \\ \bar{C}_{21} & \bar{C}_{22} & \bar{C}_{23} & 0 & 0 & \bar{C}_{26} \\ \bar{C}_{31} & \bar{C}_{32} & \bar{C}_{33} & 0 & 0 & \bar{C}_{36} \\ 0 & 0 & 0 & \bar{C}_{44} & \bar{C}_{45} & 0 \\ 0 & 0 & 0 & \bar{C}_{45} & \bar{C}_{55} & 0 \\ \bar{C}_{16} & \bar{C}_{26} & \bar{C}_{36} & 0 & 0 & \bar{C}_{66} \end{bmatrix}^{(k)} \begin{Bmatrix} \varepsilon_{xx} - \alpha_{xx}\Delta T \\ \varepsilon_{yy} - \alpha_{yy}\Delta T \\ \varepsilon_{zz} - \alpha_{zz}\Delta T \\ \gamma_{yz} \\ \gamma_{xz} \\ \gamma_{xy} - 2\alpha_{xy}\Delta T \end{Bmatrix}^{(k)} \quad (12.2.8)$$

where the $\bar{C}_{ij}^{(k)}$ are the transformed elastic coefficients in the (x, y, z) system, which are related to the elastic coefficients in the material coordinates, C_{ij} by Eq. (2.3.18). If inextensibility of transverse normals is assumed, one may use the plane stress-reduced stiffness in place of the 3-D stiffnesses. Note that the strains at a layer interface depend on the layer; i.e., $\{\varepsilon\}_P^k \neq \{\varepsilon\}_P^{k+1}$ at a point P on the interface of layers k and $k + 1$.

12.2.3 Equations of Motion

The governing equations of motion for the present layerwise theory can be derived using the principle of virtual displacements

$$0 = \int_0^T (\delta U + \delta V - \delta K) dt \quad (12.2.9)$$

where the virtual strain energy δU , virtual work done by applied forces δV , and the virtual kinetic energy δK are given by

$$\begin{aligned} \delta U &= \int_{\Omega_0} \left[\int_{-\frac{h}{2}}^{\frac{h}{2}} \left(\sigma_{xx} \delta \varepsilon_{xx} + \sigma_{yy} \delta \varepsilon_{yy} + \sigma_{zz} \delta \varepsilon_{zz} + \right. \right. \\ &\quad \left. \left. \sigma_{xy} \delta \gamma_{xy} + \sigma_{xz} \delta \gamma_{xz} + \sigma_{yz} \delta \gamma_{yz} \right) dz \right] dx dy \\ &= \int_{\Omega_0} \left\{ \sum_{I=1}^N \left[N_{xx}^I \frac{\partial \delta U_I}{\partial x} + N_{yy}^I \frac{\partial \delta V_I}{\partial y} + N_{xy}^I \left(\frac{\partial \delta U_I}{\partial y} + \frac{\partial \delta V_I}{\partial x} \right) \right. \right. \\ &\quad \left. \left. + Q_x^I \delta U_I + Q_y^I \delta V_I \right] + \sum_{I=1}^M \left[\tilde{Q}_x^I \frac{\partial \delta W_I}{\partial x} + \tilde{Q}_y^I \frac{\partial \delta W_I}{\partial y} \right. \right. \\ &\quad \left. \left. + \tilde{Q}_z^I \delta W_I + \left(\tilde{N}_{xx}^{IJ} \frac{\partial W_I}{\partial x} + \tilde{N}_{xy}^{IJ} \frac{\partial W_I}{\partial x} \right) \frac{\partial \delta W_J}{\partial x} \right. \right. \\ &\quad \left. \left. + \left(\tilde{N}_{xy}^{IJ} \frac{\partial W_I}{\partial x} + \tilde{N}_{yy}^{IJ} \frac{\partial W_I}{\partial y} \right) \frac{\partial \delta W_J}{\partial y} \right] \right\} dx dy \end{aligned} \quad (12.2.10)$$

$$\begin{aligned} \delta V &= - \int_{\Omega_0} \left[q_b(x, y) \delta w(x, y, -\frac{h}{2}) + q_t(x, y) \delta w(x, y, \frac{h}{2}) \right] dx dy \\ &\quad - \int_{\Gamma} \int_{-\frac{h}{2}}^{\frac{h}{2}} [\hat{\sigma}_{nn} \delta u_n + \hat{\sigma}_{ns} \delta u_s + \hat{\sigma}_{nz} \delta w] dz ds \\ &= - \int_{\Omega_0} (q_b \delta W_1 + q_t \delta W_M) dx dy \\ &\quad - \int_{\Gamma} \left[\sum_{I=1}^N \left(\hat{N}_{nn}^I \delta U_I^n + \hat{N}_{ns}^I \delta U_I^s \right) + \sum_{I=1}^M \hat{Q}_n^I \delta W_I \right] ds \end{aligned} \quad (12.2.11)$$

$$\begin{aligned} \delta K &= \int_{\Omega_0} \int_{-\frac{h}{2}}^{\frac{h}{2}} \rho_0 (\dot{u} \delta \dot{u} + \dot{v} \delta \dot{v} + \dot{w} \delta \dot{w}) dz dx dy \\ &= \int_{\Omega_0} \left[\sum_{I,J=1}^N I^{IJ} (\dot{U}_I \delta \dot{U}_J + \dot{V}_I \delta \dot{V}_J) + \sum_{I,J=1}^M \tilde{I}^{IJ} \dot{W}_I \delta \dot{W}_J \right] dx dy \end{aligned} \quad (12.2.12)$$

$$\mathcal{N}^I = \sum_{J=1}^M \left[\frac{\partial}{\partial x} \left(\tilde{N}_{xx}^{IJ} \frac{\partial W_J}{\partial x} + \tilde{N}_{xy}^{IJ} \frac{\partial W_J}{\partial x} \right) + \frac{\partial}{\partial y} \left(\tilde{N}_{xy}^{IJ} \frac{\partial W_J}{\partial x} + \tilde{N}_{yy}^{IJ} \frac{\partial W_J}{\partial y} \right) \right] \quad (12.2.13)$$

$$\left\{ \begin{array}{c} N_{xx}^I \\ N_{yy}^I \\ N_{xy}^I \end{array} \right\} = \int_{-\frac{h}{2}}^{\frac{h}{2}} \left\{ \begin{array}{c} \sigma_{xx} \\ \sigma_{yy} \\ \sigma_{xy} \end{array} \right\} \Phi^I dz, \quad \left\{ \begin{array}{c} \tilde{N}_{xx}^{IJ} \\ \tilde{N}_{yy}^{IJ} \\ \tilde{N}_{xy}^{IJ} \end{array} \right\} = \int_{-\frac{h}{2}}^{\frac{h}{2}} \left\{ \begin{array}{c} \sigma_{xx} \\ \sigma_{yy} \\ \sigma_{xy} \end{array} \right\} \Psi^I \Psi^J dz \quad (12.2.14)$$

$$\begin{Bmatrix} Q_x^I \\ Q_y^I \end{Bmatrix} = \int_{-\frac{h}{2}}^{\frac{h}{2}} \begin{Bmatrix} \sigma_{xz} \\ \sigma_{yz} \end{Bmatrix} \frac{d\Phi^I}{dz} dz, \quad \begin{Bmatrix} \tilde{Q}_x^I \\ \tilde{Q}_y^I \\ \tilde{Q}_z^I \end{Bmatrix} = \int_{-\frac{h}{2}}^{\frac{h}{2}} \begin{Bmatrix} \sigma_{xz} \\ \sigma_{yz} \\ \sigma_{zz} \end{Bmatrix} \Psi^I dz \quad (12.2.15)$$

$$I^{IJ} = \int_{-\frac{h}{2}}^{\frac{h}{2}} \rho_0 \Phi^I \Phi^J dz, \quad \tilde{I}^{IJ} = \int_{-\frac{h}{2}}^{\frac{h}{2}} \rho_0 \Psi^I \Psi^J dz \quad (12.2.16)$$

Substituting Eqs. (12.2.10)–(12.2.12) into Eq. (12.2.9), and deriving the Euler–Lagrange equations, we obtain

$$\delta U_I : \quad \frac{\partial N_{xx}^I}{\partial x} + \frac{\partial N_{xy}^I}{\partial y} - Q_x^I = \sum_{J=1}^N I^{IJ} \frac{\partial^2 U_J}{\partial t^2} \quad (12.2.17)$$

$$\delta V_I : \quad \frac{\partial N_{xy}^I}{\partial x} + \frac{\partial N_{yy}^I}{\partial y} - Q_y^I = \sum_{J=1}^N I^{IJ} \frac{\partial^2 V_J}{\partial t^2} \quad (12.2.18)$$

$$\delta W_I : \quad \frac{\partial \tilde{Q}_x^I}{\partial x} + \frac{\partial \tilde{Q}_y^I}{\partial y} - \tilde{Q}_z^I + \tilde{N}^I + q_b \delta_{I1} + q_t \delta_{IM} = \sum_{J=1}^M \tilde{I}^{IJ} \frac{\partial^2 W_J}{\partial t^2} \quad (12.2.19)$$

The natural (force) boundary conditions of the theory are:

$$N_{nn}^I - \hat{N}_{nn}^I = 0, \quad N_{ns}^I - \hat{N}_{ns}^I = 0, \quad (\tilde{Q}_n^I + \tilde{\mathcal{P}}^I) - \hat{Q}_n^I = 0 \quad (12.2.20)$$

where

$$\begin{aligned} N_{nn}^I &= N_{xx}^I n_x + N_{xy}^I n_y, \quad N_{ns}^I = N_{xy}^I n_x + N_{yy}^I n_y \\ \tilde{Q}_n^I &= \tilde{Q}_x^I n_x + \tilde{Q}_y^I n_y, \quad U_I^n = U_I n_x + V_I n_y, \quad U_I^s = -U_I n_x + V_I n_y \end{aligned} \quad (12.2.21)$$

$$\tilde{\mathcal{P}}^I = \sum_{J=1}^M \left[\left(\tilde{N}_{xx}^{IJ} \frac{\partial W_J}{\partial x} + \tilde{N}_{xy}^{IJ} \frac{\partial W_J}{\partial x} \right) n_x + \left(\tilde{N}_{xy}^{IJ} \frac{\partial W_J}{\partial x} + \tilde{N}_{yy}^{IJ} \frac{\partial W_J}{\partial y} \right) n_y \right] \quad (12.2.22)$$

Thus, the primary variables (displacements) and secondary variables (forces) of the layerwise theory are

$$\begin{array}{ll} \text{Primary Variables:} & U_I^n, \quad U_I^s; \quad W_I \\ \text{Secondary Variables:} & N_{nn}^I, \quad N_{ns}^I; \quad \tilde{Q}_n^I + \tilde{\mathcal{P}}^I \end{array} \quad (12.2.23)$$

Note that the form of the natural boundary conditions guarantees that the transverse shear stresses will satisfy the traction-free edge conditions on a “local” basis as the number of subdivisions through the thickness is increased (unlike the partial layerwise theories that neglect discrete layer transverse normal strain). The 2-D equations of motion can be expressed in terms of the dependent variables $(U_I(x, y, t), V_I(x, y, t), W_I(x, y, t))$ by replacing the stress components with the 3-D stress-strain relations and strain-displacement relations. The resulting system of $3n$ equations represent the semidiscretized version of Navier’s equations of motion.

12.2.4 Laminate Constitutive Equations

The laminate constitutive equations for the layerwise theory can be derived using the lamina constitutive equations (12.2.8) and the definition of stress resultants (12.2.14) and (12.2.15). We obtain

$$\begin{aligned} \left\{ \begin{array}{c} N_{xx}^I \\ N_{yy}^I \\ N_{xy}^I \end{array} \right\} &= \sum_{k=1}^{N_e} \int_{z_b^k}^{z_t^k} \left\{ \begin{array}{c} \sigma_{xx} \\ \sigma_{yy} \\ \sigma_{xy} \end{array} \right\}^{(k)} \Phi^I dz \\ &= \sum_{k=1}^{N_e} \int_{z_b^k}^{z_t^k} \begin{bmatrix} \bar{C}_{11} & \bar{C}_{12} & \bar{C}_{13} & \bar{C}_{16} \\ \bar{C}_{12} & \bar{C}_{22} & \bar{C}_{23} & \bar{C}_{26} \\ \bar{C}_{16} & \bar{C}_{26} & \bar{C}_{36} & \bar{C}_{66} \end{bmatrix}^{(k)} \left\{ \begin{array}{c} \varepsilon_{xx} - \alpha_{xx} \Delta T \\ \varepsilon_{yy} - \alpha_{yy} \Delta T \\ \varepsilon_{zz} - \alpha_{zz} \Delta T \\ \gamma_{xy} - 2\alpha_{xy} \Delta T \end{array} \right\} \Phi^I dz \\ &= \sum_{J=1}^N \begin{bmatrix} A_{11}^{IJ} & A_{12}^{IJ} & \tilde{A}_{13}^{IJ} & A_{16}^{IJ} \\ A_{12}^{IJ} & A_{22}^{IJ} & \tilde{A}_{23}^{IJ} & A_{26}^{IJ} \\ A_{16}^{IJ} & A_{26}^{IJ} & \tilde{A}_{36}^{IJ} & A_{66}^{IJ} \end{bmatrix} \left\{ \begin{array}{c} \frac{\partial U_J}{\partial x} \\ \frac{\partial V_J}{\partial y} \\ W_J \\ \frac{\partial U_J}{\partial y} + \frac{\partial V_J}{\partial x} \end{array} \right\} - \left\{ \begin{array}{c} N_{xx}^{I(T)} \\ N_{yy}^{I(T)} \\ N_{xy}^{I(T)} \end{array} \right\} \\ &\quad + \sum_{J,K=1}^M \begin{bmatrix} B_{11}^{IJK} & B_{12}^{IJK} & B_{16}^{IJK} \\ B_{12}^{IJK} & B_{22}^{IJK} & B_{26}^{IJK} \\ B_{16}^{IJK} & B_{26}^{IJK} & B_{66}^{IJK} \end{bmatrix} \left\{ \begin{array}{c} \frac{1}{2} \frac{\partial W_J}{\partial x} \frac{\partial W_K}{\partial x} \\ \frac{1}{2} \frac{\partial W_J}{\partial y} \frac{\partial W_K}{\partial y} \\ \frac{\partial W_J}{\partial x} \frac{\partial W_K}{\partial y} \end{array} \right\} \end{aligned} \quad (12.2.24)$$

$$\begin{aligned} \left\{ \begin{array}{c} \tilde{N}_{xx}^{IJ} \\ \tilde{N}_{yy}^{IJ} \\ \tilde{N}_{xy}^{IJ} \end{array} \right\} &= \sum_{k=1}^{N_e} \int_{z_b^k}^{z_t^k} \left\{ \begin{array}{c} \sigma_{xx} \\ \sigma_{yy} \\ \sigma_{xy} \end{array} \right\}^{(k)} \Psi^I \Psi^J dz \\ &= \sum_{K=1}^N \begin{bmatrix} B_{11}^{KIJ} & B_{12}^{KIJ} & \tilde{B}_{13}^{KIJ} & B_{16}^{KIJ} \\ B_{12}^{KIJ} & B_{22}^{KIJ} & \tilde{B}_{23}^{KIJ} & B_{26}^{KIJ} \\ B_{16}^{KIJ} & B_{26}^{KIJ} & \tilde{B}_{36}^{KIJ} & B_{66}^{KIJ} \end{bmatrix} \left\{ \begin{array}{c} \frac{\partial U_K}{\partial x} \\ \frac{\partial V_K}{\partial y} \\ W_K \\ \frac{\partial U_K}{\partial y} + \frac{\partial V_K}{\partial x} \end{array} \right\} - \left\{ \begin{array}{c} \tilde{N}_{xx}^{IJ(T)} \\ \tilde{N}_{yy}^{IJ(T)} \\ \tilde{N}_{xy}^{IJ(T)} \end{array} \right\} \\ &\quad + \sum_{K,P=1}^M \begin{bmatrix} D_{11}^{IJKP} & D_{12}^{IJKP} & D_{16}^{IJKP} \\ D_{12}^{IJKP} & D_{22}^{IJKP} & D_{26}^{IJKP} \\ D_{16}^{IJKP} & D_{26}^{IJKP} & D_{66}^{IJKP} \end{bmatrix} \left\{ \begin{array}{c} \frac{1}{2} \frac{\partial W_K}{\partial x} \frac{\partial W_P}{\partial x} \\ \frac{1}{2} \frac{\partial W_K}{\partial y} \frac{\partial W_P}{\partial y} \\ \frac{\partial W_K}{\partial x} \frac{\partial W_P}{\partial y} \end{array} \right\} \end{aligned} \quad (12.2.25)$$

$$\begin{aligned} \left\{ \begin{array}{c} Q_x^I \\ Q_y^I \end{array} \right\} &= \sum_{k=1}^{N_e} \int_{z_b^k}^{z_t^k} \left\{ \begin{array}{c} \sigma_{xz} \\ \sigma_{yz} \end{array} \right\}^{(k)} \frac{d\Phi^I}{dz} dz = \sum_{k=1}^{N_e} \int_{z_b^k}^{z_t^k} \begin{bmatrix} \bar{C}_{55} & \bar{C}_{45} \\ \bar{C}_{45} & \bar{C}_{44} \end{bmatrix}^{(k)} \left\{ \begin{array}{c} \gamma_{xz} \\ \gamma_{yz} \end{array} \right\}^{(k)} \frac{d\Phi^I}{dz} dz \\ &= \sum_{J=1}^N \left(\begin{bmatrix} \bar{A}_{55}^{IJ} & \bar{A}_{45}^{IJ} \\ \bar{A}_{45}^{IJ} & \bar{A}_{44}^{IJ} \end{bmatrix} \left\{ \begin{array}{c} U_J \\ V_J \end{array} \right\} + \begin{bmatrix} \bar{B}_{55}^{IJ} & \bar{B}_{45}^{IJ} \\ \bar{B}_{45}^{IJ} & \bar{B}_{44}^{IJ} \end{bmatrix} \left\{ \begin{array}{c} \frac{\partial W_J}{\partial x} \\ \frac{\partial W_J}{\partial y} \end{array} \right\} \right) \end{aligned} \quad (12.2.26)$$

$$\begin{aligned} \left\{ \begin{array}{c} \tilde{Q}_x^I \\ \tilde{Q}_y^I \end{array} \right\} &= \sum_{k=1}^{N_e} \int_{z_b^k}^{z_t^k} \left\{ \begin{array}{c} \sigma_{xz} \\ \sigma_{yz} \end{array} \right\}^{(k)} \Psi^I dz = \sum_{k=1}^{N_e} \int_{z_b^k}^{z_t^k} \begin{bmatrix} \bar{C}_{55} & \bar{C}_{45} \\ \bar{C}_{45} & \bar{C}_{44} \end{bmatrix}^{(k)} \left\{ \begin{array}{c} \gamma_{xz} \\ \gamma_{yz} \end{array} \right\}^{(k)} \Psi^I dz \\ &= \sum_{J=1}^N \left(\begin{bmatrix} \bar{D}_{55}^{IJ} & \bar{D}_{45}^{IJ} \\ \bar{D}_{45}^{IJ} & \bar{D}_{44}^{IJ} \end{bmatrix} \left\{ \begin{array}{c} U_J \\ V_J \end{array} \right\} + \begin{bmatrix} \bar{D}_{55}^{IJ} & \bar{D}_{45}^{IJ} \\ \bar{D}_{45}^{IJ} & \bar{D}_{44}^{IJ} \end{bmatrix} \left\{ \begin{array}{c} \frac{\partial W_J}{\partial x} \\ \frac{\partial W_J}{\partial y} \end{array} \right\} \right) \end{aligned} \quad (12.2.27)$$

$$\tilde{Q}_z^I = \sum_{k=1}^{N_e} \int_{z_b^k}^{z_t^k} \sigma_{zz}^{(k)} \frac{d\Psi^I}{dz} dz = \sum_{k=1}^{N_e} \int_{z_b^k}^{z_t^k} (\bar{C}_{13}\varepsilon_{xx} + \bar{C}_{23}\varepsilon_{yy} + \bar{C}_{33}\varepsilon_{zz} + \bar{C}_{36}\varepsilon_{xy})^{(k)} \frac{d\Psi^I}{dz} dz$$

$$= \sum_{J=1}^N \left[\tilde{A}_{13}^{JI} \frac{\partial U_J}{\partial x} + \tilde{A}_{23}^{JI} \frac{\partial V_J}{\partial y} + \hat{A}_{33}^{JI} W_J + \tilde{A}_{36}^{JI} \left(\frac{\partial U_K}{\partial y} + \frac{\partial V_K}{\partial x} \right) \right] - \tilde{Q}_z^{I(T)} \quad (12.2.28)$$

where N_e is the number of physical layers in the laminate, z_b^k and z_t^k are coordinates of the bottom and top of the k th layer, and the laminate stiffnesses are defined as follows:

$$\begin{aligned} A_{ij}^{IJ} &= \sum_{k=1}^{N_e} \int_{z_b^k}^{z_t^k} \bar{C}_{ij}^{(k)} \Phi^I \Phi^J dz, & \tilde{A}_{ij}^{IJ} &= \sum_{k=1}^{N_e} \int_{z_b^k}^{z_t^k} \bar{C}_{ij}^{(k)} \Phi^I \frac{d\Psi^J}{dz} dz \\ \bar{A}_{ij}^{IJ} &= \sum_{k=1}^{N_e} \int_{z_b^k}^{z_t^k} \bar{C}_{ij}^{(k)} \frac{d\Phi^I}{dz} \frac{d\Phi^J}{dz} dz, & \hat{A}_{33}^{IJ} &= \sum_{k=1}^{N_e} \int_{z_b^k}^{z_t^k} \bar{C}_{33}^{(k)} \frac{d\Psi^I}{dz} \frac{d\Psi^J}{dz} dz \\ \bar{B}_{ij}^{IJ} &= \sum_{k=1}^{N_e} \int_{z_b^k}^{z_t^k} \bar{C}_{ij}^{(k)} \frac{d\Phi^I}{dz} \Psi^J dz, & \bar{D}_{ij}^{IJ} &= \sum_{k=1}^{N_e} \int_{z_b^k}^{z_t^k} \bar{C}_{ij}^{(k)} \Psi^I \Psi^J dz \quad (12.2.29) \\ B_{ij}^{IJK} &= \sum_{k=1}^{N_e} \int_{z_b^k}^{z_t^k} \bar{C}_{ij}^{(k)} \Phi^I \Psi^J \Psi^K dz, & \tilde{B}_{ij}^{IJK} &= \sum_{k=1}^{N_e} \int_{z_b^k}^{z_t^k} \bar{C}_{ij}^{(k)} \Psi^I \Psi^J \frac{d\Psi^K}{dz} dz \\ D_{ij}^{IJKP} &= \sum_{k=1}^{N_e} \int_{z_b^k}^{z_t^k} \bar{C}_{ij}^{(k)} \Psi^I \Psi^J \Psi^K \Psi^P dz \quad (12.2.30) \end{aligned}$$

for $i, j = 1, 2, 6$. Note that when the von Kármán nonlinearity is not included, all laminate stiffnesses with three and four superscripts will not enter the governing equations.

For the nonisothermal case, the thermal stress resultants are defined as

$$\begin{aligned} \begin{Bmatrix} N_{xx}^{I(T)} \\ N_{yy}^{I(T)} \\ N_{xy}^{I(T)} \end{Bmatrix} &= \sum_{k=1}^{N_e} \int_{z_b^k}^{z_t^k} \begin{bmatrix} \bar{C}_{11} & \bar{C}_{12} & \bar{C}_{13} & \bar{C}_{16} \\ \bar{C}_{12} & \bar{C}_{22} & \bar{C}_{23} & \bar{C}_{26} \\ \bar{C}_{16} & \bar{C}_{26} & \bar{C}_{36} & \bar{C}_{66} \end{bmatrix}^{(k)} \begin{Bmatrix} \alpha_{xx} \\ \alpha_{yy} \\ \alpha_{zz} \\ 2\alpha_{xy} \end{Bmatrix}^{(k)} \Delta T \Phi^I dz \\ \begin{Bmatrix} \tilde{N}_{xx}^{IJ(T)} \\ \tilde{N}_{yy}^{IJ(T)} \\ \tilde{N}_{xy}^{IJ(T)} \end{Bmatrix} &= \sum_{k=1}^{N_e} \int_{z_b^k}^{z_t^k} \begin{bmatrix} \bar{C}_{11} & \bar{C}_{12} & \bar{C}_{13} & \bar{C}_{16} \\ \bar{C}_{12} & \bar{C}_{22} & \bar{C}_{23} & \bar{C}_{26} \\ \bar{C}_{16} & \bar{C}_{26} & \bar{C}_{36} & \bar{C}_{66} \end{bmatrix}^{(k)} \begin{Bmatrix} \alpha_{xx} \\ \alpha_{yy} \\ \alpha_{zz} \\ 2\alpha_{xy} \end{Bmatrix}^{(k)} \Delta T \Psi^I \Psi^J dz \\ \tilde{Q}_z^{I(T)} &= \sum_{k=1}^{N_e} \int_{z_b^k}^{z_t^k} (\bar{C}_{13}\alpha_{xx} + \bar{C}_{23}\alpha_{yy} + \bar{C}_{33}\alpha_{zz} + 2\bar{C}_{36}\alpha_{xy})^{(k)} \Delta T \frac{d\Psi^I}{dz} dz \quad (12.2.31) \end{aligned}$$

Note that the sum over the number of layers in the definition of the laminate stiffnesses is limited to the numerical layers over which the functions Φ^I and Ψ^I are defined. The functions Φ^I and Ψ^I are defined at the most over two adjacent numerical layers [see Eqs. (12.2.3) and (12.2.4)]. For example, for the choice of linear interpolation functions, when $\Phi^I = \Psi^I$ ($M = N$), the following expressions are obtained for a typical layer:

$$[A_{ij}]^{(k)} = \frac{\bar{C}_{ij}^{(k)} h_k}{6} \begin{bmatrix} 2 & 1 \\ 1 & 2 \end{bmatrix}, \quad [\tilde{A}_{ij}]^{(k)} = \frac{\bar{C}_{ij}^{(k)}}{2} \begin{bmatrix} -1 & 1 \\ -1 & 1 \end{bmatrix} \quad (12.2.32a)$$

$$[\bar{A}_{ij}]^{(k)} = \frac{\bar{C}_{ij}^{(k)}}{h_k} \begin{bmatrix} 1 & -1 \\ -1 & 1 \end{bmatrix}, \quad [\hat{A}_{33}]^{(k)} = \frac{\bar{C}_{33}^{(k)}}{h_k} \begin{bmatrix} 1 & -1 \\ -1 & 1 \end{bmatrix} \quad (12.2.32b)$$

$$[\bar{B}_{ij}]^{(k)} = \frac{\bar{C}_{ij}^{(k)}}{2} \begin{bmatrix} 1 & -1 \\ 1 & -1 \end{bmatrix}, \quad [\bar{D}_{ij}]^{(k)} = \frac{\bar{C}_{ij}^{(k)} h_k}{6} \begin{bmatrix} 2 & 1 \\ 1 & 2 \end{bmatrix} \quad (12.2.32c)$$

If a laminate consists of more than one layer, the above matrices must be *assembled* (see Reddy [53]). For example, $[A_{ij}]$ for a two-layer laminate takes the form

$$[A_{ij}] = \frac{1}{6} \begin{bmatrix} 2\bar{C}_{ij}^{(1)}h_1 & \bar{C}_{ij}^{(1)}h_1 & 0 \\ \bar{C}_{ij}^{(1)}h_1 & 2(\bar{C}_{ij}^{(1)}h_1 + \bar{C}_{ij}^{(2)}h_2) & \bar{C}_{ij}^{(2)}h_2 \\ 0 & \bar{C}_{ij}^{(2)}h_2 & 2\bar{C}_{ij}^{(2)}h_2 \end{bmatrix} \quad (12.2.33)$$

$$[\bar{A}_{ij}] = \begin{bmatrix} \bar{C}_{ij}^{(1)}(h_1)^{-1} & -\bar{C}_{ij}^{(1)}(h_1)^{-1} & 0 \\ -\bar{C}_{ij}^{(1)}(h_1)^{-1} & \bar{C}_{ij}^{(1)}(h_1)^{-1} + \bar{C}_{ij}^{(2)}(h_2)^{-1} & -\bar{C}_{ij}^{(2)}(h_2)^{-1} \\ 0 & -\bar{C}_{ij}^{(2)}(h_2)^{-1} & \bar{C}_{ij}^{(2)}(h_2)^{-1} \end{bmatrix} \quad (12.2.34)$$

$$[\bar{B}_{ij}] = \frac{1}{2} \begin{bmatrix} \bar{C}_{ij}^{(1)} & -\bar{C}_{ij}^{(1)} & 0 \\ \bar{C}_{ij}^{(1)} & -\bar{C}_{ij}^{(1)} + \bar{C}_{ij}^{(2)} & -\bar{C}_{ij}^{(2)} \\ 0 & \bar{C}_{ij}^{(2)} & -\bar{C}_{ij}^{(2)} \end{bmatrix} \quad (12.2.35)$$

Similar expressions hold for the other coefficients in Eq. (12.2.30).

12.3 Finite Element Model

12.3.1 Layerwise Model

The displacement finite element model corresponding to the full layerwise theory is developed by substituting an assumed interpolation of the displacement field into the principle of virtual displacements (12.2.9) for a representative finite element of the plate. Suppose that the displacement field is interpolated as

$$\begin{aligned} U_I(x, y, t) &= \sum_{j=1}^p U_I^j(t) \psi_j(x, y) \\ V_I(x, y, t) &= \sum_{j=1}^p V_I^j(t) \psi_j(x, y) \\ W_I(x, y, t) &= \sum_{j=1}^q W_I^j(t) \varphi_j(x, y) \end{aligned} \quad (12.3.1)$$

where p and q are the number of nodes per 2-D element used to approximate the in-plane and transverse deflections, respectively, and $U_I^j(t)$, $V_I^j(t)$, and $W_I^j(t)$ are the values of the displacements U_I , V_I , and W_I , respectively, at the j th node of the 2-D finite element representing the I th plane of the plate element. The functions $\psi_j(x, y)$ ($j = 1, 2, \dots, p$) and $\varphi_j(x, y)$ ($j = 1, 2, \dots, q$) are the two-dimensional Lagrangian interpolation polynomials associated with the j th node of the two-dimensional finite element.

The semidiscrete finite element equations are obtained by substituting equation (12.3.1) into the principle of virtual work in Eq. (12.2.9). Then the fully discretized equations, for the transient case, are obtained using a time approximation scheme, as discussed earlier. Here we limit our discussion to the static problems, and the case in which the same interpolation is used for all three displacements: $\varphi_j = \psi_j$ ($p = q$) and $\Psi_I = \Phi_I$ ($M = N$).

The following two-dimensional finite elements ($N = M$) are used here with isoparametric formulations:

- E4: Four-node Lagrange quadrilateral element.
- E8: Eight-node serendipity quadrilateral element.
- E9: Nine-node Lagrange quadrilateral element.
- E12: Twelve-node serendipity quadrilateral element.
- E16: Sixteen-node Lagrange quadrilateral element.

Each of these elements may be used in conjunction with one or more linear, quadratic, or cubic (denoted L,Q,C respectively) 1-D Lagrange elements through the thickness to create a wide variety of different layerwise finite elements. We use the notation E12-L6 to denote a two-dimensional E12 element with six linear subdivisions through the thickness; likewise, E9-Q3 denotes a two-dimensional E9 element with three quadratic subdivisions through the thickness.

12.3.2 Full Layerwise Model Versus 3-D Finite Element Model

The full layerwise finite element model is the same as a conventional 3-D displacement finite element model in terms of interpolation capability and problem size for a 3-D body with parallel top and bottom surfaces. A variable thickness plate must be approximated as an elementwise constant-thickness plate in order to use the present element. Virtually in all practical cases, a laminated plate structure, including a structure with dropped plies, is made up of constant-thickness laminae, and therefore the present element can be used to model such structures. The layerwise element has some analysis advantages over the conventional 3-D elements. The layerwise format maintains a 2-D type data structure similar to finite element models of 2-D ESL theories. This provides several advantages over conventional 3-D finite element models. First the volume of the input data is reduced. Secondly, the in-plane 2-D mesh and the transverse 1-D mesh can be refined independently of each other without having to reconstruct a 3-D finite element mesh. The 2-D type data structure also allows efficient formulation of the element stiffness matrices as is discussed in the next section.

Since the present layerwise plate model is developed to provide the same modeling capability as a conventional 3-D finite element model of laminated plates, it is informative to investigate the similarities and differences in these two models. First, consider the theories used to develop each model. The conventional 3-D finite element model is based on the 3-D theory of elasticity, and the associated governing equations of motion are Navier's equations. The full layerwise, 2-D laminate theory used to develop the present layerwise model is governed by a set of $3n$ coupled partial differential equations that can be viewed as the semidiscretized version of Navier's equations. Thus the governing equations of motion of the present layerwise theory

are necessarily an approximation to the exact 3-D equations of motion; however, the approximation can be made as close as desired by increasing the number of subdivisions through the thickness and/or increasing the order of interpolation through the thickness.

In contrast to the differences that exist between the governing equations of motion for these two theories both finite element models represent fully discretized versions of their respective theories; thus the modeling capabilities of the two finite element models are essentially the same. A comparison of the interpolation capability of the two finite element models reveals a close similarity. Note that both models use actual displacement components (u_1, u_2, u_3) as the primary variables (nodal degrees of freedom) and both require C^0 -continuity of these variables across element (or layer) boundaries. Further, if one compares similar element types from the two models, the interpolation of the primary variables is exactly the same. For example, an E9-Q3 layerwise element exhibits the same interpolation as a stack of three, 27 node, Lagrangian hexahedrons; an E12-L6 exhibits the same interpolation as a stack of six, 24 node, hexahedrons with cubic serendipity interpolation in the planar coordinates and linear Lagrangian interpolation in the transverse direction. Thus it is not surprising that the resulting global system of equations and subsequent solution produced by these two finite element models are exactly the same as long as the meshes, element types, and integration schemes are equivalent.

Obviously the 3-D finite element model is more general than the layerwise finite element model; the latter actually represents a special case of the former. The layerwise model assumes that the displacements, material properties, and element geometry can be approximated by a sum of conveniently separable interpolation functions (i.e., each individual 3-D interpolation function can be written as the product of a 2-D interpolation function and a 1-D interpolation function). This restriction does not imply that the displacement solution itself can be separated into the product of an in-plane function of x and y and an out-of-plane function of z ; however, in computing all volume integrals, the layerwise model can use separated numerical integration (i.e., the integration with respect to the thickness coordinate is performed independent of the integration with respect to the planar coordinates). The results from a single integration through the thickness can then be used at each Gauss point in the subsequent in-plane integration. This separated integration allows the element stiffness matrix to be computed using only a fraction of the operations required to form the stiffness matrix for a conventional 3-D finite element.

To illustrate the computational savings of the simplified, separated integration afforded by the layerwise model, the number of operations needed to form the element stiffness matrix for equivalent layerwise elements and conventional 3-D elements (see Figure 12.3.1) are tabulated in Table 12.3.1. Full quadrature is used in each case. As illustrated in Table 12.3.1, the layerwise model's separated numerical integration requires significantly fewer operations to form the element stiffness matrix. Elements 2a and 2b (see Table 12.3.1) both have 81 degrees of freedom and exhibit complete quadratic interpolation in all three coordinate directions. To form the element stiffness matrix for element 2a (i.e., 27-node, 3-D isoparametric quadratic hexahedron), a 3-D interpolation function subroutine must be called 27 times since there are 27 Gaussian quadrature points. Each time the 3-D interpolation function subroutine is called, 27 different interpolation functions must be evaluated

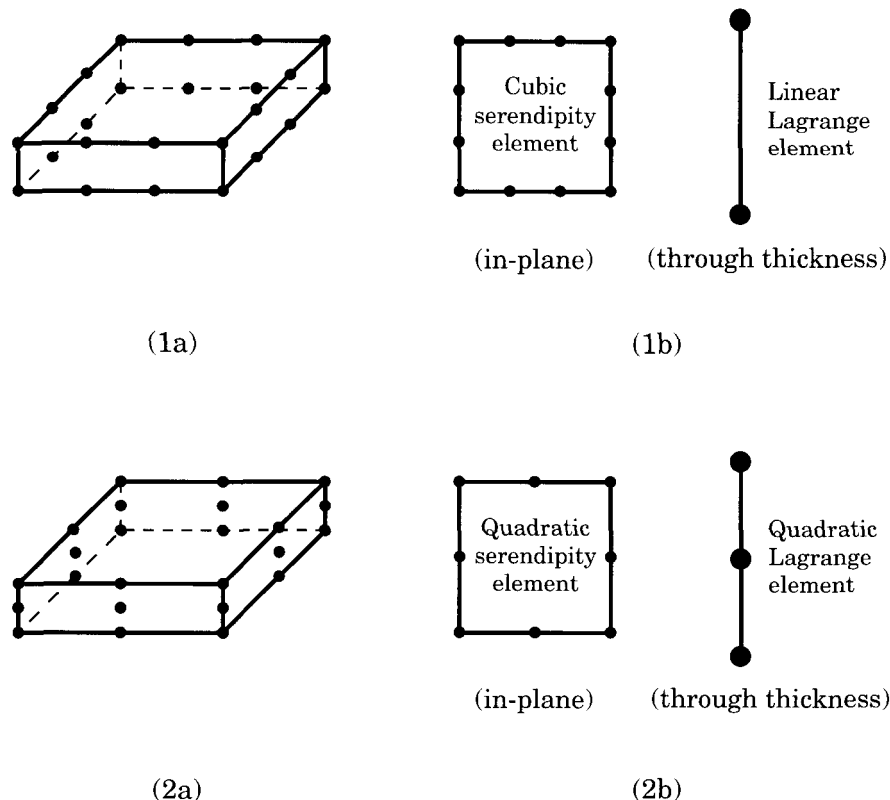


Figure 12.3.1: Various 3-D and layerwise elements used in the numerical comparison.

Table 12.3.1 Comparison of the number of operations needed to form the element stiffness matrices for equivalent elements in the conventional 3-D model and the layerwise 2-D model. Full quadrature is used in each case.

Element Type [†]	Multiplications	Additions	Assignments
1a (3-D)	1,116,000	677,000	511,000
1b (LWPT)	423,000	370,000	106,000
2a (3-D)	1,182,000	819,000	374,000
2b (LWPT)	284,000	270,000	69,000

[†] Element 1a: 72 degrees of freedom, 24-node 3-D isoparametric hexahedron with cubic in-plane interpolation and linear transverse interpolation.

Element 1b: 72 degrees of freedom, E12-L1 layerwise element.

Element 2a: 81 degrees of freedom, 27-node 3-D isoparametric hexahedron with quadratic interpolation in all three directions.

Element 2b: 81 degrees of freedom, E9-Q1 layerwise element.

and thus 272 or 729 individual interpolation functions must be evaluated. To form the element stiffness matrix for element 2b (i.e., nine-node 2-D layerwise quadrilateral element with a single quadratic layer), a 1-D interpolation function subroutine must be called 3 times and a 2-D interpolation function subroutine must be called 9 times, since there are 3 and 9 Gaussian quadrature points in the 1-D and 2-D elements, respectively. This is obviously less work than required by the 3-D element. The efficiency of the layerwise model increases (relative to the 3-D model) as more elements and/or layers are added, or as the order of the interpolation through the thickness is increased. Note that this efficient, separated integration uses standard Lagrangian interpolation through the thickness; thus certain commonly used 3-D finite elements do not have layerwise counterparts (e.g., the 20-node quadratic serendipity hexahedron element and the 32-node cubic serendipity hexahedron element).

12.3.3 Considerations for Modeling Relatively Thin Laminates

First a comment concerning “thin” and “thick” laminates is in order. In the present study we call a laminate domain *thick* if the local span-to-thickness ratio a/h is less than 20. In computing the span-to-thickness ratio, one should use the in-plane dimension of the local domain that is being modeled. Layerwise plate models are primarily intended for thick laminate situations where the simple ESL plate theories (e.g., CLPT or FSDT) are known to be inaccurate. In the analysis of thick laminates, the added computational expense of a layerwise model is justified by its improved predicting capabilities. Although a layerwise model may be primarily intended for thick plate situations, it is important to determine the limits of the layerwise model’s applicability to thin plate situations since finite element models of refined plate theories have proven to be problematic whenever the thickness dimension of the structure is greatly reduced relative to the planar dimensions. In particular, finite elements which possess full three-dimensional modeling capability can exhibit spurious transverse shear stiffness, spurious transverse normal stiffness, and ill-conditioned stiffness matrices as the span-to-thickness ratio of the structure increases. Each of these undesirable phenomena will now be discussed within the context of full layerwise finite elements and selective integration techniques will be suggested to alleviate the spurious transverse stiffnesses.

The spurious shear stiffness phenomenon is caused by an interpolation inconsistency that prevents the finite element from modeling a state of zero transverse shear stress in the presence of general nonzero bending strains. As the plate’s span-to-thickness ratio approaches the thin plate limit, the transverse shear deformation must tend toward zero relative to the bending deformation (i.e., the Kirchhoff condition). The degree to which a particular finite element fails in approximating this condition determines the amount of spurious shear stiffness the element will exhibit while deforming in a bending mode. Thus elements that are poor approximators of this condition are known to exhibit shear locking while elements which are better approximators of this condition may simply exhibit a slight overstiffness.

Next we examine the assumed form of the transverse shear strains ε_{xz} and ε_{yz} used in the layerwise finite elements to determine whether or not the Kirchhoff

condition can be satisfied in the thin plate limit. Within a specific layer of a typical finite element, the Kirchhoff condition requires that

$$\varepsilon_{yz} = \sum_{I=1}^M \sum_{j=1}^p \left(V_I^j \frac{d\Phi^I}{dz}(z_k) \psi_j(x_k, y_k) + W_I^j \Phi^I(z_k) \frac{\partial \psi_j}{\partial y}(x_k, y_k) \right) = 0 \quad (12.3.2a)$$

$$\varepsilon_{xz} = \sum_{I=1}^M \sum_{j=1}^p \left(U_I^j \frac{d\Phi^I}{dz}(z_k) \psi_j(x_k, y_k) + W_I^j \Phi^I(z_k) \frac{\partial \psi_j}{\partial x}(x_k, y_k) \right) = 0 \quad (12.3.2b)$$

where k ranges from 1 to the number of Gaussian integration points in the xy -plane of the element; M is the number of nodes through the thickness of the numerical layer; p is the number of nodes in the 2-D element. Note that Eq. (12.3.2a) exhibits an interpolation inconsistency with respect to both the y and z directions, while Eq. (12.3.2b) exhibits an interpolation inconsistency with respect to both the x and z directions. In general, these interpolation inconsistencies prevent Eqs. (12.3.2a,b) from being satisfied at all Gaussian integration points in the element xy -plane. Thus, as the span-to-thickness ratio increases, the computed solution tends to suppress the higher-order terms of the interpolation so that the Kirchhoff condition can be satisfied (i.e., spurious constraints are introduced into the model). If a reduced quadrature is used to evaluate terms contributing to the transverse shear energy (i.e., any terms containing a constitutive matrix component \bar{Q}_{ij} where $i, j = 4, 5$), then the Kirchhoff condition will not be enforced as stringently as in the case of full quadrature, since Eqs. (12.3.2a,b) will be enforced at fewer points in the domain. Thus the displacements are allowed more freedom to utilize their full interpolation capability.

In practice, reduced quadrature is required only when integrating the transverse shear terms with respect to x and y (not the thickness coordinate z), because the integrated effect of the transverse interpolation inconsistencies is insignificant compared with the contributions from the in-plane interpolation inconsistencies. Consider expanding Eqs. (12.3.2a,b) so that all of the interpolation functions are expressed as summations of simple polynomial terms. As the span-to-thickness ratio is increased, any terms that contain the transverse coordinate (z) will tend toward zero in comparison with terms that do not contain z ; therefore, the transverse interpolation inconsistency does not adversely affect the solution and therefore does not need or benefit from reduced quadrature with respect to the z direction.

Another problem that arises when modeling thin plates with finite elements possessing 3-D capability is that the accuracy of the computed transverse normal stress deteriorates rapidly as the span-to-thickness ratio increases. For relatively thick plates, the transverse normal stress is computed quite accurately; however, as the span-to-thickness ratio increases, the computed transverse normal stress actually diverges from the correct value. This phenomenon arises because of an interpolation inconsistency that prevents the finite element from modeling a state of zero transverse normal stress in the presence of general nonzero bending strains.

As the span-to-thickness ratio increases toward the thin plate limit, the strain energy associated with transverse normal strain tends toward zero relative to the bending energy. Thus the transverse normal strain must approach a functional form that is consistent with the combined Poisson effects from the dominating in-plane

strains. Setting σ_{zz} equal to zero in the constitutive equations and solving for ε_{zz} , we have

$$\varepsilon_{zz} = -\frac{1}{\bar{Q}_{33}} (\bar{Q}_{31}\varepsilon_{xx} + \bar{Q}_{32}\varepsilon_{yy} + 2\bar{Q}_{36}\varepsilon_{xy}) \quad (12.3.3a)$$

where \bar{Q}_{ij} are the transformed elastic stiffnesses. On the other hand, from the strain-displacement relations we have

$$\varepsilon_{zz} = \sum_{I=1}^M W_I \frac{d\Phi^I}{dz} \quad (12.3.3b)$$

Equations (12.3.3a,b) represent a constraint that is imposed on the solution as the thin plate limit is approached.

Expressing the strain component ε_{zz} of Eq. (12.3.3b) in terms of the finite element approximations within a typical element layer, we have

$$\begin{aligned} \varepsilon_{zz} &= \sum_{I=1}^M \sum_{j=1}^p W_I^j \frac{d\Phi^I}{dz}(z_k) \psi_j(x_k, y_k) \\ &= -\frac{1}{\bar{Q}_{33}} \sum_{I=1}^M \sum_{j=1}^p \left[\bar{Q}_{31} U_I^j \Phi^I(z_k) \frac{\partial \psi_j}{\partial x} + \bar{Q}_{32} V_I^j \Phi^I(z_k) \frac{\partial \psi_j}{\partial y} \right. \\ &\quad \left. + \bar{Q}_{36} \Phi^I(z_k) \left(U_I^j \frac{\partial \psi_j}{\partial y} + V_I^j \frac{\partial \psi_j}{\partial x} \right) \right]_{(x_k, y_k)} \end{aligned} \quad (12.3.4)$$

for $k = 1, 2, \dots, G$, where G is the number of Gaussian integration points in the element xy -plane. Note that ε_{zz} exhibits a higher-order in-plane interpolation and a lower-order transverse interpolation than the in-plane strains. In general, these interpolation inconsistencies prevent Eq. (12.3.4) from being satisfied at all Gaussian integration points in the element layer domain. As the span-to-thickness ratio increases toward the thin plate limit, the computed solution tends to suppress the higher-order terms of the interpolation so that Eq. (12.3.4) can be satisfied (i.e., spurious constraints are introduced into the model).

If a reduced quadrature is used to evaluate the terms contributing to the energy associated with transverse normal strain (i.e., any terms containing a \bar{Q}_{3i} or \bar{Q}_{i3} constitutive matrix component), then the condition given by Eq. (12.3.4) will not be enforced as stringently as in the case of full quadrature, since Eq. (12.3.4) will be enforced at fewer points in the domain. Thus the displacements are allowed more freedom to utilize their full interpolation capability.

Although selective integration can efficiently alleviate the problem of spurious transverse shear and normal stresses, such inexact integration can result in element stiffness matrices that have an excess number of zero eigenvalues. Note that the eigenvalues of an element stiffness matrix are representative of the magnitude of the force vector needed to maintain a particular mode of deformation represented by the associated eigenvector. An unconstrained layerwise finite element should have six zero eigenvalues corresponding to the six independent modes of rigid body motion (three translations and three rotations). Any additional zero eigenvalues are associated with eigenvectors representing spurious deformation modes that

produce no strain at the Gaussian integration points used in computing the element stiffness matrix. These spurious deformation modes can be superimposed on the true displacement solution without affecting the system of equations as a whole. The displacements computed in such a system may look nothing like the true solution due to the addition of one or more spurious displacement modes of arbitrary magnitude. The imposition of essential boundary conditions (necessary to prevent rigid body displacement) may or may not prevent these spurious displacement modes from occurring; thus it may be possible for spurious displacement modes to exist unsuppressed in an assembled structure that is constrained against rigid body displacement. Thus elements that possess an excessive number of zero eigenvalues must be used with caution.

An eigenvalue analysis of the layerwise finite elements is performed to determine the effect of various numerical integration schemes on the existence of spurious displacement modes. For this purpose, it is sufficient to consider a layerwise element containing a single layer. The following numerical integration schemes are considered.

F = All terms in the element stiffness matrix are computed using full integration.

S1 = A selective integration scheme in which all terms in the element stiffness matrix which contain the transverse shear stiffnesses \bar{Q}_{44} , \bar{Q}_{45} , or \bar{Q}_{55} are computed using reduced integration. All remaining terms in the element stiffness matrix are computed using full integration.

S2 = A selective integration scheme in which all terms in the element stiffness matrix which contain the stiffnesses \bar{Q}_{i3} , \bar{Q}_{i4} , or \bar{Q}_{i5} ($i = 1, 2, \dots, 6$) are computed using reduced integration. Thus all terms related to transverse shear effects or transverse normal effects are computed using reduced integration. All remaining terms in the element stiffness matrix, including those terms which correspond to strictly in-plane effects, are computed using full integration.

R = All terms in the element stiffness matrix are computed using reduced integration.

Recall from the earlier discussion that integration scheme S1 is used to remove spurious shear stress from the finite element model when the span-to-thickness ratio is large. Integration scheme S2 is used to remove both spurious transverse shear stress and spurious transverse normal stress from the finite element model when the span-to-thickness ratio is large. Integration scheme R, while not necessary, is included for comparison. Also recall that these different integration schemes are only necessary for the in-plane integration. All integrations through the thickness of the element are performed using the full integration scheme.

Table 12.3.2 shows the number of excess zero eigenvalues (i.e., the number of spurious displacement modes) exhibited by various elements under various integration schemes. Note that the three Lagrangian elements (E4, E9, E16) can exhibit spurious displacement modes unless full integration is used. The two serendipity elements do not exhibit any spurious modes except for the special case of a single isolated E8 element under uniform reduced integration.

Table 12.3.2: Number of excess zero eigenvalues that exist for various types of single, unconstrained, layerwise elements under different integration schemes.

Element Type	In-Plane Integration Scheme			
	F	S1	S2	R
E4-L1	0	2	3	7
E8-L1	0	0	0	2 [†]
E8-Q1	0	0	0	3 [†]
E9-L1	0	1	2	8
E9-Q2	0	1	3	12
E12-L1	0	0	0	0
E12-Q1	0	0	0	0
E12-C1	0	0	0	0
E16-L1	0	1	2	8
E16-Q1	0	1	3	12
E16-C1	0	1	4	16

[†] For the E8 elements, these spurious displacement modes can exist only for the case of a single isolated element. If more than one element is present, then no spurious displacement modes can exist.

12.3.4 Bending of a Simply Supported (0/90/0) Laminate

In order to investigate the influence of element type and numerical integration scheme on the accuracy of the layerwise finite element solution, a square, simply supported, symmetric cross-ply (0/90/0) laminated plate subjected to a sinusoidally distributed transverse load on the upper surface is selected. The domain of the plate is $0 < x < a, 0 < y < a, 0 < z < h$. The layers are assumed to be of equal thickness ($h_k = h/3$) and have the following material properties in the principal material coordinate system:

$$E_1 = 25 \times 10^6 \text{ psi}, \quad E_2 = E_3 = 10^6 \text{ psi}$$

$$G_{12} = 0.5 \times 10^6 \text{ psi}, \quad G_{13} = G_{23} = 0.2 \times 10^6 \text{ psi}, \quad \nu_{12} = \nu_{13} = \nu_{23} = 0.25 \quad (12.3.5)$$

This particular problem has an exact 3-D elasticity solution (see Pagano [1]) which is used to verify the displacements and stresses obtained using the layerwise finite element model. The finite element stresses are computed at the reduced Gauss points within each thickness subdivision of each element, using the computed displacements and the constitutive equations.

Due to the symmetry of the problem, only one quadrant ($a/2 < x < a, a/2 < y < a, 0 < z < h$) of the plate is modeled using the uniform, coarse meshes described in Table 12.3.3. The boundary conditions used are

$$\begin{aligned} u(x, a, z) &= u(a/2, y, z) = 0 \\ v(a, y, z) &= v(x, a/2, z) = 0 \\ w(x, a, z) &= w(a, y, z) = 0 \end{aligned} \quad (12.3.6)$$

Table 12.3.3 Finite element meshes used in the analysis of simply supported (0/90/0) plates under sinusoidally distributed transverse load.

Mesh No.	Element Type	Mesh Density	Total D.O.F.
1	E4-L6	6×6	1,029
2	E8-Q3	3×3	840
3	E9-Q3	3×3	1,029
4	E12-Q3	2×2	693
5	E16-Q3	2×2	1,029

Note that all five meshes contain the same nodal density along the edges of the computational domain, while the three meshes of Lagrangian elements contain the exact same nodal distribution throughout the domain. Five different span-to-thickness ratios are considered to test a wide range of plate-bending behavior ($a/h = 4, 10, 20, 50, 200$). Two different numerical integration schemes are compared (types F and S2 discussed earlier). Note that while the three Lagrangian elements are capable of exhibiting spurious displacement modes under S2 integration, the simply supported boundary conditions of this particular example problem prevent any of these modes from arising.

A comparison of the computed maximum transverse displacement and exact maximum transverse displacement, which occur at the centroid of the upper surface of the plate, are presented in Table 12.3.4. Note that when full quadrature is used, all elements except the E16 element (Mesh 5) exhibit a noticeable amount of artificial shear stiffening as the span-to-thickness ratio increases to 200, with the E4 element (Mesh 1) actually beginning to lock. For large span-to-thickness ratios, the spurious shear stiffening is significantly reduced by using the S2 integration scheme as shown in Table 12.3.4.

Table 12.3.4: Ratio of computed transverse displacement to exact transverse displacement at $(a/2, a/2, h)$ in a square, simply supported (0/90/0) laminate under sinusoidal transverse load.

Mesh	Integration Scheme	Span-to-Thickness Ratio, a/h				
		4	10	20	50	200
1	F	0.9815	0.9732	0.9284	0.6975	0.1280
2	F	0.9901	0.9979	0.9981	0.9959	0.9807
3	F	0.9906	0.9985	0.9987	0.9959	0.9845
4	F	0.9880	0.9960	0.9968	0.9953	0.9615
5	F	0.9907	0.9988	1.0006	1.0004	1.0001
1	S2	0.9900	0.9952	0.9945	0.9943	0.9942
2	S2	0.9873	0.9978	0.9992	0.9995	0.9992
3	S2	0.9880	0.9984	0.9998	1.0001	1.0001
4	S2	0.9980	0.9959	0.9966	0.9952	0.9650
5	S2	0.9906	0.9988	0.9997	1.0000	1.0000

Table 12.3.5 contains a comparison of computed in-plane normal stress σ_{xx} with the exact analytical value at the reduced Gauss point nearest to the point $(a/2, a/2, h)$ where σ_{xx} attains a maximum. The computed transverse normal stress σ_{zz} is compared in Table 12.3.6 with the exact analytical value at the reduced Gauss point nearest to the point $(a/2, a/2, h)$ where σ_{zz} attains a maximum. Note that as the span-to-thickness ratio increases, the computed σ_3 diverges for all elements when full quadrature is used. However, the S2 integration scheme allows accurate transverse normal stresses to be computed, even for large span-to-thickness ratios. Table 12.3.7 contains a comparison of computed transverse shear stress σ_{xz} with the exact analytical value at the reduced Gauss point nearest to the point $(a, 0, a/2)$.

Table 12.3.5: Ratio of computed σ_{xx} to exact σ_{xx} in a square, simply supported (0/90/0) laminate under sinusoidally distributed transverse load. The stresses are computed at the reduced Gauss point closest to the centroid of the upper surface of the plate $(a/2, a/2, h)$.

Mesh	Integration Scheme	Span-to-Thickness Ratio, a/h				
		4	10	20	50	200
1	F	1.0402	0.9727	0.9207	0.6900	0.1265
2	F	1.0377	1.0177	1.0135	0.9922	0.9695
3	F	1.0377	1.0177	1.0135	0.9924	0.9728
4	F	1.0402	1.0055	1.0031	1.0035	0.9828
5	F	0.9960	1.0043	1.0022	1.0042	1.0147
1	S2	1.0481	0.9959	0.9902	0.9888	0.9885
2	S2	1.0380	1.0187	1.0158	0.9997	0.9992
3	S2	1.0380	1.0187	1.0158	0.9997	0.9996
4	S2	1.0401	1.0055	1.0020	1.0000	0.9780
5	S2	1.0038	1.0038	1.0010	1.0004	1.0000

Table 12.3.6: Ratio of computed σ_{zz} to exact σ_{zz} in a square, simply supported (0/90/0) laminate under sinusoidally distributed transverse load. The stress is computed at the reduced Gauss point closest to the centroid of the upper surface of the plate $(a/2, a/2, h)$.

Mesh	Integration Scheme	Span-to-Thickness Ratio, a/h				
		4	10	20	50	200
1	F	0.9738	0.9823	0.9979	1.0724	1.2549
2	F	0.9887	1.0076	0.9959	0.8184	-4.5795
3	F	0.9887	1.0076	0.9959	0.8181	-4.6023
4	F	0.9897	0.9972	1.0055	1.0525	0.8495
5	F	0.9895	0.9947	0.9958	1.0128	1.2058
1	S2	0.9835	0.9872	0.9879	0.9881	0.9881
2	S2	0.9872	1.0059	1.0058	1.0056	0.9931
3	S2	0.9872	1.0059	1.0058	1.0054	0.9898
4	S2	0.9894	0.9965	1.0031	1.0420	1.6675
5	S2	0.9893	0.9954	0.9985	0.9962	0.9962

Table 12.3.7: Ratio of computed σ_{xz} to exact σ_{xz} in a square, simply supported (0/90/0) laminate under sinusoidal transverse load. The stress is computed at the reduced Gauss point closest to $(a, a/2, h/2)$.

Mesh	Integration Scheme	Span-to-Thickness Ratio, a/h				
		4	10	20	50	200
1	F	0.9754	0.9714	0.9360	0.7597	0.3267
2	F	0.9860	1.0135	1.0145	1.0021	1.0276
3	F	0.9860	1.0135	1.0145	1.0023	1.0296
4	F	0.9873	0.9999	1.0030	1.0210	1.2883
5	F	0.9867	0.9989	1.0000	1.0014	1.0103
1	S2	0.9857	0.9975	0.9987	0.9990	0.9990
2	S2	0.9861	1.0138	1.0148	0.9988	0.9982
3	S2	0.9861	1.0138	1.0148	0.9987	0.9970
4	S2	0.9873	0.9990	1.0030	1.0205	1.2693
5	S2	0.9868	0.9989	1.0000	1.0000	1.0000

Several generalizations can be made from the results presented in Tables 12.3.4 through 12.3.7. For relatively thick plates that undergo both bending and transverse shearing about both in-plane axes, all five element types yield accurate results using full integration and relatively coarse meshes. For relatively thin plates that undergo bending about both in-plane axes, the S2 integration scheme effectively alleviates both the spurious transverse shear stress and spurious transverse normal stress, thus allowing accurate displacements and stresses to be computed. The Lagrangian elements (E4, E9, and E16) can exhibit spurious displacement modes under S2 integration; thus one must be very cautious with these elements since it is difficult to predict whether or not the boundary conditions for a particular problem will prevent these modes from appearing.

For this simply supported cross-ply (0/90/0) laminate under sinusoidally distributed transverse load, exact solutions exist for the following three theories: (1) 3-D elasticity theory, (2) classical laminate theory (CLPT), and (3) first-order shear deformation theory (FSDT). The exact solutions from these three theories will be compared with the layerwise finite element solution of this problem. One quadrant of the thick plate ($a/h = 4$) is modeled using two finite element meshes that differ only in the refinement through the thickness. Full integration is used for both meshes. Mesh 1 (see Figure 12.3.2) features a 2×2 uniform 2-D mesh of E8-Q3 elements (i.e., one quadratic layer for each distinct material layer) for a total of 441 global degrees of freedom. Mesh 2 (not shown) features a 2×2 uniform 2-D mesh of E8-Q6 elements (i.e., two quadratic layers for each material layer) for a total of 969 global degrees of freedom.

The layerwise finite element stresses are computed via the constitutive relations at the reduced Gauss points in each finite element. For the E8-Q i elements, the reduced Gauss points correspond to the 2×2 integration points within the domain of each layer of each element. Figures 12.3.3 through 12.3.6 show the distribution of various nondimensionalized stresses σ_{xx} , σ_{zz} , σ_{yz} , and σ_{xz} , respectively, through the thickness of the plate at the reduced Gauss points closest to the position where each stress attains a maximum. Thus for Mesh 1, the stresses are computed at six

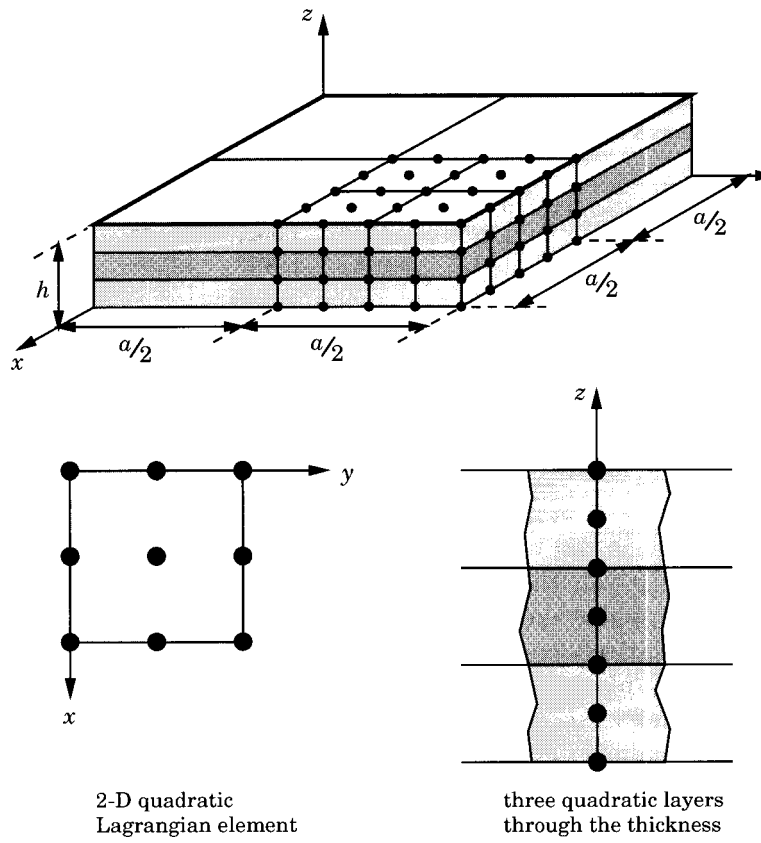


Figure 12.3.2: Mesh 1 of layerwise elements used in the finite element modeling of a quadrant of (0/90/0) laminate.

different points through the thickness, while for Mesh 2, the stresses are computed at 12 different points through the thickness. The nondimensionalized stresses, along with the corresponding reduced Gauss points, are

$$\begin{aligned}\bar{\sigma}_{xx} &= \sigma_{xx}(A, A, z) \frac{h^2}{q_0 a^2}, \quad \bar{\sigma}_{zz} = \sigma_{zz}(A, A, z) \frac{1}{q_0} \\ \bar{\sigma}_{yz} &= \sigma_{yz}(A, B, z) \frac{h}{q_0 a}, \quad \bar{\sigma}_{xz} = \sigma_{xz}(B, A, z) \frac{h}{q_0 a} \\ A &= 1.105662 \left(\frac{a}{2} \right), \quad B = 1.894338 \left(\frac{a}{2} \right)\end{aligned}\quad (12.3.7)$$

We note an excellent agreement between the layerwise finite element solution and the exact three-dimensional elasticity solution shown in Figures 12.3.3 through 12.3.6. Although not shown here, the two remaining in-plane stresses, \$\sigma_{yy}\$ and \$\sigma_{xy}\$, predicted by the layerwise finite element model also showed very close agreement with the 3-D elasticity solution. All of the stress distributions predicted by the

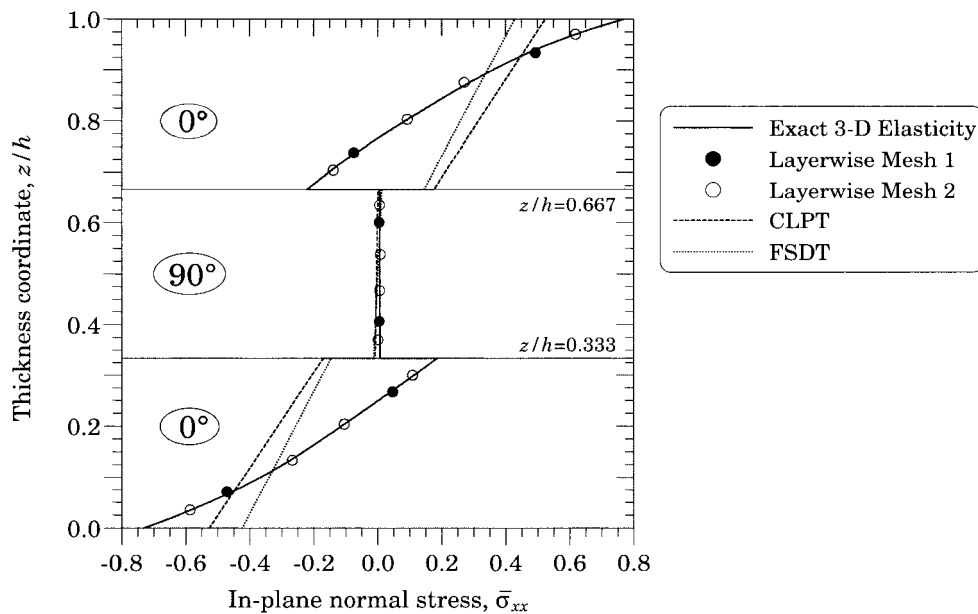


Figure 12.3.3: In-plane normal stress $\bar{\sigma}_{xx}$ distribution through the thickness of a simply supported $(0/90/0)$ laminate subjected to sinusoidally distributed transverse load ($a/h = 4$).

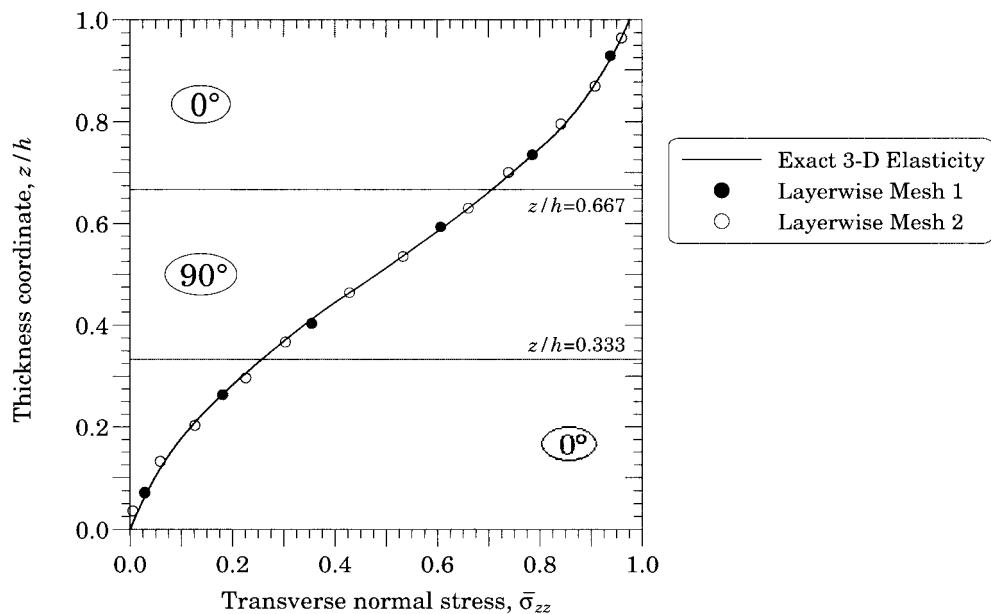


Figure 12.3.4: Transverse normal stress $\bar{\sigma}_{zz}$ distribution through the thickness of a simply supported $(0/90/0)$ laminate subjected to sinusoidally distributed transverse load ($a/h = 4$).

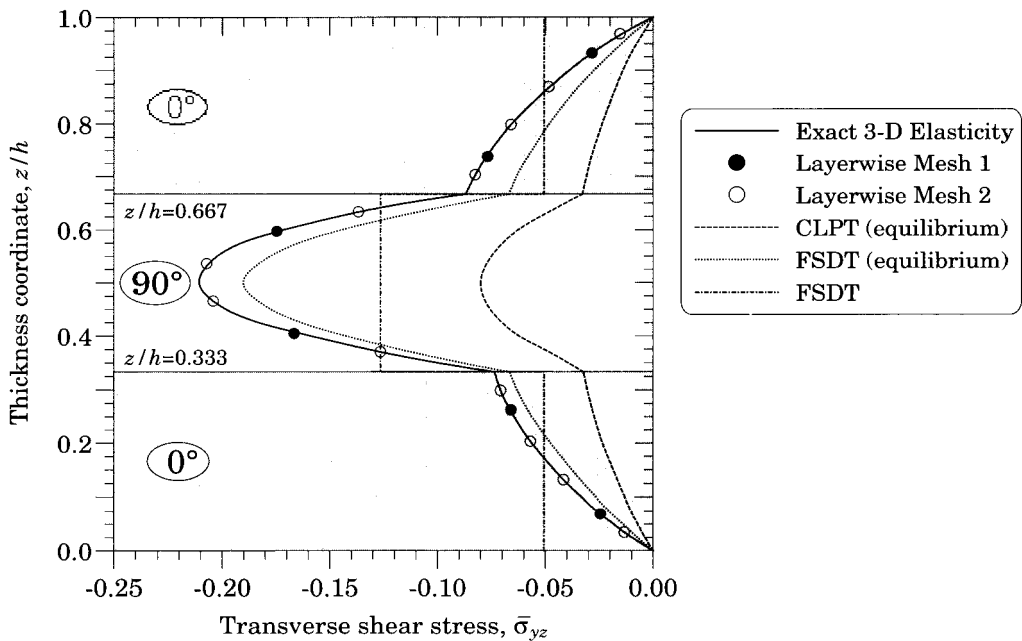


Figure 12.3.5: Transverse shear stress $\bar{\sigma}_{yz}$ distribution through the thickness of a simply supported (0/90/0) laminate subjected to sinusoidally distributed transverse load ($a/h = 4$).

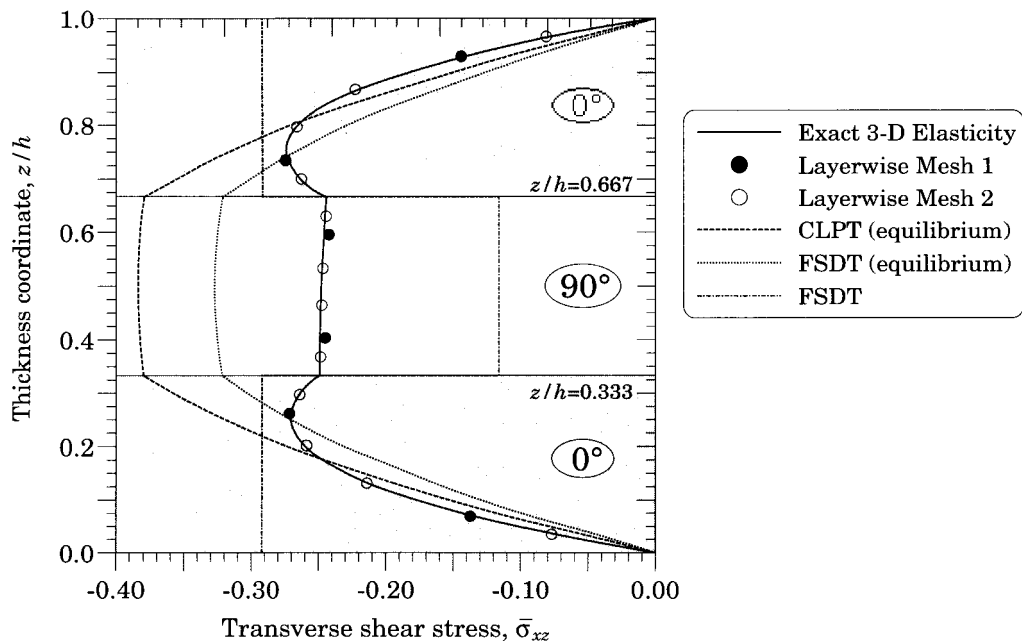


Figure 12.3.6: Transverse shear stress $\bar{\sigma}_{xz}$ distribution through the thickness of a simply supported (0/90/0) laminate subjected to sinusoidally distributed transverse load ($a/h = 4$).

single-layer theories (CLPT and FSDT) show considerable error for this thick plate ($a/h = 4$). Note that the transverse shear stresses predicted by CLPT and FSDT are computed via integration of the 3-D equilibrium equations after determining the in-plane stress field. These “equilibrium” shear stresses can also be computed for the layerwise model, thus yielding layerwise smooth shear stresses using relatively coarse refinements through the thickness; however, only the constitutive transverse shear stresses are shown here.

12.3.5 Free Edge Stresses in a $(45/-45)_s$ Laminate

Consider a symmetric angle-ply laminated plate strip $(45/-45)_s$ of length $2a$, width $2b$, and total laminate thickness $4h$, and subjected to in-plane displacements along the length at the ends. In the analysis, it is assumed that $a = 10b$ and $b = 4h$. Each of the four material layers is of equal thickness $h_k = h$ and is idealized as a homogeneous, orthotropic material with the following properties (expressed in the principal material coordinate system):

$$E_1 = 20 \times 10^6 \text{ psi}, \quad E_2 = E_3 = 2.1 \times 10^6 \text{ psi}$$

$$G_{12} = G_{23} = E_{13} = 0.85 \times 10^6 \text{ psi}, \quad \nu_{12} = \nu_{23} = \nu_{13} = 0.21 \quad (12.3.8)$$

The xy -plane is taken to be the midplane of the laminate, with the origin of the coordinate system at the centroid of the 3-D laminate. The x -coordinate is taken along the length of the plate ($-a \leq x \leq a$); the y -coordinate is taken along the width ($-b \leq y \leq b$); and the z -coordinate is taken through the thickness of the plate ($-2h \leq z \leq 2h$). The displacement boundary conditions for the laminate are

$$u(a, y, z) = u_0, \quad u(-a, y, z) = 0, \quad v(-a, y, z) = v(a, y, z) = 0, \quad w(x, y, 0) = 0 \quad (12.3.9)$$

Since the geometry and loading are symmetric about the xy -plane, only the upper half of the strip is modeled. Thus the computational domain is defined by ($-a < x < a, -b < y < b, 0 < z < 2h$). The traction-free boundary conditions for the laminate are

$$\sigma_{zz}(x, y, 2h) = 0, \quad \frac{\partial \sigma_{zz}}{\partial z}(x, y, 0) = 0 \quad (12.3.10a)$$

$$\sigma_{yz}(x, y, 0) = 0, \quad \sigma_{yz}(x, y, 2h) = 0 \quad (12.3.10b)$$

$$\sigma_{xz}(x, y, 0) = 0, \quad \sigma_{xz}(x, y, 2h) = 0 \quad (12.3.10c)$$

$$\sigma_{yz}(x, -b, z) = 0, \quad \sigma_{yz}(x, b, z) = 0 \quad (12.3.10d)$$

Most of the numerous analytical and numerical studies of the free edge effect have focused on problems that allow the use of quasi-3D analyses, for example, an infinitely long, symmetric, angle-ply plate strip subjected to an imposed uniform axial strain [i.e., $\varepsilon_1(x, y, z) = \varepsilon_0$]. For the $(45/-45)_s$ laminate, Wang and Choi [57,58] have a quasi-3D analytical solution and Whitcomb et al. [59] have a quasi-3D finite element solution. In such cases the strains and stresses are assumed to be independent of the axial coordinate x . Thus the analyst only has to be concerned with two independent variables. It should be noted that the purpose

of this numerical example is not to compare the efficiency of the layerwise finite element solution with the various quasi-3D solutions for this particular problem. The purpose of this example is simply to illustrate the ability of the layerwise plate model to accurately describe three-dimensional effects (such as free edge stresses) which are unaccounted for in conventional 2-D plate models.

The layerwise finite element model is used to compute the interlaminar stresses occurring in the boundary region near the traction-free edges in the composite strip. No attempt is made to cast the layerwise finite element model into a quasi-3D format, thus a full 3-D analysis of the finite length, composite strip is performed. The layerwise finite element solution will obviously be more computationally expensive than a comparable quasi-3D analysis; however, it is useful to verify the layerwise solution using problems which have received much attention in the literature. The finite element mesh consists of 75, two-dimensional E8-Q6 elements (5 elements along the length, 15 elements across the width, 4 quadratic subdivisions through the thickness of each material layer). All elements have the same length ($2a/5$); however, the width of the elements decreases as either of the free edges is approached. The widest elements (those elements centered on the x axis) have a width of $0.75b$ (or $12h_k$). The narrowest elements (the last two rows of elements adjacent to either of the free edges) have a width of $0.00782b$ (or $h_k/8$). The results of this analysis are presented in Figures 12.3.7 through 12.3.12, and they are discussed next.

Figures 12.3.7 through 12.3.12 show transverse stresses (σ_{zz} , σ_{yz} , σ_{xz}) computed using the layerwise finite element model. As in the previous example, the stresses are computed via the constitutive relations at the reduced Gauss points within each thickness subdivision of each element. All stresses have been nondimensionalized according to

$$\bar{\sigma}_{ij} = 20 \frac{\sigma_{ij}}{\varepsilon_0} \frac{1}{E_1}$$

where ε_0 denotes the nominal axial strain induced in the strip by the applied axial displacement of the ends (i.e., $\varepsilon_0 = u_0/2a$). It should be noted that the stresses presented in Figures 12.3.7 through 12.3.12 were taken only from the center row of fifteen elements across the width of the strip (i.e., elements centered on the line $x = a$ in the 2-D mesh). Within these elements, the axial strain (ε_{xx}) experienced a maximum variation of only 0.27%; thus the condition of uniform axial strain (as used in the quasi-3D analyses) is approximately met within this row of elements.

Figures 12.3.7 through 12.3.12 show the variation of the transverse stresses through the thickness of the strip as the free edge is approached. These stresses are computed at the reduced Gauss points which lie closest to the global yz -plane. Note that all three interlaminar stresses exhibit apparent singular behavior near the intersection of the $+45/-45$ interface and the free edge. In this particular problem, the transverse shear stress σ_{xz} exhibits the largest magnitude of the interlaminar stresses, followed by the transverse normal stress σ_{zz} . The stress distributions in Figures 12.3.7 through 12.3.9 show good qualitative agreement with results reported by Wang and Choi [58], who presented an exact elasticity solution for the associated quasi-3D problem, and Whitcomb et al. [59], who presented a displacement-based finite element solution of the associated quasi-3D problem (also see [60,61]); however, their results are not reproduced here.

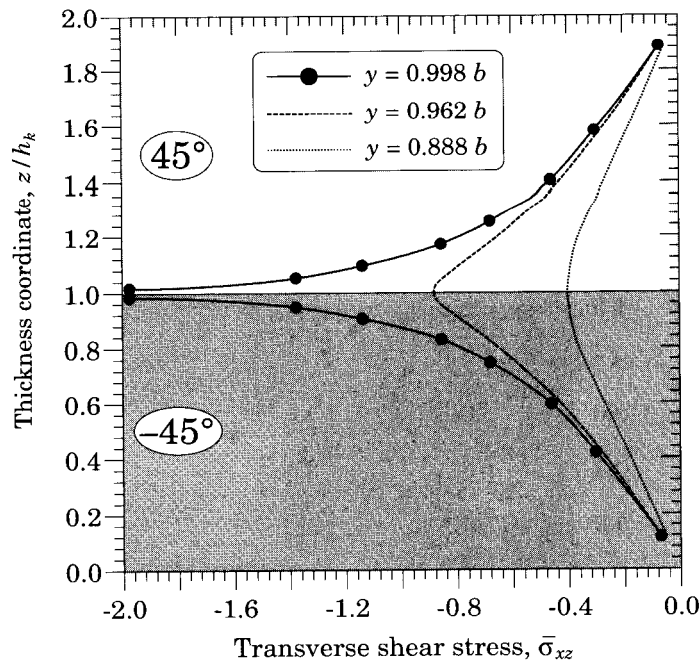


Figure 12.3.7: Distribution of transverse shear stress $\bar{\sigma}_{xz}$ through the thickness of a $(45/-45)_s$ laminate near the free edge ($x = -0.115a$).

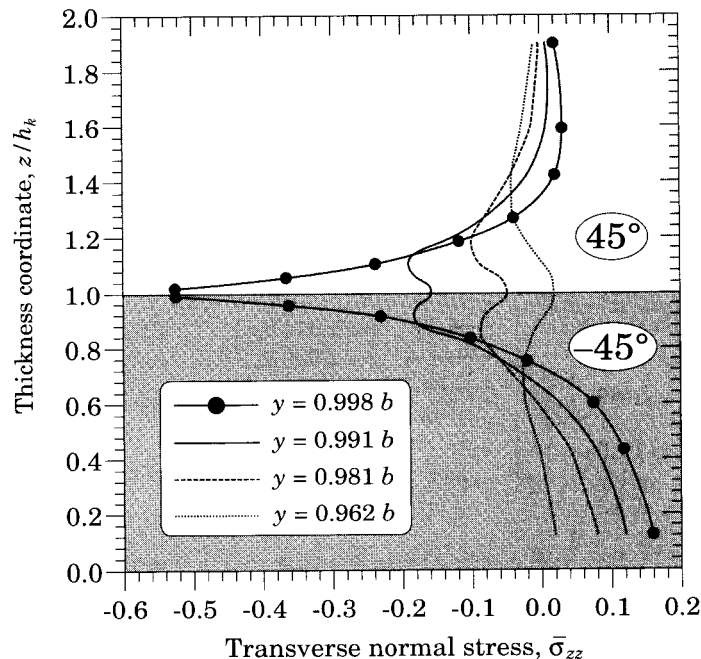


Figure 12.3.8: Distribution of transverse normal stress $\bar{\sigma}_{zz}$ through the thickness of a $(45/-45)_s$ laminate near the free edge ($x = -0.115a$).

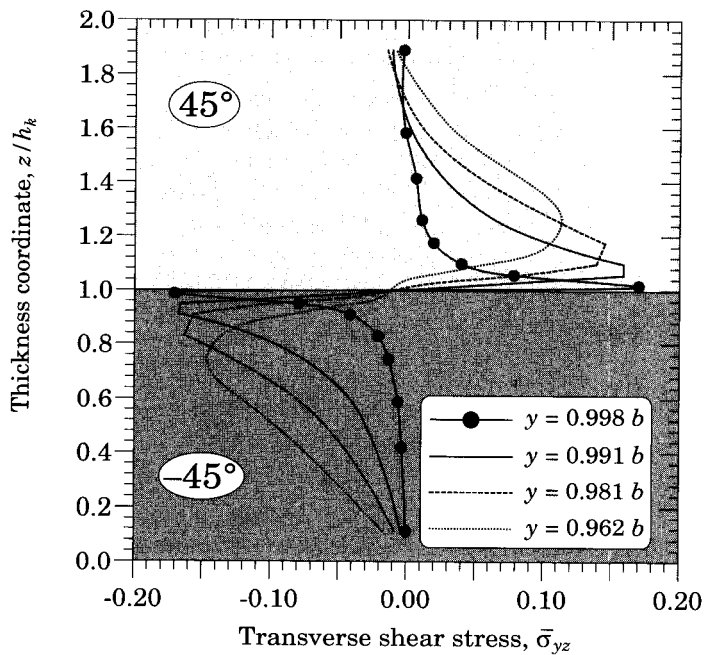


Figure 12.3.9: Distribution of transverse shear stress $\bar{\sigma}_{yz}$ through the thickness of a $(45/-45)_s$ laminate near the free edge ($x = -0.115a$).

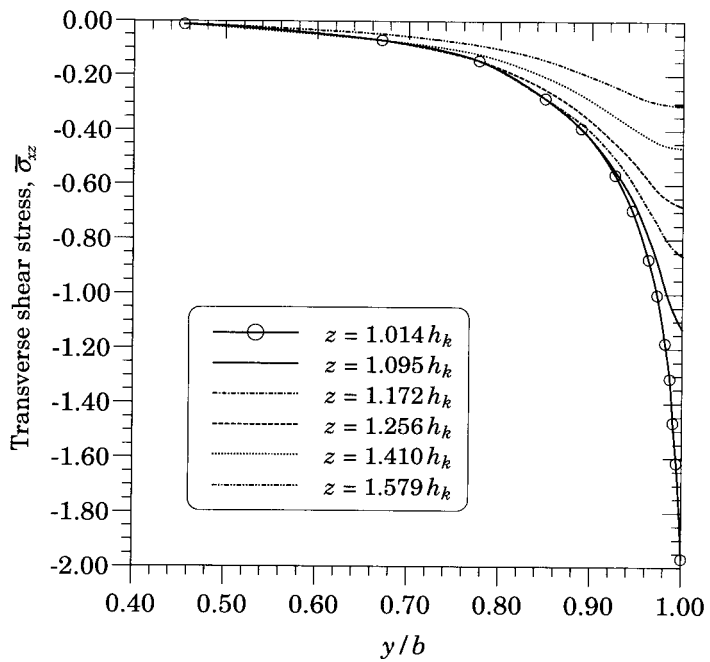


Figure 12.3.10: Distribution of transverse shear stress $\bar{\sigma}_{xz}$ across the width of a $(45/-45)_s$ laminate near the free edge ($x = -0.115a$).

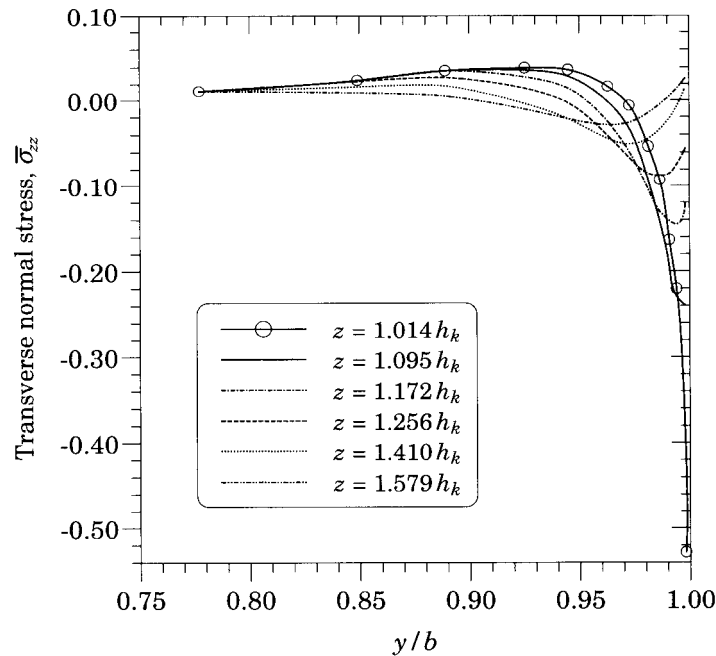


Figure 12.3.11: Distribution of transverse normal stress $\bar{\sigma}_{zz}$ across the width of a $(45/-45)_s$ laminate near the free edge ($x = -0.115a$).

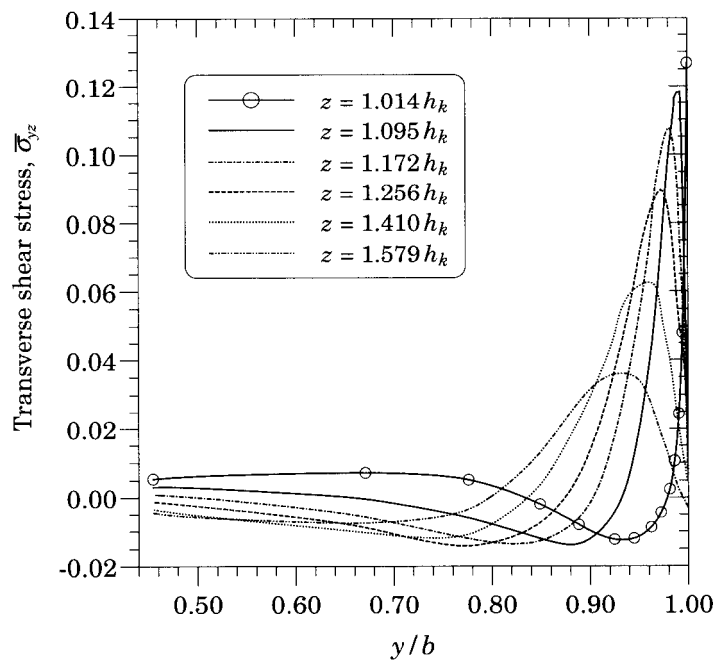


Figure 12.3.12: Distribution of transverse shear stress $\bar{\sigma}_{yz}$ across the width of a $(45/-45)_s$ laminate near the free edge ($x = -0.115a$).

An examination of Figures 12.3.7 through 12.3.9 reveals that traction-free boundary conditions equations (12.3.10a) through (12.3.10c) are apparently satisfied (within the context of the relatively coarse mesh used). Figure 12.3.9 shows that Eq. (12.3.10d) is satisfied over most of the thickness of the free edge, except in the immediate vicinity of the singular point. Note that even though Eq. (12.3.10d) is violated near the singular point, this boundary condition is still satisfied in the integral sense. Whitcomb et al. [59] suggest that this behavior is caused by the fact that the stress tensor does not have to be symmetric at a singular point (where the stress derivatives are unbounded) while most numerical methods are developed assuming a symmetric stress tensor. Whitcomb et al. [59] further reported that the region of boundary condition violation is restricted to the two elements nearest to the singular point and that this region can be made as small as desired through mesh refinement.

Figures 12.3.10 through 12.3.12 show the variation of the interlaminar stresses along the width coordinate (y) of the composite plate strip at various values of the thickness coordinate (z). There are six lines corresponding to six different z values, all of which occur in the uppermost material layer (+45). Note that all of these transverse stresses decay to zero as the distance from the free edge increases. Also note that only the stresses closest to the 45/-45 interface appear unbounded as the free edge is approached. The transverse shear stress σ_{yz} shown in Figure 12.3.12 appears to satisfy Eq. (12.3.10d) except at $z = 1.014h_k$ (again the reduced Gauss point nearest to the singular point). The transverse stress distributions shown in Figures 12.3.10 through 12.3.12 show good qualitative agreement with the quasi-3D elasticity solution presented by Wang and Choi [58], although their results are not presented here.

For this problem, the layerwise finite element stresses agree with the classical laminate theory solution for points sufficiently far from the free edge. For example, the nondimensionalized in-plane stresses at the reduced Gauss points nearest to the centroid of the strip (i.e., $x = 0.1155a$, $y = 0.2165b$) are (depending on z)

Layerwise FEM	CLPT
$2.956 < \sigma_{xx} < 2.975$	$\sigma_{xx} = 2.96$
$1.143 < \sigma_{xy} < 1.164$	$\sigma_{xy} = 1.15$
$0.0 < \sigma_{yy} < 0.012$	$\sigma_{yy} = 0.0$

While highly accurate, the layerwise models are computationally expensive, thus preventing their general use in modeling entire laminates. Fortunately, unless a laminate is extremely thick, significant three-dimensional states of stress are usually restricted to localized regions near geometric and material discontinuities such as free edges, cut-outs, delamination fronts, and matrix crack fronts, or in localized regions of intense loading. However, the localization of these 3-D stress fields does not diminish their importance, for it is in these very areas that damage initiation and propagation are most likely to occur. Therefore, we must develop procedures where a suitable theory can be used for local as well as global regions.

12.4 Variable Kinematic Formulations

12.4.1 Introduction

The ESL models, partial layerwise models, and full layerwise models each have their own advantages and disadvantages in terms of solution accuracy, solution economy, and ease of implementation. Used alone, none of these three types of models is suitable for general laminate analysis; each is restricted to a limited portion of the composite laminate modeling spectrum. However, by combining all three model types in a multiple model analysis or global-local analysis, a very wide variety of laminate problems can be solved with maximum accuracy and minimal cost. The term “multiple model analysis” is used here to denote any analysis method that uses different mathematical models and/or distinctly different levels of discretization for different subregions of the computational domain. The phrase “global-local analysis” refers to a special case of the more general multiple model analysis; the former term is typically used when there exists a particular subregion of interest that occupies a small portion of the computational domain.

All multiple model methods represent an attempt to distribute limited computational resources in an optimal manner to achieve maximum solution accuracy with minimal solution cost, subject to certain problem-specific constraints. This task often requires the joining of incompatible finite element meshes and/or incompatible mathematical models. Note that for the case of joining incompatible mathematical models, the numerical methods used to implement each of the mathematical models may be the same or different; often the finite element method is used to implement each of the models. The traditional difficulty with multiple model analyses is the maintenance of displacement continuity and force equilibrium along boundaries separating incompatible subregions.

A wide variety of multiple model methods have been reported in the literature. The analysis of composite laminates has provided the incentive for the development of many of the reported multiple model methods [62–72], due mainly to the heterogeneous nature of composite materials and the wide range of scales of interest (i.e., micromechanics level, lamina level, laminate level, and structural component level). In general, the broad spectrum of multiple model methods can be divided into two categories: (1) the sequential or multistep methods, and (2) the simultaneous methods.

Most of the sequential multiple model methods reported to date are developed for global-local analysis. Typically the global region (i.e., the entire computational domain) is analyzed with an economical, yet adequate model (often an ESL laminate model) to determine the displacement or force boundary conditions for a subsequent analysis of the local region (i.e., a small subregion of particular interest). The local region might be modeled with a highly refined mesh of the same ESL laminate elements or it might be modeled with 3-D finite elements. Two-dimensional to three-dimensional sequential global-local methods for laminated composite plates were employed, for example, by Thompson and Griffin [62], who modeled the global region using the first order shear deformation finite elements, while the local region was modeled using 3-D finite elements. The displacement field from the FSDT finite element solution of the global region was used to impose displacement boundary conditions on the local 3-D finite element model. To simplify the analysis,

the in-plane finite element discretizations of the global model and the local model were required to be compatible along the global-local boundary. One of the main criticisms of these non-iterating sequential methods [63] is that the influence of the local region on the global region is not accounted for. Specifically, displacement continuity is maintained across the global-local boundary, while the equilibrium of forces along the global-local boundary is not maintained.

This lack of force equilibrium along the global-local boundary has prompted the development of iterative, sequential, multiple model methods by Mao and Sun [64] and Whitcomb and Woo [65,66]. These sequential multiple methods attempt to iteratively establish force equilibrium along the global-local boundary, in addition to imposing displacement continuity. Each of the iterative sequential methods use the same type of mathematical model for both the global region and the local region. The method proposed by Whitcomb and Woo [65,66] requires a compatible finite element discretization along the global-local boundary while the method proposed by Mao and Sun [64] does not.

A number of simultaneous multiple model methods have been reported in the literature [67–72]. These methods are characterized by a simultaneous analysis of the entire computational domain where different subregions are modeled using different mathematical models and/or distinctly different levels of domain discretization. The simultaneous methods explicitly account for the full interaction of the different subregions and are thus directly extendible to nonlinear analysis. One simple type of simultaneous global-local method prompted by composite laminate analysis is the concept of selective ply grouping or sublaminates [67–71]. In this technique, the local region of interest is identified as a specific group of adjacent material plies, within which accurate stresses are desired. The local region spans the entire planar dimensions of the laminate. The global region is identified as that part of the computational domain lying outside the local region. Each of the material plies within the local region is individually modeled with 3-D finite elements, while the remaining plies in the global region are grouped into one or more sublaminates and modeled with 3-D finite elements. This technique amounts to modeling the sublaminates in the global region with an ESL finite element model that assumes transverse shear and transverse normal strains that are C^1 -continuous with respect to the thickness coordinate, while the individual plies in the local region are modeled using 3-D finite elements. This ply grouping concept has the disadvantage of requiring the use of 3-D finite elements over the entire planar dimensions of the laminate.

Another means for developing simultaneous multiple model methods is the use of multipoint constraint equations or Lagrange multipliers. In this technique, the variational statement is supplemented with additional integral(s) that serve to enforce compatibility between adjacent subregions. Consequently additional variables (Lagrange multipliers) are introduced into the system of algebraic equations. Within the context of ESL plate and shell models, Aminpour et al. [72] used an assumed 1-D interface function in conjunction with a hybrid variational formulation to couple subregions with incompatible mesh discretizations. In this study, only 2-D problems were addressed, and both subregions used the same type of 2-D mathematical model. The subregions differed only in their levels of discretization. While the Lagrange multiplier approach can be used to couple

subregions that use different mathematical models (e.g., 2-D/3-D modeling of plates or shells) the general implementation becomes much more cumbersome than a strict 2-D modeling; consequently this method is not often used for connecting different mathematical models.

Currently, most simultaneous 2-D to 3-D modeling of plates and shells is carried out using special transition elements [73–76]. The special transition elements are more convenient than multipoint constraints for joining subregions that use different types of mathematical models; however, they have two disadvantages. First, a different type of transition element is needed for each pair of different mathematical models that might need to be connected in a simultaneous analysis. Further, if the subregion interface has corners, then two different transition elements will be needed to complete the interface, i.e., one type for straight or curved sides and another type for corners. Second, in modeling composite laminates, a significant amount of transitioning (with respect to the transverse coordinate) is required to achieve a discrete layer 3-D representation in localized subregions of interest. The need for transitioning can be avoided by developing a transition element to connect a first-order shear deformation element (both with and without a quadratic thickness stretch) with a stack of 3-D finite elements. Davila [76] developed such a transition element and incorporated the functional interface method [72] to permit abrupt changes in the level of discretization between standard first-order shear deformation elements and the first-order shear deformation edges of the 2-D to 3-D transition elements.

Several types of simultaneous multiple model methods have been based on the hierarchical use of multiple assumed displacement fields. The earliest example of employing multiple assumed displacement fields is due to Mote [77] who combined an assumed global Ritz field with a local finite element field in the solution of beam and plate problems. Dong [78] generalized the idea of combining classical Ritz fields and finite element fields and surveyed applications of this technique.

While both full layerwise finite elements and conventional 3-D finite elements permit an accurate determination of 3-D ply level stress fields, they are computationally expensive to use; thus it is most often impractical to discretize an entire laminate with these types of elements. Fortunately, for most laminate applications, significant 3-D stress states are usually present only in localized regions of complex loading or geometric and material discontinuity. To accurately capture these localized 3-D stress fields in a tractable manner, it is usually necessary to resort to a simultaneous multiple model approach in which different subregions of the laminate are described with different types of mathematical models. The objective of such a simultaneous multiple model analysis is to match the most appropriate mathematical model with each subregion based on the physical characteristics, applied loading, expected behavior, and level of solution accuracy desired of each subregion. Thus solution economy can be maximized without sacrificing solution accuracy. In the previously mentioned works that use some form of hierarchical, multiple assumed displacement fields, both displacement fields are based on the same mathematical model; hence the subregions differ only in the level of refinement of the interpolated solution. Reddy and Robbins [79–81] were the first ones to employ hierarchical multiple assumed displacement fields to model different subregions with different mathematical models (e.g., FSDT and LWPT), which is discussed next.

12.4.2 Multiple Assumed Displacement Fields

Although simultaneous multiple model methods are simple in concept, the actual implementation of such techniques is complicated and cumbersome due mainly to the need for maintaining displacement continuity across subregion boundaries separating incompatible subdomains. To avoid such difficulties, a new hierarchical, variable kinematic finite element that provides the framework for a very general, robust, simultaneous multiple model methodology for laminated composite plates, is developed. The variable kinematic finite elements possess the following attributes:

1. The kinematics and constitutive relations of the element can be conveniently changed, thus allowing the element to represent a variety of different mathematical models from the very simple to the very complex.
2. Different types of elements can be conveniently connected together in the same computational domain, thus permitting different subregions to be described by different mathematical models. One might also think of the variable kinematic finite element as a very sophisticated, adaptable, transition element that circumvents the need for more than one type of transition element.

The hierarchical, variable kinematic finite element is developed using a multiple assumed displacement field approach, i.e., by superimposing two or more different types of assumed displacement fields in the same finite element domain. In general, the multiple assumed displacement field can be expressed as

$$u_i(x, y, z) = u_i^{ESL}(x, y, z) + u_i^{LWT}(x, y, z) \quad (12.4.1)$$

where $i = 1, 2, 3$, and $u_1 = u$, $u_2 = v$, and $u_3 = w$ are the displacement components in the x , y , and z directions, respectively. The reference plane of the plate coincides with the xy -plane. The underlying foundation of the displacement field is provided by u_i^{ESL} , which represents the assumed displacement field for any desired equivalent single-layer (ESL) theory. The second term u_i^{LWT} represents the assumed displacement field for any desired full layerwise theory. The layerwise displacement field is included as an optional, incremental enhancement to the basic ESL displacement field, so that the element can have full 3-D modeling capability when needed. Depending on the desired level of accuracy, the element may use none, part, or all of the layerwise field to create a series of different elements having a wide range of kinematic complexity. For example, discrete layer transverse shear effects can be added to the element by including u_1^{LWT} and u_2^{LWT} . Discrete layer transverse normal effects can be added to the element by including u_3^{LWT} . Displacement continuity is maintained between these different types of elements by simply enforcing homogeneous essential boundary conditions on the incremental layerwise variables, thus eliminating the need for multipoint constraints, penalty function methods, or special transition elements. It should be noted that a conventional 3-D finite element displacement field could be used instead of the full layerwise field in equation (12.4.1); however, the 2-D data structure of the full layerwise finite elements permits much easier coupling with the 2-D ESL field.

To illustrate the usefulness of a finite element based on the assumed displacement field of Eq. (12.4.1), consider a specific case where the individual displacement fields are selected as follows:

u_i^{ESL} : First-Order Shear Deformation Field

$$\begin{aligned} u_1^{ESL}(x, y, z) &= u_0(x, y) + z\phi_x(x, y) \\ u_2^{ESL}(x, y, z) &= v_0(x, y) + z\phi_y(x, y) \\ u_3^{ESL}(x, y, z) &= w_0(x, y) \end{aligned} \quad (12.4.2)$$

u_i^{LWT} : Layerwise Field of Reddy [37]

$$\begin{aligned} u_1^{LWT}(x, y, z) &= \sum_{I=1}^N U_I(x, y)\Phi^I(z) \\ u_2^{LWT}(x, y, z) &= \sum_{I=1}^N V_I(x, y)\Phi^I(z) \\ u_3^{LWT}(x, y, z) &= \sum_{I=1}^M W_I(x, y)\Psi^I(z) \end{aligned} \quad (12.4.3)$$

where (U_I, V_I, W_I) denote the nodal values of $(u_1, u_2, u_3) = (u, v, w)$, N is the number of nodes (or $N - 1$ is the number of subdivisions) through thickness, and Φ^I are the 1-D (global) interpolation functions for the discretization of the in-plane displacements through thickness, and M and Ψ^I have similar meaning for the discretization of the transverse displacement through thickness. A detailed discussion of displacement-based finite element models of the theory based solely on the displacement field in Eq. (12.4.3) was presented in the previous section. It should be noted that the layerwise field given by Eq. (12.4.3) is sufficiently general to model any of the deformation modes that can be modeled by the ESL field given in Eq. (12.4.2); thus for elements that use all the variables shown in Eqs. (12.4.2) and (12.4.3), there will be five redundant variables that must be set to zero (or ignored) to permit a unique solution for the remaining variables. The ESL variables are essential for connecting different types of elements. Therefore, the following five of the layerwise variables should be set to zero (see Figure 12.4.1):

$$U_1 = U_N = 0, \quad V_1 = V_N = 0, \quad W_1 = 0 \quad (12.4.4)$$

Parts (a) and (b) of Figure 12.4.1 illustrate a possible in-plane deformation (component $u = u_1$ only) of a transverse normal material line obtained by adding a piecewise linear layerwise displacement field to a first-order shear deformation displacement field. In this particular case, the reference plane is arbitrarily chosen to coincide with the bottom surface of the plate, and there are five nodes (i.e., planes) distributed through the thickness to define the layerwise portion of the composite displacement field. Note that in both parts (a) and (b) of Figure 12.4.1 the layerwise displacements U_I provide an incremental enhancement to the displacement u_1^{ELS} predicted by the first-order shear deformation theory as a result of setting U_1 and U_N to zero. The particular pair of U_I that are zeroed is arbitrary. The same final deformation is achieved in both parts (a) and (b); however, different pairs of U_I are zeroed, thus changing the numerical values of the remaining five nonzero variables.

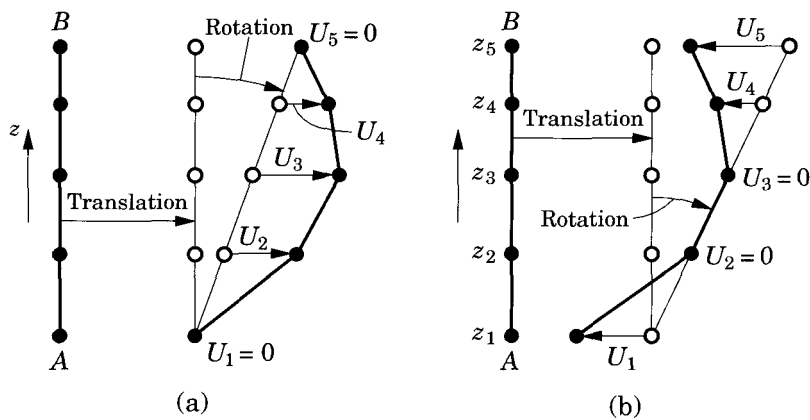


Figure 12.4.1: Superposition of a first-order shear deformation displacement field and a linear layerwise displacement field. In-plane deformation of transverse normal AB. (a) $U_1 = U_5 = 0$. (b) $U_2 = U_3 = 0$.

The location of the reference plane ($z = 0$) is arbitrary although its location affects the numerical values of the in-plane first-order shear deformation variables. If the displacements of the first-order shear deformation theory had been set to zero, then the layerwise displacements would be interpreted as total displacements.

12.4.3 Incorporation of Delamination Kinematics

A commonly occurring phenomenon in composite laminates is delamination. A delamination is simply a debonding or separation that occurs between individual material plies of a laminate (i.e., an interlaminar crack). Delaminations can occur as a result of manufacturing defects or from interlaminar normal and shear stresses brought about by local anomalies or transverse impacts. Often there may be multiple delaminations distributed through the thickness of a laminate, especially in the region surrounding an impact site. The subject of fracture mechanics has proven to be particularly useful in characterizing the severity of delaminations. For a general review of composite delamination research, the reader is referred to O'Brien [82]. The total energy release rate and its individual components have been successfully used to predict delamination onset and growth by O'Brien [82–85].

Since delamination is a common occurrence in laminates, the kinematics of single and multiple delamination should be incorporated into any general laminate model. The present multiple assumed displacement field of Eq. (12.4.1) also permits the modeling of delamination kinematics by using two or more layerwise expansions through the thickness instead of one. In this case, a separate layerwise expansion would be used for each sublaminate created by the delamination(s). Alternatively, one can model the kinematics of delamination by supplementing the composite displacement field with a simple, piecewise constant, discontinuous displacement

field that uses unit step functions of the thickness coordinate (see Barbero and Reddy [50]). Both of these methods introduce the same number of additional dependent variables. The second method is chosen here because the additional dependent variables are physically meaningful in that they represent the jump discontinuity in the displacement components across the delamination. Further, the second method allows easier modeling of multiple delaminations and easier implementation of various no-penetration contact algorithms for the delaminated surfaces (see Robbins and Reddy [52]). The supplemented composite displacement field thus becomes

$$u_i(x, y, z) = u_i^{ESL}(x, y, z) + u_i^{LWT}(x, y, z) + u_i^D(x, y, z) \quad (12.4.5)$$

$$\begin{aligned} u_1^D(x, y, z) &= \sum_{I=1}^D \mathcal{U}_I(x, y) H^I(z) \\ u_2^D(x, y, z) &= \sum_{I=1}^D \mathcal{V}_I(x, y) H^I(z) \\ u_3^D(x, y, z) &= \sum_{I=1}^D \mathcal{W}_I(x, y) H^I(z) \end{aligned} \quad (12.4.6)$$

and $H^I(z)$ are the Heaviside step functions, $H^I(z) = 1$ for $z \geq z^I$ and $H^I(z) = 0$ for $z < z^I$, and D is the number of delaminations distributed through the laminate thickness. Equation (12.4.6) represents displacement components that are piecewise constant through the laminate thickness. The delaminations are located at coordinates $z = z^I$ ($I = 1, 2, \dots, D$). Note that the I in z^I serves as a superscript and not an exponent, thus distinguishing the locations of the delaminations (z^I , $I = 1, 2, \dots, D$) from the locations of the nodes (z^J , $J = 1, 2, \dots, N$) in the layerwise expansion. Three dependent variables ($\mathcal{U}_I, \mathcal{V}_I, \mathcal{W}_I$) are introduced for each delamination. The dependent variables ($\mathcal{U}_I, \mathcal{V}_I, \mathcal{W}_I$) are interpreted as the jump discontinuities in the displacement components (u_1, u_2, u_3) at $z = z^I$ ($I = 1, 2, \dots, D$). The variable $\mathcal{W}_I(x, y)$ is the delamination opening displacement, thus the condition $\mathcal{W}_I \geq 0$ constitutes a no-penetration boundary condition for delaminated surfaces of the I th delamination. The delamination front for the I th delamination is defined as a curved or straight line in the xy -plane along which the essential boundary conditions $\mathcal{U}_I = \mathcal{V}_I = \mathcal{W}_I = 0$ are enforced.

The effect of introducing the delamination field of Eq. (12.4.5) into the composite displacement field is illustrated in Figure 12.4.2, which shows the x -component of the deformation of a transverse normal material line AB. The overall deformation of line AB is similar to that of Figure 12.4.1 with the exception of a single delamination located at $z = z^1$, where the jump discontinuity \mathcal{U}_1 is introduced. These jump discontinuities can be introduced as many times as desired for multiple delaminations (see Barbero and Reddy [50]).

In the next section we shall discuss a displacement-based finite element model of the variable kinematic displacement field in (12.4.5). A practical problem often has several regions, each requiring a different mathematical model, and the variable kinematic model allows modeling of each of them.

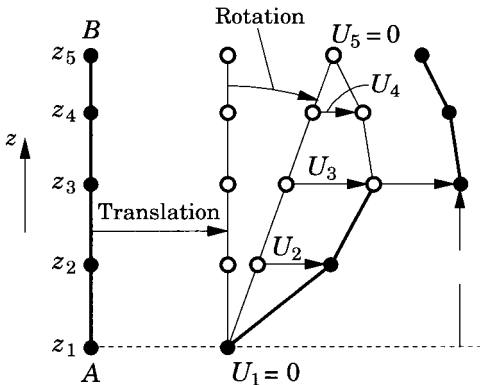


Figure 12.4.2: Superposition of a first-order shear deformation displacement field, a linear layerwise displacement field, and a piecewise constant delamination displacement field. In-plane deformation of transverse normal AB. Delamination occurs at $z = z^1$.

12.4.4 Finite Element Model

A hierarchy of three distinct types of plate elements can be obtained from the composite displacement field of Eq. (12.4.5), where the individual displacement expansions are defined by Eqs. (12.4.2), (12.4.3) and (12.4.6). The first and simplest type of element is the first-order shear deformation element (or FSDT element). This element is formed using Eq. (12.4.2) for u_i^{ESL} and suppressing u_i^{LWT} and u_i^D . The second type of element is the Type I layerwise element (or LWT1 element), which is formed using Eq. (12.4.5) but ignoring u_i^D and the expansion for u_3^{LWT} in Eq. (12.4.3). Thus, LWT1 is a partial layerwise element. Four of the layerwise variables should be set to zero (or simply ignored) to remove the redundancy from the composite displacement field (e.g., $U_1 = U_N = V_1 = V_N = 0$). Like the FSDT element, the LWT1 element assumes a state of zero transverse normal stress and thus does not explicitly account for transverse normal strain. This is implicitly achieved by using a reduced constitutive matrix similar to the FSDT element. The inclusion of Eqs. (12.4.3a) and (12.4.3b) in the LWT1 element provides discrete layer transverse shear effects, unlike the simple gross transverse shear effect included in the FSDT element. Thus the LWT1 element is applicable to thick laminates and often yields results comparable to 3-D finite elements while using approximately two thirds the number of degrees of freedom. The third and most complex element is the Type II layerwise element (or LWT2 element). This element is formed using both Eqs. (12.4.2) and (12.4.3), thus it is a full layerwise element. The composite displacement field contains five redundant variables, thus five layerwise variables are chosen (e.g., U_1, U_N, V_1, V_N, W_1) and set to zero or simply ignored. The LWT2 element explicitly accounts for all six strain components in a kinematically correct manner; i.e., the in-plane strains are C^1 -continuous through the laminate thickness while the transverse strains are C^0 -continuous through the laminate thickness. The

inclusion of the full layerwise field provides the LWT2 element with both discrete layer transverse shear effects and discrete layer transverse normal effects. The LWT2 element uses a full constitutive matrix ($\bar{Q}_{ij} = \bar{C}_{ij}$), and it is equivalent in accuracy and cost to a stack of conventional 3-D finite elements.

If delaminations are present, then both the LWT1 and LWT2 finite elements can make use of the delamination expansion of Eq. (12.4.5). The FSDT element cannot be used to model delamination since the deformation above and below the delamination cannot be separately prescribed due to the C^1 -continuity of the FSDT displacement expansion through the thickness.

Note that the various element types are created by hierarchically adding variables to the basic first-order shear deformation field. The matrix form of the finite element equations that result from the hierarchical use of Eqs. (12.4.2), (12.4.3), and (12.4.6) within a single element domain is given by

$$\begin{bmatrix} [K^{EE}] & [K^{EL}] & [K^{ED}] \\ [K^{LE}] & [K^{LL}] & [K^{LD}] \\ [K^{DE}] & [K^{DL}] & [K^{DD}] \end{bmatrix} \begin{Bmatrix} \{U^E\} \\ \{U^L\} \\ \{U^D\} \end{Bmatrix} = \begin{Bmatrix} \{F^E\} \\ \{F^L\} \\ \{F^D\} \end{Bmatrix} \quad (12.4.7)$$

where $[K^{EE}]$ represents the element stiffness matrix for an equivalent single-layer FSDT element, $[K^{LL}]$ represents the element stiffness matrix for a full layerwise element, and $[K^{DD}]$ represents the element stiffness matrix for an element based solely on the delamination field of Eq. (12.4.6). The remaining submatrices represent coupling stiffnesses between the three different displacement fields. Based on the particular type of element desired, the appropriate terms in the composite stiffness matrix are identified and computed. Since all three element types possess the first-order shear deformation variables of Eq. (12.4.2), these different types of elements can easily be simultaneously connected in the same computational domain by simply setting certain layerwise variables of Eq. (12.4.3) to zero along the incompatible boundary.

Figure 12.4.3 illustrates a hypothetical 2-D finite element mesh of variable kinematic finite elements where all three element types (FSDT, LWT1, and LWT2) are simultaneously present. The hierarchical nature of the variable kinematic elements allows interelement compatibility to be achieved by simply enforcing homogeneous boundary conditions on some or all of the incremental layerwise variables along the boundary separating two incompatible subregions. Subregion compatibility can be enforced in a strict sense or a relaxed sense by specifying the essential boundary conditions as defined below (also see Figure 12.4.3).

Strict subregion compatibility (SSC)

- At nodes on FSDT/LWT1 boundary, set $U_I = 0, V_I = 0$
- At nodes on FSDT/LWT2 boundary, set $U_I = 0, V_I = 0, W_I = 0$
- At nodes on LWT1/LWT2 boundary, set $U_I = 0, V_I = 0, W_I = 0$

Relaxed subregion compatibility (RSC)

- At nodes on FSDT/LWT1 boundary, set $U_I = 0, V_I = 0$
- At nodes on FSDT/LWT2 boundary, set $U_I = 0, V_I = 0$
- At nodes on LWT1/LWT2 boundary, set $U_I = 0, V_I = 0$

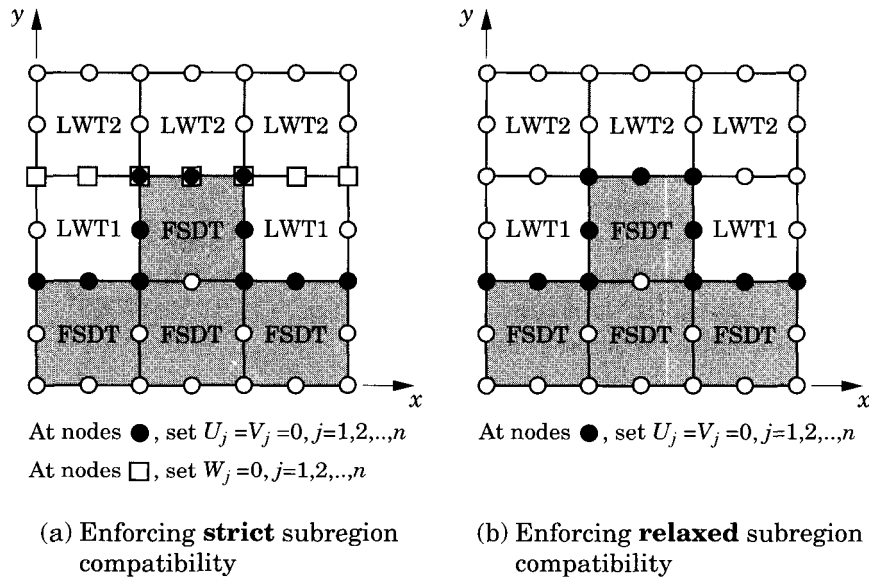


Figure 12.4.3: A simple 2-D mesh of variable kinematic finite elements. All three element types (FSDT, LWT1, and LWT2) are simultaneously present in the mesh.

for $I = 1, 2, \dots, N$. When maintaining strict subregion compatibility (SSC), all three displacement components are continuous across all types of subregion boundaries (FSDT/LWT1, LWT1/LWT2, and LWT2/FSDT). In contrast, relaxed subregion compatibility (RSC) maintains total continuity of the in-plane displacement components across all types of subregion boundaries, but it does not maintain total continuity of the transverse displacement component across FSDT/LWT2 or LWT1/LWT2 boundaries. This relaxation is often useful for obtaining accurate transverse normal stresses within LWT2 subregions, near FSDT/LWT2 or LWT1/LWT2 boundaries, since it eliminates the transverse pinching or stretching of the laminate near these boundaries, and effectively allows the transverse normal strain to react to the local dominant in-plane strains. Within those portions of LWT2 subregions sufficiently removed from FSDT/LWT2 or LWT1/LWT2 boundaries, both strict and relaxed conditions yield the same stress distributions.

The enforcing of strict or relaxed subregion compatibility via application of the appropriate homogeneous essential boundary conditions is easily automated in a finite element program and can thus be removed from the concern of the user. A significant advantage afforded by the variable kinematic elements is that once the in-plane mesh is defined, the user can then assign any of the three element types (FSDT, LWT1, and LWT2) to any of the elements in the 2-D mesh. Subsequent changes in the type of any element or group of elements can be performed with minimal effort.

12.4.5 Illustrative Examples

The problem of determining the free edge stress fields in laminates subjected to in-plane extension or bending is used to illustrate the variable kinematic finite element (VKFE) model methodology. The free edge problem is ideally suited for global-local analysis, because the 3-D stress field exists only in a boundary region (i.e., free edge) of the laminate and elsewhere only a 2-D stress state exists. Thus, the LWT2 elements can be used in the free edge (local) region and ESL elements can be used everywhere else (global region) to capture the stress fields accurately.

Free Edge Stresses in Laminates in Extension

To demonstrate the accuracy and economy afforded by the variable kinematic finite elements, a global-local analysis is performed to determine the nature of the free edge stress field in three different laminates subjected to axial extension: $(45/-45)_s$, $(45/0/-45/90)_s$, and $(45/0/-45/90/90/-45/0/45)_s$. The three laminates have length $2a$, width $2b$, and thickness $2h$. Each of the three laminates has a length-to-width ratio of 10 (i.e., $a/b = 10$). The material plies in each laminate are of equal thickness h_k . The following geometric differences exist among the three laminates:

$$\begin{aligned} (45/-45)_s \text{ laminate: } & \frac{b}{h} = 4, \quad h = 2h_k, \quad \frac{b}{h_k} = 8 \\ (45/0/-45/90)_s \text{ laminate: } & \frac{b}{h} = 15, \quad h = 4h_k, \quad \frac{b}{h_k} = 60 \\ (45/0/-45/90)_{2s} \text{ laminate: } & \frac{b}{h} = 15, \quad h = 8h_k, \quad \frac{b}{h_k} = 120 \end{aligned} \quad (12.4.8)$$

Each of the material plies in the three laminates is idealized as a homogeneous, orthotropic material; the material properties (expressed in the principal material coordinate system) are defined below.

Material plies in the four-layer laminate:

$$\begin{aligned} E_1 &= 20 \times 10^6 \text{ psi}, \quad E_2 = E_3 = 2.1 \times 10^6 \text{ psi} \\ G_{12} &= G_{23} = G_{13} = 0.85 \times 10^6 \text{ psi}, \quad \nu_{12} = \nu_{23} = \nu_{13} = 0.21 \end{aligned} \quad (12.4.9a)$$

Material plies in the eight- and sixteen-layer laminates:

$$\begin{aligned} E_1 &= 19.5 \times 10^6 \text{ psi}, \quad E_2 = E_3 = 1.48 \times 10^6 \text{ psi} \\ G_{12} &= G_{23} = G_{13} = 0.8 \times 10^6 \text{ psi}, \quad \nu_{12} = \nu_{23} = \nu_{13} = 0.3 \end{aligned} \quad (12.4.9b)$$

The origin of the global coordinate system coincides with the centroid of each of the 3-D composite laminates. The x -coordinate is taken along the length, the y -coordinate is taken across the width, and the z -coordinate is taken through the thickness of the laminate. Since the laminate is symmetric about the xy -plane, only the upper half of each laminate is modeled. Thus the computational domain is defined by $(-a < x < a, -b < y < b, 0 < z < h)$. The displacement boundary conditions for all three laminates are

$$u_1(a, y, z) = u_0, \quad u_1(-a, y, z) = u_2(-a, y, z) = u_2(a, y, z) = u_3(x, y, 0) = 0 \quad (12.4.10)$$

The slight differences in geometry and material properties among the three laminates allow comparison with solutions published in the literature. For the $(45/-45)_s$ laminate, Wang and Choi [57,58] have developed a quasi-3D elasticity solution, while Whitcomb et al. [59] produced a solution from a highly refined, quasi-3D finite element model. For the $(45/0/-45/90)_s$ and $(45/0/-45/90/90/-45/0/45)_s$ laminates, Whitcomb and Raju [61] obtained quasi-3D finite element solutions using a highly refined mesh.

The variable kinematic finite elements are used in a simultaneous multiple model analysis (global-local analysis) of these three laminates in order to accurately yet efficiently determine the free edge stresses near the middle of one of the two free edges. The global region is modeled using first-order shear deformable elements (FSDT); the local region, where accurate 3-D stresses are desired, is modeled with LWT2 elements.

First the $(45/-45)_s$ laminate will be used to assess the effects of subregion compatibility type (SSC or RSC) and size of the local LWT2 subregion on the accuracy of the computed transverse stresses near the free edge. For this purpose, five different finite element meshes are created. The 2-D, in-plane discretization for all five meshes is exactly the same, consisting of a 5×11 mesh of eight-node, quadratic, 2-D, quadrilateral finite elements (see Figure 12.4.4). All elements have the same length ($2a/5$); however, the width of the elements decreases as the free edge at (x, b, z) is approached. The widths of the eleven rows of elements, as one moves away from the refined free edge, are $h_k/16, h_k/16, h_k/8, h_k/4, h_k/2, h_k, h_k, 2h_k, 3h_k, 3h_k$, and $5h_k$ (h_k =ply thickness). The five meshes differ only in the width of the local region where LWT2 elements are used. The LWT2 elements used in the local region employ eight quadratic layers through the laminate thickness (four per material layer) as shown in Figure 12.4.5. The thickness of the numerical layers decreases as the $+45/-45$ interface is approached. From bottom to top, the layer thicknesses are $0.533h_k, 0.267h_k, 0.133h_k, 0.083h_k, 0.083h_k, 0.133h_k, 0.267h_k$, and $0.533h_k$.

Table 12.4.1 summarizes the five meshes used for the $(45/-45)_s$ laminate. Note that mesh 5 is not a global-local mesh. Mesh 5 uses LWT2 elements throughout the entire computational domain, thus serving as a control mesh for judging the accuracy of the four global-local meshes. In meshes 1 through 4, the local region (LWT2 elements) is adjacent to the free edge (x, b, z) and is centered about the plane $(0, y, z)$. In meshes 1 through 4, the length of the local region spans three fifths of the total length of the laminate; however, the width of the local region differs in each mesh ranging from $h_k/2$ to $3h_k$. Two runs are made with each of the four global-local meshes, the first using strict subregion compatibility along the FSDT-LWT2 boundary, and the second using relaxed subregion compatibility along the FSDT-LWT2 boundary.

The stresses are computed via the constitutive relations at the reduced Gauss points within the individual layers of each LWT2 element. All stresses are nondimensionalized as follows:

$$\bar{\sigma}_{ij} = \frac{20\sigma_{ij}}{\varepsilon_0 E_1} \quad (12.4.10)$$

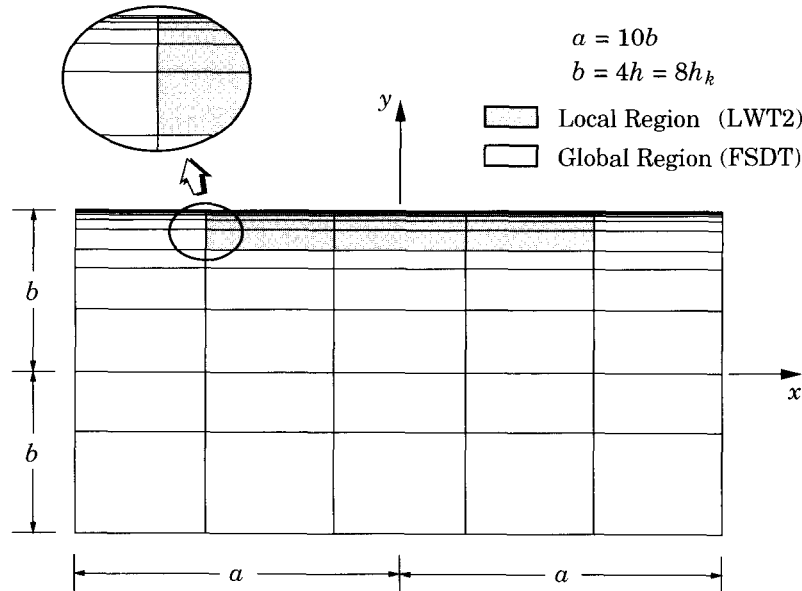


Figure 12.4.4: The 2-D mesh of variable kinematic finite elements used to model a $(45/-45)_s$ laminate under axial extension. All elements are eight-node quadrilaterals.

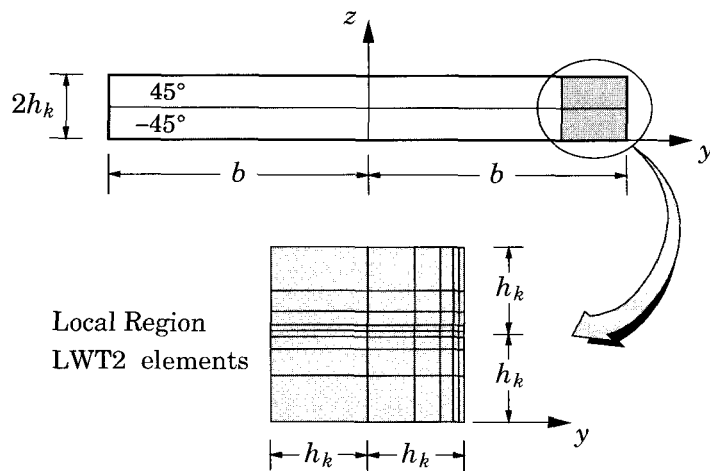


Figure 12.4.5: Discretization within the local LWT2 region, on the yz -plane. The eight-node LWT2 elements in the local region use quadratic layers.

Table 12.4.1: Description of global-local meshes for the $(45/-45)_s$ laminate under axial extension.

Remarks	Mesh 1	Mesh 2	Mesh 3	Mesh 4	Mesh 5
Number of Elements in Local LWT2 Region	3×4	3×5	3×6	3×7	5×11
Width of Local Region	$\frac{1}{2}h_k$	h_k	$2h_k$	$3h_k$	$16h_k$
Length of Local Region	$\frac{6}{5}a$	$\frac{6}{5}a$	$\frac{6}{5}a$	$\frac{6}{5}a$	$2a$
Total Number of Active DoF in VKFE Mesh (Strict Compatibility)	1,986	2,400	2,814	3,228	9,116
Total Number of Active DoF in VKFE Mesh (Relaxed Compatibility)	2,354	2,800	3,246	3,690	9,116

h_k = thickness of a single material ply. All five VKFE meshes have the exact same in-plane discretization (5×11); DoF = Degrees of Freedom.

where ε_0 is the nominal applied axial strain of $u_0/(2a)$. The stress distributions shown in Figures 12.4.6 through 12.4.8 are generated by computing the nondimensionalized stresses at a series of adjacent reduced Gauss points, and then connecting these points with straight lines.

Figures 12.4.7 and 12.4.8 show the distribution of the interlaminar stresses σ_{zz} and σ_{xz} near the free edge. The results in these two figures were obtained using relaxed subregion compatibility conditions. The stresses presented in Figure 12.4.6 are computed at the reduced Gauss points near the middle of the refined free edge, i.e., along the line $(-0.115a, 0.998b, z)$. This is also the reduced Gauss point located farthest from the FSDT/LWT2 boundary. The stresses presented in Figure 12.4.7 are computed at the reduced Gauss points closest to the line $(0, y, h_k)$, i.e., along the line $(-0.115a, y, 1.014h_k)$. All four of the global local meshes are successful in identifying the spikes in σ_{zz} and σ_{xz} that occur at the $45/-45$ interface. The results of meshes 3 and 4 are graphically indistinguishable from the results of the control mesh, mesh 5. While meshes 1 and 2 exhibit some error, they do capture the qualitative nature of the transverse stress distributions near the free edge. In meshes 1 and 2, the transverse shear stresses are predicted more accurately than the transverse normal stresses. The results also indicate that the boundary layer thickness (or the width of the local region) should be at least $2h_k$ to capture both interlaminar stresses accurately.

Figure 12.4.8 shows the effect of subregion compatibility type (strict or relaxed) on the accuracy of the transverse normal stress within the local LWT2 subregion. Only the transverse normal stress distributions are shown since similar transverse shear stress distributions were computed for both strict and relaxed subregion compatibility. Figure 12.4.8 shows the distribution of σ_{zz} across the width of the laminate, near the $+45/-45$ interface, as the free edge is approached. The stresses

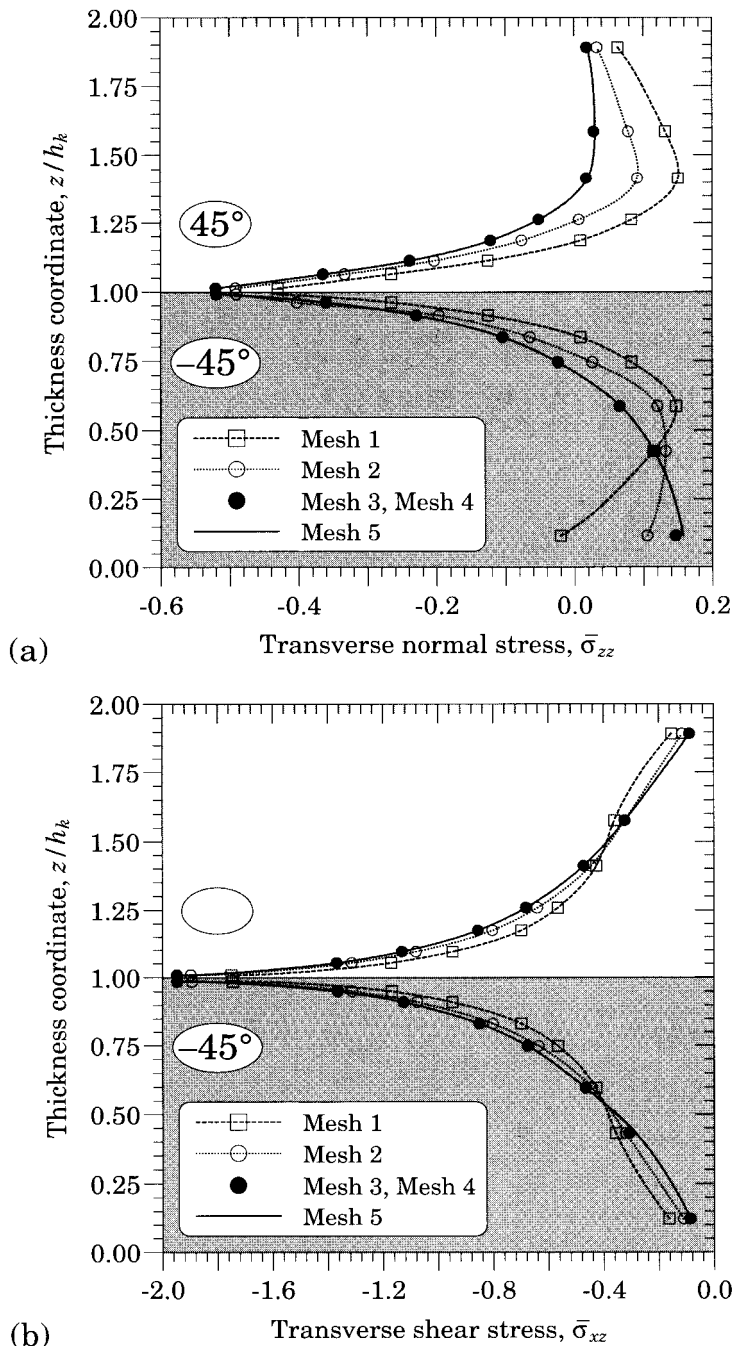


Figure 12.4.6: Interlaminar stress distribution through thickness of the $(45/-45)_s$ laminate near free edge. Results computed for meshes 1 through 5 with relaxed subregion compatibility.

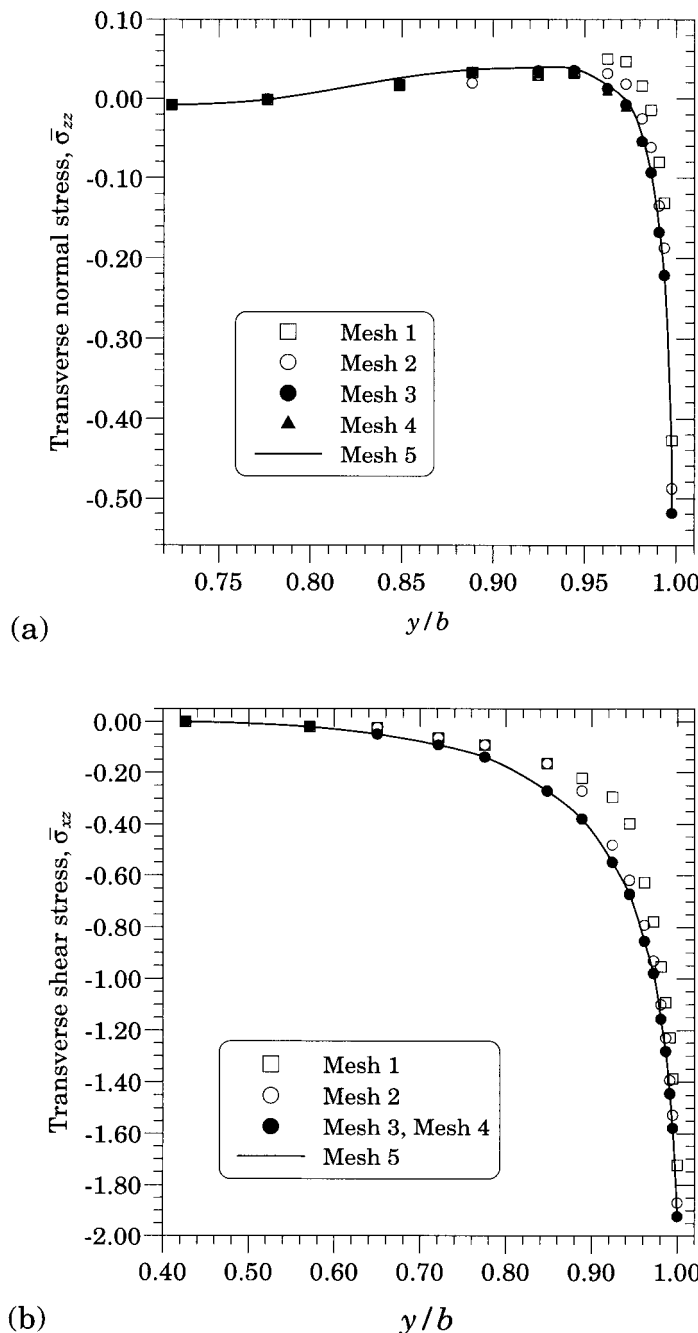


Figure 12.4.7: Interlaminar stress distribution across the width of the $(45/-45)_s$ laminate near the upper $45/-45$ interface ($z = 1.014h_k$). Results computed for meshes 1 through 5 with relaxed subregion compatibility.

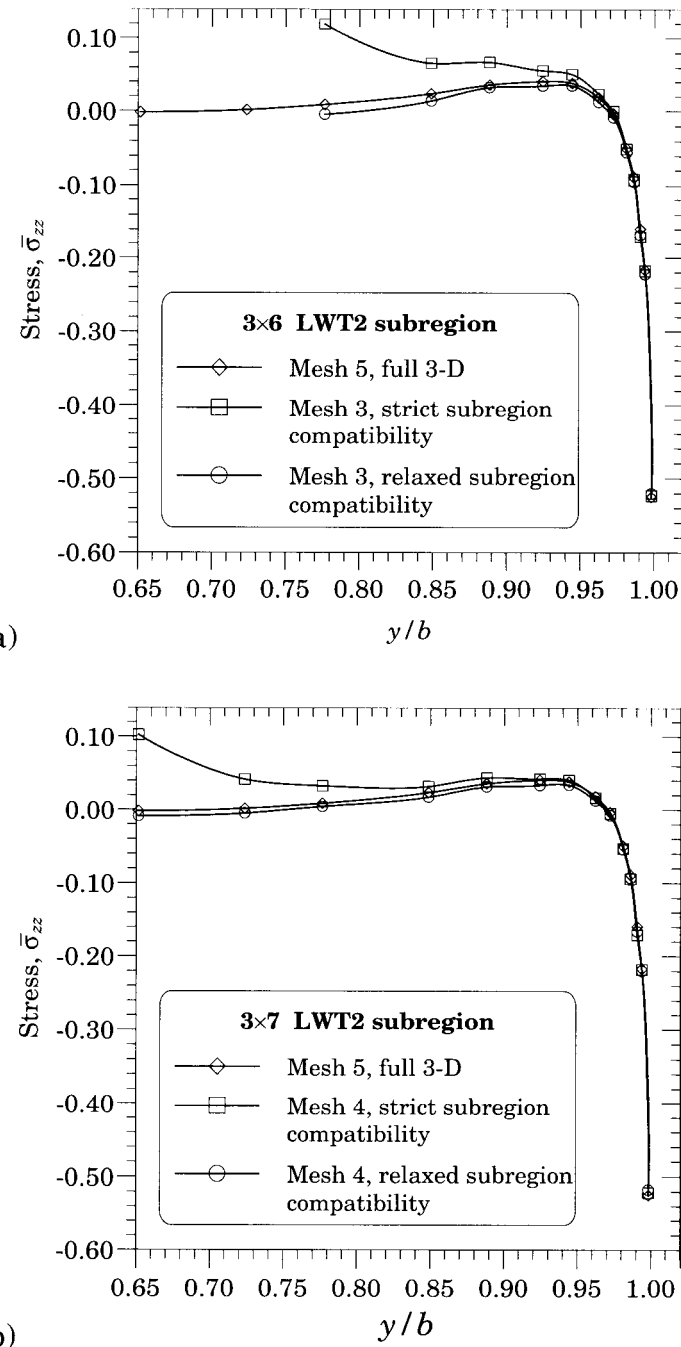


Figure 12.4.8: Stress distributions across width of the $(45/-45)_s$ laminate near the upper $45/-45$ interface ($z = 1.014h_k$). Results computed for (a) mesh 3 and (b) mesh 4 using both strict subregion compatibility and relaxed subregion compatibility.

are computed along the same line of adjacent reduced Gauss points as in Figure 12.4.7. The use of strict subregion compatibility causes significant error in the transverse normal stress near the FSDT/LWT2 boundary. This error is caused by the enforced transverse inextensibility of the laminate along the FSDT/LWT2 boundary. The FSDT elements enforce a condition of $\varepsilon_{zz} = 0$ on the edges of the LWT2 elements that form the FSDT/LWT2 boundary, thus artificially pinching or stretching the laminate thickness along the FSDT/LWT2 boundary. In contrast, the use of relaxed subregion compatibility allows the edges of the LWT2 elements that lie on the FSDT/LWT2 boundary to expand or contract in the thickness direction in response to the compatible in-plane displacement field. Thus the use of relaxed subregion compatibility permits accurate transverse normal stresses to be computed across the entire width of the LWT2 region, even near the FSDT/LWT2 boundary. The use of relaxed subregion compatibility results in a slight increase in the number of active degrees of freedom since the W_I ($I = 1, 2, \dots, N$) are not zeroed along the FSDT/LWT2 boundary (see Table 12.4.1). Thus the analyst may wish to use strict subregion compatibility provided that the LWT2 subregion is sufficiently large and provided that accurate transverse normal stresses are not needed near the FSDT/LWT2 boundary.

To illustrate the accuracy of the variable kinematic elements in determining the free edge stress field for more complex laminates, a simultaneous multiple model analysis is performed on an eight-ply $(45/0/-45/90)_s$ laminate, and a sixteen-ply $(45/0/-45/90/90/-45/0/45)_s$ laminate. Both of these laminates are subjected to axial extension similar to the previously examined $(45/-45)_s$ laminate. The in-plane discretization consists of a 5×11 2-D mesh of eight-node quadrilateral elements as shown previously in Figure 12.4.4. The local region is discretized with a 3×6 mesh of LWT2 elements. For the $(45/0/-45/90)_s$ laminate, the LWT2 elements contain 12 quadratic layers (three per material ply). Within each material ply the three quadratic layers have thicknesses of $0.25h_k$, $0.5h_k$, and $0.25h_k$ from bottom to top. For the $(45/0/-45/90/90/-45/0/45)_s$ laminate, the LWT2 elements contain 16 quadratic layers (two per material ply). Within each material ply both of the quadratic layers have thicknesses of $0.5h_k$. The $(45/0/-45/90)_s$ model contains 4,382 active degrees of freedom while the $(45/0/-45/90/90/-45/0/45)_s$ model contains 5,638 active degrees of freedom.

The computed transverse shear stress and transverse normal stress distributions for these two laminates are shown in Figures 12.4.9 and 12.4.10. The present results show excellent agreement with the quasi-3D finite element solutions of Whitcomb and Raju [61] (not included in the figure). For both laminates the maximum transverse normal stress occurs at the intersection of the 90/90 interface and the free edge, while the maximum transverse shear stress occurs at the intersection of the 45/0 and 0/-45 interfaces with the free edge. Both of these laminates have enough distinct material plies to make a full 3-D analysis prohibitively expensive, thus a sequential or simultaneous multiple model analysis is the only reasonable alternative. Many laminates have a very large number of distinct material plies, thus even with a multiple model analysis, the investigator may have to resort to using the sublaminate approach (i.e., ply grouping) within the local LWT2 region. In this case the investigator would identify a target group of adjacent material plies that would receive one or more numerical layers each, while the remaining plies

are grouped into one or more numerical layers and effectively homogenized. By performing several of these analyses, one can piece together a picture of the 3-D stress state through the laminate thickness within the local LWT2 region.

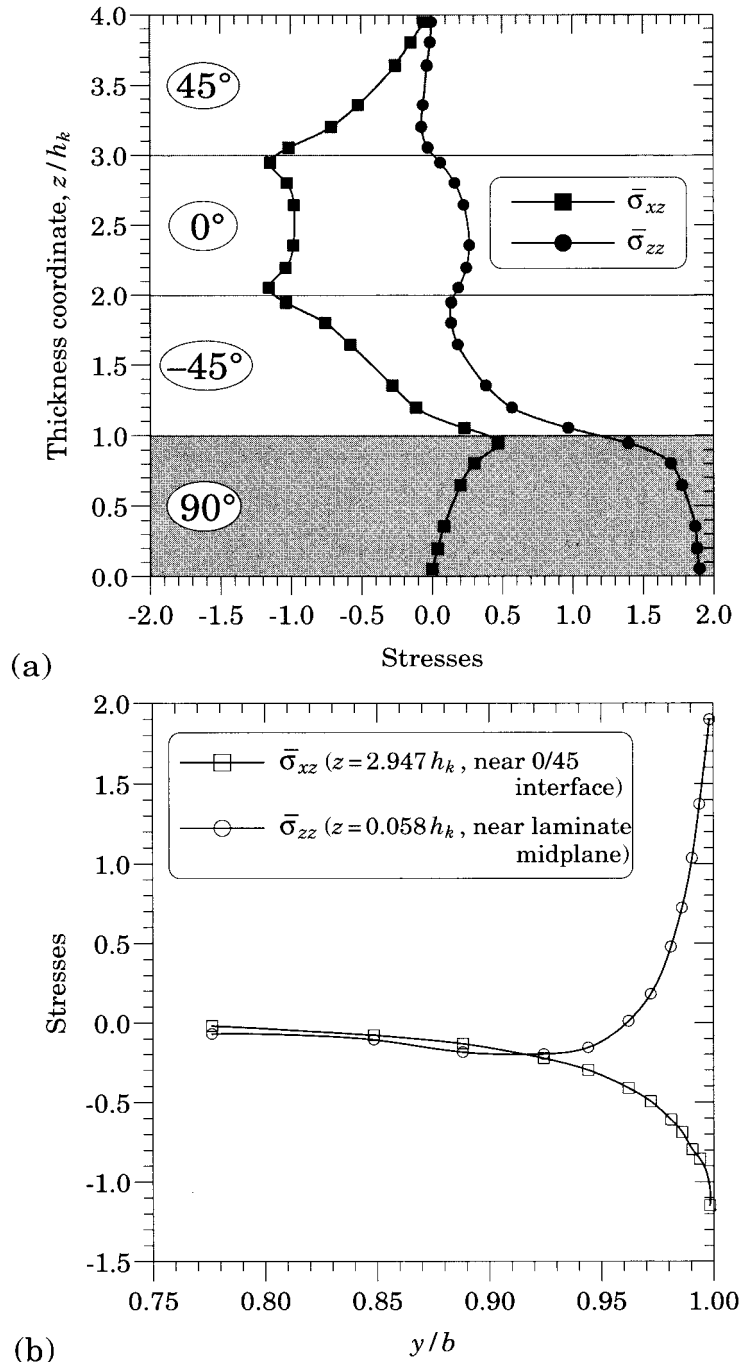


Figure 12.4.9: Interlaminar stress distributions in $(45/0/-45/90)_s$ laminate under axial extension. (a) Through the thickness near the free edge ($x = -0.115a, y = 0.998b$). (b) Across the width ($x = -0.115a$).

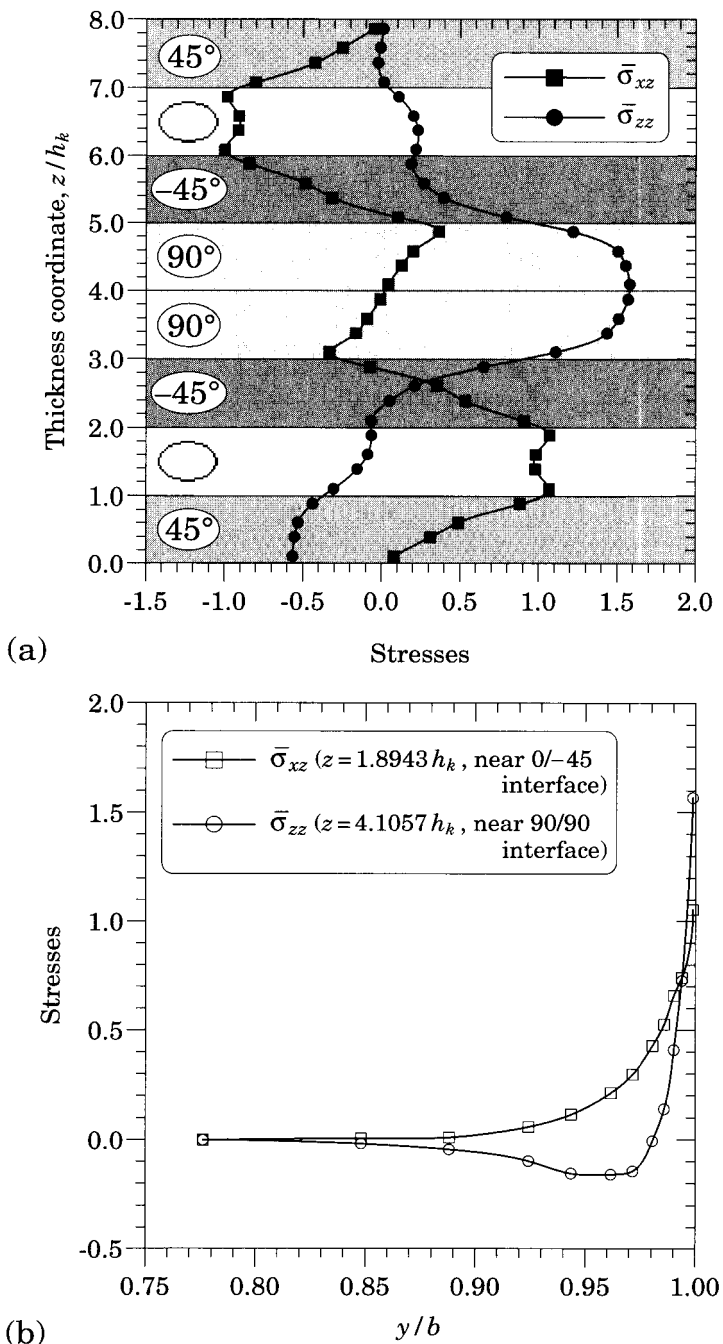


Figure 12.4.10: Interlaminar stress distributions in $(45/0/-45/90/90/-45/0/45)_s$ laminate under axial extension. (a) Through the thickness near the free edge ($x = -0.115a, y = 0.998b$). (b) Across the width ($x = -0.115a$).

Free Edge Stresses in a $(45/-45)_s$ Laminate in Bending

All of the previous examples involve the determination of free edge stress fields in laminates subjected to axial tension. To demonstrate the effectiveness of the variable kinematic finite elements for determining free edge stresses in laminates subjected to bending, consider a simply supported $(45/-45)_s$ laminate subjected to a uniform transverse load. The physical dimensions and material properties of the $(45/-45)_s$ laminate will be the same as in the axial extension example, with the exception that the origin of the coordinate system will be placed at the bottom center of one of the ends of the laminated strip. Thus the laminate occupies the domain $(0 < x < 2a, -b < y < b, 0 < z < 4h)$ where $a = 10b = 40h = 80h_k$ and h_k is the thickness of a material ply. The displacement boundary conditions are

$$u_1(a, -b, 0) = u_2(0, y, z) = u_2(2a, y, z) = u_3(0, y, 0) = u_3(2a, y, 0) = 0$$

The uniform transverse load q_0 is applied to the upper surface of the laminate and acts in the negative z direction. Note that there are no planes of symmetry in this problem, thus the computational domain consists of the entire laminate.

To accurately yet efficiently capture the free edge stresses, a global-local analysis is performed using a 2-D mesh of variable kinematic finite elements, where FSDT elements make up the majority of the computational domain, and a small patch of LWT2 elements is used to resolve the free edge stress field within a localized region of interest, which is one of the free edges. The objective of this example is to determine the effect of the width of the LWT2 region on the accuracy of the computed free edge stresses.

To investigate the effect of reducing the length of the LWT2 subregion, four different global-local meshes are created. Each mesh has a total in-plane discretization of 9×11 elements (9 elements along the laminate length, 11 elements across the laminate width). As in the previous analyses of the $(45/-45)_s$ laminate under axial extension, the in-plane mesh is highly refined over one of the free edges and is coarse over the other free edge. Note that the collective length of the central three rows of equal length elements is denoted as a_0 . The remaining six rows of elements are of equal length $(2a - a_0)/6$. The in-plane discretization of the five meshes differ in the value of a_0 ; specifically $a_0 = 2h, 4h, 8h$, and $16h$ for meshes 1 through 4, respectively. Each of the four in-plane meshes is used with both a 3×6 LWT2 subregion and 5×6 LWT2 subregion (i.e., three or five LWT2 elements in the x direction and six LWT2 elements in the y direction). The width of the LWT2 subregion is h in each case. Each of the LWT2 elements employs eleven quadratic layers through the laminate thickness: three layers in the bottom $+45^\circ$ ply, five layers in the two collective middle $-45/-45$ plies, and three layers in the top $+45^\circ$ ply. From bottom to top, the layer thicknesses are $0.6h_k, 0.3h_k, 0.1h_k, 0.1h_k, 0.3h_k, 1.2h_k, 0.3h_k, 0.1h_k, 0.1h_k, 0.3h_k$, and $0.6h_k$. By comparing the results of the 3×6 and 5×6 LWT2 subregions for each of the four meshes, the effect of LWT2 subregion length on solution accuracy can be established. Each of the global-local meshes uses relaxed subregion compatibility.

The transverse stress distributions obtained with mesh 1 ($a_0 = 2h$) are shown in Figure 12.4.11. Mesh 1 ($a_0 = 2h$) consists of both 3×6 and 5×6 LWT2 subregions. Note that while the response predicted by the 3×6 and 5×6 LWT2

subregions are qualitatively the same, there is a small quantitative difference between the two responses. This quantitative difference indicates that the shorter 3×6 LWT2 subregion (length = $2h$) is not quite adequate to capture accurately the local 3-D stress field. In particular, Figure 12.4.11b shows that the transverse shear stress distribution predicted with the 3×6 LWT2 subregion is not smooth across the FSDT/LWT2 interface which occurs at $y/b = 0.75$. Figure 12.4.11b also shows that the LWT2 subregion is not quite wide enough (width = h) to show clearly the point where σ_{zz} decays to zero. Figures 12.4.12a,b show the same results for mesh 2 where $a_0 = 4h$, with the exception that the width of the LWT2 subregion has been increased to $1.5h$ by using 3×7 and 5×7 LWT2 subregions as opposed to 3×6 and 5×6 LWT2 subregions. Note that the quantitative difference between the 3×7 and 5×7 responses is considerably smaller than for mesh 1. In Figure 12.4.12b, the disruption in the transverse shear stress distribution at the FSDT/LWT2 interface is barely detectable. Further, the increased widths of the LWT2 subregions are adequate to show the complete decay of σ_{zz} .

12.5 Application to Adaptive Structures

12.5.1 Introduction

New structural concepts are emerging in which sensors and actuators are embedded or bonded to composite laminates for high-performance structural applications. These structures are termed *adaptive structures*, which monitor their own health. Adaptive structures are particularly useful for operations in remote or hazardous locations, process monitoring, vibration isolation and control, and medical applications, to name only a few. A laminated composite structure with piezoelectric actuators and sensors, for example, receives actuation through an applied electric field (to the actuators) and sends electric signals (electric field developed in the sensors) that can be used to measure the laminate response. Actuation and sensing materials exhibit a strong coupling between their mechanical response and electrical, magnetic or thermal behavior [86] (e.g., the application of an electric field produces a deformation and deformation of the material produces an electric field). The layerwise theory is capable of representing the 3D kinematics of laminated composite structures with active elements.

The currently available analyses of piezo-laminated structures can be divided into the following classes [87–90]:

- *Uncoupled ESL models:* models that do not consider the electro-mechanical coupling. The mechanical problem is solved using an ESL theory (often CLPT) where the piezoelectric actuators actions are treated as a load (similar to a thermal stress problem). The electrical problem is not solved and the voltages in the sensors are calculated a posteriori from the solution of the mechanical problem.
- *Coupled ESL models:* models for which the mechanical problem is solved with an ESL theory, and the electrical problem is solved assuming distributions of the electric variables for each lamina of the laminate in a layerwise form.
- *Coupled Layerwise models:* models in which the full electro-mechanical coupled problem is solved using a layerwise approach.

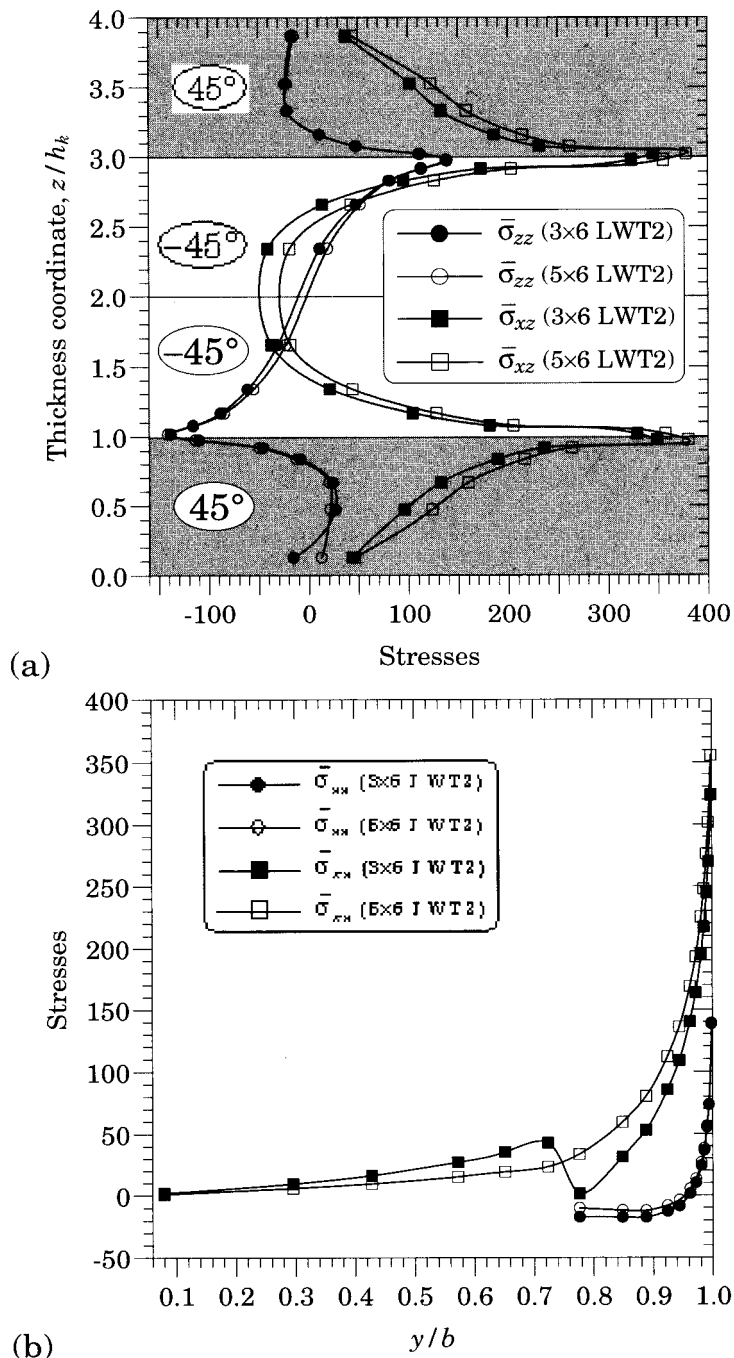


Figure 12.4.11: Interlaminar stress distributions ($\bar{\sigma} = \sigma/q_0$) in $(45/-45)_s$ laminate in bending (Mesh 1). (a) Through the thickness near the free edge at $x = a$ and $y = b$. (b) Across the width near the upper 45/-45 interface.

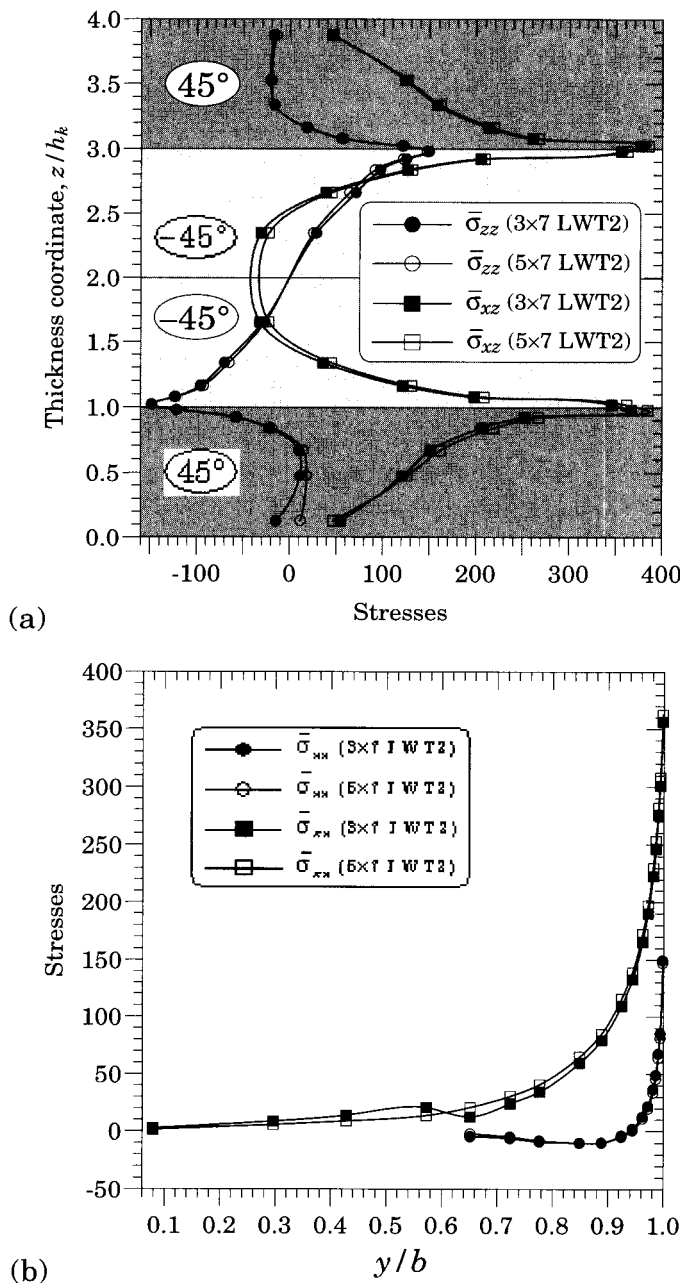


Figure 12.4.12: Interlaminar stress distributions ($\bar{\sigma} = \sigma/q_0$) in $(45/-45)_s$ laminate in bending (Mesh 2). (a) Through the thickness near the free edge at $x = a$ and $y = b$. (b) Across the width of laminate, near the upper 45/-45 interface.

Heyliger, Ramirez and Saravacos [89] used the layerwise theory of Reddy [37] to develop a general finite element formulation for the coupled electromechanical problem of piezoelectric laminated plates. Numerical results were presented for the static behavior of a thick composite plate including two piezoelectric layers. A linear variation was assumed for each variable and models with constant and variable transverse displacement were considered. Each lamina was discretized in the thickness using two or three sublayers. Three meshes were studied and full integration was used for all terms. The stresses and electrical displacements were computed at Gauss points using the constitutive law. The results are in agreement with an exact solution but the model with constant transverse displacement is less accurate. In a similar work, Saravacos, Heyliger and Hopkins [90] extended the previous finite element formulation [89] to the dynamics case.

The main objective of this section is to study an application of the layerwise displacement finite element model to adaptive structures composed of composite materials and piezoelectric inserts. The formulation includes full electromechanical coupling and allows different polynomial approximations through the thickness as well as an independent and arbitrary interpolation in the surface of the laminate [91]. Only the static linear elastic case is considered. The results obtained by the developed finite element model for a benchmark problem are discussed and compared with the respective three-dimensional closed-form solutions [91].

12.5.2 Governing Equations

Consider a laminated plate with thickness H and built with piezoelectric laminae or patches and laminae of different linear elastic materials. The piezoelectric inserts may work as sensors or actuators. A global rectangular reference frame (x, y, z) , with the z -axis aligned with the laminate thickness is used. The top and bottom planes of the laminate are denoted Ω_T and Ω_B , respectively, and the edge $\Omega \times H$ includes the laminate thickness and boundary Γ of Ω . The constitutive relations of piezoelectric materials in a piezo-laminated structure bring the electro-mechanical coupling.

The mechanical problem is governed by the 3-D equilibrium equations (the meaning of the variables should be obvious)

$$\frac{\partial \sigma_{ji}}{\partial x_j} + F_i = 0 \quad (12.5.1)$$

The boundary conditions involve specifying

$$u_i = \hat{u}_i \quad \text{or} \quad t_i \equiv \sigma_{ji} n_j = \hat{t}_i \quad (12.5.2)$$

For the electrical problem, an electro-quasi-static approximation is adopted (see Haus and Melcher [92]). This means the coupling with magnetic fields is disregarded, which is often a very good assumption for the frequencies of structural problems with piezoelectric patches (see Tiersten [86]). The electrical problem is governed by the following two differential equations (Haus and Melcher [92]):

$$\epsilon_{ijk} \frac{\partial E_i}{\partial x_j} = 0, \quad \frac{\partial D_i}{\partial x_i} - \rho_c = 0 \quad (12.5.3)$$

where E_i are the electric field components, D_i are the electric displacement components, ρ_c is the free electric charge per unit volume, and ϵ_{ijk} is the permutation symbol. The first equation in (12.5.3) implies that the electric field is irrotational; hence, it can be represented as the gradient of a scalar function φ , called the electric potential. With the introduction of the electric potential φ , the first equation in (12.5.3) is identically satisfied. Thus the governing equations for the electrical problem become

$$E_i + \frac{\partial \varphi}{\partial x_i} = 0, \quad \frac{\partial D_i}{\partial x_i} - \rho_c = 0 \quad (12.5.4)$$

The boundary condition of the electrical problem is of the form

$$\varphi^{(a)} - \varphi^{(b)} = 0 \quad \text{or} \quad n_i (D_i^{(a)} - D_i^{(b)}) = \omega_c \quad (12.5.5)$$

where ω_c is the electric free surface charge per unit area and n_i is the i th direction cosine of the unit normal vector $\hat{\mathbf{n}}$ to the surface separating mediums (a) and (b), directed from medium (b) to (a). The boundary condition for the electric displacement involves the knowledge of the electric displacement outside the domain of interest. In order to obtain a value for this, an electrical problem would have to be solved for the space outside the laminate. Usually, if the laminate is surrounded by air or vacuum and the electric field in the outside is small, it is a good assumption to consider that the electric displacement vanishes outside the laminate (see Bisegna and Maceri [93]). The material within each layer of the laminate is assumed to be homogeneous, generally anisotropic and linear elastic. The constitutive relations for a composite material layer in the global reference frame are

$$\sigma_{ij}^{(k)} = C_{ijmn}^{(k)} \varepsilon_{mn}^{(k)}, \quad D_i^{(k)} = \xi_{il}^{(k)} E_\ell^{(k)} \quad (12.5.6)$$

and for a piezoelectric material layer the constitutive equations are

$$\sigma_{ij}^{(k)} = C_{ijmn}^{(k)} \varepsilon_{mn}^{(k)} - e_{\ell ij}^{(k)} E_\ell^{(k)}, \quad D_i^{(k)} = \xi_{il}^{(k)} E_\ell^{(k)} + e_{i\ell m}^{(k)} \varepsilon_{\ell m}^{(k)} \quad (12.5.7)$$

where C_{ijmn} are the components of the fourth-order tensor of elastic moduli, $e_{\ell ij}$ are the components of the third-order tensor of piezoelectric moduli and ξ_{il} are the components of the tensor of dielectric moduli for the k th lamina. The displacements and electric potential must be continuous from point to point in the structure, and conservation of electric charge requires

$$D_z^{(k+1)} - D_z^{(k)} = \omega_c \quad (12.5.8)$$

We shall use the following layerwise expansions for the displacement field and electric potential [see Eq. (12.2.2)]

$$\begin{aligned} u(x, y, z) &= \sum_{I=1}^{N_\Phi} U^I(x, y) \Phi^I(z), & v(x, y, z) &= \sum_{I=1}^{N_\Phi} V^I(x, y) \Phi^I(z) \\ w(x, y, z) &= \sum_{I=1}^{N_\Psi} W^I(x, y) \Psi^I(z), & \varphi(x, y, z) &= \sum_{I=1}^{N_\Theta} \varphi^I(x, y) \Theta^I(z) \end{aligned} \quad (12.5.9)$$

where the numbers of functions N_Φ , N_Ψ and N_Θ considered depend on the number of layers and the degree of the assumed approximation along the thickness of each layer for the respective primary variables.

12.5.3 Finite Element Model

The finite element model presented here is similar to the one presented earlier, except that we have included the electro-mechanical coupling terms. We begin with the virtual work statement

$$0 = \int_{\Omega^e} \int_H \left(\sigma_{ij} \delta \varepsilon_{ij} - F_i \delta u_i + D_i \frac{\partial \varphi}{\partial x_i} + \rho_c \delta \varphi \right) dx dy dz \\ - \oint_{\Gamma^e} t_i \delta u_i d\Gamma^e - \oint_{\Gamma^e} (D_i n_i) \delta \varphi d\Gamma \quad (12.5.10)$$

where Ω^e denotes the midplane of a typical finite element and Γ^e denotes the boundary of the 3-D element. The stresses σ_{ij} , strains ε_{ij} and electric displacements D_i are all known in terms of the displacements (u, v, w) and electric potential φ through Eqs. (12.5.4)₁, (12.5.6), (12.5.7) and the strain-displacement relations

$$\varepsilon_{ij} = \frac{1}{2} \left(\frac{\partial u_i}{\partial x_j} + \frac{\partial u_j}{\partial x_i} \right)$$

Next, we use the following finite element approximation of $(U^I, V^I, W^I, \varphi^I)$ in the plane of the laminate [see Eq. (12.3.1)]:

$$U^I(x, y) = \sum_{K=1}^{N_{UV}^I} U_K^I a_K^I(x, y), \quad V^I(x, y) = \sum_{K=1}^{N_{UV}^I} V_K^I a_K^I(x, y) \\ W^I(x, y) = \sum_{K=1}^{N_W^I} W_K^I b_K^I(x, y), \quad \varphi^I(x, y) = \sum_{K=1}^{N_\varphi^I} \varphi_K^I c_K^I(x, y) \quad (12.5.11)$$

where $a_K^I(x, y)$, $b_K^I(x, y)$ and $c_K^I(x, y)$ are interpolation functions used for (U^I, V^I) , W^I and φ^I , respectively, and $(N_{UV}^I, N_W^I, N_\varphi^I)$ denote the associated number of degrees of freedom per element. Figure 12.5.1 illustrates a C^0 -continuous approximation of displacement component u through the thickness direction. The points (or nodes) used for the definition of the Lagrange polynomials are identified along the thickness. The number of such points is N_Φ and equals the number of layerwise approximation functions Φ^I . The function $\Phi^I(z)$, for example, corresponding to a point z_I laying at the interface connecting k th layer, where it is given by a quadratic Lagrange polynomial, and $(k+1)$ st layer, where a cubic Lagrange polynomial is considered. This function is nonzero inside layers k and $(k+1)$, and zero outside of these two layers.

Substituting the above approximation into the virtual work statement (12.5.10), we arrive at the following discrete equations for a typical element:

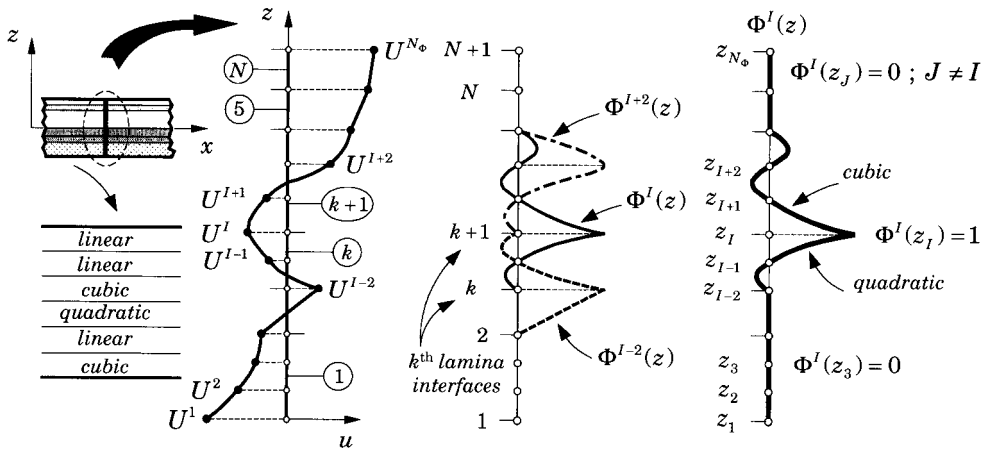


Figure 12.5.1: Examples of layerwise approximation functions Φ^I .

$$0 = \int_{\Omega^e} \int_H \left[\left(\sigma_{xx} \frac{\partial a_K^I}{\partial x} + \sigma_{yx} \frac{\partial a_K^I}{\partial y} - F_x a_K^I \right) \Phi^I + \sigma_{xz} a_K^I \frac{\partial \Phi^I}{\partial z} \right] dz dx dy \\ - \oint_{\Gamma^e} t_x a_K^I \Phi^I d\Gamma \quad (12.5.12)$$

$$0 = \int_{\Omega^e} \int_H \left[\left(\sigma_{xy} \frac{\partial a_K^I}{\partial x} + \sigma_{yy} \frac{\partial a_K^I}{\partial y} - F_y a_K^I \right) \Phi^I + \sigma_{yz} a_K^I \frac{\partial \Phi^I}{\partial z} \right] dz dx dy \\ - \oint_{\Gamma^e} t_y a_K^I \Phi^I d\Gamma \quad (12.5.13)$$

$$0 = \int_{\Omega^e} \int_H \left[\left(\sigma_{xz} \frac{\partial b_K^I}{\partial x} + \sigma_{yz} \frac{\partial b_K^I}{\partial y} - F_z b_K^I \right) \Psi^I + \sigma_{zz} b_K^I \frac{\partial \Psi^I}{\partial z} \right] dz dx dy \\ - \oint_{\Gamma^e} t_z b_K^I \Psi^I d\Gamma \quad (12.5.15)$$

$$0 = \int_{\Omega^e} \int_H \left[\left(D_x \frac{\partial c_K^I}{\partial x} + D_y \frac{\partial c_K^I}{\partial y} - \rho_c c_K^I \right) \Theta^I + \sigma_{xz} a_K^I \frac{\partial \Phi^I}{\partial x} \right] dz dx dy \\ - \oint_{\Gamma^e} (D_x n_x + D_y n_y) c_K^I \Theta^I d\Gamma \quad (12.5.15)$$

These equations can be cast into the standard form

$$[K]\{\Delta\} = \{F\} \quad (12.5.16)$$

12.5.4 An Example

Numerical results of one example problem are presented here [91]. In reasons of brevity limited results are included here, and for additional results and examples, the reader may consult the recent paper by Semedo Garcão et al. [91]. The laminate consists of a square, cross-ply, simply supported plate, with piezoelectric laminae. The exact solution was included in [91], following a development similar to the ones presented in [93,94].

Both Lagrange and conforming Hermite interpolations (continuity of the first and mixed derivatives) associated with rectangular elements are used to interpolate $(U^I, V^I, W^I, \varphi^I)$; see Reddy [53]. The stiffness matrix and load vectors are evaluated using full integration. No numerical tricks such as selective reduced integration that proved efficient in previous works are considered here. Various interpolation schemes used for the in-plane discretizations, and through-thickness approximation of a lamina are presented in Table 12.5.1. The column entitled “Plane” indicates the in-plane interpolation considered. This interpolation is made with Lagrange elements with 9 (quadratic), 16 (cubic) or 25 (quartic) nodes, or with Hermite elements with 4 degrees of freedom per node (function and its derivatives, f, f_x, f_y, f_{xy}). The column entitled “Thick” indicates the degree of Lagrange polynomials used in the thickness of each lamina or sublayer. The last two columns indicate, respectively, the number of nodes and degrees of freedom associated with the layerwise interpolation scheme for a typical lamina or sublayer. The layerwise interpolation scheme I10 considers a Lagrange element with 16 nodes and with a thickness approximation of degree 4 for (u, v) ; a Hermite element with a thickness approximation of degree 3 for w ; and a 16 node element with a degree 3 thickness approximation for φ . In the case of scheme I13, a 16-node element and cubic thickness approximation is considered for all the variables. This has the same characteristics as a cubic solid Lagrange element with 64 nodes.

The mechanical and electrical properties of the materials considered are presented in Table 12.5.2. The piezoelectric material is the PVDF and its properties are taken from [94]. In this table, the contracted notation is used for the definition of the constitutive law. The values presented refer to the material properties in the principal material coordinates.

The values used for various geometric parameters are: thickness $H = 10$ mm, and planar dimensions $a = b = 0.04$ m. The lamination scheme is (0/90/0) with equal thickness ($H/3$) layers. The domain modeled is $0 \leq x \leq a$, $0 \leq y \leq b$ and $-h/2 \leq z \leq h/2$. The geometric boundary conditions used are

$$\begin{aligned} u(x, 0, z) &= u(x, b, z) = 0; & v(0, y, z) &= v(a, y, z) = 0 \\ w(0, y, z) &= w(a, y, z) = w(x, 0, z) = w(x, b, z) = 0 \end{aligned} \quad (12.5.17)$$

Either mechanical loading or electrical input are used. When mechanical load is used, φ is set to zero on the entire boundary of the laminate. The mechanical load is taken to be

$$t_z(x, y) = 3 \times 10^5 \sin \frac{\pi x}{a} \sin \frac{\pi y}{b} \quad (12.5.18)$$

at $z = h/2$ and used stress-free boundary conditions on all other faces where displacements are not specified. When applied electric potential is used, we take

$$\begin{aligned}\varphi(0, y, z) &= \varphi(a, y, z) = \varphi(x, 0, z) = \varphi(x, b, z) = 0 \\ \varphi(x, y, -\frac{h}{2}) &= 0, \quad \varphi(x, y, \frac{h}{2}) = 200 \sin \frac{\pi x}{a} \sin \frac{\pi y}{b}\end{aligned}\quad (12.5.19)$$

The finite element discretizations used for the solution of this problem are shown in Table 12.5.3. In the column entitled “Plane” contains the in-plane discretization, number of subdivisions in the x direction times the number of subdivisions in the y direction, and the consideration of symmetry requires consideration of just one quarter of the plate. The column entitled “Thick” indicates the number of subdivisions considered in the thickness of each lamina. The number of nodes and degrees of freedom indicates the size of the problem. The discretization M4t2I9 consists of a mesh in which 4 elements are used in the x direction (4s if structural symmetry is used), with 2 subdivisions in the thickness of each lamina, considering the I9 interpolation scheme. Discretization M2t1I5 uses 2 subdivisions in the x and y directions for the complete plate, with each thickness subdivision coincident with a lamina, considering the I5 interpolation scheme.

Results are presented in Table 12.5.4–12.5.6 and Figures 12.5.2–12.5.5. The results obtained by Lage et al. [95] using a mixed layerwise finite element models are included for comparison. In the mixed model [95], displacements (u, v, w) , electric potential φ , stresses $(\sigma_{zx}, \sigma_{zy}, \sigma_{zz})$ and electric displacement D_z are used as the dependent unknowns. Here we consider for comparison the results obtained with five meshes [95], which discretize the complete plate. Bi-quadratic (eight-node) serendipity elements in the (x, y) plane and quadratic approximation in the thickness with 2 subdivisions per ply (6760 DoF) was used.

Table 12.5.4 contains values of the displacement variables at specific points, where z indicates the position in the thickness direction. All the values have errors less than 5.3% and, in general, the results are good for all the primary variables. Results for electric potential are better than for displacements. The following additional observations can be made from the numerical results presented in the tables and figures (see [91] for additional details):

- Comparing meshes M4st2I1, M4st2I2 and M4st2I3, which have only different thickness approximations, it is observed that the cubic approximation gives better results, although the quadratic approximation also yields very good results; but the linear approximation is poor.
- Meshes M4st2I6, M4st2I7 and M4st2I9 show that cubic thickness approximation is, in this case, more accurate than the 5th degree and quadratic approximations.
- Meshes M4st2I2 and M4st2I3 use 9-node elements while M4st2I6 and M4st2I7 use Hermite elements in the plane. The results for meshes M4st2I2 and M4st2I6 are very similar but M4st2I2 is slightly better. M4st2I7 is slightly more accurate than M4st2I3 for all except w .
- The in-plane interpolation and discretization influences the results, but since the plate is thick, the differences in the results are small.
- Results obtained with the mixed models [95] are all very similar but a quadratic approximation in the thickness gives better results. Comparing LL1 with M4st2I1, the accuracy in terms of displacements is the same.

Table 12.5.1: Finite element interpolation schemes for each lamina.

Interpolation Schemes	u		v		w		ϕ		Number of Nodes	Number of DoFs
	Surf.	Thick.	Surf.	Thick.	Surf.	Thick.	Surf.	Thick.		
I1	L9	1	L9	1	L9	1	L9	1	18	72
I2	L9	2	L9	2	L9	2	L9	2	27	108
I3	L9	3	L9	3	L9	3	L9	3	36	144
I4	L9	4	L9	4	L9	3	L9	3	63	162
I5	L9	4	L9	4	L9	4	L9	4	45	180
I6	H4-4	2	H4-4	2	H4-4	2	H4-4	2	12	192
I7	H4-4	3	H4-4	3	H4-4	3	H4-4	3	16	256
I8	H4-4	4	H4-4	4	H4-4	4	H4-4	4	20	320
I9	H4-4	5	H4-4	5	H4-4	5	H4-4	5	24	384
I10	L16	4	L16	4	H4-4	3	L16	3	112	288
I11	L9	3	L9	3	L25	2	L9	3	93	183
I12	L9	3	L9	3	L25	3	L9	3	100	208
I13	L16	3	L16	3	L16	3	L16	3	64	256

Li : Lagrange interpolation using i nodes.Hi-j : Hermite interpolation using i nodes and j degrees of freedom per node.

Surf. : Surface directions interpolation.

Thick. : Thickness approximation polynomial degree.

DoFs : Degrees of Freedom.

Table 12.5.2: Material properties in the material coordinates.

Material	C ₁₁ [GPa]	C ₂₂ [GPa]	C ₃₃ [GPa]	C ₁₂ [GPa]	C ₁₃ [GPa]	C ₂₃ [GPa]	C ₄₄ [GPa]	C ₅₅ [GPa]	C ₆₆ [GPa]
1	320.00	10.6	5.60	1.50	0.95	1.20	1.15	2.40	16.30
2	238.00	23.6	10.6	3.98	2.19	1.92	2.15	4.40	6.43
3	173.53	7.39	7.39	2.31	2.31	1.87	1.38	3.45	3.45
Material	e ₁₅ [C/m ²]	e ₂₄ [C/m ²]	e ₃₁ [C/m ²]	e ₃₂ [C/m ²]	e ₃₃ [C/m ²]	ξ_{11} [pF/m]	ξ_{22} [pF/m]	ξ_{33} [pF/m]	
1	0.0	0.0	0.0	0.0	0.0	30.65	26.55	26.55	
2	-0.01	-0.01	-0.13	-0.14	-0.28	110.68	106.07	106.07	
3	0.0	0.0	0.0	0.0	0.0	22.55	22.55	16.00	

Table 12.5.3: Finite element discretizations.

Discretization	Subdivisions per Ply		Number of Nodes	Problem DoFs
	Surf.	Thick.		
App. Load				
M4st2I1	4x4-S	2	567	1664
M2t1I2	2x2	1	175	318
M4st2I2	4x4-S	2	1053	3200
M4st2I3	4x4-S	2	1539	4736
M2t1I5	2x2	1	325	606
M4st2I6	4x4-S	2	395	3032
M4st2I7	4x4-S	2	475	4484
M1st1I8	1x1-S	1	52	176
M1st1I9	1x1-S	1	64	218
M4st2I9	4x4-S	2	775	7388
App. Potential				
M4st1I4	4x4-S	1	1539	2816

S: indicates that structural symmetry is accounted for, only one quarter of the plate is solved.

Table 12.5.4: Displacement components u , v , w and electric potential ϕ .

	u		v		w		ϕ	
	(0, b/2, z)	Error [%]	(a/2, 0, z)	Error [%]	(a/2, b/2, z)	Error [%]	(a/2, b/2, z)	Error [%]
App. Load Units	$z = 5.0 \text{ mm}$ [nm]		$z = 5.0 \text{ mm}$ [nm]		$z = 5.0 \text{ mm}$ [μm]		$z = 0.0 \text{ mm}$ [V]	
Exact Sol.	-171.8735		343.2618		1.5285		127.9787	
M4st2I1	-162.8555	5.247	334.5762	2.530	1.5034	1.645	126.1271	1.447
M2t1I2	-172.6304	-0.440	349.8217	-1.911	1.5232	0.351	130.5900	-2.040
M4st2I2	-171.6852	0.110	343.1651	0.028	1.5277	0.055	127.9461	0.025
M4st2I3	-171.9435	-0.041	343.4970	-0.069	1.5285	0.003	128.0024	-0.019
M2t1I5	-177.4721	-3.257	354.4165	-3.250	1.5330	-0.292	131.1849	-2.505
M4st2I6	-171.6530	0.128	342.9547	0.089	1.5275	0.067	127.9132	0.051
M4st2I7	-171.9032	-0.017	343.2639	-0.001	1.5283	0.014	127.9697	0.007
M1st1I8	-170.3784	0.870	331.5940	3.399	1.4970	2.063	127.9929	-0.011
M1st1I9	-170.4093	0.852	331.5952	3.399	1.4970	2.062	127.9933	-0.011
M4st2I9	-171.9291	-0.032	343.2786	-0.005	1.5283	0.014	127.9700	0.007
Ref. [28]	-172.5	-0.35	—	-	1.552	-1.54	128.1	-0.09
App. Poten. Units	$z = 5.0 \text{ mm}$ [pm]		$z = 5.0 \text{ mm}$ [pm]		$z = 5.0 \text{ mm}$ [nm]		$z = 0.0 \text{ mm}$ [V]	
Exact Sol.	-322.2624		-775.2442		3.3131		86.8948	
M4st1I4	-322.3629	-0.031	-775.6559	-0.053	3.3129	0.004	86.8953	-0.001
LQ [95]	-320.8	0.46	-771.9	0.43	3.316	-0.09	—	—

 $\mu\text{m} = 10^{-6} \text{ m}; \text{nm} = 10^{-9} \text{ m}; \text{pm} = 10^{-12} \text{ m}.$

$$\text{Error}[\%] = \frac{(\text{Exact} - \text{Numeric})}{\text{Exact}} \times 100.$$

Table 12.5.5: Stress components σ_{xx} , σ_{zz} , σ_{zy} and σ_{xy} .

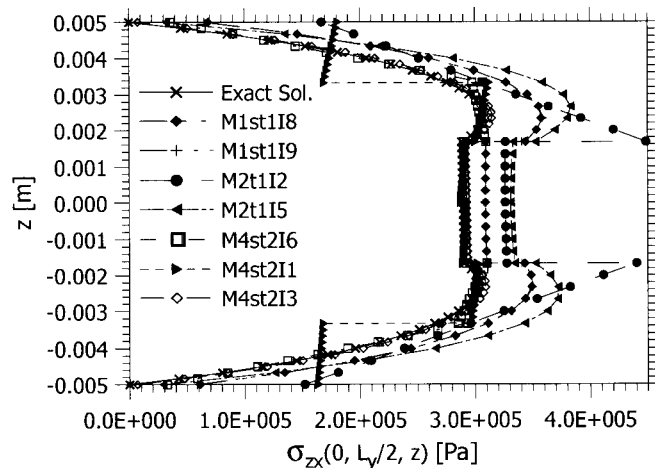
	σ_{xx}		σ_{zz}		σ_{zy}		σ_{xy}	
	(a/2, b/2, z)	Error [%]	(a/2, b/2, z)	Error [%]	(a/2, 0, z)	Error [%]	(0, 0, z)	Error [%]
App. Load Units	$z = 5.0 \text{ mm}$ [MPa]		$z = 5.0 \text{ mm}$ [KPa]		$z = 0.0 \text{ mm}$ [KPa]		$z = -5.0 \text{ mm}$ [KPa]	
Exact Sol.	3.3714		300.0000		261.4302		256.0911	
M4st2I1	3.2398	3.902	308.5588	-2.853	228.2469	12.693	250.6412	2.128
M2t1I2	3.6678	-8.793	334.8719	-11.624	296.6836	-13.485	301.9324	-17.900
M4st2I2	3.4078	-1.081	306.7711	-2.257	288.2271	-10.250	259.2187	-1.221
M4st2I3	3.4097	-1.136	300.8379	-0.279	266.7481	-2.034	259.5132	-1.336
M2t1I5	3.6779	-9.091	322.6479	-7.549	340.6215	-30.292	307.6620	-20.138
M4st2I6	3.3994	-0.831	307.1000	-2.367	285.9422	-9.376	255.1144	0.381
M4st2I7	3.4032	-0.943	301.2016	-0.401	264.4981	-1.174	255.3850	0.276
M1st1I8	3.9890	-18.318	310.2845	-3.428	302.6049	-15.750	231.6142	9.558
M1st1I9	3.9913	-18.389	309.9735	-3.324	302.0710	-15.546	231.6143	9.558
M4st2I9	3.4036	-0.955	300.5023	-0.167	265.2955	-1.479	255.3939	0.272
Ref. [28]	3.559	-5.56	301.3	-0.43	273.1	-4.47	—	—
App. Poten. Units	$z = 5.0 \text{ mm}$ [KPa]		$z = 0.0 \text{ mm}$ [Pa]		$z = 1.67 \text{ mm}$ [Pa]		$z = 5.0 \text{ mm}$ [Pa]	
Exact Sol.	4.2638		-36.2925		-232.8282		-554.2529	
M4st1I4	4.3388	-1.759	-35.3944	2.474	-228.0751	2.041	-561.5975	-1.325
LQ [95]	4.073	4.48	-37.21	-2.53	-228.0	2.09	-537.7	2.98

 $\text{KPa} = 10^3 \text{ Pa}; \text{MPa} = 10^6 \text{ Pa}.$

Table 12.5.6: Stress component σ_{zx} and electric displacement components D_x and D_z .

	σ_{zx}		σ_{zx}		D_x		D_z	
	(0, $L_y/2$, z)	Error [%]	(0, $L_y/2$, z)	Error [%]	(0, $L_y/2$, z)	Error [%]	($L_x/2$, $L_y/2$, z)	Error [%]
App. Load Units	z = 0.0 mm [kPa]		z = 2.33 mm [kPa]		z = 0.0 mm [μC/m ²]		z = 5.0 mm [μC/m ²]	
Exact Sol.	289.6226		308.0846		-2.4137		-4.9696	
M4st2I1	292.5942	-1.026	305.2003	0.936	-2.4255	-0.489	-6.4297	-29.380
M2t1I2	326.2845	-12.659	392.0923	-27.268	-2.7553	-14.152	-6.1003	-22.752
M4st2I2	292.6253	-1.037	306.8741	0.393	-2.4410	-1.130	-5.2021	-4.679
M4st2I3	292.7234	-1.071	314.6006	-2.115	-2.4419	-1.168	-5.0278	-1.172
M2t1I5	331.1318	-14.332	380.2878	-23.437	-2.7886	-15.534	-5.7064	-14.825
M4st2I6	291.4412	-0.628	304.7103	1.095	-2.4360	-0.923	-5.2043	-4.723
M4st2I7	291.5314	-0.659	312.4126	-1.405	-2.4369	-0.961	-5.0309	-1.234
M1st1I8	309.0909	-6.722	357.7194	-16.111	-2.6178	-8.454	-5.8943	-18.607
M1st1I9	309.1057	-6.727	358.7619	-16.450	-2.6178	-8.456	-5.8870	-18.461
M4st2I9	291.5245	-0.657	312.3642	-1.389	-2.4369	-0.959	-5.0137	-0.887
Ref. [95]	—	—	310.1	-0.64	-2.537	-5.10	-5.114	-2.90
App. Potential Units	z = -3.0 mm [Pa]		z = 3.0 mm [Pa]		z = 5.0 mm [μC/m ²]		z = 5.0 mm [μC/m ²]	
Exact Sol.	-218.5833		292.4657		-1.7389		-3.1003	
M4st1I4	-223.8003	-2.387	300.4777	-2.739	-1.7610	-1.267	-3.0994	0.027
Ref. [95]	—	—	292.5	0.00	-1.695	2.55	-3.107	-0.23

$\mu\text{C}/\text{m}^2 = 10^{-6} \text{ C}/\text{m}^2$.

**Figure 12.5.2:** Shear stress σ_{xz} across the thickness (Applied Load).

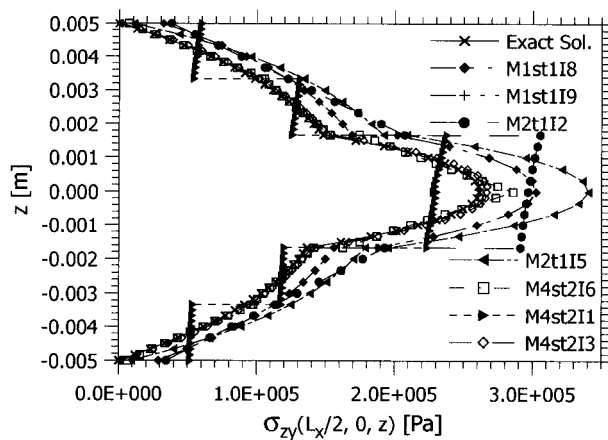


Figure 12.5.3: Shear stress σ_{yz} across the thickness (Applied Load).

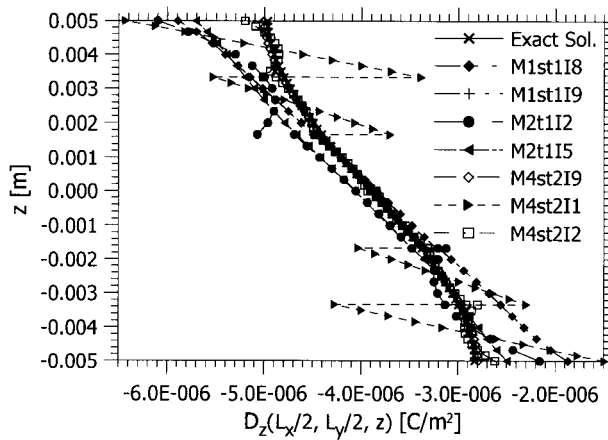


Figure 12.5.4: The electric displacement D_z across the thickness (Applied Load).

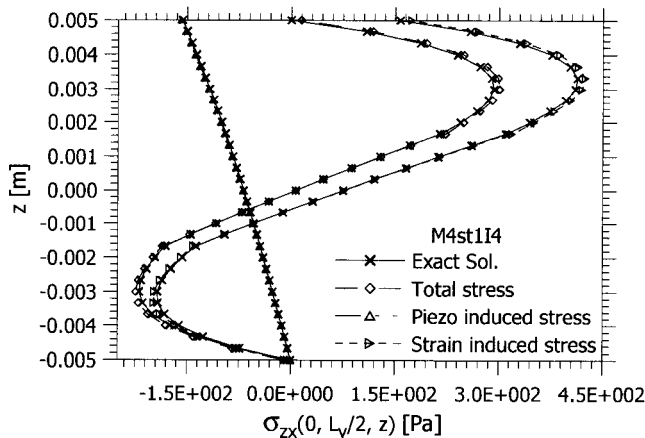


Figure 12.5.5: Shear stress σ_{xz} across the thickness (Applied Potential).

- Comparing models M2t1I2 and SQ1 it is found that M2t1I2 provides more accurate results for the displacements and electric potential, with similar computational effort.
- The mixed model (most accurate of those used in [95]) is not superior to the displacement models in the prediction of displacements and electric potential.
- The results obtained with M4st1I4 for the applied potential case are good and better than the ones provided by the mixed model.
- The accuracy of in-plane stresses (σ_{xx}, σ_{xy}) and electric displacement D_x component is more influenced by the in-plane discretization than by the thickness approximation. Although not shown, the same is true for (σ_{yy}, D_y).
- The accuracy of ($\sigma_{xz}, \sigma_{yz}, \sigma_{zz}, D_z$) is equally influenced by the in-plane and thickness approximations.
- Figures 12.5.4–12.5.6 show the stress and electric displacement distributions through thickness obtained with meshes M4st2I1, M2t1I2 and M4st2I6, for which only linear and quadratic polynomial approximation are assumed through the thickness. They show that the exact distribution is not captured, even if the in-plane discretization is very good. For meshes M4st2I1, M4st2I2 and M4st2I6, the in-plane discretization is sufficient and the distributions agree with the exact. Note that mesh M4st2I1 provides highly irregular and discontinuous distributions. Meshes M4st2I2 and M4st2I6 approximate the exact solution better for σ_{yz} (Figure 12.5.5); however, the correct solution for D_z is not captured (see Figure 12.5.6).
- Results for meshes M4st2I1, M4st2I2 and M4st2I3 show that interpolation I3 with cubic approximation through thickness is the most equilibrated, giving good results for all the secondary variables. Some values obtained with M4st2I1 and M4st2I2 are slightly better than the ones for M4st2I3, but Figures 12.5.4–12.5.6 show the differences.
- The results for meshes M4st2I2 and M4st2I6 indicate that the 9-node and Hermite elements provide similar results; M4st2I6 produces slightly better results with a little less number of degrees of freedom. Also, between M4st2I3 and M4st2I7 the Hermite interpolation behaves a little better with less number of degrees of freedom. The Hermite interpolation provides better estimate of σ_{xy} .
- Figures 12.5.4–12.5.6 indicate that interpolations I5 and I8, with 4th degree approximation through thickness, predict the correct form of the exact solution. Hence, the lack of accuracy verified with meshes M2t1I5 and M1st1I8 is due to the coarse in-plane discretization.
- In Table 12.5.5, one of the columns shows the approximation of the boundary condition at the top surface of the laminate for σ_{zz} . A good in-plane discretization and cubic or higher approximation produces good results.
- For the case of applied potential, the distribution of stresses is self-equilibrated since there are no applied external stresses. One may note the good agreement for the strain and piezoelectric induced stress contributions. The tables indicate that the displacement model with interpolation I4, using fourth degree approximation for (u, v) and cubic approximation for (w, φ) provides good results.

12.6 Layerwise Theory of Cylindrical Shells

12.6.1 Introduction

In this section an extension of the layerwise theory developed in the previous sections for laminated plates to laminated circular cylindrical shells without and with equally-spaced axial and circumferential stiffeners (see [96–110] and references therein) is presented with special emphasis on general buckling and postbuckling analysis. We use the “smeared stiffener” approach of Hutchinson and Amazio [98] (also see [99–104]). This approach is very effective when the stiffeners have identical cross section and their spacing is small compared to the buckling wave length (i.e., no skin wrinkling before global buckling). The contribution of the stiffeners is brought into the governing equations through energy considerations. The material included here comes largely from the author’s publications [105–109].

12.6.2 Unstiffened Shells

Displacements and Strains

The displacement field (u_1, u_2, u_3) in the shell is expressed as

$$\begin{aligned} u_1(x, y, z) &= \sum_{j=1}^{N+1} u_j(x, y)\phi^j(z) = u_j\phi^j \\ u_2(x, y, z) &= \sum_{j=1}^{N+1} v_j(x, y)\phi^j(z) = v_j\phi^j \\ u_3(x, y, z) &= \sum_{j=1}^{N+1} w_j(x, y)\phi^j(z) = w_j\phi^j \end{aligned} \quad (12.6.1)$$

where N is the total number of mathematical layers ($N + 1$ interfaces), (u_j, v_j, w_j) are the values of the displacements (u_1, u_2, u_3) at the j th interface, and $\phi^j(z)$ are global approximation functions with local support. In Eq. (12.6.1) summation on repeated subscripts and superscripts is used.

The strains, accounting for the von Kármán nonlinear terms in the strain-displacement relations, are given by (sum on repeated indices is implied)

$$\begin{aligned} \varepsilon_1 &= \frac{\partial u}{\partial x} + \frac{1}{2} \left(\frac{\partial w}{\partial x} \right)^2 = \frac{\partial u_i}{\partial x} \phi^i + \frac{1}{2} \left(\frac{\partial w_i}{\partial x} \phi^i \right) \left(\frac{\partial w_j}{\partial x} \phi^j \right) \\ \varepsilon_2 &= \frac{\partial v}{\partial y} + \frac{w}{R} + \frac{1}{2} \left(\frac{\partial w}{\partial y} \right)^2 = \left(\frac{\partial v_i}{\partial y} + \frac{w_i}{R} \right) \phi^i + \frac{1}{2} \left(\frac{\partial w_i}{\partial y} \phi^i \right) \left(\frac{\partial w_j}{\partial y} \phi^j \right) \\ \varepsilon_3 &= \frac{\partial w}{\partial z} = w_i \frac{d\phi^i}{dz} \\ \varepsilon_4 &= \frac{\partial v}{\partial z} + \frac{\partial w}{\partial y} - \frac{v}{R} = v_i \frac{d\phi^i}{dz} + \left(\frac{\partial w_i}{\partial y} - \frac{v_i}{R} \right) \phi^i \\ \varepsilon_5 &= \frac{\partial u}{\partial z} + \frac{\partial w}{\partial x} = u_i \frac{d\phi^i}{dz} + \frac{\partial w_i}{\partial x} \phi^i \\ \varepsilon_6 &= \frac{\partial u}{\partial y} + \frac{\partial v}{\partial x} + \frac{\partial w}{\partial x} \frac{\partial w}{\partial y} = \left(\frac{\partial u_i}{\partial y} + \frac{\partial v_i}{\partial x} \right) \phi^i + \left(\frac{\partial w_i}{\partial y} \phi^i \right) \left(\frac{\partial w_j}{\partial x} \phi^j \right) \end{aligned} \quad (12.6.2)$$

Equations of Equilibrium at Buckling

The equations of equilibrium at buckling are derived using the principle of virtual displacements (or the principle of minimum total potential energy). We have

$$0 = \delta\Pi = \delta U + \delta V \quad (12.6.3)$$

where δU is the virtual strain energy and δV is the virtual work done by the pre-buckling stresses

$$\delta U = \int_{\Omega} \int_{-\frac{h}{2}}^{\frac{h}{2}} \sigma_i \delta \varepsilon_i \, dz dA \quad (\text{sum on } i) \quad (12.6.4a)$$

$$\begin{aligned} \delta V &= \int_{\Omega} \int_{-\frac{h}{2}}^{\frac{h}{2}} \hat{\sigma}_i \delta \varepsilon_i \, dz dA \quad (\text{sum on } i) \\ &= \int_{\Omega} \left[\hat{M}_1^{ij} \frac{\partial w_i}{\partial x} \frac{\partial \delta w_j}{\partial x} + \hat{M}_6^{ij} \left(\frac{\partial w_i}{\partial x} \frac{\partial \delta w_j}{\partial x} + \frac{\partial w_i}{\partial y} \frac{\partial \delta w_j}{\partial x} \right) \right. \\ &\quad \left. + \hat{M}_2^{ij} \frac{\partial w_i}{\partial y} \frac{\partial \delta w_j}{\partial y} - p \delta W_I \right] dA \end{aligned} \quad (12.6.4b)$$

Here p denotes the pressure, and $I = 1$, when pressure is internal and $I = N + 1$ for external pressure, and quantities with a hat are specified. Substituting for δU and δV into the total potential energy principle (12.6.3), we obtain the governing equations of buckling are

$$\begin{aligned} \delta u_i : \quad &\frac{\partial M_1^i}{\partial x} + \frac{\partial M_6^i}{\partial y} - Q_1^i = 0 \\ \delta v_i : \quad &\frac{\partial M_6^i}{\partial x} + \frac{\partial M_2^i}{\partial y} - Q_2^i + \frac{1}{R} K_2^i = 0 \\ \delta w_i : \quad &\frac{\partial K_1^i}{\partial x} + \frac{\partial K_2^i}{\partial y} - \left(\frac{1}{R} M_2^i + Q_3^i \right) + \frac{\partial}{\partial x} \left(\hat{M}_1^{ij} \frac{\partial w_j}{\partial x} + \hat{M}_6^{ij} \frac{\partial w_j}{\partial y} \right) \\ &+ \frac{\partial}{\partial y} \left(\hat{M}_6^{ij} \frac{\partial w_j}{\partial x} + \hat{M}_2^{ij} \frac{\partial w_j}{\partial y} \right) + p \delta_{ii} = 0 \end{aligned} \quad (12.6.5)$$

where δ_{ij} denotes the Kronecker delta symbol and

$$M_{\alpha}^i = \int_{-\frac{h}{2}}^{\frac{h}{2}} \sigma_{\alpha} \phi^i \, dz, \quad M_{\alpha}^{ij} = \int_{-\frac{h}{2}}^{\frac{h}{2}} \sigma_{\alpha} \phi^i \phi^j \, dz \quad (\alpha = 1, 2, 6) \quad (12.6.6a)$$

$$\begin{Bmatrix} Q_1^i \\ Q_2^i \\ Q_3^i \end{Bmatrix} = \int_{-\frac{h}{2}}^{\frac{h}{2}} \begin{Bmatrix} \sigma_5 \\ \sigma_4 \\ \sigma_3 \end{Bmatrix} \frac{d\phi^i}{dz} \, dz, \quad \begin{Bmatrix} K_1^i \\ K_2^i \end{Bmatrix} = \int_{-\frac{h}{2}}^{\frac{h}{2}} \begin{Bmatrix} \sigma_5 \\ \sigma_4 \end{Bmatrix} \phi^i \, dz \quad (12.6.6b)$$

and \hat{M}_{α}^{ij} are the resultants due to specified stresses $\hat{\sigma}_{\alpha}$.

Constitutive Equations

The laminated cylindrical shell is assumed to be made up of orthotropic layers with the principal material coordinates of each layer oriented arbitrarily with respect to

the shell axis. The layer constitutive equations referred to the shell coordinates are given by

$$\begin{Bmatrix} \sigma_1 \\ \sigma_2 \\ \sigma_3 \\ \sigma_4 \\ \sigma_5 \\ \sigma_6 \end{Bmatrix} = \begin{bmatrix} c_{11} & c_{12} & c_{13} & c_{16} \\ c_{12} & c_{22} & c_{23} & c_{26} \\ c_{13} & c_{23} & c_{33} & c_{36} \\ c_{16} & c_{26} & c_{36} & c_{66} \end{bmatrix} \begin{Bmatrix} \varepsilon_1 \\ \varepsilon_2 \\ \varepsilon_3 \\ \varepsilon_4 \\ \varepsilon_5 \\ \varepsilon_6 \end{Bmatrix}, \quad \begin{Bmatrix} \sigma_4 \\ \sigma_5 \end{Bmatrix} = \begin{bmatrix} c_{44} & c_{45} \\ c_{45} & c_{55} \end{bmatrix} \begin{Bmatrix} \varepsilon_4 \\ \varepsilon_5 \end{Bmatrix} \quad (12.6.7)$$

For specially orthotropic cylinders with material principal axes coinciding with the coordinates of the cylinder, we have $c_{16} = c_{26} = c_{36} = c_{45} = 0$. Using the layer constitutive equations (12.6.7), the resultants in Eq. (12.6.6) can be expressed in terms of the strains. We have,

$$\begin{aligned} M_1^i &= \int_{-\frac{h}{2}}^{\frac{h}{2}} \sigma_1 \phi^i dz = \int_{-\frac{h}{2}}^{\frac{h}{2}} (c_{1j} \varepsilon_j) \phi^i dz, \quad (j = 1, 2, 3, 6) \\ &= D_{11}^{ij} \frac{\partial u_j}{\partial x} + D_{12}^{ij} \left(\frac{\partial v_j}{\partial y} + \frac{w_j}{R} \right) + \bar{D}_{13}^{ij} w_j + D_{16}^{ij} \left(\frac{\partial u_j}{\partial y} + \frac{\partial v_j}{\partial x} \right) \\ &\quad + \frac{1}{2} D_{11}^{ijk} \frac{\partial w_j}{\partial x} \frac{\partial w_k}{\partial x} + D_{16}^{ijk} \frac{\partial w_j}{\partial x} \frac{\partial w_k}{\partial y} + \frac{1}{2} D_{12}^{ijk} \frac{\partial w_j}{\partial y} \frac{\partial w_k}{\partial y} \\ M_2^i &= D_{12}^{ij} \frac{\partial u_j}{\partial x} + D_{22}^{ij} \left(\frac{\partial v_j}{\partial y} + \frac{w_j}{R} \right) + \bar{D}_{23}^{ij} w_j + D_{26}^{ij} \left(\frac{\partial u_j}{\partial y} + \frac{\partial v_j}{\partial x} \right) \\ &\quad + \frac{1}{2} D_{12}^{ijk} \frac{\partial w_j}{\partial x} \frac{\partial w_k}{\partial x} + D_{26}^{ijk} \frac{\partial w_j}{\partial x} \frac{\partial w_k}{\partial y} + \frac{1}{2} D_{22}^{ijk} \frac{\partial w_j}{\partial y} \frac{\partial w_k}{\partial y} \\ M_3^i &= D_{16}^{ij} \frac{\partial u_j}{\partial x} + D_{26}^{ij} \left(\frac{\partial v_j}{\partial y} + \frac{w_j}{R} \right) + \bar{D}_{36}^{ij} w_j + D_{66}^{ij} \left(\frac{\partial u_j}{\partial y} + \frac{\partial v_j}{\partial x} \right) \\ &\quad + \frac{1}{2} D_{16}^{ijk} \frac{\partial w_j}{\partial x} \frac{\partial w_k}{\partial x} + D_{66}^{ijk} \frac{\partial w_j}{\partial x} \frac{\partial w_k}{\partial y} + \frac{1}{2} D_{26}^{ijk} \frac{\partial w_j}{\partial y} \frac{\partial w_k}{\partial y} \end{aligned} \quad (12.6.8)$$

$$\begin{aligned} Q_1^i &= \int_{-\frac{h}{2}}^{\frac{h}{2}} \sigma_5 \frac{d\phi^i}{dz} dz = \int_{-\frac{h}{2}}^{\frac{h}{2}} (c_{55} \varepsilon_5 + c_{45} \varepsilon_4) \frac{d\phi^i}{dz} dz \\ &= \bar{D}_{55}^{ij} u_j + \bar{D}_{55}^{ij} \frac{\partial w_j}{\partial x} + \bar{D}_{45}^{ij} v_j + \bar{D}_{45}^{ji} \left(\frac{\partial w_j}{\partial y} - \frac{v_j}{R} \right) \\ Q_2^i &= \bar{D}_{45}^{ij} u_j + \bar{D}_{45}^{ji} \frac{\partial w_j}{\partial x} + \bar{D}_{44}^{ji} \left(\frac{\partial w_j}{\partial y} - \frac{v_j}{R} \right) \\ Q_3^i &= \int_{-\frac{h}{2}}^{\frac{h}{2}} \sigma_3 \frac{d\phi^i}{dz} dz = \int_{-\frac{h}{2}}^{\frac{h}{2}} \sigma_{3j} \varepsilon_j \frac{d\phi^i}{dz} dz \\ &= \left[\bar{D}_{13}^{ji} \frac{\partial u_j}{\partial x} + \bar{D}_{23} \left(\frac{\partial v_j}{\partial y} + \frac{v_j}{R} \right) + \bar{D}_{63}^{ji} \left(\frac{\partial u_j}{\partial y} + \frac{\partial v_j}{\partial x} \right) + \bar{D}_{33}^{ij} w_j \right. \\ &\quad \left. + \frac{1}{2} \bar{D}_{13}^{jki} \frac{\partial w_j}{\partial x} \frac{\partial w_k}{\partial x} + \bar{D}_{36}^{jki} \frac{\partial w_j}{\partial x} \frac{\partial w_k}{\partial y} + \frac{1}{2} \bar{D}_{23}^{jki} \frac{\partial w_j}{\partial y} \frac{\partial w_k}{\partial y} \right] \end{aligned} \quad (12.6.9)$$

$$\begin{aligned} K_1^i &= \int_{-\frac{h}{2}}^{\frac{h}{2}} \sigma_5 \phi^i dz = \int_{-\frac{h}{2}}^{\frac{h}{2}} (c_{55} \varepsilon_5 + c_{45} \varepsilon_4) \phi^i dz \\ &= \bar{D}_{55}^{ij} u_j + D_{55}^{ij} \frac{\partial w_j}{\partial x} + \bar{D}_{45}^{ij} v_j + D_{45}^{ji} \left(\frac{\partial w_j}{\partial y} - \frac{v_j}{R} \right) \end{aligned}$$

$$\begin{aligned} K_2^i &= \int_{-\frac{h}{2}}^{\frac{h}{2}} \sigma_4 \phi^i dz = \int_{-\frac{h}{2}}^{\frac{h}{2}} (c_{45}\varepsilon_5 + c_{44}\varepsilon_4) \phi^i dz \\ &= \bar{D}_{45}^{ij} u_j + D_{45}^{ji} \frac{\partial w_j}{\partial x} + \bar{D}_{44}^{ij} \left(\frac{\partial w_j}{\partial y} - \frac{v_j}{R} \right) \end{aligned} \quad (12.6.10)$$

$$\begin{aligned} M_1^{ij} &= D_{11}^{ijk} \frac{\partial u_k}{\partial x} + D_{12}^{ijk} \left(\frac{\partial v_k}{\partial y} + \frac{1}{R} w_k \right) + \bar{D}_{13}^{ijk} w_k + D_{16}^{ijk} \left(\frac{\partial u_k}{\partial y} + \frac{\partial v_k}{\partial x} \right) \\ &\quad + \frac{1}{2} D_{11}^{ijkl} \frac{\partial w_k}{\partial x} \frac{\partial w_\ell}{\partial x} + \frac{1}{2} D_{12}^{ijkl} \frac{\partial w_k}{\partial y} \frac{\partial w_\ell}{\partial y} + D_{16}^{ijkl} \frac{\partial w_k}{\partial x} \frac{\partial w_\ell}{\partial y} \\ M_2^{ij} &= D_{12}^{ijk} \frac{\partial u_k}{\partial x} + D_{22}^{ijk} \left(\frac{\partial v_k}{\partial y} + \frac{1}{R} w_k \right) + \bar{D}_{23}^{ijk} w_k + D_{26}^{ijk} \left(\frac{\partial u_k}{\partial y} + \frac{\partial u_k}{\partial x} \right) \\ &\quad + \frac{1}{2} D_{12}^{ijkl} \frac{\partial w_k}{\partial x} \frac{\partial w_\ell}{\partial x} + \frac{1}{2} D_{22}^{ijkl} \frac{\partial w_k}{\partial y} \frac{\partial w_\ell}{\partial y} + D_{26}^{ijkl} \frac{\partial w_k}{\partial x} \frac{\partial w_\ell}{\partial y} \\ M_6^{ij} &= D_{16}^{ijk} \frac{\partial u_k}{\partial x} + D_{26}^{ijk} \left(\frac{\partial v_k}{\partial y} + \frac{1}{R} w_k \right) + \bar{D}_{36}^{ijk} w_k + D_{66}^{ijk} \left(\frac{\partial u_k}{\partial y} + \frac{\partial v_k}{\partial x} \right) \\ &\quad + \frac{1}{2} D_{16}^{ijkl} \frac{\partial w_k}{\partial x} \frac{\partial w_\ell}{\partial x} + \frac{1}{2} D_{26}^{ijkl} \frac{\partial w_k}{\partial y} \frac{\partial w_\ell}{\partial y} + D_{66}^{ijkl} \frac{\partial w_k}{\partial x} \frac{\partial w_\ell}{\partial y} \end{aligned} \quad (12.6.11)$$

where

$$\begin{aligned} D_{\alpha\beta}^{ij} &= \int_{-\frac{h}{2}}^{\frac{h}{2}} c_{\alpha\beta} \phi^i \phi^j dz, & D_{\alpha\beta}^{ijk} &= \int_{-\frac{h}{2}}^{\frac{h}{2}} c_{\alpha\beta} \phi^i \phi^j \phi^k dz \\ D_{\alpha\beta}^{ijkl} &= \int_{-\frac{h}{2}}^{\frac{h}{2}} c_{\alpha\beta} \phi^i \phi^j \phi^k \phi^\ell dz, & D_{\alpha\beta}^{ij} &= \int_{-\frac{h}{2}}^{\frac{h}{2}} c_{\alpha\beta} \phi^i \frac{d\phi^j}{dz} dz \\ \bar{D}_{\alpha\beta}^{ijk} &= \int_{-\frac{h}{2}}^{\frac{h}{2}} c_{\alpha\beta} \phi^i \phi^j \frac{d\phi^k}{dz} dz, & \bar{D}_{\alpha\beta}^{ij} &= \int_{-\frac{h}{2}}^{\frac{h}{2}} c_{\alpha\beta} \frac{d\phi^i}{dz} \frac{d\phi^j}{dz} dz \end{aligned} \quad (12.6.12)$$

Note that $D_{\alpha\beta}^{ij}$, $\bar{D}_{\alpha\beta}^{ij}$, $D_{\alpha\beta}^{ijk}$ and $D_{\alpha\beta}^{ijkl}$ are symmetric in their subscripts and superscripts:

$$D_{\alpha\beta}^{ij} = D_{\alpha\beta}^{ji}, \quad D_{\beta\alpha}^{ij} = D_{\alpha\beta}^{ij}, \quad D_{\alpha\beta}^{ijk} = D_{\alpha\beta}^{jik} = D_{\alpha\beta}^{kji} = D_{\alpha\beta}^{ikj}, \text{ etc.} \quad (12.6.13)$$

The symmetry with respect to the superscripts is due to the definition of the integrals, and the symmetry due to the subscripts is the result of the symmetry of material stiffnesses: $Q_{\alpha\beta} = Q_{\beta\alpha}$. The coefficients with a single bar over them are **not** symmetric with respect to the superscripts.

The evaluation of $D_{\alpha\beta}^{ij}$ and $\bar{D}_{\alpha\beta}^{ij}$, for example, is discussed in detail here for information. First we recognize that ϕ^i are the global interpolation functions associated with the i th interface, and they can be expressed in terms of the approximation functions of the layer on either side of the i th interface. For linear interpolation, we have

$$\phi^i = \begin{cases} \psi_2^{(i-1)} \equiv \frac{z-z_{i-1}}{h_{i-1}}, & z_{i-1} \leq z \leq z_i \\ \psi_1^i \equiv \frac{z_i-z}{h_i}, & z_i \leq z \leq z_{i+1} \end{cases} \quad (12.6.14)$$

Thus, each mathematical layer is viewed as a 1-D finite element through the thickness, and $\psi_\alpha^{(i)}$ are the interpolation functions of the i th element ($\alpha = 1, 2$). Consequently, $[D_{\alpha\beta}]$, for example can be viewed as the assembled coefficient matrix of the element coefficients $(D_{\alpha\beta}^{ij})_k$ of the k th element,

$$(D_{\alpha\beta}^{ij})_k = \int_{z_k}^{z_{k+1}} Q_{\alpha\beta}^{(k)} \psi_i^{(k)} \phi_j^{(k)} dz, \quad [D_{\alpha\beta}]_k = Q_{\alpha\beta}^{(k)} \frac{h_k}{6} \begin{bmatrix} 2 & 1 \\ 1 & 2 \end{bmatrix} \quad (12.6.15)$$

The assembled matrix is given by

$$[D_{\alpha\beta}] = \frac{1}{6} \begin{bmatrix} 2h_1 Q_{\alpha\beta}^{(1)} & h_1 Q_{\alpha\beta}^{(1)} & 0 & 0 \\ h_1 Q_{\alpha\beta}^{(1)} & 2h_1 Q_{\alpha\beta}^{(1)} + 2h_2 Q_{\alpha\beta}^{(2)} & h_2 Q_{\alpha\beta}^{(2)} & \dots \\ 0 & h_2 Q_{\alpha\beta}^{(2)} & \dots & \dots \end{bmatrix} \quad (12.6.16)$$

Similarly, we have

$$(\bar{D}_{\alpha\beta}^{ij})_k = \int_{z_k}^{z_{k+1}} Q_{\alpha\beta}^{(k)} \phi^i \frac{d\phi^j}{dz} dz, \quad [\bar{D}_{\alpha\beta}]_k = Q^{(k)} \frac{1}{2} \begin{bmatrix} -1 & 1 \\ -1 & 1 \end{bmatrix} \quad (12.6.17)$$

and

$$[\bar{D}_{\alpha\beta}] = \frac{1}{2} \begin{bmatrix} -Q_{\alpha\beta}^{(1)} & Q_{\alpha\beta}^{(1)} & 0 & 0 \\ -Q_{\alpha\beta}^{(1)} & Q_{\alpha\beta}^{(1)} - Q_{\alpha\beta}^{(2)} & Q_{\alpha\beta}^{(2)} & \dots \\ 0 & -Q_{\alpha\beta}^{(1)} & \dots & \dots \end{bmatrix} \quad (12.6.18)$$

Similarly, other coefficients can be computed.

12.6.3 Stiffened Shells

Displacements and Strains in the Stiffeners

Now consider a cylindrical shell reinforced by eccentric axial and ring stiffeners. The stiffeners are assumed to behave like beam elements. The kinematic description of the beam elements is based on the Euler–Bernoulli beam theory:

Axial Stiffeners	Ring Stiffeners
$u_1 = u_I - z \frac{\partial w_I}{\partial x}$	$u_2 = v_I - z \frac{\partial w_I}{\partial y}$
$u_3 = w_I$	$u_3 = w_I$

(12.6.19)

Here (u_I, v_I, w_I) denote the displacement components at the I th nodal location through the shell thickness. For example, the I th node can be that on the surface of the shell.

The strains associated with the stiffeners are

$$\begin{aligned} \varepsilon_a \equiv \varepsilon_1 &= \frac{\partial u_I}{\partial x} + \frac{1}{2} \left(\frac{\partial w_I}{\partial x} \right)^2 - z \frac{\partial^2 w_I}{\partial x^2} \\ \varepsilon_c \equiv \varepsilon_2 &= \frac{\partial v_I}{\partial y} + \frac{1}{2} \left(\frac{\partial w_I}{\partial y} \right)^2 + \frac{w_I}{R} - z \frac{\partial^2 w_I}{\partial y^2} \end{aligned} \quad (12.6.20)$$

where the subscripts “a” and “c” refer to axial and circumferential stiffeners, respectively. The uniaxial stress-strain equations are used for stiffeners:

$$\sigma_a = E_a \varepsilon_a, \quad \sigma_c = E_c \varepsilon_c$$

Virtual Strain Energy of Stiffeners

The virtual strain energy for the axial stiffeners is given by

$$\begin{aligned} \delta U_a &= \frac{1}{S_a} \int_{\Omega} \left(\int_{A_a} \sigma_a \delta \varepsilon_a dA + G_a J_a \frac{\partial^2 w_I}{\partial x \partial y} \frac{\partial^2 \delta w_I}{\partial x \partial y} \right) dx dy \\ &= \int_{\Omega} \frac{1}{S_a} \left(\int_{A_a} E_a \varepsilon_a \delta \varepsilon_a dA + G_a J_a \frac{\partial^2 w_I}{\partial x \partial y} \frac{\partial^2 \delta w_I}{\partial x \partial y} \right) dx dy \\ &= \int_{\Omega} \frac{1}{S_a} \left\{ E_a A_a \left[\frac{\partial u_I}{\partial x} + \frac{1}{2} \left(\frac{\partial w_I}{\partial x} \right)^2 \right] \left(\frac{\partial \delta u_I}{\partial x} + \frac{\partial w_I}{\partial x} \frac{\partial \delta w_I}{\partial x} \right) \right. \\ &\quad + E_a \left[I_a \frac{\partial^2 w_I}{\partial x^2} \frac{\partial^2 \delta w_I}{\partial x^2} - \bar{z}_a A_a \frac{\partial^2 w_I}{\partial x^2} \left(\frac{\partial \delta u_I}{\partial x} + \frac{\partial w_I}{\partial x} \frac{\partial \delta w_I}{\partial x} \right) \right. \\ &\quad \left. \left. - \bar{z}_a A_a \frac{\partial^2 \delta w_I}{\partial x^2} \left(\frac{\partial u_I}{\partial x} + \frac{1}{2} \frac{\partial w_I}{\partial x} \frac{\partial w_I}{\partial x} \right) \right] + G_a J_a \frac{\partial^2 \delta w_I}{\partial x \partial y} \frac{\partial^2 w_I}{\partial x \partial y} \right\} dx dy \quad (12.6.21) \end{aligned}$$

where (see Figure 12.6.1)

S_a = stiffener spacing ($2\pi R/N_a$; N_a = number of axial stiffeners)

I_a = moment of inertia of the stiffener about the reference surface ($z = 0$)

$= \hat{I}_a + (\hat{z}_a)^2 A_a$; \hat{I}_a = moment of inertia about the centroid of the stiffener

\bar{z}_a = distance from the stiffener to the reference surface

J_a = Torsional constant ($G_a J_a$ = torsional rigidity) Similarly, the virtual strain energy of the circumferential stiffeners is

$$\begin{aligned} \delta U_c &= \frac{1}{S_c} \int_{\Omega} \left(\int_{A_c} E_c \varepsilon_c \delta \varepsilon_c dA + G_c J_c \frac{\partial^2 w_I}{\partial x \partial y} \frac{\partial^2 \delta w_I}{\partial x \partial y} \right) dx dy \\ &= \frac{1}{S_c} \int_{\Omega} \left\{ E_c A_c \left(\frac{\partial \delta v_I}{\partial y} + \frac{\delta w_I}{R} + \frac{\partial w_I}{\partial y} \frac{\partial \delta w_I}{\partial y} \right) \left[\frac{\partial v_I}{\partial y} + \frac{w_I}{R} + \frac{1}{2} \left(\frac{\partial w_I}{\partial y} \right)^2 \right] \right. \\ &\quad + E_c I_c \frac{\partial^2 w_I}{\partial y^2} \frac{\partial^2 \delta w_I}{\partial y^2} - \bar{z}_c A_c E_c \frac{\partial^2 w_I}{\partial y^2} \left(\frac{\partial \delta v_I}{\partial y} + \frac{\delta w_I}{R} + \frac{\partial \delta w_I}{\partial y} \frac{\partial w_I}{\partial y} \right) \\ &\quad \left. - \bar{z}_c A_c E_c \frac{\partial^2 \delta w_I}{\partial y^2} \left[\frac{\partial v_I}{\partial y} + \frac{w_I}{R} + \frac{1}{2} \left(\frac{\partial w_I}{\partial y} \right)^2 \right] + G_c J_c \frac{\partial^2 w_I}{\partial x \partial y} \frac{\partial^2 \delta w_I}{\partial x \partial y} \right\} dx dy \quad (12.6.22) \end{aligned}$$

where S_c is the stiffener spacing, $S_c = \frac{L}{N_c}$, N_c is the number of ring stiffeners, and L is the length of the cylinder.

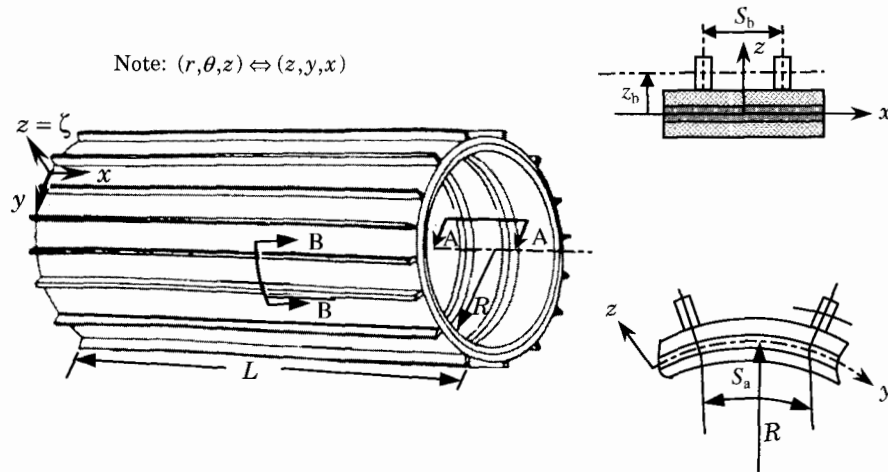


Figure 12.6.1: Schematic of a circular cylindrical shell with axial and circumferential stiffeners [101].

Equations of Equilibrium

The governing equations of stiffened composite shells with equally spaced ring and axial stiffeners can be derived using the principle of minimum total potential energy. The first variation of the total potential energy of the stiffened shell according to the linear layerwise theory is

$$\begin{aligned}
 \delta\Pi = \int_{\Omega} & \left\{ M_1^i \frac{\partial \delta u_i}{\partial x} + M_2^i \left(\frac{\partial \delta u_i}{\partial y} + \frac{1}{R} \delta w_i \right) + M_6^i \left(\frac{\partial \delta u_i}{\partial y} + \frac{\partial \delta v_i}{\partial x} \right) \right. \\
 & + Q_1^i \delta u_i + Q_2^i \delta v_i + Q_3^i \delta w_i - \frac{1}{R} K_2^i \delta v_i + K_1^i \frac{\partial \delta w_i}{\partial x} + K_2^i \frac{\partial \delta w_i}{\partial y} \\
 & + \hat{N}_1 \frac{\partial \delta w_I}{\partial x} \frac{\partial w_I}{\partial x} + \hat{N}_2 \frac{\partial \delta w_I}{\partial y} \frac{\partial w_I}{\partial y} \Big\} dx dy \\
 & + \int_{\Omega} \left\{ \frac{1}{S_a} \left[E_a A_a \frac{\partial u_I}{\partial x} \frac{\partial \delta u_I}{\partial x} + E_a I_a \frac{\partial^2 w_I}{\partial x^2} \frac{\partial^2 \delta w_I}{\partial x^2} \right. \right. \\
 & - E_a A_a \bar{z}_a \left(\frac{\partial^2 w_I}{\partial x^2} \frac{\partial \delta u_I}{\partial x} + \frac{\partial^2 \delta w_I}{\partial x^2} \frac{\partial u_I}{\partial x} \right) + G_a J_a \frac{\partial^2 w_I}{\partial x \partial y} \frac{\partial^2 \delta w_I}{\partial x \partial y} \Big] \\
 & + \frac{1}{S_c} \left[E_c A_c \left(\frac{\partial v_I}{\partial y} + \frac{w_I}{R} \right) \left(\frac{\partial \delta v_I}{\partial y} + \frac{\delta w_I}{R} \right) + E_c A_c \frac{\partial^2 \delta w_I}{\partial y^2} \frac{\partial^2 w_I}{\partial y^2} \right. \\
 & - E_c A_c \bar{z}_c \left(\frac{\partial^2 w_I}{\partial y^2} \right) \left(\frac{\partial \delta v_I}{\partial y} + \frac{\delta w_I}{R} \right) - E_c A_c \bar{z}_c \frac{\partial^2 \delta w_I}{\partial y^2} \left(\frac{\partial v_I}{\partial y} + \frac{w_I}{R} \right) \\
 & \left. \left. + G_c J_c \frac{\partial^2 w_I}{\partial x \partial y} \frac{\partial^2 \delta w_I}{\partial x \partial y} \right] \right\} dx dy \quad (\text{no sum on } I) \tag{12.6.23}
 \end{aligned}$$

where

$$\begin{aligned}\hat{N}_i &= (N_i)_{\text{shell}} + (N_i)_{\text{stiffeners}} \\ \hat{N}_1 &= \text{axial force, } \quad \hat{N}_2 = \text{lateral force}\end{aligned}\quad (12.6.24)$$

We shall assume, for buckling analysis, that

$$\hat{N}_i = \lambda \bar{N}_i \quad (\hat{N}_1 = \lambda \bar{N}_1, \quad \hat{N}_2 = \lambda \bar{N}_2) \quad (12.6.25)$$

We have

$$\begin{aligned}\bar{N}_1 &= -1, \quad \bar{N}_2 = 0, \text{ buckling under axial compressive load.} \\ \bar{N}_1 &= 0, \quad \bar{N}_2 = -1, \text{ buckling under lateral pressure.}\end{aligned}\quad (12.6.26)$$

The principle of total potential energy ($\delta\Pi = 0$) gives the following differential equations governing buckling:

$$\begin{aligned}\delta u_i : \quad &\frac{\partial M_1^i}{\partial x} + \frac{\partial M_6^i}{\partial y} - Q_1^i + \frac{E_a A_a}{S_a} \left(\frac{\partial^2 u_I}{\partial x^2} - \bar{z}_a \frac{\partial^3 w_I}{\partial x^3} \right) \delta_{iI} = 0 \\ \delta v_i : \quad &\frac{\partial M_6^i}{\partial x} + \frac{\partial M_2^i}{\partial y} - Q_2^i + \frac{K_2^i}{R} + \frac{E_c A_c}{S_c} \left[\left(\frac{\partial^2 v_I}{\partial y^2} + \frac{1}{R} \frac{\partial w_I}{\partial y} \right) - \bar{z}_c \frac{\partial^3 w_I}{\partial y^3} \right] \delta_{iI} = 0 \\ \delta w_i : \quad &\frac{\partial K_1^i}{\partial x} + \frac{\partial K_2^i}{\partial y} - Q_3^i - \frac{M_2^i}{R} + \left\{ \hat{N}_1 \frac{\partial^2 w_I}{\partial x^2} + \hat{N}_2 \frac{\partial^2 w_I}{\partial y^2} \right. \\ &+ \left[-\frac{E_a I_a}{S_a} \frac{\partial^4 w_I}{\partial x^4} - \frac{E_c I_c}{S_c} \frac{\partial^4 w_I}{\partial y^4} - \left(\frac{G_c J_c}{S_c} + \frac{G_a J_a}{S_a} \right) \frac{\partial^4 w_I}{\partial x^2 \partial y^2} + \frac{\bar{z}_a E_a A_a}{S_a} \frac{\partial^3 u_I}{\partial x^3} \right. \\ &\left. \left. + \frac{\bar{z}_c E_c A_c}{S_c} \left(\frac{\partial^3 v_I}{\partial y^3} + \frac{2}{R} \frac{\partial^2 w_I}{\partial y^2} \right) - \frac{E_c A_c}{R S_c} \left(\frac{\partial v_I}{\partial y} + \frac{1}{R} w_I \right) \right] \right\} \delta_{iI} = 0\end{aligned}\quad (12.6.27)$$

where δ_{iI} is the Kronecker delta symbol.

The Navier Solution

Here we develop exact analytical solutions of the *linear theory* [i.e., neglect the nonlinear terms in Eqs. (12.6.8)–(12.6.11)] of buckling using the Navier solution procedure. Exact analytical solutions can be developed only for simply-supported boundary conditions and for cross-ply lamination schemes.

First, we express the equilibrium equations (12.6.27) in terms of displacements:

$$\begin{aligned}D_{11}^{ij} \frac{\partial^2 u_j}{\partial x^2} + D_{16}^{ij} \left(\frac{\partial^2 u_j}{\partial x \partial y} + \frac{\partial^2 v_j}{\partial x^2} \right) + D_{12}^{ij} \left(\frac{\partial^2 u_j}{\partial x \partial y} + \frac{1}{R} \frac{\partial w_j}{\partial x} \right) + \bar{D}_{13}^{ij} \frac{\partial w_j}{\partial x} \\ + D_{16}^{ij} \frac{\partial^2 u_j}{\partial x \partial y} + D_{26}^{ij} \left(\frac{\partial^2 v_j}{\partial y^2} + \frac{1}{R} \frac{\partial w_j}{\partial y} \right) + D_{66}^{ij} \left(\frac{\partial^2 u_j}{\partial y^2} + \frac{\partial^2 v_j}{\partial x \partial y} \right) + \bar{D}_{36}^{ij} \frac{\partial w_j}{\partial y} \\ - \bar{D}_{55}^{ij} u_j - \bar{D}_{55}^{ji} \frac{\partial w_j}{\partial x} - \bar{D}_{45}^{ij} v_j - \bar{D}_{45}^{ji} \left(\frac{\partial w_j}{\partial y} - \frac{v_j}{R} \right) \\ + \frac{E_a A_a}{S_a} \left(\frac{\partial^2 u_I}{\partial x^2} - \bar{z}_a \frac{\partial^3 w_I}{\partial x^3} \right) \delta_{iI} = 0\end{aligned}\quad (12.6.28)$$

$$\begin{aligned}
& D_{16}^{ij} \frac{\partial^2 u_j}{\partial x^2} + D_{26}^{ij} \left(\frac{\partial^2 v_j}{\partial x \partial y} + \frac{1}{R} \frac{\partial w_j}{\partial x} \right) + D_{66}^{ij} \left(\frac{\partial^2 u_j}{\partial x \partial y} + \frac{\partial v_j}{\partial x^2} \right) + \bar{D}_{36}^{ij} \frac{\partial w_j}{\partial x} \\
& + D_{12}^{ij} \frac{\partial^2 u_j}{\partial x \partial y} + D_{22}^{ij} \left(\frac{\partial^2 v_j}{\partial y^2} + \frac{1}{R} \frac{\partial w_j}{\partial y} \right) + D_{26}^{ij} \left(\frac{\partial^2 u_j}{\partial y^2} + \frac{\partial^2 v_j}{\partial x \partial y} \right) + \bar{D}_{23}^{ij} \frac{\partial w_j}{\partial y} \\
& - \bar{D}_{45}^{ij} u_j - \bar{D}_{45}^{ji} \frac{\partial w_j}{\partial x} - \bar{D}_{44}^{ij} v_j - \bar{D}_{44}^{ji} \left(\frac{\partial w_j}{\partial y} - \frac{v_j}{R} \right) \\
& + \frac{1}{R} \left[\bar{D}_{45}^{ij} u_j + D_{45}^{ij} \frac{\partial w_j}{\partial x} + \bar{D}_{44}^{ij} v_j + D_{44}^{ij} \left(\frac{\partial w_j}{\partial y} - \frac{v_j}{R} \right) \right] \\
& + \frac{E_c A_c}{S_c} \left[\frac{\partial^2 v_I}{\partial y^2} + \frac{1}{R} \frac{\partial w_I}{\partial y} - \bar{z}_c \frac{\partial^3 w_I}{\partial y^3} \right] \delta_{iI} = 0
\end{aligned} \tag{12.6.29}$$

$$\begin{aligned}
& \bar{D}_{55}^{ij} \frac{\partial u_j}{\partial x} + \bar{D}_{55}^{ij} \frac{\partial^2 w_j}{\partial x^2} + \bar{D}_{45}^{ij} \frac{\partial v_j}{\partial x} + \bar{D}_{45}^{ij} \left(\frac{\partial^2 w_j}{\partial x \partial y} - \frac{1}{R} \frac{\partial v_j}{\partial x} \right) + \bar{D}_{45}^{ij} \frac{\partial u_j}{\partial y} \\
& + D_{45}^{ij} \frac{\partial^2 w}{\partial x \partial y} + \bar{D}_{44}^{ij} \frac{\partial v_j}{\partial y} + D_{44}^{ij} \left(\frac{\partial^2 w_j}{\partial y^2} - \frac{1}{R} \frac{\partial v_j}{\partial y} \right) \\
& - \frac{1}{R} \left[D_{12}^{ij} \frac{\partial u_j}{\partial x} + D_{22}^{ij} \left(\frac{\partial v_j}{\partial y} + \frac{w_j}{R} \right) + D_{26}^{ij} \left(\frac{\partial u_j}{\partial y} + \frac{\partial v_j}{\partial x} \right) + \bar{D}_{23}^{ij} w_j \right] \\
& - \bar{D}_{13}^{ij} \frac{\partial u_j}{\partial x} - \bar{D}_{23}^{ji} \left(\frac{\partial u_j}{\partial y} + \frac{w_j}{R} \right) - \bar{D}_{36}^{ji} \left(\frac{\partial u_j}{\partial y} + \frac{\partial v_j}{\partial x} \right) - \bar{D}_{33}^{ij} w_j \\
& + \left[\lambda \left(\bar{N}_1 \frac{\partial^2 w_I}{\partial x^2} + \bar{N}_2 \frac{\partial^2 w_I}{\partial y^2} \right) - \frac{E_c A_c}{R} \left(\frac{\partial v_I}{\partial y} + \frac{w_I}{R} \right) \right. \\
& + \frac{1}{S_a} \left(-E_1 I_a \frac{\partial^4 w_I}{\partial x^4} - G_a J_a \frac{\partial^4 w_I}{\partial x^2 \partial y^2} + \bar{z}_a E_a A_a \frac{\partial^3 w_I}{\partial x^3} \right) \\
& \left. - \frac{E_c I_c}{S_c} \frac{\partial^4 w_I}{\partial y^4} - G_c J_c \frac{\partial^4 w_I}{\partial x^2 \partial y^2} + \bar{z}_c A_c E_c \left(\frac{\partial^3 v_I}{\partial y^3} + \frac{2}{R} \frac{\partial^2 w_I}{\partial y^2} \right) \right] \delta_{iI} = 0
\end{aligned} \tag{12.6.30}$$

We assume the following form of the solution which satisfies the simply supported boundary conditions,

$$\begin{aligned}
u_i &= U_i^{mn} \cos \alpha_m x \cos \beta_n y \\
v_i &= V_i^{mn} \sin \alpha_m x \sin \beta_n y \\
w_i &= W_i^{mn} \sin \alpha_m x \cos \beta_n y
\end{aligned} \tag{12.6.31}$$

where $\alpha_m = m\pi/L$ and $\beta_n = n/R$ where U_i^{mn} , V_i^{mn} , and W_i^{mn} amplitudes to be determined for each mode (m, n) . Substituting Eq. (12.6.31) into Eqs. (12.6.28)-(12.6.30) and collecting coefficients of like functions, we obtain (for $D_{16}^{ij} = D_{26}^{ij} = \bar{D}_{45}^{ij} = \bar{D}_{36}^{ij} = \bar{D}_{45}^{ji} = 0$):

$$\begin{aligned}
& \left(-D_{11}^{ij} \alpha_m^2 - D_{66}^{ij} \beta_n^2 - \bar{D}_{55}^{ij} - \delta_{iI} \frac{E_a A_a}{S_a} \alpha_m^2 \right) U_j^{mn} + \alpha_m \beta_n \left(D_{12}^{ij} + D_{66}^{ij} \right) V_j^{mn} \\
& + \left[\alpha_m \left(\frac{1}{R} D_{12}^{ij} + \bar{D}_{13}^{ij} - \bar{D}_{55}^{ji} \right) + \delta_{iI} \frac{\bar{z}_a E_a A_a}{S_a} \alpha_m^3 \right] W_j^{mn} = 0
\end{aligned} \tag{12.6.32a}$$

$$\begin{aligned} & \alpha_m \beta_n \left(D_{12}^{ij} + D_{66}^{ij} \right) U_j^{mn} + \left[-D_{66}^{ij} \alpha_m^2 - D_{22}^{ij} \beta_n^2 - \bar{D}_{44}^{ij} + \frac{1}{R} \left(\bar{D}_{44}^{ij} + \bar{D}_{44}^{ji} \right) \right. \\ & \quad \left. - \frac{1}{R^2} D_{44}^{ij} - \delta_{iI} \frac{E_c A_c}{S_c} \beta_n^2 \right] V_j^{mn} + \left[-\beta_n \left(\frac{D_{22}^{ij}}{R} + \frac{D_{44}^{ij}}{R} + \bar{D}_{23}^{ji} - \bar{D}_{44}^{ji} \right) \right. \\ & \quad \left. + \delta_{iI} \frac{E_c A_c}{S_c} \left(-\frac{\beta_n}{R} - \bar{z}_c \beta_n^3 \right) \right] W_j^{mn} = 0 \end{aligned} \quad (12.6.32b)$$

$$\begin{aligned} & \left[\alpha_m \left(\frac{1}{R} D_{12}^{ij} + \bar{D}_{13}^{ji} - \bar{D}_{55}^{ij} \right) + \delta_{iI} \frac{\bar{z}_a E_a A_a}{S_c} \alpha_m^3 \right] U_j^{mn} \\ & \quad + \left[-\beta_n \left(\frac{1}{R} D_{22}^{ij} + \frac{1}{R} D_{44}^{ij} + \bar{D}_{23}^{ji} - \bar{D}_{44}^{ji} \right) + \delta_{iI} \frac{E_c A_c}{S_c} \left(-\frac{\beta_n}{R} - \bar{z}_c \beta_n^3 \right) \right] V_j^{mn} \\ & \quad + \left[-D_{55}^{ij} \alpha_m^2 - D_{44}^{ij} \beta_n^2 - \frac{1}{R^2} D_{22}^{ij} - \frac{1}{R} \bar{D}_{23}^{ji} - \frac{1}{R} \bar{D}_{23}^{ij} - \bar{D}_{33}^{ij} \right. \\ & \quad \left. + \delta_{iI} \left(-\frac{E_a I_a}{S_a} \alpha_m^4 - \frac{G_a J_a}{S_a} \alpha_m^2 \beta_n^2 - \frac{E_c I_c}{S_c} \beta_n^4 - \frac{G_c J_c}{S_c} \alpha_m^2 \beta_n^2 \right. \right. \\ & \quad \left. \left. - \frac{2 \bar{z}_c E_c A_c}{R S_c} \beta_n^2 - \frac{E_c A_c}{S_c R^2} \right) \right] W_j^{mn} = \lambda \left(\bar{N}_1 \alpha_m^2 + \bar{N}_2 \beta_n^2 \right) W_j^{mn} \delta_{iI} \end{aligned} \quad (12.6.32c)$$

For each mode (m, n) , Eqs. (12.6.32a–c) represent the eigenvalue problem

$$\begin{bmatrix} S^{11} & S^{12} & S^{13} \\ S^{12} & S^{22} & S^{23} \\ S^{13} & S^{23} & S^{33} \end{bmatrix} \begin{Bmatrix} U \\ V \\ W \end{Bmatrix} = \lambda \begin{bmatrix} M^{11} & M^{12} & M^{13} \\ M^{12} & M^{22} & M^{23} \\ M^{13} & M^{23} & M^{33} \end{bmatrix} \begin{Bmatrix} U \\ V \\ W \end{Bmatrix} \quad (12.6.33)$$

where the submatrices $S_{ij}^{\alpha\beta} = S_{ji}^{\alpha\beta}$ and $M_{ij}^{\alpha\beta} = M_{ji}^{\alpha\beta}$ ($\alpha\beta = 1, 2, 3$) can be easily identified from Eqs. (12.6.32). Note that $M_{ij}^{\alpha\beta} = 0$ for all except for $\alpha = \beta = 3$, and $M_{ij}^{33} = \bar{N}_1 \alpha_i^2 + \bar{N}_2 \beta_j^2$.

We note for the case $n = 0$, we have $V_j^{mn} = 0$, and the eigenvalue problem becomes

$$\begin{bmatrix} \hat{S}^{11} & \hat{S}^{13} \\ \hat{S}^{13} & \hat{S}^{33} \end{bmatrix} \begin{Bmatrix} U \\ W \end{Bmatrix} = \lambda \begin{bmatrix} 0 & 0 \\ 0 & \hat{M}^{33} \end{bmatrix} \begin{Bmatrix} U \\ W \end{Bmatrix} \quad (12.6.34)$$

where $\hat{S}^{\alpha\beta}$ and \hat{M}^{33} are obtained from the corresponding $S^{\alpha\beta}$ and M^{33} by setting all terms with β_n to zero. The solution of Eq. (12.6.34) gives the eigenvalues λ_{mn} , and the minimum eigenvalue is the critical buckling load.

As an example consider a simply-supported isotropic cylindrical shell (see Table 1 of Baruch and Singer [90]). The results for general instability pressure are presented in Table 12.6.1. The following geometric and material properties are used:

$$\begin{aligned} \frac{h}{R} &= 0.01217, \quad \frac{L}{R} = 4.5391, \quad \frac{A_b}{S_b h} = \frac{A_a}{S_a h} = 0.1471, \quad I_a = I_b = 0.7819 \\ \frac{z_a}{h} &= \pm 1.653, \quad \frac{z_b}{h} = \pm 1.653, \quad E = 30 \times 10^6 \text{ psi}, \quad \nu = 0.3 \end{aligned} \quad (12.6.35)$$

where $I = (Sh^3/12)$, h being the total thickness, R is the radius, and L is the length of the shell, S_a is the distance between the frames (i.e., ring stiffeners), S_b is the

distance between stringers (i.e., axial stiffeners), and z_b and z_a are the distances between the centroid of the stiffener cross section and middle surface of the shell for stringers and frames, respectively (see Figure 12.6.1). The negative sign for z_a and z_b indicates internal stiffeners. It is clear that frames on the inside of the shell give general instability loads about 10-15 percent greater than frames on the outside of the shell. Stringers are much less effective in stiffening a shell under hydrostatic pressure. Outside stringers yield critical loads greater than inside stringers.

The layerwise shell theory, which accounts for 3-D kinematics, gives lower buckling loads when compared to the single-layer shell theories. The classical shell theory overpredicts the buckling loads by 6 to 10 percent. An exception to this is seen when only one layer through the entire thickness is used. For one layer model with the layerwise shell theory, the transverse displacement is given by

$$w = w_1\phi^1 + w_2\phi^2, \quad w_1 \neq w_2$$

Table 12.6.1: General buckling pressures (lb/in^2) of stiffened isotropic ($E = 30 \times 10^6 \text{ psi}$, $\nu = 0.3$) circular cylindrical shells ($h/R = 0.01217$, $R = 82.1693$, $L = 372.9745$, $N_a = 516$ $N_c = 373$)[†].

Shell	Ref. 100	CST	FST	LWT	Mode	Error**
Unstiffened	102	103	103	111.4 (1)* 97.8 (2) 94.4 (4) 93.5 (8)	(1,4)	-10%
Ring-stiffened (External)	326	335	334	323.6 316.1 314.2 313.7	(1,3)	-6.8%
Ring-stiffened (Internal)	370	380	379	367.6 359.9 358.0 357.5	(1,3)	-6.3%
Longitudinally Stiffened (External)	106	108	108	116.1 102.5 99.1 98.3	(1,4)	-9.9%
Longitudinally Stiffened (Internal)	103	104.5	104.5	112.5 99.0 99.5 94.7	(1,4)	-10.3%
Combined (External)	346	355	354.6	333.9(8)	(1,3)	-6.3%
Combined (Internal)	377	387	386.7	365 (8)	(1,3)	-6.0%

[†] CST = classical shell theory; FST = First-order shear deformation shell theory; LWT = layerwise shell theory.

* The numbers in parentheses refer to the number of (numerical) layers.

** Percentage error = $(\text{LWT}-\text{CST})100/\text{LWT}$.

For thin shells, inextensibility of transverse normals requires $w_1 = w_2$. This constraint cannot be met in the layerwise theory with one layer model unless several layers are included in the model. Thus, it is recommended that two or more layers be used, even for isotropic shell to model with the layerwise shell theory. Note that no shear correction factors are used in the layerwise theory.

The stability of a ring-stiffened cylindrical shell considered by Jones [91] is studied next. The shell, laminated of two different isotropic layers and subjected to hydrostatic pressure, is considered. The properties of the two layers are:

$$\begin{aligned} \text{Layer 1: } & E = 44 \times 10^6 \text{ psi}, \quad \nu = 0.0, \quad h_1 = 0.04 \text{ in.} \\ \text{Layer 2: } & E = 2 \times 10^6 \text{ psi}, \quad \nu = 0.4, \quad h_2 = 0.3 \text{ in.} \end{aligned}$$

The rings are of rectangular cross section with a height of $h = 0.25$ in. and a thickness of $t = 0.06$ in., and they have the same material properties as the layer one. The inertias I and J are calculated using the relations,

$$I = \frac{th^3}{12}, \quad J = \frac{ht^3}{3}$$

The radius and length of the shell are 6 in. and 12 in., respectively.

The hydrostatic buckling pressures of the shell, as obtained by the classical and layerwise shell theories, are plotted against the ring spacing (see Figure 12.6.2) for internally-stiffened and externally stiffened cylinders. The buckling pressures obtained with the classical shell theory are larger by 7 to 9 percent for internally-stiffened shells and 7 to 20 percent for the externally stiffened shells.

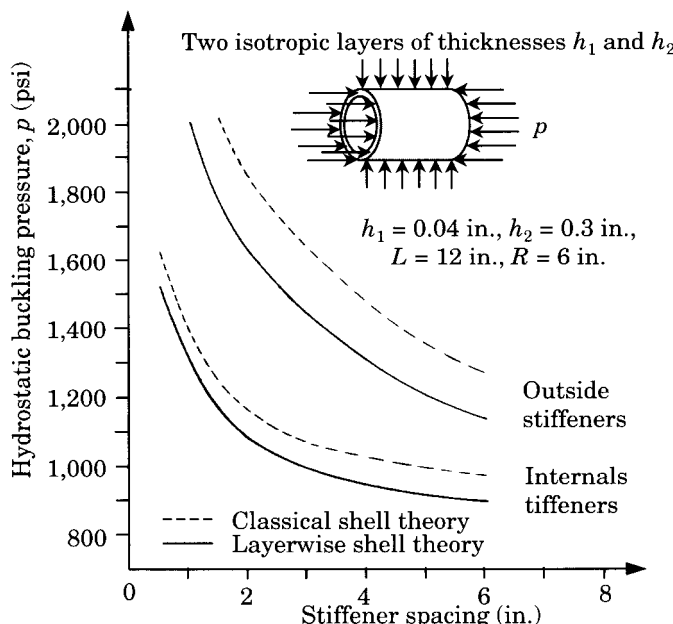


Figure 12.6.2: Hydrostatic buckling pressure of a ring-stiffened, two-layer circular cylindrical shell according to classical and layerwise shell theories.

Next, we consider an orthotropic and three-layer cross-ply (0/90/0) cylindrical shells without and with stiffeners. Table 12.6.2 contains a comparison of the buckling loads obtained with the classical shell theory and the layerwise shell theory. Figures 12.6.3 and 12.6.4 contain plots of the hydrostatic buckling pressure and axial buckling load versus stiffener spacing for orthotropic and cross-ply laminated shells. The differences between the exact solutions of the layerwise theory and the classical theory are clearly large enough to warrant the use of the layerwise shell theory.

Table 12.6.2: General buckling loads for orthotropic and cross-ply laminated graphite-epoxy circular cylindrical shells ($R = 10$ in., $L = 34.64$ in., $h = 0.12$ in., $E_1 = 30 \times 10^6$ psi, $E_2 = 0.75 \times 10^6$ psi, $G_{12} = 0.375 \times 10^6$ psi, $\nu_{12} = 0.25$).

Laminate	Axial force ($k_2 = 0$)		Lateral pressure ($k_1 = 0$)	
	CST	LWT (4)	CST	LWT(4)
0	US*	1,600.6 (3,7) [†]	1,582.4 (3,7)	60.374 (1.6)
	$S_a = 500$	3,922.0	3,624.1	93.047 (1.6)
		(1.5)	(1.5)	(1.7)
	$S_a = 1,000$	3,922.0	3,624.1	93.047 (1.7)
		(1.5)	(1.5)	(1.7)
	US	2,008.8 (3,6)	1,978.0 (3,6)	107.35 (1.5)
0/90/0	$S_a = 500$	4,904.6	4,801.3	155.6 (1.6)
		(1.4)	(1.4)	(1.6)
	$S_a = 1,000$	5,656.6	5,551.4	175.25 (1.6)
		(1.4)	(1.4)	(1.6)

[†] Mode number

*US = Unstiffened; S_a = number of axial stiffeners (outside).

12.6.4 Postbuckling of Laminated Cylinders

Introduction

In the previous section we studied linearized (eigenvalue) buckling analysis using the layerwise shell theory. The development is extended here to postbuckling analysis. The displacements are expanded in the surface of the shell by means of a double trigonometric expansion, and the Ritz method is used to obtain the nonlinear set of algebraic equations. Numerical results are presented for the postbuckling response of axially compressed multilayered cylinders for different values of shell imperfection (see Savoia and Reddy [108,109]).

Governing Equations

Consider a laminated circular cylindrical shell of total thickness h , mean radius R , and length L . The shell is laminated of N orthotropic layers with 0° or 90° orientations. The cylinder is simply supported on its edges. A local coordinate

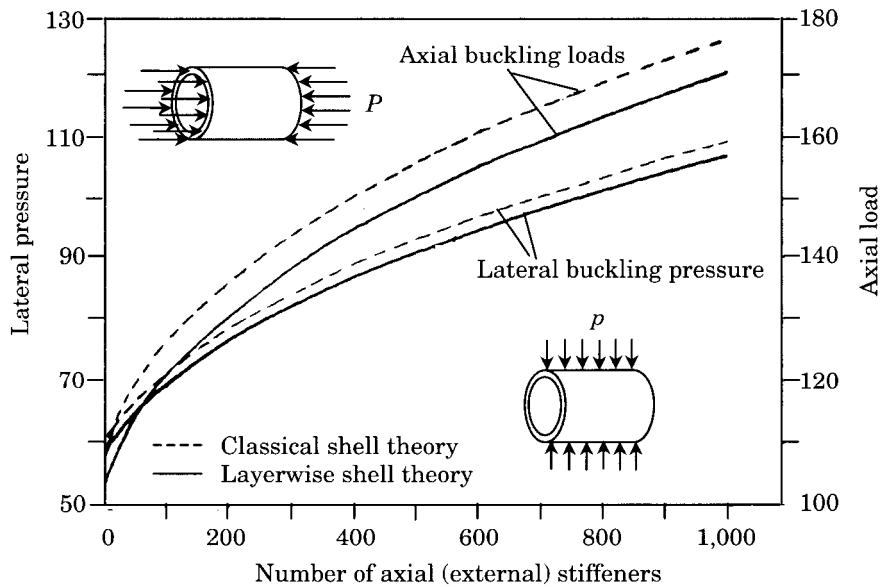


Figure 12.6.3: Lateral buckling pressure and axial buckling loads of an axially stiffened, orthotropic cylindrical shell according to the classical and layerwise shell theories.

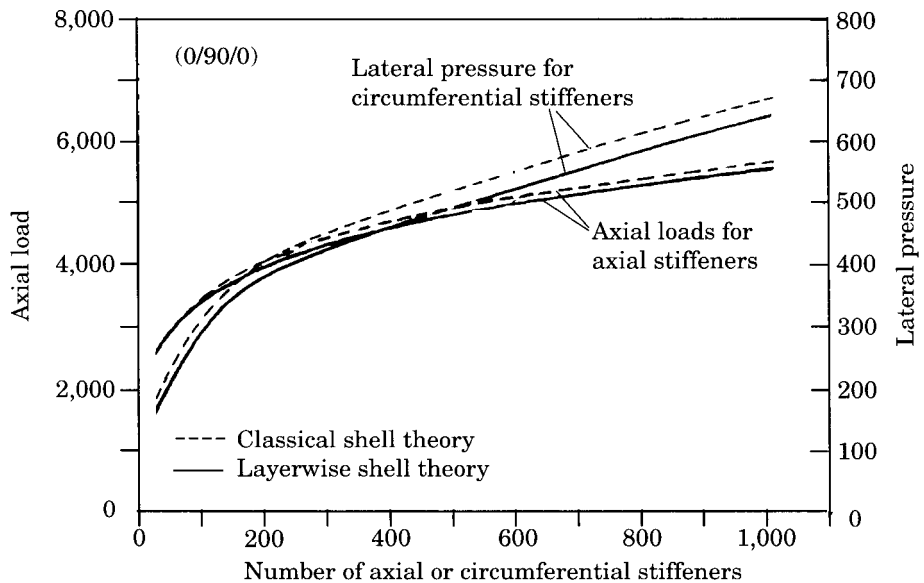


Figure 12.6.4: Lateral buckling pressure and axial buckling loads of cross-ply (0/90/0) laminated, circumferentially or axially stiffened cylindrical shells according to classical and layerwise shell theories.

system (x, y, z) is used (see Figure 12.6.5), in which x and y are in the axial and circumferential directions and z is in the direction of the outward normal to the middle surface; the corresponding displacements are designated by u , v and w . In addition \hat{w} denotes the radial deviation (i.e., geometric imperfection) of the shell from the perfectly cylindrical shape.

Considering a small shell thickness when compared with the radius of curvature R (i.e., shallow shell theory) and taking into account the nonlinear strains due to large radial displacements, the following nonlinear strain-displacement relations (see Donnell [100]) are obtained:

$$\begin{aligned}\varepsilon_1 &= \frac{\partial u}{\partial x} + \frac{\partial w}{\partial x} \left(\frac{1}{2} \frac{\partial w}{\partial x} + \frac{\partial \hat{w}}{\partial x} \right), & \varepsilon_2 &= \frac{\partial v}{\partial y} + \frac{w}{R} + \frac{\partial w}{\partial y} \left(\frac{1}{2} \frac{\partial w}{\partial y} + \frac{\partial \hat{w}}{\partial y} \right) \\ \varepsilon_3 &= \frac{\partial w}{\partial z}, & \varepsilon_4 &= \frac{\partial v}{\partial z} + \frac{\partial w}{\partial y} - \frac{v}{R}, & \varepsilon_5 &= \frac{\partial u}{\partial z} + \frac{\partial w}{\partial x} \\ \varepsilon_6 &= \frac{\partial u}{\partial y} + \frac{\partial v}{\partial x} + \frac{\partial w}{\partial x} \left(\frac{1}{2} \frac{\partial w}{\partial y} + \frac{\partial \hat{w}}{\partial y} \right) + \frac{\partial w}{\partial y} \left(\frac{1}{2} \frac{\partial w}{\partial x} + \frac{\partial \hat{w}}{\partial x} \right)\end{aligned}\quad (12.6.36)$$

Virtual Work Statement

Suppose that the circular cylindrical shell is subjected to axial load distribution q at the ends and internal and external pressure distributions p_b and p_t . The minimum total potential energy principle is used to obtain the Ritz equations. The minimum total potential energy principle states that $\delta\Pi = 0$, where $\delta\Pi$ is the first variation of the total potential energy,

$$\begin{aligned}\delta\Pi = & \int_0^L \int_0^{2\pi R} \int_{-h/2}^{h/2} \sigma_i \delta\varepsilon_i dz dy dx - \int_0^{2\pi R} \int_{-h/2}^{h/2} [q(y, z) \delta u|_{x=0} + q(y, z) \delta u|_{x=L}] dz dy \\ & - \int_0^L \int_0^{2\pi R} [p_b(x, y) \delta w|_{z=-h/2} + p_t(x, y) \delta w|_{z=h/2}] dy dx\end{aligned}\quad (12.6.37)$$

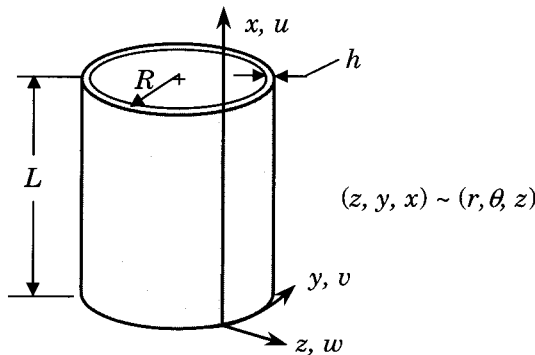


Figure 12.6.5: Geometry and coordinate system used for a cylindrical shell.

Substituting for the strains from Eq. (12.6.36) into (12.6.37) and carrying out integration through the shell thickness, we obtain

$$\begin{aligned} & \int_0^L \int_0^{2\pi R} \left\{ M_1^i \frac{\partial \delta u_i}{\partial x} + M_1^{ij} \frac{\partial \delta w_i}{\partial x} \left(\frac{\partial w_j}{\partial x} + \frac{\partial \hat{w}_j}{\partial x} \right) + M_2^i \left(\frac{\partial \delta v_i}{\partial y} + \frac{1}{R} \delta w_i \right) \right. \\ & \quad + M_2^{ij} \frac{\partial \delta w_i}{\partial y} \left(\frac{\partial w_j}{\partial y} + \frac{\partial \hat{w}_j}{\partial y} \right) + M_6^i \left(\frac{\partial \delta u_i}{\partial y} + \frac{\partial \delta v_i}{\partial x} \right) \\ & \quad \left. + M_6^{ij} \left[\frac{\partial \delta w_i}{\partial x} \left(\frac{\partial w_j}{\partial y} + \frac{\partial \hat{w}_j}{\partial y} \right) + \frac{\partial \delta w_i}{\partial y} \left(\frac{\partial w_j}{\partial x} + \frac{\partial \hat{w}_j}{\partial x} \right) \right] \right. \\ & \quad \left. + Q_3^i \delta w_i + Q_4^i \delta v_i + K_4^i \left(-\frac{1}{R} \delta v_i + \frac{\partial \delta w_i}{\partial y} \right) + Q_5^i \delta u_i + K_5^i \frac{\partial \delta w_i}{\partial x} \right\} dx dy \\ & \quad - \int_0^{2\pi R} T_i (q \delta u_i|_{x=0} + q \delta u_i|_{x=L}) dy \\ & \quad - \int_0^L \int_0^{2\pi R} [p_b(x, y) \delta w_1 + p_t(x, y) \delta w_{N+1}] dy dx = 0 \end{aligned} \quad (12.6.38)$$

where the axial load q is assumed to be constant through the thickness, and T_i is defined as

$$T_i = \int_{\frac{h}{2}}^{\frac{h}{2}} \phi^i dz = \begin{cases} t_1 & i = 1 \\ \frac{t_i + t_{i+1}}{2} & 2 \leq i \leq N \\ \frac{t_{N+1}}{2} & i = N+1 \end{cases} \quad (12.6.39)$$

Here t_i denotes the thickness of the i th layer. The laminate resultants M_α^i , M_α^{ij} , Q_α^i , and K_α^i are defined as follows:

$$\begin{aligned} M_\alpha^i &= \int_{\frac{h}{2}}^{\frac{h}{2}} \sigma_\alpha \phi^i dz \quad (\alpha = 1, 2, 6) \\ M_\alpha^{ij} &= \int_{\frac{h}{2}}^{\frac{h}{2}} \sigma_\alpha \phi^i \phi^j dz \quad (\alpha = 1, 2, 6) \\ Q_\alpha^i &= \int_{\frac{h}{2}}^{\frac{h}{2}} \sigma_\alpha \frac{d\phi^i}{dz} dz \quad (\alpha = 3, 4, 5) \\ K_\alpha^i &= \int_{\frac{h}{2}}^{\frac{h}{2}} \sigma_\alpha \phi^i dz \quad (\alpha = 4, 5) \end{aligned} \quad (12.6.40)$$

We assume that the laminated cylindrical shell is made of orthotropic layers with elastic symmetry with respect to the mean surface of the shell and material principal axes coincident with the axial and circumferential directions x and y (i.e., the cylinder is made of cross-ply lamination scheme).

The stress resultants in Eq. (12.6.40) can be expressed in terms of the generalized displacements as

$$\begin{aligned}
M_1^i &= D_{11}^{ij} \frac{\partial u_j}{\partial x} + D_{11}^{ijk} \frac{\partial w_j}{\partial x} \left(\frac{1}{2} \frac{\partial w_k}{\partial x} + \frac{\partial \hat{w}_k}{\partial x} \right) + D_{12}^{ij} \left(\frac{\partial v_j}{\partial y} + \frac{w_j}{R} \right) \\
&\quad + D_{12}^{ijk} \frac{\partial w_j}{\partial y} \left(\frac{1}{2} \frac{\partial w_k}{\partial y} + \frac{\partial \hat{w}_k}{\partial y} \right) + \bar{D}_{13}^{ij} w_j \\
M_2^i &= D_{12}^{ij} \frac{\partial u_j}{\partial x} + D_{22}^{ijk} \frac{\partial w_j}{\partial x} \left(\frac{1}{2} \frac{\partial w_k}{\partial x} + \frac{\partial \hat{w}_k}{\partial x} \right) + D_{22}^{ij} \left(\frac{\partial v_j}{\partial y} + \frac{w_j}{R} \right) \\
&\quad + D_{22}^{ijk} \frac{\partial w_j}{\partial y} \left(\frac{1}{2} \frac{\partial w_k}{\partial y} + \frac{\partial \hat{w}_k}{\partial y} \right) + \bar{D}_{23}^{ij} w_j \\
M_6^i &= D_{16}^{ij} \left(\frac{\partial u_j}{\partial y} + \frac{\partial v_j}{\partial x} \right) + D_{66}^{ijk} \left[\frac{\partial w_j}{\partial x} \left(\frac{1}{2} \frac{\partial w_k}{\partial y} + \frac{\partial \hat{w}_k}{\partial y} \right) + \frac{\partial w_j}{\partial y} \left(\frac{1}{2} \frac{\partial w_k}{\partial x} + \frac{\partial \hat{w}_k}{\partial x} \right) \right] \\
M_1^{ij} &= D_{11}^{ijk} \frac{\partial u_k}{\partial x} + D_{11}^{ijkl} \frac{\partial w_k}{\partial x} \left(\frac{1}{2} \frac{\partial w_\ell}{\partial x} + \frac{\partial \hat{w}_\ell}{\partial x} \right) + D_{12}^{ijk} \left(\frac{\partial v_k}{\partial y} + \frac{w_k}{R} \right) \\
&\quad + D_{12}^{ijkl} \frac{\partial w_k}{\partial y} \left(\frac{1}{2} \frac{\partial w_\ell}{\partial y} + \frac{\partial \hat{w}_\ell}{\partial y} \right) + \bar{D}_{13}^{ijk} w_k \\
M_2^{ij} &= D_{12}^{ijk} \frac{\partial u_k}{\partial x} + D_{12}^{ijkl} \frac{\partial w_k}{\partial x} \left(\frac{1}{2} \frac{\partial w_\ell}{\partial x} + \frac{\partial \hat{w}_\ell}{\partial x} \right) + D_{22}^{ijk} \left(\frac{\partial v_k}{\partial y} + \frac{w_k}{R} \right) \\
&\quad + D_{22}^{ijkl} \frac{\partial w_k}{\partial y} \left(\frac{1}{2} \frac{\partial w_\ell}{\partial y} + \frac{\partial \hat{w}_\ell}{\partial y} \right) + \bar{D}_{23}^{ijk} w_k \\
M_6^{ij} &= D_{16}^{ijk} \left(\frac{\partial u_k}{\partial y} + \frac{\partial v_k}{\partial x} \right) + D_{66}^{ijkl} \left[\frac{\partial w_k}{\partial x} \left(\frac{1}{2} \frac{\partial w_\ell}{\partial y} + \frac{\partial \hat{w}_\ell}{\partial y} \right) + \frac{\partial w_k}{\partial y} \left(\frac{1}{2} \frac{\partial w_\ell}{\partial x} + \frac{\partial \hat{w}_\ell}{\partial x} \right) \right] \\
Q_3^i &= \bar{D}_{13}^{ji} \frac{\partial u_j}{\partial x} + \bar{D}_{13}^{jki} \frac{\partial w_j}{\partial x} \left(\frac{1}{2} \frac{\partial w_k}{\partial x} + \frac{\partial \hat{w}_k}{\partial x} \right) + \bar{D}_{23}^{ji} \left(\frac{\partial v_j}{\partial y} + \frac{w_j}{R} \right) \\
&\quad + \bar{D}_{23}^{jki} \frac{\partial w_j}{\partial y} \left(\frac{1}{2} \frac{\partial w_k}{\partial y} + \frac{\partial \hat{w}_k}{\partial y} \right) + \bar{D}_{33}^{ij} w_j \\
Q_4^i &= \bar{D}_{44}^{ij} v_j + \bar{D}_{44}^{ji} \left(\frac{\partial w_j}{\partial y} - \frac{v_j}{R} \right), \quad Q_5^i = \bar{D}_{55}^{ij} u_j + \bar{D}_{55}^{ji} \frac{\partial w_j}{\partial x} \\
K_4^i &= \bar{D}_{44}^{ij} v_j + D_{44}^{ji} \left(\frac{\partial w_j}{\partial y} - \frac{v_j}{R} \right), \quad K_5^i = \bar{D}_{55}^{ij} u_j + D_{55}^{ji} \frac{\partial w_j}{\partial x} \tag{12.6.42}
\end{aligned}$$

where the laminate stiffnesses appearing in Eqs. (12.6.42) are defined as

$$\begin{aligned}
D_{\alpha\beta}^{ij} &= \int_{-\frac{h}{2}}^{\frac{h}{2}} C_{\alpha\beta} \phi^i \phi^j dz, & D_{\alpha\beta}^{ijk} &= \int_{-\frac{h}{2}}^{\frac{h}{2}} C_{\alpha\beta} \phi^i \phi^j \phi^k dz \\
\bar{D}_{\alpha\beta}^{ij} &= \int_{-\frac{h}{2}}^{\frac{h}{2}} C_{\alpha\beta} \phi^i \frac{d\phi^j}{dz} dz, & D_{\alpha\beta}^{ijkl} &= \int_{-\frac{h}{2}}^{\frac{h}{2}} C_{\alpha\beta} \phi^i \phi^j \phi^k \phi^\ell dz \\
\bar{D}_{\alpha 3}^{ijk} &= \int_{-\frac{h}{2}}^{\frac{h}{2}} C_{\alpha 3} \phi^i \phi^j \frac{d\phi^k}{dz} dz, & \bar{D}_{\alpha\beta}^{ij} &= \int_{-\frac{h}{2}}^{\frac{h}{2}} C_{\alpha\beta} \frac{d\phi^i}{dz} \frac{d\phi^j}{dz} dz \tag{12.6.43}
\end{aligned}$$

where $i, j, k = 1, 2, \dots, N+1$ and $\alpha, \beta = 1, 2$. The explicit form of these coefficients is given in Appendix 1 of [107]. The effect of the stiffeners can be included in the same way as was done in the buckling analysis (see [107–109]).

Ritz Equations and Numerical Examples

Suppose that the circular cylindrical shell is subjected to axial load distribution q at the ends and internal and external pressure distributions p_b and p_t . The wall imperfection is represented in terms of an increment to the radial deflection, and the increment \hat{w} is assumed to be in the same form as the displacement field. For simply-supported boundary conditions, the following solution form, which satisfies the boundary conditions $u_i = 0$ at $x = L/2$, $v_i = 0$, $w_i = 0$ and $\hat{w}_i = 0$ at $x = 0, L$ is used:

$$\begin{aligned} u_i &= U_i^{mn} \cos \alpha_m x \cos \beta_n y \quad (m = 0, \dots, M; \quad n = 0, \dots, N) \\ v_i &= V_i^{mn} \sin \alpha_m x \sin \beta_n y \quad (m = 1, \dots, M; \quad n = 1, \dots, N) \\ w_i &= W_i^{mn} \sin \alpha_m x \cos \beta_n y \quad (m = 1, \dots, M; \quad n = 0, \dots, N) \\ \hat{w}_i &= \hat{W}_i^{mn} \sin \alpha_m x \cos \beta_n y \quad (m = 1, \dots, M; \quad n = 0, \dots, N) \end{aligned} \quad (12.6.44)$$

Substitution of (12.6.44) into (12.6.42), and the result into the variational statement (12.6.38), we obtain a set of nonlinear algebraic equations (see [98,99]). Up to twelve buckling modes have been included in the analysis. The nonlinear equations are solved making use of the Riks–Wempner incremental iterative scheme in order to follow the equilibrium path through limit points. The tangent stiffness matrix, which is evaluated at each load step and iteration, can be found in [107–109].

A cross-ply (0/90/0) laminated cylindrical shell subjected to axial compression is chosen to study the effect of axial and/or ring stiffeners on the postbuckling behavior. The cylinder has the following geometric parameters, $L = 300$ cm, $R = 95.49$ cm and thickness $h = 1$ cm. The individual layers have equal thicknesses $h_i = h/3$, and the elastic coefficients are those typical of a high-modulus graphite-epoxy composite material: $E_1 = 150$ GPa, $E_2 = 7$ GPa, $G_{12} = 3.5$ GPa, $G_{23} = 1.4$ GPa, $\nu_{12} = \nu_{23} = 0.3$, where subscripts “1” and “2” denote the directions along the length and transverse to the fibers, respectively. The geometric and material characteristics of the I -shaped steel stiffeners adopted here are

$$E_a = E_c = 210\text{GPa}, \quad G_a = G_c = 80.8\text{GPa}$$

$$A_a = A_c = 1.2\text{cm}^2, \quad \bar{I}_a = \bar{I}_c = 7.2\text{cm}^4$$

$$J_a = J_c = 0.004\text{cm}^4 \quad \bar{z}_a = \bar{z}_c = 3.5\text{cm}$$

Four cases are considered: (a) unstiffened cylinder, (b) cylinder with 40 axial stiffeners, (c) cylinder with 40 ring stiffeners, and (d) cylinder with 40 axial and 40 ring stiffeners.

Figures 12.6.6–12.6.9 contain plots of the axial deflection versus the axial applied load for different values of the mode imperfections, with reference to the unstiffened, axially stiffened, ring stiffened, and axial and ring stiffened cylinders, respectively. The deformed shapes in the postbuckling path are also depicted. Note that the maximum load can be reached for very small geometric imperfections only.

For the unstiffened cylinder (Figure 12.6.6) the maximum buckling load q_{max} and the minimum post-buckling load q_{mpb} are almost coincident, and are approximately 60% of the buckling load. The postbuckling path is related to the coupling of modes (4,7) and (4,8), and its stiffness in the axial direction is approximately one-half of the membrane stiffness. For the axially stiffened cylinder (Figure 12.6.7) the reduction in the load-carrying capacity due to the smaller geometrical imperfection is only 20%. But unlike the previous case, q_{mpb} is considerably lower than q_{max} , and the postbuckling branch is characterized by a stiffness which is comparable to that of the prebuckling path; this is essentially due to the very high bending rigidity of the shapes involved during buckling (i.e., modes (1,4),(1,5),(1,6)). Moreover, it should be noted that for this cylinder, whose critical mode is characterized by a prevailingly inward radial displacement, a positive barreling ${}^3\hat{\Delta}_i^{mn} = 10^{-2}\text{cm}$ causes a reversal of the radial displacement during postbuckling and an increment of stiffness in the postbuckling path (Hutchinson and Frauenthal [99]).

The ring stiffened cylinder (Figure 12.6.8) shows the highest reduction of the load-carrying capacity, namely, 44% of the buckling load. In addition, the deformed shape is almost axisymmetric, with a high number of axial waves (modes (14,1), (14,2) and (14,3)); no minimum postbuckling load has been reached, and the postbuckling branch rapidly decreases. Higher values of the maximum load have been obtained for very small values of the geometrical imperfections ${}^3\hat{\Delta}_i^{mn} < 10^{-7}\text{cm}$. Then, in this case the linearized buckling analysis cannot yield any information about the real load-carrying capacity of the cylinder. Moreover, even the b -factor initial postbuckling analyses (Koiter [96]; Hutchinson and Amazigo [98]; Hutchinson and Frauenthal [99]) are valid in the neighborhood of the maximum load for small values of geometrical imperfections only, so that they cannot be used to predict this decreasing behavior. Finally, if axial and ring stiffeners are used (Figure 12.6.9), not only the buckling load is rapidly increased, but also a low imperfection-sensitivity occurs, and the reduction in the load-carrying capacity is approximately 20%.

12.7 Closure

In this chapter a generalized layerwise theory proposed and advanced by the author and his colleagues is described and analytical and finite element solutions of the theory are presented. The layerwise theory of Reddy [37] is based on assumed displacement field, in which the thickness variation is represented using one-dimensional finite elements and thereby reducing the 3-D continuum to a 2-D problem. The procedure has the advantage of using independent approximation of thickness variations from in-plane discretizations. Otherwise, the layerwise theory is indeed the same as the traditional 3-D displacement finite element model.

A hierarchical, displacement-based, global-local finite element model that permits an accurate, efficient, and convenient analysis of localized three-dimensional effects in laminated composite plates is also presented. By superimposing a hierarchy of assumed displacement fields in the same finite element domain, a variable kinematic finite element model is developed. All displacement fields in the hierarchy share the same assumed in-plane variation but differ in their assumed transverse variation.

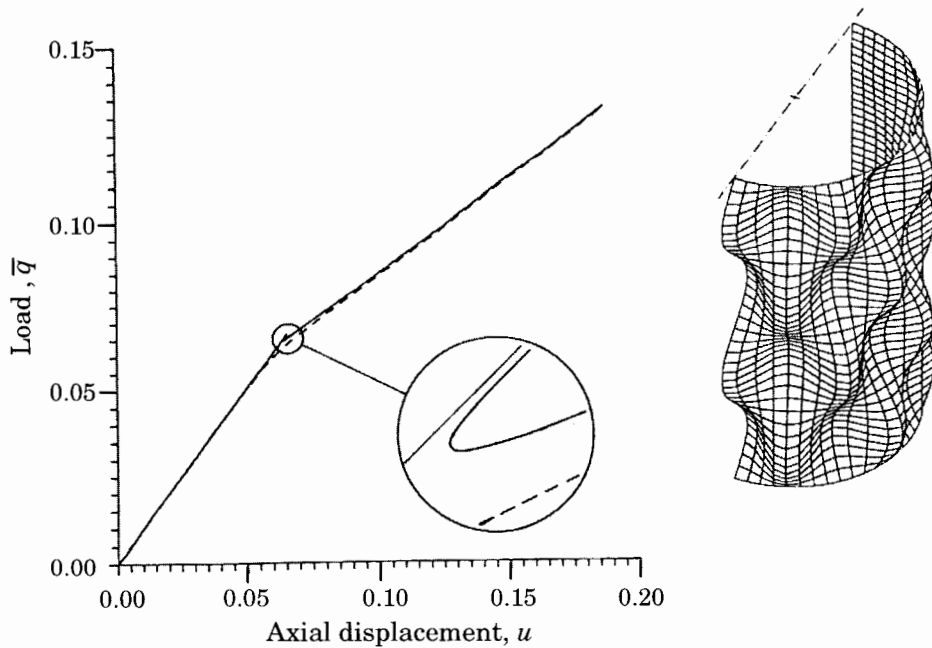


Figure 12.6.6: Plot of axial deflection (at $x=L/2$, $y=0$, $z=-h/2$) vs. load for different values of the mode imperfection (solid line: ${}^3\hat{\Delta}_i^{mn} = 10^{-5}$ cm; broken line: ${}^3\hat{\Delta}_i^{mn} = 10^{-2}$ cm); *unstiffened cylinder*.

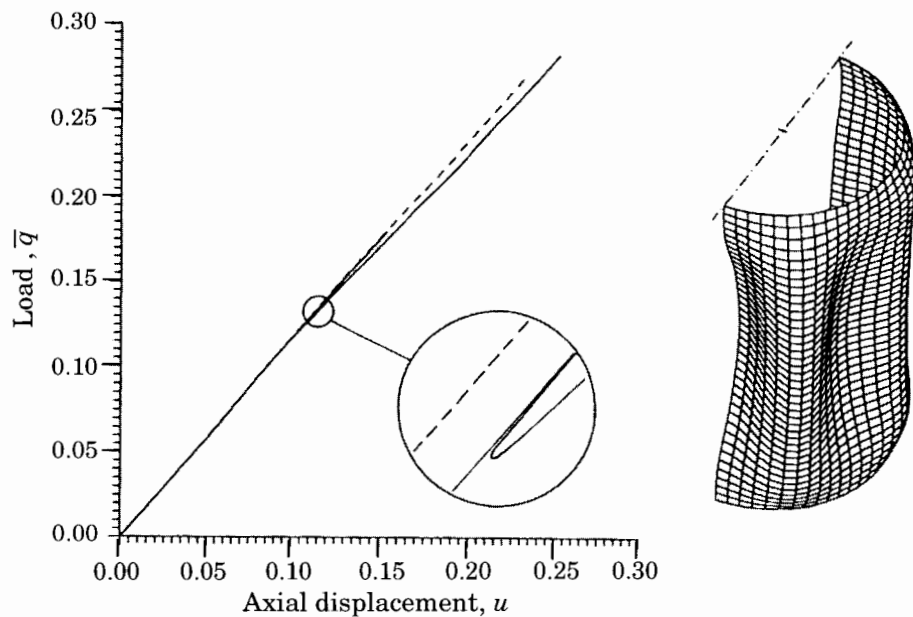


Figure 12.6.7: Plot of axial deflection (at $x=L/2$, $y=0$, $z=-h/2$) vs. load for different values of the mode imperfection; cylinder with 40 *axial stiffeners*.

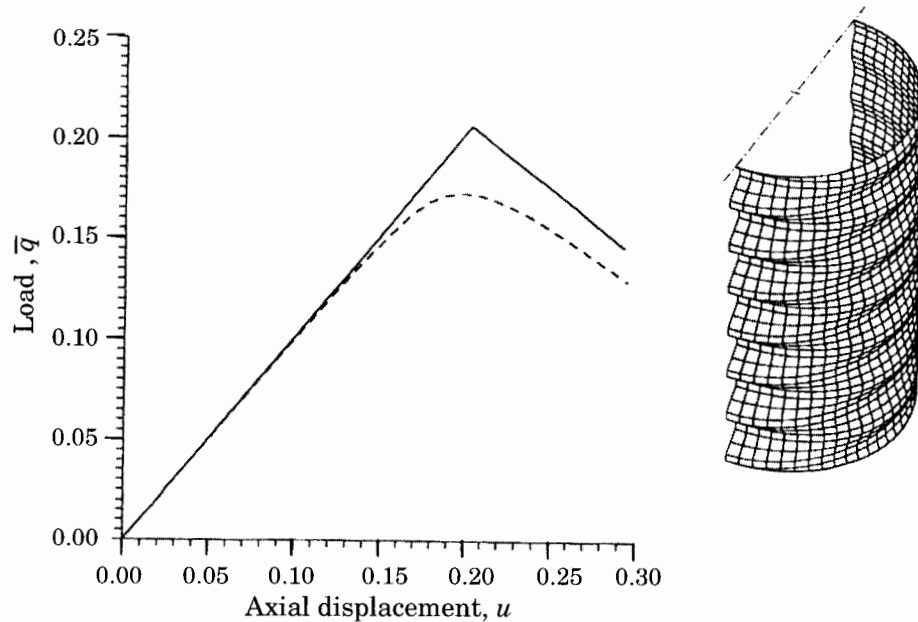


Figure 12.6.8: Plot of axial deflection (at $x=L/2$, $y=0$, $z=-h/2$) vs. load for different values of the mode imperfection; cylinder with 20 *ring stiffeners*.

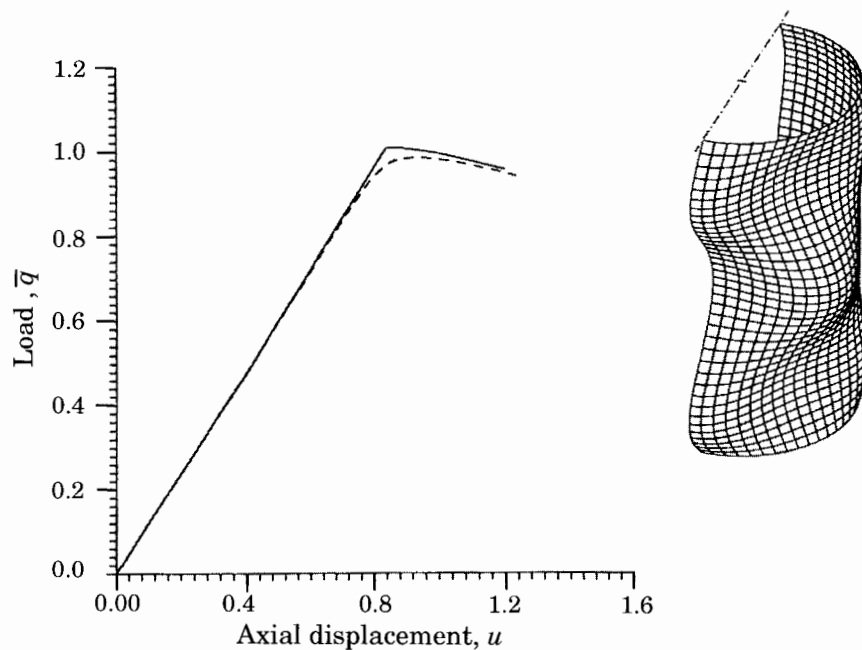


Figure 12.6.9: Plot of axial deflection (at $x=L/2$, $y=0$, $z=-h/2$) vs. load for different values of the mode imperfection; cylinder with 20 *ring stiffeners* and 40 *axial stiffeners*.

The underlying foundation of the variable kinematic element's composite displacement field is provided by a two-dimensional "equivalent single-layer" plate theory (e.g., the first-order shear deformation theory). The layerwise displacement field of Reddy [37] is included as an optional, incremental enhancement to the displacement field of the two-dimensional plate theory, so that the element can have full three-dimensional modeling capability when needed. Depending on the desired level of accuracy, an element can use none, part, or all of the layerwise field to create a hierarchy of different elements having a wide range of kinematic complexity and representing a number of different mathematical models. Discrete layer transverse shear effects and discrete layer transverse normal effects can be independently added to the element by including appropriate terms from the layerwise field. The delamination kinematics can also be included as described by Barbero and Reddy [50] and Robbins and Reddy [52].

In a 2-D mesh of variable kinematic finite elements, each one of the elements is capable of simulating any of the element types in the hierarchy. Due to the hierarchical nature of the multiple assumed displacement fields, displacement continuity can be maintained between different types of elements in the hierarchy (i.e., elements based on different mathematical models) by simply enforcing homogeneous essential boundary conditions on certain terms in the composite displacement field along the incompatible boundary. This simple process can easily be automated and subsequently removed from the concern of the user/analyst. Thus, in a single 2-D mesh of variable kinematic finite elements, it is possible to designate several different subregions that are described by elements that are based on different mathematical models. The variable kinematic elements circumvent the inconvenience and problems associated with the traditional methods of maintaining displacement continuity across incompatible subdomains (e.g., multipoint constraints, special transition elements, and penalty methods).

The layerwise theory was applied in Section 12.5 to study adaptive laminated composite structures composed of composite layers and active materials. As expected, the layerwise theory yields very accurate results for displacements as well as stresses when compared to the solutions obtained with plate theories.

The layerwise theory was extended in Section 12.6 to study buckling and postbuckling of circular cylindrical shells with or without stiffeners. Linear general buckling and nonlinear (postbuckling) analysis results are presented. In the postbuckling analysis (the Ritz method was used to reduce the continuum problem to a set of nonlinear algebraic equations, which are then solved using the Riks-Wempner iterative technique) it is observed that the magnitude of imperfection has an effect on the load-carrying capacity of the shells. The maximum load-carrying capacity of a shell can be achieved only for small imperfection (say $10^{-5} \sim 10^{-4}$ times the thickness of the shell). For large imperfections, the shell does not exhibit any obvious elastic limit load; the nonlinear load-deflection curves indicate softening structural response. Numerical results for stiffened and unstiffened cylinders show that imperfection-sensitivity is strictly related to the number of nearly simultaneous buckling modes.

We note that the variable kinematic modeling approach described here has a great potential for multi-scale modeling of composite laminates. A form of the layerwise finite element model is being incorporated into a standard commercial code.

References for Additional Reading

1. Pagano, N. J., "Exact Solutions for Composite Laminates in Cylindrical Bending," *Journal of Composite Materials*, **3**, 398–411 (1969).
2. Pagano, N. J., "Exact Solutions for Rectangular Bidirectional Composites and Sandwich Plates," *Journal of Composite Materials*, **4**, 20–34 (1970).
3. Pagano, N. J. and Hatfield, S. J., "Elastic Behavior of Multilayered Bidirectional Composites," *AIAA Journal*, **10**, 931–933 (1972).
4. Srinivas, S., Joga Rao, C. V., and Rao, A. K., "An Exact Analysis for Vibration of Simply Supported Homogeneous and Laminated Thick Rectangular Plates," *Journal of Sound and Vibration*, **12**, 187–199 (1970).
5. Srinivas, S. and Rao, A. K., "Bending, Vibration and Buckling of Simply Supported Thick Orthotropic Rectangular Plates and Laminates," *International Journal of Solids and Structures*, **6**, 1463–1481 (1970).
6. Noor, A. K., "Mixed Finite-Difference Scheme for Analysis of Simply Supported Thick Plates," *Computers and Structures*, **3**, 967–982 (1973).
7. Noor, A. K., "Free Vibrations of Multilayered Composite Plates," *AIAA Journal*, **11**, 1038–1039 (1973).
8. Savoia, M. and Reddy, J. N., "A Variational Approach to Three-Dimensional Elasticity Solutions of Laminated Composite Plates," *Journal of Applied Mechanics*, **59**, S166–S175 (1992).
9. Varadan, T. K. and Bhaskar, K., "Bending of Laminated Orthotropic Cylindrical Shells – An Elasticity Approach," *Composite Structures*, **17**, 141–156 (1991).
10. Ren, J. G., "Exact Solutions for Laminated Cylindrical Shells in Cylindrical Bending," *Composite Science and Technology*, **29**, 169–187 (1987).
11. Whitney, J. M., "The Effect of Transverse Shear Deformation in the Bending of Laminated Plates," *Journal of Composite Materials*, **3**, 534–547 (1969).
12. Swift, G. W. and Heller, R. A., "Layered Beam Analysis," *Journal of the Engineering Mechanics Division, ASCE*, **100**, 267–282 (1974).
13. Durocher, L. L. and Solecki, R., "Bending and Vibration of Isotropic Two-Layer Plates," *AIAA Journal*, **13**, 1522–1523 (1975).
14. Seide, P., "An Improved Approximate Theory for the Bending of Laminated Plates," *Mechanics Today*, **5**, 451–466 (1980).
15. Chaudhuri, R. A. and Seide, P., "Triangular Finite Element for Analysis of Thick Laminated Plates," *International Journal for Numerical Methods in Engineering*, **24**, 1203–1224 (1987).
16. Yu, Y. Y., "A New Theory of Elastic Sandwich Plates—One Dimensional Case," *Journal of Applied Mechanics*, **26**, 415–421 (1959).
17. Boal, J. L. and Reissner, E., "Three-Dimensional Theory of Elastic Plates with Transverse Inextensibility," *Journal of Mathematical Physics*, **39**, 161–181 (1961).
18. Srinivas, S., "A Refined Analysis of Laminated Composites," *Journal of Sound and Vibration*, **30**, 495–507 (1973).
19. Green, A. E. and Naghdi, P. M., "A Theory of Laminated Composite Plates," *IMA Journal of Applied Mathematics*, **29**, 1–23 (1982).
20. Rehfield, L. W. and Valisetty, R. R., "A Comprehensive Theory for Planar Bending of Composite Laminates," *Computers and Structures*, **15**, 441–447 (1983).
21. Mau, S. T., "A Refined Laminate Plate Theory," *Journal of Applied Mechanics*, **40**, 606–607 (1973).
22. Chou, P. C. and Carleone, J., "Transverse Shear in Laminated Plate Theories," *AIAA Journal*, **11**, 1333–1336 (1973).
23. Di Sciuva, M., "A Refined Transverse Shear Deformation Theory for Multilayered Anisotropic Plates," *Atti della Accademia delle Scienze di Torino*, **118**, 269–295 (1984).
24. Di Sciuva, M., "Bending, Vibration, and Buckling of Simply Supported Thick Multilayered Orthotropic Plates: An Evaluation of a New Displacement Model," *Journal of Sound and Vibration*, **105**, 425–442 (1986).

25. Di Sciuva, M., "An Improved Shear-Deformation Theory for Moderately Thick Multilayered Anisotropic Shells and Plates," *Journal of Applied Mechanics*, **54**(3), 589–596 (1987).
26. Murakami, H., "Laminated Composite Plate Theory with Improved In-Plane Responses," *Journal of Applied Mechanics*, **53**, 661–666 (1986).
27. Ren, J. G., "A New Theory of Laminated Plate," *Composite Science and Technology*, **26**, 225–239 (1986).
28. Zukas, J. A. and Vinson, J. R., "Laminated Transversely Isotropic Cylindrical Shells," *Journal of Applied Mechanics*, **38**, 400–407 (1971).
29. Waltz, T. L. and Vinson, J. R., "Interlaminar Stress in Laminated Cylindrical Shells of Composite Materials," *AIAA Journal*, **14**, 1213–1218 (1976).
30. Reddy, J. N., "A Simple Higher-Order Theory for Laminated Composite Plates," *Journal of Applied Mechanics*, **51**, 745–752 (1984).
31. Hsu, T. M. and Wang, J. T. S., "A Theory of Laminated Cylindrical Shells Consisting of Layers of Orthotropic Laminae," *AIAA Journal*, **8**, 2141–2146 (1970).
32. Rath, B. K. and Das, Y. C., "Vibration of Laminated Shells," *Journal of Sound and Vibration*, **28**(4), 737–757 (1973).
33. Mau, S. T., Tong, P., and Pian, T. H. H., "Finite Element Solutions for Laminated Plates," *Journal of Composite Materials*, **6**, 304–311 (1972).
34. Spilker, R. L., "A Hybrid-Stress Finite-Element Formulation for Thick Multilayer Laminates," *Computers and Structures*, **11**, 507–514 (1980).
35. Spilker, R. L., "An Invariant Hybrid-Stress Eight-Node Element for Thin and Thick Multilayer Laminated Plates," *International Journal for Numerical Methods in Engineering*, **20**, 573–587 (1984).
36. Hinrichsen, R. L. and Palazotto, A. N., "Nonlinear Finite Element Analysis of Thick Composite Plates Using Cubic Spline Functions," *AIAA Journal*, **24**(11), 1836–1842 (1986).
37. Reddy, J. N., "A Generalization of Two-Dimensional Theories of Laminated Composite Plates," *Communications in Applied Numerical Methods*, **3**, 173–180 (1987).
38. Barbero, E. J., Reddy, J. N., and Teply, J. L., "General Two-Dimensional Theory of Laminated Cylindrical Shells," *AIAA Journal*, **28**(3), 544–553 (1990).
39. Owen, D. R. J. and Li, Z. H., "A Refined Analysis of Laminated Plates by Finite Element Displacement Methods – I. Fundamentals and Static Analysis," *Computers and Structures*, **26**(6), 907–914 (1987).
40. Owen, D. R. J. and Li, Z. H., "A Refined Analysis of Laminated Plates by Finite Element Displacement Methods – II. Vibration and Stability," *Computers and Structures*, **26**(6), 915–923 (1987).
41. Epstein, M. and Glockner, P. G., "Nonlinear Analysis of Multilayered Shells," *International Journal of Solids and Structures*, **13**, 1081–1089 (1977).
42. Epstein, M. and Huttelmaier, H. P., "A Finite Element Formulation for Multilayered and Thick Plates," *Computers and Structures*, **16**, 645–650 (1983).
43. Lee, K. H., Senthilnathan, N. R., Lim, S. P., and Chow, S. T., "An Improved Zig-Zag Model for the Bending of Laminated Composite Plates," *Composite Structures*, **15**, 137–148 (1990).
44. Lee, K. H., Kin, W. Z., and Chow, S. T., "Bi-Directional Bending of Laminated Composite Plates Using an Improved Zig-Zag Model," *Composite Structures*, **28**, 283–294 (1994).
45. Xavier, P. B., Lee, K. H., and Chew, C. H., "An Improved Zigzag Model for the Bending of Laminated Composite Shells," *Composite Structures*, **26**, 123–138 (1993).
46. Xavier, P. B., Chew, C. H., and Lee, K. H., "Buckling and Vibration of Multilayer Orthotropic Composite Shells Using a Simple Higher-Order Layerwise Theory," *International Journal of Solids and Structures*, **32**, 3479–3497 (1995).
47. Reddy, J. N., "On the Generalization of Displacement-Based Laminate Theories," *Applied Mechanics Reviews*, **42**(11), Part 2, S213–S222 (1989).
48. Reddy, J. N., Barbero, E. J., and Teply, J. L., "A Plate Bending Element Based on a Generalized Laminate Theory," *International Journal of Numerical Methods in Engineering*, **28**, 2275–2292 (1989).

49. Barbero, E. J., Reddy, J. N., and Teply, J., "An Accurate Determination of Stresses in Thick Laminates Using a Generalized Plate Theory," *International Journal of Numerical Methods in Engineering*, **29**, 1–14 (1990).
50. Barbero, E. J. and Reddy, J. N., "Modeling of Delamination in Composite Laminates Using a Layer-Wise Plate Theory," *International Journal of Solids and Structures*, **28**(3), 373–388 (1991).
51. Robbins, D. H., Jr. and Reddy, J. N., "Modeling of Thick Composites Using a Layerwise Laminate Theory," *International Journal for Numerical Methods in Engineering*, **36**, 655–677 (1993).
52. Robbins, D. H., Jr. and Reddy, J. N., "The Effects of Kinematic Assumptions on Computed Strain Energy Release Rates for Delaminated Composite Plates," *Mathematical Modeling and Scientific Computing*, **1**(1,2), 50–66 (1993).
53. Reddy, J. N., *An Introduction to the Finite Element Method*, Second Edition, McGraw-Hill, New York, 1992.
54. Goldbery, J. L. and Schwartz, A. J., *Systems of Ordinary Differential Equations, An Introduction*, Harper and Row, New York, 1972.
55. Nosier, A., Kapania, R. K., and Reddy, J. N., "Free Vibration Analysis of Laminated Plates Using a Layerwise Theory," *AIAA Journal*, **31**(12), 2335–2346 (1993).
56. Nosier, A., Kapania, R. K., and Reddy, J. N., "Low-Velocity Impact of Laminated Composites Using a Layerwise Theory," *Computational Mechanics*, **13** (5), 360–379 (1994).
57. Wang, S. S. and Choi, I., "Boundary-Layer Effects in Composite Laminates, Part I: Free Edge Stress Singularities," *Journal of Applied Mechanics*, **49**, 541–548 (1982).
58. Wang, S. S. and Choi, I., "Boundary-Layer Effects in Composite Laminates, Part II: Free Edge Stress Solutions and Basic Characteristics," *Journal of Applied Mechanics*, **49**, 549–560 (1982).
59. Whitcomb, J. D., Raju, I. S., and Goree, J. G., "Reliability of the Finite Element Method for Calculating Free Edge Stresses in Composite Laminates," *Computers and Structures*, **15**(1), 23–37 (1982).
60. Whitcomb, J. D., "Three-Dimensional Analysis of a Post-Buckled Embedded Delamination," *Journal of Composite Materials*, **23**, 470–487 (1989).
61. Whitcomb, J. D. and Raju, I. S., "Analysis of Interlaminar Stresses in Thick Composite Laminates With and Without Edge Delamination," *Delamination and Debonding of Materials*, ASTM STP 876, W. S. Johnson (Ed.), American Society for Testing and Materials, Philadelphia, PA, 69–94 (1985).
62. Thompson, D. M. and Griffin, O. H., Jr., "2-D to 3-D Global/Local Finite Element Analysis of Cross-Ply Composite Laminates," *Journal of Reinforced Plastics and Composites*, **9**, 492–502 (1990).
63. Knight, N. F. et al., "Global/Local Methods Research Using a Common Structural Analysis Framework," *Finite Elements in Analysis and Design*, **9**, 91–112 (1991).
64. Mao, K. M. and Sun, C. T., "A Refined Global-Local Finite Element Analysis Method," *International Journal for Numerical Methods in Engineering*, **32**, 29–43 (1991).
65. Whitcomb, J. D. and Woo, K., "Application of Iterative Global/Local Finite Element Analysis. Part 1: Linear Analysis," *Communications in Numerical Methods in Engineering*, **9**(9), 745–756 (1993).
66. Whitcomb, J. D. and Woo, K., "Application of Iterative Global/Local Finite Element Analysis. Part 2: Geometrically Non-Linear Analysis," *Communications in Numerical Methods in Engineering*, **9**(9), 757–766 (1993).
67. Wang, A. S. D. and Crossman, F. W., "Calculation of Edge Stresses in Multi-Layer Laminates by Sub-Structuring," *Journal of Composite Materials*, **12**, 76–83 (1978).
68. Pagano, N. J. and Soni, S. R., "Global-Local Laminate Variational Model," *International Journal of Solids and Structures*, **19**(3), 207–228 (1983).
69. Chang, F. K., Perez, J. L., and Chang, K. Y., "Analysis of Thick Laminated Composites," *Journal of Composite Materials*, **24**, 801–821 (1990).

70. Jones, R., Callinan, R., Teh, K. K., and Brown, K. C., "Analysis of Multi-Layer Laminates Using Three-Dimensional Super Elements," *International Journal for Numerical Methods in Engineering*, **20**(3), 583–587 (1984).
71. Sun, C. T. and Liao, W. C., "Analysis of Thick Section Composite Laminates Using Effective Moduli," *Journal of Composite Materials*, **24**, 977–993 (1990).
72. Aminpour, A. A., et al., "A Global/Local Analysis Method for Treating Details in Structural Design," *Adaptive, Multilevel, and Hierarchical Computational Strategies*, ASME, AMD Vol. 157, A. K. Noor (Ed.), 119–137 (1992).
73. Surana, K. S., "Transition Finite Elements for Three-Dimensional Stress Analysis," *International Journal for Numerical Methods in Engineering*, **15**, 991–1020 (1980).
74. Surana, K. S., "Geometrically Nonlinear Formulation for the Transition Finite Elements for the Three-Dimensional Solid-Shell Transition Finite Elements," *Computers and Structures*, **15**, 549–566 (1982).
75. Liao, C. L., Reddy, J. N., and Engelstad, S. P. "A Solid-Shell Transition Element for Geometrically Nonlinear Analysis of Composite Structures," *International Journal for Numerical Methods in Engineering*, **26**, 1843–1854 (1988).
76. Davila, C., "Solid-to-Shell Transition Elements for the Computation of Interlaminar Stresses," *Second U.S. National Congress on Computational Mechanics*, Washington, D.C., August 16–18, 1993.
77. Mote, C. D., "Global-Local Finite Element," *International Journal for Numerical Methods in Engineering*, **3**, 565–574 (1971).
78. Dong, S. B., "Global-Local Finite Element Methods," *State-of-the-Art Surveys on Finite Element Technology*, A. K. Noor and W. D. Pilkey (Eds.), ASME, 451–474 (1983).
79. Reddy, J. N., and Robbins, D. H., Jr., "Analysis of Composite Laminates Using Variable Kinematic Finite Elements," *RBCM-Journal of the Brazilian Society of Mechanical Sciences*, **14**(4), 299–326 (1992).
80. Reddy, J. N. and Robbins, D. H., Jr., "A Simultaneous Multiple Model Approach for the Analysis of Composite Laminates," *Journal of the Aeronautical Society of India*, **45**, 157–177 (1993).
81. Robbins, D. H., Jr. and Reddy, J. N., "Variable Kinematic Modeling of Laminated Composite Plates," *International Journal for Numerical Methods in Engineering*, **39**, 2283–2317 (1996).
82. O'Brien, T. K., "Characterization of Delamination Onset and Growth in a Composite Laminate," *Damage in Composite Materials*, K. L. Reifsneider (Ed.), STP 775, American Society for Testing Materials, Philadelphia, PA, 140–167 (1982).
83. O'Brien, T. K., "Analysis of Local Delaminations and Their Influence on Composite Laminate Behavior," *Delamination and Debonding of Materials*, STP 877, W. S. Johnson (Ed.), American Society for Testing Materials, Philadelphia, PA, 282–297 (1985).
84. O'Brien, T. K., "Mixed-Mode Strain-Energy Release Rate Effects on Edge Delamination of Composites," *Effects of Defects in Composite Materials*, ASTM STP 836, American Society for Testing and Materials, Philadelphia, PA, 125–142 (1984).
85. O'Brien, T. K. et al., "Comparisons of Various Configurations of the Edge Delamination Test for Interlaminar Fracture Toughness," *Toughened Composites*, ASTM STP 937, N. J. Johnston (Ed.), American Society for Testing and Materials, Philadelphia, PA, 199–221 (1987).
86. Tiersten, H. F., *Linear Piezoelectric Plate Vibrations*, Plenum Press, New York (1969).
87. Benjeddou, A., "Advances in Piezoelectric Finite Element Modeling of Adaptive Structural Elements: A Survey," *Computers and Structures*, **76**, 347–363 (2000).
88. Saravanos, D. A. and Heyliger P. R., "Mechanics and Computational Models for Laminated Piezoelectric Beams, Plates and Shells," *Applied Mechanics Reviews*, **52**(10), 305–320 (1999).
89. Heyliger, P., Ramirez, G., and Saravanos, D., "Coupled Discrete-Layer Finite Elements for Laminated Piezoelectric Plates," *Communications in Numerical Methods in Engineering*, **10**, 971–981 (1994).

90. Saravanos, D. A., Heyliger, P. R., and Hopkins, D. A., "Layerwise Mechanics and Finite Elements for the Dynamic Analysis of Piezoelectric Composite Plates," *International Journal of Solids and Structures*, **34**(3), 359–378 (1997).
91. Semedo Garcão, J. E., Mota Soares, C. M., Mota Soares, C. A., and Reddy, J. N., "Analysis of Adaptive Laminated Plate Structures Using Layerwise Finite Element Models," *Computers and Structures* (to appear).
92. Haus, H. A. and Melcher, J. R., *Electromagnetic Fields and Energy*, Prentice-Hall, Englewood Cliffs, NJ (1989).
93. Bisegna, P. and Maceri, F., "An Exact Three-Dimensional Solution for Simply Supported Rectangular Piezoelectric Plates," *Journal of Applied Mechanics*, **63**, 628–638 (1996).
94. Heyliger, P., "Exact Solutions for Simply Supported Laminated Piezoelectric Plates," *Journal of Applied Mechanics*, **64**, 299–306 (1997).
95. Lage, R. G., Mota Soares, C. M., Mota Soares, C. A., Reddy, J. N., "Modelling of Piezolaminated Plates Using Layerwise Mixed Finite Elements," *Proceedings of the Sixth International Conference on Computational Structures Technology*, B.H.V. Topping and Z. Bittnar (Eds.), Civil-Comp Press, Stirling, Scotland, Paper 128 (2002).
96. Koiter, W. T., "On the stability of elastic equilibrium," Thesis, Delft, 1945; English translation issued as NASA TT-F10833 (1967).
97. Budiansky, B. and Hutchinson, J. W., "A Survey of Some Buckling Problems," *AIAA Journal*, **4**, 1505–1510 (1966).
98. Hutchinson, J. W. and Amazigo, J. C., "Imperfection-Sensitivity of Eccentrically Stiffened Cylindrical Shells," *AIAA Journal*, **5**, 392–401 (1967).
99. Hutchinson, J. W. and Frauenthal, J. C., "Elastic Postbuckling Behavior of Stiffened and Barreled Cylindrical Shells," *Journal of Applied Mechanics*, **36**, 784–790 (1969).
100. Baruch, M. and Singer, J., "Effect of Eccentricity of Stiffeners on the General Instability of Stiffened Cylindrical Shells Under Hydrostatic Pressure," *Journal of Mechanical Engineering Science*, **5**(1), 23–27 (1963).
101. Jones, R. M., "Buckling of Circular Cylindrical Shells with Multiple Orthotropic Layers and Eccentric Stiffeners," *AIAA Journal*, **6**(12), 2301–2305 (1968). *Errata*, **7**(10), 2048 (1969).
102. Arbocz, J. and Babcock, Ch. D., "Prediction of Buckling Loads Based on Experimentally Measured Initial Imperfections," *Buckling of Structures*, IUTAM Symposium, Budiansky, B. (Ed.), Springer-Verlag, Berlin, 291–311 (1974).
103. Byskov, E. and Hansen, J. C., "Postbuckling and Imperfection Sensitivity Analysis of Axially Stiffened Cylindrical Shells with Mode Interaction," *Journal of Structural Mechanics*, **8**, 205–224 (1980).
104. Simitses, G. J., "Buckling and Postbuckling of Imperfect Cylindrical Shells: a Review," *Applied Mechanics Reviews*, **39**, 1517–1524 (1986).
105. Reddy, J. N., "A Layerwise Shell Theory with Applications to Buckling and Vibration of Cross-Ply Laminated Circular Cylindrical Shells," Research Report CCMS-92-01, Center for Composite Materials and Structures, Virginia Polytechnic Institute and State University, Blacksburg, VA (1992).
106. Reddy, J. N. and Starnes, Jr., J. H., "General Buckling of Stiffened Circular Cylindrical Shells According to a Layerwise Theory," *Computers and Structures*, **49**(4), 605–616 (1993).
107. Reddy, J. N. and Savoia, M., "Postbuckling of Laminated Circular Cylindrical Shells According to the Layerwise Shell Theory," Research Report CCMS-92-02, Center for Composite Materials and Structures, Virginia Polytechnic Institute and State University, Blacksburg, VA (1992).
108. Savoia, M. and Reddy, J. N., "Layer-Wise Shell Theory for Postbuckling of Laminated Circular Cylindrical Shells," *AIAA Journal*, **30**(8), 2148–2154 (1992).
109. Savoia, M. and Reddy, J. N., "Post-Buckling Behavior of Stiffened Cross-Ply Cylindrical Shells," *Journal of Applied Mechanics*, **61**, 998–1000 (1994).
110. Donnell, L. H., *Beams, Plates and Shells*, McGraw-Hill, New York (1976).

Subject Index

- Adaptive structures, 780
 Admissible configurations, 38
 Admissible displacements, 51
 Admissible variations, 43, 53
 Alternating symbol, 5
 Analytical solution, 227, 257, 297,
 377, 439, 463, 475
 Angle-ply laminate, 142, 150
 antisymmetric, 155, 326
 Anisotropic body, 22
 Anisotropic layer, 147, 680
 Antisymmetric angle-ply laminates,
 155, 326, 353, 400, 421, 687
 Antisymmetric cross-ply laminate,
 154, 301, 348, 379, 412
 nonlinear response, 608
 third-order theory, 684
 Antisymmetric laminates,
 144, 152–155, 301, 326, 681
 Apparent moduli of an orthotropic
 material, 103
 Approximation functions, 59, 269–271
 Asymmetric laminate, 144

 Backward difference method, 363, 502
 Balanced laminate, 156
 Barlow points, 524
 Basis vectors, 4
 orthonormal, 4
 BCIZ triangle, 495
 Beam:
 bending of, 169–176, 188–192
 buckling of, 176–182, 192–197
 Euler–Bernoulli theory of, 167,
 168, 224
 nonlinear bending of, 595
 Reddy third-order theory of, 224

 Timoshenko theory of, 187, 188, 224
 vibration of, 182–187, 197–200
 Bending (static response):
 of antisymmetric angle-ply plates
 (CLPT), 329, 353
 (FSDT), 404, 426
 (TSDT), 694
 of antisymmetric cross-ply plates
 (CLPT), 308, 345, 349
 (FSDT), 381, 416
 (TSDT), 689
 of beams, 169–176, 188–192
 of doubly curved shells, 467
 of plates (FEM), 500, 511, 525
 of specially orthotropic plates, 246,
 382
 Betti's reciprocity theorem, 29
 Bifurcation, 271
 Body force, 7
 Boundary conditions:
 essential, 43, 59, 127
 force, 43, 168
 geometric, 43, 45, 59, 168
 homogeneous, 43
 natural, 43, 126, 127, 137, 735
 of beams, 169
 of cantilever (fixed-free) beams,
 50, 175
 of clamped (fixed-fixed) beams,
 173, 175, 180, 185, 190, 196, 198
 of free beams, 182, 184
 of hinged-fixed beams, 182, 184
 of simply supported beams, 172,
 180, 184, 190, 196, 198
 of simply supported plate strips,
 205, 208

- of simply supported plates, 246, 259, 271, 282, 290, 341, 439
- SS-1, 299, 300, 359, 379, 422, 465, 511, 597, 601, 625, 682
- SS-2, 301, 326, 400, 422, 511, 683
- SS-3, 597
- Buckling
 - deflection, 176
 - loads of beams, 176
 - mode, 179, 180
 - of antisymmetric angle-ply plates, (CLPT), 335, 354
 - (FSDT), 405, 428
- of antisymmetric cross-ply plates, (CLPT), 317, 347, 351
- (FSDT), 388, 419
- (TSDT), 698
- of beams, 68, 176–182, 192–197
- of circular cylindrical shells, 473
- of laminated plates (FEM), 500
- of specially orthotropic plates, 271, 285, 393
- under compressive loads, 271
- under shear load, 278
- C^0 —Continuity, 172, 699
- C^1 —Continuity, 767
- C^0 plate element, 519
- C^1 plate element, 495
- Cartesian coordinates, 4
- Cauchy stress formula, 8, 18
- Cauchy stress, 8, 18
- Central difference method, 363, 502
- Ceramic-metal, 617
- Characteristic equation, 181, 182, 184, 265, 269–271
- Characteristic polynomial,
see Characteristic equation
- Classical plate theory (CLPT):
 - assumptions of, 113
 - boundary conditions, 126
 - cylindrical bending, 131, 200
 - displacement field, 114
 - equations of motion, 119–124, 246, 297, 568
- finite element model of, 488
- strains, 116, 117
- Classical shell theory, 474
- Closed-form solution, 166, 248
- Codazzi conditions, 452
- Coefficients:
 - of hygroscopic expansion, 36
 - of mutual influence, 104
 - of thermal expansion, 35
- Collocation method, 65, 67
- Composite material, 1
- Compatibility equations, 18
- Compliance coefficients, 27
- Conditionally stable, 363
- Configuration, 13
- Conforming element:
 - rectangular element, 498
 - triangular element, 496
- Conservation of energy, 34
- Conservation of angular momentum, 20
- Conservation of linear momentum, 19
- Constant-average-acceleration method, 363, 502
- Constant strain triangle, 492
- Constitutive equations, 12, 22
 - anisotropic material, 24
 - electroelastic, 37
 - hygrothermal elastic, 36, 99
 - hyperelastic, 23, 50
 - isothermal condition, 85
 - isotropic material, 31, 32
 - monoclinic material, 25, 26
 - of a lamina, 85, 118, 119
 - orthotropic material, 26–30
 - plane stress, 33, 99–101
 - thermoelastic, 35
 - transformed, 25
- Continuum elements, 567, 631
- Continuum shell finite element, 627
- Contracted notation, 24
- Convective heat transfer coefficient, 34
- Coordinate system:
 - Cartesian, 5

- cylindrical, 6
- material, 25
- orthonormal Cartesian, 5
- rectangular Cartesian, 5
 - transformation of, 89
- Coupled ESL models, 780
- Coupled layerwise models, 780
- Cramer's rule, 308
- Critical buckling load, 68, 176, 273
- Critical time step, 363
- Cross-ply laminate, 143, 150, 699
 - antisymmetric, 154, 301, 379
- Cross product, 5
- Curl operation, 6, 11
- Cylindrical bending,
 - CLPT, 131, 200
 - FSDT, 141, 142, 214
 - FEM, 608
- Cylindrical pressure vessel, 92
- Cylindrical shell, 550, 794, 806
- Cylindrical shell panel, 551, 557, 641
- Deformation, 13
- Deformation gradient tensor, 19
- Delamination, 83, 764
- Del operator, 5
- Description of motion,
 - Eulerian, 13
 - Lagrangian, 13
 - material, 13
 - referential, 13
 - spatial, 13
- Deviatoric, 32
- Dielectric constants, 37
 - transformed, 102
- Direct methods, 58
- Direction cosines, 90
- Discrete layer theory, 728
- Displacement finite element model,
 - 500
- Dot product, 5
 - double, 10
- Dilatation, 32
- Divergence, 6, 11
- Divergence theorem, 11
- Double arrow notation, 20
- Double-dot product, 10
- Doubly-curved shells, 462, 718
- Doubly-curved shell panel, 550
- Duhamel–Neumann law, 35
- Dummy index, 5
- Dyad, 3
 - components of, 10
- Effect of bending-stretching coupling:
 - on buckling load, 209, 335, 337, 394, 406
 - on deflection, 207, 314, 317, 331, 332, 353, 388, 404
 - on frequency, 324, 339, 399, 419
 - on stresses, 313, 314, 317, 331
- Effect of bending-twisting coupling:
 - on deflection, 538
 - on frequency, 360
- Effect of lamination angle:
 - on buckling load, 213, 338, 355, 409, 428, 699
 - on deflection, 213, 333, 353, 407, 426, 533, 539, 696
 - on frequency, 213, 339, 354, 411, 428, 698
- Effect of length-to-height ratio:
 - on buckling load, 200, 201, 220, 395, 396, 409, 410, 699, 716, 717
 - on deflection, 195, 200, 217, 218, 385–387, 389, 392, 405, 407, 416, 417, 426, 427, 532, 533, 535, 636, 539, 690, 691, 694, 696, 706, 713
 - on frequency, 200, 201, 211, 223, 398–401, 410, 411, 429, 538, 540, 541, 697, 698, 716, 718
- Effect of orthotropy:
 - on buckling load, 220, 277, 289, 290, 395, 321, 322, 336, 352, 355, 420, 699
 - on deflection, 218, 314, 318, 331, 333, 350, 406, 418, 426, 427, 538, 695
 - on frequency, 284, 285, 289, 290, 324, 340, 352, 354, 400, 420, 429, 697

- on stresses, 314, 331, 406
- Effect of plate aspect ratio:**
 - on buckling load, 276, 277, 278, 321, 322, 336, 355
 - on deflection, 253, 313, 315, 318, 332, 392
 - on frequency, 285, 325, 340, 352, 354
 - on stresses, 253, 313, 315, 316
- Effect of radius-to-thickness:**
 - on deflection, 467, 468, 555, 557, 559
 - on stress, 555, 557, 559
- Effect of rotary inertia:**
 - on natural frequency, 285, 398, 399
- Effect of shear deformation:**
 - on buckling load, 395, 410, 421, 716
 - on deflection, 385–387, 405, 406, 437, 536, 538, 691, 695, 696, 705, 713
 - on frequency, 223, 398–400, 410, 420, 697–700, 716, 717
 - on stresses, 385–387, 405, 406, 437, 537, 692, 693, 705, 707, 714, 715
 - on thermal deflection, 706
- Effect of stacking sequence:**
 - on buckling load, 186, 212
 - on deflection, 186, 212
 - on natural frequency, 186, 212
- Eigenfunctions**, 264, 269–271, 360
- Eigenvalue problem**, 67, 287, 323, 337
- Eigenvalues**, 68
- Eigenvectors**, 68 *see* Eigenfunctions
- Elastic**, 22
- Elastic compliances**, 24, 27, 35
 - transformed, 97, 98
- Elastic coefficients**, 24
 - transformed, 101, 119
- Electric displacement vector**, 100
- Electric potential**, 101
- Electroelasticity**, 36
- Electrostriction**, 222
- Engineering constants**, 27–30, 86, 677
- Engineering notation**, 24
- Enthalpy function**, 37
- Entropy density**, 35
- Epsilon-delta (ϵ - δ) identity**, 5
- Equations of equilibrium**, 19
 - cylindrical bending, (CLPT), 203 (FSDT), 215
- elasticity**, 19
- Euler–Bernoulli beam theory**, 46, 169
- specially orthotropic plates**, 246
- Third-order beam theory**, 224
- Timoshenko beam theory**, 224
- Equations of motion of:**
 - antisymmetric angle-ply plates, (FSDT), 421, 422
 - antisymmetric cross-ply plates, (CLPT), 342
- classical plate theory**, 119–124, 297, 568
- cylindrical bending**,
 - (CLPT), 131
 - (FSDT), 141, 142
- elasticity (3D)**, 19
- Euler–Bernoulli beam theory**, 46–49, 226
- first-order plate theory**, 134–142, 377, 378, 575
- layerwise plate theory**, 734
- shells**, 457–460, 463, 473, 620, 719
- specially orthotropic plates**, 246
- symmetric laminates**, 356, 357
- Timoshenko beam theory**, 57, 226
- Third-order beam theory**, 57, 226
- Third-order plate theory**, 674–676
- Equivalent single-layer theory**, 109
- Error criterion**, 585
- Essential boundary condition**,
 - see* Boundary conditions
- Euler–Bernoulli beam theory**, 46, 167, 168, 224
- Euler–Bernoulli hypotheses**, 46
- Euler–Lagrange equations**, 44, 46, 49, 52, 55, 124, 136, 675, 735

- Eulerian description, 13
- Exact solution, 165
- Extensional stiffnesses, 128, 138
- Failure analysis, 648
- Failure criterion:
 - maximum stress, 648
 - Tsai–Wu, 649
- Failure mode, 654
- Fiber, 1, 81
- Fick's second law, 35
- Finite element method, 487, 567
- Finite element model of:
 - layerwise theory, 738, 785
 - plates (CLPT), 488, 572
 - plates (FSDT), 516, 578
 - plates (TSDT), 706
 - shells, 543, 622, 633
 - variable kinematic formulation, 766
- Finite strain, 15
- First-order shear deformation theory (FSDT):
 - boundary conditions, 137
 - displacement field, 132
 - equations of motion, 134–142, 575
 - finite element model of, 515
 - strains, 133, 134
- First law of thermodynamics, 34
- First Piola–Kirchhoff stress, 18
- First-ply failure, 655
- First variation, 40
- Flexure stress formula, 20
- Force boundary condition, 43
- Force resultants, 122
- Fourier's heat conduction law, 34
- Fox–Goodwin scheme, 363
- Free edge stresses, 753, 769, 779
- Frequency, *see* Vibration
- Full layerwise theory, 727
- Functional, 41
 - extrema of, 42
 - linear, 41
 - quadratic, 41
- Functionally graded plates, 613
- Fundamental lemma, 42
- Galerkin's method, 65, 66, 279
 - 363, 502
- Gauss points, 508
- Gauss quadrature, 506
- Generalized Hooke's law, 22–33, 85
- Generalized displacements, 133
- Generally orthotropic layer, 146, 150, 680
- Geometric boundary condition,
 - see* Boundary conditions
- Gibb's free energy function, 37
- Global coordinates, 503
- Global-local analysis, 759
- Gradient operator, 6
- Gradient theorem, 11
- Green–Lagrange strain tensor,
 - 14–16
- Hamilton's principle, 53–57, 457, 707, 719
- Heat conduction equation, 34
- Heat flux, 45
- Helmholtz free-energy function, 35
- Hermite interpolation, 495
- Heterogeneous body, 22
- Homogeneous, 22
- Hooke's law,
 - see* Generalized Hooke's law
- Hygroscopic expansion coefficients, 36
- Hygrothermal elasticity, 35
- Hyperelastic, 22, 23, 50
- Ideally elastic, 23
- Ill-conditioned matrix, 348, 478
- Index notation, 5
- Infinitesimal strain tensor, 16
- Initial conditions, 127, 137, 291, 441
- In-plane inertia, 323
- Integral relations, 10
- Interlaminar stresses, 726
 - see* Transverse stresses
- Internal virtual work, 44
- Internal work, 39, 44
- Interpolation functions, 487
- Invariant, 3
- Isoparametric approximation, 504

- Isotropic material, 2, 31, 32
- Jacobian matrix, 506
- Jacobian, 506
- Jordan canonical form, 478
- Kinematics, 12–16, 455
- Kinetic energy, 53
- Kinetics, 12, 454
- Kirchhoff assumptions, 113
- Kirchhoff free-edge condition, 127
- Kronecker delta, 5
- Lagrange interpolation, 491
- Lagrange multiplier method, 521
- Lagrangian description, 13
- Lamé coefficients, 452
- Lamé constants, 32
- Lamina (ply), 2, 83
- Laminate constitutive equations, 127–129, 137–139, 461, 736
- Laminated beams, 167, 187
- Laminated element, 567
- Laminated plate theories:
 - classical (CLPT), 112–131
 - first order (FSDT), 132–142
 - third order, 112
- Laminates:
 - antisymmetric, 144, 152–155, 301, 326
 - asymmetric, 144
 - angle-ply, 150, 155, 326
 - balanced, 156
 - cross-ply, 150, 154, 301
 - generally orthotropic, 150
 - single-layer, 144–147
 - specially orthotropic, 149, 150, 245
 - symmetric, 145–151
- Lamination scheme, 83
- Laplace transform, 293
- Layerwise theory:
 - displacement field of, 730
 - constitutive equations of, 736
 - equations of motion of, 734
 - finite element model of, 738, 785
 - of Reddy, 730
- stiffnesses of, 736–738
- strains of, 733
- Least squares method, 65, 66
- Lévy's method, 255, 286, 475
- Lévy solutions:
 - antisymmetric angle-ply plates, (CLPT), 353
 - (FSDT), 423
 - antisymmetric cross-ply plates, (CLPT), 342
 - (FSDT), 413
 - (TSDT), 699
- specially orthotropic plates, 255–262, 286
- Linear acceleration method, 363, 502
- Linear functional, 41
- Linearly independent set, 59
- Local coordinates, 503
- Locking:
 - membrane, 594
 - shear, 523
- Macromechanical behavior, 85
- Magnetostriction, 222
- Mass diffusitivity tensor, 35
- Mass diffusivity, 35
- Mass inertias, 122, 227, 458, 473
- Master element, 504
- Material coordinates, 13
- Material compliance matrix, 97, 98
 - transformed, 97, 98
- Material properties,
 - aluminum, 88
 - boron-epoxy, 88
 - glass-epoxy, 88
 - graphite-epoxy (AS), 88
 - graphite-epoxy (T), 88
 - graphite fabric-carbon, 30, 102
 - material 1, 525, 625, 689
 - material 2, 320, 532, 625, 694
 - steel, 88
- Material stiffnesses, 23–33
 - transformed, 96, 119
- Material strengths, 649
- Material symmetry, 25

- Matrix material, 1, 81
 Maximum stress criterion, 648
 Maxwell's relations, 36
 Mean stress, 32
 Membrane locking, *see* Locking
 Membrane strains, 117
 Mesh generation, 488
 Metric, 450
 Micromechanics, 85
 Mindlin plate theory,
 see First-order plate theory
 Minimum total potential energy, 50
 Mixed finite element model, 521
 Moisture concentration, 35
 Moment resultants, 122
 Monoclinic material, 25, 85
 Multiple model analysis,
 see Global-local analysis
 Multiple model methods, 109, 759,
 762
 Multistep methods, 759

 Natural boundary condition, 43, 126
 127, 137, 735
 Natural coordinates, 494, 504
 Navier's method, 247
 Navier's solutions:
 antisymmetric angle-ply plates,
 (CLPT), 326
 (FSDT), 402
 (TSDT), 687
 antisymmetric cross-ply plates,
 (CLPT), 301
 (FSDT), 379
 (TSDT), 684
 beam, 228
 cylindrical shell, 801
 doubly curved shells, 465
 specially orthotropic plates,
 247, 272
 Newmark's integration schemes, 362,
 502, 583
 Newton's second law, 7, 19, 44, 53
 Newton–Raphson iteration scheme,
 584
 modified, 585
 Nonconforming element:
 rectangular, 497
 triangular, 496
 Nonion form, 9
 Nonlinear analysis of:
 bending of plates, 596
 buckling of plates, 608, 645
 transient response, 612
 shell, 625, 638
 Normal derivative, 12
 Normal stress, 7, 31
 Normalized coordinates, 504
 Numerical integration, 506
 Numerical time integration,
 see Time approximation schemes

 Orthotropic lamina, 100
 Orthotropic material, 26, 85
 Orthotropic piezoelectric lamina, 118

 Partial layerwise theory, 727
 Particular solution, 59
 Particulate composites, 81
 Penalty function method, 520
 Penalty parameters, 521
 Period of vibration, 363
 Permutation symbol, 5
 Petrov–Galerkin method, 65
 Physical components, 4
 Piezoelectric effect, 36
 Piezoelectric moduli, 37, 100
 transformed, 102, 119, 438
 Piezoelectric resultants, 129, 569
 Plane of material symmetry, 25
 Plane strain, 165
 Plane stress reduced stiffnesses,
 33, 100, 677
 Plane stress, 33, 165
 Plates, 131
 classical theory of, 112–131
 first-order theory of, 132–142
 equivalent single-layer, 110
 specially orthotropic, 145, 149, 245
 third-order theory of, 671–677
 Ply, 97

- Poisson effect, 119
- Polarization charge, 36
- Polarization vector, 36
- Polyads, 10
- Postbuckling response, 645, 806
- Potential energy, 53
- Primary variables, 43, 126, 137, 227, 490, 516, 546, 676, 735
- Principle:
 - of conservation of energy, 34
 - of minimum total potential energy, 44, 50–53
 - of superposition, 27
 - of virtual displacements, 44, 45, 120, 134, 457, 631, 707, 734, 795
 - thermodynamics, 34–37
- Progressive failure, 645
- Pure extension, 17
- Pure shear, 17
- Pyroelectric constants, 37
- Pyroelectric effect, 36
- Quadratic functional, 41
- Quasi-isotropic laminate, 156
- Reciprocal relations, 28
- Rectangular Cartesian, 4
- Reddy's layerwise theory, 730
- Reddy's third-order beam theory, 224
- Reddy's third-order plate theory, 671–677
- Reduced integration, 523
- Referential description, 13
- Residual, 584
- Resultants:
 - force, 122
 - higher-order, 677
 - moment, 122
 - piezoelectric, 129
 - thermal, 128, 146, 147
- Riks–Wempner method, 585
- Ritz approximation, 62, 279, 280
 - see* Ritz method
- Ritz method, 58–62
- Rotatory inertia,
 - see* Rotary inertia
- Rotary inertia, 125
- Sanders shell theory, 449
- Scalars, 3
- Scalar product, 5
- Second law of thermodynamics, 34
- Second-order plate theory, 111
- Second Piola–Kirchhoff stress, 19
- Secondary variables, 43, 126, 137, 227, 490, 516, 546, 676, 735
- Self-starting scheme, 364
- Semidiscrete finite element model, 499, 547
- Separable solution, 361
- Sequential methods, 759
- Serendipity elements, 495
- Series solution, 166
- Set of admissible configurations, 38
- Shear correction coefficient, 57, 135
- Shear correction factors, 455
- Shear coupling, 168
- Shear-extensional coupling, 26
- Shear locking, *see* Locking
- Shear stress, 7, 31
- Shell, 449
- Simplified third order theory, 57
- Single subscript notation, 24, 85
- Spanning set, 59
- Spatial description, 13
- Specific heat, 34
- Specially orthotropic laminate, 245
- Specially orthotropic layer, 145, 150, 151, 679, 681
- Specially orthotropic plates, 245, 382
- Specially orthotropic solution, 335
- Spherical shell panel, 639, 641, 644
- Stability, *see* Buckling
- Stability, numerical, 502
- Stable equilibrium, 176
- Stacking sequence, 83
 - see* lamination scheme
- State-space approach, 260, 288, 345, 414, 425, 477, 703
- Static condensation, 308

- Stiffnesses:
- bending, 128
 - bending-extensional, 128
 - extensional, 128, 138
 - of antisymmetric angle-ply plates, 682
 - of antisymmetric cross-ply plates, 682
 - of asymmetric laminates, 144
 - of balanced laminate, 156
 - of quasi-isotropic laminate, 156
 - of single isotropic layer, 145, 678
 - of single-layer plates, 144–147, 678
 - of symmetric laminates, 680
 - laminate, 142–157
 - layerwise theory, 736, 737
- Strain-displacement relations, 13–16
- Strain:
- Green–Lagrange, 14–16, 629
 - infinitesimal, 16
 - hygrothermal, 36
 - moisture, 35
 - transformation of, 93, 94
 - thermal, 35, 36
- Strain compatibility, 18
- Strain energy, 3, 40, 50
 - complementary, 40
- Strain energy density, 23, 33, 50
- Strain gages, 87
- Strain rate tensor, 34
- Stress,
- Cauchy, 8, 18
 - deviatoric, 32
 - dyadic, 8
 - mean, 32
 - measures, 18
 - first Piola–Kirchhoff, 18
 - second Piola–Kirchhoff, 19, 629
 - single subscript notation, 24, 91
 - tensor, 8
 - transformation of, 90, 91
 - vector, 7
- Stress computation:
- of antisymmetric angle-ply plates, (CLPT), 330
 - (FSDT), 403
 - (TSDT), 688
- of antisymmetric cross-ply plates,
- (CLPT), 309
 - (FSDT), 381
 - (TSDT), 686
- of beams, 169–172
- of plates (FEM), 510, 524
- of specially orthotropic plates, 250, 383
- Subparametric formulation, 504
- Summation convention, 5, 15
- Superparametric formulation, 504
- Surface metrics, 450
- Symmetric laminate, 143, 148–151, 680
- Tangent stiffness matrix, 584
- Tensor product, 509
- Tensor, 3, 7–10
 - first-order, 10
 - Green–Lagrange strain, 14, 15
 - mass diffusivity, 35
 - product, 509
 - second-order, 10
 - third-order, 10
 - transformation of, 10
 - transpose of, 9
 - unit, 10
 - zeroth-order, 10
- Thermal coefficients of expansion, 35
 - transformed, 99, 101, 119
- Thermal conductivity tensor, 34
- Thermodynamics, 12, 34–37
- Third-order beam theory, 55–57, 224
- Third-order plate theory, 671–677
 - bending of, 689, 712
 - buckling of, 698, 712
 - displacement field of, 671–673
 - equations of motion of, 674
 - finite element model of, 706
 - stiffnesses of, 676–682
 - Lévy solution, 699
 - strains of, 674
 - vibration of, 696, 712

- Three-point bending, 172
- Time approximation schemes, 362–364
- Timoshenko beam theory, 57, 187, 188, 224
- Total Lagrangian formulation, 568, 627
- Total potential energy, 44, 50–53, 266, 279, 522
- Transformation of:
 - material coefficients, 25, 96, 97
 - strains, 93, 94
 - stresses, 90, 91
 - tensor components, 10
- Transformation matrix, 26, 636
- Transient analysis, 290, 361, 430, 612
- Transverse force resultants, 122, 135
- Transverse stresses from:
 - constitutive relations, 190, 403 686
 - equilibrium equations, 170–172, 250, 310, 382, 384, 403, 686, 688
- Tsai–Wu criterion, 649
- Uncoupled ESL models, 780
- Undetermined parameters, 58
- Uniaxial compression, 274
- Unstable equilibrium, 176
- Unsymmetric laminate, 145
- Updated Lagrangian formulation, 568, 627
- Variables,
 - primary, 43, 126, 137, 227, 490, 516, 546, 676, 735
 - secondary, 43, 126, 137, 227, 490, 516, 546, 676, 735
- Variable kinematic formulation, 759
- Variational operator, 40–42
 - properties of, 41
- Variational methods, 58
 - collocation, 65, 67, 69
 - Galerkin, 65, 66, 68, 279
 - least squares, 65, 66, 69
- Ritz, 58–62, 68, 262, 279, 280, 358
- weighted-residual, 64–68
- Vector product, 5
- Vectors, 3
 - basis, 4
 - cross product of, 5
- Vector space, 3
- Velocity feedback control, 226, 438
- Vibration, natural:
 - of antisymmetric angle-ply plates, (CLPT), 337, 354 (FSDT), 406, 428
 - of antisymmetric cross-ply plates, (CLPT), 323, 346, 351 (FSDT), 394, 419
 - of beams, 182–187, 197–200
 - of circular cylindrical shells, 473
 - of doubly curved shells, 468
 - of plates (FEM), 501, 515, 540
 - of specially orthotropic plates, 282, 285, 397
- Vibration suppression,
 - of doubly curved shells, 469
 - of laminated beams, 222
 - of laminated plates, 437
- Virtual complementary strain energy, 40
- Virtual displacements, 38, 44, 45
 - principle of, 44, 45, 120, 134, 674
- Virtual forces, 40
- Virtual strain energy, 40, 120, 134, 457, 674
- Virtual work, 38, 45, 54, 120, 134, 266, 675
- Virtual work principles, 38–46, 120
- Viscous dissipation, 34
- Voit–Kelvin notation, 24
- von Kármán nonlinearity, 567, 620, 794
- von Kármán strains, 117, 620
- Weak forms for:
 - laminated plates (CLPT), 488
 - laminated plates (FSDT), 515
 - laminated plates (TSDT), 707

midplane symmetric plates, 357
specially orthotropic plate, 266
shells, 543

Weight functions, 64

Weingarten–Gauss relations, 451

Whiskers, 1, 81

Work:

external, 45

internal, 39, 45

virtual, 38, 45, 54

f

f